癌および加齢性疾患の制御と QOL 向上を目指す創薬

平成 22 年度～平成 26 年度
私立大学戦略的研究基盤形成支援事業
研究成果報告書

平成 27 年 5 月

学校法人名　東北薬科大学
大　学　名　東北薬科大学
研究組織名　大学院薬学研究科
研究代表者　遠藤　泰之
（大学院薬学研究科・教授）

— 目　次 —

1．はしがき…… 1

2．研究成果報告書概要…… 3

3．研究発表状況

研究テーマ①

新しい作用機作をもつ癌化学療法薬の創製…… 65

研究テーマ②

エストロゲン受容体制御による加齢性疾患（骨粗鬆症、認知障害）改善薬の創製……251

研究テーマ③

癌および加齢性疾患に対する疼痛制御によるＱＯＬ向上の研究……411

平成22年度～平成26年度「私立大学戦略的研究基盤形成支援事業」（創薬研究）研究成果報告書発刊にあたって

研究代表者　遠藤　泰之

本研究プロジェクト「癌および加齢性疾患の制御とＱＯＬ向上」は、平成21年度までのハイテク･リサーチ･センター整備事業「生体内分子標的理論に基づく創薬とその臨床治療への応用」研究の研究成果を活かし、課題を集約して、さらに大きな進展を図り、東北地方における創薬研究の拠点としての役割を果たすことを目的として企画しました。

癌・加齢性疾患、あるいはこれらに付随する難治性疼痛に対する新しい治療薬の開発は高齢化社会に突入した現在、医薬科学の領域で最も社会的要請の大きい分野の一つです。本学では、ホルモン合成酵素阻害、ホルモン受容体制御などの機能を有する化合物の設計・合成・機能解析の医薬化学関連分野、疼痛制御受容体の機能解析と新規制御化合物の創製などの薬理学関連分野において、優れた実績を有しています。本プロジェクトは基礎医薬化学である分子設計・合成・活性評価から機能解析の分子生物学、薬理学、さらに臨床応用までの幅広い分野を含む８つの研究室で組織されています。本プロジェクトでは、これらの特徴ある医薬科学研究を１）天然由来化合物からの抗がん薬の創製、２）骨粗鬆症、精神疾患等の加齢性疾患制御薬の創製、３）これらの疾患に付随する難治性疼痛制御によるＱＯＬ向上の３つの研究テーマに結集し、研究の進展を図ってきました。

研究期間中に、平成23年には東日本大震災という試練もありましたが、天然由来抗がん物質の合成と構造活性相関による開発候補化合物の創製、新規エストロゲン作用化合物のうつ様行動及び認知障害の改善効果の発見、各種難治性疼痛のモルヒネ抵抗性の機構解明など、それぞれの研究テーマにおいて優れた研究成果を挙げることができました。本プロジェクトの研究成果は、医薬の開発候補化合物、リード化合物としての有用性のみならず、医薬開発の新しい方法としての端緒となることも期待しております。

平成22年度～平成26年度「私立大学戦略的研究基盤形成支援事業」
研究成果報告書概要

1 学校法人名　東北薬科大学　　2 大学名　東北薬科大学

3 研究組織名　東北薬科大学大学院薬学研究科

4 プロジェクト所在地　仙台市青葉区小松島4－4－1

5 研究プロジェクト名　癌および加齢性疾患の制御とQOL向上を目指す創薬

6 研究観点　研究拠点を形成する研究

7 研究代表者

研究代表者名	所属部局名	職名
遠藤　泰之	大学院薬学研究科	教授

8 プロジェクト参加研究者数　29　名

9 該当審査区分　理工・情報　(生物・医歯)　人文・社会

10 研究プロジェクトに参加する主な研究者

テーマ	研究者名	所属・職名	プロジェクトでの研究課題	プロジェクトでの役割
1	吉村　祐一	分子薬化学教室・教授	新規制癌性アザ糖、チオ糖及びヌクレオシド類の探索	新規抗癌薬リード化合物の創製
1	加藤　正	医薬合成化学教室・教授	抗腫瘍性抗生物質及び類縁化合物の合成	新規抗癌薬リード化合物の創製
1	山下　幸和	臨床分析化学教室・教授	アロマターゼの機能解析とホルモン依存性癌の癌化機構の解明	癌化機構の解析と新規抗癌薬リード化合物の創製
2	遠藤　泰之	創薬化学教室・教授	新規核内受容体（エストロゲン、アンドロゲン）制御化合物の分子設計及び合成	ホルモン依存性癌制御薬及び骨粗鬆症治療薬の創製
2	永田　清	環境衛生学教室・教授	核内受容体作用を簡便に検出可能なin vitro活性試験法の構築と活性評価	加齢性疾患における骨粗鬆症治療薬開発のスクリーニング
2	丹野　孝一	薬理学教室・教授	加齢性疾患モデル動物を基盤とした薬物の骨、神経系への作用解析	加齢性疾患における骨粗鬆症、精神・神経症状など生活改善薬の開発
3	櫻田　忍	機能形態学教室・教授	癌性疼痛の発症メカニズムの解明と特異的鎮痛薬の開発	癌性疼痛（難治性疼痛）の除去による癌患者のQOL向上
3	大野　勲	病態生理学教室・教授	オピオイドネットワークによる神経－免疫応答制御の解析	疼痛制御に伴う生体反応の内分泌免疫学的解析

＜研究者の変更状況＞

旧

ﾃｰﾏ	ﾌﾟﾛｼﾞｪｸﾄでの研究課題	所属・職名	研究者氏名	プロジェクトでの役割
2	加齢性疾患モデル動物を基盤とした薬物の骨、神経系への作用解析	薬理学教室・教授	只野　武	加齢性疾患における骨粗鬆症、精神・神経症状など生活改善薬の開発

（変更の時期：平成23年4月1日）

新

変更前の所属・職名	変更（就任）後の所属・職名	研究者氏名	プロジェクトでの役割
薬理学教室・准教授	薬理学教室・教授	丹野　孝一	加齢性疾患における骨粗鬆症、精神・神経症状など生活改善薬の開発

旧

ﾃｰﾏ	ﾌﾟﾛｼﾞｪｸﾄでの研究課題	所属・職名	研究者氏名	プロジェクトでの役割
1	新規制癌性アザ糖、チオ糖及びヌクレオシド類の探索	分子薬化学教室・教授	高畑　廣紀	新規抗癌薬リード化合物の創製

（変更の時期：平成26年4月1日）

新

変更前の所属・職名	変更（就任）後の所属・職名	研究者氏名	プロジェクトでの役割
分子薬化学教室・准教授	分子薬化学教室・教授	吉村　祐一	新規抗癌薬リード化合物の創製

＜研究者の追加・減員状況＞

（追加の時期：平成22年4月1日）

ﾃｰﾏ	ﾌﾟﾛｼﾞｪｸﾄでの研究課題	所属・職名	研究者氏名	プロジェクトでの役割
1	新規制癌性アザ糖、チオ糖及びヌクレオシド類の探索	分子薬化学教室・助手	名取　良浩	新規抗癌薬リード化合物の創製
1	抗腫瘍性抗生物質及び類縁化合物の合成	医薬合成化学教室・助手	成田　紘一	新規抗癌薬リード化合物の創製
1	アロマターゼの機能解析とホルモン依存性癌の癌化機構の解明	臨床分析化学教室・助手	加藤　創	癌化機構の解析と新規抗癌薬リード化合物の創製
3	オピオイドネットワークによる神経－免疫応答制御の解析	病態生理学教室・助手	河野　資	疼痛制御に伴う生体反応の内分泌免疫学的解析

（追加の時期：平成23年4月1日）

ﾃｰﾏ	ﾌﾟﾛｼﾞｪｸﾄでの研究課題	所属・職名	研究者氏名	プロジェクトでの役割
1	アロマターゼの機能解析とホルモン依存性癌の癌化機構の解明	臨床分析化学教室・講師	大野　賢一	癌化機構の解析と新規抗癌薬リード化合物の創製

（追加の時期：平成24年4月1日）

ﾃｰﾏ	ﾌﾟﾛｼﾞｪｸﾄでの研究課題	所属・職名	研究者氏名	プロジェクトでの役割
1	新規制癌性アザ糖、チオ糖及びヌクレオシド類の探索	分子薬化学教室・助教	若松　秀章	新規抗癌薬リード化合物の創製
2	加齢性疾患モデル動物を基盤とした薬物の骨、神経系への作用解析	薬理学教室・助手	根本　亙	加齢性疾患における骨粗鬆症、精神・神経症状など生活改善薬の開発

（追加の時期：平成25年4月1日）

ﾃｰﾏ	ﾌﾟﾛｼﾞｪｸﾄでの研究課題	所属・職名	研究者氏名	プロジェクトでの役割
1	新規核内受容体（エストロゲン、アンドロゲン）制御化合物の分子設計及び合成	創薬化学教室・助手	皆瀬　麻子	ホルモン依存性癌制御薬及び骨粗鬆症治療薬の創製
3	オピオイドネットワークによる神経－免疫応答制御の解析	病態生理学教室・助教	宮坂　智充	疼痛制御に伴う生体反応の内分泌免疫学的解析

（減員の時期：平成25年3月31日）

ﾃｰﾏ	ﾌﾟﾛｼﾞｪｸﾄでの研究課題	所属・職名	研究者氏名	プロジェクトでの役割
3	オピオイドネットワークによる神経－免疫応答制御の解析	病態生理学教室・助教	奥山　香織	疼痛制御に伴う生体反応の内分泌免疫学的解析

（減員の時期：平成26年3月31日）

ﾃｰﾏ	ﾌﾟﾛｼﾞｪｸﾄでの研究課題	所属・職名	研究者氏名	プロジェクトでの役割
3	癌性疼痛の発症メカニズムの解明と特異的鎮痛薬の開発	機能形態学教室・准教授	米澤　章彦	癌性疼痛（難治性疼痛）の除去による癌患者の QOL 向上

11 研究の概要（※ 項目全体を10枚以内で作成）

（1）研究プロジェクトの目的・意義及び計画の概要

癌・加齢性疾患、あるいはこれらに付随する難治性疼痛に対する新しい治療薬の開発は高齢化社会に突入した現在、医薬科学の領域で最も社会的要請の大きい分野の一つである。本学大学院薬学研究科では、平成17年度より、ハイテク・リサーチ・センター整備事業として、「生体内分子標的理論に基づく創薬とその臨床治療への応用」を実施して研究の活性化を図り、発表論文数等、目標を上回る成果を挙げている。本プロジェクトでは、東北地方における創薬研究の拠点としての役割を果たすことを念頭に、その成果を活かし、研究の焦点をより具体的に3つの研究テーマ、すなわち、①新しい作用機作をもつ癌化学療法薬の創製②エストロゲン受容体制御による加齢性疾患（骨粗鬆症、認知障害）改善薬の創製③癌および加齢性疾患に対する疼痛制御によるQOL向上の研究に集約し、全体では「癌および加齢性疾患の制御とQOL向上」をテーマとした創薬として、さらに大きな進展を図ることを目的として企画した。3つの研究テーマの具体的研究計画の概要は以下の通りである。①制癌化合物の創製に関しては天然物抗癌活性物質及び新規核酸系代謝拮抗薬等の設計・合成により新規抗癌薬のリード化合物創製に展開する。②加齢性疾患治療薬の創製に関しては、骨代謝や認知機能に関与する核内受容体制御化合物の設計・合成、転写活性化試験、動物試験に順次展開する。③癌・加齢性疾患に付随する疼痛の制御に関しては、新規ペプチド誘導体を用いた癌性疼痛時における脊髄疼痛伝達機構を明らかにする事により、癌性疼痛の発現機構を解明する。

（2）研究組織

本研究組織は、東北薬科大学大学院薬学研究科の8教室29名の研究者によって構成されており、新規化合物を設計・合成する有機化学・創薬化学系研究室から、分析・機能解析系の分析・生化学系研究室、動物試験を行なう薬理系研究室を本プロジェクトの3つの研究テーマに組織化できるように配置している。研究代表者は研究テーマ ② の責任者でもある遠藤教授が担当し、全体の統括、調整を行なうとともに、各研究者間の連携を促進するため本プロジェクトの運営会議、成果公表の取り纏め、成果発表会の企画、実行を行い、プロジェクトの充実に努めている。それぞれの研究テーマの組織は以下の通りである。

① 新しい作用機作をもつ癌化学療法薬の創製

医薬合成化学教室・加藤正教授を責任者として、分子薬化学教室（吉村祐一教授）、臨床分析化学教室（山下幸和教授）の3教室で組織し、前記教授を含み、教員11名、アソシエートスタッフ（PD相当）1名、大学院修士課程学生6名で本プロジェクトの研究を行っている。

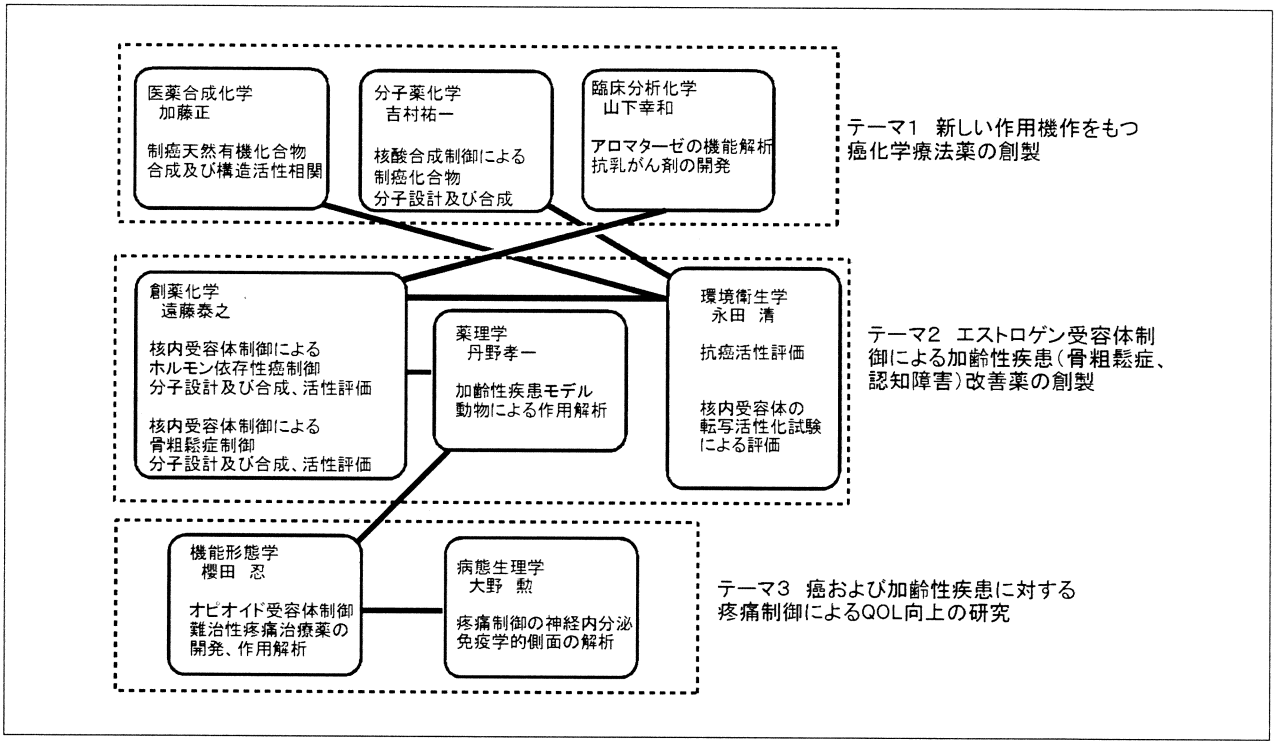
② エストロゲン受容体制御による加齢性疾患（骨粗鬆症、認知障害）改善薬の創製

創薬化学教室・遠藤泰之教授を責任者として、薬理学教室（丹野孝一教授）、環境衛生学教室（永田清教授）の3教室で組織し、前記教授を含み、教員11名、大学院博士課程学生3名、大学院修士課程学生5名で本プロジェクトの研究を行なっている。

③ 癌および加齢性疾患に対する疼痛制御によるQOL向上の研究

機能形態学教室・櫻田忍教授を責任者として、病態生理学教室（大野勲教授）との2教室で組織し、前記教授を含み、教員7名、大学院博士課程学生1名、大学院修士課程学生4名で本プロジェクトの研究を行なっている。

研究チーム間の連携に関しては、テーマ①の各研究室は、それぞれ異なる作用機構をもつ新規癌化学療法薬の合成、解析を行なっているが、得られた新規化合物の活性試験は環境衛生学教室（テーマ②）で行う計画である。テーマ②の3つの研究室は加齢性疾患治療薬の創製を目的とする新規化合物の設計・合成（創薬化学）から、転写活性試験（環境衛生学）、動物での効果解析（薬理学）まで組織化されている。テーマ③では、2つの研究室が新規ペプチドの疼痛に対する機能解析と免疫反応の両面から疼痛治療薬としての実現を目指している。以上の各研究室及び各テーマ間の連携は、以下に図示する。本プロジェクトに対しては、研究者以外に技術系職員2名、事務系職員1名が主として担当する等、大学が積極的に支援を行っている。



(3)研究施設・設備等

本研究の基盤となったハイテク・リサーチ・センター整備事業のセンター拠点およびセンター分室の総研究施設面積は 2279 ㎡(私学助成分は拠点および共用研究室 1174 ㎡)を活用し、本プロジェクトの研究者 29 名ならびにその所属する教室の PD 及び大学院生 20 名が、研究を推進している。本プロジェクトで設置した研究装置:トリプル四重極 LC-MS/MS システムの稼働時間は、ステロイド分析に有功に利用され、9326 時間、研究設備ダブルモノクロメーター式マイクロプレートリーダー及びリアルタイム PCR システムの稼働時間は、それぞれ 1571 時間、1276 時間であった。一方、ハイテク・リサーチ・センター整備事業の補助により設置した研究装置・研究設備も本プロジェクトの重要な研究設備となっており、高分解能 FT-NMR 分子構造解析システムは常時稼動し、新規化合物の構造決定に不可欠の存在として利用され、飛行時間型質量分析装置、共焦点顕微鏡画像解析装置、遺伝子タンパク解析装置、精神神経関連行動解析装置の稼働時間も、それぞれ 400 時間、384 時間、1400 時間、7033 時間と有効に活用されている。

(4)研究成果の概要 ※下記、13及び14に対応する成果には下線及び＊を付すこと。

研究プロジェクトの計画や目的・意義と関連づけて、当初の目標をどれだけ達成したか記述するとともに、新たに得られた知見などについても具体的に記述してください。

論文及び発表(項目13)は、研究テーマ毎に分け、番号をふっています。研究成果の下線はそれぞれの研究テーマの論文及び発表の番号と対応させています。

研究テーマ①新しい作用機作をもつ癌化学療法薬の創製

本研究テーマは天然物由来のがん増殖抑制効果の大きい分子標的抗がん剤の合成ルートの開発、構造活性相関の解明、さらには臨床応用可能な化合物(開発候補化合物)の創製、これまでにない構造を有する新規核酸系代謝拮抗薬の創製、アロマターゼ阻害剤及びスルファターゼ阻害剤の創製と機能解析によるホルモン依存性乳がんの制御という特徴ある3つのアプローチで研究を遂行した。

ヒストン脱アセチル化酵素(HDAC)阻害活性を有するスピルコスタチン類および p21ras ファルネシルトランスフェラーゼ阻害活性を有する TAN-1813 はいずれも微生物由来の天然有機化合物であり、新しい分子標的抗がん剤のシードとして注目されている。スピルコスタチン類の合成研究においては、収束的合成法およびマクロラクトン環化反応を基軸とする独自の方法論を用いることにより、スピルコスタチン C,D の全合成を世界に先駆けて達成した。*1 また、合成した類縁化合物の活性評価を行い、スピルコスタチン D がスピルコスタチン類の中

で最も優れたHDAC阻害活性を有することを明らかにした。*2 さらに、HDACのアイソフォーム選択性について検討したところ、マクロラクトン環の側鎖置換基の影響によりアイソフォーム選択性が大きく変化することを見出した。*3 これらの成果は今後、新しい分子標的抗がん剤を創製する上で有用な知見である。TAN-1813 の合成研究では、本化合物の C-4a 位と C-5 位の立体配置が未決定であったため、熱力学的安定性を考慮した推定構造(4aR,5S)の合成を検討した。デカリン環セグメントの合成では、フラン環を含む α,β−不飽和アルデヒドの分子内 Diels-Alder 反応を鍵工程とする方法により、デカリン環セグメントの合成を達成した。*4 もう一方のセグメントであるスクシンイミドセグメントの合成は、不斉 Michael 反応を用いることにより達成した。次に両セグメントのカップリングについて検討した。デカリンセグメントに含まれるホルミル基は立体障害により反応性が非常に低く、スクシンイミドセグメントから調製したリチウムエノラートとのカップリング反応はまったく進行しなかった。そこで、スクシンイミドセグメントにフェニルチオ基を導入した後、ヨウ化サマリウムを用いた Reformatsky 反応を行ったところ、高収率で両セグメントのカップリングに成功した。*5 さらに、得られたカップリング体をデス−マーチン試薬で酸化することにより、TAN-1813 の推定構造と等価体である化合物を合成することができた。*6

新規核酸系代謝拮抗薬の開発では、チオヌクレオシド誘導体のデザイン、合成と生物活性評価を行った。先ず、これまであまり研究例がないピラノースの含硫黄誘導体を疑似糖部とする 5'-チオチオヌクレオシド誘導体の探索を行った。目的とする疑似糖部は、cis-2-ブテン-1,4-ジオールより閉環メタセシス反応を用い、ジヒドロチオピラン骨格を構築した。得られたジヒドロチオピラン誘導体を対応するスルホキシドに変換した後、当研究室で開発した Pummerer 型チオグリコシル化反応により目的とするチオヌクレオシド誘導体の合成を達成した。*7 また、チエタン骨格が縮環した 2-oxa-6-thiabicyclo[3.2.0]heptane 骨格を疑似糖部とするイソヌクレオシド誘導体の合成も行った。*8 さらに、ジヒドロチオピラノヌクレオシドの類縁体として、ジヒドロピラノヌクレオシドの合成について検討する目的で、同誘導体合成に対応した超原子価ヨウ素試薬を利用する新規グリコシル化反応の開発にも取り組んだ。*9 開発したグリコシル化反応を利用し、新たなジヒドロピラノヌクレオシド誘導体の合成を達成した。*10 この他にも、抗癌活性と抗ウイルス活性を期待し、新規シチジンアルキルホスホネート誘導体をデザインし、その合成により、目的とするシチジンホスホネート誘導体の合成を達成した。*11 先のチオヌクレオシド誘導体に加え、ピロリジン環やピペリジン環を基本骨格とするアザ糖とそのヌクレオシド誘導体であるアザヌクレオシド類の合成についても検討した。この内、アザ糖の合成については、イリジウム触媒による不斉アリル位アルキル化反応と分子内閉環エン-インメタセシス反応により 2-イソプロピルイソファゴミンを合成した。*12 さらに、前述の不斉アリル位アルキル化反応と sp3-sp3 炭素結合生成反応を利用し、1-C-アルキル-L-アラビノイミノフラノースの合成を行った。*13 前者については、酵素阻害活性について構造活性相関研究と *In silico* ドッキングアッセイによる阻害機構の解明を行った。14 一方、後者については、さらに合成研究を進め、α-1-C-ブチル-L-アラビノフラノース誘導体を含む種々の 1 位炭素置換-L-イミノフラノース誘導体の合成を行い、α-1-C-ブチル誘導体が強い α-グリコシダーゼ阻害活性を有することを見出した。*15 さらに、1 位アリールブチル置換体の合成を行い、グリコシダーゼ阻害活性の構造活性相関について検討した。*16

一方、ホルモン依存性乳がんの制御に関して、新規アロマターゼおよびスルファターゼ阻害剤創製*17 ならびに機能解析*18を目的として、2-および 4-アミノエストロゲン並びに 4-OH-AD を母核に複素環を結合させた化合物の合成を行った。これらの化合物のアロマターゼ阻害活性について、ヒト胎盤ミクロソームを使って評価したところ、4-OH-AD にチアゾールカルボン酸を導入した化合物に強いアロマターゼ阻害活性を見出した。これに関連するエストロゲン代謝物であるカテコールエストロゲンから派生するエストロゲンオルトキノン類の一斉定量法の検討を、本研究で開発したステロイドホルモン類の LC-ESI-MS/MS 法*19 を駆使して行い、エストロゲンオルトキノンをフェナジン誘導体とすることにより、感度よく選択的に定量*20 出来ることを見出し、カテコールエストロゲンをエストロゲンオルトキノンへの変換を触媒する分子種の同定に有用であることを見出した。

研究テーマ②エストロゲン受容体制御による加齢性疾患（骨粗鬆症、認知障害）改善薬の創製

本研究テーマでは、新しい疎水性構造を用いた核内受容体制御薬の設計、合成、活性評価による新規受容体制御薬の創製、そのエストロゲン受容体制御薬を利用した精神神経系制御薬としての新たな作用の発見と機構解明、核内受容体制御系の薬物代謝酵素への関与とその評価など、核内受容体を中心とする課題の研究を推進した。

核内受容体制御リガンド設計において、新規立体的疎水性構造単位の応用は、既存の骨格の修飾では得られない、形状認識の差による活性表現の方向性の制御、新しい機構のアンタゴニズム様式等の新しい知見を

得ている。*1 組織選択的エストロゲン受容体調節に不可欠なエストロゲン受容体のアゴニスト/アンタゴニスト制御はリガンド結合による受容体構造の変化により決定付けられ、本研究での、単純な新規疎水性構造を有するジフェニルメタン骨格化合物の系統的合成により、その制御が可能であることを見出した。*2 また、エストロゲン受容体のサブタイプ α、β の選択性発現に、ハロゲンあるいはアルキル基の導入が効果的であることを見出し、選択的化合物を得ている。*3 一方、アンドロゲン受容体の新しいアンタゴニズム様式による制がん作用に着目し、我々が見出したアンドロゲン受容体拮抗リガンド BA341 の構造を基盤として、構造設計を行い、前立腺がん治療の臨床で問題となっているアンドロゲン受容体変異に対抗しうる新規アンドロゲン拮抗化合物を見出した。*4 エストロゲンと共に、重要な骨代謝制御リガンドであるビタミンD受容体の制御に関しても、新規疎水性構造を有する非セコステロイド型ビタミンD受容体アゴニストの創製に成功している。*5 受容体-リガンド相互作用の基盤となる疎水性分子間相互作用研究においても、リガンド設計に用いた新規疎水性骨格の球状の形状認識と複合体形成の基礎研究も進展している。*6 本プロジェクトで見出したエストロゲン受容体制御薬は既存の抗がんあるいは骨代謝制御に留まらず、更なる医薬分野での創製を目指し、精神神経系に対する解析についてモデル動物を用いて薬理学教室と共同で研究を開始した。BE360 が既存の選択的エストロゲン受容体制御薬(SERM)であるタモキシフェン及びラロキシフェンと比較して効果的にうつ様行動及び認知障害の両障害を改善することを見出した。*7

薬理学教室での本研究で開発された新規 SERM の精神神経系への効果の研究は、モデル動物作製と実験法の確立から開始した。アルツハイマー病やうつ病のモデル動物として用いられている嗅球摘出動物は認知障害やうつ様症状を示すが、オスと比較しメスの方がうつの症状の一つである無快感症を発現すること*8、その無快感症が中脳辺縁系のドパミン神経系の機能低下に起因していること*9 を報告した。さらに、認知障害の程度はオス及びメスで同程度であったこと*10 が判明した。これらの結果より、メスの嗅球摘出動物を用い BE360 の効果を解析した。BE360 の 100μg/day(2 週間)の慢性投与は、嗅球摘出による認知障害及び無快感症を既存の SERM であるタモキシフェンやラロキシフェンの慢性投与よりも効果的に改善した。さらに、嗅球摘出動物の子宮重量は女性ホルモンの慢性投与により有意な増加を示したが、BE360 は何ら影響を与えなかった。BE360 の作用機序を探るため分子生物学的及び免疫組織化学的に解析を行ったところ、BE360 は、抗うつ薬や抗認知症薬の反応性と関連するタンパク[cAMP response element-binding protein (CREB)のリン酸化及び脳由来神経成長因子(BDNF)発現量]の増加により海馬歯状回における神経新生を促進する可能性を明らかにした。*7、統合失調症についても、ラロキシフェンが有効であったとの報告を基に、統合失調症のモデル動物である幼若期腹側海馬障害(neonatal ventral hippocampal lesion; NVHL)ラットを用いて認知障害の指標である情報処理能力の程度を性差で比較したところメスの方がオスよりも強く障害が現れた。*11 NVHL メスラットの情報処理障害のメカニズムは、血漿エストラジオール濃度依存的ではなかった。*12 また、神経新生を抑制する薬物(MAM)を妊娠中の母親マウスに投与することにより NVHL モデルと比較してより簡便で成功率の高い神経発達障害仮説に基づいた統合失調症モデル動物の作製に成功した。*13 さらに、アンフェタミンの代謝物である *p*-hydroxyamphetamine をマウスの脳室内に投与することによっても統合失調症のモデル動物を作製することができた。*14 この結果も今後の BE360 評価のための基礎データとなる。

薬物代謝酵素活性は、医薬品の薬効および毒性発現に密接に関わっているためにその発現量を予測することが求められている。中でも肝臓や小腸での医薬品の主要な代謝酵素である CYP3A4 の発現は、核内受容体ファミリーに属する PXR や VDR によって転写制御されている。従って、PXR や VDR の ligand となりうる化合物は CYP3A4 を誘導し、薬物相互作用を引き起こすことが予測されることから、これら受容体を介した誘導評価系構築が、薬物相互作用を回避しうる新規化合物の開発に重要となる。すでに我々は肝臓系細胞株(HepG2 細胞)において CYP3A4 遺伝子転写活性化領域を利用した PXR および VDR 活性化評価系としてのレポーター遺伝子安定発現細胞株を樹立し、新たに AhR ligand である多環芳香族炭化水素類が PXR を介して CYP3A4 を誘導することを明らかにした*15。また、近年消化管における化学物質の PXR および VDR 活性化による薬物代謝関連因子(CYP3A4 や薬物トランスポーターである MDR1)の活性化による薬物相互作用が注目されていることから、PXR および VDR 活性化評価系の構築を試みた。評価系としては CYP3A4 転写活性化領域と CYP3A4 と同様に、その転写制御に PXR や VDR が関与している薬物排泄トランスポーター(MDR1)遺伝子の転写活性化領域を組み込んだレポーター遺伝子を消化管系細胞株である LS174T 細胞に導入し、各レポーター遺伝子安定発現細胞株(CYP3A4:1-2-10 細胞、MDR1:3-13 細胞)を樹立することができた。一方、薬物相互作用は、酵素誘導の他、酵素阻害によっても引き起こされることから、薬物代謝酵素阻害評価系の構

築も必要となる。そこで、薬物代謝酵素遺伝子をアデノウイルスベクターに組み込み、肝臓系細胞株に導入することで薬物代謝酵素を発現させ、化学物質による酵素阻害評価系の構築を試みた。その結果、CYP2D6 発現細胞株による活性阻害評価系を構築し、市販の健康食品についてスクリーニング調査を行うことでその有用性を示した。*16 またCYP3A4代謝活性阻害評価系については、評価の為の基本的な条件設定をほぼ決定することができた。*17 以上の結果から、新規医薬品の開発において、薬物相互作用を予測するために重要となる代表的な薬物代謝酵素の誘導および阻害評価系を構築することができた。PXR および VDR は核内受容体であり、創薬化学教室で開発された新規活性化リガンドのこれらの代謝酵素系への効果の検討も予定している。

研究テーマ③癌および加齢性疾患に対する疼痛制御による QOL 向上の研究

本研究テーマでは、がん性疼痛、各種難治性疼痛に対して、オピオイド受容体を介した有効薬の発見と機構解明、及びストレス性喘息に対するオピオイド受容体の関与と機構解明を目指して、研究を推進した。

先ず、肉腫性癌性疼痛モデルを確立し、がん性疼痛に対してはモルヒネ、オキシコドンおよびメサドンといった麻薬性鎮痛薬の鎮痛作用は著しく減弱することを見いだした*1。また、κ オピオイド受容体作動薬であるナルフラフィンの鎮痛作用も、癌性疼痛に対しては減弱することを見いだした。一方、モルヒネ抵抗性の各種難治性疼痛(神経障害性疼痛、炎症性慢性疼痛、多発性硬化症疼痛)に関しても、そのモデル動物を用い、発症メカニズムの解明ならびに有効な鎮痛薬の探索を行った。その結果、神経障害性疼痛に対してはメサドンとamidino-TAPA が*2、多発性硬化症疼痛に対してはオキシコドンとナルフラフィンが極めて有効であることを見いだした*3。また炎症性慢性疼痛に対しては、他の麻薬性鎮痛薬に比べメサドンが比較的有効であることを見いだした*4。さらに、神経障害性疼痛、炎症性慢性疼痛ならびに多発性硬化症疼痛におけるモルヒネ抵抗性には、疼痛形成時におけるそれぞれ μ 受容体の減少*5、μ 受容体のリン酸化による不活性化*6 ならびに NMDA 受容体の活性化が関与していることを見いだした。

一方、ストレス負荷により喘息反応が悪化するストレス喘息マウスモデルを用いた検討では、ストレスによる悪化がμオピオイド受容体拮抗薬を中枢神経選択的に投与されたマウスやμオピオイド受容体遺伝子欠損マウス(MORKO)では観察されなかった*7 が、中枢神経選択的に MOR を発現させた MORKO マウス(MORKO/Tg)では観察されたこと、*8 ストレスによる喘息悪化に伴うコルチコステロン遊離増加が、MORKO では低下し、MORKO/Tg では回復したこと、*9 そして、ストレスによる喘息悪化はコルチコステロン受容体拮抗薬およびコルチコステロン合成阻害薬を投与することにより軽減*10 されたことから、ストレスによる喘息悪化は、中枢神経系 MOR(nMOR)の活性化に引き続き、ストレスホルモンであるコルチコステロンが遊離され Th2免疫応答が増強することにより惹起されることを明らかにした。ストレス負荷されたマウスの気道リンパ節細胞の抗原刺激培養では、Th2 反応の増強と Th2 反応を抑制する制御性 T 細胞(Treg)の分化誘導低下が観察されたが、ストレス負荷された MORKO からの気道リンパ節細胞では観察されなかったことから、*11 ストレスによる喘息悪化は nMOR 刺激に引き続く気道局所リンパ節での Treg の分化誘導低下による Th2 反応の増強を伴うことを明らかにした。Treg は免疫寛容(Th2免疫応答の生理的抑制機構)の重要な担い手である。そこで、上記の結果から、ストレスが免疫寛容を抑制するかを検討するため、免疫寛容の誘導時にストレスを負荷したところ、ストレスにより、Treg の誘導は抑制され、Th2サイトカイン発現や喘息反応は増強した。*12 すなわち、ストレスが免疫寛容を抑制するという新たな知見を得ることができた。μ オピオイド受容体作動性鎮痛薬による免疫応答および喘息病態への影響と影響の少ない化合物構造については、健常者および喘息患者を用いて、μ オピオイド受容体遺伝子多型との関連から検討している。患者の μ オピオイド受容体一塩基多型のパターンと気道狭窄との相関から、μ オピオイド受容体を介した喘息の悪化がヒトでも示唆された。また、ヒト末梢血から分離精製した CD4+ T 細胞からの Th2サイトカイン産生が MOR アゴニスト添加で増強することを確認した。 ストレス反応において重要な役割を担う中枢性ヒスタミン受容体もストレスによる喘息悪化に関わることを明らかにした。*13

＜優れた成果があがった点＞

研究テーマ①新しい作用機作をもつ癌化学療法薬の創製

天然由来抗がん薬の合成では、スピルコスタチン C,D の初の全合成を達成*1 するとともに、マクロラクトン環の側鎖置換基が HDAC 阻害活性に与える影響について明らかにすることができた*3。また、スピルコスタチン類の合成法を応用して、2011 年に新たに発見されたブルクホルダック類の全合成も達成することができた*21。ブルクホルダック類は立体配置が未決定であったが、全合成によりその立体配置を決定することができた。さら

不斉反応を用いた短工程での合成法を開発する必要があり、現在、検討を行っている。また、TAN-1813 の合成においては、マレイミド部の構築および各保護基の脱保護条件について詳細に検討する必要があり、穏和な条件で脱保護可能な保護基の開発を含め、さらに検討を行う必要がある。疑似糖部であるチオピラノース誘導体については、以前、当研究室で開発した類似化合物の合成法を改良することで、同誘導体の合成を行った。ジヒドロピラノヌクレオシドのグリコシル化反応では、不飽和糖のアリルカチオンに対する反応では、立体異性体に加え位置異性体が発生し、その分離が困難であった。この問題を解決するため、超原子価ヨウ素を用いる酸化的グリコシル化反応を開発し、脱離反応を経由することで位置異性体の発生を回避することに成功した。エストロゲンオルトキノンは、化学的に極めて不安定な分子種でもあり、これらの物質の取り扱いは容易ではない。効果的なエストロゲンオルトキノンの捕捉ならびに質量分析法と安定同位体標識法を基盤とした迅速な内因性ステロイドのアッセイ法を目標に、適切な誘導体化を検討している。

研究テーマ②エストロゲン受容体制御による加齢性疾患（骨粗鬆症、認知障害）改善薬の創製

組織選択的エストロゲン受容体制御化合物及びアンドロゲン受容体アンタゴニストの合成において、合成法に収率及び再現性に問題がある段階があった。動物実験に供するための大量合成に適した合成法の検討を進め、反応系の濃度、反応条件の検討により、その改善に成功した。モデル動物の作成に関して、当初本プロジェクトで用いていた統合失調症モデル動物である NVHL ラットの作製は高度なテクニックが必要であり、熟練した者でも両側の海馬が破壊されている動物の成功率は 70%と決して高いものではなかった。また、ラットを用いた場合、広い飼育スペースの確保や現存のノックアウトマウスを用いて様々な解析に応用する際、マウスを用いたモデルは大変有用なものに成り得ることからマウスの統合失調症モデル動物作製に着目し、その作製に成功した。これにより、前述の問題点が解消できたものと考える。代謝系研究では、検討に用いている肝臓系細胞株は、正常な肝臓細胞の機能を一部有していないことから、実際の生体を反映した薬物相互作用の予測には不十分である。そこで iPS 細胞から肝臓細胞を分化させ、この iPS 分化肝臓細胞を用いた評価系を構築できれば、より生体に近い条件下での相互作用の予測が可能となる。現在、iPS 細胞から肝臓細胞への分化誘導を試み、分化に必要な因子の一部を同定した。

研究テーマ③癌および加齢性疾患に対する疼痛制御による QOL 向上の研究

坐骨神経周囲筋肉に肉腫細胞を移植して、坐骨神経絞扼による肉腫性癌性疼痛を発現させることに成功したが、肉腫細胞の増殖が強すぎると一次知覚神経が破壊されて痛覚麻痺が発生するといった問題が生じた。移植する肉腫細胞の量など、種々の実験条件を変更することにより、最終的に安定して癌性疼痛が測定できる実験条件を確立した。ストレスによるμオピオイド受容体刺激とグルココルチコイド（GC）遊離、免疫寛容抑制の関連は不明であり、抗原提示細胞と T 細胞サブセットの機能と GC の影響を解析する必要がある。また、μオピオイド受容体を介したストレスや μ オピオイド受容体作動性鎮痛薬による喘息悪化をヒトで解析するために、喘息の病状とμオピオイド受容体遺伝子多型との相関に対するストレス状態の影響や CD4+ T 細胞からの Th2サイトカイン産生に及ぼすμオピオイド受容体作動性鎮痛薬とμオピオイド受容体遺伝子多型との相関は例数を増やして解析する必要がある。

＜評価体制＞

（研究プロジェクトの目標等に照らした自己評価の実施や、その結果を研究費等の資源の配分へ反映させるためのルールの適切な設定、また、本プロジェクトに係る費用対効果（かけた費用に見合う効果が見られるか）について、どのように分析しているか。また、それらについて、外部（第三者）による評価を受ける体制ができているか等について記述してください。）

本プロジェクトの実施状況は、学内に於いては東北薬科大学自己評価委員会により、平成 26 年度（最終年度）終了時に、詳細な審査に基づき厳正な評価が実施される予定である。有効な研究費運用の維持に関しては創薬研究センター運営委員会を設置し、各年度の予算執行に関して随時討議を行っている。平成 24 年度終了時（中間報告作成時）における研究成果を、研究費配分に反映させる予定であったが、計画遂行が何れも順調であったため、従来の配分を維持した。また、学外有識者による本プロジェクトの外部評価体制を 24 年度に発足させた。当初構想調書、研究進捗状況報告書について、2 名の有識者に、研究の達成度、得られた成果、大学

に、ブルクホルダック A はスピルコスタチン D と同程度の HDAC1 阻害活性を有し、さらに約 5 倍のアイソフォーム選択性を有していることを明らかにした。我々の開発した方法論はスピルコスタチン類のみならず、ジスルフィド結合を有する大環状デプシペプチド類縁体の合成にも有用であることを立証することができた*22。特筆すべき点として、本研究により開発候補化合物「FK-A11」の創製に成功した*23 (その他の研究成果、特許 1,2)。核酸系代謝拮抗性抗がん薬研究では、新規ヌクレオシド誘導体に制癌活性については認められなかったものの、チオヌクレオシドの一つに抗 HIV 活性が認められた。*7 ピラノヌクレオシド合成にあたり開発した超原子価ヨウ素を利用した酸化的グリコシル化反応は、応用性に優れた合成法となった。*9,10 また、2-イソプロピルイソファゴミンと 1-C-アルキル-L-アラビノイミノフラノースが α-グリコシダーゼ阻害活性を有することが明らかとなった。*13,15 後者については、その強い α-グリコシダーゼ阻害活性に加え、動物実験でも食後過血糖の改善が認められた。*15 さらに今回開発したアザ糖誘導体の合成法は、イリジウム触媒の不斉リガンドを変えるだけで容易にエナンチオマーの合成が可能であり、*12 これらアザ糖誘導体の光学異性を含めた立体異性体の合成と構造活性相関研究への展開が期待される。ホルモン依存性乳がんの制御に関しては、エストロゲンオルトキノンの微量定量法を確立し、*20 その変換の分子種の同定並び、内因性エストラジオールによる乳がんのプロモーションメカニズム解析に有用であることが期待される。また、安定同位体基質を用いた非放射性アロマターゼ阻害活性測定法の開発*18 は、微小のアロマターゼ活性を効率良く検出することが可能とするものである。

研究テーマ②エストロゲン受容体制御による加齢性疾患(骨粗鬆症、認知障害)改善薬の創製

新規核内受容体制御化合物の創製においては、前立腺がん制御を目的としたアンドロゲン受容体アンタゴニストに関して、X 線結晶構造解析と分子モデリングを基盤として、我々が創製した BA341 の置換基変換により、アンドロゲン受容体変異に対抗しうる新規アンドロゲン拮抗化合物を見出した。*4 本プロジェクトで創製した選択的エストロゲン受容体制御薬(SERM)o-カルボランビスフェノール BE360 がうつ様行動及び認知障害を効果的に改善するという新たな活性を見出した。*7 この発見には、薬理学教室で作製したアルツハイマー病及びうつ病のメスのモデル動物*8 が重要な役割を果たした。その研究成果は、BE360 が既存の SERM であるタモキシフェン及びラロキシフェンと比較して効果的にうつ様行動及び認知障害の両障害を改善すること、*7 BE360 はエストロゲン補充療法で子宮癌へ移行する問題と成り得る子宮重量の増加を誘発しないこと、さらに、この BE360 の改善作用が海馬における CREB のリン酸化及び BDNF の増加による神経新生の促進に起因することを見出した点である。現在これらの研究成果を Behaviour Brain Research(査読有)に投稿中である。核内受容体系の代謝酵素への関与に関しては、独立に2つの転写活性化を評価しうる特徴的な細胞株の樹立が挙げられる。これは新規化合物の効率的な副作用予測のための誘導評価試験の実施に貢献できるものである。また、ヒト肝臓薬物代謝酵素である CYP3A4 の酵素誘導並びに活性阻害評価系をほぼ構築することができた*15。

研究テーマ③癌および加齢性疾患に対する疼痛制御による QOL 向上の研究

モルヒネ抵抗性を示す各種難治性疼痛(神経障害性疼痛*2、炎症性疼痛*4、多発性硬化症疼痛*3 に対して、それぞれ特異的に有効性を示す鎮痛薬を見いだした。また、神経障害性疼痛*5、炎症性慢性疼痛*6 ならびに多発性硬化症疼痛に関して、そのモルヒネ抵抗性に関わるメカニズムをそれぞれ解明した。特に炎症性慢性疼痛においては、他の難治性疼痛とは異なり、モルヒネ抵抗性が両側性に発現することを見出し、同側性と対側性のモルヒネ抵抗性発現メカニズムの違いも解明した*6。 喘息のストレス及び免疫系病態の研究では、ストレスが神経—内分泌—免疫軸を介して免疫寛容を抑制することを明らかにした本研究により、psychiatry endotype という新たな概念と治療戦略が提唱できる。また、ヒトでの喘息重症化およびをμオピオイド受容体アゴニストによる CD4+ T 細胞からの Th2サイトカイン産生の増強とμオピオイド受容体遺伝子多型との関連性を示唆する*11 結果は、μ オピオイド受容体をターゲットとした新規疼痛制御薬の開発に当たって、化合物構造と副作用の観点から重要な情報を提供する。

＜問題点＞

研究テーマ①新しい作用機作をもつ癌化学療法薬の創製

スピルコスタチン類の合成法において、重要中間体であるアリルアルコール部位を有するカルボン酸の合成法が多段階を要することから、動物実験、さらには臨床応用を指向した大量合成には不向きである。そのため、

での創薬研究拠点になりうるか、総合評価の各項目で評価及びコメントを依頼した。研究の達成度、大学での創薬研究拠点になりうるか、の 2 点では概ね達成されている、得られた成果、総合評価では優れているとの評価をいただいている。また、文部科学省からの 24 年度の中間報告(研究進捗状況報告書)の評価結果では 2 名の審査員とも、優れているとの評価をいただいている。

＜研究期間終了後の展望＞

(本プロジェクト終了後における研究の継続の有無、有の場合は今後の研究方針、無の場合は当該研究施設・装置・設備の活用方針を記述してください。)

本プロジェクトで得られた成果を総括した上で、癌および加齢性疾患の制御とQOL 向上という目標を堅持し、新しい薬理作用の発見とその機構解明を行い、新規医薬品のシードとなる化合物の創製を目指して、研究テーマや研究組織の再検討を行った上で、継続していきたいと考えている。それぞれの研究テーマについての今後の研究方針を以下に記述する。

研究テーマ①新しい作用機作をもつ癌化学療法薬の創製

天然抗がん化合物の全合成から誘導体化、高活性化合物の創製、工業的合成への合成法検討と進む方針である。スピルコスタチン類に関しては、開発した合成法を適用して引き続き類縁化合物の合成を行う予定である。臨床応用可能な HDAC 阻害剤を開発するには、高いアイソフォーム選択性が求められていることから、今回得られた構造活性相関に関する知見をもとに、さらに類縁化合物の設計・合成を行う。また、本研究により創製された開発候補化合物「FK-A11」の非臨床／臨床試験を円滑に進めるために、工業的製造法に向けた合成ルートの改良も平行して行う予定である。TAN-1813 の合成研究においては、全合成ルートの確立を第一目標として研究を継続していく予定である。本化合物の基本骨格の合成はすでに達成しているが、高度に官能基化された基質における保護基の除去は困難であった。したがって、今後は保護基について再度検討する必要があると考えている。 新規核酸系代謝拮抗薬の開発の点からは、高い活性を有する誘導体の合成には至っていない。しかし、抗 HIV 活性を有する誘導体やグリコシダーゼ阻害活性を有する誘導体が見つかるなど、当初の期待とは少しずれてはいるが有望な化合物が見出されつつある。これらは抗ウイルス薬や糖尿病治療薬のシーズの点から非常に重要な知見であり、今後の展開が期待できると考えられる。また抗HIV性ヌクレオシドの合成研究の過程で新規抗癌性ヌクレオシドを見出す可能性は十分に考えられる。以上のことから、今後もチオ糖、アザ糖を含む疑似糖の合成とこれを糖部とするヌクレオシド誘導体の合成について積極的に展開する。エストロゲンオルトキノンの選択的検出、定量法の開発により、カテコールエストロゲンとエストロゲンオルトキノンの弁別定量が可能となり、内因性エスロゲンからのエストロゲンオルトキノンの及び付加体の生成メカニズム並びにキノン生成を触媒する分子種の同定など、エストロゲンオルトキノンの genotoxicity 発現のメカニズムが解明される可能性がある。本プロジェクトで開発された安定同位体標識と LC-ESI-MS/MS 法を駆使したステロイド微量定量法は、乳がんーエストロゲンの相互関連のみならず、前立腺がんーアンドロゲン、副腎腫瘍ーアルドステロンとの相互関連を分子レベルでさらに明確にし得ると考えられる。

研究テーマ②エストロゲン受容体制御による加齢性疾患(骨粗鬆症、認知障害)改善薬の創製

本プロジェクトで創製した化合物がうつ様行動及び認知障害を効果的に改善する効果をもつことを発見したことは、加齢性疾患の制御という本プロジェクトでの密接な連携があった成果であり、この端緒を生かし、さらに具体的に以下のように進展を図りたい。統合失調症の症状が既存の SERM により改善することが報告されていることから、本プロジェクトで作製に成功した統合失調症モデルマウスを用いて、このマウスが示す陽性症状、陰性症状及び認知障害にBE360 が有効であるか否か行動薬理学的に検討し、もし、有効であればその作用機序を免疫組織化学的手法及び分子生物学的手法を用い検討する予定である。さらに、本プロジェクトでは、メスの動物しか使わなかったが、オスの各精神疾患モデル動物の異常行動に対するBE360 の有効性に関しても研究を行う予定である。また、レチノイド関連受容体が催奇形性に関与していることから、レチノイドＸ受容体アンタゴニストを環境衛生学教室と共同で催奇形性の作用機序研究や予測、阻害物質探索に展開しようとする研究も開始しており、研究プロジェクトの連携も深化しつつある。化合物の設計に関しても、新規抗アンドロゲン活性化合物、特に変異受容体に活性のある化合物の創製、選択的骨粗鬆症改善活性を有する化合物の創製など、本

研究プロジェクトの骨子である癌及び加齢性疾患の制御に関して有用なリードと作用機構に関する知見が得られることが期待される。また、本研究のコンセプトや手法が他の医薬開発や疾患研究へのインパクトを与えることが期待される。 薬物代謝に関する核内受容体の関与の研究では、新規化合物の薬物相互作用を事前に予測するために、新たに CYP3A4 以外の CYP を介した核内受容体活性化評価系及び活性阻害評価系を構築していくことが必要となる。現在、他の CYP についても評価系の構築を進めている。また創薬のターゲットにエストロゲン受容体があることから、新規化合物のエストロゲン受容体活性化評価系としてのレポーター遺伝子安定発現細胞株の構築を目指していくことが必要である。さらに iPS 細胞から肝臓細胞やエストロゲン感受性細胞を分化誘導させ、より生体に近い条件下での評価系構築を目指すことが、今後の医薬品開発に貢献していけるものと考える。

研究テーマ③癌および加齢性疾患に対する疼痛制御による QOL 向上の研究

神経障害性疼痛、炎症性慢性疼痛および多発性硬化症疼痛に対して極めて有効な鎮痛薬を見いだすことには成功したが、肉腫性癌性疼痛に対して有効な鎮痛薬を見いだすには未だ至っていない。本研究ではこれまで、肉腫性癌性疼痛に対するオピオイド性鎮痛薬の鎮痛効果を評価してきたが、今後は他の受容体やイオンチャネルをターゲットとする薬物に関しても評価を試みる予定である。喘息の新たな endotype として、psychiatry endotypeを確立するために、ストレスによるμオピオイド受容体刺激とグルココルチコイド(GC)遊離、免疫寛容抑制の関連をマウスモデル及びヒトを用いて解析する。μ オピオイド受容体遺伝子多型と喘息の発症および増悪との関連を解析することにより、個別化医療を目指す。疼痛制御薬の構造活性相関や μ オピオイド受容体を介した免疫応答機構の遺伝子レベルでの解析結果と合わせて、アレルギー疾患を合併している患者にも有効で安全に投与できるμオピオイド受容体作動性疼痛制御薬の新規合成を目指す。

＜研究成果の副次的効果＞

(研究成果の活用状況又は今後の活用計画(実用化・企業化の見通しや、特許の申請があればその申請状況・取得状況等)について、記述してください。)

研究テーマ①新しい作用機作をもつ癌化学療法薬の創製

本研究により合成したスピルコスタチン類縁化合物(約 25 種類)の生物活性評価を行い(生物／医学系研究者との共同研究)、構造活性相関を解明することができた。本研究で合成した類縁化合物の一つである「FK-A11」は、動物実験において優れた抗腫瘍効果を示すことが見いだされ (その他の研究成果、特許 1,2)、現在、東北大学病院臨床研究推進センターにおいて非臨床試験が行われている。なお、本非臨床試験は文部科学省「橋渡し研究加速ネットワークプログラムシーズ B(平成 26 年度)」の支援のもとで行われている。今後もスピルコスタチン類および TAN-1813 の類縁化合物の設計・合成と構造活性相関研究を行い、大学発の基礎研究成果を臨床応用へと繋げていきたい。 チオヌクレオシド誘導体に抗 HIV 活性を、アザ糖誘導体にグリコシダーゼ阻害活性をそれぞれ見出した。特に後者のアザ糖誘導体のうち α-1-C-ブチル-L-アラビノフラノース誘導体は動物レベルでも食後過血糖の改善効果が認められた。これらの結果は当初計画の本筋からはややはずれたものではあるが、前者は新規抗 HIV 薬の開発に、また後者は新規糖尿病治療薬の開発へと繋がることが期待される。ステロイドホルモンの水酸基のプロトン親和性誘導体化は、ステロイドホルモンの LC-ESI-MS/MS に対する応答性を飛躍的に向上させるばかりか、生体由来のステロイド試料を測定する際のマトリクス効果を減弱できるため、信頼性も向上することがあきらかとなった。本手法は、ステロイドのみならず、水酸基を有する内因性物質の LC-ESI- MS/MS 分析に広く応用可能と考えられる。

研究テーマ②エストロゲン受容体制御による加齢性疾患(骨粗鬆症、認知障害)改善薬の創製

抗がん剤、及び骨粗鬆症等の新規選択的治療薬のリード化合物とすることが、直接の目標であるが、選択的受容体活性化剤や阻害剤が生物学研究の新たな展開にも寄与するものである。本研究でも、フランス遺伝分子生物 細胞学研究所 Krezel 教授との共同研究により、本研究者らが創製した、核内受容体、レチノイド X 受容体アンタゴニストである BR1211 がマウスの記憶に対して DHA の作用に拮抗する効果を示す*18 ことが明らかになっている。また、イタリア、カラブリア大学 Bagetta 教授との神経細胞分化の研究も開始している。このように、本研究の新規リガンドが生物科学研究のツールとして用いられている。新規疎水性骨格としてのホウ素クラ

スターの計算科学的解析が、本プロジェクトを通じて生体分子とのドッキング研究を通じて発展した。複雑な分子間の molecular mechanics(分子力場計算)に必要なここで用いたホウ素クラスターのパラメータ*3, 4 は多方面に応用が可能である。本研究の基盤概念である疎水性構造にホウ素クラスターを用いる研究は本研究者が初めて考案したものであり、本年度に開催された第 15 回国際ホウ素化学シンポジウムでも、新しいホウ素の応用として認められ招待講演を行った。*1 本プロジェクトが将来のホウ素の医薬への応用に大きな影響を与えていることを示すものである。本プロジェクトでアルツハイマー病、うつ病及び統合失調症といった加齢性の精神疾患モデル動物の作製に成功したことから、今後、これらの動物を利用し新規化合物の薬効評価や副作用に関する試験が可能となった。本プロジェクトで BE360 の抗うつ及び抗認知症の効果及びその作用機序が明らかとなり、現在この結果を論文に投稿中であり、受理後、BE360 の研究成果に関して特許申請を行う予定である。樹立したレポーター遺伝子安定発現細胞株は、新規化合物のスクリーニング以外にも近年利用が増加している健康食品やサプリメント(民間生薬)による薬物相互作用の可能性を検討することにも応用可能である。実際に民間生薬である板藍根が PXR を介して CYP3A4 を誘導することを示唆する新たな知見を得ることができた。ほか、板藍根成分中の AhR ligand による CYP1A1 及び CYP1A2 遺伝子発現誘導に従来の AhR の他に PXR が関与していることを示す知見が得られた*19。

研究テーマ③癌および加齢性疾患に対する疼痛制御による QOL 向上の研究

従来明確な治療法が確立されていなかった各種難治性疼痛に対し、それぞれ特異的に有効な鎮痛薬を見いだした。Amidino-TAPA 以外は既に臨床使用されている薬物であることから、その臨床応用により難治性疼痛の治療法が確立されることが期待される。μオピオイド受容体活性化を介した喘息増悪機構の解明やμオピオイド受容体遺伝子多型と重症化や Th2サイトカイン産生増強との相関は、喘息関連因子としての MOR を示唆する。従って、新しい喘息 endotype の確立とその病態に基づくμオピオイド受容体拮抗薬によるストレス喘息の治療、μ オピオイド受容体遺伝子多型による喘息のテーラーメイド医療への展開が考えられる。また、喘息増悪の副作用の軽減を目指したμオピオイド受容体作動性疼痛制御薬の開発が可能になる。

12 キーワード(当該研究内容をよく表していると思われるものを8項目以内で記載してください。)

(1) 創薬	(2) 抗がん薬	(3) 加齢性疾患
(4) 骨粗鬆症	(5) 精神機能障害	(6) 受容体制御
(7) 難治性疼痛	(8) 鎮痛薬	

13 研究発表の状況

上記、11(4)に記載した研究成果に対応するものには＊、本報告書に全文を掲載した主要論文は○で示す。

＜雑誌論文＞

研究テーマ①新しい作用機作をもつ癌化学療法薬の創製

1. Directed synthesis of 2–spiroindolines from indole derivatives by formic acid-induced N–acyliminium ion-conjugated diene spirocyclization, H. Abe, N. Miyagawa, S. Hasegawa, T. Kobayashi, S. Aoyagi, C. Kibayashi, T. Katoh, H. Ito, *Tetrahedron Lett.*, 査読有, **2015**, *56*, 921–924.
2. ○Biochemical, biological and structural properties of romidepsin (FK228) and its analogs as novel HDAC/PI3K dual inhibitors, K. Saijo, J. Imamura, K. Narita, A. Oda, H. Shimodaira, T. Katoh, C. Ishioka, *Cancer Sci.*, 査読有, **2015**, *106*, 208–215
3. Construction of an Isonucleoside on a 2,6-Dioxobicyclo[3.2.0]heptane Skeleton. Yoshimura, Y.; Kobayashi, S.; Kaneko, H.; Suzuki, T.; Imamichi, T. *Molecules*, 査読有, **2015**, *20*, 4623-4634
4. Predicting the Structures of Complexes between Phosphoinositide 3-Kinase (PI3K) and Romidepsin-Related Compounds for the Drug Design of PI3K/Histone Deacetylase Dual Inhibitors Using Computational Docking and the Ligand-Based Drug Design Approach, A. Oda, K. Saijo, C. Ishioka, K. Narita, T. Katoh, Y. Watanabe, S. Fukuyoshi, O. Takahashi, *J. Mol. Graph.*, 査読有, **2014**, *54*, 46–53.
5. Synthesis of β-Lapachone, a Potential Anticancer Agent from the Lapacho Tree, T. Katoh, H. Monma, J. Wakasugi, K. Narita, T. Katoh, *Eur. J. Org. Chem.*, 査読有, **2014**, 7099-7103.
6. Biogenetically Inspired Total Synthesis of (+)-Liphagal: A Potent and Selective Phosphoinositide 3-Kinase α (PI3Kα) Inhibitor from the Marine Sponge *Aka coralliphaga*, Takaaki Kamishima, Takuya Kikuchi, Koichi Narita, Tadashi Katoh, *Eur. J. Org. Chem.*, 査読有, **2014**, 3443–3450.
7. Enantioselective Total Synthesis of Dysidavarone A, a Novel Sesquiterpenoid Quinone from the Marine Sponge *Dysidea avara*, Yurie Fukui, Koichi Narita, Tadashi Katoh, *Chem. Eur. J.*, 査読有, **2014**, *86*, 2436–2439.
8. ○*22 Spiruchostatin A and B, Novel Histone Deacetylase Inhibitors, Induce Apoptosis Through Reactive Oxygen Species-Mitochondria Pathway in Human Lymphoma U937 Cells, Mati Ur Rehman, Paras Jawaid, Yoko Yoshihisa, Peng Li, Qing Li Zhao, Koichi Narita, Tadashi Katoh, Takashi Kondo, Tadamichi Shimizu, *Chem. Biol. Interact.*, 査読有, **2014,** *221*, 24–34.
9. ○*21 Total synthesis of Burkholdacs A and B and 5,6,20-Tri-*epi*-burkholdac A: HDAC Inhibition and Antiproliferative Activity, Yurie Fukui, Koichi Narita, Singo Dan, Takao Yamori, Akihiro Ito, Minoru Yoshida, Tadashi Katoh, *Eur. J. Med. Chem.*, 査読有, **2014**, *76*, 301–313.
10. *16 Synthesis and Biological Evaluation of α-1-*C*-4′-Arylbutyl-L-arabinoiminofuranoses, a New Class of α-Glucosidase Inhibitors, Yoshihiro Natori, Toshihiro Sakuma, Yuichi Yoshimura, Kyoko Kinami, Yuki Hirokami, Kasumi Sato, Isao Adachi, Atsushi Kato, Hiroki Takahata, *Bioorg. Med. Chem. Lett.*, 査読有, **2014**, *24*, 3298-3301.
11. ○Asymmetric synthesis of 2,5-disubstituted 3-hydroxypyrrolidines based on stereodivergent intramolecular iridium-catalyzed allylic aminations, Yoshihiro Natori, Shunsuke Kikuchi, Takahiro Kondo, Yukako Saito, Yuichi Yoshimura, Hiroki Takahata, *Org. Biomol. Chem.*, 査読有, **2014**, *12*, 1983-1994.
12. *10 Synthesis of a Dihydropyranonucleoside Using an Oxidative Glycosylation Reaction Mediated by Hypervalent Iodine, Hiroya Kan-no, Yukako Saito, Shun Omoto, Sakie Minato, Hideaki Wakamatsu, Yoshihiro Natori, Tomozumi Imamichi, Hiroki Takahata, Yuichi Yoshimura, *Synthesis*, 査読有, **2014**, *46*, 879-886.
13. Gabapentin inhibits bortezomib-induced mechanical allodynia through supraspinal action in mice, Ryo Kitamura, Tsugunobu Andoh, Shizuka, Mizoguchi, Yukako Saito, Hiroki Takahata, Yasushi Kuraishi, *J Pharmacol Sci*, 査読有, **2014,** *124*, 502-510.
14. ○*18 Development of highly sensitive chemiliminescent assay for hydrogen peroxide under neutral conditions using acridinium ester and its application to an enzyme immunoassay, Arakawa H, Tsuruoka K, Ohno K, Tajima N, Nagano H, Luminescence, 査読有 **2014**, *29*, 374-377.
15. ○An innovative LC-MS/MS-based method for determining CYP17 and CYP19 activity in the adipose tisuue of pre- and postmenopausal and ovariectomized women using 13C-labeled steroids substrates, T. Kinoshita, S. Honma, Y. Shibata, K. Yamashita, Y. Watanabe, H. Maekubo, M. Okuyama, A. Takashima, N. Takeshita,*J. Cli. Endocrinol. Meta*b., 査読有 **2014**, *99*, 1339-1348
16. Enantioselective Total Synthesis of Otteliones A and B, Novel and Powerful Antitumor Agents from the Freshwater Plant *Ottelia alismoides*, Tadashi Katoh, *Nat. Prod. Commun.*, 査読有, **2013**, *8*, 973–980.
17. Total Synthesis of (+)-Strongylin A, a Rearranged Sesquiterpenoid Hydroquinone from a Marine Sponge, Takaaki Kamishima, Takuya Kikuchi, Tadashi Katoh, *Eur. J. Org. Chem.*, 査読有, **2013**, 4558–4563.
18. ○*1,2 Total synthesis of Bicyclic Depsipeptides Spiruchostatins C and D and Investigation of Their Histone

Deacetylase Inhibitory and Antiproliferative Activities, Koichi Narita, Yurie Fukui, Yui Sano, Takao Yamori, Akihiro Ito, Minoru Yoshida, Tadashi Katoh, *Eur. J. Med. Chem.*, 査読有, **2013**, *60*, 295–304.

19. Total Synthesis of Decahydrobenzo[*d*]xanthene Sesquiterpenoids Aureol, Strongylin A, and Stachyflin: Development of a New Strategy for the Construction of a Common Tetracyclic Core Structure, Tadashi Katoh, *Heterocycles*, 査読有, **2013**, *87*, 2199–2224.
20. Synthetic Studies on Vertihemiptellide A, a Potential Antituberculosis Agent: Synthesis of Bis-α-Sulfenylated Diketopiperazine Derivative, Koichi Narita, Suguru Atsumi, Tadashi Katoh, *J. Tohoku Pharm. Univ.*, 査読有, **2013**, 60, 55–63.
21. ○*11 Design and Synthesis of A Nucleoside and A Phosphonate Analogue Constructed on A Branched-threo-tetrofuranose Skeleton, Y. B. Kiran, Hideaki Wakamatsu, Yoshihiro Natori, Hiroki Takahata, Yuichi Yoshimura, *Tetrahedron Lett.*, 査読有, **2013**, *54*, 3949-3952.
22. A Facile Synthesis of Fully Protected *meso*-Diaminopimelic Acid (DAP) and Its Application to the Preparation of Lipophilic *N*-Acyl iE-DAP, Yukako Saito, Yuichi Yoshimura, Hideaki Wakamatsu, Hiroki Takahata, *Molecules*, 査読有, **2013**, *18*, 1162-1173.
23. Structures and absolute configurations of a short-branched fatty acid dimers from an endophytic fungus of *Aloe arborescens*, Teigo Asai, Sae Otsuki, Toru Taniguchi, Kenji Minde, Kouwa Yamashita, Hiroaki Sakurai, Tomoji Ozeki and Yoshiteru Oshima, *Tetrahedron Lett.*, 査読有 **2013**, *29*, 3402-340.
24. Benzophenones form an endophytic fungus, Graphiopsis chlorocephala, form *Paeonia lactiflora* cuktivated in the presence of a NDA^{+}-dependent HDAC inhibitor, Teigo Asai, Sae Otsuki, Hiroaki Sakurai, Kouwa Yamashita , Tomoji Ozeki and Yoshiteru Oshima, *Org. Lett.*, 査読有 **2013**, *15*, 2058-2061.
25. Structure and biomimetic synthesis of a novel a-pyrone polyketide of an endophytic penicillium sp. *Catharanthus roses* ,Teigo Asai, Dan Luo, Kouwa Yamashita and Yoshiteru Oshima, 査読有 *Org. Lett.*, 2013, *15*, 1020-1023.
26. A New Entry to the Synthesis of Primin via a *B*-Alkyl Suzuki–Miyaura Cross-Coupling Reaction, Kazuhiro Watanabe, Tomohiro Sugizaki, Yumi Tozawa, Tadashi Katoh, *Heterocycles*, 査読有, **2012**, *86*, 985–989.
27. ○*22 Characterization of Cells Resistant to the Potent Histone Deacetylase Inhibitor Spiruchostatin B (SP-B) and Effect of Overexpressed $p21^{wafl/cipl}$ on the SP-B Resistance or Susceptibility of Human Leukemia Cells, Syu-ichi Kanno, Naoyuki Maeda, Ayako Tomizawa, Shin Yomogida, Tadashi Katoh, Masaaki Ishikawa, *Int. J. Oncol.*, 査読有, **2012**, *41*, 862–868.
28. Deprotection of 3,4-Dimethoxybenzyl (^{3,4}DMB) Group on γ-Lactam Nitrogen using Phenyliodine(III) Bis(trifluoroacetate) (PIFA): Application to Isoindolinone Compounds, Kazuhiro Watanabe, Hiroaki Shibata, Yū Imai, Tadashi Katoh, *Heterocycles*, 査読有, **2012**, *84*, 1355-1361.
29. ○*22 Involvement of p21 wafl/cipl Expression in the Cytotoxicity of the Potent Histone Deacetylase Inhibitor Spiruchostatin B towards Susceptible NALM-6 Human B Cell Leukemia Cells, Syn-ichi Kanno, Naoyuki Maeda, Ayako Tomizawa, Shin Yomogida, Tadashi Katoh, Masaaki Ishikawa, *Int. J. Oncol.*, 査読有, **2012,** *40*, 1391-1396.
30. ○*23 Romidepsin (FK228) and Its Analogs Directly Inhibit PI3K Activity and Potently Induce Apoptosis as HDAC/PI3K Dual Inhibitors, Ken Saijo, Tadashi Katoh, Hideki Shimodaira, Akifumi Oda, Ohgi Takahashi, Chikashi Ishioka, *Cancer Sci.*, 査読有, **2012,** *103*, 1994-2001.
31. Synthesis of the Key Intermediate of NF-κB Inhibitor Dehydroxymethylepoxyquinomicin (DHMEQ) and Novel DHMEQ Analog, Kazuhiro Watanabe, Masato Takahashi, Etsuko Kawagoe, Tadashi Katoh, *J. Tohoku Pharm. Univ.*, 査読有, **2012**, 59, 59–67.
32. ○*15 α-1-C-Butyl-1,4-dideoxy-1,4-imino-L-arabinitol as a Second-Generation Iminosugar-Based Oral α-Glucosidase Inhibitor for Improving Postprandial Hyperglycemia, Atsushi Kato, Erina Hayashi, Saori Miyauchi, Isao Adachi, Tatsushi Imahori, Yoshihiro Natori, Yuichi Yoshimura, Robert J. Nash, Hideyuki Shimaoka, Izumi Nakagome, Jun Koseki, Shuichi Hirono, Hiroki Takahata, *J. Med. Chem.*, 査読有, **2012**, *55*, 10347-10362.
33. Asymmetric Synthesis of 1-Alkyl-2-deoxyiminofuranoses via The Iridium-catalyzed Intramolecular Cyclization of an Allylic Carbonate, Yoshihiro Natori, Shunsuke Kikuchi, Yuichi Yoshimura, Atsushi Kato, Isao Adachi, Hiroki Takahata, *Heterocycles*, 査読有, **2012**, *86*, 1401-1417.
34. Recent Advances in Cyclonucleosides: C-Cyclonucleosides and Spore Photoproducts in Damaged DNA, Yuichi Yoshimura, Hiroki Takahata, *Molecules*, 査読有, **2012**, *17*, 11630-11654.
35. A Chiral Synthesis of Iminosugars, Takahata, H. *Heterocycles*, **2012**, 査読有, *85*, 1351-1376.
36. ○*9 A New Route to N^{1}-Substituted Uracil Derivatives Using Hypervalent Iodine. Yoshimura, Y.; Kan-no, H.; Kiran, Y. B.; Natori, Y.; Saito, Y.; Takahata, H. *Synthesis,* 査読有, **2012**, *44*, 1163-1170.
37. ○ *12 Asymmetric Synthesis of 2-Propylisofagomine Using Allylic Hydroxy Group Accelerated Ring-Closing Enyne Metathesis, Taguchi, T.; Imahori, T.; Yoshimura, Y.; Kato, A.; Adachi, I.; Kawahata, M.; Yamaguchi, K.; Takahata, H. *Heterocycles*, 査読有, **2012**, *84*, 929-944.
38. An Alternative Approach to para-C-H Arylation of Phenol Palladium-Catalyzed Tandem γ-Arylation/Aromatization of 2-Cyclohexen-1-one Derivatives Imahori, T.; Tokuda, T.; Taguchi, T.; Takahata, H. *Org. Lett.*, 査読有, **2012**, *14*, 1172-1175.

39. Highly oxidized ergosterols and isariotin analogs from an entomopathogenic fungus, *Gibellula formosana*, cultivated in the presence of epigenetic modifying agents Original Research Article, Teigo Asai, Yu-Ming Chung, Hiroaki Sakurai, Tomoji Ozeki, Fang-Rong Chang, Yang-Chang Wu, Kouwa Yamashita, Yoshiteru Oshima, *Tetrahedron*, 査読有, **2012**, *29*, 5817-5823.
40. Dihydrobenzofurans as a cannabinoids receptor ligands from *Cordyceps annullata,* an entomopathogenic fungus cultivated in the presence of HDAC inhibitor, T. Asai, D. Luo, Y. Obara, T.Taniguchi, K. Monde, K. Yamashita, Y. Oshima, *Tetrahedron Lett.*, 査読有, **2012**, *53,* 2238-2243
41. ○*18 Development of RNA aptamer and its ligand binding assay on microchip electrophoresis, K. Ohno, C. Nakata, Y. Sano, F. Nishikawa, S. Nishikawa, H. Arakawa, *Curr. Chem. Genomics*, 査読有, **2012**, *6,* 1-5.
42. Aromatic polyketide glycosides from an entomopathogenic fungus, *Cordyceps indigotica,* T. Asai, T. Yamamoto, Y-M Chung, F-R. Chang, Y-C. Wu, K. Yamashita, Y. Oshima, *Tetrahedron Lett.*, 査読有, **2012**, *53,* 277-280.
43. Biomonitoring of microcystin and aflatoxin co-occurrence in aquaculture using immunohistochemistry and genotoxicity assays, E. H. Hashimoto, M. Kamogae, T. Perez Vanzella, I. M. Syllus Colus, A. P. F. Rodrigues Lourenco Bracarense, M. d. C. Bitterncourt-Oliveria, E. Itano, E. K. Kuroda, H. Katoh, S. Nagata, Y. Ueno, K.-I. Harada, E.Y. Hirooka, *Braz. Arch. Biol. Technol.*, 査読有, **2012**, *55,* 151-155.
44. Tenuipyrone, a novel skeltal polyketide from the entomopathogenic fungus, *Isaria tenuipes*, cultivated in the presence of epigenetic modifiers, T. Asai, Y-M. Chung, H.Sakurai, T. Ozeki, F-R.Chang, K.Yamashita, Y. Oshima, *Org. Lett.*, 査読有, **2012**, *20,* 513-515.
45. Effective Chemoselective Deprotection of 3,4-Dimethoxybenzyl (^{3,4}DMB) Ethers in the Presence of Benzyl and *p*-Methoxybenzyl (PMB) Ethers by Phenyliodine(III) Bis(trifluoroacetate) (PIFA), Kazuhiro Watanabe, Tadashi Katoh, *Tetrahedron Lett.*, 査読有, **2011**, *52*, 5395–5397.
46. Enantioselective Total Synthesis of (+)-Stachyflin: A Potential Anti-Influenza A Virus Agent Isolated from a Microorganism, Junji Sakurai, Takuya Kikuchi, Ohgi Takahashi, Kazuhiro Watanabe, Tadashi Katoh, *Eur. J. Org. Chem.,* 査読有, **2011**, *16*, 2948–2957.
47. Enantioselective Total Synthesis of (-)-Subglutinols A and B: Potential Immunosuppressive Agents Isolated from a Microorganism, Takuya Kikuchi, Mayuko Mineta, Jingo Ohtaka, Naoko Matsumoto, Tadashi Katoh, *Eur. J. Org. Chem.*, 査読有, **2011**, 5020–5030.
48. Total Synthesis of Bauhinoxepin J: A Biologically Active Dibenzo[*b,f*]oxepin Isolated from *Bauhinia purpurea*, Koichi Narita, Ken Nakamura, Yui Abe, Tadashi Katoh, *Eur. J. Org. Chem.*, 査読有, **2011**, 4985–4988.
49. ○*16 Docking and SAR studies of D- and L-isofagomine isomers as human β-glucocerebrosidase inhibitors, Kato, A.; Miyauchi, S.; Kato, N.; Nash, R. J.; Yoshimura, Y.; Nakagome, I.; Hirono, S.; Takahata, H.; Adachi, I. *Bioorg. Med. Chem.*, 査読有, **2011**, *19*, 3558-3568.
50. ○*7 Synthesis of 5-Thiodidehydropyranylcytosine Derivatives as Potential anti-HIV Agents, Yoshimura, Y.; Yamazaki, Y.; Saito, Y.; Natori, Y.; Imamichi, T.; Takahata, H. *Bioorg. Med. Chem. Lett.*, 査読有, **2011**, *21*, 3313-3316.
51. *14 The synthesis and biological evaluation of 1-C-alkyl-L-arabinoiminofuranoses, a novel class of α-glucosidase inhibitors, Natori, Y.; Imahori, T.; Murakami, K.; Yoshimura, Y.; Nakagawa, S.; Kato, A.; Adachi, I.; Takahata, H. *Bioorg. Med. Chem. Lett.,* 査読有, **2011**, *21*, 738-741.
52. Antimicrobial activity of various antibiotics against B-9 strain that degrades microcystin produced by cyanobacteria, K. Harada, H. Katoh, K. Tsuji, *J. Res. Inst. Meijo. Univ.*, 査読有, **2011**, *10,* 23-43.
53. *19 18-Oxycortisol measurement in adrenal vein sampling as a biomarker for subclassifying primary aldosteroism, Y. Nakamura, F. Satoh, R. Morimoto, M. Kudo, K. Takase, CE. Gometz-Sanchez, S. Honma, M. Okuyama, K. Yamashita, W. E. Rainey, H. Sasano, S. Ito, *J. Clin. Endcrinol. Metab.*, 査読有, **2011**, *96*, E1272-1278.
54. Enantioselective Total Synthesis of Novel Diterpenoid Pyrones (+)-Sesquicillin and (−)-Nalanthalide from Fungal Fermentations. Takamasa Oguchi, Kazuhiro Watanabe, Hideki Abe, Tadashi Katoh, *Heterocycles,* 査読有, **2010**, *80,* 229–250.
55. Formal Total Synthesis of Ottelione Using Iridium-Catalyzed Oxidative Desymmetrization. Takeyuki Suzuki, Kazem Ghozati, Da-Yang Zhou, Tadashi Katoh, Hiroaki Sasai. *Tetrahedron,* 査読有, **2010**, *66*, 7562–7568.
56. Spirocyclization of an *N*-Acyliminium Ion with Substituted Pyridine: Stereoselective Synthesis of Tetracyclic Spirolactams Possessing the Pyridone Nucleus, Hideki Abe, Kei-ichi Takaya, Kazuhiro Watanabe, Sakae Aoyagi, Chihiro Kibayashi, Tadashi Katoh, *Heterocycles,* 査読有, **2010**, *82,* 257-261.
57. Synthesis of Biological Activity-Oriented Natural Products, Tadashi Katoh, *Farumashia*, 査読有, **2010**, *46*, 735–737.
58. Total Synthesis of (+)-Stachyflin: a Potential Anti-influenza A Virus Agent. Kazuhiro Watanabe, Junji Sakurai, Hideki Abe, Tadashi Katoh, *Chem. Commun.*, 査読有, **2010**, *46,* 4055-4057.
59. Trends in Antimicrobial Susceptibility of Streptococcus pneumoniae in the Tohoku District of Japan: A Longitudinal Analysis from 1998 to 2007. Kazumasa Suzuki, Katsushi Nishimaki, Kaori Okuyama, Tadashi Katoh, Minoru Yasujima, Junichi Chihara, Akira Suwabe, Yoko Shibata, Choichiro Takahashi, Hiroaki

Takeda, Shiro Ida, Mitsuo Kaku, Akira Watanabe, Toshihiro Nukiwa, Kazunao Niitsuma, Keiji Kanemitsu, Motoaki Takayanagi, Isao Ohno, *Tohoku J. Exp. Med.*, 査読有, **2010**, 220, 47-57.

60. Chemoselective *O-tert*-butoxycarbonylation of phenols using 6,7-dimethoxyisoquinoline as a novel organocatalyst, Saito, Y.; Yoshimura, Y.; Takahata, H. *Tetrahedron Lett.*, 査読有, **2010**, *51*, 6915-6917
61. *8 Design and Synthesis of Isonucleosides Constructed on a 2-Oxa-6-thiabicyclo[3.2.0]heptane Scaffold Yoshimura, Y.; Asami, K.; Imamichi, T.; Kuroda, T.; Shiraki, K.; Takahata, H. *J. Org. Chem.*, 査読有, **2010**, *75*, 4161-4171
62. ○*19 Highly sensitive and specific analysis of sterol profiles in biological samples by HPLC-ESI-MS/MS, A. Honda, T. Miyazaki, T. Ikegami, J. Iwamoto, K. Yamashita, M. Numazawa, Y. Matsuzaki, *J. Steroid Biochem. Mol. Biol.*, 査読有, **2010**, *212*, 556-564
63. ○*20 Assay of labile estrogen *o*-quinones, potent carcinogenic molecular species, by high performance liquid chromatography-electrospray ionization tandem mass spectrometry with phenazine derivatization, K. Yamashita, A. Masuda, Y. Hoshino, S. Komatsu, M. Numazawa, *J. Steroid Biochem. Mol. Biol.*, 査読有, **2010**, *119*, 141-148
64. ○ *17 Probing the binding pocket of the active site of aromatase with 2-phenylaliphatic androsta-1,4-diene-3,17-dione steroids, M. Takahashi, K. Yamashita, M. Numazawa, *Steroids*, 査読有, **2010**, *75*, 230-237.
65. ○*19 Fusaric acid as a novel proton-affinitive derivatizing agent for highly sensitive quantification of hydroxysteroids by LC-ESI-MS/MS, K. Yamashita, K. Yamazaki, S. Komatsu, M. Numazawa, J. Am. Soc. Mass Spectrom.., 査読有, **2010**, *21*, 249-255.

研究テーマ②エストロゲン受容体制御による加齢性疾患（骨粗鬆症、認知障害）改善薬の創製

1. Structure-activity relationship study of diphenylamine-based estrogen receptor (ER) antagonists. Kiminori Ohta, Yuki Chiba, Asako Kaise, Yasuyuki Endo, *Bioorg. Med. Chem.*, 査読有, **2015**, *22*, 861-867.
2. The intrathecal administration of losartan, an AT1 receptor antagonist, produces an antinociceptive effect through the inhibiton of p38 MAPK phosphorylation in the mouse formalin test. Wataru Nemoto, Yoshiki Ogata, Osamu Nakagawasai, Fukie Yaoita, Takeshi Tadano, Koichi Tan-No. *Neurosci Lett.*, 査読有, **2015**, *585*, 17-22.
3. Synthesis of 2-substituted 1,3-cycloheptanedione via a Lewis acid mediated ring expansion reaction. Kohei Inomata, Yasuyuki Endo, *Heterocycles*, 査読有, **2014**, *88*, 997-1012
4. ○*3 Novel Estrogen Receptor (ER) Modulators Containing Various Hydrophobic Bent-Core Structures. Kiminori Ohta, Takumi Ogawa, Asako Kaise, Yasuyuki Endo, *Bioorg. Med. Chem.*, 査読有, **2014**, *22*, 3508-3514.
5. *3 Aliphatic Substitution of o-Carboranyl Phenols Enhances Estrogen Receptor Beta Selectivity. Kiminori Ohta, Takumi Ogawa, Asako Kaise, Akifumi Oda, Yasuyuki Endo, *Chem. Pharm. Bull.*, 査読有, **2014**, *62*, 386-391.
6. Delineation of the mechanism involved in cognitive dysfunction using schizophrenic animal models, Yasushi Yabuki, Osamu Nakagawasai, Kohji Fukunaga. *Nihon Shinkei Seishin Yakurigaku Zasshi*, 査読有, **2014**, *34*, 49-50.
7. 嗅球摘出マウスの認知障害に対するフルボキサミンの改善作用 中川西修、吉田文、高橋浩平、根本亙、八百板富紀枝、只野武、丹野孝一、東北薬科大学研究誌、査読有、**2014**、*61*、41－46
8. Angiotensin (1-7) prevents angiotensin II-induced nociceptive behavior via inhibition of p38 MAPK phosphorylation mediated through spinal Mas receptors in mice, Wataru Nemoto, Yoshiki Ogata, Osamu Nakagawasai, Fukie Yaoita, Takeshi Tadano, Koichi Tan-No. *Eur. J. Pain.*, 査読有, **2014**, 18, 1471-1479
9. Long-term feeding on powdered food causes hyperglycemia and signs of systemic illness in mice, Masahiro Tsuchiya, Fukie Niijima-Yaoita, Hiroyuki Yoneda, Ko Chiba, Shinobu Tsuchiya, Yoshihiro Hagiwara, Keiichi Sasaki, Shunji Sugawara, Yasuo Endo, Koichi Tan-No, Makoto Watanabe. *Life Sci.*, 査読有, **2014**, *103*, 8-14.
10. Functional Characterization of Wild-type and 49 CYP2D6 Allelic Variants for N-desmethyltamoxifen 4-hydroxylation Activity. Yuka Muroi, Masamitsu Takahashi, Takahiro Saito, Kanako Sakuyama, Yui Niinuma, Miyabi Ito, Chiharu Tsukada, Kiminori Ohta, Yasuyuki Endo, Akifumi Oda, Noriyasu Hirasawa, Masahiro Hiratsuka, *Drug Metabolism & Pharmacokinetics* 査読有, **2014**, [Advance Publication]Released 2014/03/18
11. 健康食品と医薬品の併用は薬物相互作用をおこす？、永田 清、熊谷 健、佐々木崇光、医薬品相互作用研究、査読無, *38*、**2014**（印刷中）.
12. ○*16 調剤薬局来局者を対象とした健康食品の使用実態調査とその情報に基づいた CYP2D6 活性阻害評価、佐々木崇光、熊谷 健、佐々木 瞳、稲見敬太、佐藤 裕。髙橋昌悟、松永民秀、頭金正博、細川正清、大森 栄、永田 清、医療薬学、査読有、**2014**, 40, 488-499
13. Histone deacetylase inhibitor valproic Acid promotes the differentiation of human induced pluripotent stem cells into hepatocyte-like cells. Kondo Y, Iwao T, Yoshihashi S, Mimori K, Ogihara R, Nagata K, Kurose K, Saito M, Niwa T, Suzuki T, Miyata N, Ohmori S, Nakamura K, Matsunaga T. *PLoS One*. 査読有, **2014** in

press

14. ○An efficient method for differentiation of human induced pluripotent stem cells into hepatocyte-like cells retaining drug metabolizing activity. Kondo Y, Iwao T, Nakamura K, Sasaki T, Takahashi S, Kamada N, Matsubara T, Gonzalez FJ, Akutsu H, Miyagawa Y, Okita H, Kiyokawa N, Toyoda M, Umezawa A, Nagata K, Matsunaga T, Ohmori S. *Drug Metab Pharmacokinet.* 査読有, **2014**, 29, 237-243.
15. ○Differentiation of human induced pluripotent stem cells into functional enterocyte-like cells using a simple method. Iwao T, Toyota M, Miyagawa Y, Okita H, Kiyokawa N, Akutsu H, Umezawa A, Nagata K, Matsunaga T, *Drug Metab Pharmacokinet*, 査読有, 29, 44-51, 2014
16. ○Alteration of the function of the UDP-glucuronosyltransferase 1A subfamily by cytochrome P450 3A4: different susceptibility for UGT isoforms and UGT1A1/7 variants. Ishii Y, Koba H, Kinoshita K, Oizaki T, Iwamoto Y, Takeda S, Miyauchi Y, Nishimura Y, Egoshi N, Taura F, Morimoto S, Ikushiro S, Nagata K, Yamazoe Y, Mackenzie PI, Yamada H, Drug Metab Dispo, 査読有, **2014**, 42, 229-238.
17. ○*3 Enhanced Estrogen Receptor Beta (ERβ) Selectivity of Fluorinated Carborane-containing ER Modulators. Kiminori Ohta, Takumi Ogawa, Asako Kaise, Yasuyuki Endo, *Bioorg. Med. Chem. Lett.*, 査読有, **2013**, 23, 6555-6558.
18. Synthesis of 2-Substituted 1,3-Cycloheptanedione via a Lewis Acid Mediated Ring Expansion Reaction. Kohei Inomata, Yasuyuki Endo, *Heterocycles* 査読有, **2013**, *88*, 997-1012.
19. Liver hydrolysate assists in the recovery from physical fatigue in a mouse model, Osamu Nakagawasai, Kotaro Yamada, Wataru Nemoto, Masahiro Fukahori, Takeshi Tadano, Koichi Tan-No. *J. Pharmacol. Sci.*, 査読有, **2013**, *123*, 328-335.
20. Angiotensin II produces nociceptive behavior through spinal AT1 receptor-mediated p38 mitogen-activated protein kinase activation in mice, Wataru Nemoto, Osamu Nakagawasai, Fukie Yaoita, Syu-Ichi Kanno, Shin Yomogida, Masaaki Ishikawa, Takeshi Tadano, Koichi Tan-No. *Mol. Pain,* 査読有, **2013**, *9*, 38.
21. Roles played by histamine in strenuous or prolonged masseter muscle activity in mice, Hiroyuki Yoneda, Fukie Niijima-Yaoita, Masahiro Tsuchiya, Hiroyuki Kumamoto, Makoto Watanabe, Hiroshi Ohtsu, Kazuhiko Yanai, Takeshi Tadano, Keiichi Sasaki, Shunji Sugawara, Yasuo Endo. *Clin. Exp. Pharmacol. Physiol.*, 査読有, **2013**, *40*, 848-855.
22. *11 統合失調症モデルラットにおける免疫組織化学染色を用いたCaMKII活性イメージング法, 矢吹悌, 中川西修, 只野武、福永浩司, *Yakugaku Zasshi,* 査読有, **2013,** 133, 501-506.
23. Influence of a long-term powdered diet on the social interaction test and dopaminergic systems in mice, Fukie Niijima-Yaoita, Masahiro Tsuchiya, Hiroko Saito, Yuka Nagasawa, Shigeo Murai, Yuichiro Arai, Osamu Nakagawasai, Wataru Nemoto, Takeshi Tadano, Koichi Tan-No. *Neurochem. Int.*, 査読有, **2013**, *63*, 309-315.
24. 継続的な運動によりうつ病発症が抑えられるメカニズムが明らかに！？, 中川西修, *ファルマシア,* 査読有, **2013,** 251, 251.
25. Combined low calcium and magnesium are risk factors for motor deficits in mice, Ryoo Taniguchi, Osamu Nakagawasai, Koichi Tan-No, Fumihiro Yamadera, Wataru Nemoto, Shoko Sato, Fukie Yaoita, Takeshi Tadano. *Biosci. Biotechnol. Biochem.*, 査読有, **2013**, *77*, 266-270.
26. Interleukin-6 modulates oxidative stress produced during the development of cisplatin nephrotoxicity, Satoru Mitazaki, Midori Hashimoto, Yui Matsuhashi, Shigeyoshi Honma, Miwako Suto, Naho Kato, Osamu Nakagawasai, Koichi Tan-No, Kouichi Hiraiwa, Makoto Yoshida, Sumiko Abe. *Life. Sci.*, 査読有, **2013**, *92*, 694-700.
27. *11 Decreased CaMK II and PKC activities in specific brain regions are associated with cognitive impairment in neonatal ventral hippocampus-lesioned rats, Yasushi Yabuki, Osamu Nakagawasai, Shigeki Moriguchi, Norifumi Shiod, Hiroshi Onogi, Koichi Tan-No, Takeshi Tadano, Kohji Fukunaga. *Neuroscience,* 査読有, **2013**, *234*, 103-115.
28. Phenylmethanesulfonyl fluoride, a serine protease inhibitor, suppresses naloxone-precipitated withdrawal jumping in morphine-dependent mice, Wataru Nemoto, Tasuku Sato, Osamu Nakagawasai, Fukie Yaoita, Jerzy Silberring, Takeshi Tadano, Koichi Tan-No. *Neuropeptides,* 査読有, **2013**, *47*, 187-191.
29. *8 Chronic fluvoxamine treatment changes 5-HT2A/2C receptor-mediated behavior in olfactory bulbectomized mice, Akira Oba, Osamu Nakagawasai, Hiroshi Onogi, Wataru Nemoto, Fukie Yaoita, Yuichiro Arai, Koichi Tan-No, Takeshi Tadano. *Life. Sci.*, 査読有, **2013**, *92*, 119-124.
30. ○Hepatocyte nuclear factor 6 activates the transcription of CYP3A4 in hepatocyte-like cells differentiated from human induced pluripotent stem cells, Sasaki T, Takahashi S, Numata Y, Narita M, Tanaka Y, Kumagai T, Kondo Y, Matsunaga T, Ohmori S, Nagata K. *Drug Metab. Pharmacokinet.*, 査読有, **2013**, *28*, 250-259.
31. ○*3 Estrogenic activity of B-fluorinated o-carborane-1,2-bisphenol synthesized via SNAr reaction. Kiminori Ohta, Takumi Ogawa, Yasuyuki Endo, *Bioorg. Med. Chem.Lett.* 査読有, **2012**, *22*, 4728-4730.
32. Facile Synthesis and Estrogen Activity of Arylpyrrole-based Bisphenol Derivatives. Kiminori Ohta, Fumi Taguchi, and Yasuyuki Endo, *Heterocycles*, 査読有, **2012**, *86*, 165-170.
33. ○*4 Development of androgen receptor ligands by application of ten-vertex *para*-carborane as a novel hydrophobic core structure, Shinya Fujii, Kiminori Ohta, Tokuhito Goto, Akifumi Oda, Hiroyuki Masuno, Yasuyuki Endo, Hiroyuki Kagechika, *Med. Chem. Commun.* 査読有, **2012**, *3*, 680-684.

34. Structural Activity-relationship Study on Benzoic Acid Part of Diphenylamine-based Retinoids, Kiminori Ohta, Emiko Kawachi, Koichi Shudo, Hiroyuki Kagechika, Bioorg. Med. Chem. Lett, 査読有, **2012**, 23, 81-84.
35. *1 ホウ素クラスターを用いた実践的創薬研究, 太田公規, 遠藤泰之, ファルマシア, 査読有, **2012**, *48*, 504-508.
36. 記憶・学習障害の発現メカニズムの解明とその予防薬, 只野武, 中川西修, 師尾仁, 金森正剛, 新島富紀枝, 丹野孝一, *日本未病システム学会雑誌*, 査読有, **2012**, *18*, 43-49.
37. Pharmacological evaluation of catalepsy in low calcium and/or magnesium deficient feeding mice, Osamu Nakagawasai, Ryoo Taniguchi, Koichi Tan-No, Fumihiro Yamadera, Wataru Nemoto, Fukie Yaoita, Takeshi Tadano. *Health,* 査読有, **2012**, *4*, 1138-1144.
38. Enhanced behavioral response to 5-HT-related agonists in postweaning protein malnourished mice, Shoko Sato, Osamu Nakagawasai, Takafumi Hayashi, Atsuko Oikawa, Fukie Yaoita, Koichi Tan-No, Takeshi Tadano, Tsuneyoshi Suzuki. *Biol. Pharm. Bull.,* 査読有, **2012**, *35*, 1697-702.
39. Roles of histamine in exercise-induced fatigue: favouring endurance and protecting against exhaustion, Fukie Niijima-Yaoita, Masahiro Tsuchiya, Hiroshi Ohtsu, Kazuhiko Yanai, Shunji Sugawara, Yasuo Endo, Takeshi Tadano. *Biol. Pharm. Bull.,* 査読有, **2012**, *35*, 91-97.
40. TNF-a/actinomycin D-mediated Hepg2 cells in the presence of iron as a model of hepatocyte injury, Takahashi S, Miura A, Sasaki H, Sakaguchi S, Nagata K, *J ohoku Pharm Univ.* 査読有, **2012**, *59*, 67-74.
41. Mechanisms of CYP3A Induction by Glucocorticoids in Human Fetal Liver Cells. Matsunaga T, Maruyama M, Matsubara T, Nagata K, YamazoeY, Ohmori S. *Drug Metab Pharmacokinet.* 査読有, **2012**, *27*, 653-657.
42. Effects of Hypoxia-inducible Factor-1α Chemical Stabilizer, CoCl2 and Hypoxia on Gene Expression of CYP3As in Human Fetal Liner Cells, Eiji Suzuki, Tamihide Matsunaga, Akiko Aonuma, Takamitsu Sasaki, Kiyoshi Nagata, Shigeru Ohmori, *Drug Metab. Pharmacokinet.*, 査読有, **2012**, *27*, 398-404.
43. ○*15 Polycyclic Aromatic Hydrocarbons Activate CYP3A4 Gene Transcription through Human Pregnane X Receptor, Takeshi Kumagai, Hiroyuki Suzuki, Takamitsu Sasaki, Shuhei Sakaguchi, Shinichi Miyairi, Yasushi Yamazoe, Kiyoshi Nagata, *Drug Metab. Pharmacokinet.*, 査読有, **2012**, *27*, 200-206.
44. *5 Boron Cluster-based Development of Potent Non-Secosteroidal Vitamin D Receptor Ligands: Direct Observation of Hydrophobic Interaction between Protein Surface and Carborane, Shinya Fujii,a, Hiroyuki Masuno, Yoshiyuki Taoda, Atsushi Kano, Angsuma Wongmayura, Makoto Nakabayashi, Nobutoshi Ito, Masato Shimizu, Emiko Kawachi, Tomoya Hirano, Yasuyuki Endo, Aya Tanatani, Hiroyuki Kagechika, *J. Am. Chem. Soc.* 査読有, **2011**, *133*, 20933-20941.
45. ○*4 Crystal Structure, Docking Study and Structure-activity Relationship of Carborane-containing Androgen, Kiminori Ohta, Tokuhito Goto, Shinya Fujii, Masatoshi Kawahata, Akifumi Oda, Shigeru Ohta, Kentaro Yamaguchi, Shuichi Hirono, Yasuyuki Endo, *Bioorg. Med. Chem.* 査読有, **2011**, *19*, 3540-3548.
46. *18 RXR-gamma is Implicated in Docosahexaenoic Acid Modulation of Despair Behaviors and Working Memory in Mice, Marta Wietrzych-Schindler , Monika Szyszka-Niagolov, Kiminori Ohta, Yasuyuki Endo, Efrén Pérez, Angel R. de Lera, Pierre Chambon, Wojciech Krezel, *Biological Psychiatry*, 査読有, **2011**, 69, 788-794.
47. ○*4 *p*-Carborane Based Androgen Antagonists Active in LNCaP Cells with a Mutated Androgen Receptor, Shinya Fujii, Ayumi Yamada, Keiko Tomita, Mao Nagano, Tokuhito Goto, Kiminori Ohta, Takashi Harayama, Yasuyuki Endo, Hiroyuki Kagechika, *Med. Chem. Commun.* 査読有, **2011**, *2*, 877-880.
48. Executive functions of postweaning protein malnutrition in mice, Shoko Sato, Osamu Nakagawasai, Koichi Tan-No, Fukie Niijima, Tsuneyoshi Suzuki, Takeshi Tadano. *Biol. Pharm. Bull.,* 査読有, **2011**, *34*, 1413-1417.
49. ○*14 p-Hydroxyamphetamine causes prepulse inhibition disruption in mice: contribution of serotonin neurotransmission, Hiroshi Onogi, Osamu Nakagawasai, Atsushi Sato, Satoru Mitazaki, Kohta Nakaya, Kenya Watanabe, Fukie Niijima-Yaoita, Koichi Tan-No, Yuichiro Arai, Tsuneaki Kikuchi, Takeshi Tadano. *Behav. Brain Res.* 査読有, **2011**, *224*, 159-165.
50. *14 Alpha1,6-fucosyltransferase-deficient mice exhibit multiple behavioral abnormalities associated with a schizophrenia-like phenotype: importance of the balance between the dopamine and serotonin systems, Tomohiko Fukuda, Hirokazu Hashimoto, Natsumi Okayasu, Akihiko Kameyama, Hiroshi Onogi, Osamu Nakagawasai, Takahiro Nakazawa, Tomoyo Kurosawa, Yan Hao, Tomoya Isaji, Takeshi Tadano, Hisashi Narimatsu, Naoyuki Taniguchi, Jianguo Gu. *J. Biol. Chem.,* 査読有, **2011**, *286*, 18434-18443.
51. Intraplantar injection of gangliosides produces nociceptive behavior and hyperalgesia via a glutamate signaling mechanism, Shun Watanabe, Koichi Tan-No, Takeshi Tadano, Hideyoshi Higashi. *Pain*, 査読有, **2011**, *152*, 327-334.
52. ○*14 Pharmacological characterizations of memantine-induced disruption of prepulse inhibition of the acoustic startle response in mice: involvement of dopamine D_2 and 5-HT_{2A} receptors, Kohta Nakaya, Osamu Nakagawasai, Yuichiro Arai, Hiroshi Onogi, Atsushi Sato, Fukie Niijima, Koichi Tan-No, Takeshi Tadano. *Behav. Brain Res.* 査読有, **2011**, *218*, 165-173.
53. モルヒネの鎮痛耐性および身体的依存形成におけるシステインプロテアーゼの関与, 丹野孝一, *東*

北薬科大学研究誌, **2011,** *58,* 29-34.

54. Association between Cancer Risk and Drug-metabolizing Enzyme Gene (CYP2A6, CYP2A13, CYP4B1, SULT1A1, GSTM1, and GSTT1) Polymorphisms in Cases of Lung Cancer in Japan, Yuichiro Tamaki, Tomio Arai, Haruhiko Sugimura, Takamitsu Sasaki, Masashi Honda, Yuka Muroi, Yoichi Matsubara, Shuichi Kanno, Masaaki Ishikawa, Noriyasu Hirasawa, Mashiro Hiratsuka, *Drug Metab. Pharmacokinet.*, 査読有, **2011**, *26*, 516-522.
55. Tumor Necrosis Factor-Alpha–Nuclear Factor-Kappa B-Signaling Enhances St2b2 Expression during 12-*O*-Tetradecanoylphorbol-13-acetate-Induced Epidermal Hyperplasia, Toshihiro Matsuda, Miki Shimada, Akira Sato, Takanori Akase, Kouichi Yoshinari, Kiyoshi Nagata, Yasushi Yamazoe, *Biol. Pharm. Bull.*, 査読有, **2011**, *34*, 183-190.
56. Progression of Alcoholic and Non-alcoholic Steatohepatitis: Common Metabolic Aspects of Innate Immune System and Oxidative Stress, Shuhei Sakaguchi, Shougo Takahashi, Takamitsu Sasaki, Takeshi Kumagai, Kiyoshi Nagata, *Drug Metab. Pharmacokinet.*, 査読有, **2011**,*26*, 30-46.
57. Asymmetric intramolecular aldol reaction mediated by (S)-N-substituted–N-(2-pyrrolidinylmethyl)amine to prepare Wieland-Miescher ketone, Yuichi Akahane, Kohei Inomata, Yasuyuki Endo, *Heterocycles*, 査読有, **2010**, *82*, 1727-1737.
58. *6 Conformational Control of Benzyl-o-carboranylbenzene Derivatives and Molecular Encapsulation of Acetone into the Dynamically-formed Space of 1,3,5-Tris(2-benzyl-o-carboran- 1-yl)benzene, Chalermkiat Songkram, Kiminori Ohta, Kentaro Yamaguch, Fabio Pichierri, Yasuyuki Endo, *Inorg. Chem.* 査読有, **2010**, *49*, 11174–11183.
59. ○*4 Design and Synthesis of Potent Androgen Receptor (AR) Antagonists Bearing a p-Carborane Cage: Promising Ligand for Antiandrogen Withdrawal Syndrome, Tokuhito Goto, Kiminori Ohta, Shinya Fujii, Shigeru Ohta, Yasuyuki Endo, *J. Med. Chem.*, 査読有, **2010**, *53*, 4917-4926.
60. ○*8,9 Influence of olfactory bulbectomy on maternal behavior and dopaminergic function in nucleus accumbens in mice. Atsushi Sato, Osamu Nakagawasai, Koichi Tan-No, Hiroshi Onogi, Fukie Niijima, Takeshi Tadano. *Behav. Brain Res.* 査読有, **2010**, *215*, 141-145.
61. ○*14 p-Hydroxyamphetamine causes prepulse inhibition disruptions in mice: contribution of dopamine neurotransmission, Hiroshi Onogi, Osamu Nakagawasai, Koichi Tan-No, Satoru Mitazaki, Atsushi Sato, Kohta Nakaya, Fukie Niijima, Yuichiro Arai, Tsuneaki Kikuchi, Takeshi Tadano. *Behav. Brain Res.* 査読有, **2010**, *214*, 349-356.
62. Effects of atomoxetine on levels of monoamines and related substances in discrete brain regions in mice intermittently deprived of rapid eye movement sleep, Fukie Niijima, Hiroko Saito, Shigeo Murai, Yuichiro Arai, Osamu Nakagawasai, Koichi Tan-No, Hiromi Watanabe, Hajime Hiraga, Takeshi Tadano. *Biol. Pharm. Bull.*, 査読有, **2010**, *33*, 617-621.
63. ○*8,9 Effect of non-selective dopaminergic receptor agonist on disrupted maternal behavior in olfactory bulbectomized mice. Atsushi Sato, Osamu Nakagawasai, Koichi Tan-No, Hiroshi Onogi, Fukie Niijima, Takeshi Tadano. *Behav. Brain Res.* 査読有, **2010**, *210*, 251-256.
64. ○*14 Central administration of p-hydroxyamphetamine produces a behavioral stimulant effect in rodents: evidence for the involvement of dopaminergic systems, Hiroshi Onogi, Masato Hozumi, Osamu Nakagawasai, Yuichiro Arai, Seiichiro Ishigaki, Atsushi Sato, Seiichi Furuta, Fukie Niijima, Koichi Tan-No, Takeshi Tadano. *Psychopharmacology,* 査読有, **2010**, *208,* 323-331.
65. ○*14 Behavioral and neurochemical characterization of mice deficient in the N-type Ca2+ channel alpha1B subunit, Osamu Nakagawasai, Hiroshi Onogi, Satoru Mitazaki, Atsushi Sato, Kenya Watanabe, Hiroko Saito, Shigeo Murai, Kohta Nakaya, Manabu Murakami, Eiki Takahashi, Koichi Tan-No, Takeshi Tadano. *Behav. Brain Res.* 査読有, **2010**, *208*, 224-230.
66. Suppressive effects by cysteine protease inhibitors on naloxone-precipitated withdrawal jumping in morphine-dependent mice. Koichi Tan-No, Tasuku Sato, Masakazu Shimoda, Osamu Nakagawasai, Fukie Niijima, Shunsuke Kawamura, Seiichi Furuta, Takumi Sato, Susumu Satoh, Jerzy Silberring, Lars Terenius, Takeshi Tadano. *Neuropeptide.* 査読有, **2010**, *44*, 279-283.
67. Functional characterization of genetic polymorphisms identified in the promoter region of the xanthine oxidase gene, Mutsumi Kudo, Takamitsu Sasaki, Masaaki Ishikawa, Noriyasu Hirasawa, Mashiro Hiratsuka, *Drug Metab. Pharmacokinet.*, 査読有, **2010**,*25*, 599-603.
68. ○Malondialdehyde-modified low density lipoprotein (MDA-LDL)-induced cell growth was suppressed by polycyclic aromatic hydrocarbons (PAHs), Hiroyuki Suzuki, Takamitsu Sasaki, Takeshi Kumagai, Shuhei Sakaguchi, Kiyoshi Nagata, *J. Toxicol. Sci.*, 査読有, **2010**, *35*, 137-147

研究テーマ③癌および加齢性疾患に対する疼痛制御によるQOL向上の研究

1. Distinct Selectivity of Gangliosides Required for $CD4^+$ T and $CD8^+$ T Cell Activation, Inokuchi J, Nagafuku M, Ohno I, Suzuki A. Biochim. Biophys. Acta., 査読有, 2015, 1851, 98-106.
2. ストレスによる免疫トレランスの解消, 河野資、大野勲, *臨床免疫・アレルギー科,* 査読無, *2014, 61,* 682-688

3. Spinal ERK2 activation through δ_2-opioid receptors contributes to nociceptive behavior induced by intrathecal injection of leucine-enkephalin, Takaaki Komatsu, Soh Katsuyama, Hirokazu Mizoguchi, Chikai Sakurada, Minoru Tsuzuki, Shinobu Sakurada, Tsukasa Sakurada, *Peptides*, 査読有, **2014**, *54*, 131-139
4. ○*6 Potential involvement of μ-opioid receptor dysregulation on the reduced antinociception of morphine in the inflammatory pain state in mice, Yuta Aoki, Hirokazu Mizoguchi, Chizuko Watanabe, Kumiko Takeda, Tsukasa Sakurada, Shinobu Sakurada, *J. Pharmacol. Sci.*, 査読有, **2014**, *124*, 258-266.
5. ○*4 Differential alternation of the antinociceptive effect of narcotic analgesics on the inflammatory pain state, Yuta Aoki, Hirokazu Mizoguchi, Chizuko Watanabe, Tsukasa Sakurada, Shinobu Sakurada, *Neurosci. Lett.*, 査読有, **2014**, *560*, 122-125.
6. Involvement of multiple μ-opioid receptor subtypes on the presynaptic or postsynaptic inhibition of spinal pain transmission, Hirokazu Mizoguchi, Hirokazu Takagi, Chizuko Watanabe, Akihiko Yonezawa, Takumi Sato, Tsukasa Sakurada, Shinobu Sakurada, *Peptides*, 査読有, **2014**, *51*, 15-25.
7. ○*10 The involvement of glucocorticoids in psychological stress-induced exacerbations of experimental allergic asthma, Kaoru Okuyama, Kazuhisa Dobashi, Tomomitsu Miyasaka, Naoki Yamazaki, Toshiaki Kikuchi, Ichiro Sora, Motoaki Takayanagi, Hirohito Kita, Isao Ohno, *Int. Arch. Allergy Immunol.*, 査読有, **2014**, *163*, 297-306.
8. *8, 9, 11 ストレスによる気道炎症の修飾, 大野勲, *喘息*, 査読無, **2104**, *27*, 63-68.
9. Involvement of spinal release of α-neo-endorphin on the antinociceptive effect of TAPA, Hirokazu Mizoguchi, Takashi Kon-no, Hiroyuki Watanabe, Chizuko Watanabe, Akihiko Yonezawa, Takumi Sato, Tsukasa Sakurada, Shinobu Sakurada, *Peptides*, 査読有, **2013**, *50*, 139-144.
10. ○Distinct physiological role of amidino-TAPA-sensitive and DAMGO-insensitive μ-opioid receptor splice variants in the mouse spinal cord, Hirokazu Mizoguchi, Chizuko Watanabe, Takayuki Higashiya, Satoshi Takeda, Kaori Moriyama, Yuta Aoki, Takashi Kon-no, Hirokazu Takagi, Akihiko Yonezawa, Takumi Sato, Tsukasa Sakurada, Shinobu Sakurada, *Eur. J. Pharmacol.*, 査読有, **2013**, *711*, 80-86.
11. Involvement of peripheral cannabinoid and opioid receptors in β-caryophyllene-induced antinociception, Soh Katsuyama, Hirokazu Mizoguchi, Hikari Kuwahata, Takaaki Komatsu, Kohshi Nagaoka, Hitoshi Nakamura, Giacinto Bagetta, Tsukasa Sakurada, Shinobu Sakurada, *Eur. J. Pain*, 査読有, **2013**, *17*, 664-675.
12. Peripherally injected linalool and bergamot essential oil attenuate mechanical allodynia via inhibiting spinal ERK phosphorylation, Hikari Kuwahata, Takaaki Komatsu, Soh Katsuyama, Maria Tiziana Corasaniti, Giacinto Bagetta, Shinobu Sakurada, Tsukasa Sakurada, Kazuo Takahama, *Pharmacol. Biochem. Behav.*, 査読有, **2013**, *103*, 735-741.
13. Contribution of $CD4^+$ T cells and dendritic cells to female-dominant antigen-induced Th2 cytokine production by bronchial lymph node cells, Kaoru Okuyama, Masatoshi Suenaga, Shyunya Furuki, Tasuku Kawano, Yuichi Ohkawara, Motoaki Takayanagi, Toshiaki Kikuchi, Isao Ohno, *Int. Arch. Allergy Immunol.*, 査読有, **2013**, *161*, 58-65.
14. ○Heterogeneity of gangliosides among T cell subsets, Jin-ichi Inokuchi, Masakazu Nagafuku, Isao Ohno, Akemi Suzuki, *Cell. Mol. Life Sci.*, 査読有, **2013**, *70*, 3067-75.
15. *8, 9 オピオイド受容体とアレルギー炎症, 大野勲, *呼吸*, 査読無, **2013**, *32*, 20-24.
16. 気管支喘息における気道リモデリングの分子病態とその予防, 大野勲, 山内広平, *臨床免疫・アレルギー科*, 査読無, **2013**, *59*, 83-88.
17. ラット射精機能評価モデルを用いた副作用解析と治療薬探索、米澤章彦、渡辺千寿子、溝口広一、河谷正仁、木村行雄、櫻田忍、*自律神経*, 査読有, **2012**, *49*, 74-75.
18. Non-opioid nociceptive activity of human dynorphin mutants that cause neurodegenerative disorder spinocerebellar ataxia type 23, Hiroyuki Watanabe, Hirokazu Mizoguchi, Dineke S. Verbeek, Alexander Kuzmin, Fred Nyberg, Oleg Krishtal, Shinobu Sakurada, Georgy Bakalkin, *Peptides*, 査読有, **2012**, *35*, 306-310.
19. The involvement of the spinal release of glutamate and nitric oxide in peripheral noxious stimulation-induced pain-related behaviors--study in mouse spinal microdialysis, Chizuko Watanabe, Hirokazu Mizoguchi, Giacinto Bagetta, Shinobu Sakurada, *Neurosci Lett.*, 査読有, **2012**, *515*, 111-114.
20. Understanding anomalous adaptation in chronic pain for successful development of disease modifying drugs, Giacinto Bagetta, Shinobu Sakurada, *Curr. Opin. Pharmacol.*, 査読有, **2012**, *12*, 1-3.
21. ○*2 New vistas in opioid control of pain, Hirokazu Mizoguchi, Chizuko Watanabe, Tsukasa Sakurada, Shinobu Sakurada, *Curr. Opin. Pharmacol.*, 査読有, **2012**, *12*, 87-91.
22. ○Higher sensitivity of male $CD4^+$ T cells to suppressive effects of $CD8^+$ T cells on IL-5 production compared with female $CD4^+$ T cells, Kaori Okuyama, Tsuyoshi Kashimura, Tasuku Kawano, Yuichi Ohkawara, Motoaki Takayanagi, Toshiaki Kikuchi, Isao Ohno, *Int. Arch. Allergy Immunol.*, 査読有, **2012**, *158*, 35-41.
23. ○*8, 9 μ–opioid receptor-mediated alterations of allergen-induced immune responses of bronchial lymph node cells in a murine model of stress asthma. Kaori Okuyama, Soichiro Ide, Shinobu Sakurada, Kazumasu Sasaki, Ichiro Sora, Gen Tamura, Yuichi Ohkawara, Motoaki Takayanagi, Isao Ohno, *Allergol, Int.*, 査読有, **2012**, *61*, 245-258.
24. ○CD4 and CD8 T cells require different membrane gangliosides for activation, Masakazu Nagafuku, Kaori

Okuyama, Onimaru Y, Akemi Suzuki, Odagiri Y, Yamashita T, Iwasaki K, Fujiwara M, Motoaki Takayanagi, Isao Ohno, Jin-ichi Inokuchi, *Proc. Natl. Acad. Sci. USA*, 査読有, **2012**, *109*, E336-342.

25. Inhibition of ERK phosphorylation by substance P N-terminal fragment decreases capsaicin-induced nociceptive response, Takaaki Komatsu, Hirokazu Mizoguchi, Mika Sasaki, Chikai Sakurada, Minoru Tsuzuki, Shinobu Sakurada, Tsukasa Sakurada, *Neuropharmacology*, 査読有, **2011**, *61*, 608-613.
26. Antinociceptive effects of spinally administered nociceptin/orphanin FQ and its N-terminal fragments on capsaicin-induced nociception, Soh Katsuyama, Hirokazu Mizoguchi, Takaaki Komatsu, Chikai Sakurada, Minoru Tsuzuki, Shinobu Sakurada, Tsukasa Sakurada, *Peptides*, 査読有, **2011**, *32*, 1530-1535.
27. Partial involvement of NMDA receptors and glial cells in the nociceptive behaviors induced by intrathecally administered histamine, Hirokazu Mizoguchi, Takaaki Komatsu, Yoko Iwata, Chizuko Watanabe, Hiroyuki Watanabe, Tohru Orito, Soh Katsuyama, Akihiko Yonezawa, Kenji Onodera, Tsukasa Sakurada, Shinobu Sakurada, *Neurosci Lett.*, 査読有, **2011**, *495*, 83-87.
28. ○Dermorphin tetrapeptide analogs as potent and long-lasting analgesics with pharmacological profiles distinct from morphine, Hirokazu Mizoguchi, Giacinto Bagetta, Tsukasa Sakurada, Shinobu Sakurada, *Peptides*, 査読有, **2011**, *32*, 421-427.
29. Involvement of glial cells in the nociceptive behaviors induced by a high-dose of histamine administered intrathecally, Hirokazu Mizoguchi, Takaaki Komatsu, Yoko Iwata, Chizuko Watanabe, Hiroyuki Watanabe, Tohru Orito, Soh Katsuyama, Akihiko Yonezawa, Kenji Onodera, Tsukasa Sakurada, Shinobu Sakurada, *Eur. J. Pharmacol.*, 査読有, **2011**, *653*, 21-25.
30. Temporal profile of vascular changes induced by systemic nitroglycerin in the meningeal and cortical districts, Rosaria Greco, Cristina Meazza, Antonina Stefania Mangione, Marta Allena, Monica Bolla, Diana Amantea, Hirokazu Mizoguchi, Giorgio Sandrini, Giuseppe Nappi, Cristina Tassorelli, *Cephalalgia*, 査読有, **2011**, *31*, 190-198.
31. ○Involvement of mouse μ-opioid receptor splice variants in the spinal antinociception induced by the dermorphin tetrapeptide analog amidino-TAPA, Hirokazu Mizoguchi, Chizuko Watanabe, Takayuki Higashiya, Satoshi Takeda, Kaori Moriyama, Akihiko Yonezawa, Takumi Sato, Takaaki Komatsu, Tsukasa Sakurada, Shinobu Sakurada, *Eur. J. Pharmacol.*, 査読有, **2011**, *651*, 66-72.
32. Intraplantar injection of bergamot essential oil induces peripheral antinociception mediated by opioid mechanism, Tsukasa Sakurada, Hirokazu Mizoguchi, Hikari Kuwahata, Soh Katsuyama, Takaaki Komatsu, Luigi Antonio Morrone, Maria Tiziana Corasaniti, Giacinto Bagetta, Shinobu Sakurada, *Pharmacol. Biochem. Behav.*, 査読有, **2011**, *97*, 436-443.
33. 高齢者の喘息でも好酸球は重要なのでしょうか？ 大野勲, *アレルギーの臨床*, 査読無, **2011**, *31*, 335.
34. 糖鎖によるアレルギー性免疫応答の調節, 奥山香織, 大野勲, 永福正和, 井ノ口仁一, *呼吸*, 査読無, **2011**, *30*, 223-229.
35. T cell subsets related with a sex difference in IL-5 production, Kaori Okuyama, Yuka Hamanaka, Tasuku Kawano, Yuichi Ohkawara, Motoaki Takayanagi, Toshiaki Kikuchi, Isao Ohno. *Int. Arch. Allergy Immunol.*, 査読有, **2011**, *155*, 21-26.
36. The cannabinoid 1 receptor antagonist AM251 produces nocifensive behavior via activation of ERK signaling pathway, Soh Katsuyama, Hirokazu Mizoguchi, Takaaki Komatsu, Kohshi Nagaoka, Shinobu Sakurada, Tsukasa Sakurada, *Neuropharmacology*, 査読有, **2010**, *59*, 534-541.
37. ○Lack of a rewarding effect and a locomotor-enhancing effect of the selective μ-opioid receptor agonist amidino-TAPA, Hirokazu Mizoguchi, Chizuko Watanabe, Shin Osada, Maya Yoshioka, Yuta Aoki, Sanae Natsui, Akihiko Yonezawa, Syu-ichi Kanno, Masaaki Ishikawa, Tsukasa Sakurada, Shinobu Sakurada, *Psychopharmacology (Berl)*, 査読有, **2010**, *212*, 215-225.
38. Role of supraspinal and spinal α_1-adrenergic receptor subtypes in micturition reflex in conscious rats, Masaru Yoshizumi, Kazumasa Matsumoto-Miyai, Akihiko Yonezawa, Masahito Kawatani, *Am. J. Physiol. Renal. Physiol.*, 査読有, **2010**, *299*, F785-791.
39. Neuropharmacology of the essential oil of bergamot, Giacinto Bagetta, Luigi Antonio Morrone, Laura Rombolà, Diana Amantea, Rossella Russo, Laura Berliocchi, Shinobu Sakurada, Tsukasa Sakurada, Domenicantonio Rotiroti, Maria Tiziana Corasaniti, *Fitoterapia*, 査読有, **2010**, *81*, 453-461.
40. Characterization of intrathecally administered hemokinin-1-induced nociceptive behaviors in mice, Chizuko Watanabe, Hirokazu Mizoguchi, Akihiko Yonezawa, Shinobu Sakurada, *Peptides*, 査読有, **2010**, *31*, 1613-1616
41. *7 喘息モデルとオピオイド, 大野勲, *アレルギー・免疫*, 査読無, **2010**, *17*, 1851-1858.
42. *7 喘息と脳機能, 大野勲, *臨床免疫・アレルギー科*, 査読無, **2010**, *54*, 332-338.
43. *7 喘息と脳機能, 大野勲, *International Review of Asthma & COPD*, 査読無, **2010**, *12*, 29-34.
44. *7 気管支喘息と精神的ストレス, 大野勲, *臨床病理*, 査読無, **2010**, *58*, 292-299.
45. *7 ストレス喘息とμオピオイド受容体, 大野勲, *アレルギーと神経ペプチド*, 査読無, **2010**, *6*, 4-9.
46. ○Gender differences in transcriptional regulation of IL-5 expression by bronchial lymph node cells in a mouse model of asthma, Kana Wada, Kaori Okuyama, Yuichi Ohkawara, Motoaki Takayanagi, Isao Ohno, *Respirology*, 査読有, **2010**, *15*, 629-635.

47. Trends in antimicrobial susceptibility of *Streptococcus pneumoniae* in the Tohoku district of Japan: a longitudinal analysis from 1998 to 2007, Kazumasa Suzuki, Katsushi Nishimaki, Kaori Okuyama, Tadashi Katoh, Minoru Yasujima, Junichi Chihara, Akira Suwabe, Yoko Shibata, Choichiro Takahashi, Hiroaki Takeda, Shiro Ida, Mitsuo Kaku, Akira Watanabe, Toshihiro Nukiwa, Kazunao Niitsuma, Keiji Kanemitsu, Motoaki Takayanagi, Isao Ohno, *Tohoku J. Exp. Med.*, 査読有, **2010**, *220*, 47-57.
48. ○The involvement of μ-opioid receptors in the central nervous system in the worsening of allergic airway inflammation by psychological stress in mice, Kaori Okuyama, Kana Wada, Shinobu Sakurada, Hirokazu Mizoguchi, Hiroshi Komatsu, Ichiro Sora, Gen Tamura, Yuichi Ohkawara, Motoaki Takayanagi, Isao Ohno, *Int. Arch. Allergy Immunol.*, 査読有, **2010**, *152*, 342-352.

＜図書＞

研究テーマ①新しい作用機作をもつ癌化学療法薬の創製

1. 「よくわかる薬学機器分析」(藤岡稔大、二村典行、大庭義史、山下幸和　編)、廣川書店、2015.
2. 「免疫測定法 －基礎から先端まで－」大野賢一（小林典裕、上田宏、三宅司郎、荒川秀俊　編)、講談社、2014.
3. Studies in Natural Products Chemistry, Vol. 43, Tadashi Katoh, ed. by Atta-ur-Rahman, Elsevier, Amsterdam, 2014, p.1–39
4. 「よくわかる薬学分析化学」(二村典行、大庭義史、山下幸和　編)、廣川書店、2014.
5. 構造解析概説、「パートナー分析化学 II」、山下幸和（山口政俊、升島　努、能田　均編)、南江堂、2012、43-51.
6. Development of Novel Proton-Affinitive Derivatives for Simultaneous Analysis of Testosterone and Dihydrotestosterone in Human Serum and Prostate Tissue by LC-ESI-MS/MS, 「Testosterone: Biochemistry, therapeutic use and rophysiological effects」, Kouwa Yamashita (ed. by Kanstantin Chichinadze), Nova Scientific Publishers Inc, **2012**, 145-158.

研究テーマ②エストロゲン受容体制御による加齢性疾患(骨粗鬆症、認知障害)改善薬の創製

1. 内因性敗血症及びそのショックモデルの作成と病態･薬効評価、敗血症の診断/治療の実情と病態･メカニズムをふまえた開発戦略、坂口　修平、永田　清、技術情報協会、21-27、2013.
2. エンドトキシン感受性コントロールモデルその臨床的意義､敗血症の診断/治療の実情と病態･メカニズムをふまえた開発戦略、坂口　修平、永田　清、技術情報協会、16-20、2013.
3. Methamphetamines: Abuse, Health Effects and Treatment Options, "Pharmacological actions of p-hydroxyamphetamine in the central nervous system", Osamu Nakagawasai, Hiroshi Onogi, Satoru Mitazaki, Masato Hozumi, Koichi Tan-No, Yuichiro Arai, Tsuneaki Kikuchi, Takeshi Tadano (Editors, Jorg Ornoy and Xiaoling He), Nova Science Publishers, 2012, 14 (187-200)
4. 「エンドトキシン・自然免疫研究 15 －飛躍する自然免疫研究－」敗血症モデルとしての TNF-α 誘導肝細胞死と酸化ストレス、坂口修平、 髙橋昌悟、 熊谷　健、 佐々木崇光、 永田　清、 医学図書出版、53-57、2012.
5. Neuropeptide Degradation Related to the Expression of the Physiological Action of Neuropeptides, "Neuropeptides in Neuroprotection and Neuroregeneration", Chikai Sakurada, Hirokazu Mizoguchi, Takaaki Komatsu, Shinobu Sakurada, Tsukasa Sakurada (Edited by F.J. Nyberg), CRC Press, 2012, 17 (27-43)
6. 天然物合成で活躍した反応：実験のコツとポイント、加藤 正 (有機合成化学協会 編)、化学同人、2011, p.82–83, p.134–135.
7. 化学物質の代謝・代謝的活性化､「考える衛生化学」､永田　清（平山晃久　編集)､廣川書店､125-152、2011.
8. チトクロム P-450 を介した薬物代謝、創薬研究のストラテジー、佐々木崇光、永田　清、（奥山　茂、斉藤亜紀良、山田久陽　編集）金芳堂、京都、187-193、2011.
9. 薬物代謝酵素の個人変動の要因、予防医学としての衛生化学　—健康と環境—、永田　清、（吉原紘一、繪柳玲子　編集）広川書店、 241-251、2010.
10. 医薬品の毒性に影響する要因、医薬品安全性学　（第２版）、永田　清、（吉田武美、竹内幸一　編集）広川書店、49-67、2010.
11. 酵素誘導、薬物代謝学　（第３版）医療薬学・医薬品開発の基礎として、永田　清、（加藤隆一、山添康、横井毅　編集）、東京化学同人、127-139、2010.

研究テーマ③癌および加齢性疾患に対する疼痛制御による QOL 向上の研究

1. ベンゾジアゼピン系抗不安薬､「緩和医療薬学」､溝口広一（日本緩和医療薬学会 編)、南江堂、2013、1 (71)
2. 疼痛治療における鎮痛補助薬の有効性と限界２—抗てんかん薬：抑制性神経活性化薬、「薬局 64」、佐野元彦、溝口広一、高瀬久光、2013、9 (90-98)

3. Capter 212: Endomorphins, "Handbook of Biological Active Peptides 2nd Edition", Hirokazu Mizoguchi, Tsukasa Sakurada, Shinobu Sakurada (Edited by Abba Kastin), Elsevier, 2013, 6(1556-1561)
4. 「機能形態学 改訂 3 版」、櫻田忍、櫻田司、櫻田誓、米澤章彦、溝口広一（櫻田忍、櫻田司 編）、南江堂、2013、332(1-332)
5. 尿路系、「トワイクロス先生のがん緩和ケア処方薬」、溝口広一（武田文和、鈴木勉 監訳）、医学書院、2013、11(487-497)
6. 栄養と血液、「トワイクロス先生のがん緩和ケア処方薬」、溝口広一（武田文和、鈴木勉 監訳）、医学書院、2013、14(499-512)
7. Neuropeptide Degradation Related to the Expression of the Physiological Action of Neuropeptides, "Neuropeptides in Neuroprotection and Neuroregeneration", Chikai Sakurada, Hirokazu Mizoguchi, Takaaki Komatsu, Shinobu Sakurada, Tsukasa Sakurada (Edited by F.J. Nyberg), CRC Press, 2012, 17(27-43)
8. Ethnopharmacological Approaches Used to Identify Medicinal Plants, "HERVAL MEDICINES: Development and Validation of Plant-Derived Medicines for Human Health", Tsukasa Sakurada, Hirokazu Mizoguchi, Soh Katsuyama, Takaaki Komatsu, Hikari Kuwahata, Laura Rombola, Giacinto Bagetta, Maria Tiziana Corasaniti, Shinobu Sakurada (Edited by Giacinto Bagetta, Marco Cosentino, Maria Tiziana Corasaniti, Shinobu Sakurada), CRC Press, 2011, 23(27-49)
9. Mechanisms and Clinical Relevance of Herb-Drug Interactions from the Perspectives of Pharmacokinetics, "HERVAL MEDICINES: Development and Validation of Plant-Derived Medicines for Human Health", Laura Berliocchi, Rossella Russo, Hirokazu Mizoguchi, Maria Tiziana Corasaniti (Edited by Giacinto Bagetta, Marco Cosentino, Maria Tiziana Corasaniti, Shinobu Sakurada), CRC Press, 2011, 35(243-277)
10. Contribution of Herbal Medicine to Human Health: A Brief History, "HERVAL MEDICINES: Development and Validation of Plant-Derived Medicines for Human Health", Luigi Antonio Morrone, Laura Rombola, Diana Amantea, Hirokazu Mizoguchi, Maria Tiziana Corasaniti (Edited by Giacinto Bagetta, Marco Cosentino, Maria Tiziana Corasaniti, Shinobu Sakurada), CRC Press, 2011, 31(381-411)

＜学会発表＞

学会名、発表者名、発表標題名、開催地、発表年月（西暦）について記入してください（左記の項目が網羅されていれば、項目の順序を入れ替えても可）。また、現在から発表年次順に遡り、通し番号を付してください。

研究テーマ①新しい作用機作をもつ癌化学療法薬の創製

1. PTP1B 阻害活性を有するダイシダバロン B および C の全合成研究, 成田紘一, 福井友理恵, 佐藤江里, 安達剛史, 加藤　正, 日本薬学会第 135 年会, 神戸, 2015 年 3 月
2. カンナビノイド受容体アゴニスト活性を有するフェルギネン B の全合成研究, 佐々木　理, 成田紘一, 加藤　正, 日本薬学会第 135 年会, 神戸, 2015 年 3 月
3. 海洋天然物であるイリマキノン、イソスポンジアキノン、スメノクアロンおよび スメノスポンジンの全合成, 加藤　武, 熱海　秀, 佐藤廣河, 平間美佳, 成田紘一, 加藤　正, 日本薬学会第 135 年会, 神戸, 2015 年 3 月
4. 選択的 PI3Kα 阻害物質(+)-リファガールの全合成, 菊地拓也, 神島尭明, 成田紘一, 加藤　正, 日本薬学会第 135 年会, 神戸, 2015 年 3 月
5. イナミドの三成分連結反応におけるカップリングパートナーの影響、若松秀章、石井彩香、菊地洋平、木村翔、名取良浩、吉村祐一、日本薬学会第 135 年会、神戸、2015 年 3 月
6. C1 位に 4-アリールブチル基が置換したイミノフラノース誘導体の不斉合成とその酵素阻害活性評価、名取良浩、佐久間俊嘉、木南今日子、加藤敦、足立伊佐雄、吉村祐一、日本薬学会第 135 年会、神戸、2015 年 3 月
7. 超原子価ヨウ素とジセレニドによる酸化的エーテル環化反応の検討、斎藤有香子、植松拓也、名取良浩、若松秀章、吉村祐一、日本薬学会第 135 年会、神戸、2015 年 3 月
8. 1-C-n-ブチル-L-イミノ糖誘導体の触媒的不斉合成とα-グルコシダーゼ阻害作用に対する構造活性相関、佐久間俊嘉、名取良浩、加藤敦、足立伊佐雄、中川進平、吉村祐一、日本薬学会第 135 年会、神戸、2015 年 3 月
9. 違法薬物分析を指向した LC-MS による構造解析法の検討 加藤創, 渡邊将樹, 菊池悠子, 栗屋麻実, 山下幸和, 原田健一, 宮城薬剤師学術フォーラム 2014, 仙台, 2014 年 11 月
10. 胆汁酸のピコリルエステル化による高感度 LC-MS 分析 加藤 創, 三塚進, 加藤杏奈, 阿邊満夕子, 池田麻希, 山下幸和, 日本薬学会第 135 年会, 神戸, 2015 年 3 月
11. コレステロールの前駆体および水酸化代謝物の LC-ESI-MS/MS 分析 小松祥子, 千葉淳, 都澤優, 宮本和明, 山下幸和, 日本薬学会第 135 年会, 神戸, 2015 年 3 月
12. Dvelopement of New Glycosylation Reactions and Its Application to the Synthesis of Nucleoside Derivatives. Yoshimura Yuichi. 3rd SNU Mini-Symposium on Medicinal Chemistry, Seoul, Korea, Feb, 2015
13. PTP1B 阻害活性を有する ダイシダバロン A の全合成, 福井友理恵, 成田紘一, 加藤　正, 第 40 回反応と合成の進歩シンポジウム, 仙台, 2014 年, 11 月

14. Syntheses of Stavudine and Its 4'-Substituted Analogue Using Hypervalent Iodine Mediated Oxidative Glycosylation. Yuichi Yoshimura, Hiroya Kan-no, Yoshihiro Natori, Yukako Saito, Hideaki Wakamatsu. 第2回国際会議（兼）第7回 有機触媒シンポジウム，東京，2014年11月
15. イナミドを基質としたパラジウム触媒による三成分連結反応、若松秀章、菊地洋平、石井彩香、木村翔、高橋彩乃、柳澤里佳、名取良浩、高畑廣紀、吉村祐一、第40回反応と合成の進歩シンポジウム、仙台、2014年11月
16. イナミドを用いた三成分連結反応におけるボロン酸及びハロゲン化アリールの効果、若松秀章、石井彩香、菊地洋平、木村翔、高橋彩乃、柳澤里佳、名取良浩、吉村祐一、第53回日本薬学会東北支部大会、いわき、2014年10月
17. *15　C1位に4-アリールブチル基が置換したイミノ糖誘導体の不斉合成とそのα-グルコシダーゼ阻害活性評価、名取良浩、佐久間俊嘉、加藤敦、足立伊佐雄、吉村祐一、第53回日本薬学会東北支部大会、いわき、2014年10月
18. p21*ras* ファルネシルトランスフェラーゼ阻害物質 TAN-1813 の合成研究，成田紘一，加藤　正，第53回日本薬学会東北支部大会，いわき，2014年10月
19. Chaetomium属糸状菌が生産する新規芳香族ポリケチド類に関する研究 山本崇史，浅井禎吾，森田峻太郎，山下幸和，藤井勲，大島吉輝，第53回日本薬学会東北支部大会，いわき，2014年10月
20. キリギリス内糸状菌が生産する新規二次代謝物の探索 布木純，浅井禎吾，山下幸和，大島吉輝，第53回日本薬学会東北支部大会，いわき，2014年10月
21. Aldosteroneの dimethylethylsilyl および dimethylisopropylsilyl 誘導体化と GC-MS 分析 小松祥子，大池裕貴，山下幸和，第53回日本薬学会東北支部大会，いわき，2014年10月
22. 硫化水素の生物発光検出に関する基礎的研究 大野賢一，岩渕理子，山下　幸和，第53回日本薬学会東北支部大会，いわき，2014年10月
23. 新規 HDAC/PI3K 二重阻害剤としてのデプシペプチド類縁体の抗腫瘍活性の検討，西條　憲，李仁，成田紘一，加藤　正，下平秀樹，石岡千加史，第73回日本癌学会学術総会，横浜，2014年9月
24. 抗がん活性天然物マンデラリド A の合成に向けて：Ag(I) 触媒による *cis*-2,5-DHF および 3,6-DHP の合成，渡邉一弘，日本薬学会 第13回化学系若手研究者セミナー，仙台，2014年9月
25. ルテニウム触媒を用いたエンイナミドを基質とする閉環反応、若松秀章、小椋玲奈、坂上舞依子、花田美幸、竹下光弘、佐々木好美、高畑廣紀、吉村祐一、第44回複素環化学討論会、札幌、2014年9月
26. *15 1-C-n-ブチル-L-イミノフラノース誘導体の不斉合成と その酵素阻害活性評価、佐久間俊嘉、名取良浩、中川進平、加藤敦、足立伊佐雄、吉村祐一、第44回複素環化学討論会、札幌、2014年9月
27. *In Vitro* and *In Vivo* Antitumor Effects of Romidepsin Analogs as Novel PI3K/HDAC dual Inhibitors, Jin Lee, Ken Saijo, Koichi Narita, Tadashi Katoh, Hideki Shimodaira, Chikashi Ishioka, The 9th International Symposium of the Institute Network, Osaka, Japan, June, 2014
28. *In vitro* および *in vivo* における PI3K/HDAC 二重阻害剤としての FK228 類縁体の抗腫瘍効果の評価，李　仁，西條　憲，下平秀樹，成田紘一，加藤　正，石岡千加史，第18回日本がん分子標的治療学会，仙台，2014年6月
29. トリアゾール環を側鎖に持つ D-イミノフラノース誘導体の合成と生物活性評価、名取良浩、盛友莉恵、吉村祐一、佐藤香純、加藤敦、足立伊佐雄、高畑廣紀、日本薬学会第134年会、熊本、2014年3月
30. 2,6-2 置換ピペリデン誘導体の合成と有機触媒への応用、酒井華恵、吉村祐一、高畑廣紀、日本薬学会第134年会、熊本、2014年3月
31. *15 β-1-C-n-ブチル-L-イミノ糖誘導体の触媒的不斉合成と α-グルコシダーゼ阻害作用に対する構造活性相関、佐久間俊嘉、名取良浩、吉村祐一、加藤敦、足立伊佐雄、中川進平、高畑廣紀、日本薬学会第134年会、熊本、2014年3月
32. 3'-デオキシ-4'-チオヌクレオシドの合成研究、伊藤文、吉村祐一、名取良浩、高畑廣紀、日本薬学会第134年会、熊本、2014年3月
33. *10 新規酸化的グリコシル化反応を利用したヌクレオシド誘導体の合成、菅野裕也、植松拓也、若松秀章、名取良浩、斎藤有香子、吉村祐一、高畑廣紀、日本薬学会第134年会、熊本、2014年3月
34. イナミドを基質としたパラジウム触媒による炭素炭素結合形成反応、若松秀章、吉村祐一、柳澤里佳、高橋彩乃、名取良浩、高畑廣紀、日本薬学会第134年会、熊本、2014年3月
35. 抗腫瘍活性を有するダイシダバロン A の全合成、福井友理恵、成田紘一、加藤　正、日本薬学会第134年会、熊本、2014年3月
36. *5, 6 p21^{ras} ファルネシルトランスフェラーゼ阻害物質 TAN-1813 の合成研究、成田紘一、加藤　正、日本薬学会第134年会、熊本、2014年3月
37. 抗腫瘍活性を有するβ-ラパコンの簡便合成、加藤　武、門間博充、若杉　潤、成田紘一、加藤　正、日本薬学会第134年会、熊本、2014年3月
38. LC-ESI-MS/MS 法による 3β-HS 活性評価を目的とした基礎検討、小松祥子，太齋ひとみ，山下　幸和，沼澤光輝，日本薬学会第134年会，熊本，2014年3月

39. ツツジ科植物内生糸状菌を資源とした新規天然物の探索、大槻紗恵、浅井貞悟、山下幸和、大島吉輝日本薬学会第 134 年会, 熊本, 2014 年 3 月
40. エピジェネティックな二次代謝活性化法を利用するイチイ内生糸状菌を資源とした新規天然物の探索、布木　純、浅井貞悟、山下幸和、河治久実、児玉栄一、大島吉輝、日本薬学会第 134 年会, 熊本, 2014 年 3 月
41. *21 Enhancement of Radiation-Induced Apoptosis by a Potent Histone Deacetylase Inhibitor Spiruchoustatin-B, Mati ur Rehman, Paras Jawaid, Koichi Narita, Tadashi Katoh, Tadamichi Shimizu, Takashi Kondo, The 1st GI-CORE Medical Science and Engineering Symposium, Sapporo, Japan, Febrary, February, 2014
42. 抗インフルエンザ A ウイルス活性を有するストロンギリン A の全合成、神島尭明、加藤　正、第 39 回反応と合成の進歩シンポジウム、福岡、2013 年、11 月
43. 酸化的グリコシル化反応を利用したスタブジン及び 4'-置換スタブジンの新規合成法、菅野裕也、植松拓也、吉村祐一、高畑廣紀、第 31 回メディシナルケミストリーシンポジウム、広島、2013 年 11 月
44. *10 Design and Synthesis of Nucleoside Phosphonate Constructed on a Branched-tetrofuranose Skeleton, Yuichi Yoshimura, Y. B. Kiran, Hideaki Wakamatsu, Yoshihiro Natori, Hiroki Takahata, The 40th International Symposium on Nucleic Acids Chemistry, Yokohama, November 2013
45. イリジウム触媒を用いた分子内環化反応を基盤とする置換ピロリジン体の立体選択的合成、名取良浩、菊地俊輔、近藤孝洋、斎藤有香子、吉村祐一、高畑廣紀、第 39 回反応と合成の進歩シンポジウム、福岡、2013 年 11 月
46. 遷移金属錯体を用いたイナミドに対する位置選択的炭素鎖導入法の開発、若松秀章、柳澤里佳, 高橋 彩乃、名取良浩、吉村祐一、高畑廣紀、第 52 回日本薬学会東北支部大会、仙台、2013 年 10 月
47. クリックケミストリーを利用したトリアゾール環を側鎖に持つ D-イミノフラノース誘導体の合成研究、盛友莉恵、名取良浩、吉村祐一、高畑廣紀、第 52 回日本薬学会東北支部大会、仙台、2013 年 10 月
48. α-1-*C*-アルキル-D-アラビノース型イミノ糖誘導体の合成とその糖加水分解酵素阻害活性評価、名取良浩、渡邊靖香、佐久間俊嘉、千葉由稀、吉村祐一、高畑廣紀、第 52 回日本薬学会東北支部大会、仙台、2013 年 10 月
49. *5, 6 p21^{ras} ファルネシルトランスフェラーゼ阻害物質 TAN-1813 の合成研究、成田紘一、加藤　正、第 52 回日本薬学会東北支部大会、仙台、2013 年 10 月
50. 抗腫瘍活性を有するダイシダバロン A の全合成、福井友理恵、成田紘一、加藤　正、第 52 回日本薬学会東北支部大会、仙台、2013 年 10 月
51. 抗インフルエンザ A ウイルス活性を有するストロンギリン A の全合成、神島尭明、加藤　正、第 52 回日本薬学会東北支部大会、仙台、2013 年 10 月
52. ピコリル誘導体化による生体内微量胆汁酸の高感度分析法の確立、加藤杏奈、三塚　進、加藤　創、山下幸和、第 52 回日本薬学会東北支部大会、仙台、2013 年 10 月
53. *19 アンドロゲンの高感度質量分析法の開発と唾液試料への応用、田村智美、長谷川智美、大野賢一、山下幸和、第 52 回日本薬学会東北支部大会、仙台、2013 年 10 月
54. LC-ESI-MS/MS 法による水酸化ステロイドのメタボローム解析（VII）—ステロール類のピコリン酸およびN-メチルピペリジンカルボン酸誘導体の調製—、小松祥子、都澤　優、千葉　淳、山崎敬子、山下幸和、沼澤光輝、第 52 回日本薬学会東北支部大会、仙台、2013 年 10 月
55. 植物、節足動物内生糸状菌を資源とした新規天然物の探索、布木　純、浅井貞悟、山下幸和、大島吉輝、第 52 回日本薬学会東北支部大会、仙台、2013 年 10 月
56. シャクヤク内生糸状菌 Graphinosis chlorocephala が産生する新規ベンゾフェノン類に関する研究、大槻紗恵、浅井貞悟、山下幸和、河治久実、児玉栄一、大島吉輝、第 52 回日本薬学会東北支部大会、仙台、2013 年 10 月
57. *1,2 Total Synthesis of the Bicyclic Depsipeptides -Spiruchostatins A, B, C and D- and Investigation of Their HDAC Inhibitory and Antiproliferative Activities, Yurie Fukui, Koichi Narita, Tadashi Katoh, 13th International Conference on the Chemistry of Antibiotics and Other Bioactive Compounds (ICCA-13), Yamanashi, Japan, September, 2013
58. Synthetic Study Toward Marine Natural Products Related to Illimaquione, Suguru Atsumi, Koichi Narita, Tadashi Katoh, 13th International Conference on the Chemistry of Antibiotics and Other Bioactive Compounds (ICCA-13), Yamanashi, Japan, September, 2013
59. The First Total Synthesis of (+)-Strongylin A; A Potential Anti-Influenza A Virus Agent, Takaaki Kamishima, Tadashi Katoh, 13th International Conference on the Chemistry of Antibiotics and other bioactive compounds (ICCA-13), Yamanashi, Japan, September, 2013
60. Palladium Catalyzed Three-Component Coupling of Ynamides, Hideaki Wakamatsu, Yuichi Yoshimura, Rika Yanagisawa, Ayano Takahashi, Yoshihiro Natori, Hiroki Takahata, International Symposium for the 70th Anniversary of the Tohoku Branch of the Chemical Society of Japan, Sendai, September, 2013
61. *15 1-アルキル-L-イミノフラノース誘導体の不斉合成と α-グルコシダーゼ阻害作用に対する構造活性相関研究、佐久間俊嘉、名取良浩、吉村祐一、加藤敦、足立伊佐雄、高畑廣紀、第 30 回有機合成

化学セミナー、岡山、2013 年 9 月
62. 3'-デオキシ-4'-チオヌクレオシド類の合成研究、伊藤文、吉村祐一、高畑廣紀、第 30 回有機合成化学セミナー、岡山、2013 年 9 月
63. 6-メチル 1,2,3,6-テトラヒドロピコリン酸の合成と有機触媒への応用、酒井華恵、吉村祐一、若松秀章、名取良浩、高畑廣紀、第 30 回有機合成化学セミナー、岡山、2013 年 9 月
64. *10 新規グリコシル化反応の開発を基盤とするヌクレオシド誘導体の合成と医薬品化学研究、吉村祐一、有機合成化学研究セミナー、室蘭、2013 年 7 月
65. *9The Synthesis of α-1-C-Alkyl-1,4-dideoxy-1,4-imino-L-arabinitol, A Novel Class of Iminosugar-Based α-Glucosidase Inhibitors, Yoshihiro Natori, Yuichi Yoshimura, Atsushi Kato, Isao Adachi, Hiroki Takahata, 18th European Symposium on Organic Chemistry (ESOC 2013), Marseille, France, July, 2013
66. Transition Metal Catalyzed Carbon-Carbon Bond Forming Reaction of Ynamides, Hideaki Wakamatsu, Yuichi Yoshimura, Ayano Takahashi, Yoshimi Sasaki, Yoshihiro Natori, Hiroki Takahata, The 20th International Symposium on Olefin Metathesis and Related Chemistry, Nara, July, 2013
67. Synthesis of Dihydropyran Derivatives Using Ag(I)-Catalyzed Cyclization: Model Studies Toward Southern Half of Mandelalide A, Kazuhiro Watanabe, Rich G Carter, 68th ACS Northwest Regional Meeting (NORM13), Corvallis, Oregon, USA, July, 2013
68. *20 Microdetermination of labile estrogen-o-quinones and their cysteine/glutathione conjugates by high performance liquid chromatography-electrospray ionization tandem mass spectrometry, Kouwa Yamashita, Miki Shiratori, Emi Kondo, Sachiko Komatsu, Hajime Katoh, Ken-ichi Ohno, 39th International Symposium on High Performance Liquid Phase Separations and Related Technique, Amsterdam, The Netherlands, June, 2013.
69. *23 HDAC/PI3K Dual Inhibitor としての Romidepsin(FK228)新規類縁体の開発と最適化、李 仁、西條 憲、下平秀樹、成田紘一、加藤 正、石岡千加史、第 17 回日本がん分子標的治療学会、京都、2013 年 6 月
70. *3, 22 分子内に S-S 結合を持つ大環状デプシペプチド類の合成と活性評価、加藤 正、文部科学省新学術領域研究「がん研究分野の特性等を踏まえた支援活動」化学療法基盤支援活動班・ミニ班会議、東京、2013 年 5 月
71. *15 α-1-C-アルキル-1,4-ジデオキシ-1,4-イミノ-L-アラビニトールの不斉合成とその α-グルコシダーゼ阻害活性評価、名取良浩、今堀龍志、吉村祐一、加藤敦、足立伊佐雄、広野修一、高畑廣紀、第 11 回次世代を担う有機化学シンポジウム、東京、2013 年 5 月
72. Synthesis of 6-Methyl-1,2,3,6-tetrahydropicolic Acid as a Potential Organocatalyst, Hanae Sakai, Yuichi Yoshimura, Hideaki Wakamatsu, Yoshihiro Natori, Hiroki Takahata, 4th UK/Japan Conference in Catalytic Asymmetric Synthesis, Sendai, April, 2013
73. *13 The Synthesis of α-1-*C*-Alkyl-1,4-dideoxy-1,4-imino-D-arabinitols and their Biological Activities, Yoshihiro Natori, Yasuka Watanabe, Yuichi Yoshimura, Atsushi Kato, Isao Adachi, Hiroki Takahata, The 23rd French-Japanese Symposium on Medicinal and Fine Chemistry, Nagasaki, May, 2013
74. *13 次世代型イミノ糖である α-1-*C*-alkyl-LAB の特性と生物活性について（第 1 報）、足立伊佐雄、加藤敦、林恵利奈、中川進平、名取良浩、吉村祐一、高畑廣紀、日本薬学会第 133 年会、横浜、2013 年 3 月
75. *13 次世代型イミノ糖である α-1-*C*-alkyl-LAB の特性と生物活性について（第 2 報）、加藤敦、林恵利奈、足立伊佐雄、今堀龍志、名取良浩、吉村祐一、島岡秀行、中込泉、小関準、広野修一、高畑廣紀、日本薬学会第 133 年会、横浜、2013 年 3 月
76. *9 超原子価ヨウ素試薬を利用したグリコシル化反応の開発とヌクレオシド合成への応用、菅野裕也、吉村祐一、Kiran, Y. B.、名取良浩、斎藤有香子、高畑廣紀、日本薬学会第 133 年会、横浜、2013 年 3 月
77. *13 C1 位に 4-アリールブチル基を導入した L-アラビノイミノ糖誘導体の不斉合成と生物活性評価、名取良浩、今堀龍志、吉村祐一、嶋田陽介、加藤敦、足立伊佐雄、高畑廣紀、日本薬学会第 133 年会、横浜、2013 年 3 月
78. α-1-*C*-アルキル-D-アラビノイミノ糖誘導体の触媒的不斉合成とその生物活性評価、渡邊靖香、佐久間俊嘉、名取良浩、吉村祐一、佐藤香純、加藤敦、足立伊佐雄、高畑廣紀、日本薬学会第 133 年会、横浜、2013 年 3 月
79. *13 1-*C*-*n*-ブチル-L-イミノフラノース誘導体の触媒的不斉合成、佐久間俊嘉、渡邉はるか、名取良浩、吉村祐一、中川進平、加藤敦、足立伊佐雄、高畑廣紀、日本薬学会第 133 年会、横浜、2013 年 3 月
80. *14 コンピュータリガンドドッキングによる α-glucosidase 阻害剤 α-1-C-Butyl-LAB の maltase 及び β-glucosidase に対する結合様式解析、中込泉、小関準、山乙教之、合田浩明、林恵利奈、足立伊佐雄、今堀龍志、名取良浩、吉村祐一、加藤敦、高畑廣紀、広野修一、日本薬学会第 133 年会、横浜、2013 年 3 月
81. α 位置換 *meso*-ジアミノピメリン酸誘導体の合成研究、斎藤有香子、吉村祐一、高畑廣紀、日本薬学会第 133 年会，横浜、2013 年 3 月
82. イナミドを基質としたパラジウム触媒による三成分連結反応の開発、若松秀章、吉村祐一、高畑廣紀、日本薬学会第 133 年会、横浜、2013 年 3 月

83. 抗インフルエンザ活性を有するストロンギリンAの全合成、神島尭明、渡邉一弘、加藤　正、日本薬学会第133年会、横浜、2013年3月
84. 抗腫瘍活性を有するダイシダバロンAの全合成研究, 福井友理恵, 成田紘一、加藤　正、日本薬学会第133年会、横浜 、2013年3月
85. ジベンゾ[*b,f*]オキセピン骨格を有するバウヒノキセピンHの全合成研究、成田紘一、加藤　正、日本薬学会第133年会、横浜、2013年3月
86. LC-ESI-MS/MS法による水酸化ステロイドのメタボローム解析（VI）ーステロイド硫酸抱合体の定量法の最適化ー、小松祥子、齋藤彩夏、榊　教克、山下幸和、沼澤光輝、日本薬学会第133年会, 横浜, 2013年3月
87. *20 LC-ESI-MS/MS法による水酸化ステロイドのメタボローム解析（V）ー安定同位体標識カテコールエストロゲン-GSH付加体の調製ー、山下幸和、近藤恵美、白取未希、小松祥子、加藤　創、大野賢一、沼澤光輝、日本薬学会第133年会, 横浜, 2013年3月
88. ジフルオロジニトロベンゼンを用いた絶対配置決定法の開発（XVII） 二級アミン誘導体のコンフォメーション解析、加藤　創、渡邊将樹、菊池悠子、原田健一、山下幸和、日本薬学会第133年会, 横浜, 2013年3月
89. 糸状菌二次代謝を活性化するNAD依存型HDAC阻害剤の探索とそれを用いた新規天然物の創出、森田峻太郎、浅井貞悟、谷口　透、門出健次、櫻井博章、尾関智二、山下幸和、大島吉輝、日本薬学会第133年会, 横浜, 2013年3月
90. HDAC阻害剤を用いた多様な糸状菌ポリケチドの創出ーChaetomium indicum由来スピロラクトン型ポリケチド類の単離構造決定ー山本崇史、浅井貞悟、谷口　透、門出健次、山下幸和、大島吉輝、日本薬学会第133年会, 横浜, 2013年3月
91. *18 Development of estradiol ELISA for efficient screening of aromatase inhibitor, Ken-ichi Ohno, Tamaki Matsui, Kouwa Yamashita, International Symposium for Neuroscience 2013, sedai, February 2013.
92. *1,2 Total Synthesis of the Bicyclic Depsipeptides – Spiruchostatins A, B, C, and D- and Investigation of Their HDAC Inhibitory and Antiproliferative Activities, Koichi Narita, Yurie Fukui, Yui Sano, Takao Yamori, Akihiro Ito, Minoru Yoshida, Tadashi Katoh, International Symposium for Neurosciences 2013, Sendai, Japan, February, 2013
93. *9 Development of Oxidative Glycosylation Reaction For Nucleoside Synthesis Based on Hypervalent Iodine Chemistry, Yuichi Yoshimura, First Japan-USA Organocatalytic Symposium, Hawaii, December, 2012
94. *20 ヒストン脱アセチル化酵素(HDAC)阻害剤ブルクホルダックAの全合成、福井友理恵、成田紘一、加藤　正、第38回反応と合成の進歩シンポジウム、東京、2012年11月
95. *13 Synthesis of 1-*C*-Substituted-L-arabinoiminofuranoses and Evaluation of Biological Activities as Novel Class of α-Glucosidase Inhibitors, Yoshihiro Natori, Yuichi Yoshimura, Atsushi Kato, Isao Adachi, Shuichi Hirono, Hiroki Takahata, 13th Tetrahedron Symposium – Asia Edition, Taipei, Taiwan, November, 2012
96. *16 C1位に4-アリールブチル基を組み込んだL-アラビノイミノフラノースの触媒的不斉合成と生物活性評価、名取良浩、吉村祐一、高畑廣紀、嶋田陽介、加藤敦、足立伊佐雄、第38回反応と合成の進歩シンポジウム、東京、2012年11月
97. *11 Synthetic Study of Novel Nucleoside Phosphonate Analog as a Potential Anti-HIV Agent, Y. B. Kiran, Yuichi Yoshimura, Yoshihiro Natori, Hiroki Takahata, IKCOC-12, 京都、2012年11月
98. *11 新規ヌクレオシドホスホネート誘導体の合成研究、吉村祐一、Y. B. Kiran, 高畑廣紀、第30回メディシナルケミストリーシンポジウム、東京、2012年11月
99. *19 Pyridine-carboxylates as Proton-affinitive Derivatives in HPLC-ESI-MS/MS Analysis of Hydroxysteroids, Kouwa Yamashita, Sachiko Komatsu, Hajime Katoh, Ken-ichi Ohno, 29th LC/MS Montreux Symposium, Montreux, Switzerland, November, 2012.
100. *18 LC-ESI-MS/MSによるアロマターゼ活性測定法」の開発および従来法との比較、小松祥子、鈴木直樹、高橋　透、山下幸和、沼澤光輝、第51回日本薬学会東北支部大会、青森、2012年10月
101. 改良 Marfey 法の二級アミンへの適用－DLA 誘導体の溶出挙動とコンフォメーションの解明－ 加藤　創、渡邊将樹、菊池悠子、山下幸和、原田健一、第51回日本薬学会東北支部大会、青森、2012年10月
102. *23 Prediction of the Complex Structure Between PI3K and Romidepsin (FK228) for Drug Design of PI3K/HDAC Dual Inhibitors, AKifumi Oda, Ken Saijo, Chikashi Ishioka, Tadashi Katoh, Shuichi Fukuyoshi, Ryoichi Nakagaki, Ohgi Takahashi, 生命医薬情報学連合大会、東京、2012年10月
103. *21 ヒストン脱アセチル化酵素(HDAC)阻害剤ブルクホルダックAの全合成、福井友理恵、成田紘一、加藤　正、 第51回日本薬学会東北支部大会、青森、2012年10月
104. イリジウム触媒的分子内閉環反応を基盤とするピロリジンアルカロイドの合成、菊地俊輔、名取良浩、近藤孝洋、吉村祐一、高畑廣紀、第42回複素環化学討論会、京都、2012年10月
105. イリジウム触媒的分子内環化反応を機軸とする(+)-bulgecinine および(+)-preussin の合成、菊地俊輔、近藤孝洋、名取良浩、吉村祐一、高畑廣紀、第51回日本薬学会東北支部大会、青森、2012年10月
106. *9 超原子価ヨウ素試薬を利用したグリコシル化反応の開発とヌクレオシド合成への応用、菅野裕也、吉村祐一、高畑廣紀、第51回日本薬学会東北支部大会、青森、2012年10月
107. *13 Asymmetric synthesis and biological evaluations of 1-alkyl L-*arabino*iminofuranoses, Yoshihiro Natori,

Tatsushi Imahori, Yuichi Yoshimura, Atsushi Kato, Isao Adachi, Hiroki Takahata, 第6回武田科学振興財団薬科学シンポジウム、2012年9月

108.新規ヌクレオシド誘導体合成を指向したグリコシル化反応の開発、吉村祐一、平成24年度化学系学協会東北支部、秋田、2012年9月

109.酸化的グリコシル化反応を利用したジヒドロピラノヌクレオシドの合成、菅野裕也、吉村祐一、高畑廣紀、第29回有機合成化学セミナー、静岡、2012年9月

110.*13 L-アラビノイミノフラノースをベースとした食後過血糖改善薬の合成研究、加藤敦、林恵利奈、中川進平、足立伊佐雄、中込泉、小関準、広野修一、名取良浩、今堀龍志、吉村祐一、高畑廣紀、第31回日本糖質学会年会、鹿児島、2012年9月

111.光計測を利用した活性酸素検出法の開発、大野賢一、平成24年度日本薬学会東北支部第1回物理・分析系若手セミナー、仙台、2012年9月

112.*19 Use of proton-affinitive derivatization in HPLC-positive-ESI-MS analysis of biologically important carboxylic acids, Hajime Kato, Shin Mitsuzuka, Kouwa Yamashita, Mitsuteru Numazawa, 19th Internationa Mass Spectrometry Conference, Kyoto, September 2012

113.*13 The Synthesis of 1-*C*-alkyl-L-arabinoiminofuranoses as novel class of α-glucosidase inhibitors, Yoshihiro Natori, Tatsushi Imahori, Yuichi Yoshimura, and Hiroki Takahata, 13th Belgian Organic Synthesis Symposium, Leuven, July, 2012.

114.*22 新規HDAC/PI3K二重阻害剤としてのロミデプシン(FK228)類縁体の同定、西條　憲、加藤　正、石岡千加史、第16回日本がん分子標的治療学会、北九州、2012年6月

115.*21 HDAC阻害剤ブルックホルダックAの全合成、福井友理恵、成田紘一、佐藤静香、渡邉一弘、加藤　正、日本薬学会第132年会、札幌、2012年3月

116.*1,2 スピルコスタチンCおよびDの合成と活性評価、成田紘一、福井友理恵、佐藤静香、渡邉一弘、加藤　正、日本薬学会第132年会、札幌、2012年3月

117.*4 $p21^{ras}$ ファルネシルトランスフェラーゼ阻害物質TAN-1813の合成研究、渡邉一弘、千田一慶、佐藤静香、成田紘一、加藤　正、日本薬学会第132年会、札幌、2012年3月

118.*13 C1位に4-アリールブチル基を導入したL-アラビノイミノ糖誘導体の触媒的不斉合成、名取良浩、今堀龍志、吉村祐一、中川進平、加藤敦、足立伊佐雄、高畑廣紀、日本薬学会第132年会、札幌、2012年3月

119.*10 Isofagomine類のβ-glucocerebrosidaseに対する結合親和性と構造活性相関について、加藤敦、中川進平、足立伊佐雄、中込泉、広野修一、吉村祐一、高畑廣紀、日本薬学会第132年会、札幌、2012年3月

120.*9 ジヒドロピラノヌクレオシドの合成、吉村祐一、尾本瞬、湊咲絵、斎藤有香子、名取良浩、高畑廣紀、日本薬学会第132年会、札幌、2012年3月

121.基質－触媒間相互作用によるタンデムエン－インメタセシス反応の方向性自在制御、今堀龍志、宇野亨、栗原清二、高畑廣紀、日本薬学会第132年会、札幌、2012年3月

122.低分子生体成分ミミック体の創出を基盤とする創薬化学研究、高畑廣紀、日本薬学会第132年会、札幌、2012年3月

123.2,3-Dihydrobenzofurans from *Cordyceps annullata*, an entomopathogenic fungus, cultivated with a HDAC inhibitor, and their cannabinoid receptors agonist activity 羅 丹, 浅井禎吾, 山下幸和, 大島吉輝, 日本薬学会第132年会, 札幌, 2012年3月

124.*19 LC-ESI-MS/MS法による水酸化ステロイドのメタボローム解析 (III) —エストロゲン分析におけるfusarate誘導体の有用性について—小松祥子, 太齋ひとみ, 山下幸和, 沼澤光輝, 日本薬学会第132年会, 札幌, 2012年3月

125.LC-ESI-MS/MS法による水酸化ステロイドのメタボローム解析 (IV) —27ステロイドの一斉分析—山下幸和, 小松祥子, 加藤 創, 大野賢一, 沼澤光輝, 本間誠次郎, 日本薬学会第132年会, 札幌, 2012年3月

126.ジフルオロジニトロベンゼンを用いた絶対配置決定法の開発 (XVI) 二級アミンへの適用加藤 創, 渡邊将樹, 山下幸和, 原田健一, 日本薬学会第132年会, 札幌, 2012年3月

127.エピジェネティック制御を利用した新規有用物質の探索; 昆虫寄生糸状菌 *Isaria tenuipes* 由来新規四環式ポリケチド *tenuipyrone* の単離構造決定, 浅井禎吾, Yu-Ming Chung, 櫻井博章, 尾関智二, 山下幸和, 大島吉輝, 日本薬学会第132年会, 札幌, 2012年3月

128.HDAC阻害剤を用いた昆虫寄生糸状菌 *Cordyceps indigotica* および植物内生糸状菌 *Chaetomiun indicum* 由来新規芳香族ポリケチド類の創出, 山本崇志, 浅井禎吾, 山下幸和, 大島吉輝, 日本薬学会第132年会, 札幌, 2012年3月

129.Synthesis of Nucleoside Derivatives using Novel Glycosylation Reaction, Yuichi Yoshimura, Hiroki Takahata, 6th International Conference on Cutting-Edge Organic Chemistry in Asia (ICCEOCA-6), Hong Kong, December, 2011

130.*13 Catalytic Enantioselective Synthesis and Biological Evaluation of C1-Alkyl-L-arabino-Iminofuranose Derivatives as α-Glycosidase Inhibitor, Yoshihiro Natori, Tatsushi Imahori, Keichi Murakami, Yuichi Yoshimura, Shinpei Nakagawa, Atsushi Kato, Isao Adachi, Hiroki Takahata, 8th AFMC International Medicinal Chemistry Symposium (AIMECS11), Tokyo, November-December, 2011.

131.*7 Design and Synthesis of 5'-Thio-pyrano-nucleosides as Potential Anti-HIV Agents, Yuichi Yoshimura, Yoshiko Yamazaki, Yukako Saito, Yoshihiro Natori, Tomozumi Imamichi, and Hiroki Takahata, 8th AFMC International Medicinal Chemistry Symposium (AIMECS11), Tokyo, November-December, 2011

132.*14 Docking and SAR studies of D- and L-isofagomine isomers as human β-glucocerebrosidase inhibitors, Atsushi Kato, Saori Miyauchi, Izumi Nakagome, Yuichi Yoshimura, Shuichi Hirono, Hiroki Takahara, and Isao Adachi, 8th AFMC International Medicinal Chemistry Symposium (AIMECS11), Tokyo, November-December, 2011.

133.*7 Design and Synthesis of a Novel Ring-expanded Dihydrothiopyranyl Nucleosides, Yoshiko Yamazaki, Yuichi Yoshimura, Yukako Saito, Yoshihiro Natori, Tomozumi Imamichi, Hiroki Takahata, 15th SIGMA-ALDRICH Organic Synthesis Meeting, Belgium, December, 2011

134.ジアミノピメリン酸誘導体の合成研究とその応用、斎藤有香子、吉村祐一、高畑廣紀、第37回反応と合成の進歩シンポジウム、徳島、2011年11月

135.*18 $^{13}C_3$-Androstenedione を用いる LC-MS/MS による新しい CYP19 活性測定法, 本間誠次郎, 前久保仁恵, 笹本英彦, 山下幸和, 沼澤光輝, 第19回日本ステロイドホルモン学会学術集会, 福岡, 2011年11月

136.*19 LC-ESI-MS/MS によるヒト末梢血中 18-oxoF および 18-OHF 測定法の開発, 前久保仁恵, 奥山光伸, 本間誠次郎, 笹本英彦, 斉藤守信, 山下幸和, 第19回日本ステロイドホルモン学会学術集会, 福岡, 2011年11月

137.*19 $^{13}C_3$-progesterone を用いた CYP17 活性測定法の開発、笹本英彦, 本間誠次郎, 山下幸和, 第19回日本ステロイドホルモン学会学術集会, 福岡, 2011年11月

138.*22 Total Synthesis of the Bicyclic Depsipeptide HDAC Inhibitors Spiruchostatins A, B and FK228 (FR901228), Koichi Narita, Kazuhiro Watanabe, Takao Yamori, Minoru Yoshida, Tadashi Katoh, 8th AFMC International Medicinal Chemistry Symposium (AIMECS 11), Tokyo, November, 2011

139.ジベンゾ[*b,f*]オキセピン骨格を有するバウヒノキセピンJの合成、成田紘一, 阿部 結, 中村 健, 加藤 正、第37回反応と合成の進歩シンポジウム、徳島、2011年11月

140.エピジェネティックな酵素阻害剤を利用した昆虫寄生糸状菌 *Cordyceps indigotica* 由来新規芳香族ポリケチド類の単離構造決定、山本崇史, 浅井禎吾, 山下幸和, 大島吉輝, 第50回日本薬学会東北支部大会,仙台, 2011年10月

141.HDAC 阻害剤を利用した昆虫寄生糸状菌 *Cordyceps annullata* 由来新規ジヒドロベンゾフラン類の単離構造決定、羅 丹, 浅井禎吾, 山下幸和, 大島吉輝, 第 50 回記念 日本薬学会東北支部大会, 仙台, 2011年10月

142.*20 エストロゲンオルトキノンによるタンパク修飾 (I) —L-Cys、N-Ac-L-Cys および GSH 共有結合体の調製とカテコール/キノン平衡—白取未希, 加藤 創, 山下幸和, 沼澤光輝, 第50回日本薬学会東北支部大会,仙台, 2011年10月

143.合成副腎皮質ホルモン類のフザリン酸エステル化を用いた LC-ESI-MS/MS による微量定量法の開発, 小松祥子, 山下幸和, 沼澤光輝, 第50回記念 日本薬学会東北支部大会, 仙台, 2011年10月

144.*19 LC-ESI-MS/MS 法によるカテコール型エストロゲンのプロファイリング、加藤 創, 小松祥子, 山下幸和, 沼澤光輝, 第50回記念 日本薬学会東北支部大会,仙台, 2011年10月

145.双環性ヘテロ環化合物の制御構築に向けた置換基効果を活用する方向選択的分子内タンデムエン-インメタセシス反応の開発、今堀龍志、宇野亨、栗原清二、高畑廣紀、第41回複素環化学討論会、熊本、2011年10月

146.*N*-アリールイミダゾール-酸複合アシル基転移触媒によるアルコールの速度論的光学分割、今堀龍志、清田祐基、八巻玲太、高畑廣紀、第41回複素環化学討論会、熊本、2011年10月

147.イリジウム触媒的環化反応を鍵工程とするピロリジン誘導体の立体選択的合成、菊地俊輔、名取良浩、近藤孝洋、吉村祐一、高畑廣紀、第50回日本薬学会東北支部例会、仙台、2011年10月

148.*13 The Synthesis and Biological Evaluation of 1-C-Alkyl-L-arabinoiminofuranoses, A Novel Class of α-Glucosidase Inhibitors, Yoshihiro Natori, Tatsushi Imahori, Yoshimura Yuichi, Hiroki Takahata, 22nd French-Japanese Symposium of Medicinal and Fine Chemistry, Rouen, France, September, 2011

149.3-ヒドロキシピペコリン酸を基本骨格とする有機分子触媒の合成と不斉 Mannich 反応への応用、吉村祐一、大原千明、宮川達徳、高畑廣紀、第4回有機触媒シンポジウム、東京、2011年9月

150.*13 C1 位アルキル L-アラビノイミノフラノース誘導体の触媒的不斉合成とその生物活性評価、名取良浩、今堀龍志、吉村祐一、中川進平、加藤敦、足立伊佐雄、高畑廣紀、第53回天然有機化合物討論会要旨集、大阪、2011年9月

151.*13 イリジウム触媒的環化反応を鍵工程とする C1-アルキルイミノフラノース誘導体の不斉合成研究、菊地俊輔、名取良浩、吉村祐一、高畑廣紀、第28回有機合成化学セミナー、山形、2011年8-9月

152.*22 Total Synthesis of the Bicyclic Depsipeptide HDAC Inhibitors Spiruchostatins A, B and FK228 (FR901228), Koichi Narita, Kazuhiro Watanabe, Takao Yamori, Minoru Yoshida, Tadashi Katoh, Italian-Japanese International Seminar for Neuroscience, Sendai, September, 2011

153.Synthesis of Iminosugars Including Hydroxypipecolic Acid Derivatives: Evaluation of Glycosidase Inhibitory Activity and Application as an Organocatalyst, Yuichi Yoshimura, Hiroki Takahata, 2nd Annual World

Congress of Catalytic Asymmetric Synthesis-2011, Beijing, China, August, 2011.
154.*12 D-および L-isofagomine 類の合成とグリコシダーゼ阻害活性、加藤敦、宮内沙織、中川進平、足立伊佐雄、中川泉、広野修一、吉村祐一、高畑廣紀、第 30 回日本糖質学会年会、新潟、2011 年 7 月
155.ジアリールジアゾメタンの分子内不斉 C–H 挿入反応：スチルベノイド二量体マキシモールＡの触媒的不斉合成、名取良浩、浪江亮介、南部寿則、橋本俊一、Symposium on Molecular Chirality 2011、東京, 2011 年 5 月
156.クロスメタセシス反応を用いた官能基導入 *meso*-ジアミノピメリン酸の合成研究、斎藤有香子、吉村祐一、高畑廣紀、日本薬学会第 131 年会、静岡、2011 年 3 月
157.*13 C1 置換 L-アラビノイミノ糖誘導体の触媒的不斉合成、名取良浩、今堀龍志、吉村祐一、中川進平、加藤敦、足立伊佐雄、高畑廣紀、日本薬学会第 131 年会、静岡、2011 年 3 月
158.ラジカル環化反応を用いた炭素架橋シクロヌクレオシドの合成、吉村祐一、和知克典、山崎佳子、高畑廣紀、日本薬学会第 131 年会、静岡、2011 年 3 月
159.2-シクロヘキセン-1-オンのタンデム γ-アリール化/芳香環化反応によるフェノールの para-C-H アリール化代替法、今堀龍志、田口竜也、高畑廣紀、日本薬学会第 131 年会、静岡、2011 年 3 月
160.*14 β-Glucocerebrosidase に対する 1-*N* 型イミノ糖の親和性と構造活性相関について、加藤敦、小池有理子、足立伊佐雄、中込泉、広野修一、高畑廣紀、日本薬学会第 131 年会、静岡、2011 年 3 月
161.フザリン酸エステルを用いた合成副腎皮質ホルモン類の LC-ESI-MS/MS による微量定量法小松祥子, 高橋円香, 山下幸和, 沼澤光輝, 日本薬学会第 131 年会, 静岡, 2011 年 3 月
162.*19　LC-ESI-MS/MS 法による水酸化ステロイドのメタボローム解析 (II) —C_{21}-ステロイド代謝物—山下幸和, 小松祥子, 高橋円香, 佐々木春奈, 千葉かおり, 沼澤光輝, 奥山光伸, 中川利沙, 本間誠次郎, 日本薬学会第 131 年会, 静岡, 2011 年 3 月
163.*19　LC-ESI-MS/MS 法による水酸化ステロイドのメタボローム解析 (I) —エストロゲン代謝物について—加藤 創, 小松祥子, 橘 優衣, 山下幸和, 沼澤　光輝, 日本薬学会第 131 年会, 静岡, 2011 年 3 月
164.抗結核作用および抗マラリア作用を有するバウヒノキセピン J の合成、成田紘一, 中村　健, 渡邉一弘, 加藤　正、日本薬学会第 131 年会、静岡、2011 年 3 月
165.超原子価ヨウ素(Ⅲ)試薬 PIFA を用いた 3,4-ジメトキシベンジル基の選択的な脱保護反応の開発、渡邉一弘, 成田紘一, 佐藤静香, 加藤　正、日本薬学会第 131 年会、静岡、2011 年 3 月
166.(–)-サブグルチノール A および B の全合成、菊地拓也, 大高仁吾, 峯田真由子, 小口剛正, 成田紘一, 渡邉一弘, 加藤　正、日本薬学会第 131 年会、静岡、2011 年 3 月
167.*19 質量分析法を基盤とした脂質メタボローム解析法の構築 —水酸化ステロイド分子を中心に山下幸和, 平成 22 年度日本薬学会東北支部講演会 第 32 回東北薬学セミナー, 仙台, 2010 年 12 月
168.Oxidative Desymmetrization of Diols by Iridium Catalyst, Takeyuki Suzuki, Kazem Ghozati, Shuhei Takatani, Tadashi Katoh, Hiroaki Sasaia, 2010 International Chemical Congress of Pacific Basin Societies (PACIFICHEM 2010), Honolulu, December, 2010
169.Synthetic Study of *Kopsia* Alkaloid Lapidilectine B, Hideki Abe, Takuya Kikuchi, Kazuhiro Watanabe, Sakae Aoyagi, Chihiro Kibayashi, Tadashi Katoh, Hisanaka Ito, 2010 International Chemical Congress of Pacific Basin Societies (PACIFICHEM 2010), Honolulu, December, 2010
170.Enantioselective Total Synthesis of (−)-Candelalides A, B and C: Potential Kv1.3 Blocking Immunosuppressive Agents, Kazuhiro Watanabe, Takamasa Oguchi, Hideki Abe, Tadashi Katoh, 2010 International Chemical Congress of Pacific Basin Societies (PACIFICHEM 2010), Honolulu, December, 2010
171.Synthesis of *meso*-diaminopimelic acid and its application to the biologically active peptides, Yukako Saito, Tomokazu Watanabe, Yuichi Yoshimura, Hiroki Takahata, Pacifichem 2010, Honolulu, Hawaii, U.S.A., December, 2010
172.2,6-Dioxabicyclo[3.2.0]heptane 骨格を有するイソヌクレオシドのデザインと合成、吉村祐一、小林学史、金子仁美、鈴木剛、高畑廣紀、第 28 回メディシナルケミストリーシンポジウム、京都、2010 年 11 月
173.*19 質量分析法を基盤とする水酸化ステロイド類のメタボロミクス解析、山下幸和, 小松祥子, 加藤創, 沼澤光輝, 奥山光伸, 中川利沙, 本間誠次郎, 第 18 回日本ステロイドホルモン学会学術集会, 名古屋, 2010 年 11 月
174.超原子価ヨウ素試薬 PIFA を用いたジメトキシベンジル基の選択的脱保護、渡邉一弘、成田紘一、佐藤静香、加藤　正、第 36 回反応と合成の進歩シンポジウム、名古屋、2010 年 11 月
175.*22 新規ヒストン脱アセチル化酵素阻害薬 Spiruchostatin B によるヒト B 細胞由来白血病細胞株 NALM-6 に対する Apoptosis 発現機構について、前田直就、菅野秀一、冨澤亜也子、蓬田伸、加藤　正、石川正明、第 49 回日本薬学会東北支部大会、郡山、2010 年 10 月
176.超原子価ヨウ素試薬 PIFA を活用したジメトキシベンジル基の選択的脱保護の検討、渡邉一弘、成田紘一、佐藤静香、加藤　正、第 49 回日本薬学会東北支部大会、郡山、2010 年 10 月
177.抗結核作用および抗マラリア作用を有するバウヒノキセピン J の合成、成田紘一、中村　健、渡邉一弘、加藤　正、第 49 回日本薬学会東北支部大会、郡山、2010 年 10 月
178.カンデラリド A,B,C の全合成、渡邉一弘、小口剛正、成田紘一、佐藤静香、加藤　正、第 40 回複素環化学討論会、仙台、2010 年 10 月

179.イミダゾール- 酸複合有機分子触媒によるアルコールの速度論的光学分割、今堀龍志、八巻玲太、高畑廣紀、第 40 回複素環化学討論会、仙台、2010 年 10 月
180.*7 ジヒドロチオピランを疑似糖部とする新規ヌクレオシド誘導体のデザインと合成、山崎佳子、吉村祐一、斎藤有香子、高畑廣紀、第 40 回複素環化学討論会、仙台、2010 年 10 月
181.*13 L-アラビノース型 1-アルキルイミノフラノース誘導体の触媒的不斉合成、名取良浩、今堀龍志、村上景一、吉村祐一、高畑廣紀、第 49 回日本薬学会東北支部大会、郡山、2010 年 10 月
182.LC-ESI-MS/MS によるプロスタグランジン誘導体の微量定量と薬物動態測定への応用、加藤 創, 山下幸和, 沼澤光輝, 第 49 回日本薬学会東北支部大会, 郡山, 2010 年 10 月
183.*19 LC-ESI-MS/MS による合成副腎皮質ホルモン剤の微量定量および薬物動態測定への応用、小松祥子, 高橋円香, 山下幸和, 沼澤光輝, 第 49 回日本薬学会東北支部大会, 郡山, 2010 年 10 月
184.Microcystin 分解性微生物 B-9 株による環状ペプチドの特異的加水分解、加藤 創, 辻 清美, 原田健一, 第 35 回日本医用マススペクトル学会, 名古屋, 2010 年 9 月
185.6,7-ジメトキシイソキノリンを有機触媒とするフェノール類の Boc 化反応、斎藤有香子、吉村祐一、高畑廣紀、第 3 回有機触媒シンポジウム、仙台、2010 年 9 月
186.電子供与基置換イソキノリンを触媒とするフェノール類の Boc 化反応、斎藤有香子、吉村祐一、高畑廣紀、日本プロセス化学会 2010 サマーシンポジウム、東京、2010 年 7 月
187.*19 LC-ESI-MS/MS によるステロイド類の一斉分離分析法の開発と疾病診断への応用、小松祥子, 山下幸和, 高橋円香, 沼澤光輝, 第 23 回バイオメディカル分析科学シンポジウム, 松島, 2010 年 7 月
188.抗腫瘍活性物質 GKK1032 類の合成研究、菊地拓也、阿部秀樹、渡邉一弘、加藤 正、第 21 回万有仙台シンポジウム、仙台、2010 年 6 月
189.*19 ステロイド類の LC-ESI-MS/MS のためのプロトン親和性誘導体の開発 (II) —□[5]-3□-ヒドロキシステロイド類の微量定量への応用—山下幸和, 小松祥子, 沼澤光輝, 宮代好通, 奥山光伸, 本間誠次郎, 日本薬学会第 130 年会, 岡山, 2010 年 3 月
190.*19 ステロイド類の LC-ESI-MS/MS のためのプロトン親和性誘導体の開発 (I) —高感度分析のための誘導体の最適化—小松祥子, 山崎敬子, 高橋円香, 山下幸和, 沼澤光輝, 日本薬学会第 130 年会, 岡山, 2010 年 3 月
191.*17 2-Phenylaliphatic androsta-1,4-diene-3,17-dione によるアロマターゼの可逆的ならびに不可逆的阻害 高橋円香, 山下幸和, 沼澤光輝, 日本薬学会第 130 年会, 岡山, 2010 年 3 月
192.*15 Synthesis of isofagomine, Hiroki Takahata, 21nd French-Japanese Symposium of Medicinal and Fine Chemistry, Kyoto, April, 2010.

研究テーマ②エストロゲン受容体制御による加齢性疾患(骨粗鬆症、認知障害)改善薬の創製

1. キラルアミンのプロトン化を制御因子とするエナンチオ二元的分子内アルドール反応、本田 翔太, 猪股 浩平, 遠藤 泰之、日本薬学会第 135 年会、神戸、2015 年 3 月
2. 硫黄含有複素環を用いた新規エストロゲン受容体リガンドの探索、青砥 沙也加、田口 史, 皆瀬 麻子, 太田 公規, 遠藤 泰之、日本薬学会第 135 年会、神戸、2015 年 3 月
   m-カルボランを中心骨格とする新規抗腫瘍性化合物の開発、皆瀬 麻子, 遠藤 泰之、日本薬学会第 135 年会、神戸、2015 年 3 月
3. ER サブタイプ選択性を有した SERM を目指したジフェニルメタン誘導体の疎水性構造変換、小島友寛、佐藤学、小川卓巳、太田公規、遠藤泰之、日本薬学会第 135 年会、神戸、2015 年 3 月
4. Concanavalin A 誘発性 sickness behavior に対する肝臓水解物の改善効果、中川西修、山田耕太郎、佐藤慎、宮昂平、小潟佳輝、根本亙、櫻井英知、丹野孝一、日本薬学会第 135 年会、神戸、2015 年 3 月
5. 1 型糖尿病モデルマウスの神経障害性疼痛に対する脊髄アンジオテンシン系の関与、根本亙、小潟佳輝、中川西修、八百板富紀枝、只野武、丹野孝一、日本薬学会第 135 年会、神戸、2015 年 3 月
6. 糖尿病誘発性アロディニアに対する脊髄アンジオテンシン系の関与、小潟佳輝、根本亙、中川西修、八百板富紀枝、只野武、丹野孝一、第 24 回神経行動薬理若手研究者の集い、名古屋、2015 年 3 月
7. ストレプトゾトシン誘発糖尿病性神経障害性疼痛における脊髄アンジオテンシン系の関与、小潟佳輝、根本亙、中川西修、八百板富紀枝、只野武、丹野孝一、第 88 回日本薬理学会年会、名古屋、2014 年 3 月
8. スカブロニン G メチルエステルは、海馬神経新生促進作用によって抗認知症効果を引き起こす、中川西修、林嘉蓉、根本亙、小原祐太郎、八百板富紀枝、荒井裕一朗、只野武、小早川優、中田雅久、丹野孝一、第 88 回日本薬理学会年会、名古屋、2015 年 3 月
9. ロサルタンの脊髄クモ膜下腔内投与による抗侵害刺激作用について、根本亙、小潟佳輝、中川西修、八百板富紀枝、只野武、丹野孝一、第 88 回日本薬理学会年会、名古屋、2015 年 3 月
10. Scabronine G-methylester attenuates hippocampal neurogenesis impairment and the memory deficits induced by olfactory bulbectomy. Jia Rong Lin, Osamu Nakagawasai, Wataru Nemoto, Yutaro Obara, Fukie Yaoita, Yu Kobayakawa, Masahisa Nakada, Koichi Tan-No, 第 24 回神経行動薬理若手研究者の集い、名古屋、2015 年 3 月
11. メチルアゾキシメタノールを用いた統合失調症モデルマウスの作製、中川西修、手塚大介、根本亙、八百板富紀枝、只野武、丹野孝一、第 16 回応用薬理シンポジウム、松島、2014 年 12 月

12. 疼痛伝達機構における脊髄アンジオテンシン系の役割、根本亙、小潟佳輝、中川西修、八百板富紀枝、只野武、丹野孝一、第16回応用薬理シンポジウム、松島、2014年12月
13. 含硫黄複素環を有する新規エストロゲン受容体リガンドの合成と活性評価、青砥沙也加、田口史、皆瀬麻子、太田公規、遠藤泰之、第32回メディシナルケミストリーシンポジウム、神戸、2014年11月
14. カルボラニルフェノールグリセロール誘導体の抗アンドロゲン活性とその構造活性相関、皆瀬麻子、阿部孝俊、太田公規、小田彰史、遠藤泰之、第32回メディシナルケミストリーシンポジウム、神戸、2014年11月
15. トロポロン誘導体の抗腫瘍活性における構造活性相関、太田公規、皆瀬麻子、遠藤泰之、第32回メディシナルケミストリーシンポジウム、神戸、2014年11月
16. NMDA受容体遮断薬MK-801誘発性記憶障害に対する緑茶成分テアニンの改善効果、宮昂平、中川西修、根本亙、八百板富紀枝、丹野孝一、宮城薬剤師学術フォーラム2014、仙台、2014年11月
17. Angiotensin IIおよびIII誘発性疼痛関連行動の発現機序の解明、日野栞、根本亙、中川西修、八百板富紀枝、丹野孝一、宮城薬剤師学術フォーラム2014、仙台、2014年11月
18. 新規アゾトロポロン誘導体の細胞増殖抑制活性、太田 公規, 皆瀬 麻子, 遠藤 泰之、日本薬学会第135年会、神戸、2015年3月ピリジニルメチルアミン誘導体を用いるエナンチオ二元的分子内不斉アルドール反応、本田翔太, 猪股浩平, 遠藤泰之、第53回日本薬学会東北支部大会, いわき、2014年10月
19. 断続的断眠ストレス負荷誘発性腸管輸送能の亢進状態における腸管α2アドレナリン受容体の発現について、髙橋由衣、八百板富紀枝、名村幸大、西館俊介、菅野秀一、石川正明、米澤章彦、根本亙、中川西修、只野武、丹野孝一、第53回日本薬学会東北支部大会、いわき、2014年10月
20. 断続的断眠ストレス負荷誘発性異常行動に対するADHD治療薬の効果について、名村幸大、八百板富紀枝、永澤佑佳、西館俊介、髙橋由衣、土谷昌広、荒井裕一朗、根本亙、中川西修、只野武、丹野孝一、第53回日本薬学会東北支部大会、いわき、2014年10月
21. 長期粉末食飼育による低不安行動の発現におけるGABA-A受容体の関与、西館俊介、八百板富紀枝、名村幸大、髙橋由衣、土谷昌広、荒井裕一朗、根本亙、中川西修、只野武、丹野孝一、第53回日本薬学会東北支部大会、いわき、2014年10月
22. ロサルタンの抗侵害刺激作用について、根本亙、小潟佳輝、中川西修、八百板富紀枝、只野武、丹野孝一、第126回日本薬理学会近畿部会、和歌山、2014年10月
23. A novel evaluation system for inhibition of CYP3A4 activity by dietary supplements, Yu Sato, Shogo Takahashi, Takamitsu Sasaki, Takeshi Kumagai, Kiyoshi Nagata, 19 th ISSX/29 th JSSX annual meeting, Sanfrancisco, October, 2014.
24. Cyclin dependent kinase 1 involved in reculation of CYP2D6 expression, Keita Inami, Takamitsu Sasaki, Syu-ichi Kanno, Takeshi Kumagai, Kiyoshi Nagata, 19 th ISSX/29 th JSSX annual meeting, Sanfrancisco, October, 2014.
25. *19 Effect of Ban-Lan-Gen on transactivation of the CYP1A1 and CYP1A2 genes, Takeshi Kumagai, Takayuki Kiyomatsu, Takamitsu Sasaki, Kiyoshi Nagata, 19 th ISSX/29 th JSSX annual meeting, Sanfrancisco, October, 2014.
26. 食習慣の質的低下がマウス不安関連行動に及ぼす影響について、八百板富紀枝、西館俊介、髙橋由衣、名村幸大、土谷昌広、荒井裕一朗、根本亙、中川西修、只野武、丹野孝一、第65回日本薬理学会北部会、福島、2014年9月
27. 糖尿病性神経障害性疼痛における脊髄アンジオテンシンIIの関与、小潟佳輝、根本亙、中川西修、八百板富紀枝、只野武、丹野孝一、第65回日本薬理学会北部会、福島、2014年9月
28. *1 Carborane as Three Dimensional Hydrophobic Pharmacophore in Medicinal Drug Design. Yasuyuki Endo, Kiminori Ohta, Takumi Ogawa, Tokuhito Goto, Asako Kaise, 15th International Symposium on Boron Chemistry (IMEBORON XV), Prague, Czech Republic, August, 2014. (Invited Lecture)
29. Role of the spinal angiotensin system in nociceptive transmission, Wataru Nemoto, Osamu Nakagawasai, Fukie Yaoita, Koichi Tan-No, 生体機能と創薬シンポジウム2014、大阪、2014年8月
30. *13 胎生期メチルアゾキシメタノール処理マウスが神経発達障害仮説に基づいた統合失調症モデルに成り得るか？、中川西修、手塚大介、根本亙、八百板富紀枝、荒井裕一朗、只野武、丹野孝一、第18回活性アミンに関するワークショップ、香川、2014年8月
31. Angiotensin II type 1 receptor-mediated increase in spinal p38 MAPK phosphorylation leads to the induction of nociceptive behavior in mice, Osamu Nakagawasai, Wataru Nemoto, Yoshiki Ogata, Fukie Yaoita, Takeshi Tadano, Koichi Tan-No, International Narcotics Research Conference 2014, モントリオール、2014年7月
32. Antagonistic effect of angiotensin (1-7) on angiotensin II-induced nociceptive behavior in mice, Wataru Nemoto, Yoshiki Ogata, Osamu Nakagawasai, Fukie Yaoita, Takeshi Tadano, Koichi Tan-No, International Narcotics Research Conference 2014, モントリオール、2014年7月
33. *7, 8 嗅球摘出マウスの短期記憶障害と海馬神経新生抑制に対する新規選択的エストロゲン受容体モジュレーターBE360の改善効果、中川西修、佐々木俊裕、斎藤智恵、深澤鈴、星杏奈、根本亙、八百板富紀枝、小川卓巳、太田公規、遠藤泰之、丹野孝一、平成26年度東北薬科大学創薬研究センターシンポジウム、仙台、2014年6月

34. アンジオテンシン (1-7) はアンジオテンシン II 誘発性疼痛関連行動を抑制する、小潟佳輝、根本亙、中川西修、青木聡美、川田悠貴、嶋脇佳子、日野栞、八百板富紀枝、丹野孝一、平成 26 年度東北薬科大学創薬研究センターシンポジウム、仙台、2014 年 6 月
35. 脊髄疼痛伝達機構におけるアンジオテンシン II 代謝物の役割、根本亙、小潟佳輝、青木聡美、川田悠貴、嶋脇佳子、日野栞、中川西修、八百板富紀枝、只野武、丹野孝一、日本薬学会第 134 年会、熊本、2014 年 3 月
36. *8 嗅球摘出マウスの記憶障害及び神経新生に対するメマンチンの改善効果について、中川西修、磯野仁一、根本亙、守屋孝洋、八百板富紀枝、荒井裕一朗、只野武、丹野孝一、日本薬学会第 134 年会、熊本、2014 年 3 月
37. 肝臓水解物の肉体疲労改善効果、山田耕太郎、中川西修、根本亙、櫻井英知、只野武、丹野孝一、日本農芸化学会 2014 年度大会、東京、2014 年 3 月
38. 新規キサンチンオキシダーゼ阻害剤の創製、　太田公規、石井康博、遠藤泰之、日本薬学会第 133 年会、2014 年 3 月
39. *4 新規カルボラン含有 AR アンタゴニストの開発：　カルボラン環上炭素の位置異性と活性との関係、皆瀬麻子、阿部孝俊、太田公規、遠藤泰之、日本薬学会第 133 年会、熊本、2014 年 3 月
40. アンジオテンシン II 誘発性侵害行動に対するアンジオテンシン (1-7) の拮抗効果、根本亙、中川西修、八百板富紀枝、只野武、丹野孝一、第 87 回日本薬理学会年会、仙台、2014 年 3 月
41. *4 カルボラニルフェニルグリセロール誘導体におけるカルボラン環上炭素の位置異性と抗アンドロゲン活性の関係 皆瀬麻子、阿部孝俊、太田公規、遠藤泰之、第 31 回メディシナルケミストリーシンポジウム、広島、2013 年 11 月
42. キサンチンオキシダーゼ阻害活性を有するトリアジン誘導体、太田公規、石井康博、遠藤泰之、第 31 回メディシナルケミストリーシンポジウム、広島、2013 年 11 月
43. 肝臓水解物は肉体疲労を軽減する、中川西修、山田耕太郎、根本亙、櫻井英知、只野武、丹野孝一、第 16 回日本補完代替医療学会、金沢、2013 年 11 月
44. 中枢疲労バイオマーカーとしてのグルタミン酸、小野木弘志、中川西修、丹野孝一、菊池恒明、只野武、第 16 回日本補完代替医療学会、金沢、2013 年 11 月
45. Pharmacokinetic function of hepatocyte-like cells derived from human iPS cells-derived, Yuki Kondo, Takahiro Iwao, Takamitsu Sasaki, Kiyoshi Nagata, Kouichi Kurose, Takashi Horikawa, Takuro Niwa, Satoshi Yamaori, Shigeru Ohmori, Katsunori Nakamura, Tamihide Matsunaga, 28 th, JSSX annual meeting, 東京, October, 2013.
46. 疎水性構造の変換によるジフェニルメタン誘導体の ER サブタイプ選択性、小島友寛、佐藤　学、小川卓巳、太田公規、遠藤泰之、第 52 回日本薬学会東北支部大会、東北大学、2013 年 10 月
47. *2 アダマンタンを疎水性骨格とするエストロゲン受容体リガンドの探索：　疎水性構造の変換による活性制御、青砥沙也加、皆瀬麻子、太田公規、遠藤泰之、第 52 回日本薬学会東北支部大会、東北大学、2013 年 10 月
48. *6 Design and synthesis of artificial molecular receptors with 1,3,5-tris(o-carboranyl)arene structure, Kiminori Ohta, Chalermkiat Songkram, Kentaro Yamaguchi, Pichierri Fabio, Yasuyuki Endo, International Symposium for the 70th Anniversary of the Tohoku Branch of the Chemical Society of Japan, Sendai, Japan, Sep, 2013
49. 断続的断眠ストレス負荷誘発性マウス腸管輸送能亢進状態における α2 アドレナリン受容体の関与、八百板富紀枝、下道麻夏、荒井香、齊藤貴之、根本亙、中川西修、只野武、丹野孝一、第 64 回日本薬理学会北部会、旭川、2013 年 9 月
50. CYP2D6 活性阻害評価系の構築と健康食品の使用実態調査に基づいた薬物相互作用の解析、佐々木瞳、佐々木崇光、稲見敬太、熊谷　健、永田　清、第 23 回日本医療薬学会年会、仙台、2013 年 9 月.
51. 新規 P450 活性阻害実験系の開発と健康食品による薬物代謝活性阻害評価、佐藤　裕，髙橋昌悟，石橋幸奈，根本あゆみ，齋藤詩奈子，角間元美，榊　聡美，伏見　彩，佐々木崇光，熊谷　健，永田清 、フォーラム 2013 衛生薬学・環境トキシコロジー、福岡、2013 年 9 月.
52. ヒト iPS 細胞由来肝細胞を用いた薬物代謝酵素誘導評価、松永民秀、近藤祐樹、荻原留理、岩尾岳洋、永田　清、黒瀬光一、堀川隆司、丹波卓朗，山折　大、大森　栄、中村克徳、フォーラム 2013 衛生薬学・環境トキシコロジー、福岡、2013 年 9 月.
53. CYP3A4 遺伝子発現誘導に及ぼす健康食品の影響、熊谷　健，中澤洋一，工藤裕太，齋藤雄大、竹屋里恵，笠原　彩、佐々木崇光，永田　清、フォーラム 2013 衛生薬学・環境トキシコロジー、福岡、2013 年 9 月.
54. *7 嗅球摘出マウスの認知障害に対する新規化合物 BE360 の改善効果、中川西修、佐々木俊裕、斎藤智恵、深澤鈴、星杏奈、根本亙、八百板富紀枝、荒井裕一朗、只野武、小川卓巳、太田公規、遠藤泰之、丹野孝一、第 17 回活性アミンに関するワークショップ、福井、2013 年 8 月
55. *7 嗅球摘出マウスのうつ様行動に対する新規化合物 BE360 の改善効果、中川西修、佐々木俊裕、斎藤智恵、深澤鈴、星杏奈、根本亙、八百板富紀枝、小川卓巳、太田公規、遠藤泰之、只野武、丹野孝一、生体機能と創薬シンポジウム 2013、福岡、2013 年 8 月
56. アンジオテンシン II 誘発性疼痛関連行動におけるアストロサイトの関与、根本亙、長谷川大地、中川西修、八百板富紀枝、只野武、丹野孝一、生体機能と創薬シンポジウム 2013、福岡、2013 年 8 月

57. *7, 8 嗅球摘出マウスのうつ様行動に対する新規化合物 BE360 の改善効果、中川西修、佐々木俊裕、斎藤智恵、深澤鈴、星杏奈、根本亙、八百板富紀枝、小川卓巳、太田公規、遠藤泰之、只野武、丹野孝一、生体機能と創薬シンポジウム 2013、福岡、2013 年 8 月
58. *7, 8 嗅球摘出マウスの認知障害に対する新規化合物 BE360 の改善効果、中川西修、佐々木俊裕、斎藤智恵、深澤鈴、星杏奈、根本亙、八百板富紀枝、荒井裕一朗、只野武、小川卓巳、太田公規、遠藤泰之、丹野孝一、第 17 回活性アミンに関するワークショップ、福井、2013 年 8 月
59. 粉末食飼育はマウスの糖代謝機構を障害し、行動異常を誘発する、千葉航、土谷昌広、八百板富紀枝、米田博行、渡邉誠、佐々木啓一、坪井明人、服部佳功、日本老年歯科医学会第 24 回学術大会、大阪、2013 年 6 月
60. 肝分化 iPS 細胞への LETF 同時導入による CYP3A4 発現影響、佐藤　裕、高橋昌悟、佐々木崇光、松永民秀、永田　清、2013 年度 P450、UGT、SULT 研究会、宮崎、2013 年 6 月.
61. 多環芳香族炭化水素による CYP2D6 および CYP3A4 の発現調節機構の解析、稲見敬太、佐々木崇光、熊谷　健、菅野秀一、永田　清、2013 年度 P450、UGT、SULT 研究会、宮崎、2013 年 6 月.
62. *6　カルボランの特性を利用した tripodal ホスト化合物の創製、太田公規、Chalermkiat Songkram、川幡正俊、山口健太郎、遠藤泰之、第 11 回次世代を担う有機化学シンポジウム、東京、2013 年 5 月
63. メチルフェニデートの自発的交替行動障害改善効果における一酸化窒素合成酵素の関与、八百板富紀枝、永澤佑佳、齊藤貴之、荒井香、下道麻夏、土谷昌広、根本亙、中川西修、荒井裕一朗、只野武、丹野孝一、第 86 回日本薬理学会年会、福岡、2013 年 3 月
64. *11, 12 幼若期腹側海馬障害ラットの行動及び生化学的変化に対する性別及び性周期の影響、小野木弘志、中川西修、根本亙、大場憲、菊池恒明、丹野孝一、只野武、第 86 回日本薬理学会年会、福岡、2013 年 3 月
65. *11 認知機能改善薬 ST101 は統合失調症モデルラットの認知障害を改善する、矢吹悌、中川西修、丹野孝一、福永浩司、第 86 回日本薬理学会年会、福岡、2013 年 3 月
66. *8, 9 うつ病モデルにおける母性行動の解析、中川西修、佐藤敦、 根本亙、 八百板富紀枝、只野武、丹野孝一、神経行動薬理若手研究者の集い、福岡、2013 年 3 月
67. *8 Role of antidepressant on DOI-induced head-twitch response in olfactory bulbectomized mice, Osamu Nakagawasai, Akira Oba, Hiroshi Onogi, Wataru Nemoto, Fukie Yaoita, Takeshi Tadano, Koichi Tan-No, International Symposium for Neurosciences, 仙台、2013 年 3 月
68. Angiotensin II induces nociceptive behavior accompanied by p38 MAPK phosphorylation mediated through spinal AT1 receptors, Wataru Nemoto, Osamu Nakagawasai, Fukie Yaoita, Syu-Ichi Kanno, Shin Yomogida, Masaaki Ishikawa, Takeshi Tadano, Koichi Tan-No, International Symposium for Neurosciences, 仙台、2013 年 3 月
69. Influence of a long-term powdered diet on the social interaction test in mice: the role of dopaminergic systems, Fukie Yaoita, Masahiro Tsuchiya, Hiroko Saito, Yuka Nagasawa, Shigeo Murai, Yuichiro Arai, Osamu Nakagawasai, Wataru Nemoto, Takeshi Tadano, Koichi Tan-No, International Symposium for Neurosciences, 仙台、2013 年 3 月
70. Preparation of Wieland-Miescher ketone analogues via enantiodivergent intramolecular aldol reaction mediated by a chiral triamine, Kohei Inomata, Takashi Nagamine, Yasuyuki Endo, The 23rd French-Japanese Symposium on Medicinal and Fine Chemistry, Nagasaki, May, 2013
71. キサンチンオキシダーゼ阻害剤の探索、太田公規、小川真澄、伊藤将、遠藤泰之、日本薬学会第 133 年会、横浜、2013 年 3 月
72. ２－メトキシエストラジオールをリード化合物とした新規疎水性骨格を有するチューブリン重合阻害剤の開発、皆瀬麻子、太田公規、遠藤泰之、日本薬学会第 133 年会、横浜、2013 年 3 月
73. 2-置換-シクロヘプタン-1,3-ジオンの実用的合成、猪股浩平、遠藤泰之、日本薬学会第 133 年会、横浜、2013 年 3 月
74. HepG2 細胞を用いた鉄存在下 actinomycin D による TNF-α 誘導肝細胞死に対する NO の防御効果と HO-1 の関与、 坂口修平、佐々木　瞳、高橋昌悟、佐々木崇光、熊谷　健、永田　清、日本薬学会第 133 年会、 横浜、2013 年 3 月.
75. 健康食品による CYP1A1/1A2 遺伝子発現誘導の検討、熊谷　健、笠原　彩、齋藤雄大、永田　清、日本薬学会第 133 年会、 横浜、2013 年 3 月
76. Cytochrome P450 3A4 活性の UDP-glucurin.osyltransferase(UGT)2B7 による抑制:UGT2B7 と calnexin の C 末端 cytosolic tail 置換による抑制作用の消失、宮内　優、石井祐次、永田　清、山添　康、マッケンジー・ピーター、山田英之、日本薬学会第 133 年会、横浜、2013 年 3 月.
77. Hepatic differentiation of human induced pluripotent stem cells by using factors involved in liver function and development, Takamitu Sasaki、Yoshihiro Numata、Shogo Takahashi、Takeshi Kumagai、Tamihide Matsunaga、Kiyoshi Nagata, International Symposium for Neurosciences 2013、仙台、 2013 年 2 月
78. *4 カルボラン化合物 BA321 の新規選択的アンドロゲン受容体モジュレーターとしての作用上部良輔，松本 千穂，富成司，稲田 全規，遠藤 泰之，宮浦 千里、第 85 回日本生化学会大会、福岡、2012 年 12 月
79. エストロゲン代謝物を基にデザインした新規カルボラン含有チューブリン重合阻害剤、皆瀬麻子、太田公規、遠藤泰之、第 30 回メディシナルケミストリーシンポジウム、東京、2012 年 11 月

80. 新規キサンチンオキシダーゼ（XO）阻害剤の探索、太田公規、小川真澄、伊藤将、遠藤泰之、第 30 回メディシナルケミストリーシンポジウム、東京、2012 年 11 月
81. 乳酸菌 Enterococcus faecalis の代替医療に関する薬理学的検証、只野武、川畑哲郎、辰野貴則、島野康子、高野文英、中川西修、丹野孝一、太田富久、第 15 回日本補完代替医療学会、東京、2012 年 11 月
82. Post-translational of cytochrome P450 3A4 activity through protrin-protein interactions with UDP-glucuronosyltransferase 2B7 and 1A9:The UGT domain(s) contributing to the interaction, Miyauchi Y, Nagata K, Yamazoe Y, Mackenzie PI, Yamada H, 27th JSSX Annual Meeting, 千葉, November 2012.
83. Generation of human induced pluripotent stem cell derived enterocytes with peptide transport function, Iwao T, Nakamura K, Nagata K, Matsunaga T, 27th JSSX Annual Meeting, 千葉, November 2012.
84. Small molecule compounds enhance differentiation to hepatocytes from induced pluripotent stem cells, Kondo Y, Iwao T, Yoshihashi S, Mimori K, Sugiyama R, Sasaki T, Nagata K, Kurose K, Niwa T, Yamaori S, Nakamura K, Matsunaga T, 27th JSSX Annual Meeting, 千葉, November 2012.
85. Cytochrome P450 3A1 alters the function of UDP-glucuronosyltransferase 2B3 which lacks potencial glycosylation sites, Nakamura T, Miyauchi Y, Takeda T, Yamazoe Y, Nagata k, Mackenzie PI, Yamada H, Yuji Ishii Y, 27th JSSX Annual Meeting, 千葉, November 2012.
86. Cytochrome P450 3A4 alters the affinity of UDP-glucuronosyltransferase 1A isoforms toward UDP-glucuronic acid, Kinoshita K, Koba H, Miyauchi Y, Ikushiro S, Yamazoe Y, Nagata K, Macknzie PI, Yamada H, Yuji Ishii Y, 27th JSSX Annual Meeting, 千葉, November 2012.
87. MicroRNA enhances the expression of CYP genes in HepG2 cells and hepatocyte-like cells differentiated from human induced pluripotent stem cells, Sasaki T, Numata Y, Kanno T, Chiba F, Takahashi R, Yoshida M, Matsunaga T, Nagata K, 27 th, JSSX annual meeting, Tokyo, November , 2012.
88. Identification of a novel transactivation mechanism of the MRP3 gene, Numata Y, Sasaki T, Kanno T, Chiba F, Takahashi R, Yoshida M, Kanno S, Nagata K, 27 th, JSSX annual meeting, Tokyo, November, 2012.
89. 健康食品による CYP3A4 遺伝子発現誘導の検討、齋藤 雄大、笠原 彩、中澤 洋一、熊谷 健、永田 清、第 51 回日本薬学会東北支部大会、青森、2012 年 10 月.
90. 健康食品によるシトクロム P450 活性阻害の検討、齋藤詩奈子、髙橋 昌悟、角間 元美、榊 聡美、伏見 彩、佐々木崇光、永田 清、第 51 回日本薬学会東北支部大会、青森、2012 年 10 月.
91. HNF6 導入時期による肝分化 iPS 細胞の薬物代謝酵素発現への影響、沼田 喜弘、佐々木崇光、千葉 文博、菅野 高弘、高橋 里菜、吉田美都里、松永 民秀、永田 清、第 51 回日本薬学会東北支部大会、青森、2012 年 10 月.
92. microRNA 導入による肝薬物代謝酵素発現への影響、菅野 高弘、佐々木崇光、沼田 喜弘、千葉 文博、吉田美都里、高橋 里菜、松永 民秀、永田 清、第 51 回日本薬学会東北支部大会、青森、2012 年 10 月.
93. 幼若期マウスにおける低タンパク食飼育の記憶関連行動に対する影響、佐藤祥子、中川西修、林貴史、及川淳子、八百板富紀枝、丹野孝一、只野武、鈴木常義、第 51 回日本薬学会東北支部大会、青森、2012 年 10 月
94. *8 うつ病モデル動物の 5-HT $_{2A/2C}$ 受容体関連行動の変化と抗うつ薬の影響、大場憲、中川西修、丹野孝一、小野木弘志、根本亙、八百板富紀枝、玉田淳一、只野武、第 51 回日本薬学会東北支部大会、青森、2012 年 10 月
95. マウス咬筋長時間活動におけるヒスタミンの役割：ブラキシズムと顎関節症の抗ヒスタミン薬による予防・治療を視野にした基礎研究、米田博行、土谷昌広、八百板富紀枝、佐々木啓一、菅原俊二、遠藤康男、第 16 回日本ヒスタミン学会、岡山、2012 年 10 月
96. *11 統合失調症モデル、新生仔期腹側海馬損傷ラットの認知機能障害のメカニズム、矢吹悌、森口茂樹、塩田倫史、中川西修、小野木弘志、丹野孝一、只野武、 福永浩司、次世代を担う創薬・医療薬理シンポジウム 2012、大阪、2012 年 9 月
97. ラット C6 グリオーマ細胞における GDNF の遺伝子発現に関する ERK5 の役割、根本亙、第 11 回生物化学者若手研究セミナー、仙台、2012 年 9 月
98. 受動拡散型ヌクレオチドトランスポーター1 を介したアデノシン取り込みによるマウス海馬神経幹細胞の増殖・分化調節機構、針生彩、鈴木悠子、Choi Sun、Choi Doo-Sup、八百板富紀枝、丹野孝一、守屋孝洋、中畑則道、第 63 回日本薬理学会北部会、新潟、2012 年 9 月
99. マウスにおける食習慣の質的低下による情動行動への影響について、八百板富紀枝、土谷昌広、斉藤弘子、村井繁夫、荒井裕一朗、根本亙、中川西修、只野武、丹野孝一、第 63 回日本薬理学会北部会、新潟、2012 年 9 月
100. アンジオテンシン II 誘発性疼痛関連行動における p38 MAPK の関与、根本亙、中川西修、八百板富紀枝、菅野秀一、蓬田伸、石川正明、只野武、丹野孝一、第 63 回日本薬理学会北部会、新潟、2012 年 9 月
101. Enantiodivergent intramolecular aldol reaction depending on a conformational change of chiral triamine, Kohei Inomata, Takashi Nagamine, Yasuyki Endo, International conference catalysis of organic synthesis, Moskow, 2012 年 9 月
102. *8 嗅球摘出マウスの記憶障害に対する BDNF の改善効果について、磯野仁一、中川西修、根本亙、

八百板富紀枝、只野武、守屋孝洋、丹野孝一、第16回活性アミンに関するワークショップ、札幌、2012年8月

103. 低カルシウム・マグネシウム食飼育によるカタレプシー発現と黒質ドパミン神経について、谷口亮央、中川西修、八百板富紀枝、根本亙、荒井裕一朗、只野武、妻木良二、丹野孝一、第16回活性アミンに関するワークショップ、札幌、2012年8月

104. 健康食品と医薬品における薬物相互作用解明を目指した健康食品使用実態調査、小西麻美子、奥崎恭子、北畠知美、佐藤　裕、佐々木崇光、熊谷　健、榊原明美、鈴木　匡、松永民秀、頭金正博、細川正清、大森　栄、永田　清、医療薬学フォーラム2012　第20回クリニカルファーマシーシンポジウム、福岡、2012年7月.

105. DP-glucuronosyltransferase (UGT) 2B7 and 1A9 suppress Cytochrome P450 3A4 function: Evidence for the involvement of the cytosolic tail of UGT in the suppression, Yuu Miyauchi, Yuji Ishii, Kiyoshi Nagata, Yasushi Yamazoe, Peter I. Mackenzie, Hideyuki Yamada, 19th International Symposium on Microsomes and Drug Oxidations, 12th European Regional ISSX Meeting, Netherlands, July, 2012.

106. Alteration in the function of the UDP-glucuronosyltransferase 1A subfamily by Cytochrome P450 3A4: Different susceptibility of UGT isoforms and UGT1A7 variants, Yuji Ishii, Hiroki Koba, Toshiya Oizaki, Yuki Iwamoto, Shinichi Ikushiro, Kiyoshi Nagata, Yasushi Yamazoe, Peter I. Mackenzie, Hideyuki Yamada, 19th International Symposium on Microsomes and Drug Oxidations, 12th European Regional ISSX Meeting, Netherlands, July, 2012.

107. Enhanced expression of Cytochrome P450 genes by hepatocyte nuclear factor-6 in hepatocyte-like cells differentiated from human induced puluripotent stem cells, Shogo Takahashi, Yoshihiro Numata, Masayo Narita, Yutaka Tanaka, Takamitsu Sasaki, Tamihide Matsunaga, Kiyoshi Nagata, 19th International Symposium on Microsomes and Drug Oxidations, 12th European Regional ISSX Meeting, Netherlands, July, 2012.

108. Differentiation into functional enterocyte-like cells from human induced pluripotent stem cells, Takahito Iwao, Kiyoshi Nagata, Tamihide Matsunaga, 19th International Symposium on Microsomes and Drug Oxidations, 12th European Regional ISSX Meeting, Netherlands, July, 2012.

109. *6 電子不足π平面と活性化C-H水素によるアニオン認識、伊藤将、太田公規、遠藤泰之、第9回ホスト・ゲストシンポジウム、札幌、2012年5月

110. *6 カルボラン誘導体とシクロデキストリンの複合体形成と結合様式、太田公規、今野俊輔、遠藤泰之、第9回ホスト・ゲストシンポジウム、札幌、2012年5月

111. *6 カルボラン誘導体とシクロデキストリンの複合体形成と結合様式、太田公規、今野俊輔、遠藤泰之，第8回ホスト・ゲスト化学シンポジウム、札幌、2012年5月

112. *6 電子不足π平面と活性化C-H水素によるアニオン認識、伊藤将、太田公規、遠藤泰之，第8回ホスト・ゲスト化学シンポジウム、札幌、2012年5月

113. *9 うつ病動物モデルの母性行動障害と中脳辺縁系ドパミン神経、中川西修、佐藤敦、長谷川大記、根本亙、八百板富紀枝、只野武、丹野孝一、平成24年度東北薬科大学創薬研究センターシンポジウム、仙台、2012年5月

114. 断続的断眠ストレス負荷誘発性交替行動障害に対するメチルフェニデート改善作用について、八百板富紀枝、永澤佑佳、土谷昌広、中川西修、根本亙、荒井裕一朗、只野武、丹野孝一、平成24年度東北薬科大学創薬研究センターシンポジウム、仙台、2012年5月

115. *4 変異アンドロゲン受容体（ＡＲ）にも有効な新規カルボラン含有ＡＲアンタゴニストの創製，皆瀬麻子、後藤徳仁、藤井晋也、太田公規、遠藤泰之、日本薬学会第132年会、札幌、2012年3月

116. o-カルボランの特異的反応を利用したフッ素選択的蛍光センサーの開発，伊藤将、太田公規、遠藤泰之，日本薬学会第132年会、札幌、2012年3月

117. *2 エストロゲン活性を有するジフェニルメタン誘導体の疎水性構造活性相関、佐藤学、北尾聡一朗、太田公規、遠藤泰之、日本薬学会第132年会、札幌、2012年3月

118. 2-置換-シクロヘプタン-1,3-ジオンの合成とエナンチオ二元的分子内不斉アルドール反応への適用、猪股浩平，長峰高志，遠藤泰之、日本薬学会第132年会、札幌、2012年3月

119. C—B結合開裂反応によるホウ酸生成を利用した細胞内d-ブロック金属イオンの11B NMRプローブ、北村　正典、鈴木　利宙、安部　良、上野　毅、遠藤　泰之、国嶋　崇隆、青木　伸、日本薬学会第132年会、札幌、2012年3月

120. 新規カルボラン含有アニオンレセプターの構築と蛍光によるアニオン認識、太田公規、高橋周平、山﨑広人、遠藤泰之、日本薬学会第132年会、札幌、2012年3月

121. Androgen rceptor-Estrogen Receptor Dual Ligands for Anti-cancer Drugs, Yasuyuki Endo, JSPS Japan-Spain Joint Research Project, Institut de Ciència de Materials de Barcelona (C.S.I.C.) Campus U.A.B., Barcelona, Spain, March, 2012.

122. In vitroでの酸化ストレスモデルとしての鉄存在下actinomaycinDによるTNF-α誘導肝細胞障害の構築とNOの影響、坂口修平、三浦彩佳、高橋昌悟、佐々木崇光、熊谷　健、永田　清、日本薬学会第132年会、札幌、2012年3月

123. *8, 11, 13 精神神経疾患の発症機序解明の為のモデル動物作製、中川西修、第190回つくばブレインサイエンス、筑波、2012年2月

124.*11 Roles of serotonergic neurons and their effects on prepulse inhibition deficits in a neurodevelopmental model of schizophrenia, Satoru Mitazaki, Osamu Nakagawasai, Koichi Tan-No, Sumiko Abe, NRF-JSPS Asian Science Seminar 2012, ソウル、2012 年 2 月

125.*9 Maternal behavior and dopaminergic function in a model of depression, Osamu Nakagawasai, Atsushi Sato, Hiroshi Onogi, Yuichiro Arai, Fukie Yaoita, Tsuneaki Kikuchi, Koichi Tan-No, Takeshi Tadano, NRF-JSPS Asian Science Seminar 2012, ソウル、2012 年 2 月

126.*2 Design and Synthesis of Estrogen Receptor Modulators: Controlling of the Agonist/Antagonist Balance in *m*-Carborane Bisphenol Derivatives, Kiminori Ohta, Takumi Ogawa, Shigeru Ohta, Yasuyuki Endo, AIMECS11, Tokyo, Japan, Nov, 2011.

127.*4 Development of Novel AR Antagonists Active in LNCaP Cells with Mutated Androgen Receptor, Ayumi Yamada, Shiya Fujii, Keiko Tomita, Mao Nagano, Takashi Harayama, Kiminori, Ohta, Yasuyuki Endo, Hiroyuki Kagechika, AIMECS11, Tokyo, Japan, Nov, 2011.

128.*4 Design and Synthesis of Novel Carborane-containing AR Antagonists Having a Glycerol Moiety Based on the Co-crystal Structure of Bicalutamide with hAR LBD, Asako Kaise, Tokuhito Goto, Shinya Fujii, Kiminori Ohta, Yasuyuki Endo, AIMECS11, Tokyo, Japan, Nov, 2011.

129.Brønsted 酸量応答型キラルアミンによる分子内不斉アルドール反応を用いた Wieland- Miescher ケトンアナログのエナンチオ二元的合成研究、猪股浩平，長峰高志，遠藤泰之、第 37 回反応と合成の進歩シンポジウム，徳島，2011 年 11 月

130.*8 記憶・学習障害の発現メカニズムの解明とその予防薬、只野武、中川西修、師尾仁、金森正剛、新島富紀枝、丹野孝一、第 18 回日本未病システム学会、名古屋、2011 年 11 月

131.Hetero-oligomerization of UDP-glucuronosyltransferases and cytochrome P450 3A4: Analysis by fluorescence resonance energy transfer (FRET) and modulation of CYP3A4 activity by UGTs, Yuu Miyauchi, Yuji Ishii, Toshiya Oizaki, Yasushi Yamazoe, Kiyoshi Nagata, Peter I. Mackenzie, Hideyuki Yamada, 26th JSSX annual meeting, Hitoshima, November, 2011.

132.Effect of cytochrome P450 3A4 on the function of UDP-glucuronosyltransferase 1A3: Alteration of affinity roward UDP-glucuronic acid, Kousuke Kinoshita, Yuji Ishii, Yuu Miyauchi, Toshiya Oizaki, Shinichi Ikushiro, Yasushi Yamazoe, Kiyoshi Nagata, Peter I. Mackenzie, Hideyuki Yamada, 26th JSSX annual meeting, Hitoshima, November, 2011.

133.Indirubin, a compornent of Ban-Lan-Gen, activates CYP3A4 gene transcription through human pregnane X receptor, Takeshi Kumagai, Ryosuke Sugawara, Machi Miura, Takamitsu Sasaki, Shinichi Miyairi, Kiyoshi Nagata, 26th ISSX annual meeting, Hitoshima, November, 2011.

134.Effect of quercetin on differentiation into hepatocyte-like cells from human induced pluripotent stem cells, Yuki Kondo, Takahiro Iwao, Masayoshi Saito, Takuro Niwa, Kouichi Kurose, Kiyoshi Nagata, Tamihide Matsunaga, 26th JSSX annual meeting, Hitoshima, November, 2011.

135.Differentiation into the enterocyte-like cells from human induced pluripotent stem cells, Takahiro Iwao, Kiyoshi Nagata, Tamihide Matsunaga, 26th JSSX annual meeting, Hitoshima, November, 2011.

136.Hepatocyte nuclear factor-6 enhances expression of CYP3A4 in HepG2 cells and hepatocyte-like cells differentiated from human induced pluripotent stem cells, Takamitsu Sasaki, Yutaka Tanaka, Shogo Takahashi, Takeshi Kumagai, Shuhei Sakaguchi, Tamihide Matsunaga, Kiyoshi Nagata, 26th JSSX annual meeting, Hitoshima, November, 2011.

137.凍結 P450 発現アデノウイルス感染細胞を用いた薬物代謝評価系の構築、安藤寛美、佐藤　裕、高橋昌悟、佐々木崇光、永田　清、第 50 回記念日本薬学会東北支部大会、仙台、2011 年 10 月.

138.板藍根による CYP3A4 活性誘導の検討*、菅原亮輔、熊谷　健、三浦真知、高橋昌悟、佐々木崇光、坂口修平、宮入伸一、永田　清、第 50 回記念日本薬学会東北支部大会、仙台、2011 年 10 月

139.iPS 細胞を用いた肝分化誘導法の検討、山田健太、佐々木崇光、高橋昌悟、松永民秀、永田　清、第 50 回記念日本薬学会東北支部大会、仙台、2011 年 10 月.

140.Comparison of Catalytic Properties between Human UDP- glucuronocyltransferase 1A7*3, an Allelic Variant and its Wild-type 1A7*1, Hiroki Koba, Yuji Ishii, Toshiya oizaki, Arief nurrochmad, Shin-ichi Ikushiro, Yasushi Yamazoe, Kiyoshi Nagata, Peter I Mackenzie, Hideyuki Yamada, 25th JSSX annual meeting, Tokyo, October, 201 1.

141.Protein-protein Association of Cytochrome P450 and UDP-glucuronocyltransferase: Its Relevance to Enzyme Function, Yuji Ishii, Yuu Miyauchi, Hiroki Koba, Shuso Takeda, Kiyoshi Nagata, Peter I Mackenzie, Yasushi Yamazoe, Hideyuki Yamada, 25th JSSX annual meeting, Tokyo, October, 2011.

142.*2 ジフェニルメタン骨格への新規疎水性部位導入による ER リガンドの創製、佐藤 学、北尾聡一朗、太田公規、遠藤泰之、第 50 回日本薬学会東北支部大会、仙台、2011 年 10 月

143.*11 新生仔期腹側海馬（NVH）損傷ラットにおける認知機能障害と CaMKII 活性低下の関連性、矢吹悌、森口茂樹、塩田倫史、中川西修、小野木弘志、丹野孝一、只野武、福永浩司、第 50 回記念日本薬学会東北支部大会、仙台、2011 年 10 月

144.断続的断眠ストレス負荷誘発性不注意行動に対する Methylphenidate の改善作用について、永澤佑佳、八百板富紀枝、土谷昌広、中川西修、荒井裕一朗、丹野孝一、只野武、第 62 回日本薬理学会北部会、仙台、2011 年 9 月

145.*14 p-Hydroxyamphetamine 脳室内投与による行動異常と脳内ドパミン神経系の関与、小野木弘志、中川西修、三反崎聖、丹野孝一、只野武、菊池恒明、第 62 回日本薬理学会北部会、仙台、2011 年 9 月
146.Involvement of the p53 tumor-suppressor protein in the development of antinociceptive tolerance to morphine, Koichi Tan-No, Masakazu Shimoda, Kenya Watanabe, Osamu Nakagawasai, Fukie Yaoita, Syu-ichi Kanno, Masaaki Ishikawa, Georgy Bakalkin, Takeshi Tadano, Italian-Japanese International Seminar for Neurosciences, 仙台、2011 年 9 月
147.*14 Serotonergic mechanisms contribute to sensorimotor gating deficits induced by p-hydroxyamphetamine, Osamu Nakagawasai, Hiroshi Onogi, Koichi Tan-No, Fukie Yaoita, Takeshi Tadano, Italian-Japanese International Seminar for Neurosciences, 仙台、2011 年 9 月
148.*6 Conformational Control of Benzyl-o-carboranylbenzene Derivatives and Molecular Encapsulation of Acetone in the Dynamically Formed Space of 1,3,5-Tris(2-benzyl-o-carboran-1-yl)benzene, Kiminori Ohta, Chalermkiat Songkram, Yamaguchi Kentaro, Fabio Pichierri, Yasuyuki Endo, IME Boron XIV, Niagara falls, Canada, Sep, 2011
149.Design and Synthesis of Diphenylamine-based Novel Anion Receptors Bearing o-Carborane Cages, Shuhei Takahashi, Hiroto Yamazaki, Kiminori Ohta, Yasuyuki Endo, IME Boron XIV, Niagara falls, Canada, Sep, 2011
150.*4 Design and Synthesis of Novel AR Antagonists having a glycerol moiety, Asako Kaise, Tokuhito Goto, Shinya Fujii, Kiminori Ohta, Yasuyuki Endo, IME Boron XIV, Niagara falls, Canada, Sep, 2011
151.*4 Development of Novel Carborane-based Androgen Receptor Antagonists Effective for Mutated Receptor, Ayumi Yamada, Shiya Fujii, Keiko Tomita, Mao Nagano, Takashi Harayama, Kiminori Ohta, Yasuyuki Endo, Hiroyuki Kagechika, IME Boron XIV, Niagara falls, Canada, Sep, 2011
152.*8, 9 うつ病モデル動物の母性行動について、中川西修、佐藤敦、小野木弘志、八百板富紀枝、丹野孝一、只野武、第 15 回活性アミンに関するワークショップ、徳島、2011 年 8 月
153.*8,11,14 精神疾患解明を目指した動物モデルの作製、中川西修、平成 23 年度日本薬学会東北支部総会・学術講演会、仙台、2011 年 7 月
154.*6 ベンジル-o-カルボラニルベンゼンのコンフォメーション制御とアセトン分子の包接、太田公規、Songkram Chalermkiat、Fabio Pichierri、山口健太郎、遠藤泰之、第 7 回ホスト・ゲスト化学シンポジウム、広島、2011 年 5 月
155.カルボラン C-H 水素を利用した水素結合形成とイオン認識、太田公規、山﨑広人、川幡正俊、山口健太郎、遠藤泰之、第 9 回次世代を担う有機化学シンポジウム、東京、2011 年 5 月
156.ジアリールアミン骨格を利用したアニオンレセプターの構築と蛍光によるアニオン認識、髙橋周平，山﨑広人，太田公規，遠藤泰之、日本薬学会第 134 年会，静岡，2011 年 3 月
157.ベンジル型キラルアミンを用いる分子間不斉アルドール反応によるキラル 4 級炭素の構築、田中皓祐，猪股浩平，遠藤泰之、日本薬学会第 134 年会，静岡，2011 年 3 月
158.*2 SNAr 反応を利用したカルボラン含有エストロゲン受容体リガンドの合成、太田公規，小川卓巳，後藤徳仁，遠藤泰之、日本薬学会第 134 年会，静岡，2011 年 3 月
159.*4 共結晶構造を基にした効果的な抗アンドロゲン化合物の創製、皆瀬麻子，後藤　徳仁，藤井　晋也，太田　公規，遠藤　泰之、日本薬学会第 134 年会，静岡，2011 年 3 月
160.*12 幼若期腹側海馬障害雌性ラットにおける性周期依存的な行動変化、小野木弘志、中川西修、佐藤敦、中谷孝太、望月成美、荒井裕一朗、八百板（新島）富紀枝、丹野孝一、只野武、第 84 回日本薬理学会年会、横浜、2011 年 3 月
161.断続的な断眠ストレス負荷誘発性マウス交替行動障害に対するメチルフェニデートの効果、永澤佑佳、八百板（新島）富紀枝、中川西修、丹野孝一、荒井裕一朗、只野武、第 84 回日本薬理学会年会、横浜、2011 年 3 月
162.*8 病態解明を目指した動物モデルの作製、只野武、第 20 回神経行動薬理若手研究者の集い、東京、2011 年 3 月
163.*11 新生仔期腹側海馬（NVH）損傷ラット前脳における CaMKII 機能低下と行動異常、矢吹悌、森口茂樹、中川西修、小野木弘志、只野武、塩田倫史、福永浩司、第 20 回神経行動薬理若手研究者の集い、東京、2011 年 3 月
164.*12 幼若期腹側海馬障害雌性ラットにおける性周期依存的な自発運動量の変化、小野木弘志、中川西修、佐藤敦、中谷孝太、望月成美、荒井裕一朗、八百板富紀枝、丹野孝一、只野武、第 20 回神経行動薬理若手研究者の集い、東京、2011 年 3 月
165.痛みにおける末梢ガングリオシドの機能、渡辺俊、丹野孝一、只野武、東秀好、第 20 回神経行動薬理若手研究者の集い、東京、2011 年 3 月
166.*1 新規立体的疎水性構造の活用による受容体機能制御とその創薬への応用、遠藤泰之、創薬懇話会 2010 in 蔵王（招待講演），2010 年 11 月
167.カルボランの特性を利用した人工クロライドイオンチャネルの創製、太田公規，山﨑広人，川幡正俊，山口健太郎，遠藤泰之、第 29 回メディシナルケミストリーシンポジウム，京都，2010 年 11 月
168.バイオジェニックス“エンテロコッカス・フェカリス加熱処理菌”の健康維持に対する研究、青木香代子、得津嘉男、室井真人、石田理津子、相坂麻紗子、岩佐広行、只野武、第 17 回日本未病システム学会学術総会、沖縄、2010 年 11 月

169.未病治療における乳酸菌の有用性、只野武、大河原雄一、角 朝希、住谷夏紀、菅野秀一、石川正明、第17回日本未病システム学会学術総会、沖縄、2010年11月
170.運動負荷による骨格筋の疲労に対するヒスタミンの効果について、八百板（新島）富紀枝、土谷昌広、大津浩、谷内一彦、中川西修、丹野孝一、菅原俊二、遠藤康男、只野武、第14回日本ヒスタミン学会、川崎、2010年10月
171.アンジオテンシンⅡ脊髄クモ膜下腔内投与による疼痛関連行動、鈴木義紀、丹野孝一、中川西修、新島富紀枝、菅野秀一、蓬田伸、石川正明、只野武、第49回日本薬学会東北支部大会、郡山、2010年10月
172.ピロリジニルメチルアミンアナログを用いる Wieland-Miescher ケトンのエナンチオ選択的合成、赤羽優一，猪股浩平，遠藤泰之、第40回複素環化学討論会，仙台，2010 年 10 月
173.ジフェニルアミン骨格を利用したアニオンレセプターの創製、高橋周平，山﨑広人，太田公規，遠藤泰之、第49回日本薬学会東北支部大会，郡山，2010年10月
174.*4 グリセロール基を有する新規 AR アンタゴニストの創製、皆瀬麻子，後藤徳仁，藤井晋也，太田公規，遠藤泰之、第49回日本薬学会東北支部大会，郡山，2010年10月
175.ベンジル型キラルアミンによる分子内および分子間不斉アルドール反応に関する研究、田中皓祐，長峰高志，猪股浩平，遠藤泰之、第49回日本薬学会東北支部大会，郡山，2010年10月
176.MRP3 における新規転写誘導機構の解明、沼田喜弘，佐々木崇光、佐藤　渉、松井怜美、鳥谷部貴祥、山添　康、永田　清、第49回日本薬学会東北支部大会、福島、2010年10月.
177.CYP3A4 転写活性に影響を与える FBS 中成分の同定、福士素子、熊谷　健，佐々木崇光、永田　清、第49回日本薬学会東北支部大会、福島、2010年10月
178.*1 Application of Carboranes for Medicinal Drug Design Utilizing Their Globular Geometry and Hydrophobicity. Yasuyuki Endo, JSPS Japan-Spain Joint Research Project, Institut de Ciència de Materials de Barcelona (C.S.I.C.) Campus U.A.B., Barceloan, Spain, September, 2010
179.*9 うつ病が報酬機能や母性行動に与える影響－モデル動物を用いた検討－、中川西修、佐藤敦、小野木弘志、中谷孝太、望月成美、新島富紀枝、丹野孝一、只野武、第12回応用薬理シンポジウム、横浜、2010年9月
180.未病治療におけるサプリメントの有用性－薬理学的検証を中心として－、只野武、第12回応用薬理シンポジウム、横浜、2010年9月
181.N 型カルシウムチャネル α1B サブユニット欠損マウスの行動及び神経化学的特徴、中川西修、小野木弘志、三反崎聖、佐藤 敦、渡辺研弥、斉藤弘子、村井繁夫、中谷孝太、望月成美、村上学、高橋英機、新島富紀枝、丹野孝一、只野武、第40回日本神経精神薬理学会、仙台、2010年9月
182.アンジオテンシンⅡ脊髄クモ膜下腔内投与による ERK の活性化を介した疼痛関連行動、鈴木義紀、丹野孝一、中川西修、新島富紀枝、菅野秀一、蓬田伸、石川正明、只野武、第61回日本薬理学会北部会、札幌、2010年9月
183.Memantine 誘発性 prepulse inhibition 障害における中枢ドパミン・セロトニン受容体の関与、中谷孝太、中川西修、荒井裕一朗、小野木弘志、佐藤敦、新島富紀枝、丹野孝一、只野武、第61回日本薬理学会北部会、札幌、2010年9月
184.*11 新生仔期腹側海馬損傷ラットの前頭前皮質における興奮性神経伝達機能低下と統合失調症様行動評価、矢吹悌、森口茂樹、中川西修、小野木弘志、只野武、福永浩司、第61回日本薬理学会北部会、札幌、2010年9月
185.*11 新生仔期腹側海馬損傷ラット前頭前皮質と海馬における CaMKⅡの機能低下、矢吹悌、森口茂樹、中川西修、小野木弘志、只野武、福永浩司、第14回活性アミンに関するワークショップ、仙台、2010年8月
186.*12 統合失調症雌性ラットモデルが示すプレパルスインヒビッション障害の性周期依存的な変化、小野木弘志、中川西修、佐藤敦、中谷孝太、望月成美、新島富紀枝、丹野孝一、只野武、第14回活性アミンに関するワークショップ、仙台、2010年8月
187.*12 統合失調症雌性ラットモデルにおける脳内情報処理障害の検討、小野木弘志、中川西修、佐藤敦、中谷孝太、望月成美、新島富紀枝、丹野孝一、只野武、第14回神経科学領域における分子モニタリングシンポジウム、静岡、2010年6月
188.*9 嗅球摘出マウスの母性行動と報酬機能におけるドパミン神経系の関与、佐藤敦、中川西修、小野木弘志、中谷孝太、望月成美、新島富紀枝、丹野孝一、只野武、第14回神経科学領域における分子モニタリングシンポジウム、静岡、2010年6月
189.*6 Conformational Controls of Benzyl-o-carboranylbenzene Derivatives and Molecular Encapsulation of Acetone, Kiminori Ohta, Chalermkiat Songkram, Masatoshi Kawahata, Kentaro Yamaguchi, Pichierri Fabio, Yasuyuki Endo, 5th International Symposium on Macrocyclic & Supramolecular Chemistry, Nara, Japan, June, 2010
190.Design, Synthesis, and Anion Binding Properties of Novel Receptors with Dipyrromethan Units, Harunobu Akiyama, Kiminori Ohta, Yasuyuki Endo, 5th International Symposium on Macrocyclic & Supramolecular Chemistry, Nara, Japan, June, 2010

研究テーマ③癌および加齢性疾患に対する疼痛制御によるQOL向上の研究

1. *3 Effects of narcotic analgesics on the multiple sclerosis-related pain, Hirokazu Mizoguchi, Takahiro Sumi, Chizuko Watanabe, Asuna Ohtsuki, Hiroshi Nagase, Shinobu Sakurada, 第88回日本薬理学会年会, 名古屋, 2015年3月
2. Possible roles for $CD8^+$ T cells in female-dominant IL-4 production in allergic asthma, MIYASAKA Tomomitsu, ITO Chihiro, DOBASHI-OKUYAMA Kaori, SATO Miki, MASUDA Chiaki, KAWANO Tasuku, OHKAWARA Yuichi, KIKUCHI Toshiaki, TAKAYANAGI Motoaki, OHNO Isao., 第43回日本免疫学会総会、京都、2014年12月
3. The increased susceptibility to asthma with the impairment of respiratory tolerance by psychological stress, ISHIGAKI Takahiro, KAWANO Tasuku, MIYASAKA Tomomitsu, OHKAWARA Yuichi, TAKAYANAGI Motoaki, OHNO Isao., 第43回日本免疫学会総会、京都、2014年12月
4. *3 多発性硬化症疼痛に対するオピオイド性鎮痛薬の効果、溝口広一、渡辺千寿子、長瀬博、櫻田忍、第126回日本薬理学会近畿部会、和歌山、2014年10月
5. *2 神経障害性疼痛に対するmethadoneの脊髄鎮痛作用、角貴祐、溝口広一、渡辺千寿子、櫻田忍、第126回日本薬理学会近畿部会、和歌山、2014年10月
6. *2, 3 各種難治性疼痛に対する麻薬性鎮痛薬の効果、角貴祐、溝口広一、渡辺千寿子、櫻田忍、第65回日本薬理学会北部会、福島、2014年9月
7. アレルギー性気道炎症の性差におけるCD4+T細胞ならびにCD8+T細胞の役割、宮坂智充、伊藤ちひろ、佐藤美希、奥山香織、河野資、大河原雄一、菊地利明、高柳元明、大野勲、第48回東北アレルギー懇話会、山形、2014年7月
8. 肺炎球菌に対する防御機構とワクチン、宮坂智充、赤堀ゆきこ、石井恵子、大野勲、川上和義、第25回日本生体防御学会学術総会、仙台、2014年7月
9. *12 喘息の病態発症と精神的ストレスによる免疫寛容の抑制、石垣貴裕、河野資、宮坂智充、大河原雄一、高柳元明、大野勲、第２６回日本アレルギー学会春期臨床大会、京都、2014年5月
10. アレルギー性気道炎症における$CD8^+$T細胞の関与、佐藤美希、宮坂智充、伊藤ちひろ、奥山香織、河野資、大河原雄一、菊地利明、高柳元明、大野勲、第２６回日本アレルギー学会春期臨床大会、京都、2014年5月
11. アレルギー性気道炎症の性差におけるCD８+T細胞の関与、伊藤ちひろ、宮坂智充、奥山香織、河野資、大河原雄一、菊地利明、高柳元明、大野勲、第５４回日本呼吸器学会学術講演会、大阪、2014年4月
12. *12 精神的ストレスによる免疫寛容の抑制と喘息の病態発症、石垣貴裕、河野資、宮坂智充、大河原雄一、高柳元明、大野勲、第５４回日本呼吸器学会学術講演会、大阪、2014年4月
13. *4, 6 Antinociceptive effect of narcotic analgesics against mechanical allodynia in inflammatory pain state, Yuta Aoki, Hirokazu Mizoguchi, Chizuko Watanabe, Akihiko Yonezawa, Shinobu Sakurada, 第87回日本薬理学会年会, 仙台, 2014年3月
14. *1 The antinociceptive effect of opioid analgesics in neuropathic cancer pain, Ryou Sugawara, Hirokazu Mizoguchi, Chizuko Watanabe, Akihiko Yonezawa, Syu-ichi Kanno, Masaaki Ishikawa, Hiroshi Nagase, Shinobu Sakurada, 第87回日本薬理学会年会, 仙台, 2014年3月
15. *2 Antinociceptive effect of narcotic analgesics in neuropathic pain state, Takahiro Sumi, Hirokazu Mizoguchi, Chizuko Watanabe, Akihiko Yonezawa, Shinobu Sakurada, 第87回日本薬理学会年会, 仙台, 2014年3月
16. Antipruritic effect of kappa-opioid receptor agonist in mice, Takahiro Niida, Hirokazu Mizoguchi, Chizuko Watanabe, Akihiko Yonezawa, Hiroshi Nagase, Shinobu Sakurada, 第87回日本薬理学会年会、仙台、2014年3月
17. T細胞分化制御機構におけるスフィンゴ糖脂質発言の意義、永福正和、大野勲、鈴木明身、井ノ口仁一、第一回糖鎖免疫学術集会　Glycoimmunolgy 2014、東京、2014年2月
18. Possible roles for CD4+ T cells and CD8+ T cells in sex differences in Th2 cytokine-mediated allergic airway inflammation, Chihiro Ito, Tomomitsu Miyasaka, Kaori Okuyama, Tasuku Kawano, Yuichi Ohkawara, Toshiaki Kikuchi, Motoaki Takayanagi, Isao Ohno, 第42回日本免疫学会学術集会、幕張、2013年12月
19. *12 免疫寛容に対する精神的ストレスの影響と喘息の病態発症、河野資、石垣貴裕、酒井百恵、佐久間美佳、冨田さゆみ、宮坂智充、大河原雄一、高柳元明、大野勲、第６３回日本アレルギー学会秋期学術大会、東京、2013年11月
20. *13 中枢神経系１型および２型ヒスタミン受容体を介した精神的ストレスによるアレルギー性気道炎症の悪化、宮坂智充、奥山香織、河野資、大河原雄一、高柳元明、大野勲、第６３回日本アレルギー学会秋期学術大会、東京、2013年11月
21. *13 気管支喘息におけるストレス誘発性気道炎症の悪化に対する中枢性ヒスタミン受容体の関与、宮坂智充、奥山香織、河野資、大河原雄一、高柳元明、大野勲、第１７回日本ヒスタミン学会、松江、2013年11月
22. *12 精神的ストレスによる免疫寛容の抑制と喘息病態の発症、石垣貴裕、河野資、酒井百恵、宮坂智充、大河原雄一、高柳元明、大野勲、第52回日本薬学会東北支部大会、仙台、2013年10月
23. アレルギー性気道炎症の性差におけるCD８+T細胞の関与、伊藤ちひろ、奥山香織、宮坂智充、河

野資，大河原雄一，菊地利明，高柳元明，大野勲、第 52 回日本薬学会東北支部大会，仙台，2013 年 10 月

24. 脊髄疼痛伝達機構に対する μ 受容体サブクラスの多様的制御の解析、高木宏和、溝口広一、渡辺千寿子、米澤章彦、櫻田忍、第 52 回日本薬学会東北支部大会、仙台、2013 年 10 月
25. デルモルフィン誘導体 TAPA の脊髄鎮痛作用発現機構、今野崇、溝口広一、渡辺千寿子、米澤章彦、櫻田忍、第 52 回日本薬学会東北支部大会、仙台、2013 年 10 月
26. *1 神経絞扼性癌性疼痛における麻薬性鎮痛薬の効果、菅原陵、溝口広一、渡辺千寿子、米澤章彦、菅野秀一、石川正明、櫻田忍、第 52 回日本薬学会東北支部大会、仙台、2013 年 10 月
27. 神経障害性疼痛における末梢性 TRPV1 受容体及び NMDA 受容体の関与、遠藤有里子、溝口広一、渡辺千寿子、米澤章彦、櫻田忍、第 52 回日本薬学会東北支部大会、仙台、2013 年 10 月
28. *2 神経障害性疼痛における各種麻薬性鎮痛薬の効果、角貴祐、溝口広一、渡辺千寿子、米澤章彦、櫻田忍、第 52 回日本薬学会東北支部大会、仙台、2013 年 10 月
29. CB1 受容体拮抗薬 AM251 は ERK の活性化を介して疼痛関連行動を起こす、長岡高史、勝山壮、溝口広一、小松生明、渡辺千寿子、米澤章彦、櫻田司、櫻田忍、第 52 回日本薬学会東北支部大会、仙台、2013 年 10 月
30. *3 多発性硬化症疼痛に対する麻薬性鎮痛薬の効果、溝口広一、渡辺千寿子、米澤章彦、長瀬博、櫻田司、櫻田忍、第 33 回鎮痛薬・オピオイドペプチドシンポジウム、神戸、2013 年 9 月
31. *6 Phosphorylation of mu opioid receptor reduced morphine analgesia in inflammatory pain state, Yuta Aoki, Hirokazu Mizoguchi, Chizuko Watanabe, Akihiko Yonezawa, Tsukasa Sakurada, Shinobu Sakurada, International Narcotic Research Conference, Cairns (Australia), 2013 年 7 月
32. *2,5 Effectiveness of amidino-TAPA against morphine-resistant neuropathic pain, Hirokazu Mizoguchi, Chizuko Watanabe, Akihiko Yonezawa, Tsukasa Sakurada, Shinobu Sakurada, International Narcotic Research Conference, Cairns (Australia), 2013 年 7 月
33. *12 精神的ストレスによる免疫寛容の抑制と喘息の病態発症、河野資、石垣貴裕、佐久間美佳、冨田さゆみ、奥山香織、大河原雄一、高柳元明、大野勲、第４７回東北アレルギー懇話会、福島、2013 年 7 月
34. Impact of obesity and glucose intolerance on allergic airways inflammation in a murine asthma model, Yuichi Ohkawara, Yoshiaki Ohkashiwa, Chisa Narukawa, Masakazu Nagafuku, Osamu Nakagawasai, Tasuku Kawano, Motoaki Takayanagi, Jin-ichi Inokuchi, Isao Ohno, The 23rd Congress of Interasma Japan / North Asia, Tokyo, 2013 年 6 月
35. *12 Respiratory tolerance is inhibited by the exposure to psychological stress in mice, Tasuku Kawano, Takahiro Ishigaki, Mika Sakuma, Sayumi Tomita, Tomomitsu Miyasaka, Kaori Okuyama, Yuichi Ohkawara, Motoaki Takayanagi, Isao Ohno, The 23rd Congress of Interasma Japan / North Asia, Tokyo, 2013 年 6 月
36. The contribution of CD4+ T and CD8+ T cells to sex differences in allergic airway inflammation, Chihiro Ito, Kaori Okuyama, Tasuku Kawano, Yuichi Ohkawara, Toshiaki Kikuchi, Motoaki Takayanagi, Isao Ohno, The 23rd Congress of Interasma Japan / North Asia, Tokyo, 2013 年 6 月
37. Contribution of CD4+ T cells and dendritic cells to female-dominant antigen-induced Th2 cytokine production by bronchial lymph node cells, Isao Ohno, Tomomitsu Miyasaka, Kaori Okuyama, Toshiaki Kikuchi, Tasuku Kawano, Yuichi Ohkawara, Motoaki Takayanagi, The 23rd Congress of Interasma Japan / North Asia, Tokyo, 2013 年 6 月
38. *13 The involvement of H1 receptors in the central nervous system in psychological stress-induced asthma exacerbation, Isao Ohno, Kaori Okuyama, Tasuku Kawano, Yuichi Ohkawara, Motoaki Takayanagi, The 23rd Congress of Interasma Japan / North Asia, Tokyo, 2013 年 6 月
39. *12 精神的ストレスによる免疫寛容の抑制と喘息の病態発症、河野資、石垣貴裕、佐久間美佳、冨田さゆみ、奥山香織、大河原雄一、高柳元明、大野勲、アレルギー・好酸球研究会 2013、東京、2013 年 6 月
40. アレルギー性気道炎症の性差における $CD4^+$T および $CD8^+$T 細胞の関与、伊藤ちひろ、奥山香織、河野資、大河原雄一、菊地利明、高柳元明、大野勲、アレルギー・好酸球研究会 2013、東京、2013 年 6 月
41. *12 精神的ストレスによる免疫寛容の抑制と喘息発症、河野資、石垣貴裕、佐久間美佳、冨田さゆみ、奥山香織、大河原雄一、高柳元明、大野勲、第 25 回日本アレルギー学会春季臨床大会、横浜、2013 年 5 月
42. *13 中枢性 1 型ヒスタミン受容体を介した精神的ストレスによる気管支喘息悪化、奥山香織、河野資、大河原雄一、高柳元明、大野勲、第 25 回日本アレルギー学会春季臨床大会、横浜、2013 年 5 月
43. アレルギー性気道炎症の性差における $CD4^+$T および $CD8^+$T 細胞の関与、奥山香織、伊藤ちひろ、河野資、大河原雄一、菊地利明、高柳元明、大野勲、第 25 回日本アレルギー学会春季臨床大会、横浜、2013 年 5 月
44. 内臓肥満と気管支喘息増悪の関係—マウスモデルを用いた検討—、大河原雄一、大柏芳彰、生川千紗、永福正和、奥山香織、河野資、高柳元明、井ノ口仁一、大野勲、第 25 回日本アレルギー学会春季臨床大会、横浜、2013 年 5 月

45. 喘息病態における抗原特異的 Th2 サイトカイン産生の性差、奥山香織、末永正俊、古木俊也、河野資、大河原雄一、菊地利明、高柳元明、大野勲、第５３回日本呼吸器学会学術講演会、東京、2013 年 4 月
46. *13 精神的ストレスによるアレルギー性気道炎症の悪化における中枢神経系１型ヒスタミン受容体の関与、奥山香織、怡土達也、河野資、大河原雄一、高柳元明、大野勲、第５３回日本呼吸器学会学術講演会、東京、2013 年 4 月
47. *6 Involvement of phosphorylation of μ-opioid receptors on the bilateral reduction of morphine analgesia in inflammatory pain state, Yuta Aoki, Hirokazu Mizoguchi, Chizuko Watanabe, Akihiko Yonezawa, Shinobu Sakurada, 第 86 回日本薬理学会年会, 福岡, 2013 年 3 月
48. Distinct physiological role of MOR-1J and MOR-1L on the mouse brain, Hirokazu Mizoguchi, Chizuko Watanabe, Akihiko Yonezawa, Tsukasa Sakurada, Shinobu Sakurada, 第 86 回日本薬理学会年会, 福岡, 2013 年 3 月
49. Involvement of spinal dynorphin in the mechanism of morphine resistance to allodynia after peripheral nerve injury, Takaaki Komatsu, Soh katsuyama, Chikai Sakurada, Shinobu Sakurada, Tsukasa Sakurada, 第 86 回日本薬理学会年会, 福岡, 2013 年 3 月
50. Intrathecal morphine-3-glucuronide induces nociception through δ_2-opioid receptors in the spinal cord, Takaaki Komatsu, Shinobu Sakurada, Tsukasa Sakurada, International Symposium for Neurosciences 2013, 仙台, 2013 年 2 月
51. *6 Phosphorylation of μ opioid receptor reduced morphine analgesia in inflammatory pain state, Yuta Aoki, Hirokazu Mizoguchi, Chizuko Watanabe, Akihiko Yonezawa, Shinobu Sakurada, International Symposium for Neurosciences 2013, 仙台, 2013 年 2 月
52. Involvement of peripheral TRPV1 receptor in neuropathic pain, Yuriko Endo, Hirokazu Mizoguchi, Chizuko Watanabe, Akihiko Yonezawa, Shinobu Sakurada, International Symposium for Neurosciences 2013, 仙台, 2013 年 2 月
53. Analysis of histamine H_4 receptor-mediated scratching behavior in mice, Shota Fujiwara, Hirokazu Mizoguchi, Chizuko Watanabe, Akihiko Yonezawa, Kazuhiko Yanai, Hiroshi Ohtsu, Shinobu Sakurada, International Symposium for Neurosciences 2013, 仙台, 2013 年 2 月
54. Spinal antinociceptive effect of endomorphins in inflammatory pain and neuropathic pain, Ryo Odagiri, Hirokazu Mizoguchi, Chizuko Watanabe, Akihiko Yonezawa, Shinobu Sakurada, International Symposium for Neurosciences 2013, 仙台, 2013 年 2 月
55. *3 Different effectiveness of narcotic analgesics on multiple sclerosis-related chronic pain, Asuna Otsuki, Hirokazu Mizoguchi, Chizuko Watanabe, Akihiko Yonezawa, Shinobu Sakurada, International Symposium for Neurosciences 2013, 仙台, 2013 年 2 月
56. *1 The antinociceptive effect of morphine in neuropathic cancer pain, Ryo Sugawara, Hirokazu Mizoguchi, Chizuko Watanabe, Akihiko Yonezawa, Shinobu Sakurada, International Symposium for Neurosciences 2013, 仙台, 2013 年 2 月
57. *10 The involvement of glucocorticoids in asthma exacerbations induced by psychological stress, Kaori Okuyama, Tasuku Kawano, Yuichi Ohkawara, Ichiro Sora, Motoaki Takayanagi, Isao Ohno, International Symposium for Neuroscience 2013, Sendai, 2013 年 2 月
58. 肥満がアレルギー性気道炎症に及ぼす多様性についてーマウスモデルを用いた検討—、大河原雄一、永福正和、生川千紗、奥山香織、河野資、高柳元明、井ノ口仁一、大野勲、第 62 回日本アレルギー学会秋季学術大会、大阪、2012 年 11 月
59. 気管支喘息重症度の性差における $CD4^+$T および $CD8^+$T 細胞の関与、奥山香織、渡部紗香、伊藤ちひろ、河野資、大河原雄一、菊地利明、高柳元明、大野勲、第 62 回日本アレルギー学会秋季学術大会、大阪、2012 年 11 月
60. 抗原誘導性 Th2 サイトカイン産生の性差　～樹状細胞の機能の性差～、奥山香織、末永正俊、古木俊也、河野資、大河原雄一、菊地利明、高柳元明、大野勲、第 62 回日本アレルギー学会秋季学術大会、大阪、2012 年 11 月
61. *10 ストレスホルモンによるアレルギー性気道反応の増悪、奥山香織、山崎直希、河野資、大河原雄一、高柳元明、大野勲、第 62 回日本アレルギー学会秋季学術大会、大阪、2012 年 11 月
62. *13 中枢性１型ヒスタミン受容体を介した精神的ストレス誘発性気管支喘息悪化、奥山香織、怡土達也、河野資、大河原雄一、高柳元明、大野勲、第１６回日本ヒスタミン学会、岡山、2012 年 10 月
63. 喘息モデルマウスを用いた気管支喘息重症度の性差の解析～$CD8^+$ T 細胞の関与～、伊藤ちひろ、渡部紗香、奥山香織、河野資、大河原雄一、菊地利明、高柳元明、大野勲、第５１回日本薬学会東北支部大会、青森、2012 年 10 月
64. Distinct physiological role of the MOR-1 splice variants in the mouse brain, Hirokazu Mizoguchi, Chizuko Watanabe, Akihiko Yonezawa, Tsukasa Sakurada, Shinobu Sakurada, Society for Neuroscience Neuroscience 2012, New Orleans (UAS), 2012 年 10 月
65. マウスにおける H_4 受容体を介したかゆみ関連行動、冨士原翔太、溝口広一、渡辺千寿子、米澤章彦、櫻田忍、第 51 回日本薬学会東北支部大会、青森市、2012 年 10 月

66. H_4 受容体選択的マウス掻痒行動の特徴、冨士原翔太、溝口広一、渡辺千寿子、米澤章彦、櫻田忍、第 16 回日本ヒスタミン学会、岡山市、2012 年 10 月
67. Involvement of H_1 receptor in pain related behaviors induced by nociceptin and its metabolites in the mouse spinal cord, Shinobu Sakurada, NEW TRENDS IN PAIN RESEARCH From Basic Research to Clinical Translation, Calabria (Italy), 2012 年 9 月
68. 難治性疼痛に対する脊髄 endomorphins の効果、小田桐遼、青木祐太、溝口広一、渡辺千寿子、米澤章彦、櫻田忍、第 63 回日本薬理学会北部会、新潟市、2012 年 9 月
69. *3 多発性硬化症疼痛に対する麻薬性鎮痛薬の効果、大槻明日奈、溝口広一、渡辺千寿子、米澤章彦、櫻田忍、第 63 回日本薬理学会北部会、新潟市、2012 年 9 月
70. 射精の生理学 世界の update、米澤章彦、櫻田忍、木村行雄、第 23 回日本性機能学会学術総会、東京、2012 年 9 月
71. アレルギー性気道炎症の性差～気管支リンパ節細胞によるサイトカイン発現の解析～、奥山香織、末永正俊、古木俊也、河野資、大河原雄一、菊地利明、高柳元明、大野勲、第４６回東北アレルギー懇話会、仙台、2012 年 7 月
72. 抗原誘導性 Th２サイトカイン産生の性差～樹状細胞の機能の性差～、奥山香織、末永正俊、古木俊也、河野資、大河原雄一、菊地利明、高柳元明、大野勲、アレルギー・好酸球研究会 201、東京、2012 年 6 月
73. T 細胞による IL-5 産生の性差—若齢マウスと成熟マウスの比較—、奥山香織、岡田優、河野資、大河原雄一、菊地利明、高柳元明、大野勲、第２４回日本アレルギー学会春季臨床大会、東京、2012 年 5 月
74. T 細胞による IL-5 産生の性差～$CD8^+$T の制御能に対する $CD4^+$T の感受性の性差、奥山香織、河野資、大河原雄一、菊地利明、高柳元明、大野勲、第５２回日本呼吸器学会学術講演会、神戸、2012 年 4 月
75. 神経因性疼痛モデルマウスに対する β-Caryophyllene 局所投与による抗アロディニア効果、勝山壮、小松生明、長岡高史、中村仁、櫻田忍、櫻田司、日本薬学会第 132 年会、札幌、2012 年 3 月
76. 抗がん剤による神経障害ならびに下痢発現メカニズム解明における多施設共同研究（第 2 報）：抗がん剤による脊髄後根神経節における TRP チャネル機能変化と鎮痛薬による改善の可能性、中川貴之、趙萌、高瀬久光、酒井寛泰、吉澤一巳、鈴木雅美、葛巻直子、佐野元彦、川出義浩、伊勢雄也、溝口広一、金子周司、徳山尚吾、成田年、日本薬学会第 132 年会、札幌、2012 年 3 月
77. *6 炎症性疼痛時のモルヒネ効果減弱に関する脊髄 μ 受容体の変化、青木祐太、溝口広一、渡辺千寿子、米澤章彦、櫻田忍、第 85 回日本薬理学会年会、京都、2012 年 3 月
78. μ 受容体作動薬 ADAMB の脊髄における抗侵害作用発現機序、青木祐太、溝口広一、渡辺千寿子、米澤章彦、櫻田忍、第 21 回神経行動薬理若手研究者の集い、京都、2012 年 3 月
79. $CD4^+$T および $CD8^+$T による IL-5 産生制御の性差、奥山香織、河野資、大河原雄一、菊地利明、高柳元明、大野勲、第６１回日本アレルギー学会秋季学術大会、東京、2011 年 11 月
80. 肥満、インスリン抵抗性と喘息との関係—ガングリオシド（GM3）欠損肥満マウスモデルを用いた検討—、大河原雄一、奥山香織、永福正和、河野資、高柳元明、井ノ口仁一、大野勲、第６１回日本アレルギー学会秋季学術大会、東京、2011 年 11 月
81. ガングリオシド分子種によるアレルギー性気道炎症の制御、大野勲、奥山香織、永福正和、大河原雄一、河野資、高柳元明、井ノ口仁一、第６１回日本アレルギー学会秋季学術大会、東京、2011 年 11 月
82. T 細胞による IL-5 産生性差の機序—$CD8^+$T 細胞の制御能の性差、奥山香織、樫村剛志、河野資、大河原雄一、菊地利明、高柳元明、大野勲、第５０回日本薬学会東北支部大会、仙台、2011 年 10 月
83. 東北地方における肺炎球菌薬剤耐性化と抗菌剤使用に関する臨床疫学的調査、大野勲、大河原雄一、第６０回日本感染症学会東日本地方会学術集会、山形、2011 年 10 月
84. *10 グルココルチコイド受容体を介した精神的ストレスによる喘息病態の悪化、奥山香織、山崎直樹、河野資、大河原雄一、高柳元明、大野勲、第１５回日本ヒスタミン学会、盛岡、2011 年 10 月
85. ラット射精機能評価モデルを用いた治療薬探索と副作用解析、米澤章彦、木村行雄、河谷正仁、櫻田忍、第 64 回日本自律神経学会総会、秋田、2011 年 10 月
86. ADAMB の脊髄における抗侵害作用の発現機序について、青木祐太、溝口広一、渡辺千寿子、米澤章彦、櫻田忍、第 50 回記念日本薬学会東北支部大会、仙台、2011 年 10 月
87. 災害支援医薬品活用システムの構築の必要性、山田清文、曽良一郎、池田和隆、溝口広一、第 21 回日本臨床精神神経薬理学会・第 41 回日本神経精神薬理学会合同年会、東京、2011 年 10 月
88. Endomorphin 前駆体産生遺伝子の探索、小田桐遼、溝口広一、渡辺千寿子、米澤章彦、櫻田忍、第 62 回日本薬理学会北部会、仙台、2011 年 9 月
89. *6 炎症性慢性疼痛時における morphine 鎮痛作用の減弱機構、青木祐太、溝口広一、渡辺千寿子、米澤章彦、櫻田忍、第 62 回日本薬理学会北部会、仙台、2011 年 9 月
90. *3 多発性硬化症疼痛に対する麻薬性鎮痛薬の効果、大槻明日奈、溝口広一、渡辺千寿子、米澤章彦、櫻田忍、第 5 回日本緩和医療薬学会年会、千葉、2011 年 9 月
91. *6 炎症性慢性疼痛時における morphine の鎮痛作用減弱について、青木祐太、溝口広一、渡辺千寿子、米澤章彦、櫻田忍、第 5 回日本緩和医療薬学会年会、千葉、2011 年 9 月

92. *3 多発性硬化症疼痛の実験動物モデルとその特異的治療薬の探索、溝口広一、櫻田忍、第5回日本緩和医療薬学会年会、千葉、2011年9月
93. Characterization of the antinociceptive tolerance of new μ opioid receptor agonist amidino-TAPS and amidino-TAPA, Shota Fujiwara, Hirokazu Mizoguchi, Chizuko Watanabe, Akihiko Yonezawa, Shinobu Sakurada, Italian-Japanese International Seminar for Neurosciences, Sendai (Japan), 2011年9月
94. Identification of the gene for endomorphin precursor, Ryo Odagiri, Hirokazu Mizoguchi, Chizuko Watanabe, Akihiko Yonezawa, Shinobu Sakurada, Italian-Japanese International Seminar for Neurosciences, Sendai (Japan), 2011年9月
95. *3 Different effectiveness of narcotic analgesics on multiple sclerosis-related chronic pain, Asuna Otsuki, Hirokazu Mizoguchi, Chizuko Watanabe, Akihiko Yonezawa, Shinobu Sakurada, Italian-Japanese International Seminar for Neurosciences, Sendai (Japan), 2011年9月
96. *6 Mechanism of reduced morphine analgesia in inflammatory pain state, Yuta Aoki, Hirokazu Mizoguchi, Chizuko Watanabe, Akihiko Yonezawa, Shinobu Sakurada, Italian-Japanese International Seminar for Neurosciences, Sendai (Japan), 2011年9月
97. 東日本大震災における緊急支援医薬品の活用状況と管理・供給上の問題点、山田清文、曽良一郎、池田和隆、溝口広一、山脇成人、医療薬学フォーラム2011、旭川、2011年7月
98. GM3関連スフィンゴ糖脂質依存性CD4-T細胞機能とアレルギー性気道炎症、大野勲、奥山香織、永福正和、大河原雄一、河野資、高柳元明、井ノ口仁一、第45回東北アレルギー懇話会、盛岡、2011年7月
99. マウス喘息モデルにおける食餌性肥満による気道炎症増悪とインスリン抵抗性について、大河原雄一、奥山香織、河野資、大野勲、アレルギー・好酸球研究会2011、東京、2011年6月
100. $CD4^+$T および $CD8^+$T による IL-5 産生制御の性差、奥山香織、河野資、大河原雄一、菊地利明、高柳元明、大野勲、アレルギー・好酸球研究会2011、東京、2011年6月
101. Pathogenic activities of dynorphin A mutants that cause human neurodegenerative disorder spinocerebellar ataxia type 23: induction of nociceptive behaviors in mice through non-opioid mechanism, Hiroyuki Watanabe, Dineke S. Verbeek, Hirokazu Mizoguchi, Fred Nyberg, Shinobu Sakurada, Georgy Bakalkin, International Narcotics Research Conference 2011, Florida (USA), 2011年6月
102. IL-5 産生の性差に関与するT細胞サブセットの解析、奥山香織、濱中悠賀、河野資、大河原雄一、高柳元明、菊地利明、大野勲、第51回日本呼吸器学会学術講演会、東京、2011年4月
103. 新規μ-受容体作動薬 amidino-TAPS と amidino-TAPA の鎮痛耐性、富士原翔太、溝口広一、渡辺千寿子、米澤章彦、櫻田忍、第20回神経行動薬理若手研究者の集い、震災により誌上発表、2011年3月
104. Endomorphin 前駆体産生遺伝子の探索、小田桐遼、溝口広一、渡辺千寿子、米澤章彦、櫻田忍、第20回神経行動薬理若手研究者の集い、震災により誌上発表、2011年3月
105. *3 多発性硬化症疼痛に対する麻薬性鎮痛薬の効果、大槻明日奈、溝口広一、渡辺千寿子、米澤章彦、櫻田忍、第20回神経行動薬理若手研究者の集い、震災により誌上発表、2011年3月
106. *6 炎症生慢性疼痛時におけるμオピオイド受容体の変動、青木祐太、溝口広一、渡辺千寿子、米澤章彦、櫻田忍、第20回神経行動薬理若手研究者の集い、震災により誌上発表、2011年3月
107. ラット勃起機能に及ぼす冬虫夏草の影響、米澤章彦、萬谷優、蛯子学、渡辺千寿子、溝口広一、木村行雄、櫻田忍、第21回日本性機能学会東部総会、震災により誌上発表、2011年3月
108. *10, 11 神経-内分泌-免疫軸からみたアレルギーの分子病態：神経-内分泌-免疫軸からみたストレス喘息、大野勲、第60回日本アレルギー学会秋季学術大会、東京、2010年11月
109. T細胞サブセットにおけるIL-5産生の性差の解析、奥山香織、河野資、大河原雄一、菊地利明、高柳元明、大野勲、第60回日本アレルギー学会秋季学術大会、東京、2010年11月
110. *7 精神的ストレス誘発性喘息の病態とμ-オピオイド受容体の関与、奥山香織、河野資、大河原雄一、曽良一郎、櫻田忍、高柳元明、大野勲、第60回日本アレルギー学会秋季学術大会、東京、2010年11月
111. 肥満と喘息発症・増悪との関連 —食餌性肥満マウス喘息モデルを用いた基礎的検討-、大河原雄一、河野資、奥山香織、高柳元明、大野勲、第60回日本アレルギー学会秋季学術大会、東京、2010年11月
112. GM3ガングリオシド分子種による $CD4^+$T 選択的機能制御とアレルギー性気道炎症、大野勲、奥山香織、永福正和、大河原雄一、河野資、高柳元明、井ノ口仁一、第60回日本アレルギー学会秋季学術大会、東京、2010年11月
113. 抗菌剤使用と肺炎球菌薬剤耐性化に関する臨床疫学的調査、遠藤夕貴、高橋佐衣、黒田あゆみ、菅野雄貴、鈴木一正、西巻雄司、奥山香織、河野資、大河原雄一、大野勲、保嶋実、茆原順一、諏訪部章、柴田陽光、高橋長一郎、武田博明、井田士朗、賀来満夫、渡辺彰、貫和敏博、新妻一直、金光敬二、第7回みやぎ薬剤師学術大会、仙台、2010年11月
114. *7 ストレス誘発性喘息におけるμ-オピオイド受容体による病態修飾の解析、奥山香織、河野資、櫻田忍、曽良一郎、田村弦、大河原雄一、高柳元明、大野勲、第14回日本ヒスタミン学会、川崎、2010年10月
115. 抗菌剤使用と肺炎球菌薬剤耐性化に関する臨床疫学的研究、大野勲、鈴木一正、西巻雄司、奥山香織、保嶋実、茆原順一、諏訪部章、柴田陽光、高橋長一郎、武田博明、井田士朗、賀来満夫、渡辺

彰、貫和敏博、新妻一直、金光敬二、第４９回日本薬学会東北支部大会、郡山、2010 年 10 月
116.SS-4690-1 誘発痒み関連行動の発現機構、溝口広一、勝山壮、藤村務、櫻田忍、第 20 回国際痒みシンポジウム、東京、2010 年 10 月
117.2`6`-dimethylphenylalanine を持つ新規 dermorphin N 末端テトラペプチド誘導体の抗侵害作用、東谷崇之、溝口広一、渡辺千寿子、米澤章彦、佐々木有亮、安保明博、櫻田忍、第 49 回日本薬学会東北支部大会、郡山、2010 年 10 月
118.アロディニア形成における足蹠スペルミンの関与、徳永幸子、溝口広一、渡辺千寿子、米澤章彦、櫻田忍、第 49 回日本薬学会東北支部大会、郡山、2010 年 10 月
119. *6 炎症性慢性疼痛時における μ オピオイド受容体の変動、青木祐太、溝口広一、渡辺千寿子、米澤章彦、櫻田忍、第 49 回日本薬学会東北支部大会、郡山、2010 年 10 月
120.サブスタンス P によるモルヒネ抗侵害刺激作用の増強効果—サブスタンス P N-末端代謝物の関与、真井健吾、小松生明、佐々木美佳、櫻田司、櫻田忍、第 49 回日本薬学会東北支部大会、郡山、2010 年 10 月
121.ヒスタミン誘発疼痛関連行動における脊髄グリア細胞の関与、波岡陽子、溝口広一、小松生明、勝山壮、渡辺千寿子、櫻田司、櫻田忍、第 14 回日本ヒスタミン学会、川崎、2010 年 10 月
122.痛みとかゆみの受容におけるヒスタミン受容体の役割、櫻田忍、第 14 回日本ヒスタミン学会、川崎、2010 年 10 月
123.植物由来成分リナロールの末梢性抗侵害刺激作用におけるオピオイド受容体サブタイサブタイプの関与、真井健吾、勝山壮、桑波田日香里、小松生明、Giacinto Bagetta、櫻田忍、櫻田司、第 4 回日本緩和医療薬学会、鹿児島、2010 年 9 月
124.Dermorphin 誘導体 Try-D-Arg-Phe-Sar-OH 誘発性抗侵害作用の発現機構の解明、渡辺千寿子、溝口広二、渡邉廣行、伊藤周徳、米澤章彦、櫻田忍、第 4 回日本緩和医療薬学会、鹿児島、2010 年 9 月
125. Essential oil of bergamot reduces pain behavior induced by formalin in mice, Alessandra Levato, Diana Amantae, Valentina Regio, Hirokazu Mizoguchi, Shinobu Sakurada, Tsukasa Sakurada, Domenicantonio Rotiroti, Giacinto Bagetta, Maria Tiziana Corasaniti, Laura Berliocchi, MOLECULAR TARGETS FOR NOVEL PAIN THERAPEUTICS From Basic Research to Clinical Translation, Calabria (Italy), 2010 年 9 月
126.Lack of the rewarding effect and locomotor-enhancing effect of mu-opioid receptor agonist amidino-TAPA, Yu Banya, Hirokazu Mizoguchi, Chizuko Watanabe, Akihiko Yonezawa, Tsukasa Sakurada, Shinobu Sakurada, MOLECULAR TARGETS FOR NOVEL PAIN THERAPEUTICS From Basic Research to Clinical Translation, Calabria (Italy), 2010 年 9 月
127.*6 Changes in μ-opioid receptor on the mouse spinal cord in inflammatory pain state, Yuta Aoki, Hirokazu Mizoguchi, Chizuko Watanabe, Akihiko Yonezawa, Shinobu Sakurada, MOLECULAR TARGETS FOR NOVEL PAIN THERAPEUTICS From Basic Research to Clinical Translation, Calabria (Italy), 2010 年 9 月
128. Spermine-induced mechanical allodynia in the mouse hind-paw, Yukiko Tokunaga, Hirokazu Mizoguchi, Chizuko Watanabe, Akihiko Yonezawa, Shinobu Sakurada, MOLECULAR TARGETS FOR NOVEL PAIN THERAPEUTICS From Basic Research to Clinical Translation, Calabria (Italy), 2010 年 9 月
129.Neuropathic pain promotes the expression of the autophagic markers LC3 and beclin in the mouse spinal cord, Maria Maiaru, Rossella Russo, Alessandra Levato, Laura Rombola, Hirokazu Mizoguchi, Giacinto Bagetta, Maria Tiziana Corasaniti, Laura Berliocchi, MOLECULAR TARGETS FOR NOVEL PAIN THERAPEUTICS From Basic Research to Clinical Translation, Calabria (Italy), 2010 年 9 月
130.Mu_2-opioid receptors involve in the antinociceptive activity induced by Tyr-W-MIF-1 in the mouse spinal site, Hiroyuki Watanabe, Shinobu Sakurada, Georgy Bakalkin, MOLECULAR TARGETS FOR NOVEL PAIN THERAPEUTICS From Basic Research to Clinical Translation, Calabria (Italy), 2010 年 9 月
131. Differential phenotype features of neuropathic pain in mice bearing a dystonic genotype, Laura Berliocchi, Alessandra Levato, Luigi Antonio Morrone, Antonio Pisani, Annalisa Tassone, Hirokazu Mizoguchi, Giacinto Bagetta, Maria Tiziana Corasaniti, MOLECULAR TARGETS FOR NOVEL PAIN THERAPEUTICS From Basic Research to Clinical Translation, Calabria (Italy), 2010 年 9 月
132.*2,5 A peptidic analgesic for treatment to morphine-resistant intractable pain, Hirokazu Mizoguchi, Chizuko Watanabe, Akihiko Yonezawa, Shinobu Sakurada, MOLECULAR TARGETS FOR NOVEL PAIN THERAPEUTICS From Basic Research to Clinical Translation, Calabria (Italy), 2010 年 9 月
133.Roles of histamine in pain perception: Studies using histamine-related genes knockout mice, Kazuhiko Yanai, Shinobu Sakurada, MOLECULAR TARGETS FOR NOVEL PAIN THERAPEUTICS From Basic Research to Clinical Translation, Calabria (Italy), 2010 年 9 月
134.Intrathecal morphine-3-glucuronide induces nociception through δ_2-opioid receptors in the spinal cord, Takaaki Komatsu, Shinobu Sakurada, Tsukasa Sakurada, MOLECULAR TARGETS FOR NOVEL PAIN THERAPEUTICS From Basic Research to Clinical Translation, Calabria (Italy), 2010 年 9 月
135.Nociceptin-mediated nociceptive spinal transmission system, Shinobu Sakurada, MOLECULAR TARGETS FOR NOVEL PAIN THERAPEUTICS From Basic Research to Clinical Translation, Calabria (Italy), 2010 年 9 月
136.*6 Changes in μ-opioid receptor on the mouse spinal cord in inflammatory pain state, Yuta Aoki, Hirokazu Mizoguchi, Chizuko Watanabe, Akihiko Yonezawa, Shinobu Sakurada, New Perspectives in Neuroscience:

Joint Meeting of Young Italian and Japanese Neuroscientists, Naples (Italy), 2010 年 9 月

137. Spermine-induced mechanical allodynia in the mouse hind-paw, Yukiko Tokunaga, Hirokazu Mizoguchi, Chizuko Watanabe, Akihiko Yonezawa, Shinobu Sakurada, New Perspectives in Neuroscience: Joint Meeting of Young Italian and Japanese Neuroscientists, Naples (Italy), 2010 年 9 月

138. Synergistic action of dopamine D_2-like and 5-HT_{2C} receptor agonists on ejaculation, but not penile erection in rats, Yu Banya, Akihiko Yonezawa, Masaru Yoshizumi, Chizuko Watanabe, Hirokazu Mizoguchi, Yukio Kimura, Masahito Kawatani, Shinobu Sakurada, New Perspectives in Neuroscience: Joint Meeting of Young Italian and Japanese Neuroscientists, Naples (Italy), 2010 年 9 月

139. Antinociceptive mechanism of epibatidine anlogue ABT-594 in mice, Takafumi Hayashi, Soh Katsuyama, Hitoshi Nakamura, Tsuneyosi Suzuki, Shinobu Sakurada, New Perspectives in Neuroscience: Joint Meeting of Young Italian and Japanese Neuroscientists, Naples (Italy), 2010 年 9 月

140. *2, 5 難治性疼痛治療薬としての新規ペプチド性鎮痛薬 amidino-TAPA の特性、溝口広一、櫻田忍、第 20 回日本臨床精神神経薬理学会・第 40 回日本神経精神薬理学会合同年会、仙台、2010 年 9 月

141. 東北地方で分離された肺炎球菌のペニシリン結合蛋白（PBP）遺伝子変異と経口 β-ラクタム剤感受性に関する臨床疫学的調査、大野勲、鈴木一正、西巻雄司、奥山香織、保嶋実、茆原順一、諏訪部章、柴田陽光、高橋長一郎、武田博明、井田士朗、賀来満夫、渡辺彰、貫和敏博、新妻一直、金光敬二、第 91 回日本呼吸器学会東北地方会、山形、2010 年 9 月

142. *7 The involvement of μ–opioid receptors in the central nervous system in the worsening of allergic aiway inflammation by psychological stress in mice, Kaori Okuyama, Shinobu Sakurada, Hirokazu Mizoguchi, Hiroshi Komatsu, Ichiro Sora, Gen Tamura, Yuichi Ohkawara, Motoaki Takayanagi, Isao Ohno, New perspectives in neuroscience, Naples, 2010 年 9 月

143. ラットにおける spontaneous seminal emission とその射精機能評価への応用—α_1アドレナリン受容体遮断薬の射精障害解析—、伊勢慎之介、米澤章彦、渡辺千寿子、溝口広一、渥美久義、木村行雄、河谷正仁、櫻田忍、第 14 回活性アミンに関するワークショップ、仙台、2010 年 8 月

144. ラットの spontaneous seminal emission 発現における脊髄 5-HT_2 受容体サブタイプの役割、萬谷優、米澤章彦、善積克、渡辺千寿子、溝口広一、木村行雄、河谷正仁、櫻田忍、日本性機能学会第 21 回学術総会、名古屋、2010 年 8 月

145. Distinct physiological role of spinal mMOR-1 splice variants, Hirokazu Mizoguchi, Chizuko Watanabe, Akihiko Yonezawa, Tsukasa Sakurada, Shinobu Sakurada, International Narcotics Research Conference 2010, Malmö (Sweden), 2010 年 7 月

146. Lack of the rewarding effect and locomotor-enhancing effect of mu-opioid receptor agonist amidino-TAPA, Yuta Aoki, Hirokazu Mizoguchi, Chizuko. Watanabe, Akihiko Yonezawa, Tsukasa Sakurada, Shinobu Sakurada, International Narcotics Research Conference 2010, Malmö (Sweden), 2010 年 7 月

147. *7 ストレス誘発性喘息における μ-オピオイド受容体による病態修飾の解析、奥山香織、河野資、櫻田忍、曽良一郎、田村弦、高柳元明、大野勲、第 21 回日本生体防御学会、仙台、2010 年 7 月

148. アレルギー性気道炎症における GM3 関連糖脂質の関与、大野勲、奥山香織、永福正和、大河原雄一、和田佳奈、河野資、高柳元明、井ノ口仁一、第４４回東北アレルギー懇話会、八戸、2010 年 7 月

149. IL-5 産生の性差に関与する T 細胞サブセットの解析、櫻井佳奈、奥山香織、河野資、大河原雄一、菊地利明、高柳元明、大野勲、アレルギー・好酸球研究会 2010、東京、2010 年 6 月

150. アレルギー性気道炎症における GM3 関連糖脂質の機能解析、大野勲、奥山香織、永福正和、大河原雄一、和田佳奈、河野資、高柳元明、井ノ口仁一、第５０回日本呼吸器学会、京都、2010 年 4 月

＜研究成果の公開状況＞（上記以外）

平成 26 年度創薬研究センターシンポジウム（平成 26 年 6 月 14 日）
研究成果発表（口頭 8 題）

1. カルボラニルフェニルグリセロール誘導体における AR アンタゴニスト活性とカルボラン炭素の位置異性との関係（皆瀬麻子、阿部孝俊、太田公規、遠藤泰之）
2. 1-C-n-ブチル-L-イミノ糖誘導体の触媒的不斉合成とα-グルコシダーゼ阻害活性評価（佐久間俊嘉、名取良浩、加藤　敦、足立伊佐雄、中川進平、吉村祐一）
3. PTP1B 阻害活性を有するダイシダバロン A の全合成　（福井友理恵、成田紘一、加藤　正）
4. アンドロゲンの高感度質量分析法の開発と唾液試料への応用（大野賢一、内海晴香、田村智美、長谷川智美、山下幸和）
5. 板藍根含有成分の CYP1A1/1A2 遺伝子発現誘導に及ぼす PXR の影響（熊谷　健、清松孝行、佐々木崇光、永田　清）
6. 嗅球摘出マウスの短期記憶障害と海馬神経新生抑制に対する新規選択的エストロゲン受容体モジュレーターBE360 の改善効果（中川西修、佐々木俊裕、斎藤智恵、深澤　鈴、星　杏奈、根本　亙、八百板富紀枝、小川卓巳、太田公規、遠藤泰之、丹野孝一）
7. 炎症性疼痛下における麻薬性鎮痛薬の鎮痛作用減弱機構（溝口広一、渡辺千寿子、櫻田　忍）
8. アレルギー性気道炎症の性差における CD8 陽性 T 細胞の関与（伊藤ちひろ、宮坂智充、奥山香織、佐藤美希、増田千愛、河野　資、大河原雄一、菊地利明、高柳元明、大野　勲）

研究成果発表（ポスター9 題）

1. 次世代 SERM を目指したジフェニルメタン誘導体の疎水性構造変換（小島友寛、佐藤　学、小川卓巳、太田公規、遠藤泰之）
2. クリックケミストリーを用いた D-イミノフラノース誘導体の合成と酵素阻害活性評価（名取良浩、盛友莉恵、加藤　敦、足立伊佐雄、吉村祐一)
3. 膠芽腫治療薬の創製を指向したセスキテルペンキノンおよびセスキテルペンベンゾオキサゾール類の合成研究（熱海　秀、加藤　武、成田紘一、加藤　正）
4. ピコリル誘導体化による生体内微量胆汁酸の高感度分析法の確立（加藤　創、加藤杏奈、三塚　進、山下幸和）
5. AhR を介さない多環芳香族炭化水素による CYP 誘導機構の解明（稲見敬太、佐々木崇光、菅野秀一、熊谷　健、永田　清）
6. アデノウイルスを用いた新規 CYP3A4 活性阻害実験系の開発と健康食品による薬物代謝活性阻害評価（佐藤　裕、髙橋昌悟、佐々木崇光、熊谷　健、永田　清）
7. アンジオテンシン (1-7) はアンジオテンシン II 誘発性疼痛関連行動を抑制する（小潟佳輝、根本　亙、中川西修、青木聡美、川田悠貴、嶋脇佳子、日野　栞、八百板富紀枝、丹野孝一）
8. Hemokinin-1 誘発性疼痛関連行動の発現機構（渡辺千寿子、溝口広一、櫻田　忍）
9. 精神的ストレスによる免疫寛容の抑制と喘息発症の感受性増大（石垣貴裕、河野　資、宮坂智充、大河原雄一、高柳元明、大野　勲）

特別講演 3 題

1. CYP 基質構造からの代謝予測（内閣府食品安全委員会/東北大学名誉教授　山添　康）
2. ダイオキシンによる性未成熟と育児破綻：機構と解決法（九州大学大学院　薬学研究院　分子衛生薬学分野教授　山田　英之）
3. 環境中親電子物質のケミカルバイオロジー：化学修飾を介したシグナル伝達変動および毒性発現とそれらを制御する活性イオウ分子（筑波大学　医学医療系　環境生物学分野教授　熊谷　嘉人）

平成 25 年度創薬研究センターシンポジウム（平成 25 年 5 月 25 日）
研究成果発表（口頭 8 題）

1. 化合物ライブラリーの構築とランダムスクリーニングからの創薬展開（太田公規、皆瀬麻子、遠藤泰之 ）
2. 超原子価ヨウ素試薬を利用したグリコシル化反応の開発と応用（菅野裕也、吉村祐一、Y.B.Kiran、名取良浩、斎藤有香子、高畑廣紀）
3. 抗インフルエンザ A ウイルス活性を有するストロンギリン A の全合成（神島尭明、加藤　正）
4. 酵素イムノアッセイによる非放射性アロマターゼ活性測定法の開発（大野賢一、松井　環、山下幸和）
5. 健康食品である板藍根の CYP3A4 発現誘導に及ぼす影響（熊谷　健、菅原亮輔、三浦真知、佐々木崇光、宮入伸一、永田　清）
6. 脊髄疼痛伝達機構におけるアンジオテンシン II の役割について（根本亙、中川西修、八百板富紀枝、三浦圭裕、長谷川大地、大友光平、大堀彩、岡本駿、只野武、丹野孝一）
7. 多発性硬化症疼痛に対する麻薬性鎮痛薬の効果（溝口広一、渡辺千寿子、米澤章彦、櫻田忍）

8. 精神的ストレスによる免疫寛容の抑制と喘息の病態発症（石垣貴裕、河野資、佐久間美佳、冨田さゆみ、奥山香織、宮坂智充、大河原雄一、高柳元明、大野勲）

研究成果発表（ポスター9 題）
1. エストロゲン代謝物を基にデザインした新規抗腫瘍性化合物の探索（皆瀬麻子, 太田公規, 遠藤泰之）
2. 3'-デオキシ-4'-チオヌクレオシド誘導体の合成研究（伊藤　文、吉村祐一、高畑廣紀）
3. スピルコスタチン類の全合成とその HDAC 阻害およびヒトがん細胞増殖抑制活性の評価（福井友理恵、成田紘一、加藤　正）
4. LC-ESI-MS/MS 法によるステロイド硫酸抱合体定量法の最適化（小松祥子, 齋藤彩夏, 榊教克, 山下幸和, 沼澤光輝）
5. MRP3 遺伝子発現誘導に関与する MAPK 経路の解析（稲見敬太、佐々木崇光、沼田喜弘、船越広大、新井　悠、菅野秀一、熊谷　健、永田　清）
6. 粉末食飼育マウスにおける social interaction の障害について（八百板富紀枝、荒井香、下道麻夏、齊藤貴之、土谷昌広、斉藤弘子、村井繁夫、荒井裕一朗、根本亙、中川西修、只野武、丹野孝一）
7. μ 受容体作動薬 ADAMB の脊髄における抗侵害作用発現機序（青木祐太、溝口広一、渡辺千寿子、米澤章彦、櫻田忍）
8. 精神的ストレスによるアレルギー性気道炎症の悪化における中枢神経系 1 型ヒスタミン受容体の関与（中出仁美、蛭田祥子、奥山香織、怡土達也、宮坂智充、河野資、大河原雄一、高柳元明、大野勲）
9. アレルギー性気道炎症の性差における $CD4^+$T および $CD8^+$T 細胞の関与（伊藤ちひろ、奥山香織、渡部紗加、宮坂智充、河野資、大河原雄一、菊池利明、高柳元明、大野勲）

特別講演 3 題
1. 食用植物成分クルクミンをリードとする創薬研究（東北大学 大学院薬学研究科教授・岩渕好治）
2. アカデミアからの日本発医薬品創出へ向けて（独立行政法人　医薬品医療機器総合機構 (PMDA) 審査センター長・矢守隆夫）
3. すべては全合成から始まる（早稲田大学 理工学研究所　栄誉フェロー・名誉教授・竜田邦明）

平成 24 年度創薬研究センターシンポジウム（平成 24 年 5 月 29 日）
研究成果発表（口頭 8 題）
1. 前立腺がんの根治を目指した新規 pureAR アンタゴニストの創製（皆瀬麻子、後藤徳仁、太田公規、遠藤泰之）
2. Synthesis of novel nucleoside phosphonate derivatives as potential anti-HIV agents (Y. B. Kiran, Yuichi Yoshimura, Yoshihiro Natori, Hiroki Takahata)
3. リパーゼによる位置選択的な脱アセチル化反応を基軸とする(Z)-4-ヒドロキシタモキシフェンの合成（渡邉一弘、伊藤拓也、加藤亜沙美、千田一慶、加藤正）
4. カテコールエストロゲンならびにエストロゲンオルトキノンおよびその生体成分との付加体の定量法の関する研究（加藤創、橘優衣、白取未希、武藤健史、山下幸和、沼澤光輝）
5. 肝特異的転写因子 NHF-6 による薬物代謝酵素発現誘導：新規薬物代謝研究ツールを志向した肝分化 iPS 細胞樹立への応用（佐々木崇光、沼田喜弘、成田昌代、高橋昌悟、田中大、松永民秀、永田清）
6. 断続的断眠ストレス負荷誘発性交代行動障害に対するメチルフェニデートの改善効果について（八百板富紀枝、永澤佑佳、土谷昌広、中川西修、根本亙、荒井祐一朗、只野武、丹野孝一）
7. 多発性硬化症疼痛の実験モデルの確立とその特異的治療薬の探索（溝口広一、渡辺千寿子、米澤章彦、櫻田忍）
8. 気管支喘息重傷度の性差：$CD8^+$T 細胞の制御能に対する $CD4^+$T 細胞の感受性の性差（奥山香織、樫村剛志、河野資、大河原雄一、菊池利明、高柳元明、大野勲）

研究成果発表（ポスター9 題）
1. カルボランの特異的反応を利用した高選択的フッ素アニオンセンサーの開発（伊藤将、太田公規、遠藤泰之）
2. 新規生物活性ヌクレオシドの創製を目指したジヒドロピラノヌクレオシドの合成研究（菅野裕也、吉村祐一、高畑廣紀）
3. ヒストン脱アセチル化酵素(HDAC)阻害剤ブルクホルダック A の全合成（福井友理、成田紘一、加藤正）
4. Estrone および formestane の複素環誘導体の調整法（小松祥子、佐藤忍、早坂幸恵、山下幸和、沼澤光輝）
5. 消化管における薬物動態関連遺伝子の発現誘導評価系構築（熊谷健、中澤洋一、野崎智紀、佐々木崇光、永田清）
6. うつ病動物モデルの母性行動障害と中脳辺縁系ドパミン神経（中川西修、佐藤敦、長谷川大記、根本亙、八百板富紀枝、只野武、丹野孝一）

7. 化学的侵害刺激による脊髄内神経伝達物質の遊離量の変化（渡辺千寿子、溝口広一、米澤章彦、櫻田忍）
8. 炎症性慢性疼痛下における morphine の鎮痛作用減弱機構（青木裕太、溝口広一、渡辺千寿子、米澤章彦、櫻田忍）
9. グルココルチコイド受容体を介した精神的ストレスによる喘息病態の悪化（奥山香織、山崎直樹、河野資、大河原雄一、高柳元明、大野勲）

特別講演 3 題
1. 抗がん剤開発の課題：大学からの視点で（東北大加齢研・石岡千加史）
2. アレルギーにおける脂質関連核内受容体と好酸球活性化と性差（秋田大医・茆原純一）
3. 痛みと心身相関（九大医・久保千春）

共催シンポジウム等
1. セミナー（平成 27 年 3 月 6 日）
   氏家悠佳助教（和歌山県立医科大学薬理学教室）
   免疫細胞制御に基づく神経障害性疼痛治療標的の探索
2. セミナー（平成 26 年 8 月 27 日）
   Michela Crudo 博士（Calabria 大学）
   Long-term molecular and behavioral effects of alcohol on the GABAergic system of zebrafish
3. 講演会（平成 26 年 8 月 22 日）
   Richard G Lea Associate Professor（University of Nottingham）
   内分泌撹乱物質と生殖・妊娠
4. 国際交流学術セミナー（平成 26 年 3 月 22 日）
   Giacinto Bagetta 教授（Calabria 大学）
   Dissection of dual role of inflammatory mediators in ischemic stroke for validating novel neurotherapeutics
   岸岡史郎教授（和歌山県立医科大学医学部）
   Effects of formalin-induced inflammatory pain on the development of tolerance to and physical dependence on nicotine in mice
5. セミナー（平成 25 年 10 月 2 日）
   豊岡尚樹教授（富山大学大学院理工学研究部）
   富山発新薬開発を目指したメディシナルケミストリー
   武田敬教授（広島大学大学院医歯薬保健学研究院）
   炭素陰イオンの三次元的アニオンリレーを機軸とする有機合成反応
6. 講演会（平成 25 年 7 月 1 日）
   Hirohito Kita,M.D.(Mayo Clinic Rochester
   好酸球機能の多様性と特異性
7. セミナー（平成 25 年 6 月 25 日）
   高須清誠教授（京都大学大学院薬学研究科）
   小員環ひずみを利用する機能性分子の創薬
   大嶋孝志教授（九州大学大学院薬学研究科）
   化学選択的アシル化反応の開発とその機構解明
8. 講演会（平成 25 年 5 月 21 日）
   Prof.Robert M. Williams(Colorado State University)
   Tetrahydroisoquinoline Antitumor Alkaloids;Total Synthesis,Mechanism of Action and Biosynthesis
9. 国際交流学術シンポジウム（平成 25 年 2 月 26 日）
   Prof.Laura Berliocchi(Calabria University)Antinociceptive proprieties of bergamot essential oil(BEO)
   岸岡史郎教授（和歌山県立医科大学）Endogenous opioid system participates in the nicotine-induced physical dependence through alpha7 nicotinic acetylcholine receptor but not alpha4beta2 in mice
   Dr.Damiana Scuteri(Calabria University)Characterization of alpha2-deltal expression and response to chronic treatment with gabapentin in amouse model of neuropathic pain
   櫻田司教授（第一薬科大学）Involvement of peripheral opioid and cannabinoid receptors in antinociception induced by bergamot essential oil and β-caryophyllene
   善積克助教（秋田大学）Mechanisms of locus coeruleus activation by gabapentinoids
   小松生明准教授（第一薬科大学）Intrathecal morphine-3-glucuronide induces nociception through δ_2-opioid receptors in the spinal cord
   渡辺俊博士 Gangliosides produce nociceptive behavior and hyperalgesia via glutamate signals
   長瀬博教授（北里大学）Study and development of a novel antitussive drug,TRK-851
   Prof.Giacinto Bagetta(Calabria University)Is there a role for autophagy in pain processing?
10. 特別講演会（平成 24 年 7 月 27 日）
    藤村務准教授（順天堂大学大学院医学研究科）
    がんにおけるバイオマーカーの探査とメタボロミクス解析

11. 特別講演会（平成 22 年 12 月 8 日）
高山廣光教授（千葉大学大学院薬学研究院）生物活性アルカロイドの探索と不斉全合成
12. 特別講演会（平成 22 年 7 月 15 日）
Prof. Clara Viñas (Institut de Ciència de Materials de Barcelona Campus U.A.B)
Expanding the possibilities of boron based molecules for application in medicine and molecular materials
Prof. Francesc Teixidor (Institut de Ciència de Materials de Barcelona Campus U.A.B)
Boron clusters: a route from catalysis to molecularly derived materials

インターネットでの公開状況

本プロジェクトの目的、研究計画概要（http://www.tohoku-pharm.ac.jp/new/index.cgi?eid=173）及び平成 22、23 年度研究成果概要（http://www.tohoku-pharm.ac.jp/new/index.cgi?eid=284）をインターネット上に公開している。

また、平成 24 年に提出した「研究進捗状況報告書の概要」（http://www.tohoku-pharm.ac.jp/new/index.cgi?eid=318）をインターネット上に公開している。

14 その他の研究成果等

「13 研究発表の状況」で記述した論文、学会発表等以外の研究成果、企業との連携実績があれば具体的に記入してください。また、上記、11(4)に記載した研究成果に対応するものには下線及び＊を付してください。
※ 論文や学会発表等になじまない研究である場合は、本欄を充実させること

特許

1. 発明の名称：＊新規ホスファチジルイノシトール 3 キナーゼ阻害剤および医薬組成物
発明者：石岡千加史、西條 憲、加藤 正
出願番号：特願 2011-217378 (出願日 平成 23 年 9 月 30 日)
2. 発明の名称：＊Novel Phosphatidylinositol-3-kinase Inhibitor and Pharmaceutical Composition
発明者：石岡千加史、西條 憲、加藤 正
国際特許出願番号：PCT/JP2012/074 (出願日 2012 年 9 月 25 日)
国際特許公開番号：WO2013/047509 (公開日 2013 年 4 月 4 日)
3. 発明の名称：ヘルパーT 細胞の選択的機能制御法
発明者、井ノ口仁一、永福正和、大野勲、奥山香織
特許番号：特許第 5232241 (登録日：平成 25 年 3 月 29 日)
4. Agent for ameliorating postprandial hyperglycemia, and pyrrolidine iminosugar or salt thereof
Kato, A.; Adachi, I.; Takahata, H.; Imahori, T.
PCT Int. Appl. (2011), WO 2011058975 A1 20110519.
5. 発明の名称 ステロイドの測定方法 特許権者 あすか製薬株式会社
発明者 沼澤光輝 山下幸和
出願番号 特願 2005-324856 (登録日平成 22 年 11 月 26 日)
6. 発明の名称：AMP 活性化プロテインキナーゼ活性化剤
発明者：山田耕太郎、三浦直良、中川西修、丹野孝一
国際公開番号；WO2015/022927 A1（出願日 2014 年 8 月 11 日）

15 「選定時」及び「中間評価時」に付された留意事項とそれへの対応

＜「選定時」に付された留意事項＞

留意事項が付されていない場合は「該当なし」と記載してください。

3つの研究テーマ個々は優れた提案を含んでいるため、相互に関連した統一目標を設定されたい。

＜「選定時」に付された留意事項への対応＞

付された留意事項に対し、どのような対応策を講じ、また、それにより、どのような成果があがったか等について、詳細に記載してください。

留意事項に対して、3つの研究テーマ間の連携も重視、本プロジェクトでの協力関係を最大限生かせるよう計画した。研究テーマ①癌化学療法薬の創製では、各研究室は、HDAC 阻害、代謝拮抗、アロマターゼ阻害と、それぞれ異なる作用機構をもつ新規癌化学療法薬の合成、解析を行っているが、得られた新規化合物の活性試験は、作用機構に従い、環境衛生学教室（テーマ②）あるいは、活性試験に適した共同研究者と行なうよう具体化した。研究テーマ②はエストロゲン受容体制御による加齢性疾患薬の創製がテーマであるが、創薬化学教室においては、核内受容体制御による癌化学療法薬（ホルモン依存性がん治療薬）の設計・合成も行うこととした。その結果、前立腺がん治療で問題となっている変異アンドロゲン受容体（既存の薬剤抵抗性）に有効な化合物を得ている。また、テーマ①に属する臨床分析化学教室は、エストロゲン及びその毒性代謝物の分析をもって、テーマ②と関連しており、密接な連携を図ることとした。テーマ②の薬理学教室及びテーマ③で疼痛制御を目指す機能形態学教室は動物実験における共通の基盤をもっており、各々の病態動物の作成の協力を図ることとした。3つの研究テーマでの統一した目標は、癌化学療法薬、加齢性疾患（骨粗鬆症、認知障害）改善薬、難治性疼痛治療薬の3つの分野で。画期的な新薬あるいは、その端緒となる成果を得て、その情報を公開することであり、現在、精力的に研究を展開している。

＜「中間評価時」に付された留意事項＞

留意事項が付されていない場合は「該当なし」と記載してください。

該当なし

＜「中間評価時」に付された留意事項への対応＞

付された留意事項に対し、どのような対応策を講じ、また、それにより、どのような成果があがったか等について、詳細に記載してください。

留意事項としての指摘はなかったが、評価コメントの中で大学院生・PD の活用、外部評価の実施、基礎研究から目標である創薬を視野に入れた研究への展開への期待などが示されていた。大学院生の活用に関しては薬学6年制による大学院生の減少等、致し方ない面もあるが、PD の活用と共に努力していきたい。外部評価は、評価体制の項で記述したように平成 24 年度後半に行った。医薬品の開発には新規活性化合物の発見からは長い期間が必要であるが、本プロジェクトで見出した化合物の特許出願、非臨床試験への適用など、成果を活かす努力を続けている。

16 施設・装置・設備・研究費の支出状況（実績概要）

（千円）

年度・区分		支出額	内訳						
			法人負担	私学助成	共同研究機関負担	受託研究等	寄付金	その他（　　）	備考
平成22年度	施設								
	装置	61,950	30,975	30,975					
	設備	19,189	6,397	12,792					
	研究費	24,253	13,519	10,734					
平成23年度	施設								
	装置								
	設備								
	研究費	27,729	14,731	12,998					
平成24年度	施設								
	装置								
	設備								
	研究費	28,206	14,236	13,970					
平成25年度	施設								
	装置								
	設備								
	研究費	24,000	12,988	11,012					
平成26年度	施設								
	装置								
	設備								
	研究費	24,000	12,344	11,656					
総額	施設								
	装置	61,950	30,975	30,975					
	設備	19,189	6,397	12,792					
	研究費	128,188	67,818	60,370					
総計		209,327	105,190	104,137					

17 施設・装置・設備の整備状況 （私学助成を受けたものはすべて記載してください。）

《施　設》（私学助成を受けていないものも含め、使用している施設をすべて記載してください。）　（千円）

施設の名称	整備年度	研究施設面積	研究室等数	使用者数	事業経費	補助金額	補助主体
教育研究棟 創薬研究センター （ハイテク・リサーチ・センター）	H22 （H17）	2,278.94 ㎡ （2,293.12㎡）	8研究室 ＋ 中央機器 センター	49　人	（293,117）	（142,163）	（私学助成）

※ 私学助成による補助事業として行った新増築により、整備前と比較して増加した面積

(H17) 1,174 ㎡

《装置・設備》（私学助成を受けていないものは、主なもののみを記載してください。）　（千円）

装置・設備の名称	整備年度	型番	台数	稼働時間数	事業経費	補助金額	補助主体
（研究装置） トリプル四重極 LC-MS/MSシステム	H22	TSQ Vantage AM	1式	9326 h	61,950	30,975	私学助成
高分解能FT-NMR 分子構造解析システム	H17	JNM-AL400	1式	常時稼働	59,850	29,925	〃
飛行時間型質量分析装置	〃	autoflex-SY Reflectron System	1式	400 h	41,958	20,979	〃
（研究設備） ダブルモノクロメーター式 マイクロプレートリーダー	H22	InfiniteM1000-TPCOI	1式	1571 h	10,946	7,297	私学助成
リアルタイムPCRシステム	〃	1.StepOnePlus-E 2.autoMACS	1式	1276 h	8,243	5,495	〃
共焦点顕微鏡画像解析装置	H17	TIRF-C1Plus	1式	384 h	25,830	17,220	〃
遺伝子タンパク解析装置	〃	PALM-MBⅢ-A	1式	1400 h	25,095	16,730	〃
精神神経関連行動解析装置	〃	--	1式	7033 h	24,780	16,520	〃

18 研究費の支出状況

【テーマ1】

（千円）

年度	平成 22 年度			
小科目	支出額	積算内訳		
		主な使途	金額	主な内容
教育研究経費支出				
消耗品費	6,106	薬品	2,879	試薬
		実験材料	2,453	試料，実験用品
		その他	773	文房具，OA用品
通信運搬費		郵便・運搬		ｻﾝﾌﾟﾙ配送等
印刷製本費		論文等印刷		論文印刷，文献複写
旅費交通費	749	学会・研究発表	749	学会参加，研究打合せ
報酬・委託料	76	委託	19	分析・検査，英文校正
		支払報酬	58	講演料等
（修繕費）	926	設備修繕	926	機器修理・ﾒﾝﾃﾅﾝｽ
（諸会費）	58	学会等参加	58	学会，ｼﾝﾎﾟｼﾞｳﾑ
計	7,915			
アルバイト関係支出				
人件費支出（兼務職員）		--		--
教育研究経費支出		--		--
計				
設備関係支出（1個又は1組の価格が500万円未満のもの）				
教育研究用機器備品	1,188	機械器具	1,188	送風定温乾燥器 WFO-500 他
図書	16	和・洋書	16	Metathesis in Natural Product Synthesis
計	1,204			
研究スタッフ関係支出				
ﾘｻｰﾁ・ｱｼｽﾀﾝﾄ				--
ﾎﾟｽﾄ・ﾄﾞｸﾀｰ				--
研究支援推進経費				--
計				

【テーマ1】

（千円）

年度	平成 23 年度			
小科目	支出額	積算内訳		
		主な使途	金額	主な内容
教育研究経費支出				
消耗品費	5,929	薬品	3,304	試薬
		実験材料	2,503	試料，実験用品
		その他	122	文房具，OA用品
通信運搬費	1	郵便・運搬	1	ｻﾝﾌﾟﾙ配送等
印刷製本費	217	論文等印刷	217	論文印刷，文献複写
旅費交通費	1,023	学会・研究発表	1,023	学会参加，研究打合せ
報酬・委託料	70	委託	57	分析・検査，英文校正
		支払報酬	13	講演料等
（修繕費）	867	設備修繕	867	機器修理・ﾒﾝﾃﾅﾝｽ
（諸会費）	50	学会等参加	50	学会，ｼﾝﾎﾟｼﾞｳﾑ
計	8,157			
アルバイト関係支出				
人件費支出（兼務職員）	3,453	ｱｼｽﾀﾝﾄ・ｽﾀｯﾌ	3,453	学内1人、月給、10ヶ月
教育研究経費支出		--		--
計	3,453			
設備関係支出（1個又は1組の価格が500万円未満のもの）				
教育研究用機器備品	865	機械器具	865	ｹﾐｽﾄﾌﾟﾗｻﾞ CP-300 他
図書	27	和・洋書	27	Steroid Analysis
計	892			
研究スタッフ関係支出				
ﾘｻｰﾁ・ｱｼｽﾀﾝﾄ				--
ﾎﾟｽﾄ・ﾄﾞｸﾀｰ				--
研究支援推進経費				--
計				

【テーマ1】

（千円）

年度	平成　24　年度			
小科目	支出額	積算内訳		
		主な使途	金額	主な内容
教育研究経費支出				
消耗品費	5,785	薬品	2,753	試薬
		実験材料	2,874	試料，実験用品
		その他	159	文房具，OA用品
通信運搬費	1	郵便・運搬	1	ｻﾝﾌﾟﾙ配送等
印刷製本費	19	論文等印刷	19	論文印刷，文献複写
旅費交通費	1,220	学会・研究発表	1,220	学会参加，研究打合せ
報酬・委託料	30	委託	30	分析・検査，英文校正
		支払報酬		講演料等
（修繕費）	136	設備修繕	136	機器修理・ﾒﾝﾃﾅﾝｽ
（諸会費）	58	学会等参加	58	学会，ｼﾝﾎﾟｼﾞｳﾑ
計	7,249			
アルバイト関係支出				
人件費支出（兼務職員）	4,206	ｱｿｼｴｲﾄ・ｽﾀｯﾌ	4,206	学内1人、月給、12ヶ月
教育研究経費支出		--		--
計	4,206			
設備関係支出（1個又は1組の価格が500万円未満のもの）				
教育研究用機器備品	1,751	機械器具	1,751	ｵｿﾞﾝ発生装置 SO-03UN-OX 他
図書		和・洋書		
計	1,751			
研究スタッフ関係支出				
リサーチ・アシスタント				--
ポスト・ドクター				--
研究支援推進経費				--
計				

【テーマ1】

（千円）

年度	平成　25　年度			
小科目	支出額	積算内訳		
		主な使途	金額	主な内容
教育研究経費支出				
消耗品費	5,762	薬品	3,119	試薬
		実験材料	2,272	試料，実験用品
		その他	371	文房具，OA用品
通信運搬費	1	郵便・運搬	1	ｻﾝﾌﾟﾙ配送等
印刷製本費	132	論文等印刷	132	論文印刷，文献複写
旅費交通費	1,349	学会・研究発表	1,349	学会参加，研究打合せ
報酬・委託料	124	委託	78	分析・検査，英文校正
		支払報酬	46	講演料等
（修繕費）	304	設備修繕	304	機器修理・ﾒﾝﾃﾅﾝｽ
（諸会費）		学会等参加		学会，ｼﾝﾎﾟｼﾞｳﾑ
計	7,672			
アルバイト関係支出				
人件費支出（兼務職員）		--		--
教育研究経費支出		--		--
計				
設備関係支出（1個又は1組の価格が500万円未満のもの）				
教育研究用機器備品	1,328	機械器具	1,328	HPLCﾎﾟﾝﾌﾟ LC-20AD 他
図書		和・洋書		
計	1,328			
研究スタッフ関係支出				
リサーチ・アシスタント				--
ポスト・ドクター				--
研究支援推進経費				--
計				

【テーマ1】

（千円）

年度	平成 26 年度			
小科目	支出額	積算内訳		
		主な使途	金額	主な内容
教育研究経費支出				
消耗品費	6,065	薬品	3,295	試薬
		実験材料	2,542	試料，実験用品
		その他	228	文房具，OA用品
通信運搬費	7	郵便・運搬	7	ｻﾝﾌﾟﾙ配送等
印刷製本費		論文等印刷		論文印刷，文献複写
旅費交通費	603	学会・研究発表	603	学会参加，研究打合せ
報酬・委託料	19	委託	19	分析・検査，英文校正
		支払報酬		講演料等
（修繕費）	141	設備修繕	141	機器修理・ﾒﾝﾃﾅﾝｽ
（諸会費）	5	学会等参加	5	学会，ｼﾝﾎﾟｼﾞｳﾑ
計	6,840			
アルバイト関係支出				
人件費支出（兼務職員）		--		--
教育研究経費支出		--		--
計				
設備関係支出（1個又は1組の価格が500万円未満のもの）				
教育研究用機器備品	2,160	機械器具	2,160	ﾎﾟｰﾀﾌﾞﾙ水素発生器 他
図書		和・洋書		
計	2,160			
研究スタッフ関係支出				
リサーチ・アシスタント				--
ポスト・ドクター				--
研究支援推進経費				--
計				

【テーマ2】

（千円）

年度	平成 22 年度			
小科目	支出額	積算内訳		
		主な使途	金額	主な内容
教育研究経費支出				
消耗品費	7,616	薬品	3,534	試薬
		実験材料	2,953	試料，実験用品
		その他	1,129	文房具，OA用品
通信運搬費		郵便・運搬		ｻﾝﾌﾟﾙ配送等
印刷製本費	95	論文等印刷	95	論文印刷，文献複写
旅費交通費		学会・研究発表		学会参加，研究打合せ
報酬・委託料	266	委託	178	分析・検査，英文校正
		支払報酬	88	講演料等
（修繕費）	74	設備修繕	74	機器修理・ﾒﾝﾃﾅﾝｽ
（諸会費）		学会等参加		学会，ｼﾝﾎﾟｼﾞｳﾑ
計	8,051			
アルバイト関係支出				
人件費支出（兼務職員）		--		--
教育研究経費支出		--		--
計				
設備関係支出（1個又は1組の価格が500万円未満のもの）				
教育研究用機器備品	849	機械器具	849	ﾀﾞｲﾔﾌﾗﾑ型真空ﾎﾟﾝﾌﾟ DTC-41 他
図書		和・洋書		--
計	849			
研究スタッフ関係支出				
リサーチ・アシスタント				--
ポスト・ドクター				--
研究支援推進経費				--
計				

【テーマ2】

（千円）

年度	平成　23　年度			
小科目	支出額	積算内訳		
		主な使途	金額	主な内容
教育研究経費支出				
消耗品費	8,169	薬品	4,288	試薬
		実験材料	3,143	試料，実験用品
		その他	737	文房具，OA用品
通信運搬費	1	郵便・運搬	1	ｻﾝﾌﾟﾙ配送等
印刷製本費	148	論文等印刷	148	論文印刷，文献複写
旅費交通費	146	学会・研究発表	146	学会参加，研究打合せ
報酬・委託料	320	委託	320	分析・検査，英文校正
		支払報酬		講演料等
（修繕費）	217	設備修繕	217	機器修理・ﾒﾝﾃﾅﾝｽ
（諸会費）		学会等参加		学会，ｼﾝﾎﾟｼﾞｳﾑ
計	9,000			
アルバイト関係支出				
人件費支出（兼務職員）		--		--
教育研究経費支出		--		--
計				
設備関係支出（1個又は1組の価格が500万円未満のもの）				
教育研究用機器備品		機械器具		--
図書		和・洋書		--
計				
研究スタッフ関係支出				
リサーチ・アシスタント				--
ポスト・ドクター				--
研究支援推進経費				--
計				

【テーマ2】

（千円）

年度	平成　24　年度			
小科目	支出額	積算内訳		
		主な使途	金額	主な内容
教育研究経費支出				
消耗品費	6,764	薬品	3,593	試薬
		実験材料	2,542	試料，実験用品
		その他	629	文房具，OA用品
通信運搬費	1	郵便・運搬	1	ｻﾝﾌﾟﾙ配送等
印刷製本費	152	論文等印刷	152	論文印刷，文献複写
旅費交通費		学会・研究発表		学会参加，研究打合せ
報酬・委託料	248	委託	241	分析・検査，英文校正
		支払報酬	7	講演料等
（修繕費）	50	設備修繕	50	機器修理・ﾒﾝﾃﾅﾝｽ
（諸会費）		学会等参加		学会，ｼﾝﾎﾟｼﾞｳﾑ
計	7,215			
アルバイト関係支出				
人件費支出（兼務職員）		--		--
教育研究経費支出		--		--
計				
設備関係支出（1個又は1組の価格が500万円未満のもの）				
教育研究用機器備品	1,785	機械器具	1,785	ｵｰﾄｻﾝﾌﾟﾗｰ　他
図書		和・洋書		--
計	1,785			
研究スタッフ関係支出				
リサーチ・アシスタント				--
ポスト・ドクター				--
研究支援推進経費				--
計				

【テーマ2】

（千円）

年度	平成 25 年度			
小科目	支出額	積算内訳		
		主な使途	金額	主な内容
教育研究経費支出				
消耗品費	7,456	薬品	4,666	試薬
		実験材料	2,342	試料，実験用品
		その他	448	文房具，OA用品
通信運搬費	5	郵便･運搬	5	ｻﾝﾌﾟﾙ配送等
印刷製本費	49	論文等印刷	49	論文印刷，文献複写
旅費交通費		学会･研究発表		学会参加，研究打合せ
報酬･委託料	125	委託	125	分析･検査，英文校正
		支払報酬		講演料等
（修繕費）	65	設備修繕	65	機器修理･ﾒﾝﾃﾅﾝｽ
（諸会費）		学会等参加		学会，ｼﾝﾎﾟｼﾞｳﾑ
計	7,700			
アルバイト関係支出				
人件費支出（兼務職員）		--		--
教育研究経費支出		--		--
計				
設備関係支出（1個又は1組の価格が500万円未満のもの）				
教育研究用機器備品	1,300	機械器具	1,300	超低温ﾌﾘｰｻﾞｰMDF-U33V-PJ
図書		和･洋書		--
計	1,300			
研究スタッフ関係支出				
リサーチ･アシスタント				--
ポスト･ドクター				--
研究支援推進経費				--
計				

【テーマ2】

（千円）

年度	平成 26 年度			
小科目	支出額	積算内訳		
		主な使途	金額	主な内容
教育研究経費支出				
消耗品費	7,190	薬品	3,358	試薬
		実験材料	3,260	試料，実験用品
		その他	572	文房具，OA用品
通信運搬費	1	郵便･運搬	1	ｻﾝﾌﾟﾙ配送等
印刷製本費	320	論文等印刷	320	論文印刷，文献複写
旅費交通費	230	学会･研究発表	230	学会参加，研究打合せ
報酬･委託料	216	委託	203	分析･検査，英文校正
		支払報酬	13	講演料等
（修繕費）	422	設備修繕	422	機器修理･ﾒﾝﾃﾅﾝｽ
（賃借料）	1	設備賃借費	1	容器使用料
計	8,380			
アルバイト関係支出				
人件費支出（兼務職員）		--		--
教育研究経費支出		--		--
計				
設備関係支出（1個又は1組の価格が500万円未満のもの）				
教育研究用機器備品	620	機械器具	620	CO2ｲﾝｷｭﾍﾞｰﾀｰ
図書		和･洋書		--
計	620			
研究スタッフ関係支出				
リサーチ･アシスタント				--
ポスト･ドクター				--
研究支援推進経費				--
計				

【テーマ3】

（千円）

年度	平成　22　年度			
小科目	支出額	積算内訳		
		主な使途	金額	主な内容
教育研究経費支出				
消耗品費	4,184	薬品	2,679	試薬
		実験材料	1,464	試料，実験用品
		その他	40	文房具，OA用品
通信運搬費	2	郵便･運搬	2	ｻﾝﾌﾟﾙ配送等
印刷製本費		論文等印刷		論文印刷，文献複写
旅費交通費	1,262	学会･研究発表	1,262	学会参加，研究打合せ
報酬･委託料		委託		分析･検査，英文校正
		支払報酬		講演料等
（修繕費）		設備修繕		機器修理･ﾒﾝﾃﾅﾝｽ
（諸会費）		学会等参加		学会，ｼﾝﾎﾟｼﾞｳﾑ
計	5,448			
アルバイト関係支出				
人件費支出（兼務職員）		--		--
教育研究経費支出		--		--
計				
設備関係支出（1個又は1組の価格が500万円未満のもの）				
教育研究用機器備品	786	機械器具	786	ﾏｲﾊﾞｲｵ VT-208 他
図書		和･洋書		--
計	786			
研究スタッフ関係支出				
ﾘｻｰﾁ･ｱｼｽﾀﾝﾄ				--
ﾎﾟｽﾄ･ﾄﾞｸﾀｰ				--
研究支援推進経費				--
計				

【テーマ3】

（千円）

年度	平成　23　年度			
小科目	支出額	積算内訳		
		主な使途	金額	主な内容
教育研究経費支出				
消耗品費	5,301	薬品	2,430	試薬
		実験材料	2,872	試料，実験用品
		その他		文房具，OA用品
通信運搬費	2	郵便･運搬	2	ｻﾝﾌﾟﾙ配送等
印刷製本費	315	論文等印刷	315	論文印刷，文献複写
旅費交通費	416	学会･研究発表	416	学会参加，研究打合せ
報酬･委託料	7	委託		分析･検査，英文校正
		支払報酬	7	講演料等
（修繕費）	186	設備修繕	186	機器修理･ﾒﾝﾃﾅﾝｽ
（諸会費）		学会等参加		学会，ｼﾝﾎﾟｼﾞｳﾑ
計	6,227			
アルバイト関係支出				
人件費支出（兼務職員）		--		--
教育研究経費支出		--		--
計				
設備関係支出（1個又は1組の価格が500万円未満のもの）				
教育研究用機器備品		機械器具		--
図書		和･洋書		--
計				
研究スタッフ関係支出				
ﾘｻｰﾁ･ｱｼｽﾀﾝﾄ				--
ﾎﾟｽﾄ･ﾄﾞｸﾀｰ				--
研究支援推進経費				--
計				

【テーマ3】

（千円）

年度	平成　24　年度			
小科目	支出額	積算内訳		
		主な使途	金額	主な内容
教育研究経費支出				
消耗品費	4,232	薬品	1,504	試薬
		実験材料	2,728	試料，実験用品
		その他		文房具，OA用品
通信運搬費	0	郵便・運搬	0	ｻﾝﾌﾟﾙ配送等
印刷製本費	170	論文等印刷	170	論文印刷，文献複写
旅費交通費	1,340	学会・研究発表	1,340	学会参加，研究打合せ
報酬・委託料	257	委託	257	分析・検査，英文校正
		支払報酬		講演料等
（修繕費）		設備修繕		機器修理・ﾒﾝﾃﾅﾝｽ
（諸会費）		学会等参加		学会，ｼﾝﾎﾟｼﾞｳﾑ
計	6,000			
アルバイト関係支出				
人件費支出（兼務職員）		--		--
教育研究経費支出		--		--
計				
設備関係支出（1個又は1組の価格が500万円未満のもの）				
教育研究用機器備品		機械器具		--
図書		和・洋書		
計				
研究スタッフ関係支出				
リサーチ・アシスタント				--
ポスト・ドクター				--
研究支援推進経費				--
計				

【テーマ3】

（千円）

年度	平成　25　年度			
小科目	支出額	積算内訳		
		主な使途	金額	主な内容
教育研究経費支出				
消耗品費	5,328	薬品	2,421	試薬
		実験材料	2,907	試料，実験用品
		その他		文房具，OA用品
通信運搬費		郵便・運搬		ｻﾝﾌﾟﾙ配送等
印刷製本費	209	論文等印刷	209	論文印刷，文献複写
旅費交通費	360	学会・研究発表	360	学会参加，研究打合せ
報酬・委託料	103	委託		分析・検査，英文校正
		支払報酬	103	講演料等
（修繕費）		設備修繕		機器修理・ﾒﾝﾃﾅﾝｽ
（諸会費）		学会等参加		学会，ｼﾝﾎﾟｼﾞｳﾑ
計	6,000			
アルバイト関係支出				
人件費支出（兼務職員）		--		--
教育研究経費支出		--		--
計				
設備関係支出（1個又は1組の価格が500万円未満のもの）				
教育研究用機器備品		機械器具		--
図書		和・洋書		--
計				
研究スタッフ関係支出				
リサーチ・アシスタント				--
ポスト・ドクター				--
研究支援推進経費				--
計				

【テーマ3】

（千円）

年　度	平成　26　年度			
小科目	支出額	積算内訳		
		主な使途	金額	主な内容
教育研究経費支出				
消耗品費	5,713	薬品	2,380	試薬
		実験材料	3,330	試料，実験用品
		その他	3	文房具，OA用品
通信運搬費		郵便･運搬		ｻﾝﾌﾟﾙ配送等
印刷製本費		論文等印刷		論文印刷，文献複写
旅費交通費	153	学会･研究発表	153	学会参加，研究打合せ
報酬･委託料	134	委託		分析･検査，英文校正
		支払報酬	134	講演料等
（修繕費）		設備修繕		機器修理･ﾒﾝﾃﾅﾝｽ
（諸会費）		学会等参加		学会，ｼﾝﾎﾟｼﾞｳﾑ
計	6,000			
アルバイト関係支出				
人件費支出（兼務職員）		--		--
教育研究経費支出		--		--
計				
設備関係支出（1個又は1組の価格が500万円未満のもの）				
教育研究用機器備品		機械器具		--
図書		和･洋書		
計				
研究スタッフ関係支出				
リサーチ･アシスタント				--
ポスト･ドクター				--
研究支援推進経費				--
計				

研究テーマ①

新しい作用機作をもつ癌化学療法薬の創製

Cancer Science
Japanese Cancer Association JCA
Open Access

Biochemical, biological and structural properties of romidepsin (FK228) and its analogs as novel HDAC/PI3K dual inhibitors

Ken Saijo,[1] Jin Imamura,[1] Koichi Narita,[2] Akifumi Oda,[3] Hideki Shimodaira,[1] Tadashi Katoh[2] and Chikashi Ishioka[1]

[1]Department of Clinical Oncology, Institute of Development, Aging and Cancer, Tohoku University, Sendai; [2]Laboratory of Synthetic and Medicinal Chemistry, Faculty of Pharmaceutical Sciences, Tohoku Pharmaceutical University, Sendai; [3]Institute of Medical, Pharmaceutical and Health Sciences, Kanazawa University, Ishikawa, Japan

Key words

Drug development, dual inhibitor, HDAC, PI3K, romidepsin

Correspondence

Chikashi Ishioka, Department of Clinical Oncology, Institute of Development, Aging and Cancer, Tohoku University, Sendai 980-8575, Japan.
Tel: +81-22-717-854; Fax: +81-22-717-8548;
E-mail: chikashi@idac.tohoku.ac.jp

Funding information

Ministry of Education, Culture, Sports, Science and Technology (MEXT) KAKENHI (24300339). (25830110). (26460034). Gonryo Medical Foundation

Received July 18, 2014; Revised November 29, 2014; Accepted December 2, 2014

Cancer Sci **106** (2015) 208–215

doi: 10.1111/cas.12585

Romidepsin (FK228, depsipeptide) is a potent histone deacetylase (HDAC) inhibitor that has FDA approval for the treatment of cutaneous and peripheral T-cell lymphomas. We have previously reported that FK228 and its analogs have an additional activity as phosphatidylinositol 3-kinase (PI3K) inhibitors, and are defined as HDAC/PI3K dual inhibitors. Because a combination of an HDAC inhibitor and a PI3K inhibitor induces apoptosis in human cancer cells in a synergistic manner, development of an HDAC/PI3K dual inhibitor will provide an attractive novel drug for cancer therapy. Using structure-based optimization of the analogs, FK-A11 was identified as the most potent analog. FK-A11 inhibited phosphorylation of AKT and accelerated histone acetylation at lower concentrations, resulting in stronger cytotoxic effects than FK228 and the other analogs in human cancer cells. In this study, we have characterized the biochemical, biological and structural properties of FK228 analogs as PI3K inhibitors. First, FK-A11 is an ATP competitive PI3K inhibitor. Second, FK-A11 is a pan-p110 isoform inhibitor. Third, FK-A11 selectively inhibits PI3K among 22 common cellular kinases. Fourth, conformational changes of FK228 analogs by reduction of an internal disulfide bond have no effect on PI3K inhibitory activity, unlike HDAC inhibitory activity. Finally, molecular modeling of PI3K-FK228 analogs and analyses of the binding affinities identified the structure that defines potency for PI3K inhibitory activity. These results prove our concept that a series of FK228 analogs are HDAC/PI3K dual inhibitors. These findings should help in the development of FK228 analogs as novel HDAC/PI3K dual inhibitors.

Phosphatidylinositol 3-kinase (PI3K), an ubiquitously expressed lipid kinase, phosphorylates phosphatidylinositol-4,5-biphosphate (PIP2), generating phosphatidylinositol-3,4,5-triphosphate (PIP3).[1] PIP3 serves as a second messenger in the signal transduction pathway,leading to cancer cell initiation, proliferation and survival.[2] Class I PI3K is composed of a catalytic subunit, p110, and a regulatory subunit, p85 or p101. The catalytic subunit consists of four isoforms: p110α, β, γ and δ.[3] In many human cancers, the PI3K pathway is frequently activated through gain of function mutations in the *PIK3CA* gene that encodes p110α.[4] Therefore, the catalytic subunits of PI3K are considered to be potential drug targets for cancer therapy.[5,6]

In addition to genetic mutations, epigenetic changes, such as dysregulation of histone deacetylases (HDAC), contribute to cancer cell initiation and growth, by altering the cell phenotype and gene expression and by disturbing homeostasis.[7] Thus, HDAC inhibitors are newly emerging drugs for cancer therapeutics.[8,9] Romidepsin (FK228, depsipeptide) is an HDAC inhibitor with high inhibitory activity for class I HDAC.[10] FK228 is a bicyclic depsipeptide that is structurally characteristic compared with other HDAC inhibitors. Reduction of the internal disulfide bond changes the conformation of FK228 to the open form, producing free sulfhydryl groups that can interact with the catalytic active pocket of HDAC.[10] FK228 is approved by the FDA for the treatment of patients with cutaneous T-cell lymphoma or peripheral T-cell lymphoma.[11,12]

Recently, it has been reported that the combination of an HDAC inhibitor and a kinase inhibitor, such as epidermal growth factor receptor (EGFR) tyrosine kinase inhibitor or PI3K inhibitor, overcomes kinase inhibitor resistance and induces apoptosis in human solid cancers in a synergistic manner.[13–15] Therefore, development of inhibitors targeting both HDAC and PI3K would be advantageous as anticancer drug candidates. Indeed, a single molecule dual inhibitor of HDAC and PI3K is under investigation in a phase I clinical trial.[16]

We have previously demonstrated that FK228 and its analogs directly inhibit PI3K activity and potently induce apoptosis through HDAC/PI3K dual inhibition.[17] In other words, FK228 and its analogs have been identified as novel HDAC/PI3K dual inhibitors. However, no additional finding of

© 2014 The Authors. Cancer Science published by Wiley Publishing Asia Pty Ltd on behalf of Japanese Cancer Association.
This is an open access article under the terms of the Creative Commons Attribution-NonCommercial-NoDerivs License, which permits use and distribution in any medium, provided the original work is properly cited, the use is non-commercial and no modifications or adaptations are made.

FK228 as a kinase inhibitor has been reported to date. Here, we describe the biochemical, biological and structural properties of FK228 and its analogs as PI3K inhibitors. These findings provide important clues for the development of more potent FK228 analogs as HDAC/PI3K dual inhibitors.

Materials and Methods

Reagents. LY294002 and suberoylanilide hydroxamic acid (SAHA) were purchased from Cayman Chemical Company (Ann-Arbor, MI, USA). Wortmannin was purchased from Millipore (Billerica, MA, USA). FK228 and its analogs were synthesized and provided by T. K. from Tohoku Pharmaceutical University.[18]

Kinase assay. PI3K (p110α/p85α) activity and other 20 common cellular kinase activities were evaluated by the mobility shift assay (Carna Biosciences, Kobe, Japan).[19] Individual activity for the four p110 isoforms, α, β, γ and δ, was measured using an homogenous time-resolved fluorescence (HTRF) assay (PI3K assay kit; Millipore). Mammalian target of rapamaycin (mTOR) activity was measured using a K-LISA mTOR activity kit (Millipore). The detailed methods of each assay are described in Supplementary Document S1.

Enzyme kinetic assay. The PI3K assay for Lineweaver–Burk analysis was performed using an ADP-Glo assay kit (Promega, Madison, WI, USA). PI3K activity was assayed at five different ATP concentrations (5, 10, 25, 50 and 100 μM), with 40 nM PI3Kα, 25 μM PIP2 and FK-A11 (0, 2.5, 5 and 10 μM). A Lineweaver–Burk plot was developed by plotting $1/v$ (reaction velocity) against 1/[ATP] (ATP concentration).

HDAC activity assay. FK228 and its analogs, except for FK-A21 and FK-A22, were evaluated for HDAC inhibitory activity using the Screening Committee of Anticancer Drugs (SCADS). The HDAC inhibitory activities of FK-A21 and FK-A22 were evaluated using an HDAC inhibitor screening kit (Cayman Chemical Company) as described in Supplementary Document S1.

Cell lines. The human cancer cell lines used in this study included the prostate cancer cell line PC3 and the colorectal cancer cell line HCT116. PC3 was obtained from the Cell Resource Center (Institute of Development, Aging, and Cancer, Tohoku University, Sendai, Japan). HCT116 was purchased from the ATCC (Mannassas, VA, USA).

Western blot analysis. Western blotting was conducted as previously described,[17] using antibodies described in Supplementary Document S1.

Cell proliferation assay. A cell proliferation assay was performed with a Cell Counting Kit-8 (Dojindo Laboratories, Kumamoto, Japan) as previously described.[17] Cells (8×10^3 per well) were seeded and incubated in 96-well plates for 24 h. Compounds were added to the cells and further cultured for 24 h at 37°C. The ratios of surviving cells to control cells treated with 0.5 or 1% DMSO were calculated.

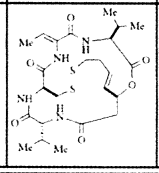
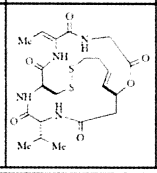
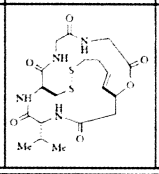
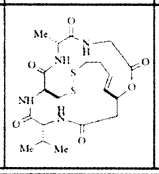
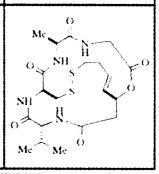
Molecular modeling of the PI3K-FK228 analog and HDAC1-FK228 analog complexes. A computational docking simulation of PI3K and FK-A11 was carried out using the predicted PI3K-FK228 complex structure previously described.[17] The structure of the PI3K (p110α H1047R/p85α)–wortmannin complex (Protein Data Bank ID: 3HHM) was used to obtain the PI3K template structure. The HDAC1 template structure was obtained from the protein data bank (ID: 4BXK). Conformational searches of docking complexes were performed using LMOD and OMEGA (OpenEye Scientific Software, Boston, MA, USA).[20] Subsequently, the docking calculations were carried out using the calculation method FRED, to obtain Chemgauss 4 scores that suggest the binding affinities.[21]

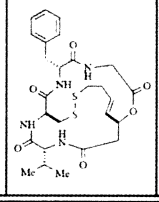
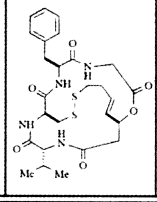
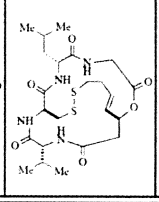
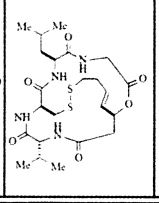
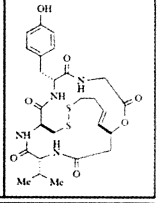
Results

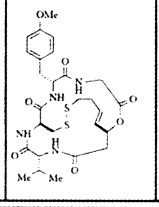
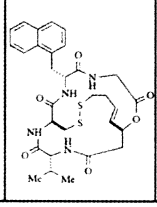
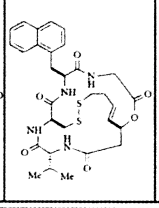
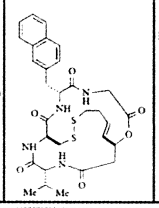
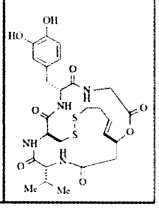
Search for novel FK228 analogs with potent HDAC/PI3K dual inhibitory activity in cell-free systems. In our previous study, we reported that FK-A5 was the most potent PI3K inhibitor identified among FK228 and its 10 analogs.[17] From the perspective of chemical constitution, FK-A5 has a characteristic structure, possessing a benzyl group at the C7 position. To identify a more potent PI3K inhibitor, most of the additional 14 analogs (FK-A7, FK-A8, FK-A9, FK-A10, FK-A11, FK-A12, FK-A13, FK-A15, FK-A17, FK-A18, FK-A20, FK-A21, FK-A22 and SP-4) were synthesized by modification of the benzyl group at the C7 position. PI3K inhibitory activities were evaluated in a cell-free system (Fig. 1). Among the newly synthesized analogs, FK-A11, FK-A12 and FK-A20 were more potent than the other analogs. In particular, FK-A11 was the most potent PI3K inhibitor, with activity exceeding that of both FK228 and FK-A5. The IC_{50} values against p110α of FK-A11, FK-A5 and FK228 were 6.7, 27.3 and 57.1 μM, respectively (Figs 1 and 2a). FK-A11 has 4-fold and 8.5-fold stronger activity than FK-A5 and FK228, respectively. From a structural viewpoint, the benzyl group at the C7 position of FK-A5 was replaced by a naphthylmethyl group which consists of a fused pair of benzene rings in FK-A11 (Fig. 1). In addition to the PI3K inhibitory activity, FK-A11 was also a more potent HDAC inhibitor, exceeding both FK228 and FK-A5. The IC_{50} values against HDAC1 of FK-A11, FK-A5 and FK228 were 0.64, 2.5 and 3.6 nM, respectively (Fig. 1). FK-A12 and FK-A20 were weaker HDAC inhibitors than FK228, FK-A5 and FK-A11. Although FK-A11 and FK-A12 are stereoisomers with respect to the C7 position, their HDAC inhibitory activities were different. These results indicated that FK-A11 was the most potent HDAC/PI3K dual inhibitor among the FK228 analogs synthesized so far.

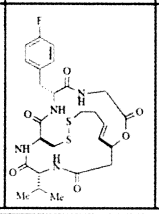
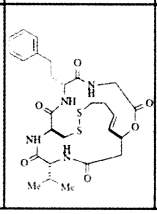
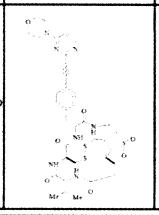
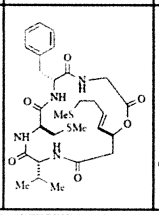
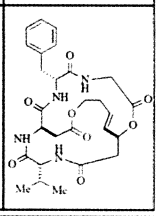
Inhibitory effects of FK228 analogs on PI3K, HDAC and cell proliferation in human cancer cell lines. A prostate cancer cell line PC3 and a human colon cancer cell line HCT116 were cultured in the presence of FK228 analogs, an HDAC inhibitor SAHA, a PI3K inhibitor LY294002, or a combination of SAHA and LY294002. The data with PC3 cells showed that FK-A11 inhibited the phosphorylation of AKT, a downstream component of PI3K, at lower concentrations than that observed with FK228 and FK-A5 (Fig. 2b). As for HDAC inhibition, FK-A11 increased acetylated histones at nM-range concentrations similar to FK228 and FK-A5 (Fig. 2c). In cell proliferation assay in PC3 cells, FK-A11 exhibited stronger cytotoxic effects than any other FK228 analog and the combination of SAHA and LY294002 (Fig. 2d). Furthermore, to elucidate the contribution of HDAC/PI3K dual inhibition to the cytotoxic effects, the effects of some FK228 analogs were compared. FK-A11 and FK-A12 are stereoisomers with similar PI3K inhibitory activity but different HDAC inhibitory activity. FK-A11 has 17.3-fold stronger HDAC inhibitory activity than FK-A12 (Fig. 1). In comparison of the cytotoxic effects, FK-A12 showed weaker cytotoxic effects than FK-A11 at the lower concentrations, 10 and 100 nM (Fig. 2d). The cytotoxic effects of FK-A11 and FK-A12 were similar at the concentrations of 1 and 10 μM (Fig. 2d). In addition, SP-3 and FK-A3 with weaker PI3K inhibitory activity than FK228, and with similar HDAC inhibitory activity to FK228 have been evaluated. Both SP-3 and FK-A3 did not potentiate cytotoxic effects

© 2014 The Authors. Cancer Science published by Wiley Publishing Asia Pty Ltd on behalf of Japanese Cancer Association.

Compound		FK228	FK-A1	FK-A2	FK-A3	FK-A4
IC50	HDAC1	3.6 ±0.46 nM	7.8 ±0.44 nM	45 ±7.7 nM	4.2 ± 0.14 nM	340.0 ± 20 nM
	P110α	57.1 μM	26.2 μM	139 μM	>100 μM	120 μM
Structure						

Compound		FK-A5	FK-A6	**FK-A7**	**FK-A8**	**FK-A9**
IC50	HDAC1	2.5 ± 1.1 nM	19.4 ± 2.5 nM	0.96 ± 0.14 nM	11.4 ± 4.1 nM	0.41 ± 0.26 nM
	P110α	27.3 μM	24.7 μM	32.2 μM	44.7 μM	14.1 μM
Structure						

Compound		**FK-A10**	**FK-A11**	**FK-A12**	**FK-A13**	**FK-A15**
IC50	HDAC1	0.54 ± 0.025 nM	0.64 ±0.3 nM	11.1 ± 2.7 nM	6.3 ± 0.39 nM	9.3 ± 0.64 nM
	P110α	26.7 μM	6.7 μM	7.2 μM	8.5 μM	21.2 μM
Structure						

Compound		**FK-A17**	**FK-A18**	**FK-A20**	**FK-A21**	**FK-A22**
IC50	HDAC1	5.8 ± 0.54 nM	5.2 ± 0.42 nM	27.7 ± 2.3 nM	No activity	No activity
	P110α	20.2 μM	18.6 μM	8.19 μM	27.1 μM	20.2 μM
Structure						

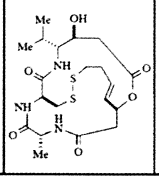
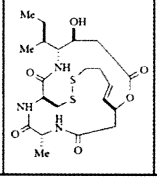
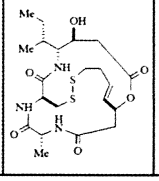
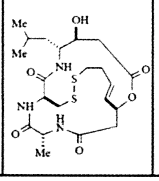
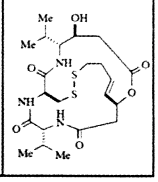
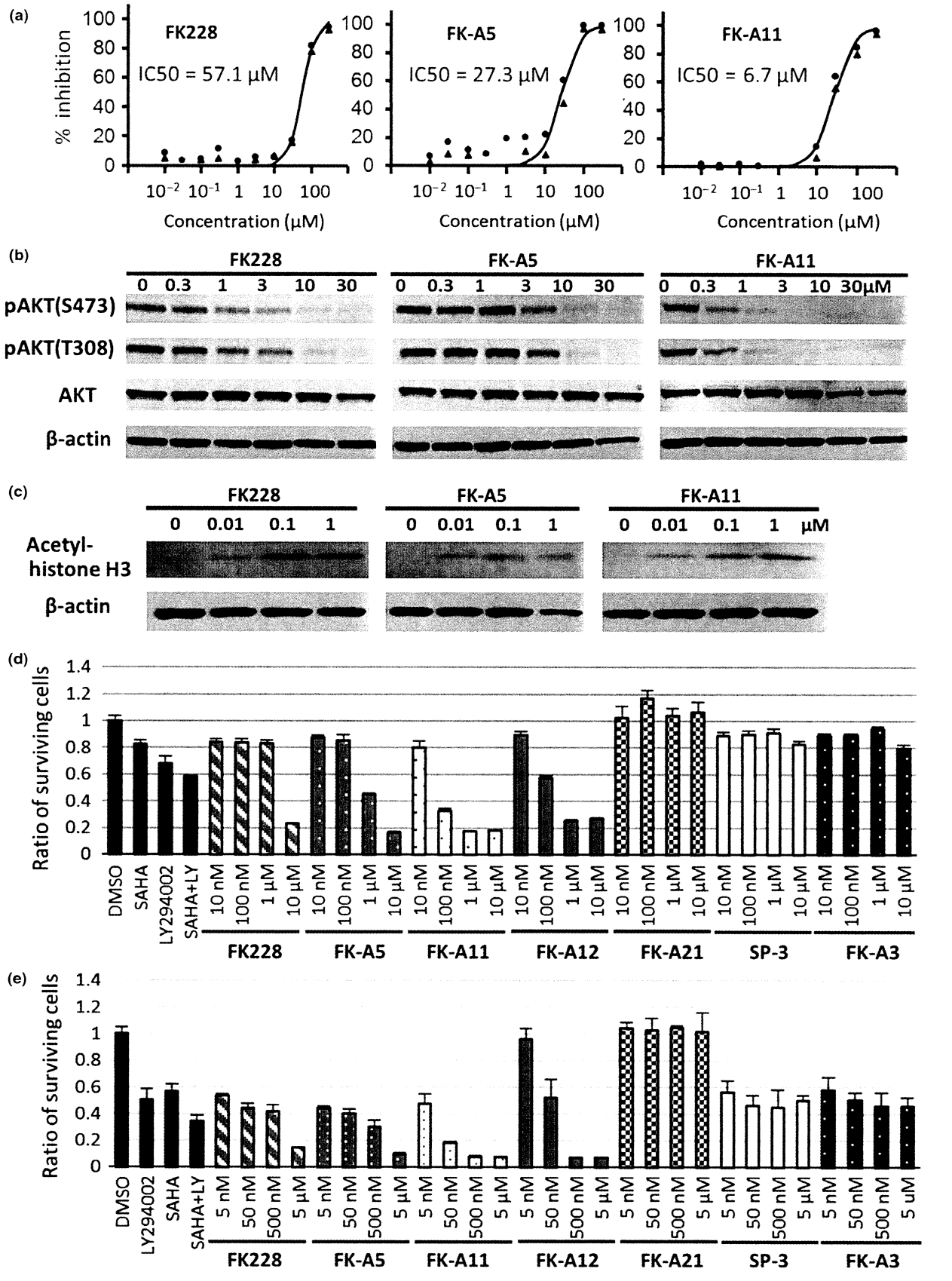
Compound		SP-1 spiruchostatin A	SP-2 spiruchostatin B	SP-3 5"epispiruchostatinB	**SP-4 spiruchostatin C**	SP-5 spiruchostatin D
IC50	HDAC1	3.3±0.51 nM	2.2 ± 0.12 nM	2.4 ± 0.35 nM	0.93 ± 0.20 nM	0.75 ± 0.18 nM
	P110α	41.4 μM	41.8 μM	107.0 μM	Not examined	Not examined
Structure						

Fig. 1. Chemical structures and IC_{50} values for p110α and HDAC1. The chemical structures of FK228 and the analogs are shown. The additional 14 analogs are written in bold letters on gray backgrounds. Their IC_{50} values for HDAC1 (mean ± SD) and for p110α are indicated. IC_{50} values for HDAC1 were assayed by Screening Committee of Anticancer Drugs (SCADS) and by using HDAC inhibitor screening kit. IC_{50} values were determined as the mean ± SD of the concentrations calculated from at least three independent dose-response curves. Inhibition of PI3K activity was evaluated by a mobility shift assay. Data are the mean of two experiments performed in duplicate. IC_{50} values were calculated from concentration versus % inhibition curves by fitting to a four-parameter logistic curve.

© 2014 The Authors. Cancer Science published by Wiley Publishing Asia Pty Ltd on behalf of Japanese Cancer Association.



© 2014 The Authors. Cancer Science published by Wiley Publishing Asia Pty Ltd on behalf of Japanese Cancer Association.

Fig. 2. Effects of FK228, FK-A5 and FK-A11 on inhibition of PI3K activity and cell proliferation. (a) Inhibition of PI3K activity was evaluated by a mobility shift assay. The activity in the control reaction was defined as 0% inhibition. Percent inhibition of each test reaction was calculated. The experiments were carried out in duplicate. The two independent percent inhibition values for each concentration were plotted. (b) Western blot analysis of phosphorylated AKT in PC3 cells. Cells were treated for 3 h with various concentrations of FK228, FK-A5 and FK-A11. (c) Western blot analysis of acetyl-histone H3 in PC3 cell. Cells were treated for 3 h with various concentrations of FK228, FK-A5 and FK-A11. (d) PC3 cell proliferation assay. Cells were treated for 24 h with DMSO, 50 μM LY294002 (LY), 2.5 μM SAHA, a combination of 50 μM LY and 2.5 μM SAHA, FK228, FK-A5 and FK-A11 at concentrations of 10 and 100 nM and 1 and 10 μM. The ratio of surviving cells to the control treated with 1% DMSO was calculated. (e) HCT116 cell proliferation assay. Cells were treated for 24 h with 0.5% DMSO as the control, 50 μM LY, 2.5 μM SAHA, a combination of 50 μM LY and 2.5 μM SAHA, FK228, FK-A5, FK-A11, FK-A12, FK-A21, SP-3 and FK-A3 at concentrations of 5, 50 and 500 nM and 5 μM.

even at concentrations of 1 and 10 μM (Fig. 2d). Similar cytotoxic effects of FK228 analogs were observed in HCT116 cells that were more sensitive to HDAC inhibitors than PC3 cells (Fig. 2e). These results indicate that PI3K inhibition clearly potentiates the cytotoxic effect of HDAC inhibition, and that FK-A11 is the most potent inhibitor. FK-A21 with PI3K inhibitory activity and without HDAC inhibitory activity exhibited no cytotoxic effect (Fig. 2d,e). Moreover, FK-A21 did not inhibit AKT phosphorylation in cells in spite of PI3K inhibitory activity confirmed in the cell free mobility shift assay (Suppl. Fig. S1). DMSO had no toxicity on cell proliferation in both cell lines.

FK-A11, an ATP competitive PI3K inhibitor. We previously reported that FK228 binds to the ATP-binding pocket of p110α based on a study with a docking model. Furthermore, this model is supported by the fact that the PI3K inhibitory activity of FK228 was weakened at a high concentration of ATP in an *in vitro* assay.[17] We also predicted that FK-A5 would bind to the ATP-binding pocket of p110α.[22] To investigate whether FK-A11 is an ATP competitive PI3K inhibitor, an *in vitro* ATP competition assay and a docking simulation were performed. In the *in vitro* assay, the PI3K activity was measured at various concentrations of ATP in the absence and presence of increasing concentrations of FK-A11. Lineweaver–Burk plot analysis showed that FK-A11 changed K_m (the Michaelis constant) without affecting V_{max} (the max velocity), indicating the apparent mode of competitive inhibition with ATP (Fig. 3). In the docking model, FK-A11 was predicted to bind to the ATP-binding site of p110α, similarly to FK228 and FK-A5. FK-A11 occupied the ATP-binding pocket of p110α with its naphthalene moiety localized to a deep portion of the pocket (Fig. 4a–c). These results indicated that FK-A11 is an ATP competitive PI3K inhibitor.

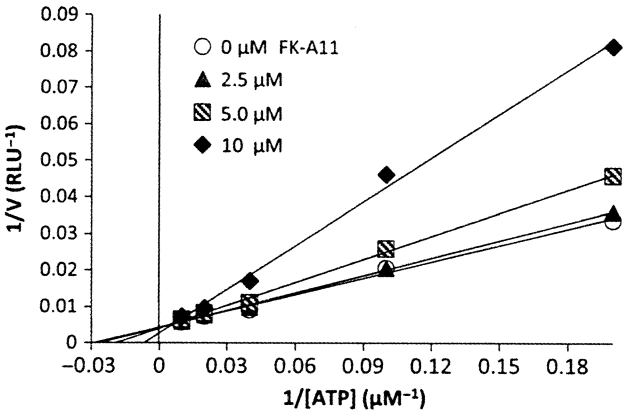


Fig. 3. Lineweaver–Burk plot of the inhibition of PI3K activity with FK-A11. PI3K activity assay was performed at five concentrations of ATP (5, 10, 25, 50 and 100 μM), 40 nM PI3Kα and 25 μM PIP2 in the absence or presence of increasing concentrations of FK-A11. $1/v$ (reaction velocity) was plotted versus 1/[ATP] (ATP concentration).

FK-A11, a selective PI3K kinase inhibitor. To elucidate the kinase selectivity, the inhibitory activities of FK-A11 for 21 kinases were assessed using a mobility shift assay. In addition, inhibition of mTOR activity was measured by using a K-LISA mTOR activity kit (Millipore). At a concentration of 10 μM, FK-A11 inhibited PI3K by 81%, whereas it inhibited the other 21 kinases by only 0–32.3% (Table 1). FK-A11 showed no mTOR inhibitory activity at 10 μM (Table 1), and very weak inhibitory activity even at higher concentrations of 50 and 100 μM (Suppl. Fig. S2). These results indicated that FK-A11 is a selective PI3K inhibitor.

FK-A11, a pan-PI3K inhibitor. The catalytic subunit of class I PI3K, p110 has four isoforms: α, β, γ and δ.[3] To investigate whether FK-A11 inhibits each isoform, an HTRF assay was performed. FK-A11 inhibited all four p110 isoforms similar to wortmannin, a pan-PI3K inhibitor (Fig. 5). The percent inhibition of each isoform, α, β, γ and δ by 3 μM FK-A11 was 41.2, 17.1, 10.5 and 32.9%, respectively (Fig. 5b). These results indicated that FK-A11 is a pan-PI3K inhibitor.

Effects of conformational changes of FK228 analogs on PI3K inhibitory activity. Reducing activity, such as that generated by glutathione reductase, changes FK228 to an open form, exposing the free sulfhydryl group that is involved in HDAC inhibition.[10] To investigate whether the conformational change by reduction is also related to PI3K inhibition, FK-A21 and FK-A22 were designed and synthesized based on the FK-A5 structure (Fig. 1). Because both FK-A21 and FK-A22 lack the internal disulfide bond, their conformations should not be affected by reduction. FK-A21 always retains the open form because the disulfide bond is replaced with two methylthio groups. In contrast, FK-A22 always retains the closed form because it has a lactone substructure. Both FK-A21 and FK-A22 did not inhibit HDAC activity because they lack free sulfhydryl groups (Fig. 1). In contrast, the IC_{50} values of FK-A21 and FK-A22 for PI3K were approximately equivalent to that of FK-A5 (Fig. 1). These results indicated that the conformational change induced by reduction does not affect PI3K inhibitory activity, and that the active site of FK228 analogs for PI3K inhibition is different from that for HDAC inhibition.

Evaluation of the binding affinities of FK228, FK-A5 or FK-A11 for PI3K and its drug-resistant mutants using computational docking simulations. To investigate whether FK-A11 interacts with PI3K similar to FK228 and FK-A5, Chemgauss 4 scores that indicate the intensity of the binding affinity were calculated in computational docking simulations. The scores showed that FK-A11 has a higher affinity for PI3K than FK228 and FK-A5, in accordance with the results of an *in vitro* kinase assay (Table 2 and Fig. 2a). Drug resistant PI3K mutants have been discovered by *PIK3CA* mutagenesis in yeast. The mutants were I800L and I800M with substitution of isoleucine located in the ATP-binding pocket of p110α.[23] Computational docking simulations of the two PI3K mutants and FK-A11 were carried out, so that Chemgauss 4 scores showed reduced affini-

© 2014 The Authors. Cancer Science published by Wiley Publishing Asia Pty Ltd on behalf of Japanese Cancer Association.

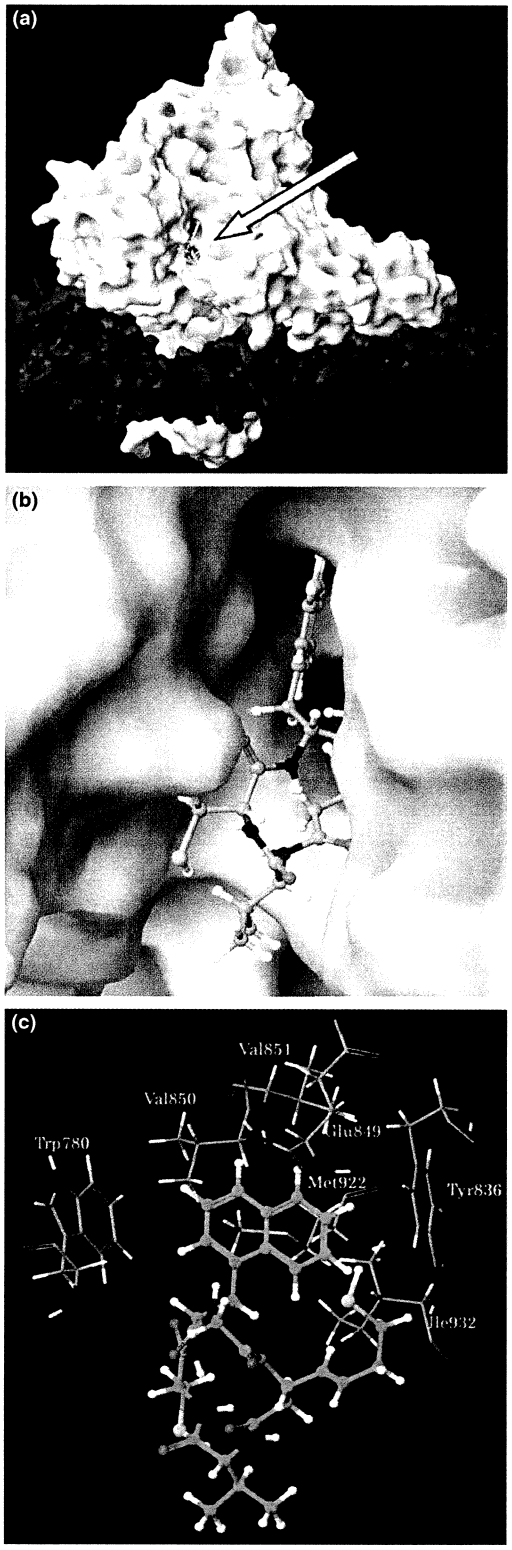


Fig. 4. Molecular modeling of PI3K-FK-A11 complex. (a) Molecular surface structure. White and red components represent p110α and p85α, respectively. FK-A11 in the complex is indicated by the yellow arrow. (b) The enlarged picture around FK-A11 in the ATP-binding pocket. (c) Hydrophobic amino acids around the naphthalene ring of FK-A11 in the PI3K-FK-A11 complex.

Table 1. Inhibitory activities of FK-A11 for 22 kinases

Kinase	% inhibition at 10 μM FK-A11
ABL	12.6
ALK	13.6
EML4-ALK	0.3
EGFR	3.4
FGFR1	15.3
FLT3	4.7
IGF1R	−3.8
JAK3	2.6
MET	0.3
PDGFRα	5.4
SRC	−1.5
AKT1	0.4
BRAF	19.9
Erk1	5.3
Erk2	6.5
MAP2K1(MEK)	30.9
MAP3K1	32.3
MAP3K2	18.8
p38α	7.1
RAF1	20.5
PI3K(p110α)	81
mTOR	−7.6

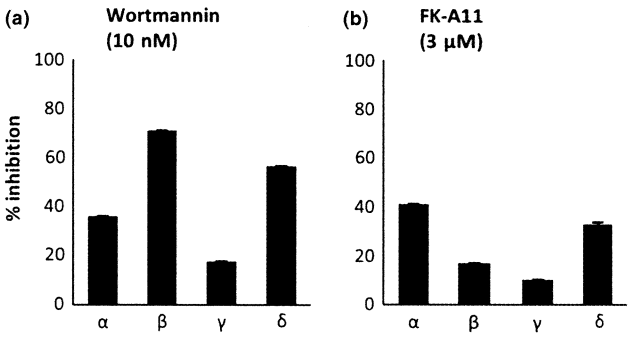


Fig. 5. Inhibition profiles of FK-A11 for p110α isoforms. Enzyme activities of p110 isoforms, α, β, γ and δ, were measured using a homogenous time-resolved fluorescence (HTRF) assay. 10 nM wortmannin (a) or 3 μM FK-A11 (b) was incubated with a solution containing each PI3K isoform protein, 10 μM PIP2, 25 μM ATP and 2 mM DTT. Percent inhibition of the enzyme activity by the compounds was calculated with the following formula. Percent inhibition = [(readout value of inhibited activity − that of normal activity)/(readout value of biotinylated-PIP3 − that of normal activity)] × 100.

Table 2. Binding affinity of FK228 and its analogs to PI3K based on computational docking simulations using FRED program

PI3K-ligand complex	Chemgauss 4 score†
PI3K–FK228	−4.33
PI3K–FK-A5	−5.2
PI3K–FK-A11	−8.95
PI3K(p110α I800L)–FK-A11	−2.17
PI3K(p110α I800M)–FK-A11	−1.41

†Lower score means higher affinity.

© 2014 The Authors. Cancer Science published by Wiley Publishing Asia Pty Ltd on behalf of Japanese Cancer Association.

ties of FK-A11 for these mutants compared with wild type p110α (Table 2). These results indicated that stronger PI3K inhibition by FK-A11 is based on stronger binding to the ATP-binding pocket of PI3K.

Evaluation of the binding affinities of FK228 and FK-A11 for HDAC1 using computational docking simulations. We generated molecular docking models of HDAC1-FK228 (data not shown) and HDAC1-FK-A11 complexes (Fig. 6). Subsequently calculated Chemgauss 4 scores showed higher binding affinity of FK-A11 than that of FK228 for HDAC1 (Table 3). In a molecular model of HDAC1-FK-A11 complex, the free sulfhydryl group of FK-A11 interacted with the active-site zinc. Moreover, the naphthylmethyl group of FK-A11 interacted with Tyr204 or Cys273 in HDAC1 (Fig. 6).

Discussion

We have previously identified FK228 and its analogs as HDAC/PI3K dual inhibitors.[17] In this study, we investigated the biochemical, biological and structural properties of FK228 analogs, focusing on FK-A11, from the viewpoint of the kinase inhibitory activities. In search for novel analogs, we identified FK-A11 as the most potent HDAC/PI3K dual inhibitor. FK-A11 inhibits PI3K with 8.5-fold more potency, and inhibits HDAC1 with 5.6-fold more potency than FK228. As a kinase inhibitor, FK-A11 highly selectively inhibited PI3K among 22 kinases tested (Table 1). Based on pharmacokinetic properties and isoform selectivity for the ATP-binding site, PI3K inhibitors have been classified into the following three groups.[6,24] The first group of inhibitors are pan-PI3K inhibitors, which are able to bind to all class I PI3K and include LY294002, wortmannin, GDC-0941 and ZSTK474.[24–26] The second group of inhibitors are isoform-specific inhibitors which have been developed to overcome the toxicity of a pan-PI3K inhibitor and include idelalisib (CAL-101), which targets p110δ.[27] The third group of inhibitors is PI3K/mTOR dual inhibitors that share similar structures in the ATP-binding sites of PI3K and mTOR. FK-A11 inhibited all four of the class I PI3K isoforms (Fig. 5). In contrast, FK-A11 did not inhibit mTOR (Table 2). Therefore, FK228 analogs are classified as pan-PI3K inhibitors.

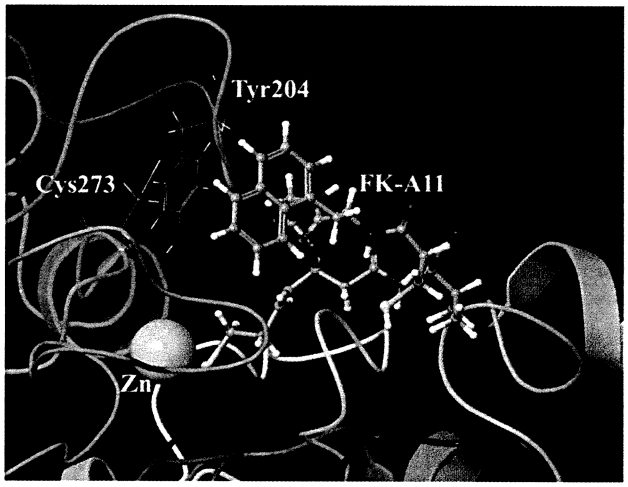


Fig. 6. Molecular modeling of HDAC1-FK-A11 complex. The enlarged picture around the active-site zinc and FK-A11. The sulfhydryl group of FK-A11 interacted with zinc. The naphthylmethyl group of FK-A11 was located closely to Tyr204 and Cys273.

Table 3. Binding affinity of FK228 and FK-A11 to HDAC1 based on computational docking simulations using FRED program

HDAC1-ligand complex	Chemgauss 4 score†
HDAC1–FK228	0.198
HDAC1–FK-A11	−1.771

†Lower score means higher affinity.

Considerable interest has centered on the effect of reduction on PI3K inhibitory activity, because reductase activity changes FK228 to an open structure that is active for HDAC inhibition.[10] To elucidate the effect of reduction, we synthesized FK-A21 and FK-A22 with conformations that are not affected by reduction. Both compounds inhibited PI3K, but did not inhibit HDAC as expected (Fig. 1). Despite the PI3K inhibitory activity confirmed in the cell free mobility shift assay, FK-A21 exhibited no activity in cells (Fig. 2 and Suppl. Fig. S1). We assumed that this depends on the instability of FK-A21 in cells: as previously reported, the reduced open form of FK228 increases the instability in cells.[10] Our results indicate that the potential structural site for PI3K inhibition is different from that for HDAC inhibition.

All previously described PI3K inhibitors bind to the ATP-binding site of the p110.[28–30] FK-A11 is also an ATP competitive PI3K inhibitor based on the results of the ATP competition assay and the docking simulation (Figs 3 and 4). In the docking simulations, FK-A11 has higher affinity to PI3K than FK228 and FK-A5 (Table 2). This result correlates with the potency of PI3K inhibitory activity. The surface of the ATP-binding pocket in p110α is surrounded by hydrophobic residues, and there is some space created by the hydrophobic residues around the naphthalene ring of FK-A11 (Fig. 4c). The interaction between the aromatic rings of the ligand and the hydrophobic aromatic residues of the internal binding pocket, the so-called π–π staking interaction, may play an important role in allowing for higher affinity. The naphthalene ring of FK-A11 could approach closer to the hydrophobic aromatic residues of the ATP-binding pocket, and could confer a stronger π–π stacking interaction than the phenyl ring of FK-A5. Similarly, in docking simulations for HDAC1, FK-A11 had higher affinity than FK228 (Table 3). The naphthalene ring of FK-A11 might contribute to higher affinity not only for PI3K but also for HDAC1 (Fig. 6).

When compared to combination therapy involving several drugs, a single dual target inhibitor is expected to have advantages, such as a simpler pharmacokinetic property, lower toxicity, higher compliance and more efficient clinical benefit.[16] Therefore, development of the dual target inhibitor will provide an attractive novel drug for cancer therapy. Because the combination of an HDAC inhibitor and a PI3K inhibitor induces apoptosis in a synergistic manner, development of an HDAC/PI3K dual inhibitor is especially attractive. We anticipate that our investigation might prompt ideas for the further development of novel analogs as HDAC/PI3K dual inhibitors.

Acknowledgments

This work was supported by the Ministry of Education, Culture, Sports, Science and Technology (MEXT) KAKENHI grant numbers 24300339, 25830110 and 26460034, and the Gonryo Medical Foundation.

© 2014 The Authors. Cancer Science published by Wiley Publishing Asia Pty Ltd on behalf of Japanese Cancer Association.

Disclosure Statement

Chikashi Ishioka received research grants from Chugai Pharmaceutical Co., Ltd., Taiho Pharmaceutical Co., Ltd., Daiichi-Sankyo Co., Ltd. and Merck Serono Co., Ltd. The other authors have no conflict of interest to declare.

References

1 Fruman DA, Meyers RE, Cantley LC. Phosphoinositide kinases. *Annu Rev Biochem* 1998; **67**: 481–507.
2 Cantley LC. The phosphoinositide 3-kinase pathway. *Science* 2002; **296**: 1655–7.
3 Hennessy BT, Smith DL, Ram PT, Lu Y, Mills GB. Exploiting the PI3K /AKT pathway for cancer drug discovery. *Nat Rev Drug Discov* 2005; **4**: 988–1004.
4 Samuels Y, Wang Z, Bardelli A *et al.* High frequency of mutations of the PIK3CA gene in human cancers. *Science* 2004; **304**: 554.
5 Vogt PK, Gymnopoulos M, Hart JR. PI 3-kinase and cancer: changing accents. *Curr Opin Genet Dev* 2009; **19**: 12–7.
6 Martini M, Ciraolo E, Gulluni F, Hirsch E. Targeting PI3K in cancer: any good news? *Front Oncol* 2013; **3**: 108.
7 West AC, Johnstone RW. New and emerging HDAC inhibitors for cancer treatment. *J Clin Invest* 2014; **124**: 30–9.
8 Bolden JE, Peart MJ, Johnstone RW. Anticancer activities of histone deacetylase inhibitors. *Nat Rev Drug Discov* 2006; **5**: 769–84.
9 Lane AA, Chabner BA. Histone deacetylase inhibitors in cancer therapy. *J Clin Oncol* 2009; **27**: 5459–68.
10 Furumai R, Matsuyama A, Kobashi N *et al.* FK228 (depsipeptide) as a natural prodrug that inhibits class I histone deacetylases. *Cancer Res* 2002; **62**: 4916–21.
11 Bertino EM, Otterson GA. Romidepsin: a novel histone deacetylase inhibitor for cancer. *Expert Opin Investig Drugs* 2011; **20**: 1151–8.
12 Mummaneni P, Shord SS. Epigenetics and oncology. *Pharmacotherapy* 2014; **34**: 495–505.
13 Nakagawa T, Takeuchi S, Yamada T *et al.* EGFR-TKI resistance due to BIM polymorphism can be circumvented in combination with HDAC inhibition. *Cancer Res* 2013; **73**: 2428–34.
14 Chakraborty AR, Robey RW, Luchenko VL *et al.* MAPK pathway activation leads to Bim loss and histone deacetylase inhibitor resistance: rationale to combine romidepsin with an MEK inhibitor. *Blood* 2013; **121**: 4115–25.
15 Yoshioka T, Yogosawa S, Yamada T, Kitawaki J, Sakai T. Combination of a novel HDAC inhibitor OBP-801/YM753 and a PI3K inhibitor LY294002 synergistically induces apoptosis in human endometrial carcinoma cells due to increase of Bim with accumulation of ROS. *Gynecol Oncol* 2013; **129**: 425–32.
16 Qian C, Lai CJ, Bao R *et al.* Cancer network disruption by a single molecule inhibitor targeting both histone deacetylase activity and phosphatidylinositol 3-kinase signaling. *Clin Cancer Res* 2012; **18**: 4104–13.
17 Saijo K, Katoh T, Shimodaira H, Oda A, Takahashi O, Ishioka C. Romidepsin (FK228) and its analogs directly inhibit phosphatidylinositol 3-kinase activity and potently induce apoptosis as histone deacetylase/phosphatidylinositol 3-kinase dual inhibitors. *Cancer Sci* 2012; **103**: 1994–2001.
18 Narita K, Kikuchi T, Watanabe K *et al.* Total synthesis of the bicyclic depsipeptide HDAC inhibitors spiruchostatins A and B, 5″-epi-spiruchostatin B, FK228 (FR901228) and preliminary evaluation of their biological activity. *Chemistry* 2009; **15**: 11174–86.
19 Kitagawa D, Yokota K, Gouda M *et al.* Activity-based kinase profiling of approved tyrosine kinase inhibitors. *Genes Cells* 2013; **18**: 110–22.
20 Kolossvary I, Guida WC. Low mode search. An efficient, automated computational method for conformational analysis: application to cyclic and acyclic alkanes and cyclic peptides. *J Am Chem Soc* 1996; **118**: 5011–9.
21 McGann MR, Almond HR, Nicholls A, Grant JA, Brown FK. Gaussian docking functions. *Biopolymers* 2003; **68**: 76–90.
22 Oda A, Saijo K, Ishioka C *et al.* Predicting the structures of complexes between phosphoinositide 3-kinase (PI3K) and romidepsin-related compounds for the drug design of PI3K/histone deacetylase dual inhibitors using computational docking and the ligand-based drug design approach. *J Mol Graph Model* 2014; **54**: 46–53.
23 Zunder ER, Knight ZA, Houseman BT, Apsel B, Shokat KM. Discovery of drug-resistant and drug-sensitizing mutations in the oncogenic PI3K isoform p110 alpha. *Cancer Cell* 2008; **14**: 180–92.
24 Akinleye A, Avvaru P, Furqan M, Song Y, Liu D. Phosphatidylinositol 3-kinase (PI3K) inhibitors as cancer therapeutics. *J Hematol Oncol* 2013; **6**: 88.
25 Folkes AJ, Ahmadi K, Alderton WK *et al.* The identification of 2-(1H-indazol-4-yl)-6-(4-methanesulfonyl-piperazin-1-ylmethyl)-4-morpholin-4-yl-t hieno[3,2-d]pyrimidine (GDC-0941) as a potent, selective, orally bioavailable inhibitor of class I PI3 kinase for the treatment of cancer. *J Med Chem* 2008; **51**: 5522–32.
26 Yaguchi S, Fukui Y, Koshimizu I *et al.* Antitumor activity of ZSTK474, a new phosphatidylinositol 3-kinase inhibitor. *J Natl Cancer Inst* 2006; **98**: 545–56.
27 Lannutti BJ, Meadows SA, Herman SE *et al.* CAL-101, a p110delta selective phosphatidylinositol-3-kinase inhibitor for the treatment of B-cell malignancies, inhibits PI3K signaling and cellular viability. *Blood* 2011; **117**: 591–4.
28 Walker EH, Pacold ME, Perisic O *et al.* Structural determinants of phosphoinositide 3-kinase inhibition by wortmannin, LY294002, quercetin, myricetin, and staurosporine. *Mol Cell* 2000; **6**: 909–19.
29 Vadas O, Burke JE, Zhang X, Berndt A, Williams RL. Structural basis for activation and inhibition of class I phosphoinositide 3-kinases. *Sci Signal* 2011; **4**: re2.
30 Kong D, Yamori T. ZSTK474 is an ATP-competitive inhibitor of class I phosphatidylinositol 3 kinase isoforms. *Cancer Sci* 2007; **98**: 1638–42.

Supporting Information

Additional supporting information may be found in the online version of this article:

Fig. S1. Western blot analysis of phosphorylated AKT and acetyl-histones in PC3 cells treated with FK-A5 or FK-A21.

Fig. S2. The effect of FK-A11 on inhibition of mTOR activity.

Doc. S1 Detailed materials and methods.

© 2014 The Authors. Cancer Science published by Wiley Publishing Asia Pty Ltd on behalf of Japanese Cancer Association.

Chemico-Biological Interactions 221 (2014) 24–34

Contents lists available at ScienceDirect

Chemico-Biological Interactions

journal homepage: www.elsevier.com/locate/chembioint

Spiruchostatin A and B, novel histone deacetylase inhibitors, induce apoptosis through reactive oxygen species-mitochondria pathway in human lymphoma U937 cells

Mati Ur Rehman [a], Paras Jawaid [b], Yoko Yoshihisa [a], Peng Li [b], Qing Li Zhao [b], Koichi Narita [c], Tadashi Katoh [c], Takashi Kondo [b,*], Tadamichi Shimizu [a]

[a] Department of Dermatology, Graduate School of Medicine and Pharmaceutical Science, University of Toyama, 2630 Sugitani, Toyama 930-0194, Japan
[b] Department of Radiological Sciences, Graduate School of Medicine and Pharmaceutical Science, University of Toyama, 2630 Sugitani, Toyama 930-0194, Japan
[c] Laboratory of Synthetic and Medicinal Chemistry, Faculty of Chemical Pharmaceutical Science, Tohoku Pharmaceutical University, Aoba-ku, Sendai 981-8558, Japan

ARTICLE INFO

Article history:
Received 14 May 2014
Received in revised form 30 June 2014
Accepted 11 July 2014
Available online 29 July 2014

Keywords:
Spiruchostatin A
Spiruchostatin B
HDAC inhibitors
Apoptosis
ROS

ABSTRACT

Spiruchostatin A (SP-A) and spiruchostatin B (SP-B) are the potent histone deacetylase inhibitors (HDACi), that has the potential for chemotherapy of leukemia but the exact mechanism of these compounds remains unclear. In the present study, the role of reactive oxygen species (ROS) production and the mechanism involved in the apoptosis was investigated in human lymphoma U937 cell. When the U937 cells were treated with SP-A and SP-B for 24 h at different concentrations, evidence of apoptotic features, including increase in DNA fragmentation and changes in nuclear morphology, were obtained. SP-B showed maximum potency to induce apoptosis, while SP-A was less potent. Apoptosis was also determined by increase in the fraction of sub-G1 cells and Annexin V-FITC staining cells. SP-A and SP-B induced apoptosis was accompanied by significant increase in the formation of intracellular reactive oxygen species (ROS). Pre-treatment with *N*-acetyl-L-cysteine (NAC), significantly inhibited the SP-A and SP-B mediated apoptosis, suggesting a vital role of ROS involved in the lethality of both agents. Moreover, SP-A and SP-B treatment resulted in the loss of mitochondrial membrane potential (MMP), and Fas, caspase-8 and caspase-3 activation. In addition Bid activation and the release of cytochrome-c to the cytosol was also observed. In this study, we suggest that a marked induction of intracellular ROS mediated mitochondrial pathway and the Fas plays a role in the SP-A and SP-B induced apoptosis. Taken together, our data provides further insights of the mechanism of action of SP-A and SP-B and their potential application as novel chemotherapeutic agents.

© 2014 Elsevier Ireland Ltd. All rights reserved.

1. Introduction

Acetylation and deacetylation of histones play a crucial role to control transcriptional activity of different genes through affecting the interaction between DNA and histones [1,2]. Histones acetylation and deacetylation is regulated by a balance between two specific enzymes, histone acetyltransferases (HATs) and histone deacetylase (HDAC) [3,4]. Aberrant regulation of HATs and HDAC activity has been reported to play an important role in uncontrolled cancer growth [5,6]. Increased HDAC activity was reported in several human cancer cell lines and therefore HDAC inhibition is considered as the novel strategy in the cancer treatment [7,8]. Recently, histone deacetylase inhibitors (HDACi) have gained much attention and emerged as promising anti-cancer agents [9], because of their diverse mode of action which include disruption of co-repressor complexes, ROS induction, death receptors up-regulation, generation of lipid second messengers (e.g. ceramide), interference with chaperone protein function [10,11]. Until now, several HDACi have been identified and on the basis of their structural features they were divided into different classes [12]. FK228 (romidepsin) and suberoylanilide hydroxamic acid (SAHA) has

Abbreviations: SP-A, Spiruchostatin A; SP-B, Spiruchostatin B; ROS, reactive oxygen species; HDAC, histone deacetylase; MMP, mitochondrial membrane potential; NAC, *N*-acetyl-L-cysteine; FITC, fluorescein isothiocyanate; HATs, histone acetyltransferases; HDACi, histone deacetylase inhibitors; CTCL, cutaneous T-cell lymphoma; SAHA, suberoylanilide hydroxamic acid; SCLC, small cell lung cancer; DCFH-DA, dichlorofluorescein diacetate; DMSO, dimethyl sulfoxide; DTT, dithiothreitol; HE, hydroethidine; pNA, chromophore p-nitroanilide; TCA, trichloroacetic acid; TMRM, tetramethylrhodamine methyl ester.

* Corresponding author. Tel.: +81 76 434 7267; fax: +81 76 434 5190.
E-mail address: kondot@med.u-toyama.ac.jp (T. Kondo).

http://dx.doi.org/10.1016/j.cbi.2014.07.004
0009-2797/© 2014 Elsevier Ireland Ltd. All rights reserved.

already been approved by US Food and Drug administration (FDA), for the treatment of cutaneous T cell lymphoma (CTCL) [13], and others such as valproic acid and MS-275 are still in clinical trials [13,14].

In spite of the fact that HDAC inhibitors are promising anti-cancer agents, the molecular mechanism involved in the cell death after treatment with HDAC inhibitors remain unclear, but the induction of oxidative stress seems to be common theme involved in the cell death caused by HDAC inhibitors [15]. In solid tumor and leukemia cells, HDAC inhibitors have been reported to induce apoptosis through ROS generation [16]. Recently, Spiruchostatin A and B, the structurally similar 15-membered bicyclic depsipeptides, were successfully isolated from a culture broth of *Pseudomonas* sp. [17]. Both agents were found to possess potent HDAC inhibitory activity and have the potential for chemotherapy of leukemia [18,19]. Previously, the HDAC inhibitory activity of these agents were tested against the panel of 39 cancer cell line, in which SP-B was found to be the most potent inhibitor of HDAC1 and it showed the most potent inhibitory activity as compared to other HDACi including FK228 and SP-A [19]. Like other HDACi, SP-A and SP-B also characterized by the biological effects which include growth inhibition, cell cycle arrest and induction of p21 expression [3,20].

The purpose of this study is to determine the possible apoptosis inducing activity of SP-A and SP-B, and the detail molecular mechanism involved. To date, no report has regarded the effects of these compounds on ROS production and apoptosis in human lymphoma U937 cells. Therefore, this study was undertaken to further clarify the molecular mechanism involved in the apoptosis induced by SP-A and SP-B in human lymphoma U937 cells.

2. Materials and methods

2.1. Chemicals

Spiruchostatin A and B were kindly provided by Prof. Tadashi Katoh (Faculty of Pharmaceutical Sciences, Tohoku Pharmaceutical University, Sendai, Japan). Both agents were dissolved in dimethyl sulfoxide (DMSO) and stored at −20 °C. The agents were diluted with culture media to prepare serial concentrations just before the use. The Annexin V-FITC kit was from Immunotech (Marseille, France). RNase A was purchased from Nacalai Tesque (Kyoto, Japan). DCFH-DA and HE was from molecular probes (Eugene). The FLICE/caspase-8 colorimetric protease assay kit was obtained from MBL (Nagoya, Japan). Antibodies against caspase-3, Bid, Bcl-2, Ac-H3, Ac-H4 and secondary horseradish peroxide (HRP)-conjugated anti-rabbit or anti-mouse IgG were obtained from Cell Signaling technology (Danvers M.A.). Anti-β-actin was from Sigma Aldrich (Saint Louis) and anti-cytochrome-c pAb, anti Bax and Fas were purchased from Santa Cruz Biotechnology Inc (CA). Anti caspase-8 was from R&D systems (Minneapolis, USA). All other reagents were of analytical grade.

2.2. Cell culture

A human myelomonocytic lymphoma cell lines, U937 and Molt-4 were obtained from Human Sciences Research Resource Bank (Japan Human Sciences Foundation, Tokyo, Japan). HL-60 cells were kindly provided as a gift by Emeritus Prof. Yoshisada Fujiwara, Kobe University. The cells were grown in RPMI 1640 culture medium supplemented with 10% heat-inactivated fetal bovine serum (FBS) at 37 °C in humidified air with 5% CO_2.

2.3. Cell cycle analysis

For flow cytometry, cells were fixed with 70% ice cold ethanol at least for 2 h or stored overnight at −20 °C, and subsequently treated with 0.25 mg/ml RNase A (Nacalai Tesque, Kyoto, Japan) and 50 μg/ml PI to obtain the distribution of PI-based cell-cycle phases. The samples were finally run on an Epics XL flow cytometer (Beckman Coulter, Fullerton, CA) [21].

2.4. DNA fragmentation assay

For the detection of apoptosis the percentage of DNA fragmentation was assessed up till 24 h post treatment using the method of Sellins and Cohen [22], with minor modifications. Briefly, approximately 3×10^6 cells were lysed using 200 μl of lysis buffer (10 mM Tris, 1 mM EDTA and 0.2% Triton X-100, pH 7.5) and centrifuged at 13,000*g* for 10 min. Subsequently, each DNA sample in the supernatant and the resulting pellet was precipitated in the 25% trichloroacetic acid (TCA) at 4 °C overnight and quantified using a diphenylamine reagent after hydrolysis in 5% TCA at 90 °C for 20 min. The percentage of fragmented DNA in each sample was calculated as the amount of DNA in the supernatant divided by total DNA for that sample (supernatant plus pellet).

2.5. Morphological detection of apoptosis

The morphological changes in the cells were examined by Giemsa staining. To identify the apoptotic cells after treatment with SP-A and SP-B, cells were harvested after 24 h of incubation at 37 °C, were washed with PBS and collected by centrifugation. Then the cells were fixed with methanol and acetic acid (3:1) and spread on the glass slides. After drying, staining was performed with 5% Giemsa solution (pH 6.8) for 5 min [23].

2.6. Detection of apoptosis using Annexin V-FITC/PI staining

To determine early apoptosis and secondary necrosis, phosphatidylserine (PS) externalization of apoptosis was determined by analysis of propidium iodide (PI) and fluorescein isothiocyanate (FITC)-labeled Annexin V (Immunotech, Marseille, France) using Flow cytometry (Epics XL, Beckman-Coulter, Miami, FL) [24] according to the instructions of the manufacturer. Briefly, cells were treated with SP-A and SP-B at different concentrations for 24 h at 37 °C, cells were collected, washed with cold PBS at 4 °C and centrifuged at 1200 rpm for 3 min. The resulting pellet was mixed with the binding buffer of the Annexin V-FITC kit. FITC-labeled Annexin V (5 μl) and PI (5 μl) were added to the 490 μl suspension and mixed gently. After incubation at 4 °C for 20 min in the dark, the cells were analyzed with a flow cytometry.

2.7. Assessment of intracellular reactive oxygen species (ROS)

Evaluation of intracellular H_2O_2 was performed by flow cytometry using the fluorescence generate in the cells loaded with the peroxide-sensitive fluorescent probe, a H_2O_2 sensitive dye, dichlorofluorescein diacetate (DCFH-DA) (Molecular probes, Eugene, OR). DCFH-DA rapidly diffuses in to the cytosol of cells where it is hydrolyzed to the non-fluorescent, oxidation sensitive DCFH. In the presence of cytosolic peroxide, DCFH is rapidly oxidized to the non-diffusible, fluorescent DCF.

Briefly, after treatment with SP-A and SP-B for different time periods, the cells were collected and washed with PBS, and were stained with 10 μM of DCFH-DA at 37 °C for 30 min. The fraction of DCF fluorescence positive cells was measured by flow cytometry as the proportion of cells containing intracellular H_2O_2 [25].

Hydroethidine (HE, Molecular Probes, Eugene) was used to determine superoxide generation using the method of Gorman et al [26].

2.8. Measurement of mitochondrial membrane potential (MMP)

To measure changes in MMP, U937 cells were harvested at different time periods and stained with 10 nM tetramethylrhodamine methyl ester (TMRM) (Molecular Probes) for 15 min at 37 °C in 1 ml of PBS, followed by the immediate flow cytometry of red TMRM fluorescence (excitation at 488 nm; emission at 575 nm).

2.9. Measurement of caspase-8 activity

To measure caspase-8 activity, a FLICE/caspase-8 colorimetric protease assay kit (MBL, Nagoya, Japan) was used according to manufacturer's instructions. The assay is based on the spectrophotometric detection of chromophore p-nitroanilide (pNA), a substrate of activated caspase-8. The pNA absorbance was quantified using a spectrophotometer at a wavelength of 400 nm (Beckman Instruments Inc., Fullerton, CA) [27].

2.10. Western blot analysis for proteins

Cells were collected and washed with cold PBS. They were lysed at a density of 2.5×10^6 cells/70 μl of RIPA buffer (50 mM Tris–HCl, 150 mM NaCl, 1% Nonidet P-40 (v/v), 1% sodium deoxycholate, 0.05% SDS, 1 μg of each aprotinin, pepstatin and leupeptin and 1 mm phenylmethyl sulfonyl fluoride) for 20 min. Following brief sonification, the lysates were centrifuged at 12,000g for 10 min at 4 °C, and the protein content in the supernatant was measured using the Bio- Rad protein assay kit (Bio-Rad, Hercules, CA). Protein lysates were denatured at 96 °C for 5 min after mixing with 2 μl SDS-loading buffer, applied on an SDS polyacrylamide gel for electrophoresis, and transferred to nitrocellulose membrane. Western blot analysis was performed to detect caspase-3, caspase-8, Bid, Bax, Bcl-2, Fas, Ac-H3 and Ac-H4 expression using specific antibodies. Blots were then probed with either secondary horseradish peroxide (HRP)-conjugated anti-rabbit or anti-mouse IgG antibodies obtained from Cell Signaling. Band signals were visualized on a luminescent image analyzer (LAS 4000, Fujifilm Co., Tokyo, Japan) by using chemiluminescence ECL detection reagents (Amersham Biosciences, Buckinghamshire, UK).

For the preparation of cytosolic extracts, 5×10^7 cells were harvested and washed with 10 ml ice-cold PBS then centrifuged at 600g for 5 min and the supernatant was removed. Cells were re-suspended in 300 μl of 1× Cytosol Extraction Buffer Mix containing DTT and a Protease inhibitor according to the manufacturer's instruction and then incubated on ice for 10 min. Cells were homogenized in an ice-cold dounce tissue grinder and then centrifuged at 3000 rpm for 10 min at 4 °C to remove nuclei and debris. The supernatant was collected and centrifuged again at 13,000 rpm for 30 min at 4 °C. The resulting supernatant was used as the soluble cytosolic fraction. Protein contents in cytosolic fraction were determined as described above. Following SDS–PAGE, Western blotting was performed to detect cytochrome-c release into cytosol using anti-cytochrome-c pAb (Santa Cruz Biotechnology Inc., Santa Cruz, CA) and anti-β-actin mAb was used as a control (Sigma).

2.11. Statistical analysis

All values are expressed as the means ± S.D. of the respective test or control group. Statistical significance between the control group and test groups was evaluated by either Student's *t*-test or one-way ANOVA. Values of $p < 0.05$ were considered to be significant. All experiments were performed in triplicate.

3. Results

3.1. Induction of apoptosis by SP-A and SP-B

The chemical structures of the HDAC inhibitors used in this study are shown in (Fig. 1). U937 cells were treated in a concentration-dependent manner for 24 h, followed by the colorimetric DNA fragmentation assay, a hallmark of apoptosis. As illustrated in Fig. 2 A, the results showed significant increase in the DNA fragmentation (%) with SP-A 30 nM and SP-B at 10 and 30 nM concentration as compared to control, respectively. While, 10 nM of SP-A does not induced any cell death in U937 cells. Further time-dependent analysis considering these two doses showed no DNA fragmentation at initial 6 and 12 h. However, DNA fragmentation was apparent at 18 h and increased at 24 h with SP-B (10 and 30 nM) and SP-A (30 nM) treatment (Fig. 2B and C). Thus, 10 and 30 nM of SP-A and SP-B were often used in this study. DNA fragmentation analysis was also done using human promyelocytic leukemia cells (HL-60) and Molt-4 cells. Both SP-A and SP-B induced apoptosis in a similar manner with those observed in U937 cells. Taken together these findings indicate that SP-A and SP-B induce apoptosis in human leukemia cells in a concentration- and time-dependent manner (Fig. 2D and E).

Increased apoptosis was observed in U937 cells, as evidenced by DNA fragmentation analysis. Human lymphoma U937 cells were most susceptible to SP-A and SP-B treatment as compared to Molt-4 and HL-60 cells. Based on the finding U937 cells were selected to evaluate the detail mechanism involved in the apoptosis induced by SP-A and SP-B.

Further, to examined the HDAC inhibition we analyzed the effects of SP-A and SP-B on acetylation of histones using Western blot, time dependent increase in the acetylated histone H3 and H4 levels were seen with SP-A and SP-B 30 nM (Fig. 2F).

The cell morphology indicate that cells treated with SP-A and SP-B for 24 h showed typical signs of apoptosis, i.e. cytoplasmic aggregation, nuclear condensation, and fragmentation (Fig. 3A). Even at higher concentration of 100 nM, no signs of necrosis were observed (data not shown). Annexin V-FITC and PI double staining has been used extensively to distinguish between cells in early and late apoptosis. In this study we measured early and late apoptosis induced by SP-A (3–30 nM) and SP-B (3–30 nM) for 24 h in U937 cells. Flow cytometry using Annexin V-FITC and PI staining showed that treatment with SP-A (30 nM) and SP-B (10, 30 nM) caused significant apoptosis in U937 cells compared to control in a concentration dependent manner ($p < 0.01$). Interestingly, SP-B 10 nM induced significantly higher apoptosis than that of SP-A 10 nM (Fig. 3B and C).

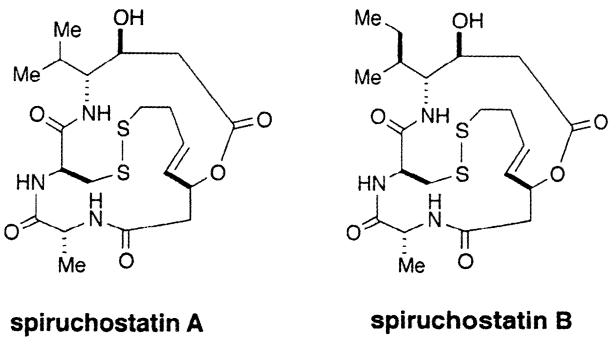


Fig. 1. Chemical structure of the Spiruchostatin A and Spiruchostatin B.

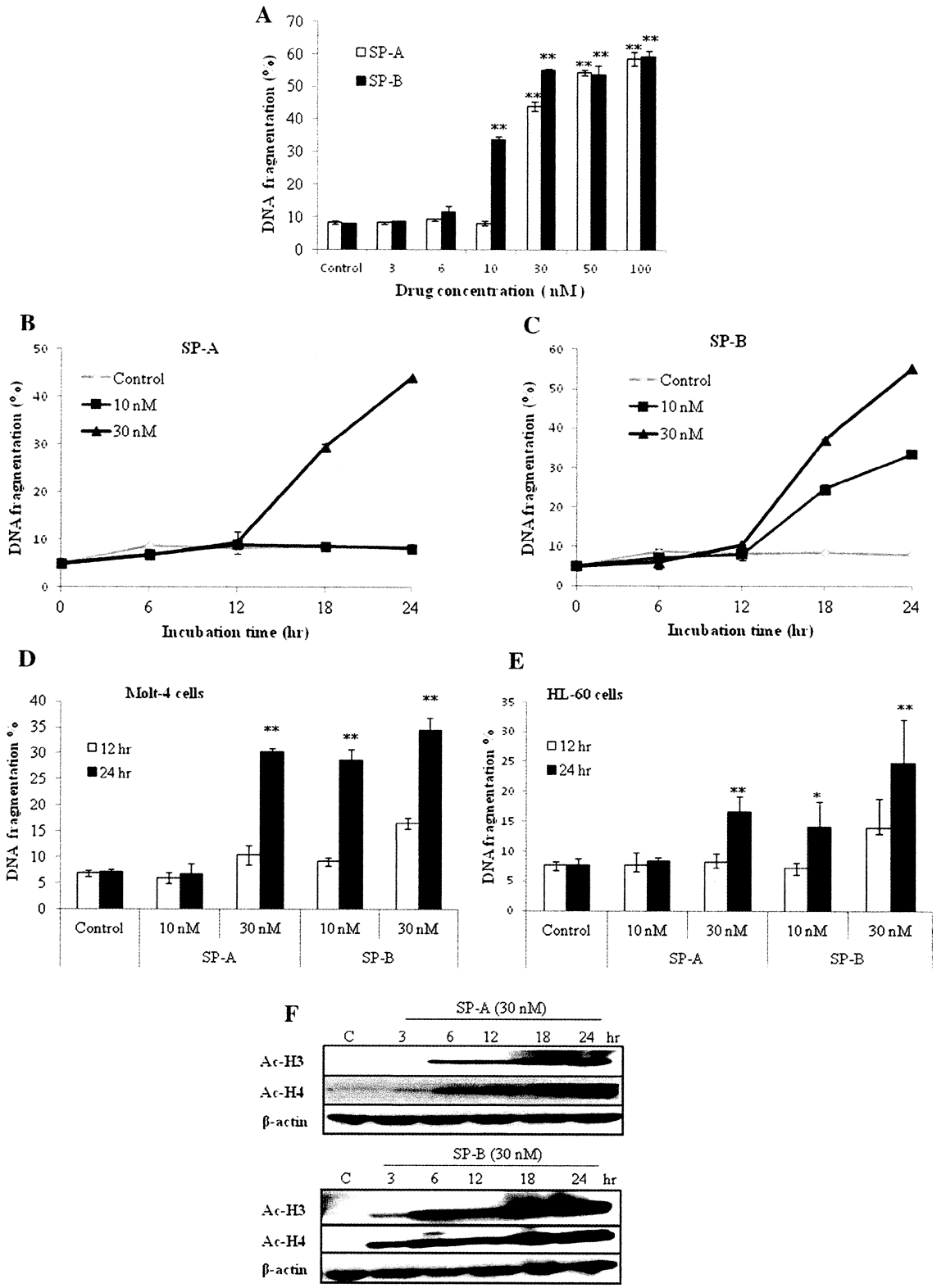


Fig. 2. DNA fragmentation induced by SP-A and SP-B. (A) U937 cells were treated with SP-A and SP-B at different concentrations (3–100 nM) for 24 h followed by DNA fragmentation assay. (B) Time-dependent induction of DNA fragmentation by SP-A 10 and 30 nM in U937 cells. (C) Time-dependent induction of DNA fragmentation by SP-B 10 and 30 nM in U937 cells. (D) Molt-4 cells were treated with SP-A and SP-B 10 and 30 nM for 12 and 24 h followed by DNA fragmentation assay. (E) HL-60 cells were treated with SP-A and SP-B 10 and 30 nM for 12 and 24 h followed by DNA fragmentation assay. (F) SP-A and SP-B 30 nM caused a time-dependent increase in acetylated histone H3 and acetylated histone H4 levels. Where indicated, values for the treated cells are significantly different to the untreated cells at the same time point at $^{*}p < 0.05$; $^{**}p < 0.01$. The results are presented as the mean ± S.D. ($n = 3$).

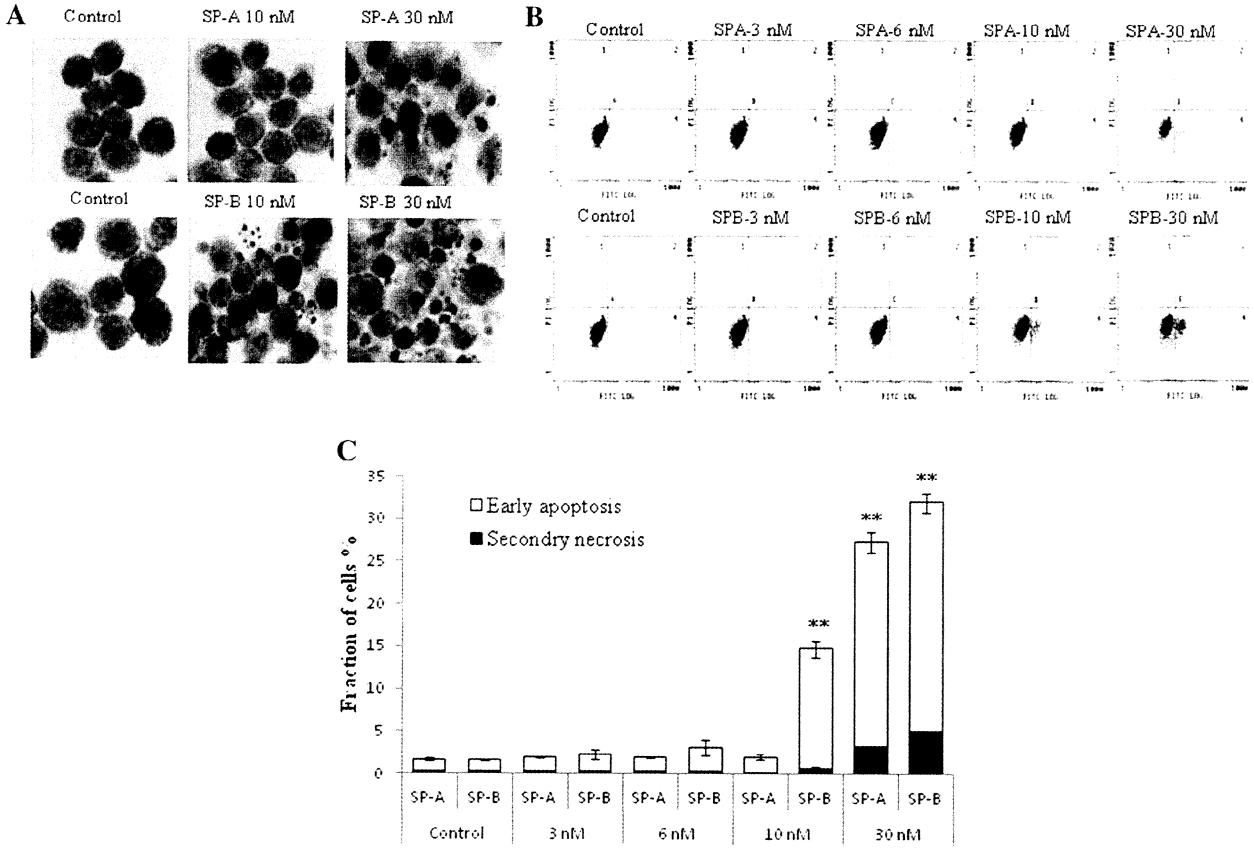


Fig. 3. Assessment of apoptosis. (A) Morphological features of apoptosis after treatment of U937 cells with 10 and 30 nM SP-A and SP-B for 24 h. Signs of apoptosis were detected by Giemsa staining and then examined under microscope at ×400 magnification. (B) Representative flow cytometric histograms of Annexin V-FITC/PI staining are shown (C) U937 cells were treated with 3, 6, 10 and 30 nM SP-A and SP-B. The cells were stained with Annexin V-FITC and PI for flow cytometry after 24 h. Where indicated, values for the treated cells are significantly different to the untreated cells at the same time point at $^{*}p < 0.05$; $^{**}p < 0.01$.

3.2. Effects of SP-A and SP-B on cell cycle distribution

Cell cycle distributions were examined in SP-A and SP-B treated U937 cells. U937 cells were treated with or without SP-A and SP-B (10 and 30 nM) for 18 and 24 h. As shown in Table 1, after 24 h incubation, the percentage of cells in sub-G1 population increased from 2.3 ± 1.2% to 27.0 ± 6.4% with SP-A 30 nM, from 3.0 ± 0.2% to 25.1 ± 1.9% with SP-B 10 nM and 36.7 ± 0.8% with SP-B 30 nM as compared to control. This increase in the percentage of sub-G1 population was determined by a decrease of cells in the G1 and G_2/M phases, which was caused by apoptosis.

3.3. SP-A and SP-B induced ROS generation in U937 cells

Induction of ROS has been implicated in the lethality of several HDACs inhibitors, however a detailed analysis of its role in SP-A and SP-B induced apoptosis has not been studied yet. Exposure of U937 cells with SP-A and SP-B 30 nM does not induce any profound change in ROS production at initial 3 and 6 h but a peak in the ROS generation was observed at 14 h with both the agents, more profound increased in the ROS production was observed with SP-B 30 nM as evidenced by the oxidation-sensitive dye dichlorofluorescein diacetate (DCFH-DA) (Fig. 4A–C). To confirm the role

Table 1
Cell cycle analysis by flow-cytometry. Data are mean ± S.D.; $n = 3$.

	18 h				24 h			
	SubG1 (%)	G0/G1 (%)	S (%)	G2/M (%)	SubG1 (%)	G0/G1 (%)	S (%)	G2/M (%)
SP-A								
Control	2.5 ± 0.7	37.6 ± 2.5	33.5 ± 0.8	19.7 ± 0.8	2.3 ± 1.2	36.5 ± 3	34.5 ± 1.3	23.5 ± 0.6
10 nM	2.0 ± 0.3	36.4 ± 4.9	33.3 ± 1.0	21.0 ± 4.8	2.9 ± 1.4	35.0 ± 4.7	34.4 ± 3.4	23.8 ± 2.0
30 nM	7.9 ± 0.2	14.8 ± 1.9	44.7 ± 1.6	24.0 ± 1.1	**27.0 ± 6.4****	18.2 ± 2.3	37.0 ± 3.9	16.7 ± 2.9
SP-B								
Control	2.1 ± 0.8	39.0 ± 3.1	33.5 ± 0.8	19.7 ± 0.8	3.0 ± 0.2	36.3 + 3.3	34.5 ± 1.3	23.0 ± 1.0
10 nM	**5.3 ± 1.7***	22.3 ± 5.1	39.4 ± 6.0	25.7 ± 1.4	**25.1 ± 1.9****	25.3 ± 4.6	35.8 ± 4.1	17.0 ± 3.0
30 nM	**12.3 ± 2.7****	13.1 ± 2.3	46.8 ± 5.6	17.4 ± 3.1	**36.7 ± 0.8****	19.2 ± 2.3	37.3 ± 5.0	10.0 ± 1.0

* $p < 0.05$ vs control.
** $p < 0.01$ vs control.

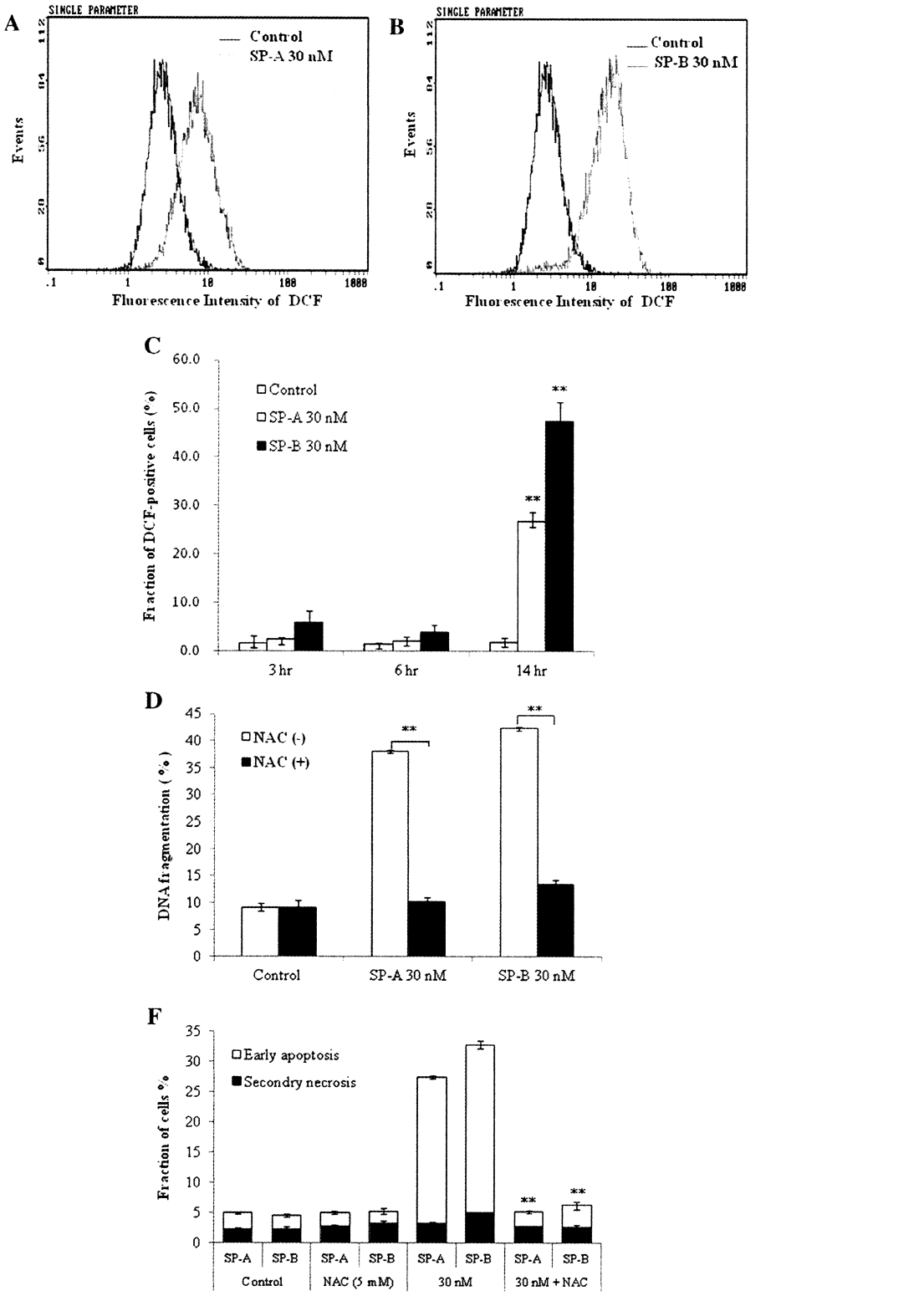


Fig. 4. Effects of SP-A and SP-B on generation of intracellular ROS in U937 cells. (A and B) U937 cells were treated with 30 nM SP-A and SP-B for 14 h. SP-A and SP-B treated U937 cells exhibited an increase in DCF fluorescence compared with the control cells. One representative photomicrograph from three independent experiments is shown. (C) Induction of intracellular ROS generation by SP-A and SP-B. U937 cells were treated with SP-A and SP-B 30 nM for 3, 6 and 14 h. The cells were subjected to 10 μM DCFH-DA staining, were incubated at 37 °C for 30 min before measuring of the intracellular ROS by flow cytometry. Where indicated, values for the treated cells are significantly different to the untreated cells at the same time point at $^{**}p < 0.01$. The results are expressed as means ± S.D. ($n = 3$). (D and E) U937 cells were pre-treated with or without 5 mM NAC for 1 h and stimulated with SP-A and SP-B 30 nM for 24 h followed by measurement of apoptosis with DNA fragmentation assay and Annexin V-FITC/PI staining, $^{**}p < 0.01$ as compared to treatment alone. The results are expressed as means ± S.D. ($n = 3$).

of ROS production in the apoptosis induced by SP-A and SP-B, cells were pre-treated with 5 mM NAC (*an antioxidant, N-acetyl-L-cysteine*) for 1 h. NAC pre-treatment significantly inhibited the apoptosis induced by SP-A and SP-B ($p < 0.01$) (Fig. 4D and E), suggesting a crucial role of ROS generation in the apoptosis induction by these agents.

3.4. Measurement of mitochondrial membrane potential

To assess the effects of SP-A and SP-B on the mitochondrial apoptotic pathway, mitochondrial membrane potential of U937 cells treated with SP-A (10, 30 nM) and SP-B (10, 30 nM) was evaluated. A significant time and concentration-dependent MMP loss was observed (Fig 5C and D).

3.5. Effects of SP-A and SP-B on activation of extrinsic pathway of apoptosis

To determine the involvement of extrinsic pathway of apoptosis, effects of SP-A and SP-B on Fas and caspase 8 were investigated. The Fas receptor is a death receptor on the surface of cells that leads to one of the apoptotic pathways, extrinsic pathway, through DISC assembly and subsequent caspase-8 activation. SP-A and SP-B induced a clear time-dependent increase in the protein expression of Fas at 30 nM concentration (Fig. 6A). Simultaneously, increased in the cleaved caspase-8 protein expression following treatment with SP-A (30 nM) and SP-B (10, 30 nM) for 24 h was observed. Moreover, increased caspase-8 activity was also observed with SP-A (30 nM) and SP-B (10, 30 nM) as compared to control (Fig. 6B and C).

3.6. SP-A and SP-B induced caspase activation

Caspases play a key role in the apoptosis signaling pathways. To investigate the role of caspase-3 in the apoptosis induced by SP-A and SP-B. Cells were treated with SP-A and SP-B, activation of caspase cascade was determined by Western blot using caspase 3 specific antibody. An increased in the cleaved form of caspase-3 was observed following treatment with SP-A (30 nM) and SP-B (10, 30 nM) for 18 and 24 h (Fig 7).

3.7. Changes in the apoptosis-related proteins

Bcl-2 family proteins with anti- or pro-apoptotic functions cause the release of cytochrome-c from the mitochondrial membrane, leading to the activation of caspase cascade. In this study, Western blot analysis revealed the activation of Bid following treatment with SP-A 30 nM and SP-B (10, 30 nM) for 18 and 24 h in the U937 cells. The expression of pro-apoptotic Bax and an anti-apoptotic Bcl-2 remained unchanged (Fig 8A). In addition, cytochrome-c release from mitochondria to cytosol was induced by SP-A (30 nM) and SP-B (10, 30 nM) at 24 h (Fig 8B).

4. Discussion

SP-A and SP-B have been reported for the potent HDAC inhibitory activity [18,19], however the molecular mechanism involved

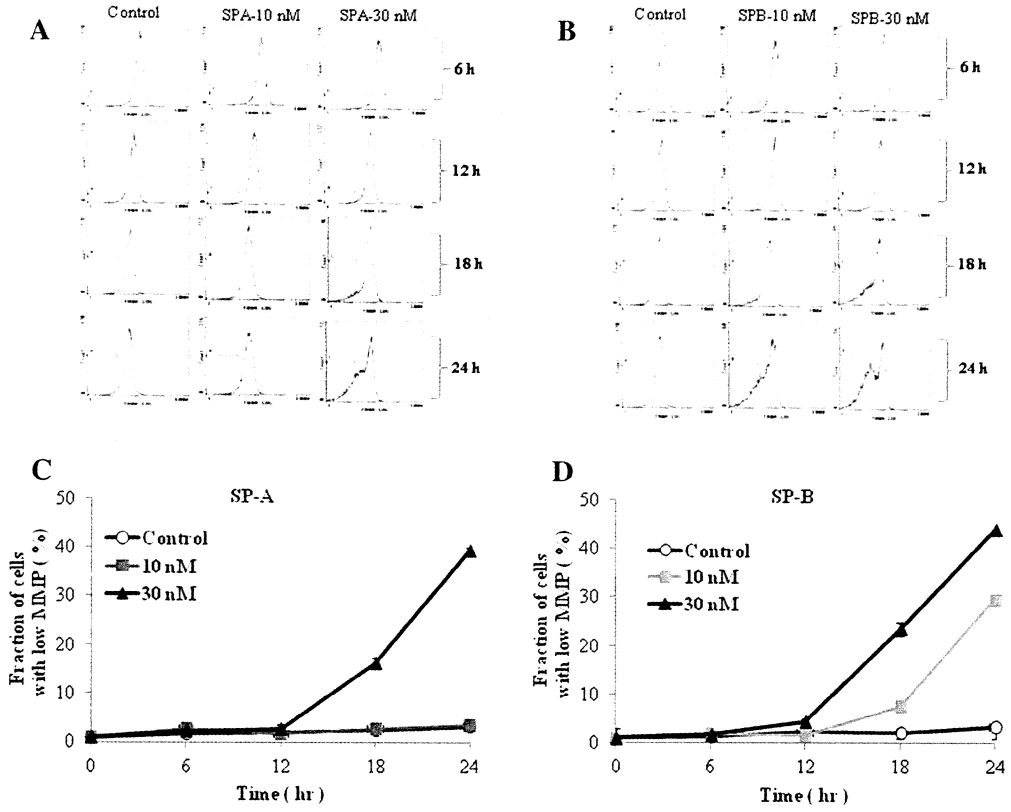


Fig. 5. Effects of SP-A and SP-B on mitochondrial membrane potential. (A and B) Representative flow cytometric histograms of SP-A and SP-B induced MMP loss. (C) Time-dependent effects of SP-A 10 and 30 nM on the mitochondrial membrane potential of U937 cells. (D) Time-dependent effects of SP-B 10 and 30 nM on the mitochondrial membrane potential of U937 cells. The loss of MMP was observed in the cells treated with SP-A and SP-B, as determined by flow cytometry using TMRM staining. The results are expressed as means ± S.D. ($n = 3$).

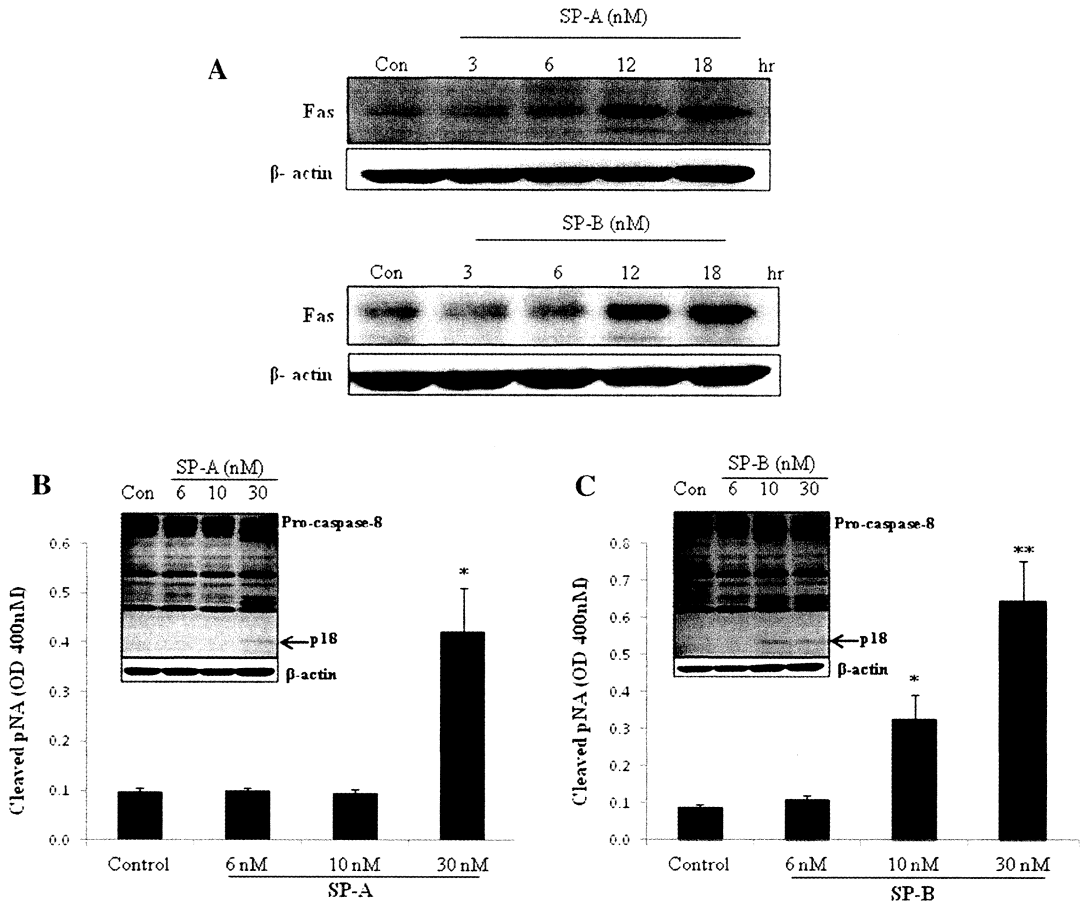


Fig. 6. Effects of SP-A and SP-B on Fas and caspase-8 activation. (A) Time-dependent changes of Fas expression after treatment with SP-A and SP-B 30 nM in U937 cells. (B) Concentration-dependent changes in the protein expression of caspase-8 after treatment with SP-A for 24 h. The caspase-8 activity in U937 cells induced by SP-A was also measured with FLICE/caspase-8 colorimetric protease kit (C) Concentration-dependent changes in the protein expression of caspase-8 after treatment with SP-B for 24 h. The caspase-8 activity in U937 cells induced by SP-B was also measured with FLICE/caspase-8 colorimetric protease kit. Where indicated, values for the treated cells are significantly different to the untreated cells at the same time point at $^{*}p < 0.05$, $^{**}p < 0.01$. The results are presented as the mean ± S.D. ($n = 3$), as determined by one way ANOVA.

in the lethality of these agents needs further investigation. This is the first report that evaluated the apoptosis activity of these agents in U937 cells. Both SP-A and SP-B share many structural activities with FK228, which is already approved for the treatment of CTCL. Both compounds possess intermolecular disulfide bond that is in FK228 reduced intra-cellularly to provide the zinc-binding group and ROS may be generated in the redox-cycling reaction and take part in apoptosis [18,28].

Recently, several HDAC inhibitors have been reported to induce apoptosis through ROS generation including FK228, SAHA, trichostatin A, sodium butyrate, MS275 and LAQ-824. [15,29,30]. Suberoylanilide hydroxamic acid (SAHA) and FK228 were reported to induce a cell death pathway by cleavage of Bid [31,32]. A recent study showed that FK228 induce apoptosis via ROS generation, and FK228-induced apoptosis was attenuated by pre-incubation with NAC (*N*-acetyl cysteine), suggesting that ROS production is likely involved in the mode of action of FK228 in solid cancer cell lines, caused mitochondrial damage and apoptosis [28] In consistent, we have demonstrated that in human lymphoma U937 cells, a marked increase in the ROS production was observed with SP-A and SP-B. Pre-incubation with NAC significantly blocked the generation of ROS and apoptosis induced by SP-A and SP-B, supporting the notion that ROS production is involved in the death mechanism. In term of differences between SP-A and SP-B, we did not detect any clear differences between these two structurally similar compounds but both the agents can induce apoptosis associated with increase in p21 [20]. Therefore, it might be possible that these agents can induce apoptosis via a ROS production and p21 increase as FK228 does, or indirectly by the activation of NAD (P) H oxidase and xanthine oxidase [33,34]. However, further future investigations are necessary to rule out the source of this ROS generation. In this study we mainly detected changes in ROS level by DCFH-DA probe, which is more sensitive towards hydrogen peroxide [35]. Unfortunately, we did not detect any significant changes with other probes like HE (data not shown).

The mechanism involved in the HDAC inhibitors induced cell death is still unclear. Although, oxidative stress has been identified as a mechanism involved in the lethality of HDAC inhibitors but the manner by which HDACi induce oxidative stress is poorly understood. Two distinct mechanisms are apparently involved; one involves the mitochondrial injury, while other implicates the modulation of anti-oxidant levels. HDACi induces expression of Bid, which binds to and disrupts the mitochondrial membrane and resulted in increased ROS and apoptosis [31,36]. Previously, in osteosarcoma and chronic lymphocytic leukemia cells, depsipeptide has been reported to induce apoptosis selectively via a caspase-8 (extrinsic) pathway [37,38]. Depsipeptide induced apoptosis via activation of mitochondrial pathway, independent

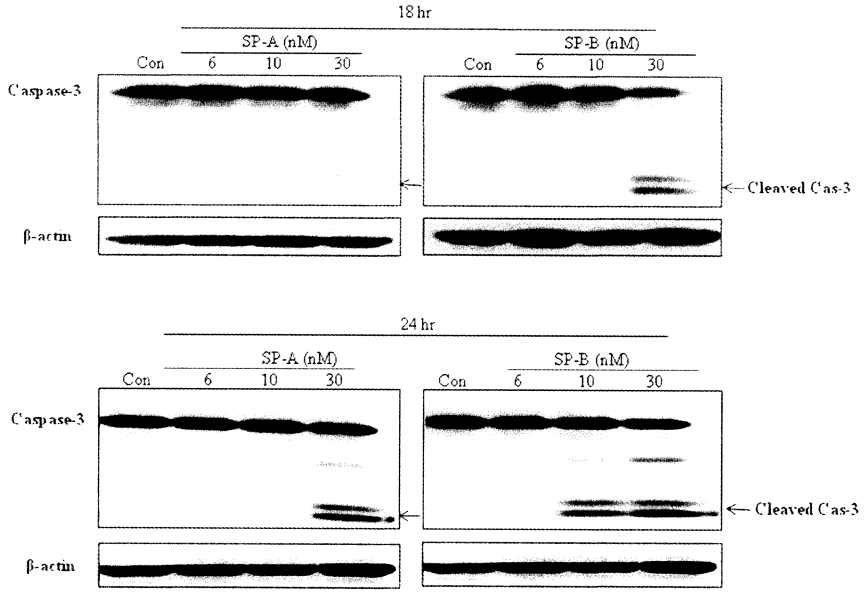


Fig. 7. Effects of SP-A and SP-B on activation of caspase-3. Concentration-dependent changes in the expression of caspase 3 after 18 and 24 h incubation with SP-A and SP-B. Date is representative of three independent experiments.

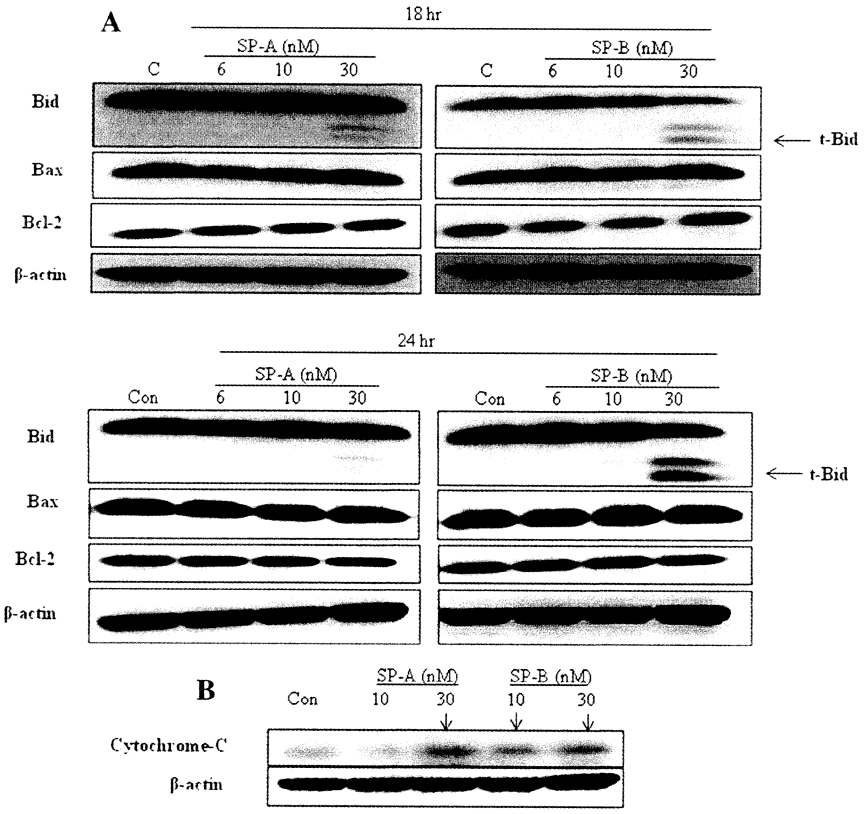


Fig. 8. Effects of SP-A and SP-B on apoptosis related proteins and release of cytochrome-c. (A) U937 cells were treated with SP-A and SP-B in a dose-dependent manner for 18 and 24 h. The cell lysates were harvested for Western blot analysis. Changes in expressions of Bax, Bcl-2, and Bid induced by SP-A and SP-B. (B) Release of cytochrome-c (Cyt-c) in cytosolic fraction after treatment with SP-A and SP-B for 24 h. One representative picture from three independent experiments is shown.

of caspase activation in acute leukemia cells [32] and in the small cell lung cancer (SCLC) induced caspase dependent apoptosis via mitochondrial pathway without the involvement of death receptor pathway [39]. In contrast to these reports, findings with SP-A and SP-B demonstrate the involvement of both the extrinsic and intrinsic pathway of apoptosis. The discrepancy in between the current

and previous report can be resolved by accounting the fact that the induction of different cell pathways by different HDACi may be dependent on the different targets and the cell type used. In this study, treatment with SP-A and SP-B significantly caused MMP loss in a time-dependent manner with a concurrent release of cytochrome-c into the cytosol. These findings suggest the involvement of mitochondria in SP-A and SP-B induced cell death. The involvement of the extrinsic pathway is suggested by the increased Fas and caspase-8 activation with SP-A and SP-B treatment. The extrinsic pathway is due to the direct interaction of cell surface receptors, such as Fas, with caspase-8, that in turn activates downstream effector caspases.

Bcl-2 family proteins are involved in pro- or anti-apoptotic processes by interacting with the mitochondria [40]. HDACi, alter the factors that are involved in the regulation of intrinsic pathway. Bid activation, can initiate the intrinsic pathway [9]. In consistent, our findings also revealed activation of Bid with both SP-A and SP-B treatment. Bid can be cleaved by caspase-8 and the cleaved Bid as the carboxyl-terminal fragment translocates to the mitochondria to induce the release of cytochrome-c [41,42]. These two apoptotic pathways may be interconnected by the caspase-8-mediated cleavage of Bid, which triggers the activation of the mitochondrial pathway.

In conclusion, the current study is the first to demonstrate that SP-A and SP-B induces apoptosis in human lymphoma U937 cells. SP-A and SP-B treatment resulted in increased accumulation of ROS and pre-treatment with NAC significantly prevented the apoptosis induced by these agents suggesting the involvement of ROS-dependent pathways in the cell death. Additionally, FAS activation may also play an important role in the SP-A and SP-B induced apoptosis. Our findings may help the potential application of these agents as future chemo-therapeutics agents.

Conflict of Interest

The author has no conflict of interest.

Transparency Document

The Transparency document associated with this article can be found in the online version.

Acknowledgements

None.

References

[1] P.A. Marks, V.M. Richon, R.A. Rifkind, Histone deacetylase inhibitors: inducers of differentiation or apoptosis of transformed cells, J. Natl. Cancer Inst. 92 (2000) 1210–1216.
[2] C. Nervi, U. Borello, F. Fazi, V. Buffa, P.G. Pelicci, G. Cossu, Inhibition of histone deacetylase activity by trichostatin A modulates gene expression during mouse embryogenesis without apparent toxicity, Cancer Res. 61 (2001) 1247–1249.
[3] C.A. Hassig, S.L. Schreiber, Nuclear histone acetylases and deacetylases and transcriptional regulation: HATs off to HDACs, Curr. Opin. Chem. Biol. 1 (1997) 300–308.
[4] T. Kouzarides, Histone acetylases and deacetylases in cell proliferation, Curr. Opin. Genet. Dev. 9 (1999) 40–48.
[5] S. Timmermann, H. Lehrmann, A. Polesskaya, A.H. Bellan, Histone acetylation and disease, Cell. Mol. Life Sci. 58 (2001) 728–736.
[6] W.D. Cress, E. Seto, Histone deacetylases, transcriptional control, and cancer, J. Cell. Physiol. 184 (2000) 1–16.
[7] A.Al. Janadi, S.R. Chandana, B.A. Conley, Histone deacetylation: an attractive target for cancer therapy?, Drugs R D 9 (2008) 369–383
[8] M.J. Lee, Y.S. Kim, S. Kummar, G. Giaccone, J.B. Trepel, Histone deacetylase inhibitors in cancer therapy, Curr. Opin. Oncol. 20 (2008) 639–649.
[9] J.E. Bolden, M.J. Peart, R.W. Johnstone, Anticancer activities of histone deacetylase inhibitors, Nat. Rev. Drug Discov. 5 (2006) 769–784.
[10] R.R. Rosato, S. Grant, Histone deacetylase inhibitors: insights into mechanisms of lethality, Expert Opin. Ther. Targets 9 (2005) 809–824.
[11] R.W. Johnstone, J.D. Licht, Histone deacetylase inhibitors in cancer therapy: is transcription the primary target?, Cancer Cell 4 (2003) 13–18
[12] O.H. Kramer, M. Gottlicher, T. Heinzel, Histone deacetylase as a therapeutic target, Trends Endocr. Met. 12 (2001) 294–300.
[13] P.A. Marks, W.S. Xu, Histone deacetylase inhibitors: potential in cancer therapy, J. Cell. Biochem. 107 (2009) 600–608.
[14] J.Y. Yoon, G. Ishdori, B.A. Graham, J.B. Johnston, S.B. Gibson, Valproic acid enhances fludarabine-induced apoptosis mediated by ROS and involving decreased AKT and ATM activation in B-cell-lymphoid neoplastic cells, Apoptosis 19 (2014) 191–200.
[15] R.R. Rosato, S.C. Maggio, J.A. Almenara, S.G. Payne, P. Atadja, S. Spiegel, P. Duent, S. Grant, The histone deacetylase inhibitor LAQ824 induces human leukemia cell death through a process involving XIAP down-regulation, oxidative injury, and the acid sphingomyelinase-dependent generation of ceramide, Mol. Pharmacol. 69 (2006) 216–225.
[16] A. Martirosyan, S. Leonard, X. Shi, B. Griffith, P. Gannett, J. Strobl, Actions of a histone deacetylase inhibitor NSC3852 (5-nitroso-8-quinolinol) link reactive oxygen species to cell differentiation and apoptosis in MCF-7 human mammary tumor cells, J. Pharmacol. Exp. Ther. 317 (2006) 546–552.
[17] Y. Masuoka, A. Nagai, K.S. Ya, K. Furihata, K. Nagai, K.I. Suzuki, Y. Hayakawa, H. Seto, Spiruchostatins A and B, novel gene expression-enhancing substances produced by *Pseudomonas* sp., Tetrahedron Lett. 42 (2001) 41–44.
[18] S.J. Crabb, M. Howell, H. Rogers, M. Ishfaq, A.Y. George, K. Carey, B.M. Pickering, P. East, R. Mitter, S. Maeda, P.W.M. Johnson, P. Townsend, K.S. Ya, M. Yoshida, A. Ganesan, G. Packham, Characterisation of the in vitro activity of the depsipeptide histone deacetylase inhibitor spiruchostatin A, Biochem. Pharmacol. 76 (2008) 463–475.
[19] K. Narita, T. Kikuchi, K. Watanabe, T. Takizawa, T. Oguchi, K. Kudo, K. Matsuhara, H. Abe, T. Yamori, M. Yoshida, T. Katoh, Total synthesis of the bicyclic depsipeptide HDAC inhibitors spiruchostatins A and B, 5″-epi-spiruchostatin B, FK228 (FR901228) and preliminary evaluation of their biological activity, Chem. Eur. J. 15 (2009) 11174–11186.
[20] S. Kanno, N. Maeda, A. Tomizawa, S. Yomogida, T. Katoh, M. Ishikawa, Involvement of p21waf1/cip1 expression in the cytotoxicity of the potent histone deacetylase inhibitor spiruchostatin B towards susceptible NALM-6 human B cell leukemia cells, Int. J. Oncol. 40 (2012) 1391–1396.
[21] Y. Furusawa, Y. Fujiwara, M.A. Hassan, Y. Tabuchi, A. Morita, A. Enomoto, T. Kondo, Inhibition of DNA-dependent protein kinase promotes ultrasound-induced cell death including apoptosis in human leukemia cells, Cancer Lett. 322 (2012) 107–112.
[22] K.S. Sellins, J.J. Cohen, Gene induction by gamma irradiation leads to DNA fragmentation in lymphocytes, J. Immunol. 139 (1987) 3199–3206.
[23] M. Li, T. Kondo, Q.L. Zhao, F.J. Li, K. Tanabe, Y. Arai, Z.C. Zhou, M. Kasuya, Apoptosis induced by cadmium in human lymphoma U937 cells through Ca2+-calpain and caspase-mitochondria-dependent pathways, J. Biol. Chem. 275 (2000) 39702–39709.
[24] Z.G. Cui, T. Kondo, L.B.J. Feril, K. Waki, O. Inanami, M. Kuwabara, Effects of antioxidants on X-ray- or hyperthermia-induced apoptosis in human lymphoma U937 cells, Apoptosis 9 (2004) 757–763.
[25] P. Jawaid, M.U. Rehman, Y. Yoshihisa, P. Li, Q.L. Zhao, M.A. Hassan, Y. Miyamoto, T. Shimizu, T. Kondo, Effects of SOD/catalase mimetic platinum nanoparticles on radiation induced apoptosis in human lymphoma U937 cells, Apoptosis 19 (2014) 1006–1016.
[26] A. Gorman, A. McGowan, T.G. Cotter, Role of peroxide and superoxide anion during tumour cell apoptosis, FEBS Lett. 404 (1997) 27–33.
[27] K. Ahmed, Q.L. Zhao, Y. Matsuya, D.Y. Yu, L.B.F. Jr, H. Nemoto, T. Kondo, Rapid and transient intracellular oxidative stress due to novel macrosphelides trigger apoptosis via Fas/caspase-8-dependent pathway in human lymphoma U937 cells, Chem. Biol. Interact. 170 (2007) 86–89.
[28] H. Mizutani, Y. Hiraku, S.T. Oikawa, M. Murata, K. Ikemura, T. Iwamoto, Y. Kagawa, M. Okuda, S. Kawanishi, Romidepsin (FK228), a potent histone deacetylase inhibitor, induces apoptosis through the generation of hydrogen peroxide, Cancer Sci. 101 (2010) 2214–2219.
[29] R.R. Rosato, J.A. Almenara, S. Grant, The histone deacetylase inhibitor MS-275 promotes differentiation or apoptosis in human leukemia cells through a process regulated by generation of reactive oxygen species and induction of p21CIP1/WAF1 1, Cancer Res. 63 (2003) 3637–3645.
[30] R.R. Rosato, J.A. Almenara, S.C. Maggio, S. Coe, P. Atadja, P. Dent, S. Grant, Role of histone deacetylase inhibitor-induced reactive oxygen species and DNA damage in LAQ-824/fludarabine antileukemic interactions, Mol. Cancer Ther. 7 (2008) 3285–3297.
[31] A.A. Ruefli, M.J. Ausserlechner, D. Bernhard, V.R. Sutton, K.M. Tainton, R. Kofler, M.J. Smyth, R.W. Johnstone, The histone deacetylase inhibitor and chemotherapeutic agent suberoylanilide hydroxamic acid (SAHA) induces a cell-death pathway characterized by cleavage of Bid and production of reactive oxygen species, Proc. Natl. Acad. Sci. U.S.A. 98 (2011) 10833–10838.
[32] M.J. Peart, K.M. Tainton, A.A. Ruefli, A.E. Dear, K.A. Sedelies, L.A. O'Reilly, N.J. Waterhouse, J.A. Trapani, R.W. Johnstone, Novel mechanisms of apoptosis induced by histone deacetylase inhibitors, Cancer Res. 63 (2003) 4460–4471.
[33] H. Mizutani, S.T. Oikawa, Y. Hiraku, S. Oikawa, M. Kojima, S. Kawanishi, Mechanism of apoptosis induced by a new topoisomerase inhibitor through the generation of hydrogen peroxide, J. Biol. Chem. 277 (2002) 30684–30689.

[34] H. Mizutani, S.T. Oikawa, Y. Hiraku, M. Kojima, S. Kawanishi, Mechanism of apoptosis induced by doxorubicin through the generation of hydrogen peroxide, Life Sci. 76 (2005) 1439–1453.
[35] K.I. Setsukinai, Y. Urano, K. Kakinumas, Development of novel fluorescence probes that can reliably detect reactive oxygen species and distinguish specific species, J. Biol. Chem. 278 (2003) 3170–3175.
[36] C.P. Miller, M.M. Singh, N.R.D. Valle, C.A. Manton, J. Chandra, Therapeutic strategies to enhance the anticancer efficacy of histone deacetylase inhibitors, J. Biomed. Biotechnol. (2011), http://dx.doi.org/10.1155/2011/514261.
[37] T. Imai, A. Adachi, K. Nishijo, M. Ohgusgi, M. Okada, T. Yasumi, K. Watanabe, R. Nishikomori, T. Nakayama, S. Yonehara, J. Toguchida, T. Nakahata, FR901228 induces tumor regression associated with induction of Fas ligand and activation of Fas signaling in human osteosarcoma cells, Oncogene 22 (2003) 9231–9342.
[38] J.L. Aron, M.R. Parthun, G. Marcucci, S. Kitada, A.P. Mone, M.E. Davis, T. Shen, T. Murphy, J. Wickham, C. Kanakry, D.M. Lucas, J.C. Reed, M.R. Grever, J.C. Byrd, Depsipeptide (FR901228) induces histone acetylation and inhibition of histone deacetylase in chronic lymphocytic leukemia cells concurrent with activation of caspase 8-mediated apoptosis and down regulation of c-FLIP protein, Blood 102 (2003) 652–658.
[39] S. Doi, H. Soda, M. Oka, J. Tsurutani, T. Kitazaki, Y. Nakamura, M. Fukuda, Y. Yamada, S. Kamihira, S. Kohno, The histone deacetylase inhibitor FR901228 induces caspase-dependent Apoptosis via the mitochondrial pathway in small cell lung cancer cells, Mol. Cancer Ther. 3 (2004) 1397–13402.
[40] Y. Tsujimoto, S. Shimizu, Bcl-2 family: life-or-death switch, FEBS Lett. 466 (2000) 6–10.
[41] K. Ahmed, Z.L. Wei, Q.L. Zhao, N. Nakajima, T. Matsunaga, M. Ogasawara, T. Kondo, Role of fatty acid chain length on the induction of apoptosis by newly synthesized catechin derivatives, Chem. Biol. Interact. 185 (2010) 182–188.
[42] H. Li, H. Zhu, C.J. Xu, J. Yuan, Cleavage of BID by caspase 8 mediates the mitochondrial damage in the Fas pathway of apoptosis, Cell 94 (1998) 491–501.

European Journal of Medicinal Chemistry 76 (2014) 301–313

Contents lists available at ScienceDirect

European Journal of Medicinal Chemistry

journal homepage: http://www.elsevier.com/locate/ejmech

Original article

Total synthesis of burkholdacs A and B and 5,6,20-tri-*epi*-burkholdac A: HDAC inhibition and antiproliferative activity

Yurie Fukui [a], Koichi Narita [a], Singo Dan [b], Takao Yamori [b,c], Akihiro Ito [d], Minoru Yoshida [d], Tadashi Katoh [a,*]

[a] *Laboratory of Synthetic and Medicinal Chemistry, Faculty of Pharmaceutical Sciences, Tohoku Pharmaceutical University, 4-4-1 Komatsushima, Aoba-ku, Sendai 981-8558, Japan*
[b] *Division of Molecular Pharmacology, Cancer Chemotherapy Center, Japanese Foundation for Cancer Research, 3-10-6 Ariake, Koto-ku, Tokyo 135-8550, Japan*
[c] *Pharmaceuticals and Medical Devices Agency (PMDA), 3-3-2 Kasumigaseki, Chiyoda-ku, Tokyo 100-0013, Japan*
[d] *Chemical Genetics Laboratory, RIKEN, 2-1 Hirosawa, Wako-shi, Saitama 351-0198, Japan*

ARTICLE INFO

Article history:
Received 17 January 2014
Received in revised form
12 February 2014
Accepted 16 February 2014
Available online 18 February 2014

Keywords:
Burkholdacs
Histone deacetylase inhibitors
Natural products
Bicyclic depsipeptide
Total synthesis

ABSTRACT

The bicyclic depsipeptide histone deacetylase (HDAC) inhibitors burkholdacs A and B were efficiently synthesized in a highly convergent and unified manner. The synthesis features the amide coupling of a D-valine-D-cysteine- or D-*allo*-isoleucine-D-cysteine-containing segment with a D-methionine-containing segment to directly assemble the corresponding *seco*-acids, key precursors for macrolactonization. Using the same methodology, 5,6,20-tri-*epi*-burkholdac A was also synthesized. HDAC inhibitory assays and cell-growth inhibition analyses of the synthesized depsipeptides demonstrated the potency order of this class of bicyclic depsipeptides as compared to the clinically approved depsipeptide FK228 (romidepsin). Novel structure–activity relationships within this class of compounds were also revealed.

© 2014 Elsevier Masson SAS. All rights reserved.

1. Introduction

In 2011, Brady et al. reported the isolation and structural elucidation of the two new bicyclic depsipeptide histone deacetylase (HDAC) inhibitors, burkholdacs A (**1**) and B (**2**) (Fig. 1) [1]. These compounds were identified through the systematic overexpression of transcription factors associated with natural product gene clusters encoded within *Burkholderia thilandensis* E264 [1]. The stereochemistry at the C5, C6 and C20 positions could not be unambiguously assigned at that time. The stereostructures of **1** and **2** were proposed as compounds **3** and **4** in Fig. 1, respectively, based on the biosynthesis gene cluster that contains only one epimerase domain [1]. Through two independent total syntheses by Ganesan et al. in 2011 [2] and by Ye et al. in 2012 [3], the stereochemistry of the two new HDAC inhibitors, which includes their absolute configurations, was determined, as shown in structures **1** and **2**.

In the course of our continuing research on the synthesis and biological evaluation of bicyclic depsipeptide HDAC inhibitors including FK228 (romidepsin) (**5**) [4] and the spiruchostatins A (**6**) [4,5], B (**7**) [4,6], C (**8**) [7] and D (**9**) [7], we became interested in the synthesis of **1** and **2** and their analogues with the aim of identifying novel mechanism-based anticancer agents [8]. Several total syntheses of **5**–**7** by other groups have been published in the literature [9]. In this study, we describe our total synthesis of **1** and **2** and the earlier proposed stereostructure **3** by applying a synthetic strategy developed previously in our laboratory [4–7]. The synthesized compounds **1**–**3** were subjected to HDAC inhibition assays and antiproliferative analyses to establish the potency order for this class of bicyclic depsipeptide HDAC inhibitors (**1**–**3** and **5**–**9**).

2. Results and discussion

2.1. Chemistry

2.1.1. Synthetic plan for burkholdacs A (*1*) and B (*2*)

Our synthetic plan for **1** and **2** is outlined in Scheme 1. We envisioned that target molecules **1** and **2** could be synthesized via the macrolactonization of the corresponding *seco*-acids **10** and **11**, followed by disulfide bond formation. The key macrolactonization

* Corresponding author.
E-mail address: katoh@tohoku-pharm.ac.jp (T. Katoh).

http://dx.doi.org/10.1016/j.ejmech.2014.02.044
0223-5234/© 2014 Elsevier Masson SAS. All rights reserved.

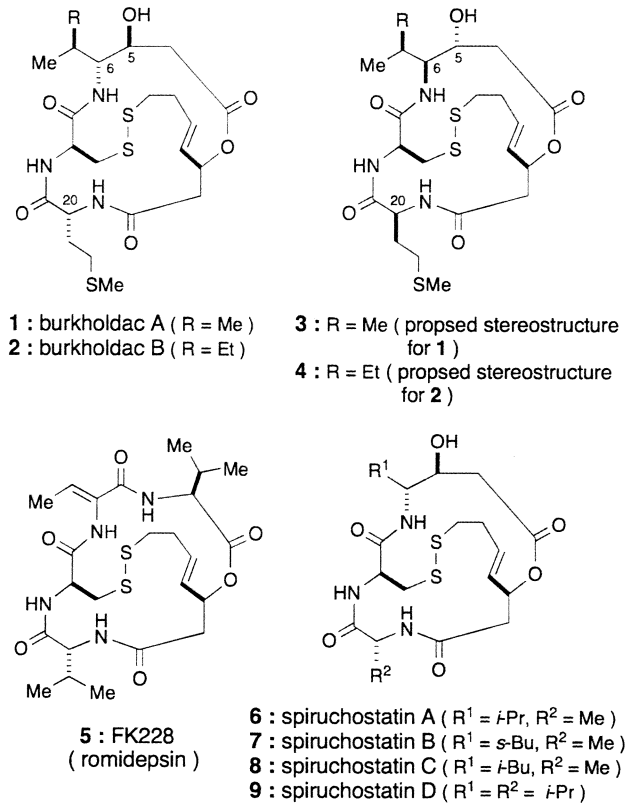


Fig. 1. Revised (**1**, **2**) and Brady's original (**3**, **4**) structures of burkholdacs A and B, FK228 (romidepsin) (**5**) and spiruchostatins A–D (**6**–**9**). *i*-Pr = isopropyl, *s*-Bu = *sec*-butyl, *i*-Bu = isobutyl.

precursors **10** and **11** could be prepared through the direct coupling of the D-valine-D-cysteine-containing segment **12** and D-*allo*-isoleucine-D-cysteine-containing segment **13**, respectively, with the D-methionine-containing segment **14**. The segment **14** was to be formed by condensation of commercially available D-methionine methyl ester (**15**) with the known carboxylic acid **16** (previously prepared from L-malic acid in our laboratory [4–6]). The two segments **12** and **13** were obtained as previously described in our total synthesis of **6** and **7** [4–6].

2.1.2. Synthesis of burkholdac A (*1*)

We initially pursued the synthesis of **1**. For the synthesis, the key segment **14** was efficiently prepared, as shown in Scheme 2. The condensation of **15** with **16** [4–6] afforded the desired coupling product **17** in excellent yield. Subsequent saponification of the methyl ester moiety in **17** furnished the requisite segment **14** in quantitative yield.

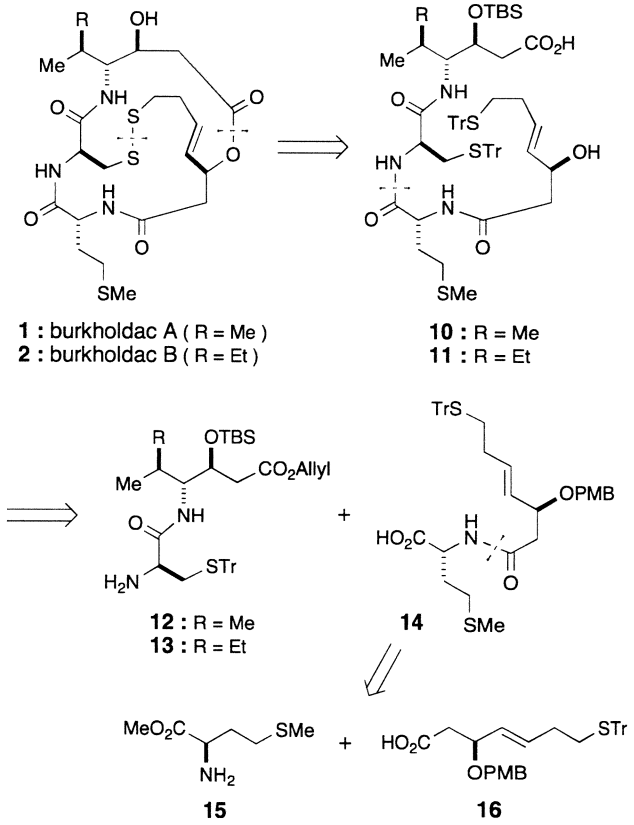
Subsequently, the synthesis of **1** was accomplished by assembling the two segments **12** [4,5] and **14**, as shown in Scheme 3. Thus, treatment of **12** and **14** with HATU (1.3 equiv) and HOAt (1.3 equiv) in the presence of *i*-Pr_2NEt (2.6 equiv) in CH_2Cl_2 at −30 °C for 3 h afforded the desired condensation product **18** in 83% yield without appreciable epimerization at the C20 stereogenic centre (burkholdacs numbering). The condensation product **18** was then converted to the requisite *seco*-acid **10** with an overall yield of 74% using alcohol **19** via the successive removal of both the PMB- and allyl-protecting groups. Notably, the sensitive methyl sulfide function present in the C20 side chain remained intact during the oxidative deprotection step (cf. DDQ, CH_2Cl_2/H_2O, rt, 3 h). The critical macrolactonization of **10** was successfully achieved by employing the Shiina method [10] [MNBA (1.3 equiv), DMAP (3.0 equiv), CH_2Cl_2 (10 mM), rt, 12 h], which afforded the expected cyclization product **20** in 79% yield. Subsequent disulfide bond formation accompanied by oxidative *S*-Tr deprotection of **20** was efficiently achieved by brief exposure to I_2 in a dilute CH_2Cl_2/MeOH solution (0.5 mM) at ambient temperature, which resulted in the production of the desired disulfide **21** in 81% yield. Finally, deprotection of the TBS group in **21** (89%) led to the completion of the total synthesis of **1**. The spectroscopic properties (IR, ^1H and ^{13}C NMR, and MS) of the synthesized sample **1** were identical to those reported for natural **1** [1].

2.1.3. Synthesis of burkholdac B (*2*)

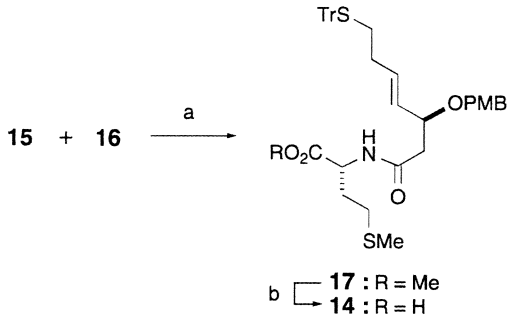
As shown in Scheme 4, using segments **13** [4,6] and **14** as the starting materials, **2** was synthesized in a manner similar to that described for the synthesis of **1** (cf. Scheme 3). The spectroscopic properties (IR, ^1H and ^{13}C NMR, and MS) of the synthesized sample **2** were identical with those reported for natural **2** [1].

2.1.4. Synthesis of 5,6,20-tri-epi-burkholdac A (*3*)

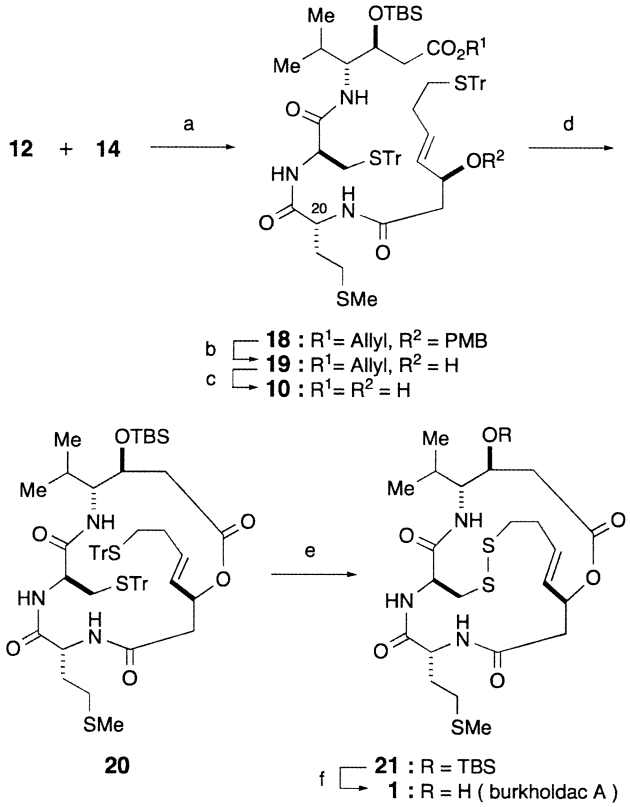
Moreover, we synthesized the Brady's proposed stereoisomer, 5,6,20-tri-*epi*-burkholdac A (**3**), to assess its biological activity. Using *N*-Boc-L-valinal (**26**) [11] as the starting material, the key segment **35** was synthesized according to a method developed previously in our laboratory [4,5] (Scheme 5). The other key segment **37** was readily prepared via the condensation of commercially available L-methionine methyl ester (*ent*-**15**) with



Scheme 1. Synthetic plan for burkholdacs A (**1**) and B (**2**). TBS = *tert*-butyldimethylsilyl, Tr (trityl) = triphenylmethyl, PMB = 4-methoxybenzyl.



Scheme 2. Synthesis of segment **14**. (a) PyBOP, *i*-Pr_2NEt, MeCN, rt, 99%; (b) LiOH, MeOH, rt, 100%. PyBOP = (benzotriazol-1-yloxy)tripyrrolidinophosphonium hexafluorophosphate.



Scheme 3. Synthesis of burkholdac A (**1**). (a) HATU, HOAt, *i*-Pr_2NEt, CH_2Cl_2, −30 °C, 83%; (b) DDQ, CH_2Cl_2/H_2O, rt, 87%; c) $Pd(PPh_3)_4$, morpholine, THF, rt, 85%; (d) MNBA, DMAP, CH_2Cl_2, rt, 79%; (e) I_2, CH_2Cl_2/MeOH, rt, 81%; (f) HF·pyridine, pyridine, rt, 89%. HATU = *O*-(7-azabenzotriazol-1-yl)-*N*,*N*,*N*',*N*'-tetramethyluronium hexafluorophosphate, HOAt = 1-hydroxy-7-azabenzotriazole, DDQ = 2,3-dichloro-5,6-dicyano-1,4-benzoquinone, MNBA = 2-methyl-6-nitrobenzoic anhydride, DMAP = 4-dimethylaminopyridine.

carboxylic acid **16** (Scheme 6). The final target molecule **3** was synthesized, as shown in Scheme 7, through condensation of the two segments **35** and **37** in a manner similar to that described for the synthesis of **1** (cf. Schemes 2 and 3).

2.2. Biological evaluation

The synthesized compounds **1**–**3** were evaluated for their HDAC inhibitory activity and their cell-growth inhibitory activity to determine the order of their potency and reveal some novel aspects of structure–activity relationships (SARs) within this class of compounds.

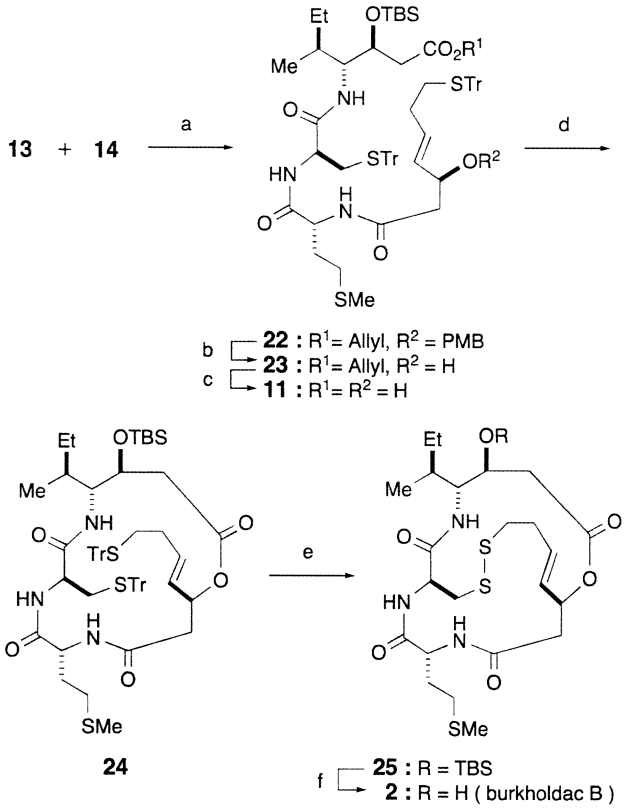
2.2.1. HDAC inhibition assay

HDAC enzymes are zinc metalloenzymes that catalyze the hydrolysis of acetylated lysine residues on proteins, particularly histones [12]. There are 18 human HDAC isoforms, which are grouped into the following four major classes: class I (HDACs 1, 2, 3 and 8), class II (class IIa: HDACs 4, 5, 7 and 9; class IIb: HDACs 6 and 10), and class IV (HDAC 11) are Zn^{2+}-dependent metallohydrolases, while class III HDACs (7 members) are NAD^+-dependent sirtuins [13]. The inhibition of class I HDACs is considered to be a useful mechanism for anticancer agents, whereas the inhibition of class IIb HDACs may cause undesirable side effects such as serious cardiac hypertrophy [14]. In 2009, FK228 has been approved by the Food and Drug Administration in USA for treatment of cutaneous T-cell lymphoma [15]. However, this anticancer agent is associated with an unresolved cardiotoxicity that probably arises from insufficient class selectivity [15,16]. Therefore, the potent and selective inhibition of class I enzymes is highly desirable in next-generation cancer chemotherapy [17].

Compounds **1**–**3** were tested for their HDAC inhibitory activity against HDAC1 (class I) and HDAC6 (class IIb) enzymes to determine their degree of potency and isoform selectivity. In this assay, FK228 was used as a positive control. As summarized in Table 1, **1** and **2** exhibited extremely potent inhibitory activity against HDAC1 in the low nanomolar range (IC_{50} = 1.0–1.2 nM). Their potencies were observed to be approximately three-fold higher than that of FK228 (IC_{50} = 3.6 nM). In contrast, the unnatural stereoisomer **3** exhibited much lower inhibitory activity (IC_{50} = 336.6 nM) than the natural products (**1**: IC_{50} = 1.0 nM, **2**: IC_{50} = 1.2 nM), suggesting that the stereochemistry at the C5, C6 and C20 positions plays a key role in determining the pronounced HDAC1 inhibition efficacy. Combined with our previous data for spiruchostatins A (**6**), B (**7**), C (**8**) and D (**9**) [4,7], the potency order was estimated to be **9** (IC_{50} = 0.75 nM) ≥ **8** (IC_{50} = 0.93 nM) ≈ **1** (IC_{50} = 1.0 nM) ≥ **2** (IC_{50} = 1.2 nM) > **7** (IC_{50} = 2.2 nM) > **6** (IC_{50} = 3.3 nM) ≥ FK228 (**5**) (IC_{50} = 3.6 nM). As expected for HDAC6 inhibitory activity, both **1** and **2** were essentially inactive (**1**: IC_{50} = 1975 nM, **2**: IC_{50} = 992 nM). Isoform selectivity (class I/IIb) is expressed, for convenience, as a selective index (SI) value (HDAC6 IC_{50}/HDAC1 IC_{50}). Along with our previous data [4,7], the order of the selectivity was then determined to be **1** (SI = 1645) > **2** (SI = 992) > **7** (SI = 636) > **6** (SI = 485) > **8** (SI = 346) ≥ **9** (SI = 320) > FK228 (**5**) (SI = 108). Notably, the isoform selectivity of **1** and **2** is nine-to-fifteen-fold higher than that of FK228, which represents, to the best of our knowledge, the highest level of class I/II selectivity among the naturally occurring bicyclic depsipeptides known to date. In addition, a good correlation between enzymatic (HDAC1) activity and cellular HDAC inhibition efficacy [expressed as the EC_{10000} (effective concentration for 100 times increased induction) value measured via the p21 promoter assay] was determined for all of the compounds. From these results, it was revealed that structural alteration of the side chain at the C20 position is quite effective for improving the isoform selectivity without loss of the potent HDAC inhibitory activity.

2.2.2. Cell-growth inhibition assay

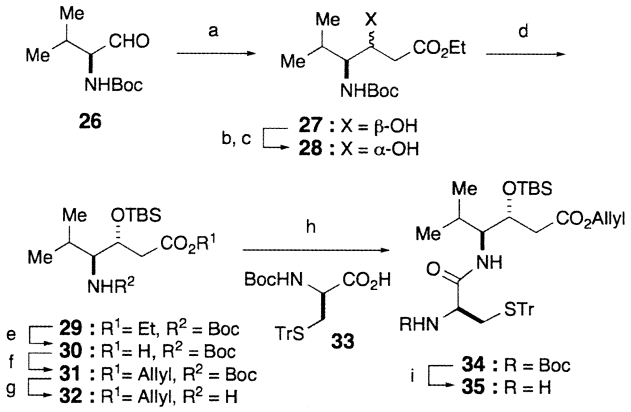
Next, the growth–inhibitory activity of compounds **1**–**3** was evaluated at the Japanese Foundation for Cancer Research simultaneously with FK228 as a reference compound using a panel of 39 human cancer cell lines [18]. The number of cell lines and their origin (organ) are as follows: 5 breast, 6 central nervous system (brain), 1 melanoma, 5 ovary, 2 kidney, 6 stomach and 2 prostate.



Scheme 4. Synthesis of burkholdac B (**2**). (a) HATU, HOAt, *i*-Pr_2NEt, CH_2Cl_2, −30 °C, 92%; (b) DDQ, CH_2Cl_2/H_2O, rt, 82%; (c) $Pd(PPh_3)_4$, morpholine, THF, rt, 94%; (d) MNBA, DMAP, CH_2Cl_2, rt, 81%; (e) I_2, CH_2Cl_2/MeOH, rt, 79%; (f) HF·pyridine, pyridine, rt, 97%.

Dose-response curves were measured at five different concentrations (from 10^{-10} to 10^{-6} M or from 10^{-8} to 10^{-4} M) for each compound, and the concentration causing 50% cell growth inhibition (GI_{50}) was compared with that of the control.

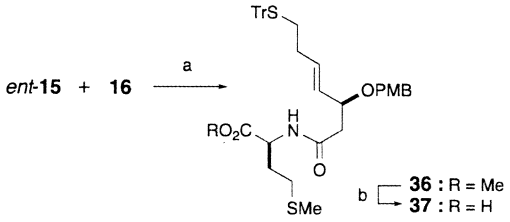
The GI_{50} values of the tested compounds **1**–**3** along with those for FK228 are shown in Table 2. Compounds **1** and **2** exhibited extremely potent growth–inhibitory activity against nearly all of the 39 cell lines in the sub-nanomolar to nanomolar range. Notably, the efficacy of **1** and **2** was superior to that of FK228 on brain cancer (SF-539, **1**: GI_{50} = 0.72 nM, **2**: GI_{50} = 0.70 nM), colon cancer (HCC2998, **1**: GI_{50} = 0.67 nM; KM-12, **1**: GI_{50} = 0.76 nM; HT-29, **1**: GI_{50} = 0.65 nM, **2**: GI_{50} = 0.74 nM; HCT-116, **1**: GI_{50} = 0.51 nM, **2**: GI_{50} = 0.51 nM), lung cancer (NCI-H23, **1**: GI_{50} = 0.64 nM; NCI-H226, **1**: GI_{50} = 0.47 nM; NCI-H522, **1**: GI_{50} = 0.20 nM, **2**: GI_{50} = 0.42 nM; NCI-H460, **1**: GI_{50} = 0.91 nM, **2**: GI_{50} = 0.53 nM; A549, **1**: GI_{50} = 0.57 nM, **2**: GI_{50} = 0.85 nM; DMS114, **1**: GI_{50} = 0.97 nM), melanoma cancer (LOX-IMVI, **1**: GI_{50} = 0.50 nM), ovary cancer (OVCAR-8, **1**: GI_{50} = 0.68 nM, **2**: GI_{50} = 0.72 nM; SK-OV-3, **1**: GI_{50} = 0.78 nM), stomach cancer (MKN1, **1**: GI_{50} = 0.67 nM) and prostate cancer (DU-145, **1**: GI_{50} = 0.82 nM) cells. In contrast, **3** exhibited fairly decreased activity against all of the 39 cell lines (GI_{50} = 230–15000 nM). The potency order of the bicyclic depsipeptides, including **5**–**9** (based on our previous data [4,7]), was estimated using the MG-MID value (mean value of GI_{50} over all of the cell lines tested) to be **1** (2.1 nM) ≥ **2** (3.2 nM) ≥ **9** (3.8 nM) > **7** (5.6 nM) ≈ FK228 (**5**) (6.2 nM) > **6** (15 nM) > **8** (28 nM). These results indicate that the antiproliferative activity of **1** and **2** is two-to-three-fold higher than that of FK228. Considering both the HDAC inhibitory and antiproliferative activities, **1** and **2** seem to be promising candidates for the development of novel anticancer agents with higher efficacy and lower toxicity.



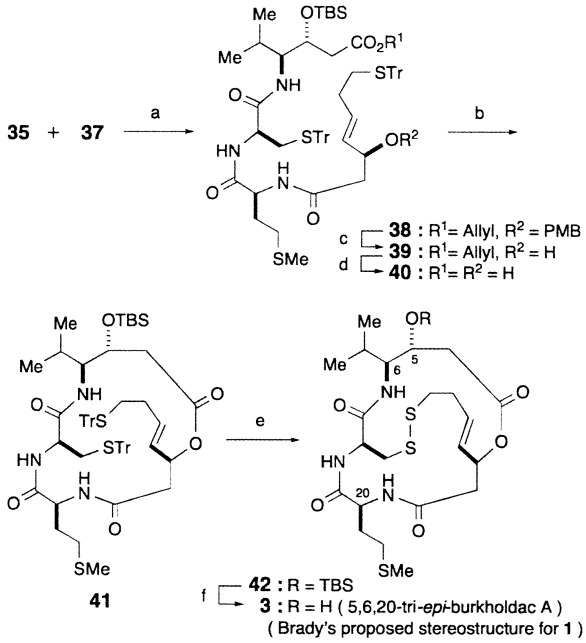
Scheme 5. Synthesis of segment **35**. (a) LDA, CH_3CO_2Et, THF, −78 °C; at −78 °C, add. **26**, 57% for **27**, 30% for **28** (**27**/**28** 2:1); (b) Jones reagent, acetone, 0 °C to rt, 86%; (c) KBH_4, MeOH, −40 °C, 79% for **28**, 5% for **27** (**28**/**27** 16:1); (d) TBSCl, imidazole, DMF, rt, 99%; (e) 1 M NaOH, EtOH, rt; (f) allyl bromide, K_2CO_3, DMF, rt, 81% (2 steps); (g) TMSOTf, 2,6-lutidine, CH_2Cl_2, rt; MeOH, rt; (h) **33**, PyBOP, *i*-Pr_2NEt, MeCN, rt, 68% (2 steps); (i) TMSOTf, 2,6-lutidine, CH_2Cl_2, rt; MeOH, rt; 98%. LDA = lithium diisopropylamide, TMSOTf = trimethylsilyl trifluoromethanesulfonate.

3. Conclusion

The total synthesis of burkholdacs A (**1**) and B (**2**) and 5,6,20-tri-*epi*-burkholdac A (**3**) was achieved in a highly convergent and



Scheme 6. Synthesis of segment **37**. (a) PyBOP, *i*-Pr_2NEt, CH_2Cl_2, 0 °C to rt, 81%; (b) 1 M LiOH, MeOH, rt, 98%.



Scheme 7. Synthesis of 5,6,20-tri-*epi*-burkholdac A (**3**) (Brady's proposed stereostructure for **1**). (a) HATU, HOAt, *i*-Pr_2NEt, CH_2Cl_2, −30 °C, 81%; (b) DDQ, CH_2Cl_2/H_2O, rt, 83%; (c) $Pd(PPh_3)_4$, morpholine, THF, rt, 74%; (d) MNBA, DMAP, CH_2Cl_2, rt, 84%; (e) I_2, CH_2Cl_2/MeOH, rt, 85%; (f) HF·pyridine, pyridine, rt, 89%.

unified manner. Using the results of a preliminary biological evaluation of the synthesized compounds **1**–**3** and our previously obtained data for FK228 (**5**) and the spiruchostatins A–D (**6**–**9**), the order of the efficacy of the naturally occurring bicyclic depsipeptide HDAC inhibitors was established. Notably, the burkholdacs (**1** and **2**) were determined to be superior to **5** with respect to their HDAC1 inhibitory activity, isoform selectivity towards HDAC1 over HDAC6 and antiproliferative activity. These results should be useful for the design and development of anticancer agents with therapeutic potential that target the isoform-selective inhibition of HDACs. We are currently synthesizing additional analogues of burkholdacs with the aim of exploring their SARs. In addition, further investigation of the activity of the synthetic samples using animal models is in progress.

4. Experimental

4.1. Chemistry

All reactions involving air- and moisture-sensitive reagents were carried out using oven dried glassware and standard syringe-septum cap techniques. Routine monitorings of reaction were

Table 1
HDAC inhibitory activity of burkholdacs A (**4**) and B (**5**) and 5,6,20-tri-*epi*-burkholdac A (**3**).

Compound	IC_{50}[a] (nM)			EC_{10000}[e] (nM)
	HDAC1 (class I)[b]	HDAC6 (class IIb)[b]	SI[d]	Cell HDAC
1	1.2	1975	1645	1.4
2	1.0	992	992	0.76
3	336.6	>10,000	–	>200
FK228[c]	3.6	390	108	3.8

[a] Concentration that induces 50% inhibition against HDACs.
[b] Enzyme assay was performed in the presence of 100 μM dithiothreitol (DTT).
[c] Positive control used in this study was synthesized in our laboratory [4].
[d] Selectivity index (HDAC6 IC_{50}/HDAC1 IC_{50}) as the selectivity towards class I HDAC1 over class IIb HDAC6.
[e] The concentration that induces luciferase activity 100-fold higher than basal level.

Table 2
Growth inhibition of burkholdacs A (**1**) and B (**2**) and 5,6,20-tri-*epi*-burukholdac A (**3**) against a panel of 39 human cancer cell lines.

Origin of cancer	Cell line	GI_{50}[a] (nM)			FK228[b]
		1	**2**	**3**	
Breast	HBC-4	3.0	3.8	1300	6.9
	BSY-1	4.0	5.0	1600	8.5
	HBC-5	7.8	2.3	1900	13
	MCF-7	2.0	2.8	1800	4.2
	MDA-MB-231	1.8	2.6	1800	5.5
Central nervous system (Brain)					
	U-251	2.2	4.4	410	3.9
	SF-268	1.8	4.1	960	4.9
	SF-295	3.0	2.3	1600	4.0
	SF-539	0.72	0.70	1800	3.6
	SNB-75	3.6	1.4	1000	7.2
	SNB-78	460[c]	11	1700	9.6
Colon	HCC2998	0.67	2.6	1700	3.1
	KM-12	0.76	3.6	1600	3.4
	HT-29	0.65	0.74	1400	3.3
	HCT-15	300	100[c]	15,000[c]	450[c]
	HCT-116	0.51	0.51	540	3.1
Lung	NCI-H23	0.64	3.3	1600	4.6
	NCI-H226	0.47	2.7	1700	8.9
	NCI-H522	0.20[d]	0.42[d]	360	1.8[d]
	NCI-H460	0.91	0.53	1800	3.0
	A549	0.57	0.85	1400	2.6
	DMS273	3.0	2.7	2300	5.8
	DMS114	0.97	3.2	1300	3.6
Melanoma ovary	LOX-IMVI	0.50	2.5	230[d]	2.5
	OVCAR-3	2.2	2.8	1800	4.6
	OVCAR-4	5.8	5.0	1800	20
	OVCAR-5	1.0	1.6	1300	2.8
	OVCAR-8	0.68	0.72	1900	5.5
	SK-OV-3	0.78	1.9	1700	3.3
Kidney	RXF-631L	1.3	2.3	4000	6.6
	ACHN	3.4	6.6	4400	20
Stomach	St-4	8.1	1.1	3400	22
	MKN1	0.67	2.5	1400	3.2
	MKN7	4.1	10	2100	4.9
	MKN28	8.5	16	1900	17
	MKN45	7.6	14	3700	14
	MKN74	1.8	2.9	1500	3.0
Prostate	DU-145	0.82	3.1	1500	6.0
	PC-3	4.4	8.3	1600	18
MG-MID[e]		2.1	3.2	1600	6.2

[a] Concentration that induces 50% inhibition of cell growth compared to the control.
[b] Positive control used in this study was synthesized in our laboratory [4].
[c] The least sensitive cell.
[d] The most sensitive cell.
[e] Mean value of GI_{50} over all cell lines tested.

carried out using glass-supported Merck silica gel 60 F_{254} TLC plates. Flash column chromatography was performed on Kanto Chemical Silica Gel 60N (spherical, neutral 40–50 nm) with the solvents indicated.

All solvents and reagents were used as supplied with following exceptions. Tetrahydrofuran (THF) was freshly distilled from Na metal/benzophenone under argon. *N,N*-Dimethylformamide (DMF), CH_2Cl_2, MeCN, pyridine, *i*-Pr_2NH, and *i*-Pr_2NEt were distilled from calcium hydride under argon.

Measurements of optical rotations were performed with a JASCO DIP-370 automatic digital polarimeter. ^1H and ^{13}C NMR spectra were measured with a JEOL AL-400 (400 MHz) spectrometer. Chemical shifts were expressed in ppm using Me_4Si ($\delta = 0$) as an internal standard. The following abbreviations are used: singlet (s), doublet (d), triplet (t), quartet (q), multiplet (m) and broad (br). Infrared (IR) spectral measurements were carried out with a JASCO FT/IR-4100 spectrometer. Low- and High-resolution mass (HRMS) spectra were measured on a JEOL JMS-DX 303/JMA-DA 5000 SYSTEM high resolution mass spectrometer.

4.1.1. (R)-Methyl 2-[(S,E)-3-(4-methoxybenzyloxy)-7-(tritylthio) hept-4-enamide]-4- (methylthio)butanoate (17)

i-Pr_2NEt (0.32 mL, 1.9 mmol) was added dropwise to a stirred solution of **16** (146 mg, 0.27 mmol) and D-methionine methyl ester (**15**) (108 mg, 0.54 mmol) in MeCN (15 mL) containing (benzotriazol-1-yloxy)tripyrrolidinophosphonium hexafluorophosphate (PyBOP) (281 mg, 0.54 mmol) at 0 °C under argon, and stirring was continued for 2 h at room temperature. The reaction mixture was diluted with EtOAc (120 mL), and the organic layer was washed successively with 10% aqueous HCl (2 × 40 mL), saturated aqueous $NaHCO_3$ (2 × 40 mL) and brine (2 × 40 mL), then dried over Na_2SO_4. Concentration of the solvent in vacuo afforded a residue, which was purified by column chromatography (hexane/EtOAc 2:1) to give **17** (183 mg, 99%) as a colorless oil. $[\alpha]25_D$ −15.2 (*c* 1.00, $CHCl_3$); ^1H NMR (400 MHz, $CDCl_3$): δ 1.82–1.91 (1H, m), 1.99–2.17 (3H, m), 2.02 (3H, s), 2.21–2.25 (2H, m), 2.36–2.43 (3H, m), 2.51 (1H, dd, J = 8.8, 15.1 Hz), 3.73 (3H, s), 3.79 (3H, s), 4.10 (1H, dt, J = 2.9, 8.3 Hz), 4.31 (1H, d, J = 11.2 Hz), 4.51 (1H, d, J = 10.7 Hz), 4.65–4.70 (1H, m), 5.32 (1H, dd, J = 7.8, 15.6 Hz), 5.59 (1H, dt, J = 6.8, 15.1 Hz), 6.83 (2H, d, J = 8.3 Hz), 7.01 (1H, d, J = 8.3 Hz), 7.19–7.45 (17H, m); ^{13}C NMR (100 MHz, $CDCl_3$): δ 15.4, 29.9, 31.2, 31.4, 31.8, 42.7, 51.3, 52.3, 55.3, 66.6, 70.0, 76.7, 113.8 (3C), 126.6 (2C), 127.9 (6C), 129.6 (6C), 129.7 (2C), 129.9, 130.3, 133.0, 144.9 (3C), 159.3, 170.6, 172.4; IR (neat): 3438, 1734, 1647, 1514, 1443, 1363, 1300, 1248, 1174, 1077, 1032, 972 cm^{-1}; HRMS (EI): *m/z* calcd for $C_{40}H_{45}NO_5S_2$ (M^+) 683.2739, found 683.2741.

4.1.2. (R)-2-[(S,E)-3-(4-Methoxybenzyloxy)-7-(tritylthio)hept-4-enamide]-4-(methylthio)butanoic acid (14)

1 M LiOH (0.64 mL, 0.64 mmol) was added dropwise to a stirred solution of **17** (110 mg, 0.16 mmol) in MeOH (3.2 mL) at room temperature. After 3 h, 10% aqueous HCl was added to the mixture at 0 °C until the pH was 6. The resulting mixture was extracted with EtOAc (3 × 20 mL), and the combined extracts were washed with saturated aqueous $NaHCO_3$ (2 × 10 mL) and brine (2 × 10 mL), then dried over Na_2SO_4. Concentration of the solvent in vacuo afforded a residue, which was purified by column chromatography ($CHCl_3$/MeOH 10:1) to give **14** (107 mg, 100%) as a white amorphous solid. $[\alpha]25_D$ −3.2 (*c* 1.00, $CHCl_3$); ^1H NMR (400 MHz, $CDCl_3$): δ 1.84–1.91 (1H, m), 1.99 (3H, s), 2.10–2.24 (5H, m), 2.40–2.52 (4H, m), 3.76 (3H, s), 4.07–4.12 (1H, m), 4.26 (1H, d, J = 10.7 Hz), 4.41 (1H, d, J = 10.3 Hz), 4.57–4.61 (1H, m), 5.29 (1H, dd, J = 7.3, 15.4 Hz), 5.57 (1H, dt, J = 6.8, 15.1 Hz), 6.80–6.84 (3H, m), 7.15–7.4 (17H, m); ^{13}C NMR (100 MHz, $CDCl_3$): δ 15.2, 29.8, 31.2, 31.3, 42.3, 51.8, 55.2, 66.5, 66.9, 70.0, 76.4, 113.8 (3C), 126.5 (2C), 127.8 (6C), 128.5, 129.6 (6C), 129.7 (2C), 130.0, 133.1, 144.8 (3C), 159.2, 171.7, 175.2; IR (neat): 3358, 3085, 2916, 1729, 1644, 1613, 1514, 1443, 1248, 1175, 1077, 1034, 970, 748, 701 cm^{-1}; HRMS (FAB): *m/z* calcd for $C_{39}H_{43}NO_5S_2Na$ (M^+ + Na) 692.2480, found 692.2454.

4.1.3. (3S,4R)-Allyl 3-(tert-butyldimethylsiloxy)-4-{(S)-2-[(R)-2-[(S,E)-3-(4-methoxybenzyloxy)-7-(tritylthio)hept-4-enoylamino]-4-(methylthio)butanoylamino]-3-tritylthio(propionylamino)}-5-methylhexanoate (18)

i-Pr_2NEt (71 μL, 0.42 mmol) was added dropwise to a stirred solution of **12** (106 mg, 0.16 mmol) and **14** (107 mg, 0.16 mmol) in CH_2Cl_2 (3.2 mL) containing *O*-(7-azabenzotriazol-1-yl)-*N,N,N′,N′*-tetramethyluronium hexafluorophosphate (HATU) (79.1 mg, 0.21 mmol) and 1-hydroxy-7-azabenzotriazole (HOAt) (28.3 mg, 0.21 mmol) at −30 °C under argon. After 3 h, the reaction mixture was diluted with $CHCl_3$ (30 mL). The organic layer was washed successively with 10% aqueous HCl (2 × 10 mL), saturated aqueous $NaHCO_3$ (2 × 10 mL) and brine (2 × 10 mL), then dried over Na_2SO_4. Concentration of the solvent in vacuo afforded a residue, which was purified by column chromatography (hexane/EtOAc 1:1) to give **18** (175 mg, 83%) as a colorless viscous liquid. $[\alpha]25_D$ +10.8 (*c* 1.02, $CHCl_3$); ^1H NMR (400 MHz, $CDCl_3$): δ 0.01 (3H, s), 0.05 (3H, s), 0.79–0.84 (6H, m), 0.82 (9H, s), 1.66–1.73 (1H, m), 1.88–1.98 (2H, m), 1.97 (3H, s), 2.05–2.23 (4H, m), 2.30–2.45 (5H, m), 2.47–2.55 (2H, m), 2.73 (1H, dd, J = 8.3, 13.2 Hz), 3.74–3.80 (1H, m), 3.79 (3H, s), 3.87 (1H, dd, J = 5.4, 7.8 Hz), 4.01 (1H, dt, J = 3.4, 8.1 Hz), 4.09–4.17 (1H, m), 4.15 (1H, d, J = 10.2 Hz), 4.35–4.42 (1H, m), 4.37 (1H, d, J = 10.7 Hz), 4.45–4.55 (2H, m), 5.18–5.31 (3H, m), 5.45 (1H, dt, J = 6.8, 15.4 Hz), 5.82–5.92 (1H, m), 5.99 (1H, d, J = 10.2 Hz), 6.63 (1H, d, J = 7.3 Hz), 6.83 (2H, d, J = 8.8 Hz), 7.05 (1H, d, J = 7.3 Hz), 7.13–7.44 (32H, m); ^{13}C NMR (100 MHz, $CDCl_3$): δ −4.7, −4.6, 15.1, 16.8, 17.9, 20.4, 25.8 (3C), 27.9, 30.1, 30.6, 31.3, 31.4, 33.0, 39.6, 42.5, 52.1, 52.6, 55.3, 58.3, 65.3, 66.6, 67.1, 69.5, 70.1, 76.5, 114.0 (3C), 118.4 (3C), 126.6 (6C), 126.8 (2C), 127.9 (6C), 128.1 (6C), 128.7, 129.5 (6C), 129.7, 129.8 (2C), 130.0, 132.1, 133.1, 144.3 (3C), 144.8 (3C), 159.4, 169.7, 171.21, 171.22, 171.6; IR (neat): 3435, 2929, 2855, 1683, 1638, 1556, 1541, 1515, 1248, 1171, 1082, 1035, 828, 744, 701 cm^{-1}; HRMS (FAB): *m/z* calcd for $C_{77}H_{94}N_3O_8S_3Si$ (M^+ + H) 1312.5972, found 1312.5957.

4.1.4. (3S,4R)-Allyl 3-(tert-butyldimethylsiloxy)-4-{(S)-2-[(R)-2-[(S,E)-3-hydroxy-7-(tritylthio)hept-4-enoylamino]-4-(methylthio) butanoylamino]-3-tritylthio(propionylamino)}-5-methylhexanoate (19)

2,3-dichloro-5,6-dicyano-1,4-benzoquinone (DDQ) (64 mg, 0.23 mmol) was added in small portions to a stirred solution of **18** (146 mg, 0.11 mmol) in CH_2Cl_2/H_2O 9:1 (11 mL) at room temperature. After 3 h, the mixture was diluted with $CHCl_3$ (60 mL), and the organic layer was washed with saturated aqueous $NaHCO_3$ (2 × 20 mL) and brine (2 × 20 mL), then dried over Na_2SO_4. Concentration of the solvent in vacuo afforded a residue, which was purified by column chromatography (hexane/EtOAc, 1:1) to give **19** (114 mg, 87%) as a colorless viscous liquid. $[\alpha]25_D$ +6.4 (*c* 1.00, $CHCl_3$); ^1H NMR (400 MHz, $CDCl_3$): δ 0.00 (3H, s), 0.05 (3H, s), 0.79–0.84 (6H, m), 0.81 (9H, s), 1.86–1.97 (2H, m), 2.02–2.10 (3H, m), 2.06 (3H, s), 2.17–2.23 (3H, m), 2.30–2.33 (1H, m), 2.40 (1H, dd, J = 7.3, 15.6 Hz), 2.51–2.55 (3H, m), 2.63 (1H, dd, J = 8.3, 12.9 Hz), 3.30 (1H, br s), 3.89–3.97 (1H, m), 3.92–3.97 (1H, m), 4.14–4.18 (1H, m), 4.33–4.37 (1H, m), 4.42–4.54 (3H, m), 5.19–5.31 (2H, m), 5.36 (1H, dd, J = 6.3, 15.4 Hz), 5.49 (1H, dt, J = 6.8, 15.1 Hz), 5.81–5.91 (2H, m), 6.49 (1H, d, J = 7.8 Hz), 7.14–7.45 (32H, m); ^{13}C NMR (100 MHz, $CDCl_3$): δ −4.8, −4.7, 15.4, 16.9, 17.9, 20.2, 25.7 (3C), 28.0, 30.3, 30.4, 31.25, 31.33, 33.2, 39.4, 44.1, 52.6, 53.1, 58.5, 65.3, 66.6, 67.0, 69.3, 69.8, 118.4, 126.6 (3C), 126.8 (3C), 127.8 (6C), 128.0 (6C), 129.48 (6C), 129.53 (6C), 129.9, 132.0, 132.5, 144.3 (3C), 144.8 (3C), 170.0, 170.9,

171.5, 171.6; IR (neat): 3438, 2958, 2930, 2854, 1736, 1635, 1550, 1489, 1443, 1252, 1181, 1036, 828, 741, 701 cm^{-1}; HRMS (FAB): *m/z* calcd for $C_{69}H_{86}N_3O_7S_3Si$ (M^+ + H) 1192.5397, found 1192.5396.

4.1.5. (3S,4R)-3-(Tert-butyldimethylsiloxy)-4-{(S)-2-[(R)-2-[(S,E)-3-hydroxy-7-(tritylthio)hept-4-enoylamino]-4-(methylthio) butanoylamino]-3-tritylthio(propionylamino)}-5-methylhexanoic acid (**10**)

Morpholine (18.8 L, 0.22 mmol) was added dropwise to a stirred solution of **19** (117 mg, 97 μmol) in THF (10 mL) containing $Pd(PPh_3)_4$ (13.0 mg, 11 μmol) at room temperature under argon. After 30 min, the reaction mixture was diluted with EtOAc (30 mL). The organic layer was washed with 10% aqueous HCl (2 × 10 mL) and brine (2 × 10 mL), then dried over Na_2SO_4. Concentration of the solvent in vacuo afforded a residue, which was purified by column chromatography ($CHCl_3$/MeOH 20:1) to give **10** (98.9 mg, 85%) as a white amorphous solid. [α]25D +2.2 (*c* 1.00, $CHCl_3$); ^1H NMR (400 MHz, $CDCl_3$): δ 0.05 (6H, s), 0.80–0.87 (15H, m), 1.91–2.12 (5H, m), 2.04 (3H, s), 2.19–2.25 (3H, m), 2.33 (1H, dd, *J* = 2.9, 13.4 Hz), 2.40 (1H, dd, *J* = 4.4, 15.9 Hz), 2.49–2.53 (4H, m), 2.72 (1H, dd, *J* = 8.3, 12.4 Hz), 3.75–3.84 (1H, m), 4.07–4.13 (2H, m), 4.33–4.38 (1H, m), 4.49–4.54 (1H, m), 5.34 (1H, dd, *J* = 5.9, 15.6 Hz), 5.47 (1H, dt, *J* = 6.8, 15.1 Hz), 6.32 (1H, d, *J* = 10.3 Hz), 6.81 (1H, d, *J* = 7.3 Hz), 7.15–7.44 (31H, m); ^{13}C NMR (100 MHz, $CDCl_3$): δ −4.8, −4.5, 15.4, 16.4, 17.9, 20.3, 25.7 (3C), 27.7, 29.7, 30.2, 31.28, 31.32, 33.2, 39.7, 44.2, 53.30, 53.34, 59.3, 66.2, 67.0, 69.0, 69.8, 126.6 (3C), 126.9 (3C), 127.9 (6C), 128.1 (6C), 129.5 (6C), 129.6 (6C), 130.1, 132.3, 144.3 (3C), 144.8 (3C), 170.4, 171.5, 172.0, 173.9; IR (neat): 3435, 2955, 1646, 1557, 1541, 1507, 1437, 1396, 1255, 1184, 1088, 1011, 953, 742, 702 cm^{-1}; HRMS (FAB): *m/z* calcd for $C_{66}H_{82}N_3O_7S_3Si$ (M^+ + H) 1152.5084, found 1152.5062.

4.1.6. (2S,6R,9S,12R,13S)-13-(Tert-butyldimethylsilyloxy)-12-isopropyl-6-[2-(methylthio)ethyl]-2-[(E)-4-(tritylthio)but-1-enyl]-9-tritylthiomethyl-1-oxa-5,8,11-triazacyclopentadecane-4,7,10,15-tetraone (**20**)

A solution of **10** (119 mg, 0.10 mmol) in CH_2Cl_2 (10 mL) was added very slowly to a stirred solution of 2-methyl-6-nitrobenzoic anhydride (MNBA) (46.3 mg, 0.14 mmol) in CH_2Cl_2 (100 mL, 1.0 mM concentration) containing 4-dimethylaminopyridine (DMAP) (38 mg, 0.31 mmol) at room temperature over 14 h. After 1 h, the mixture was diluted with CH_2Cl_2 (100 mL), and the organic layer was washed successively with saturated aqueous $NaHCO_3$ (2 × 40 mL), water (2 × 40 mL) and brine (2 × 40 mL), then dried over Na_2SO_4. Concentration of the solvent in vacuo afforded a residue, which was purified by column chromatography (hexane/EtOAc, 1:1) to give **20** (89.0 mg, 79%) as a white amorphous solid. [α]25D −7.7 (*c* 1.01, $CHCl_3$); ^1H NMR (400 MHz, $CDCl_3$): δ 0.00 (3H, s), 0.08 (3H, s), 0.81–0.84 (6H, m), 0.87 (9H, s), 2.02–2.26 (7H, m), 2.06 (3H, s), 2.35–2.52 (4H, m), 2.58–2.70 (2H, m), 2.75 (1H, dd, *J* = 4.4, 12.7 Hz), 3.26–3.31 (1H, m), 3.40–3.46 (1H, m), 3.66–3.70 (1H, m), 4.08–4.12 (1H, m), 4.34–4.37 (1H, m), 5.40 (1H, dd, *J* = 6.8, 15.1 Hz), 5.56–5.60 (1H, m), 5.70 (1H, dt, *J* = 6.8, 15.1 Hz), 6.45 (1H, br s), 6.88 (1H, d, *J* = 5.9 Hz), 7.11 (1H, d, *J* = 10.3 Hz), 7.18–7.41 (30H, m); ^{13}C NMR (100 MHz, $CDCl_3$): δ −4.8, −4.1, 15.1, 15.5, 17.9, 20.5, 25.7 (3C), 27.3, 29.3, 30.3, 31.0, 31.3, 31.7, 42.0, 42.1, 52.9, 58.0, 58.9, 66.6, 66.9, 68.8, 71.5, 126.6 (3C), 126.8 (3C), 127.9 (6C), 128.0 (6C), 128.6, 129.49 (6C), 129.52 (6C), 133.3, 144.4 (3C), 144.8 (3C), 169.8, 170.16, 170.18, 171.8; IR (neat): 3430, 2955, 2928, 2857, 1733, 1715, 1648, 1575, 1540, 1507, 1490, 1445, 1260, 1082, 832, 771, 747, 699 cm^{-1}; HRMS (FAB): *m/z*: calcd for $C_{66}H_{80}N_3O_6S_3Si$ (M^+ + H) 1134.4979, found 1134.4996.

4.1.7. (1S,5S,6R,9S,20R,E)-5-(Tert-butyldimethylsilyloxy)-6-isopropyl-20-[2-(methylthio)ethyl]-2-oxa-11,12-dithia-7,19,22-triazabicyclo[7.7.6]docos-15-ene-3,8,18,21-tetraone (**21**)

A solution of **20** (89 mg, 78 μmol) in CH_2Cl_2/MeOH 9:1 (20 mL) was added dropwise to a vigorously stirred solution of I_2 (198 mg, 0.78 mmol) in CH_2Cl_2/MeOH 9:1 (157 mL, 0.5 mM concentration) over 10 min at room temperature. After 10 min, the reaction was quenched with 0.2 M ascorbic acid/citric acid buffer (10 mL, adjusted to pH 4.0) at room temperature, and the resulting mixture was extracted with $CHCl_3$ (3 × 50 mL). The combined extracts were washed with brine (2 × 50 mL), then dried over Na_2SO_4. Concentration of the solvent in vacuo afforded a residue, which was purified by column chromatography ($CHCl_3$/MeOH 30:1) to give **21** (40.8 mg, 81%) as a white amorphous solid. [α]25D +27.4 (*c* 0.81, $CHCl_3$); ^1H NMR (400 MHz, CD_3OD): δ −0.07 (3H, s), 0.00 (3H, s), 0.72 (3H, d, *J* = 6.8 Hz), 0.74 (9H, s), 0.79 (3H, d, *J* = 6.8 Hz), 1.87–1.95 (1H, m), 1.92 (3H, s), 2.00–2.06 (1H, m), 2.19–2.25 (1H, m), 2.37–2.61 (6H, m), 2.67–2.75 (2H, m), 2.79–2.83 (2H, m), 3.01–3.24 (3H, m), 4.06–4.09 (1H, m), 4.59–4.62 (2H, m), 5.46–5.47 (1H, m), 5.73–5.85 (2H, m), 6.84 (1H, d, *J* = 8.8 Hz), 7.47 (1H, d, *J* = 7.3 Hz), 8.38 (1H, br s); ^{13}C NMR (100 MHz, CD_3OD): δ −4.7, −4.0, 15.1, 18.1, 18.9, 21.6, 26.3 (3C), 30.5, 31.0, 31.3, 33.4, 41.4, 41.6, 42.1, 56.7, 57.3, 63.9, 69.1, 71.4, 79.5, 130.1, 132.4, 170.5, 170.9, 173.9, 174.3; IR (neat): 3342, 2957, 2928, 2856, 1744, 1662, 1542, 1432, 1257, 1158, 1137, 1080, 833, 776, 755 cm^{-1}; HRMS (FAB): *m/z* calcd for $C_{28}H_{50}N_3O_6S_3Si$ (M^+ + H) 648.2631, found 648.2629.

4.1.8. Burkholdac A (**1**)

HF·pyridine (2.5 mL) was added to a stirred solution of **21** (32.0 mg, 49 μmol) in pyridine (5 mL) at room temperature. After 14 h, the reaction mixture was diluted with EtOAc (60 mL), and the organic layer was washed successively with 3% aqueous HCl (3 × 15 mL), saturated aqueous $NaHCO_3$ (2 × 15 mL) and brine (2 × 15 mL), then dried over Na_2SO_4. Concentration of the solvent in vacuo afforded a residue, which was purified by column chromatography ($CHCl_3$/MeOH 10:1) to give **1** (23.4 mg, 89%) as a white amorphous solid. [α]25D −57.3 (*c* 0.16, MeOH), {lit [3]. [α]20D −54 (*c* 0.23 in MeOH)}. ^1H NMR (400 MHz, CD_3CN): δ 0.78 (3H, d, *J* = 6.3 Hz), 0.88 (3H, d, *J* = 6.8 Hz), 1.92–1.99 (1H, m), 2.02 (3H, s), 2.13–2.21 (1H, m), 2.36–2.43 (1H, m), 2.48–2.75 (9H, m), 2.88 (1H, dd, *J* = 7.3, 13.2 Hz), 3.02–3.05 (1H, m), 3.14–3.24 (3H, m), 4.04–4.09 (1H, m), 4.33–4.39 (1H, m), 4.62 (1H, dt, *J* = 3.9, 9.3 Hz), 5.43–5.45 (1H, m), 5.80 (1H, d, *J* = 12.2 Hz), 6.01–6.07 (1H, m), 6.78 (1H, d, *J* = 8.8 Hz), 7.17 (1H, br s), 7.29 (1H, d, *J* = 6.8 Hz); ^{13}C NMR (100 MHz, CD_3CN): δ 15.1, 19.7, 21.1, 30.4, 30.6, 31.2, 33.3, 40.8, 40.9 (2C), 41.7, 56.3, 56.8, 63.2, 69.1, 71.6, 131.4, 132.4, 169.9, 171.7, 171.8, 172.8; IR (neat): 3361, 3335, 2960, 2921, 2849, 1733, 1717, 1683, 1654, 1541, 1523, 1508, 1263, 1162, 1020, 983, 754 cm^{-1}; HRMS (FAB): *m/z* calcd for $C_{22}H_{36}N_3O_6S_3$ (M^+ + H) 534.1766, found 534.1769. The ^1H and ^{13}C NMR, and MS spectrum are identical with those reported for natural burkholdac A [1].

4.1.9. (3S,4R,5R)-Allyl 3-(tert-butyldimethylsiloxy)-4-{(S)-2-[(R)-2-[(S,E)-3-(4- methoxybenzyloxy)-7-(tritylthio)hept-4-enoylamino]-4-(methylthio)butanoylamino]-3- tritylthio(propionylamino)}-5-methylheptanoate (**22**)

i-Pr_2NEt (0.17 L, 1.0 mmol) was added dropwise to a stirred solution of **13** (260 mg, 0.39 mmol) and **14** (258 mg, 0.39 mmol) in CH_2Cl_2 (7.7 mL) containing HATU (190 mg, 0.50 mmol) and HOAt (68.1 mg, 0.50 mmol) at −30 °C under argon. After 3 h, the reaction mixture was diluted with $CHCl_3$ (40 mL). The organic layer was washed successively with 10% aqueous HCl (2 × 15 mL), saturated aqueous $NaHCO_3$ (2 × 15 mL) and brine (2 × 15 mL), then dried over Na_2SO_4. Concentration of the solvent in vacuo afforded a residue, which was purified by column chromatography (hexane/EtOAc 1:1)

to give **22** (471 mg, 92%) as a colorless viscous liquid. [α]25D +12.8 (*c* 1.00, $CHCl_3$); ^1H NMR (400 MHz, $CDCl_3$): δ 0.00 (3H, s), 0.06 (3H, s), 0.78–0.85 (6H, m), 0.83 (9H, s), 1.01–1.12 (1H, m), 1.15–1.24 (1H, m), 1.65–1.79 (2H, m), 1.88–1.97 (1H, m), 1.97 (3H, s), 2.04–2.15 (2H, m), 2.17–2.23 (2H, m), 2.30–2.47 (5H, m), 2.50–2.55 (2H, m), 2.73 (1H, dd, *J* = 8.3, 13.2 Hz), 3.78 (3H, s), 3.84–3.94 (2H, m), 4.00 (1H, dt, *J* = 3.4, 8.3 Hz), 4.10–4.17 (1H, m), 4.14 (1H, d, *J* = 10.7 Hz), 4.35–4.42 (1H, m), 4.37 (1H, d, *J* = 11.2 Hz), 4.43–4.54 (2H, m), 5.17–5.30 (3H, m), 5.44 (1H, dt, *J* = 6.8, 15.1 Hz), 5.81–5.91 (1H, m), 5.99 (1H, d, *J* = 10.2 Hz), 6.61 (1H, d, *J* = 7.8 Hz), 6.83 (2H, d, *J* = 8.3 Hz), 7.04 (1H, d, *J* = 7.3 Hz), 7.13–7.44 (32H, m); ^{13}C NMR (100 MHz, $CDCl_3$): δ −4.8, −4.5, 11.7, 13.6, 15.0, 17.9, 20.4, 25.7 (3C), 27.2, 30.0, 30.6, 31.2, 31.3, 32.9, 34.0, 40.0, 42.5, 51.9, 52.5, 55.2, 55.9, 65.2, 67.0, 69.4, 70.0, 76.4, 113.9 (2C), 118.3, 126.6 (3C), 126.7 (3C), 127.8 (6C), 128.0 (6C), 129.47 (6C), 129.49 (6C), 129.6, 129.8 (2C), 130.0, 132.0, 133.0, 144.2 (3C), 144.8 (3C), 159.3, 169.6, 171.1, 171.2, 171.5; IR (neat): 3287, 3059, 2957, 2928, 2856, 1733, 1639, 1539, 1514, 1443, 1248, 1172, 1084, 831, 744, 700 cm^{-1}; HRMS (FAB): *m/z* calcd for $C_{78}H_{96}N_3O_8S_3Si$ (M^+ + H) 1326.6129, found 1326.6110.

*4.1.10. (3S,4R,5R)-Allyl 3-(tert-butyldimethylsiloxy)-4-{(S)-2-[(R)-2-[(S,E)-3-hydroxy-7-(tritylthio)hept-4-enoylamino]-4-(methylthio)butanoylamino]-3-tritylthio(propionylamino)}-5-methylheptanoate (**23**)*

DDQ (161 mg, 0.71 mmol) was added in small portions to a stirred solution of **22** (471 mg, 0.36 mmol) in CH_2Cl_2/H_2O 9:1 (18 mL) at room temperature. After 3 h, the mixture was diluted with $CHCl_3$ (60 mL), and the organic layer was washed with saturated aqueous $NaHCO_3$ (2 × 20 mL) and brine (2 × 20 mL), then dried over Na_2SO_4. Concentration of the solvent in vacuo afforded a residue, which was purified by column chromatography (hexane/EtOAc, 1:1) to give **23** (353 mg, 82%) as a colorless viscous liquid. [α]25D +12.3 (*c* 1.01, $CHCl_3$); ^1H NMR (400 MHz, $CDCl_3$): δ 0.00 (3H, s), 0.06 (3H, s), 0.78–0.86 (6H, m), 0.83 (9H, s), 1.05–1.12 (1H, m), 1.17–1.24 (1H, m), 1.72–1.78 (1H, m), 1.86–1.95 (1H, m), 2.01–2.09 (3H, m), 2.04 (3H, s), 2.17–2.23 (3H, m), 2.32 (1H, dd, *J* = 2.4, 13.7 Hz), 2.41 (1H, dd, *J* = 7.3, 16.1 Hz), 2.49–2.63 (5H, m), 3.40 (1H, d, *J* = 2.9 Hz), 3.87–3.97 (2H, m), 4.14 (1H, dt, *J* = 3.4, 7.2 Hz), 4.33–4.37 (1H, m), 4.39–4.52 (3H, m), 5.18–5.30 (2H, m), 5.39 (1H, dd, *J* = 6.3, 15.4 Hz), 5.49 (1H, dt, *J* = 6.8, 15.6 Hz), 5.79–5.88 (1H, m), 5.91 (1H, d, *J* = 10.3 Hz), 6.52 (1H, d, *J* = 7.8 Hz), 7.15–7.43 (31H, m); ^{13}C NMR (100 MHz, $CDCl_3$): δ −4.8, −4.5, 11.6, 13.7, 15.3, 17.9, 25.7 (3C), 27.0, 30.3, 30.4, 31, 2, 31.3, 33.1, 34.1, 39.9, 44.0, 52.6, 53.0, 56.1, 65.2, 66.6, 66.9, 69.3, 69.8, 118.3, 126.6 (3C), 126.8 (3C), 127.8 (6C), 128.0 (6C), 129.45 (6C), 129.52 (6C), 129.9, 132.0, 132.5, 144.2 (3C), 144.8 (3C), 170.0, 170.9, 171.5, 171.6; IR (neat): 3277, 3059, 2956, 2927, 2855, 1736, 1636, 1543, 1490, 1443, 1387, 1251, 1084, 836, 743, 700 cm^{-1}; HRMS (FAB): *m/z* calcd for $C_{70}H_{88}N_3O_7S_3Si$ (M^+ + H) 1206.5554, found 1206.5562.

*4.1.11. (3S,4R,5R)-3-(Tert-butyldimethylsiloxy)-4-{(S)-2-[(R)-2-[(S,E)-3-hydroxy-7-(tritylthio)hept-4-enoylamino]-4-(methylthio)butanoylamino]-3-tritylthio(propionylamino)}-5-methylheptanoic acid (**11**)*

Morpholine (51 μL, 0.59 mmol) was added dropwise to a stirred solution of **23** (353 mg, 0.29 mmol) in THF (15 mL) containing $Pd(PPh_3)_4$ (33.8 mg, 29 μmol) at room temperature under argon. After 30 min, the reaction mixture was diluted with EtOAc (30 mL), and the organic layer was washed with 10% aqueous HCl (2 × 10 mL) and brine (2 × 10 mL), then dried over Na_2SO_4. Concentration of the solvent in vacuo afforded a residue, which was purified by column chromatography ($CHCl_3$/MeOH 20:1) to give **11** (320 mg, 94%) as a white amorphous solid. [α]25D +4.8 (*c* 1.13, $CHCl_3$); ^1H NMR (400 MHz, $CDCl_3$): δ 0.04 (3H, s), 0.05 (3H, s), 0.77–0.85 (6H, m), 0.85 (9H, s), 1.04–1.11 (1H, m), 1.16–1.23 (1H, m), 1.75–1.81 (1H, m), 1.89–1.96 (1H, m), 2.01–2.10 (3H, m), 2.01 (3H, s), 2.18–2.34 (4H, m), 2.39 (1H, dd, *J* = 3.9, 16.1 Hz), 2.46–2.56 (4H, m), 2.70 (1H, dd, *J* = 8.3, 11.9 Hz), 3.89–3.94 (1H, m), 4.07–4.11 (2H, m), 4.32–4.37 (1H, m), 4.52 (1H, dd, *J* = 7.8, 12.7 Hz), 5.34 (1H, dd, *J* = 5.9, 15.6 Hz), 5.47 (1H, dt, *J* = 6.8, 15.1 Hz), 6.41 (1H, d, *J* = 10.2 Hz), 6.88 (1H, d, *J* = 7.3 Hz), 7.14–7.42 (31H, m); ^{13}C NMR (100 MHz, $CDCl_3$): δ −4.8, −4.4, 11.8, 13.5, 15.3, 17.8, 25.7 (3C), 27.1, 30.2, 30.4, 31.2, 31.3, 33.0, 34.1, 40.1, 44.0, 53.1, 53.4, 56.9, 66.5, 66.9, 68.8, 69.7, 126.6 (3C), 126.8 (3C), 127.8 (6C), 128.0 (6C), 129.4 (6C), 129.5 (6C), 129.9, 132.3, 144.2 (3C), 144.8 (3C), 170.3, 171.6, 171.9, 174.3; IR (neat): 3285, 3059, 3018, 2957, 2927, 2856, 1714, 1642, 1539, 1489, 1471, 1443, 1252, 1085, 836, 751, 700 cm^{-1}; HRMS (FAB): *m/z* calcd for $C_{67}H_{83}N_3O_7S_3SiNa$ (M^+ + Na) 1188.5060, found 1188.5057.

*4.1.12. (2S,6R,9S,12R,13S)-12-[(S)-Isobutyl]-13-(tert-butyldimethylsilyloxy)-6-[2-(methylthio)ethyl]-2-[(E)-4-(tritylthio)but-1-en-1-yl]-9-tritylthiomethyl-1-oxa-5,8,11-triazacyclopentadecane-4,7,10,15-tetraone (**24**)*

A solution of **11** (320 mg, 0.27 mmol) in CH_2Cl_2 (27 mL) was added very slowly to a stirred solution of MNBA (123 mg, 0.36 mmol) in CH_2Cl_2 (270 mL, 1.0 mM concentration) containing DMAP (101 mg, 0.82 mmol) at room temperature over 14 h. After 1 h, the mixture was diluted with CH_2Cl_2 (200 mL), and the organic layer was washed successively with saturated aqueous $NaHCO_3$ (2 × 80 mL), water (2 × 80 mL) and brine (2 × 80 mL), then dried over Na_2SO_4. Concentration of the solvent in vacuo afforded a residue, which was purified by column chromatography (hexane/EtOAc, 1:1) to give **24** (256 mg, 81%) as a white amorphous solid. [α]25D −6.0 (*c* 1.00, $CHCl_3$); ^1H NMR (400 MHz, $CDCl_3$): δ 0.00 (3H, s), 0.08 (3H, s), 0.83 (3H, d, *J* = 6.8 Hz), 0.89–0.93 (3H, m), 0.89 (9H, s), 1.04–1.12 (1H, m), 1.18–1.27 (1H, m), 1.87–1.92 (1H, m), 2.00–2.20 (4H, m), 2.05 (3H, s), 2.22–2.30 (2H, m), 2.36–2.66 (4H, m), 2.59–2.66 (2H, m), 2.72 (1H, dd, *J* = 10.2, 18.3 Hz), 3.34–3.41 (2H, m), 3.82 (1H, dt, *J* = 2.0, 9.8 Hz), 4.16 (1H, dt, *J* = 4.4, 9.8 Hz), 4.34 (1H, dd, *J* = 7.3, 14.6 Hz), 5.41 (1H, dd, *J* = 6.8, 15.6 Hz), 5.59–5.64 (1H, m), 5.71 (1H, dt, *J* = 6.8, 15.1 Hz), 6.48 (1H, d, *J* = 7.3 Hz), 7.00 (1H, d, *J* = 4.9 Hz), 7.16 (1H, d, *J* = 10.3 Hz), 7.25–7.49 (30H, m); ^{13}C NMR (100 MHz, $CDCl_3$): δ −4.9, −4.0, 12.0, 12.9, 15.1, 17.8, 25.6 (3C), 27.3, 29.5, 30.2, 30.9, 31.3, 31.8, 34.0, 41.8, 42.2, 52.9, 57.0, 57.8, 66.6, 66.8, 68.6, 71.5, 126.6 (3C), 126.8 (3C), 127.8 (6C), 128.0 (6C), 128.1, 129.45 (6C), 129.48 (6C), 133.1, 144.4 (3C), 144.7 (3C), 169.8, 170.17, 170.24, 171.9; IR (neat): 3286, 3057, 2956, 2928, 2855, 1732, 1683, 1669, 1652, 1541, 1444, 1255, 1184, 1084, 834, 742, 699 cm^{-1}; HRMS (FAB): *m/z* calcd for $C_{67}H_{81}N_3O_6S_3SiNa$ (M^+ + Na) 1170.4954, found 1170.4971.

*4.1.13. (1S,5S,6R,9S,20R,E)-6-[(S)-Isobutyl]-5-(tert-butyldimethylsilyloxy)-20-[2-(methylthio)ethyl]-2-oxa-11,12-dithia-7,19,22-triazabicyclo[7.7.6]docos-15-ene-3,8,18,21-tetraone (**25**)*

A solution of **24** (246 mg, 0.21 mmol) in CH_2Cl_2/MeOH 9:1 (50 mL) was added dropwise to a vigorously stirred solution of I_2 (544 mg, 2.1 mmol) in CH_2Cl_2/MeOH 9:1 (420 mL, 0.5 mM concentration) over 10 min at room temperature. After 10 min, the reaction was quenched with 0.2 M ascorbic acid/citric acid buffer (20 mL, adjusted to pH 4.0) at room temperature, and the resulting mixture was extracted with $CHCl_3$ (3 × 50 mL). The combined extracts were washed with brine (2 × 50 mL), then dried over Na_2SO_4. Concentration of the solvent in vacuo afforded a residue, which was purified by column chromatography ($CHCl_3$/MeOH 30:1) to give **25** (112 mg, 79%) as a white amorphous solid. [α]25D +13.1 (*c* 1.01, $CHCl_3$); ^1H NMR (400 MHz, $CDCl_3$): δ 0.09 (3H, s), 0.16 (3H, s), 0.86–0.96 (6H, m), 0.93 (9H, s), 1.20–1.27 (1H, m), 1.36–1.43 (1H, m), 1.88 (1H, ddd, *J* = 2.4, 6.8, 14.0 Hz), 2.02–2.10 (1H, m), 2.19 (3H, s), 2.28–

2.36 (1H, m), 2.49–2.83 (8H, m), 2.96–3.14 (4H, m), 3.54–3.65 (1H, m), 4.41 (1H, dt, J = 4.4, 8.8 Hz), 4.86 (1H, dt, J = 3.4, 10.3 Hz), 4.98–5.02 (1H, m), 5.67–5.71 (2H, m), 6.33–6.41 (1H, m), 6.76 (1H, d, J = 6.8 Hz), 7.13 (1H, d, J = 6.8 Hz), 7.52 (1H, d, J = 3.9 Hz); ^{13}C NMR (100 MHz, $CDCl_3$): δ −5.0, −4.3, 11.9, 14.5, 15.5, 17.9, 25.7 (3C), 25.8, 27.7, 28.0, 31.3, 34.5, 36.2, 40.0, 40.4, 41.3, 53.7, 57.3, 61.0, 67.0, 68.9, 129.3, 132.4, 168.9, 169.0, 170.1, 171.0; IR (neat): 3341, 2957, 2929, 2857, 1745, 1662, 1543, 1432, 1257, 1158, 1138, 1080, 949, 837, 756 cm^{-1}; HRMS (FAB): m/z calcd for $C_{29}H_{52}N_3O_6S_3Si$ (M^+ + H) 662.2788, found 662.2783.

4.1.14. Burkholdac B (**2**)

HF·pyridine (1.2 mL) was added to a stirred solution of **25** (77.3 mg, 0.12 mmol) in pyridine (2.3 mL) at room temperature. After 14 h, the reaction mixture was diluted with EtOAc (60 mL), and the organic layer was washed successively with 3% aqueous HCl (3 × 15 mL), saturated aqueous $NaHCO_3$ (2 × 15 mL) and brine (2 × 15 mL), then dried over Na_2SO_4. Concentration of the solvent in vacuo afforded a residue, which was purified by column chromatography ($CHCl_3$/MeOH 10:1) to give **2** (62.0 mg, 97%) as a white amorphous solid. [α]25$_D$ −57.8 (c 1.00, MeOH), {lit. [2]. [α]32$_D$ −62.6 (c 0.34, MeOH)}. ^{1}H NMR (400 MHz, CD_2Cl_2): δ 0.88 (3H, d, J = 6.8 Hz), 0.91 (3H, t, J = 7.3 Hz), 1.16–1.24 (1H, m), 1.48–1.54 (1H, m), 1.99–2.09 (2H, m), 2.17 (3H, s), 2.20–2.29 (1H, m), 2.42–2.51 (1H, m), 2.61–2.68 (5H, m), 2.73–2.79 (2H, m), 2.88–2.93 (2H, m), 3.11 (1H, d, J = 13.7 Hz), 3.20–3.28 (2H, m), 3.32–3.36 (1H, m), 4.29 (1H, dt, J = 8.3, 4.4 Hz), 4.55–4.57 (1H, m), 4.83 (1H, dt, J = 8.8, 3.4 Hz), 5.49–5.51 (1H, m), 5.72 (1H, d, J = 15.6 Hz), 6.31 (1H, t, J = 11.7 Hz), 6.77 (1H, d, J = 9.3 Hz), 7.25 (1H, d, J = 7.3 Hz), 7.46 (1H, d, J = 2.9 Hz); ^{13}C NMR (100 MHz, CD_2Cl_2): δ 11.7, 15.56, 15.58, 27.5, 28.6, 31.5, 33.7, 36.6, 39.9, 41.1, 41.4, 41.8, 55.0, 57.6, 61.8, 68.5, 71.1, 129.5, 133.4, 169.4, 170.5, 171.4, 172.1; IR (neat): 3376, 2957, 2924, 2855, 1736, 1685, 1656, 1543, 1524, 1439, 1273, 1162, 980, 753 cm^{-1}; HRMS (FAB): m/z calcd for $C_{23}H_{38}N_3O_6S_3$ (M^+ + H) 548.1923, found 548.1924. The ^{1}H and ^{13}C NMR, and MS spectrum are identical with those reported for natural burkholdac B [1].

4.1.15. (3S,4S)-Ethyl 4-(tert-butoxycarbonylamino)-3-hydroxy-5-methylhexanoate (**27**) and its (3R,4S)-isomer (**28**)

A solution of EtOAc (6.0 mL, 62 mmol) in THF (8 mL) was added slowly to a stirred solution of lithium diisopropylamide (LDA) (62 mmol) [prepared from n-BuLi in hexane (1.6 M solution, 38.7 mL, 62 mmol) and i-Pr$_2$NH (9.3 mL, 65 mmol)] in THF (30 mL) at −78 °C. After 30 min, (2S)-2-(*tert*-butoxycarbonylamino)-3-methylbutylaldehyde (*N*-Boc-L-valinal) (**26**) [11] (3.66 g, 18 mmol) in THF (30 mL) was added to the above mixture at −78 °C. After 40 min, the reaction was quenched with 2 M HCl (20 mL) at −78 °C, and the resulting mixture was extracted with EtOAc (2 × 100 mL). The combined extracts were washed with saturated aqueous $NaHCO_3$ (2 × 50 mL) and brine (2 × 50 mL), then dried over Na_2SO_4. Concentration of the solvent in vacuo afforded a residue, which was purified by column chromatography (hexane/EtOAc 5:1 → 4:1) to give **27** (2.98 g, 57%, less polar) and **28** (1.56 g, 30%, more polar).

Compound 27: colorless oil; [α]25$_D$ −39.8 (c 1.03, $CHCl_3$); ^{1}H NMR (400 MHz, $CDCl_3$): δ 0.96 (3H, d, J = 6.8 Hz), 1.00 (3H, d, J = 6.8 Hz), 1.28 (3H, t, J = 7.1 Hz), 1.44 (9H, s), 1.83–1.91 (1H, m), 2.45 (1H, dd, J = 2.7, 16.7 Hz), 2.55 (1H, dd, J = 9.8, 16.7 Hz), 3.15 (1H, t, J = 9.5 Hz), 3.29 (1H, d, J = 2.9 Hz), 4.17 (2H, q, J = 6.8 Hz), 4.24–4.28 (1H, m), 4.85 (1H, d, J = 9.3 Hz); ^{13}C NMR (100 MHz, $CDCl_3$): δ 14.1, 19.5, 19.8, 28.4 (3C), 30.4, 39.1, 59.6, 60.8, 67.1, 79.1, 156.4, 173.7; IR (neat): 3393, 2977, 1716, 1507, 1392, 1367, 1309, 1279, 1247, 1174, 1042, 1023, 869, 777 cm^{-1}; HRMS (EI): m/z calcd for $C_{14}H_{27}NO_5$ (M^+) 289.1889, found 289.1882.

Compound 28: colorless oil; [α]25$_D$ +9.0 (c 1.02, $CHCl_3$); ^{1}H NMR (400 MHz, $CDCl_3$): δ 0.88 (3H, d, J = 7.3 Hz), 0.95 (3H, d, J = 6.8 Hz), 1.28 (3H, t, J = 7.3 Hz), 1.44 (9H, s), 2.09–2.17 (1H, m), 2.46 (1H, dd, J = 9.8, 17.1 Hz), 2.59 (1H, dd, J = 2.0, 17.1 Hz), 3.30 (1H, d, J = 4.9 Hz), 3.50–3.56 (1H, m), 3.90–3.96 (1H, m), 4.18 (2H, dq, J = 6.8, 2.0 Hz), 4.43 (1H, br d, J = 10.2 Hz); ^{13}C NMR (100 MHz, $CDCl_3$): δ 14.1, 16.2, 20.1, 27.5, 28.3 (3C), 38.4, 58.7, 60.8, 69.2, 79.5, 156.4, 173.2; IR (neat): 3450, 3369, 2965, 1716, 1698, 1524, 1391, 1367, 1308, 1251, 1173, 1069, 984, 869, 775 cm^{-1}; HRMS (EI): m/z calcd for $C_{14}H_{27}NO_5$ (M^+) 289.1889, found 289.1891.

4.1.16. Conversion of compound **27** to compound **28**

2.6 M Jones reagent (5.2 mL, 14 mmol) was added dropwise to a stirred solution of **27** (2.68 g, 9.2 mmol) in acetone (80 mL) at 0 °C, and stirring was continued for 1 h at room temperature. The mixture was diluted with Et_2O (200 mL). The organic layer was washed with saturated aqueous $NaHCO_3$ (2 × 50 mL) and brine (2 × 50 mL), then dried over Na_2SO_4. Concentration of the solvent in vacuo afforded a residue, which was purified by column chromatography (hexane/EtOAc 8:1 → 4:1) to give (*S*)-ethyl 4-(*tert*-butoxycarbonylamino)-5-methyl-3-oxohexanoate (2.26 g, 86%) as a colorless oil.

KBH_4 (2.13 g, 40 mmol) was added in small portions to a stirred solution of the above product (2.26 g, 7.9 mmol) in MeOH (80 mL) at −40 °C. After 5 h, the reaction was quenched with 10% aqueous citric acid at 0 °C (adjusted to pH 3). After concentration of the reaction mixture in vacuo, water (30 mL) was added, and the resulting mixture was extracted with CH_2Cl_2 (4 × 30 mL). The combined extracts were washed with brine (2 × 30 mL), then dried over Na_2SO_4. Concentration of the solvent in vacuo afforded a residue, which was purified by column chromatography (hexane/EtOAc 5:1 → 4:1) to give **28** (1.80 g, 79%) along with **27** (112 mg, 5%). The IR, ^{1}H and ^{13}C NMR, mass spectra of these samples were identical with those recorded for **27** and **28**, respectively.

4.1.17. (3R,4S)-Ethyl 4-(tert-butoxycarbonylamino)-3-(tert-butyldimethylsiloxy)-5-methylhexanoate (**29**)

tert-Butyldimethylsilyl chloride (TBSCl) (1.26 g, 8.4 mmol) was added to stirred solution of **28** (807 mg, 2.8 mmol) in DMF (20 mL) containing imidazole (1.14 g, 17 mmol) at room temperature. After 24 h, the reaction mixture was diluted with Et_2O (120 mL), and the organic layer was washed successively with 3% aqueous HCl (2 × 30 mL), saturated aqueous $NaHCO_3$ (2 × 30 mL) and brine (2 × 30 mL), then dried over Na_2SO_4. Concentration of the solvent in vacuo afforded a residue, which was purified by column chromatography (hexane/EtOAc 10:1 → 5:1) to give **29** (1.11 g, 99%) as a colorless oil. [α]25$_D$ −5.0 (c 1.00, $CHCl_3$); ^{1}H NMR (400 MHz, $CDCl_3$): δ 0.04 (3H, s), 0.09 (3H, s), 0.87–0.88 (12H, m), 0.92 (3H, d, J = 6.8 Hz), 1.27 (3H, t, J = 7.3 Hz), 1.43 (9H, s), 1.93–1.99 (1H, m), 2.43 (1H, dd, J = 5.9, 15.1 Hz), 2.53 (1H, dd, J = 6.2, 15.6 Hz), 3.47–3.53 (1H, m), 4.07–4.22 (3H, m), 4.46 (1H, br d, J = 10.7 Hz); ^{13}CNMR (100 MHz, $CDCl_3$): δ −4.9, −4.7, 14.1, 16.8, 18.0, 20.6, 25.7 (3C), 27.9, 28.4 (3C), 40.0, 59.5, 60.5, 70.1, 78.9, 155.9, 171.9; IR (neat): 3455, 3377, 2960, 2931, 1719, 1703, 1390, 1366, 1304, 1254, 1174, 1082, 837, 777 cm^{-1}; HRMS (EI): m/z calcd for $C_{20}H_{41}NO_5Si$ (M^+) 403.2754, found 403.2850.

4.1.18. (3R,4S)-Allyl 4-(tert-butoxycarbonylamino)-3-(tert-butyldimethylsiloxy)-5-methylhexanoate (**31**)

1 M NaOH (14 mL, 14 mmol) was added dropwise to a stirred solution of **29** (1.11 g, 2.8 mmol) in EtOH (30 mL) at room temperature. After 6 h, the mixture was diluted with 10% aqueous HCl (30 mL) at 0 °C, and the resulting mixture was extracted with EtOAc (3 × 30 mL). The combined extracts were washed with brine (2 × 20 mL), then dried over Na_2SO_4. Concentration of the

solvent in vacuo afforded (3*R*,4*S*)-4-(*tert*-butoxycarbonylamino)-3-(*tert*-butyldimethylsiloxy)-5-methylhexanoic acid (**30**) (1.03 g), which was used for the next reaction without further purification.

Allyl bromide (0.48 mL, 5.5 mmol) was added to a stirred solution of the crude carboxylic acid **30** (1.03 g, 2.8 mmol) in DMF (30 mL) containing K_2CO_3 (1.16 g, 8.3 mmol) at room temperature. After 6 h, the reaction was diluted with water (10 mL), and the resulting mixture was extracted with Et_2O (4 × 30 mL). The combined extracts were washed successively with 3% aqueous HCl (2 × 20 mL), saturated aqueous $NaHCO_3$ (2 × 20 mL) and brine (2 × 20 mL), then dried over Na_2SO_4. Concentration of the solvent in vacuo afforded a residue, which was purified by column chromatography (hexane/EtOAc 5:1) to give **31** (927 mg, 81%, 2 steps) as a pale yellow oil. $[\alpha]25_D$ −6.0 (*c* 1.00, $CHCl_3$); ^1H NMR (400 MHz, $CDCl_3$): δ 0.04 (3H, s), 0.10 (3H, s), 0.87–0.88 (12H, m), 0.93 (3H, d, J = 6.8 Hz), 1.43 (9H, s), 1.91–2.00 (1H, m), 2.47 (1H, dd, J = 7.3, 15.6 Hz), 2.57 (1H, dd, J = 5.8, 15.6 Hz), 3.48–3.53 (1H, m), 4.21 (1H, dd, J = 6.8, 12.7 Hz), 4.43 (1H, br d, J = 10.7 Hz), 4.53–4.63 (2H, m), 5.23–5.35 (2H, m), 5.88–5.97 (1H, m); ^{13}C NMR (100 MHz, $CDCl_3$): δ −4.9, −4.7, 16.7, 17.9, 20.5, 25.7 (3C), 27.9, 28.4 (3C), 40.0, 59.5, 65.3, 70.1, 79.0, 118.5, 132.0, 155.9, 171.5; IR (neat): 3453, 3374, 2960, 2931, 2858, 1714, 1704, 1504, 1390, 1366, 1254, 1172, 1083, 990, 837, 777, 666 cm^{-1}; HRMS (EI): *m/z* calcd for $C_{21}H_{41}NO_5Si$ (M^+) 415.2754, found 415. 2752.

4.1.19. (3R,4S)-Allyl 4-[(S)-2-(tert-butoxycarbonylamino)-3-(tritylthio)propanamido]-3-(tert-butyldimethylsiloxy)-5-methylhexanoate (34)

Trimethylsilyl trifluoromethanesulfonate (TMSOTf) (0.69 mL, 3.8 mmol) was added to a stirred solution of **31** (200 mg, 0.48 mmol) in CH_2Cl_2 (10 mL) in the presence of 2,6-lutidine (0.56 mL, 4.8 mmol) at room temperature. After 30 min, MeOH (1.6 mL) was added to the reaction mixture at 0 °C, and stirring was continued for 3 h at room temperature. The reaction mixture was concentrated in vacuo to afford (3*R*,4*S*)-allyl 4-amino-3-(*tert*-butyldimethylsiloxy)-5-methylhexanoate (**32**) (151 mg) as a colorless oil, which was immediately used for the next reaction due to its instability (prone to form a γ-lactam ring).

i-Pr_2NEt (0.25 mL, 1.5 mmol) was added dropwise to a stirred solution of the crude amine **32** (151 mg, 0.48 mmol) and *N*-Boc-*S*-trityl-D-cysteine (**33**) (333 mg, 0.72 mmol) in MeCN (16 mL) containing PyBOP (300 mg, 0.58 mmol) at room temperature under argon. After 3 h, the mixture was diluted with Et_2O (80 mL), and the organic layer was washed successively with 3% aqueous HCl (2 × 30 mL), saturated aqueous $NaHCO_3$ (2 × 30 mL) and brine (2 × 30 mL), then dried over Na_2SO_4. Concentration of the solvent in vacuo to afford a residue, which was purified by column chromatography (hexane/EtOAc 1:1) to give **34** (247 mg, 68%, 2 steps) as a colorless oil. $[\alpha]25_D$ −3.2 (*c* 1.00, $CHCl_3$); ^1H NMR (400 MHz, $CDCl_3$): δ 0.00 (3H, s), 0.05 (3H, s), 0.81 (3H, d, J = 6.3 Hz), 0.83 (9H, s), 0.86 (3H, d, J = 6.8 Hz), 1.42 (9H, s), 1.91–1.99 (1H, m), 2.44 (1H, dd, J = 6.3, 17.1 Hz), 2.50–2.58 (2H, m), 2.70–2.78 (1H, m), 3.80–3.86 (1H, m), 3.92 (1H, dt, J = 6.3, 5.4 Hz), 4.14 (1H, dt, J = 6.8, 4.4 Hz), 4.44–4.57 (2H, m), 4.70–4.76 (1H, m), 5.18–5.30 (2H, m), 5.80–5.90 (1H, m), 6.08 (1H, d, J = 10.7 Hz), 7.19–7.43 (15H, m); ^{13}C NMR (100 MHz, $CDCl_3$): δ −4.8, −4.6, 16.6, 17.9, 20.4, 25.7 (3C), 27.9, 28.2 (3C), 33.7, 39.7, 53.8, 57.9, 65.2, 67.2, 69.8, 80.2, 118.4, 126.8 (3C), 128.0 (6C), 129.5 (6C), 132.0, 144.4 (3C), 155.2, 170.3, 171.5; IR (neat): 3327, 2959, 2930, 2857, 1717, 1683, 1491, 1367, 1254, 1173, 1093, 937, 836, 751, 701 cm^{-1}; HRMS (EI): *m/z* calcd for $C_{43}H_{60}N_2O_6SSi$ (M^+) 760.3941, found 760.3934.

4.1.20. (3R,4S)-Allyl 4-[(S)-2-amino-3-(tritylthio)propanamido]-3-(tert-butyldimethylsiloxy)-5- methylhexanoate (35)

TMSOTf (0.29 mL, 1.6 mmol) was added dropwise to a stirred solution of **34** (241 mg, 0.32 mmol) in CH_2Cl_2 (4 mL) containing 2,6-lutidine (0.37 mL, 3.2 mmol) at room temperature. After 1 h, MeOH (0.7 mL) was added to the reaction mixture at 0 °C, and stirring was continued for 1 h at room temperature. The mixture was concentrated in vacuo to afford a residue, which was purified by column chromatography (hexane/EtOAc 5:1) to give **35** (206 mg, 98%) as a white amorphous solid. $[\alpha]25_D$ −4.2 (*c* 1.00, $CHCl_3$); ^1H NMR (400 MHz, $CDCl_3$): δ 0.00 (3H, s), 0.03 (3H, s), 0.82–0.85 (15H, m), 1.30 (2H, br s), 1.93–2.01 (1H, m), 2.45 (1H, dd, J = 6.8, 15.6 Hz), 2.47–2.56 (2H, m), 2.75 (1H, dd, J = 3.9, 12.7 Hz), 3.04 (1H, dd, J = 3.9, 8.8 Hz), 3.74–3.79 (1H, m), 4.14 (1H, dd, J = 6.3, 11.2 Hz), 4.46 (1H, dd, J = 5.4, 13.2 Hz), 4.53 (1H, dd, J = 5.9, 13.2 Hz), 5.20 (1H, d, J = 10.7 Hz), 5.28 (1H, dd, J = 1.5, 17.1 Hz), 5.81–5.90 (1H, m), 7.08 (1H, d, J = 9.3 Hz), 7.18–7.44 (15H, m); ^{13}C NMR (100 MHz, $CDCl_3$): δ −4.7, −4.6, 16.9, 17.9, 20.6, 25.7 (3C), 27.8, 37.4, 40.0, 54.1, 57.7, 65.2, 66.9, 69.9, 118.4, 126.7 (3C), 127.9 (6C), 129.6 (6C), 132.0, 144.6 (3C), 171.5, 172.8; IR (neat): 3369, 3312, 2958, 2929, 2856, 1736, 1673, 1508, 1255, 1174, 1092, 936, 836, 777, 743, 701, 676 cm^{-1}; HRMS (FAB): *m/z* calcd for $C_{38}H_{53}N_2O_4SSi$ ($M^+ + H$) 661.3466, found 661.3476.

4.1.21. (S)-Methyl 2-[(S,E)-3-(4-methoxybenzyloxy)-7-(tritylthio) hept-4-enamide]-4-(methylthio)butanoate (36)

i-Pr_2NEt (0.15 L, 0.91 mmol) was added dropwise to a stirred solution of **16** (70.9 mg, 0.13 mmol) and L-methionine methyl ester (***ent*-15**) (51.9 mg, 0.26 mmol) in MeCN (6.5 mL) containing PyBOP (135 mg, 0.26 mmol) at 0 °C under argon, and stirring was continued for 2 h at room temperature. The reaction mixture was diluted with EtOAc (30 mL), and the organic layer was washed successively with 10% aqueous HCl (2 × 10 mL), saturated aqueous $NaHCO_3$ (2 × 10 mL) and brine (2 × 10 mL), then dried over Na_2SO_4. Concentration of the solvent in vacuo afforded a residue, which was purified by column chromatography (hexane/EtOAc 2:1) to give **36** (87.0 mg, 98%) as a colorless oil. $[\alpha]25_D$ 1.8 (*c* 1.00, $CHCl_3$); ^1H NMR (400 MHz, $CDCl_3$): δ 1.84–1.91 (1H, m), 2.04 (3H, s), 2.05–2.16 (3H, m), 2.21–2.23 (2H, m), 2.36–2.49 (4H, m), 3.70 (3H, s), 3.78 (3H, s), 4.08–4.13 (1H, m), 4.25 (1H, d, J = 12.2 Hz), 4.52 (1H, d, J = 11.2 Hz), 4.68 (1H, dd, J = 7.3, 12.7 Hz), 5.35 (1H, dd, J = 8.3, 15.1 Hz), 5.59 (1H, dt, J = 6.8, 15.6 Hz), 6.83 (2H, d, J = 8.8 Hz), 6.87 (1H, d, J = 8.3 Hz), 7.19–7.45 (17H, m); ^{13}C NMR (100 MHz, $CDCl_3$): δ 15.3, 29.8, 31.2, 31.4, 31.8, 43.0, 51.3, 52.3, 55.2, 66.5, 69.8, 76.3, 113.8 (3C), 126.6 (2C), 127.8 (6C), 129.5 (6C), 129.6 (2C), 129.9, 130.2, 133.1, 144.8 (3C), 159.2, 170.3, 172.2; IR (neat): 3327, 3057, 2952, 2917, 1743, 1652, 1443, 1248, 1174, 1080, 1034, 822, 744, 701 cm^{-1}; HRMS (EI): *m/z* calcd for $C_{40}H_{45}NO_5S_2$ (M^+) 683.2739, found 683.2737.

4.1.22. (S)-2-[(S,E)-3-(4-methoxybenzyloxy)-7-(tritylthio)hept-4-enamide]-4-(methylthio)butanoic acid (37)

1 M LiOH (1.2 mL, 1.2 mmol) was added dropwise to a stirred solution of **36** (213 mg, 0.31 mmol) in MeOH (6.2 mL) at room temperature. After 3 h, 10% aqueous HCl was added to the mixture at 0 °C until the pH was 6. The resulting mixture was extracted with EtOAc (3 × 20 mL), and the combined extracts were washed with saturated aqueous $NaHCO_3$ (2 × 10 mL) and brine (2 × 10 mL), then dried over Na_2SO_4. Concentration of the solvent in vacuo afforded a residue, which was purified by column chromatography ($CHCl_3$/MeOH 10:1) to give **37** (203 mg, 98%) as a white amorphous solid. $[\alpha]25_D$ −4.6 (*c* 1.00, $CHCl_3$); ^1H NMR (400 MHz, $CDCl_3$): δ 1.84–1.93 (1H, m), 2.00 (3H, s), 2.07–2.18 (3H, m), 2.21–2.25 (2H, m), 2.39–2.51 (4H, m), 3.77 (3H, s), 4.11 (1H, dt, J = 8.3, 3.4 Hz), 4.24 (1H, d, J = 10.7 Hz), 4.51 (1H, d, J = 11.7 Hz), 4.63–4.67 (1H, m), 5.32 (1H, dd, J = 8.3, 15.6 Hz), 5.59 (1H, dt, J = 6.8, 15.1 Hz), 6.82 (2H, d,

J = 8.3 Hz), 7.07 (1H, d, J = 8.3 Hz), 7.05–7.45 (17H, m); ^{13}C NMR (100 MHz, $CDCl_3$): δ 15.2, 29.8, 31.2, 31.3, 31.4, 42.7, 51.6, 55.2, 66.5, 69.8, 76.2, 113.8 (3C), 126.6 (2C), 127.8 (6C), 129.5 (6C), 129.6, 129.7 (2C), 130.0, 133.4, 144.8 (3C), 159.2, 171.7, 175.1; IR (neat): 3336, 3015, 2918, 1733, 1614, 1541, 1514, 1489, 1444, 1248, 1177, 1034, 822, 747, 701 cm^{-1}; HRMS (FAB): m/z calcd for $C_{39}H_{44}NO_5S_2$ (M^+ + H) 670.2661, found 670.2684.

*4.1.23. (3R,4S)-Allyl 3-(tert-butyldimethylsiloxy)-4-{(S)-2-[(S)-2-[(S,E)-3-(4- methoxybenzyloxy)-7-(tritylthio)hept-4-enoylamino]-4-(methylthio)butanoylamino]-3-tritylthio(propionylamino)}-5-methylhexanoate (**38**)*

i-Pr$_2$NEt (66 μL, 0.39 mmol) was added dropwise to a stirred solution of **35** (99.1 mg, 0.15 mmol) and **37** (100 mg, 0.15 mmol) in CH_2Cl_2 (3.0 mL) containing HATU (74.1 mg, 0.20 mmol) and HOAt (26.5 mg, 0.20 mmol) at −30 °C under argon. After 3 h, the reaction mixture was diluted with $CHCl_3$ (30 mL). The organic layer was washed successively with 10% aqueous HCl (2 × 10 mL), saturated aqueous $NaHCO_3$ (2 × 10 mL) and brine (2 × 10 mL), then dried over Na_2SO_4. Concentration of the solvent in vacuo afforded a residue, which was purified by column chromatography (hexane/EtOAc 1:1) to give **38** (159 mg, 81%) as a colorless viscous liquid. [α]25D −1.2 (*c* 1.00, $CHCl_3$); ^{1}H NMR (400 MHz, $CDCl_3$): δ 0.00 (3H, s), 0.04 (3H, s), 0.72 (3H, d, J = 6.3 Hz), 0.80 (9H, s), 0.85 (3H, d, J = 6.3 Hz), 1.72–1.81 (2H, m), 1.94–2.00 (1H, m), 1.94 (3H, s), 2.11–2.15 (2H, m), 2.19–2.44 (7H, m), 2.54 (1H, dd, J = 3.9, 15.6 Hz), 2.65 (2H, d, J = 6.8 Hz), 3.76–3.78 (1H, m), 3.78 (3H, s), 4.05 (1H, dt, J = 8.3, 3.4 Hz), 4.17–4.22 (4H, m), 4.44–4.56 (3H, m), 5.17–5.33 (3H, m), 5.56 (1H, dt, J = 6.3, 15.6 Hz), 5.80–5.90 (1H, m), 6.25–6.31 (2H, m), 6.80–6.90 (3H, m), 7.17–7.42 (32H, m); ^{13}C NMR (100 MHz, $CDCl_3$): δ −4.8, −4.7, 15.2, 17.5, 17.9, 20.3, 25.7 (3C), 28.4, 30.0, 30.6, 31.2, 31.4, 33.7, 39.4, 42.9, 52.6, 53.1, 55.3, 59.0, 65.3, 66.6, 67.2, 69.3, 69.9, 76.4, 113.9 (2C), 118.3, 126.6 (3C), 126.8 (3C), 127.9 (6C), 128.0 (6C), 129.52 (6C), 129.54 (6C), 129.6 (2C), 129.9, 130.2, 132.1, 133.2, 144.4 (3C), 144.8 (3C), 159.3, 169.3, 171.05, 171.09, 172.0 ppm; IR (neat): 3319, 2957, 2929, 2856, 1733, 1645, 1514, 1444, 1250, 1176, 1083, 1035, 836, 743, 701 cm^{-1}; HRMS (FAB): m/z calcd for $C_{77}H_{94}N_3O_8S_3Si$ (M^+ + H) 1312.5972, found 1312.5948.

*4.1.24. (3R,4S)-Allyl 3-(tert-butyldimethylsiloxy)-4-{(S)-2-[(S)-2-[(S,E)-3-hydroxy-7-(tritylthio)hept-4-enoylamino]-4-(methylthio)butanoylamino]-3-tritylthio(propionylamino)}-5-methylhexanoate (**39**)*

DDQ (93.1 mg, 0.34 mmol) was added in small portions to a stirred solution of **38** (212 mg, 0.16 mmol) in CH_2Cl_2/H_2O 9:1 (16 mL) at room temperature. After 3 h, the mixture was diluted with $CHCl_3$ (60 mL), and the organic layer was washed with saturated aqueous $NaHCO_3$ (2 × 20 mL) and brine (2 × 20 mL), then dried over Na_2SO_4. Concentration of the solvent in vacuo afforded a residue, which was purified by column chromatography (hexane/EtOAc, 1:1) to give **39** (158 mg, 83%) as a colorless viscous liquid. [α]25D −7.7 (*c* 1.01, $CHCl_3$); ^{1}H NMR (400 MHz, $CDCl_3$): δ 0.00 (3H, s), 0.04 (3H, s), 0.78 (3H, d, J = 6.3 Hz), 0.80 (9H, s), 0.87 (3H, d, J = 6.8 Hz), 1.81–1.88 (1H, m), 1.90–1.99 (1H, m), 2.02–2.14 (3H, m), 2.03 (3H, s), 2.18–2.22 (2H, m), 2.27 (1H, dd, J = 9.3, 15.1 Hz), 2.55–2.69 (5H, m), 2.59 (1H, dd, J = 5.4, 12.7 Hz), 2.66 (1H, dd, J = 7.8, 13.2 Hz), 3.25 (1H, d, J = 3.4 Hz), 3.80 (1H, dt, J = 9.8, 6.3 Hz), 4.14–4.18 (2H, m), 4.29 (1H, dd, J = 6.8, 13.2 Hz), 4.35–4.41 (1H, m), 4.40 (1H, dd, J = 4.9, 13.7 Hz), 4.54 (1H, dd, J = 5.9, 13.2 Hz), 5.18–5.30 (2H, m), 5.38 (1H, dd, J = 6.3, 15.6 Hz), 5.53 (1H, dt, J = 6.8, 15.1 Hz), 5.80–5.90 (1H, m), 6.17 (1H, d, J = 10.2 Hz), 6.51–6.56 (2H, m), 7.18–7.52 (30 H, m); ^{13}C NMR (100 MHz, $CDCl_3$): δ −4.8 (2C), 15.2, 17.3, 17.9, 20.3, 25.7 (3C), 28.3, 30.15, 30.21, 31.3, 31.4, 33.6, 39.5, 42.9, 52.7, 52.9, 58.8, 65.4, 66.6, 67.1, 68.9, 69.2, 118.5, 126.6 (3C), 126.8 (3C), 127.8 (6C), 128.0 (6C), 129.47 (6C), 129.52 (6C), 130.0, 131.9, 132.3, 144.3 (3C), 144.8 (3C), 169.5, 170.8, 171.8, 172.0; IR (neat): 3340, 3318, 2958, 2928, 1732, 1634, 1539, 1444, 1255, 1179, 1094, 836, 743, 700 cm^{-1}; HRMS (FAB): m/z: calcd for $C_{69}H_{86}N_3O_7S_3Si$ (M^+ + H) 1192.5397, found 1192.5406.

*4.1.25. (3R,4S)-3-(Tert-butyldimethylsiloxy)-4-{(S)-2-[(S)-2-[(S,E)-3-hydroxy-7-(tritylthio)hept-4-enoylamino]-4-(methylthio)butanoylamino]-3-tritylthio(propionylamino)}-5-methylhexanoic acid (**40**)*

Morpholine (15.6 μL, 0.18 mmol) was added dropwise to a stirred solution of **39** (100 mg, 84 μmol) in THF (10 mL) containing $Pd(PPh_3)_4$ (11 mg, 9.5 μmol) at room temperature under argon. After 30 min, the reaction mixture was diluted with EtOAc (30 mL), and the organic layer was washed with 10% aqueous HCl (2 × 10 mL) and brine (2 × 10 mL), then dried over Na_2SO_4. Concentration of the solvent in vacuo afforded a residue, which was purified by column chromatography ($CHCl_3$/MeOH 20:1) to give **40** (71.6 mg, 74%) as a white amorphous solid. [α]25D −13.8 (*c* 1.00, $CHCl_3$); ^{1}H NMR (400 MHz, $CDCl_3/CD_3OD$ 9:1): δ 0.03 (6H, s), 0.74 (3H, d, J = 7.3 Hz), 0.81 (3H, d, J = 7.3 Hz), 0.84 (9H, s), 1.83–1.92 (1H, m), 1.95–2.01 (1H, m), 2.01 (3H, s), 2.03–2.09 (3H, m), 2.17–2.20 (2H, m), 2.29 (1H, dd, J = 9.3, 14.1 Hz), 2.32–2.39 (3H, m), 2.48–2.52 (2H, m), 2.54–2.57 (2H, m), 3.71–3.76 (1H, m), 4.02–4.06 (2H, m), 4.33–4.38 (1H, m), 4.44 (1H, t, J = 7.1 Hz), 5.39 (1H, dd, J = 5.9, 15.1 Hz), 5.51 (1H, dt, J = 6.3, 15.6 Hz), 6.59 (1H, d, J = 9.8 Hz), 7.15–7.44 (32H, m); ^{13}C NMR (100 MHz, $CDCl_3/CD_3OD$ 9:1): δ −5.1, −4.7, 15.1, 16.1, 17.7, 20.3, 25.6 (3C), 27.6, 29.5, 29.9, 30.8, 31.2, 31.3, 33.4, 43.0, 52.5, 52.7, 59.3, 66.4, 67.0, 68.6, 69.5, 126.5 (3C), 126.7 (3C), 127.7 (6C), 127.9 (6C), 129.3 (6C), 129.4 (6C), 131.2, 132.4, 144.2 (3C), 144.7 (3C), 170.2, 171.9, 172.2, 172.5; IR (neat): 3420, 2956, 2927, 2855, 1646, 1577, 1489, 1444, 1253, 1184, 1083, 1034, 969, 836, 743, 700, 622 cm^{-1}; HRMS (FAB): m/z calcd for $C_{66}H_{81}N_3O_7S_3SiK$ (M^+ + K) 1190.4643, found 1190.4653.

*4.1.26. (2S,6S,9S,12S,13R)-13-(Tert-butyldimethylsilyloxy)-12-isopropyl-6-[2-(methylthio)ethyl]-2-[(E)-4-(tritylthio)but-1-enyl]-9-tritylthiomethyl-1-oxa-5,8,11-triazacyclopentadecane-4,7,10,15-tetraone (**41**)*

A solution of **40** (81.2 mg, 70 μmol) in CH_2Cl_2 (7 mL) was added very slowly to a stirred solution of MNBA (31.3 mg, 91 μmol) in CH_2Cl_2 (70 mL, 1.0 mM concentration) containing DMAP (25.7 mg, 0.21 mmol) at room temperature over 14 h. After 1 h, the mixture was diluted with CH_2Cl_2 (100 mL), and the organic layer was washed successively with saturated aqueous $NaHCO_3$ (2 × 40 mL), water (2 × 40 mL) and brine (2 × 40 mL), then dried over Na_2SO_4. Concentration of the solvent in vacuo afforded a residue, which was purified by column chromatography (hexane/EtOAc, 1:1) to give **41** (66.3 mg, 84%) as a white amorphous solid. [α]25D −7.6 (*c* 1.00, $CHCl_3$); ^{1}H NMR (400 MHz, $CDCl_3/CD_3OD$ 9:1): δ −0.03 (3H, s), 0.14 (3H, s), 0.90–0.98 (15H, m), 1.85–1.94 (1H, m), 1.97–2.04 (1H, m), 2.10–2.14 (1H, m), 2.10 (3H, s), 2.25–2.37 (6H, m), 2.46–2.55 (3H, m), 2.63–2.75 (3H, m), 3.65 (1H, dd, J = 7.8, 14.6 Hz), 3.78 (1H, dt, J = 10.7, 2.4 Hz), 4.07 (1H, dt, J = 10.2, 3.4 Hz), 4.45 (1H, dd, J = 7.3, 16.1 Hz), 5.45–5.54 (2H, m), 5.67 (1H, dt, J = 5.9, 14.6 Hz), 6.52 (1H, d, J = 10.2 Hz), 7.02 (1H, d, J = 8.3 Hz), 7.28–7.51 (30H, m), 7.93 (1H, d, J = 8.3 Hz); ^{13}C NMR (100 MHz, $CDCl_3/CD_3OD$ 9:1): δ −5.4, −4.6, 14.4, 15.2, 17.8, 20.2, 25.6 (3C), 26.4, 30.0, 31.0, 31.2, 31.3, 31.9, 40.5, 41.5, 51.7, 53.0, 57.9, 66.5, 67.1, 67.7, 70.8, 126.5 (3C), 126.7 (3C), 127.7 (6C), 127.9 (6C), 128.1, 129.4 (12C), 132.5, 144.3 (3C), 144.7 (3C), 169.1, 170.1, 171.4, 171.8; IR (neat): 3443, 2959, 2930, 1733, 1645, 1540, 1444, 1387, 1256, 1219, 1180, 1126, 1084, 1035, 834, 743, 700 cm^{-1}; HRMS (FAB): m/z calcd for $C_{66}H_{80}N_3O_6S_3Si$ (M^+ + H) 1134.4979, found 1134.4974.

*4.1.27. (1S,5R,6S,9S,20S,E)-5-(Tert-butyldimethylsilyloxy)-6-isopropyl-20-[2-(methylthio)ethyl]-2-oxa-11,12-dithia-7,19,22-triazabicyclo[7.7.6]docos-15-ene-3,8,18,21-tetraone (**42**)*

A solution of **41** (56 mg, 49 μmol) in CH_2Cl_2/MeOH 9:1 (13 mL) was added dropwise to a vigorously stirred solution of I_2 (127 mg, 0.49 mmol) in CH_2Cl_2/MeOH 9:1 (98 mL, 0.5 mM concentration) over 10 min at room temperature. After 10 min, the reaction was quenched with 0.2 M ascorbic acid/citric acid buffer (10 mL, adjusted to pH 4.0) at room temperature, and the resulting mixture was extracted with $CHCl_3$ (3 × 50 mL). The combined extracts were washed with brine (2 × 50 mL), then dried over Na_2SO_4. Concentration of the solvent in vacuo afforded a residue, which was purified by column chromatography ($CHCl_3$/MeOH 30:1) to give **42** (27.4 mg, 85%) as a white amorphous solid. $[\alpha]25_D$ −105.5 (*c* 1.01, $CHCl_3$); ^{1}H NMR (400 MHz, $CDCl_3/CD_3OD$ 9:1): δ 0.05 (3H, s), 0.15 (3H, s), 0.77 (3H, d, *J* = 5.4 Hz), 0.80–0.82 (12H, m), 2.02 (3H, s), 2.09–2.27 (3H, m), 2.31–2.47 (5H, m), 2.54–2.60 (3H, m), 2.80–2.87 (2H, m), 3.32–3.46 (2H, m), 3.75–3.83 (2H, m), 4.02–4.07 (1H, m), 4.78–4.83 (1H, m), 5.56 (1H, d, *J* = 4.4 Hz), 5.65–5.73 (2H, m), 7.04 (1H, d, *J* = 7.3 Hz), 7.13 (1H, d, *J* = 10.2 Hz), 7.96 (1H, d, *J* = 5.9 Hz); ^{13}C NMR (100 MHz, $CDCl_3/CD_3OD$ 9:1): δ −5.5, −4.4, 14.6, 14.7, 17.8, 20.5, 25.7 (3C), 26.3, 27.9, 29.6, 30.8, 31.4, 40.0, 40.3, 42.9, 53.9, 56.7, 60.0, 69.0, 69.6, 130.5 (2C), 170.0, 170.1, 170.3, 171.3; IR (neat): 3389, 3308, 2957, 2928, 2856, 1741, 1660, 1541, 1430, 1301, 1249, 1167, 1092, 947, 838, 778, 756 cm^{-1}; HRMS (FAB): *m/z*: calcd for $C_{28}H_{50}N_3O_6S_3Si$ (M^+ + H) 648.2631, found 648.2639.

*4.1.28. 5,6,20-Tri-epi-burkholdac A (**3**)*

HF·pyridine (2.0 mL) was added to a stirred solution of **42** (26 mg, 40 μmol) in pyridine (4 mL) at room temperature. After 14 h, the reaction mixture was diluted with EtOAc (60 mL), and the organic layer was washed successively with 3% aqueous HCl (3 × 15 mL), saturated aqueous $NaHCO_3$ (2 × 15 mL) and brine (2 × 15 mL), then dried over Na_2SO_4. Concentration of the solvent in vacuo afforded a residue, which was purified by column chromatography ($CHCl_3$/MeOH 10:1) to give **3** (18.9 mg, 89%) as a white amorphous solid. $[\alpha]25_D$ −114.3 (*c* 0.38, $CHCl_3$); ^{1}H NMR (400 MHz, CD_3CN): δ 0.74 (3H, d, *J* = 6.8), 0.75 (3H, d, *J* = 6.8 Hz), 2.00 (3H, s), 2.00–2.09 (4H, m), 2.20 (1H, dd, *J* = 3.4, 13.7 Hz), 2.24–2.33 (2H, m), 2.36–2.44 (2H, m), 2.47–2.56 (3H, m), 2.61 (1H, dd, *J* = 6.8, 12.9 Hz), 3.13–3.35 (2H, m), 3.41 (1H, d, *J* = 7.3 Hz), 3.60 (1H, dt, *J* = 2.9, 10.2 Hz), 3.73–3.78 (1H, m), 3.84–3.90 (1H, m), 4.67 (1H, br s), 5.49–5.51 (1H, m), 5.69 (1H, d, *J* = 15.6 Hz), 5.84 (1H, br s), 6.88–6.90 (1H, m), 6.96 (1H, d, *J* = 9.8 Hz), 7.37 ppm (1H, d, *J* = 4.9 Hz); ^{13}C NMR (100 MHz, CD_3CN): δ 15.1, 15.6, 20.9, 28.3, 29.1, 30.3, 31.5, 41.07, 41.13, 41.30, 41.33, 43.8, 54.9, 60.0, 69.8, 69.9, 131.0, 131.4, 170.6, 171.0, 171.3, 172.1; IR (neat): 3383, 3301, 2961, 2923, 1733, 1717, 1653, 1541, 1507, 1429, 1286, 1245, 1166, 1021, 974, 754 cm^{-1}; HRMS (FAB): *m/z*: calcd for $C_{22}H_{36}N_3O_6S_3$ (M^+ + H) 534.1766, found 534.1764.

4.2. Biological evaluation

4.2.1. HDACs preparation and enzyme inhibition assay [19]

In a 100-mm dish, 293T cells (1–2 × 10^7) were grown for 24 h and transiently transfected with 10 μg each of the vector pcDNA3-HDAC1 for human HDAC1 or pcDNA3-mHDA2/HDAC6 for mouse HDAC6, using the LipofectAMINE2000 reagent (Invitrogen). After successive cultivation in DMEM for 24 h, the cells were washed with PBS and lysed by sonication in lysis buffer containing 50 mM Tris–HCl (pH 7.5), 120 mM NaCl, 5 mM EDTA, and 0.5% NP40. The soluble fraction collected by microcentrifugation was precleared by incubation with protein A/G agarose beads (Roche). After the cleared supernatant had been incubated for 1 h at 4 °C with 4 μg of an anti-FLAG M2 antibody (Sigma–Aldrich Inc.) for HDAC1 and HDAC6, the agarose beads were washed three times with lysis buffer and once with histone deacetylase buffer consisting of 20 mM Tris–HCl (pH 8.0), 150 mM NaCl, and 10% glycerol. The bound proteins were released from the immune complex by incubation for 1 h at 4 °C with 40 μg of the FLAG peptide (Sigma–Aldrich Inc.) in histone deacetylase buffer (200 μL). The supernatant was collected by centrifugation. For the enzyme assay, 10 μL of the enzyme fraction was added to 1 μL of fluorescent substrate (2 mM Ac-KGLGK(Ac)-MCA) and 9 μL of histone deacetylase buffer, and the mixture was incubated at 37 °C for 30 min. The reaction was stopped by the addition of 30 μL of trypsin (20 mg/mL) and incubated at 37 °C for 15 min. The released aminomethylcoumarin (AMC) was measured using a fluorescence plate reader. The 50% inhibitory concentrations (IC_{50}) were determined as the means with SD calculated from at least three independent dose–response curves.

4.2.2. Cell HDAC inhibition assay (p21 promoter assay) [19]

A luciferase reporter plasmid (pGW-FL) was constructed by cloning the 2.4 kb genomic fragment containing the transcription start site into HindIII and SmaI sites of the pGL3-Basic plasmid (Promega Co., Madison, WI). Mv1Lu (mink lung epithelial cell line) cells were transfected with the pGW-FL and a phagemid expressing neomycin/kanamycin resistance gene (pBK-CMV, Stratagene, La Jolla, CA) with the Lipofectamine reagent (Life Technology, Rockville, MD, USA). After the transfected cells had been selected by 400 μg mL^{-1} Geneticin (G418, Life Technology), colonies formed were isolated. One of the clones was selected and named MFLL-9. MFLL-9 expressed a low level of luciferase, whose activity was enhanced by TSA in a dose-dependent manner. MFLL-9 cells (1 × 10^5) cultured in a 96-well multi-well plate for 24 h were incubated for 20 h in the medium containing various concentrations of drugs. The luciferase activity of each cell lysate was measured with a LucLite luciferase Reporter Gene Assay Kit (Packard Instrument Co., Meriden, CT) and recorded with a Luminescencer-JNR luminometer (ATTO, Tokyo, Japan). Data were normalized to the protein concentration in cell lysates. Concentrations at which a drug induces the luciferase activity 100-fold higher than the basal level are presented as the 10,000% effective concentration 10,000% (EC_{10000}). The human wild-type p21 promoter luciferase fusion plasmid, WWP-Luc, was a kind gift from Dr. B. Vogelstein.

4.2.3. Cell-growth inhibition assay [18]

This experiment was carried out at the Cancer Chemotherapy Center, Japanese Foundation for Cancer Research. The screening panel consisted of the following 39 human cancer cell lines (HCC panel): breast cancer HBC-4, BSY-1, HBC-5, MCF-7, and MDA-MB-231; brain cancer U-251, SF-268, SF-295, SF-539, SNB-75, and SNB-78; colon cancer HCC2998, KM-12, HT-29, HCT-15, and HCT-116; lung cancer NCI-H23, NCI-H226, NCI-H522, NCI-H460, A549, DMS273, and DMS114; melanoma LOX-IMVI; ovarian cancer OVCAR-3, OVCAR-4, OVCAR-5, OVCAR-8, and SK-OV-3; renal cancer RXF-631L and ACHN; stomach cancer St-4, MKN1, MKN7, MKN28, MKN45, and MKN74; prostate cancer DU-145 and PC-3. The GI_{50} (50% cell growth inhibition) value for these cell lines was determined by using the sulforhodamine B colorimetric method.

Acknowledgments

We are grateful to the Screening Committee of New Anticancer Agents, which is supported by a Grant-in-Aid for Scientific Research on Priority Area 'Cancers' from the Ministry of Education, Culture, Sports, Science and Technology, Japan (MEXT), for assistance with the biological evaluation of compounds **1**–**3**. This study was also

supported by a Grant-in-Aid for the Strategic Research Foundation Program at Private Universities (2010–2014) and a Grant-in-Aid for Scientific Research (C) (No. 24590017, 2012–2014) from MEXT.

Appendix A. Supplementary data

Supplementary data related to this article can be found at http://dx.doi.org/10.1016/j.ejmech.2014.02.044.

References

[1] J.B. Biggins, C.D. Gleber, S.F. Brady, Organic Letters 13 (2011) 1536–1539.
[2] H. Benelkerbir, A.M. Donlevy, G. Packham, A. Ganesan, Organic Letters 13 (2011) 6337–6344.
[3] J. Liu, X. Ma, Y. Liu, Z. Wang, S. Kwong, Q. Ren, S. Tang, Y. Meng, Z. Xu, T. Ye, Synlett 23 (2013) 783–787.
[4] K. Narita, T. Kikuchi, K. Watanabe, T. Takizawa, T. Oguchi, K. Kudo, K. Matsuhara, H. Abe, T. Yamori, M. Yoshida, T. Katoh, Chemistry – A European Journal 15 (2009) 11174–11186.
[5] T. Takizawa, K. Watanabe, K. Narita, K. Kudo, T. Oguchi, H. Abe, T. Katoh, Heterocycles 76 (2008) 275–290.
[6] T. Takizawa, K. Watanabe, K. Narita, T. Oguchi, H. Abe, T. Katoh, Chemical Communications (2008) 1677–1679.
[7] K. Narita, Y. Fukui, Y. Sano, T. Yamori, A. Ito, M. Yoshida, T. Katoh, European Journal of Medicinal Chemistry 60 (2013) 295–304.
[8] (a) K. Saijo, C. Ishioka, T. Katoh, PCT WO 047509 A1, 2013;
(b) K. Saijo, T. Katoh, H. Shimodaira, A. Oda, O. Takahashi, C. Ishioka, Cancer Science 103 (2012) 1994–2001.
[9] **Total synthesis of FK228(5) by other groups:** (a) S. Wen, G. Packham, A. Ganesan, Journal of Organic Chemistry 73 (2008) 9353–9361;
(b) T.J. Greshock, D.M. Johns, Y. Noguchi, R.M. Williams, Organic Letters 10 (2008) 613–616;
(c) K.W. Li, J. Wu, W. Xing, J.A. Simon, Journal of the American Chemical Society 118 (1996) 7237–7238. Total synthesis of spiruchostatin A (6) by other groups;
(d) N.A. Calandra, Y.L. Cheng, K.A. Kocak, J.S. Miller, Organic Letters 11 (2009) 1971–1974;
(e) Y. Iijima, A. Munakata, K. Shin-ya, A. Ganesan, T. Doi, T. Takahashi, Tetrahedron Letters 50 (2009) 2970–2972;
(f) T. Doi, Y. Iijima, K. Shin-ya, A. Ganesan, T. Takahashi, Tetrahedron Letters 47 (2006) 1177–1180;
(g) A. Yurek-George, F. Habens, M. Brimmell, G. Packham, A. Ganesan, Journal of the American Chemical Society 126 (2004) 1030–1031. Total synthesis of spiruchostatin B (7) by other grup;
(h) S. Fuse, K. Okada, Y. Iijima, A. Munakata, K. Machida, T. Takahashi, M. Takagi, K. Shin-ya, T. Doi, Organic and Biomolecular Chemistry 9 (2011) 3825–3833.
[10] (a) I. Shiina, T. Katoh, S. Nagai, M. Hashizume, Chemical Record 9 (2009) 305–320;
(b) I. Shiina, A. Sasaki, T. Kikuchi, H. Fukui, Chemistry Asian Journal 3 (2008) 462–472;
(c) I. Shiina, Chemical Reviews 107 (2007) 239–273;
(d) I. Shiina, M. Hashizume, Tetrahedron 62 (2006) 7934–7939;
(e) I. Shiina, M. Kubota, H. Oshiumi, M. Hashizume, Journal of Organic Chemistry 69 (2004) 1830–1882.
[11] E.P. Johnson, M.P. Hubieki, A.P. Combs, C.A. Teleha, Synthesis (2011) 4023–4026.
[12] (a) X.J. Yang, E. Seto, Nature Reviews Molecular Cell Biology 9 (2008) 206–218;
(b) T. Kouzarides, Cell 128 (2007) 693–705;
(c) B.E. Bernstein, A. Meissner, E.S. Lander, Cell 128 (2007) 669–681;
(d) P. Trojer, D. Reinberg, Cell 125 (2006) 213–217.
[13] (a) O. Witt, H.E. Deubzer, T. Milde, I. Oehme, Cancer Letters 277 (2009) 8–21;
(b) M. Haberland, R.L. Montgomery, E.N. Olson, Nature Reviews Genetics 10 (2009) 32–42;
(c) M.A. Holbert, R. Marmorstein, Current Opinion in Structural Biology 15 (2005) 673–680;
(d) S. Voelt-Mahlknecht, A.D. Ho, U. Mahlnecht, International Journal of Molecular Medicine 16 (2005) 589–598;
(e) A.J.M. De Ruijter, A.H. Van Gennip, H.N. Caron, S. Kemp, A.B.P. Van Kuilenburg, Biochemical Journal 370 (2003) 737–749.
[14] (a) G.P. Delcuve, D.H. Khan, J.R. Davie, Expert Opinion on Therapeutic Targets 17 (2013) 29–41;
(b) O. Khan, T. La, B. Nicholas, Immunology and Cell Biology 90 (2012) 85–94;
(c) M. Rius, F. Lyko, Oncogene 31 (2012) 4257–4267;
(d) T.A. McKinsey, Journal of Molecular and Cellular Cardiology 51 (2011) 491–496;
(e) A.P. Kozikowski, K.V. Butler, Current Pharmaceutical Design 14 (2008) 505–528;
(f) A.V. Bieliauskas, M.K.H. Pflum, Chemical Society Reviews 37 (2008) 1402–1413;
(g) S. Senese, K. Zaragoza, S. Minardi, I. Muradore, S. Ronzoni, A. Passafaro, L. Bernard, G.F. Draetta, M. Alcalay, C. Seiser, S. Chiocca, Molecular and Cellular Biology 27 (2007) 4784–4795;
(h) P. Kahnberg, A.J. Lucke, M.P. Glenn, G.M. Boyle, J.D.A. Tyndall, P.G. Parsons, D.P. Fairlie, Journal of Medicinal Chemistry 49 (2006) 7611–7622;
(i) S. Chang, T.A. McKinsey, C.L. Zhang, J.A. Richardson, J.A. Hill, E.N. Olson, Molecular and Cellular Biology 24 (2004) 8467–8476.
[15] (a) B.E. Gryder, Q.H. Sodji, A.K. Oyelere, Future Medicinal Chemistry 4 (2012) 505–524;
(b) G. Giannini, W. Cabri, C. Fattorusso, M. Rodriquez, Future Medicinal Chemistry 4 (2012) 1439–1460;
(c) K.M. Van der Molen, W. McCulloch, C.J. Pearce, N.H. Oberlies, Journal of Antibiotics 64 (2011) 525–531;
(d) C. Grant, F. Rahman, R. Piekarz, C. Peer, R. Frye, R.W. Robey, E.R. Gardner, W.D. Figg, S.E. Bates, Expert Review of Anticancer Therapy 10 (2010) 997–1008.
[16] M.H. Shah, P. Binkley, K. Chan, J. Xiao, D. Arbogast, M. Collamore, Y. Farra, D. Young, M. Grever, Clinical Cancer Research 12 (2006) 3997–4003.
[17] (a) P. Gupta, R.C. Reid, A. Iyer, M. Sweet, D.P. Fairlie, Current Topics in Medicinal Chemistry 12 (2012) 1479–1499;
(b) H. Pan, J. Cao, W. Xu, Anti-Cancer Agents in Medicinal Chemistry 12 (2012) 247–270.
[18] (a) S. Yaguchi, Y. Fukui, I. Koshimizu, H. Yoshimi, T. Matsuno, H. Gouda, S. Hirono, K. Yamazaki, T. Yamori, Journal of the National Cancer Institute 98 (2006) 545–556;
(b) T. Yamori, Cancer Chemotherapy and Pharmacology 52 (Suppl. 1) (2003) 74–79;
(c) S. Dan, T. Tsunoda, O. Kitahara, R. Yanagawa, H. Zembutsu, T. Katagiri, K. Yamazaki, Y. Nakamura, T. Yamori, Cancer Research 62 (2002) 1139–1147;
(d) T. Yamori, A. Matsunaga, S. Sato, K. Yamazaki, A. Komi, K. Ishizu, I. Mita, H. Edatsugi, Y. Matsuba, K. Takezawa, O. Nakanishi, H. Kohno, Y. Nakajima, H. Komatsu, T. Andoh, T. Tsuruo, Cancer Research 59 (1999) 4042–4049.
[19] G.M. Shivashimpi, S. Amagai, T. Kato, N. Nishino, S. Maeda, T.G. Nishino, M. Yoshida, Bioorganic and Medicinal Chemistry 15 (2007) 7830–7839.

Organic & Biomolecular Chemistry

PAPER

Asymmetric synthesis of 2,5-disubstituted 3-hydroxypyrrolidines based on stereodivergent intramolecular iridium-catalyzed allylic aminations†

Cite this: *Org. Biomol. Chem.*, 2014, **12**, 1983

Yoshihiro Natori, Shunsuke Kikuchi, Takahiro Kondo, Yukako Saito, Yuichi Yoshimura and Hiroki Takahata*

Received 11th November 2013,
Accepted 23rd January 2014

DOI: 10.1039/c3ob42229a

www.rsc.org/obc

Intramolecular iridium-catalyzed allylic aminations of homochiral (*E*)-6-*N*-nosylaminohept-2-en-1-yl methyl carbonates were investigated. The relative position of the 2,5-substituents of the resulting pyrrolidines was found to be controlled by using both enantiomers (**4** and **5**) of the appropriate chiral ligand, demonstrating a simple and highly stereodivergent synthetic protocol. Selected *trans*- and *cis*-2,5-disubstituted 3-hydroxypyrrolidines (**2a** and **18a**) were converted to (+)-bulgecinine (**6**) and (+)-preussin (**7**), respectively.

Introduction

Substituted pyrrolidines are very important scaffolds in a variety of biologically active substances and occur in various natural products such as cocaine, hyacinthacine A1, stemonine and kaitocephalin as well as pharmacologically active compounds, such as trandolapril (an angiotensin converting enzyme inhibitor) (Fig. 1).[1] The broad range of biological activities of highly functionalized pyrrolidines underlines the importance of having a diversity of versatile and efficient stereoselective methods for their preparation readily available.[2]

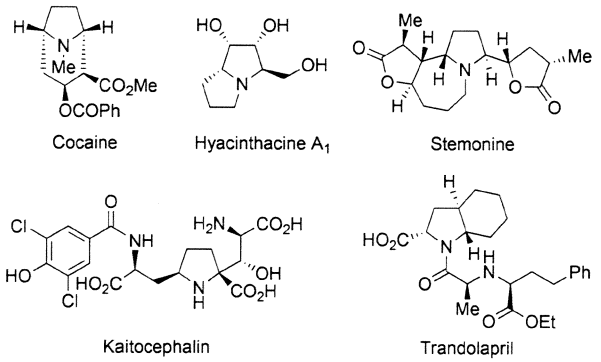


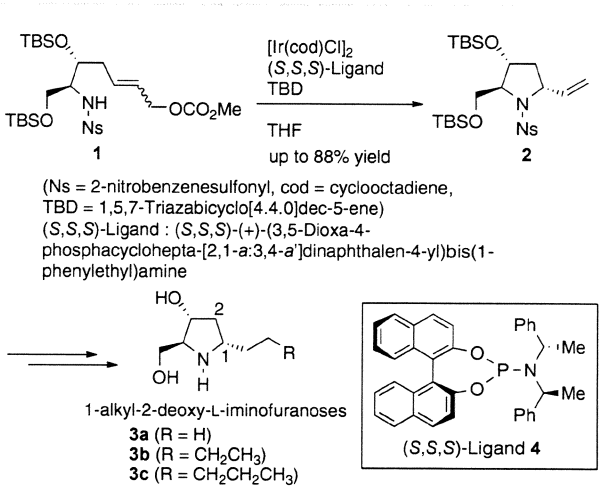
Fig. 1 Bioactive substances including substituted pyrrolidine structure.

Faculty of Pharmaceutical Sciences, Tohoku Pharmaceutical University, Sendai 981-8558, Japan

† Electronic supplementary information (ESI) available. See DOI: 10.1039/c3ob42229a

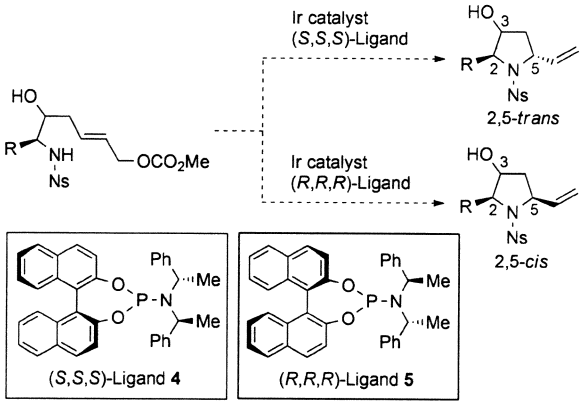
Two main strategies for the stereoselective preparation of highly substituted pyrrolidines have evolved: either asymmetric 1,3-dipolar cycloaddition or a sequential approach in which linear molecules containing the stereocenters are first constructed, followed by diastereoselective cyclization.

We recently reported on the stereoselective synthesis of *trans*-2,5-disubstituted 3-hydroxypyrrolidine derivatives *via* an intramolecular iridium (Ir)-catalyzed allylic amination with allylic carbonates as the starting compounds in preparing 1-alkyl-2-deoxy-L-iminofuranoses (**3a–c**) which were used in a structure–activity relationship (SAR) study of imino sugars (Scheme 1).[3]

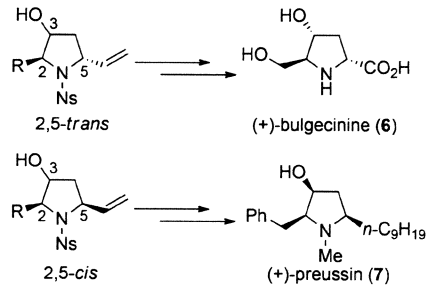


Scheme 1 Preparation of 1-alkyl-2-deoxyiminofuranoses *via* allylic amination as a key step.

This journal is © The Royal Society of Chemistry 2014



Scheme 2 Preparation of 2,5-*trans*/*cis* pyrrolidine derivatives controlled by chiral ligands.



Scheme 3 Key intermediates for the syntheses of (+)-bulgecinine (**6**) and (+)-preussin (**7**).

High levels of diastereoselectivity at the C-2 and C-5 positions in cyclizations by the addition of amine N–H functionalities to unsaturated carbon–carbon bonds are currently possible.[4] However, there is a drawback of this approach in that the selectivity of the cyclization process is predetermined by the configuration of the substrate and usually only one of a pair of diastereomers is produced. As a continuation of our interest in the development of this type of intramolecular Ir-catalyzed allylic amination, we found that the 2,5-*trans*/*cis* diastereoselectivity in cyclizations leading to pyrrolidine formation can be controlled using both enantiomers (**4** and **5**) of the appropriate chiral ligand as shown in Scheme 2.

Accordingly, we report on the use of this strategy for the stereodivergent synthesis of 2,5-disubstituted-3-hydroxypyrrolidine alkaloids such as (+)-bulgecinine (**6**) and (+)-preussin (**7**) (Scheme 3).

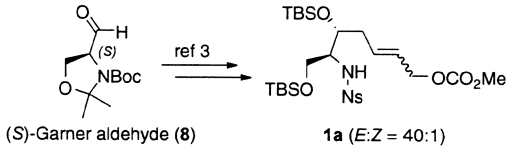
Results and discussion

Diastereoselective cyclization reactions of allylic carboxylate catalyzed by $[Ir(cod)Cl]_2$ and a chiral phosphoroamidate ligand (4 or 5)

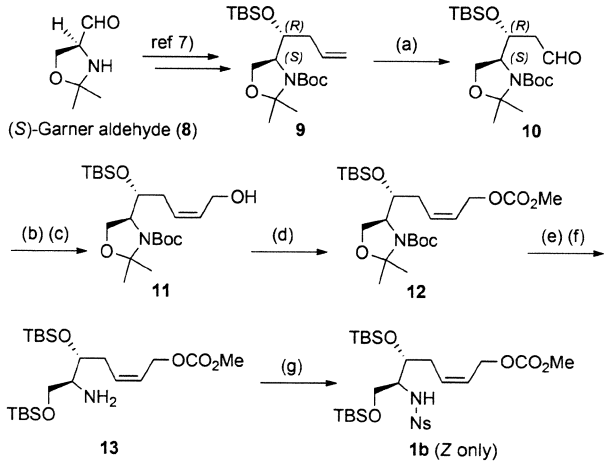
A configurational change to obtain both *trans*/*cis* diastereomers of 2,6-disubstituted piperidines was achieved for Ir-catalyzed allylic cyclization reactions using external chiral ligands, as reported by Helmchen.[5a,b] On the other hand, to the best of our knowledge, a similar approach to produce both 2,5-*trans*/*cis* diastereomers in cyclizations of pyrrolidine has scarcely been investigated.[5c] We planned to examine the Ir-catalyzed cyclization reaction of allylic carbonate using the (*S*,*S*,*S*)- or (*R*,*R*,*R*)-ligand (**4** or **5**). Additionally, it was of interest to examine the effect of the geometry of the double-bond (*E*/*Z*) on this cyclization. Therefore, we required both *E* and *Z* isomers of the cyclization precursor. The cyclization precursor **1a** (*E* : *Z* = 40 : 1) is available from the (*S*)-Garner aldehyde (**8**) following a previously reported procedure, which provides mainly the *E* isomer (Scheme 4).[3]

The *Z* isomer **1b** of the cyclization precursor was prepared by a *Z*-selective Horner–Wadsworth–Emmons reaction using Ando's reagent[6] as a key step, starting with the known alkene **9**[7] (Scheme 5). Ozonolysis of alkene **9** afforded the aldehyde **10** (93%), which was subjected to Ando olefination followed by reduction to give the (*Z*)-allylic alcohol **11** in 46% yield (2 steps). A series of transformations (1, methyl carbonation of the hydroxy group; 2, hydrolysis of the *N*-Boc oxazolidine ring; 3, protection of both the hydroxyl and amino groups) from **11** gave the cyclization precursor **1b** (*Z* only) in good yield.

With both cyclization precursors **1a** (*E* : *Z* = 40 : 1) and **1b** (*Z* only) in hand, the key diastereoselective cyclization using **4**



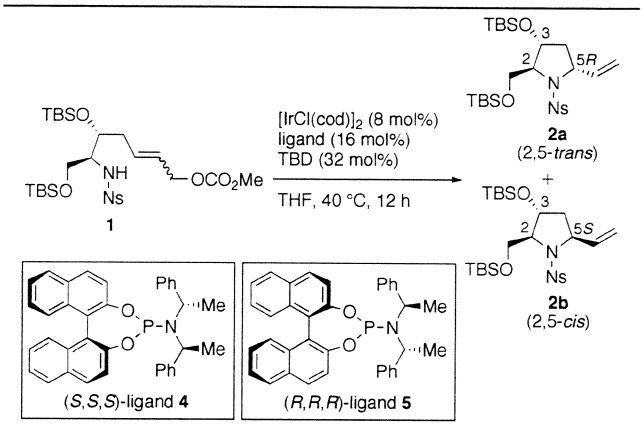
Scheme 4 Preparation of cyclization precursor **1a** (*E* : *Z* = 40 : 1).



Scheme 5 Preparation of cyclization precursor **1b** (*Z* only) (a) O_3/CH_2Cl_2/−78 °C then PPh_3/−78 °C to rt/93%, (b) ethyl diphenylphosphonoacetate/NaH/THF/−78 to 0 °C, (c) DIBAL-H/CH_2Cl_2/−78 °C/46% (2 steps), (d) methyl chloroformate/DMAP/pyridine/CH_2Cl_2/rt/98%, (e) CF_3CO_2H/CH_2Cl_2/0 °C to rt, (f) TBSCl/imidazole/CH_2Cl_2/0 °C to rt/93% (2 steps), (g) NsCl/Et_3N/DMAP/0 °C to rt/91%.

This journal is © The Royal Society of Chemistry 2014

Table 1 Allylic amination reaction of allylic carbonate **1**



Entry	Substrate	Ligand	**2a** : **2b**[a]	Yield[b] (%)
1	**1a** (*E* : *Z* = 40 : 1)	(*S*,*S*,*S*)	12 : 1	78[c]
2	**1a** (*E* : *Z* = 40 : 1)	(*R*,*R*,*R*)	1 : 6	74
3	**1b** (*Z* = only)	(*S*,*S*,*S*)	1 : 2.4	95
4	**1b** (*Z* = only)	(*R*,*R*,*R*)	3.5 : 1	99
5	**1a** (*E* : Z = 40 : 1)	$P(OPh)_3$	1 : 1	58
6	**1b** (*Z* = only)	$P(OPh)_3$	1 : 1	50

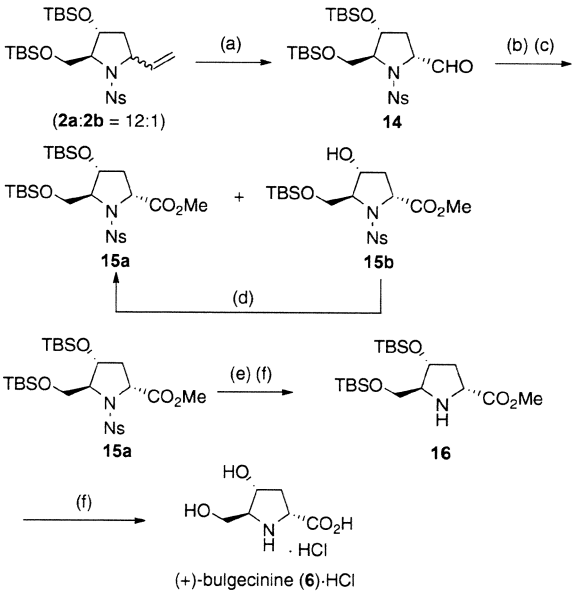
[a] Combined yield of two diastereomers. [b] Determined by ^{1}H-NMR analysis of the crude mixture. [c] The reaction afforded a similar result on the gram scale (>2 g of **1**) (cod = cyclooctadiene, TBD = 1,5,7-triazabicyclo[4.4.0]dec-5-ene).

or 5 as a ligand was examined (Table 1).[8] In a previous study,[3] the cyclization of **1a** (*E* : *Z* = 40 : 1) catalyzed by $[Ir(cod)Cl]_2$ (8 mol%), the (*S*,*S*,*S*)-ligand **4** (16 mol%) and the TBD (32 mol%) was carried out. The cyclization reaction proceeded smoothly to provide the desired (5*R*)-vinyl pyrrolidine derivative **2** in 78% yield with a high diastereoselectivity (**2a** : **2b** = 12 : 1) (entry 1). On the other hand, the cyclization of **1a** using the (*R*,*R*,*R*)-ligand **5** to confirm the ligand effect for C5 stereochemistry of the cyclization product expectedly resulted in the reversal of the major diastereomer with moderate diastereoselectivity (**2a** : **2b** = 1 : 6) (entry 2). Next, when the substrate **1b** (*Z* isomer only) was reacted under the same conditions, the selectivity of the amination of **1b** (*Z* isomer only) catalyzed by (*S*,*S*,*S*)- and (*R*,*R*,*R*)-ligand (**4** and **5**) was low. In contrast, the diastereoselectivity was interestingly reversed (entries 3 and 4). The geometry of the allylic carbonate part was very important in terms of diastereoselectivity, although the reason for this remains unclear. It has been reported that the intermolecular Ir-catalyzed allylic amination of the (*Z*)-isomer preferentially yielded the linear amination product with a high *Z*-selectivity instead of the branched substituted product.[9] However, no *endo* cyclization occurred in the absence of a seven membered product. Because these results were very interesting, additional study is needed. When we used $P(OPh)_3$ as the achiral ligand, no diastereoselectivity was observed, resulting in no substrate control (entries 5 and 6).

Thus the 2,5-*trans*/*cis* diastereoselectivity of the cyclization can be easily controlled by external control, using both enantiomers (**4** and **5**) of the appropriate chiral ligand to produce both 2,5-*trans*/*cis*-substituted pyrrolidine derivatives, which are expected to function as useful synthons in preparing pyrrolidine alkaloids.

The synthesis of (+)-bulgecinine·HCl having 2,5-*trans* substituted groups

First, we examined the synthesis of an enantiomer of (−)-bulgecinine (**6**) which is a common aglycon substituent of bulgecins A, B, and C isolated from *Pseudomonas acidophila* or *Pseudomonas mesoacidophila*,[10] starting from the 2,5-*trans* substituted pyrrolidine derivative **2a** as the synthon. Because of its unique antibacterial activities,[11] the unusual amino acid core of bulgecinine (**6**) has attracted considerable attention as targets of total synthesis and biological studies. In fact, a number of syntheses of natural (−)-bulgecinine (**6**) have been reported in the literature.[12] However, a few research groups reported on the synthesis of the enantiomer (+)-bulgecinine (**6**).[12d,13] Accordingly, we planned its preparation along with our continuous interest in the biological activities of both enantiomers.[14] Our stereoselective synthesis of (+)-bulgecinine (**6**)·HCl started with the ozonolysis of a diastereomixture of **2** (**2a** : **2b** = 12 : 1) to furnish the desired aldehyde **14** in 84% yield (Scheme 6). The aldehyde was oxidized under mild conditions followed by esterification of the resulting carboxylic acid with CH_2N_2 to provide two separable methyl esters (the desired ester **15a** (67%) and the mono-TBS protected ester **15b** (28%)). At this stage, the position of the hydroxyl group in **15b** was unknown. Its position was determined to be at C-4, because



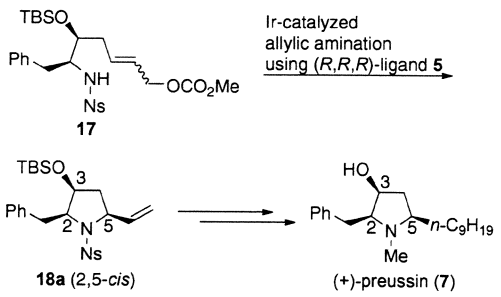
Scheme 6 Asymmetric synthesis of (+)-bulgecinine (**6**) hydrochloride (a) $O_3/CH_2Cl_2/-78$ °C then $Me_2S/-78$ °C/84%, (b) $NaClO_2/NaH_2PO_4{\cdot}2H_2O$/2-methyl-2-butene/*t*-BuOH : H_2O (4 : 1)/rt, (c) CH_2N_2 (Et_2O solution)/Et_2O/0 °C to rt/**15a**(67%), **15b** (28%) (2 steps), (d) TBSOTf/2,6,-lutidine/CH_2Cl_2/rt/94%, (e) PhSH/ K_2CO_3/MeCN/40 °C/94%, and (f) 6 N HCl/100 °C/83%.

acetylation of the hydroxyl group gave the secondary acetoxy product (see ESI†). The mono-TBS protected ester **15b** was protected by a TBS group to afford **15a** in good yield. The deprotection of the Ns group under standard conditions was carried out to give the amine **16** in high yield. Finally, deprotection of TBS groups using 6 N HCl was carried out to provide (+)-bulgecinine (**6**)·HCl. Optical rotation data of our synthesized (+)-bulgecinine (**6**)·HCl were in agreement with the $[\alpha]_D$ value of (−)-bulgecinine (***ent*-6**)·HCl reported by Datta's research group[12f] (our synthesized (+)-bulgecinine (**6**)·HCl; $[\alpha]_D^{25}$ = −11.6 (*c* 0.65, 1 N HCl), previously reported (−)-bulgecinine (***ent*-6**)·HCl; $[\alpha]_D^{25}$ = +11.71 (*c* 0.65, 1 N HCl)).

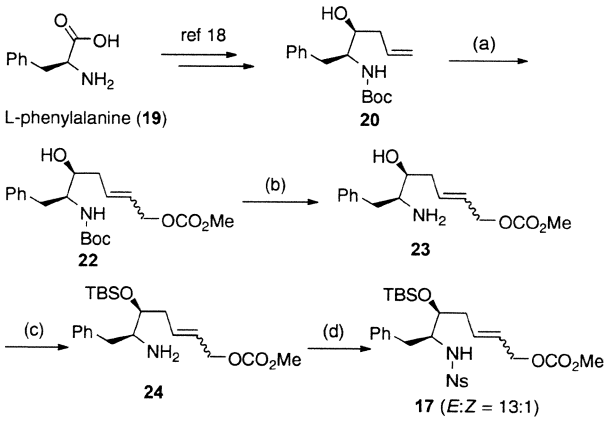
The synthesis of (+)-preussin (7) having 2,5-*cis* substituted groups

Next, we commenced the synthesis of (+)-preussin (7) containing a 2,5-*cis* substituted pyrrolidine derivative. (+)-Preussin (7) was isolated from a liquid fermentation broth of *Aspergillus ochraceus* in 1988.[15] It shows a broad spectrum of antifungal activity and has also shown growth-inhibitory and cytotoxic effects on human cancer cells.[15a,16] Numerous reports on the synthesis of (+)-preussin (7) as an attractive target have appeared in the literature.[17] Encouraged by the result of the cyclization reaction in Table 1 (entry 2), it was expected that the efficient asymmetric synthesis of a 2,3,5-trisubstituted pyrrolidine such as (+)-preussin (7) with *cis*-2,5-disubstituted pyrrolidine would be possible. We chose **17** as a precursor of the intramolecular allylic amination using (*R*,*R*,*R*)-ligand **5** to provide the 2,5-*cis* cyclization product **18a** as a major isomer (Scheme 7).

We embarked on the preparation of the cyclization precursor **17** starting with the known alcohol **20**[18] derived from L-phenylalanine (**19**) (Scheme 8). An olefin cross metathesis (Grubbs II catalyst) of **20** and (*Z*)-but-2-ene-1,4-diyl dimethyl dicarbonate (**21**) (5 eq.) afforded the allylic carbonate **22** as a mixture of *E* and *Z* isomers in good yield. At this stage, the ratio of *E* and *Z* isomers remained undetermined because of difficulties associated with the ^{1}H-NMR analysis. After deprotection of the Boc group using trifluoroacetic acid, sequential protection of the hydroxyl with a TBS group and the amine with an Ns group afforded the cyclization precursor **17** in high



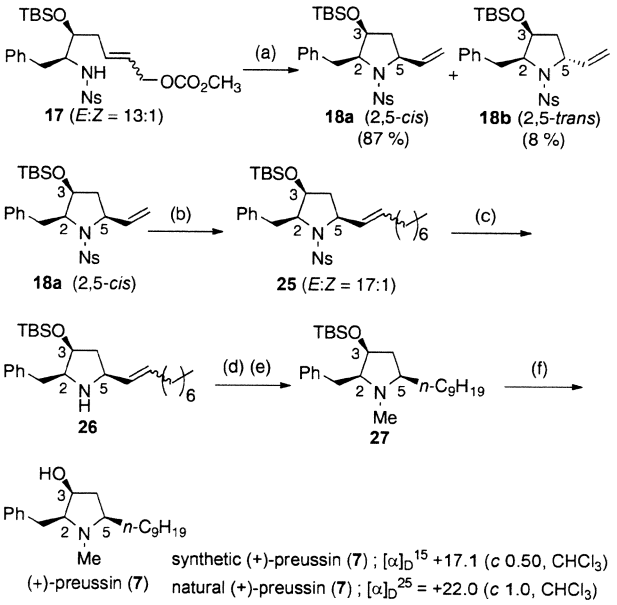
Scheme 7 Synthetic plan for (+)-preussin (**7**) *via* Ir-catalyzed allylic amination using (*R*,*R*,*R*)-ligand **5**.



Scheme 8 Preparation of cyclization precursor **17**. (a) MeO_2CO **21** OCO_2Me/Grubbs 2nd catalyst (5 mol%)/CH_2Cl_2/rt/89%, (b) CF_3CO_2H/CH_2Cl_2/0 °C to rt, (c) TBSCl/imidazole/CH_2Cl_2/0 °C to rt/76% (2 steps), and (d) NsCl/Et_3N/DMAP/0 °C to rt/97%.

yield. The ratio of *E* and *Z* isomers of **17** was then determined from its ^{1}H-NMR spectrum (*E* : *Z* = 13 : 1).

With the cyclization precursor **17** in hand, the diastereoselective cyclization of the allylic carbonate was examined under similar conditions using the (*R*,*R*,*R*)-ligand **5** (Scheme 9). Predictably, the desired product **18a** (2,5-*cis*) was obtained in good yield with high diastereoselectivity (**18a**: 87%, **18b**: 8%).[19] Next, we converted the obtained pyrrolidine derivative **18a** into (+)-preussin (7) *via* several steps. An olefin



Scheme 9 Asymmetric synthesis of (+)-preussin (**7**). (a) $[IrCl(cod)]_2$ (8 mol%)/(*R*,*R*,*R*)-ligand **5** (16 mol%)/TBD (32 mol%)/THF/40 °C/4 h/**8a** (87%) and **18b** (8%), (b) 1-nonene (10 eq.)/Grubbs 2nd catalyst (15 mol%)/CH_2Cl_2/40 °C/80%, (c) PhSH/K_2CO_3/CH_3CN/40 °C/91%, (d) formaldehyde (37% in water)/MeOH/rt (e), H_2 (balloon)/PtO_2/rt/50% (2 steps), and (f) TBAF/THF/ rtf 83%.

This journal is © The Royal Society of Chemistry 2014

cross metathesis between the pyrrolidine derivative **18a** and 1-nonene provided the alkene **25**, the Ns group of which was then removed under standard conditions by treatment with thiophenol in the presence of K_2CO_3 to give the amine **26**.

The reductive methylation of **26** afforded the amine **27** in moderate yield. Finally, the amine **27** was treated with TBAF to provide (+)-preussin (7) in good yield. The spectral data for the synthesized (+)-preussin (7) were in full agreement with reported values for naturally occurring (+)-preussin (7).[15]

Conclusion

In summary, the intramolecular iridium-catalyzed allylic cyclization of (*E*)-allylic methyl carbonates by an exchange in both enantiomers of the (*S*,*S*,*S*)-ligand **4** or the (*R*,*R*,*R*)-ligand **5** afforded the 2,5-*trans*/*cis* pyrrolidine derivatives, accompanied by the interconversion of diastereoselectivities. The stereodivergent ring construction was applied to the syntheses of the 2,5-*trans*/*cis* pyrrolidine alkaloids (+)-bulgecinine (**6**)·HCl and (+)-preussin (7). Because a wide variety of natural products and medicinally relevant compounds with 2,5-*trans*/*cis* substituted pyrrolidine structures exist, this amination reaction promises to be very useful for the synthesis of such compounds.

Experimental

General methods

Infrared (IR) spectra were recorded on a Perkin-Elmer 1600 series FT-IR spectrometer. Mass spectra (MS) were recorded on a JEOL JMN-DX 303/JMA-DA 5000 spectrometer. Microanalyses were performed on a Perkin-Elmer CHN 2400 Elemental Analyzer. Optical rotations were measured with a JASCO DIP-360 or JASCO P-1020 digital polarimeter. ^{1}H-NMR spectra were recorded on a JEOL JNM-AL 400 (400 MHz) spectrometer, using tetramethylsilane as an internal standard. The following abbreviations are used: s = singlet, d = doublet, t = triplet, q = quartet, m = multiplet, br = broad. ^{13}C-NMR spectra were recorded on a JEOL JNM-AL 400 (400 MHz) spectrometer. Chemical shifts are reported relative to the internal standard ($CDCl_3$; δ 77.00). Column chromatography was carried out on Merck Silica Gel 60 (230–400 mesh) or KANTO Silica Gel 60N (40–50 μm) for flash chromatography. All non-aqueous reactions were carried out under an argon atmosphere. Additionally, methyl carboxylate **1a**,[3] alkene **9**[7] and allylic alcohol **20**[18] were known products, and they were prepared according to a reported procedure.

(*S*)-*tert*-Butyl 4-[(*R*)-1-{(*tert*-butyldimethylsilyl)oxy}-3-oxopropyl]-2,2-dimethyloxazolidine-3-carboxylate (10). Ozone was bubbled through a stirred solution of the alkene **9** (1.91 g, 4.96 mmol) in CH_2Cl_2 (50 mL) at −78 °C. The solution was stirred at −78 °C for 1 h, at which time the solution became blue, and then oxygen was bubbled through the solution until it became colorless. Triphenylphosphine (1.95 g, 7.44 mmol) was then added to the stirred solution at −78 °C and then it was allowed to warm to room temperature over 18 h under an argon atmosphere. The solvents were removed under reduced pressure, and the residue was purified by silica gel column chromatography (*n*-hexane–EtOAc = 50 : 1 → 5 : 1) to give aldehyde **10** (937 mg, 93%) as a white solid.

M.p. 47–49 °C; $[\alpha]_D^{28}$ −23.5 (*c* 0.86, $CHCl_3$); ^{1}H-NMR (400 MHz, $CDCl_3$) δ 0.06 (s, 3H), 0.10 (s, 3H), 0.87 (s, 9H), 1.47 (s, 15H), 2.53–2.63 (m, 2H), 3.87–3.91 (m, 1H), 4.02 (m, 2H), 4.35 (m, 1H), 9.83 (m, 1H); ^{13}C-NMR (100 MHz, $CDCl_3$) δ −4.9, −4.3, 14.1, 18.0, 24.7, 25.6, 25.7, 27.3, 28.3, 31.6, 48.4, 61.4, 64.3, 67.9, 80.6, 94.1, 153.3, 201.1; IR (KBr) cm^{-1}: 3007, 2976, 2933, 2896, 2859, 1714, 1475, 1393, 1365, 1300, 1257, 1210, 1178, 1101, 1084, 1060; EI-MS (*m*/*z*): 388 (M^+ + 1). HRMS calcd for $C_{19}H_{38}NO_5Si$: 388.2519, found: 388.2511. Anal. calcd for $C_{19}H_{37}NO_5Si$: C, 58.88; H, 9.62; N, 3.61. Found: C, 59.23; H, 10.02; N, 3.62.

(*S*)-*tert*-Butyl 4-[(*R*,*Z*)-1-{(*tert*-butyldimethylsilyl)oxy}-5-hydroxypent-3-en-1-yl]-2,2-dimethyloxazolidine-3-carboxylate (11). NaH (60% dispersion in mineral oil, 273 mg, 6.83 mmol) was added to a solution of ethyl diphenylphosphonoacetate (1.8 mL, 6.83 mmol) in THF (23 mL) at 0 °C. After stirring at 0 °C for 30 min, the suspension was cooled to −78 °C. A solution of aldehyde **10** (883 mg, 2.28 mmol) in THF (23 mL) was added to the suspension *via* a cannula at −78 °C. After stirring at −78 °C for 30 min, the reaction mixture was warmed to 0 °C. The reaction was quenched with water (20 mL) and extracted with ethyl acetate (2 × 30 mL). The combined organic layers were washed with brine (30 mL), and dried over anhydrous Na_2SO_4. Filtration and evaporation *in vacuo* furnished the crude product, which was purified by silica gel column chromatography (*n*-hexane–EtOAc = 50 : 1) to afford a mixture of the desired α,β-unsaturated ester and inseparable byproduct (887 mg).

The obtained mixture of α,β-unsaturated ester and inseparable byproduct (887 mg) was dissolved in CH_2Cl_2 (19 mL). DIBAL-H (1.5 M solution in toluene, 3.2 mL, 4.79 mmol) was added dropwise to the solution at −78 °C. After stirring at −78 °C for 1 h, the reaction was quenched with water (10 mL). 10% aqueous solution of potassium sodium tartrate (20 mL) was added to the mixture and the resulting mixture was then stirred vigorously at room temperature for 5 h. The separated aqueous layer was extracted with CH_2Cl_2 (3 × 20 mL), and the combined extracts were dried over anhydrous Na_2SO_4. Filtration and evaporation *in vacuo* furnished the crude product, which was purified by silica gel column chromatography (*n*-hexane–EtOAc = 10 : 1) to afford alcohol **11** (436 mg, 46%, 2 steps) as a colorless oil.

$[\alpha]_D^{25}$ −42.8 (*c* 1.29, $CHCl_3$); ^{1}H-NMR (400 MHz, $CDCl_3$) δ 0.06 (s, 3H), 0.08 (s, 3H), 0.90 (s, 9H), 1.48 (s, 15H), 2.13–2.40 (m, 3H), 3.84–3.90 (m, 2H), 4.03 (m, 1H), 4.11–4.19 (m, 3H), 5.68–5.74 (m, 2H); ^{13}C-NMR (100 MHz, $CDCl_3$) δ −4.6, −4.3, 14.1, 18.0, 22.6, 25.2, 25.9, 27.0, 28.5, 31.6, 32.7, 58.4, 60.3, 63.1, 69.8, 80.5, 127.6, 130.7; IR (neat) cm^{-1}: 3434, 2931, 2858, 1694, 1682, 1473, 1463, 1393, 1254, 1208, 1174, 1097, 1075; EI-MS (*m*/*z*): 416 (M^+ + 1). HRMS calcd for $C_{21}H_{42}NO_5Si$: 416.2832, found: 416.2850.

This journal is © The Royal Society of Chemistry 2014

(*S*)-*tert*-Butyl 2,2-dimethyl-4-{(*R*,*Z*)-11,11,12,12-tetramethyl-3-oxo-2,4,10-trioxa-11-silatridec-6-en-9-yl}oxazolidine-3-carboxylate (12). Methyl chloroformate (0.24 mL, 3.1 mmol) was added to a solution of allylic alcohol **11** (261 mg, 0.627 mmol), DMAP (18.4 mg, 0.151 mmol) and pyridine (0.51 mL, 6.27 mmol) in CH_2Cl_2 (6.3 mL) at room temperature. After stirring at room temperature for 13 h, the reaction was quenched with water (5 mL). The whole mixture was extracted with CH_2Cl_2 (20 mL). The extract was washed with water (3 × 10 mL) and brine (10 mL), and dried over anhydrous Na_2SO_4. Filtration and evaporation *in vacuo* furnished the crude product, which was purified by silica gel column chromatography (*n*-hexane–EtOAc = 20 : 1) to afford methyl carbonate **12** (290 mg, 98%) as a colorless oil.

$[\alpha]_D^{24}$ −43.4 (*c* 0.92, $CHCl_3$); ^{1}H-NMR (400 MHz, $CDCl_3$) δ 0.05 (s, 3H), 0.07 (s, 3H), 0.90 (s, 9H), 1.48 (s, 15H), 2.25 (dd, *J* = 6.8, 12.2 Hz, 2H), 3.78 (s, 3H), 3.87–3.91 (m, 2H), 4.09–4.11 (m, 1H), 4.35 (brs, 1H), 4.61–4.71 (m, 2H), 5.62–5.75 (m, 2H); ^{13}C-NMR (100 MHz, $CDCl_3$) δ −4.5, −4.3, 18.0, 25.3, 25.9, 26.2, 26.6, 28.4, 33.7, 54.7, 60.9, 62.6, 63.4, 63.6, 69.2, 80.1, 94.0, 124.6, 131.2, 155.7; IR (neat) cm^{-1}: 2957, 2932, 2858, 1755, 1694, 1463, 1445, 1367, 1265, 1208, 1176, 1096, 1075; EI-MS (*m*/*z*): 474 (M^+ + 1). HRMS calcd for $C_{23}H_{44}NO_7Si$: 474.2887, found: 474.2891.

(5*R*,6*S*,*Z*)-6-Amino-5,7-bis{(*tert*-butyldimethylsilyl)oxy}hept-2-en-1-yl methyl carbonate (13). To a solution of **12** (42.0 mg, 0.0887 mmol) in CH_2Cl_2 (1.0 mL) was added TFA (1.0 mL) at 0 °C. After the mixture was stirred at 0 °C for 1 h, the solvents were removed under reduced pressure. Traces of TFA were removed from a mixture by azeotropic distillations with toluene (2 × 5 mL) under reduced pressure at room temperature.

The residue was dissolved in CH_2Cl_2 (1.0 mL). Imidazole (90.5 mg, 1.33 mmol) and TBSCl (53.5 mg, 0.355 mmol) were added to this solution at 0 °C. The reaction was stirred at room temperature for 15 h, and then quenched with water (5 mL). The whole mixture was extracted with CH_2Cl_2 (3 × 10 mL). The combined organic layers were dried over anhydrous Na_2SO_4. Filtration and evaporation *in vacuo* furnished the crude product, which was purified by silica gel column chromatography (*n*-hexane–EtOAc = 10 : 1) to afford amine **13** (37.1 mg, 93%, 2 steps) as a colorless oil.

$[\alpha]_D^{25}$ −19.9 (*c* 1.10, $CHCl_3$); ^{1}H-NMR (400 MHz, $CDCl_3$) δ 0.06 (s, 12H), 0.89 (s, 9H), 0.90 (s, 9H), 2.23–2.27 (m, 1H), 2.46–2.53 (m, 1H), 2.83 (m, 1H), 3.45 (dd, *J* = 7.2, 9.7 Hz, 1H), 3.66–3.76 (m, 2H), 3.78 (s, 3H), 4.69 (d, *J* = 7.2 Hz, 2H), 5.63–5.69 (m, 1H), 5.74–5.83 (m, 1H); ^{13}C-NMR (100 MHz, $CDCl_3$) δ −5.4, −5.3, −4.7, −4.3, 18.0, 18.2, 25.7, 25.8, 25.9, 30.8, 54.7, 56.6, 63.8, 64.9, 73.0, 124.5, 131.9, 155.7; IR (neat) cm^{-1}: 3372, 2956, 2930, 2887, 2858, 1749, 1589, 1472, 1463, 1444, 1409, 1389, 1361, 1267, 1085, 1006; EI-MS (*m*/*z*): 447 (M^+). HRMS calcd for $C_{21}H_{45}NO_5Si_2$: 447.2836, found: 447.2821.

(5*R*,6*S*,*Z*)-5,7-Bis{(*tert*-butyldimethylsilyl)oxy}-6-(2-nitrophenylsulfonamido)hept-2-en-1-yl methyl carbonate (1b). To a solution of amine **13** (250 mg, 0.559 mmol), Et_3N (0.14 mL, 1.01 mmol) and DMAP (16.4 mg, 0.134 mmol) in CH_2Cl_2 (45 mL) was added 2-nitrobenzenesulfonyl chloride (149 mg, 0.670 mmol) at 0 °C. The mixture was stirred at room temperature for 3 h. After evaporation, the residue was diluted with EtOAc (30 mL). The whole mixture was washed successively with brine (15 mL), 5% $KHSO_4$ (15 mL) and brine (15 mL), and dried over anhydrous Na_2SO_4. Filtration and evaporation *in vacuo* furnished the crude product, which was purified by silica gel column chromatography (*n*-hexane–EtOAc = 20 : 1 → 15 : 1) to afford **1b** (323 mg, 91%) as a white solid.

M.p. 56–59 °C; $[\alpha]_D^{23}$ +41.4 (*c* 1.10, $CHCl_3$); ^{1}H-NMR (400 MHz, $CDCl_3$) δ −0.16 (s, 3H), −0.08 (s, 3H), 0.05 (s, 3H), 0.06 (s, 3H), 0.78 (s, 9H), 0.85 (s, 9H), 2.40 (dd, *J* = 6.3, 6.3 Hz, 2H), 3.48–3.58 (m, 2H), 3.71 (dd, *J* = 5.3, 10.1 Hz, 1H), 3.78 (s, 3H), 4.02–4.06 (m, 1H), 4.62–4.65 (m, 2H), 5.66–5.76 (m, 3H), 7.69–7.75 (m, 2H), 7.86–7.88 (m, 1H), 8.09–8.12 (m, 1H); ^{13}C-NMR (100 MHz, $CDCl_3$) δ −5.9, −5.6, −4.6, −4.3, 18.0, 18.1, 25.7, 25.8, 31.8, 54.8, 59.9, 61.1, 63.7, 71.7, 125.2, 125.4, 130.4, 130.6, 132.9, 133.2, 135.1, 155.7; IR (KBr) cm^{-1}: 3338, 3090, 3050, 2958, 2934, 2888, 2858, 1752, 1665, 1593, 1548, 1472, 1463, 1442, 1415, 1368, 1347, 1307, 1208, 1175, 1125, 1102, 1080, 1004; FAB-MS (*m*/*z*): 633 (M^+ + 1); HRMS calcd for $C_{27}H_{49}N_2O_9Si_2$: 633.2697, found: 633.2701. Anal. calcd for $C_{27}H_{48}N_2O_9SSi$: C, 51.24; H, 7.64; N, 4.43. Found: C, 51.34; H, 7.85; N, 4.37.

(2*S*,3*R*,5*R*)-3-{(*tert*-Butyldimethylsilyl)oxy}-2-[{(*tert*-butyldimethylsilyl)oxy}methyl]-1-{(2-nitrophenyl)sulfonyl}-5-vinylpyrrolidine (2a)

(2*S*,3*R*,5*S*)-3-{(*tert*-Butyldimethylsilyl)oxy}-2-[{(*tert*-butyldimethylsilyl)oxy}methyl]-1-{(2-nitrophenyl)sulfonyl}-5-vinylpyrrolidine (2b). (Table 1, entry 1)

To a solution of $[Ir(cod)Cl]_2$ (8.5 mg, 0.0130 mmol, 8 mol%) and (*S*,*S*,*S*)-(+)-(3,5-dioxa-4-phosphacyclohepta[2,1-*a*:3,4-*a*']-dinaphthalen-4-yl)bis(1-phenylethyl)amine ((*S*,*S*,*S*)-ligand) **4** (13.6 mg, 0.025 mmol, 16 mol%) in THF (0.45 mL) was added dry 1,5,7-triazabicyclo[4.4.0]dec-5-ene (TBD) (7.0 mg, 0.050 mmol, 32 mol%). After the mixture was stirred at room temperature for 1 h, a solution of allylic carbonate **1a** (*E* : *Z* = 40 : 1, 100 mg, 0.158 mmol) in THF (1.0 mL) was added to the reaction mixture *via* a cannula. After stirring at 40 °C for 12 h, the mixture was concentrated and the residue was purified by silica gel column chromatography (*n*-hexane–EtOAc = 30 : 1) to give the cyclic compound **2** (**2a** : **2b** = 12 : 1) (68.7 mg, 78%, combined yield of **2a** and **2b**) as a white solid.

These compound data were collected using partially separated **2a** (pure) or **2b** (pure).

2a: m.p. 90–92 °C; $[\alpha]_D^{24}$ +137.2 (*c* 0.96, $CHCl_3$); ^{1}H-NMR (400 MHz, $CDCl_3$) δ 0.08 (s, 6H), 0.09 (s, 3H), 0.10 (s, 3H), 0.86 (s, 9H), 0.90 (s, 9H), 1.69 (d, *J* = 13.5 Hz, 1H), 2.51–2.58 (m, 1H), 3.48 (dd, *J* = 8.3, 10.1 Hz, 1H), 3.96 (dd, *J* = 3.4, 10.6 Hz, 1H), 4.07 (dd, *J* = 2.9, 8.2 Hz, 1H), 4.45 (m, 2H), 4.79 (d, *J* = 8.6 Hz, 1H), 5.06 (d, *J* = 15.9 Hz, 1H), 5.72–5.81 (m, 1H), 7.53–7.63 (m, 3H), 8.14 (d, *J* = 6.8 Hz, 1H); ^{13}C-NMR (100 MHz, $CDCl_3$) δ −5.5, −5.4, −5.0, −4.9, 17.9, 18.2, 25.7, 25.9, 39.6, 64.1, 64.3, 71.9, 74.8, 117.4, 123.7, 130.6, 131.0, 132.8, 135.8, 138.3, 148.9; IR (KBr) cm^{-1}: 3097, 3030, 2932, 2886, 2888,

This journal is © The Royal Society of Chemistry 2014

1584, 1548, 1472, 1352; FAB-MS (*m/z*): 557 (M^+ + 1); HRMS calcd for $C_{25}H_{45}N_2O_6SSi_2$: 557.2539, found: 557.2529.

2b: m.p. 94–96 °C; $[\alpha]_D^{24}$ +27.2 (*c* 0.76, $CHCl_3$); ^{1}H-NMR (400 MHz, $CDCl_3$) δ −0.08 (s, 3H), −0.05 (s, 3H), 0.09 (s, 3H), 0.10 (s, 3H), 0.69 (s, 9H), 0.91 (s, 9H), 1.88–2.02 (m, 2H), 3.43 (dd, *J* = 9.7, 11.6 Hz, 1H), 3.86–3.90 (dd, *J* = 3.9, 11.6 Hz, 2H), 4.30 (d, *J* = 3.4 Hz, 1H), 4.36–4.42 (dd, *J* = 7.3, 17.4 Hz, 1H), 5.08 (d, *J* = 10.1 Hz, 1H), 5.18 (d, *J* = 17.4 Hz, 1H), 5.83–5.92 (m, 1H), 7.51–7.54 (m, 1H), 7.61–7.68 (m, 2H), 7.99–8.01 (m, 1H); ^{13}C-NMR (100 MHz, $CDCl_3$) δ −5.5, −5.4, −5.0, 17.9, 18.3, 25.6, 25.9, 41.1, 62.6, 64.4, 71.2, 72.4, 115.7, 123.8, 130.9, 131.0, 132.8, 133.3, 139.2, 149.0; IR (KBr) cm^{-1}: 3095, 2956, 2932, 2859, 2886, 1548, 1473, 1440; FAB-MS (*m/z*): 557 (M^+ + 1); HRMS calcd for $C_{25}H_{45}N_2O_6SSi_2$: 557.2539, found: 557.2538.

Diastereomeric ratio (**2a** : **2b**) was determined by ^{1}H-NMR analysis of the crude reaction mixture. The ratio was calculated from two peaks (**2a**: 5.72–5.81 ppm (m, 1H), **2b**: 5.83–5.92 (m, 1H)).

(Table 1, entry 2)

To a solution of $[Ir(cod)Cl]_2$ (7.6 mg, 0.0114 mmol, 8 mol%) and (*S*,*S*,*S*)-(+)-(3,5-dioxa-4-phosphacyclohepta[2,1-*a* : 3,4-*a*′]-dinaphthalen-4-yl)bis(1-phenylethyl)amine ((*R*,*R*,*R*)-ligand) **5** (12.3 mg, 0.0227 mmol, 16 mol%) in THF (0.5 mL) was added 1,5,7-triazabicyclo[4.4.0]dec-5-ene (6.3 mg, 0.0454 mmol, 32 mol%). After the mixture was stirred at room temperature for 1 h, a solution of allylic carbonate **1a** (*E* : *Z* = 40 : 1, 90.0 mg, 0.142 mmol) in THF (1.1 mL) was added to the reaction mixture *via* a cannula. After stirring at 40 °C for 12 h, the mixture was concentrated and the residue was purified by silica gel column chromatography (*n*-hexane–EtOAc = 30 : 1) to give the cyclic compound **2** (**2a** : **2b** = 1 : 6) (58.5 mg, 74%, combined yield of **2a** and **2b**) as a white solid.

(Table 1, entry 3)

To a solution of $[Ir(cod)Cl]_2$ (8.9 mg, 0.0133 mmol, 8 mol%) and (*S*,*S*,*S*)-(+)-(3,5-dioxa-4-phosphacyclohepta[2,1-*a*:3,4-*a*′]-dinaphthalen-4-yl)bis(1-phenylethyl)amine ((*S*,*S*,*S*)-ligand) **4** (14.4 mg, 0.0266 mmol, 16 mol%) in THF (0.5 mL) was added 1,5,7-triazabicyclo[4.4.0]dec-5-ene (7.4 mg, 0.0533 mmol, 32 mol%). After the mixture was stirred at room temperature for 1 h, a solution of allylic carbonate **1a** (*Z* only, 105.4 mg, 0.167 mmol) in THF (1.1 mL) was added to the reaction mixture *via* a cannula. After stirring at 40 °C for 12 h, the mixture was concentrated and the residue was purified by silica gel column chromatography (*n*-hexane–EtOAc = 30 : 1) to give the cyclic compound **2** (**2a** : **2b** = 1 : 2.4) (88.6 mg, 95%, combined yield of **2a** and **2b**) as a white solid.

(Table 1, entry 4)

To a solution of $[Ir(cod)Cl]_2$ (8.9 mg, 0.0133 mmol, 8 mol%) and (*R*,*R*,*R*)-(+)-(3,5-dioxa-4-phosphacyclohepta[2,1-*a* : 3,4-*a*′]-dinaphthalen-4-yl)bis(1-phenylethyl)amine ((*R*,*R*,*R*)-ligand) **5** (14.4 mg, 0.0266 mmol, 16 mol%) in THF (0.5 mL) was added 1,5,7-triazabicyclo[4.4.0]dec-5-ene (7.4 mg, 0.0533 mmol, 32 mol%). After the mixture was stirred at room temperature for 1 h, a solution of allylic carbonate **1a** (*Z* only, 105.4 mg, 0.167 mmol) in THF (1.1 mL) was added to the reaction mixture *via* a cannula. After stirring at 40 °C for 12 h, the mixture was concentrated and the residue was purified by silica gel column chromatography (*n*-hexane–EtOAc = 30 : 1) to give the cyclic compound **2** (**2a** : **2b** = 3.5 : 1) (92.1 mg, 99%, combined yield of **2a** and **2b**) as a white solid.

(Table 1, entry 5)

To a solution of $[Ir(cod)Cl]_2$ (9.4 mg, 0.0134 mmol, 8 mol%) and triphenyl phosphite (7.3 μL, 0.0278 mmol, 16 mol%) in THF (0.5 mL) was added 1,5,7-triazabicyclo[4.4.0]dec-5-ene (7.8 mg, 0.056 mmol, 32 mol%). After the mixture was stirred at room temperature for 1 h, a solution of allylic carbonate **1a** (*E* : *Z* = 9 : 1, 111 mg, 0.175 mmol) in THF (1.1 mL) was added to the reaction mixture *via* a cannula. After stirring at 40 °C for 12 h, the mixture was concentrated and the residue was purified by silica gel column chromatography (*n*-hexane–EtOAc = 30 : 1 → 15 : 1) to give the cyclic compound **2** (**2a** : **2b** = 1 : 1) (56.5 mg, 58%, combined yield of **2a** and **2b**) as a white solid and starting material **1a** (41.1 mg, 37%) as a pale yellow oil.

(Table 1, entry 6)

To a solution of $[Ir(cod)Cl]_2$ (6.9 mg, 0.0102 mmol, 8 mol%) and triphenyl phosphite (5.4 μL, 0.0205 mmol, 16 mol%) in THF (0.4 mL) was added 1,5,7-triazabicyclo[4.4.0]dec-5-ene (7.0 mg, 0.050 mmol, 32 mol%). After the mixture was stirred at room temperature for 1 h, a solution of allylic carbonate **1b** (*Z* only, 81.0 mg, 0.128 mmol) in THF (0.8 mL) was added to the reaction mixture *via* a cannula. After stirring at 40 °C for 12 h, the mixture was concentrated and the residue was purified by silica gel column chromatography (*n*-hexane–EtOAc = 30 : 1 → 15 : 1) to give the cyclic compound **2** (**2a** : **2b** = 1 : 1) (35.6 mg, 50%, combined yield of **2a** and **2b**) and starting material **1b** (26.7 mg, 33%) as white solids.

(2*R*,4*R*,5*S*)-4-{(*tert*-Butyldimethylsilyl)oxy}-5-[{(*tert*-butyldimethylsilyl)oxy}methyl]-1-{(2-nitrophenyl)sulfonyl}pyrrolidine-2-carbaldehyde (14). Ozone was bubbled through a stirred solution of **2** (**2a** : **2b** = 12 : 1, 877 mg, 1.57 mmol) in CH_2Cl_2 (62 mL) at −78 °C. The solution was stirred at −78 °C for 1 h, at which time the solution became blue, and then oxygen was bubbled through the solution until it became colorless. Dimethyl sulfide (0.58 mL, 7.84 mmol) was added to the stirred solution at −78 °C and then it was allowed to warm to room temperature over 10 h under an argon atmosphere. The solvents were removed under reduced pressure, and the residue was purified by silica gel column chromatography (*n*-hexane–EtOAc = 10 : 1 → 3 : 1) to give aldehyde **14** (736 mg, 84%) as a white solid.

m.p. 132–134 °C; $[\alpha]_D^{19}$ +129.8 (*c* 1.08, $CHCl_3$); ^{1}H-NMR (400 MHz, $CDCl_3$) δ −0.05 (s, 3H), −0.01 (s, 3H), 0.04 (s, 3H), 0.08 (s, 3H), 0.83 (s, 9H), 0.83 (s, 9H), 2.04 (d, *J* = 13.5 Hz, 1H), 2.49–2.56 (ddd, *J* = 2.9, 9.2, 13.5 Hz, 1H), 3.38 (dd, *J* = 7.3, 10.6 Hz, 1H), 3.62 (dd, *J* = 3.4, 10.6 Hz, 1H), 4.09 (dd, *J* = 3.4, 7.3 Hz, 1H), 4.39 (dd, *J* = 2.4, 9.2 Hz, 2H), 7.66 (m, 3H), 8.11 (m, 1H), 9.63 (d, *J* = 2.4 H, 1 Hz); ^{13}C-NMR (100 MHz, $CDCl_3$) δ −5.7, −5.6, −5.0, −4.9, 17.8, 18.1, 25.6, 25.8, 39.1, 62.3, 68.0, 71.1, 73.7, 124.4, 130.4, 132.0, 133.9, 135.0, 148.1, 202.0; IR (KBr) cm^{-1}: 3703, 2958, 2932, 2859, 2888, 1736, 1543, 1473; FAB-MS (*m/z*): 559 (M^+ + 1). HRMS calcd for $C_{24}H_{43}N_2O_7SSi_2$: 559.2329, found: 559.2312.

This journal is © The Royal Society of Chemistry 2014

(2*R*,4*R*,5*S*)-Methyl 4-{(*tert*-butyldimethylsilyl)oxy}-5-[{(*tert*-butyldimethylsilyl)oxy}methyl]-1-{(2-nitrophenyl)sulfonyl}pyrrolidine-2-carboxylate (15a)

(2*R*,4*R*,5*S*)-Methyl 5-[{(*tert*-butyldimethylsilyl)oxy}methyl]-4-hydroxy-1-{(2-nitrophenyl)sulfonyl}pyrrolidine-2-carboxylate (15b). A solution of $NaClO_2$ (0.73 M aqueous solution, 1.1 mL) was added to a solution of aldehyde **14** (49.9 mg, 0.0893 mmol), 2-methyl-2-butene (0.42 mL, 3.96 mmol) and $NaH_2PO_4{\cdot}2H_2O$ (97.5 mg, 0.625 mmol) in *t*-BuOH (3 mL) at 0 °C. After stirring at room temperature for 1 h, the reaction mixture was quenched with water (5 mL). The whole mixture was extracted with EtOAc (3 × 15 mL) and the combined organic layers were dried over Na_2SO_4. After filtration, the filtrate was concentrated under reduced pressure.

The residue was dissolved in Et_2O (2 mL) and the solution was cooled to 0 °C. CH_2N_2 in Et_2O (excess) was added to the solution at 0 °C. After stirring at room temperature for 14 h, the solvents were removed under reduced pressure, and the residue was purified by silica gel column chromatography (*n*-hexane–EtOAc = 30 : 1) to give ester **15a** (35.3 mg, 67%) and ester **15b** (11.7 mg, 28%) as colorless oils.

15a: $[\alpha]_D^{16}$ +64.8 (*c* 1.04, $CHCl_3$); ^{1}H-NMR (400 MHz, $CDCl_3$) δ −0.06 (s, 3H), −0.02 (s, 3H), 0.03 (s, 3H), 0.05 (s, 3H), 0.82 (s, 9H), 0.84 (s, 9H), 2.14 (d, *J* = 13.0 Hz, 1H), 2.46–2.53 (ddd, *J* = 4.4, 9.7, 13.5 Hz, 1H), 3.45 (dd, *J* = 7.3, 10.6 Hz, 1H), 3.58 (s, 3H), 3.74 (dd, *J* = 3.4, 10.6 Hz, 1H), 3.94 (dd, *J* = 2.4, 6.8 Hz, 1H), 4.41 (d, *J* = 3.4, 1H), 4.69 (d, *J* = 8.7, 1H), 7.63–7.67 (m, 3H), 8.36 (m, 1H); ^{13}C-NMR (100 MHz, $CDCl_3$) δ −5.6, −5.0, −4.9, 17.8, 18.2, 25.5, 25.8, 38.0, 52.1, 62.4, 70.1, 74.8, 124.2, 131.0, 131.5, 133.0, 135.7, 148.2, 171.6; IR (neat) cm^{-1}; 3099, 2953, 2931, 2886, 2858, 1765, 1544, 1472; FAB-MS (*m*/*z*): 589 (M^+ + 1). HRMS calcd for $C_{25}H_{45}N_2O_8SSi_2$: 589.2435, found: 589.2452.

15b: $[\alpha]_D^{26}$ +151.1 (*c* 1.07, $CHCl_3$); ^{1}H-NMR (400 MHz, $CDCl_3$) δ −0.06 (s, 3H), −0.01 (s, 3H), 0.83 (s, 9H), 1.99–2.06 (m, 1H), 2.67–2.75 (m, 1H), 3.64 (s, 3H), 3.69–3.71 (m, 2H), 4.28–4.30 (m, 2H), 4.61 (d, *J* = 8.7 Hz, 1H), 7.65–7.73 (m, 3H), 8.09–8.12 (m, 1H); ^{13}C-NMR (100 MHz, $CDCl_3$) δ −5.7, −5.6, 18.1, 27.8, 37.8, 53.0, 61.4, 62.9, 72.0, 75.3, 76.7, 124.4, 130.7, 131.6, 133.7, 134.2, 175.1; IR (neat) cm^{-1}: 3465, 3098, 2955, 2857, 1732, 1591, 1547, 1471, 1440, 1359, 1256, 1218, 1163, 1115; FAB-MS (*m*/*z*): 475 (M^+ + 1). HRMS calcd for $C_{19}H_{31}N_2O_8SSi$: 475.157, found: 475.1562.

Acetylation of mono-TBS protected ester 15b

(2*R*,4*R*,5*S*)-Methyl 4-acetoxy-5-[{(*tert*-butyldimethylsilyl)oxy}-methyl]-1-{(2-nitrophenyl)sulfonyl}pyrrolidine-2-carboxylate (28). Ac_2O (8.6 mg 0.0843 mmol) was added to a mixture of 15b (20.0 mg, 0.0421 mmol), pyridine (10.0 mg, 0.126 mmol) and DMAP (0.47 mg, 0.00421 mmol) in CH_2Cl_2 (0.8 mL) at 0 °C. The reaction mixture was stirred at 0 °C for 2 h, and the reaction was quenched with water (1 mL). The whole mixture was extracted with EtOAc (2 × 10 mL). The organic extracts were washed with brine (5 mL), and dried over anhydrous Na_2SO_4. Filtration and evaporation *in vacuo* furnished the crude product, which was purified by silica gel column chromatography (*n*-hexane–EtOAc = 5 : 1) to afford **28** as a colorless oil (16.8 mg, 77%).

$[\alpha]_D^{25}$ +95.0 (*c* 2.05, $CHCl_3$); ^{1}H-NMR (400 MHz, $CDCl_3$) δ −0.14 (s, 3H), −0.03 (s, 3H), 0.78 (s, 9H), 2.02 (s, 3H), 2.23 (d, *J* = 14.0 Hz, 1H), 2.69 (ddd, *J* = 5.3, 8.7, 14.0 Hz, 1H), 3.65 (s, 3H), 3.78–3.86 (m, 2H), 4.20 (brs, 1H), 4.76 (d, *J* = 8.7 Hz), 5.16 (d, *J* = 5.3 Hz), 7.67–7.71 (m, 3H), 8.19–8.21 (m, 1H); ^{13}C-NMR (100 MHz, $CDCl_3$) δ −5.8, −5.7, 18.0, 20.9, 25.7, 35.7, 52.3, 61.9, 62.5, 68.6, 124.5, 130.9, 131.7, 133.4, 135.6, 170.4, 171.7; IR (neat) cm^{-1}: 2954, 2930, 2858, 1759, 1739, 1547; EI-MS (*m*/*z*): 517 (M^+ + 1). HRMS calcd for $C_{21}H_{33}N_2O_9SSi$: 517.1676, found: 517.1686.

After this acetylation reaction (**15b** → **28**), the chemical shift value of C4-H changed the most (C4-H of the compound **15b**: 4.28–4.30 ppm (m, C*H*(CH)(CH_2)OH), C4-H of the compound **28**: 5.16 ppm (d, *J* = 5.3 Hz, C*H*(CH)(CH_2)OAc)). Additionally, HMBC analysis of **28** revealed the relation between C4-H and carbonyl carbon of the acetoxy group.

(2*R*,4*R*,5*S*)-Methyl-4-(*tert*-butyldimethylsilyloxy)-5-(*tert*-butyldimethylsilyloxy methyl)pyrrolidine-2-carboxylate (16). PhSH (90 μL, 0.85 mmol) was added to a mixture of **15a** (166 mg, 0.28 mmol) and K_2CO_3 (195 mg, 1.41 mmol) in CH_3CN (6.4 mL) at room temperature. The reaction mixture was stirred at 40 °C for 2 h. After filtration, the filtrate was concentrated *in vacuo*. The residue was diluted with CH_2Cl_2 (50 mL), and the whole mixture was separated. The organic layer was washed with 10% $Na_2S_2O_3$ (15 mL) and brine (15 mL), and dried over anhydrous Na_2SO_4. The residue was purified by silica gel column chromatography (*n*-hexane–EtOAc = 20 : 1) to give amine **16** (107 mg, 94%) as a pale yellow oil.

$[\alpha]_D^{20}$ −7.9 (*c* 1.01, $CHCl_3$); ^{1}H-NMR (400 MHz, $CDCl_3$) δ 0.03 (s, 6H), 0.05 (s, 6H), 0.85 (s, 9H), 0.89 (s, 9H), 2.04 (m, 1H), 2.04–2.09 (m, 1H), 2.22–2.29 (ddd, *J* = 4.8, 8.7, 13.5 Hz, 1H), 3.16–3.20 (m, 1H), 3.36–3.40 (dd, *J* = 7.7, 10.6 Hz, 1H), 3.54–3.58 (dd, *J* = 4.8, 10.1 Hz, 1H), 3.72 (s, 3H), 3.80–3.83 (dd, *J* = 3.4, 8.7 Hz, 1H), 4.14–4.17 (m, 1H); ^{13}C-NMR (100 MHz, $CDCl_3$) δ −5.5, −5.4, −4.8, −4.8, 25.6, 25.9, 37.9, 52.1, 58.5, 64.6, 67.5, 73.0, 132.0, 175.6; IR (neat) cm^{-1}: 3684, 3664, 2955, 2931, 2896, 1743, 1543, 1472; FAB-MS (*m*/*z*): 404 (M^+ + 1). HRMS calcd for $C_{19}H_{42}NO_4Si_2$: 404.2652, found: 404.2649.

(+)-Bulgecinine (6)·hydrochloride

The solution of amine **16** (40 mg, 0.099 mmol) in 6 N HCl (3.0 mL) was stirred at 100 °C for 12 h. After cooling to room temperature, the reaction mixture was washed with CH_2Cl_2 (5 mL). The aqueous layer was evaporated *in vacuo*, and (+)-bulgecinine (**6**)·hydrochloride (16.2 mg, 83%) was obtained as a brown amorphous solid.

$[\alpha]_D^{18}$ −11.9 (*c* 1.62, 1 N HCl) ((−)-bulgecinine (*ent*-**6**)·HCl; $[\alpha]_D^{25}$ = +11.71 (*c* 0.65, 1 N HCl)[12f]); ^{1}H-NMR (400 MHz, D_2O) δ 2.18 (ddd, *J* = 4.9, 9.3, 14.1 Hz, 1H), 2.52 (ddd, *J* = 5.4, 8.8, 14.1 Hz, 1H), 3.62–3.81 (m, 3H), 4.31 (dd, *J* = 4.4, 8.8 Hz, 1H), 4.41 (dd, *J* = 4.9, 8.8 Hz, 1H); ^{13}C-NMR (100 MHz, D_2O) δ 36.8, 58.7, 59.1, 68.2, 71.2, 172.7; IR (KBr) cm^{-1}: 3367, 1733, 1627, 1361, 1249; FAB-MS (*m*/*z*):162 (M^+ + 1). HRMS calcd for $C_6H_{12}NO_4$: 162.0766, found: 162.0767.

This journal is © The Royal Society of Chemistry 2014

(5*S*,6*S*)-6-{(*tert*-Butoxycarbonyl)amino}-5-hydroxy-7-phenylhept-2-en-1-yl methyl carbonate (22). A solution of alcohol **20** (1.52 g, 5.22 mmol) and (*Z*)-but-2-ene-1,4-diyl dimethyl dicarbonate (**21**) (5.33 g, 26.1 mmol) in CH_2Cl_2 (104 mL) was degassed with argon for 30 min. Grubbs catalyst 2nd generation (222 mg, 0.261 mmol, 1 mol%) was added to the solution. The reaction was stirred at room temperature for 12 h. After concentration *in vacuo*, the residue was purified by flash chromatography (*n*-hexane–Et_2O = 3 : 1 → 2 : 1) to give a methyl carbonate **22** (1.76 g, 89%) as a brown oil.

$[\alpha]_D^{27}$ −16.5 (*c* 0.68, $CHCl_3$); ^{1}H-NMR (400 MHz, $CDCl_3$) *E* isomer δ 1.34 (brs, 1H), 1.41 (s, 9H), 2.21–2.31 (m, 1H), 2.84–2.95 (m, 2H), 3.61 (brs, 1H), 3.73–3.75 (m, 1H), 3.77 (s, 3H), 4.56 (d, *J* = 5.9 Hz, 2H), 5.63–5.70 (m, 1H), 5.73–5.80 (m, 1H), 7.19–7.31 (m, 5H); *Z* isomer δ 1.34 (brs, 1H), 1.41 (s, 9H), 2.21–2.31 (m, 1H), 2.84–2.95 (m, 2H), 3.61 (brs, 1H), 3.73–3.75 (m, 1H), 3.77 (s, 3H), 4.87 (d, *J* = 9.3 Hz, 2H), 5.63–5.70 (m, 1H), 5.73–5.80 (m, 1H), 7.19–7.31 (m, 5H); ^{13}C-NMR (100 MHz, $CDCl_3$) (mixture of *E*/*Z* isomers) δ 28.3, 29.7, 37.7, 38.6, 54.7, 55.4, 68.1, 70.3, 79.4, 126.4, 127.0, 128.5, 129.3, 132.3, 138.3, 155.6, 156.0; IR (neat) cm^{-1}: 3428, 3030, 2115, 1748, 1668, 1505, 1455, 1393, 1367, 1268, 1170; EI-MS (*m*/*z*): 379 (M^+); HRMS calcd for $C_{20}H_{29}NO_6$: 379.1995, found: 379.1991.

(5*S*,6*S*)-6-Amino-5-(*tert*-butyldimethylsilyloxy)-7-phenylhept-2-en-1-yl methyl carbonate (24). To a solution of **22** (221 mg, 0.583 mmol) in CH_2Cl_2 (2.7 mL) was added TFA (2.7 mL) at 0 °C. After the mixture was stirred at room temperature for 1 h, the solvents were removed under reduced pressure. Traces of TFA were removed from a mixture by azeotropic distillations with toluene (2 × 10 mL) under reduced pressure at room temperature.

The residue was dissolved in CH_2Cl_2 (2.7 mL). Imidazole (298 mg, 4.37 mmol) and TBSCl (176 mg, 1.17 mmol) were added to this solution at 0 °C. After being stirred at room temperature for 14 h, the reaction was quenched with water (10 mL). The whole mixture was extracted with CH_2Cl_2 (3 × 20 mL). The combined organic layers were dried over anhydrous Na_2SO_4. Filtration and evaporation *in vacuo* furnished the crude product, which was purified by silica gel column chromatography (*n*-hexane–Et_2O = 6 : 1 → 1 : 1) to afford **24** (174 mg, 76%, 2 steps) as a colorless oil.

$[\alpha]_D^{23}$ +2.9 (*c* 1.30, $CHCl_3$); ^{1}H-NMR (400 MHz, $CDCl_3$) *E* isomer δ 0.03 (s, 3H), 0.05 (s, 3H), 0.88 (s, 9H), 1.50 (brs, 2H), 2.21–2.28 (m, 1H), 2.34–2.46 (m, 2H), 2.78–2.82 (m, 1H), 2.86–2.91 (m, 1H), 3.60 (dt, *J* = 3.8, 5.8 Hz, 1H), 3.71 (s, 3H), 4.53 (d, *J* = 6.3 Hz, 2H), 5.58–5.65 (m, 1H), 5.74 (ddd, *J* = 6.8, 7.3, 15.4 Hz, 1H), 7.11–7.16 (m, 3H), 7.21–7.25 (m, 2H); *Z* isomer δ 0.04 (s, 3H), 0.05 (s, 3H), 0.88 (s, 9H), 1.50 (br, s, 2H), 2.21–2.28 (m, 1H), 2.34–2.46 (m, 2H), 2.78–2.82 (m, 1H), 2.86–2.91 (m, 1H), 3.60 (dt, *J* = 3.8, 5.8 Hz, 1H), 3.69 (s, 3H), 4.66 (m, 2H), 5.58–5.65 (m, 1H), 5.74 (ddd, *J* = 6.8, 7.3, 15.4 Hz, 1H), 7.11–7.16 (m, 3H), 7.21–7.25 (m, 2H); ^{13}C-NMR (100 MHz, $CDCl_3$) (mixture of *E*/*Z* isomers) δ −4.7, −4.6, −4.2, −4.1, 18.0, 25.7, 25.8, 36.7, 40.4, 40.6, 54.3, 54.6, 55.9, 67.8, 68.2, 74.7, 124.7, 125.8, 126.1, 128.4, 129.1, 131.6, 132.9, 139.6, 155.5, 155.6; IR (neat) cm^{-1}: 3383, 3028, 2955, 2930, 2857, 1748, 1603, 1495, 1443, 1382, 1361, 1268, 1067; EI-MS (*m*/*z*): 393 (M^+); HRMS calcd for $C_{21}H_{35}NO_4Si$: 393.2335, found: 393.2341. Anal. calcd for $C_{21}H_{35}NO_4Si$: C, 64.08; H, 8.96; N, 3.56. Found: C, 63.88; H, 9.16; N, 3.46.

(5*S*,6*S*)-5-(*tert*-Butyldimethylsilyloxy)-6-(2-nitrophenylsulfonamido)-7-phenylhept-2-en-1-yl methyl carbonate (17). To a solution of amine **24** (1.71 g, 4.34 mmol), Et_3N (1.1 mL, 7.82 mmol) and DMAP (127 mg, 1.04 mmol) in CH_2Cl_2 (43 mL) was added 2-nitrobenzenesulfonyl chloride (1.16 g, 5.21 mmol) at 0 °C. The mixture was stirred at room temperature for 12 h. After evaporation, the residue was diluted with EtOAc (100 mL). The whole mixture was washed successively with brine (15 mL), 5% $KHSO_4$ (15 mL) and brine (15 mL), and dried over anhydrous Na_2SO_4. Filtration and evaporation *in vacuo* furnished the crude product, which was purified by silica gel column chromatography (*n*-hexane–Et_2O = 6 : 1 → 3 : 1) to afford **17** (2.44 g, 97%) as a pale yellow oil.

$[\alpha]_D^{26}$ +52.6 (*c* 1.21, $CHCl_3$); ^{1}H-NMR (400 MHz, $CDCl_3$) *E* isomer δ 0.09 (s, 3H), 0.14 (s, 3H), 0.96 (s, 9H), 2.14 (ddd, *J* = 6.3, 6.8, 13.6 Hz, 1H), 2.32 (ddd, *J* = 6.8, 7.2, 14.1 Hz, 1H), 2.60 (dd, *J* = 9.2, 14.1 Hz, 1H), 2.87 (dd, *J* = 6.3, 14.0 Hz, 1H), 3.73–3.82 (m, 5H), 4.54 (d, *J* = 5.8 Hz, 2H), 5.47–5.54 (m, 1H), 5.60–5.65 (m, 1H), 5.73, (d, *J* = 8.2 Hz, 1H), 6.95–6.99 (m, 5H), 7.51–7.59 (m, 2H), 7.71–7.74 (m, 2H); *Z* isomer δ 0.12 (s, 3H), 0.17 (s, 3H), 0.96 (s, 9H), 2.14 (ddd, *J* = 6.3, 6.8, 13.6 Hz, 1H), 2.32 (ddd, *J* = 6.8, 7.2, 14.1 Hz, 1H), 2.60 (dd, *J* = 9.2, 14.1 Hz, 1H), 2.87 (dd, *J* = 6.3, 14.0 Hz, 1H), 3.73–3.82 (m, 5H), 4.63 (d, *J* = 4.8 Hz, 2H), 5.47–5.54 (m, 1H), 5.60–5.65 (m, 1H), 5.78 (d, *J* = 8.2 Hz, 1H), 6.95–6.99 (m, 5H), 7.51–7.59 (m, 2H), 7.71–7.74 (m, 2H); ^{13}C-NMR (100 MHz, $CDCl_3$) (mixture of *E*/*Z* isomers) δ −4.7, −4.6, −4.2, 17.9, 25.7, 25.8, 31.2, 36.1, 37.1, 37.9, 54.7, 59.6, 60.3, 63.5, 68.0, 72.8, 73.1, 125.3, 125.4, 126.4, 126.5, 126.8, 128.1, 128.2, 128.8, 128.9, 129.6, 129.7, 130.8, 131.6, 132.7, 132.8, 132.9, 134.9, 137.3; IR (neat) cm^{-1}: 3583, 3375, 3028, 2955, 2930, 2887, 2858, 1748, 1673, 1595, 1539, 1496, 1471, 1443, 1409, 1361, 1269, 1218, 1167, 1074; FAB-MS (*m*/*z*): 579 (M^+ + 1). HRMS calcd for $C_{27}H_{39}N_2O_8SSi$: 579.2196, found: 579.2182.

The *E*/*Z* isomer ratio was determined by ^{1}H-NMR analysis (*E* isomer; 4.54 (d, *J* = 5.8 Hz, 2H), *Z* isomer; 4.63 (d, *J* = 4.8 Hz, 2H)).

(2*S*,3*S*,5*S*)-2-Benzyl-3-(*tert*-butyldimethylsilyloxy)-1-(2-nitrophenylsulfonyl)-5-vinylpyrrolidine (18a)

(2*S*,3*S*,5*R*)-2-Benzyl-3-(*tert*-butyldimethylsilyloxy)-1-(2-nitrophenylsulfonyl)-5-vinylpyrrolidine (18b). To a solution of $[Ir(cod)Cl]_2$ (16.2 mg, 0.0241 mmol, 8 mol%) and (*R*,*R*,*R*)-(+)-(3,5-dioxa-4-phosphacyclohepta[2,1-*a* : 3,4-*a*']dinaphthalen-4-yl)bis(1-phenylethyl)amine ((*R*,*R*,*R*)-ligand) **5** (26.0 mg, 0.0481 mmol, 16 mol%) in THF (0.84 mL) was added 1,5,7-triazabicyclo[4.4.0]dec-5-ene (13.4 mg, 0.0963 mmol, 32 mol%). After the mixture was stirred for 1 h at room temperature, a solution of allylic carbonate **17** (*E* : *Z* = 13 : 1, 174 mg, 0.301 mmol) in THF (2.0 mL) was added to the reaction mixture *via* a cannula. After stirring for 4 h at 40 °C, the mixture was cooled to room temperature. The reaction was quenched with *sat.* NH_4Cl (5 mL), and the whole mixture was

This journal is © The Royal Society of Chemistry 2014

extracted with EtOAc (3 × 20 mL). The combined organic layers were dried over anhydrous Na_2SO_4. Filtration and evaporation *in vacuo* furnished the crude product, which was purified by silica gel column chromatography (*n*-hexane–Et_2O = 20 : 1 → 8 : 1) to afford **18a** (132 mg, 87%) as a white solid and **18b** (12.0 mg, 8%) as a white solid.

18a: m.p. 77–80 °C; $[\alpha]_D^{28}$ +71.5 (*c* 1.03, $CHCl_3$); ^{1}H-NMR (400 MHz, $CDCl_3$) δ −0.01 (s, 3H), 0.02 (s, 3H), 0.88 (s, 9H), 1.72–1.80 (m, 1H), 2.13–2.20 (m, 1H), 2.87 (dd, *J* = 6.3, 14.5 Hz, 1H), 3.08 (dd, *J* = 6.3, 14.0 Hz, 1H), 4.13–4.30 (m, 3H), 5.04 (d, *J* = 10.6 Hz, 1H), 5.06 (d, *J* = 17.4 Hz, 1H), 5.73 (ddd, *J* = 7.2, 10.1, 17.4 Hz, 1H), 7.14–7.18 (m, 1H), 7.22–7.30 (m, 4H), 7.53–7.59 (m, 2H), 7.63–7.67 (m, 1H), 7.79 (d, *J* = 8.2 Hz, 1H); ^{13}C-NMR (100 MHz, $CDCl_3$) δ −5.2, −4.9, 18.1, 25.8, 35.8, 38.7, 59.9, 65.0, 71.3, 115.8, 123.8, 126.2, 128.0, 130.3, 131.1, 131.9, 133.6, 138.3, 139.3, 148.4; IR (KBr) cm^{-1}: 3091, 3028, 2952, 2894, 2860, 1547, 1495, 1465, 1370, 1346, 1258, 1169, 1124, 1067; FAB-MS (*m*/*z*): 503 (M^+ + 1). HRMS calcd for $C_{25}H_{35}N_2O_5SSi$: 503.2036, found: 503.2041. Anal. calcd for $C_{25}H_{34}N_2O_5SSi$: C, 59.73; H, 6.82; N, 5.57. Found: C, 59.60; H, 6.98; N, 5.52.

18b: m.p. 119–121 °C; $[\alpha]_D^{27}$ +23.9 (*c* 0.85, $CHCl_3$); ^{1}H-NMR (400 MHz, $CDCl_3$) δ −0.01 (s, 3H), 0.03 (s, 3H), 0.88 (s, 9H), 1.61–1.66 (m, 1H), 1.90–1.98 (m, 1H), 3.08 (dd, *J* = 2.9, 14.0 Hz, 1H), 3.17 (dd, *J* = 7.2, 14.0 Hz, 1H), 4.11–4.18 (m, 1H), 4.36 (dt, *J* = 2.4, 6.8 Hz, 1H), 4.45 (dt, *J* = 6.8, 10.1 Hz, 1H), 4.69 (d, *J* = 10.1 Hz, 1H), 5.01 (d, *J* = 16.9 Hz, 1H), 5.23 (ddd, *J* = 9.7, 9.7, 16.9 Hz, 1H), 7.17–7.22 (m, 1H), 7.25–7.29 (m, 2H), 7.43 (d, *J* = 7.2 Hz, 2H), 7.55–7.65 (m, 3H), 8.00 (d, *J* = 8.2 Hz, 1H); ^{13}C-NMR (100 MHz, $CDCl_3$) δ −5.1, −5.0, 18.2, 25.9, 36.4, 39.1, 60.4, 65.9, 70.8, 117.6, 123.8, 126.1, 126.6, 128.0, 128.4, 130.5, 131.2, 132.3, 133.1, 136.2, 137.3, 139.0, 147.9; IR (KBr) cm^{-1}: 3086, 3031, 2955, 2886, 2857, 1740, 1661, 1541, 1464, 1370, 1344, 1300, 1255, 1163, 1067; FAB-MS (*m*/*z*): 503 (M^+ + 1). HRMS calcd for $C_{25}H_{35}N_2O_5SSi$: 503.2036, found: 503.2042.

(2*S*,3*S*,5*S*)-2-Benzyl-3-(*tert*-butyldimethylsilyloxy)-1-(2-nitrophenylsulfonyl)-5-(non-1-enyl)pyrrolidine (25). A solution of **18a** (264 mg, 0.525 mmol) and 1-nonene (0.91 mL, 5.25 mmol) in CH_2Cl_2 (5.3 mL) was degassed with argon for 10 min. The solution was heated to 40 °C and 3 portions of Grubbs catalyst 2nd generation (each 22.3 mg, 0.0262 mmol, 5 mol%) were added after (0 h, 4 h, 10 h).

The reaction was stirred for an additional 14 h for a total reaction time of 24 h and then cooled to room temperature and concentrated. The residue was purified by flash chromatography (*n*-hexane–Et_2O = 15 : 1) to give a compound **25** (252 mg, 80%) as a colorless oil.

$[\alpha]_D^{17}$ +34.2 (*c* 1.36, $CHCl_3$); ^{1}H-NMR (400 MHz, $CDCl_3$) *E* isomer δ 0.03 (s, 3H), 0.07 (s, 3H), 0.91–0.97 (m, 12H), 1.30–1.37 (m, 10H), 1.76 (dt, *J* = 8.7, 12.6 Hz, 1H), 1.99–2.06 (m, 2H), 2.16–2.23 (m, 1H), 2.94 (dd, *J* = 6.3, 14.5 Hz, 1H), 3.13 (dd, *J* = 6.3, 14.5 Hz, 1H), 4.10–4.29 (m, 2H), 4.34 (dd, *J* = 6.3, 12.6 Hz, 1H), 5.40 (dd, *J* = 7.7, 15.5 Hz, 1H), 5.49–5.56 (m, 1H), 7.19–7.35 (m, 5H), 7.57–7.61 (m, 2H), 7.66–7.70 (m, 1H), 7.83 (d, *J* = 7.2 Hz, 1H); *Z* isomer δ 0.05 (s, 3H), 0.08 (s, 3H), 0.91–0.97 (m, 12H), 1.30–1.37 (m, 10H), 1.76 (dt, *J* = 8.7, 12.6 Hz, 1H), 1.99–2.06 (m, 2H), 2.16–2.23 (m, 1H), 2.74–2.77 (m, 1H), 2.85 (dd, *J* = 6.8, 14.1 Hz, 1H), 3.78–3.85 (m, 2H), 4.56 (dd, *J* = 7.8, 15.6 Hz, 1H), 5.40 (dd, *J* = 7.7, 15.5 Hz, 1H), 5.49–5.56 (m, 1H), 7.19–7.35 (m, 5H), 7.57–7.61 (m, 2H), 7.66–7.70 (m, 1H), 7.83 (d, *J* = 7.2 Hz, 1H); ^{13}C-NMR (100 MHz, $CDCl_3$) (mixture of *E*/*Z* isomers) δ −5.2, −4.8, 14.1, 18.1, 22.5, 22.6, 25.8, 28.8, 28.9, 29.1, 31.7, 31.8, 32.0, 35.8, 39.2, 59.8, 64.9, 71.4, 123.7, 126.1, 128.0, 128.1, 130.2, 130.8, 131.0, 131.8, 132.3, 132.8, 133.4, 138.5, 148.4; IR (neat) cm^{-1}: 3030, 2928, 2856, 1548, 1497, 1471, 1373, 1254, 1167, 1128, 1063; FAB-MS (*m*/*z*): 601 (M^+ + 1). HRMS calcd for $C_{32}H_{49}N_2O_5SSi$: 601.3131, found: 601.3112.

E/*Z* isomer ratio was determined by ^{1}H-NMR analysis (*E* isomer: 4.34 (dd, *J* = 6.3, 12.6 Hz, 1H), *Z* isomer: 4.56 (dd, *J* = 7.8, 15.6 Hz, 1H)).

(2*S*,3*S*,5*S*)-2-Benzyl-3-(*tert*-butyldimethylsilyloxy)-5-(non-1-enyl)pyrrolidine (26). PhSH (574 μL, 5.63 mmol) was added to a mixture of **25** (1.12 g, 1.86 mmol) and K_2CO_3 (1.29 g, 9.31 mmol) in CH_3CN (42 mL) at room temperature. The reaction mixture was stirred at 40 °C for 12 h. After filtration, the filtrate was concentrated *in vacuo*. The residue was diluted with CH_2Cl_2 (100 mL), and the whole mixture was washed with 10% $Na_2S_2O_3$ (30 mL). The water layer was extracted with CH_2Cl_2 (2 × 50 mL). The combined organic layers were dried over anhydrous Na_2SO_4. After filtration and evaporation, the residue was purified by silica gel column chromatography (*n*-hexane–Et_2O = 10 : 1 → 1 : 2) to give amine **26** (705 mg, 91%) as a pale yellow oil.

$[\alpha]_D^{21}$ −16.5 (*c* 1.55, $CHCl_3$); ^{1}H-NMR (400 MHz, $CDCl_3$) *E* isomer δ 0.02 (s, 3H), 0.06 (s, 3H), 0.86 (t, *J* = 7.2 Hz, 3H), 0.93 (s, 9H), 1.25–1.33 (m, 10H), 1.52–1.58 (m, 1H), 1.92–2.01 (m, 2H), 2.15 (ddd, *J* = 5.8, 8.2, 13.8 Hz, 1H), 2.77–2.90 (m, 2H), 3.05 (m, 1H), 3.43 (dt, *J* = 6.8, 7.5 Hz, 1H), 4.14–4.17 (m, 1H), 5.45–5.56 (m, 2H), 7.16–7.29 (m, 5H); *Z* isomer δ 0.01 (s, 3H), 0.05 (s, 3H), 0.86 (t, *J* = 7.2 Hz, 3H), 0.93 (s, 9H), 1.25–1.33 (m, 10H), 1.45–1.47 (m, 1H), 1.92–2.01 (m, 2H), 2.27–2.31 (m, 1H), 2.77–2.90 (m, 2H), 3.05 (m, 1H), 3.81 (dt, *J* = 7.2, 8.2 Hz, 1H), 4.12–4.13 (m, 1H), 5.34–5.45 (m, 2H), 7.16–7.29 (m, 5H); ^{13}C-NMR (100 MHz, $CDCl_3$) (mixture of *E*/*Z* isomers) δ −5.0, −4.2, 14.1, 18.2, 22.5, 22.6, 25.9, 26.0, 28.8, 29.1, 31.7, 31.8, 32.2, 36.1, 43.0, 59.6, 65.9, 66.0, 73.7, 125.9, 128.3, 128.9, 131.7, 132.9, 140.4; IR (neat) cm^{-1}: 3424, 3029, 2956, 2929, 2856, 2121, 1638, 1496, 1468, 1362, 1254, 1081; EI-MS (*m*/*z*): 415 (M^+). HRMS calcd for $C_{26}H_{45}NOSi$: 415.3270, found: 415.3255.

(2*S*,3*S*,5*R*)-2-Benzyl-3-(*tert*-butyldimethylsilyloxy)-1-methyl-5-nonylpyrrolidine (27). HCHO (37% in H_2O, 146 μL, 1.80 mmol) was added to a solution of amine **26** (50.3 mg, 0.121 mmol) in MeOH (7.3 mL) at room temperature. After stirring at room temperature for 10 min, PtO_2 (27.6 mg, 0.121 mmol) was added to the reaction mixture. The resulting mixture was stirred under hydrogen at atmospheric pressure for 20 h. The mixture was then filtered through a filter paper, and the filter paper was washed with MeOH. The filtrates were concentrated *in vacuo*, and the residue was purified by silica gel column chromatography (*n*-hexane–Et_2OAc = 30 : 1) to afford amine **27** (26.3 mg, 50%, 2 steps) as a colorless oil.

This journal is © The Royal Society of Chemistry 2014

$[\alpha]_D^{27}$ +24.2 (*c* 1.45, $CHCl_3$); ^{1}H-NMR (400 MHz, $CDCl_3$) δ −0.10 (s, 3H), −0.03 (s, 3H), 0.87–0.90 (m, 12H), 1.27–1.45 (m, 16H), 1.71 (m, 1H), 2.04–2.06 (m, 1H), 2.21–2.26 (m, 4H), 2.47 (m, 1H), 2.75–2.79 (m, 1H), 3.03 (ddd, J = 7.2, 7.3, 7.8 Hz, 1H), 4.14–4.17 (m, 1H), 7.14–7.20 (m, 1H), 7.24–7.28 (m, 4H); ^{13}C-NMR (100 MHz, $CDCl_3$) δ −5.0, −4.3, 14.1, 18.2, 22.7, 26.0, 26.7, 29.3, 29.5, 29.6, 29.7, 29.9, 31.2, 40.3, 66.0, 71.1, 73.4, 125.6, 128.1, 129.1; IR (neat) cm^{-1}: 3028, 2927, 2855, 2782, 1604, 1497, 1463, 1361, 1255, 1140; FAB-MS (*m*/*z*): 432 (M^+ + 1). HRMS calcd for $C_{27}H_{50}NOSi$: 432.3662, found: 432.3662.

(+)-Preussin (7)

TBAF (1.0 M in THF, 76 μL, 0.076 mmol) was added to a solution of amine **27** (19.2 mg, 0.0445 mmol) in THF (2 mL) at 0 °C. After stirring at room temperature for 22 h, the solvents were removed under reduced pressure. The residue was purified by flash chromatography (*n*-hexane–EtOAc = 4 : 1) to give a (+)-preussin (7) (11.7 mg, 83%) as a colorless oil.

$[\alpha]_D^{15}$ +17.1 (*c* 0.50, $CHCl_3$). (natural (+)-preussin (7); $[\alpha]_D^{25}$ = +22.0 (*c* 1.0, $CHCl_3$)[15a]) ^{1}H-NMR (400 MHz, $CDCl_3$) δ 0.86 (t, J = 7.2 Hz, 3H), 1.26 (m, 16H), 1.43 (dd, J = 6.3, 13.5 Hz, 1H), 1.69–1.72 (m, 1H), 2.13–2.25 (m, 2H), 2.27 (m, 1H), 2.35 (s, 3H), 2.83–2.93 (m, 1H), 3.82 (m, 1H), 7.18–7.22 (m, 1H), 7.28–7.31 (m, 4H); ^{13}C-NMR (100 MHz, $CDCl_3$) δ 14.1, 22.7, 26.3, 29.3, 29.6, 29.9, 31.9, 33.6, 34.8, 38.6, 39.3, 65.9, 70.4, 73.6, 126.1, 128.4, 129.3, 139.3; IR (neat) cm^{-1}: 3338, 2925, 2854, 2344, 1730, 1604, 1496, 1456; FAB-MS (*m*/*z*): 318 (M^+ + 1). HRMS calcd for $C_{21}H_{36}NO$: 318.2797, found: 318.2794.

Acknowledgements

This work supported in part by a Grant-in-Aid for Young Scientists (B) (no. 23790138) (Y.N.) from JSPS and by a grant of the Strategic Research Foundation Grant-aided Project for Private Universities from the Ministry of Education, Culture, Sport, Science, and Technology, Japan (MEXT), 2010–2014.

Notes and references

1 (*a*) J. R. Lewis, *Nat. Prod. Rep.*, 2001, **18**, 95–128; (*b*) D. O'Hagan, *Nat. Prod. Rep.*, 2000, **17**, 435–446.

2 (*a*) C. Mothes, C. Caumes, A. Guez, H. Boullet, T. Gendrineau, S. Darses, N. Delsuc, R. Moumné, B. Oswald, O. Lequin and P. Karoyan, *Molecules*, 2013, **18**, 2307–2327; (*b*) I. Dragutan, V. Dragutan, C. Mitan, H. C. Vosloo, L. Delaude and A. Demonceau, *Beilstein J. Org. Chem.*, 2011, **7**, 699–716; (*c*) B. L. Stocker, E. M. Dangerfield, A. L. Win-Mason, G. W. Haslett and M. S. M. Timmer, *Eur. J. Org. Chem.*, 2010, 1615–1637; (*d*) J. P. Wolfe, *Eur. J. Org. Chem.*, 2007, 571–582; (*e*) P.-Q. Huang, *Synlett*, 2006, 1133–1149; (*f*) F.-X. Felpin and J. Lebreton, *Eur. J. Org. Chem.*, 2003, 3693–3712; (*g*) H. Yoda, *Curr. Org. Chem.*, 2002, **6**, 223–243; (*h*) M. Pichon and B. Figadère, *Tetrahedron: Asymmetry*, 1996, **7**, 927–964 and references cited therein.

3 Y. Natori, S. Kikuchi, Y. Yoshimura, A. Kato, I. Adachi and H. Takahata, *Heterocycles*, 2012, **86**, 1401–1417.

4 (*a*) A. Minatti and K. Muñiz, *Chem. Soc. Rev.*, 2007, **36**, 1142–1152; (*b*) D. M. D'Souza and T. J. J. Müller, *Chem. Soc. Rev.*, 2007, **36**, 1095–1108; (*c*) N. Toyooka and H. Nemoto, in *New Methods for the Asymmetric Synthesis of Nitrogen Heterocycles*, ed. J. L. Vicario, D. Badia and L. Carrillo, 2005, pp. 149–163; (*d*) H. Takahata, H. Bandoh and T. Momose, *J. Org. Chem.*, 1992, **57**, 4401–4404.

5 (*a*) C. Gnamm, K. Brödner, C. M. Krauter and G. Helmchen, *Chem.-Eur. J.*, 2009, **15**, 10514–10532; (*b*) C. Gnamm, C. M. Krauter, K. Brödner and G. Helmchen, *Chem.-Eur. J.*, 2009, **15**, 2050–2054; (*c*) M. Gärtner, S. Mader, K. Seehafer and G. Helmchen, *J. Am. Chem. Soc.*, 2011, **133**, 2072–2075. However, no details of formation of pyrrolidine were described in ESI.†

6 (*a*) K. Ando, *J. Org. Chem.*, 1999, **64**, 6815–6821; (*b*) K. Ando, *J. Org. Chem.*, 1998, **63**, 8411–8416; (*c*) K. Ando, *J. Org. Chem.*, 1997, **62**, 1934–1939.

7 S. N. Murthy and Y. V. D. Nageswar, *Synthesis*, 2011, 755–758.

8 A chiral (*S*,*S*,*S*)-ligand **4** was purchased from Sigma-Aldrich Co. A chiral (*R*,*R*,*R*)-ligand **5** was prepared according to a reported procedure. K. Tissot-Croset, D. Polet and A. Alexakis, *Angew. Chem., Int. Ed.*, 2004, **43**, 2426–2428.

9 R. Takeuchi and M. Kashio, *J. Am. Chem. Soc.*, 1998, **120**, 8647–8655.

10 (*a*) S. Shinagawa, M. Maki, K. Kintaka, A. Imada and M. Asai, *J. Antibiot.*, 1985, **38**, 17–23; (*b*) A. Imada, K. Kintaka, M. Nakao and S. Shinagawa, *J. Antibiot.*, 1982, **35**, 1400–1403.

11 S. Shinagawa, F. Kashara, Y. Wada, S. Harada and M. Asai, *Tetrahedron*, 1984, **40**, 3465–3470.

12 (*a*) B. Das and D. N. Kumar, *Synlett*, 2011, 1285–1287; (*b*) K. Show, P. K. Upadhyay and P. Kumar, *Tetrahedron: Asymmetry*, 2011, **22**, 1234–1238; (*c*) S. Chandrasekhar, G. Chandrashekar, K. Vijeendera and G. D. Sarma, *Tetrahedron: Asymmetry*, 2006, **17**, 2864–2869; (*d*) B. M. Trost, D. B. Horne and M. J. Woltering, *Chem.-Eur. J.*, 2006, **12**, 6607–6620; (*e*) S. P. Chavan, C. Praveen, P. Sharma and U. R. Kalkote, *Tetrahedron Lett.*, 2005, **46**, 439–441; (*f*) J. K. Khalaf and A. Datta, *J. Org. Chem.*, 2004, **69**, 387–390; (*g*) K. A. Holt, J. P. Swift, M. E. B. Smith, S. J. C. Taylor and R. McCague, *Tetrahedron Lett.*, 2002, **43**, 1545–1548; (*h*) A. Krasinski and J. Jurczak, *Tetrahedron Lett.*, 2001, **42**, 2019–2021; and references cited therein.

13 (*a*) A. Madau, G. Porzi and S. Sandri, *Tetrahedron: Asymmetry*, 1996, **7**, 825–830; (*b*) Y. Yuasa, J. Ando and S. Shibuya, *J. Chem. Soc., Perkin Trans. 1*, 1996, 793–802; (*c*) Y. Yuasa, J. Ando and S. Shibuya, *J. Chem. Soc., Chem. Commun.*, 1994, 1383–1384; (*d*) C. Schmeck and L. S. Hegedus, *J. Am. Chem. Soc.*, 1994, **116**, 9927–9934.

14 (*a*) A. Kato, E. Hayashi, S. Miyauchi, I. Adachi, T. Imahori, Y. Natori, Y. Yoshimura, R. J. Nash, H. Shimaoka,

This journal is © The Royal Society of Chemistry 2014

I. Nakagome, J. Koseki, S. Hirono and H. Takahata, *J. Med. Chem.*, 2012, **55**, 10347–10362; (*b*) Y. Natori, T. Imahori, K. Murakami, Y. Yoshimura, S. Nakagawa, A. Kato, I. Adachi and H. Takahata, *Bioorg. Med. Chem. Lett.*, 2011, **21**, 738–741; (*c*) Y. Saito, S. Takahashi, N. Azerb, A. T. Eldefrawi, M. E. Eldefrawi and H. Takahata, *Heterocycles*, 2009, **79**, 1043–1060; (*d*) Y. Yoshimura, C. Ohara, T. Imahori, Y. Saito, A. Kato, S. Miyauchi, I. Adachi and H. Takahata, *Bioorg. Med. Chem.*, 2008, **16**, 8273–8286; (*e*) Y. Saito, N. Okamoto and H. Takahata, *Beils. J. Org. Chem.*, 2007, **3**, 37; (*f*) A. Kato, N. Kato, E. Kano, I. Adachi, K. Ikeda, L. Yu, T. Okamoto, Y. Banba, H. Ouchi, H. Takahata and N. Asano, *J. Med. Chem.*, 2005, **48**, 2036–2044; (*g*) H. Takahata, Y. Banba, H. Ouchi, H. Nemoto, A. Kato and I. Adachi, *J. Org. Chem.*, 2003, **68**, 3603–3607; (*h*) H. Takahata and M. Shimizu, *Amino Acids*, 2003, **24**, 267–272; (*i*) H. Takahata, Y. Banba, H. Ouchi, H. Nemoto, A. Kato and I. Adachi, *J. Org. Chem.*, 2003, **68**, 3603–3607.

15 (*a*) J. H. Johnson, D. W. Phillipson and A. D. Kahle, *J. Antibiot.*, 1989, **42**, 1184–1185; (*b*) R. E. Schwartz, J. Liesch, O. Hensens, L. Zitano, S. Honeycutt, G. Garrity, R. A. Fromtling, J. Onishi and R. Monaghan, *J. Antibiot.*, 1988, **41**, 1774–1779.

16 T. V. Achenbach, E. P. Slater, H. Brummerhop, T. Bach and R. Müller, *Antimicrob. Agents Chemother.*, 2000, **44**, 2794–2801.

17 (*a*) R. Britton and B. Kang, *Nat. Prod. Rep.*, 2013, **30**, 227–236; (*b*) R. Chowdhury and S. K. Ghosh, *Synthesis*, 2011, 1936–1945; (*c*) K.-J. Xiao, Y. Wang, K.-Y. Ye and P.-Q. Huang, *Chem.-Eur. J.*, 2010, **16**, 12792–12796; (*d*) J. A. Draper and R. Britton, *Org. Lett.*, 2010, **12**, 4034–4037; (*e*) F. D. Davis, J. Zhang, H. Qiu and Y. Wu, *Org. Lett.*, 2008, **10**, 1433–1436; (*f*) N. Gogoi, J. Boruwa and N. C. Barua, *Eur. J. Org. Chem.*, 2006, 1722–1725; (*g*) M. B. Bertrand and J. P. Wolfe, *Org. Lett.*, 2006, **8**, 2353–2356; (*h*) S. Canova, V. Bellosta and J. Cossy, *Synlett*, 2004, 1811–1813; (*i*) F. A. Davis and J. Deng, *Tetrahedron*, 2004, **60**, 5111–5115; (*j*) M. Okue, H. Watanabe, K. Kasahara, M. Yoshida, S. Horinouchi and T. Kitahara, *Biosci., Biotechnol., Biochem.*, 2002, **66**, 1093–1096 and references cited therein.

18 G. Veerasa, *Synth. Commun.*, 2000, **30**, 1479–1487.

19 On the gram scale (>2 g of **17**), the diastereoselectivity was slightly decreased in a 75% (**18a**) : 14% (**18b**) ratio.

This journal is © The Royal Society of Chemistry 2014

Research article

LUMINESCENCE
The Journal of Biological and Chemical Luminescence

Received: 18 December 2012, Revised: 16 May 2013, Accepted: 24 May 2013 Published online in Wiley Online Library

(wileyonlinelibrary.com) DOI 10.1002/bio.2555

Development of a highly sensitive chemiluminescent assay for hydrogen peroxide under neutral conditions using acridinium ester and its application to an enzyme immunoassay

Hidetoshi Arakawa,* Keiko Tsuruoka, Ken-ichi Ohno, Noriko Tajima and Hiromi Nagano

ABSTRACT: We developed a highly sensitive chemiluminescent (CL) assay for hydrogen peroxide using 10-methyl-9-(phenoxycarbonyl) acridinium fluorosulfonate (PMAC) that produced chemiluminescence under neutral conditions and applied it to an enzyme immunoassay (EIA). One picomole of hydrogen peroxide could be detected using the optimized PMAC-CL method and 6.2×10^{-20} mol β-D-galactosidase (β-gal) could be detected by combining an indoxyl derivative substrate and the proposed PMAC-CL method. This highly sensitive CL β-gal assay was applied to an EIA for thyroid-stimulating hormone (TSH) using β-gal as a label enzyme; 0.02–100.0 μU/mL TSH in human serum could be assayed directly and with high reproducibility. Copyright © 2013 John Wiley & Sons, Ltd. Copyright © 2013 John Wiley & Sons, Ltd.

Keywords: chemiluminescence; PMAC; hydrogen peroxide; β-D-galactosidase; TSH; EIA

Introduction

Several types of changes occur in biogenic substances during the disease process. Therefore, rapid and precise determination of these changes facilitates effective diagnosis, optimal therapy, evaluation of treatment efficacy, and monitoring of drug side effects.

Because biogenic materials are comprised of an enormous variety of substances, highly specific and sensitive measurement techniques are needed for the detection or quantitative determination of a specific substance in a biological fluid. Several sensitive methods are used including colorimetric analysis, fluorescence and luminescence. Among these, the chemiluminescence (CL) technique is rapid and has high sensitivity. This method has been applied to the measurement of biogenic substances (1) and the sensitive detection of labeled enzymes in enzyme immunoassays (EIA) or DNA probe assays (2,3). In particular, EIA can determine specific substances in complex biological materials without isolation or purification, and has been widely applied in the field of clinical chemistry. Horseradish peroxidase, β-D-galactosidase (β-gal) and alkaline phosphatase are widely used as label enzymes in EIA. We found that reducing substances, such as indoxyl derivatives (4) and catecholamine (5), reacted with dissolved oxygen under basic conditions to produce H_2O_2. In these assays, the concentration of H_2O_2 was determined using a luminol CL method. However, because this method proceeded under basic conditions or using catalytic reagent, some disadvantages were noted, including nonspecific reactions caused by the generation of other reactive oxygen species. In this study, the conditions for a highly sensitive assay of H_2O_2 were studied using 10-methyl-9-(phenoxycarbonyl) acridinium fluorosulfonate (PMAC), which produces CL under neutral conditions. In addition, conditions for the measurment of β-gal activity using an indoxyl derivative substrate, as well as CL-EIA using β-gal, were studied.

Experimental

Materials

PMAC was purchased from Dojin Do Laboratories (Kumamoto, Japan). Hydrogen peroxide was obtained from Mitsubishi Gas Chemical (Tokyo, Japan). β-Gal was obtained from Roche Molecular Biochemicals (Indianapolis, IN, USA). 5-Bromo-4-chloro-3-indolyl-β-D-galactoside (X-gal) and hexadecyltrimethylammonium chloride were purchased from Wako Pure Chemical Industries, Ltd (Osaka Japan).

β-Gal-labeled anti-(thyroid-stimulating hormone) (TSH) antibody and 96-well plates coated with anti-TSH antibody were from Eiken Chemical Company (Tokyo, Japan). Other chemicals were of analytical reagent grade.

* Correspondence to: H. Arakawa, School of Pharmacy, Showa University, Shinagawa-ku, Tokyo 142–8555, Japan. Email: arakawa@pharm.showa-u.ac.jp

School of Pharmacy, Showa University, Shinagawa-ku, Tokyo142-8555, Japan

Copyright © 2013 John Wiley & Sons, Ltd.

Preparation and reagent

For the CL reagent (5×10^{-6} mol/L), 2 mg of PMAC was dissolved in 10 mL of 0.1 mol/L KCl, and kept at 4°C (5×10^{-4} mol/L), and diluted 100 times (5×10^{-6} mol/L) with 0.1 mol/L KCl just before use.

Preparation of 0.2 mmol/L X-gal solution. X-Gal (3.74 mg) was dissolved in 50 mL of 0.01 mol/L sodium phosphate buffer (pH 8.0) containing 0.5 mmol/L $MgCl_2$ and 0.1% bovine serum albumin (BSA; PB assay buffer) and stored at 4°C.

Procedure

Measurement for H_2O_2. A 20-μL aliquot of 0.1 mol/L sodium hydrogen carbonate, 20 μL of 5 mmol/L cationic surfactant and 50 μL of CL reagent were added sequentially to 100 μL of H_2O_2 solution. CL intensity was measured for 10 s after 15 s of mixing.

Measurement of β-gal. An 10-μL aliquot of β-gal diluted in PB assay buffer and 20 μL of 0.2 mmol/L X-gal were mixed, and incubated at 37°C for 1 h. Ninety microliters of 0.1 mol/L sodium bicarbonate, 20 μL of 5 mmol/L hexadecyltrimethylammonium chloride and 50 μL of CL reagent (5×10^{-6} mol/L PMAC in 0.1 mol/L KCl) were added sequentially to 30 μL of the reaction mixture. CL intensity was measured for 10 s after 15 s of mixing.

CL-EIA for TSH. Twenty microliters of serum and 100 μL of β-gal-labeled anti-TSH antibody solution were added successively to a microtiter plate immobilized with anti-TSH antibody, and left overnight at 25°C. After washing the plate three times with saline, 200 μL of 0.2 mol/L X-gal solution was added and incubated at 37°C. After 2 h, 50 μL of stop solution was added to the plate. The β-gal activity in reaction mixture was measured using the CL method described above.

Results and discussion

Measurement of H_2O_2 using the acridinium CL-EIA method

Fluorescence and CL methods have been developed for the measurment of H_2O_2, but most of these are carried out under strongly basic conditions (6) or using catalytic agents (7). In this report, we studied the usefulness of PMAC, a phenyl ester of acridinium esters, for the measurement of hydrogen peroxide. Unlike CL reactions such as luminol, PMAC reacts with H_2O_2 to produce strong CL in neutral conditions without the need for catalytic agents. Fig. 1 shows the principle of the CL reaction of PMAC. PMAC reacts with H_2O_2 to produce an excited state of *N*-methyl acridone via a dioxetane structure. This excited state of *N*-methyl acridone is thought to produce luminescence as it returns to the ground state (8).

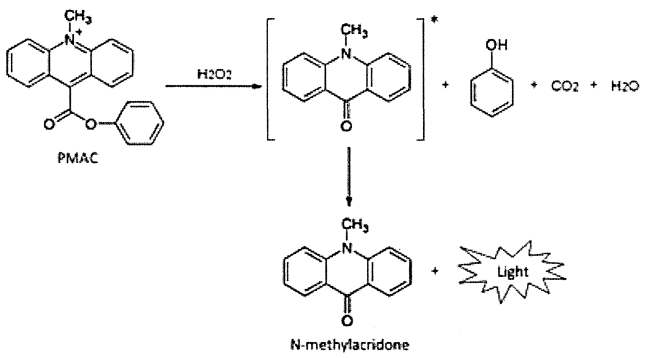


Figure 1. CL reaction of PMAC with H_2O_2.

To establish a highly sensitive and rapid determination of H_2O_2, the following conditions were studied: reaction pH, salt concentration, type and concentration of surfactant used as an enhancer, concentrations of PMAC and KCl, and time course of CL.

Effects of pH and sodium hydrogen carbonate solution on CL intensity. Sodium phosphate (pH 3–9) and sodium carbonate (pH 8.2–11) buffers were tested. The results showed that use of sodium phosphate buffer failed to produce adequate CL intensity. Sodium carbonate buffer is typically used for CL reactions with luminol. When sodium carbonate buffer was used, higher CL intensities were demostrated in the higher pH range of the buffer, but no significant differences in the signal-to-noise (S/N) ratios were found. Chen et al. reported that peroxycarboxylic salt, produced by reacting H_2O_2 and sodium hydrogen carbonate, exerts strong oxidative and sensitization effects for CL (9). Here, we also studied the effect of sodium hydrogen carbonate on CL intensities over a similar pH range. Higher S/N ratios were obtained using sodium hydrogen carbonate solution compared with sodium carbonate solution (data not shown).

Next, the effects of different concentrations (0.001–1 mol/L) of sodium hydrogen carbonate buffer (pH 8.2) were studied. The result indicated that the highest CL intensity and S/N ratio were obtained with 0.1 mol/L sodium hydrogen carbonate. This concentration was used in subsequent experiments.

Effect of surfactants. In measuring CL intensity, the addition of surfactants induces stronger emissions due to catalytic effects introduced by molecular assembly of the surfactants, similar to the enrichment effects of a reactive molecular ion or the confinement effects of excitation products. In this study, we tested the effects nine different surfactants: five cationic (cethyldimethylethylammonium bromide, tetradecyltrimethylammonium bromide, cetylpyridinium bromide, hexadecyltrimethylammonium chloride and triethylben zylammonium chloride); two anionic (sodium dodecyl sulfate and sodium *n*-dodecylbenzenesulfonate); and two non-ionic (Triton X-100 and Tween 20). The results showed slightly increased CL when using cationic surfactants, with two showing particularly strong CL. The addition of anionic surfactants resulted in lowered CL levels. Subsequent studies were carried out using hexadecyltrimethylammonium chloride (5 mmol/L) which gave the highest S/N ratio. It was thought that the cationic surface increased the efficiency of the reaction between PMAC and hydrogen peroxide, as seen in lucigenin chemiluminescence (10).

Effect of KCl concentration. The effects of different concentrations (0–1 mol/L) of KCl were analyzed. CL intensity was not affected by KCl concentrations and high blank values were demonstrated between 0 and 0.05 mol/L. No significant difference in S/N ratios was found in the test conditions. Subsequent studies were carried out with 0.1 mol/L KCl which showed a lower blank value.

Effect of PMAC concentration. The effect of PMAC concentrations (5×10^{-8}–5×10^{-4} mol/L) on CL intensity was studied. The results indicated higher CL intensities with higher PMAC concentrations. Subsequent studies were carried out with 5×10^{-6} mol/L of PMAC, which gave a high S/N ratio.

CL time course. The time course of CL intensities was studied between 10 s and 15 min after addition of the CL reagent. As

Copyright © 2013 John Wiley & Sons, Ltd.

LUMINESCENCE
The Journal of Biological and Chemical Luminescence

indicated in Fig. 2, strong CL appeared immediately after addition of the CL reagent and reached a maximum in 45 s, then declined gradually and remained stable for 15 min. In subsequent studies, to facilitate a more rapid assay, the reaction was measured and integrated between 15 and 25 s after addition of CL reagent.

Standard curve of H_2O_2 using the PMAC-CL method and reproducibility. The following results were obtained under optimized conditions for the H_2O_2 assay.

Fig. 3 shows the standard curve for H_2O_2 and indicates satisfactory linearity. The linear calibration range was 10^{-12}–10^{-9} mol/assay, with a limit of detection (LOD) of 10^{-12} mol/assay (blank ± 3 SD). The sensitivity of this PMAC-CL method was higher than that of isoluminol-m-POD (microperoxidase) (LOD, 10 pmol). The reproducibility of this method was studied in seven repeated experiments and the coefficient of variance (CV%) was examined at each point on the standard curve. The results indicated CV values between 2.2 and 7.5 % (mean, 5.5%).

A highly sensitive assay for β-gal using the PMAC-CL method and its application to CL-EIA

We applied the H_2O_2 assay using the PMAC-CL system to the measurement of β-gal activity with X-gal as the substrate and an EIA of TSH.

The principle CL assay for this β-gal system is the detection of H_2O_2 produced by hydrolysis of X-gal by β-gal with PMAC.

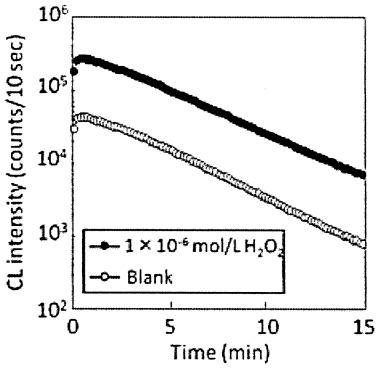


Figure 2. Time course of CL intensity of the reaction of PMAC and H_2O_2 in the presence (•) and abscence (○) of H_2O_2.

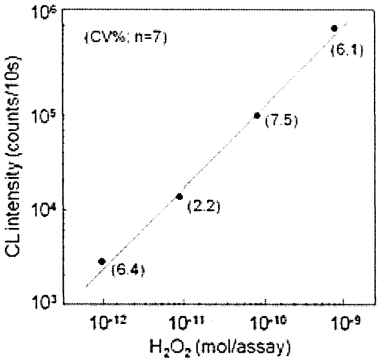


Figure 3. Standard curve of H_2O_2 and its coefficient of variation (CV%).

Optimal conditions for β-gal assay. To establish a highly sensitive measurement system for β-gal activity, reaction pH, salt concentration, substrate concentration and reaction time were studied. As a result, the following conditions were chosen: the assay buffer was 0.01 mol/L sodium phosphate buffer pH 8.0 containing 0.5 mmol/L $MgCl_2$ and 0.1% BSA, and the X-gal concentration was 0.2 mmol/L and the reaction time was 1 h to facilitate a more rapid performance of the immunoassay.

Standard curve and reproducibility of the β-gal assay. The measurable range of β-gal was 6.2×10^{-20}– 6.2×10^{-16} mol/assay, with a LOD of 6.2×10^{-20} mol/assay (blank ± 3 SD). This PMAC-CL method demonstrated higher sensitivity than previously reported CL detection methods using isoluminol-m-POD (11) or 3-(2'-spiroadamantane)-4-methoxy-4-(3''-β-D-galactopyranosyloxyphenyl)-1,2-dioxetane (12). The reproducibility of the reaction was studied and satisfactory CV values were obtained (8.1–10.6%, mean 9.6%, $n=7$). This CL method was subsequently applied to CL-EIA using β-gal as the labeling enzyme.

Measurement of TSH by CL-EIA using β-gal as the labeling enzyme

To confirm the usefulness of β-gal, a CL-EIA for TSH was developed. For this purpose, an anti-(human TSH) monoclonal antibody and β-gal-labeled anti-(human TSH) antibody conjugate were used as a solid-phase antibody and an enzyme-labeled antibody, respectively.

Standard curve of TSH in CL-EIA. Optimal conditions for the TSH immunoassay were studied and determined as described above.

Fig. 4(a) shows the standard curve for TSH obtained using this method. The measurement range for TSH was 0.02–100.0 μU/mL. The result showed a satisfactory level of sensitivity for measurement of clinical TSH concentrations. The reproducibility of the assay demonstrated a CV range of 3.1–9.0% with a mean of 5.7% ($n=6$).

Linearity of diluted samples. To determine serum TSH, the accuracy of this assay was evaluated by studying the linearity of measured TSH in diluted serum. Three different human serum samples (A, B and C) were analyzed at 1:1, 1:2, 1:4, 1:8 and 1:16 dilutions with phosphate-buffered saline (PBS) containing 0.1% BSA. The results showed linearity from near the origin for all serum samples, indicating that this assay method is applicable to determination of human serum TSH with a satisfactory level of accuracy. Dilution curves are shown in Fig. 4(b).

Correlation between the proposed method and another conventional method. TSH levels in human sera were analyzed using the proposed method and compared with those determined using another conventional method. A CL-EIA kit (Abbott Diagnostic Division) using acridinium ester-labeled anti-TSH antibody was used as the conventional method.

As shown in Fig. 5, 90 human serum samples were tested. Comparitive analysis demonstrated a correlation coefficient of 0.946 (regression formula: $y=0.903x+1.136$) and correlation of TSH low-levels < 10 μU/mL showed inside of Fig. 5, indicating that this assay is applicable as a routine assay in clinical practice.

Copyright © 2013 John Wiley & Sons, Ltd.

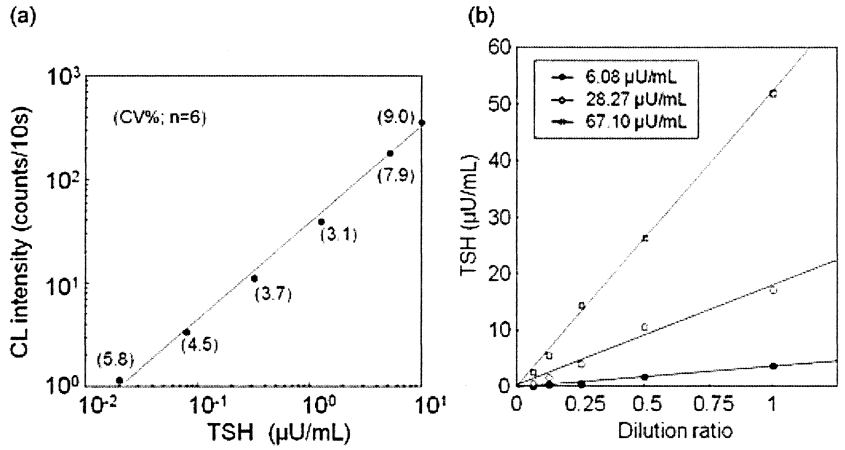


Figure 4. Standard curve of TSH and its coefficient of variation (CV%) (a) and dilution curves of human serum samples (b).

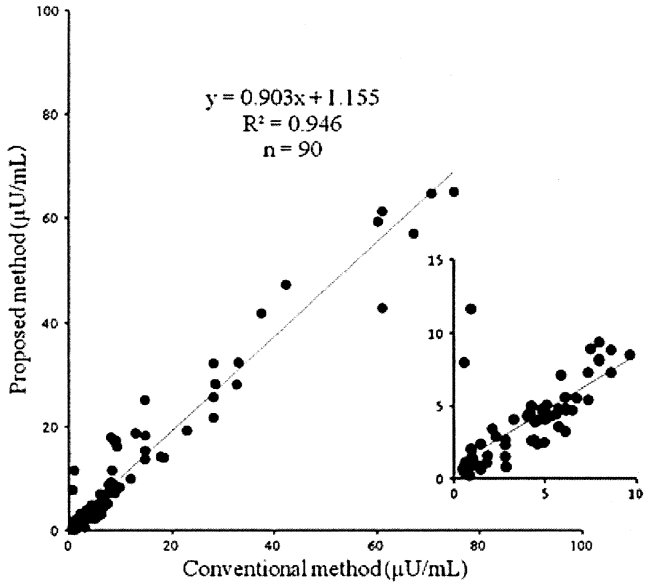


Figure 5. Correlation of serum TSH levels between the proposed method and the conventional method: CL-EIA using acridinium ester-labeled antibody.

Conclusion

In this study, we developed a CL assay of H_2O_2 using PMAC as a luminescence probe. This assay system was used to determine β-gal activity.

The LODs of H_2O_2 and β-gal were 10^{-12} and 10^{-20} mol/assay, respectively. This method was applied to an EIA for TSH. The developed CL-EIA was highly sensitive and could also be applied to the analysis of clinical specimens.

References

1. Arakawa H, Masuda K, Tajima N, Maeda M. Chemiluminescence assay for tetrahydrobiopterin based on the generation of hydrogen peroxide using isolumino/microperoxidase in the presence of 1-methoxy PMS. Luminescence 2007;22:245–50.
2. Arakawa H, Maeda M, Tsuji A. Chemiluminescence enzyme immunoassay of cortisol using peroxidase as label. Anal Bichem 1979;97:248–54.
3. Kricka LJ. Clinical applications of chemiluminescence. Anal Chim Acta 2003;500:279–86.
4. Arakawa H, Maeda M, Tsuji A. Chemiluminescent assay of various enzymes using indoxyl derivatives as substrate and its applications to enzyme immunoassay and DNA probe assay. Anal Biochem 1991;199:238–42.
5. Arakawa H, Kanemitu M, Maeda M. Chemiluminescent assay for catecholamines by the generation of hydrogen peroxide on basic solution and the use of isoluminol–microperoxidase. Anal Sci 1999;15:1269–72.
6. Zaitsu K, Ohkura Y. New fluorogenic substrates for horseradish peroxidase: rapid and sensitive assays for hydrogen peroxide and the peroxidase. Anal Biochem 1980;109:109–13.
7. Maeda M, Arakawa H, Tsuji A. Chemiluminescent assay of various enzyme activities and its application to enzyme immunoassays. J Biolumin Chemilumin 1989;4:140–8.
8. McCapra F. Chemical mechanisms in bioluminescence. Acc Chem Res 1976:9:201–8.
9. Chen H, Lin L, Lin Z, Guo G, Lin J. Chemiluminescence arising from the decomposition of peroxymonocarbonate and enhanced by CdTe quantum dots. J Phys Chem A 2010;114:10049–58.
10. Kamidate T, Yoshida K, Kaneyasu T, Segawa T, Watanabe H. Micelle-enhanced lucigenin chemiluminecence for the determination of catecholamines. Anal Sci 1990;6:645–9.
11. Arakawa H, Ikegami T, Maeda M, Tsuji A. Chemiluminescent enzyme immunoassay for alpha-fetoprotein using β-D-galactosidase as label and 5-bromo- 4-chloro-3-indolyl-β-D-galactopyranoside as substrate. J Biolumin Chemilumin 1993;8:135–9.
12. Bronstein I, Edwards B, Voyta JC. 1,2-Dioxetanes: novel chemiluminescent enzyme substrates applications to immunoassay. J Biolumin Chemilumin 1989;4:99–11.

Copyright © 2013 John Wiley & Sons, Ltd.

An Innovative LC-MS/MS-Based Method for Determining CYP 17 and CYP 19 Activity in the Adipose Tissue of Pre- and Postmenopausal and Ovariectomized Women Using ^{13}C-Labeled Steroid Substrates

Toshihiko Kinoshita, Seijiro Honma, Yasuhiro Shibata, Kouwa Yamashita, Yoko Watanabe, Hitoe Maekubo, Mitsunobu Okuyama, Akiko Takashima, and Naoki Takeshita

Department of Obstetrics and Gynecology (T.K., A.T., N.T.), Toho University Medical Center Sakura Hospital, Chiba 285-8741, Japan; Department of Analytical Research (S.H., Y.W., H.M., M.O.), ASKA Pharma Medical Co Ltd, Kawasaki 213-8522, Japan; Department of Urology (Y.S.), Gunma University Graduate School of Medicine, Maebashi 371-8511, Japan; and Department of Clinical Analysis (K.Y.), Tohoku Pharmaceutical University, Sendai 981-8558, Japan

Context: Does adipose tissue produce steroid hormones like an endocrine organ?

Object: To clarify whether adipose tissue produces sex steroid hormone like an endocrine organ, we estimated several key steroid hormone levels, as well as CYP17 and CYP19 activity, in ovariectomized, pre- and postmenopausal women by liquid chromatography-tandem mass spectrometry (LC-MS/MS).

Subjects and Methods: The subjects were 19 premenopausal (n = 12), postmenopausal (n = 4), and ovariectomized women (n = 3) aged 27–68 years. Serum, visceral adipose and sc adipose samples were taken from these subjects and stored at −70°C. The levels of cortisol, cortisone, progesterone (Prog), androstenedione, dehydroepiandrosterone, estrone, estradiol (E2), and T in serum and adipose tissue were estimated simultaneously by LC-MS/MS. CYP17 and CYP19 activity in tissues were assayed with the use of ^{13}C-labeled steroid precursors and LC-MS/MS-based estimation of the metabolites.

Results: E2 and Prog levels in the sera of postmenopausal or ovariectomized women were less than 10% of those in premenopausal women. No marked variations were seen in other hormones. Estrone, androstenedione, dehydroepiandrosterone, and Prog levels in the visceral and sc tissues of postmenopausal and ovariectomized women were 9–60 times higher than those in serum, whereas E2 and T levels were 3- to 7-fold higher than those in serum, and cortisol and cortisone levels were 20% of those found for serum. CYP17 in adipose tissue was found to have 17-hydroxylase and 20,17-lyase activity, with each catalytic activity being essentially equal. Therefore, CYP17 in adipose tissue is of the testicular/ovarian type but not adrenal type, which has 17-hydroxylase activity dominant. The presence of CYP19 activity in adipose tissue was approximately 3% of CYP17.

Conclusion: Our findings suggest that adipose tissue acts as an endocrine organ, with CYP17 and CYP19 activity playing an essential role in sex steroid hormone biosynthesis. ***(J Clin Endocrinol Metab* 99: 1339–1347, 2014)**

Abbreviations: A-dione, androstenedione; $^{13}C_3$-A-Dione, androstenedione-2,3,4-$^{13}C_3$; $^{13}C_3$-DHT, dihydrotestosterone-2,3,4-$^{13}C_3$; $^{13}C_3$-E2, estradiol-2,3,4-$^{13}C_3$; $^{13}C_3$-E1, estrone-2,3,4-$^{13}C_3$; $^{13}C_4$-estradiol, estradiol-1,2,3,4-$^{13}C_4$; $^{13}C_4$-estrone, estrone-1,2,3,4-$^{13}C_4$; $^{13}C_3$-17-OH-Prog, 17-hydroxyprogesterone-2,3,4-$^{13}C_3$; Cortisol-d4, cortisol-9,11,12,12-$^2H_4$; $^{13}C_3$-Prog, progesterone-2,3,4-$^{13}C_3$; $^{13}C_3$-T, testosterone-2,3,4-$^{13}C_3$; DHEA, dehydroepiandrosterone; DHT, dihydrotestosterone; DMSO, dimethylsulfoxide; E1, estrone; E2, estradiol; E1-PFB-HP, estrone-3-PFB-17-hydrazinopyridinium; E2-PFB-PY, E2–3-PFB-17-pyridinium; HP, hydrazino-2-methylpyridine; IS, Internal standard; LC-MS/MS, liquid chromatography-tandem mass spectrometry; LOQ, limit of quantification; NADPH, nicotinamide adenine dinucleotide phosphate reduced; PI, picolinoyl ester; Prog, progesterone.

ISSN Print 0021-972X ISSN Online 1945-7197
Printed in U.S.A.
Copyright © 2014 by the Endocrine Society
Received October 8, 2013. Accepted January 21, 2014.
First Published Online January 23, 2014

The Endocrine Society. Downloaded from press.endocrine.org by [${individualUser.displayName}] on 15 April 2015. at 01:03 For personal use only. No other uses without permission. . All rights reserved.

It has been reported that although serum estradiol (E2) falls considerably after menopause, the incidence of hormone-dependent breast and endometrial cancers is high and the serum E2 levels of patients with these diseases are higher than those in healthy persons (1–3). Moreover, it has been reported that the prevalence of osteoporosis in people with high body fat levels after menopause is low, whereas that of cardiovascular-related diseases, breast cancer, or endometrial cancer is high. These findings suggest that estrogen may be produced in adipose tissue and therefore influence the onset of these diseases (4). The gene expression and enzyme activities of CYP19, which produces estrogen in the ovary and adipose tissue, have been widely studied (5–7).

A number of groups have already demonstrated that steroid hormones such as androgen, estrogen, and corticoid are taken up by visceral and sc adipose tissues and that some androgen is converted into estrogen therein by an intracrine mechanism (8, 9). In addition to CYP19, gene expression and enzyme activities such as CYP11A, 3β-hydroxysteroid dehydrogenase, 17β-hydroxysteroid dehydrogenase, 5α-reductase, sulfatase, and steroidogenic acute regulatory protein, which participate in steroid biosynthesis and metabolic processes, are also detected in adipose tissue. As such, adipose tissue has recently come to be thought of as an endocrine organ (9–15). However, consensus has not been reached as to whether CYP17 is present in adipose tissue, which is essential for sex steroid production (11). One of the reasons for this is that a reliable analytical method for evaluation of steroid biosynthesis in adipose tissues is still lacking. Steroid assays have recently been reexamined using liquid chromatography-tandem mass spectrometry (LC-MS/MS) instead of conventional RIA (2, 15).

The main goal of our study was to exactly determine the levels of steroid hormones simultaneously in the sera and visceral and sc adipose tissue of ovariectomized women using a LC-MS/MS analytical technique to clarify any differences between ovariectomized and menopausal women and thereby determine whether CYP17 is an essential enzyme for sex steroid hormone biosynthesis in adipose tissue. Thus, we have developed a new in vitro tracer method that enables us to measure CYP17 and CYP19 activities by combining the tissue culture in the presence of a ^{13}C-labeled steroid precursor with the LC-MS/MS technique to detect ^{13}C-labeled metabolites.

Materials and Methods

Subjects and samples

The subjects were 19 women aged 27–68 years who had undergone abdominal operations for gynecopathy in the Obstetrics and Gynecology Department at Toho University Medical Center Sakura Hospital. This study was approved by the Toho University Medical Center Sakura Hospital Ethics Committee. Informed consent was obtained from each subject prior to their operation. Patients were not administered hormone-based drugs beforehand. Subjects were categorized as premenopausal (n = 12; n = 5 follicular phase, n = 7 luteal phase), postmenopausal (n = 4), or ovariectomized (n = 3). The average age and body mass index of the premenopausal women were 40.2 ± 6.9 years (range 27–48) and 25.9 ± 4.9 kg/m^2, respectively, those of the postmenopausal women 59.0 ± 7.5 years (range 51–68) and 24.4 ± 4.6 kg/m^2, respectively, and those of the ovariectomized women 37.3 ± 6.1 years (range 34–44) and 23.1 ± 5.2 kg/m^2, respectively. All operations were performed under general anesthesia, and sc adipose (1 g) and visceral adipose tissue (1 g) samples were collected from the hypogastric incision region and peripheral caul tissues, respectively. Blood was collected at the same time to provide 1 mL of serum. All tissue and serum samples were frozen and stored at −70°C until analysis.

Materials and reagents

Estrone (E1), E2, cortisol, dehydroepiandrosterone (DHEA), androstenedione (A-dione), T, progesterone (Prog), and dihydrotestosterone (DHT) were purchased from Aldrich and Steroids. Progesterone-2,3,4-$^{13}C_3$ ($^{13}C_3$-Prog), estrone-1,2,3,4-$^{13}C_4$ ($^{13}C_4$-estrone), and estradiol-1,2,3,4-$^{13}C_4$ ($^{13}C_4$-estradiol) were purchased from Hayashi Junsei Chemical Co, Ltd, and androstenedione-2,3,4-$^{13}C_3$ ($^{13}C_3$-A-Dione), estrone-2,3,4-$^{13}C_3$ ($^{13}C_3$-E1), estradiol-2,3,4-$^{13}C_3$ ($^{13}C_3$-E2), testosterone-2,3,4-$^{13}C_3$ ($^{13}C_3$-T), and dihydrotestosterone-2,3,4-$^{13}C_3$ ($^{13}C_3$-DHT) were purchased from Isoscience. 17-Hydroxyprogesterone-2,3,4-$^{13}C_3$ ($^{13}C_3$-17-OH-Prog) was synthesized from $^{13}C_3$-Prog (16). DHEA-4,5,6-$^2H_3$, cortisol-9,11,12,12-$^2H_4$ (Cortisol-d4), testosterone-16,16,17-$^2H_3$, and dihydrotestosterone-16,16,17-$^2H_3$ were purchased from C/D/N Isotopes. InertSep SI (60 mg, 3 mL), Bond Elut C18 (30 mg, 3 mL business), and Oasis MAX (60 mg, 3 mL) were purchased from GL Science, Varian, and Waters, respectively. 4-Dimethylaminopyridine, 2-methyl-6-nitrobenzoic anhydride, picolinic acid, pentafluorobenzylbromide, and 2-fluoro-1-methylpyridinium p-toluenesulfonate were purchased from Tokyo Chemical Industry Co, Ltd. 6-Methylestrone and 6-methylestradiol were provided by Professor Numazawa (Tohoku Pharmaceutical College, Sendai, Japan). Chlormadinone was obtained from ASKA Pharmaceutical Co, Ltd.

Liquid chromatography-tandem mass spectrometry

An API-4000 instrument (Applied Biosystems Inc) was used for LC-MS/MS, and measurements were performed in positive-ion mode with a Cadenza CD-C18 (3 × 250 mm, 3.5 μm; Waters) or Xterra MS-C18 column (100 mm × 2.1 mm, 3.5 μm; Waters). Measurements were performed with 1% formic acid and a methanol/acetonitrile mixture as mobile phase, with different gradients, and a flow rate of 0.4 mL/min. The tandem mass spectrometry conditions were as follows: declustering potential: 100 V; spray voltage: 5500 V; collision energy: 40 eV; nitrogen curtain gas: 12 cpi (gas pressure): ion source temperature: 550°C.

Hormone measurement in adipose tissue

Previously weighed adipose tissue samples were cut with scissors and homogenized in water (10 mL/g) using an Ultra-Turrax homogenizer (IKA) with cooling. Internal standards (ISs) were added to the homogenate, which was then extracted with EtOAc (3 vol) and the solvent evaporated on a rotary evaporator at 40°C. The

The Endocrine Society. Downloaded from press.endocrine.org by [${individualUser.displayNa...], ...pril 2015. at 01:03 For personal use only. No other uses without permission. . All rights reserved.

extract was then analyzed using the salivary hormone analysis method described by Kido et al (17). The estrogen fraction obtained was converted to its pentafluorobenzyl ether with pentafluorobenzylbromide reagent using the method of Arai et al (18). The product was dissolved in 15% EtOAc/hexane (1 mL) and applied to an InertSept IS cartridge column for separation into E1–3-PFB and E2–3-PFB fractions with 15%–50% EtOAc/hexane (3.5 mL). E2–3-PFB was further derivatized to E2–3-PFB-17-pyridinium (E2-PFB-PY) using the method of Arai et al. Five percent 2-methylpyridinehydrazine reagent was added to the E1 derivative fraction and left at room temperature for 1 hour, as described by Higashi (19), to obtain estrone-3-PFB-17-hydrazinopyridinium (E1-PFB-HP). The reaction mixture was applied to an InterSept IS cartridge and eluted with 15% EtOAc/hexane (4 mL). The E1 and E2 derivative fractions were combined and analyzed by LC-MS/MS. The following ions (mass to charge ratio) were detected: E1-PFB-hydrazino-2-methylpyridine (HP): 556.3/375.3; $^{13}C_4$-E1-PFB-HP: 560.3/379.3; E2–3-PFB-17-PY: 544.2/339.0; $^{13}C_4$-E2–3-PFB-17-PY: 548.2/343.2; cortisol: 363.3/121.2; cortisone: 361.2/121.2; Prog: 315.3/97.2; DHEA-picolinoyl ester (PI): 394.3/175.1; T-PI: 394.3/150.2; DHT-PI: 396.4/121.2; A-dione: 287.2/109; cortisol-d4: 367.3/121.2; $^{13}C_3$-Prog: 318/100.2; T-PI-d3: 397.3/150.2; A-Dione-1,2,4,6,7,16,16-$^2H_4$: 294.2/113; DHEA 3-picolinoyl ester-2,2,4,6-$^2H_4$: 398.1/179.4. Validation of serum analysis was conducted with 0.2 mL of hormone-free serum. From testing for within-run reproducibility (n = 5) and between-run reproducibility (n = 5, 3 d) the lower limit of quantification (LOQ) was within 20%, and the LOQ for concentration higher than that were determined from tests in which it was set to within 15%, as follows: cortisol, cortisone: 150 pg/mL; Prog: 10 pg/mL; DHEA: 10 pg/mL; T: 5 pg/mL; A-dione: 10 pg/mL; E1: 2.5 pg/mL; E2: 2.5 pg/mL. Validation of adipose tissue analysis was conducted with 100 mg of tissue. Estimation was the same as for serum: cortisol, cortisone: 300 pg/g; Prog: 20 pg/g; DHEA: 20pg/g; T: 10 pg/g; A-dione: 20 pg/g; and E1: 5 pg/g; E2: 5 pg/g.

Measurement of CYP17 and CYP19 activity in adipose tissue

CYP17 activity

Tissue samples were homogenized for 1 minute in an Ultra-Turrax homogenizer (IKA) in an ice bath, after which 0.1 M Tris buffer (pH 7.6, 1 g/mL) was added. The resulting mixture was homogenized using a Teflon-glass homogenizer. The supernatant was obtained from the homogenate by refrigerated centrifugation (1000 rpm × 2 min, 4°C). Nicotinamide adenine dinucleotide phosphate reduced (NADPH; 2 mg per 50 μL) and $^{13}C_3$-Prog [500 ng per 25 μL, dimethylsulfoxide (DMSO) solution] were added to the supernatant (200 μL) in a test tube and the mixture adjusted to 0.5 mL with buffer and then incubated at 37°C for various times. After the reaction, DHEA-2,2,4,6-$^2H_4$ (1 ng) and chlormadinone (1 ng) were added as ISs and the mixture extracted with EtOAc (5 mL). The extract was dissolved in 20% methanol (1 mL) and applied to a Bound Elut C18 cartridge (Varian). After washing successively with water (1 mL) and 30% acetonitrile/water (3 mL), the steroid fraction was eluted with 80% acetonitrile/water (3 mL). Part of the steroid fraction was analyzed by LC-MS/MS to estimate nonderivatized steroids. The remainder was treated with picolinoyl reagents and T and DHT analyzed and estimated using the method described by Kido et al (17).

The following ions were measured (mass to charge ratio): $^{13}C_3$-17-OH-Prog: 334.2/111.8; $^{13}C_3$-A-Dione: 290.2/112.0; $^{13}C_3$-T-PI: 397.3/256.3; $^{13}C_3$-DHT-PI: 399.4/206.1; DHEA-PI-d4: 398.1/179.4; and chlormadinone; 398.1/179.4. Enzyme activity was provided as picomoles per hour per milligram wet tissue. The LOQ was 40 picograms per gram for $^{13}C_3$-17-OHProg, 40 pg/g for $^{13}C_3$-A-Dione, 20 pg/g for $^{13}C_3$-T, and 20 pg/g for $^{13}C_3$-DHT.

CYP19 activity

The supernatant (100 μL) and NADPH (2 mg) were added to a test tube containing $^{13}C_3$-A-Dione (250 ng per 50 μL, DMSO solution) and the mixture adjusted to 0.5 mL with buffer and then incubated at 37°C for various times. After the reaction, 6-methylestrone (100 pg) and 6-methylestradiol (100 pg) were added as ISs and the mixture extracted with EtOAc (5 mL). The extract dissolved in 20% methanol was applied to a Bound Elut C18 cartridge (Varian). After washing with water (1 mL) and 30% acetonitrile/water (3 mL), estrogen was eluted with 80% acetonitrile/water (3 mL). The extract obtained was used in an analytical procedure to determine the phenol fraction of salivary hormone as described by Kido et al (17). The E1 and E2 fractions were then combined and analyzed by LC-MS/MS.

The following ions were measured (mass to charge ratio): $^{13}C_3$-E1–3-PFB-17-HP: 560.3/379.3; $^{13}C_3$-E2–3-PFB-17-PY: 548.2/343.2; 6-methylestrone-3-PFB-17-HP: 570.24/389.4; and 6-methylestradiol-PFB-17-PY: 558.3/353.1. Enzyme activity was provided as picomoles per hour per milligram wet tissue. The LOQs were 10 pg/g for $^{13}C_3$-E1 and $^{13}C_3$-E2, respectively.

Comparison of CYP19 activity obtained by radiometry and LC-MS/MS

Tris buffer (0.10 M; pH 7.6, 50.5 mL) was added to rat ovary (50.5 mg) and homogenized with a Teflon homogenizer. The resulting homogenate was diluted to three concentrations (10, 1, and 0.1 mg/mL). NADPH (2 mg) and $^{13}C_3$-A-dione (250 ng/25 μL, DMSO solution) or 1β-^{3}H-A-dione (1.0 μCi) were added as substrate to each homogenate (400 μL) and adjusted to 0.5 mL with buffer. The reaction mixture was incubated for 120 minutes at 37°C, and then the specimen was analyzed by LC-MS/MS in the same manner as above after addition of an IS. In the case of 1β-^{3}H-A-dione as substrate, the activity was determined by method the incorporation of tritium from the substrate into water as described by Simpson et al (6).

Statistical analysis

Data are indicated as mean ± SD. Spearman rank correlation coefficients were calculated. Statistical comparisons of the mean differences between two groups were performed using a Mann-Whitney *U* test. The significance level was set to $P < .05$. All data were analyzed using Dr. SPSS software version 11.0. (SPSS, Inc).

Results

Hormone levels in serum

Table 1 shows the mean levels of serum steroid hormones for pre- and postmenopausal and ovariectomized women. The serum E2 and Prog levels in postmenopausal and ovariectomized women were less than 7 and 40 pg/mL, respectively, thus indicating a significant decrease ($P < .001$) with respect to the values found for premenopausal women. Although DHEA and A-dione levels de-

The Endocrine Society. Downloaded from press.endocrine.org by [${individualUser.displayN...} ...April 2015. at 01:03 For personal use only. No other uses without permission. . All rights reserved.

Table 1. The Hormone Levels in Serum and Adipose Tissues of Premenopausal, Postmenopausal, and Ovariectomized Women

State	Compounds	Units	Serum	Visceral		Subcutaneous	
Premenopausal (n = 12)	Cortisol	ng/mL, g	82.00 ± 30.45	17.31 ± 19.45	(0.20)	12.56 ± 13.45	(0.15)
	Cortisone	ng/mL, g	22.06 ± 4.44	4.15 ± 4.04	(0.19)	3.49 ± 3.40	(0.16)
	DHEA	ng/mL, g	4.09 ± 2.85	30.53 ± 21.40	(7.46)	33.41 ± 40.02	(8.16)
	T	ng/mL, g	0.17 ± 0.10	0.22 ± 0.15	(1.26)	0.18 ± 0.15	(1.03)
	Prog	ng/mL, g	5.77 ± 5.30	110.91 ± 116.37	(19.2)	66.19 ± 71.31	(11.4)
	A-dione	ng/mL, g	1.06 ± 0.72	10.81 ± 8.54	(10.1)	5.47 ± 3.53	(5.14)
	E1	pg/mL, g	39.54 ± 27.54	572.13 ± 452.91	(14.4)	402.15 ± 317.43	(10.1)
	E2	pg/mL, g	70.49 ± 59.11	109.57 ± 130.62	(1.55)	103.16 ± 102.87	(1.46)
Postmenopausal (n = 4)	Cortisol	ng/mL, g	110.20 ± 55.30	12.35 ± 13.81	(0.11)	14.14 ± 20.04	(0.13)
	Cortisone	ng/mL, g	23.03 ± 9.86	3.31 ± 2.72	(0.14)	2.27 ± 1.93	(0.10)
	DHEA	ng/mL, g	1.64 ± 0.25	18.95 ± 16.37	(11.5)	16.63 ± 13.06	(10.1)
	T	ng/mL, g	0.15 ± 0.09	0.16 ± 0.12	(1.04)	0.17 ± 0.15	(1.15)
	Prog	ng/mL, g	0.04 ± 0.02	0.71 ± 0.24	(18.7)	0.52 ± 0.14	(13.7)
	A-dione	ng/mL, g	0.40 ± 0.31	5.82 ± 4.86	(14.4)	4.48 ± 2.77	(11.1)
	E1	pg/mL, g	30.00 ± 25.00	429.00 ± 487.00	(14.1)	260.00 ± 231.00	(8.61)
	E2	pg/mL, g	7.00 ± 5.00	30.00 ± 28.00	(4.29)	23.00 ± 13.00	(3.32)
Ovariectomized (n = 3)	Cortisol	ng/mL, g	61.06 ± 35.52	10.34 ± 10.14	(0.17)	4.15 ± 1.72	(0.07)
	Cortisone	ng/mL, g	16.31 ± 8.49	3.78 ± 1.15	(0.23)	1.46 ± 0.93	(0.09)
	DHEA	ng/mL, g	1.95 ± 1.08	34.00 ± 8.34	(17.4)	33.65 ± 26.01	(17.2)
	T	ng/mL, g	0.12 ± 0.09	0.28 ± 0.24	(2.35)	0.37 ± 0.27	(3.16)
	Prog	ng/mL, g	0.04 ± 0.00	2.24 ± 1.28	(61.5)	2.17 ± 2.72	(59.7)
	A-dione	ng/mL, g	0.35 ± 0.10	8.32 ± 6.29	(23.8)	5.93 ± 5.76	(16.9)
	E1	pg/mL, g	16.00 ± 12.00	292.00 ± 123.00	(17.7)	259.00 ± 94.00	(15.7)
	E2	pg/mL, g	5.00 ± 4.00	26.00 ± 21.00	(5.27)	36.00 ± 30.00	(7.24)

Values in parentheses are the mean hormone levels in tissue/mean plasma levels.

creased slightly with aging, no variation was observed for E1, T, cortisol, or cortisone in either group. Moreover, no correlation was found between the serum hormone levels and body mass index found for premenopausal women.

Hormone levels in adipose tissue

Table 1 also shows the mean hormone levels in adipose tissue. No significant difference between visceral and sc adipose tissue was found for any of the eight hormones studied. However, E2 concentrations in the adipose tissue of premenopausal women were significantly higher than those in postmenopausal and ovariectomized women ($P < .01$). The DHEA, A-dione, Prog, and E1 levels in adipose tissue for pre- and postmenopausal and ovariectomized women were significantly higher (9–60 times) than those in serum ($P < .001$). Tissue to serum ratios for E2 were 5.3–7.2 for the ovariectomized group, 3.0–4.3 for the postmenopausal group, and 1.5–1.6 for the premenopausal group; therefore, the involvement of adipose tissue in the ovariectomized group is large. On the other hand, ratios for T for each group were 2.4–3.2, 1.0–1.2, and 1.0–1.3, respectively, and the effect of adipose is considerably low. In contrast, cortisol and cortisone levels in adipose tissue were significantly lower (<20%) than the values found in serum. The correlation

Table 2. The Correlation Coefficients Between Hormone Levels of Serum and Adipose Tissue

	Group 1 (n = 19) Adipose Tissue				Group 2 (n = 12) Adipose Tissue				Group 3 (n = 7) Adipose Tissue			
	Visceral		Subcutaneous		Visceral		Subcutaneous		Visceral		Subcutaneous	
Steroids	r	*P* Value	r	*P* Value	r	*P* Value	r	*P* Value	r	*P* Value	r	*P* Value
Cortisol	0.382	.106	0.425	.070	0.287	.366	0.385	.217	0.429	.337	0.536	.215
Cortisone	0.529	.035	0.034	.200	0.539	.108	0.358	.310	0.771	.072	0.371	.468
DHEA	0.438	.079	0.343	.177	0.616	.033	0.322	.307	0.300	.624	0.300	.624
T	0.651	.003	0.456	.050	0.437	.155	0.462	.131	0.685	.090	0.613	.144
Prog	0.830	.001	0.866	.001	0.881	.004	0.833	.010	0.667	.219	0.103	.870
A-dione	0.475	.040	0.357	.133	0.147	.649	0.161	.618	0.821	.023	0.750	.052
E1	0.659	.002	0.792	.001	0.545	.067	0.769	.003	0.750	.050	0.750	.050
E2	0.730	.001	0.638	.004	0.730	.007	0.665	.026	0.873	.010	0.829	.021

Group 1 was premenopausal, postmenopausal, and ovariectomized women. Group 2 was premenopausal women. Group 3 was postmenopausal women and ovariectomized women.

The Endocrine Society. Downloaded from press.endocrine.org by [${individualUser.displayNa...] on 07 April 2015. at 01:03 For personal use only. No other uses without permission. . All rights reserved.

between serum and adipose tissue levels for all eight hormones studied is shown in Table 2, which shows that the serum E2 levels for postmenopausal and ovariectomized women ($< r = 0.80$) are strongly correlated with those for adipose tissue. Cortisol, cortisone, and DHEA do not show such a correlation.

Method for measuring CYP17 activity

To demonstrate the presence of CYP17 in human adipose tissue, we used this method on rat testicular tissue, for which the existence of CYP17 is already known, to serve as a positive control group. We examined by tandem mass spectrometry the ^{13}C products biosynthesized in both tissues using ^{13}C-labeled compounds. Figure 1 shows the results of the enzymatic reaction when changing the amount of substrate and tissue. The main products in adipose tissue were 17-OH-Prog and A-Dione, with T and DHT levels being less than 1% of that for A-Dione. A similar result was obtained for rat testis. These in vitro tests clearly indicate both 17-hydroxylase and 17,20-lyase activities in adipose tissue.

Method for measuring CYP19 activity

To demonstrate the presence of CYP19 in human adipose tissue, we used this method on rat ovarian tissue, for

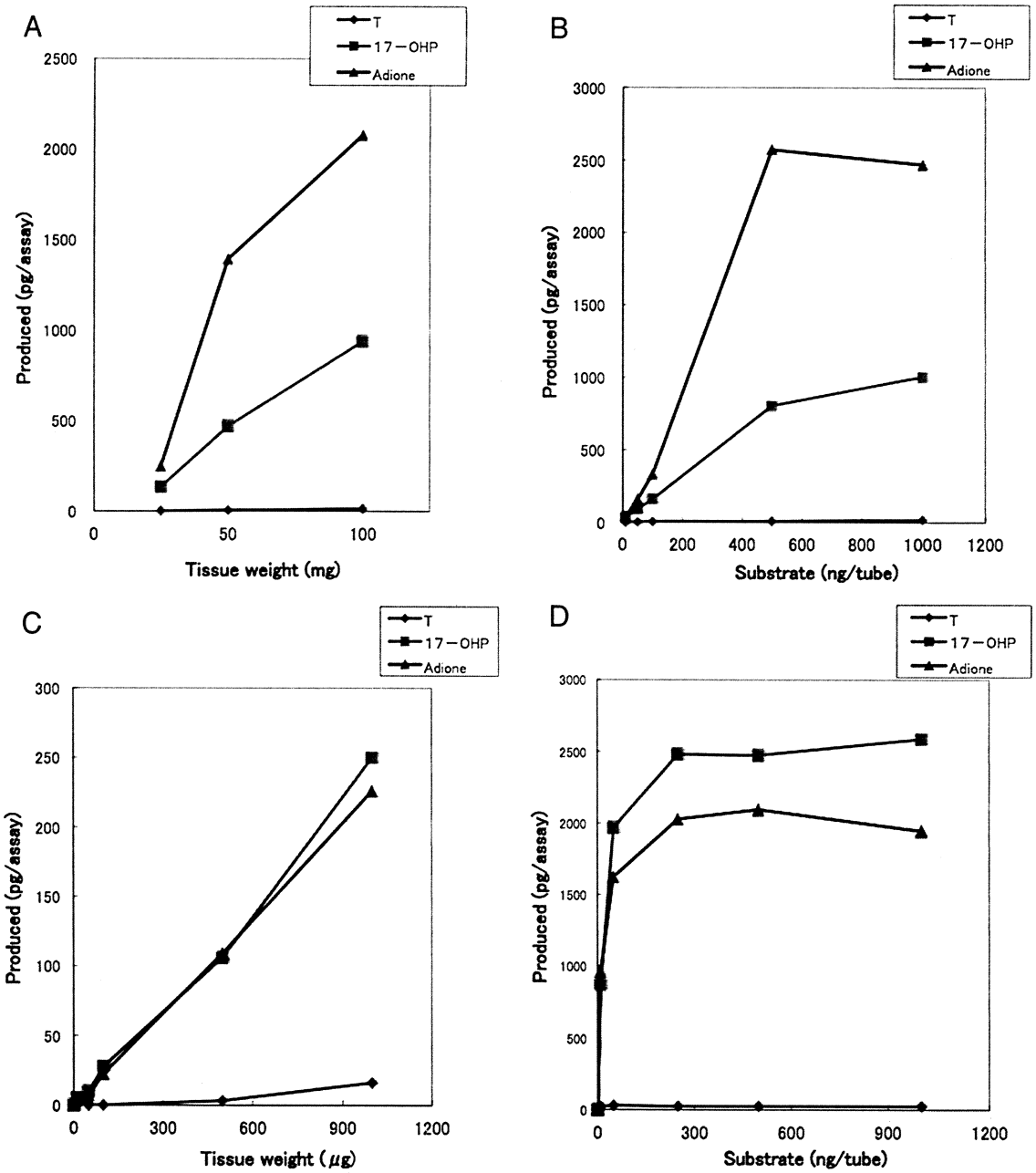


Figure 1. Formation of ^{13}C-17-OH-Prog and ^{13}C-A-Dione from ^{13}C-Prog by CYP17 in human sc and rat testicular tissue. A and B, Subcutaneous adipose tissue. C and D, Rat testis.

The Endocrine Society. Downloaded from press.endocrine.org by [${individualUser.displayN... 119 ...April 2015. at 01:03 For personal use only. No other uses without permission. . All rights reserved.

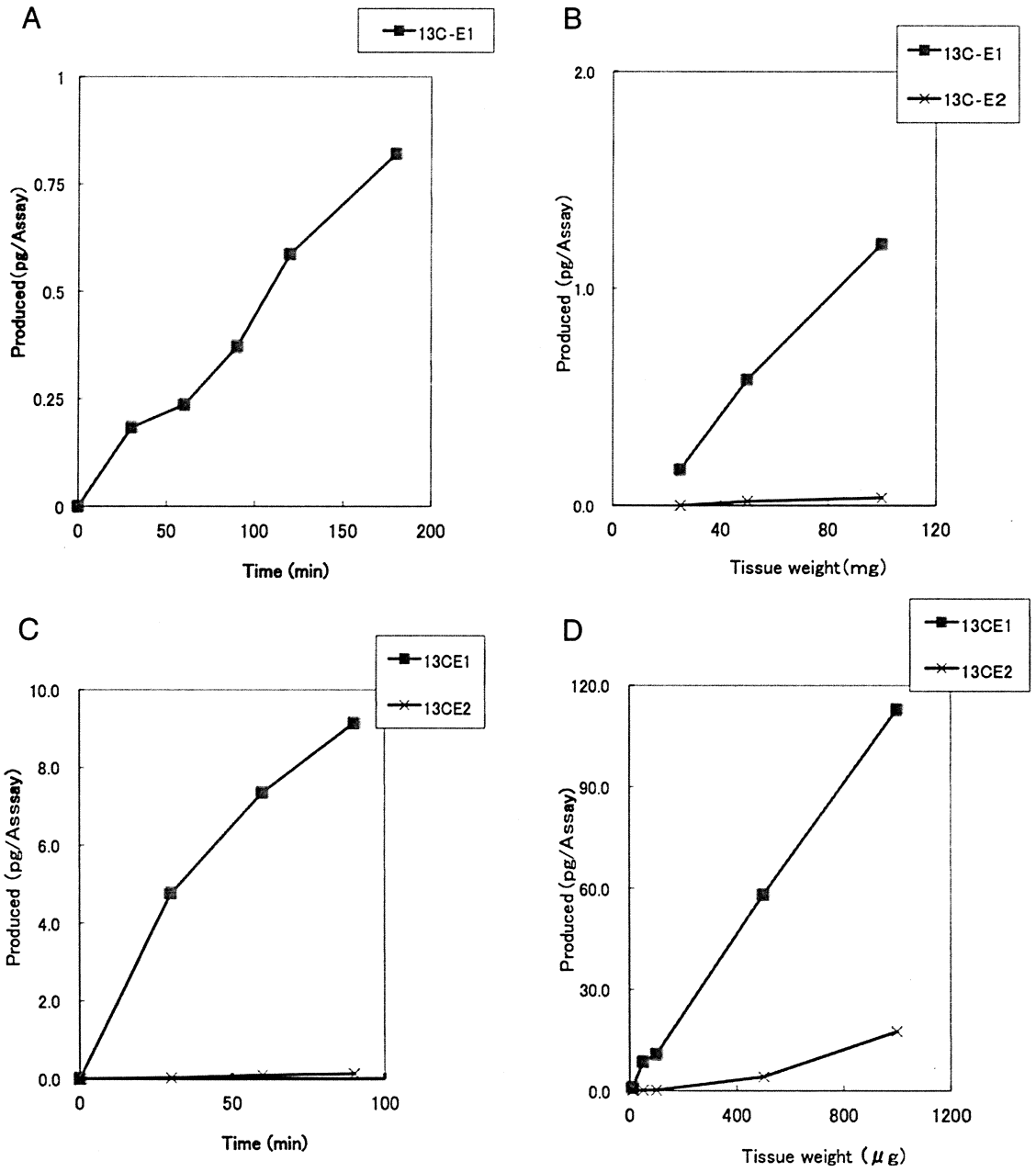


Figure 2. Formation of ^{13}C-estrone and ^{13}C-estradiol from ^{13}C-A-Dione by CYP19 in human sc and rat ovarian tissue. A and B, Subcutaneous adipose tissue. C and D, Rat ovary.

which the existence of CYP19 is already known, to serve as a positive control group. Figure 2 shows the results of the enzymatic reaction when changing the incubation time and the amount of tissue. The main enzyme product produced in rat ovary and human adipose tissue was E1, thus confirming the presence of CYP19 in both. E2 production was approximately 1% of that for E1.

As for the in vitro measurement of CYP19 activity, the LC-MS/MS method was compared with the radiometric method described by Simpson et al (6) using rat ovary tissue. The correlation between these two methods was good ($r = 0.93$). The lower limit of E1 quantification for the LC-MS/MS method is 10 pg/g, and the detection limit for the radiometric method is three times background. A comparison of the two methods showed that the sensitivity of the method combining ^{13}C-labeled steroid precursors with LC-MS/MS was 6 times higher than for the Simpson method.

CYP17 and CYP19 activity in adipose

Table 3 shows the results of the CYP17 and CYP19 activity in adipose tissues. The mean total CYP17 activity (17-OH-Prog + A-dione) values for sc tissue were significantly higher than those for visceral tissue, whereas the mean total CYP19 activity for sc tissue did not differ significantly from that for visceral tissue. CYP17 activity in

The Endocrine Society. Downloaded from press.endocrine.org by [${individualUser.displayNa...], ...pril 2015. at 01:03 For personal use only. No other uses without permission. . All rights reserved.

Table 3. Comparison With CYP17 and CYP19 Activity in Human Adipose Tissues

Adipose Tissue	Sample Number	CYP17		CYP19		Total Activity	
		^{13}C-17-OH-Prog pmol/g · h	^{13}C-A-Dione pmol/g · h	^{13}C-E1 pmol/g · h	^{13}C-E2 pmol/g · h	CYP17 pmol/g · h	CYP19 pmol/g · h
Visceral	1	0.293	0.409	0.011	0.001[a]	0.702	0.012
	2	0.087[a]	0.154[a]	0.010	0.000[a]	0.241	0.010
	3	0.612	0.685	0.013	0.000[a]	1.298	0.013
	4	1.170	1.228	0.031	0.001	2.398	0.031
	Mean	0.541	0.619	0.016	0.000	1.160	0.017
	SD	0.472	0.460	0.010	0.000	0.932	0.010
Subcutaneous	1	0.672	0.303	0.040	0.001[a]	0.976	0.041
	2	0.634	0.613	0.029	0.000[a]	1.247	0.029
	3	3.090	3.143	0.002[a]	0.000[a]	6.233	0.002
	4	1.275	1.360	0.082	0.003	2.635	0.085
	Mean	1.418	1.355	0.038	0.001	2.773[b]	0.039
	SD	1.153	1.272	0.033	0.001	2.419	0.035

Incubation time was 1 hour for CYP17 and 2 hours for CYP19.

[a] Under minimum limit of determination.

[b] $P < .05$

both adipose tissues was about 70 times higher than CYP19 activity, and CYP17 and CYP19 activities tended to be high in sc adipose than in visceral adipose tissue.

Discussion

The serum E2 and Prog levels in postmenopausal and ovariectomized women were found to be less than 10% of those in premenopausal women, with E1 and A-dione levels decreasing by 50%. These results agree well with other reports (20–22). DHEA and A-dione levels presented a strong correlation with aging, whereas E2 levels did not. This may be due to the influence of the premenopausal estrous cycle. A comparison of the ratios of hormone levels in the serum and adipose tissues of pre- and postmenopausal and ovariectomized women led to the following three groups. In the first group (all subjects), E1, Prog, DHEA, and A-dione levels in adipose tissues were significantly higher (5–60 times) than in the serum level. As shown in Table 2, the serum E1 and E2 levels of ovariectomized and pre- and postmenopausal women were positively correlated with those in both adipose tissues (more than r = 0.66), strongly suggesting that estrogen is produced in adipose tissues and secreted into the blood. The enzyme activity of CYP19 in adipose tissues is positively correlated with age and is considered to be one of the causes of postmenopausal breast and endometrial cancer (3, 5, 22–24). DHEA, which was present at high levels in adipose tissue, was not clearly correlated with the levels in serum. It therefore remains unclear whether DHEA is produced from pregnenolone in adipose tissue or is taken up from the blood.

In the second group (postmenopausal and ovariectomized women), the E2 and T levels in adipose tissue were 1–7 times higher than those in serum as shown in Table 1, whereas the E1 and A-dione levels were about 9–24 times higher than those in serum. This finding suggests that 17β-hydroxysteroid dehydrogenase activity in adipose tissue may be weak and agrees with previous reports (12, 25). In the third group (pre- and postmenopausal and ovariectomized women), the cortisol and cortisone levels in adipose tissue were significantly lower than in serum, with ratios of approximately 20% of those for serum. The level of DHEA in adipose tissue of postmenopausal and ovariectomized women is highest in the estimated hormone, and a part of DHEA may be converted from DHEA sulfate by sulfatase (Table 1). Feher and Bodrogi (26) have reported that E1, DHEA, T, A-dione, Prog, and 17-OH-Prog levels in adipose tissue were significantly higher than those in serum.

Our study of CYP19 showed that estrogen is produced from $^{13}C_3$-A-Dione, a precursor labeled with a stable isotope, and that the ratio of $^{13}C_3$-E1 to $^{13}C_3$-E2 was 8:1. Radiometric methods have traditionally been used to assay CYP19 activity by measuring the tritium-labeled water released from A-dione-1β-^{3}H. The main drawback of this method is that tritium can also be released by nonenzymatic oxidation. As such, the LC-MS/MS technique is essential to determine trace estrogen levels (~0.5–5 pg) and to clarify whether CYP19 activity is present in previously unexamined tissue and whether CYP19 activity correlates with clinical characteristics. As shown in Table 1, the differences in estrogen levels between serum and adipose tissue must be caused by factors that control the *CYP19* gene activity in the ovary and adipose tissue. In fact, many researchers reported about the differences in the promoter region of the *CYP19* gene and in the reg-

The Endocrine Society. Downloaded from press.endocrine.org by [${individualUser.displayN... 121 ...April 2015. at 01:03 For personal use only. No other uses without permission. . All rights reserved.

ulator levels as glucocorticoid, cytokine, TNF-α, and FSH (5, 7, 27, 28).

It has also been reported that the CYP19 regulator in visceral and sc adipose tissue, including breast adipose tissue, is mainly glucocorticoid, cytokine, and TNF-α rather than the FSH found in ovarian tissue (5, 23, 28). More recently Zhao et al (29) have reported that injecting this *CYP19* gene from human adipose tissue into aromatase knockout mice induced expression of an estrogen tumor similar to that found in humans.

CYP17 is found as two types: the adrenal type, which has much more 17α-hydroxylase than 17,20-lyase activity and in which cortisol is mainly produced, and the ovarian/testicular type, which has much more 17,20-lyase than 17-hydroxylase and in which sex hormones are mainly produced. Hence, it is extremely important to determine whether the CYP17 found in sc adipose is of the former or the latter type. As shown in Figure 1, in an in vitro enzymatic reaction with adipose tissue, we found that 17α-OH-Prog was produced initially by the action of CYP17 followed by production of the same amount of A-dione shortly afterward due to lyase activity. The amounts of T and DHT, which are other C19 steroids, were very low. To the best of our knowledge, this is the first study to show that the CYP17 activity present in adipose tissue is of the testicular/ovarian type, which has both hydroxylase and lyase activities. It has been reported that the differences in the two catalytic activities of CYP17 in each organ depend on the quantity of cytochrome b5 (30, 31). However, details of this mechanism are still unclear. Valle et al (9) and Mackenzie et al (14) have reported that the activity of CYP17 does not exist in adipose tissue. The reason that our results differ is probably either because CYP17 exists as an isozyme or it is unstable in adipose tissue, thus meaning that it could not be detected for technical reasons.

In 2002, Puche et al (32) detected *CYP17* gene expression and activity in adipose tissue. During a study of the catalytic action of the enzyme with ^{14}C-labeled Prog, only the production of 17-OH-Prog was found and no A-dione could be detected. As a result, these findings proposed that the CYP17 in adipose tissue may be of the adrenal type and that A-dione could not be detected due to a limitation of the test method used. Our finding that the CYP17 in adipose tissue has both hydroxylase and lyase activity is also supported by the results of Feher and Bodrogi (26), who reported that the levels of 17-OH-Prog and A-dione in adipose tissue were 4–10 times higher than in serum. Because we obtained a similar result (Table 1), it can be concluded that these steroid compounds are probably produced in adipose tissue. Consequently, CYP17 probably exists as the isozyme type in adipose tissue (33).

We also compared CYP17 and CYP19 activities in visceral and sc adipose tissue. Our findings showed that CYP17 activity in these tissues is 70-times higher than CYP19 activity. We therefore suggest that adipose tissue acts as an endocrine organ, with CYP17 and CYP19 activity playing an essential role in sex steroid hormone biosynthesis.

Conclusion

The serum E2 levels of postmenopausal and ovariectomized women were 10% of those in premenopausal women. Moreover, E1, DHEA, A-dione, and Prog levels in adipose tissue of postmenopausal and ovariectomized women were 9–60 times higher than in serum, whereas E2 levels in adipose tissue were 1–7 times higher than those in serum. No significant differences in hormone levels in sc and visceral adipose tissue were seen between pre- and postmenopausal women. A new tracer approach for determining CYP17 and CYP19 activity in adipose tissue has confirmed the presence of CYP17 and CYP19 activity in visceral and sc adipose tissue, with the former being 70 times stronger than the latter.

Acknowledgments

Address all correspondence and requests for reprints to: Yasuhiro Shibata, PhD, MD, Department of Urology, Gunma University Graduate School of Medicine 3-39-22 Showa-machi, Maebashi, Gunma 371-8511, Japan. E-mail: yash@gunma-u.ac.jp or Toshihiko Kinoshita, Department of Obstetrics and Gynecology, Toho University Medical Center, Sakura Hospital, 564-1 Shimoshizu Sakura City, Ciba 285-8741, Japan. E-mail: kino@sakura.med.toho-u.ac.jp.

Disclosure Summary: The authors have nothing to declare.

References

1. **Key TJ.** Endogenous oestrogens and breast cancer risk in premenopausal and postmenopausal women. *Steroids.* 2011;76:812–815.
2. **Lepine J, Audet-Walsh E, Gregoire J, et al.** Circulating estrogens in endometrial cancer cases and their relationship with tissular expression of key estrogen biosynthesis and metabolic pathways. *J Clin Endocrinol Metab.* 2010;95:2689–2698.
3. **Huhtinen K, Desai R, Stahle M, et al.** Endometrial and endometriotic concentrations of estrone and estradiol are determined by local metabolism rather than circulating levels. *J Clin Endocrinol Metab.* 2012;97:4228–4235.
4. **Lonning PE, Haynes BP, Straume AH, et al.** Recent data on intratumor estrogens in breast cancer. *Steroids.* 2011;76:786–791.
5. **Bulun SE, Simpson ER.** Breast cancer and expression of aromatase in Brest adipose tissue. *Trends Endocrinol Metab.* 1994;5:113–120.
6. **Simpson ER, Merrill JC, Hollub AJ, Graham-Lorence S, Mendelson CR.** Regulation of estrogen biosynthesis by human adipose cells. *Endocrine Rev.* 1989;10:136–148.
7. **Simpson ER.** Role of aromatase in sex steroid action. *J Mol Endocrinol.* 2000;25:149–156.

The Endocrine Society. Downloaded from press.endocrine.org by [${individualUser.displayNa... ...pril 2015. at 01:03 For personal use only. No other uses without permission. . All rights reserved.

8. **Deslypere JP, Verdonck L, Vermeulen A.** Fat tissue: a steroid reservoir and site of steroid metabolism. *J Clin Endocrinol Metab.* 1985; 61:564–570.
9. **Valle LD, Toffolo V, Nardi A, et al.** Tissue-specific transcriptional initiation and activity of steroid sulfatase complementing dehydroepiandrosterone sulfate uptake and intracrine steroid activations in human adipose tissue. *J Endocrinol.* 2006;190:129–139.
10. **Kershaw EE, Flier JS.** Adipose tissue as an endocrine organ. *J Clin Endocrinol Metab.* 2004;89:2548–2556.
11. **Belanger C, Luu-The VL, Dupont P, Tchernof A.** Adipose tissue intracrinology: potential importance of local androgen/estrogen metabolism in the regulation of adiposity. *Hormone Metab Res.* 2002; 34:737–745.
12. **Blouin K, Nadeau M, Mailloux J, et al.** Pathways of adipose tissue androgen metabolism in women: depot differences and modulation by adipogenesis. *Am J Physiol Endocrinol Metab.* 2009;296:E244–E255.
13. **Montes-Nieo R, Insenser M, Martinez-Garcia MA, Escobar-Morreale HF.** A nontargeted proteomic study of the influence of androgen excess on human visceral and subcutaneous adipose tissue proteomes. *J Clin Endocrinol Metab.* 2013;98:E576–E585.
14. **Mackenzie SM, Hudat SS, Sattar N, Fraser R, Connell JMC, Davies E.** Depot-specific steroidogenic gene transcription in human adipose tissue. *Clin Endocrinol (Oxf).* 2008;69:848–854.
15. **Blair IA.** Analysis of estrogens in serum and plasma from postmenopausal women: past present and future. *Steroids.* 2010;75:297–306.
16. **Bailey EJ, Barton DHR, Elks J, Templeton JF.** Compounds related to the steroid hormones. Part IX. Oxygenation of steroid ketones in strongly basic medium: a new method of preparation of 17α-hydroxypregnan-20-ones. *J Chem Soc.* 1962;1578–1591.
17. **Kido T, Tung DV, Manh HD, et al.** High cortisol and cortisone levels are associated with breast milk dioxin concentrations in Vietnamese women. *Eur J Endocrinol.* 2014;170:131–139.
18. **Arai S, Miyashiro Y, Shibata Y, et al.** New quantification method for estradiol in the prostatic tissues of benign prostatic hyperplasia using liquid chromatography-tandem mass spectrometry. *Steroid.* 2010; 75:13–19.
19. **Higashi T.** Salivary hormone measurement using LC/MS/MS: specific and patient-friendly tool for assessment of endocrine function. *Biol Pharm Bull.* 2012;35:1401–1408.
20. **Badeau M, Vihma V, Mikkola TS, Tiitinen A, Tikkanen MJ.** Estradiol fatty acid esters in adipose tissue and serum of pregnant and pre- and postmenopausal women. *J Clin Endocrinol Metab.* 2007; 92:4327–4331.
21. **Yamatani H, Takahashi K, Yoshida T, Takata K, Kurachi H.** Association of estrogen with glucocorticoid levels in visceral fat in postmenopausal women. *Menopause.* 2013;20(4):437–442.
22. **Simpson ER.** Sources of estrogen and their importance. *J Steroid Biochem Mol Biol.* 2003;86:225–230.
23. **Meseguer A, Puche C, Cabero A.** Sex steroid biosynthesis in white adipose tissue. *Horm Metab Res.* 2002;34:731–736.
24. **Szymczak J, Milewicz A, Thijssen JHH, Blankenstein MA, Daroszewski J.** Concentration of sex steroids in adipose tissue after menopause. *Steroids.* 1998;63:319–321.
25. **Blouin K, Richard C, Belanger C, et al.** Local androgen inactivation in abdominal visceral adipose tissue. *J Clin Endocrinol Metab.* 2003; 88:5944–5950.
26. **Feher T, Bodrogi L.** A comparative study of steroid concentrations in human adipose tissue and the peripheral circulation. *Clin Chim Acta.* 1982;126:135–141.
27. **Bulun SE, Sebastian S, Takayama K, Suzuki T, Sasano H, Shozu M.** The human CYP19 (aromatase P450) gene: update on physiologic roles and genomic organization of promoters. *J Steroid Biochem Mol Biol.* 2003;86:219–224.
28. **Zhao Y, Agarwal VR, Mendelson CR, Simpson ER.** Transcriptional regulation of CYP19 gene (aromatase) expression in adipose stromal cells in primary culture. *J Steroid Biochem Mol Biol.* 1997;61: 203–210.
29. **Zhao H, Pearson EK, Brooks DC, et al.** A humanized pattern of aromatase expression is associated with mammary hyperplasia in mice. *Endocrinology.* 2012;153:2701–2713.
30. **Yamaoka M, Hara T, Hitaka T, et al.** Orteronel (TAK-700), a novel non-steroidal 17,20-lyase inhibitor: effect on steroid synthesis in human and monkey adrenal cells and serum steroid levels in cynomolgus monkeys. *J Steroid Biochem Mol Biol.* 2012;129:115–128.
31. **Idkowiak J, Randell T, Dhir V, et al.** A missense mutation in the human cytochrome b5 gene causes 46, xy disorder of sex development due to true isolated 17,20 lyase deficiency. *J Clin Endocrinol Metab.* 2012;97:E465–E475.
32. **Puche C, Jose M, Cabero A, Meseguer A.** Expression and enzymatic activity of the P450c17 gene in human adipose tissue. *Eur J Endocrinol.* 2002;146:223–229.
33. **Sharp L, Cardy AH, Cotton SC, Little J.** CYP17 gene polymorphisms: prevalence and associations with hormone levels and related factors. *Am J Epidemiol.* 2004;160:729–740.

The Endocrine Society. Downloaded from press.endocrine.org by [${individualUser.displayNa...pril 2015. at 01:03 For personal use only. No other uses without permission. . All rights reserved.

European Journal of Medicinal Chemistry 60 (2013) 295–304

Contents lists available at SciVerse ScienceDirect

European Journal of Medicinal Chemistry

journal homepage: http://www.elsevier.com/locate/ejmech

Original article

Total synthesis of bicyclic depsipeptides spiruchostatins C and D and investigation of their histone deacetylase inhibitory and antiproliferative activities

Koichi Narita [a], Yurie Fukui [a], Yui Sano [a], Takao Yamori [b], Akihiro Ito [c], Minoru Yoshida [c], Tadashi Katoh [a,*]

[a] Laboratory of Synthetic and Medicinal Chemistry, Faculty of Pharmaceutical Sciences, Tohoku Pharmaceutical University, 4-4-1 Komatsushima, Aoba-ku, Sendai 981-8558, Japan
[b] Division of Molecular Pharmacology, Cancer Chemotherapy Center, Japanese Foundation for Cancer Research, 3-10-6 Ariake, Koto-ku, Tokyo 135-8550, Japan
[c] Chemical Genetics Laboratory, RIKEN, 2-1 Hirosawa, Wako-shi, Saitama 351-0198, Japan

ARTICLE INFO

Article history:
Received 27 October 2012
Received in revised form
8 December 2012
Accepted 11 December 2012
Available online 21 December 2012

Keywords:
Spiruchostatins
Histone deacetylase inhibitors
Natural products
Bicyclic depsipeptide
Total synthesis

ABSTRACT

The bicyclic depsipeptide histone deacetylase (HDAC) inhibitors spiruchostatins C and D were synthesized for the first time in a highly convergent and unified manner. The method features the amide coupling of a D-leucine–D-cysteine- or D-valine–D-cysteine-containing segment with a D-alanine- or D-valine-containing segment to directly assemble the corresponding *seco*-acids, key precursors of macrolactonization. The HDAC inhibitory assay and cell-growth inhibition analysis of the synthesized depsipeptides determined the order of potency of spiruchostatins A–D in comparison with the clinically approved depsipeptide FK228 (romidepsin). Novel aspects of structure–activity relationships (SAR) were revealed.

© 2012 Elsevier Masson SAS. All rights reserved.

1. Introduction

Histone deacetylase (HDAC) inhibitors have attracted significant attention because of their potentials as novel mechanism-based anticancer agents [1]. It has been reported that HDAC inhibitors exhibit prominent antitumour activity in several human tumour xenograft models by inducing transcriptional events involved in growth arrest, differentiation and apoptotic cell death [1,2]. HDAC enzymes remove an acetyl group from the lysine residues of the core histones, leading to a changed chromatin structure that impacts transcriptional activity [3]. There are 18 human HDAC isoforms, which are grouped into four major classes: class I (HDACs 1, 2, 3 and 8), class II (class IIa: HDACs 4, 5, 7 and 10; class IIb: HDACs 6 and 10), and class IV (HDAC 11) are Zn^{2+}-dependent metallohydrolases, while class III HDACs (7 members) are NAD^{+}-dependent sirtuins [4]. The inhibition of class I HDACs is considered to be a useful mechanism for anticancer agents, whereas the inhibition of class II HDACs may cause undesirable side effects such as serious cardiac hypertrophy [5]. Therefore, the potent and selective inhibition of class I enzymes is highly desirable in cancer chemotherapy.

In 2009, the Food and Drug Administration (FDA) in the USA approved the bicyclic depsipeptide HDAC inhibitor FK228 (romidepsin, **1**, Fig. 1) for the treatment of cutaneous T cell lymphoma (CTCL) [6]. However, this anticancer agent is associated with an unresolved cardiotoxicity issue [6b,7], which highlights the need for further identification and development of new HDAC inhibitors with high efficacy and low toxicity [1n,4a]. FK228 was originally isolated from a culture broth of *Chromobacterium violaceum* (No. 968) by Fujisawa Pharmaceutical Co. Ltd. (now Astellas Pharma Inc.) in 1994 [8]. The structural features of this natural product include a 16-membered bicyclic depsipeptide consisting of (*Z*)-2-amino-2-butenoic acid, L-valine, D-cysteine, D-valine, (3*R*,4*E*)-3-hydroxy-7-mercapto-4-heptenoic acid and a characteristic disulfide bond linkage [8b]. Subsequent to the discovery of FK228, the structurally similar 15-membered bicyclic depsipeptide HDAC inhibitors — spiruchostatins A (**2**) [9], B (**3**) [9], C (**4**) [10,11] and D (**5**) [12] — were successively isolated from a culture broth of the *Pseudomonas* sp. by Shin-ya and Yamanouchi Pharmaceutical Co. Ltd. (now Astellas Pharma Inc.).

The attractive biological properties and unique structural features of **1**–**5** have made them intriguing and timely targets for

* Corresponding author. Tel./fax: +81 22 727 0135.
E-mail address: katoh@tohoku-pharm.ac.jp (T. Katoh).

0223-5234/$ – see front matter © 2012 Elsevier Masson SAS. All rights reserved.
http://dx.doi.org/10.1016/j.ejmech.2012.12.023

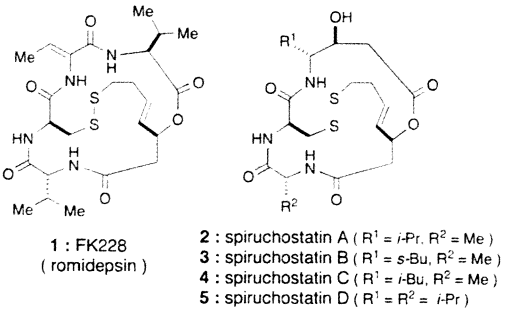


Fig. 1. Structures of FK228 (romidepsin) (**1**) and spiruchostatins A (**1**), B (**2**), C (**3**) and D (**4**). *i*-Pr = isopropyl, *s*-Bu = *sec*-butyl, *i*-Bu = isobutyl.

total synthesis. Several total syntheses of FK228 (**1**) [13], spiruchostatins A (**2**) [13a,14] and B (**3**) [13a,15] have been published. However, to the best of our knowledge, the total synthesis of spiruchostatins C (**4**) and D (**5**) has not been reported, and their biological properties have not been described in the patent literatures [10,12]. We have previously presented the total synthesis of **1**–**3** using a highly convergent and unified scheme [13a,14c,15b], and demonstrated that **1**–**3** exhibit a potent class I HDAC inhibitory activity (IC_{50} = 2.2–3.6 nM) [13a]. During our efforts on the synthesis and biological evaluation of the bicyclic depsipeptide HDAC inhibitors, we became interested in the biological potencies of **4** and **5** as compared with those of **1**–**3**. In this paper, we describe the total synthesis of **4** and **5** for the first time applying the synthetic strategy developed in our laboratory [13a]. HDAC inhibition assay and antiproliferative analysis of the synthesized **4** and **5** were also performed to establish the potency order of the bicyclic depsipeptides family (**1**–**5**).

2. Results and discussion

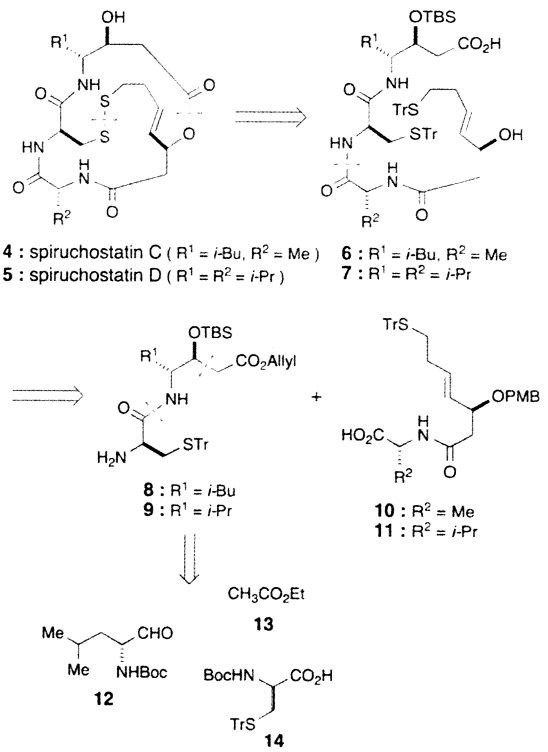
2.1. Chemistry

2.1.1. Synthetic plan for spiruchostatins C (*4*) and D (*5*)

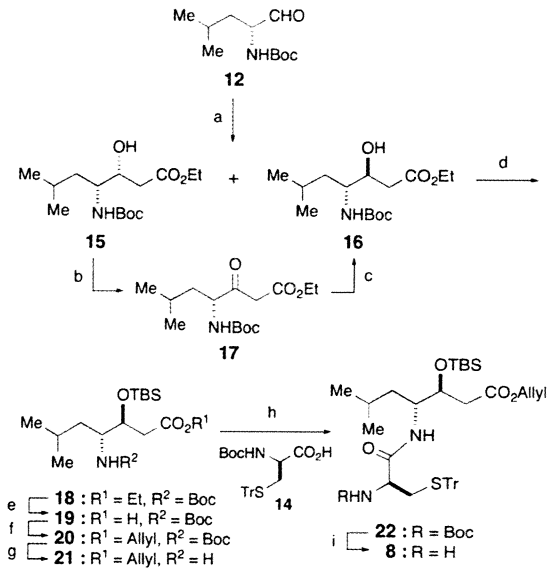
Our synthetic plan for spiruchostatins C (**4**) and D (**5**) is outlined in Scheme 1. We envisioned that the targeted molecules **4** and **5** could be synthesized by the macrolactonization of the corresponding *seco*-acids **6** and **7**, followed by disulfide bond formation. The key element of this scheme is the highly convergent assembly of **6** and **7** by the direct coupling of a D-leucine–D-cysteine-containing segment **8** and a D-alanine-containing segment **10** and a D-valine–D-cysteine-containing segment **9** and a D-valine-containing segment **11**, respectively. The segment **8** was to be prepared by the aldol coupling of *N*-Boc-D-leucinal (**12**) with ethyl acetate (**13**) and subsequent condensation with the D-cysteine derivative **14**. The remaining three segments **9**, **10** and **11** were obtained by our previously described total synthesis of **1**–**3** [13a].

2.1.2. Synthesis of segment *8*

The synthesis of **8**, starting from the known *N*-Boc-D-leucinal (**12**) [16], is shown in Scheme 2; the route is based on our previous study [13a]. Thus, the aldol coupling of **12** with the lithium enolate of ethyl acetate (**13**) gave the desired coupling product **16** (33%) and the undesired stereoisomer **15** (54%). The conversion of **15** to **16** was achieved by Jones oxidation (80%) and the stereoselective reduction of the resulting ketone **17** (90%). The ethyl ester **16** was then transformed to the allyl ester **21** via a four-step operation involving the *tert*-butyldimethylsilyl (TBS) protection of the hydroxy group in **16** (99%), the saponification of the ester moiety in the resulting TBS ether **18**, the formation of an allyl ester from



Scheme 1. Synthetic plan for spiruchostatins C (**4**) and D (**5**). TBS = *tert*-butyldimethylsilyl, Tr (trityl) = triphenylmethyl, Boc = *tert*-butoxycarbonyl, PMB = 4-methoxybenzyl.

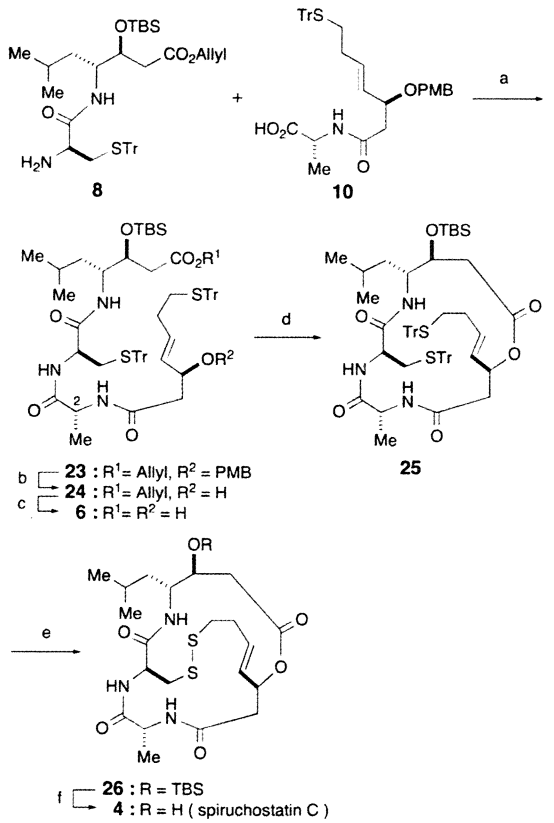


Scheme 2. Synthesis of segment **8**. (a) LDA, CH_3CO_2Et (**13**), THF, −78 °C; at −78 °C, add. **12**, 54% for **15**, 33% for **16** (**15**/**16** *ca.* 3:2); (b) Jones reagent, acetone, 0 °C to rt, 80%; (c) KBH_4, MeOH, −40 °C, 90%; (d) TBSCl, imidazole, DMF, rt, 99%; (e) 1 M NaOH, EtOH, rt; (f) allyl bromide, K_2CO_3, DMF, rt. 77% (2 steps); (g) TMSOTf, 2,6-lutidine, CH_2Cl_2, rt; MeOH, rt; (h) **14**, PyBOP, *i*-Pr_2NEt, MeCN, rt, 69% (2 steps); (i) TMSOTf, 2,6-lutidine, CH_2Cl_2, rt, 88%. LDA = lithium diisopropylamide, TMSOTf = trimethylsilyl trifluoromethanesulfonate, PyBOP = (benzotriazol-1-yloxy)tripyrrolidinophosphonium hexafluorophosphate.

the liberated carboxylic acid **19** (77% in two steps) and the deprotection of the *N*-Boc group in **20**. The condensation of the amine **21** with *N*-Boc-*S*-trityl-L-cysteine (**14**) furnished the desired coupling product **22** with a 69% yield from **20**. Finally, the deprotection of the *N*-Boc group in **22** afforded the requisite segment **8** in 88% yield.

2.1.3. Synthesis of spiruchostatin C (4)

After obtaining the key segment **8**, we performed the synthesis of the first target spiruchostatin C (**4**), as shown in Scheme 3. The condensation of **8** with segment **10** proceeded well under the mild conditions [HATU (1.3 equiv), HOAt (1.3 equiv), *i*-Pr_2NEt (2.6 equiv), −30 °C, 6 h] explored in our previous studies [13a]. The desired coupling product **23** was obtained in 84% yield without appreciable epimerization at the C2 stereogenic centre (D-alanine part in **23**). The coupling product **23** was converted to the requisite *seco*-acid **6** with an overall yield of 98% using the alcohol **24** by the successive removal of both the PMB and allyl protecting groups. The subsequent macrolactonization of **6** was achieved by employing the Shiina method [17] [MNBA (1.3 equiv), DMAP (3.0 equiv), CH_2Cl_2 (10 mM), rt, 12 h], which resulted in the desired cyclization product **25** in 75% yield. Finally, simultaneous *S*-Tr deprotection and disulfide bond formation of **25** (95%) followed by the deprotection of the TBS group of the resulting disulfide **26** (91%) furnished spiruchostatin C (**4**), $[\alpha]_D^{25} = -59.4°$ (c = 0.20 in $CHCl_3$) {lit. [10] $[\alpha]_D^{25} = -60.0°$ (c = 0.10 in $CHCl_3$)}. The spectroscopic properties (IR, ^1H and ^{13}C NMR, and MS) of the synthetic sample **4** were identical with those reported for natural **4** [10].



Scheme 3. Synthesis of spiruchostatin C (**4**). (a) HATU, HOAt, *i*-Pr_2NEt, CH_2Cl_2, −30 °C, 84%; (b) DDQ, CH_2Cl_2/H_2O, rt, 99%; (c) $Pd(PPh_3)_4$, morpholine, THF, rt, 99%; (d) MNBA, DMAP, CH_2Cl_2, rt, 75%; (e) I_2, MeOH/CH_2Cl_2, rt, 95%; (f) HF·pyridine, pyridine, rt, 91%. HATU = *O*-(7-azabenzotriazol-1-yl)-*N*,*N*,*N*′,*N*′-tetramethyluronium hexafluorophosphate, HOAt = 1-hydroxy-7-azabenzotriazole, DDQ = 2,3-dichloro-5,6-dicyano-1,4-benzoquinone, MNBA = 2-methyl-6-nitrobenzoic anhydride, DMAP = 4-dimethylaminopyridine.

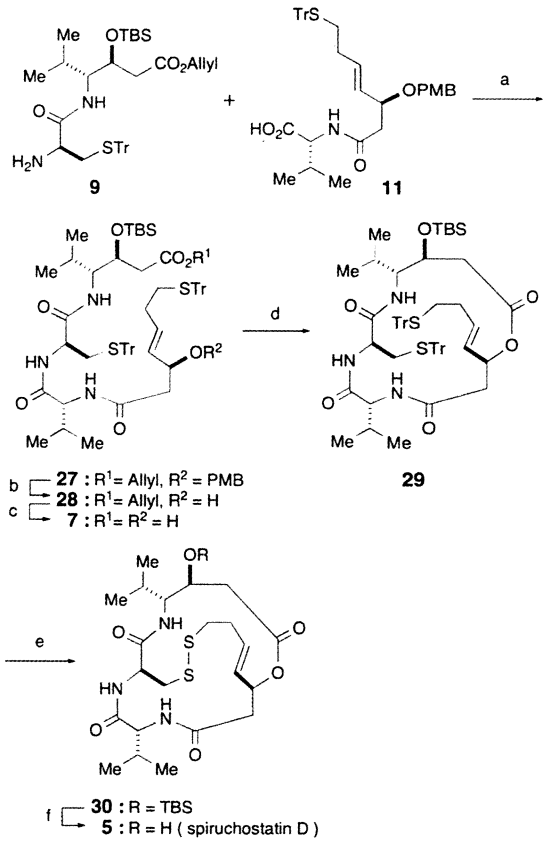
2.1.4. Synthesis of spiruchostatin D (5)

As shown in Scheme 4, using segments **9** [13a] and **11** [13a] as the starting materials, the second target spiruchostatin D (**5**) was synthesized in a manner similar to that described for **4** (cf. Scheme 3). The spectroscopic properties (IR, ^1H and ^{13}C NMR, and MS) of the synthesized sample **5** were identical with those reported for natural **5** [12]. The optical rotation of synthesized **5** {$[\alpha]_D^{25} = -59.2°$ (c = 0.29 in MeOH)} corresponded to that of natural **5** {$[\alpha]_D^{25} = -65.3°$ (c = 0.20 in MeOH)} [12].

2.2. Biological evaluation

2.2.1. HDAC inhibition assay

The synthesized spiruchostatins C (**4**) and D (**5**) were tested for their HDAC inhibitory activity against HDAC1 (class I) and HDAC6 (class IIb) to determine the degree of potency and isoform selectivity. In this assay, FK228 was used as a positive control. As summarized in Table 1, the two compounds **4** and **5** that were tested exhibited extremely potent inhibitory activity against HDAC1 in the sub-nanomolar range (IC_{50} = 0.75–0.93 nM). The potencies of **4** and **5** were observed to be 3-to-4-fold higher than that of FK228. Combined with our previous data for spiruchostatins A (**2**) and B (**3**) [13a], the order of potency was estimated to be **5** (IC_{50} = 0.75 nM) ≥ **4** (IC_{50} = 0.93 nM) > **3** (IC_{50} = 2.2 nM) ≥ **2** (IC_{50} = 3.3 nM) ≈ FK228 (**1**) (IC_{50} = 3.6 nM). Spiruchostatin D (**5**)



Scheme 4. Synthesis of spiruchostatin D (**5**). (a) HATU, HOAt, *i*-Pr_2NEt, CH_2Cl_2, −30 °C, 94%; (b) DDQ, CH_2Cl_2/H_2O, rt, 79%; (c) $Pd(PPh_3)_4$, morpholine, THF, rt, 90%; (d) MNBA, DMAP, CH_2Cl_2, rt, 85%; (e) I_2, MeOH/CH_2Cl_2, rt, 88%; (f) HF·pyridine, pyridine, rt, 93%.

Table 1
HDAC inhibitory activity of spiruchostatins C (**4**) and D (**5**).

Compound	IC_{50}[a] (nM)		SI[d]
	HDAC1 (class I)[b]	HDAC6 (class IIb)[b]	
4	0.93	320	346
5	0.75	240	320
FK228[c]	3.6	390	108

[a] Concentration that induces 50% inhibition against HDACs.
[b] Enzyme assay was performed in the presence of 100 μM dithiothreitol (DTT).
[c] Positive control used in this study was synthesized in our laboratory.
[d] Selectivity index (HDAC6 IC_{50}/HDAC1 IC_{50}) as the selectivity toward class I HDAC1 over class IIb HDAC6.

exhibited the most potent HDAC1 inhibitory activity among the spiruchostatins family (**2**–**5**), suggesting that sterically bulky terminal-branched alkyl groups are preferable for the R^1 and R^2 side chains in the spiruchostatins (cf. Fig. 1). As expected for HDAC6 inhibitory activity, both **4** and **5** were essentially inactive (**4**: IC_{50} = 320 nM, **5**: IC_{50} = 240 nM), which is similar to the behavior exhibited by FK228 (IC_{50} = 390 nM). Isoform selectivity (class I/IIb) is expressed, for convenience, as a selective index (SI) value (HDAC6 IC_{50}/HDAC1 IC_{50}). The isoform selectivity of **4** (SI = 346) and **5** (SI = 320) is approximately 3-fold higher than that of FK228 (SI = 108). These results suggested that the minor structural alteration of the R^1 and R^2 side chains in spiruchostatins improves HDAC inhibitory activity and isoform selectivity. This is in agreement with a previous SAR study on synthetic FK228 analogues reported by Ganesan et al. [18].

2.2.2. Cell-growth inhibition assay

The growth-inhibitory activity of compounds **4** and **5** was evaluated simultaneously with FK228, a reference compound, using a panel of 39 human cancer cell lines at the Japanese Foundation for Cancer Research [19]. The number of cell lines and their origin (organ) are as follows: 5 breast, 6 central nervous system (brain), 1 melanoma, 5 ovary, 2 kidney, 6 stomach and 2 prostate. Dose–response curves were measured at five different concentrations (10^{-10}–10^{-6} or 10^{-8}–10^{-4} M) for each compound, and the concentration causing 50% cell-growth inhibition (GI_{50}) was compared with that of the control. The GI_{50} values of the tested compounds **4** and **5** along with FK228 are shown in Table 2. Compound **5** exhibited extremely potent growth-inhibitory activity against almost all 39 cell lines in the sub-nanomolar to nanomolar range and its efficacy was superior to that of FK228. In contrast, compound **4** exhibited decreased activity compared to FK228. The order of potency, combined with our previous data for **2** and **3** [13a], was estimated by the MG-MID value (mean value of GI_{50} over all cell lines tested) to be **5** (3.8 nM) ≥ **3** (5.6 nM) ≈ FK228 (**1**) (6.2 nM) > **2** (15 nM) > **4** (28 nM).

Considering the HDAC inhibitory and antiproliferative activities, spiruchostatin D (**5**) seems to be a promising candidate for the development of novel anticancer agents with high efficacy and low toxicity. Interestingly, the order of potency in antiproliferative activity is not necessarily in agreement with that in HDAC inhibitory activity. This is probably influenced by bioavailability and/or cell permeability. Another possible explanation for this discrepancy is that this class of HDAC inhibitors has an additional mechanism of action, albeit the molecular target is unknown at present. This hypothetical issue is now under investigation in our laboratories.

3. Conclusion

We have achieved the first total synthesis of spiruchostatins C (**4**) and D (**5**) in a highly convergent and unified manner. The present synthesis demonstrated that our explored synthetic strategy has the potential for producing spiruchostatin analogues that possess various alkyl side chains. The preliminary biological evaluation of the synthesized **4** and **5** together with our previous data for **2** and **3** determined the order of the efficacy of the spiruchostatins family (**2**–**5**). These results would be useful for the design and development of anticancer agents with therapeutic potential that target the isoform-selective inhibition of HDACs. Further investigations concerning the synthesis of unnatural spiruchostatin analogues and SAR study are currently underway and will be reported in due course.

Table 2
Growth inhibition of spiruchostatins C (**4**) and D (**5**) against a panel of 39 human cancer cell lines.

Origin of cancer	Cell line	GI_{50}[a] (nM)		
		4	**5**	FK228[b]
Breast	HBC-4	20	4.1	6.9
	BSY-1	25	5.2	8.5
	HBC-5	150	18	13
	MCF-7	47	2.9	4.2
	MDA-MB-231	14	1.7	5.5
Central nervous system (brain)	U-251	52	2.7	3.9
	SF-268	25	3.5	4.9
	SF-295	32	5.1	4.0
	SF-539	10[c]	0.58	3.6
	SNB-75	10[c]	1.9	7.2
	SNB-78	78	41	9.6
Colon	HCC2998	11	1.5	3.1
	KM-12	10[c]	2.6	3.4
	HT-29	10[c]	2.2	3.3
	HCT-15	3800[d]	210[d]	450[d]
	HCT-116	10[c]	1.3	3.1
Lung	NCI-H23	10[c]	2.5	4.6
	NCI-H226	53	4.0	8.9
	NCI-H522	10[c]	0.39[c]	1.8[c]
	NCI-H460	16	2.8	3.0
	A549	10[c]	0.97	2.6
	DMS273	32	5.1	5.8
	DMS114	10[c]	3.6	3.6
Melanoma	LOX-IMVI	10[c]	1.8	2.5
Ovary	OVCAR-3	16	2.2	4.6
	OVCAR-4	58	4.7	20
	OVCAR-5	10[c]	1.2	2.8
	OVCAR-8	10[c]	2.7	5.5
	SK-OV-3	15	2.3	3.3
Kidney	RXF-631L	35	5.9	6.6
	ACHN	130	21	20
Stomach	St-4	190	16	22
	MKN1	16	2.0	3.2
	MKN7	150	5.8	4.9
	MKN28	130	9.5	17
	MKN45	100	9.6	14
	MKN74	15	2.9	3.0
Prostate	DU-145	10[c]	4.0	6.0
	PC-3	23	8.7	18
MG-MID[e]		28	3.8	6.2

[a] Concentration that induces 50% inhibition of cell growth compared to the control.
[b] Positive control used in this study was synthesized in our laboratory.
[c] The most sensitive cell.
[d] The least sensitive cell.
[e] Mean value of GI_{50} over all cell lines tested.

4. Experimental

4.1. Chemistry

All reactions involving air- and moisture-sensitive reagents were carried out using oven dried glassware and standard syringe-septum cap techniques. Routine monitorings of reaction were carried out using glass-supported Merck silica gel 60 F_{254} TLC

plates. Flash column chromatography was performed on Kanto Chemical Silica Gel 60N (spherical, neutral 40–50 nm) with the solvents indicated.

All solvents and reagents were used as supplied with following exceptions. Tetrahydrofuran (THF) was freshly distilled from Na metal/benzophenone under argon. *N,N*-dimethylformamide (DMF), CH_2Cl_2, MeCN, pyridine, *i*-Pr_2NH, and *i*-Pr_2NEt were distilled from calcium hydride under argon.

Measurements of optical rotations were performed with a JASCO DIP-370 automatic digital polarimeter. ^1H and ^{13}C NMR spectra were measured with a JEOL AL-400 (400 MHz) spectrometer. Chemical shifts were expressed in ppm using Me_4Si ($\delta = 0$) as an internal standard. The following abbreviations are used: singlet (s), doublet (d), triplet (t), quartet (q), multiplet (m) and broad (br). Infrared (IR) spectral measurements were carried out with a JASCO FT/IR-4100 spectrometer. Low- and high-resolution mass (HRMS) spectra were measured on a JEOL JMS-DX 303/JMA-DA 5000 SYSTEM high-resolution mass spectrometer.

4.1.1. (3R,4R)-ethyl 4-(tert-butoxycarbonylamino)-3-hydroxy-6-methylheptanoate (**15**) and its (3S,4R)-isomer (**16**)

A solution of EtOAc (3.05 mL, 31 mmol) in THF (3 mL) was added slowly to a stirred solution of lithium diisopropylamide (LDA) (31 mmol) [prepared from *n*-BuLi in hexane (1.6 M solution, 20.6 mL, 33 mmol) and *i*-Pr_2NH (4.4 mL, 31 mmol)] in THF (15 mL) at −78 °C. After 30 min, (2*R*)-2-(*tert*-butoxycarbonylamino)-4-methylpentylaldehyde (*N*-Boc-D-leucinal) (**12**) [16] (1.98 g, 9.2 mmol) in THF (9 mL) was added to the above mixture at −78 °C. After 40 min, the reaction was quenched with 2 M HCl (10 mL) at −78 °C, and the resulting mixture was extracted with EtOAc (2 × 50 mL). The combined extracts were washed with saturated aqueous $NaHCO_3$ (2 × 30 mL) and brine (2 × 30 mL), then dried over Na_2SO_4. Concentration of the solvent in vacuo afforded a residue, which was purified by column chromatography (hexane/EtOAc 5:1 → 4:1) to give **15** (1.51 g, 54%, less polar) and **16** (0.93 g, 33%, more polar).

Compound **15**: colorless oil; $[\alpha]_D^{25}$ +33.8 (*c* 1.00, $CHCl_3$); IR (neat): 3441, 3381, 2957, 2933, 2870, 1714, 1695, 1513, 1506, 1470, 1455, 1392, 1367, 1327, 1251, 1173, 1114, 1098, 1046, 1027 cm^{-1}; ^1H NMR (400 MHz, $CDCl_3$): δ 0.93 (6H, d, J = 6.8 Hz), 1.25–1.28 (1H, m), 1.27 (3H, t, J = 7.3 Hz), 1.44–1.56 (1H, m), 1.44 (9H, s), 1.63–1.68 (1H, m), 2.47–2.58 (2H, m), 3.41 (1H, d, J = 2.9 Hz), 3.62 (1H, d, J = 5.4 Hz), 4.02 (1H, s), 4.17 (2H, dd, J = 6.8, 6.8 Hz), 4.79 (1H, d, J = 9.8 Hz); ^{13}C NMR (100 MHz, $CDCl_3$): δ 14.0, 22.2, 22.9, 24.7, 28.3 (3C), 38.8, 41.6, 51.9, 60.7, 69.7, 79.0, 156.0, 173.2; HRMS (EI): *m/z* calcd for $C_{15}H_{29}NO_5$ (M^+) 303.2046, found 303.2039.

Compound **16**: colorless oil; $[\alpha]_D^{25}$ +20.2 (*c* 1.00, $CHCl_3$); IR (neat): 3444, 3371, 2977, 2957, 2935, 2871, 1714, 1695, 1522, 1391, 1367, 1252, 1174, 1043, 1026 cm^{-1}; ^1H NMR (400 MHz, $CDCl_3$): δ 0.91 (3H, d, J = 6.3 Hz), 0.94 (3H, d, J = 6.8 Hz), 1.27 (3H, t, J = 7.3 Hz), 1.32–1.35 (2H, m) 1.44 (9H, s), 1.64–1.71 (1H, m), 2.46–2.48 (2H, m), 3.54 (1H, d, J = 2.9 Hz), 3.67 (1H, br s), 4.01 (1H, br s), 4.17 (2H, dd, J = 6.8, 7.3 Hz), 4.68 (1H, d, J = 8.8 Hz); ^{13}C NMR (100 MHz, $CDCl_3$): δ 14.1, 21.5, 23.6, 24.7, 28.3 (3C), 38.1, 38.8, 52.7, 60.7, 71.3, 79.4, 156.1, 172.7; HRMS (EI): *m/z* calcd for $C_{15}H_{29}NO_5$ (M^+) 303.2046, found 303.2039.

4.1.2. (R)-ethyl 4-(tert-butoxycarbonylamino)-6-methyl-3-oxoheptanoate (**17**)

2.6 M Jones reagent (2.21 mL, 5.8 mmol) was added dropwise to a stirred solution of **15** (1.16 g, 3.8 mmol) in acetone (40 mL) at 0 °C, and stirring was continued for 1 h at room temperature. The mixture was diluted with Et_2O (150 mL). The organic layer was washed with saturated aqueous $NaHCO_3$ (2 × 40 mL) and brine (2 × 40 mL), then dried over Na_2SO_4. Concentration of the solvent in vacuo afforded a residue, which was purified by column chromatography (hexane/EtOAc 8:1 → 4:1) to give **17** (0.98 g, 86%) as a colorless oil. $[\alpha]_D^{25}$ +18.4 (*c* 1.03, $CHCl_3$); IR (neat): 3358, 2961, 2935, 2872, 1748, 1714, 1513, 1391, 1367, 1317, 1252, 1167, 1044, 1030 cm^{-1}; ^1H NMR (400 MHz, $CDCl_3$): δ 0.95 (3H, d, J = 3.1 Hz), 0.96 (3H, d, J = 3.4 Hz), 1.28 (3H, t, J = 7.3 Hz), 1.36–1.42 (1H, m), 1.45 (9H, s), 1.56–1.77 (1H, m), 3.55 (2H, dd, J = 15.6, 15.6 Hz), 4.20 (2H, dd, J = 7.3, 7.3 Hz), 4.34–4.39 (1H, m), 4.93 (1H, d, J = 7.3 Hz); ^{13}C NMR (100 MHz, $CDCl_3$): δ 14.1, 21.6, 23.2, 24.8, 28.3 (3C), 39.9, 46.3, 58.2, 61.4, 80.1, 155.5, 167.0, 172.7; HRMS (EI): *m/z* calcd for $C_{15}H_{27}NO_5$ (M^+) 301.1889, found 301.1883.

4.1.3. Conversion of compound **17** to compound **16** by stereoselective reduction

KBH_4 (1.30 g, 4.3 mmol) was added in small portions to a stirred solution of **17** (1.30 g, 4.3 mmol) in MeOH (40 mL) at −40 °C. After 5 h, the reaction was quenched with 10% aqueous citric acid at 0 °C (adjusted to pH 3). After concentration of the reaction mixture in vacuo, water (15 mL) was added, and the resulting mixture was extracted with CH_2Cl_2 (4 × 15 mL). The combined extracts were washed with brine (2 × 15 mL), then dried over Na_2SO_4. Concentration of the solvent in vacuo afforded a residue, which was purified by column chromatography (hexane/EtOAc 5:1 → 4:1) to give **16** (1.04 g, 90%). The IR, ^1H and ^{13}C NMR, mass spectra of this sample were identical with those recorded for compound **16**.

4.1.4. (3S,4R)-ethyl 4-(tert-butoxycarbonylamino)-3-(tert-butyldimethylsiloxy)-6-methylheptanoate (**18**)

tert-butyldimethylsilyl chloride (TBSCl) (1.15 g, 7.7 mmol) was added to a stirred solution of **16** (0.78 g, 2.3 mmol) in DMF (30 mL) containing imidazole (1.04 g, 15 mmol) at room temperature. After 24 h, the reaction mixture was diluted with Et_2O (120 mL), and the organic layer was washed successively with 3% aqueous HCl (2 × 30 mL), saturated aqueous $NaHCO_3$ (2 × 30 mL) and brine (2 × 30 mL), then dried over Na_2SO_4. Concentration of the solvent in vacuo afforded a residue, which was purified by column chromatography (hexane/EtOAc 10:1 → 5:1) to give **18** (1.08 g, 99%) as a colorless oil. $[\alpha]_D^{25}$ +15.5 (*c* 1.01, $CHCl_3$); IR (neat): 3371, 3273, 2957, 2931, 2901, 2857, 1703, 1504, 1472, 1390, 1366, 1284, 1253, 1174, 1094, 1051, 1028, 1007, 836, 777 cm^{-1}; ^1H NMR (400 MHz, $CDCl_3$): δ 0.01 (3H, s), 0,07 (3H, s), 0.84 (9H, br s), 0.84–0.90 (6H, m), 1.21–1.25 (5H, m), 1.40 (9H, s), 1.57–1.65 (1H, m), 2.40 (1H, d, J = 6.4 Hz), 3.61 (1H, s), 4.06–4.16 (3H, m), 4.39 (1H, d, J = 8.3 Hz); ^{13}C NMR (100 MHz, $CDCl_3$): δ −4.9, −4.8, 14.1, 18.0, 21.5, 23.7, 24.6, 25.7 (3C), 28.3 (3C), 38.5, 39.8, 53.0, 60.4, 71.7, 78.8, 155.3, 171.2; HRMS (EI): *m/z* calcd for $C_{21}H_{43}NO_5Si$ (M^+) 417.2911, found 417.2893.

4.1.5. (3S,4R)-allyl 4-(tert-butoxycarbonylamino)-3-(tert-butyldimethylsiloxy)-6-methylheptanoate (**20**)

1 M NaOH (16 mL, 16 mmol) was added dropwise to a stirred solution of **18** (1.30 g, 3.1 mmol) in EtOH (30 mL) at room temperature. After 6 h, the mixture was diluted with 10% aqueous HCl (20 mL) at 0 °C, and the resulting mixture was extracted with EtOAc (3 × 30 mL). The combined extracts were washed with brine (2 × 20 mL), then dried over Na_2SO_4. Concentration of the solvent in vacuo afforded (3*S*,4*R*)-4-(*tert*-butoxycarbonylamino)-3-(*tert*-butyldimethylsiloxy)-6-methylheptanoic acid (**19**) as a white amorphous solid, which was used for the next reaction without further purification.

Allyl bromide (0.54 mL, 6.2 mmol) was added to a stirred solution of **19** (1.21 g, 3.1 mmol) in DMF (30 mL) containing K_2CO_3 (1.31 g, 9.4 mmol) at room temperature. After 6 h, the reaction was diluted with water (15 mL) at room temperature, and the resulting mixture was extracted with Et_2O (4 × 30 mL). The combined

extracts were washed successively with 3% aqueous HCl (2 × 20 mL), saturated aqueous $NaHCO_3$ (2 × 20 mL) and brine (2 × 20 mL), then dried over Na_2SO_4. Concentration of the solvent in vacuo afforded a residue, which was purified by column chromatography (hexane/EtOAc 5:1) to give **20** [1.03 g, 77% (2 steps from **18**)] as a pale yellow oil. $[\alpha]_D^{25}$ +16.1 (*c* 1.03, $CHCl_3$); IR (neat): 2956, 2930, 2898, 2857, 1739, 1717, 1703, 1389, 1366, 1253, 1171, 1095, 836, 777 cm^{-1}; ^1H NMR (400 MHz, $CDCl_3$): δ −0.02 (3H, s), −0.05 (3H, s), 0.82 (9H, s), 0.82–0.88 (6H, m), 1.19–1.24 (2H, m), 1.38 (9H, s), 1.55–1.63 (1H, m), 2.42 (2H, d, J = 6.4 Hz), 3.59 (1H, br s), 4.16 (1H, br s), 4.35 (1H, d, J = 8.3 Hz), 4.48–4.57 (2H, m), 5.17–5.29 (2H, m), 5.82–5.92 (1H, m); ^{13}C NMR (100 MHz, $CDCl_3$): δ −4.8, −4.7, 18.0, 21.6, 23.7, 24.6, 25.8 (3C), 28.3 (3C), 38.5, 39.7, 53.1, 65.3, 70.5, 71.7, 118.4, 132.0, 155.3, 171.0; HRMS (EI): *m/z* calcd for $C_{22}H_{43}NO_5Si$ (M^+) 429.2911, found 429. 2927.

*4.1.6. (3S,4R)-allyl 4-[(S)-2-(tert-butoxycarbonylamino)-3-(tritylthio)propanamido]-3-(tert-butyldimethylsiloxy)-6-methylheptanoate (**22**)*

Trimethylsilyl trifluoromethanesulfonate (TMSOTf) (2.13 mL, 12 mmol) was added to a stirred solution of **20** (632 mg, 1.5 mmol) in CH_2Cl_2 (30 mL) in the presence of 2,6-lutidine (1.70 mL, 15 mmol) at room temperature. After 1 h, MeOH (5.0 mL) was added to the reaction mixture at 0 °C, and stirring was continued for 1 h at room temperature. The reaction mixture was concentrated in vacuo to afford (3S,4R)-allyl 4-amino-3-(*tert*-butyldimethylsiloxy)-6-methylheptanoate (**21**) as a colorless oil, which was immediately used for the next reaction due to its instability (prone to form a γ-lactam ring).

i-Pr_2NEt (0.37 mL, 2.21 mmol) was added dropwise to a stirred solution of the crude amine **21** (480 mg, 15 mmol) and *N*-Boc-*S*-trityl-D-cysteine (**14**) [13a] (1.02 g, 2.21 mmol) in MeCN (50 mL) containing (benzotriazol-1-yloxy)tripyrrolidinophosphonium hexafluorophosphate (PyBOP) (918 mg, 1.8 mmol) at room temperature under argon. After 3 h, the mixture was diluted with Et_2O (80 mL), and the organic layer was washed successively with 3% aqueous HCl (2 × 30 mL), saturated aqueous $NaHCO_3$ (2 × 30 mL) and brine (2 × 30 mL), then dried over Na_2SO_4. Concentration of the solvent in vacuo afforded a residue, which was purified by column chromatography (hexane/EtOAc 1:1) to give **22** (781 mg, 69%, 2 steps from **20**) as a colorless oil. $[\alpha]_D^{25}$ +5.0 (*c* 1.00, $CHCl_3$); IR (neat): 2956, 2930,1736, 1692, 1512, 1492, 1366, 1252, 1169, 833, 777, 700 cm^{-1}; ^1H NMR (400 MHz, $CDCl_3$): δ −0.01 (3H, s), 0.05 (3H, s), 0.83–0.88 (6H, m), 0.85 (9H, s), 1.25–1.31 (2H, m), 1.40 (9H, s), 1.52–1.58 (1H, m), 2.41–2.51 (3H, m), 2.76 (1H, dd, J = 6.8, 6.8 Hz), 3.88–3.98 (2H, m), 4.10–4.14 (1H, m), 4.53–4.56 (2H, m), 4.72 (1H, d, J = 6.8 Hz), 5.21–5.33 (2H, m), 5.85–5.94 (1H, m), 6.08 (1H, d, J = 8.3 Hz), 7.19–7.42 (15H, m); ^{13}C NMR (100 MHz, $CDCl_3$): δ −4.7, −4.6, 18.0, 21.5, 23.9, 24.5, 25.8 (3C), 28.2 (3C), 33.4, 38.7, 39.8, 51.8, 53.5, 65.3, 67.1, 71.7, 80.3, 118.5, 126.8 (3C), 128.0 (6C), 129.6 (6C), 132.0, 144.5 (3C), 149.8, 170.0, 170.9 ppm; HRMS (FAB): *m/z* calcd for $C_{44}H_{62}N_2O_6SSi$ (M^+) 774.4098, found 774.4091.

*4.1.7. (3S,4R)-allyl 4-[(S)-2-amino-3-(tritylthio)propanamido]-3-(tert-butyldimethylsiloxy)-6-methylheptanoate (**8**)*

TMSOTf (0.90 mL, 5.0 mmol) was added dropwise to a stirred solution of **22** (781 mg, 1.0 mmol) in CH_2Cl_2 (11 mL) containing 2,6-lutidine (0.91 mL, 5.0 mmol) at room temperature. After 1 h, MeOH (2.2 mL) was added to the reaction mixture at 0 °C, and stirring was continued for 1 h at room temperature. The mixture was concentrated in vacuo to afford a residue, which was purified by column chromatography (hexane/EtOAc 2:1) to give **8** (593 mg, 88%) as a white amorphous solid. $[\alpha]_D^{25}$ +3.8 (*c* 1.00, $CHCl_3$); IR (neat): 2954, 2929, 2895, 2856, 1736, 1671, 1508, 1471, 1445, 1254, 1172, 1084, 835, 777, 743, 700 cm^{-1}; ^1H NMR (400 MHz, $CDCl_3$): δ 0.82–0.89 (6H, m), 0.86 (9H, s), 1.25–1.37 (2H, m), 1.49–1.51 (1H, m), 2.42–2.52 (2H, m), 2.58 (1H, dd, J = 8.3, 8.3 Hz), 2.69 (1H, dd, J = 3.4, 3.9 Hz), 3.10 (1H, dd, J = 3.4, 3.9 Hz), 3.89–3.94 (1H, m), 4.11–4.15 (1H, m) 4.55 (2H, d, J = 5.9 Hz), 5.22–5.33 (2H, m), 5.85–5.94 (1H, m), 7.14 (1H, d, J = 9.3 Hz), 7.21 (2H, d, J = 7.3 Hz), 7.26–7.44 (15H, m); ^{13}C NMR (100 MHz, $CDCl_3$): δ −4.7, −4.6, 17.9, 21.6, 23.8, 24.6, 25.8 (3C), 37.3, 38.3, 40.1, 51.5, 53.7, 65.3, 66.8, 71.8, 118.5, 126.7 (3C), 127.9 (6C), 129.6 (6C), 132.0, 144.6, 171.0, 172.2; HRMS (FAB): *m/z* calcd for $C_{39}H_{55}N_2O_4SSi$ (M^+ + H) 674.3574, found 675.3662.

*4.1.8. (3S,4R)-allyl 3-(tert-butyldimethylsiloxy)-4-{(S)-2-[(R)-2-[(S,E)-3-(4-methoxybenzyloxy)-7-(tritylthio)hept-4-enoylamino]propionylamino]-3-tritylthio(propionylamino)}-6-methylheptanoate (**23**)*

i-Pr_2NEt (73 μL, 0.43 mmol) was added dropwise to a stirred solution of **8** (108 mg, 0.16 mmol) and (*R*)-2-[(*S,E*)-3-(4-methoxybenzyloxy)-7-(tritylthio)hept-4-enamido]propanoic acid (**10**) [13a] (100 mg, 0.16 mmol) in CH_2Cl_2 (3.2 mL) containing *O*-(7-azabenzotriazol-1-yl)-*N,N,N′,N′*-tetramethyluronium hexafluorophosphate (HATU) (81.2 mg, 0.21 mmol) and 1-hydroxy-7-azabenzotriazole (HOAt) (28.6 mg, 0.21 mmol) at −30 °C under argon. After 3 h, the reaction mixture was diluted with $CHCl_3$ (30 mL). The organic layer was washed successively with 10% aqueous HCl (2 × 10 mL), saturated aqueous $NaHCO_3$ (2 × 10 mL) and brine (2 × 10 mL), then dried over Na_2SO_4. Concentration of the solvent in vacuo afforded a residue, which was purified by column chromatography (hexane/EtOAc 1:1) to give **23** (169 mg, 84%) as a colorless viscous liquid. $[\alpha]_D^{25}$ +12.0 (*c* 1.00, $CHCl_3$); IR (neat): 282, 2956, 2930, 1735, 1626, 1541, 1512, 1444, 1247, 1172, 1083, 835, 743, 699 cm^{-1}; ^1H NMR (400 MHz, $CDCl_3$): δ −0.01 (3H, s), 0.05 (3H, s), 0.81–0.86 (15H, m), 1.16 (3H, d, J = 7.3), 1.32 (2H, m), 1.45–1.48 (1H, m), 2.08–2.12 (2H, m), 2.19–2.23 (2H, m), 2.31 (1H, dd, J = 3.4, 2.9 Hz), 2.40–2.52 (4H, m), 2.83 (1H, dd, J = 7.3, 7.8 Hz), 3.79 (3H, s), 3.89–4.02 (2H, m), 4.06–4.14 (3H, m), 4.19–4.27 (1H, m), 4.36 (1H, d, J = 10.7 Hz), 4.53–4.55 (2H, m), 5.19–5.45 (4H, m), 5.85–5.94 (1H, m), 6.19 (1H, d, J = 9.3 Hz), 6.53 (1H, d, J = 8.3 Hz), 6.82–6.84 (2H, m), 6.96 (1H, d, J = 6.3 Hz), 7.14–7.29 (20H, d), 7.36–7.43 (12H, m); ^{13}C NMR (100 MHz, $CDCl_3$): δ −4.7, −4.6, 17.0, 18.0, 21.5, 23.8, 24.7, 25.8 (3C), 29.6, 31.2, 33.1, 39.1, 39.6, 42.4, 49.0, 52.1, 52.2, 55.3, 65.2, 66.6, 66.9, 70.0, 71.7, 76.4, 113.9 (2C), 118.3, 126.6 (3C), 126.8 (3C), 127.8 (6C), 128.0 (6C), 129.48 (6C), 129.52 (8C), 129.6, 129.8 (2C), 132.1, 144.3 (3C), 144.8 (3C), 159.4, 169.3, 171.2, 171.23, 172.0; HRMS (FAB): *m/z* calcd for $C_{76}H_{92}N_3O_8S_2Si$ (M^+ + H) 1266.7665, found 1266.6104.

*4.1.9. (3S,4R)-allyl 3-(tert-butyldimethylsiloxy)-4-{(S)-2-[(R)-2-[(S,E)-3-hydroxy-7-(tritylthio)hept-4-enoylamino]propionylamino]-3-tritylthio(propionylamino)}-6-methylheptanate (**24**)*

2,3-dichloro-5,6-dicyano-1,4-benzoquinone (DDQ) (73.5 mg, 0.27 mmol) was added in small portions to a stirred solution of **23** (160 mg, 0.13 mmol) in CH_2Cl_2/H_2O 9:1 (13 mL) at room temperature. After 3 h, the reaction mixture was diluted with $CHCl_3$ (60 mL), and the organic layer was washed with saturated aqueous $NaHCO_3$ (2 × 20 mL) and brine (2 × 20 mL), then dried over Na_2SO_4. Concentration of the solvent in vacuo afforded a residue, which was purified by column chromatography (hexane/EtOAc 3:2) to give **24** (147 mg, 99%) as a colorless viscous liquid. $[\alpha]_D^{25}$ +10.4 (*c* 1.00, $CHCl_3$); IR (neat): 3283, 2955, 2929, 1734, 1626, 1525, 1489, 1444, 1253, 1169, 1090, 833, 742, 699, 675 cm^{-1}; ^1H NMR (400 MHz, $CDCl_3$): δ 0.01 (3H, s), 0.06 (3H, s), 0.83–0.88 (15H, m), 1.26–1.34 (5H, m), 1.47–1.54 (1H, m), 2.04–2.09 (2H, m), 2.17–2.26 (2H, m), 2.31 (1H, dd, J = 2.4, 2.4 Hz), 2.41–2.54 (4H, m), 2.71 (1H, dd, J = 7.3, 7.3 Hz), 3.08 (1H, d, J = 1.9 Hz), 3.91–3.96 (1H, m), 4.09–4.22 (2H, m), 4.30–4.35 (2H, m), 4.48–4.57 (2H,m), 5.20–5.48 (4H, m), 5.84–5.94 (1H, m), 6.06 (1H, d,

J = 7.3 Hz), 6.14 (1H, d, J = 9.3 Hz), 6.89 (1H, d, J = 8.3 Hz), 7.17–7.31 (18H, m), 7.37–7.43 (12H, m); ^{13}C NMR (100 MHz, $CDCl_3$): δ −4.7, −4.6, 17.5, 18.0, 21.5, 23.8, 24.7, 25.8 (3C), 31.28, 31.34, 33.3, 39.3, 39.6, 43.9, 49.6, 52.3 (2C), 65.3, 66.6, 66.9, 69.7, 71.7, 118.3, 126.6 (3C), 126.9 (3C), 127.9 (6C), 128.1 (6C), 129.5 (6C), 129.6 (6C), 130.0, 132.1, 132.5, 144.3 (3C), 144.9 (3C), 169.5, 171.3, 171.6, 171.8; HRMS (FAB): m/z calcd for $C_{68}H_{84}N_3O_7S_2Si$ (M^+ + H) 1146.6180, found 1146.5529.

*4.1.10. (7S,11R,14S,17R,18S,E)-18-(tert-butyldimethylsilyloxy)-7-hydroxy-17-isobutyl-11-methyl-9,12,15-trioxo-1,1,1,-triphenyl-14-tritylthiomethyl-2-thia-10,13,16-triazaicos-5-en-20-oic acid (**6**)*

Morpholine (7.3 μL, 84 μmol) was added dropwise to a stirred solution of **24** (47.8 mg, 42 μmol) in THF (4.2 mL) containing $Pd(PPh_3)_4$ (4.8 mg, 4.2 μmol) at room temperature under argon. After 30 min, the reaction mixture was diluted with EtOAc (30 mL), and the organic layer was washed with 10% aqueous HCl (2 × 10 mL) and brine (2 × 10 mL), then dried over Na_2SO_4. Concentration of the solvent in vacuo afforded a residue, which was purified by column chromatography ($CHCl_3$/MeOH 20:1) to give **6** (45.7 mg, 99%) as a white amorphous solid. $[\alpha]_D^{25}$ −11.2 (c 1.00, $CHCl_3$); IR (neat): 3295, 3081, 3058, 3018, 2955, 2928, 2856, 1714, 1659, 1651, 1644, 1635, 1538, 1488, 1444, 1256, 1094, 835, 752, 700 cm^{-1}; ^{1}H NMR (400 MHz, $CDCl_3$): δ 0.07 (6H, d, J = 4.9 Hz), 0.79–0.91 (15H, m), 1.35 (3H, d, J = 7.3 Hz), 1.38–1.49 (2H, m), 1.52–1.57 (1H, m), 2.02–2.07 (2H, m), 2.17–2.26 (3H, m), 2.31–2.37 (2H, m), 2.44 (1H, dd, J = 3.4, 3.9 Hz), 2.53 (1H, dd, J = 6.3, 6.3 Hz), 2.82 (1H, dd, J = 6.8, 6.8 Hz), 3.86–3.96 (2H, m), 4.25–4.35 (3H, m), 5.28–5.44 (2H, m), 6.38 (1H, d, J = 5.9 Hz), 6.54 (1H, d, J = 8.3 Hz), 7.06 (1H, d, J = 8.3 Hz), 7.15–7.30 (18H, m), 7.34–7.43 (12H, m); ^{13}C NMR (100 MHz, $CDCl_3$): δ −4.7, −4.5, 17.2, 17.9, 21.4, 24.0, 24.8, 25.8 (3C), 29.7, 31.3, 33.1, 39.9, 39.96, 44.03, 50.3, 52.6, 53.1, 66.7, 66.8, 69.7, 71.7, 126.7 (3C), 127.0 (3C), 127.9 (6C), 128.1 (6C), 129.4 (6C), 129.6 (6C), 132.0, 132.1, 144.1 (3C), 144.8, 170.4, 172.25, 172.30, 172.4; HRMS (FAB): m/z calcd for $C_{65}H_{80}N_3O_7S_2Si$ (M^+ + H) 1106.5542, found 1106.5216.

*4.1.11. (2S,6R,9S,12R,13S)-13-(tert-butyldimethylsiloxy)-12-isobutyl-6-methyl-2-[(E)-4-(tritylthio)but-1-enyl]-9-tritylthiomethyl-1-oxa-5,8,11-triazacyclopentadecane-4,7,10,15-tetraone (**25**)*

A solution of **6** (45.7 mg, 41 μmol) in CH_2Cl_2 (4.1 mL) was added very slowly to a stirred solution of 2-methyl-6-nitrobenzoic anhydride (MNBA) (18.5 mg, 54 μmol) in CH_2Cl_2 (41 mL, 1.0 mM concentration) containing 4-dimethylaminopyridine (DMAP) (18.5 mg, 54 μmol) at room temperature over 14 h. After 1 h, the mixture was diluted with CH_2Cl_2 (50 mL), and the organic layer was washed successively with saturated aqueous $NaHCO_3$ (2 × 20 mL), water (2 × 20 mL) and brine (2 × 20 mL), then dried over Na_2SO_4. Concentration of the solvent in vacuo afforded a residue, which was purified by column chromatography (hexane/EtOAc 1:1) to give **25** (33.5 mg, 75%) as a white amorphous solid. $[\alpha]_D^{25}$ −9.3 (c 1.01, $CHCl_3$); IR (neat): 3468, 3323, 2954, 2927, 1735, 1651, 1537, 1489, 1444, 1259, 1094, 832, 743, 700, 668 cm^{-1}; ^{1}H NMR (400 MHz, $CDCl_3$): δ 0.01 (3H, s), 0.05 (3H, s), 0.78–0.93 (15H, m), 1.22–1.40 (5H, m), 1.72–1.83 (1H, m), 1.94–2.08 (2H, m), 2.16–2.20 (2H, m), 2.33–2.41 (2H, m), 2.47–2.53 (2H, m), 2.71 (1H, d, J = 13.2 Hz), 3.28–3.35 (2H, m), 3.70 (1H, br s), 4.18 (1H, t, J = 6.3, 6.8 Hz), 4.30–4.33 (1H, m), 5.29–5.35 (1H, m), 6.23 (1H, br s), 6.60 (1H, br s), 6.94 (1H, d, J = 7.3 Hz), 7.18–7.40 (30H, m); ^{13}C NMR (100 MHz, $CDCl_3$): δ −4.7, −4.3, 17.20, 17.9, 21.3, 23.8, 25.0, 25.8 (3C), 31.1, 31.3, 32.5, 38.8, 39.4, 41.5, 50.4, 53.1, 54.4, 66.7, 69.8, 70.2, 77.2, 126.7 (3C), 126.8 (3C), 127.9 (6C), 128.0 (6C), 128.5, 129.50 (6C), 129.54 (6C), 131.9, 144.5 (3C), 144.8 (3C), 169.4, 169.9, 170.5, 171.5; HRMS (FAB): m/z calcd for $C_{65}H_{78}N_3O_6S_2Si$ (M^+ + H) 1088.5389, found 1088.5118.

*4.1.12. (1S,5S,6R,9S,20R,E)-5-(tert-butyldimethylsilyloxy)-6-isobutyl-20-methyl-2-oxa-11,12-dithia-7,19,22-triazabicyclo[7.7.6]docos-15-ene-3,8,18,21-tetraone (**26**)*

A solution of **25** (33.5 mg, 31 μmol) in CH_2Cl_2/MeOH 9:1 (7.5 mL) was added dropwise to a vigorously stirred solution of I_2 (78.4 mg, 0.31 mmol) in CH_2Cl_2/MeOH 9:1 (62 mL, 0.5 mM concentration) over 10 min at room temperature. After 10 min, the reaction was quenched with 10% aqueous $Na_2S_2O_3$ (30 mL) at room temperature. The resulting mixture was diluted with CH_2Cl_2 (90 mL), and the organic layer was washed with saturated aqueous $NaHCO_3$ (2 × 30 mL) and brine (2 × 30 mL), then dried over Na_2SO_4. Concentration of the solvent in vacuo afforded a residue, which was purified by column chromatography ($CHCl_3$/MeOH 30:1) to give **26** (17.6 mg, 95%) as a white amorphous solid. $[\alpha]_D^{25}$ −3.4 (c 1.00, $CHCl_3$); IR (neat): 3426, 2953, 2857, 1747, 1653, 1541, 1259, 1146, 1127, 833 cm^{-1}; ^{1}H NMR (400 MHz, $CDCl_3$): δ 0.09 (3H, s), 0.13 (3H, s), 0.89–0.93 (15H, m), 1.50 (3H, d, J = 7.3 Hz), 1.54–1.66 (2H, m), 1.96–2.05 (1H, m), 2.44–2.57 (3H, m), 2.64–2.70 (3H, m), 3.03–3.11 (2H, m), 3.21 (2H, dd, J = 7.3, 7.3 Hz), 3.41 (1H, br s), 4.24–4.31 (1H, m), 4.50–4.54 (1H, m), 4.91 (1H, br s), 5.64–5.68 (2H, m), 5.88 (1H, s), 6.08 (1H, br s) 6.72 (1H, d, J = 9.8 Hz), 7.47 (1H, d, J = 6.8 Hz); ^{13}C NMR (100 MHz, $CDCl_3$): δ −4.8, −4.3, 16.7, 17.9, 21.1, 23.7, 25.3, 25.7 (3C), 33.3, 38.8, 38.9, 39.9, 40.6, 40.9, 52.2, 54.5, 55.9, 69.3, 70.8, 129.6, 132.5, 168.5, 168.8, 171.2, 171.3; HRMS (FAB): m/z calcd for $C_{27}H_{48}N_3O_6S_2Si$ (M^+ + H) 601.8941, found 602.2757.

*4.1.13. Spiruchostatin C (**4**)*

HF pyridine (0.55 mL) was added to a stirred solution of **26** (35.4 mg, 58 μmol) in pyridine (1.1 mL) at room temperature. After 14 h, the reaction mixture was diluted with EtOAc (60 mL), and the organic layer was washed successively with 3% aqueous HCl (3 × 15 mL), saturated aqueous $NaHCO_3$ (2 × 15 mL) and brine (2 × 15 mL), then dried over Na_2SO_4. Concentration of the solvent in vacuo afforded a residue, which was purified by column chromatography ($CHCl_3$/MeOH 10:1) to give **4** (spiruchostatin C) (26.0 mg, 93%) as a white amorphous solid. $[\alpha]_D^{25}$ −59.4 (c 0.20, $CHCl_3$) {lit. [10] $[\alpha]_D^{25}$ −60.0 (c 0.10, $CHCl_3$)}; IR (neat): 3455, 3369, 3311, 2998, 2953, 2868, 1728, 1659, 1546, 1530, 1275, 1161 cm^{-1}; ^{1}H NMR (400 MHz, $CDCl_3$): δ 0.92 (6H, d, J = 6.3), 1.50–1.56 (4H, m), 1.59–1.68 (1H, m), 2.05–2.13 (1H, m), 2.42 (1H, dd, J = 11.7, 11.7 Hz), 2.57 (1H, d, J = 13.2 Hz), 2.64–2.76 (5H, m), 2.99–3.06 (1H, m), 3.17–3.20 (2H, m), 3.30 (1H, br s), 3.41 (1H, dd, J = 7.3, 7.3 Hz), 4.23–4.29 (1H, m), 4.34–4.41 (1H, m), 4.84–4.89 (1H, m) 5.46 (1H, br s), 5.67 (1H, d, J = 15.1 Hz), 5.93 (1H, d, J = 3.4 Hz), 6.36 (1H, t, J = 12.2, 13.7 Hz), 6.72 (1H, d, J = 9.3 Hz), 7.49 (1H, d, J = 7.3 Hz); ^{13}C NMR (100 MHz, $CDCl_3$): δ 16.6, 21.2, 23.5, 25.2, 29.7, 32.9, 38.7, 38.8, 40.7, 41.1, 52.3, 54.8, 56.3, 70.6, 70.9, 128.7, 133.5, 168.8, 170.8, 171.0, 171.6; HRMS (FAB): m/z calcd for $C_{21}H_{34}N_3O_6S_2$ (M^+ + H) 487.6332, found 488.1890. The IR, ^{1}H and ^{13}C NMR, and HRMS spectrum are essentially identical with those reported for natural spiruchostatin C [10].

*4.1.14. (3S,4R)-allyl 3-(tert-butyldimethylsiloxy)-4-{(S)-2-[(R)-2-[(S,E)-3-(4-methoxybenzyloxy)-7-(tritylthio)hept-4-enoylamino]isovaleroylamino]-3-tritylthio(propionylamino)}-5-methylhexanoate (**27**)*

i-Pr_2NEt (0.17 mL, 1.0 mmol) was added dropwise to a stirred solution of 4-[(*S*)-2-amino-3-(tritylthio)propanamido]-3-(*tert*-butyldimethylsiloxy)-5-methylhexanoate (**9**) [13a] (258 mg, 0.39 mmol) and (*R*)-2-[(*S*,*E*)-3-(4-methoxybenzyloxy)-7-(tritylthio) hept-4-enamido]-3-methylbutanoic acid (**11**) [13a] (247 mg, 0.39 mmol) in CH_2Cl_2 (8.0 mL) containing HATU (193 mg, 0.51 mmol) and HOAt (69.2 mg, 0.51 mmol) at −30 °C under argon. After 3 h, the reaction mixture was diluted with $CHCl_3$ (50 mL). The organic layer was washed successively with 10% aqueous HCl (2 × 20 mL), saturated aqueous $NaHCO_3$ (2 × 20 mL) and brine

(2 × 20 mL), then dried over Na_2SO_4. Concentration of the solvent in vacuo afforded a residue, which was purified by column chromatography (hexane/EtOAc 2:1) to give **27** (469 mg, 94%) as a colorless viscous liquid. $[\alpha]_D^{25}$ +5.6 (*c* 1.00, $CHCl_3$); IR (neat): 3290, 3058, 2958, 2930, 2857, 1734, 1637, 1540, 1514, 1444, 1389, 1248, 1173, 1092, 1036, 830, 743, 700 cm^{-1}; ^1H NMR (400 MHz, $CDCl_3$): δ 0.02 (3H, s), 0.06 (3H, s), 0.68 (3H, d, *J* = 6.8 Hz), 0.76–0.86 (9H, m), 0.82 (9H, s), 1.86–2.13 (4H, m), 2.17–2.23 (2H, m), 2.34–2.57 (6H, m), 2.76 (1H, dd, *J* = 7.8, 12.9 Hz), 3.75–3.82 (1H, m), 3.78 (3H, s), 3.93–4.02 (2H, m), 4.09 (1H, dd, *J* = 5.9, 7.3 Hz), 4.15–4.22 (2H, m), 4.39 (1H, d, *J* = 10.7 Hz), 4.46 (1H, dd, *J* = 5.9, 13.2 Hz), 4.53 (1H, dd, *J* = 5.9, 12.7 Hz), 5.18–5.31 (3H, m), 5.49 (1H, dt, *J* = 6.8, 15.5 Hz), 5.81–5.91 (1H, m), 6.01 (1H, d, *J* = 10.2 Hz), 6.30 (1H, d, *J* = 7.8 Hz), 6.80 (2H, d, *J* = 8.3 Hz), 7.03 (1H, d, *J* = 7.8 Hz), 7.16–7.45 (32H, m); ^{13}C NMR (100 MHz, $CDCl_3$): δ −4.7, −4.6, 16.9, 17.6, 17.9, 19.5, 20.3, 25.7 (3C), 28.0, 29.9, 31.2, 31.3, 33.2, 39.4, 42.5, 52.4, 55.3, 58.4, 58.5, 65.2, 66.5, 67.1, 69.4, 70.0, 76.5, 113.8 (2C), 118.3, 126.6 (3C), 126.8 (3C), 127.9 (6C), 128.1 (6C), 129.5 (12C), 129.7, 129.9 (2C), 129.9, 132.1, 133.2, 144.3 (3C), 144.8 (3C), 159.3, 169.8, 171.1, 171.2, 171.6; HRMS (FAB): *m/z* calcd for $C_{77}H_{93}N_3O_8S_2SiNa$ (M^+ + Na) 1318.5810, found 1318.5787.

*4.1.15. (3S,4R)-allyl 3-(tert-butyldimethylsiloxy)-4-{(S)-2-[(R)-2-[(S,E)-3-hydroxy-7-(tritylthio)hept-4-enoylamino]isovaleroylamino]-3-tritylthio(propionylamino)}-5-methylhexanate (**28**)*

DDQ (166 mg, 0.73 mmol) was added in small portions to a stirred solution of **27** (469 mg, 0.37 mmol) in CH_2Cl_2/H_2O 9:1 (18 mL) at room temperature. After 3 h, the reaction mixture was diluted with $CHCl_3$ (60 mL), and the organic layer was washed with saturated aqueous $NaHCO_3$ (2 × 20 mL) and brine (2 × 20 mL), then dried over Na_2SO_4. Concentration of the solvent in vacuo afforded a residue, which was purified by column chromatography (hexane/EtOAc 1:1) to give **28** (336 mg, 79%) as a colorless viscous liquid. $[\alpha]_D^{25}$ +11.2 (*c* 1.00, $CHCl_3$); IR (neat): 3270, 3058, 2958, 2928, 2856, 1736, 1673, 1633, 1549, 1490, 1444, 1390, 1254, 1174, 1093, 837, 743, 700, 674 cm^{-1}; ^1H NMR (400 MHz, $CDCl_3$): δ 0.00 (3H, s), 0.05 (3H, s), 0.79–0.85 (9H, m), 0.81 (9H, s), 0.92 (3H, d, *J* = 6.8 Hz), 1.87–1.92 (1H, m), 2.05 (1H, d, *J* = 7.3 Hz), 2.17–2.26 (4H, m), 2.33 (1H, dd, *J* = 2.7, 13.7 Hz), 2.41 (1H, dd, *J* = 7.3, 15.6 Hz), 2.49–2.61 (4H, m), 3.43 (1H, br s), 3.73–3.78 (1H, m), 3.99 (1H, dd, *J* = 8.3, 14.9 Hz), 4.17 (1H, dt, *J* = 3.4, 7.2 Hz), 4.23 (1H, dd, *J* = 4.9, 8.3 Hz), 4.33–4.37 (1H, m), 4.49 (1H, dd, *J* = 5.9, 13.3 Hz), 4.52 (1H, dd, *J* = 5.9, 13.2 Hz), 5.19–5.31 (2H, m), 5.36 (1H, dd, *J* = 5.9, 15.4 Hz), 5.51 (1H, dt, *J* = 6.3, 15.5 Hz), 5.81–5.93 (2H, m), 6.04 (1H, d, *J* = 8.3 Hz), 6.93 (1H, d, *J* = 8.3 Hz), 7.17–7.43 (30H, m); ^{13}C NMR (100 MHz, $CDCl_3$): δ −4.7, −4.7, 16.9, 17.4, 17.9, 19.5, 20.2, 25.7 (3C), 28.1, 29.7, 31.30, 31.34, 33.3, 39.34, 44.0, 52.6, 58.5, 58.6, 65.3, 66.6, 67.0, 69.3, 69.8, 118.4, 126.6 (3C), 126.8 (3C), 127.9 (6C), 128.0 (6C), 129.48 (6C), 129.54 (6C), 129.9, 132.0, 132.5, 144.3 (3C), 144.8 (3C), 170.2, 170.9, 171.6, 171.7 ppm; HRMS (FAB): *m/z* calcd for $C_{69}H_{86}N_3O_7S_2Si$ (M^+ + H) 1159.5598, found 1160.5654.

*4.1.16. (7S,11R,14S,17R,18S,E)-18-(tert-butyldimethylsilyloxy)-7-hydroxy-11,17-diisopropyl-9,12,15-trioxo-1,1,1-triphenyl-14-tritylthiomethyl-2-thia-10,13,16-triazaicos-5-en-20-oic acid (**7**)*

Morpholine (46 μL, 0.53 mmol) was added dropwise to a stirred solution of **28** (308 mg, 0.27 mmol) in THF (13 mL) containing $Pd(PPh_3)_4$ (30.7 mg, 27 μmol) at room temperature under argon. After 30 min, the reaction mixture was diluted with EtOAc (30 mL), and the organic layer was washed with 10% aqueous HCl (2 × 10 mL) and brine (2 × 10 mL), then dried over Na_2SO_4. Concentration of the solvent in vacuo afforded a residue, which was purified by column chromatography ($CHCl_3$/MeOH 20:1) to give **7** (270 mg, 90%) as a white amorphous solid. $[\alpha]_D^{25}$ −0.8 (*c* 1.00, $CHCl_3$); ^1H NMR (400 MHz, $CDCl_3$): δ 0.00 (6H, s), 0.74–0.79 (9H, m), 0.79 (9H, s), 0.87 (3H, d, *J* = 6.8 Hz), 1.94–2.02 (3H, m), 2.12–2.36 (6H, m), 2.41–2.50 (2H, m), 2.63–2.68 (1H, m), 3.69–3.75 (1H, m), 4.02–4.07 (2H, m), 4.18–4.21 (1H, m), 4.27–4.32 (1H, m), 5.32 (1H, dd, *J* = 5.9, 15.4 Hz), 5.41 (1H, dt, *J* = 6.4, 15.1 Hz), 6.22 (1H, d, *J* = 9.8 Hz), 6.33 (1H, br s), 7.02 (1H, br s), 7.10–7.42 (30H, m); ^{13}C NMR (100 MHz, $CDCl_3$): δ −4.8, −4.5, 16.7, 17.4, 17.9, 19.5, 20.3, 25.7 (3C), 27.9, 29.6, 31.3, 33.2, 39.7, 43.9, 53.2, 58.8, 59.0, 66.5, 66.9, 69.1, 69.6, 126.6 (3C), 126.7 (3C), 128.5 (6C), 128.6 (6C), 129.45 (6C), 129.51 (6C), 131.5, 132.5, 144.3 (3C), 144.8 (3C), 170.4, 171.5, 172.2, 174.0; IR (neat): 282, 3058, 2958, 1717, 1637, 1544, 1489, 1438, 1388, 1255, 1181, 1120, 1093, 1034, 836, 744, 723, 699 cm^{-1}; HRMS (FAB): *m/z* calcd for $C_{66}H_{81}N_3O_7S_2SiK$ (M^+ + K) 1158.4922, found 1158.4901.

*4.1.17. (2S,6R,9S,12R,13S)-13-(tert-butyldimethylsiloxy)-6,12-diisopropyl-2-[(E)-4-(tritylthio)but-1-enyl]-9-tritylthiomethyl-1-oxa-5,8,11-triazacyclopentadecane-4,7,10,15-tetraone (**29**)*

A solution of **7** (34.8 mg, 31 μmol) in CH_2Cl_2 (3.0 mL) was added very slowly to a stirred solution of MNBA (13.9 mg, 31 μmol) in CH_2Cl_2 (30 mL, 1.0 mM concentration) containing DMAP (11.4 mg, 93 μmol) at room temperature over 14 h. After 1 h, the mixture was diluted with CH_2Cl_2 (50 mL), and the organic layer was washed successively with saturated aqueous $NaHCO_3$ (2 × 20 mL), water (2 × 20 mL) and brine (2 × 20 mL), then dried over Na_2SO_4. Concentration of the solvent in vacuo afforded a residue, which was purified by column chromatography (hexane/EtOAc 1:1) to give **29** (28.9 mg, 85%) as a white amorphous solid. $[\alpha]_D^{25}$ −6.3 (*c* 0.64, $CHCl_3$); ^1H NMR (400 MHz, $CDCl_3$): δ −0.10 (3H, s), 0.00 (3H, s), 0.76–0.80 (6H, m), 0.80 (9H, s), 0.95 (3H, d, *J* = 6.8 Hz), 1.00 (3H, d, J = 6.8 Hz), 1.93–2.09 (4H, m), 2.16–2.20 (2H, m), 2.31 (1H, dd, *J* = 6.3, 16.1 Hz), 2.38 (1H, dd, *J* = 2.9, 16.6 Hz), 2.45–2.52 (2H, m), 2.61 (1H, d, *J* = 8.3 Hz), 3.24–3.29 (2H, m), 3.54–3.60 (1H, m), 3.94–3.99 (2H, m), 5.37 (1H, dd, *J* = 6.8, 15.4 Hz), 5.44–5.49 (1H, m), 5.67 (1H, dt, *J* = 6.3, 15.6 Hz), 6.11 (1H, d, *J* = 7.8 Hz), 6.60 (1H, d, *J* = 4.9 Hz), 7.20–7.43 (31H, m); ^{13}C NMR (100 MHz, $CDCl_3$): δ −4.9, −3.9, 15.6, 17.9, 18.6, 19.4, 20.5, 25.8 (3C), 27.2, 29.7, 30.4, 30.9, 31.4, 32.0, 41.2, 42.1, 58.3, 59.6, 66.6, 66.9, 68.9, 72.2, 126.6 (3C), 126.8 (3C), 127.9 (6C), 128.0 (6C), 128.2, 129.47 (6C), 129.52 (6C), 133.4, 144.4 (3C), 144.8 (3C), 169.6, 170.1, 170.6, 173.1 ppm; IR (neat): 3468, 3323, 2954, 2927, 1735, 1651, 1537, 1489, 1444, 1259, 1094, 832, 743, 700, 668 cm^{-1}; HRMS (FAB): *m/z* calcd for $C_{66}H_{79}N_3O_6S_2SiNa$ (M^+ + Na) 1124.5077, found 1124.5040.

*4.1.18. (1S,5S,6R,9S,20R,E)-5-(tert-butyldimethylsilyloxy)-6,20-diisopropyl-2-oxa-11,12-dithia-7,19,22-triazabicyclo[7.7.6]docos-15-ene-3,8,18,21-tetraone (**30**)*

A solution of **29** (45.0 mg, 42 μmol) in CH_2Cl_2/MeOH 9:1 (17 mL) was added dropwise to a vigorously stirred solution of I_2 (170 mg, 0.67 mmol) in CH_2Cl_2/MeOH 9:1 (84 mL, 0.5 mM concentration) over 10 min at room temperature. After 10 min, the reaction was quenched with 10% aqueous $Na_2S_2O_3$ (30 mL) at room temperature. The resulting mixture was diluted with CH_2Cl_2 (90 mL), and the organic layer was washed with saturated aqueous $NaHCO_3$ (2 × 30 mL) and brine (2 × 30 mL), then dried over Na_2SO_4. Concentration of the solvent in vacuo afforded a residue, which was purified by column chromatography ($CHCl_3$/MeOH 30:1) to give **30** (36.1 mg, 88%) as a white amorphous solid. $[\alpha]_D^{25}$ +13.6 (*c* 0.28, $CHCl_3$); IR (neat): 3335, 2956, 1747, 1670, 1541, 1258, 1158, 948, 831, 781 cm^{-1}; ^1H NMR (400 MHz, $CDCl_3$): δ 0.10 (3H, s), 0.16 (3H, s), 0.79 (3H, d, *J* = 6.8 Hz), 0.83 (9H, s), 0.87 (3H, d, *J* = 6.8 Hz), 0.95 (3H, d, *J* = 6.8 Hz), 0.99 (3H, d, *J* = 6.8 Hz), 2.06–2.14 (1H, m), 2.18–2.26 (1H, m), 2.47–2.53 (3H, m), 2.58–2.91 (6H, m), 3.04 (1H, dd, *J* = 7.3, 13.2 Hz), 3.70–3.72 (1H, m), 4.07 (1H, t, *J* = 5.2 Hz), 4.75 (1H, dt, *J* = 3.4, 9.8 Hz), 4.95–4.99 (1H, m), 5.54 (1H, d, *J* = 15.1 Hz), 5.61–5.62 (1H, m), 5.71 (1H, d, *J* = 4.4 Hz), 6.50 (1H, t, *J* = 13.4 Hz), 6.62

(1H, d, J = 9.8 Hz), 7.00 (1H, J = 6.8 Hz); ^{13}C NMR (100 MHz, $CDCl_3$): δ −4.8, −4.2, 17.0, 18.0, 19.1, 19.8, 21.0, 25.7 (3C), 29.0, 29.2, 35.2, 39.2, 40.6, 41.3, 44.2, 53.6, 61.8, 62.8, 67.4, 68.7, 128.3, 133.4, 168.8, 169.1, 170.0, 171.2 ppm; HRMS (FAB): m/z calcd for $C_{28}H_{49}N_3O_6S_2Si$ (M^+ + H) 615.2832, found 615.2914.

*4.1.19. Spiruchostatin D (**5**)*

HF·pyridine (0.55 mL) was added to a stirred solution of **30** (35.4 mg, 58 μmol) in pyridine (1.1 mL) at room temperature. After 14 h, the reaction mixture was diluted with EtOAc (60 mL), and the organic layer was washed successively with 3% aqueous HCl (3 × 15 mL), saturated aqueous $NaHCO_3$ (2 × 15 mL) and brine (2 × 15 mL), then dried over Na_2SO_4. Concentration of the solvent in vacuo afforded a residue, which was purified by column chromatography ($CHCl_3$/MeOH 10:1) to give **5** (spiruchostatin D) (26.8 mg, 93%) as a white amorphous solid. $[\alpha]_D^{25}$ −59.2 (c 0.29, MeOH) {lit. [12] $[\alpha]_D^{25}$ −65.3 (c 0.20, MeOH)}; ^{1}H NMR (400 MHz, $CDCl_3$): δ 0.93 (3H, d, J = 6.8 Hz), 1.04 (3H, d, J = 6.8 Hz), 1.07 (3H, d, J = 6.8 Hz), 1.09 (3H, d, J = 7.3 Hz), 2.25–2.34 (1H, m), 2.36–2.44 (1H, m), 2.46–2.54 (1H, m), 2.62 (1H, d, J = 13.2 Hz), 2.66–2.79 (5H, m), 2.98–3.15 (3H, m), 3.38 (1H, d, J = 6.8, 13.2 Hz), 3.51–3.57 (1H, m), 4.10 (1H, t, J = 5.1 Hz), 4.56–4.58 (1H, m), 4.93–4.98 (1H, m), 5.50–5.52 (1H, m), 5.68 (1H, d, J = 15.1 Hz), 5.92–5.95 (1H, m), 6.54 (1H, t, J = 12.7 Hz), 6.74 (1H, d, J = 9.3 Hz), 7.39 (1H, d, J = 7.3 Hz); ^{13}C NMR (100 MHz, $CDCl_3$): δ 19.3, 19.6, 19.7, 20.6, 29.1, 29.6, 34.0, 39.7, 40.2, 40.8, 42.6, 54.3, 62.1, 63.4, 69.4, 70.4, 128.1, 133.9, 168.9, 170.0, 171.0, 171.8 ppm; IR (neat): 3375, 3342, 2964, 2932, 2875, 1731, 1660, 1534, 1519, 1266, 1162, 979, 911, 755, 733 cm^{-1}; HRMS (FAB): m/z calcd for $C_{20}H_{32}N_3O_6S_2$ (M^+ + H) 501.196, found 501.2057. The IR, ^{1}H and ^{13}C NMR, and HRMS spectrum are essentially identical with those reported for natural spiruchostatin D [12].

4.2. Biological evaluation

4.2.1. HDACs preparation and enzyme inhibition assay [20]

In a 100-mm dish, 293 T cells (1–2 × 10^7) were grown for 24 h and transiently transfected with 10 μg each of the vector pcDNA3-HDAC1 for human HDAC1 or pcDNA3-mHDA2/HDAC6 for mouse HDAC6, using the LipofectAMINE2000 reagent (Invitrogen). After successive cultivation in DMEM for 24 h, the cells were washed with PBS and lysed by sonication in lysis buffer containing 50 mM Tris–HCl (pH 7.5), 120 mM NaCl, 5 mM EDTA, and 0.5% NP40. The soluble fraction collected by microcentrifugation was precleared by incubation with protein A/G agarose beads (Roche). After the cleared supernatant had been incubated for 1 h at 4 °C with 4 μg of an anti-FLAG M2 antibody (Sigma–Aldrich Inc.) for HDAC1 and HDAC6, the agarose beads were washed three times with lysis buffer and once with histone deacetylase buffer consisting of 20 mM Tris–HCl (pH 8.0), 150 mM NaCl, and 10% glycerol. The bound proteins were released from the immune complex by incubation for 1 h at 4 °C with 40 μg of the FLAG peptide (Sigma–Aldrich Inc.) in histone deacetylase buffer (200 μL). The supernatant was collected by centrifugation. For the enzyme assay, 10 μL of the enzyme fraction was added to 1 μL of fluorescent substrate (2 mM Ac-KGLGK(Ac)-MCA) and 9 μL of histone deacetylase buffer, and the mixture was incubated at 37 °C for 30 min. The reaction was stopped by the addition of 30 μL of trypsin (20 mg/mL) and incubated at 37 °C for 15 min. The released aminomethylcoumarin (AMC) was measured using a fluorescence plate reader. The 50% inhibitory concentrations (IC_{50}) were determined as the means with SD calculated from at least three independent dose–response curves.

4.2.2. Cell-growth inhibition assay [19]

This experiment was carried out at the Cancer Chemotherapy Center, Japanese Foundation for Cancer Research. The screening panel consisted of the following 39 human cancer cell lines (HCC panel): breast cancer HBC-4, BSY-1, HBC-5, MCF-7, and MDA-MB-231; brain cancer U-251, SF-268, SF-295, SF-539, SNB-75, and SNB-78; colon cancer HCC2998, KM-12, HT-29, HCT-15, and HCT-116; lung cancer NCI-H23, NCI-H226, NCI-H522, NCI-H460, A549, DMS273, and DMS114; melanoma LOX-IMVI; ovarian cancer OVCAR-3, OVCAR-4, OVCAR-5, OVCAR-8, and SK-OV-3; renal cancer RXF-631L and ACHN; stomach cancer St-4, MKN1, MKN7, MKN28, MKN45, and MKN74; prostate cancer DU-145 and PC-3. The GI_{50} (50% cell-growth inhibition) value for these cell lines was determined by using the sulforhodamine B colorimetric method.

Acknowledgements

We are grateful to the Screening Committee of New Anticancer Agents supported by a Grant-in-Aid for Scientific Research on Priority Area 'Cancer' from the Ministry of Education, Culture, Sports, Science and Technology, Japan (MEXT) for the biological evaluation of compounds **4** and **5**. This study was supported by a Grant-in-Aid for the Strategic Research Foundation Program at Private Universities (2010–2014) from MEXT and a Grant-in-Aid for Scientific Research (C) (Nos. 21590018 and 24590017) from MEXT.

Appendix A. Supplementary data

Supplementary data related to this article can be found at http://dx.doi.org/10.1016/j.ejmech.2012.12.023.

References

[1] (a) S. Kanno, N. Maeda, A. Tomizawa, S. Yomogida, T. Katoh, M. Ishikawa, Int. J. Oncol. 41 (2012) 862–868;
(b) S. Kanno, N. Maeda, A. Tomizawa, S. Yomogida, T. Katoh, M. Ishikawa, Int. J. Oncol. 40 (2012) 1391–1396;
(c) T. Ai, H. Cui, L. Chen, Curr. Med. Chem. 19 (2012) 475–487;
(d) O. Khan, N.B. La Thangue, Immunol. Cell. Biol. 90 (2012) 85–94;
(e) P. Perego, V. Zuco, L. Gatti, F. Zunino, Biochem. Pharmacol. 83 (2012) 987–994;
(f) B.N. Singh, H. Zhou, J. Li, T. Tipton, B. Wang, G. Shao, E.N. Gilbert, Q. Li, S.-W. Jiang, Future Oncol. 7 (2011) 1415–1428;
(g) R. Harrod, Leuk. Res. 35 (2011) 1436–1437;
(h) B. Venugopal, T.R.J. Evans, Curr. Med. Chem. 18 (2011) 1658–1671;
(i) E.M. Bertino, G.A. Otterson, Expert Opin. Inv. Drugs 20 (2011) 1151–1158;
(j) S. Consalvi, V. Saccone, L. Giordani, G. Minetti, C. Mozzetta, P.L. Puri, Mol. Med. 17 (2011) 457–465;
(k) V. Carafa, A. Nebbioso, L. Altucci, Recent Pat. Anti-Cancer Drug Discov. 6 (2011) 131–145;
(l) A. Quintás-Cardama, F.P.S. Santos, G. Garcia-Manero, Leukemia 25 (2011) 226–235;
(m) P.A. Marks, Expert Opin. Inv. Drugs 19 (2010) 1049–1066;
(n) P. Bertrand, Eur. J. Med. Chem. 45 (2010) 2095–2116;
(o) A.A. Lane, B.A. Chabner, J. Clin. Oncol. 27 (2009) 5459–5468;
(p) X. Ma, H.H. Ezzeldin, R.B. Diasio, Drugs 69 (2009) 1911–1934.
[2] (a) G.R. Leggatt, B. Gabrielli, Immunol. Cell. Biol. 90 (2012) 33–38;
(b) A.K. Oyelere, P.C. Chen, W. Guerrant, S.C. Mwakwari, R. Hood, Y. Zhang, Y. Fan, J. Med. Chem. 52 (2009) 456–468;
(c) L.M. Butler, D.B. Agus, H.I. Scher, B. Higgins, A. Rose, C. Cordon-Cardo, H.T. Thaler, R.A. Rifkind, P.A. Marks, V.M. Richon, Cancer Res. 60 (2000) 5165–5170;
(d) A. Saito, T. Yamashita, Y. Mariko, Y. Nosaka, K. Tsuchiya, T. Ando, T. Suzuki, T. Tsuruo, O. Nakanishi, Proc. Natl. Acad. Sci. U S A 96 (1999) 4592–4597;
(e) R.D. Glick, S.L. Swendeman, D.C. Coffey, R.A. Rifkind, P.A. Marks, V.M. Richon, M.P. La Quaglia, Cancer Res. 59 (1999) 4392–4399.
[3] (a) X.J. Yang, E. Seto, Nat. Rev. Mol. Cell. Biol. 9 (2008) 206–218;
(b) T. Kouzarides, Cell 128 (2007) 693–705;
(c) B.E. Bernstein, A. Meissner, E.S. Lander, Cell 128 (2007) 669–681;
(d) P. Trojer, D. Reinberg, Cell 125 (2006) 213–217.
[4] (a) O. Witt, H.E. Deubzer, T. Milde, I. Oehme, Cancer Lett. 277 (2009) 8–21;
(b) M. Haberland, R.L. Montgomery, E.N. Olson, Nat. Rev. Genet. 10 (2009) 32–42;
(c) M.A. Holbert, R. Marmorstein, Curr. Opin. Struct. Biol. 15 (2005) 673–680;
(d) S. Voelt-Mahlknecht, A.D. Ho, U. Mahlnecht, Int. J. Mol. Med. 16 (2005) 589–598;

(e) A.J.M. De Ruijter, A.H. Van Gennip, H.N. Caron, S. Kemp, A.B.P. Van Kuilenburg, Biochem. J. 370 (2003) 737–749.
[5] (a) T.A. McKinsey, J. Mol. Cell. Cardiol. 51 (2011) 491–496;
(b) A.P. Kozikowski, K.V. Butler, Curr. Pharm. Des. 14 (2008) 505–528;
(c) A.V. Bieliauskas, M.K.H. Pflum, Chem. Soc. Rev. 37 (2008) 1402–1413;
(d) S. Senese, K. Zaragoza, S. Minardi, I. Muradore, S. Ronzoni, A. Passafaro, L. Bernard, G.F. Draetta, M. Alcalay, C. Seiser, S. Chiocca, Mol. Cell. Biol. 27 (2007) 4784–4795;
(e) P. Kahnberg, A.J. Lucke, M.P. Glenn, G.M. Boyle, J.D.A. Tyndall, P.G. Parsons, D.P. Fairlie, J. Med. Chem. 49 (2006) 7611–7622;
(f) S. Chang, T.A. McKinsey, C.L. Zhang, J.A. Richardson, J.A. Hill, E.N. Olson, Mol. Cell. Biol. 24 (2004) 8467–8476.
[6] (a) K.M. Van der Molen, W. McCulloch, C.J. Pearce, N.H. Oberlies, J. Antibiot. 64 (2011) 525–531;
(b) C. Grant, F. Rahman, R. Piekarz, C. Peer, R. Frye, R.W. Robey, E.R. Gardner, W.D. Figg, S.E. Bates, Expert Rev. Anticancer Ther. 10 (2010) 997–1008.
[7] M.H. Shah, P. Binkley, K. Chan, J. Xiao, D. Arbogast, M. Collamore, Y. Farra, D. Young, M. Grever, Clin. Cancer Res. 12 (2006) 3997–4003.
[8] (a) H. Ueda, H. Nakajima, Y. Hori, T. Fujita, M. Nishimura, T. Goto, M. Okuhara, J. Antibiot. 47 (1994) 301–310;
(b) N. Shigematsu, H. Ueda, S. Takase, H. Tanaka, J. Antibiot. 47 (1994) 311–314;
(c) H. Ueda, T. Manda, S. Matsumoto, S. Mukumoto, F. Nishigaki, I. Kawamura, K. Shimomura, J. Antibiot. 47 (1994) 315–323;
(d) M. Okuhara, T. Goto, T. Fujita, Y. Hori, H. Ueda (Fujisawa Pharmaceutical Co. Ltd., Japan), JP 3141296A (1991).
[9] Y. Masuoka, A. Nagai, K. Shin-ya, K. Furihata, K. Nagai, K. Suzuki, Y. Hayakawa, H. Seto, Tetrahedron Lett. 42 (2001) 41–44.
[10] N. Shindo, A. Terada, M. Mori, N. Amino, K. Hayata, K. Nagai, Y. Hayakawa, K. Shin-ya, Y. Masuoka (Yamanouchi Pharmaceutical Co. Ltd., Japan), JP 348340A (2001).
[11] Recently, Klausmeyer et al. reported the isolation and structural elucidation of a novel spiruchostatin congener from *Burkholderia thailandensis* and assigned it an improper name 'spiruchostatin C'. To avoid nomenclatural confusions, maybe it should be named as one of a series of burkholdacs such as 'burkholdac C', see: P. Klausmeyer, S.M. Shipley, K.M. Zuck, T.G. McCloud J. Nat. Prod. 74 (2011) 2039–2044.
[12] K. Nagai, M. Taniguchi, N. Shindo, Y. Terada, M. Mori, N. Amino, K. Suzumura, I. Takahashi, M. Amase (Yamanouchi Pharmaceutical Co. Ltd., Japan), PCT WO 20460 A1 (2004).
[13] (a) K. Narita, T. Kikuchi, K. Watanabe, T. Takizawa, T. Oguchi, K. Kudo, K. Matsuhara, H. Abe, T. Yamori, M. Yoshida, T. Katoh, Chem. Eur. J. 15 (2009) 11174–11186;
(b) S. Wen, G. Packham, A. Ganesan, J. Org. Chem. 73 (2008) 9353–9361;
(c) T.J. Greshock, D.M. Johns, Y. Noguchi, R.M. Williams, Org. Lett. 10 (2008) 613–616;
(d) K.W. Li, J. Wu, W. Xing, J.A. Simon, J. Am. Chem. Soc. 118 (1996) 7237–7238.
[14] (a) N.A. Calandra, Y.L. Cheng, K.A. Kocak, J.S. Miller, Org. Lett. 11 (2009) 1971–1974;
(b) Y. Iijima, A. Munakata, K. Shin-ya, A. Ganesan, T. Doi, T. Takahashi, Tetrahedron Lett. 50 (2009) 2970–2972;
(c) T. Takizawa, K. Watanabe, K. Narita, K. Kudo, T. Oguchi, H. Abe, T. Katoh, Heterocycles 76 (2008) 275–290;
(d) T. Doi, Y. Iijima, K. Shin-ya, A. Ganesan, T. Takahashi, Tetrahedron Lett. 47 (2006) 1177–1180;
(e) A. Yurek-George, F. Habens, M. Brimmell, G. Packham, A. Ganesan, J. Am. Chem. Soc. 126 (2004) 1030–1031.
[15] (a) S. Fuse, K. Okada, Y. Iijima, A. Munakata, K. Machida, T. Takahashi, M. Takagi, K. Shin-ya, T. Doi, Org. Biomol. Chem. 9 (2011) 3825–3833;
(b) T. Takizawa, K. Watanabe, K. Narita, T. Oguchi, H. Abe, T. Katoh, Chem. Commun. (2008) 1677–1679.
[16] E.P. Johnson, M.P. Hubieki, A.P. Combs, C.A. Teleha, Synthesis (2011) 4023–4026.
[17] (a) I. Shiina, T. Katoh, S. Nagai, M. Hashizume, Chem. Rec. 9 (2009) 305–320;
(b) I. Shiina, A. Sasaki, T. Kikuchi, H. Fukui, Chem. Asian J. 3 (2008) 462–472;
(c) I. Shiina, Chem. Rev. 107 (2007) 239–273;
(d) I. Shiina, M. Hashizume, Tetrahedron 62 (2006) 7934–7939;
(e) I. Shiina, M. Kubota, H. Oshiumi, M. Hashizume, J. Org. Chem. 69 (2004) 1822–1830.
[18] A. Yurek-George, A.R.L. Ceil, A.H.K. Mo, S. Wen, H. Rogers, F. Habens, S. Maeda, M. Yoshida, G. Packham, A. Ganesan, J. Med. Chem. 50 (2007) 5720–5726.
[19] (a) S. Yaguchi, Y. Fukui, I. Koshimizu, H. Yoshimi, T. Matsuno, H. Gouda, S. Hirono, K. Yamazaki, T. Yamori, J. Natl. Cancer Inst. 98 (2006) 545–556;
(b) T. Yamori, Cancer Chemother. Pharmacol. 52 (Suppl. 1) (2003) 74–79;
(c) S. Dan, T. Tsunoda, O. Kitahara, R. Yanagawa, H. Zembutsu, T. Katagiri, K. Yamazaki, Y. Nakamura, T. Yamori, Cancer Res. 62 (2002) 1139–1147;
(d) T. Yamori, A. Matsunaga, S. Sato, K. Yamazaki, A. Komi, K. Ishizu, I. Mita, H. Edatsugi, Y. Matsuba, K. Takezawa, O. Nakanishi, H. Kohno, Y. Nakajima, H. Komatsu, T. Andoh, T. Tsuruo, Cancer Res. 59 (1999) 4042–4049.
[20] G.M. Shivashimpi, S. Amagai, T. Kato, N. Nishino, S. Maeda, T.G. Nishino, M. Yoshida, Bioorg. Med. Chem. 15 (2007) 7830–7839.

Tetrahedron Letters 54 (2013) 3949–3952

Contents lists available at SciVerse ScienceDirect

Tetrahedron Letters

journal homepage: www.elsevier.com/locate/tetlet

Design and synthesis of a nucleoside and a phosphonate analogue constructed on a branched-*threo*-tetrofuranose skeleton

Y. B. Kiran, Hideaki Wakamatsu, Yoshihiro Natori, Hiroki Takahata *, Yuichi Yoshimura *

Faculty of Pharmaceutical Sciences, Tohoku Pharmaceutical University, 4-4-1 Komatsushima, Aoba-ku, Sendai 981-8558, Japan

ARTICLE INFO

Article history:
Received 21 April 2013
Revised 11 May 2013
Accepted 14 May 2013
Available online 22 May 2013

Keywords:
Nucleoside
Nucleoside phosphonate
Nucleotide
Glycosylation
Antiviral

ABSTRACT

The synthesis of a novel nucleoside phosphonate constructed on a branched-*threo*-tetrofuranose scaffold, as a potential antiviral agent, is described. The pseudosugar moiety served as the nucleoside skeleton was produced starting from 2-butyne-1,4-diol in 10-steps. Glycosylation with the pseudosugar involved stereoselective neighboring group participation of *p*-anisyl group and gave the nucleoside derivative in 94% yield. After manipulating the protecting group and introduction of a methylenephosphate unit, the synthesis of the target novel cytidine phosphonate was achieved. The resulting nucleoside, a synthetic intermediate of the nucleoside phosphonate, would also be expected to serve as a useful building block for the synthesis of novel antisense/antigene derivatives.

© 2013 Elsevier Ltd. All rights reserved.

Drug development based on nucleosides/nucleotides has resulted in the development of various medicines, the most typical examples of which are antimetabolites for use in combatting cancer and viruses. To date, a wide variety of antitumor, antiherpes and anti-HIV drugs based on nucleoside analogues are approved and used in the clinic.[1] Also drug development focused on antisense, antigene, aptamer and RNAi has long been a subject of interest. These 'nucleic acid medicines' are highly attractive since they can directly suppress or block transcription and the action of proteins that cause diseases.[2] However, many problems remain to be solved before the widespread use of nucleic acid medicines is to be achieved. This impedes the development of nucleic acid medicines. As a result, only a few nucleic acid-based drugs have been approved and their uses are limited to topical treatment.[3] One such problem to be overcome is the instability of oligo(deoxy)nucleotides (ONs) in serum due to the nuclease-catalyzed hydrolysis of the phosphodiester linkage. To avoid this problem, ONs containing modified nucleotide units are frequently used.[4] From these points of view, it is obvious that a study of the synthesis of nucleoside derivatives with emphasis on structural novelty would greatly contribute to the development of nucleic acid medicines as well as nucleoside antimetabolites. As part of our ongoing studies related to the synthesis of nucleoside derivatives,[5] we were prompted to consider a nucleoside phosphonate constructed on a novel nucleoside skeleton. Nucleoside phosphonates are promising as antiviral agents. They can bypass the conversion of nucleosides to active triphosphate forms since nucleoside phosphonate derivatives are able to skip the first phosphorylation step. An alkylphosphate unit in their structure mimics a phosphate moiety, which permits them to act as a nucleoside monophosphate.[6] In this study, we report on the synthesis of a nucleoside derivative **1** bearing a branched-*threo*-tetrofuranose scaffold as a pseudosugar moiety and a nucleoside phosphonate derivative **2** obtained from **1**. The nucleoside phosphonate **2** is promising as an anti-HIV agent since it is structurally similar to PMDTA,[7] a known anti-HIV nucleoside phosphonate. In addition, the nucleoside derivative **1** has primary and secondary hydroxyl groups in appropriate positions of the sugar moiety and might serve as a useful building block, for example, **3**, to create a novel antisense and antigene ONs (Fig. 1). This characteristic structure of nucleoside phosphonate **2** is also unique as a mimic of cidofovir, an anti-HCMV drug (vide infra).

Our first attempt to synthesize a nucleoside derivative **1** having a branched-*threo*-tetrofuranose skeleton started from 2-butyne-1,4-diol (**4**) and was intended to produce **1** as a racemic mixture. The reduction of **4** with lithium aluminum hydride under standard conditions[8] gave the (*E*)-butenediol **5** which was silylated at one primary hydroxyl group to give a mono alcohol **6**. The epoxidation of **6** by treatment with *m*CPBA afforded the epoxide **7** in good yield. To construct the pseudosugar skeleton, it was necessary to introduce a C1 unit equivalent to an aldehyde into **7**. This was achieved by nucleophilic attack of an anion generated from di(thiophenyl)methane. Lithiation of di(thiophenyl)methane by treatment with *n*-butyllithium produced the corresponding anion which, on reaction with **7**, gave the diol derivative **8** in 57%. The nucleophilic attack of the anion occurred selectively from the less

* Corresponding authors. Tel.: +81 22 727 0145; fax: +81 22 275 2013.
E-mail address: yoshimura@tohoku-pharm.ac.jp (Y. Yoshimura).

0040-4039/$ - see front matter © 2013 Elsevier Ltd. All rights reserved.
http://dx.doi.org/10.1016/j.tetlet.2013.05.062

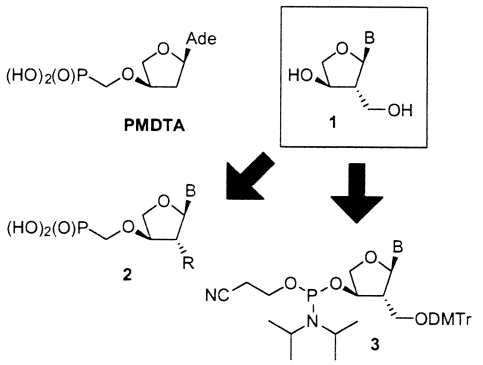
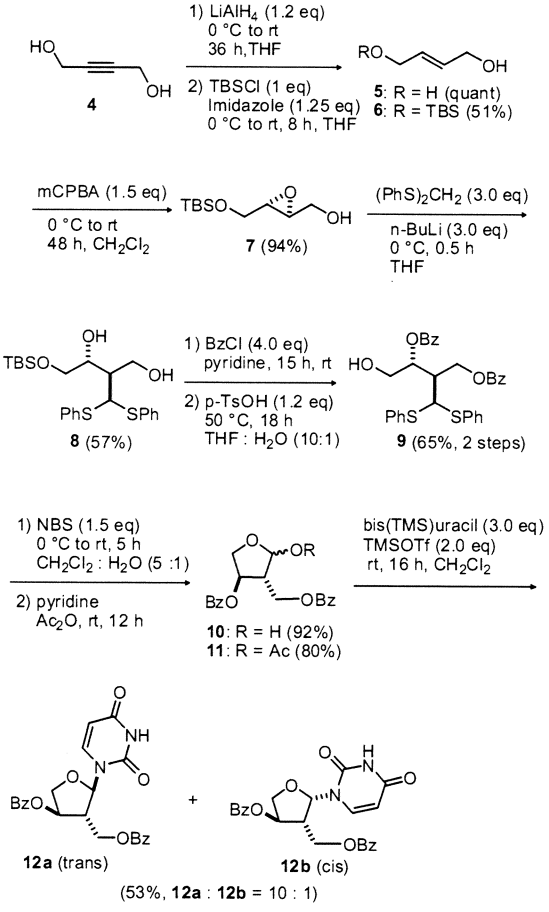


Figure 1. Structures of nucleoside **1** constructed on a branched-*threo*-tetrofuranose scaffold and nucleoside phosphonate **2**.

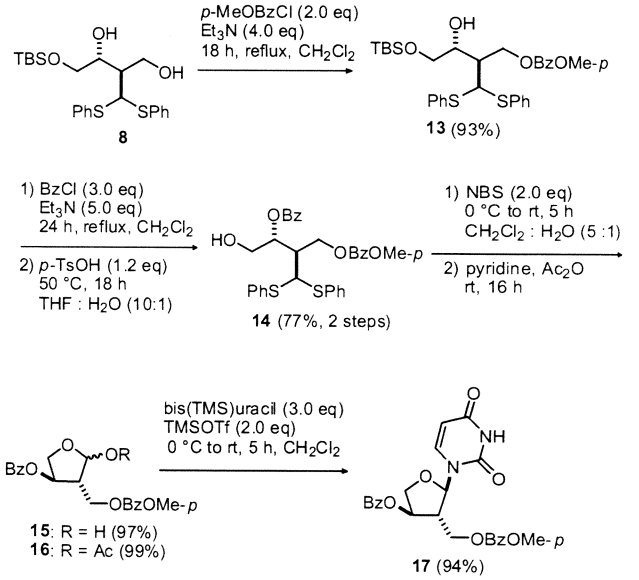
hindered side and gave **8** as a single isomer. The diol portion of **8** was protected by introducing a benzoyl group and the resulting crude product was subsequently treated with *p*-TsOH to remove the TBS group giving the dibenzoate **9**. Conversion of the di(thiophenyl)methyl unit to an aldehyde was achieved by reacting **9** with NBS[9] to spontaneously form a hemiacetal structure giving **10** in excellent yield. Acetylation of **10** in pyridine gave the pseudosugar donor **11** which was subjected to the glycosylation reaction under Vorbrüggen conditions.[10] Treatment of **11** with bis(trimethylsilyl)uracil in the presence of TMSOTf gave a mixture of **12a** and **12b** in 53% yield as an anomeric mixture in a ratio of 10:1 to **12a**:**12b** (Scheme 1).

The fact that the glycosylation gave a mixture of products in moderate yield prompted us to modify the synthetic route to the target nucleoside in order to find a more efficient glycosylation reaction. To complete this task, we intended to introduce a more electron-donating acyl group at the primary hydroxyl group of the pseudosugar donor, by which the effect of neighboring group participation would be enhanced to stabilize the intermediate for the glycosylation reaction[11] (vide infra). Compound **8** was selectively acylated with a *p*-anisyl (*p*-MeOBz) group at the primary hydroxyl group to give the *p*-anisyl derivative **13**. Following the synthetic scheme described above, the *p*-anisyl derivative **13** was converted into the pseudosugar donor **16** in four-steps. The glycosylation of **16** using the Vorbrüggen method[10] gave the nucleoside derivative **17** as a single isomer in 94% yield (Scheme 2).[12] It is noteworthy that yield and selectivity were both improved as we expected.

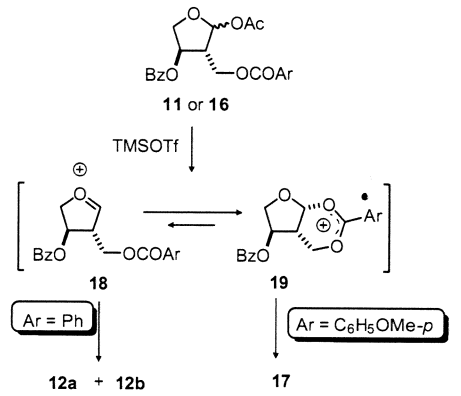
From the results mentioned above, a proposed mechanism for the glycosylation reaction is shown in Scheme 3. In both of the reaction from the pseudosugar donors **11** and **16**, the reaction with TMSOTf generates the oxocarbenium ion **18**. In addition, the



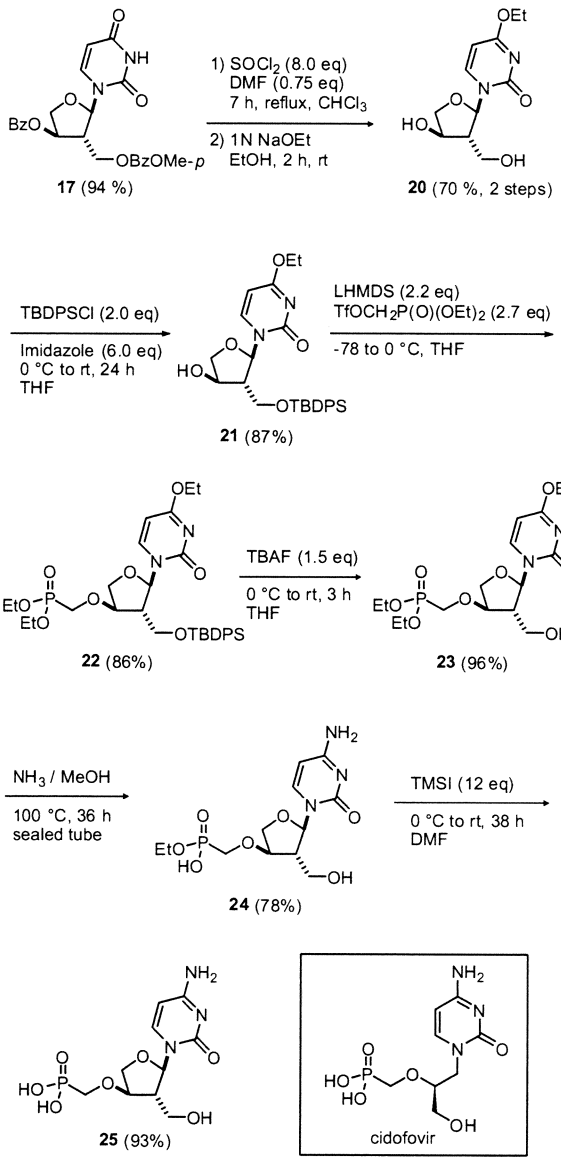
Scheme 1. Synthesis of a nucleoside derivative constructed on a branched-*threo*-tetrofuranose scaffold.



Scheme 2. Modified synthesis of a nucleoside derivative constructed on a branched-*threo*-tetrofuranose scaffold.



Scheme 3. Postulated reaction mechanism of glycosylation reaction.



Scheme 4. Synthesis of nucleoside phosphonate **25**.

neighboring group participation of the acyl group would form the cyclic acyloxonium ion **19**. It is clear that **18** and **19** are in equilibrium with each other and that **19** would be the more stabilized form.[11] When silylated uracil only reacts with **18**, the reaction gives a mixture of anomers. On the other hand, the reaction of **19** with silylated uracil would exclusively give one isomer having a 1′,2′-trans stereochemistry. In the case of **11**, the reaction predominantly gave **12a** with only minor amounts of **12b** being formed. This result suggests that the oxocarbenium ion **18** partly contributes, although most of the reaction proceeds through **19**. To realize a further shift in the equilibrium toward **19**, the more electron-donating *p*-anisyl group was introduced, as described above. Indeed, the reaction of **16** gave the nucleoside **17** as the sole product, which is consistent with our proposed mechanism (Scheme 3).

Completion of the synthesis of a nucleoside constructed on a branched-*threo*-tetrofuranose scaffold led us to our second project, that is, the synthesis of a nucleoside phosphonate derivative. Compound **17** was converted into a 4-ethoxypyrimidone derivative in preparation for its assembly into a nucleoside phosphonate and the conversion of uracil into cytosine, since our final target was the production of a cytidine phosphonate derivative. Treatment of **17** with the Vilsmeyer reagent gave a 4-chloropyrimidone derivative.[13] This unstable intermediate was quickly treated with sodium ethoxide to give the deprotected 4-ethoxypyrimidone derivative **20**. After again protecting the primary hydroxyl group with a TBDPS group, the resulting **21** was assembled by the reaction with diethyl [(trifluoromethanesulfonyl)oxy]methanephosphonate and LHMDS[14] to give the phosphonate **22** in 86% yield. After deprotection of the silyl group, the conversion of **22** to a cytosine derivative via reacting it with methanolic ammonia at 100 °C in a sealed tube gave compound **24**, one ethyl group of which was unexpectedly deprotected. Finally, deprotection of remaining ethyl group by treatment with TMSI gave the desired cytidine phosphonate **25** in good yield (Scheme 4).

In conclusion, we report on the design and synthesis of a novel nucleoside constructed on a branched-*threo*-tetrofuranose skeleton which has the potential to serve as a useful nucleotide building block for synthesizing novel ONs for antisense and antigene applications. As a demonstration of its synthetic usefulness, we also synthesized a new cytidine phosphonate **25** from the obtained nucleoside. It is interesting to note that the cytidine phosphonate **25** has a unique structure that is analogous to cidofovir[15] as well as PMDTA[7] and would be expected to have promise for use as an antiviral agent. Biological evaluations of **25** are currently in progress and the results will be reported elsewhere.

Acknowledgements

This work was supported in part by a Grant-in-Aid for Scientific Research (No. 24590143, Y.Y.) from JSPS and by a grant of Strategic Research Foundation Grant-aided Project for Private Universities from Ministry of Education, Culture, Sport, Science, and Technology, Japan (MEXT), 2010–2014.

Supplementary data

Supplementary data associated with this article can be found, in the online version, at http://dx.doi.org/10.1016/j.tetlet.2013.05.062.

References and notes

1. (a) Elnaggar, M.; Giovannetti, E.; Peters, G. J. *Curr. Pharm. Des.* **2012**, *18*, 2811–2829; (b) Razonable, R. R. *Mayo Clin. Proc.* **2011**, *86*, 1009–1026; (c) Cihlar, T.; Ray, A. S. *Antiviral Res.* **2010**, *85*, 39–58; (d) Meng, W. D.; Qing, F. L. *Curr. Top. Med. Chem.* **2006**, *6*, 1499–1528.
2. (a) Fukuda, N. *Med. Chem.* **2006**, *2*, 13–19; (b) Frederickson, R. M. *Mol. Ther.* **2005**, *12*, 775–776.
3. Keefe, A. D.; Pai, S.; Ellington, A. *Nat. Rev. Drug Disc.* **2010**, *9*, 537–550.
4. (a) Burnett, J. C.; Rossi, J. J. *Chem. Biol.* **2012**, *19*, 60–71; (b) Lebreton, J.; Escudier, J. M.; Arzel, L.; Len, C. *Chem. Rev.* **2010**, *110*, 3371–3418; (c) Bramsen, J. B.; Laursen, M. B.; Nielsen, A. F.; Hansen, T. B.; Bus, C.; Langkjaer, N.; Babu, B. R.; Hojland, T.; Abramov, M.; Van Aerschot, A.; Odadzic, D.; Smicius, R.; Haas, J.; Andree, C.; Barman, J.; Wenska, M.; Srivastava, P.; Zhou, C.; Honcharenko, D.; Hess, S.; Muller, E.; Bobkov, G. V.; Mikhailov, S. N.; Fava, E.; Meyer, T. F.; Chattopadhyaya, J.; Zerial, M.; Engels, J. W.; Herdewijn, P.; Wengel, J.; Kjems, J. *Nucleic Acids Res.* **2009**, *37*, 2867–2881.
5. (a) Yoshimura, Y.; Yamazaki, Y.; Saito, Y.; Natori, Y.; Imamichi, T.; Takahata, H. *Bioorg. Med. Chem. Lett.* **2011**, *21*, 3313–3316. Recent works:; (b) Yoshimura, Y.; Yamazaki, Y.; Saito, Y.; Takahata, H. *Tetrahedron* **2009**, *65*, 9091–9102; (c) Yoshimura, Y.; Ohta, M.; Imahori, T.; Imamichi, T.; Takahata, H. *Org. Lett.* **2008**, *10*, 3449–3452; (d) Yoshimura, Y.; Asami, K.; Matsui, H.; Tanaka, H.; Takahata, H. *Org. Lett.* **2006**, *8*, 6015–6018.
6. Ray, A. S.; Hostetler, K. Y. *Antiviral Res.* **2011**, *92*, 277–291.
7. Wu, T.; Froeyen, M.; Kempeneers, V.; Pannecouque, C.; Wang, J.; Busson, R.; De Clercq, E.; Herdewijn, P. *J. Am. Chem. Soc.* **2005**, *127*, 5056–5065.
8. Organ, M. G.; Cooper, J. T.; Rogers, L. R.; Soleymanzadeh, F.; Paul, T. *J. Org. Chem.* **2000**, *65*, 7959–7970.
9. Sato, K.; Akai, S.; Shoji, H.; Sugita, N.; Yoshida, S.; Nagai, Y.; Suzuki, K.; Nakamura, Y.; Kajihara, Y.; Funabashi, M.; Yoshimura, J. *J. Org. Chem.* **2008**, *73*, 1234–1242.

10. (a) Vorbrüggen, H.; Krolikiewicz, K.; Bennua, B. *Chem. Ber.* **1981**, *114*, 1234–1255; (b) Ueda, T.; Watanabe, S.-I. *Chem. Pharm. Bull.* **1985**, *33*, 3689–3695.
11. Naka, T.; Minakawa, N.; Abe, H.; Kaga, D.; Matsuda, A. *J. Am. Chem. Soc.* **2000**, *122*, 7233–7243.
12. The stereochemistry of **17** was determined by NOE experiments after converting to compound **21** in which 0.3% of NOE at H-1′ was observed when irradiated at H-3′ and 1.2% of NOE was observed at H-6 of pyrimidine ring when irradiated at H-2′.
13. Matsuda, A.; Itoh, H.; Takenuki, K.; Sasaki, T.; Ueda, T. *Chem. Pharm. Bull.* **1988**, *36*, 945–953.
14. Saneyoshi, H.; Deschamps, J. R.; Marquez, V. E. *J. Org. Chem.* **2010**, *75*, 7659–7669.
15. De Clercq, E.; Holy, A. *Nat. Rev. Drug Disc.* **2005**, *4*, 928–940.

Characterization of cells resistant to the potent histone deacetylase inhibitor spiruchostatin B (SP-B) and effect of overexpressed p21$^{waf1/cip1}$ on the SP-B resistance or susceptibility of human leukemia cells

SYU-ICHI KANNO[1], NAOYUKI MAEDA[1], AYAKO TOMIZAWA[1], SHIN YOMOGIDA[1], TADASHI KATOH[2] and MASAAKI ISHIKAWA[1]

[1]Department of Clinical Pharmacotherapeutics; [2]Laboratory of Synthetic Medicinal Chemistry, Department of Chemical Pharmaceutical Science, Tohoku Pharmaceutical University, Aoba-ku, Sendai 981-8558, Japan

Received March 9, 2012; Accepted May 10, 2012

DOI: 10.3892/ijo.2012.1507

Abstract. We previously showed that the B cell leukemia cell line NALM-6 had the highest susceptibility among a number of leukemia cell lines to spiruchostatin B (SP-B), a potent histone deacetylase (HDAC) inhibitor. We also showed that SP-B-induced cytotoxicity depended on induction of apoptosis that was mediated by p21$^{waf1/cip1}$ expression. In the present study, we generated and characterized a stable, SP-B-resistant NALM-6 cell line (NALM-6/SP-B) by continuous exposure to SP-B, starting with a low SP-B concentration. NALM-6/SP-B cells were also more resistant to FK228, which has a similar chemical structure to SP-B, and were slightly more resistant to the P-gp substrates doxorubicin and vincristine than parental cells, but displayed similar susceptibility to other HDAC inhibitors and to paclitaxel as the parental cells. There was little change in the basal mRNA expression of *HDAC1*, *p53*, *Bax*, *Bcl-2*, *Fas*, *caspase-3*, *c-Myc* and *MDR1* in NALM-6/SP-B compared to parental cells, but the mRNA expression of *p21$^{waf1/cip1}$* was decreased. The introduction of an exogenous p21$^{waf1/cip1}$ expression vector restored SP-B induction of NALM-6/SP-B cell apoptosis. Moreover, overexpressed p21$^{waf1/cip1}$ enhanced SP-B induction of the apoptosis of the human erythroleukemia leukemia cell line K562 which is less susceptible to SP-B than NALM-6 cells. These results suggest that downregulation of *p21$^{waf1/cip1}$*, which is a characteristic feature of NALM-6/SP-B cells, was important for their resistance to SP-B, and that this SP-B resistance could be overcome by the introduction of exogenous p21$^{waf1/cip1}$. Furthermore, introduction of p21$^{waf1/cip1}$ to other leukemia cells such as K562 may enhance their susceptibility to SP-B. This is the first report of the characterization of SP-B-resistant cells and of the effect of overexpressed p21$^{waf1/cip1}$ on the resistance or susceptibility of human leukemia cells to SP-B.

Correspondence to: Dr Syu-ichi Kanno, Department of Clinical Pharmacotherapeutics, Tohoku Pharmaceutical University, 4-4-1 Komatsushima, Aoba-ku, Sendai 981-8558, Japan
E-mail: syu-kan@tohoku-pharm.ac.jp

Key words: spiruchostatin, histone deacetylase inhibitor, p21$^{waf1/cip1}$, drug resistant, apoptosis

Introduction

The acetylation status of histones plays an important role in the regulation of gene expression by altering chromatin structure. Histone deacetylases (HDAC) facilitate a closed chromatin structure and hence transcriptional repression. HDAC function is commonly affected in human cancers. Therefore, inhibition of HDAC represents a novel therapeutic approach for cancer therapy. In our previous study, we compared the activity of structurally similar bicyclic depsipeptide compounds using a panel of 39 human cancer cell lines and found that spiruchostatin B (SP-B) was the most potent inhibitor of HDAC1 and displayed the most potent growth-inhibitory activity (1).

The anti-tumor effects of HDAC inhibitors (HDIs) have been shown to be mediated by various signaling mechanisms. One such mechanism involves release of HDAC1 from its binding to the p21$^{waf1/cip1}$ promoter, including to the Sp1 sites on this promoter, which results in enhanced histone acetylation around these promoter sites and strong activation of the expression of the cyclin-dependent kinase inhibitor p21$^{waf1/cip1}$ (2). p21$^{waf1/cip1}$ was initially identified as a cell cycle regulatory protein that can cause cell cycle arrest (3). Therefore, p21$^{waf1/cip1}$ is a key gene expression target of HDI anti-tumor activity, and induction of p21$^{waf1/cip1}$ by inhibition of HDAC function is critical for HDI blockage of cell cycle progression (4-7). Indeed, we have shown that NALM-6, a B cell leukemia cell line that has higher expression of *p21$^{waf1/cip1}$* mRNA compared with other typical leukemia cell lines, was susceptible to SP-B-induced cytotoxicity that depended on induction of apoptosis (8). This result suggests that the introduction of exogenous p21$^{waf1/cip1}$ into human leukemia cells that have a low susceptibility to SP-B will enhance their susceptibility to SP-B.

There are several major problems with the use of anti-cancer drugs for the chemotherapy of cancer patients. One such problem

is the acquisition of drug resistance by tumor cells. Development of resistance to chemotherapy is therefore a major concern with any new therapy. It is well established that one mechanism of resistance to chemotherapeutic agents involves the expression of MDR1 (P-glycoprotein, P-gp), which can induce increased efflux of anticancer agents from tumor cells (9). P-gp is a major contributor to the resistance of cancer cells to FK228, a chemical with a similar structure to that of SP-B (10-12). It has also been shown that treatment with other HDIs such as suberoylanilide hydroxamic acid (SAHA, vorinostat) can result in the acquisition of irreversible and multidrug resistance-independent HDI resistance in HCT colon tumor cells (13,14). To date, there has been no report on the establishment of an SP-B-resistant human leukemia cell line, characterization of such an SP-B-resistant cell line or determination of what molecule might reverse such resistance.

In the present study, we generated and characterized a stable, SP-B-resistant NALM-6 cell (NALM-6/SP-B) line by continuous exposure of the cells to SP-B, starting with a low concentration. We also tested whether introduction of exogenous p21$^{waf1/cip1}$ would reverse the SP-B resistance of NALM-6/SP-B cells, or enhance the susceptibility of the K562 human erythroleukemia leukemia cell line, which is less susceptible to SP-B than NALM-6 cells, to SP-B-induced apoptosis. The ultimate aims of this study were to better understand the acquisition of resistance or susceptibility to SP-B with a view of its clinical application for the chemotherapy of leukemia.

Materials and methods

Materials and cell culture. SP-B was prepared as previously described (1,15). Trichostatin A (TSA), sodium butyrate (NaB) and all other reagents, unless stated, were of the highest grade available and were supplied by either Sigma (St. Louis, MO, USA) or Wako Pure Chemical Industries, Ltd (Osaka, Japan). All cells were supplied by the Cell Resource Center for Biomedical Research, Tohoku University (Sendai, Japan). Cells were routinely cultured using standard methods as described in our previous report (16).

Cytotoxicity and apoptosis. Cytotoxicity was assessed using the MTT (3-(4,5-dimethylthiazol-2-yl)-2,5-diphenyl tetrazolium bromide) assay, and apoptosis was estimated based on nuclear morphological observation using by our previously described method (17).

Establishment of a spiruchostatin B-resistant cell line, NALM-6/SP-B. NALM-6/SP-B cells were obtained using a modification of a method for obtaining Ara-C-resistant cells (17). NALM-6 parental cells were cultured in increasing concentrations of SP-B, starting at 0.1 nM. Viable cells were then passaged into a higher concentration of NALM-6 in 0.1 nM increments until a concentration of 6 nM SP-B was reached. NALM-6/SP-B cells were then maintained in complete RPMI-1640 medium containing 6 nM SP-B.

RNA isolation and quantitative real-time polymerase chain reaction (qPCR) assay. The mRNA expression level of *p21$^{waf1/cip1}$* (GenBank Accession no. NM_000389.4), *HDAC1* (NM_004964.2), *p53* (NM_000546.4), *Bax* (NM_138761.3), *Bcl-2* (NM_000633.2), *Fas* (NM_000043.3), *caspase-3* (*Cas-3*, NM_004346.3), *c-Myc* (NM_002467.3), or *multidrug resistance* (*MDR1*, NM_000927.3) in NALM-6 or NALM-6/SP-B cells was quantified using the real-time polymerase chain reaction (qPCR) with a Light Cycler (Roche, Basel, Switzerland). Briefly, total-RNA was extracted from each cell line with the Isogen reagent (Nippon Gene, Tokyo, Japan) and 0.1 μg of total-RNA was then reverse transcribed to single-strand cDNA using the RverTra Ace® qPCR RT Kit (Toyobo, Osaka, Japan). Aliquots of the cDNA preparations were subjected to qPCR analysis using SYBR® Premix Ex Taq™ (Takara Bio, Shiga, Japan) to quantify the expression of each target gene and of the internal standard *β-actin* (GenBank Accession no. NM_001101.3) using Light Cycler. The primer pairs used were from the QuantiTect® Primer Assay (Qiagen, Valencia, CA, USA) or were Takara Perfect Real Time Primers (Takara Bio). The results of all assays were checked with the melting curves to confirm the presence of single PCR products.

Plasmid constructs and transfection studies. The p21$^{waf1/cip1}$ gene was isolated from parental NALM-6 cells by PCR using KOD plus DNA polymerase (Toyobo) and was cloned into pcDNA 3.1 Directional TOPO® Expression vector (Invitrogen), according to the protocol supplied by the manufacturer. Briefly, the sequences of the primers used were 5'-CACCATGTCAGAACCGGCTGG GGATG-3' for the upstream primer (sense strand, residues 126-147), and 5'-TTAGGGCTTCCTCTTGGAGAAGATC AGC-3' for the downstream primer (antisense strand, residues 593-620), both of which were synthesized by Operon (Tokyo, Japan), and which yielded a product of about 0.5 kb. PCR amplification was performed for 1 cycle at 94°C for 2 min, which was immediately followed by 30 cycles of 15 sec at 94°C (dissociation), 30 sec at 61°C (primer annealing), and 2 min at 68°C (extension). The PCR products were resolved by electrophoresis on a 1% agarose gel and the gel was stained with ethidium bromide and imaged. The identity of the PCR product was confirmed by direct sequence analysis. The open reading frame of *p21$^{waf1/cip1}$* that was generated by PCR was then inserted into the pcDNA 3.1 expression vector. The obtained cDNA sequence was analyzed and confirmed to be identical with the reported sequence. Empty vectors were used as controls in the experiments.

NALM-6/SP-B or K562 cells were transfected with the pcDNA 3.1 plasmid DNA alone (Empty) or with pcDNA 3.1 containing *p21$^{waf1/cip1}$* cDNA, using the Neon™ Transfection System (Invitrogen) according to the instructions provided by the manufacturer. Briefly, 70-90% confluent cells were harvested and then washed twice with PBS. Subsequently, $2x10^5$ cells were transfected with 1 μg of plasmid in a volume of 10 μl using a Neon tip and electroporation. The conditions of electroporation were: 1,325 V for K562 cells or 1,410 V for NALM-6/SP-B cells, a pulse length of 10 msec, and a total of 3 pulses. The cells were then cultured for 18 h without antibiotics and used for the cytotoxicity assay.

Western blotting. Changes in the expression level of the p21$^{waf1/cip1}$ protein were detected using western blotting as described in our previous report (18). All antibodies used were purchased from Cell Signaling Technology Inc. (Beverly, MA, USA).

Table I. The cytotoxicity of anti-cancer drugs towards NALM-6 and NALM-6/SP-B.

Drugs (concentration)	IC_{50} NALM-6	IC_{50} NALM-6/SP-B	Index
SP-B (nM)	1.6 (1.03-2.73)	9.9 (5.98-16.55)	x5.9
FK228 (nM)	2.1 (1.31-3.54)	10.3 (6.48-16.36)	x4.8
TSA (nM)	33.3 (23.13-48.08)	36.5 (24.08-55.45)	x1.1
NaB (mM)	0.86 (0.668-1.120)	1.3 (0.88-2.10)	x1.6
DOX (nM)	15.8 (9.99-25.23)	42.6 (24.84-73.06)	x2.7
VCR (nM)	3.4 (2.10-5.53)	8.9 (5.53-14.43)	x2.6
TAX (nM)	4.5 (2.26-9.13)	5.4 (2.85-10.45)	x1.2

The cells were treated with the anti-cancer drugs for 72 h and subsequently cytotoxicity was assessed using the MTT assay. Data were calculated relative to each control group and are expressed as the concentration which results in 50% cell growth inhibition (IC_{50}). The range of values obtained is shown in brackets under each result.

Statistical analysis. Statistical analysis of the results was performed using a one-way analysis of variance (ANOVA) followed by the Williams' type multiple comparison test or a Bonferroni test among multiple groups. A p-value of <0.05 was considered statistically significant.

Results

Characteristics of SP-B-resistant NALM-6 cells. We first established an SP-B-resistant cell line termed NALM-6/SP-B. We had previously calculated that 50% cell growth inhibition (IC_{50}) of parental NALM-6 cells by SP-B after 24 h of culture occurred at an SP-B concentration of 5.2 nM (8). We therefore aimed to develop NALM-6 cells that were resistant to SP-B concentrations of up to 6 nM. Whereas SP-B was cytotoxic towards the parental cells at concentrations of SP-B above 1 nM following incubation for 72 h, SP-B did not induce any significant decrease in cell survival of NALM-6/SP-B cells, even at SP-B concentrations of up to 6 nM (Fig. 1). As indicated in Table I, the IC_{50} of SP-B for NALM-6/SP-B cells was 5.9-fold higher than that for parental cells. We additionally compared the effect of other HDIs such as FK228, TSA and NaB, as well as the effect of several typical chemotherapeutic agents, on the growth of NALM-6 and NALM-6/SP-B cells. Although NALM-6/SP-B cells were more resistant to FK228 than the parental cells (4.8-fold higher resistance), the parental and resistant cells showed similar susceptibility to the effects of the other HDIs and of paclitaxel (Taxol; TAX). NALM-6/SP-B cells were slightly more resistant to the P-gp substrates doxorubicin (DOX)

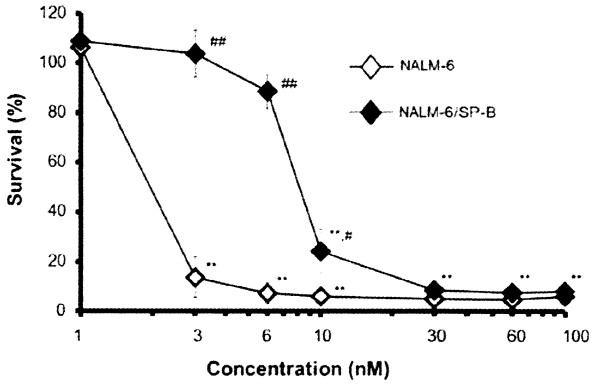


Figure 1. Cytotoxicity of SP-B towards NALM-6 (parent) cells or NALM-6/SP-B (resistant) cells over 72 h. Cells were incubated with the indicated concentrations of SP-B for 72 h, following which cell survival was assayed using the MTT assay. Survival (%) was calculated relative to the control (SP-B vehicle). The results are means ± SEM of three individual studies. $^{**}p<0.01$ compared with control. $^{\#}p<0.05$, $^{\#\#}p<0.01$ compared with parental NALM-6 cells.

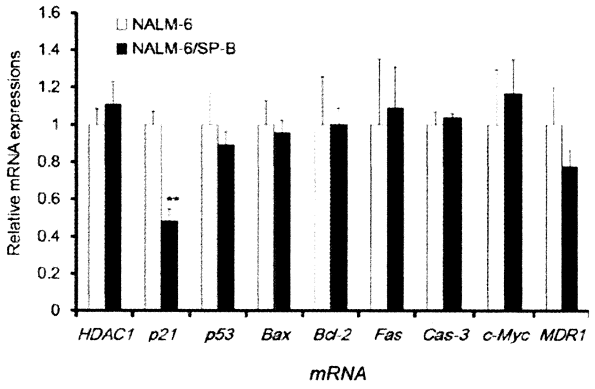


Figure 2. Comparison of the expression of representative mRNA in NALM-6 (parent) and NALM-6/SP-B (resistant) cells. Expression of the indicated mRNA was quantified using qPCR. Changes in mRNA expression are expressed as fold change in mRNA level relative to the mRNA expression of NALM-6 cells. $^{**}p<0.01$ compared to expression in NALM-6 cells. The results are means ± SEM of three individual studies.

and vincristine (VCR) than the parental cells, but this increased resistance was not statistically significant. To further ascertain the characteristics of NALM-6/SP-B cells, we compared the mRNA expression of 9 genes related to cellular growth or apoptosis, including *HDAC1*, *p21*$^{waf1/cip1}$, *p53*, *Bax*, *Bcl-2*, *Fas*, *Cas-3*, *c-Myc*, and *MDR1* in NALM-6/SP-B and control NALM-6 cells using qPCR (Fig. 2). The mRNA expression of *p21*$^{waf1/cip1}$ was significantly decreased in NALM-6/SP-B cells to less than half the level of parental cells, but the mRNA expression level of the other genes showed little difference between the two cell types. Thus, downregulation of *p21*$^{waf1/cip1}$ appeared to be a characteristic of NALM-6/SP-B cells that is important for their resistance to SP-B.

The introduction of exogenous p21$^{waf1/cip1}$ *leads to the reversal of SP-B resistance.* Fig. 2 shows that, of the mRNAs expression tested, only *p21*$^{waf1/cip1}$ mRNA expression was decreased in

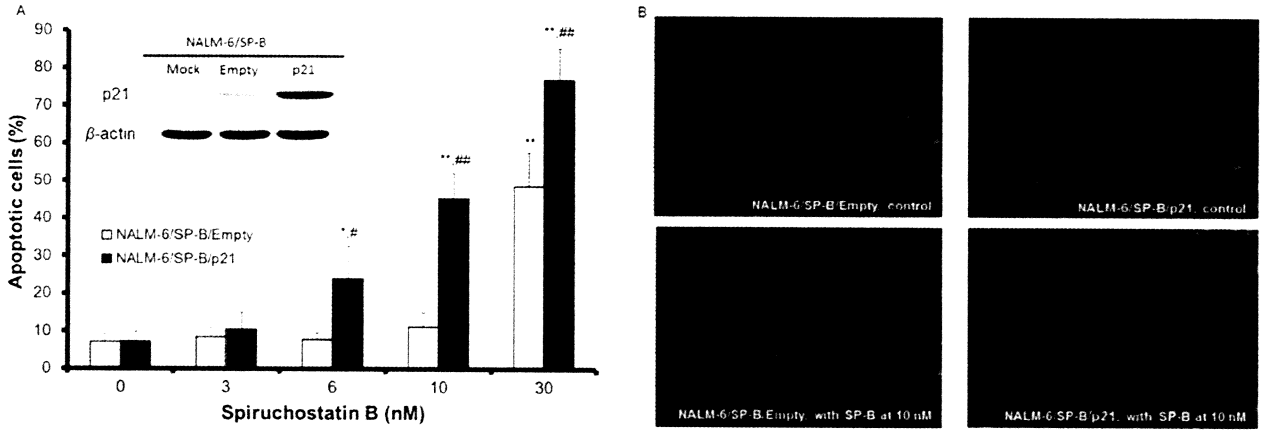


Figure 3. Effect of overexpressed p21$^{waf1/cip1}$ on apoptosis of NALM-6/SP-B cells. NALM-6/SP-B cells were transfected with empty vector (Empty or NALM-6/SP-B/Empty), with a p21$^{waf1/cip1}$ expression vector (p21 or NALM-6/SP-B/p21) or without vector (Mock). (A, inset) p21$^{waf1/cip1}$ protein expression was analyzed by western blotting using β-actin as a loading control. A representative blot of three independent experiments is shown. (A, bar graph) The percentage of apoptotic cells within each group was calculated following staining of cell nuclei with H33342. Apoptotic nuclei were defined by chromatin condensation and partition into multiple bodies. White bars, NALM-6/SP-B/Empty; black bars, NALM-6/SP-B/p21. The results are means ± SEM of three individual studies. *p<0.05, **p<0.01 compared with the respective control. $^{\#}$p<0.05, $^{\#\#}$p<0.01 compared with NALM-6/SP-B/Empty. (B) Representative photographs of control and SP-B-treated cells whose nuclei were stained with H33342 (magnification, x400).

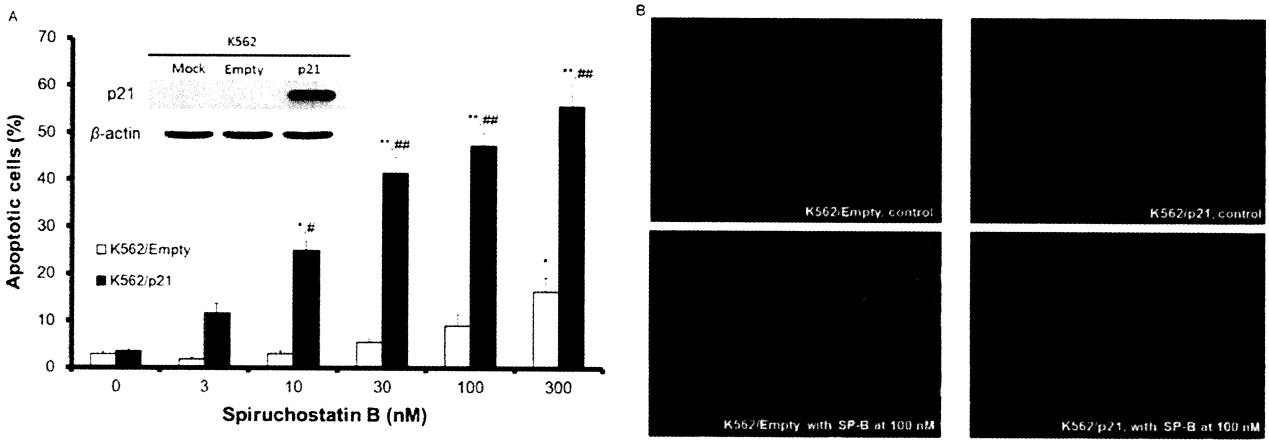


Figure 4. Effect of overexpressed p21$^{waf1/cip1}$ on apoptosis of K562 cells. K562 cells were transfected with empty vector (Empty or K562/Empty), with a p21$^{waf1/cip1}$ expression vector (p21 or K562/p21) or without vector (Mock). (A, inset) p21$^{waf1/cip1}$ protein expression was analyzed by western blotting using β-actin as a loading control. A representative blot of three independent experiments is shown. (A, graph) The percentage of apoptotic cells within each group was calculated following staining of cell nuclei with H33342. Apoptotic nuclei were defined by chromatin condensation and partition into multiple bodies. White bars, K562/Empty; black bars, K562/p21. The results are means ± SEM of three individual studies. *p<0.05, **p<0.01 compared with the respective control. $^{\#}$p<0.05, $^{\#\#}$p<0.01 compared with K562/Empty. (B) Representative photographs of control and SP-B-treated cells whose nuclei were stained with H33342 (magnification, x400).

NALM-6/SP-B cells. We therefore next constructed a p21$^{waf1/cip1}$ expression vector, and attempted to reverse the SP-B resistance of NALM-6/SP-B cells by transfection of this vector. As shown in the inset to Fig. 3A, the p21$^{waf1/cip1}$ protein was strongly expressed in NALM-6/SP-B cells 24 h after transfection with the p21$^{waf1/cip1}$ expression vector. Overexpression of p21$^{waf1/cip1}$ was maintained following incubation for 48 h, there was little change of in cell viability, cell cycle arrest or induction of apoptosis of p21$^{waf1/cip1}$ overexpressing NALM-6/SP-B (NALM-6/SP-B/p21) cells compared to NALM-6/SP-B cells (data not shown). These results suggest that introduction of exogenous p21$^{waf1/cip1}$ alone is not sufficient to critically affect cell growth or the induction of apoptosis in NALM-6/SP-B cells. Although apoptosis of NALM-6/SP-B/Empty (transfected with empty control vector) cells was not induced by SP-B at SP-B concentrations of 10 nM or less over a 24-h incubation, apoptosis of NALM-6/SP-B/p21 cells was induced by SP-B at concentrations starting from 6 nM and there was a concentration-dependent increase in NALM-6/SP-B/p21 cell apoptosis between 6 and 30 nM of SP-B. Incubation with 10 nM SP-B for 24 h induced morphological changes typical of apoptosis such as chromatin condensation and apoptotic bodies in NALM-6/SP-B/p21 cells, but induced little change in the morphology of NALM-6/SP-B/Empty cells (Fig. 3B). The percentage cell survival of NALM-6/SP-B/Empty and NALM-6/SP-B/p21 cells following incubation for 48 h with SP-B at concentrations of 3,

6, 10 and 30 nM was 99.8, 91.1, 88.4 and 10.2%, and 73.3, 62.7, 47.5 and 3.4%, respectively. These data indicate that induction of exogenous $p21^{waf1/cip1}$ expression reversed the SP-B resistance of the NALM-6/SP-B cells.

The introduction of exogenous $p21^{waf1/cip1}$ enhances the susceptibility of another leukemia cell line to SP-B-induced apoptosis. Our previous results indicated that the human erythroleukemia cell line K562 was considerably less susceptible to SP-B than typical leukemia cell lines (8). Thus, the IC_{50} of SP-B for K562 cells was more than 100-fold higher than that for the parental NALM-6 cells. To determine whether introduction of exogenous $p21^{waf1/cip1}$ expression improves the susceptibility of leukemia cells to SP-B, we transfected K562 cells with $p21^{waf1/cip1}$ and analyzed its effect on the susceptibility of these cells to apoptosis induced by SP-B (Fig. 4A and B). As shown in the inset to Fig. 4A, the $p21^{waf1/cip1}$ protein was expressed in K562 cells 24 h after $p21^{waf1/cip1}$ transfection (K562/p21). Following SP-B treatment of K562 control cells (transfected with empty vector, K562/Empty), there was no significant induction of apoptosis by SP-B compared to non-treated cells at SP-B concentrations of up to 100 nM, although apoptosis of these cells was increased at an SP-B concentration of 300 nM. Apoptosis was induced by SP-B in K562/p21 cells in an SP-B concentration-dependent manner and apoptosis of these cells was significantly increased compared to K562/Empty cells at all SP-B concentrations tested between 10 and 300 nM (Fig. 4A). The percentage cell survival of K562/Empty or K562/p21 cells following incubation for 48 h with SP-B at concentrations of 3, 10, 30, 100 and 300 nM was 102.8, 98.4, 87.4, 72.8 and 28.4%, and 85.2, 79.9, 38.2, 19.1 and 13.8%, respectively. Thus, expression of exogenous $p21^{waf1/cip1}$ enhanced the susceptibility of K562 cells to SP-B.

Discussion

Our previous report showed that SP-B is the most potent HDI for a typical human leukemia cell line and further demonstrated that the expression of $p21^{waf1/cip1}$ plays a pivotal role in SP-B induction of apoptosis and in the resulting anti-tumor activity of SP-B (8). In the present study, we developed and characterized SP-B-resistant NALM-6 cells, and, by comparing SP-B-resistant and -susceptible leukemia cells, showed that the introduction of exogenous $p21^{waf1/cip1}$ into cells reversed their SP-B resistance and enhanced their susceptibility to SP-B.

The SP-B-resistant NALM-6 cells we established were also resistant to FK228 (Table I). All previously established FK228-resistant cells are highly resistant to FK228 compared with parental cells and this resistance depends on increased expression of the P-gp protein that is encoded by the *MDR1* gene (10-12). These previously established FK228-resistant cells acquired drug resistance within a short period (continuous culture for 1 to 3 months) compared with the SP-B-resistant cells that we established (continuous culture for almost 6 months). The SP-B concentration and the culture period necessary for acquisition of resistance to SP-B in this study suggest that it was more difficult to achieve SP-B resistance than FK228 resistance. Furthermore, SP-B resistance had little effect on *MDR1* mRNA expression in NALM-6 cells. However, despite the fact that *MDR1* mRNA expression of NALM-6/SP-B was nearly the same as that of parental cells (Fig. 2), the NALM-6/SP-B cells displayed lower susceptibility to DOX and VCR, which are better substrates for P-gp, than the parental cells (Table I). A previous DNA microarray analysis study indicated that the level of $p21^{waf1/cip1}$ is significantly decreased in DOX-resistant acute myelocytic leukemia cells (19). This result suggests that a decline in $p21^{waf1/cip1}$ contributes to lower sensitivity to DOX. Our data further showed that NALM-6/SP-B cells are slightly more resistant to VCR than parental cells, but show similar resistance to TAX. Both VCR and TAX are M-phase-specific drugs that stabilize microtubules. A previous study indicated that cytotoxicity and apoptosis induced by these agents were potentiated by overexpression of $p21^{waf1/cip1}$ in sarcoma cells (20). In contrast, enforced expression of $p21^{waf1/cip1}$ in leukemia cells attenuated TAX-mediated apoptosis (21). Thus, the involvement of $p21^{waf1/cip1}$ in the action of M-phase-specific drugs may be cell specific. Yamada *et al* (11), using cDNA microarray analysis, showed that gene expression of $p21^{waf1/cip1}$ increased in FK228-resistant KU812 cells established from a patient with myeloid leukemia in blastic crisis. Unexpectedly, in our study, NALM-6/SP-B showed decreased $p21^{waf1/cip1}$ mRNA expression compared with parental cells (Fig. 2). We propose that the underlying mechanism is as follows: SP-B has a stronger effect on $p21^{waf1/cip1}$ expression than other HDIs (8); therefore, continuous exposure of NALM-6 parental cells to SP-B might lead to counteraction of HDI effects on $p21^{waf1/cip1}$ expression, resulting in downregulation of $p21^{waf1/cip1}$ mRNA expression. Such a decrease may not occur following continuous exposure of cells to other HDIs, which have a lower effect on histone deacetylases, and therefore on $p21^{waf1/cip1}$ expression.

As shown in Fig. 2, although endogenous $p21^{waf1/cip1}$ mRNA expression was decreased in NALM-6 cells that had acquired SP-B resistance, neither the mRNA expression of *HDAC1* nor that of other transcription factors such as *p53* or *c-Myc*, or of apoptosis-related genes showed any change. This *HDAC1* result is in contrast to HL-60 human promyelocytic leukemia cells that are resistant to HDIs, which have been shown to possess significantly higher levels of HDAC1 than parental cells (22). Several other studies in which p53 was assayed as a representative apoptosis-related transcription factor indicated that HDI-induced apoptosis involves the p53 pathway (23,24). In contrast, it has also been shown that HDI induces apoptosis through a p53-independent pathway in leukemia cells (25,26). Our result suggests that the SP-B resistance of NALM-6 cells does not involve p53 expression. Indeed, SP-B did not change p53 expression and pifithrin-α, an inhibitor of p53, and did not affect SP-B-induced apoptosis in either parental NALM-6 or NALM-6/SP-B cells (data not shown). The mRNA expression of the proto-oncogene *c-Myc*, in addition to that of $p21^{waf1/cip1}$, has been shown to be a useful indicator of the anti-tumor activity of FK228 (27). Moreover, cDNA microarray analysis of a human acute T cell leukemia cell line (CEM) has shown that HDIs regulate not only *c-Myc*, but also other genes such as *Bax*, *Bcl-2* and *Cas-3* that are involved in the intrinsic apoptotic pathway (28). Another study has proposed that FR901228 (also called FK228) can upregulate the Fas system in osteosarcoma cells, resulting in caspase activation (29). However, as mentioned above, no significant change in the mRNA levels of these previously reported signals was observed in the SP-B-resistant NALM-6 cells. Here, we demonstrated

that the decrease in *p21$^{waf1/cip1}$* mRNA expression was a unique characteristic of the SP-B-resistant NALM-6 cells. This is how induction of apoptosis by SP-B in NALM-6/SP-B was reversed, by the introduction of exogenous p21$^{waf1/cip1}$ expression, which compensated for the decrease in endogenous p21$^{waf1/cip1}$ in the resistant cells (Fig. 3).

Recent studies have shown that p21$^{waf1/cip1}$ can mediate both pro- and anti-apoptotic functions in response to anti-tumor agents depending on the cell type and the cellular context (30). As shown in Fig. 4A and B, overexpressed p21$^{waf1/cip1}$ enhanced SP-B-induced apoptosis in K562 cells. This result suggests that p21$^{waf1/cip1}$ has pro-apoptotic functions in K562 cells. Furthermore, the enhancing effect of exogenous p21$^{waf1/cip1}$ on the susceptibility of K562 cells to SP-B-induced apoptosis was stronger than its effect on the reversal of the resistance of NALM-6/SP-B cells to SP-B (Fig. 3). In other words, overexpressed p21$^{waf1/cip1}$ could not completely reverse the resistance of NALM-6/SP-B so that it had the same level of SP-B susceptibility as the parental cells. Most studies on induction of apoptosis by p21$^{waf1/cip1}$ were reported using cells that expressed a non-functional p53 mutant (30). It has already been reported that K562 cells harbor mutated p53 (31,32), and that NALM-6 cells express wild-type p53 (18,32). The ability of overexpressed p21$^{waf1/cip1}$ to enhance SP-B-induced apoptosis is assumed to depend on p53 status. Elucidation of the relationship between p53 status and p21$^{waf1/cip1}$ expression may lead to the establishment of effective SP-B chemotherapy for leukemia patients.

In conclusion, NALM-6 cells that were resistant to SP-B showed a unique decrease in the mRNA expression of *p21$^{waf1/cip1}$*. The introduction of exogenous p21$^{waf1/cip1}$ not only reversed the SP-B resistance of these NALM-6 cells, but also enhanced the susceptibility of K562 cells to apoptosis induced by SP-B. Based on these results, introduction of exogenous p21$^{waf1/cip1}$ into tumor cells in a clinical setting should improve tumor resistance to SP-B or may lead to successful chemotherapy using SP-B. Our findings may be useful when establishing a therapeutic strategy using SP-B.

References

1. Narita K, Kikuchi T, Watanabe K, *et al*: Total synthesis of the bicyclic depsipeptide HDAC inhibitors spiruchostatins A and B, 5''-epi-spiruchostatin B, FK228 (FR901228) and preliminary evaluation of their biological activity. Chemistry 15: 11174-11186, 2009.
2. Ocker M and Schneider-Stock R: Histone deacetylase inhibitors: signalling towards p21cip1/waf1. Int J Biochem Cell Biol 39: 1367-1374, 2007.
3. Xiong Y, Zhang H and Beach D: D type cyclins associate with multiple protein kinases and the DNA replication and repair factor PCNA. Cell 71: 505-514, 1992.
4. Han JW, Ahn SH, Kim YK, *et al*: Activation of p21(WAF1/Cip1) transcription through Sp1 sites by histone deacetylase inhibitor apicidin: involvement of protein kinase C. J Biol Chem 276: 42084-42090, 2001.
5. Fournel M, Trachy-Bourget MC, Yan PT, *et al*: Sulfonamide anilides, a novel class of histone deacetylase inhibitors, are antiproliferative against human tumors. Cancer Res 62: 4325-4330, 2002.
6. Archer SY, Meng S, Shei A and Hodin RA: p21(WAF1) is required for butyrate-mediated growth inhibition of human colon cancer cells. Proc Natl Acad Sci USA 95: 6791-6796, 1998.
7. Sambucetti LC, Fischer DD, Zabludoff S, *et al*: Histone deacetylase inhibition selectively alters the activity and expression of cell cycle proteins leading to specific chromatin acetylation and antiproliferative effects. J Biol Chem 274: 34940-34947, 1999.
8. Kanno SI, Maeda N, Tomizawa A, Yomogida S, Katoh T and Ishikawa M: Involvement of p21$^{waf1/cip1}$ expression in the cytotoxicity of the potent histone deacetylase inhibitor spiruchostatin B towards susceptible NALM-6 human B cell leukemia cells. Int J Oncol 40: 1391-1396, 2012.
9. Szakacs G, Annereau JP, Lababidi S, *et al*: Predicting drug sensitivity and resistance: profiling ABC transporter genes in cancer cells. Cancer Cell 6: 129-137, 2004.
10. Xiao JJ, Huang Y, Dai Z, *et al*: Chemoresistance to depsipeptide FK228 [(E)-(1S,4S,10S,21R)-7-[(Z)-ethylidene]-4,21-diiso propyl-2-oxa-12,13-dithia-5,8,20,23-tetraazabicyclo[8,7,6]-tricos -16-ene-3,6,9,22-pentanone] is mediated by reversible MDR1 induction in human cancer cell lines. J Pharmacol Exp Ther 314: 467-475, 2005.
11. Yamada H, Arakawa Y, Saito S, Agawa M, Kano Y and Horiguchi-Yamada J: Depsipeptide-resistant KU812 cells show reversible P-glycoprotein expression, hyper-acetylated histones, and modulated gene expression profile. Leuk Res 30: 723-734, 2006.
12. Matsubara H, Watanabe M, Imai T, *et al*: Involvement of extracellular signal-regulated kinase activation in human osteosarcoma cell resistance to the histone deacetylase inhibitor FK228 [(1S,4S,7Z,10S,16E,21R)-7-ethylidene-4,21-bis(propan-2-yl)-2-oxa-12,13-dit hia-5,8,20,23-tetraazabicyclo[8.7.6] tricos-16-ene-3,6,9,19,22-pentone]. J Pharmacol Exp Ther 328: 839-848, 2009.
13. Imesch P, Dedes KJ, Furlato M, Fink D and Fedier A: MLH1 protects from resistance acquisition by the histone deacetylase inhibitor trichostatin A in colon tumor cells. Int J Oncol 35: 631-640, 2009.
14. Dedes KJ, Dedes I, Imesch P, von Bueren AO, Fink D and Fedier A: Acquired vorinostat resistance shows partial cross-resistance to 'second-generation' HDAC inhibitors and correlates with loss of histone acetylation and apoptosis but not with altered HDAC and HAT activities. Anticancer Drugs 20: 321-333, 2009.
15. Takizawa T, Watanabe K, Narita K, Oguchi T, Abe H and Katoh T: Total synthesis of spiruchostatin B, a potent histone deacetylase inhibitor, from a microorganism. Chem Commun (Camb): 1677-1679, 2008.
16. Kanno S, Kakuta M, Kitajima Y, *et al*: Preventive effect of trimidox on oxidative stress in U937 cell line. Biol Pharm Bull 30: 994-998, 2007.
17. Kanno S, Hiura T, Ohtake T, *et al*: Characterization of resistance to cytosine arabinoside (Ara-C) in NALM-6 human B leukemia cells. Clin Chim Acta 377: 144-149, 2007.
18. Kanno S, Higurashi A, Watanabe Y, Shouji A, Asou K and Ishikawa M: Susceptibility to cytosine arabinoside (Ara-C)-induced cytotoxicity in human leukemia cell lines. Toxicol Lett 152: 149-158, 2004.
19. Song JH, Choi CH, Yeom HJ, Hwang SY and Kim TS: Monitoring the gene expression profiles of doxorubicin-resistant acute myelocytic leukemia cells by DNA microarray analysis. Life Sci 79: 193-202, 2006.
20. Li W, Fan J, Banerjee D and Bertino JR: Overexpression of p21(waf1) decreases G2-M arrest and apoptosis induced by paclitaxel in human sarcoma cells lacking both p53 and functional Rb protein. Mol Pharmacol 55: 1088-1093, 1999.
21. Ahmed W, Rahmani M, Dent P and Grant S: The cyclin-dependent kinase inhibitor p21(CIP1/WAF1) blocks paclitaxel-induced G2M arrest and attenuates mitochondrial injury and apoptosis in p53-null human leukemia cells. Cell Cycle 3: 1305-1311, 2004.
22. Fiskus W, Rao R, Fernandez P, *et al*: Molecular and biologic characterization and drug sensitivity of pan-histone deacetylase inhibitor-resistant acute myeloid leukemia cells. Blood 112: 2896-2905, 2008.
23. Bandyopadhyay D, Mishra A and Medrano EE: Overexpression of histone deacetylase 1 confers resistance to sodium butyrate-mediated apoptosis in melanoma cells through a p53-mediated pathway. Cancer Res 64: 7706-7710, 2004.
24. Condorelli F, Gnemmi I, Vallario A, Genazzani AA and Canonico PL: Inhibitors of histone deacetylase (HDAC) restore the p53 pathway in neuroblastoma cells. Br J Pharmacol 153: 657-668, 2008.
25. Vrana JA, Decker RH, Johnson CR, *et al*: Induction of apoptosis in U937 human leukemia cells by suberoylanilide hydroxamic acid (SAHA) proceeds through pathways that are regulated by Bcl-2/Bcl-XL, c-Jun, and p21CIP1, but independent of p53. Oncogene 18: 7016-7025, 1999.

26. Insinga A, Monestiroli S, Ronzoni S, *et al*: Inhibitors of histone deacetylases induce tumor-selective apoptosis through activation of the death receptor pathway. Nat Med 11: 71-76, 2005.
27. Sasakawa Y, Naoe Y, Inoue T, *et al*: Effects of FK228, a novel histone deacetylase inhibitor, on tumor growth and expression of p21 and c-myc genes in vivo. Cancer Lett 195: 161-168, 2003.
28. Peart MJ, Smyth GK, van Laar RK, *et al*: Identification and functional significance of genes regulated by structurally different histone deacetylase inhibitors. Proc Natl Acad Sci USA 102: 3697-3702, 2005.
29. Imai T, Adachi S, Nishijo K, *et al*: FR901228 induces tumor regression associated with induction of Fas ligand and activation of Fas signaling in human osteosarcoma cells. Oncogene 22: 9231-9242, 2003.
30. Liu S, Bishop WR and Liu M: Differential effects of cell cycle regulatory protein p21(WAF1/Cip1) on apoptosis and sensitivity to cancer chemotherapy. Drug Resist Updat 6: 183-195, 2003.
31. Law JC, Ritke MK, Yalowich JC, Leder GH and Ferrell RE: Mutational inactivation of the p53 gene in the human erythroid leukemic K562 cell line. Leuk Res 17: 1045-1050, 1993.
32. Filippini G, Griffin S, Uhr M, *et al*: A novel flow cytometric method for the quantification of p53 gene expression. Cytometry 31: 180-186, 1998.

Involvement of p21$^{waf1/cip1}$ expression in the cytotoxicity of the potent histone deacetylase inhibitor spiruchostatin B towards susceptible NALM-6 human B cell leukemia cells

SYU-ICHI KANNO[1], NAOYUKI MAEDA[1], AYAKO TOMIZAWA[1], SHIN YOMOGIDA[1], TADASHI KATOH[2] and MASAAKI ISHIKAWA[1]

[1]Department of Clinical Pharmacotherapeutics, [2]Laboratory of Synthetic Medicinal Chemistry, Department of Chemical Pharmaceutical Science, Tohoku Pharmaceutical University, 4-4-1 Komatsushima, Aoba-ku, Sendai 981-8558, Japan

Received October 21, 2011; Accepted December 2, 2011

DOI: 10.3892/ijo.2011.1323

Abstract. Spiruchostatin B (SP-B) is a potent histone deacetylase (HDAC) inhibitor that has potential for the chemotherapy of leukemia. The aim of this study was to study the susceptibility of human leukemia cell lines to SP-B. We found that NALM-6 human B cell leukemia cells are the most susceptible to SP-B. There was a low correlation between the expression of *HDAC1* mRNA and HDI susceptibility of leukemia cells. NALM-6 has higher endogenous *p21$^{waf1/cip1}$* mRNA expression than other leukemia cells. SP-B-induced cytotoxicity was mediated by induction of histone acetylation via inhibition of HDACs, and this effect of SP-B was associated with apoptosis, which was mediated by caspase activation in NALM-6 cells. SP-B time-dependently increased the size of the sub-G1 (apoptotic) peak, and this effect correlated with SP-B induction of cellular apoptotic features such as changes in nuclear morphology. SP-B significantly increased p21$^{waf1/cip1}$ expression prior to induction of apoptosis. In conclusion, NALM-6 cells, which have a higher expression of *p21$^{waf1/cip1}$* mRNA than other leukemia cell lines, were susceptible to SP-B-induced cytotoxicity that resulted in induction of apoptosis. Our findings may be useful when establishing a therapeutic strategy based on SP-B.

Introduction

Since inhibition of histone deacetylase (HDAC) activity reverses the epigenetic silencing frequently observed in cancer, various HDAC inhibitors (HDIs) have been developed for therapeutic purposes (1). Studies of leukemia have provided examples for the functional implications of HDACs in cancer development and progression, as well as their relevance for therapeutic targeting (2). There has been intensive research regarding the clinical use of HDIs (3), and clinical trials involving systemic HDI treatment have been reported (4). Different classes of agents with HDAC inhibitor activity exert different biological effects, possibly because of additional distinct effects on mechanisms of cell regulation.

The chemical structures of typical HDIs that were used for experiments in this study are shown in Fig. 1. Sodium butyrate (NaB) is a short-chain acid that is produced by anaerobic bacterial fermentation of dietary fibers, which has been shown to inhibit HDAC activity (5). Trichostatin A (TSA) is a naturally occurring hydroxamate that is a potent HDI (6), but is considered too toxic for clinical development (7). Romidepsin (FK228), which is a more potent HDI than either of the above chemicals, is a naturally occurring 16-membered bicyclic depsipeptide that was isolated from *Chromobacterium violaceum* in 1994 (8). Preclinical studies with FK228 in leukemia patients demonstrated that it effectively induced apoptosis at concentrations at which HDAC inhibition occurs (9). Subsequently, structurally similar 15-membered bicyclic depsipeptides, spiruchostatins A and B, isolated from a culture broth of *Pseudomonas sp.* by Masuoka *et al* in 2001 (10), were also found to exhibit potent HDAC inhibitory activity (11,12). In a previous study, we compared the activity of these depsipeptide compounds using a panel of 39 human cancer cell lines and found that spiruchostatin B (SP-B) was the most potent inhibitor of HDAC1 and displayed the most potent growth-inhibitory activity (13).

The anti-tumor effects of HDIs have been shown to be mediated by various signaling mechanisms. The induction of p21$^{waf1/cip1}$ and the resulting blockage of cell cycle progression are critical for the anti-tumor activities of all HDIs (14-17). This induction is independent of p53 and correlates with alterations in proteins associated with the p21$^{waf1/cip1}$ promoter, including an increase in the acetylation of histones (18,19).

The aims of this study were to better understand the signaling mechanism of SP-B anti-tumor activity with a view to its clinical application, we examined the susceptibility of human leukemia cell lines to SP-B. Our study suggests that the human B cell leukemia NALM-6 cell line, which has higher

Correspondence to: Dr Syu-Ichi Kanno, Department of Clinical Pharmacotherapeutics, Tohoku Pharmaceutical University, 4-4-1 Komatsushima, Aoba-ku, Sendai 981-8558, Japan
E-mail: syu-kan@tohoku-pharm.ac.jp

Key words: spiruchostatin, histone deacetylase inhibitor, p21$^{waf1/cip1}$, human leukemia cell lines, NALM-6

p21$^{waf1/cip1}$ expression than other leukemia cells, is the most susceptible to SP-B. These data may prove useful with respect to the clinical application of SP-B.

Materials and methods

Materials and cell culture. SP-B and FK228 were prepared as previously described (13,20). TSA, and all other reagents, unless stated, were of the highest grade available and were supplied by either Sigma (St. Louis, MO, USA) or Wako Pure Chemical Industries, Ltd (Osaka, Japan). Normal human leukocyte cDNA was purchased from OriGene Technologies Inc (Rockville, MD, USA). All cells were supplied by the Cell Resource Center for Biomedical Research, Tohoku University (Sendai, Japan). Cells were routinely cultured using standard methods as described in our previous reports (21).

Cytotoxicity and apoptosis. Cytotoxicity was assessed using the MTT [3-(4,5-dimethylthiazol-2-yl)-2,5-diphenyl tetrazolium bromide] assay, and apoptosis was estimated by nuclear morphological observation or by analysis of qualitative damage to genomic DNA (DNA fragmentation) using a modification of our previously described method (22).

Cell cycle analyses by flow cytometry. Analyses of the cell cycle were performed by flow cytometry using a FACSCalibur flow cytometer (Becton Dickinson, San Jose, CA, USA) with CELLQuest Pro software (BD Biosciences). Data analyses for cell cycle distribution were performed on linear propidium iodide (PI) histograms using the mathematical software ModFit LT 2.0 (Verity Software House; Topsham, ME, USA).

RNA isolation and quantitative real-time polymerase chain reaction (qPCR) assay. The mRNA expression level of *p21$^{waf1/cip1}$* (GenBank Accession no. NM_000389.4), *HDAC1* (NM_004964.2), in human leukemia cells was quantified using the real-time polymerase chain reaction (qPCR) with a Light Cycler (Roche, Basel, Switzerland). Briefly, total RNA was extracted from each cell line with the Isogen reagent (Nippon Gene, Tokyo, Japan) and 0.1 μg of total RNA was then reverse transcribed to single-strand cDNA using the RverTra Ace® qPCR RT Kit (Toyobo, Osaka, Japan). Aliquots of the cDNA preparations were subjected to qPCR analysis using SYBR® Premix Ex Taq™ (Takara Bio, Shiga, Japan) to quantify the expression of each target gene and of the internal standard β-actin (GenBank Accession no. NM_001101.3) using Light Cycler. The primer pairs used were from the QuantiTect® Primer Assay (Qiagen, Valencia, CA) or were Takara Perfect Real Time Primers (Takara Bio). The results of all assays were checked with the melting curves to confirm the presence of single PCR products.

Western blotting. Changes in the expression level of apoptosis related proteins or of the p21$^{waf1/cip1}$ protein were detected using Western blotting as described in our previous reports (23). All antibodies used were purchased from Cell signaling Technology, Inc. (Beverly, MA, USA). Protein levels were analyzed by enhanced chemiluminescence with an ECL plus Western blotting detection system (Amersham, Arlington Heights, IL, USA).

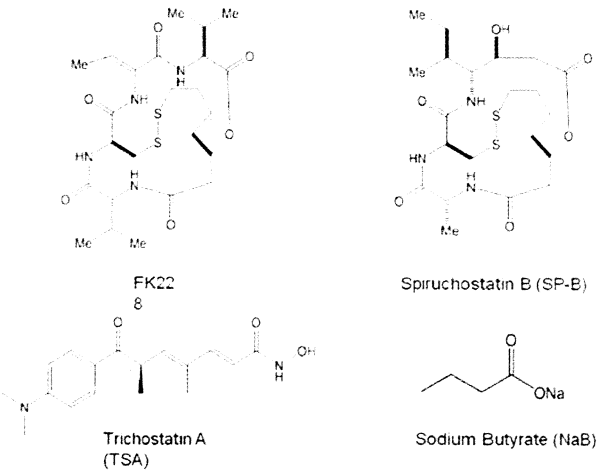


Figure 1. Chemical structures of HDIs.

Statistical analysis. Statistical analysis of the results was performed using a one-way analysis of variance (ANOVA) followed by the Williams' type multiple comparison test or a Bonferroni test among multiple groups. A $p<0.05$ was considered significant.

Results

Susceptibility of human leukemia cell lines to HDIs. We first examined the susceptibility of human leukemia cell lines to the cytotoxicity of typical HDIs; SP-B, TSA, or NaB, by incubation of the cells with HDIs for 24 h. Susceptibility was estimated by analysis of cell growth using the MTT assay, in which the HDI concentration that induced 50% cell growth inhibition (IC_{50}) was calculated using GraphPad Prism software version 4.0 (Table I). SP-B displayed the most potent cytotoxicity towards each leukemia cell line, showing cytotoxicity at nanomolar (nM) concentrations. Compared to SP-B, TSA showed moderate cytotoxicity at micromolar (μM) concentrations towards all leukemia cell lines except for NALM-6 cells. All cell lines were considerably less susceptible to NaB. Thus, SP-B has potent cytotoxic effects on leukemia cells. In addition, NALM-6 cells were the most susceptible of all of the leukemia cells tested to the cytotoxic activity of all of the HDIs. To determine the factor(s) that makes human leukemia cells susceptible to HDIs, we carried out qPCR to assess the mRNA levels of *HDAC1* and *p21$^{waf1/cip1}$* in the leukemic cells compared to normal human leukocytes (Fig. 2). Compared to control, the mRNA expression of *HDAC1* was higher in MOLT-4 (2.0-fold higher) and K562 (2.3-fold higher) cells. The mRNA expression of *p21$^{waf1/cip1}$* was extremely high in NALM-6 (3.8-fold higher than control), but its expression in the other leukemia cells was lower than in normal leukocytes.

SP-B-induced cytotoxicity and apoptosis in NALM-6 cells. Since NALM-6 was the most susceptible cell line to SP-B, as shown in Table I, we used this cell line to confirm that SP-B-induced cytotoxicity depends on apoptosis and HDAC inhibition. We first determined the best conditions for SP-B treatment of NALM-6 cells for induction of cytotoxicity.

Table I. HDAC inhibitor-induced cytotoxicity in human leukemia cell lines.[a]

Cell line	Characteristic	SP-B (nM)	TSA (μM)	NaB (mM)
NALM-6	B cell leukemia	5.168 (2.981-8.960)	0.085 (0.050-0.144)	1.232 (0.837-1.811)
U937	Diffuse histiocytic lymphoma	27.47 (19.050-39.600)	2.840 (1.669-4.833)	11.19 (8.164-15.350)
MOLT-4	T cell leukemia	29.87 (16.130-55.310)	1.405 (0.680-2.902)	7.947 (5.815-10.860)
HL-60	Promyelocytic	64.22 (40.960-100.700)	1.840 (1.063-3.186)	10.03 (7.351-13.680)
K562	Erythroleukemia	536.4 (319.100-901.800)	35.79 (2.135-59.998)	>10

[a]Cytotoxicity was assessed using the MTT assay following incubation of the cells with the indicated HDIs for 24 h. Data were calculated relative to each control group and are expressed as the concentration which induces 50% cell growth inhibition (IC_{50}). The range of values obtained is shown in brackets under each result.

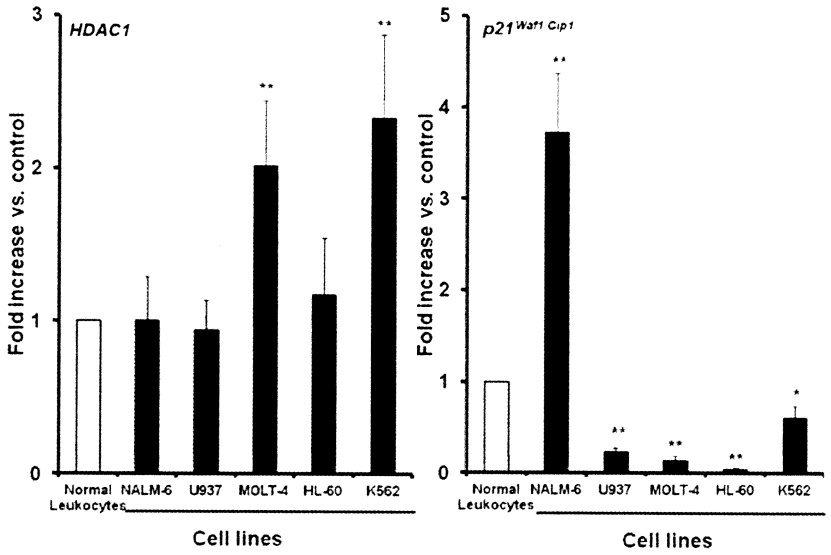


Figure 2. Comparison of *HDAC1* or *p21*$^{waf1/cip1}$ mRNA expression in human leukemia cell lines. mRNA expression was analyzed using qPCR and data are expressed as fold change in the mRNA level relative to normal human leukocytes. $^{*}p<0.05$, $^{**}p<0.01$ compared to expression in normal human leukocytes.

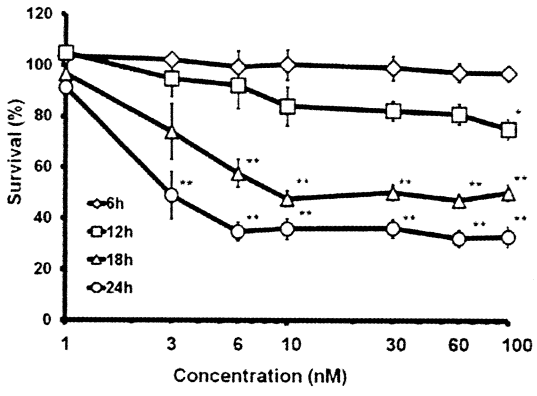


Figure 3. SP-B-induced cytotoxicity towards NALM-6 cells. NALM-6 cells were incubated with the indicated concentrations of SP-B for the indicated times. Cytotoxicity was assessed using the MTT assay, survival (%) was calculated relative to the control (SP-B vehicle). The results are means ± SEM of three individual studies. $^{*}p<0.05$, $^{**}p<0.01$ compared with the control group under the indicated culture condition.

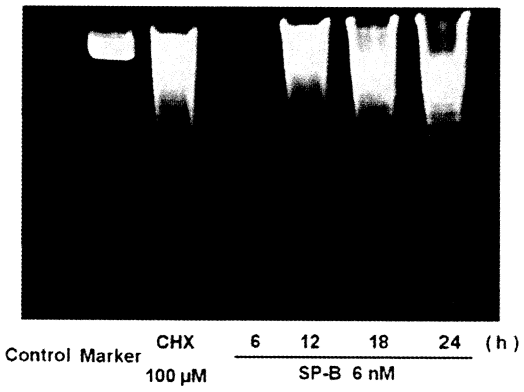


Figure 4. SP-B induces DNA damage (DNA fragmentation). SP-B-induced damage to genomic DNA was qualitatively estimated by agarose gel electrophoresis following incubation of NALM-6 cells with 6 nM SP-B for the indicated times. Cycloheximide (CHX) was used as a positive control and no SP-B vehicle as a negative control. DNA samples were electrophoresed on 1.4% agarose gel containing ethidium bromide, visualized under UV light, and photographed.

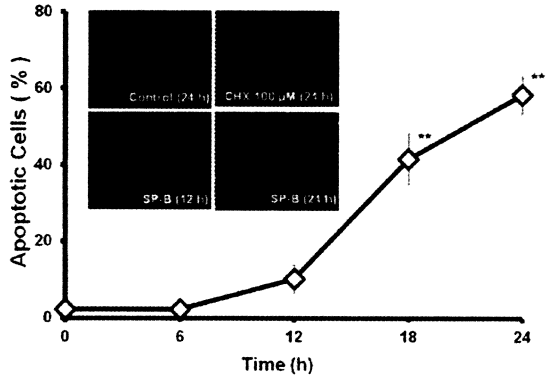


Figure 5. SP-B induces changes in nuclear morphology. NALM-6 cells were treated with 6 nM SP-B or with 100 mM cycloheximide (CHX, positive control) or with a negative control (SP-B vehicle) for the indicated times. Cell nuclei were then stained with H33342. Apoptotic nuclei, which were characterized by chromatin condensation followed by partition into multiple bodies (magnification, x400), were counted and the percentage of apoptotic cells was calculated. The results are means ± SEM of three individual studies. $^{**}p<0.01$ compared with control group.

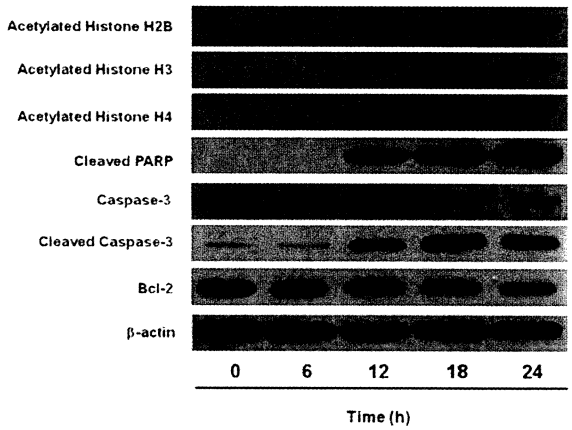


Figure 6. Western blotting analysis of SP-B-induced changes in the level of acetylated histones and apoptosis-related proteins. Cells were incubated with 6 nM SP-B for the indicated times and expression of the indicated proteins was then analyzed by Western blotting using expression of β-actin as a loading control. Experiments shown are representative of a minimum of three separate experiments.

SP-B had significant cytotoxic effects on NALM-6 cells at concentrations greater than or equal to 6 nM, and following incubation for 18 h (Fig. 3). Interestingly, there was little change in the cytotoxic effects of SP-B at concentrations between 6 and 100 nM, when incubated with cells for 24 h. Based on these data we used SP-B at a concentration of 6 nM for the rest of the study. We next analyzed the effect of SP-B on apoptosis. Apoptosis is characterized by oligonucleosomal DNA fragmentation, qualitative damage to genomic DNA and nuclear morphological changes such as chromatin condensation. Since treatment with high doses of cycloheximide (CHX) is known to induce apoptosis in human B leukocytes (24), we used 100 μM CHX as positive control for induction of apop-

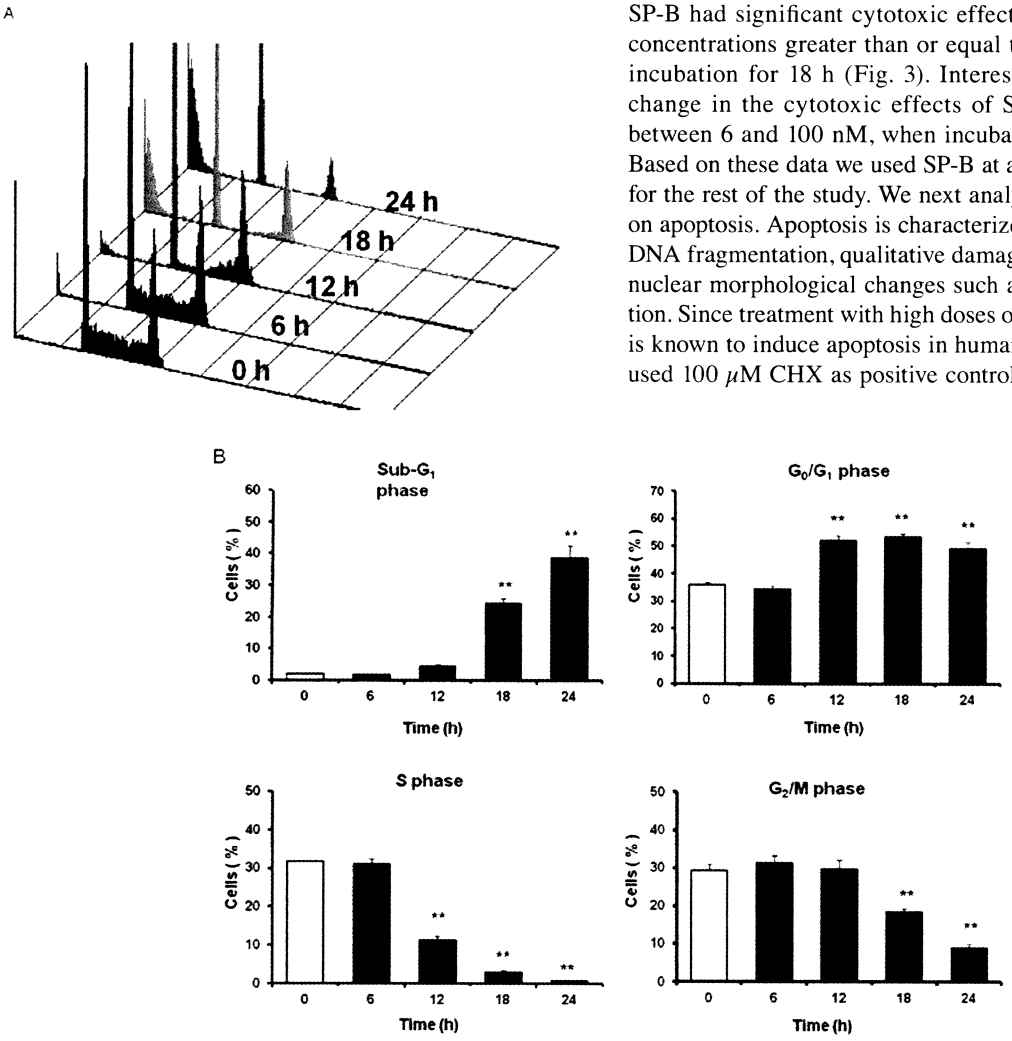


Figure 7. Effects of SP-B on the cell cycle. (A) Representative cell cycle profiles obtained using FACS of NALM-6 cells treated for the indicated times with 6 nM SP-B. (B) The percentage of cells at the indicated stage of the cell cycle in response to SP-B was assessed in NALM-6. The results are means ± SEM of three individual studies. $^{**}p<0.01$ compared with control group.

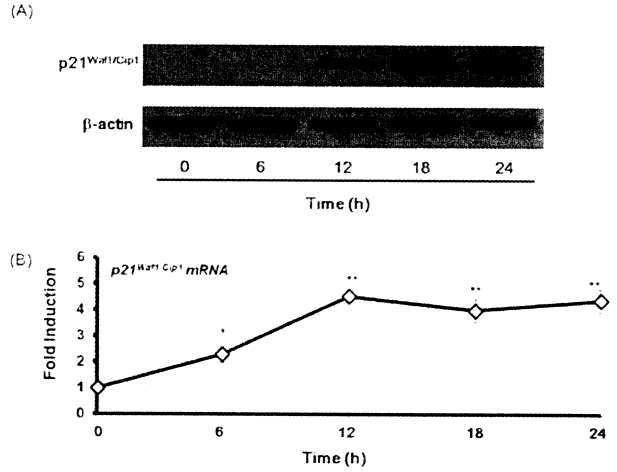


Figure 8. SP-B induces $p21^{waf1/cip1}$ protein and mRNA expression. NALM-6 cells were incubated with SP-B for the indicated times. (A) $p21^{waf1/cip1}$ protein expression was analyzed by Western blotting using β-actin as a loading control. The experiment shown is representative of two separate experiments. (B) *p21waf1/cip1* mRNA expression was analyzed using qPCR. The results are means ± SEM of three individual studies. *p<0.05, **p<0.01 compared with control.

tosis in this study. SP-B at a concentration of 6 nM induced DNA fragmentation (Fig. 4) and nuclear morphological change (Fig. 5) following treatment of the cells for more than 12 h and 18 h, respectively. Thus, SP-B induces cellular changes that are characteristic of apoptosis. To confirm the mechanisms by which SP-B induces apoptosis and HDAC inhibition we analyzed the expression of apoptosis related proteins and acetylated histone proteins respectively using Western blotting (Fig. 6). There were no change in these proteins following incubation for 6 h with SP-B, but the expression of acetylated histones H2B, H3 and H4, of cleaved PARP and of cleaved caspase-3, as well as the degradation of total caspase-3 and Bcl-2 proteins were increased following incubation for 12 h or longer. Hence, HDAC inhibition by SP-B was associated with induction of apoptosis and acetylation of histones, which in turn led to cytotoxic effects.

SP-B induces cell cycle arrest and up-regulates p21waf1/cip1 expression. We next examined the effect of SP-B on cell cycle progression in NALM-6 cells by FACS analysis of cells stained with PI (Fig. 7A and B). SP-B time-dependently increased the size of the sub-G_1 (apoptotic) peak, and this effect correlated with SP-B induction of cellular apoptotic features such as changes in nuclear morphology (see Fig. 5). Following 12 h incubation with SP-B, G_0/G_1 arrest was accompanied by a marked decrease in the number of cells in the S phase and, at later times of incubation by a decrease in the number of cells in the G_2/M phase. Since induction of $p21^{waf1/cip1}$ results in a blockage of cell cycle progression, and since $p21^{waf1/cip1}$ is also a well-established and key gene expression target of HDIs (14-17), we hypothesized that these affects of SP-B on the cell cycle were dependent on SP-B induction of the transcription factor $p21^{waf1/cip1}$. Indeed, the protein and mRNA levels of p21waf1/cip1 clearly increased in a time-dependent manner following incubation with SP-B (Fig. 8A and B, respectively).

Discussion

At least 80 clinical trials are currently underway in which the anti-tumor activities of at least 11 different HDAC inhibitory agents are being tested on cancers including both hematological and solid malignancies (25). It is therefore desirable to develop useful and highly potent HDIs. In the present study, SP-B was the most potent HDI in terms of induction of cytotoxic effects against several typical human leukemia cell lines (Table I). It is commonly assumed that powerful cytotoxic reagents affect normal cells leading to side effects. However, in our experimental *in vitro* study SP-B did not have significant cytotoxic effects towards normal leukocytes that were supplied by healthy volunteers (data not shown).

Several tumors, including hematological malignancies, are known to have higher HDAC expression than their normal counterparts (26, 27). In addition, clinical studies suggest that the level of *HDAC1* mRNA could potentially serve as a marker for patients with gastric (28), lung (29), or breast (30) cancers. We postulated that the cytotoxic effects of HDIs might be significantly higher on leukemia cell lines that have higher expression of *HDAC1* mRNA. However, there was only a modest correlation between *HDAC1* mRNA expression and SP-B cytotoxicity (Fig. 2). Unexpectedly, K562, which shows a low susceptibility to SP-B, displayed the highest expression of *HDAC1* mRNA of the leukemia cells tested. These data could imply that there is a low correlation between the expression of *HDAC1* mRNA and the HDI susceptibility of leukemia cells.

It has been reported that $p21^{waf1/cip1}$ plays a pivotal role in the anti-tumor activities of all HDIs (14-17). Indeed, the mRNA expression of *p21waf1/cip1* was markedly increased in NALM-6 cells, which was the cell line that was most susceptible to HDIs in this study. Our data suggest that higher p21waf1/cip1 mRNA expression contributes to susceptibility to HDIs. However, it is unlikely that susceptibility to HDIs including SP-B is dependent solely on *p21waf1/cip1* mRNA expression. This is because *p21waf1/cip1* mRNA expression was only increased in NALM-6 cells and not in the other HDI-susceptible cell lines, in which expression of *p21waf1/cip1* mRNA was even lower than that of normal leukocytes. Therefore it appears that high *p21waf1/cip1* mRNA expression is unique to NALM-6.

HDI-induced cytotoxicity has been shown to involve induction of apoptosis that is mediated by caspase activation and Bcl-2 inhibition (31). Our data showed SP-B cytotoxicity following incubation with concentrations of SP-B ≥6 nM for 18 h (Fig. 3). Prior to this time point, after 12 h incubation, SP-B induced apoptosis, as indicated by DNA fragmentation (Fig. 4) and increased changes in nuclear morphology (Fig. 5). We showed that SP-B-induced apoptosis is mediated by caspase activation, since it was accompanied by the cleavage of PARP, which is a major substrate of executioner caspases including caspase-3. Both histone acetylation and changes in the level of apoptosis-related proteins were simultaneously detected following incubation with SP-B for 12 h (Fig. 6). These results support the hypothesis that SP-B-induced cytotoxicity is mediated by induction of histone acetylation via inhibition of HDAC, and that this effect of SP-B is associated with apoptosis, which was mediated by caspase activation. Notably, induction of apoptosis following incubation with SP-B was not observed at incubation times of <12 h in this study. The kinetics of histone acetylation induced

by HDIs have been previously reported, and it was shown that the histone acetylation induced by spiruchostatin A and FK228 is delayed compared with HDIs such as TSA that have a different chemical structure (11). Since SP-B has structural similarity with the former compounds, longer times of incubation were expected for the effect of SP-B on histone acetylation to become evident in NALM-6. As shown in Fig. 7, the change in cell cycle distribution induced by SP-B was primarily a decrease in S phase and a shift to the G_0/G_1 phase, followed by an increased in the sub-G_1 phase that was accompanied by a later decrease in the G_2/M phase. It is well established that *p21$^{waf1/cip1}$* is a negative regulator of the cell cycle, regulates gene transcription, and modulates apoptosis (32). Induction of p21$^{waf1/cip1}$ is a commonly used marker of HDAC inhibition (33). The induction of p21$^{waf1/cip1}$ by SP-B that we observed supports previous data that p21$^{waf1/cip1}$ is involved in events involving HDAC inhibition. Thus, after 6 h incubation with SP-B, there was little change in cell cycle distribution or in apoptotic features, and only a small increase in *p21$^{waf1/cip1}$* mRNA expression (Fig. 8A). However, after 12 h incubation with SP-B, there was a significant increase in both the mRNA and protein expression of p21$^{waf1/cip1}$ (Fig. 8), which was accompanied by SP-B induction of apoptosis and cell cycle arrest (Figs. 4-7).

In conclusion, NALM-6 cells, which have higher expression of *p21$^{waf1/cip1}$* mRNA than other leukemia cell lines, were susceptible to SP-B-induced cytotoxicity that resulted in induction of apoptosis. Expression of *p21$^{waf1/cip1}$* mRNA has prognostic significance in acute lymphoblastic leukemia (34). Interactions between therapy and biomarkers, as well as the emergence of p21$^{waf1/cip1}$ as a prognostic indicator, provide clues as to the underlying biology of leukemia. Our findings may be useful when establishing a therapeutic strategy for SP-B.

References

1. Abujamra AL, Dos Santos MP, Roesler R, Schwartsmann G and Brunetto AL: Histone deacetylase inhibitors: a new perspective for the treatment of leukemia. Leuk Res 34: 687-695, 2010.
2. Leone G, D'Alo F, Zardo G, Voso MT and Nervi C: Epigenetic treatment of myelodysplastic syndromes and acute myeloid leukemias. Curr Med Chem 15: 1274-1287, 2008.
3. Paris M, Porcelloni M, Binaschi M and Fattori D: Histone deacetylase inhibitors: from bench to clinic. J Med Chem 51: 1505-1529, 2008.
4. Wagner JM, Hackanson B, Lubbert M and Jung M: Histone deacetylase (HDAC) inhibitors in recent clinical trials for cancer therapy. Clin Epigenetics 1: 117-136, 2010.
5. Davie JR: Inhibition of histone deacetylase activity by butyrate. J Nutr 133: S2485-S2493, 2003.
6. Yoshida M, Kijima M, Akita M and Beppu T: Potent and specific inhibition of mammalian histone deacetylase both in vivo and in vitro by trichostatin A. J Biol Chem 265: 17174-17179, 1990.
7. Elaut G, Torok G, Vinken M, *et al*: Major phase I biotransformation pathways of Trichostatin a in rat hepatocytes and in rat and human liver microsomes. Drug Metab Dispos 30: 1320-1328, 2002.
8. Ueda H, Nakajima H, Hori Y, *et al*: FR901228, a novel antitumor bicyclic depsipeptide produced by Chromobacterium violaceum No. 968. I. Taxonomy, fermentation, isolation, physico-chemical and biological properties, and antitumor activity. J Antibiot (Tokyo) 47: 301-310, 1994.
9. Byrd JC, Marcucci G, Parthun MR, *et al*: A phase 1 and pharmacodynamic study of depsipeptide (FK228) in chronic lymphocytic leukemia and acute myeloid leukemia. Blood 105: 959-967, 2005.
10. Masuoka Y, Nagai A, Shin-Ya K, *et al*: Spiruchostatins A and B, novel gene expression-enhancing substances produced by Pseudomonas sp. Tetrahedron Lett 42: 41-44, 2001.
11. Crabb SJ, Howell M, Rogers H, *et al*: Characterisation of the in vitro activity of the depsipeptide histone deacetylase inhibitor spiruchostatin A. Biochem Pharmacol 76: 463-475, 2008.
12. Davidson SM, Townsend PA, Carroll C, *et al*: The transcriptional coactivator p300 plays a critical role in the hypertrophic and protective pathways induced by phenylephrine in cardiac cells but is specific to the hypertrophic effect of urocortin. Chembiochem 6: 162-170, 2005.
13. Narita K, Kikuchi T, Watanabe K, *et al*: Total synthesis of the bicyclic depsipeptide HDAC inhibitors spiruchostatins A and B, 5''-epi-spiruchostatin B, FK228 (FR901228) and preliminary evaluation of their biological activity. Chemistry 15: 11174-11186, 2009.
14. Han JW, Ahn SH, Kim YK, *et al*: Activation of p21(WAF1/Cip1) transcription through Sp1 sites by histone deacetylase inhibitor apicidin: involvement of protein kinase C. J Biol Chem 276: 42084-42090, 2001.
15. Fournel M, Trachy-Bourget MC, Yan PT, *et al*: Sulfonamide anilides, a novel class of histone deacetylase inhibitors, are antiproliferative against human tumors. Cancer Res 62: 4325-4330, 2002.
16. Archer SY, Meng S, Shei A and Hodin RA: p21(WAF1) is required for butyrate-mediated growth inhibition of human colon cancer cells. Proc Natl Acad Sci USA 95: 6791-6796, 1998.
17. Sambucetti LC, Fischer DD, Zabludoff S, *et al*: Histone deacetylase inhibition selectively alters the activity and expression of cell cycle proteins leading to specific chromatin acetylation and antiproliferative effects. J Biol Chem 274: 34940-34947, 1999.
18. Gui CY, Ngo L, Xu WS, Richon VM and Marks PA: Histone deacetylase (HDAC) inhibitor activation of p21WAF1 involves changes in promoter-associated proteins, including HDAC1. Proc Natl Acad Sci USA 101: 1241-1246, 2004.
19. Ocker M and Schneider-Stock R: Histone deacetylase inhibitors: signalling towards p21cip1/waf1. Int J Biochem Cell Biol 39: 1367-1374, 2007.
20. Takizawa T, Watanabe K, Narita K, Oguchi T, Abe H and Katoh T: Total synthesis of spiruchostatin B, a potent histone deacetylase inhibitor, from a microorganism. Chem Commun (Camb): 1677-1679, 2008.
21. Kanno S, Kakuta M, Kitajima Y, *et al*: Preventive effect of trimidox on oxidative stress in U937 cell line. Biol Pharm Bull 30: 994-998, 2007.
22. Kanno S, Hiura T, Ohtake T, *et al*: Characterization of resistance to cytosine arabinoside (Ara-C) in NALM-6 human B leukemia cells. Clin Chim Acta 377: 144-149, 2007.
23. Kanno S, Higurashi A, Watanabe Y, Shouji A, Asou K and Ishikawa M: Susceptibility to cytosine arabinoside (Ara-C)-induced cytotoxicity in human leukemia cell lines. Toxicol Lett 152: 149-158, 2004.
24. Lemaire C, Andreau K, Souvannavong V and Adam A: Specific dual effect of cycloheximide on B lymphocyte apoptosis: involvement of CPP32/caspase-3. Biochem Pharmacol 58: 85-93, 1999.
25. Tan J, Cang S, Ma Y, Petrillo RL and Liu D: Novel histone deacetylase inhibitors in clinical trials as anti-cancer agents. J Hematol Oncol 3: 5, 2010.
26. Kim MS, Kwon HJ, Lee YM, *et al*: Histone deacetylases induce angiogenesis by negative regulation of tumor suppressor genes. Nat Med 7: 437-443, 2001.
27. Marquard L, Poulsen CB, Gjerdrum LM, *et al*: Histone deacetylase 1, 2, 6 and acetylated histone H4 in B- and T-cell lymphomas. Histopathology 54: 688-698, 2009.
28. Choi JH, Kwon HJ, Yoon BI, *et al*: Expression profile of histone deacetylase 1 in gastric cancer tissues. Jpn J Cancer Res 92: 1300-1304, 2001.
29. Sasaki H, Moriyama S, Nakashima Y, *et al*: Histone deacetylase 1 mRNA expression in lung cancer. Lung Cancer 46: 171-178, 2004.
30. Zhang Z, Yamashita H, Toyama T, *et al*: Quantitation of HDAC1 mRNA expression in invasive carcinoma of the breast*. Breast Cancer Res Treat 94: 11-16, 2005.
31. Peart MJ, Tainton KM, Ruefli AA, *et al*: Novel mechanisms of apoptosis induced by histone deacetylase inhibitors. Cancer Res 63: 4460-4471, 2003.
32. Abbas T and Dutta A: p21 in cancer: intricate networks and multiple activities. Nat Rev Cancer 9: 400-414, 2009.
33. Arts J, Angibaud P, Marien A, *et al*: R306465 is a novel potent inhibitor of class I histone deacetylases with broad-spectrum antitumoral activity against solid and haematological malignancies. Br J Cancer 97: 1344-1353, 2007.
34. Roman-Gomez J, Castillejo JA, Jimenez A, *et al*: 5' CpG island hypermethylation is associated with transcriptional silencing of the p21(CIP1/WAF1/SDI1) gene and confers poor prognosis in acute lymphoblastic leukemia. Blood 99: 2291-2296, 2002.

Cancer Science
The official journal of the Japanese Cancer Association JCA

Romidepsin (FK228) and its analogs directly inhibit phosphatidylinositol 3-kinase activity and potently induce apoptosis as histone deacetylase/phosphatidylinositol 3-kinase dual inhibitors

Ken Saijo,[1] Tadashi Katoh,[2] Hideki Shimodaira,[1] Akifumi Oda,[3] Ohgi Takahashi[3] and Chikashi Ishioka[1,4]

[1]Department of Clinical Oncology, Institute of Development, Aging and Cancer, Tohoku University, Sendai; [2]Laboratory of Synthetic and Medicinal Chemistry, Department of Chemical Pharmaceutical Sciences; [3]Laboratory of Pharmaceutical Physical Chemistry, Faculty of Pharmaceutical Sciences, Tohoku Pharmaceutical University, Sendai, Japan

(Received March 14, 2012/Revised June 21, 2012/Accepted August 17, 2012/Accepted manuscript online August 24, 2012/Article first published online October 12, 2012)

Activation of phosphatidylinositol 3-kinase (PI3K) signaling is involved in carcinogenesis and cancer progression. The PI3K inhibitors are considered candidate drugs for cancer treatment. Here, we describe a drug screening system for novel PI3K inhibitors using *Saccharomyces cerevisiae* strains with deleterious mutations in the ATP-binding cassette transporter genes, because wild-type *S. cerevisiae* uses drug efflux pumps for reducing intracellular drug concentrations. By screening the chemical library of the Screening Committee of Anticancer Drugs, we identified the histone deacetylase (HDAC) inhibitor romidepsin (FK228) and its novel analogs. *In vitro* PI3K activity assays confirmed that these compounds directly inhibit PI3K activity at μM-range concentrations. FK-A5 analog was the most potent inhibitor. Western blotting revealed that these compounds inhibit phosphorylation of protein kinase B and downstream signaling components. Molecular modeling of the PI3K–FK228 complex indicated that FK228 binds to the ATP-binding pocket of PI3K. At μM-range concentrations, FK228 and FK-A5 show potent cytotoxicity, inducing apoptosis even in HDAC inhibitor-resistant cells. Furthermore, HDAC/PI3K dual inhibition by FK228 and FK-A5 at μM-range concentrations potentiates the apoptosis induction, mimicking the effect of combining specific HDAC and PI3K inhibitors. In this study, we showed that FK228 and its analogs directly inhibit PI3K activity and induce apoptosis at μM-range concentrations, similar to HDAC/PI3K dual inhibition. In future, optimizing the potency of FK228 and its analogs against PI3K may contribute to the development of novel HDAC/PI3K dual inhibitors for cancer treatment. (*Cancer Sci* 2012; 103: 1994–2001)

Phosphatidylinositol 3-kinase (PI3K) phosphorylates phosphatidylinositol 4,5-bisphosphate (PIP2) at the 3-OH group of the inositol ring, generating phosphatidylinositol 3,4,5-trisphosphate (PIP3).[1] In turn, PIP3 activates protein kinase B (AKT) and downstream molecules, leading to increased cell growth, proliferation, and survival.[2] Class IA PI3K is composed of a catalytic subunit, p110, and a regulatory subunit, p85. *PIK3CA* encodes p110α, and is frequently mutated in human cancers.[3] Because almost all of the mutations are functionally active,[4] activation of PI3K is likely to play a crucial role in carcinogenesis and cancer progression. Phosphatase and tensin homologue deleted on chromosome 10 (PTEN) dephosphorylates PIP3 to PIP2 as the catalytic counterpart of PI3K.[5] In addition to *PIK3CA* mutations, inactivating mutations in, or loss of, *PTEN* have also been observed in human cancers, supporting the involvement of PI3K in cancer.[6] Therefore, inhibitors of PI3K are considered to be candidate drugs for cancer therapy. Indeed, some PI3K inhibitors have entered clinical trials, but efforts are still underway to develop new PI3K inhibitors.[7]

To discover novel PI3K inhibitors, we took advantage of a drug screening system that uses a strain of the yeast *Saccharomyces cerevisiae* with deleterious mutations in ATP-binding cassette (ABC) transporter genes. We used this strain because intracellular drug concentrations in yeast with wild-type ABC transporter genes are efficiently reduced by drug efflux pumps.[8] The screening system is based on growth inhibition induced by overexpression of membrane-localized p110α in yeast, in which no endogenous p110 homolog is expressed.[9] Conversion of the essential PIP2 pool to PIP3 by exogenous p110α expression impairs yeast growth by altering morphogenesis and vesicular trafficking.[10] The PI3K inhibitor LY294002 is reportedly able to reverse this p110α-induced growth inhibition.[10] Similarly, other compounds with the ability to inhibit PI3K can rescue cells from p110α-induced growth inhibition. Using this system, we screened the deposited chemical library of the Screening Committee of Anticancer Drugs (SCADS) and thereby isolated a histone deacetylase (HDAC) inhibitor, romidepsin (FK228), and its analogs. FK228 is a potent HDAC inhibitor, with recent approval for the treatment of cutaneous T-cell lymphoma.[11] The HDAC inhibitors have pleiotropic antitumor activities, because of their ability to act on non-histone targets.[12] However, there is no evidence that HDAC inhibitors have kinase inhibitory activities. Here, we showed that FK228 and its analogs directly inhibit PI3K activity, and we evaluated their cytotoxicity as HDAC/PI3K dual inhibitors.

Materials and Methods

Plasmids. The plasmid pSJ01 is a CEN/ARS URA3 vector, which expresses p110α plus the palmitoylation signal from H-Ras (p110α–CAAX) under the control of *GAL1* promoter. To generate pSJ01, the full-length open reading frame PIK3CA cDNA (a gift from Peter K. Vogt, The Scripps Research Institute, La Jolla, CA, USA) was amplified by PCR adding the CAAX motif immediately before the stop codon. The plasmid pSJ21 is a CEN/ARS LEU2 vector, which expresses wild-type PTEN. pRS315 and pRS316 are CEN/ARS LEU2 and URA3 vectors, respectively, and they were used as control vectors.[13]

Yeast strains and media. Yeast strains used were YPH499 (*MATa, ura3-52, lys2-801, ade2-101, trp1-Δ63, his3-Δ200, leu2-Δ1*) and AD1-9 (*MATα, Δyor1, Δsnq2, Δpdr5, Δpdr10, Δpdr11, Δycf1, Δpdr3, Δpdr15, Δpdr1, Δhis1, Δura3*). YPH499

[4]To whom correspondence should be addressed.
E-mail: chikashi@idac.tohoku.ac.jp

doi: 10.1111/cas.12002
© 2012 Japanese Cancer Association

was purchased from Stratagene (La Jolla, CA, USA). AD1-9 was gifted by Nader Nourizad (Stanford University, Stanford, CA, USA). In AD1-9, to append another auxotrophic selection marker, generating AD1-9_*leu2*, *LEU2* was disrupted by means of a *hisG-URA3-hisG* cassette.[14] A general non-selective yeast growth medium, YPD broth, or agar was used. Synthetic minimal medium (SD) contained glucose and lacked auxotrophic markers uracil (U) and leucine (L). In synthetic galactose medium (SGal), glucose was replaced with galactose.

Chemical library. The SCADS deposited chemical library was kindly provided by SCADS, supported by a Grant-in-Aid for Scientific Research on Innovative Areas and Scientific Support Programs for Cancer Research from the Ministry of Education, Culture, Sports, Science and Technology, Japan. The library was composed of three 96-well plates. All compounds were dissolved in DMSO.

Chemicals. LY294002 and suberoylanilide hydroxamic acid (SAHA) were purchased from Cayman Chemical (Ann-Arbor, MI, USA). Trichostatin A was purchased from Sigma-Aldrich (St. Louis, MI, USA). FK228 and its analogs were synthesized and provided by T. K.

Screening system for PI3K inhibitors using *S. cerevisiae*. The sets of plasmids, pRS316 and pRS315, pSJ01 (expressing p110α) and pRS315, and pSJ01 and pSJ21 (coexpressing p110α and PTEN) were transformed into AD1-9_*leu2*. The transformants were incubated overnight in SD-U-L and adjusted to an A_{600} of 0.3. We inoculated 10 μL transformant cells to 200 μL aliquots of SGal-U-L media containing each test compound. The aliquots were then incubated with shaking in 96-well plates for 24 h at 30°C. Compounds that showed an increase in A_{600} value among the transformants expressing p110α were identified as candidates.

***In vitro* PI3K assay.** PI3K activity was evaluated by an electrophoretic mobility shift assay (Carna Biosciences, Kobe, Japan). Compound solutions (1000 nM PIP2, 50 μM ATP, 5 mM MgCl, and 21 nM PI3K [p110α/p85α]) were prepared with assay buffer containing 2 mM DTT (Carna Biosciences) and mixed and incubated in a 384-well microplate for 5 h at room temperature. To evaluate the ATP-competitive effect, PI3K activity was also examined under a higher concentration of ATP (500 μM) and a shorter incubation period (2 h). Reaction mixtures were then applied to the LabChip (Caliper Life Sciences, Hopkinton, MA, USA), and the product, PIP3, and substrate, PIP2, peaks were separated and quantified. The PI3K reaction was evaluated by the product ratio, calculated from peak heights of the product and substrate.

Molecular modeling of the PI3K–FK228 complex. Construction and conformational analysis of the PI3K–FK228 complex structure models were carried out using eHiTS (SimBioSys, San Francisco, CA, USA). The structure of the PI3K (p110α H1047R/p85α)–wortmannin complex (Protein Data Bank Identification Code: 3HHM) was used to obtain the PI3K template structure. FK228 is a pro-drug and is structurally changed in cells to a reduced active form for HDAC inhibition.[15] Therefore, the structure of reduced FK228 was applied in this docking simulation. The top-ranked docking model, according to the eHiTS score, was adopted and displayed.

Cell lines. The human cancer cell lines used in this study were the prostate cancer cell line PC3 (Cell Resource Center, Institute of Development, Aging, and Cancer, Tohoku University, Sendai, Japan) and the colorectal cancer cell lines HCT116 and RKO (both ATCC, Manassas, VA, USA), and CO115 (kindly provided by John M. Mariadason, Ludwig Institute for Cancer Research, Melbourne, Vic., Australia). Cells were cultured in RPMI-1640 medium (Sigma-Aldrich) containing 10% FBS.

Western blot analysis. Cells treated with test compounds were harvested and lysed in a buffer (500 mM Tris-HCl [pH 7.5], 100 mM NaCl, 2 mM EDTA, 1 mM sodium orthovanadate, 1% Tergitol-type NP-40, and 1% protease inhibitor cocktail; Sigma-Aldrich). Cell lysates were separated by SDS-PAGE, followed by electroblotting onto PVDF membranes (Millipore, Billerica, MA, USA). Rabbit polyclonal antibodies for AKT, phosphorylated AKT (Ser473), phosphorylated AKT (Thr308), phosphorylated GSK-3β (Ser9), phosphorylated mTOR (Ser2448), phosphorylated p70S6K (Thr389), phosphorylated 4E-BP1 (Thr37/46), phosphorylatedMEK1/2 (Ser217/221), and phosphorylated ERK1/2 (Thr202/Tyr204) were all purchased from Cell Signaling Technology (Danvers, MA, USA). Other antibodies were purchased as follows: anti-β-actin monoclonal antibody (Sigma-Aldrich), anti-PARP1/2 polyclonal antibody (Santa Cruz Biotechnology, Santa Cruz, CA, USA), anti-acetyl-Histone H3 and anti-acetyl-histone H4 (Upstate Biotechnology, Lake Placid, NY, USA), and Alexa Fluor 680 as a secondary antibody (Invitrogen, Carlsbad, CA, USA). Immunoreactive bands were detected using the Odyssey Infrared Imaging System (LI-COR Biosciences, Lincoln, NE, USA).

Cell proliferation assay. The colorectal cancer cell lines HCT116, CO115, and RKO were used. A total of 8×10^3 cells per well were seeded and incubated into 96-well plates for 24 h. They were then treated with compounds and further cultured for 24 h at 37°C. Cell viability was assayed by quantifying the uptake and digestion of 2-(2-methoxy-4-nitrophenyl)-3-(4-nitrophenyl)-5-(2,4-disulfophenyl)-2H-tetrazolium monosodium salt (Dojindo Laboratories, Kumamoto, Japan) using a SpectraMax M2e. We calculated the ratio of surviving cells to controls treated with 1% DMSO alone.

Cell cycle analysis by FACS. HCT116 cells were seeded into six-well plates at a concentration of 2×10^5 per well, exposed to the compounds at various concentrations, cultured for 24 h, collected, and sorted by FACS using the Cytomics FC 500 flow cytometry system (Beckman Coulter, Brea, CA, USA).

Results

Human PI3K induces growth inhibition in *S. cerevisiae*. Ectopic expression of human p110α inhibited the growth of the YPH499 strain of yeast. In contrast, coexpression of wild-type PTEN in p110α-expressing yeast rescued this growth inhibition (Fig. 1A,B). In YPH499, the PI3K inhibitor LY294002 partially rescued the growth inhibition in the transformants expressing p110α (Fig. 1B), as previously reported.[10] Similar results were observed with AD1-9 (data not shown), a drug-sensitive strain due to the deletion of seven ABC transporters.[16] We compared the sensitivity of AD1-9 to the PI3K inhibitor LY294002 with that of the wild-type strain YPH499. The growth inhibition induced by p110α expression was rescued at a LY294002 concentration of 50 μM in YPH499 (Fig. 1C); in contrast, this rescue was achieved at 5 μM LY294002 in AD1-9 (Fig. 1D). This result indicates that AD1-9 is approximately 10 times more sensitive to LY294002 compared to YPH499; therefore, AD1-9 was used for drug screening.

Screening of chemical library. We screened the SCADS deposited chemical library using the yeast screening system. All compounds were tested at two different concentrations, 0.5 and 5 μM. No compounds recovered the cells at a concentration of 0.5 μM (data not shown). However, at a concentration of 5 μM, some compounds rescued the p110α-induced growth inhibition, as with LY294002 (Fig. 1E). As a result, we identified seven compounds as candidate PI3K inhibitors; these included an HDAC inhibitor, FK228, and its analogs (Fig. 1E). The structures of FK228 and its analogs and their IC_{50} values for HDAC1 and HDAC6 examined by SCADS are shown in Figure 2. All of them strongly inhibited HDAC1 in a selective manner.

Inhibition of PI3K activity by FK228 and its analogs. Eleven compounds including the seven screened compounds (FK228,

© 2012 Japanese Cancer Association

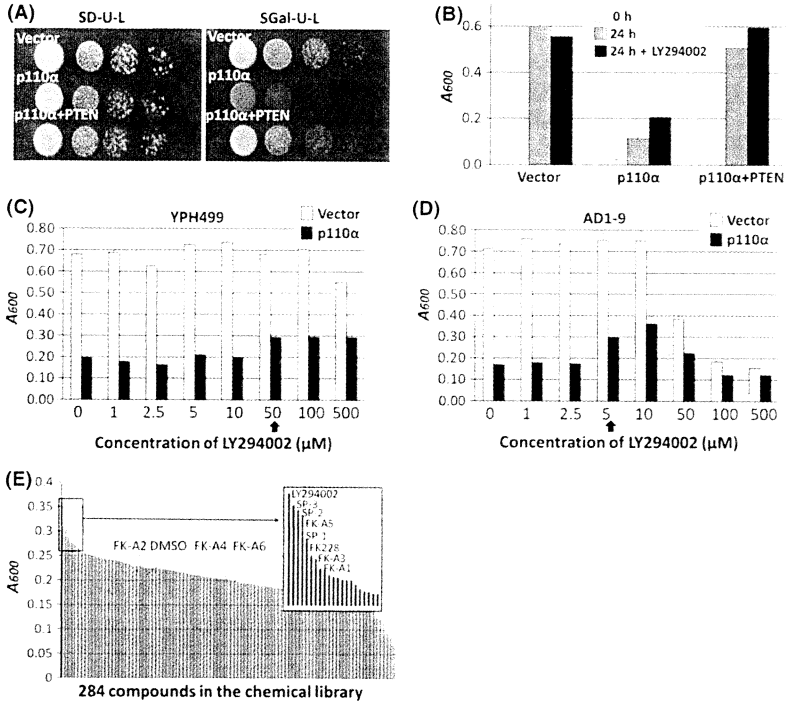


Fig. 1. Identification of FK228 and its analogs as candidate phosphatidylinositol 3-kinase (PI3K) inhibitors using *Saccharomyces cerevisiae*. (A) YPH499 was cotransformed with the following sets of *URA3* and *LEU2* marked vectors: top row, pRS316 and pRS315; second row, pSJ01 (p110α) and pRS315; and third row, pSJ01 and pSJ21 (PTEN). Serial 10-fold dilutions of the transformants were deposited on solid synthetic minimal medium–uracil –leucine (SD-U-L) and synthetic galactose medium (SGal)-U-L media. (B) YPH499 transformants were incubated in SGal-U-L medium, with or without 50 μM LY294002. Then A_{600} was measured as an indicator of yeast growth. (C,D) Transformants of YPH499 and AD1-9 expressing p110α were cultured in SGal-U-L medium containing various concentrations of LY294002. Sensitivity for LY294002 was compared by detecting the concentration at which growth inhibition was rescued (arrow). (E) Screening results of the chemical library of the Screening Committee of Anticancer Drugs. AD1-9 transformants expressing p110α were cultured in SGal-U-L media containing each compound. A_{600} values are the mean of experiments carried out in triplicate. Test compounds are arranged according to A_{600} values in the figure. LY294002, DMSO, and FK228 and its analogs are indicated.

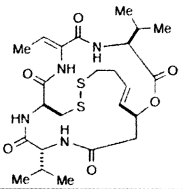
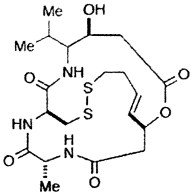
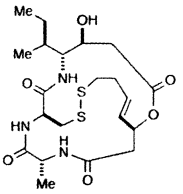
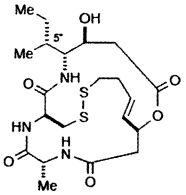
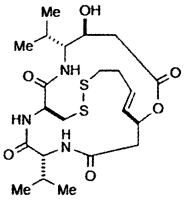
SP-1, SP-2, SP-3, FK-A1, FK-A3, and FK-A5) and four other FK228 analogs (SP-5, FK-A2, FK-A4, and FK-A6) were examined for PI3K inhibition at a concentration of 20 μM by mobility shift assay. All compounds directly inhibited PI3K activity (Fig. 3A). Of these, FK-A5 was the most potent, whereas SP-3 was the weakest (Fig. 3A). Next, we determined the IC_{50} for PI3K activity. The IC_{50} values of FK228, FK-A5, SP-3, and LY294002 were 57.1, 26.2, 107.0 and 0.7 μM, respectively (Fig. 3B–E). FK-A5 showed double the activity of FK228 and 4-fold the activity of SP-3, but its activity was 37-fold less than that of LY294002. These data indicate that FK228 and its analogs directly inhibit PI3K activity, but that the potency of inhibitory activity differs among analogs.

Molecular modeling of the PI3K–FK228 complex. All known PI3K inhibitors are ATP-competitive inhibitors;[17] therefore, we investigated whether FK228 was capable of binding to the ATP-binding site of p110α. As shown in Figure 4, the ATP-binding pocket of p110α was occupied by reduced FK228. Additionally, PI3K inhibitory activity of FK228 was weakened under the high concentration of ATP *in vitro* assay (Fig. 3F). The IC_{50} values of FK228 under the standard ATP concentration (50 μM) and high ATP concentration (500 μM) were 57.2 and 125.0 μM, respectively. These data suggest that FK228 is an ATP-competitive PI3K inhibitor.

Inhibition of AKT phosphorylation and downstream signaling by FK228 and FK-A5. We used PC3 cells to evaluate FK228 and FK-A5-mediated inhibition of the AKT pathway by Western blotting, because PC3 cells are PTEN-null and show constitutively active AKT.[18] FK228 and FK-A5 as well as LY294002 inhibited the AKT phosphorylation within 30 min, without altering total AKT levels, at a concentration of 10 μM (Fig. 5A). Next, we investigated the effect of various concentrations of FK228 and FK-A5 on AKT and its downstream signaling components. FK228 and FK-A5 inhibited phosphorylation of AKT, GSK-3β, mTOR, p70S6K, and 4E-BP1 in a dose-dependent manner at μM-range concentrations. As for the Ras-MAP kinase pathway, another major signaling pathway involved in cell proliferation, the level of phosphorylated MEK1/2 was unaltered, but the level of phosphorylated ERK1/2 was reduced slightly by the addition of 30 μM FK228 or FK-A5. These results indicate that FK228 and FK-A5 act primarily through the AKT signaling pathway and that they are capable of exerting inhibitory activity on other kinases.

Antiproliferative effects of FK228, FK-A5, and SP-3. Among the FK228 analogs, FK-A5 is the most potent PI3K inhibitor, and SP-3 is the weakest (Fig. 3A). However, those analogs retain almost equal activity as HDAC inhibitors (Fig. 2). To examine the antiproliferative effects of FK228, FK-A5, and SP-3, we used the HDAC inhibitor-resistant cell lines RKO and CO115 as well as the HDAC inhibitor-sensitive cell line HCT116.[19,20] HCT116, RKO, and CO115 are colorectal cancer cells with microsatellite instability. In RKO and CO115 cells, biallelic frameshift mutations occur in the $(A)_9$ repeat of exon 1 of *HDAC2*, leading to the loss of HDAC2.[19,20] This loss induces apoptotic protease-activating factor-1 expression, which dysregulates apoptosis and renders the cells resistant to HDAC inhibitors.[20] In HDAC inhibitor-sensitive HCT116 cells, SAHA at a concentration of 2.5 μM, and FK228, FK-A5, and SP-3 at nM-range concentrations inhibited cell growth by 30–60% (Fig. 6). In contrast, CO115 and RKO were more resistant to these HDAC inhibitors than HCT116 cells (Fig. 6). Similar results were observed when 250 nM trichostatin A was used as another HDAC inhibitor (Fig. S1). All three cell lines examined were sensitive to LY294002, which reduced cell counts by 41–51%. The combination of LY294002 and SAHA caused enhanced antiproliferative effects in HCT116 cells, but not in RKO or CO115 cells. The combination of LY294002 and FK228, FK-A5, or SP-3 at nM-range concentrations resulted in enhanced antiproliferative effects in HCT116 cells. Conversely, in RKO and CO115 cells, these combinations did not enhance antiproliferative effects, resulting in an effect almost identical to that of LY294002 monotherapy. At concentrations of 5 and 50 μM to inhibit PI3K activity, FK228 or FK-A5 monotherapy showed potent antiproliferative (cytotoxic) effects, reducing 80–90% of cell counts, even in HDAC inhibitor-resistant cells. However, SP-3, with its poor PI3K

doi: 10.1111/cas.12002
© 2012 Japanese Cancer Association

Compound	Structure	HDAC1 IC50	HDAC6 IC50
FK228 $C_{24}H_{36}N_4O_6S_2$ MW:540.70		0.0036 μM	0.39 μM
SP-1 spiruchostatin A $C_{20}H_{31}N_3O_6S_2$ MW:473.61		0.0033 μM	1.60 μM
SP-2 spiruchostatin B $C_{21}H_{33}N_3O_6S_2$ MW:487.63		0.0022 μM	1.40 μM
SP-3 5″-*epi*-spiruchostatin B $C_{21}H_{33}N_3O_6S_2$ MW:487.63		0.0024 μM	3.90 μM
SP-5 spiruchostatin D $C_{22}H_{35}N_3O_6S_2$ MW:501.66		Not examined	Not examined

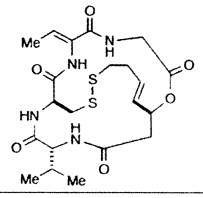
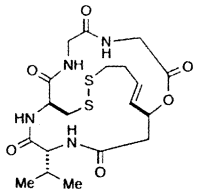
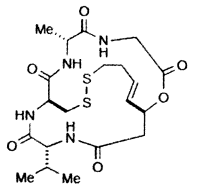
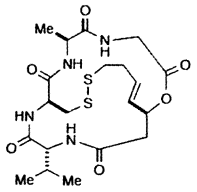
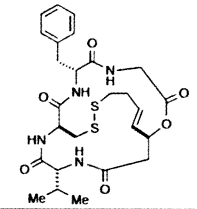
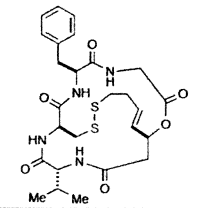
Compound	Structure	HDAC1 IC50	HDAC6 IC50
FK-A1 $C_{21}H_{30}N_4O_6S_2$ MW:498.62		0.0078 μM	3.20 μM
FK-A2 $C_{19}H_{28}N_4O_6S_2$ MW:472.58		0.045 μM	4.80 μM
FK-A3 $C_{20}H_{30}N_4O_6S_2$ MW:486.61		0.0042 μM	3.20 μM
FK-A4 $C_{20}H_{30}N_4O_6S_2$ MW:486.61		0.34 μM	2.10 μM
FK-A5 $C_{26}H_{34}N_4O_6S_2$ MW:562.70		0.0025 μM	1.60 μM
FK-A6 $C_{26}H_{34}N_4O_6S_2$ MW:562.70		0.019 μM	2.90 μM

Fig. 2. Structures and histone deacetylase (HDAC) inhibitory activity of FK228 and its analogs. The structures of FK228 and the analogs examined in this study and their IC_{50} values for HDAC1 and HDAC6 are shown.

inhibitory activity, did not potentiate the antiproliferative effect at μM-range concentrations. These results suggest that inhibition of PI3K activity enhances the cytotoxicity of FK228 or FK-A5 at μM-range concentrations.

Effects of FK228, FK-A5, and SP-3 on apoptosis and cell cycle. We carried out a FACS analysis of cell death induced by FK228 and FK-A5. HCT116 cells were treated with LY294002, SAHA, FK228, or FK-A5 under the same conditions as in the cell proliferation assay. The cell cycle phases at which HDAC inhibitors induce arrest are reported to differ depending on the drug concentration and cell line.[21–23] In this experiment, SAHA induced G_2/M arrest in HCT116 cells (Fig. 7A). FK228 and FK-A5 at nM-range concentrations also induced G_2/M arrest (Fig. 7B). In contrast, inhibition of PI3K was reported to induce G_0/G_1 arrest.[24,25] In agreement with the previous reports, LY294002 induced G_0/G_1 arrest (Fig. 7A). The combination of LY294002 and SAHA, and combinations of LY294002 with either FK228 or FK-A5 at nM-range concentrations increased the sub-G_1 fraction to approximately 40%, indicating apoptosis induction (Fig. 7A,B). At a concentration of 5 μM, FK228 or FK-A5 increased the sub-G_1 fraction to 37%, and the DNA histograms were similar to those of combination therapy with LY294002 and an HDAC inhibitor (Fig. 7A,B). Apoptosis induction by FK228 and FK-A5 was

© 2012 Japanese Cancer Association

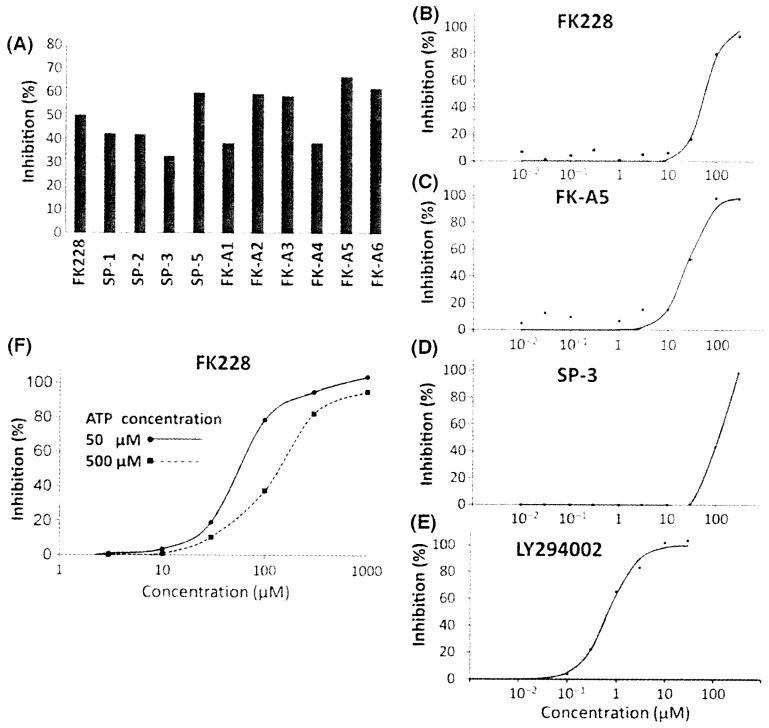


Fig. 3. Effects of FK228 and its analogs on phosphatidylinositol 3-kinase (PI3K) activity. (A) Inhibition of PI3K activity was evaluated by mobility shift assay. The read-out value of a control reaction (complete reaction mixture) was set as a 0% inhibition, and the percentage inhibition of each test solution was calculated at a concentration of 20 μM. Data are the mean of two experiments carried out in duplicate. (B–E) IC_{50} values of FK228, FK-A5, SP-3, and LY294002 were calculated from concentration versus % inhibition curves by fitting to a four-parameter logistic curve. (F) Inhibition of PI3K activity of FK228 was evaluated under the conditions of two different ATP concentrations, 50 and 500 μM. Each concentration versus % inhibition curve is shown.

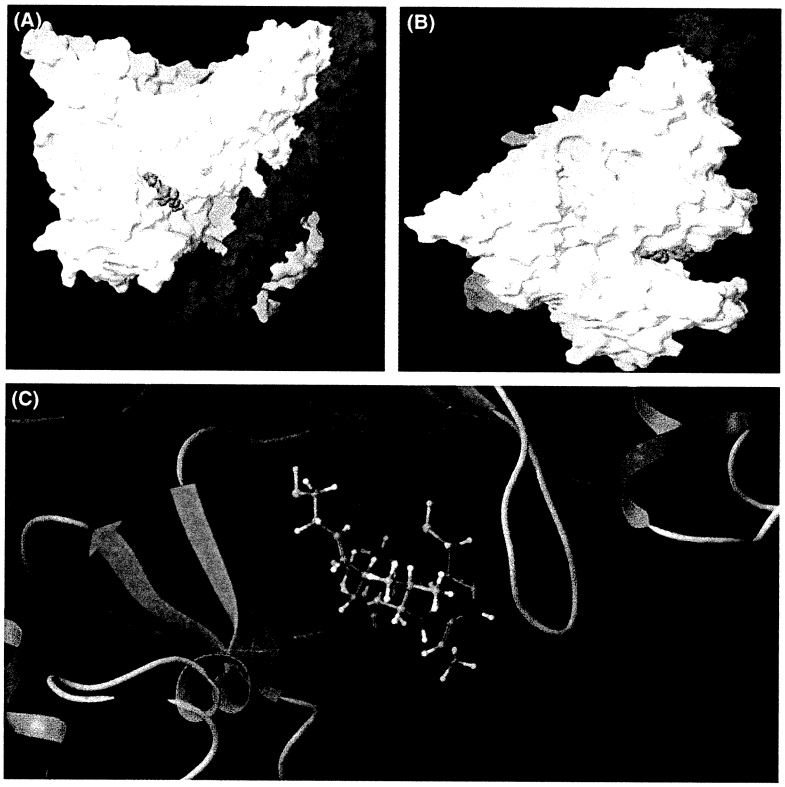


Fig. 4. Molecular modeling of the phosphatidylinositol 3-kinase (PI3K)–FK228 complex. (A) Molecular surface structure of the PI3K–FK228 complex model. Orange, reduced form of FK228; red, p85α; white, p110α. (B) Side view of Fig. 4(A). (C) Enlarged picture around the ligand. A ball and stick model shows the reduced FK228 in the PI3K ribbon and line drawing.

supported by increased expression of cleaved PARP (Fig. 7C). FK228 and FK-A5 at a concentration of 5 μM caused the greatest elevation in the level of cleaved PARP, potently inducing apoptosis, in accordance with the results from the FACS analysis. Furthermore, FK228 and FK-A5 at this concentration simultaneously inhibited AKT phosphorylation and accelerated histone acetylation (Fig. 7C). Similar results were observed in CO115 treated with FK-A5 (Fig. 7D). In contrast, SP-3 did not

doi: 10.1111/cas.12002
© 2012 Japanese Cancer Association

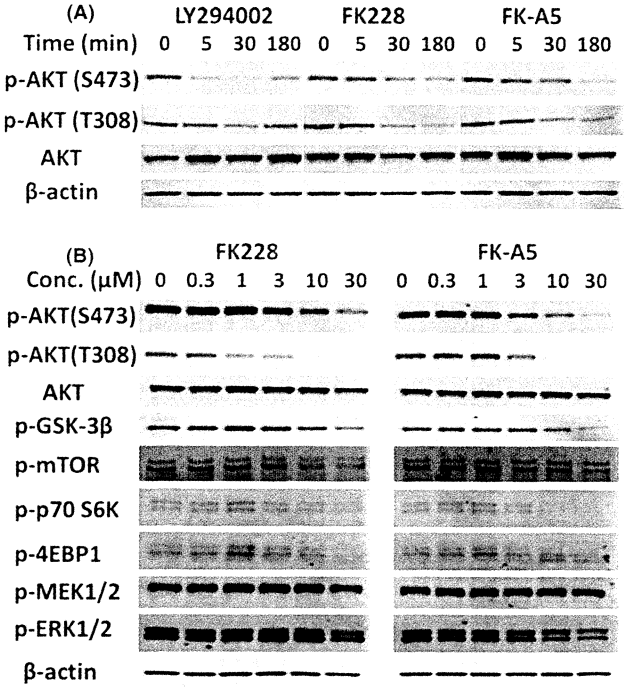


Fig. 5. Western blot analysis of protein kinase B (AKT) and its downstream components in cells treated with FK228 or FK-A5. (A) Evaluation of the experimental time course. PC3 cells were treated with LY294002, FK228, or FK-A5 at a concentration of 10 μM. (B) Effect of various concentrations of FK228 or FK-A5 on AKT and its downstream signaling components. PC3 cells were treated with FK228 or FK-A5 for 3 h.

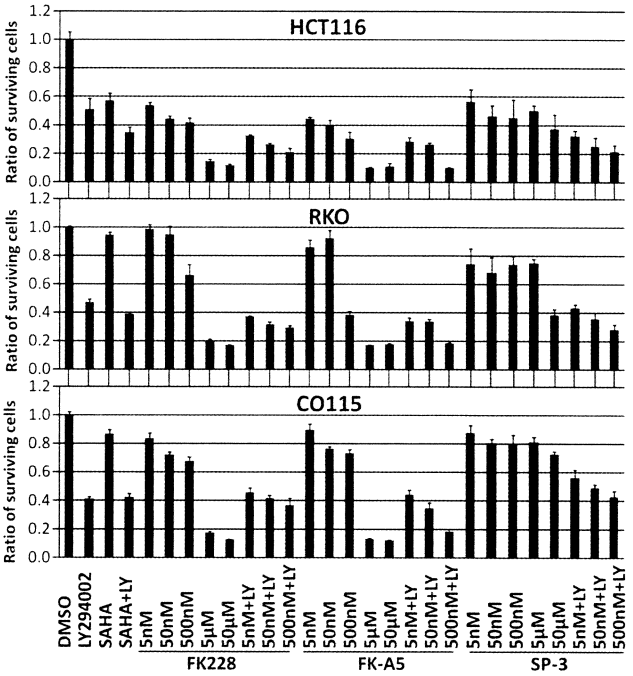


Fig. 6. Antiproliferative effects of FK228, FK-A5, and SP-3. HCT116, RKO, and CO115 colorectal cancer cells were treated with: DMSO; 50 μM LY294002 (LY); 2.5 μM suberoylanilide hydroxamic acid (SAHA); a combination of 50 μM LY with 2.5 μM SAHA; FK228, FK-A5, or SP-3 at concentrations of 5, 50, 500 nM, 5, and 50 μM; and a combination of 50 μM LY with FK228, FK-A5, or SP-3 at concentrations of 5, 50, and 500 nM. The cell viability was assayed 24 h after treatment. The ratio of surviving cells to the controls treated with 1% DMSO was calculated.

inhibit AKT phosphorylation, although it acetylated histone (Fig. 7D). These results indicate that μM-range concentrations of FK228 and FK-A5 potently induce apoptosis through HDAC/PI3K dual inhibition.

Discussion

In this study, we identified FK228 and its analogs as novel PI3K inhibitors. FK228 is a potent HDAC inhibitor, with recent approval for use in the treatment of cutaneous T-cell lymphoma.[11] The HDAC inhibitors have pleiotropic antitumor activities because of their ability to act on non-histone targets.[12] However, until now, there have been no reports documenting its function as a kinase inhibitor. In this study, we add a new mechanism of direct PI3K inhibition to the pleiotropic functions of FK228 in antitumor activity.

Kodani *et al.*[26] reported that 2–10 nM FK228 inhibited AKT phosphorylation and suppressed the PI3K/AKT pathway in A549 lung cancer cells, although they did not elucidate the mechanism for this in their study. They showed that 5 nM FK228 dephosphorylated AKT in 24 h, but not in 6 or 12 h.[26] In contrast, we showed that AKT dephosphorylation by FK228 began in 5 min, in a manner similar to that for LY294002 (Fig. 5A). In addition, we showed that the concentration at which FK228 had PI3K inhibitory activity was within the μM-range. Thus, we speculated that the suppression of the AKT pathway by FK228 reported by Kodani *et al.*[26] does not occur by direct inhibition of PI3K, but through another indirect mechanism, such as epigenetic alteration. This study is the first to show that FK228 directly inhibits PI3K activity.

FK228 is structurally changed in cells to a reduced active form for HDAC inhibition.[15] Therefore, it is assumed that the reduced FK228 is also active for PI3K inhibition. Supporting that, *in vitro* PI3K assay was carried out under conditions containing 2 mM DTT which is expected to reduce FK228 and its analogs. In Figures 5 and 7, FK228 and FK-A5 inhibited the AKT signaling pathway in cells at lower concentrations than *in vitro* IC_{50} values. We speculated that reduction power *in vitro* might be insufficient compared to that in cells, for changing FK228 and FK-A5 to active form.

The results of the cell proliferation assay revealed that μM-range concentrations of FK228 or FK-A5 resulted in potent cytotoxicity, even in HDAC inhibitor-resistant cells (Fig. 6). Furthermore, the results of FACS and Western blotting showed that the cause of cell death was apoptosis. We suggest that HDAC/PI3K dual inhibition by FK228 or FK-A5 at μM-range concentrations contributes to the potent apoptosis induction because: (i) FK228 and FK-A5 at μM concentrations inhibited AKT phosphorylation and acetylated histones simultaneously (Fig. 7C,D); (ii) both apoptosis and the effects on the cell cycle induced by FK228 or FK-A5 at μM-range concentrations mimicked the effects of a combination of individual HDAC and PI3K inhibitors as measured by FACS analyses (Fig. 7A, B); and (iii) SP-3 with poor PI3K inhibitory activity could not potentiate the cytotoxic effect. The combination of an HDAC inhibitor with a PI3K inhibitor was shown to result in cytotoxic synergy[27], therefore, a HDAC/PI3K dual inhibitor could contribute greatly to the treatment of refractory cancer.

FK228 and its analogs are potent HDAC inhibitors, capable of inhibiting HDAC1 at nM-range concentrations.[28] In contrast, the PI3K inhibitory activity of these compounds is shown within the μM range. Of these analogs, FK-A5 and FK-A6 were the most potent PI3K inhibitors (Fig. 3A). FK-A5

© 2012 Japanese Cancer Association

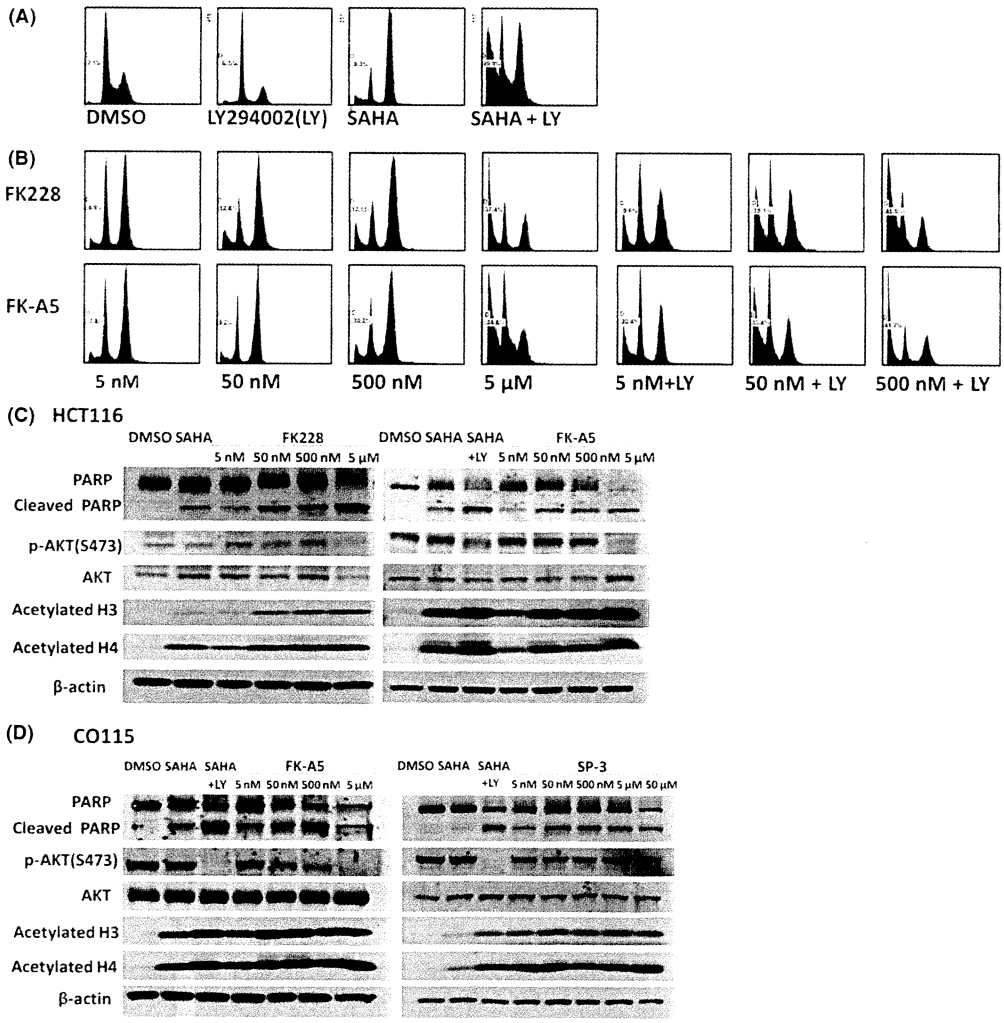


Fig. 7. Effects of FK228, FK-A5, and SP-3 on apoptosis, cell cycle, protein kinase B (AKT) phosphorylation, and histone acetylation. (A,B) HCT116 colorectal cancer cells were treated with: DMSO; 50 μM LY294002 (LY); 2.5 μM suberoylanilide hydroxamic acid (SAHA); a combination of 50 μM LY with 2.5 μM SAHA; FK228 or FK-A5 at concentrations of 5, 50, 500 nM, and 5 μM; and a combination of 50 μM LY with FK228 or FK-A5 at concentrations of 5, 50, and 500 nM. The cells were harvested 24 h after treatment. (C,D) Western blot analysis of poly(ADP-ribose) polymerase (PARP) cleavage, AKT dephosphorylation, and histone acetylation by FK228, FK-A5, or SP-3 in HCT116 and CO115 cells cultured as indicated in Fig. 6.

and FK-A6 are stereoisomers and have a characteristic structure, possessing a benzyl group in position 7 (Fig. 2). If their structural differences are found to be responsible for the greater potency compared with other analogs, this would provide us with a clue regarding optimization of the PI3K inhibitory activity of these compounds.

In conclusion, we showed that FK228 and its analogs directly inhibit PI3K activity and potently induce apoptosis through HDAC/PI3K dual inhibition at μM-range concentrations. Further studies are required to identify analogs that can inhibit PI3K more potently.

Acknowledgments

This study was supported by the Ministry of Education, Culture, Sports, Science and Technology, Japan, the Ministry of Health, Labour and Welfare, Japan, and the Japan Science and Technology Agency.

Disclosure Statement

Chikashi Ishioka received a research grant from Chugai Pharmaceutical Co. and Novartis Pharma K.K., and also recieved lecture fees from Taiho Pharmaceutical Co. None of the other authors has any conflict of interest.

References

1 Fruman DA, Meyers RE, Cantley LC. Phosphoinositide kinases. *Annu Rev Biochem* 1998; **67**: 481–507.
2 Cantley LC. The phosphoinositide 3-kinase pathway. *Science* 2002; **296**: 1655–7.
3 Samuels Y, Wang Z, Bardelli A *et al.* High frequency of mutations of the PIK3CA gene in human cancers. *Science* 2004; **304**: 554.
4 Ikenoue T, Kanai F, Hikiba Y *et al.* Functional analysis of PIK3CA gene mutations in human colorectal cancer. *Cancer Res* 2005; **65**: 4562–7.

doi: 10.1111/cas.12002
© 2012 Japanese Cancer Association

5 Maehama T, Dixon JE. The tumor suppressor, PTEN/MMAC1, dephosphorylates the lipid second messenger, phosphatidylinositol 3,4,5-trisphosphate. *J Biol Chem* 1998; **273**: 13375–8.
6 Salmena L, Carracedo A, Pandolfi PP. Tenets of PTEN tumor suppression. *Cell* 2008; **133**: 403–14.
7 Kong D, Yamori T. Advances in development of phosphatidylinositol 3-kinase inhibitors. *Curr Med Chem* 2009; **16**: 2839–54.
8 Barberis A, Gunde T, Berset C, Audetat S, Luthi U. Yeast as a screening tool. *Drug Discovery Today: Technologies* 2005; **2**: 187–92.
9 Cid V, Rodríguez-Escudero I, Andrés-Pons A *et al.* Assessment of PTEN tumor suppressor activity in nonmammalian models: the year of the yeast. *Oncogene* 2008; **27**: 5431–42.
10 Rodríguez-Escudero I, Roelants FM, Thorner J, Nombela C, Molina M, Cid VJ. Reconstitution of the mammalian PI3K/PTEN/Akt pathway in yeast. *Biochem J* 2005; **390**: 613–23.
11 Bertino EM, Otterson GA. Romidepsin: a novel histone deacetylase inhibitor for cancer. *Expert Opin Investig Drugs* 2011; **20**: 1151–8.
12 Xu W, Parmigiani R, Marks P. Histone deacetylase inhibitors: molecular mechanisms of action. *Oncogene* 2007; **26**: 5541–52.
13 Sikorski RS, Hieter P. A system of shuttle vectors and yeast host strains designed for efficient manipulation of DNA in *Saccharomyces cerevisiae*. *Genetics* 1989; **122**: 19–27.
14 Alani E, Cao L, Kleckner N. A method for gene disruption that allows repeated use of USR3 selection in the construction of multiply disrupted yeast strains. *Genetics* 1987; **116**: 541–5.
15 Furumai R, Matsuyama A, Kobashi N *et al.* FK228 (depsipeptide) as a natural prodrug that inhibits class I histone deacetylases. *Cancer Res* 2002; **62**: 4916–21.
16 Rogers B, Decottignies A, Kolaczkowski M, Carvajal E, Balzi E, Goffeau A. The pleitropic drug ABC transporters from *Saccharomyces cerevisiae*. *J Mol Microbiol Biotechnol* 2001; **3**: 207–14.
17 Walker EH, Pacold ME, Perisic O *et al.* Structural determinants of phosphoinositide 3-kinase inhibition by wortmannin, LY294002, quercetin, myricetin, and staurosporine. *Mol Cell* 2000; **6**: 909–19.
18 Grunwald V, DeGraffenried L, Russel D, Friedrichs WE, Ray RB, Hidalgo M. Inhibitors of mTOR reverse doxorubicin resistance conferred by PTEN status in prostate cancer cells. *Cancer Res* 2002; **62**: 6141–5.
19 Ropero S, Fraga MF, Ballestar E *et al.* A truncating mutation of HDAC2 in human cancers confers resistance to histone deacetylase inhibition. *Nat Genet* 2006; **38**: 566–9.
20 Hanigan CL, van Engeland M, De Bruine AP *et al.* An inactivating mutation in HDAC2 leads to dysregulation of apoptosis mediated by APAF1. *Gastroenterology* 2008; **135**: 1654–64.
21 Richon VM, Sandhoff TW, Rifkind RA, Marks PA. Histone deacetylase inhibitor selectively induces p21WAF1 expression and gene-associated histone acetylation. *Proc Natl Acad Sci U S A* 2000; **97**: 10014–9.
22 Nakajima H, Kim YB, Terano H, Yoshida M, Horinouchi S. FR901228, a potent antitumor antibiotic, is a novel histone deacetylase inhibitor. *Exp Cell Res* 1998; **241**: 126–33.
23 Hartlapp I, Pallasch C, Weibert G, Kemkers A, Hummel M, Re D. Depsipeptide induces cell death in Hodgkin lymphoma-derived cell lines. *Leuk Res* 2009; **33**: 929–36.
24 Dan S, Yoshimi H, Okamura M, Mukai Y, Yamori T. Inhibition of PI3K by ZSTK474 suppressed tumor growth not via apoptosis but G0/G1 arrest. *Biochem Biophys Res Commun* 2009; **379**: 104–9.
25 Reagan-Shaw S, Ahmad N. RNA interference-mediated depletion of phosphoinositide 3-kinase activates forkhead box class O transcription factors and induces cell cycle arrest and apoptosis in breast carcinoma cells. *Cancer Res* 2006; **66**: 1062–9.
26 Kodani M, Igishi T, Matsumoto S *et al.* Suppression of phosphatidylinositol 3-kinase/Akt signaling pathway is a determinant of the sensitivity to a novel histone deacetylase inhibitor, FK228, in lung adenocarcinoma cells. *Oncol Rep* 2005; **13**: 477–83.
27 Wozniak MB, Villuendas R, Bischoff JR *et al.* Vorinostat interferes with the signaling transduction pathway of T-cell receptor and synergizes with phosphoinositide-3 kinase inhibitors in cutaneous T-cell lymphoma. *Haematologica* 2010; **95**: 613–21.
28 Narita K, Kikuchi T, Watanabe K *et al.* Total synthesis of the bicyclic depsipeptide HDAC inhibitors Spiruchostatins A and B, 5"-epi-Spiruchostatin B, FK228 (FR901228) and preliminary evaluation of their biological activity. *Chem Eur J* 2009; **15**: 11174–86.

Supporting Information

Additional Supporting Information may be found in the online version of this article:

Fig. S1. Antiproliferative effects of trichostatin A.

Please note: Wiley-Blackwell are not responsible for the content or functionality of any supporting materials supplied by the authors. Any queries (other than missing material) should be directed to the corresponding author for the article.

© 2012 Japanese Cancer Association

Journal of
Medicinal
Chemistry

Featured Article

pubs.acs.org/jmc

α-1-C-Butyl-1,4-dideoxy-1,4-imino-L-arabinitol as a Second-Generation Iminosugar-Based Oral α-Glucosidase Inhibitor for Improving Postprandial Hyperglycemia

Atsushi Kato,*[,†] Erina Hayashi,[†] Saori Miyauchi,[†] Isao Adachi,[†] Tatsushi Imahori,[‡] Yoshihiro Natori,[‡] Yuichi Yoshimura,[‡] Robert J. Nash,[§] Hideyuki Shimaoka,[∥] Izumi Nakagome,[⊥] Jun Koseki,[⊥] Shuichi Hirono,[⊥] and Hiroki Takahata*[,‡]

[†]Department of Hospital Pharmacy, University of Toyama, Toyama 930-0194, Japan

[‡]Faculty of Pharmaceutical Sciences, Tohoku Pharmaceutical University, Sendai 981-8558, Japan

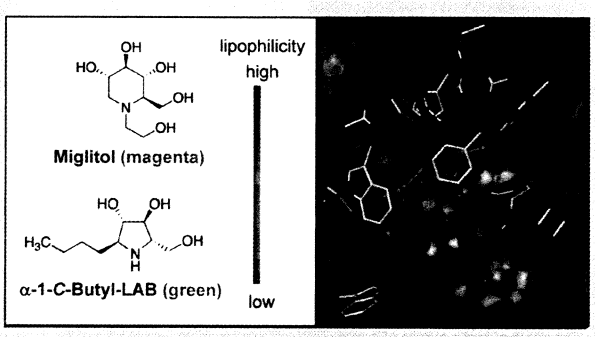
[§]Institute of Biological, Environmental and Rural Sciences/Phytoquest Limited, Plas Gogerddan, Aberystwyth, Ceredigion SY23 3EB, United Kingdom

[∥]S-BIO Business Division, Simitomo Bakelite Company Limited, Tokyo 140-0002, Japan

[⊥]School of Pharmaceutical Sciences, Kitasato University, Tokyo 108-8641, Japan

Supporting Information

ABSTRACT: We report on the synthesis and the biological evaluation of a series of α-1-C-alkylated 1,4-dideoxy-1,4-imino-L-arabinitol (LAB) derivatives. The asymmetric synthesis of the derivatives was achieved by asymmetric allylic alkylation, ring-closing metathesis, and Negishi cross-coupling as key reactions. α-1-C-Butyl-LAB is a potent inhibitor of intestinal maltase, isomaltase, and sucrase, with IC_{50} values of 0.13, 4.7, and 0.032 μM, respectively. Matrix-assisted laser desorption ionization time-of-flight mass spectrometric analysis revealed that this compound differs from miglitol in that it does not influence oligosaccharide processing and the maturation of glycoproteins. A molecular docking study of maltase-glucoamylase suggested that the interaction modes and the orientations of α-1-C-butyl-LAB and miglitol are clearly different. Furthermore, α-1-C-butyl-LAB strongly suppressed postprandial hyperglycemia at an early phase, similar to miglitol in vivo. It is noteworthy that the effective dose was about 10-fold lower than that for miglitol. α-1-C-Butyl-LAB therefore represents a new class of promising compounds that can improve postprandial hyperglycemia.



■ INTRODUCTION

Diabetes mellitus, one of the most common chronic metabolic diseases, occurs when the pancreas produces insufficient levels of insulin, or when the body cannot effectively use the insulin it produces.[1−3] Type 2 diabetes is induced by a combination of factors, including lifestyle and genetic factors. Today, the worldwide prevalence of diabetes is taking on pandemic dimensions, as changing lifestyles lead to reduced physical activity and increased obesity. In 2010, 285 million people were suffering from diabetes, and this number is estimated to increase to 439 million by 2030.[4] In recent years, it has been proposed that acute blood glucose elevations induce vascular damage through direct action on the vascular endothelium and finally cause myocardial infarctions, coronary heart disease, and cerebral apoplexy.[5] Therefore, the careful control of blood glucose levels can delay or protect at-risk subjects from developing cardiovascular diseases.[6−9] Antidiabetic drugs are currently classified into several different mechanistic classes (e.g., insulin secretagogues such as sulfonylureas, insulin sensitizers such as biguanides and thiazolidinediones, insulin mimetics such as glucagon-like peptide analogues and agonists, α-glucosidase inhibitors, and DPP IV inhibitors). However, some of these drugs have unacceptable side effects in some patients or lose their effectiveness over time. Therefore, the search for new antidiabetic drugs has continued to attract considerable interest.

Among these drugs, α-glucosidase inhibitors are oral antidiabetic agents which suppress postprandial hyperglycemia by inhibiting the hydrolysis of disaccharides such as maltose, isomaltase, and sucrose in the brush border membrane and delaying the absorption of carbohydrates from the small intestine. A recent metaregression analysis revealed that a close relationship exists between 2 h postprandial glucose levels and cardiovascular risk below the diabetic threshold,[10] and there is growing epidemiological evidence to show that an association

Received: September 11, 2012
Published: October 29, 2012

ACS Publications © 2012 American Chemical Society

between postprandial hyperglycemia and macrovascular complications exists in diabetic individuals.[11−13] Therefore, α-glucosidase inhibitors have considerable potential for preventing these cardiovascular risks. At present, a large number of compounds mimicking the structures of monosaccharides or oligosaccharides have been discovered from natural sources, which include thiosugars.[14−16] Among them, N-containing α-glucosidase inhibitors belong to two different main chemical classes. The first class is carbasugar-based inhibitors such as acarbose and voglibose. Carbasugars are carbocyclic analogues of hexopyranoses in which the ring oxygen has been replaced by carbon.[17] 5a-Carba-α-D-glucopyranosylamines such as validamine,[18] valienamine,[19] and valiolamine[20] in particular have proved to be important lead compounds for the development of clinically important antidiabetic agents. The first commercially available antidiabetic α-glucosidase inhibitor acarbose was introduced into the market in Germany in 1990 and has since been successfully marketed in Europe and Latin America. Voglibose was designed from valiolamine. It was produced by the reductive amination of valiolamine with dihydroxyacetone and was intended to function as an oral antidiabetic agent.[21] The second class of α-glucosidase inhibitors is iminosugar-based inhibitors such as miglitol. Iminosugars are sugar mimics with a nitrogen atom in place of the ring oxygen of monosaccharides. Miglitol was designed from 1-deoxynojirimycin (DNJ). DNJ has an excellent α-glucosidase inhibitory activity in vitro,[22] whereas its efficacy in vivo is only moderate.[23] Therefore, a large number of DNJ derivatives have been prepared in the hopes of increasing in vivo activity for this class of compounds.[24−26] Finally, *N*-(hydroxyethyl)-DNJ (miglitol) was reported to be the most favorable inhibitor out of a large number of in vitro active agents, and it was introduced into the market in 1999 as a more potent second-generation α-glucosidase inhibitor.

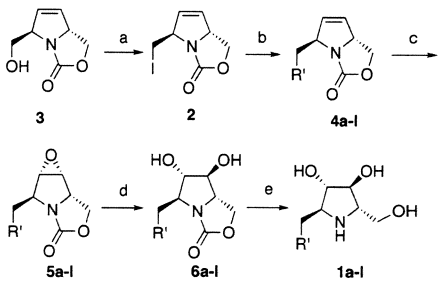
Although the mechanisms of action against intestinal enzymes for these two classes of α-glucosidase inhibitors are similar, each has a distinct clinical strategy. The most important arguing point is whether absorption from the intestinal tract is of benefit to the clinical effects. Glycosidases, which are involved in several important anabolic and catabolic processes, act not only on intestinal digestion but also on lysosomal catabolism and the post-translational modification of glycoproteins. The inhibition of liver and lysosomal glycosidases is occasionally responsible for the development of serious hepatic dysfunctions.[27] Thus, carbasugar-based drugs were designed to not cross the intestinal membranes. Acarbose is poorly absorbed from the gastrointestinal tract, the mean systemic bioavailability being only between 0.5% and 1.6%.[28] Similarly, voglibose is designed with a propanediol group from valiolamine for the purpose of disrupting its absorption. However, this poor absorption means that the drug stays in the intestine and colon for a long period of time and is associated with a high frequency of side effects such as flatulence, diarrhea, and hypoglycemia. In contrast, the iminosugar-based drug miglitol was designed to be nearly completely absorbed from the intestinal tract and may possess systemic effects in addition to affecting the intestinal border.[29,30] Previous experiments showed that the plasma half-life of miglitol is 2.4 h with a plasma peak concentration of 1.1 mg/L and a peak T_{max} of 2.3 h after an oral administration of 2 mg/kg of body weight.[31] Moreover, these studies revealed that there are two different glucose suppression mechanisms associated with miglitol, both direct and indirect. It directly and reversibly inhibits the α-glucosidase enzyme, and it induces the secretion of the glucagon-like peptide-1 (GLP-1). GLP-1 is a gut incretin hormone that is considered to be a promising therapeutic agent for type 2 diabetes because it stimulates β-cell proliferation, insulin secretion, and sensitivity in a glucose-dependent manner.[32,33] However, this absorption activity invites the risk of potential hepatic dysfunction.

Thus, our strategy has been to design effective iminosugar-type α-glucosidase inhibitors that affect postprandial hyperglycemia that not only show strong inhibitory effects against maltase, isomaltase, and sucrase but also do not interfere with the processing of glycoproteins. As part of our research program aimed at developing new potent and selective α-glucosidase inhibitors, we reported that the synthetic enantiomer 1,4-dideoxy-1,4-imino-L-arabinitol (LAB) is a more active and selective inhibitor of α-glucosidases than the natural product 1,4-dideoxy-1,4-imino-D-arabinitol (DAB).[34] In addition, the introduction of a branched carbon chain at the C4 position led to an improved sucrase inhibition (IC_{50} = 0.66 μM).[35] Considering this remarkable activity, we envisaged that a further improvement in activity might be gained in the case of structures having a longer side chain. To test this hypothesis, a series of α-1-*C*-alkylated LAB derivatives were then prepared by asymmetric allylic alkylation (AAA), ring-closing metathesis (RCM), and Negishi cross-coupling as key reactions. We herein describe the synthesis and biological evaluation of a series of α-1-*C*-alkylated LAB derivatives, which includes their suppressive effects on blood glucose levels using a carbohydrate loading test and their effects on whole cell glycoproteins, as determined by matrix-assisted laser desorption ionization time-of-flight mass spectrometric (MALDI-TOF MS) analysis. We also studied the selectivity of α-1-*C*-butyl-LAB for intestinal α-glucosidases vs intestinal β-glycosidases and lysosomal β-glucocerebrosidase. An additional aim was to demonstrate the molecular docking properties of α-1-*C*-butyl-LAB with maltase with the intention of determining the extent of difference from miglitol.

■ CHEMISTRY

Initially, the bicyclic 2,5-dihydropyrrole **2** was selected as the common intermediate for the synthesis of **1a−l** (Scheme 1).[36] The iodide **2** was prepared by iodination of oxazolidinol **3**, obtained by a modified Trost procedure.[37] With the iodide **2** in hand, Csp^3−Csp^3 bond formation using metal-catalyzed cross-

Scheme 1. Synthesis of α-l-*C*-Alkyl-LAB[a]



[a]Reagents: (a) I_2, Ph_3P, imidazole, CH_2Cl_2; (b) bis(l,5-cyclooctadiene)nickel(0), (*S*,*S*)-2,6-bis(4-isopropyl-2-oxazolin-2-yl)-pyridine, then alkylzinc bromide, *N*,*N*-dimethylacetamide; (c) ethylenediaminetetraacetic acid, 1,1,1-trifluoroacetone, Oxone, $NaHCO_3$, CH_3CN, H_2O; (d) trifluoroacetic acid, THF/H_2O; (e) NaOH, EtOH/H_2O.

dx.doi.org/10.1021/jm301304e | J. Med. Chem. 2012, 55, 10347−10362

coupling was examined owing to homologation of the alkyl substituents. Among the several procedures examined, the Negishi cross-coupling reaction developed by Fu et al.[38,39] was successful and gave the desired alkyl-substituted oxazolidinones **4a–l** (Table 1). The epoxidation of olefin in **4a–l** with the dioxirane, generated in situ from Oxone with 1,1,1-trifluoroacetone, resulted in the stereoselective formation of epoxides **5a–l**. Since the alkyl substituents of **4** are oriented toward the axial position of an approximate planar bicycloxazolone in a molecular model, the stereochemistry of the epoxide was deduced to be *anti* with respect to the alkyl substituents. Ring-opening of the epoxide with aqueous TFA stereoselectively proceeded to provide diols **6a–l**. The stereochemistries of diols of **6c** were determined to be 6α and 7β configurations, because an NOE correlation was observed between the hydrogen at C-5 and the hydrogen at C-7. Finally, the oxazolinones **6a–l** were transformed by basic hydrolysis into the desired iminosugars **1a–l** (Table 2).[40]

Table 1. Negishi Cross-Coupling of 2 with Alkylzinc Halides Using Catalytic $Ni(COD)_2$ in the Presence of a Tridentate Nitrogen Ligand [(*R,R*)-*i*-Pr-Pybox]

entry	R′ZnX	product	yield[a] (%)
1	MeZnI	**4a**	69
2	EtZnI	**4b**	63
3	*n*-PrZnBr	**4c**	78
4	*n*-BuZnBr	**4d**	63
5	n-$C_5H_{11}ZnBr$	**4e**	69
6	n-$C_6H_{13}ZnBr$	**4f**	69
7	n-$C_7H_{15}ZnBr$	**4g**	68
8	n-$C_8H_{17}ZnBr$	**4h**	72
9	n-$C_9H_{19}ZnBr$	**4i**	66
10	n-$C_{10}H_{21}ZnBr$	**4j**	71
11	$Ph(CH_2)_3ZnBr$	**4k**	73
12	$(CH_3)_2CH(CH_2)_2ZnBr$	**4l**	76

[a]Isolated yield.

Table 2. Yields of the Three-Step Sequence from 4 to 1

entry	R′	product	yield[a] (%)
1	Me	**1a**	51
2	Et	**1b**	58
3	*n*-Pr	**1c**	43
4	*n*-Bu	**1d**	52
5	n-C_5H_{11}	**1e**	55
6	n-C_6H_{13}	**1f**	59
7	n-C_7H_{15}	**1g**	35
8	n-C_8H_{17}	**1h**	49
9	n-C_9H_{19}	**1i**	30
10	n-$C_{10}H_{21}$	**1j**	45
11	$Ph(CH_2)_3$	**1k**	55
12	$(CH_3)_2CH(CH_2)_2$	**1l**	62

[a]Isolated yield.

Next the tetrols **7** and **8** were prepared from an enantiomer (2*R*,5*R* configuration), **9**, of the known *ent*-**9**,[34] as shown in Scheme 2. Treatment of the Weinreb amide **9** with propylmagnesium bromide gave the ketone **10** in 78% yield, which was reduced with DIBAL-H to afford the β-alcohol **11** and the α-alcohol **12** in a ratio of 4:1. On the other hand, the reduction of **10** with $NaBH_4$ provided **12** and **11** in a 2:1 ratio with inverse selectivity. These selectivities were previously observed in a similar example by Trost et al.[37] Epoxidation of **11** included the relative amount of two epoxides, **13**, which were cleaved by hydrolysis to give the same triol **14** as a single diastereomer. Probably, S_N2 attack of water occurs from the sterically less hindered side of both epoxides to produce the same product **14**.[34] Finally, hydrogenolysis of **14** afforded the desired tetrol **7**. Similarly, **12** was transformed via **15** and **16** into **8**.

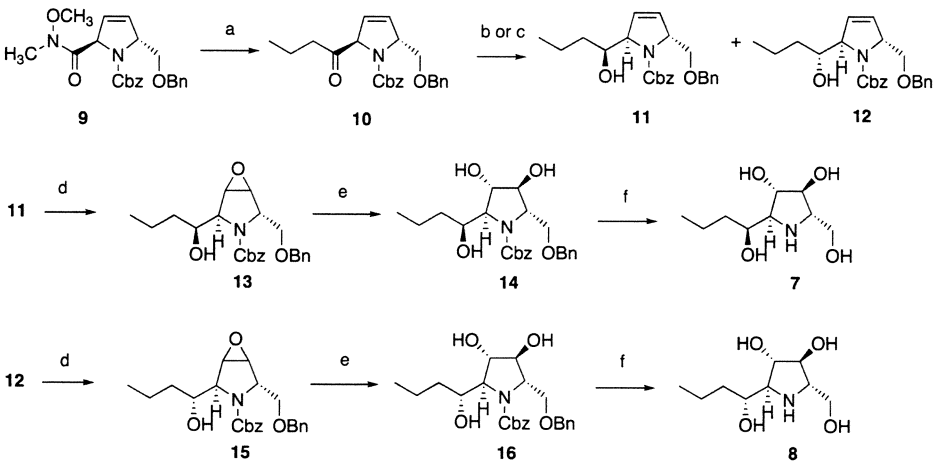
In addition, the *N*-butyl derivative **17** of **1c** and compound **18** with a 3-butyl substituent in place of the 3-hydroxy of **1c** were prepared as exhibited in Scheme 3. Reductive amino alkylation of **1c** with butyraldehyde in the presence of $NaBH_3CN$ gave *N*-butyl-1-*C*-butyl-LAB (**17**). Next the epoxide of **5c** was cleaved by *n*-butyllithium in the presence of CuI to provide **19**, which was hydrolyzed with base to give 1,3-*C*-dibutyl-LAB (**18**).

■ BIOLOGICAL RESULTS AND DISCUSSION

Evaluation of *N*- or 1-*C*-Butyl-LAB and -DNJ Derivatives as Glycosidase Inhibitors. In connection with our recent work concerning the synthesis of pyrrolidine-based iminosugars with a branched carbon chain of biological interest,[35,41] we turned our attention to the design of potent and selective α-glucosidase inhibitors with the goal of reducing postprandial hyperglycemia. We first evaluated *N*-butyl-LAB and α-1-*C*-butyl-LAB, since a previous structure–activity relationship study indicated that the natural product DAB is a good inhibitor, but the enantiomer LAB is a more potent inhibitor of α-glucosidases.[42] *N*-Butyl-1-deoxynojirimycin (*N*-butyl-DNJ) and α-1-*C*-butyl-DNJ were also tested to extend our understanding of the effect of introducing an alkyl substituent into an iminosugar. We found that the inhibitory potency of the parent DNJ was slightly better than that of LAB against α-glucosidases (Table 3). However, DNJ showed a broad inhibition spectrum against β-glucosidases, β-galactosidases, and trehalases. The introduction of an *N*-butyl substituent into LAB and DNJ reduced their effectiveness as glycosidase inhibitors. In sharp contrast, the introduction of a butyl chain at C-1 of LAB to give α-1-*C*-butyl-LAB dramatically improved its inhibitory potency against sucrase, with an IC_{50} value of 0.032 μM. We were also intrigued by the fact that α-1-*C*-butyl-LAB showed no significant inhibition toward liver and lysosomal β-glucosidases and β-galactosidases, even at a concentration of 1000 μM. α-1-*C*-Butyl-DNJ was a potent inhibitor of isomaltase, whereas this compound was also a good inhibitor of human lysosome β-glucocerebrosidase, with an IC_{50} value of 70 μM. Previous reports pointed out that these nonspecific inhibitions may cause undesirable side effects in the treatment of diabetes. In sharp contrast, α-1-*C*-butyl-LAB showed no significant inhibition toward β-glucocerebrosidase. To clarify the structural basis of the interaction of α-1-*C*-butyl-DNJ and α-1-*C*-butyl-LAB with human β-glucocerebrosidase, we constructed three-dimensional structures of the human β-glucocerebrosidase complexed with α-1-*C*-butyl-LAB or α-1-*C*-butyl-DNJ. As shown in Figure 1, α-1-*C*-butyl-DNJ and α-1-*C*-butyl-LAB were found to bind to β-glucocerebrosidase with the same orientation. Both α-1-*C*-butyl-DNJ and α-1-*C*-butyl-LAB interacted with aromatic groups such as Tyr313 and Phe246. However, the estimated binding energy (ΔE) of α-1-*C*-butyl-DNJ (-219.08 kcal mol^{-1}) with β-glucocerebrosidase indicated that it was more stable than 1-*C*-butyl-LAB (-185.87 kcal mol^{-1}) (Table 4). These differences ($\Delta\Delta E$) in binding energies

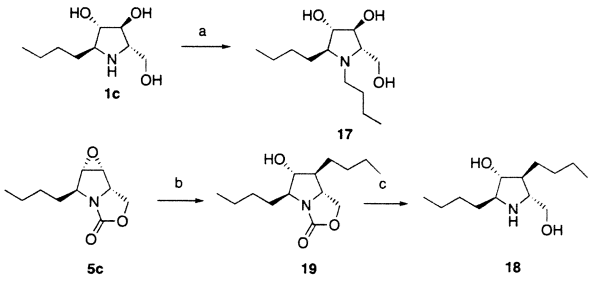
dx.doi.org/10.1021/jm301304e | J. Med. Chem. 2012, 55, 10347–10362

Scheme 2. Synthesis of 7 and 8[a]



[a]Reagents: (a) PrMgBr, THF, 78%; (b) DIBAL-H, Et_2O, 65% for **11**, 18% for **12**; (c) $NaBH_4$, MeOH, 24% for **11**, 51% for **12**; (d) ethylenediaminetetraacetic acid, 1,1,1-trifluoroacetone, Oxone, $NaHCO_3$, CH_3CN, H_2O, 83% for **13**, 80% for **15**; (e) trifluoroacetic acid, THF/H_2O, 93% for **14**, 16% for **16**; (f) H_2, 5% Pd–C, concd HCl, MeOH, 68% for **7**, 94% for **8**.

Scheme 3. Synthesis of 17 and 18[a]

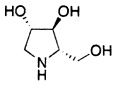
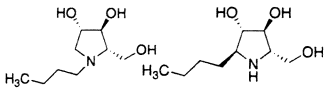
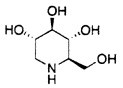
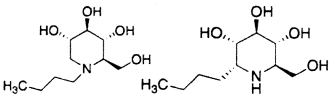


[a]Reagents: (a) $NaBH_3CN$, butyraldehyde, CH_3OH, 46%; (b) CuI, Et_2O, then *n*-BuLi, *n*-hexane, 23%; (c) NaOH, EtOH/H_2O, 38%.

may explain the differences in inhibition potency against β-glucocerebrosidase.

Optimization of the α-1-*C*-Alkyl Chain Length. On the basis of these findings, it clearly appeared that the addition of an alkyl chain at C-1 of LAB might lead to the production of highly potent and selective inhibitors of intestinal maltase and sucrase. Thus, we focused on the anomeric position and whether extending the alkyl chain at this position could influence the inhibition activities of LAB (Figure 2). Of these compounds, the introduction of short (ethyl and propyl) and longer (decyl and undecyl) groups reduced the inhibition activities compared to that of LAB (Table 5). Furthermore, we found that the inhibitory potency of α-1-*C*-alkyl-LAB against isomaltase derivatives decreased with increasing length of the alkyl chain. There is, therefore, a minimum 1-C-alkyl chain length requirement for achieving a strong inhibition of maltase and sucrase, with a butyl group being optimal. To check if the change from LAB to DNJ in the iminosugar part had an influence on activity toward intestinal α-glucosidases, we prepared α-1-C-alkyl-DNJs **19**–**21**. This comparison revealed that the inhibitory activity of α-1-C-alkyl-DNJs against maltase and sucrase was even weaker than that of α-1-C-alkyl-LABs. For example, α-1-*C*-butyl-DNJ (**19**) is 92-fold and 119-fold less active on maltase and sucrase than the corresponding α-1-C-butyl-LAB (**1c**). In contrast, α-1-C-octyl-DNJ (**21**) is 625-fold more potent as an isomaltase inhibitor than α-1-*C*-octyl-LAB (**1g**). These results suggest that the change from LAB to DNJ in the iminosugar portion of the molecule results in a dramatic enhancement in enzyme specificity and α-1-C-alkyl-LAB was clearly different from α-1-C-alkyl-DNJ. For comparison, we next investigated whether the introduction of different substituents in the anomeric position had an influence on the inhibition activities of intestinal maltase, isomaltase, and sucrase (Table 5). Changing the butyl group to a 4-phenylbutyl group or a 4-methylpentyl group at the C-1 position results in a greater specificity for inhibiting maltase; **1k** and **1l** showed almost the same inhibition potency against maltase, with IC_{50} values of 0.22 and 0.19 μM, respectively, but its inhibition toward isomaltase and sucrose was reduced. It is noteworthy that the C-1′ OH group dramatically changed the inhibition potency and spectrum. We previously reported that the 1-*C*-hydroxymethyl derivative of LAB, as in L-DMDP, was found to display inhibitory activity toward intestinal maltase, isomaltase, and sucrase, with IC_{50} values of 1.2, 0.77, and 0.62 μM, respectively.[43] These values are comparable to those of LAB. In contrast, remarkable reductions in isomaltase inhibition were observed in the case of α-1-*C*-{(*R*)-1-hydroxybutyl}-LAB (**8**), which is indeed a 1004-fold weaker inhibitor than L-DMDP, while α-1-*C*-{(*S*)-1-hydroxybutyl}-LAB (**7**) showed a comparable inhibition toward maltase and sucrase. The *N*-butylation (**17**) and 3-*C*-butylation (**18**) of α-1-*C*-butyl-LAB obviously decreased the affinity for these α-glucosidases. Acarbose showed inhibitory activity against maltase and sucrase, with IC_{50} values of 0.18 and 2.9 μM, respectively. However, acarbose exhibited less than a 50% inhibition of isomaltase even at concentrations as high as 1000 μM. Voglibose was found to be a much stronger inhibitor than acarbose. The IC_{50} inhibitory activities toward maltase, isomaltase, and sucrase were 0.12, 5.2, and 37 μM, respectively. Miglitol showed potent inhibitory activity against maltase and sucrase, with IC_{50} values of 1.3 and 1 μM, respectively, but these values were weaker than those of voglibose. In addition, the most striking difference between miglitol and α-1-*C*-butyl-LAB is that miglitol showed an unfavorable inhibition against rat intestinal cellobiase and lactase, with IC_{50} values of 164 and 41 μM, respectively,

Table 3. Concentration of Iminosugars Giving 50% Inhibition of Various Glycosidases

	IC_{50} (μM)					
						
Enzyme	LAB	*N*-Butyl-LAB	1-*C*-Butyl-LAB (**1c**)	DNJ	*N*-Butyl-DNJ	α-1-*C*-Butyl-DNJ
α-Glucosidase						
Rat intestinal maltase	0.93	63	0.13	0.36	2.1	12
Rat intestinal isomaltase	0.36	54	4.7	0.30	2.7	0.45
Rat intestinal sucrase	1.0	73	0.032	0.21	58	3.8
β-Glucosidase						
Rat intestinal cellobiase	NI[a]	NI	NI	520	NI	NI
Bovine liver	NI	NI	NI	210	NI	120
Human β-glucocerebrosidase	NI	NI	NI	195	399	70
β-Galactosidase						
Rat intestinal lactase	415	NI	NI	26	274	230
Bovine liver	NI	NI	NI	NI	NI	152
Trehalase						
Rat intestinal trehalase	75	NI	NI	42	38	167
Porcine kidney	131	NI	NI	41	36	172

[a]NI = no inhibition (less than 50% inhibition at 1000 μM).

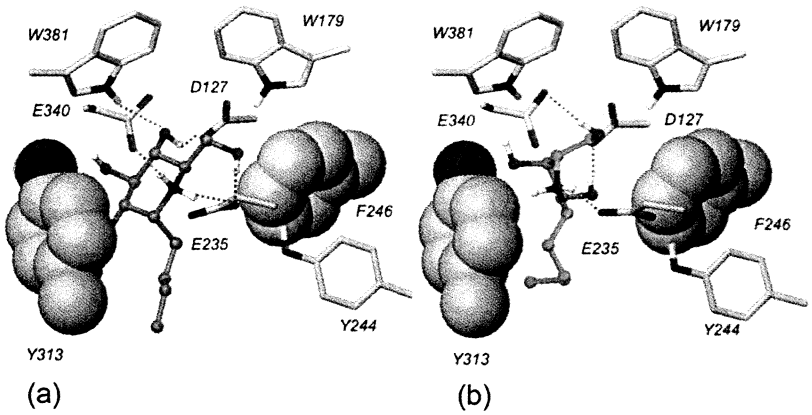


Figure 1. Docking view of (a) α-1-C-butyl-DNJ and (b) α-1-C-butyl-LAB with human β-glucocerebrosidase.

Table 4. Inhibitory Activity (IC_{50}), IFDScore, and Binding Energy of α-1-C-Butyl-DNJ and α-1-C-Butyl-LAB for Human β-Glucocerebrosidase

	IC_{50} (μM)	IFDScore	Δ(IFDScore)	ΔE (kcal/mol)	$\Delta\Delta E$ (kcal/mol)
α-1-C-butyl-DNJ	70	−890.68	−1.53	−219.08	−33.21
α-1-C-butyl-LAB	NI[a]	−889.14	0.00	−185.87	0.00

[a]NI = less than 50% inhibition at 1000 μM.

whereas α-1-C-butyl-LAB had no effect on these enzymes (data not shown). On the basis of a comparison of these commercially available inhibitors, the α-1-C-butyl-LAB prepared in this study obviously has potential for clinical use.

Structural Modification of Whole Cell *N*-Linked Oligosaccharides. The lumen of the endoplasmic reticulum (ER) is a highly specialized compartment for the folding and oligomeric assembly of secretory proteins, plasma membrane proteins, and proteins destined for the various organelles of the vacuolar system.[44,45] The conformational maturations of these functional glycoproteins are determined not only by the amino acid sequence but also by post-translational modifications and by a variety of chaperones and folding enzymes such as ER α-glucosidases and α-mannosidases.[46,47] The *N*-linked glycosylation of nascent proteins involves the transfer of $Glc_3Man_9GlcNAc_2$ from a dolichol precursor to the asparagine residue of the Asn-X-Ser/Thr glycosylation sequon of a protein. The oligosaccharide is subsequently processed by the sequential action of trimming glycosidases in the ER, prior to the production of hybrid and complex oligosaccharide structures in the Golgi.[48,49] This process of trimming commences with ER α-glucosidase I, which removes the outer α-1,2-linked glucose residue from the oligosaccharide, followed by the removal of the remaining two glucose residues through the action of an ER α-glucosidase II. In many cases, misfolded and genetic mutant

dx.doi.org/10.1021/jm301304e | J. Med. Chem. 2012, 55, 10347−10362

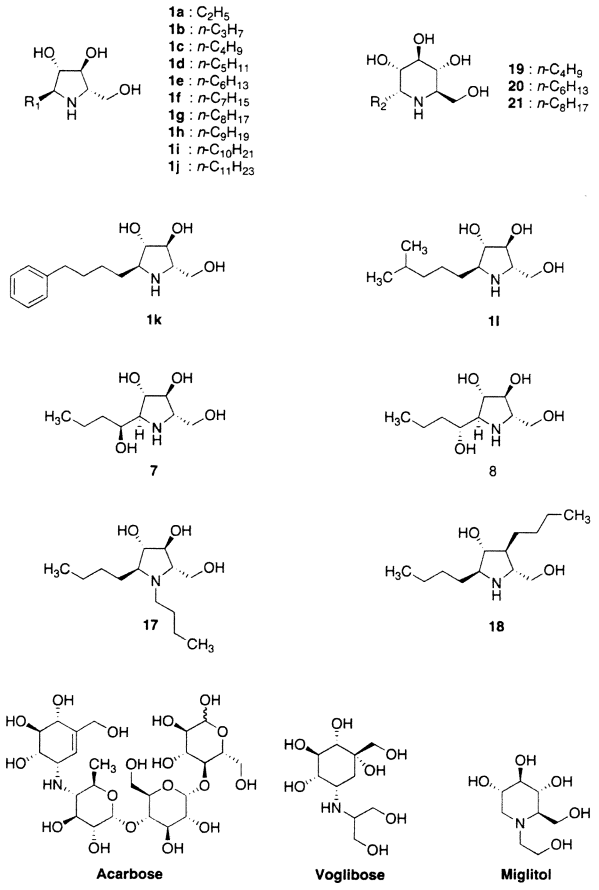


Figure 2. Chemical structures of α-1-*C*-alkylated LAB derivatives and sugar-mimic α-glucosidase inhibitors.

proteins are retained in the ER and are eventually degraded by ER-associated degradation (ERAD).[47,50,51] Thus, considering the fact that α-glucosidase inhibitors could be clinically used as antidiabetes agents, it is important that they do not disrupt the folding and maturation processes of glycoproteins. Previous studies have reported that DNJ, which is a parent compound of miglitol, inhibited not only intestinal α-glycosidases but also the processing ER enzymes α-glucosidase I and II.[52,53] Therefore, the use of DNJ could drastically change the glycan structures on glycoproteins, since it could prevent the transformation of high mannose- or hybrid-type glycans into complex-type glycans. To examine the effect of miglitol and α-1-*C*-butyl-LAB on whole cell *N*-linked oligosaccharide structures, we used the recently established chemoselective glycoblotting technique and MALDI-TOF MS analysis.[54] Human hepatocellular carcinoma HepG2 cells were treated with either 500 μM miglitol or 500 μM α-1-C-butyl-LAB for 48 h. All of the *N*-linked oligosaccharides were selectively captured onto new high-density hydrazide beads, which permitted them to be efficiently purified from cell homogenates. The captured *N*-linked oligosaccharides were subjected to on-bead methyl esterification to stabilize the sialic acids for the simultaneous quantitation of neutral and sialylated oligosaccharides by MALDI-TOF MS. As shown in Figure 3b and Table 6, a 48 h treatment with 500 μM miglitol resulted in immature $Glc_3Man_9GlcNAc_2$ (m/z 2799), $Glc_2Man_9GlcNAc_2$ (m/z 2637), and $Glc_1Man_9GlcNAc_2$ (m/z 2475) being accumulated. The presence of these glucose-residue-containing oligosaccharide structures is highly indicative of the inhibition of the processing enzymes α-glucosidase I and II. In sharp contrast, the control and α-1-C-butyl-LAB had very similar patterns (Figure 3a,c). These results clearly indicate that there is a risk associated with the use of miglitol, since it could increase the expression of immature high-mannose-type *N*-linked oligosaccharides, whereas α-1-C-butyl-LAB did not appear to have any effect on the processing α-glucosidases.

Table 5. IC_{50} Values (μM) for α-1-C-Alkyl-LAB against Intestinal α-Glucosidases, Compared with α-1-C-Alkyl-DNJs 19 and 20, Acarbose, Voglibose, and Miglitol

	IC_{50} (μM)		
compound	maltase	isomaltase	sucrase
α-1-C-ethyl-LAB (**1a**)	2.6	11	0.68
α-1-C-propyl-LAB (**1b**)	1.7	47	0.26
α-1-C-butyl-LAB (**1c**)	0.13	4.7	0.032
α-1-C-pentyl-LAB (**1d**)	0.71	18	0.19
α-1-C-hexyl-LAB (**1e**)	0.51	11	0.11
α-1-C-heptyl-LAB (**1f**)	0.38	16	0.24
α-1-C-octyl-LAB (**1g**)	0.32	75	0.45
α-1-C-nonyl-LAB (**1h**)	0.84	171	1.4
α-1-C-decyl-LAB (**1i**)	1.2	606	1.7
α-1-C-undecyl-LAB (**1j**)	3.9	NI	13
α-1-C-(4-phenylbutyl)-LAB (**1k**)	0.22	14	0.31
α-1-C-(4-methylpentyl)-LAB (**1l**)	0.19	12	0.24
α-1-C-{(*S*)-1-hydroxybutyl}-LAB (**7**)	3.3	96	0.68
α-1-C-{(*R*)-1-hydroxybutyl}-LAB (**8**)	89	773	5.7
N-butyl-α-1-C-butyl-LAB (**17**)	25	NI	8.8
1,3-C-dibutyl-LAB (**18**)	NI[a]	NI	NI
α-1-C-butyl-DNJ (**19**)	12	0.45	3.8
α-1-C-hexyl-DNJ (**20**)	4.7	0.31	2.4
α-1-C-octyl-DNJ (**21**)	2.1	0.12	1.5
acarbose	0.18	NI	2.9
voglibose	0.12	5.2	0.37
miglitol	1.3	39	1.0

[a]NI = less than 50% inhibition at 1000 μM.

Carbohydrate Loading Test. A recent metaregression analysis revealed that 2 h postprandial glucose levels and cardiovascular risk were closely related.[10] Furthermore, there is a substantial body of epidemiological evidence that points to an association between postprandial hyperglycemia and macrovascular complications.[12,55] Therefore, α-glucosidase inhibitors have considerable potential for reducing the risk of these diseases. The iminosugar-based α-glucosidase inhibitor miglitol differs from carbasugar-type α-glucosidase inhibitors such as acarbose and voglibose, because it is rapidly and completely absorbs in the upper region of the small intestine.[31] This pharmacokinetic property consequently enables the strong and early phase suppression of postprandial hyperglycemia, with no or minimal gastrointestinal complications. We then investigated the influence of α-1-C-butyl-LAB and miglitol, which was used as a positive control, on blood glucose levels after an in vivo maltose loading (Figure 4). The control group was loaded with saline only. When compared to the control, α-1-C-butyl-LAB caused significantly lower blood glucose levels at 15 and 30 min compared to a placebo administration (Figure 4b). Moreover, treatment with α-1-C-butyl-LAB led to a 43.9% decrease of the area under the curve (AUC) at a dose of 0.25 mg/kg of body weight. It was interesting to note that the remaining blood

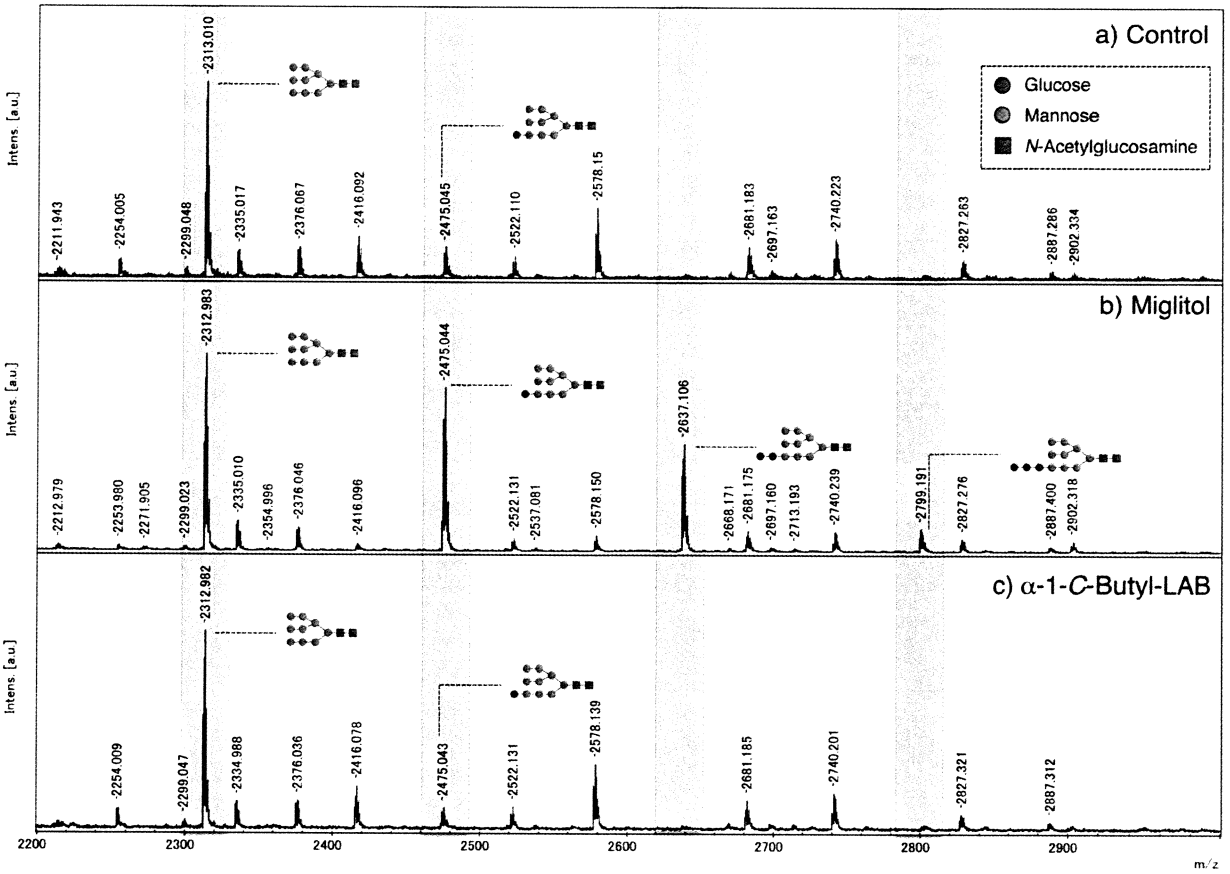


Figure 3. MALDI-TOF MS spectra showing the effects of α-glucosidase-inhibiting iminosugars on whole cell glycoproteins. Relative expression levels of glucose residues containing *N*-linked oligosaccharides on human hepatocelluar carcinoma HepG2 cells cultured for 48 h with or without 500 μM (b) miglitol and (c) α-1-C-butyl-LAB. Structural identification of glycans was performed by MS analysis and the use of a database for glycan structures (http://web.expasy.org/glycomod/).

Table 6. Structures and Proportion (%) of Isolated Whole Cell *N*-Linked Oligosaccharide Peaks from the Control and 500 μM Miglitol- and 500 μM α-1-*C*-Butyl-LAB-Treated HepG2 Cells

● Glucose ● Mannose ■ *N*-Acetylglucosamine

m/z	Estimated glycan composition ('GlycoMod' database)	Structure:	% Area		
			Control	α-1-*C*-butyl-LAB	Miglitol
2313	$(Hex)_6 + (Man)_3(GlcNAc)_2$		5.96	7.13	10.67
2475	$(Hex)_7 + (Man)_3(GlcNAc)_2$		1.22	1.02	9.63
2637	$(Hex)_8 + (Man)_3(GlcNAc)_2$		0.00	0.00	6.69
2799	$(Hex)_9 + (Man)_3(GlcNAc)_2$		0.00	0.00	1.54

glucose levels were slightly higher with α-1-*C*-butyl-LAB than with the placebo at 60 and 120 min (Figure 4b). This behavior with strong and early phase suppression of postprandial hyperglycemia was similar to that observed for miglitol (Figure 4a). For comparison, we next investigated the influence of α-1-C-butyl-LAB using a sucrose loading test (Figure 5). The administration of sucrose (2.5 g/kg of body weight, po) to fasted mice resulted in a rapid increase in blood glucose concentrations from 80 ± 8 mg/dL to a maximum of 181 ± 16 mg/dL after 30 min. Thereafter blood glucose levels recovered to the pretreatment level at 120 min. α-1-C-Butyl-LAB resulted in significantly lower blood glucose levels at 15, 30, and 60 min than placebo administration (Figure 5b). Moreover, the AUC for plasma glucose from 0 to 60 min after α-1-C-butyl-LAB administration was reduced by 49.1% at a dose of 0.1 mg/kg of body weight and 69.2% at a dose of 0.5 mg/kg of body weight, compared with the AUC for the control. This behavior was similar to that observed for miglitol administration (Figure 5a).

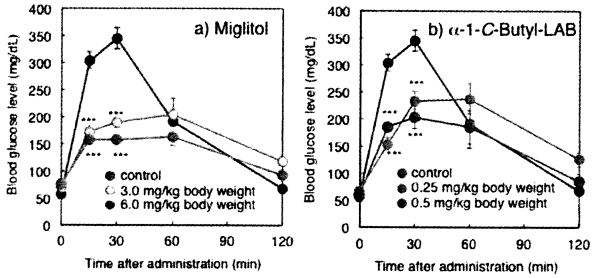


Figure 4. Effects of miglitol (a) and α-1-C-butyl-LAB (b) on blood glucose levels. Blood glucose concentrations of male ddY mouse after an oral load with maltose, 2.5 g/kg of body weight, with (a) 3.0 (light green) and 6.0 (green) mg/kg of body weight miglitol and (b) 0.25 (orange) and 0.5 (red) mg/kg of body weight α-1-C-butyl-LAB. The control group was loaded with saline (purple). Each value represents the mean ± SEM (n = 5). Three asterisks indicate a significant difference (p < 0.001) compared with the control.

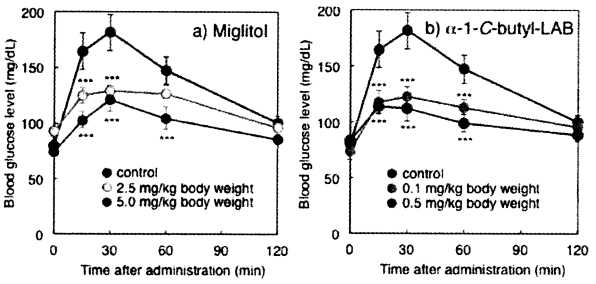


Figure 5. Effects of miglitol (a) and α-1-C-butyl-LAB (b) on blood glucose levels. Blood glucose concentrations of male ddY mouse after an oral load with sucrose, 2.5 g/kg of body weight, with (a) 2.5 (light green) and 5.0 (green) mg/kg of body weight miglitol and (b) 0.1 (orange) and 0.5 (red) mg/kg of body weight α-1-C-butyl-LAB. The control group was loaded with saline (blue). Each value represents the mean ± SEM (n = 5). Three asterisks indicate a significant difference (p < 0.001) compared with the control.

The administration of miglitol led to the suppression of the blood glucose levels in a dose-dependent manner; as a consequence, the AUC for plasma glucose from 0 to 60 min after miglitol administration was reduced by 40.5% at a dose of 2.5 mg/kg of body weight and 58.7% at a dose of 5.0 mg/kg of body weight. Remarkably, the effective doses of α-1-C-butyl-LAB were about 10 times lower than those of miglitol in both disaccharide loading tests. The LAB derivative showed a suppressive effect against postprandial hyperglycemia at a does of only 0.1−0.5 mg/kg of body weight (Figures 4 and 5). A recent study suggested that miglitol suppresses glucose levels via two different mechanisms, namely, the direct inhibition of α-glucosidase and, indirectly, via affecting the secretion of GLP-1.[56,57] GLP-1 is released from the intestine in response to nutrients and exerts a potent insulin-releasing effect on pancreatic β-cells.[32,33] The important point to note is that the GLP-1 release effect appears only when it is administered orally.[13] Further studies will clearly be needed to more completely understand the mechanisms of α-1-C-butyl-LAB, but our results could be interpreted to mean that it affects to GLP-1 secretion because this compound is not only an iminosugar but also an absorbable α-glucosidase inhibitor similar to miglitol. On the basis of these findings and by comparison with our results for miglitol, it appears that α-1-C-butyl-LAB is absorbed from the upper region of the small intestine, much the same as miglitol, and it causes less diarrhea than acarbose and voglibose.

Docking Studies of α-1-C-Butyl-LAB and Miglitol with Intestinal Maltase. In piperidine pyranoside mimics such as α-1-C-butyl-DNJ and miglitol, there is usually a good overlap between the structure of the glycoside and inhibition by the corresponding iminosugar mimic. However, α-1-C-butyl-LAB is an unusual L-type pyrrolidine iminosugar, and it does not seem to overlap extensively with D-type piperidine iminosugars. To understand the structural basis of the interaction of α-1-C-butyl-LAB and miglitol with maltase, we first determined the mode of inhibition and the inhibition constant (K_i) of miglitol and α-1-C-butyl-LAB from Lineweaver−Burk plots. As shown in Figure 6, miglitol and α-1-C-butyl-LAB inhibited maltase in a competitive manner, with K_i values of 0.46 and 0.085 μM, respectively. This result suggests that α-1-C-butyl-LAB occupies the active site of this enzyme, much the same as miglitol. Thus, we next attempted to construct three-dimensional structures of the N-terminal catalytic domain of maltase-glucoamylase (ntMGAM) of rat complexed with α-1-C-butyl-LAB. For comparison, we also constructed three-dimensional structures of rat ntMGAM complexed with α-1-C-butyl-DNJ or miglitol. As shown in Figure 7, α-1-C-butyl-LAB, α-1-C-butyl-DNJ, and miglitol were observed to bind to the hydrophobic pocket consisting of Trp376, Trp516, Trp613, and Phe649 of rat ntMGAM. However, it was suggested that the orientations of the butyl groups of α-1-C-butyl-LAB and α-1-C-butyl-DNJ are different. The butyl group of α-1-C-butyl-LAB has a favorable interaction with the hydrophobic pocket (Trp376, Leu405, and Ile441), while the butyl groups of α-1-C-butyl-DNJ bind to the other hydrophobic pocket (Trp481, Met519) (Figure 7). The interaction between the butyl group of α-1-C-butyl-LAB and the hydrophobic pocket of ntMGAM looks important for ligand binding, which conforms to the study[58] by Aguilar-Moncayo et al. pointing out the critical role of aglyconic interactions in glycosidase binding. The hydroxyethyl group of miglitol also binds to the same hydrophobic pocket as α-1-C-butyl-DNJ, but miglitol has an additional interaction with hydrophilic residues (Asp616 and Arg600) of rat ntMGAM. The interactions between rat ntMGAM and α-1-C-butyl-LAB,

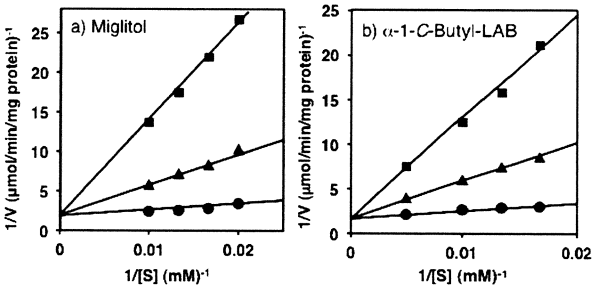


Figure 6. Lineweaver−Burk plots of miglitol (a) and α-1-C-butyl-LAB (b) inhibition of rat intestinal maltase. An increasing concentration of maltose or sucrose was used to determine the K_i values, and the data were plotted as $1/V$ versus $1/[S]$. (a) The concentrations of miglitol were 0 μM (closed circles), 2.0 μM (closed triangles), and 5.0 μM (closed squares). The calculated K_i value was 0.46 μM. (b) The concentrations of α-1-C-butyl-LAB were 0 μM (closed circles), 0.2 μM (closed triangles), and 0.75 μM (closed squares). The calculated K_i value was 0.085 μM.

dx.doi.org/10.1021/jm301304e | J. Med. Chem. 2012, 55, 10347−10362

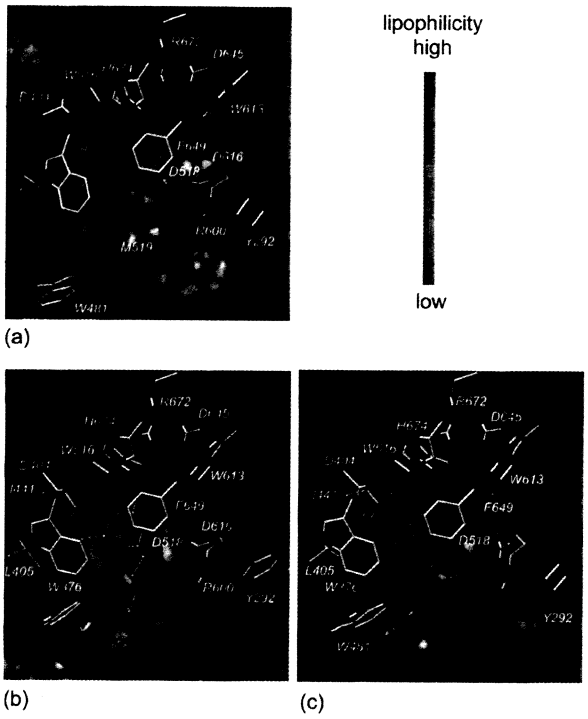


Figure 7. View of interactions of (a) α-1-C-butyl-LAB, (b) α-1-C-butyl-DNJ, and (c) miglitol with rat ntMGAM.

α-1-C-butyl-DNJ, or miglitol are illustrated in Figure 8. Miglitol and α-1-C-butyl-DNJ are positioned to form hydrogen bonds with Asp404, Asp518, Asp616, and His674 of rat ntMGAM, while α-1-C-butyl-LAB can form hydrogen bonds with Asp518, Asp616, Trp613, and Asp645 of rat ntMGAM. For the purpose of clarifying the difference, the binding energies between the compounds and rat ntMGAM were calculated. The binding energies (ΔE) for α-1-C-butyl-LAB, α-1-C-butyl-DNJ, and miglitol were −269.97, −236.53, and −261.36 kcal mol^{-1} (Table 7). These results were consistent with the experimental results (IC_{50}) showing that miglitol and α-1-C-butyl-LAB have higher inhibitory activities against maltase of rat ntMGAM than α-1-C-butyl-DNJ. For further confirmation, we also constructed the three-dimensional models of the α-1-C-butyl-LAB−human ntMGAM complex. The docking calculation was performed under the same conditions as the docking calculations of rat ntMGAM using the X-ray structures of human ntMGAM (PDB IDs 2QLY, 2QMJ, 3CTT, and 3L4W). The binding energy (ΔE), as estimated from the three-dimensional structures of the compound with human ntMGAM, suggested that α-1-C-butyl-LAB would be an inhibitor of human maltase as well as that from the rat (Table 8). Furthermore, the binding free energy (ΔG) estimated by the MM-GBSA method using Prime in the Schrödinger Suite strongly supported that α-1-C-butyl-LAB has inhibition activity in human ntMGAM.

■ CONCLUSIONS

In this study, we report on the design and synthesis of a series of α-1-C-alkylated LAB derivatives by AAA, RCM, and Negishi cross-coupling as key reactions. Among the produced compounds, α-1-C-butyl-LAB showed potent inhibitory activity toward intestinal maltase, isomaltase, and sucrase, with IC_{50} values of 0.20, 4.7, and 0.032 μM, respectively. The following

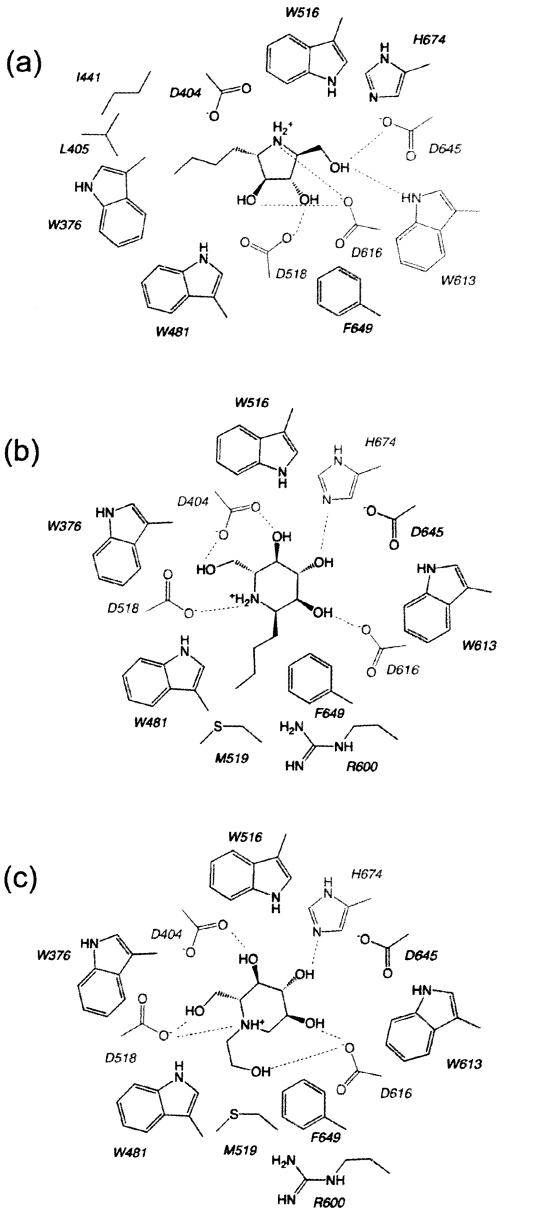


Figure 8. Schematic interaction diagrams between rat ntMGAM and (a) α-1-C-butyl-LAB, (b) α-1-C-butyl-DNJ, and (c) miglitol. Hydrogen bonds are depicted by dashed lines.

Table 7. Inhibitory Activity (IC_{50}) and Binding Energy (ΔE) of α-1-C-Butyl-LAB, α-1-C-Butyl-DNJ, and Miglitol with Rat ntMGAM

	IC_{50} (μM)	ΔE (kcal/mol)
α-1-C-butyl-LAB	0.13	−269.97
α-1-C-butyl-DNJ	12	−236.53
miglitol	1.3	−261.36

are the main features of α-1-C-butyl-LAB: (a) It does not inhibit intestinal β-glycosidases and lysosomal β-glucocerebrosidase even at concentrations as high as 1000 μM. (b) MALDI-TOF MS analysis revealed that it obviously differs from miglitol in that it does not disrupt oligosaccharide processing and the

Table 8. Binding Energy (ΔE) and Binding Free Energy (ΔG) Estimated for α-1-*C*-Butyl-LAB with Human and Rat ntMGAM

	ΔE (kcal/mol)	ΔG (kcal/mol)
rat ntMGAM	−269.97	−42.13
human ntMGAM	−260.51	−46.99

maturation of glycoproteins. (c) It showed a strong and early phase suppression of postprandial hyperglycemia, and the effective dose was 10 times lower than that for miglitol. (d) Both α-1-*C*-butyl-LAB and miglitol are competitive inhibitors, whereas molecular docking studies revealed that the interaction modes and the orientations of the alkyl chain of α-1-*C*-butyl-LAB and miglitol are clearly different. Each alkyl group has a favorable interaction, but with different hydrophobic pockets. (e) Docking calculations using X-ray structures of human ntMGAM (PDB IDs 2QLY, 2QMJ, 3CTT, and 3L4W) suggested that the binding conformations and orientations of α-1-*C*-butyl-LAB and miglitol in human ntMGAM are similar to those in rat ntMGAM. α-1-*C*-Butyl-LAB therefore represents a new class of promising compounds that have the potential for treating postprandial hyperglycemia.

■ EXPERIMENTAL SECTION

General Experimental Procedures. Infrared (IR) spectra were recorded on a Perkin-Elmer 1600 series FT-IR spectrometer. Mass spectra were recorded on a JEOL JMN-DX 303/JMA-DA 5000 spectrometer. Microanalyses were performed on a Perkin-Elmer CHN 2400 elemental analyzer. Optical rotations were measured with a JASCO DIP-360 or JASCO P-1020 digital polarimeter. Proton nuclear magnetic resonance (^{1}H NMR) spectra were recorded on a JEOL JNM-EX 270 (270 MHz), Varian Gemini-300 (300 MHz), JEOL JNM-AL 400 (400 MHz), Varian Unity-500 (500 MHz), or JNM-LA (600 MHz) spectrometer using tetramethylsilane as the internal standard. The following abbreviations are used: s = singlet, d = doublet, t = triplet, q = quartet, m = multiplet, br = broad. Column chromatography was carried out on Merck silica gel 60 (230−400 mesh) or KANTO silica gel 60N (40−50 mm) for flash chromatography. The purity of all final compounds was established to be ≥95% by HPLC analysis (Agilent 1220 Infinity LC system). HPLC conditions: TSKgel NH_2-100 3 μm column (4.6 mm ×15 cm) using CH_3CN/H_2O = 90/10 (flow rate 1.0 mL/min) as the eluent and refractive index detector (retention time 17.2 min for compound **1c**).

Preparation of Iminosugars and Their Alkyl Derivatives. 1-Deoxynojirimycin was isolated from the roots of *Adenophora triphylla* according to the literature.[59] The 1-*C*-alkyl-DNJ derivatives **19**−**21** were prepared according to the method reported previously.[60,61] LAB was prepared from xylitol according to the literature.[62] The *N*-butylation of LAB and DNJ was performed by treatment with the butyl bromide and K_2CO_3 in dimethylformamide. The reaction mixture was evaporated in vacuo, and the residual syrup was redissolved in MeOH and applied to an Amberlist 15 column (H^+ form), eluted with 0.5 M NH_4OH, and concentrated. The eluate was finally purified by Dowex 1-X2 (OH^- form) and Amberlite CG-50 (NH_4^+ form) column chromatography with water as the eluent. Acarbose was purchased from LKT Laboratories Inc. (St. Paul, MN). Voglibose and miglitol were purchased from Wako Pure Chemical Industries, Ltd. (Osaka, Japan).

Typical Procedure for α-1-*C*-Alkyl-LAB. *Preparation of (5R,7aR)-5-(Iodomethyl)-1,7a-dihydropyrrolo[1,2-c]oxazol-3(5H)-one (2).* Iodine chips (11.3 g, 44.5 mmol) were added to a solution of alcohol **3** (3.45 g, 22.2 mmol), triphenylphosphine (14.6 g, 55.6 mmol), and imidazole (3.79 g, 55.6 mmol) in CH_2Cl_2 (89 mL) at 0 °C. After being stirred at room temperature for 6 h, the reaction was quenched with 1.0 M aq sodium thiosulfate. The water layer was extracted with CH_2Cl_2 (2 × 40 mL). The organic layers were combined and dried over anhydrous Na_2SO_4. Filtration and evaporation in vacuo furnished the crude product, which was purified by column chromatography (silica gel, 80 g, hexane/EtOAc = 2/1) to provide **2** (5.16 g, 88%) as a pale yellow oil. $[\alpha]_D^{23}$ = +141.6 ($CHCl_3$, *c* = 1.00). ^{1}H NMR ($CDCl_3$, 400 MHz): δ 3.29−3.37 (m, 2H), 4.24 (dd, *J* = 8.7, 6.8 Hz, 1H), 4.64 (t, *J* = 8.7 Hz, 1H), 4.79 (br s, 1H), 4.86−4.90 (m, 1H), 6.03 (d, *J* = 6.3 Hz, 1H), 6.08 (d, *J* = 6.8 Hz, 1H). ^{13}C NMR ($CHCl_3$, 100 MHz): δ 8.60, 64.51, 67.20, 68.84, 130.73, 133.28, 162.11. IR (neat, cm^{-1}): 1749. HRMS (EI): *m*/*z* calcd for $C_7H_8NO_2I$ (M^+) 264.9600, found 264.9603.

Preparation of Alkylzinc Bromide (n-Propylzinc Bromide). Iodine chips (127 mg, 0.50 mmol) were added to a suspension of zinc powder (981 mg, 15.0 mmol) in *N*,*N*-dimethylacetamide (10 mL) at room temperature. After being stirred for 10 min, the resulting mixture changed from a dark brown suspension to a colorless suspension. 1-Bromopropane (0.91 mL, 10.0 mmol) was added by syringe, and the reaction mixture was stirred at 80 °C for 3 h. The concentration in *N*,*N*-dimethylacetamide was ~0.75 M.

*Typical Procedure for Negishi Coupling (**4c**).* Yellow bis(1,5-cyclooctadiene)nickel(0) (48.4 mg, 0.176 mmol, 16 mol %) and (*S*,*S*)-2,6-bis(4-isopropyl-2-oxazolin-2-yl)pyridine (106 mg, 0.352 mmol, 32 mol %) were added to *N*,*N*-dimethylacetamide (7.0 mL) under an argon atmosphere, and the resulting mixture was stirred for 30 min at room temperature. The resulting deep-blue solution was added to a solution of the *n*-propylzinc bromide (in *N*,*N*-dimethylacetamide, 4.7 mL, 3.52 mmol) and **2** (291 mg, 1.10 mmol). After being stirred for 20 h, the reaction was quenched with iodine chips (440 mg). After being stirred for 10 min, the dark-brown mixture was passed through a short pad of silica gel (eluting with AcOEt/hexane = 1/1) (to remove *N*,*N*-dimethylacetamide, inorganic salts, and iodine). The filtrate was then concentrated, and the residue was purified by flash chromatography (silica gel, 20 g, eluting with hexane/EtOAc = 3/1) to provide **4c** (156 mg, 78%) as a colorless oil.

*(5S,7aR)-5-Butyl-1,7a-dihydropyrrolo[1,2-c]oxazol-3(5H)-one (**4c**).* $[\alpha]_D^{24}$ = +175.4 ($CHCl_3$, *c* = 1.08). ^{1}H NMR ($CDCl_3$, 400 MHz): δ 0.91 (t, *J* = 6.8 Hz, 3H), 1.34−1.58 (m, 6H), 4.20 (dd, *J* = 8.2, 5.3 Hz, 1H), 4.54 (br s, 1H), 4.58 (t, *J* = 8.7 Hz, 1H), 4.72−4.77 (m, 1H), 5.85 (ddd, *J* = 6.3, 1.4 Hz, 1H), 6.02 (ddd, *J* = 6.3, 2.4 Hz, 1H). ^{13}C NMR ($CHCl_3$, 100 MHz): δ 13.94, 22.44, 28.30, 34.02, 63.82, 67.41, 68.72, 127.97, 135.23, 162.98. IR (neat, cm^{-1}): 2930, 1752. HRMS (EI): *m*/*z* calcd for $C_{10}H_{15}NO_2$ (M^+) 181.1103, found 181.1099.

*Typical Procedure for Epoxidation (**5c**).* To a vial with **4c** (158.0 mg, 0.872 mmol) were added 6.4 mL of CH_3CN and 4.4 mL of 4 × 10^{-4} M ethylenediaminetetraacetic acid in H_2O. The solution was cooled to 0 °C, and 1,1,1-trifluoroacetone (977 mg, 8.72 mmol) was added. A mixture of solid Oxone (2.68 g, 4.36 mmol) and $NaHCO_3$ (549 mg, 6.54 mmol) was added in four portions over 45 min. The reaction was stirred for 2 h at 0 °C, then diluted with 5 mL of H_2O, and extracted with CH_2Cl_2 (3 × 15 mL). The organic layers were combined and dried over anhydrous Na_2SO_4. Filtration and evaporation in vacuo furnished the crude product (231 mg), which was purified by column chromatography (silica gel, 6 g, Et_2O) to provide epoxide **5c** (171 mg, 99%) as a colorless oil.

*(1aR,1bS,6S,6aS)-6-Butyltetrahydrooxireno[2′,3′:3,4]pyrrolo[1,2-c]oxazol-4(1aH)-one (**5c**).* $[\alpha]_D^{22}$ = +48.2 ($CHCl_3$, *c* = 0.12). ^{1}H NMR ($CDCl_3$, 400 MHz): δ 0.90 (t, *J* = 7.2 Hz, 3H), 1.26−1.58 (m, 6H), 3.54 (d, *J* = 2.9 Hz, 1H), 3.61 (d, *J* = 2.9 Hz, 1H), 3.97 (dd, *J* = 8.7, 4.3 Hz, 1H), 4.03 (dd, *J* = 9.2, 4.8 Hz, 1H), 4.46 (dd, *J* = 9.2, 4.3 Hz, 1H), 4.53 (t, *J* = 8.7 Hz, 1H). ^{13}C NMR ($CDCl_3$, 100 MHz): δ 13.91, 22.39, 28.19, 29.73, 55.27, 57.20, 58.77, 60.42, 64.65, 162.56. IR (neat, cm^{-1}): 2959, 2933, 1754. HRMS (EI): *m*/*z* calcd for $C_{10}H_{15}NO_3$ (M^+) 197.1052, found 197.1054.

*Typical Procedure for the Preparation of a Diol (**6c**).* Trifluoroacetic acid (0.78 mL, 10.5 mmol) was added to a solution of the epoxide **5c** (171 mg, 0.867 mmol) in THF/H_2O (3/2, 7.5 mL). After being stirred at 80 °C for 72 h, the reaction mixture was cooled to room temperature and concentrated. The product was purified by flash chromatography (silica gel, 10 g, Et_2O only → Et_2O/CH_3OH = 20/1) to yield diol **6c** (136 mg, 74%) as a colorless oil.

*(5S,6S,7S,7aS)-5-Butyl-6,7-dihydroxytetrahydropyrrolo[1,2-c]-oxazol-3(1H)-one (**6c**).* $[\alpha]_D^{23}$ = +22.2 ($CHCl_3$, c = 0.46). ^{1}H NMR ($CDCl_3$, 400 MHz): δ 0.90–0.95 (m, 3H), 1.25–1.69 (m, 6H), 3.65–3.67 (m, 1H), 3.84–3.88 (m, 1H), 3.90–3.98 (m, 2H), 4.34 (dd, J = 9.7, 3.9 Hz, 1H), 4.52 (dd, J = 9.2, 7.7 Hz, 1H). ^{13}C NMR ($CHCl_3$, 100 MHz): δ 13.99, 22.42, 28.20, 32.81, 61.99, 65.29, 66.85, 80.93, 83.74, 162.45. IR (neat, cm^{-1}): 3377, 1731. HRMS (EI): m/z calcd for $C_{10}H_{17}NO_4$ (M^+) 215.1158, found 215.1162.

*Typical Procedure for Hydrolysis (**1c**).* NaOH (143 mg, 3.58 mmol) was added to a solution of diol **6c** (71.0 mg, 0.330 mmol) in EtOH/H_2O (2:1, 4.2 mL), and the mixture was refluxed for 12 h. The reaction mixture was cooled to room temperature and concentrated. The product was purified by flash chromatography (silica gel, 10 g, Et_2O/MeOH/25% NH_3(aq) = 80/20/1 → Et_2O/MeOH/25% NH_3(aq) = 0/100/2) to yield **1c** (38.0 mg, 61%) as a white amorphous solid.

*α-1-C-Ethyl-LAB (**1a**).* $[\alpha]_D^{24}$ = −57.9 (CH_3OH, c = 1.37). ^{1}H NMR (CD_3OD, 400 MHz): δ 0.98 (t, J = 7.5 Hz, 3H), 1.39–1.50 (m, 1H), 1.65–1.75 (m, 1H), 2.78 (dt, J = 7.7, 5.3 Hz, 1H), 2.95 (dt, J = 6.3, 4.3 Hz, 1H), 3.56–3.61 (m, 2H), 3.64–3.68 (m, 1H), 3.75 (t, J = 6.8 Hz, 1H). ^{13}C NMR (CD_3OD, 100 MHz): δ 11.32, 27.97, 63.29, 64.19, 64.35, 79.67, 83.34. IR (KBr, cm^{-1}): 3297, 2922. HRMS (EI): m/z calcd for $C_7H_{15}NO_3$ (M^+) 161.1052, found 161.1056.

*α-1-C-Propyl-LAB (**1b**).* $[\alpha]_D^{24}$ = −46.7 (CH_3OH, c = 1.18). ^{1}H NMR (CD_3OD, 400 MHz): δ 0.96 (t, J = 7.2 Hz, 3H), 1.35–1.55 (m, 3H), 1.63–1.74 (m, 1H), 2.92–2.97 (m, 1H), 3.04 (dd, J = 6.3, 3.9 Hz, 1H), 3.60–3.65 (m, 2H), 3.68–3.72 (m, 1H), 3.79 (t, J = 6.3 Hz, 1H). ^{13}C NMR (CD_3OD, 100 MHz): δ 14.42, 20.77, 36.83, 62.54, 62.65, 64.55, 79.00, 82.97. IR (KBr, cm^{-1}): 3223, 2929. HRMS (EI): m/z calcd for $C_8H_{17}NO_3$ (M^+) 175.1208, found 175.1207.

*α-1-C-Butyl-LAB (**1c**).* $[\alpha]_D^{27}$ = −47.7 (CH_3OH, c = 1.00). ^{1}H NMR (CD_3OD, 400 MHz): δ 0.93 (t, J = 6.8 Hz, 3H), 1.28–1.45 (m, 5H), 1.64–1.72 (m, 1H), 2.83 (dt, J = 7.7, 5.3 Hz, 1H), 2.94 (dt, J = 6.3, 4.3 Hz, 2H), 3.63–3.67 (m, 1H), 3.74 (t, J = 6.3 Hz, 1H). ^{13}C NMR (CD_3OD, 100 MHz): δ 14.33, 23.77, 29.83, 34.45, 62.67, 62.87, 64.56, 79.13, 83.10. IR (KBr, cm^{-1}): 3285. HRMS (EI): m/z calcd for $C_9H_{19}NO_3$ (M^+) 189.1365, found 189.1360.

*α-1-C-Pentyl-LAB (**1d**).* $[\alpha]_D^{24}$ = −53.5 (CH_3OH, c = 1.44). ^{1}H NMR (CD_3OD, 400 MHz): δ 0.91 (t, J = 7.0 Hz, 3H), 1.24–1.50 (m, 7H), 1.60–1.73 (m, 1H), 2.81–2.86 (m, 1H), 2.93–2.97 (m, 1H), 3.55–3.59 (m, 2H), 3.63–3.67 (m, 1H), 3.74 (t, J = 6.5 Hz, 1H). ^{13}C NMR (CD_3OD, 100 MHz): δ 14.39, 23.66, 27.46, 33.14, 35.32, 62.65, 63.34, 64.40, 79.64, 83.68. IR (KBr, cm^{-1}): 3285, 2926. HRMS (EI): m/z calcd for $C_{10}H_{21}NO_3$ (M^+) 203.1521, found 203.1519.

*α-1-C-Hexyl-LAB (**1e**).* $[\alpha]_D^{24}$ = −51.1 (CH_3OH, c = 1.18). ^{1}H NMR (CD_3OD, 400 MHz): δ 0.90 (t, J = 6.3 Hz, 3H), 1.25–1.48 (m, 9H), 1.62–1.72 (m, 1H), 2.86 (dd, J = 12.5, 7.2 Hz, 1H), 2.97 (dd, J = 10.9, 6.0 Hz, 1H), 3.56–3.60 (m, 2H), 3.64–3.68 (m, 1H), 3.75 (t, J = 6.5 Hz, 1H). ^{13}C NMR (CD_3OD, 100 MHz): δ 14.41, 23.67, 27.70, 30.54, 32.94, 35.26, 62.69, 63.23, 64.41, 79.57, 83.58. IR (KBr, cm^{-1}): 3286, 2924, 2853. HRMS (EI): m/z calcd for $C_{11}H_{23}NO_3$ (M^+) 217.1678, found 217.1685.

*α-1-C-Heptyl-LAB (**1f**).* $[\alpha]_D^{24}$ = −46.1 (CH_3OH, c = 1.00). ^{1}H NMR (CD_3OD, 400 MHz): δ 0.90 (t, J = 6.8 Hz, 3H), 1.20–1.50 (m, 11H), 1.60–1.75 (m, 1H), 2.84 (dd, J = 12.6, 7.7 Hz, 1H), 2.96 (dd, J = 10.6, 6.3 Hz, 1H), 3.55–3.59 (m, 2H), 3.64–3.68 (m, 1H), 3.74 (t, J = 6.5 Hz, 1H). ^{13}C NMR (CD_3OD, 100 MHz): δ 14.43, 23.73, 27.77, 30.39, 30.86, 33.01, 35.32, 62.67, 63.29, 64.41, 79.61, 83.64. IR (KBr, cm^{-1}): 3286, 2923. HRMS (EI): m/z calcd for $C_{12}H_{25}NO_3$ (M^+) 231.1834, found 231.1824.

*α-1-C-Octyl-LAB (**1g**).* $[\alpha]_D^{23}$ = −44.2 (CH_3OH, c = 0.70). ^{1}H NMR (CD_3OD, 400 MHz): δ 0.89 (t, J = 7.0 Hz, 3H), 1.30–1.47 (m, 13H), 1.67–1.73 (m, 1H), 2.89–2.94 (m, 1H), 3.01–3.06 (m, 1H), 3.59–3.63 (m, 2H), 3.69 (m, 1H), 3.77 (t, J = 6.8 Hz, 1H). ^{13}C NMR (CD_3OD, 100 MHz): δ 14.43, 23.73, 27.68, 30.41, 30.64, 30.82, 33.05, 34.79, 62.69, 62.98, 64.65, 79.15, 83.12. IR (KBr, cm^{-1}): 3287, 2924, 2852. HRMS (EI): m/z calcd for $C_{13}H_{27}NO_3$ (M^+) 245.1991, found 245.1982.

*α-1-C-nonyl-LAB (**1h**).* $[\alpha]_D^{23}$ = −45.5 (CH_3OH, c = 1.33). ^{1}H NMR (CD_3OD, 400 MHz): δ 0.89 (t, J = 6.8 Hz, 3H), 1.22–1.50 (m, 15H), 1.62–1.72 (m, 1H), 2.84 (dd, J = 12.5, 7.2 Hz, 1H), 2.97 (m, 1H), 3.55–3.60 (m, 2H), 3.64–3.68 (m, 1H), 3.74 (t. J = 6.8 Hz, 1H). ^{13}C NMR (CD_3OD, 100 MHz): δ 14.45, 23.73, 27.77, 30.47, 30.71, 30.89, 33.07, 35.31, 62.69, 63.28, 64.42, 79.61, 83.63. IR (neat, cm^{-1}): 3289, 2923, 2852. HRMS (EI): m/z calcd for $C_{14}H_{29}NO_3$ (M^+) 259.2147, found 259.2151.

*α-1-C-Decyl-LAB (**1i**).* $[\alpha]_D^{22}$ = −36.5 (CH_3OH, c = 0.41). ^{1}H NMR (CD_3OD, 400 MHz): δ 0.90 (t, J = 6.5 Hz, 3H), 1.24–1.51 (m, 17H), 1.65–1.75 (m, 1H), 2.86 (dd, J = 12.3, 7.5 Hz, 1H), 2.97 (dd, J = 10.6, 6.3 Hz, 1H), 3.57–3.61 (m, 2H), 3.67 (dd, J = 11.6, 4.3 Hz, 1H), 3.77 (t, J = 6.7 Hz, 1H). ^{13}C NMR (CD_3OD, 100 MHz): δ 14.45, 23.73, 27.68, 30.47, 30.67, 30.74, 30.82, 33.07, 34.81, 62.71, 62.94, 64.60, 79.18, 83.15. IR (KBr, cm^{-1}): 3289, 2923, 2852. HRMS (EI): m/z calcd for $C_{15}H_{31}NO_3$ (M^+) 273.2304, found 273.2304.

*α-1-C-Undecyl-LAB (**1j**).* $[\alpha]_D^{23}$ = −37.8 (CH_3OH, c = 1.00). ^{1}H NMR (CD_3OD, 400 MHz): δ 0.89 (t, J = 6.3 Hz, 3H), 1.29–1.50 (m, 19H), 1.63–1.75 (m, 1H), 2.86 (dd, J = 12.3, 7.5 Hz, 1H), 2.97 (dd, J = 10.6, 6.3 Hz, 1H), 3.57–3.61 (m, 2H), 3.65–3.69 (m, 1H), 3.75 (t, J = 6.5 Hz, 1H). ^{13}C NMR (CD_3OD, 100 MHz): δ 14.46, 23.74, 27.77, 30.48, 30.71, 30.75, 30.80, 30.89, 33.08, 35.29, 62.70, 63.25, 64.43, 79.58, 83.61. IR (KBr, cm^{-1}): 3290, 2922. HRMS (EI): m/z calcd for $C_{16}H_{33}NO_3$ (M^+) 287.2460, found 287.2461.

*α-1-C-(4-Phenylbutyl)-LAB (**1k**).* $[\alpha]_D^{24}$ = −35.7 (CH_3OH, c = 0.88). ^{1}H NMR (CD_3OD, 400 MHz): δ 1.39–1.53 (m, 3H), 1.62–1.74 (m, 3H), 2.62 (t, J = 7.7 Hz, 2H), 2.84–2.89 (m, 1H), 2.96–3.00 (m, 1H), 3.56–3.60 (m, 2H), 3.65–3.68 (m, 1H), 3.75 (t, J = 6.5 Hz, 1H). ^{13}C NMR (CD_3OD, 100 MHz): δ 27.33, 32.81, 34.93, 36.80, 62.76, 63.02, 64.53, 79.39, 83.40, 126.68, 129.28, 129.42, 143.78. IR (KBr, cm^{-1}): 3367, 3028, 2931, 2851. HRMS (EI): m/z calcd for $C_{15}H_{23}NO_3$ (M^+) 265.1678, found 265.1669.

*α-1-C-(4-Methylpentyl)-LAB (**1l**).* $[\alpha]_D^{24}$ = −44.8 (CH_3OH, c = 0.75). ^{1}H NMR (CD_3OD, 400 MHz): δ 0.89 (d, J = 6.8 Hz, 6H), 1.19–1.68 (m, 7H), 2.87–2.91 (m, 1H), 2.97–3.02 (m, 1H), 3.57–3.61 (m, 2H), 3.65–3.69 (m, 1H), 3.76 (t, J = 6.8 Hz, 1H). ^{13}C NMR (CD_3OD, 100 MHz): δ 22.97, 22.99, 25.56, 29.12, 35.33, 40.25, 62.88, 63.00, 64.55, 79.39, 83.40. IR (KBr, cm^{-1}): 3277, 2957, 2928, 2870. HRMS (EI): m/z calcd for $C_{11}H_{23}NO_3$ (M^+) 259.2147, found 259.2151.

*Preparation of α-1-C-{(S)-1-Hydroxybutyl}-LAB (**7**) and α-1-C-{(R)-1-Hydroxybutyl}-LAB (**8**). (2R,5R)-Benzyl 2-{(Benzyloxy)methyl}-5-butyryl-2,5-dihydro-1H-pyrrole-1-carboxylate (**10**).* To a suspension of the Mg chips (208 mg, 8.54 mmol) in THF (8.5 mL) was added 1-bromopropane (0.66 mL, 7.32 mmol) dropwise over 5 min at room temperature, and the reaction mixture was refluxed for 1 h. The resulting green-black solution was cooled to room temperature. To the reaction mixture was added a solution of Weinreb amide **9** (1.00 g, 2.44 mmol) in THF (5 mL), and the reaction was stirred for 3 h. The reaction mixture was poured into a two-layer mixture of Et_2O (15 mL) and saturated aqueous NH_4Cl (15 mL) at 0 °C. The aqueous layer was separated and extracted with EtOAc (30 mL). The combined organic layers were washed with saturated aqueous $NaHCO_3$ (15 mL) and brine (15 mL), dried over Na_2SO_4, and concentrated to yield a yellow oil. The residue was purified by flash chromatography (silica gel, 40 g, hexane/EtOAc = 4/1) to yield **10** (720 mg, 75%) as a pale yellow oil. $[\alpha]_D^{23}$ = +349.6 ($CHCl_3$, c = 1.96). ^{1}H NMR ($CDCl_3$, 400 MHz): (major) δ 0.75 (t, J = 7.2 Hz, 3H), 1.33–1.66 (m, 2H), 2.11 (dt, J = 17.4, 7.7 Hz, 1H), 2.23 (dt, J = 17.4, 7.7 Hz, 1H), 3.80 (dd, J = 9.2, 5.8 Hz, 1H), 3.91 (dd, J = 9.7, 2.9 Hz, 1H), 4.52 (d, J = 2.9 Hz, 1H), 4.88–4.91 (m, 1H), 5.10–5.14 (m, 3H), 5.66 (dt, J = 6.3, 1.9 Hz, 1H), 6.06 (dt, J = 6.3, 1.9 Hz, 1H), 7.23–7.38 (m, 10H); (minor) δ 0.89 (t, J = 7.2 Hz, 3H), 1.33–1.66 (m, 2H), 2.34 (dt, J = 17.4, 7.2 Hz, 1H), 2.46 (dt, J = 17.4, 7.2 Hz, 1H), 3.57 (dd, J = 9.2, 5.8 Hz, 1H), 3.74 (dd, J = 9.7, 2.9 Hz, 1H), 4.42 (d, J = 6.3 Hz, 1H), 4.78–4.82 (m, 2H), 4.99–5.02 (m, 3H), 5.72 (dt, J = 6.3, 1.9 Hz, 1H), 6.02 (dt, J = 6.3, 1.9 Hz, 1H), 7.23–7.38 (m, 10H). ^{13}C NMR ($CDCl_3$, 100 MHz): δ 13.55, 13.69, 16.48, 16.65, 38.94, 40.15, 64.56, 65.48, 67.18, 67.34, 69.12, 70.23, 73.24, 73.38, 74.29, 74.37, 124.87, 124.96, 126.96, 127.44, 127.46, 127.59, 127.64, 127.69, 128.12, 128.15, 128.20, 128.27, 128.34, 128.39, 128.47, 128.51, 128.55, 132.17, 132.22, 135.94, 136.22, 138.03, 138.20, 153.62, 206.44, 207.07. IR (neat, cm^{-1}): 2962, 2874, 1714.

HRMS (EI): m/z calcd for $C_{11}H_{23}NO_4$ (M^+) 233.1627, found 233.1638.

(2R,5R)-Benzyl 2-((Benzyloxy)methyl)-5-{(S)-1-hydroxybutyl}-2,5-dihydro-1H-pyrrole-1-carboxylate (11). To a solution of ketone **10** (264 mg, 0.668 mmol) in Et_2O (4.5 mL) at 0 °C was added DIBAL-H (0.89 mL, 1.5 M in hexane, 1.34 mmol) dropwise over 5 min. After being stirred at this temperature for 2 h, the mixture was quenched by addition of EtOAc (5 mL) and 1 M aqueous potassium sodium tartrate (5 mL). The resulting mixture was stirred vigorously at room temperature for 2 h and then was extracted with EtOAc (2 × 15 mL). The combined organic layers were washed with brine (10 mL) and dried over anhydrous Na_2SO_4. Filtration and evaporation in vacuo furnished the crude product, which was purified by column chromatography (silica gel, 15 g, hexane/EtOAc = 3/1 → hexane/EtOAc = 2/1) to give **11** (172 mg, 65%) as a colorless oil and **12** (47.8 mg, 18%) as a colorless oil. $[\alpha]_D^{23}$ = +227.2 ($CHCl_3$, c = 0.98). ^{1}H NMR ($CDCl_3$, 400 MHz): (major) δ 0.90 (t, J = 7.2 Hz, 3H), 1.20–1.34 (m, 4H), 3.56 (dd, J = 9.2, 5.8 Hz, 1H), 3.71 (dd, J = 9.2, 2.9 Hz, 1H), 3.84–3.88 (m, 1H), 4.09 (d, J = 9.7 Hz, 1H), 4.34–4.49 (m, 2H), 4.61–4.64 (m, 1H), 4.86–4.87 (m, 1H), 5.08 (d, J = 2.4 Hz, 2H), 5.70 (dt, J = 6.8, 1.9 Hz, 1H), 5.89 (dt, J = 6.8, 1.9 Hz, 1H), 7.22–7.35 (m, 10H); (minor) δ 0.88 (t, J = 7.2 Hz, 3H), 1.20–1.34 (m, 4H), 3.52–3.58 (m, 1H), 3.67–3.721 (m, 1H), 3.84–3.88 (m, 1H), 4.09 (m, 1H), 4.34–4.49 (m, 2H), 4.61–4.64 (m, 1H), 4.86–4.87 (m, 1H), 5.03–5.09 (m, 2H), 5.70–5.72 (m, 1H), 5.88–6.01 (m, 1H), 7.22–7.35 (m, 10H). ^{13}C NMR ($CDCl_3$, 100 MHz): δ 14.11, 19.46, 33.50, 65.35, 67.38, 70.27, 72.09, 72.33, 73.16, 127.42, 127.52, 127.65, 128.09, 128.16, 128.21, 128.30, 128.38, 128.54, 129.55, 136.12, 138.12, 155.73. IR (neat, cm^{-1}): 3430, 2957, 1683. HRMS (EI): m/z calcd for $C_{24}H_{29}NO_4$ (M^+) 395.2097, found 395.2097.

(2S,3S,4S,5S)-Benzyl-2-{(benzyloxy)methyl}-3,4-dihydroxy-5-{(S)-1-hydroxybutyl}pyrrolidine-1-carboxylate (14). To a vial containing **11** (122 mg, 0.308 mmol) were added CH_3CN (3.1 mL) and 4 × 10^{-4} M ethylenediaminetetraacetic acid in H_2O (2.1 mL). The solution was cooled to 0 °C, and 1,1,1-trifluoroacetone (345 mg, 3.08 mmol) was added. A mixture of solid Oxone (947 mg, 1.54 mmol) and $NaHCO_3$ (245 mg, 2.31 mmol) was added in four portions over 45 min. The reaction was stirred for 2 h at 0 °C, then diluted with 5 mL of H_2O, and extracted with EtOAc (2 × 15 mL). The organic layers were combined and dried over anhydrous Na_2SO_4. Filtration and evaporation in vacuo furnished the crude product, which was purified by column chromatography (silica gel, 6 g, Et_2O) to provide a mixture of epoxides **13** (105 mg, 83%) as a colorless oil. Trifluoroacetic acid (0.25 mL, 3.37 mmol) was added to a solution of the epoxides **13** (102 mg, 0.248 mmol) in THF/H_2O (3/2, 2.5 mL). After being stirred at 70 °C for 12 h, the reaction mixture was cooled to room temperature, quenched by addition of saturated aqueous $NaHCO_3$ (5 mL), and extracted with EtOAc (3 × 5 mL). The combined organic layers were washed with brine (5 mL) and dried over anhydrous Na_2SO_4. Filtration and evaporation in vacuo furnished the crude product, which was purified by column chromatography (silica gel, 5 g, hexane/EtOAc = 2/1 → hexane/EtOAc = 1/1) to yield diol **14** (100 mg, 93%) as a colorless oil. $[\alpha]_D^{22}$ = −+57.8 ($CHCl_3$, c = 1.21). ^{1}H NMR ($CDCl_3$, 400 MHz, ca.1:1 mixture): δ 0.86 (t, J = 6.8 Hz, 3H), 0.97 (t, J = 6.8 Hz, 3H), 1.25–1.61 (m, 8H), 3.50–3.58 (m, 2H), 3.84–4.15 (m, 10H), 4.28–4.57 (m, 6H), 4.76–5.17 (m, 6H), 7.20–7.35 (m, 10H). ^{13}C NMR ($CDCl_3$, 100 MHz): δ 14.03, 14.30, 19.46, 19.62, 36.61, 36.69, 67.32, 67.38, 67.76, 67.81, 68.48, 69.26, 70.84, 73.08, 73.65, 73.88, 74.09, 76.03, 77.64, 79.73, 80.69, 128.15, 128.22, 128.26, 128.52, 128.54, 128.55, 128.64, 128.86, 128.92, 128.99, 136.37, 136.45, 136.68, 136. 82, 154.80, 154.83. IR (neat, cm^{-1}): 3390, 2958, 2927, 1683. HRMS (EI): m/z calcd for $C_{24}H_{31}NO_6$ (M^+) 429.2151, found 429.2146.

α-1-C-{(S)-1-Hydroxybutyl}-LAB (7). Pd/C (5% Pd, 9.8 mg, 10 wt %) was added to a stirred solution of diol **14** (98.4 mg, 0.229 mmol) in MeOH (2.3 mL) and concentrated HCl (3 drops). The reaction mixture was stirred for 10 h under a balloon of H_2. The reaction mixture was filtered through Celite (eluting with MeOH) and concentrated in vacuo. The product was purified by flash chromatography (silica gel, 3 g, Et_2O/MeOH/25% NH_3(aq) = 80/20/1 →Et_2O/MeOH/25% NH_3(aq) = 0/100/2) to yield **7** (32.0 mg, 68%) as a white amorphous solid. $[\alpha]_D^{22}$ = −17.1 (CH_3OH, c = 1.32). ^{1}H NMR (CD_3OD, 400 MHz): δ 0.97 (t, J = 7.2 Hz, 3H), 1.36–1.64 (m, 4H), 3.37–3.40 (m, 2H), 3.77–3.90 (m, 3H), 3.97 (t, J = 6.8 Hz, 1H), 4.23 (t, J = 6.8 Hz, 1H). ^{13}C NMR (CD_3OD, 100 MHz): δ 14.24, 19.96, 36.67, 58.62, 64.77, 66.01, 69.72, 75.09, 76.64. IR (neat, cm^{-1}): 3350, 2962. HRMS (FAB): m/z calcd for $C_9H_{20}NO_4$ (M + H^+) 206.1392, found 206.1394.

(2R,5R)-Benzyl 2-{(Benzyloxy)methyl}-5-{(R)-1-hydroxybutyl}-2,5-dihydro-1H-pyrrole-1-carboxylate (12). To a solution of ketone **10** (360 mg, 0.915 mmol) in MeOH (6 mL) at 0 °C was added $NaBH_4$ (69.2 mg, 1.83 mmol). After being stirred at this temperature for 1 h, the mixture was quenched by addition of H_2O (5 mL). The resulting mixture was extracted with EtOAc (2 × 25 mL). The combined organic layers were washed with brine (15 mL) and dried over anhydrous Na_2SO_4. Filtration and evaporation in vacuo furnished the crude product, which was purified by column chromatography (silica gel, 15 g, hexane/EtOAc = 3/1 → hexane/EtOAc = 2/1) to give **11** (87.5 mg, 24%) as a colorless oil and **12** (183 mg, 51%) as a colorless oil. $[\alpha]_D^{22}$ = +234.6.0 ($CHCl_3$, c = 0.80). ^{1}H NMR ($CDCl_3$, 400 MHz): (major) δ 0.91 (t, J = 6.8 Hz, 3H), 1.10–1.60 (m, 4H), 3.54 (dd, J = 9.2, 6.3 Hz, 1H), 3.68 (dd, J = 9.2, 2.4 Hz, 1H), 3.94 (br s, 1H), 4.34–4.43 (m, 3H), 4.51–4.70 (m, 2H), 5.07 (d, J = 6.8 Hz, 2H), 5.82–5.88 (m, 2H), 7.22–7.36 (m, 10H); (minor) δ 0.81 (t, J = 6.8 Hz, 3H), 1.10–1.60 (m, 4H), 3.81–3.91 (m, 2H), 4.16 (br s, 1H), 4.51–4.70 (m, 5H), 5.03–5.22 (m, 2H), 5.82–5.96 (m, 2H), 7.22–7.36 (m, 10H). ^{13}C NMR ($CDCl_3$, 100 MHz): δ 14.11, 18.51, 19.08, 35.13, 64.83, 65.77, 66.88, 67.38, 70.30, 72.07, 73.16, 73.27, 74.11, 126.76, 127.11, 127.39, 127.43, 127.65, 128.22, 128.23, 128.30, 128.39, 128.54, 129.05, 136.08, 138.13, 155.89, 155.90. IR (neat, cm^{-1}): 3435, 2933, 2871, 1682. HRMS (EI): m/z calcd for $C_{24}H_{29}NO_4$ (M^+) 395.2097, found 395.2097.

(2S,3S,4S,5S)-Benzyl 2-{(Benzyloxy)methyl}-3,4-dihydroxy-5-{(R)-1-hydroxybutyl}pyrrolidine-1-carboxylate (16). To a vial with **12** (155 mg, 0.392 mmol) were added CH_3CN (3.9 mL) and 4 × 10^{-4} M ethylenediaminetetraacetic acid in H_2O (2.6 mL). The solution was cooled to 0 °C, and 1,1,1-trifluoroacetone (439 mg, 3.08 mmol) was added. A mixture of solid Oxone (1.21 g, 1.96 mmol) and $NaHCO_3$ (312 mg, 2.94 mmol) was added in four portions over 45 min. The reaction was stirred for 2 h at 0 °C, then diluted with 5 mL of H_2O, and extracted with EtOAc (2 × 15 mL). The organic layers were combined and dried over anhydrous Na_2SO_4. Filtration and evaporation in vacuo furnished the crude product, which was purified by column chromatography (silica gel, 6 g, Et_2O) to provide a mixture of epoxides **15** (129 mg, 80%) as a colorless oil. Trifluoroacetic acid (0.30 mL, 4.04 mmol) was added to a solution of the epoxides **13** (125 mg, 0.304 mmol) in THF/H_2O (3/2, 3.0 mL). After being stirred at 70 °C for 12 h, the reaction mixture was cooled to room temperature, quenched by addition of saturated aqueous $NaHCO_3$ (5 mL), and extracted with EtOAc (3 × 5 mL). The combined organic layers were washed with brine (5 mL) and dried over anhydrous Na_2SO_4. Filtration and evaporation in vacuo furnished the crude product, which was purified by column chromatography (silica gel, 5 g, hexane/EtOAc = 2/1 → hexane/EtOAc = 1/1) to yield diol **14** (21.0 mg, 16%) as a colorless oil. $[\alpha]_D^{20}$ = +77.3 ($CHCl_3$, c = 0.19). ^{1}H NMR ($CDCl_3$, 400 MHz): (major) δ 0.94 (t, J = 6.8 Hz, 3H), 1.33–1.88 (m, 4H), 3.45–3.57 (m, 1H), 3.67–4.09 (m, 5H), 4.29–4.37 (m, 1H), 4.45–4.59 (m, 2H), 5.02–5.17 (m, 2H), 7.18–7.35 (m, 10H); (minor) δ 0.78 (t, J = 6.8 Hz, 3H), 1.33–1.88 (m, 4H), 3.45–3.57 (m, 1H), 3.67–4.09 (m, 5H), 4.29–4.37 (m, 1H), 4.45–4.59 (m, 2H), 5.02–5.17 (m, 2H), 7.18–7.35 (m, 10H). ^{13}C NMR ($CDCl_3$, 100 MHz): δ 13.78, 13.99, 19.08, 19.30, 29.70, 38.19, 67.11, 67.40, 67.59, 68.61, 68.77, 71.18, 72.53, 73.50, 73.74, 74.49, 74.97, 79.62, 80.55, 81.07, 81.68, 127.95, 128.26, 128.35, 128.54, 128.60, 135.99, 136.38, 136.67, 155.16, 156.61. IR (neat, cm^{-1}): 3390, 2958, 2927, 1674. HRMS (EI): m/z calcd for $C_{24}H_{31}NO_6$ (M^+) 429.2151, found 429.2150.

α-1-C-{(R)-1-Hydroxybutyl}-LAB (8). Pd/C (5% Pd, 2.1 mg, 10 wt %) was added to a stirred solution of diol **16** (20.6 mg, 0.0480 mmol) in MeOH (1.0 mL) and concentrated HCl (1 drop). The reaction mixture was stirred for 10 h under a balloon of H_2. The reaction

mixture was filtered through Celite (eluting with MeOH) and concentrated in vacuo. The product was purified by flash chromatography (silica gel, 2 g, Et_2O/MeOH/25% NH_3(aq) = 80/20/1 → Et_2O/MeOH/25% NH_3(aq) = 0/100/2) to yield **8** (9.30 mg, 94%) as a white amorphous solid. $[\alpha]_D^{22} = -11.6$ (CH_3OH, $c = 0.10$). ^1H NMR (CD_3OD, 400 MHz): δ 0.97 (t, $J = 7.2$ Hz, 3H), 1.39–1.57 (m, 4H), 3.20–3.23 (m, 1H), 3.34–3.38 (m, 1H), 3.75–3.88 (m, 3H), 3.97–4.02 (m, 2H), 4.88 (br s, 1H). ^{13}C NMR (CD_3OD, 100 MHz): δ 14.16, 19.64, 37.61, 58.98, 64.92, 67.73, 68.68, 76.16, 76.43. IR (neat, cm^{-1}): 3367, 2931. HRMS (FAB): m/z calcd for $C_9H_{20}NO_4$ ($M + H^+$) 206.1392, found 206.1384.

N-Butyl-α-1-C-butyl-LAB (17). Sodium borocyanohydride (9.9 mg, 0.15 mmol) and butyraldehyde (30 μL, 0.32 mmol) were added to the solution of (2*S*,3*S*,4*S*,5*S*)-2-butyl-5-(hydroxymethyl)pyrrolidine-3,4-diol (19 mg, 0.10 mmol) in MeOH (2.0 mL) at 0 °C, and the resulting solution was stirred for 2 h at the same temperature. Then the solvent was removed under reduced pressure. The residue was purified by silica gel SiO_2 column chromatography to obtain **17** (11.2 mg, 46%). $[\alpha]_D^{20} = +36.9$ ($CHCl_3$, $c = 1.01$). ^1H NMR (400 MHz, $CDCl_3$): δ 0.87–0.94 (m, 6H), 1.25–1.50 (m, 9H), 1.58–1.67 (m, 1H), 2.57–2.72 (m, 2H), 2.85 (br s, 1H), 3.07 (br d, $J = 10.1$ Hz, 1H), 3.72–3.81 (m, 2H), 3.86 (br s, 1H), 4.11 (br d, $J = 3.4$ Hz, 1H), 4.20 (br s, 3H). ^{13}C NMR (100 MHz, $CDCl_3$): δ 13.92, 14.03, 20.58, 22.85, 25.24, 28.36, 29.50, 46.56, 58.90, 67.74, 69.45, 79.97, 80.42. IR (neat) cm^{-1} 3391, 2959, 2873, 2344, 2173. HRMS (EI): m/z calcd for $C_{13}H_{27}NO_3$ (M^+) 245.1991, found 245.1980.

(5S,6R,7S,7aR)-5,7-Dibutyltetrahydro-6-hydroxypyrrolo[1,2-c]-oxazol-3(1H)-one (19). CuI (84.6 mg, 0.44 mmol) was dried under reduced pressure, and Et_2O (0.7 mL) was added under an argon atmosphere. The solution was cooled at 0 °C, and *n*-BuLi (1.6 M hexane solution, 0.55 mL, 0.50 mmol) was added. The solution was stirred until the yellow color disappeared. The resulting solution was utilized as the ether solution of *n*-Bu_2CuLi. The prepared ether solution of *n*-Bu_2CuLi was added to the solution of **5c** (43.2 mg, 0.22 mmol) in Et_2O (0.7 mL) at −20 °C under an argon atmosphere. The solution was stirred until the starting material disappeared on TLC. Then a saturated aqueous solution of NH_4Cl was added to quench the reaction. The resulting mixture was extracted with CH_2Cl_2 and dried over Na_2SO_4. The solvent was removed under reduced pressure, and the residue was purified by silica gel column chromatography (Et_2O) to afford **19** (13 mg, 23%). $[\alpha]_D^{24} = +11.5$ ($CHCl_3$, $c = 1.30$). ^1H NMR (400 MHz, $CDCl_3$): δ 0.88–0.94 (m, 6H), 1.20–1.55 (m, 10H), 1.60–1.69 (m, 2H), 1.83–1.88 (m, 1H), 3.57–3.74 (m, 2H), 3.72 (dd, $J = 7.7$, 5.3 Hz, 1H), 4.19 (dd, $J = 9.2$, 3.9 Hz, 1H), 4.47 (t, $J = 8.7$ Hz, 1H). ^{13}C NMR (100 MHz, $CDCl_3$): δ 13.85, 13.98, 22.54, 22.94, 28.24, 30,10, 30.50, 33.82, 52.85, 62.13, 66.27, 67.47, 84.92, 161.30. IR (KBr, cm^{-1}): 3426, 1733, 1398, 1227. HRMS (EI): m/z calcd for $C_{14}H_{25}NO_3$ (M^+) 255.1843, found 255.1832.

(2S,3R,4S,5R)-2,4-Dibutyl-5-(hydroxymethyl)pyrrolidin-3-ol (18). To the solution of **19** (13 mg, 0.051 mmol) in EtOH (0.4 mL) were added H_2O (0.2 mL) and NaOH (20 mg, 0.5 mmol) at room temperature. The solution was refluxed at 100 °C for 1 h. Then the solvent was removed under reduced pressure. The residue was purified by silica gel SiO_2 column chromatography (MeOH) to obtain **18** (4.4 mg, 38%). $[\alpha]_D^{20} = -15.6$ (CH_3OH, $c = 0.44$). ^1H NMR (400 MHz, CD_3OD): δ 0.89–0.96 (m, 6H), 1.25–1.80 (m, 13H), 2.90–3.05 (m, 2H), 3.43 (t, $J = 8.2$ Hz, 1H), 3.55 (dd, $J = 11.6$, 7.2 Hz, 1H), 3.64 (dd, $J = 11.6$, 3.7 Hz, 1H). ^{13}C NMR (100 MHz, CD_3OD): δ 14.28, 14.32, 23.81, 24.01, 29.96, 30.79, 30.89, 33.10, 33.28, 35.17, 63.87, 64.04, 64.13, 82.38. IR (KBr, cm^{-1}): 3375, 1561, 1467. HRMS (EI): m/z calcd for $C_{14}H_{25}NO_3$ (M^+) 229.2042, found 229.2049.

Assay of Enzyme Inhibition. Brush border membranes were prepared from the rat small intestine according to the method of Kessler et al.[63] and were assayed at pH 5.8 for rat intestinal maltase, isomaltase, sucrase, cellobiase, and lactase using the appropriate disaccharides as substrates. For rat intestinal maltase activities, the reaction mixture contained 25 mM maltose and the appropriate amount of enzyme, and the incubations were performed for 10–30 min at 37 °C. The reaction was stopped by heating at 100 °C for 3 min. After centrifugation (600*g*, 10 min), 0.05 mL of the resulting reaction mixture was added to 3 mL of the glucose CII-test reagent (Wako Pure Chemical Industries, Osaka, Japan). The absorbance at 505 nm was measured to determine the amount of the released D-glucose. Kinetic parameters were determined by the double-reciprocal-plot method of Lineweaver–Burk at increasing concentrations of the appropriate maltose.

Glycoblotting. The human hepatocelluar carcinoma HepG2 cell line was obtained from the European Collection of Cell Cultures (ECACC 85011430). Cells were cultured in low-glucose Dulbecco's modified Eagle's medium (Invitrogen, Carlsbad, CA), supplemented with 10% fetal calf serum (Invitrogen), and maintained in a humidified incubator at 37 °C with 5% CO_2. *N*-Linked oligosaccharide analysis was performed on HepG2 cells after treatment for 48 h with miglitol or α-1-*C*-butyl-LAB, which gave additional *N*-linked oligosaccharide in the MALDI-TOF MS profiles derived from HepG2 homogenates (Figure 3b,c) in comparison to untreated controls (Figure 3a). Cell pellets were homogenized in 0.5% Triton X-100 solution. The solubilized proteinaceous materials were reduced by dithiothreitol (DTT) at 60 °C for 30 min followed by alkylation with 10 μL of 123 mM iodoacetamide (IAA) by incubation in the dark at 25 °C for 60 min. The mixture was then treated with 10 μL of 40 units/μL trypsin at 37 °C for 60 min, followed by heat inactivation of the enzyme at 90 °C for 10 min. After being cooled to room temperature, *N*-glycans were enzymatically released from trypsin-digested glycopeptides by incubation with 5 units of PNGase F (Roche Applied Science, Switzerland) at 37 °C for 16 h. PNGase F-treated samples were dropped onto BlotGlyco beads (Sumitomo Bakelite Co., Tokyo, Japan) in a filter plate, and this was followed by addition of 2% acetic acid/acetonitrile. After incubation at 80 °C for 60 min to covalently ligate glycans onto the beads, the beads were washed with 2 M guanidine hydrochloride, distilled water, and 1% triethylamine/methanol to remove nonspecifically bound impurities. After washing, the beads were treated with 10% acetic anhydride/methanol for 30 min at ambient temperature to quench the hydrazide groups. The beads were then washed serially with 10 mM hydrochloric acid, distilled water, methanol, and dimethyl sulfoxide (DMSO). On-bead methyl esterification was performed by the reaction with 500 mM 1-methyl-3-*p*-tolyltriazene/DMSO solution at 60 °C for 60 min. After the beads were washed with methanol and distilled water, the trapped glycans were finally released and recovered as N^{π}-((aminooxy)acetyl)-tryptophanylarginine methyl ester (aoWR) derivatives by adding 20 mM aoWR and 2% acetic acid/acetonitrile and incubated at 80 °C for 1 h. The resulting aoWR-labeled glycans were recovered by washing the beads with distilled water, and the collected solution was further purified with a solid-phase extraction column (Cleanup column, Sumitomo Bakelite Co.) to remove the excess aoWR. The purified solution was mixed with 2,5-dihydroxybenzoic acid solution and subsequently subjected to MALDI-TOF analysis.

MALDI-TOF MS Analysis. All measurements were performed with an Autoflex III TOF/TOF mass spectrometer equipped with a reflector and controlled by the FlexControl 3.0 software package (Bruker Daltonics GmbH, Bremen, Germany), according to a general protocol reported previously.[51] The peaks were detected generally as a formula of $[M + H]^+$ ions. In MALDI-TOF MS reflector mode, ions generated by a Smartbeam (pulsed UV nitrogen laser, $\lambda = 337$ nm, 5 Hz) were accelerated to a kinetic energy of 23.5 kV. Masses were automatically annotated by using FlexAnalysis 2.0. External calibration of MALDI mass spectra was carried out using singly charged monoisotopic peaks of a mixture of human angiotensin II (m/z 1046.542), bombesin (m/z 1619.823), adrenocorticotropin (18–39) (m/z 2465.199), and somatostatin 28 (m/z 3147.472). All measurements were performed as follows: 1 mL of the sample solution was mixed with 1 mL of 2,5-dihydroxybenzoic acid (10 mg/mL in 30% ACN), and 1 mL of the resulting mixture was subjected to MALDI-TOF mass analysis. Structural identification of glycans was performed by MS analysis and the use of a database for glycan structures[64] (http://web.expasy.org/glycomod/).

Disaccharide Loading Test. The animal experimental protocols in this study were approved by the Animal Experiments Committee of the University of Toyama (S-2010 UH-2). Male ddY mice (29–33 g)

after an overnight fast were used for acute disaccharide loading tests. Maltose (2.5 g/kg of body weight) or sucrose (2.5 g/kg of body weight) as well as the inhibitor, miglitol, was dissolved in 0.9% NaCl solution and administered to the mice via a stomach tube. A control group was loaded with saline only. Blood samples for glucose measurements were obtained from the tail vein at 0, 15, 30, 60, and 120 min after disaccharide loading. The blood glucose levels were measured by a portable kit, StatStrip Xpress (Nova Biomedical Co. Ltd., Waltham, MA). The AUC over a period of 60 min after disaccharide loading was calculated by the trapezoidal method.

Homology Modeling of the Rat *N*-Terminal Catalytic Domain of ntMGAM. The α-glucosidase activities are associated with two small intestinal membrane-bound enzymes: maltase-glucoamylase and sucrase-isomaltase. The *N*-terminal catalytic domain of maltase-glucoamylase (ntMGAM) has a preference for short linear α-1,4 oligosaccharides such as maltose.[65] To investigate the inhibitory activity of α-1-*C*-butyl-LAB on the hydrolysis of maltose in rats, we first constructed a three-dimensional model of rat ntMGAM using homology modeling with Prime 1.5 (Schrödinger, Portland, OR), because the three-dimensional structure of rat ntMGAM has not been determined experimentally. The amino acid sequence of rat ntMGAM was taken from the UniProtKB-Swiss-Prot database (accession number Q6P7A9). Sequences homologous to the rat ntMGAM against the Protein Data Bank (PDB) were performed using a BLAST search, and the three-dimensional structures of human ntMGAM were subsequently found (sequence identity between rat ntMGAM and human ntMGAM, 45%). Four representative structures of human ntMGAM were obtained by clustering 12 three-dimensional structures of human ntMGAM taken from the PDB on the basis of side chain structures around the ligand (PDB IDs 2QLY, 2QMJ, 3CTT, and 3L4W). Using four template structures of human ntMGAM, we constructed the homology models of rat ntMGAM. The stereochemical quality evaluation using PROCHECK indicated that the four homology models are reasonable.[66]

Docking Studies of α-1-*C*-Butyl-LAB, α-1-*C*-Butyl-DNJ, and Miglitol with Rat ntMGAM. Docking calculations of α-1-*C*-butyl-LAB, α-1-*C*-butyl-DNJ, and miglitol with the homology models of rat ntMGAM were carried out using the standard precision mode for Glide 5.5 in the Schrödinger suite. The top three poses ranked with GlideScore[67] were minimized by an OPLS2005 force field, and the docking model that exhibited the most stable interaction energy was then selected as the best model. The binding free energies between rat ntMGAM and the compounds were calculated accurately by combining an OPLS2005 force field with the GB/SA continuum solvation model to include the effect of solvent.[68] The binding energy was estimated as follows: $\Delta E = E_{complex} - (E_{protein} - E_{ligand})$. Here, $E_{complex}$, $E_{protein}$, and E_{ligand} are the molecular mechanics energies of the complex structure, the protein structure, and the ligand structure, respectively.

Docking Studies of α-1-*C*-Butyl-LAB and α-1-*C*-Butyl-DNJ with Human β-Glucocerebrosidase. The docking calculations of α-1-*C*-butyl-LAB and α-1-*C*-butyl-DNJ with β-glucocerebrosidase were carried out using the X-ray of human β-glucocerebrosidase (PDB ID 2NSX) and Induced Fit Docking[69] in the Schrödinger package. For the initial docking process of the Induced Fit Docking, van der Waals (vdW) radii of both the ligand and the receptor were scaled to 0.5 to soften the surfaces of the protein and the ligand, and Asn396 was temporarily mutated to alanine because multiple X-ray structures showed that the orientation of the side chain of Asn396 changes. The ligands were then redocked back into the new receptor using the default vdW radii scaling (1.0 receptor, 0.8 ligand), and Asn396 mutated to alanine was restored in the final docking. The standard precision mode was used in the docking analysis. IFDScore was the sum of the docking energy, receptor strain, and solvation terms. Finally, the top pose ranked by IFDScore was minimized by an OPLS2005 force field.

■ ASSOCIATED CONTENT

Ⓢ Supporting Information

General experimental protocols and ^{1}H and ^{13}C NMR spectra of the compounds. This material is available free of charge via the Internet at http://pubs.acs.org.

■ AUTHOR INFORMATION

Corresponding Author

*Phone: +81-76-434-7868 (A.K.); +81-22-727-0144 (H.T.). E-mail: kato@med.u-toyama.ac.jp (A.K.); takahata@tohoku-pharm.ac.jp (H.T.).

Notes

The authors declare no competing financial interest.

■ ACKNOWLEDGMENTS

We thank Dr. Naoki Asano (BioApply Co., Ltd.) for valuable discussions on the α-1-*C*-alkyl-DNJ derivatives and Takahito Kunimatsu and Shinpei Nakagawa (University of Toyama) for their experimental contribution. This work was supported by a Grant-in-Aid for Scientific Research (C) (23590127) (A.K.) from the Japanese Society for the Promotion of Science (JSPS).

■ ABBREVIATIONS USED

LAB, 1,4-dideoxy-1,4-imino-L-arabinitol; DAB, 1,4-dideoxy-1,4-imino-D-arabinitol; DNJ, 1-deoxynojirimycin; DMDP, (2*R*,5*R*)-bis(dihydroxymethyl)-(3*R*,4*R*)-dihydroxypyrrolidine; IC_{50}, concentration of compound required to induce 50% inhibition; ER, endoplasmic reticulum; MALDI-TOF MS, matrix-assisted laser desorption ionization time-of-flight mass spectrometry; AUC, area under the curve; ntMGAM, *N*-terminal catalytic domain of maltase-glucoamylase; AAA, asymmetric allylic alkylation; RCM, ring-closing metathesis

■ REFERENCES

(1) Tuomilehto, J.; Lindström, J.; Eriksson, J. G.; Valle, T. T.; Hämäläinen, H.; Ilanne-Parikka, P.; Keinänen-Kiukaanniemi, S.; Laakso, M.; Louheranta, A.; Rastas, M.; Salminen, V.; Uusitupa, M. (for the Finnish Diabetes Prevention Study Group). Prevention of type 2 diabetes mellitus by changes in lifestyle among subjects with impaired glucose tolerance. *N. Engl. J. Med.* **2001**, *344*, 1343−1350.

(2) Lyssenko, V; Jonsson, A.; Almgren, P.; Pulizzi, N.; Isomaa, B.; Tuomi, T.; Berglung, G.; Alshuler, D.; Nilsson, P.; Groop, L. Clinical risk factors, DNA variants, and the development of type 2 diabetes. *N. Engl. J. Med.* **2008**, *359*, 2220−2232.

(3) McCarthy, M. I. Genomics, type 2 diabetes, and obesity. *N. Engl. J. Med.* **2010**, *363*, 2339−2350.

(4) Shaw, J. E.; Sicree, R. A.; Zimmet, P. Z. Global estimates of the prevalence of diabetes for 2010 and 2030. *Diabetes Res. Clin. Pract.* **2010**, *87*, 4−14.

(5) Gerich, J. E. Clinical significance, pathogenesis, and management of postprandial hyperglycemia. *Arch. Intern. Med.* **2003**, *163*, 1306−1316.

(6) UK Prospective Diabetes Study Group.. Intensive blood-glucose control with sulphonylureas or insulin compared with conventional treatment and risk of complications in patients with type 2 diabetes (UKPDS 33). *Lancet* **1998**, *352*, 837−853.

(7) UK Prospective Diabetes Study Group.. Effect of intensive blood-glucose control with metformin on complications in overweight patients with type 2 diabetes (UKPDS 34). *Lancet* **1998**, *352*, 854−865.

(8) Stratton, I. M.; Adler, A. I.; Neil, H. A. W.; Matthws, D. R.; Manley, S. E.; Cull, C. A.; Hadden, D.; Turner, R. C.; Holman, R. R. Association of glycaemia with macrovascular and microvascular complications of type 2 diabetes (UKPDS 35): prospective observational study. *BMJ [Br. Med. J.]* **2000**, *321*, 405−412.

(9) Hanefeld, M.; Cagatay, M.; Petrowitsch, T.; Neuse, D.; Petzinna, D.; Rupp, M. Acarbose reduces the risk for myocardial infarction in type 2 diabetic patients: meta-analysis of seven long-term studies. *Eur. Heart J.* **2004**, *25*, 10−16.
(10) Coutinho, M.; Gerstein, H. C; Wang, Y.; Yusuf, S. The relationship between glucose and incident cardiovascular events. A metaregression analysis of published data from 20 studies of 95,783 individuals followed for 12.4 years. *Diabetes Care* **1999**, *22*, 233−240.
(11) Bonora, E.; Muggeo, M. Postprandial blood glucose as a risk factor for cardiovascular disease in type II diabetes: the epidemiological evidence. *Diabetologia* **2001**, *44*, 2107−2114.
(12) Ceriello, A. Postprandial hyperglycemia and diabetes complications: is it time to treat? *Diabetes* **2005**, *54*, 1−7.
(13) Iwasa, M.; Yamada, Y.; Kobayashi, H.; Yasuda, S.; Kawamura, I.; Sumi, S.; Shiraki, T.; Yamaki, T.; Ushikoshi, H.; Hattori, A.; Aoyama, T.; Nishigaki, K.; Takemura, G.; Fujiwara, H; Minatoguchi, S. Both stimulation of GLP-1 recepters and inhibiton of glycogenolysis additively contribute to a protective effect of oral miglitol against ishaemia-reperfusion injury in rabbits. *Br. J. Pharmacol.* **2011**, *164*, 119−131.
(14) Asano, N.; Nash, R. J.; Molyneux, R. J.; Fleet, G. W. J. Sugar-mimic glycosidase inhibitors: natural occurrence, biological activity and prospects for therapeutic application. *Tetrahedron: Asymmetry* **2000**, *11*, 1645−1680.
(15) Sim, L.; Jayakanthan, K.; Mohan, S.; Nasi, R.; Johnston, B. D.; Pinto, B. M.; Rose, D. R. New glucosidase inhibitors from an ayurvedic herbal treatment for type 2 diabetes: structures and inhibition of human intestinal maltase-glucoamylase with compounds from *Salacia reticulata*. *Biochemistry* **2010**, *49*, 443−451.
(16) Eskandari, R.; Jones, K.; Rose, D. R.; Pinto, B. M. Selectivity of 3′-O-methylponkoranol for inhibition of N- and C-terminal maltase glucoamylase and sucrase isomaltase, potential therapeutics for digestive disorders or their sequelae. *Bioorg. Med. Chem. Lett.* **2011**, *21*, 6491−6494.
(17) Ogawa, S. Synthetic studies on glycosidase inhibitors composed of 5a-carba-sugars. *Carbohydrate Mimics: Concepts and Methods*; Chapleur, Y., Ed.; Wiley-VCH: Weinheim, Germany, 1998; pp 87−106.
(18) Horii, S.; Iwasa, T.; Mizuta, E.; Kameda, Y. Studies on validamycins, new antibiotics. VI. Validamine, hydroxyvalidamine and validatol, new cyclitols. *J. Antibiot.* **1971**, *24*, 59−63.
(19) Kameda, Y.; Asano, N.; Yoshikawa, M.; Matsui, K. Valienamine as an α-glucosidase inhibitor. *J. Antibiot.* **1980**, *33*, 1575−1576.
(20) Kameda, Y.; Asano, N.; Yoshikawa, M.; Takeuchi, M.; Yamaguchi, T.; Matsui, K. Valiolamine, a new α-glucosidase inhibiting aminocyclitol produced by *Streptomyces hygroscopicus*. *J. Antibiot.* **1984**, *37*, 1301−1307.
(21) Horii, S; Fukase, H.; Matsuo, T.; Asano, N.; Matsui, K. Synthesis and α-D-glucosidase inhibitory activity of N-substituted valiolamine derivatives as potential oral antidiabetic agents. *J. Med. Chem.* **1986**, *29*, 1038−1046.
(22) Kato, A.; Kato, N.; Kano, E.; Adachi, I.; Ikeda, K.; Yu, L.; Okamoto, T.; Banba, Y.; Ouchi, H.; Takahata, H.; Asano, N. Biological properties of D- and L-1-deoxyazasugars. *J. Med. Chem.* **2005**, *48*, 2036−2044.
(23) Junge, B.; Matzke, M.; Stltefuss, J. In *Handbook of Experimental Pharmacology*; Kuhlmann, J., Puls, W., Eds.; Springer-Verlag: New York, 1996; Vol. *119*, p 411.
(24) Cauderay, M.; Tappy, L.; Temler, E.; Jequier, E.; Hillebrand, I.; Felber, J. P. Effect of α-glucohydrolase inhibitors (Bay m1099 and Bay o1248) on sucrose metabolism in normal men. *Metabolism* **1986**, *35*, 472−477.
(25) Madar, Z.; Olefsky, J. Effect of the α-glucosidase inhibitor Bay-O-1248 on the metabolic response of nondiabetic and diabetic rats to a high-carbogydrate diet. *Am. J. Clin. Nutr.* **1986**, *44*, 206−211.
(26) Taylor, R. H.; Barker, H. M.; Bowey, E. A.; Canfield, J. E. Regulation of absorption of dietary carbohydrate in man by two new glycosidase inhibitors. *Gut* **1986**, *27*, 1471−1478.
(27) Wisselaar, H. A.; van Dongen, J. M.; Reuser, A. J. Effects of *N*-hydroxyethyl-1-deoxynojirimycin (BAY m 1099) on the activity of neutral- and acid α-glucosidases in human fibroblasts and HepG2 cells. *Clin. Chim. Acta* **1989**, *182*, 41−52.
(28) Putter, J. In *Enzyme Inhibitors*; Brodech, E., Ed.; Verlag Chemie: Weinheim, Germany, 1980; p 139.
(29) Joubert, P. H.; Venter, H. L.; Foukaridis, G. N. The effect of miglitol and acarbose after an oral glucose load: a novel hypoglycaemic mechanism? *Br. J. Clin. Pharmacol.* **1990**, *30*, 391−396.
(30) Bischoff, H. Pharmacology of α-glucosidase inhibition. *Eur. J. Clin. Invest.* **1994**, *24*, 3−10.
(31) Arh, H. J.; Boberg, M; Brendei, E.; Krause, H. P.; Steinke, W. Pharmacokinetics of miglitol. Absorption, distribution, metabolism, and excretion following administration to rats, dogs, and man. *Arzneimittelforschung* **1997**, *47*, 734−745.
(32) Kreymann, B.; Williams, G.; Ghatei, M. A.; Bloom, S. R. Glucagon-like peptide-1 7-36: a physiological incretin in man. *Lancet* **1987**, *2*, 1300−1304.
(33) Zander, M.; Madsbad, S.; Madsen, J. L.; Holst, J. J. Effect of 6-week course of glucagon-like peptide 1 on glycaemic control, insulin sensitivity, and beta-cell function in type 2 diabetes: a parallel-group study. *Lancet* **2002**, *359*, 824−830.
(34) Asano, N.; Ikeda, K.; Yu, Li.; Kato, A.; Takebayashi, K.; Adachi, I.; Kato, I.; Ouchi, H.; Takahata, H.; Fleet, G. W. J. The L-enantiomers of D-sugar-mimicking iminosugars are noncompetitive inhibitors of D-glycohydrolase? *Tetrahedron: Asymmetry* **2005**, *16*, 223−229.
(35) da Cruz, F. P.; Newberry, S.; Jenkinson, S. F.; Wormald, M. R.; Butters, T. D.; Alonzi, D. S.; Nakagawa, S.; Becq, F.; Norez, C.; Nash, R. J.; Kato, A.; Fleet, G. W. J. 4-C-Me-DAB and 4-C-Me-LAB—enantiomeric alkyl-branched pyrrolidine iminosugars—are specific and potent α-glucosidase inhibitors; acetone as the sole protecting group. *Tetrahedron Lett.* **2011**, *52*, 219−223.
(36) Natori, Y.; Imahori, T.; Murakami, K.; Yoshimura, Y.; Nakagawa, S.; Kato, A.; Adachi, I.; Takahata, H. The synthesis and biological evaluation of 1-C-alkyl-L-arabinoiminofuranoses, a novel class of α-glucosidase inhibitors. *Bioorg. Med. Chem. Lett.* **2011**, *21*, 738−741.
(37) Trost, B. M.; Horne, D. B.; Woltering, M. J. Palladium-catalyzed DYKAT of butadiene monoepoxide: enantioselective total synthesis of (+)-DMDP, (−)-bulgecinine, and (+)-broussonetine G. *Chem.—Eur. J.* **2006**, *12*, 6607−6620.
(38) Fu, G. C.; Zhou, J. S. Cross-couplings of unactivated secondary alkyl halides: room-temperature nickel-catalyzed Negishi reactions of alkyl bromides and iodides. *J. Am. Chem. Soc.* **2003**, *125*, 14726−14727.
(39) Phapale, V. B.; Buñuel, E.; García-Iglesias, M.; Cárdenas, D. J. Ni-catalyzed cascade formation of $C(sp^3)$-$C(sp^3)$ bonds by cyclization and cross-coupling reactions of iodoalkanes with alkyl zinc halides. *Angew. Chem., Int. Ed.* **2007**, *46*, 8790−8795.
(40) Calveras, J.; Egido-Gabás, M.; Gómez, L.; Casas, J.; Parella, T.; Joglar, J.; Bujons, J.; Clapés, P. Dihydroxyacetone phosphate aldolase catalyzed synthesis of structurally diverse polyhydroxylated pyrrolidine derivatives and evaluation of their glycosidase inhibitory properties. *Chem.—Eur. J.* **2009**, *15*, 7310−7328.
(41) Best, D.; Jenkinson, S. F.; Saville, A. W.; Alonzi, D. S.; Wormald, M. R.; Butters, T. D.; Norez, C.; Becq, F.; Bleriot, Y.; Adachi, I.; Kato, A.; Fleet, G. W. J. Cystic fibrosis and diabetes: isoLAB and isoDAB, enantiomeric carbon-branched pyrrolidine iminosugars. *Tetrahedron Lett.* **2010**, *51*, 4170−4174.
(42) Scofield, A. M.; Fellows, L. E.; Nash, R. J.; Fleet, G. W. J. Inhibition of mammalian digestive disaccharides by polyhydroxy alkaloids. *Life Sci.* **1986**, *39*, 645−650.
(43) Best, D.; Wang, C.; Weymouth-Wilson, A. C.; Clarkson, R. A.; Wilson, F. X.; Nash, R. J.; Miyauchi, S.; Kato, A.; Fleet, G. W. J. Looking glass inhibitors: scalable syntheses of DNJ, DMDP, and (3*R*)-3-hydroxy-L-bulgecinine from D-glucuronolactone and of L-DNJ, L-DMDP, and (3*S*)-3-hydroxy-D-bulgecinine from L-glucuronolactone. DMDP inhibits β-glucosidases and β-galactosidases whereas L-DMDP

is a potent and specific inhibitor of α-glucosidases. *Tetrahedron: Asymmetry* **2010**, *21*, 311−319.
(44) Ellgaard, L.; Molinari, M.; Helenius, A. Setting the standards: quality control in the secretory pathway. *Science* **1999**, *286*, 1882−1888.
(45) Kopito, R. R. ER quality control: the cytoplasmic connection. *Cell* **1997**, *88*, 427−430.
(46) Hammond, C.; Braakman, I.; Helenius, A. Role of N-linked oligosaccharide recognition, glucose trimming, and calnexin in glycoprotein folding and quality control. *Proc. Natl. Acad. Sci. U.S.A.* **1994**, *91*, 913−917.
(47) Hosokawa, N.; Wada, I.; Hasegawa, K.; Yorifuji, T.; Tremblay, L. O.; Herscovics, A.; Nagata, K. A novel ER α-mannosidase-like protein accelerates ER-associated degradation. *EMBO Rep.* **2001**, *2*, 415−422.
(48) Hubbard, S. C.; Ivatt, R. J. Synthesis and processing of asparagines-linked oligosaccharides. *Annu. Rev. Biochem.* **1981**, *50*, 555−583.
(49) Elbein, A. D. Inhibitors of the biosynthesis and processing of *N*-linked oligosaccharides. *CRC Crit. Rev. Biochem.* **1984**, *16*, 21−49.
(50) Kopito, R. R. ER quality control: the cytoplasmic connection. *Cell* **1997**, *88*, 427−430.
(51) Bonifacino, J. S.; Weissman, A. M. Ubiqitin and the control of protein in the secretory and the endoplasmic pathways. *Annu. Rev. Cell Dev. Biol.* **1998**, *14*, 19−57.
(52) Elbein, A. D. Glycosidase inhibitors: inhibitors of *N*-linked oligosaccharide processing. *FASEB J.* **1991**, *5*, 3055−3063.
(53) Asano, N.; Oseki, K.; Kizu, H; Matsui, K. Nitrogen-in-the-ring pyranoses and furanoses: structural basis of inhibition of mammalian glycosidases. *J. Med. Chem.* **1994**, *37*, 3701−3706.
(54) Furukawa, J.; Shinohara, Y.; Kuramoto, H.; Miura, Y.; Shimaoka, H.; Kurogochi, M.; Nakano, M.; Nishimura, S. I. Comprehensive approach to structural and functional glycomics based on chemoselective glycoblotting and sequential tag conversion. *Anal. Chem.* **2008**, *80*, 1094−1101.
(55) Dailey, G. Early and intensive therapy for management of hyperglycemia and cardiovascular risk factors in patients with type 2 diabetes. *Clin. Ther.* **2011**, *33*, 665−678.
(56) Arakawa, M.; Ebato, C.; Mita, T.; Fujitani, Y.; Shimizu, T.; Watada, H.; Kawamori, R.; Hirose, T. Miglitol suppresses the postprandial increase in interleukin 6 and enhances active glucagon-like peptide 1 secretion in viscerally obese subjects. *Metabolism* **2008**, *57*, 1299−1306.
(57) Aoki, K.; Kamiyama, H.; Yoshimura, K.; Shibuya, M.; Masuda, K.; Terauchi, Y. Miglitol administered before breakfast increased plasma active glucagon-like peptide-1 (GLP-1) levels after lunch in patients with type 2 diseases treated with sitagliptin. *Acta Diabetol.* **2012**, *49*, 225−230.
(58) Aguilar-Moncayo, M.; Takai, T.; Higaki, K.; Mena-Barragán, T.; Hirano, Y.; Yura, K.; Li, L.; Yu, Y.; Ninomiya, H.; García-Moreno, M. I.; Ishii, S.; Sakakibara, Y.; Ohno, K.; Nanba, E.; Ortiz Mellet, C.; García Fernández, J. M.; Suzuki, Y. Tuning glycosidase inhibition through aglycone interactions: pharmacological chaperones for Fabry disease and GM1 gangliosidosis. *Chem. Commun.* **2012**, *48*, 6514−6516.
(59) Kato, A.; Yamashita, Y.; Nakagawa, S.; Koike, Y.; Adachi, I.; Hollinshead, J.; Nas, R. J.; Ikeda, K.; Asano, N. 2,5-Dideoxy-2,5-imino-D-aritol as a new class of pharmacological chaperone for Fabry disease. *Bioorg. Med. Chem.* **2010**, *18*, 3790−3794.
(60) Godin, G.; Compain, P.; Masson, G.; Martin, O. R. A general strategy for the practical synthesis of nojirimycin *C*-glycosides and analogues. Extension to the first reported example of an iminosugar 1-phosphonate. *J. Org. Chem.* **2002**, *67*, 6960−6970.
(61) Godin, G.; Compain, P.; Martin, O. R. General access to iminosugar *C*-glycoside building blocks by means of cross-metathesis: a gateway to glycoconjugate mimetics. *Org. Lett.* **2003**, *5*, 3269−3272.
(62) Fleet, G. W. J.; Nicholas, S. J.; Smith, P. W.; Evans, S. V.; Fellows, L. E.; Nash, R. J. Potent competitive inhibition of α-galactosidase and α-glucosidase activity by 1,4-dideoxy-1,4-iminopentitols: synthesis of 1,4-dideoxy-1,4-imino-D-lyxitol and of both enantiomer of 1,4-dideoxy-1,4-iminoarabinitol. *Tetrahedron Lett.* **1985**, *26*, 3127−3130.
(63) Kessler, M.; Acuto, O.; Strelli, C.; Murer, H.; Semenza, G. A. A modified procedure for the rapid preparation of efficiently transporting vesicles from small intestinal brush border membranes. Their use in investigating some properties of D-glucose and choline transport systems. *Biochem. Biophys. Acta* **1978**, *506*, 136−154.
(64) Cooper, C. A.; Gasteiger, E.; Packer, N. GlycoMod—a software tool for determining glycosylation compositions from mass spectrometric data. *Proteomics* **2001**, *1*, 340−349.
(65) Sim, L.; Willemsma, C.; Mohan, S.; Naim, H. Y.; Pinto, B. M.; Rose, D. R. Structural basis for substrate selectivity in human maltase-glucoamylase and sucrase-isomaltase *N*-terminal domains. *J. Biol. Chem.* **2010**, *285*, 17763−70.
(66) Laskowski, R. A.; MacArthur, M. W.; Moss, D. S.; Thornton, J. M. *PROCHECK*: a program to check the stereochemical quality of protein structures. *J. Appl. Crystallogr.* **1993**, *26*, 283−291.
(67) Friesner, R. A.; Banks, J. L.; Murphy, R. B.; Halgren, T. A.; Klicic, J. J.; Mainz, D. T. Glide: a new approach for rapid, accurate docking and scoring. 1. Method and assessment of docking accuracy. *J. Med. Chem.* **2004**, *47*, 1739−1749.
(68) Still, W. C.; Tempczyk, A.; Hawlely, R. C.; Hendrickson, T. Semianalytical treatment of solvation for molecular mechanics and dynamics. *J. Am. Chem. Soc.* **1990**, *112*, 6127−6129.
(69) Sherman, W.; Day, T.; Jacobson, M. P.; Friesner, R. A.; Farid, R. Novel procedure for modeling ligand/receptor induced fit effects. *J. Med. Chem.* **2006**, *49*, 534−553.

A New Route to N^1-Substituted Uracil Derivatives Using Hypervalent Iodine

Yuichi Yoshimura,* Hiroya Kan-no, Y. B. Kiran, Yoshihiro Natori, Yukako Saito, Hiroki Takahata*

Faculty of Pharmaceutical Sciences, Tohoku Pharmaceutical University, 4-4-1 Komatsushima, Aoba-ku, Sendai, 981-8558, Japan
Fax +81(22)2752013; E-Mail: yoshimura@tohoku-pharm.ac.jp

Received: 21.02.2012; Accepted: 24.02.2012

Abstract: In continuation of our previous study, oxidative coupling reactions of uracil with allylsilane or enol ethers were examined using diacetoxyiodobenzene. The reaction of persilylated uracil with 3,4-dihydro-2*H*-pyran in the presence of TMSOTf and $PhI(OAc)_2$ resulted in the formation of a dihydropyranyluracil derivative, although the yield was low. In an extension of the oxidative coupling reaction, a novel glycosylation reaction using glycal derivatives as substrates was also developed. The treatment of persilylated uracil and 3,4-dihydro-2*H*-pyran with $(PhSe)_2$ and $PhI(OAc)_2$ in the presence of a catalytic amount of TMSOTf gave a 2,3-*anti*-derivative of 1-(3-phenylselanyltetrahydropyran-2-yl)uracil stereoselectively and in good yield.

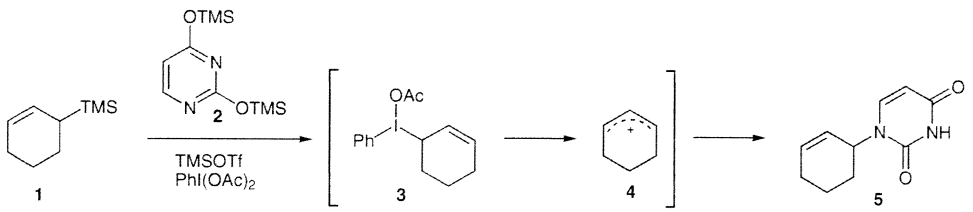
Key words: hypervalent iodine, nucleoside, oxidative coupling, glycosylation, glycal

Nucleoside derivatives are widely used clinically as drugs and as biological tools. There is no doubt about the importance of developing new nucleoside derivatives, since they promise to contribute to the progress of medical treatment and biological chemistry. The three general methods for the synthesis of nucleoside derivatives include: 1) synthesis starting from a natural nucleoside,[1] 2) construction of a nucleobase moiety on an appropriate sugar portion after manipulation,[2] and 3) glycosylation of a base with an appropriately modified sugar.[3] Although the transformation of naturally occurring nucleosides is a straightforward method for preparing new derivatives, it is obvious that limitations to obtaining new compounds with structural diversity exist. In contrast, the third method, which involves a glycosylation reaction, has an advantage in that various nucleoside derivatives containing different base moieties can be synthesized from a common sugar-intermediate in a minimum number of steps. In the past, we synthesized a wide variety of nucleoside derivatives by developing novel glycosylation reactions.[4–6]

An example of this is the use of a Pummerer-type thioglycosylation reaction for the synthesis of 4′-thionucleosides.[4] This reaction involves two steps: 1) oxidation of a sulfide to the corresponding sulfoxide and 2) a trimethylsilyl trifluoromethanesulfonate (TMSOTf)-catalyzed coupling reaction of the sulfoxide with persilylated nucleobases. Recently, the concept of the thioglycosylation reaction coupled with oxidation was applied to the synthesis of carbocyclic nucleosides.[6] As a result, we successfully developed a hypervalent iodine-catalyzed reaction for condensing a base and a pseudosugar by which a basic carbocyclic nucleoside skeleton was constructed.[6] The reaction, as with the Pummerer-type thioglycosylation, involves 2 steps:[6] 1) the generation of the carbocation **4** by the oxidative reaction of an allylsilane **1** with diacetoxyiodobenzene [$PhI(OAc)_2$] and TMSOTf, and 2) the subsequent addition of bis(trimethylsilyl)uracil (**2**) as shown in Scheme 1.

In this report, some preliminary applications of the oxidative coupling reaction to allylsilane or enol ether using a TMSOTf/$PhI(OAc)_2$ system are described. In addition, the results triggered the development of a novel glycosylation reaction using oxidative conditions. The synthesis of a 2′-phenylselenonucleoside from a glycal derivative using the TMSOTf/$PhI(OAc)_2$/$(PhSe)_2$ system is also reported.

Initially, the reaction of allyltrimethylsilane (**6**) and bis(trimethylsilyl)uracil (**2**) was examined using the conditions reported in a previous report.[6] Although the conditions for the reaction of allyltrimethylsilane (**6**) were modified slightly, 1-allyluracil (**10a**) was obtained in 69% yield from **6** on treatment with 1 equivalent of $PhI(OAc)_2$, TMSOTf, and **2** in dichloromethane (Table 1, entry 1). The same principles were applied to the reaction of benzyltrimethylsilane (**7**), but no trace of the desired **10b** was



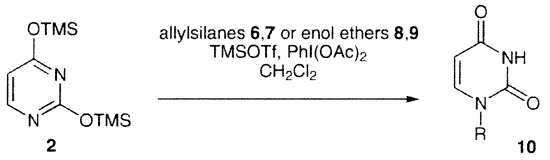
Scheme 1 Our previous study

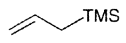
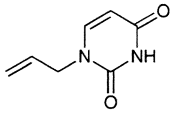
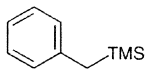
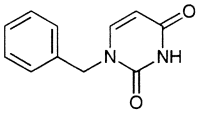
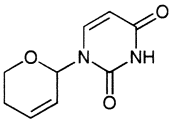
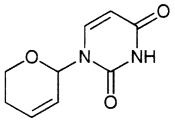
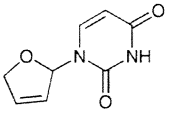
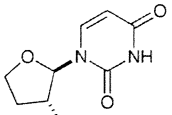
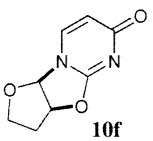
SYNTHESIS 2012, 44, 1163–1170
Advanced online publication: 22.03.2012
DOI: 10.1055/s-0031-1290749; Art ID: SS-2012-C0184-ST
© Georg Thieme Verlag Stuttgart · New York

detected (entry 2). The reason is not clear at this time. One plausible explanation is that the electrophilic substitution of the phenyl ring might preferentially occur under the conditions used. The reaction of 3,4-dihydro-2*H*-pyran (**8**) was examined next. As in the case mentioned above, the reaction conditions for preparing **10c** from **8** needed to be optimized. After several attempts, it was found that a dihydropyranyluracil derivative **10c** was produced in 31% yield when **8** was treated with $PhI(OAc)_2$ (1.5 equiv), TMSOTf (0.4 equiv), and **2** (2.0 equiv) at –40 °C to room temperature (entry 3). It was found that 0.2 equivalent of $Cu(OTf)_2$, instead of TMSOTf, also catalyzed the reaction.[7] However, when **8** was reacted with **2** under the above conditions in the presence of $Cu(OTf)_2$ at room temperature, **10c** was formed in 24% yield (entry 4). Although other metal triflates, for example, $Sc(OTf)_3$ and $Y(OTf)_3$, were found to catalyze the reaction, the yields were lower than that obtained using $Cu(OTf)_2$ (data not shown). The oxidative coupling reaction was also applied to 2,3-dihydrofuran (**9**). In contrast to the results for **8**, the reaction gave an inseparable mixture of dihydrofuryl derivatives **10d** and **10e**[8] in 5.5% yield along with O-cyclo derivative **10f** in 8.9% yield (entry 5).

Even though, except for **10a**, none of the yields shown in Table 1 were completely satisfactory, it is important to note that the oxidative coupling reaction proceeded with enol ethers and gave a nitrogen-substituted product. A proposed mechanism for the oxidative coupling reaction is shown in Scheme 2.[9] When the dihydropyran **8** or **9** re-

Table 1 Summary of the Oxidative Coupling of Bis(TMS)uracil **2** with Allylsilanes and Enol Ethers



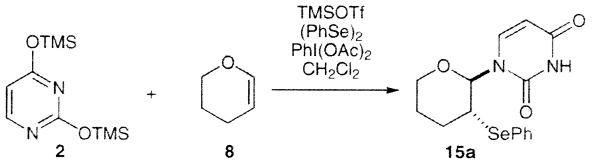
Entry	Compound	Product	Yield (%)
1	 **6**	 **10a**	69
2	 **7**	 **10b**	ND[a]
3	 **8**	 **10c**	31[b]
4	 **8**	 **10c**	24[c]
5	 **9**	 **10d**  **10e**  **10f**	5.5 (**10d**/**10e** = 3:1), 8.9 (**10f**)[d,e]

[a] Not detected.
[b] Method A: $PhI(OAc)_2$ (1.5 equiv), TMSOTf (0.4 equiv), and **2** (2.0 equiv) at –40 °C to r.t.
[c] Method B: $PhI(OAc)_2$ (1.5 equiv), $Cu(OTf)_2$ (0.2 equiv), and **2** (2.0 equiv) at r.t.
[d] Method C: $PhI(OAc)_2$ (1.5 equiv), TMSOTf (0.4 equiv), and **2** (2.0 equiv) at 0 °C to r.t.
[e] The ratio was determined based on ^1H NMR spectroscopy.

 © Georg Thieme Verlag Stuttgart · New York

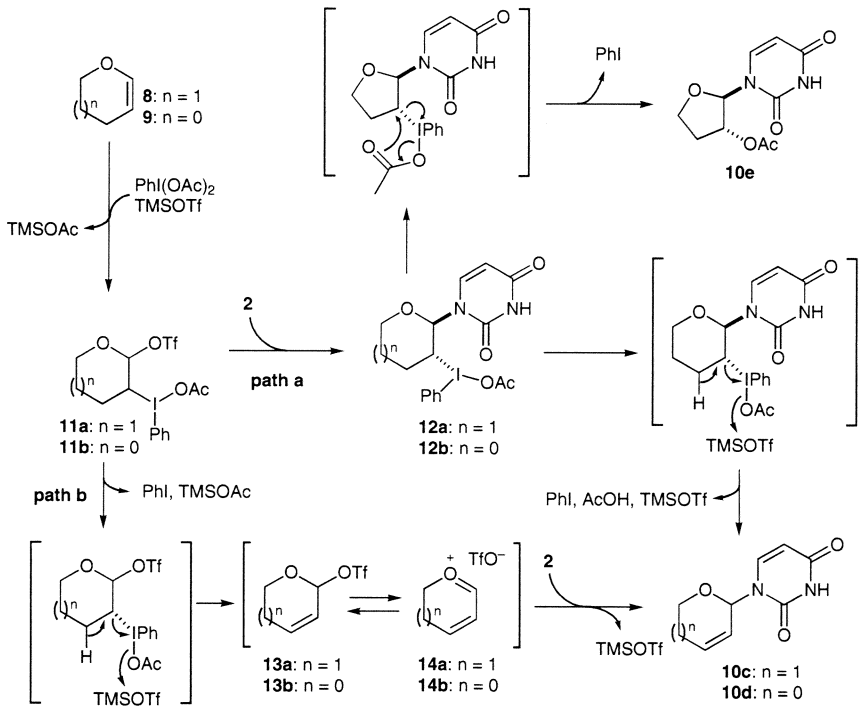
acts with PhI(OAc)$_2$ in the presence of TMSOTf, an acetoxyiodobenzene derivative **11a,b** is initially produced. Two pathways shown in Scheme 2 are possible for the conversion of **11a,b** into the N^1-substituted uracils **10c** and **10d**: the nucleophilic attack of bis(TMS)uracil **2** occurs prior to the elimination (path a) or an allylic carbocation **14a,b** generated from **11a,b** reacts with **2** (path b). Since the formation of **10e** and **10f** from dihydrofuran **9** was observed, the preferred pathway for the oxidative coupling reaction appears to involve path a, rather than path b (Scheme 2). In the case of the reaction with **8**, the elimination would generally proceed with **10c** being formed via **12a** as depicted in Scheme 2. In the case of **9**, however, a similar 2-iodophenyl intermediate **12b** preferentially gives rise to the 2,2′-O-cyclo derivative **10f**. The reason why the reaction of **9** prefers the intramolecular nucleophilic attack to the elimination is not clear at this time. The conformational flexibility of the tetrahydrofuran ring in the reaction of **9** might make the formation of five-membered ring system easy. The above mechanism explains why the reaction gave only poor yields: it is likely that the formation of an allyl cation like **14a,b**, through path b, may compete and this would result in the formation of dihydropyrans and furans.

To improve the yields in the oxidative coupling reaction, the use of a co-catalyst was examined. Very recently, Singh and Wirth reported on a new selenium-catalyzed cyclization of γ,δ-unsaturated carboxylic acids to 3,6-dihydro-2*H*-pyran-2-ones using hypervalent iodine as an oxidant in the presence of catalytic amounts of diphenyl diselenide [(PhSe)$_2$].[10] Given the proposed reaction mechanism, we hypothesized that the instability of the intermediate **11a,b** (or competing path b) might be a factor in the low yield of the oxidative coupling reaction and that this could be avoided if (PhSe)$_2$ was used as a co-catalyst. When **2** and **8** were treated with PhI(OAc)$_2$ and (PhSe)$_2$ in the presence of catalytic amounts of TMSOTf, the *trans*-isomer of 1-(3-phenylselanyltetrahydropyran-2-yl)uracil (**15a**) was selectively produced, as shown in Scheme 3.[11] The result differed from the one expected and was deemed to be important, since this reaction has the potential for use in producing 2′-deoxynucleosides as well as dideoxydidehydronucleosides such as **10c** and **10d**, which constitute an important class of antiviral agents[12] (Scheme 3).



Scheme 3 Synthesis of 1-(3-phenylselanyltetrahydropyran-2-yl)uracil (**15a**)

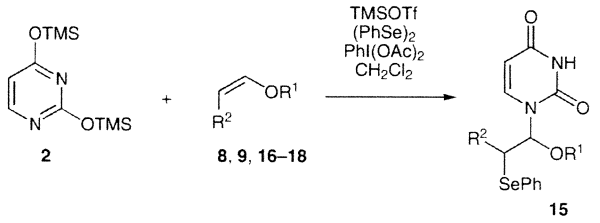
The oxidative coupling of **2** with enol ethers and glycals using the TMSOTf/PhI(OAc)$_2$/(PhSe)$_2$ system was examined and the results are summarized in Table 2. As described above, the reaction with **8** gave **15a** stereoselectively and in 73% yield (Table 2, entry 1). Similarly, reaction with **9** furnished 1-(3-phenylselanyltetrahydrofuran-2-yl)uracil (**15b**) in 31% yield (entry 2). In

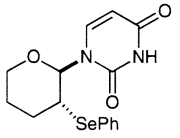
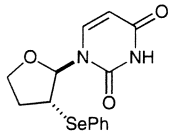
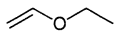
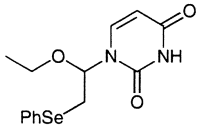
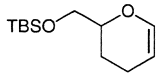
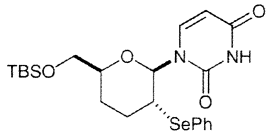
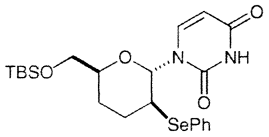
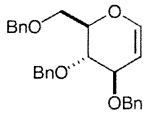
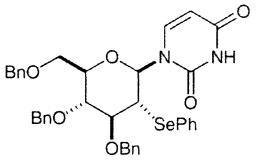
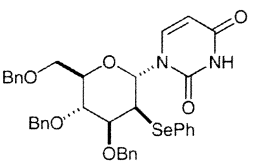


Scheme 2 A proposed reaction mechanism for the oxidative coupling of 3,4-dihydro-2*H*-pyran (**8**) and dihydrofuran **9** with TMSOTf/PhI(OAc)$_2$

© Georg Thieme Verlag Stuttgart · New York

Table 2 Summary of the Oxidative Coupling Reaction of Bis(TMS)uracil **2** with Enol Ethers Using TMSOTf/PhI(OAc)$_2$/(PhSe)$_2$ System



Entry	Compound	Product	Yield (%)
1	 **8**	 **15a**	73[a]
2	 **9**	 **15b**	31[a]
3	 **16**	 **15c**	69[b]
4	 **17**	 **15d** +  **15e**	80[c] (**15d**/**15e** = 2:1[d])
5	 **18**	 **15f** +  **15g**	64[c] (**15f**/**15g** = 1:1[d])

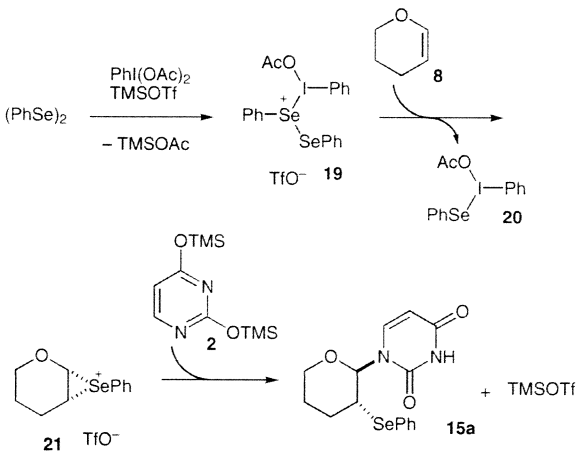
[a] Performed at r.t.
[b] Performed at –5 °C.
[c] Performed at –20 °C.
[d] The ratio was determined based on ^{1}H NMR spectroscopy.

both cases, the reaction selectively produced the *trans*-isomer and the best results were obtained when the reaction was conducted at room temperature. In contrast, the reaction with the ethyl vinyl ether (**16**) at room temperature gave 1-(1-ethoxy-2-phenylselanylethyl)uracil (**15c**) in low yield (data not shown). The reaction of **2** with **16** at –5 °C, on the other hand, afforded **15c** in 69% yield (entry 3). In all of the above cases, 1 equivalent of PhI(OAc)$_2$ and (PhSe)$_2$ in the presence of 0.1 equivalent of TMSOTf were employed. When the same reactions were performed with 0.5 equivalent of (PhSe)$_2$, the isolated yields of the products were decreased (data not shown). As an extension, the oxidative coupling of the glycal derivatives **17**[13] and **18**, which can be considered to constitute a new gly-

© Georg Thieme Verlag Stuttgart · New York

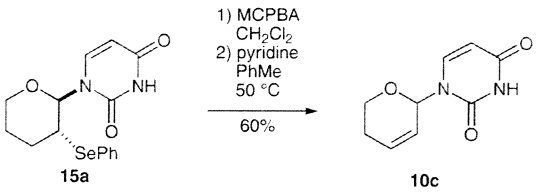
cosylation reaction applicable to the synthesis of 2′-deoxy- and 2′,3′-dideoxydidehydronucleosides, were tried. The reaction of **17** gave **15d** and **15e** in 80% yield with the predominant formation of β-nucleoside **15d** (entry 4).[14] On the other hand, the oxidative glycosylation reaction of D-glucal **18** gave a mixture of **15f** and **15g** in 64% yield and lacked stereoselectivity (entry 5).

A proposed reaction mechanism for the oxidative coupling under TMSOTf/PhI(OAc)$_2$/(PhSe)$_2$ system is shown in Scheme 4. Diphenyl diselenide is oxidized to a phenylselenium derivative **19** by the action of TMSOTf and PhI(OAc)$_2$. The phenylselenium derivative **19** then reacts with an enol ether, for example, dihydropyran **8**, to form an episelenium ion **21**. Nucleophilic attack of **2** to **21** results in the formation of **15a** along with the regeneration of TMSOTf that can be used in the next cycle of the reaction. During the course of the oxidative coupling, a hypervalent iodine derivative **20**, formed along with **19**, might have the ability to convert **8** into **21**. However, at least 1 equivalent of diphenyl diselenide was required to achieve the yields described above. The results suggest that **20** could not act as an electrophilic selenium reagent in this reaction.



Scheme 4 Proposed reaction mechanism for the oxidative coupling for the TMSOTf/PhI(OAc)$_2$/(PhSe)$_2$ system

Until now, we have not succeeded in the direct formation of dihydropyranyluracil derivatives, for example, **10c** as originally planned. One of the reasons for this is the instability of the dihydropyranyluracil under the acidic conditions of the reactions. Even in the case of the *syn*-elimination of selenoxide derivatives of nucleosides, the addition of a base is frequently required.[15] Indeed, the conversion of **15a** into **10c** was achieved using the two-step synthesis shown in Scheme 5 and pyridine was needed as an additive. We attempted to add triethylamine in the conditions in entry 1 of Table 2. However, this resulted in the suppression of the reaction with decreased yields (data not shown).



Scheme 5 Synthesis of **10c**

In conclusion, in continuation of our previous study, the development of a novel oxidative coupling reaction of persilylated uracil with allylsilanes and enol ethers to produce a dihydropyranyluracil derivative in the presence of TMSOTf and PhI(OAc)$_2$ is presented. As an extension of the oxidative coupling reaction, a novel glycosylation reaction starting from glycal derivatives by using a TMSOTf/PhI(OAc)$_2$/(PhSe)$_2$ system was also developed. The latter promises to serve as a new route to the synthesis of 2′-deoxynucleosides and dideoxydidehydronucleosides, which are medicinally and biologically important class of compounds.

Melting points are uncorrected. NMR spectra were recorded at 400 MHz (^{1}H), 100 MHz (^{13}C) using $CDCl_3$ as a solvent. As an internal standard, TMS was used for $CDCl_3$. Mass spectra were recorded using EI and CI ionization modes. Isobutane was used as the reagent gas in CI mass spectra. Silica gel used for chromatography was from Fuji Silysia PSQ 100B. When the reagents sensitive to moisture were used, the reaction was performed under argon atmosphere.

N^1-Allyluracil (10a)

To a solution of bis(trimethylsilyl)uracil (**2**; 138 μL, 0.53 mmol), PhI(OAc)$_2$ (171 mg, 0.53 mmol), and allyltrimethylsilane (84 μL, 0.53 mmol) in CH_2Cl_2 (3 mL) was added TMSOTf (96 μL, 0.53 mmol) at 0 °C. The mixture was stirred at r.t. for 1 h. To the mixture were added excess of solid $NaHCO_3$ (ca. 1 g) and sat. aq $NaHCO_3$ (0.5 mL). The mixture was diluted with CH_2Cl_2 (30 mL) and dried (Na_2SO_4). After filtration, the filtrate was concentrated under reduced pressure, and the residue was purified by silica gel column chromatography (50–100% EtOAc in hexane) to give **10a** (55.6 mg, 69%); white crystals; mp 100–101 °C.

IR (KBr): 921, 1201, 1466, 1688, 2927 cm^{-1}.

^{1}H NMR (400 MHz, $CDCl_3$): δ = 4.36 (td, J = 1.9, 3.6 Hz, 2 H), 5.28 (d, J = 16.9 Hz, 1 H), 5.33 (d, J = 10.1 Hz, 1 H), 5.73 (dd, J = 1.9, 8.2 Hz, 1 H), 5.93–5.83 (m, 1 H), 7.15 (d, J = 8.2 Hz, 1 H), 8.69 (br s, 1 H).

^{13}C NMR (100 MHz, $CDCl_3$): δ = 50.0, 102.5, 119.5, 131.4, 143.7, 150.8, 163.7.

EI-MS: m/z = 152 [M$^+$].

HRMS (EI): m/z calcd for $C_7H_8N_2O_2$: 152.0586 [M$^+$]; found: 152.0580.

N^1-(5,6-Dihydro-2*H*-pyran-2-yl)uracil (10c)

Method A (Table 1, entry 3): To a solution of bis(trimethylsilyl)uracil (**2**; 256 μL, 1.0 mmol), PhI(OAc)$_2$ (241 mg, 0.75 mmol), and 3,4-dihydro-2*H*-pyran (**8**; 45.6 μL, 0.50 mmol) in CH_2Cl_2 (5 mL) was added TMSOTf (36.3 μL, 0.20 mmol) at –40 °C. After allowing to reach r.t. in 2 h, the mixture was stirred at r.t. overnight. The reaction was quenched with sat. aq $NaHCO_3$ (5 mL) and extracted with CH_2Cl_2 (3 × 15 mL). The combined organic layers were washed with brine (10 mL) and dried (Na_2SO_4). After filtration, the filtrate was concentrated under reduced pressure, and the residue was puri-

© Georg Thieme Verlag Stuttgart · New York

fied by silica gel column chromatography (75–100% EtOAc in hexane) to give **10c** (30.2 mg, 31%).

Method B (Table 1, entry 4): To a solution of bis(trimethylsilyl)uracil (**2**; 256 μL, 1.0 mmol), $PhI(OAc)_2$ (241 mg, 0.75 mmol) and 3,4-dihydro-2*H*-pyran (**8**; 45.6 μL, 0.50 mmol) in CH_2Cl_2 (3 mL) was added TMSOTf (36.3 μL, 0.20 mmol) at 0 °C. After stirring at r.t. for 2 h, the reaction was quenched with sat. aq $NaHCO_3$ (5 mL) and extracted with CH_2Cl_2 (3 × 15 mL). The combined organic layers were washed with brine (10 mL) and dried (Na_2SO_4). After filtration, the filtrate was concentrated under reduced pressure, and the residue was purified by silica gel column chromatography (75–100% EtOAc in hexane) to give **10c** (25.3 mg, 24%); white crystals; mp 113–115 °C.

IR (KBr): 820, 1243, 1385, 1676, 3019 cm^{-1}.

^1H NMR (400 MHz, $CDCl_3$): δ = 2.01–2.34 (m, 2 H), 3.86–3.96 (m, 2 H), 5.64 (d, *J* = 10.6 Hz, 1 H), 5.72 (d, *J* = 8.2 Hz, 1 H), 6.36–6.40 (m, 2 H), 7.42 (d, *J* = 8.2 Hz, 1 H), 9.00 (br s, 1 H).

^{13}C NMR (100 MHz, $CDCl_3$): δ = 24.4, 61.7, 77.6, 102.1, 123.7, 133.1, 140.9, 150.7, 163.1.

EI-MS: *m/z* = 194 [M^+].

HRMS (EI): *m/z* calcd for $C_9H_{10}N_2O_3$: 194.0691 [M^+]; found: 194.0695.

1-(2,3-Dihydrofuran-5-yl)uracil (10d)

Method C (Table 1, entry 5): To a solution of bis(trimethylsilyl)uracil (**2**; 256 μL, 1.0 mmol), $PhI(OAc)_2$ (241 mg, 0.75 mmol), and dihydrofuran **9** (37.8 μL, 0.50 mmol) in CH_2Cl_2 (5 mL) was added TMSOTf (36.3 μL, 0.20 mmol) at 0 °C. After allowing to reach r.t., the mixture was stirred at r.t. for 4 h. The reaction was quenched with sat. aq $NaHCO_3$ (5 mL) and extracted with CH_2Cl_2 (3 × 15 mL). The combined organic layers were washed with brine (10 mL) and dried (Na_2SO_4). After filtration, the filtrate was concentrated under reduced pressure, and the residue was purified by silica gel column chromatography (50 → 75 → 100% EtOAc in hexane) to give a mixture of **10d** and **10e** (5 mg, **10d**/**10e** = 3:1, 5.5%) as less polar products and **10f** (8 mg, 8.9%) as a more polar product.

10d and 10e

^1H NMR (400 MHz, $CDCl_3$): δ = 1.24 (s, 0.75 H), 2.14–2.17 (m, 0.25 H), 2.26–2.36 (m, 0.25 H), 4.15 (td, *J* = 6.7, 9.2 Hz, 0.25 H), 4.34 (td, *J* = 3.5, 8.7 Hz, 0.25 H), 4.71–4.76 (m, 0.75 H), 4.81–4.87 (m, 0.75 H), 5.37 (dt, *J* = 1.9, 4.4 Hz, 0.25 H), 5.71–5.74 (m, 1.25 H), 5.83–5.85 (m, 0.75 H), 6.44–6.46 (m, 0.75 H), 7.00–7.02 (m, 0.75 H), 7.08 (d, *J* = 8.2 Hz, 0.75 H), 7.23 (d, *J* = 8.2 Hz, 0.25 H), 8.67 (br s, 0.25 H), 8.73 (br s, 0.25 H).

EI-MS: *m/z* = 180 [M^+] (**10d**).

CI-MS: *m/z* = 241 [M^+ + 1] (**10e**).

10f

White crystals; mp 248–250 °C (sublimed).

^1H NMR (400 MHz, $CDCl_3$): δ = 2.17–2.24 (m, 1 H), 2.48 (d, *J* = 4.6, 14.3 Hz, 1 H), 4.23–4.30 (m, 2 H), 5.41 (t, *J* = 5.3 Hz, 1 H), 6.12 (d, *J* = 7.2 Hz, 1 H), 6.50 (d, *J* = 5.3 Hz, 1 H), 7.71 (d, *J* = 7.2 Hz, 1 H).

EI-MS: *m/z* = 180 [M^+].

HRMS (EI): *m/z* calcd for $C_8H_8N_2O_3$: 180.0535 [M^+]; found: 180.0536.

Oxidative Coupling Reaction of Bis(TMS)uracil (2) with Enol Ethers Using TMSOTf/$PhI(OAc)_2$/$(PhSe)_2$ System; General Procedure

To a solution of bis(trimethylsilyl)uracil (**2**; 138 μL, 0.53 mmol), $PhI(OAc)_2$ (171 mg, 0.53 mmol), $PhSe)_2$ (165 mg, 0.53 mmol), and enol ether (0.53 mmol) in CH_2Cl_2 (3 mL) was added TMSOTf (9.6 μL, 0.053 mmol) at the temperature shown in Table 2. After stirring at the same temperature for 1 h, the reaction was quenched with sat. aq $NaHCO_3$ (5 mL) and extracted with CH_2Cl_2 (3 × 15 mL). The combined organic layers were washed with brine (10 mL) and dried (Na_2SO_4). After filtration, the filtrate was concentrated under reduced pressure, and the residue was purified by silica gel column chromatography (Table 2).

***N*^{1}-[*trans*-3-(Phenylselanyl)tetrahydro-2*H*-pyran-2-yl]uracil (15a)**

By the general procedure described above, compound **15a** (128.6 mg, 73%) was obtained from 3,4-dihydro-2*H*-pyran (**8**; 45.6 μL, 0.50 mmol) after purification by silica gel column chromatography (33 → 50 → 75% EtOAc in hexane); white foam.

IR (KBr): 744, 1066, 1257, 1688, 3056 cm^{-1}.

^1H NMR (400 MHz, $CDCl_3$): δ = 1.81–1.67 (m, 3 H), 2.44 (d, *J* = 13.0 Hz, 1 H), 3.23 (dt, *J* = 3.9, 10.6 Hz, 1 H), 3.64 (t, *J* = 12.1 Hz, 1 H), 4.08 (d, *J* = 13.0 Hz, 1 H), 5.36 (dd, *J* = 1.9, 8.2 Hz, 1 H), 5.69 (d, *J* = 10.1 Hz, 1 H), 6.98 (d, *J* = 8.2 Hz, 1 H), 7.34–7.22 (m, 3 H), 7.53 (d, *J* = 6.8 Hz, 2 H), 8.14 (br s, 1 H).

^{13}C NMR (100 MHz, $CDCl_3$): δ = 26.9, 30.8, 43.6, 68.6, 85.6, 102.4, 126.8, 128.6, 129.3, 135.8, 139.2, 150.3, 162.7.

EI-MS: *m/z* = 352 [M^+].

HRMS (EI): *m/z* calcd for $C_{15}H_{16}N_2O_3Se$: 352.0326 [M^+]; found: 352.0320.

***N*^{1}-[*trans*-3-(Phenylselanyl)tetrahydrofuran-2-yl]uracil (15b)**

By the general procedure described above, compound **15b** (52 mg, 31%) was obtained from dihydrofuran **9** (37.8 μL, 0.53 mmol) after purification by silica gel column chromatography (33 → 50 → 75% EtOAc in hexane); white foam.

IR (KBr): 744, 1066, 1257, 1688, 3056 cm^{-1}.

^1H NMR (400 MHz, $CDCl_3$): δ = 2.10–2.17 (m, 1 H), 2.36–2.43 (m, 1 H), 3.81–3.87 (m, 1 H), 4.12 (q, *J* = 7.8 Hz, 1 H), 4.20–4.25 (m, 1 H), 5.62 (d, *J* = 8.3 Hz, 1 H), 5.93 (d, *J* = 3.9 Hz, 1 H), 7.14 (d, *J* = 8.3 Hz, 1 H), 7.28–7.34 (m, 3 H), 7.64 (d, *J* = 4.2 Hz, 2 H), 8.09 (br s, 1 H).

^{13}C NMR (100 MHz, $CDCl_3$): δ = 31.2, 43.5, 69.0, 92.9, 102.1, 126.8, 126.6, 129.3, 135.6, 139.6, 150.0, 163.2.

EI-MS: *m/z* = 338 [M^+].

HRMS (EI): *m/z* calcd for $C_{14}H_{14}N_2O_3Se$: 338.0170 [M^+]; found: 338.0160.

***N*^{1}-[1-Ethoxy-2-(phenylselanyl)ethyl]uracil (15c)**

By the general procedure described above, compound **15c** (125 mg, 69%) was obtained from ethyl vinyl ether (**16**; 138 μL, 0.53 mmol) after purification by silica gel column chromatography (9% EtOAc in CH_2Cl_2); whitish brown solid; mp 99.0–101.0 °C.

IR (KBr): 762, 1332, 1626, 1701, 3057 cm^{-1}.

^1H NMR (400 MHz, $CDCl_3$): δ = 1.21 (t, *J* = 7.2 Hz, 3 H), 3.17 (dd, *J* = 5.7, 12.9 Hz, 1 H), 3.27 (dd, *J* = 5.7, 12.9 Hz, 1 H), 3.56 (q, *J* = 7.2 Hz, 2 H), 5.67 (dd, *J* = 1.5, 7.8 Hz, 1 H), 5.88 (t, *J* = 5.7 Hz, 1 H), 7.25–7.27 (m, 3 H), 7.36 (d, *J* = 8.2 Hz, 1 H), 7.51–7.53 (m, 2 H), 9.07 (br s, 1 H).

^{13}C NMR (100 MHz, $CDCl_3$): δ = 14.6, 31.7, 53.4, 65.4, 84.6, 102.5, 127.5, 129.2, 133.1, 138.6, 150.8, 163.3.

EI-MS: *m/z* = 340 [M^+].

HRMS (EI): *m/z* calcd for $C_{14}H_{16}N_2O_3Se$: 340.0329 [M^+]; found: 340.0321.

1-[(2*R,3*R**,6*S**)-6-{[(*tert*-Butyldimethylsilyl)oxy]methyl}-3-(phenylselanyl)tetrahydro-2*H*-pyran-2-yl]uracil (15d) and 1-[(2*S**,3*S**,6*S**)-6-{[(*tert*-Butyldimethylsilyl)oxy]methyl}-3-(phenylselanyl)tetrahydro-2*H*-pyran-2-yl]uracil (15e)**

By the general procedure described above, compounds **15d** (135 mg, 51%) and **15e** (75 mg, 29%) were obtained from **17**[13] (121 mg,

© Georg Thieme Verlag Stuttgart · New York

0.53 mmol) after purification by silica gel column chromatography (33% EtOAc in hexane).

15d
White crystals; mp 174.0–176.0 °C.

IR (KBr): 689, 776, 1386, 1667, 1703, 2953 cm^{-1}.

^1H NMR (400 MHz, $CDCl_3$): δ = 0.00 (s, 6 H), 0.89 (s, 9 H), 1.46–1.55 (m, 1 H), 1.72–1.80 (m, 2 H), 2.42–2.45 (m, 1 H), 3.16 (s, 1 H), 3.55 (dd, *J* = 1.9, 10.2 Hz, 1 H), 3.61–3.69 (m, 2 H), 5.40 (dd, *J* = 1.9, 8.2 Hz, 1 H), 5.82 (d, *J* = 10.2 Hz, 1 H), 7.00 (d, *J* = 8.2 Hz, 1 H), 7.22–7.30 (m, 3 H), 7.54–7.55 (m, 2 H), 9.16 (br s, 1 H).

^{13}C NMR (100 MHz, $CDCl_3$): δ = –5.3, 18.2, 25.7, 28.7, 30.2, 43.5, 65.4, 78.8, 85.2, 102.2, 126.7, 128.5, 129.3, 135.8, 139.2, 150.3, 162.8.

EI-MS: *m/z* = 496 [M^+].

HRMS (EI): *m/z* calcd for $C_{22}H_{32}N_2O_4SeSi$: 496.1308 [M^+]; found: 496.1295.

15e
White crystals; mp 165.0–167.0 °C.

IR (KBr): 649, 775, 1387, 1666, 1705, 2952 cm^{-1}.

^1H NMR (400 MHz, $CDCl_3$): δ = 0.00 (s, 6 H), 0.82 (s, 9 H), 1.80–1.97 (m, 3 H), 2.16–2.21 (m, 1 H), 3.14–3.21 (m, 1 H), 3.71 (dd, *J* = 5.3, 10.5 Hz, 1 H), 3.79 (dd, *J* = 6.7, 10.5 Hz, 1 H), 3.98 (s, 1 H), 5.32 (dd, *J* = 1.9, 8.2 Hz, 1 H), 6.02 (d, *J* = 10.5 Hz, 1 H), 6.96 (d, *J* = 8.2 Hz, 1 H), 7.14–7.23 (m, 3 H), 7.46–7.47 (m, 2 H), 8.52 (br s, 1 H).

^{13}C NMR (100 MHz, $CDCl_3$): δ = –5.5, 18.1, 25.8, 26.1, 26.5, 43.6, 62.7, 74.9, 81.5, 102.1, 126.9, 128.5, 129.3, 135.6, 139.2, 150.0, 162.6.

EI-MS: *m/z* = 496 [M^+].

HRMS (EI): *m/z* calcd for $C_{22}H_{32}N_2O_4SeSi$: 496.1308 [M^+]; found: 496.1299.

N^1-(3,4,6-Tri-*O*-benzyl-2-deoxy-2-*O*-phenylselanyl-β-D-*gluco*-pyranosyl)uracil (15f) and N^1-(3,4,6-Tri-*O*-benzyl-2-deoxy-2-*O*-phenylselanyl-α-D-*gluco*-pyranosyl)uracil (15g)
By the general procedure described above, compounds **15f,g** (231 mg, 64%) were obtained as an inseparable mixture from tri-*O*-benzyl-D-glucal (**18**; 220 mg, 0.53 mmol) after purification by silica gel column chromatography (33% EtOAc in hexane).

^1H NMR (400 MHz, $CDCl_3$): δ = 3.30 (t, *J* = 10.1 Hz, 0.5 H), 3.60–3.88 (m, 4.5 H), 4.24 (s, 0.5 H), 4.39 (t, *J* = 6.8 Hz, 0.5 H), 4.42–4.55 (m, 3.5 H), 4.60–4.64 (m, 1 H), 4.86 (d, *J* = 10.6 Hz, 0.5 H), 4.91 (d, *J* = 10.1 Hz, 0.5 H), 4.99 (d, *J* = 10.1 Hz, 0.5 H), 5.13 (dd, *J* = 2.2, 8.0 Hz, 0.5 H), 5.33 (dd, *J* = 1.9, 7.8 Hz, 0.5 H), 5.91 (d, *J* = 10.6 Hz, 0.5 H), 6.29 (d, *J* = 10.6 Hz, 0.5 H), 6.83–6.88 (m, 1 H), 7.16–7.53 (m, 20 H), 8.61 (br s, 0.5 H), 9.01 (br s, 0.5 H).

^{13}C NMR (100 MHz, $CDCl_3$): δ = 46.6, 51.4, 67.4, 68.2, 71.1, 71.7, 73.0, 73.3, 73.4, 75.1, 76.1, 76.2, 77.4, 78.7, 79.0, 82.5, 101.8, 102.5, 127.6, 127.7, 127.7, 127.8, 127.9, 128.0, 128.1, 128.2, 128.2, 128.3, 128.4, 128.4, 128.5, 128.6, 129.3, 129.4, 134.6, 135.1, 136.6, 137.4, 137.7, 137.7, 137.8, 137.8, 139.5, 150.1, 150.2, 162.6, 162.7.

EI-MS: *m/z* = 684 [M^+].

HRMS (EI): *m/z* calcd for $C_{37}H_{36}N_2O_6Se$: 684.1739 [M^+]; found: 684.1752.

Acknowledgment

This work was supported in part by a Grant-in-Aid for Scientific Research (No. 21590119), JSPS (Y.Y.) and by a grant of Strategic Research Foundation Grant-aided Project for Private Universities from Ministry of Education, Culture, Sport, Science, and Technology, Japan (MEXT).

References

(1) Recent reports: (a) Fan, X.; Wang, Y.; Qu, Y.; Xu, H.; He, Y.; Zhang, X.; Wang, J. *J. Org. Chem.* **2011**, *76*, 982. (b) Peacock, H.; Maydanovych, O.; Beal, P. A. *Org. Lett.* **2010**, *12*, 1044. (c) Plant, A.; Thompson, P.; William, D. M. *J. Org. Chem.* **2009**, *74*, 4870. (d) Smith, D. B.; Kalayanov, G.; Sund, C.; Winqvist, A.; Pinho, P.; Maltseva, T.; Morisson, V.; Leveque, V.; Rajyaguru, S.; Le, Pogam. S.; Najera, I.; Benkestock, K.; Zhou, X.-X.; Maag, H.; Cammack, N.; Martin, J. A.; Swallow, S.; Johansson, N. J.; Klumpp, K.; Smith, M. *J. Med. Chem.* **2009**, *52*, 219. (e) Spitale, R. C.; Heller, M. G.; Pelly, A. J.; Wedekind, J. E. *J. Org. Chem.* **2007**, *72*, 8551.

(2) Recent reports: (a) Dalençon, S.; Youcef, R. A.; Pipelier, M.; Maisonneuve, V.; Dubreuil, D.; Huet, F.; Legoupy, S. *J. Org. Chem.* **2011**, *76*, 8059. (b) Saneyoshi, H.; Deschamps, J. R.; Marquez, V. E. *J. Org. Chem.* **2010**, *75*, 7659. (c) Jiang, M. X.-W.; Jin, B.; Gage, J. L.; Priour, A.; Savela, G.; Miller, M. J. *J. Org. Chem.* **2006**, *71*, 4164.

(3) Recent reports: (a) Huang, Q.; Herdewijin, P. *J. Org. Chem.* **2011**, *76*, 3742. (b) Reddy, P. G.; Chun, B.-W.; Zhang, H.-R.; Rachakonda, S.; Ross, B. S.; Sofia, M. J. *J. Org. Chem.* **2011**, *76*, 3782. (c) Seth, P. P.; Vasquez, G.; Allerson, C. A.; Berdeja, A.; Gaus, H.; Kinberger, G. A.; Prakash, T. P.; Migawa, M. T.; Bhat, B.; Swayze, E. E. *J. Org. Chem.* **2010**, *75*, 1569. (d) Prévost, M.; St-Jean, O.; Guindon, Y. *J. Am. Chem. Soc.* **2010**, *132*, 12433. (e) Stauffer, C. S.; Datta, A. *J. Org. Chem.* **2008**, *73*, 4166. (f) Sabatino, D.; Damha, M. J. *J. Am. Chem. Soc.* **2007**, *129*, 8259. (g) Jean-Baptiste, L.; Yemets, S.; Legay, R.; Lequeux, T. *J. Org. Chem.* **2006**, *71*, 2352. (h) Neogi, A.; Majhi, T. P.; Mukhopadhyay, R.; Chattopadyay, P. *J. Org. Chem.* **2006**, *71*, 3291. (i) Gagneron, J.; Gosselin, G.; Mathé, C. *J. Org. Chem.* **2005**, *70*, 6891.

(4) (a) Yoshimura, Y.; Yamazaki, Y.; Saito, Y.; Natori, Y.; Imamichi, T.; Takahata, H. *Bioorg. Med. Chem. Lett.* **2011**, *21*, 3313. (b) Yoshimura, Y.; Yamazaki, Y.; Saito, Y.; Takahata, H. *Tetrahedron* **2009**, *65*, 9091. (c) Yoshimura, Y.; Yamazaki, Y.; Kawahata, M.; Yamaguchi, K.; Takahata, H. *Tetrahedron Lett.* **2007**, *48*, 4519. (d) Yoshimura, Y.; Kuze, T.; Ueno, M.; Komiya, F.; Haraguchi, K.; Tanaka, H.; Kano, F.; Yamada, K.; Asami, K.; Kaneko, N.; Takahata, H. *Tetrahedron Lett.* **2006**, *47*, 591. (e) Yoshimura, Y.; Kitano, K.; Yamada, K.; Satoh, H.; Watanabe, M.; Miura, S.; Sakata, S.; Sasaki, T.; Matsuda, A. *J. Org. Chem.* **1997**, *62*, 3140. (f) Yoshimura, Y.; Kitano, K.; Satoh, H.; Watanabe, M.; Miura, S.; Sakata, S.; Sasaki, T.; Matsuda, A. *J. Org. Chem.* **1996**, *61*, 822.

(5) (a) Yoshimura, Y.; Asami, K.; Imamichi, T.; Kuroda, T.; Shiraki, K.; Tanaka, H.; Takahata, H. *J. Org. Chem.* **2010**, *75*, 4161. (b) Yoshimura, Y.; Asami, K.; Matsui, H.; Tanaka, H.; Takahata, H. *Org. Lett.* **2006**, *8*, 6015.

(6) Yoshimura, Y.; Ohta, M.; Imahori, T.; Imamichi, T.; Takahata, H. *Org. Lett.* **2008**, *10*, 3449.

(7) During the course of our investigation, the intramolecular oxidative C–N bond forming reaction using $Cu(OTf)_2$ and $PhI(OAc)_2$ has been reported: Cho, S. H.; Yoon, J.; Chang, S. *J. Am. Chem. Soc.* **2011**, *133*, 5996.

(8) The H-H COSY spectrum of **10d** and **10e** showed that there is no cross peak corresponding to the correlation between H1′ and H2′ of **10e**. This revealed that a dihedral angle of H1′-C1′-C2′-H2′ should be around 90°. From this result, **10e** was determined to be a 1′,2′-*trans*-isomer.

(9) The C2-acylglycosylation of glycals with $PhI(OCOR)_2$ in the presence of $Et_2O{\cdot}BF_3$ was reported to proceed via a C2-phenyliodonium (I^{III}) intermediate: Shi, L.; Kim, Y.-J.; Gin, D. Y. *J. Am. Chem. Soc.* **2001**, *123*, 6939.

© Georg Thieme Verlag Stuttgart · New York

(10) Singh, F. V.; Wirth, T. *Org. Lett.* **2011**, *13*, 6504.
(11) In contrast, the reaction of glycal derivatives with $(PhSe)_2$, $PhI(OAc)_2$, and NaN_3 gave 2-azido-1-phenylseleno-glycoside selectively: (a) Litjens, R. E. J. N.; den Heeten, R.; Timmer, M. S. M.; Overkleeft, H. S.; van der Marel, G. A. *Chem.–Eur. J.* **2005**, *11*, 1010. (b) Jiaang, W.-T.; Chang, M.-Y.; Tseng, P.-H.; Chen, S.-T. *Tetrahedron Lett.* **2000**, *41*, 3127. (c) Santoyo-Gonzalez, F.; Calvo-Flores, F. G.; García-Mendoza, P.; Hernández-Mateo, F.; Isac-García, J.; Robles-Díaz, R. *J. Org. Chem.* **1993**, *58*, 6122.
(12) For example, see: (a) De Clercq, E. *Biochem. Pharmacol.* **2011**, *82*, 99. (b) Esté, J. A.; Cihlar, T. *Antiviral Res.* **2010**, *85*, 25. (c) Meadows, D. C.; Gervey-Hague, J. *ChemMedChem* **2006**, *1*, 16. (d) Imamichi, T. *Curr. Pharm. Design* **2004**, *10*, 4039.
(13) Imanieh, H.; Quayle, P.; Voaden, M.; Conway, J. *Tetrahedron Lett.* **1992**, *33*, 543.
(14) The stereochemistries of **15d,e** were determined by NOE experiments: **15d** showed a NOE (3.1%) between H-6 of the uracil ring and one of the methylene protons on the siloxymethyl group on C6 of tetrahydropyran. On the other hand, in the case of **15e**, NOEs (9.9% and 2.3%) were found between the H-2 of tetrahydropyran (anomeric proton) and the methylene protons of the siloxymethyl group. The stereochemistries of **15f,g** were estimated by comparison with the ^1H NMR spectra of **15d,e**.
(15) (a) Díaz, Y.; El-Laghdach, A.; Matheu, M. I.; Castillón, S. *J. Org. Chem.* **1997**, *62*, 1501. (b) Wilson, L.; Lotta, D. *Tetrahedron Lett.* **1990**, *31*, 1815.

 © Georg Thieme Verlag Stuttgart · New York

HETEROCYCLES, Vol. 84, No. 2, 2012, pp. 929 - 944. © 2012 The Japan Institute of Heterocyclic Chemistry
Received, 2nd July, 2011, Accepted, 4th August, 2011, Published online, 15th August, 2011
DOI: 10.3987/COM-11-S(P)74

ASYMMETRIC SYNTHESIS OF 2-PROPYLISOFAGOMINE USING ALLYLIC HYDROXY GROUP ACCELERATED RING-CLOSING ENYNE METATHESIS≠

Tatsuya Taguchi,[a] Tatsushi Imahori, [a] Yuichi Yoshimura, [a] Atsushi Kato,[b] Isao Adachi,[b] Masatoshi Kawahata,[c] Kentaro Yamaguchi,[c] and Hiroki Takahata [a]*

[a]Faculty of Pharmaceutical Sciences, Tohoku Pharmaceutical University, Sendai 981-8558, Japan : takahata@tohoku-pharm.ac.jp

[b]Department of Hospital Pharmacy, University of Toyama, Toyama 930-0194, Japan

[c]Faculty of Pharmaceutical Sciences, Tokushima Bunri University, Kagawa Campus, Sanuki, 769-2193, Japan

Abstract – An asymmetric synthesis of 2-propylisofagomine **5** using allylic hydroxy group accelerated ring-closing enyne metathesis (AHA-RCEM) was conducted with high diastereoselectivity in 13% overall yield starting from the commercially available (*E*)-hex-2-ol.

INTRODUCTION

Iminosugars belong to the family of polyhydroxylated alkaloids. Many iminofuranose and iminopyranose analogs are potent α- and β-glycosidase inhibitors[1] and also have antidiabetic, anticancer, and antiviral properties. *N*-Butyl-1-deoxynojirimycin (DNJ) **1** (Zavesca™) is used in the treatment of Gaucher disease. Another iminosugar, Miglitol **2**, which is commercially available in the USA and Canada, is used for the treatment of type II diabetes (GLYSET™). In addition, *Galacto*-DNJ (Migalastat) **3** has been shown to inhibit lysosomal a-galactosidase and is currently in phase III clinical trials for the treatment of Fabry's disease (Figure 1).[2] The chemical and biological properties of iminosugars have been extensively reviewed in past years.[3]

The search for anomer selective β-glycosidase inhibitors has led to the development of a new class of sugar-mimics, 1-*N*-iminosugars with a nitrogen atom at the anomeric position. The first example of such compounds, the 1-*N*-iminosugar isofagomine **4**, was first designed by Bols *et al.*[4] as an apparent transition

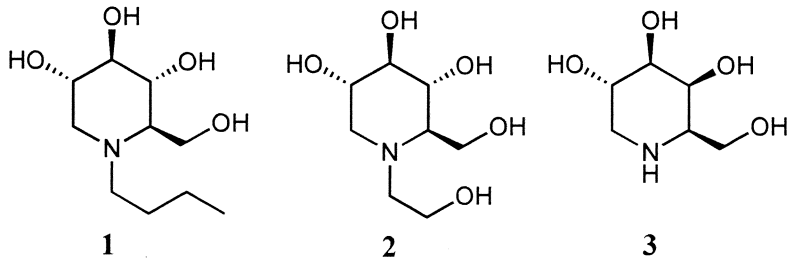


Figure 1. Clinical drugs of iminosugars

state analog that mimics the carbocationic form of the oxycarbenium-like transition state in which the positive charge resides at the anomeric carbon. Isofagomine has been found to be a selective and very strong inhibitor of β-glucosidase [K_i = 0.11 mM, from sweet almonds][4] and isofagomine derivatives have recently received a great deal of attention because they are new candidates for the therapeutic treatment of Gaucher's disease. They are currently in Phase II of clinical development. Gaucher's disease is a lysosomal storage disorder caused by inherited genetic mutations in the GBA gene, which results in deficient activity of glucocerebrosidase (GCase). Deficient GCase activity leads to the progressive accumulation of glucosylceramide (GlcCer). A very promising therapeutic strategy of the treatment of Gaucher's disease involves the use of small molecule pharmacological chaperones, often competitive enzyme inhibitors, to facilitate the proper folding and trafficking of the lysosomal enzymes.[5] In Gaucher's disease, disfunctional lysosomes cause hepatosplenomegaly, anaemia, bone lesions, and, in more severe cases, central nervous system impairment.[6] It has been reported that isofagomine is a more effective pharmacological chaperone for GCase.[7] As a consequence, the development of new stereoselective and versatile procedures for the synthesis of isofagomine-type iminosugars constitutes an area of considerable interest.[8] Recently, the synthesis of 6-alkyl isofagomines and their potent inhibition for Gcase were reported.[9] However, the synthesis of 2-alkyl isofagomines remains unexplored. Here we wish to report a synthesis of 2-propylisofagomine **5** using allylic hydroxy group accelerated ring-closing enyne metathesis (AHA-RCEM) developed by us[10] (Figure 2).

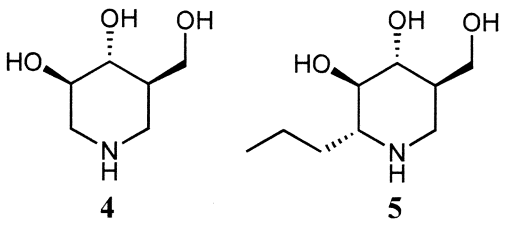
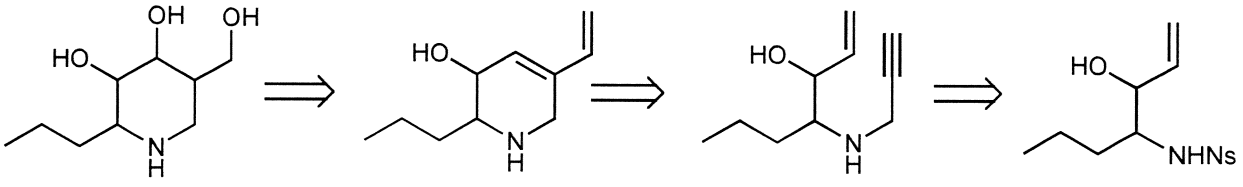


Figure 2. Structures of isofagomine and 2-propylisofagomine

RESULTS AND DISCUSSION

Our strategy for the synthesis of 2-propylisofagomine is outlined in Scheme 1, which shows that the desired iminosugars **A** can be produced from cyclic diene **B** by several operation. The piperidene core could be prepared by the AHA-RCEM of the terminal alkyne **C** as a key step. Therefore, we embarked on a synthesis of the precursor C, which is available from the known chiral *N*-nosyl allylic amine **D**.



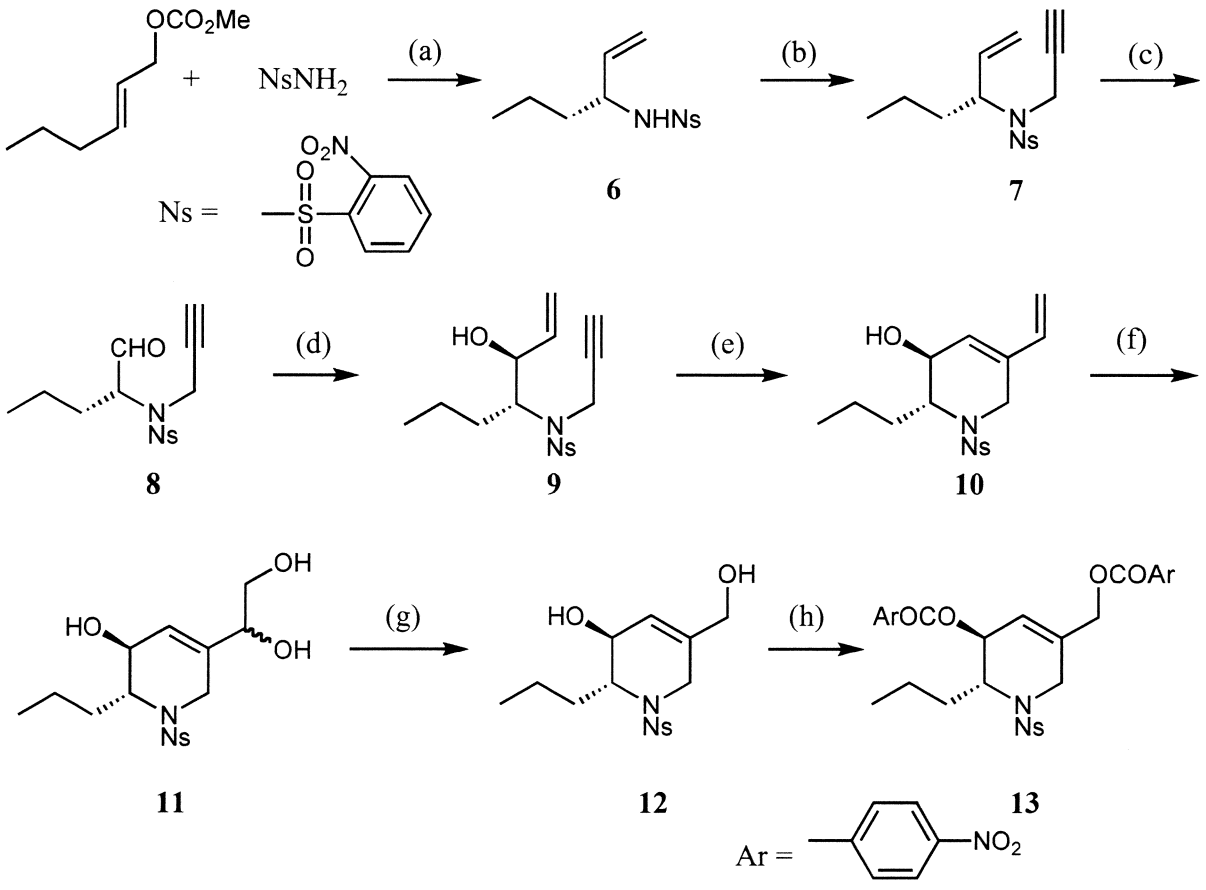
A **B** **C** **D**

Scheme 1. Retrosynthesis of 2-propylisofagomines

In initial experiments, an asymmetric allylic amination between *N*-(*o*-nosyl)amine and carbonate provided the known (*R*)-*N*-hexenylnosylamide **6** in 82% yield with 94% ee using the procedure reported by Weihofen *et al.*[11] The propargylation of **6** with propargyl bromide in the presence of potassium carbonate quantitatively gave the acetylene product **7** in quantitative yield, which, on ozonolysis, afforded the aldehyde **8** in 88% yield.[12] The vinylation of **8** with vinylmagnesium chloide in THF at –78 °C proceeded stereoselectively to give the allyl alcohol **9** as a single diasterteomer in 66% yield. Although the stereochemistry of **9** remains unclear in this stage, we tentatively concluded that it is 3*S*,4*R* in the light of the Felkin-Anh model. Having the precursor **9**, the AHA-RCEM of **9** was carried out using Grubb's I (10 mo%) as a catalyst at room temperature in a short reaction time to afford cyclic diene **10** in 85% yield. Treatment of **10** with AD-mix-β as a bulky oxidant resulted in the highly regioselective dihydroxylation of terminal olefin to provide diol **11** (81%).[13] Oxidative cleavage of the diol **11** with $NaIO_4$, followed by reduction with $NaBH_4$, gave the allyl alcohol **12** (94% over two steps). In this stage, the stereochemistry of **12** was determined by a X-ray crystallographic analysis of **13** obtained by the di-*p*-nitrobenzoate to be 2*R*,3*S* (Figure 3).

With **12** in hand, we attempted to perform a hydroxylation at the 4 position of **12** by hydroboration followed by oxidation. The olefin **12** was treated with BH_3-THF complex (6 equiv.) at room temperature for 13 h, followed by oxidation with 3 M NaOH and 30% H_2O_2 to give a separable mixture of triols **14a** and **14b** in 72% yield.[14] Unfortunately, a ratio of the two diastereomeric triols was about 1:1 with no selectivity. We concluded that **14a** was produced *via* transition state **A** with chelation between the hydroxy group at the 3 position and the borane reagent. Accordingly, the preparation of the desired triol

14b resulted in low selectivity. Therefore, we hypothesized that the hydroboration of a protected silyl ether **15** could preferentially produce the desired isomer *via* transition state **B** due to steric repulsion between boran reagent and bulky *O*-silylated group. In practice, the hydroboration-oxidation of **15** produced the expected product **16** as a single isomer in 60% yield. Removal of the TBDPS group by treatment with TBAF smoothly furnished the triol **17** in 96% yield. Finally, deprotection of Ns group with benzenethiol in the presence of K_2CO_3 gave the desired 2-propylisofagomine **5** in 82% yield. Since a nuclear Overhauser effect (NOE) was observed between axial hydrogens at the 2 and 4 positions and also between axial hydrogenes at 3 and 5 positions as shown in Figure 3, the stereochemistry of **5** was confirmed to be 2*R*,3*R*,4*R*,5*R*. In addition, **14a** was transformed with denosylation into **18** in 90% yield.



Scheme 2. (a) *o*-$NsNH_2$/1,5,7-triazabicyclo[4,4,0]dec-5-ene (TBD)/cat. $[Ir(COD)Cl]_2$/(*S,S,S*)-(+)-(3,5-dioxa-4-phosphacyclohepta[2,1-3,4-a']dinaphtalen-4-yl)bis(1-phenylethyl)amine/Et_3N/THF/82%, (b) propargyl bromide/ K_2CO_3/MeCN/quant., (c) O_3/ Me_2S/ CH_2Cl_2/88%, (d) vinylmagunesium chloride/THF/66%, (e) cat. Grubbs'1st/CH_2Cl_2/82%, (f) AD-mix-b®/*tert*-BuOH-H_2O/81%, (g) (1) $NaIO_4$/EtOH-H_2O, (2) $NaBH_4$/ EtOH-H_2O/94%, (h) *p*-nitorobenzoyl chloride/ DMAP/ CH_2Cl_2/99%

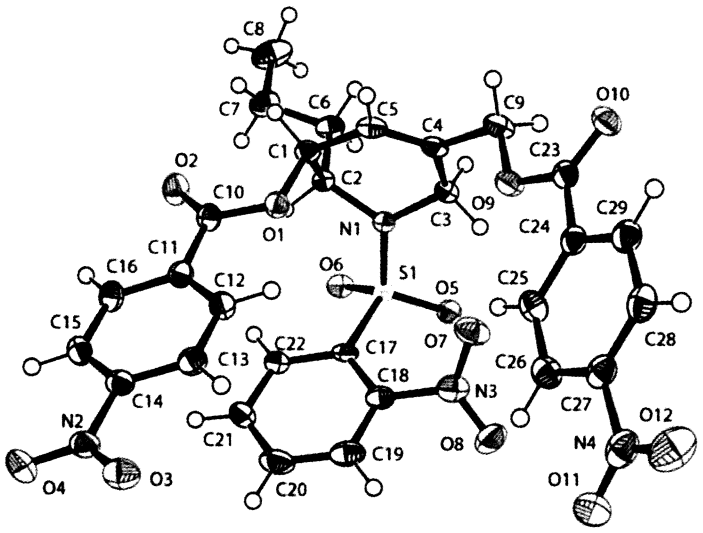
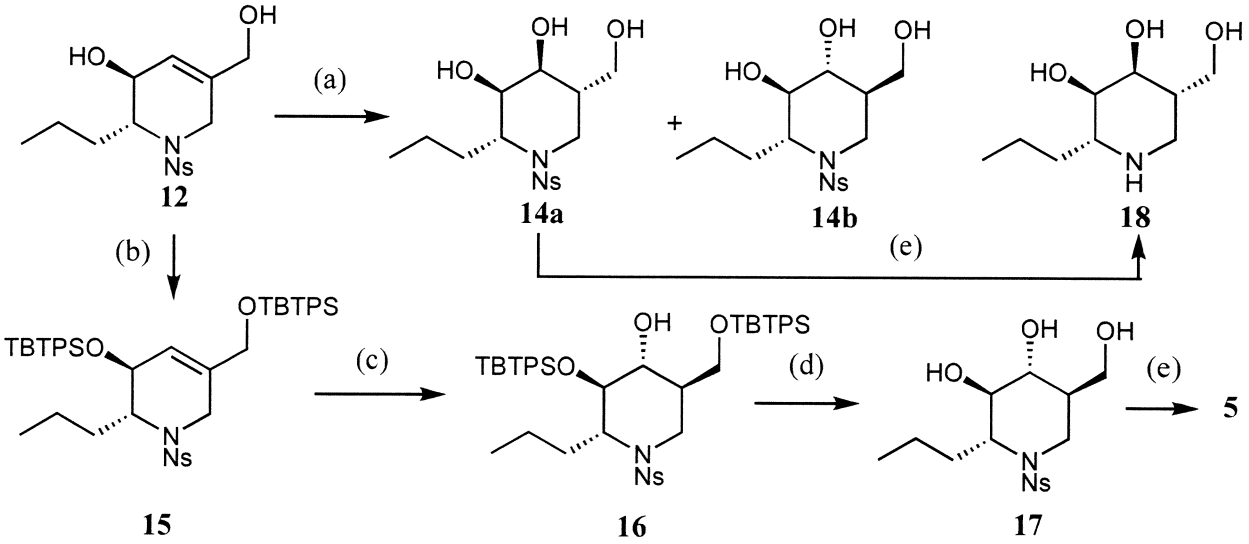


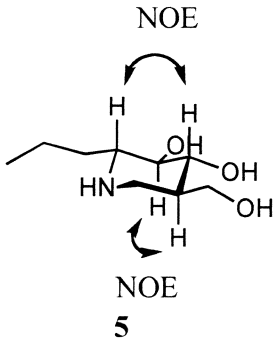
Figure 3. ORTEP diagram of **13**



Figure 4. Transition state in the hydroboration of **12** and **15**



Scheme 3. (a) (1)BH_3-THF/THF, (2) 3M NaOH/30% H_2O_2/37% for **14a**/35%, for **14b**, (b) TBDPSCl/imidazole/DMAP/ CH_2Cl_2/93%, (c) BH_3-THF/THF, (2) 3M NaOH/30% H_2O_2/60%, (d) TBAF/THF/96%, (e) benzenethiol/K_2CO_3/MeCN/82%/ for **5**, for 90% for **18**



5

Figure 5. NOE experiment of **5**

Having obtained the 2-propylisofagomines **5** and **18**, their ability to serve as inhibitors of several glucosidases was examined. The results are shown in Table 1. We were disappointed to find that 2-propylisofagimine **5** did not show potent inhibitory activity toward β-glucosidases in less than 50% inhibition at 1000 μM. Since isofagomine has been reported to be a very strong inhibitor of β-glucosidase, this finding was surprising. Although the reason remains unclear, the inhibitory activities would be strongly suppressed by the presence of a 2-propyl substituent. On the other hand, **18** exhibited moderate inhibition towards a-fucosidase (entry 8).

Table 1. Concentration of **5** and **18** for require to achieve 50% inhibition of several glycosidases

entry	enzyme	**5**	**18**
	β-glucosidase		
1	almond	NI	NI
2	bovine liver	NI	NI
3	rat intestinal cellobiase	NI	NI
	α-glucosidase		
4	rice	NI	NI
5	yeast	NI	NI
6	rat intestinal maltase	NI	NI
7	rat intestinal sucrase	NI	NI
	α-fucosidase		
8	bovine epididydymis	NI	253

NI: less than 50% inhibition at 1000 μM.

In summary, 2-propylisofagomine **5** was stereoselectively prepared from the carbonate in 13% overall yield using AHA-RCEM as a key step.

EXPERIMENTAL

Infrared (IR) spectra were recorded on a Perkin-Elmer 1600 series FT-IR spectrometer. Mass spectra (MS) were recorded on a JEOL JMN-DX 303/JMA-DA 5000 spectrometer. Microanalyses were performed on a Perkin-Elmer CHN 2400 Elemental Analyzer. Optical rotations were measured with a JASCO DIP-360 or JASCO P-1020 digital polarimeter. Proton nuclear magnetic resonance (^{1}H NMR) spectra were recorded on JEOL JNM-AL 400 (400 MHz) spectrometer, using tetramethylsilane as an internal standard. The following abbreviations are used: s = singlet, d = doublet, t = triplet, q = quartet, m = multiplet, br = broad. Column chromatography was carried out on Merck Silica gel 60 (230-400 mesh) or KANTO Silica Gel 60N (40-50 mm) for flash chromatography.

(*R*)-*N*-(Hex-1-en-3-yl)-2-nitorobenzenesulfonlyamide (6)

A mixture of dried TBD (62.0 mg, 0.45 mmol), $[Ir(COD)Cl]_2$ (68.2 mg, 0.10 mmol), (*S*,*S*,*S*)-(+)-(3,5-dioxa-4-phosphacyclohepta [2,1-3,4-a']dinaphtalen-4-yl)bis(1-phenylethyl)amine (111.4 mg, 0.41 mmol) in THF (5 mL) was stirred for 2 h under Ar. To the mixture were successively (*E*)-hex-2-enyl methyl carbonate (791.1 mg, 5.0 mmol)、*o*-nitrobenzenesulfonylamide (1.21 g, 6 mmol), and NEt_3 (0.71 mL, 5.0 mmol) and the whole was stirred at room temperature for 37 h. After evaporation, the residue was purified by silica gel chromatography (*n*-hexane : EtOAc = 15 : 1) to give **6** (1.17 g, 82%, 94% ee) as an oil; Pale yellow oil. $[\alpha]^{27}_D$ +122.7 (*c* 1.0, $CHCl_3$). ^{1}H-NMR (400 MHz, $CDCl_3$) δ: 0.88 (3H, t, *J* = 7.25 Hz), 1.25-1.41 (2H, m), 1.47-1.54 (2H, m), 3.94-4.01 (1H, m), 4.91 (1H, d, *J* = 10.63 Hz), 5.01 (1H, d, *J* = 16.90 Hz), 5.27 (1H, d, *J* = 8.21 Hz), 5.53 (1H, ddd, *J* = 7.25, 9.66, 17.39 Hz), 7.68-7.73 (2H, m), 7.83-7.87 (1H, m), 8.08-8.12 (1H, m). ^{13}C-NMR (100 MHz, $CDCl_3$) δ: 13.6, 18.5, 37.7, 57.4, 116.2, 125.2, 131.0, 132.6, 133.3, 135.1, 137.3, 147.8. IR (neat) cm^{-1} : 3338, 2961, 1645, 1538, 1442, 1415, 1362, 1170. HPLC (Column AD-H): *n*-hexane : *i*-PrOH = 9 : 1, Flow Rate 1.5 mL/min, retention time 44.3 min (major), 48.7 min (minor), 33.9 °C, 254 nm. EI-MS (m/z) 284 (M^+). HRMS Calcd for $C_{12}H_{16}N_2O_4S$: 284.0831 Found 284.0836.

(*R*)-*N*-(Hex-1-en-3-yl)-2-nitro-*N*-(prop-2-ynyl)benzenesulfonlyamine (7)

To a mixture of **6** (1.10 g, 3.87 mmol) in acetonitrile (8.3 mL) was successively addd propargyl bromide (0.6 mL, 7.74 mmol) and K_2CO_3 (1.08 g, 7.74 mmol). The whole was refluxedfor 16 h. After filtration through cotton, the filtrate eas evaporated. The filtrate was purified with chromatography (*n*-hexane : EtOAc = 5 : 1) to yield **7** (1.25 g, quant.).

Pale yellow oil. $[\alpha]^{26}_D$ +59.8 (*c* 1.0, $CHCl_3$). ^{1}H-NMR (400 MHz, $CDCl_3$) δ: 0.90 (3H, t, *J* = 7.25 Hz), 1.30-1.44 (2H, m), 1.65-1.77 (2H, m), 2.18 (1H, t, *J* = 1.93 Hz), 4.10 (1H, dd, *J* = 2.42, 81.14 Hz), 4.10 (1H, dd, *J* = 2.42, 46.36 Hz), 4.45 (1H, q, *J* = 6.76 Hz), 5.13-5.18 (2H, m), 5.81 (1H, ddd, *J* = 5.8, 11.11, 16.90, Hz), 7.62-7.69 (3H, m), 8.13-8.15 (1H, m). ^{13}C-NMR (100 MHz, $CDCl_3$) δ: 13.7, 19.4, 32.9, 33.8, 60.2, 72.5, 79.6, 118.1, 124.0, 131.3, 131.5, 133.5, 133.8, 135.5. IR (neat) cm^{-1} : 3292, 2961, 2935, 2124,

1642, 1547, 1439, 1425, 1373, 1164. EI-MS (m/z) 322 (M^+). HRMS Calcd for $C_{15}H_{18}N_2O_4S$: 322.0987 Found 322.0986.

(*R*)-2-Nitro-*N*-(1-oxopentan-2-yl)-*N*-(prop-2-ynyl)benzenesulfonamide (8)

A solution of **7** (1.22 g, 3.79 mmol) in CH_2Cl_2 (200 mL) was bubbled with ozone at –78 °C. After passing of excess ozone, Me_2S was slowly added to the solution at the same temperature. The whole was stirred at room temperature for 3 h. After evaporation, the residue was purified by silica gel chromatography (*n*-hexane : EtOAc = 40 : 1) to yield **8** (1.08 g, 88%).

Crystal. mp : 82-83 °C. $[\alpha]^{23}_D$ -61.2 (*c* 1.0, $CHCl_3$). ^{1}H-NMR (400 MHz, $CDCl_3$) δ: 0.87 (3H, t, *J* = 7.25 Hz), 1.20-1.30 (1H, m), 1.38-1.47 (1H, m), 1.64-1.74 (1H, m), 1.97-2.06 (1H, m), 2.28 (1H, t, *J* = 2.42 Hz), 4.20 (1H, dd, *J* = 4.35, 10.63), 7.69-7.77 (3H, m), 4.22 (1H, dd, *J* = 2.42, 90.80 Hz), 4.22 (1H, dd, *J* = 2.42, 127.50 Hz), 8.14-8.16 (1H, m), 9.77 (1H, s). ^{13}C-NMR (100 MHz, $CDCl_3$) δ: 13.4, 19.0, 28.2, 34.8, 65.8, 74.5, 78.0, 124.6, 131.5, 132.0, 133.1, 134.1, 147.8, 199.8. IR (KBr) cm^{-1} : 3280, 2968, 2935, 2126, 1590, 1542, 1466, 1435, 1373, 1356, 1165. EI-MS (m/z) 324 (M^+). HRMS Calcd for $C_{14}H_{16}N_2O_5S$: 324.0780 Found 324.0767. Anal. Calcd for $C_{14}H_{16}N_2O_5S$: C, 51.84; H, 4.97; N, 8.64. Found C, 51.87; H, 4.93; N, 8.61.

***N*-(3*S*,4*R*)-3-(Hydroxyhept-1-en-4-yl)-2-nitro-*N*-(prop-2-ynyl)benzenesulfonamide (9)**

Vinylmagunesium chloride (1.86 mL, 2.76 mmol) in THF (1.86 mL) was quickly added to a solution of **8** (300 mg, 0.92 mmol) in THF (9.2 mL) at -78 °C under Ar. Immediately, aq. NH_4Cl was added to the reaction mixture. After evaporation, water and CH_2Cl_2 were added to the residue. The mixture was separated and the aqueous layer was extracted with CH_2Cl_2 three tomes. The combined organic solvents were dried with Na_2SO_4 and evaporated. The residue was purified by silica gel chromatography (CH_2Cl_2 : Et_2O = 40 : 1) to yield **9** (215.1 mg, 66%). Pale yellow oil. $[\alpha]^{24}_D$ -62.2 (*c* 1.0, $CHCl_3$). ^{1}H-NMR (400 MHz, $CDCl_3$) δ: 0.80 (3H, t, *J* = 7.25 Hz), 1.03-1.09 (1H, m), 1.26-1.33 (1H, m), 1.46-1.52 (1H, m), 1.67-1.75 (1H, m), 2.12 (1H, d, *J* = 4.83 Hz), 2.21 (1H, t, *J* = 2.42 Hz), 3.91 (1H, dt, *J* = 2.89, 10.62 Hz), 4.36 (1H, dd, *J* = 2.42, 124.60 Hz), 4.36 (1H dd, *J* = 2.42, 86.93 Hz), 4.57 (1H, sex, *J* = 2.42 Hz), 5.20 (1H, dt, *J* = 1.45, 10.62 Hz), 5.33 (1H, dt, *J* = 1.45, 15.94 Hz), 5.95 (1H, ddd, *J* = 4.35, 10.62, 17.39 Hz), 7.61-7.63 (1H, m), 7.69 (2H, ddd, *J* = 2.42, 3.86, 6.76), 8.17-8.20 (1 H, m). ^{13}C-NMR (100 MHz, $CDCl_3$) δ: 13.5, 19.1, 27.1, 33.6, 61.7, 72.2, 75.1, 80.0, 115.6, 123.8, 131.4, 131.5, 133.2, 133.8, 137.9, 147.8. IR (neat) cm^{-1} : 3546, 3291, 2961, 1544, 1438, 1373, 1347, 1160. EI-MS (m/z) 352 (M^+). HRMS Calcd for $C_{16}H_{20}N_2O_5S$: 352.1093 Found 352.1096.

(2*S*,3*S*)-1-(2-Nitrophenylsulfonyl)-2-propyl-5-vinyl-1, 2, 3, 6-tetrahydropyridin-3-ol (10)

A mixture of **9** (247.4 mg, 0.70 mmol) and Grubbs'1st (57.6 mg, 0.070 mmol) in CH_2Cl_2 (35 mL) was stirred at roomtemperature for 2.5 h under Ar. After evaporation, the residue was purified by silica gel chromatography (CH_2Cl_2 : EtOAc = 40 : 1) to yield **10** (202.3 mg, 82%).

Oil. $[\alpha]^{26}_{D}$ +78.6 (*c* 1.0, $CHCl_3$). ^{1}H-NMR (400 MHz, $CDCl_3$) δ: 0.84 (3H, t, *J* = 7.25 Hz), 1.18-1.50 (4H, m), 2.16 (1H, d, *J* = 9.66 Hz), 3.80 (1H, d, *J* = 17.87), 3.94-4.00 (2H, m), 4.49 (1H, d, *J* = 17.87 Hz), 5.22 (1H, d, *J* = 11.11 Hz), 5.32 (1H, d, *J* = 17.39 Hz), 5.86 (1H, d, *J* = 5.31 Hz), 6.31 (2H, dd, *J* = 11.11, 17.89 Hz), 7.63-7.73 (3H, m), 8.16-8.18 (1H, m). ^{13}C-NMR (100 MHz, $CDCl_3$) δ: 13.8, 19.5, 31.4, 40.1, 59.2, 66.2, 115.2, 124.2, 125.2, 131.5, 131.8, 133.5, 133.7, 135.4, 135.7, 147.7. IR (neat) cm^{-1} : 3539, 2961, 2929, 1609, 1543, 1439, 1372, 1345, 1163. EI-MS (m/z) 352 (M^+). HRMS Calcd for $C_{16}H_{20}N_2O_5S$: 352.1093 Found 352.1096.

1-((5*S*,6*R*)-5-Hydroxy-1-(2-nitrophenylsulfonyl)-6-propyl-1,2,5,6-tetrahydropyridin-3-yl)ethane-1,2-diol (11)

A mixture of **10** (56 mg, 0.159 mmol) and AD-mix-β® (513 mg) in *t*-BuOH (0.8 mL) and H_2O (0.8 mL) was stirred at room temperature for 12 h. After addition of Na_2SO_3 (253 mg), Na_2SO_4 was added to the mixture. The whole was filtrated through Celite and the filtrate was evaporated. The residue was purified by silica gel chromatography (CH_2Cl_2 : MeOH = 15 : 1) to yield **11** (49.8 mg, 81%).

Amorphous. ^{1}H-NMR (400 MHz, $CDCl_3$) δ: 0.83-0.87 (6H, m), 1.23-1.49 (8H, m), 3.64-3.80 (6H, m), 3.89-3.92 (4H, m), 4.20-4.33 (4H, m), 5.93-5.97 (2H, m), 7.65-7.72 (6H, m), 8.16-8.18 (2H, m). EI-MS (m/z) 368 (M^+ -H_2O). HRMS Calcd for $C_{16}H_{20}N_2O_6S$ (-H_2O) : 368.1042 Found 368.1048.

(2*R*,3*R*)-5-(Hydroxymethyl)-1-(2-nitrophenylsulfonyl)-2-propyl-1,2,3,6-tetrahydropyridin-3-ol (12)

A mixture of **11** (141.8 mg, 0.37 mmol) and $NaIO_4$ (119.3 mg, 0.56 mmol) in EtOH (2.6 mL) and H_2O (2.6 mL) was stirred at room temperature for 1.5 h. $NaBH_4$ (22.1 mg, 0.56 mmol) was added to the reaction mixture and the the whole was stirred at room temperature for 0.5 h. After evaporation, water and CH_2CH_2 were added to the residue. The mixture was separated and the aqueous layer was extracted with CH_2CH_2 6 times. The combined organic solvents were dried with Na_2SO_4 and evaporated. The residue was washed with a small amounts of Et_20 and CH_2Cl_2 to yield and dried in vauo to yield **8a** (123.8 mg, 94%). Needle crystal. mp: 180-181 °C. $[\alpha]^{26}_{D}$ +32.2 (*c* 1.0, MeOH). ^{1}H-NMR (400 MHz, $CDCl_3$) δ: 0.85 (3H, t, *J* = 7.25 Hz), 1.21-1.25 (2H, m), 1.34-1.39 (2H, m), 2.08 (1H, d, *J* = 9.18 Hz), 3.70 (1H, d, *J* = 18.35 Hz), 3.93 (2H, t, *J* = 6.77 Hz), 4.16 (2H, s), 4.31 (1H, d, *J* = 18.35 Hz), 5.90 (1H, d, *J* = 5.80 Hz), 7.63-7.71 (3H, m), 8.16-8.19 (1H, m). ^{13}C-NMR (100 MHz, $CDCl_3$) δ: 13.6, 19.4, 31.3, 40.9, 59.2, 63.1, 65.3, 119.7, 123.9, 131.0, 131.7, 133.4, 135.2, 138.5, 147.8. IR (KBr) cm^{-1} : 3281, 2965, 2935, 1544, 1461, 1435, 1374, 1350, 1161. EI-MS (m/z) 338 (M^+ -H_2O). HRMS Calcd for $C_{15}H_{18}N_2O_5S$ (-H_2O): 338.0936 Found 338.0929. Anal. Calcd for $C_{15}H_{20}N_2O_6S$: C, 50.55; H, 5.66; N, 7.86. Found C, 50.62; H, 5.61; N, 7.83.

((5*S*,6*R*)-5-(4-Nitrobenzoyloxyl)-1-(2-nitrophenylsulfonyl)-6-propyl-1,2,5,6-tetrahydropyridin-3-yl)-methyl 4-nitrobenzenoate (13)

A mixture of 12 (88.4 mg, 0.25 mmol), DMAP (77.1 mg, 0.63 mmol), and *p*-nitorobenzoyl chloride

(118.0 mg, 0.63 mmol) in CH_2Cl_2 (4 mL) was stirred at room temperature for 1 h. Aqueous $NaHCO_3$, water, and CH_2Cl_2 were successively added to the mixture and the whole was separated. The aqueous layer was extracted with CH_2Cl_2 twice and the combined organic solvents were dried with Na_2SO_4. After evaporation, the residue was purified by silica gel chromatography (CH_2Cl_2) to yield **13** (161.2 mg, 99%). Crystal. mp: 163-165 °C. $[\alpha]^{28}_D$ +150.7 (*c* 1.0, $CHCl_3$). ^{1}H-NMR (400 MHz, $CDCl_3$) δ: 0.92 (3H, t, *J* = 7.25 Hz), 1.32-1.45 (2H, m), 1.56-1.62 (2H, m), 3.84 (1H, d, *J* = 18.35 Hz), 4.30 (1H, t, *J* = 7.25 Hz), 4.56 (1H, d, *J* = 18.35), 4.95 (2H, s), 5.32 (1H, d, *J* = 5.80 Hz), 6.10 (1H, d, *J* = 5.31 Hz), 7.47-7.54 (2H, m), 7.58-7.61 (1H, m), 8.01-8.04 (3H, m), 8.19-8.22 (2H, m), 8.31 (4H, q, *J* = 9.18 Hz). ^{13}C-NMR (100 MHz, $CDCl_3$) δ: 13.9, 19.6, 31.6, 41.4, 55.6, 65.7, 68.6, 77.2, 119.4, 123.4, 123.7, 124.4, 131.0, 131.8, 133.4, 134.3, 134.9, 137.6, 150.6, 150.8, 164.2, 164.3. IR (KBr) cm^{-1} : 2962, 1721, 1608, 1528, 1439, 1349, 1162. EI-MS (m/z) 654 (M^+). HRMS Calcd for $C_{29}H_{26}N_4O_{12}S$: 654.1268 Found 654.1293. Anal. Calcd for $C_{29}H_{26}N_4O_{12}S$: C, 53.21; H, 4.00; N, 8.56. Found C, 53.18; H, 3.78; N, 8.48.

Table 2. Crystal data and structure refinement for **13**

Identification code	a0808291kwh	
Empirical formula	C29 H26 N4 O12 S	
Formula weight	654.60	
Temperature	120 K	
Wavelength	0.71073 ≈	
Crystal system	Monoclinic	
Space group	P21	
Unit cell dimensions	a = 11.3639(14) ≈	α= 90°.
	b = 11.6881(15) ≈	β= 109.783(1)°.
	c = 12.0016(15) ≈	γ = 90°.
Volume	1500.0(3) ≈^{3}	
Z	2	
Density (calculated)	1.449 Mg/m^3	
Absorption coefficient	0.180 mm^{-1}	
F(000)	680	
Crystal size	0.30 x 0.30 x 0.05 mm^3	
Theta range for data collection	1.80 to 27.27°.	
Index ranges	-13<=h<=14, -8<=k<=14, -15<=l<=14	
Reflections collected	7464	
Independent reflections	4125 [R(int) = 0.0166]	
Completeness to theta = 25.00∞	99.2%	
Absorption correction	None	
Refinement method	Full-matrix least-squares on F^2	

Data / restraints / parameters	4125 / 1 / 416
Goodness-of-fit on F^2	1.036
Final R indices [I>2sigma(I)]	R1 = 0.0270, wR2 = 0.0665
R indices (all data)	R1 = 0.0299, wR2 = 0.0682
Absolute structure parameter	-0.01(6)
Largest diff. peak and hole	0.178 and -0.282 e.$\approx^{-3}$

Table 3. Atomic coordinates (x 10^4) and equivalent isotropic displacement parameters ($\approx^2$x 10^3) for **13**. U(eq) is defined as one third of the trace of the orthogonalized U^{ij} tensor.

	x	y	z	U(eq)
C(1)	9178(2)	13038(2)	5470(2)	22(1)
C(2)	8765(2)	11868(2)	4921(2)	21(1)
C(3)	10755(2)	10981(2)	6295(2)	25(1)
C(4)	11236(2)	12178(2)	6575(2)	24(1)
C(5)	10539(2)	13093(2)	6192(2)	24(1)
C(6)	9024(2)	11719(2)	3759(2)	25(1)
C(7)	8030(2)	12298(2)	2724(2)	34(1)
C(8)	8281(3)	12149(3)	1570(2)	49(1)
C(9)	12571(2)	12284(2)	7388(2)	29(1)
C(10)	7371(2)	13719(2)	5850(2)	24(1)
C(11)	6842(2)	14000(2)	6802(2)	23(1)
C(12)	7552(2)	13930(2)	7995(2)	25(1)
C(13)	7030(2)	14228(2)	8848(2)	26(1)
C(14)	5799(2)	14571(2)	8470(2)	24(1)
C(15)	5060(2)	14641(2)	7291(2)	26(1)
C(16)	5599(2)	14351(2)	6448(2)	26(1)
C(17)	7776(2)	10374(2)	6980(2)	21(1)
C(18)	8231(2)	10203(2)	8201(2)	25(1)
C(19)	7502(2)	10422(2)	8896(2)	32(1)
C(20)	6326(2)	10878(2)	8388(2)	40(1)
C(21)	5867(2)	11091(2)	7187(2)	37(1)
C(22)	6578(2)	10811(2)	6480(2)	28(1)
C(23)	13566(2)	12455(2)	9460(2)	25(1)
C(24)	13391(2)	12432(2)	10638(2)	24(1)
C(25)	12275(2)	12046(2)	10752(2)	29(1)
C(26)	12176(2)	11938(2)	11867(2)	31(1)
C(27)	13186(2)	12235(2)	12839(2)	29(1)

C(28)	14281(2)	12674(2)	12751(2)	32(1)
C(29)	14379(2)	12765(2)	11635(2)	31(1)
N(1)	9381(1)	10978(2)	5804(2)	22(1)
N(2)	5244(2)	14901(2)	9375(2)	29(1)
N(3)	9521(2)	9843(2)	8838(2)	31(1)
N(4)	13108(2)	12033(2)	14029(2)	36(1)
O(1)	8546(1)	13322(1)	6313(1)	26(1)
O(2)	6819(1)	13826(2)	4807(1)	34(1)
O(3)	5925(1)	14899(2)	10417(1)	34(1)
O(4)	4134(1)	15153(2)	9038(1)	40(1)
O(5)	9391(1)	9012(1)	6559(1)	25(1)
O(6)	7572(1)	9718(1)	4900(1)	27(1)
O(7)	10363(1)	10365(2)	8628(1)	40(1)
O(8)	9696(2)	9088(2)	9582(2)	50(1)
O(9)	12497(1)	12286(2)	8572(1)	30(1)
O(10)	14565(1)	12599(1)	9327(1)	30(1)
O(11)	12194(2)	11527(2)	14100(2)	45(1)
O(12)	13981(2)	12356(2)	14884(1)	53(1)
S(1)	8560(1)	9919(1)	5994(1)	19(1)

(2*R*,3*R*,4*S*,5*S*)-5-(Hydroxymethyl)-1-(2-nitrophenylsulfonyl)-2-propypiperidine-3,4-diol (14a) and (2*R*,3*R*,4*R*,5*R*)-5-(Hydroxymethyl)-1-(2-nitrophenylsulfonyl)-2-propypiperidine-3,4-diol (14b). BH_3·THF (1.90 mL, 3.42 mmol) was dropwise added to a solution of **12** (204.3 mg, 0.57 mmol) in THF (1.93 mL) at 0 °C. The whole was stirred at room temperature for 13 h. 3M NaOH (1.90 mL, 5.7 mmol) and 30% H_2O_2 (1.90 mL, 57 mmol) were successively added to reaction mixture at 0 °C and thn the whole was stirred at room temperature for 2.5 h. After evaporation, water and CH_2Cl_2 were added to the residue. The mixture separated and the aqueous layer was extracted with CH_2Cl_2 6 times. The combined organic solvents were dried with Na_2SO_4 and evaporated. The residue was purified by silica gel chromatography (CH_2Cl_2 : MeOH= 20 : 1) to yield **14a** (79.0 mg, 37%) and **14b** (74.7 mg, 35%). **(14a):** Amorphous. $[\alpha]^{26}_D$ -27.5 (*c* 1.0, $CHCl_3$). ^{1}H-NMR (400 MHz, $CDCl_3$) δ: 0.87 (3H, t, *J* = 7.25 Hz), 1.20-1.35 (3H, m), 2.21-2.03 (1H, m), 2.64 (1H, d, *J* = 3.86 Hz), 2.90 (1H, dd, *J* = 12.56, 14.49 Hz), 3.05 (1H, d, *J* = 6.76 Hz), 3.49 (2H, d, *J* = 5.31 Hz), 3.73 (1H, ddd, *J* = 3.86, 6.76, 10.63 Hz), 3.79-3.93 (4H, m), 4.10-4.13 (1H, m), 7.60-7.62 (1H, m), 7.67-7.70 (2H, m), 8.12-8.14 (1H, m). ^{13}C-NMR (100 MHz, $CDCl_3$) δ: 13.8, 19.5, 30.8, 39.0, 41.5, 59.6, 63.5, 69.7, 70.0, 123.9, 131.4, 131.6, 133.4, 133.9, 147.8. IR (KBr) cm^{-1} : 3445, 2964, 2938, 1544, 1467, 1439, 1368, 1167. EI-MS (m/z) 374 (M^+). HRMS Calcd for $C_{15}H_{22}N_2O_7S$: 374.1148 Found 374.1161. **(14b):** Amorphous. $[\alpha]^{26}_D$ -126.7 (*c* 1.0, $CHCl_3$). ^{1}H-NMR (400 MHz, $CDCl_3$)

δ: 0.73 (3H, t, *J* = 7.25 Hz), 0.84-0.92 (1H, m), 1.00-1.14 (2H, m), 1.93 (1H, q, *J* = 5.31), 3.56-3.69 (3H, m), 3.73-3.84 (3H, m), 3.79-3.92 (3H, m), 4.11 (1H, t, *J* = 7.32 Hz), 7.65-7.70 (3H, m), 8.07-8.09 (1H, m). ^{13}C-NMR (100 MHz, $CDCl_3$) δ: 13.6, 19.5, 32.1, 41.1, 42.2, 60.9, 61.9, 71.1, 72.0, 124.0, 130.6, 131.6, 133.4, 134.0, 147.5. IR (KBr) cm^{-1} : 3392, 2936, 1542, 1372, 1168. EI-MS (m/z) 374 (M^+). HRMS Calcd for $C_{15}H_{22}N_2O_7S$: 374.1148 Found 374.1161.

(2*R*,3*S*)-3-(*tert*-Butyldiphenylsilyloxy)-5-((*tert*-butyldiphenylsilyloxy)methyl)-1-(2-nitrophenyl-sulfonyl)-2-propyl-1,2,3,6-tetrahydropyridine (15) A mixture of **12** (181 mg, 0.51 mmol), imidazole (90.8 mg, 1.32 mmol), DMAP (22.6 mg, 0.18 mol) and TBDPSCl (0.34 mL, 1.27 mmol) in CH_2Cl_2 (10 mL) was stirred at room temperature for 8 h. The mixture was filtrated through celite and the filtrate was washed with brine. The washed solvent was dried with Na_2SO_4 and evaporated. The residue was purified by silica gel chromatography (*n*-hexane : EtOAc = 10 : 1) to yield **15** (393.5 mg, 93%). Oil. $[\alpha]^{27}_D$ -1.3 (*c* 1.0, $CHCl_3$). ^{1}H-NMR (400 MHz, $CDCl_3$) δ: 0.77 (3H, t, *J* = 7.25 Hz), 0.96 (9H, s), 1.01 (9H, s), 1.12-1.26 (4H, m), 3.66 (1H, d, *J* = 18.35 Hz), 3.83 (1H, d, *J* = 18.35 Hz), 3.97 (1H, d, *J* = 5.31 Hz), 4.05 (2H, d, *J* = 13.04 Hz), 4.21 (1H, t, *J* = 7.25 Hz), 5.65 (1H, d, *J* = 4.83 Hz), 7.32-7.46 (13H, m), 7.51-7.72 (10H, m), 8.45 (1H, d, *J* = 7.72). ^{13}C-NMR (100 MHz, $CDCl_3$) δ: 13.8, 19.1, 19.2, 19.4, 27.0, 40.1, 59.6, 64.7, 67.9, 120.3, 124.2, 127.7, 127.8, 127.9, 129.8, 129.9, 130.0, 131.8, 132.8, 133.7, 134.3, 135.3, 135.4, 135.7, 135.9, 136.6. IR (KBr) cm^{-1} : 2959, 2932, 1736, 1590, 1546, 1472, 1428, 1346, 1161. EI-MS (m/z) 832 (M^+). HRMS Calcd for $C_{47}H_{56}N_4O_6SSi_2$: 832.3398 Found 832.3381.

(2*R*,3*R*,4*R*,5*R*)-3-(*tert*-Butyldiphenylsilyloxy)-5-((*tert*-butyldiphenylsilyloxy)methyl)-1-(2-nitrophenyl-sulfonyl)-2-propylpiperidin-4-ol (16). BH_3-THF (4.1 mL, 4.1 mmol) was dropwise added to a solution of **15** (339.1 mg, 0.41 mmol) in THF (1.4 mL) at 0 °C. The whole was stirred at room temperature for 16.5 h. 3M NaOH (1.37 mL, 4.1 mmol) and 30% H_2O_2 (1.37 mL, 12 mmol) were successively added to reaction mixture at 0 °C and thn the whole was stirred at room temperature for 2.5 h. After evaporation, water and CH_2Cl_2 were added to the residue. The mixture separated and the aqueous layer was extracted with CH_2Cl_2 4 times. The combined organic solvents were dried with Na_2SO_4 and evaporated. The residue was purified by silica gel chromatography (*n*-hexane : EtOAc = 10 : 1) to yield **16** (208.8 mg, 60%). Amorphous. $[\alpha]^{21}_D$ -32.3 (*c* 0.50, $CHCl_3$). ^{1}H-NMR (400 MHz, $CDCl_3$) δ: 0.79 (3H, t, *J* = 7.25 Hz), 0.93-1.06 (18H, m), 1.27 (2H, t, *J* = 7.25), 1.63-1.73 (2H, m), 1.90 (1H, q, *J* = 5.80), 2.34 (1H, d, *J* = 4.35 Hz), 3.35-3.52 (2H, m), 3.61-3.78 (3H, m), 3.86-3.96 (2H, m), 7.25-7.68 (23H, m), 7.99-8.01 (1H, m). ^{13}C-NMR (100 MHz, $CDCl_3$) δ: 13.8, 19.1, 19.2, 19.7, 27.0, 27.1, 32.2, 33.96, 38.52, 40.3, 42.6, 43.3, 60.1, 70.6, 72.3, 123.8, 127.6, 127.7, 127.8,129.7, 130.9, 133.1, 133.4, 133.7, 134.0, 134.2, 136.2. IR (KBr) cm^{-1} : 3567, 2959, 2931, 1546, 1472, 1428, 1373, 1174. EI-MS (m/z) 850 (M^+). HRMS Calcd for $C_{47}H_{58}N_2O_7SSi_2$: 850.3503 Found 850.3499.

(2*R*,3*R*,4*R*,5*R*)-5-(Hydroxymethyl)-2-propylpiperidine-3,4-diol (2-(*n*-propyl)isofagomine) (5). A

solution of **16** (194 mg, 0.049 mmol) and TBAF (0.56 mL, 0.575 mol) in THF(5.6 mL) was stirred at room temperature for 2.5 h. To the reaction solvent was added sat. aq. $NaHCO_3$. After evaporation, water and CH_2CH_2 were added to the residue. The mixture separated and the aqueous layer was extracted with CH_2CH_2 5 times. The combined organic solvents were dried with Na_2SO_4 and evaporated. The residue was purified by silica gel chromatography (CH_2Cl_2 : MeOH = 20 : 1) to yield **17** (82.3 mg, 96%). **17** ^{13}C-NMR (100 MHz, $CDCl_3$) δ: 13.3, 19.3, 31.9, 40.7, 42.2, 60.7, 61.5, 70.6, 71.5, 123.7, 130.3, 131.4, 133.3, 133.6, 147.4. Without further purification, K_2CO_3 (152.1 mg, 1.10 mmol) and PhSH (68.5 mL, 0.66 mmol) were added to a solution of **17** (82.3 mg, 0.219 mmol). The mixture was stirred at room temperature for 16 h. After filtration, the filtrate was evaporated. The residue was purified by silica gel chromatography (MeOH) to yield **5** (33.8 mg, 82%). Viscous solid. $[\alpha]^{23}_D$ +46.6 (*c* 0.65, H_2O) as hydrocloride salt. ^{1}H-NMR (400 MHz, CD_3OD) δ: 0.95 (3H, t, *J* = 7.25 Hz), 1.29-1.1.40 (2H, m), 1.48-1.56 (1H, m), 1.66-1.73 (1H, m), 1.81-1.90 (1H, m), 2.39-2.51 (2H, m), 3.03 (1H, t, *J* = 9.18 Hz), 3.12-3.23 (2H, m), 3.54 (1H, dd, *J* = 6.76, 11.11 Hz), 3.77 (1H, dd, *J* = 3.86, 10.63 Hz). ^{13}C-NMR (100 MHz, CD_3OD) δ: 14.5, 19.7, 35.0, 46.0, 47.8, 61.4, 62.4, 75.7, 77.6. IR (KBr) cm^{-1} : 3369, 2962, 1071. EI-MS (m/z) 189 (M^+). HRMS Calcd for $C_9H_{19}NO_3$: 189.1365 Found 189.1371.

(2*R*,3*R*,4*S*,5*S*)-5-(Hydroxymethyl)-2-propylpiperidine-3,4-diol (18) . A mixture of **14a** (31.6 mg, 0.084 mmol), K_2CO_3 (59.7 mg, 0.43 mmol) and PhSH (27 μL, 0.26 mmol) in acetonitrile (2.2 mL) was stirred at room temperature for 18.5 h. After filtration, the filtrate was evaporated. The residue was purified by silica gel chromatography (MeOH : 10% NH_4OH = 40 : 1) to yield **18** (14.3 mg, 90%).

Viscous solid. $[\alpha]^{25}_D$ -15.6 (*c* 0.53, H_2O) as hydrochloride. ^{1}H-NMR (400 MHz, CD_3OD) δ: 0.95 (3H, t, *J* = 7.32 Hz), 1.28-1.1.53 (3H, m), 1.57-1.66 (1H, m), 1.93-2.01 (1H, m), 2.73 (1H, dd, *J* = 7.81, 13.17 Hz), 2.92-3.00 (2H, m), 3.55 (1H, q, *J* = 2.93 Hz), 3.62-3.71 (2H, m), 3.77 (1H, dd, *J* = 2.93, 4.88 Hz). ^{13}C-NMR (100 MHz, CD_3OD) δ: 14.5, 20.5, 32.9, 42.4, 42.9, 58.7, 62.6, 69.3, 71.5. IR (KBr) cm^{-1} : 3402, 2960, 1063. EI-MS (m/z) 189 (M^+). HRMS Calcd for $C_9H_{19}NO_3$: 189.1365 Found 189.1374.

Bioassay of **5** and **18**

The enzymes α-glucosidase (from rice, assayed at pH 5.0), β-glucosidases (from almond, pH 5.0; from bovine liver, pH 6.8), α-L-fucosidase (from bovine epididymis, pH 5.5), were purchased from Sigma–Aldrich Co. Brush border membranes were prepared from the rat small intestine according to the method of Kessler *et al.*, [15] and were assayed at pH 5.8 for rat intestinal maltase, sucrase, and cellobiase, using the appropriate disaccharides as substrates. For rice α-glucosidase and rat intestinal maltase activities, the reaction mixture contained 25 mM maltose and the appropriate amount of enzyme, and the incubations were performed for 10–30 min at 37 °C was stopped by heating at 100 °C (600 g; 10 min), 0.05 mL of the resulting reaction mixture were added to 3 mL of the Glucose CII-test Wako (Wako Pure Chemical Ind., Osaka, Japan). The absorbance at 505 nm was measured to determine the amount of the

released D-glucose. Other glycosidase activities were determined using an appropriate *p*-nitrophenyl glycoside as substrate at the optimum pH of each enzyme. The reaction mixture contained 2 mM of the substrate and the appropriate amount of enzyme. The reaction was stopped by adding 2 mL of 400 mM Na_2CO_3. The released *p*-nitrophenol was measured spectrometrically at 400 nm.

ACKNOWLEDGEMENT

This study was financially supported by a Grant-in-Aid for Scientific Research from the Japan Society for the Promotion of Science (JSPS).

REFERENCES AND NOTES

≠Dedicated to Professor AI Padwa, on the occasion of his 75th birthday, in admiration of his many contributions of heterocyclic chemistry.

1. (a) B. Winchester and G. W. J. Fleet, *Glycobiology,* 1992, **2**, 199; (b) T. D Butters, R. A. Dwek, and F. M. Platt, *Chem. Rev.*, 2000, **100**, 4683; (c) R.-W. Wang and F.-L. Qing, *Org. Lett.,* 2005, **7**, 2189; (d) P. Sears, and C.-H. Wong, *Angew. Chem. Int. Ed.,* 1999, **38**, 2300; (e) N. Asano, R. J. Nash, R. J. Molyneux, and D. W. J. Fleet, *Tetrahedron: Asymmetry*, 2000, **11**, 1.
2. P. Compain and O. R. Martin, 'Iminosugars—From Synthesis to Therapeutic Applications,'John Wiley & Sons Ltd: West Sussex England, 2007.
3. (a) D. J. Wardro and S. L. Waidyarachchi, *Nat. Produ. Rep.*, 2010, **27**, 1431; (b) B. L. Stocker, E. M. Dangerfield, A. L. Win-Mason, G. W. Haslett, and M. S. M. Timmer, *Euro. J. Org. Chem.*, 2010, 1615.
4. M. Bols, *Acc. Chem. Res.,* 1998, **31**, 1.
5. V. H. Lillelund, H. H. Jensen, X. Liang, and M. Bols, *Chem. Rev.,* 2002, **102**, 515.
6. J.-Q. Fan, *Trends Pharmacol. Sci.,* 2003, **24**, 355.
7. (a) R. L. Lieberman, B. A. Wustman, P. Huertas, A. C. Jr., Powe, C. W. Pine, R. Khanna, M. G. Schlossmacher, D. Ringe, and G. A. Petsko, *Nature Chemical Biology,* 2007, **3**, 101; (b) Z. Yu, A. R. Sawkar, L. J. Whalen, C.-H. Wong, and J. W. Kelly, *J. Med. Chem.,* 2007, **50**, 94.
8. (a) E. Lindback, O. Lopez, J. G. Fernandez-Bolanos, S. P. A. Sauer, and M. Bols, *Org. Lett.,* 2011, **13**, 2908; (b) P. Gupta, S. Dharuman, and Y. D. Vankar, *Tetrahedron: Asymmetry*, 2010, **21**, 2966; (c) A. Rives, Y. Genisson, V. Faugeroux, N. Saffon, and M. Baltas, *Synthesis*, 2009, 3251; (d) Y. Mihara, H. Ojima, T. Imahori, Y. Yoshimura, H. Ouchi, and H. Takahata, *Heterocycles*, 2007, **72**, 633; (e) H. Ouchi, Y. Mihara, and H. Takahata, *J. Org. Chem.*, 2005, **70**, 5207.
9. X. Zhu, K. A. Sheth, S. Li, H-H. Chang, and J.-Q. Fan, *Angew. Chem. Int. Ed.* 2005, **44**, 7450.
10. T. Imahori, H. Ojima, Y. Yoshimura, and H. Takahata, *Chem. Eur. J.*, 2008, **14**, 10762.

11. (a) R. Weihofen, O. Tverskoy, and G. Helmchen, *Angew. Chem. Int. Ed.,* 2006, **45**, 5546; (b) R. Weihofen, A. Dahnz, O. Tverskoy, and G. Helmchen, *Chem. Commun.*, 2005, 3541.
12. The use of cat. OsO_4 in the presence of $NaIO_4$ resulted in low yields (20~30%).
13. The use of AD- mix-α® produced **11** in less than 75% yield.
14. The use of 3.2 eq. BH_3-THF gave **14a,b** in 61% yield, with the recovery of **12** (16%).
15. M. Kessler, O. Acuto, C. Strelli, H. Murer, and G. Semenza, *Biochem. Biophys. Acta*, 1978, **506**, 136.

Open Access

Development of RNA Aptamer and its Ligand Binding Assay on Microchip Electrophoresis

Ken-ichi Ohno[a], Chikara Nakata[a], Yoshihiro Sano[a], Fumiko Nishikawa[b], Satoshi Nishikawa[b] and Hidetoshi Arakawa*[,a]

[a]*School of Pharmacy Showa University, 1-5-8 Hatanodai, Shinagawa, Tokyo 142-8555, Japan*

[b]*Institute for Biological Resources and Functions, National Institute of Advanced Industrial Science and Technology (AIST), 1-1-1 Higashi, Tsukuba, Ibaraki 305-8566, Japan*

Abstract: Microchip electrophoresis (ME) coupled with fluorescence detection was used to estimate the binding activity of aptamer in each systematic evolution of ligands by exponential enrichment (SELEX) round for a target molecule. This approach is a non-radioisotopic, rapid and simple platform, and electrophoretic separation appears to be an effective technique for aptamers of oligonucleotide molecules. We tried to obtain gonadotropin-specific RNA aptamer by the above approach. As a result, the peaks of aptamers based on the conformational differences between them were separated and detected on the electropherograms. Moreover, the intensity of peak of unbound aptamer was decreased with progression through the SELEX rounds, suggesting that RNA aptamer with high affinity was obtained by the proposed method.

Keywords: Aptamer, conformational differences, fluorescence detection, intercalating dyes, microchip electrophoresis, SELEX.

INTRODUCTION

Antigen-antibody reaction is a sensitive and selective biological response against viruses, bacteria and exogenous substances. Antibodies have specific affinity for the corresponding target molecules (antigens), and are considered the most useful and powerful tool for analytical, biochemical and clinical techniques, such as enzyme-linked and radioimmunoassay, immunoprecipitation, immunostaining and western blotting, because their target molecules are easily identified and captured from complex matrices, including blood, cells, tissues, and other biological and artificial fluids. In recent years, several biosensors have been developed that use antibody coupled with the detection systems of surface plasmon resonance (SPR) [1], quartz crystal microbalance (QCM) [2] and fluorescence resonance energy transfer (FRET) [3]. However, it is difficult and requires a lot of effort and time to prepare and obtain target-specific antibodies, especially monoclonal antibodies, because of *in vivo* materials from animal sources, in addition, the difficulty depends on the target molecules and the biological properties of immunological tolerance and toxic potential. These constraints place limits on the range of antibodies available to us.

On the other hand, aptamers are single-stranded DNA and RNA oligonucleotides that fold into unique secondary or ternary structures, such as hairpin, bulge, pseudoknot and G-quartet, which have the potential to capture a ligand (target) molecule similarly to antibodies. By *in vitro* selection, namely, systematic evolution of ligands by exponential enrichment (SELEX) [4, 5], it is possible in principle to prepare and obtain aptamers easily for unlimited target molecules. There have been several different kinds of aptamers developed for amino acids, medicines, nucleic acids, vitamins, peptides and proteins [6]. The SELEX approach is based on affinity selection from a very large DNA or RNA library with random sequences. In general, SELEX is carried out by the following three-step process that forms a single round, which consists of (i) the isolation of DNAs or RNAs bound to target molecules from a reaction mixture of DNA or RNA library by affinity-based techniques, (ii) the amplification of the isolated DNAs or RNAs by (RT-)PCR and (iii) the estimation of the affinity for a target molecule. Several assay techniques such as nitrocellulose filtration, affinity chromatography and affinity bead-based assay have been employed for studies on the binding activities of aptamers with their target molecules, but these techniques only enable semi-quantitative measurement.

In our previous report, aptamer-based binding assays with intercalating dyes of ethidium bromide (EtBr), SYBR Gold and SYBR Green II have already been described using microchip electrophoresis (ME) coupled with fluorescence detection [7]. ME and capillary electrophoresis are useful for many kinds of ligand binding assays because of their high separation efficiency as a B/F separation system and the minimal sample volume. Our approach has the advantages that the unbound (free) aptamer can be separated from aptamer-protein complex on a microchip in a short time, and there is no need to prepare modifications such as fluorescence labeling and immobilization as shown in Fig. (**1**). It was observed that the intensity of peaks of unbound aptamers was decreased with the increase in the corresponding protein concentration, and then each calibration curve was obtained with high sensitivity as expected. In this study, by using ME to estimate the binding activity in SELEX rounds,

*Address correspondence to this author at the School of Pharmacy, Showa University, 1-5-8 Hatanodai, Shinagawa, Tokyo 142-8555, Japan; Tel: +81-3-3784-8194; Fax: +81-3-3784-8247;
E-mail: arakawa@pharm.showa-u.ac.jp

1875-3973/12 2012 Bentham Open

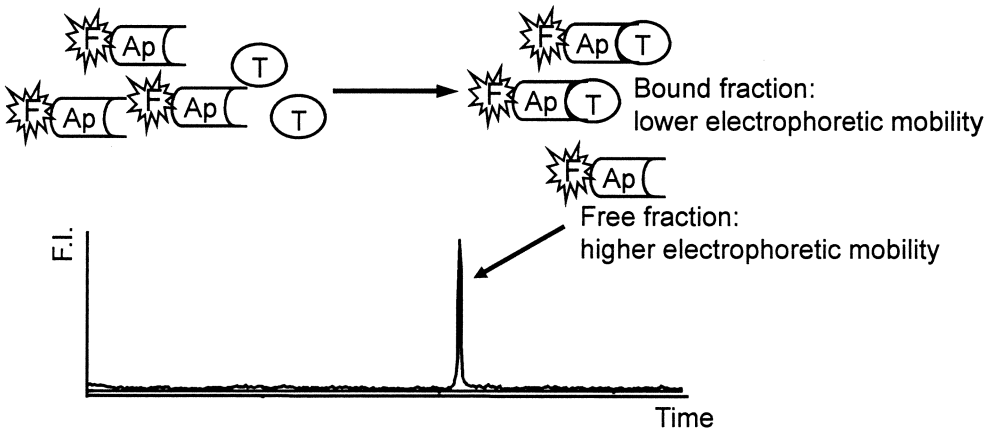


Fig. (1). Principle of aptamer-based binding assay by microchip electrophoresis: Ap, aptamer; F, fluorescent intercalating dye; T, target molecule; F.I., fluorescence intensity.

we have tried to develop an efficient novel RNA aptamer for human menopausal gonadotropin (hMG) related to human chorionic gonadotropin (hCG) and applied it to aptamer-based binding assay, since our previous report demonstrates the clinical significance of developing a sensitive immunoassay of hCG for use in quality control and diagnosis [8].

EXPERIMENTAL

Materials and Methods

Template DNA for RNA library and primers for PCR amplification and RNA synthesis were obtained from Takara Bio Inc. (Shiga, Japan). Template DNA (60 bases) was designed with primer sequences of 15 bases at both ends for PCR amplification and a randomized sequence of 30 bases in the middle region. The sequences are as follows:

template DNA: 5'-GGTAGATACGATGGA-N30-CATGAC GCGCAGCCA-3', 5'-end primer: 5'-AGTAATACGACTC ACTATAGGTAGATACGATGGA-3' (the underlined sequence is T7 promoter region), 3'-end primer: 5'-TGGCTGCGCGTCATG-3'.

SELEX Procedure

SELEX was carried out in accordance with a previous report. In brief, the single-stranded template DNA (4.5 nmol) was converted into double-stranded DNA by PCR, by the following procedure: 94 °C for 1 min (94 °C for 1 min, 55 °C for 1 min, 72 °C for 1 min) x 3 cycles, with 3'-end primer (4.5 nmol). The reaction mixture was re-amplified by PCR, by the following procedure: (94 °C for 1 min, 55 °C for 1 min, 72 °C for 1 min) x 3 cycles, with 5'-end and 3'-end primers (1 nmol each), and the resultant solution was purified by ethanol precipitation. For RNA synthesis, PCR product of 79 base pairs was subjected to *in vitro* transcription with T7 RNA polymerase (T7 Ampliscribe kit, Epicentre Technology) and purified by spin down with a Bio-spin 30 (Bio-Rad Laboratories, Hercules, CA). The obtained 60 bases RNA library was used for SELEX, in which the appropriate amount of RNA was dissolved with 50 mmol/L Tris-HCl buffer (pH 7.6) containing 5 mmol/L $MgCl_2$, 25 mmol/L NaCl and 25 mmol/L KCl, and was heated at 90 °C for 2 min and then slowly cooled to room temperature. The RNA solution was premixed with target molecule (hMG) and incubated at room temperature for 0.5–60 min, and the reaction mixture was passed through a nitrocellulose filter (HAWP filter, 0.45 μm, Millipore). The RNAs bound to hMG were retained on the filter, and recovered with the same buffer heated at 90 °C for 5 min. The recovered RNA was again passed through a fresh nitrocellulose filter to remove proteins and RNAs nonspecifically bound to the filter. The eluted RNA was recovered and purified by ethanol precipitation. The purified RNA was reverse-transcribed with avian myeloblastosis virus (AMV, Wako Pure Chemicals) with 3'-end primer at 42 °C for 60 min, and the obtained cDNA was amplified by PCR, 94 °C for 1 min (94 °C for 1 min, 55 °C for 0.75 min, 72 °C for 1 min) x 10–15 cycles, with 5'-end and 3'-end primers. The PCR product was recovered by ethanol precipitation, and transcribed into RNA with T7 RNA polymerase at 37 °C for 2 h, and the reaction mixture was purified by 8% (w/v) polyacrylamide gel electrophoresis (PAGE) on gel containing 7 mol/L urea. The amount of newly obtained RNA library was determined by absorption spectrometry at 260 nm and subjected to the next SELEX round.

Microchip Electrophoresis

For aptamer-based binding assay with RNA obtained in each round, ME was performed using a cosmo-*i* SV1100 from Hitachi Electronics Engineering Co. Ltd. (Tokyo, Japan), and a Hitachi Chemical microchip, which is designed in a cross type channels for the injection with a 10 mm and the separation with a 45 mm in length, a 0.1 mm in width and a 0.03 mm in depth, and is fabricated with polymethyl methacrylate (PMMA) as shown in Fig. (**2**). The channel was filled with 0.5% hydroxypropyl methylcellulose (HPMC, Sigma-Aldrich, St. Louis, MO) in 1 x TBE buffer containing 0.5 μg/mL EtBr or 10,000-fold dilution of SYBR Green II (Invitrogen, Carlsbad, CA) for fluorescence detection. The sample solutions were prepared with RNA libraries and hMG protein as described in the SELEX procedure and were incubated for 30 min at room temperature; then, fluorescein as the internal standard was added before the measurements. The sample solution (10 μL) was subjected to ME in triplicate.

The electrophoresis was performed with an injection voltage of 300 V for 60 sec, and at separation and return

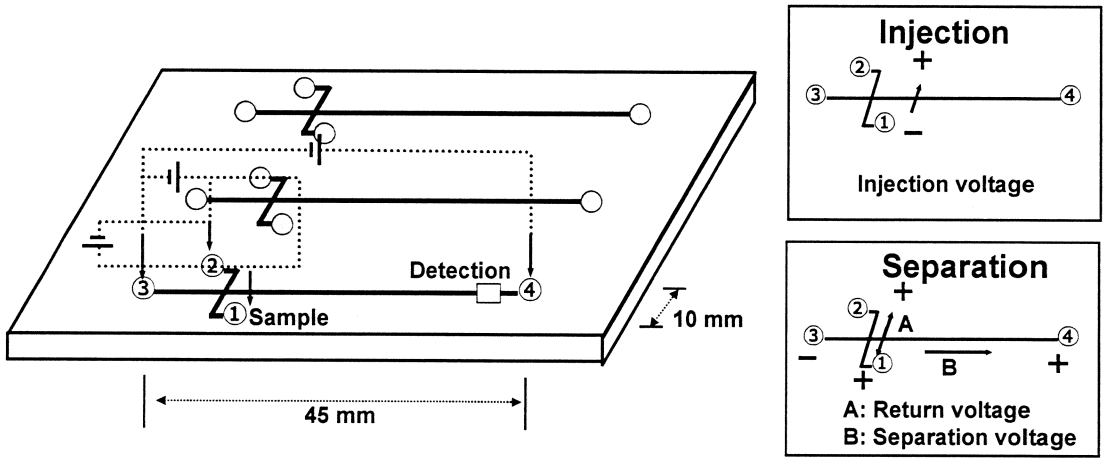


Fig. (2). Schematic illustration of microchip electrophoresis.

voltages of 750 V and 180 V, respectively, for 180 sec simultaneously. On the obtained electropherograms, the peak height for RNA was normalized with the peak height for fluorescein as the internal standard.

RESULTS AND DISCUSSION

RNA template (60 bases) was initially obtained from single-stranded DNA template (60 bases) by PCR and subsequent *in vitro* transcription, and was subjected to 12 successive rounds of selection. In the first round of selection, the randomized RNA library, which contains approximately 10^{15} molecules (4.5 nmol), was mixed and incubated with 0.5 nmol hMG. As SELEX rounds progressed, the binding conditions were restricted to refine RNA library to those RNAs with higher affinity for hMG. Over the whole SELEX rounds, the reaction time was gradually decreased; in addition, the amounts of template RNAs and hMG and number of PCR cycles were decreased in the last two rounds. As a result, specific RNA libraries were obtained in each round, and the detailed SELEX conditions and the resultant amounts of recovered RNA are shown in Table **1**.

Next, to estimate the binding activity of each round of RNAs, the reaction mixture of RNAs and hMG was subjected to ME using EtBr for ligand binding assay after each round of selection. Typical electropherograms are shown in Fig. (**3**), which were produced using the 11th generation of RNA (G11 RNA). As shown in Fig. (**3A**), an electropherogram of one peak around 60 sec was obtained using unheated G11 RNA alone. However, the heated G11 RNA provided two major peaks (Fig. **3B**), suggesting that, by heating and slowly cooling, RNA molecules would fold into unique secondary and ternary conformations (functional structures) from a non-specific single-stranded conformation. This result is consistent with our previous reports of the separation and detection of single nucleotide polymorphisms (SNPs) by capillary electrophoresis on the basis of single-strand DNA conformation polymorphism (SSCP) [9, 10]. Furthermore, the different kinds of conformations could be

Table 1. Conditions and Results of SELEX

Generation	Template RNA (pmol)	hMG (pmol)	Reaction time (min)	PCR (cycle)	Recovered RNA (pmol)
1	2000	500	60	15	5688
2	2844	711	45	15	6004
3	2002	501	30	15	5072
4	2454	614	20	15	5508
5	2754	689	10	15	5238
6	2619	655	5	15	5358
7	2679	670	2.5	15	5400
8	2524	631	1.5	15	4692
9	2346	587	1	15	4836
10	2418	605	0.5	15	5040
11	1000	250	0.5	10	1212
12	500	125	0.5	10	645

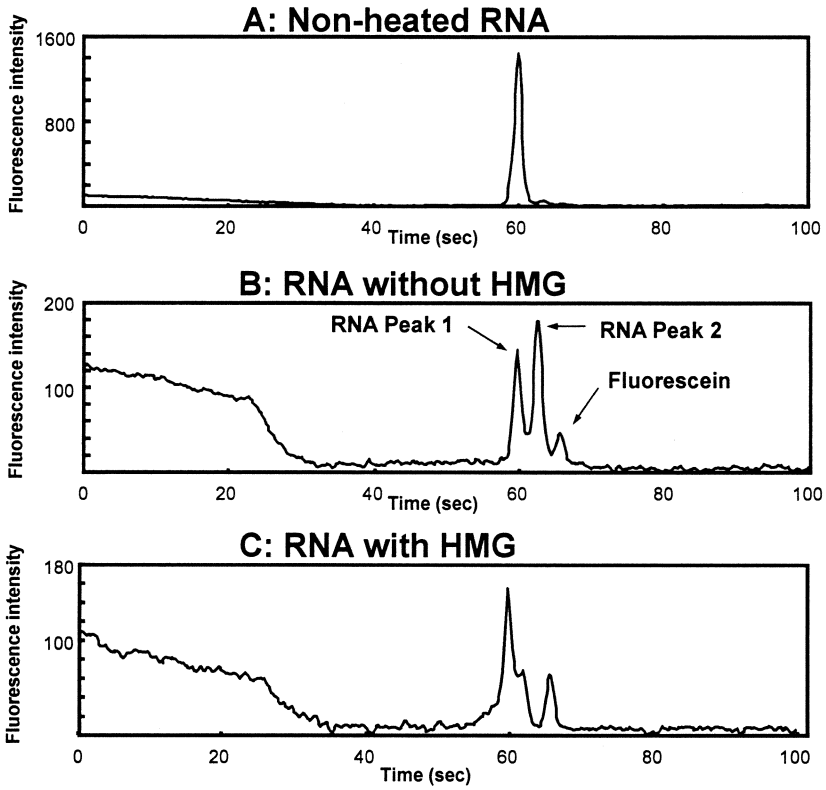


Fig. (3). Electropherograms for aptamer-based binding assays.

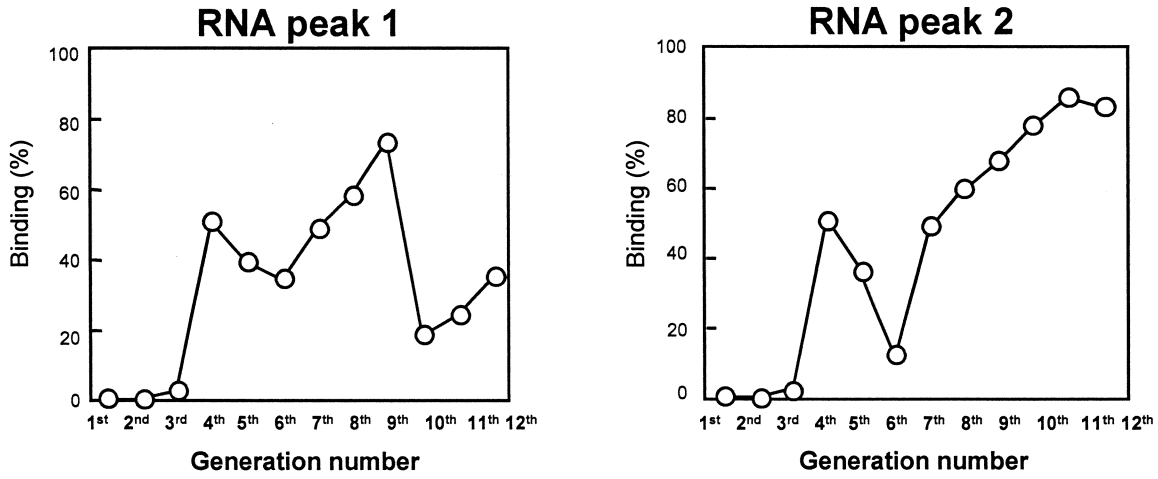


Fig. (4). Binding activities of aptamers obtained in each round for hMG.

efficiently separated on ME. Fig. (**3C**) shows the result of the reaction mixture of G11 RNA and hMG, indicating that the second peak (peak 2) of G11 RNA was decreased in the presence of hMG, but the first peak (peak 1) showed little change. Therefore, peak 2 should correspond to the RNAs with higher affinity for hMG compared with peak 1. On the other hand, no peak corresponding to RNA-hMG complex was observed under the proposed separation mode and conditions. Fig. (**4**) shows the binding activities of G1–G12 RNAs obtained from the peak heights of peaks 1 and 2. The binding activities of peak 2 were improved with the increase in the rounds of selection. Among G1–G12 RNAs, peak 2 of G11 RNA showed the highest binding activity for hMG, so G11 RNA was applied to aptamer-based binding assay with EtBr and SYBR Green II for highly sensitive fluorescence detection. As a result, the intensity of peak 2 of G11 RNA was decreased with an increase in hMG concentration, and then the standard curves for hMG were obtained over the concentration range of 1–200 pmol/assay using EtBr, and 0.1–10 pmol/assay using SYBR Green II as shown in Fig. (**5**). The reasons for the sensitivity are that SYBR Green II exhibits higher fluorescence quantum yield with single-stranded RNA, and its excitation wavelength is suitable for the blue LED of the light source on the device. In the pro-

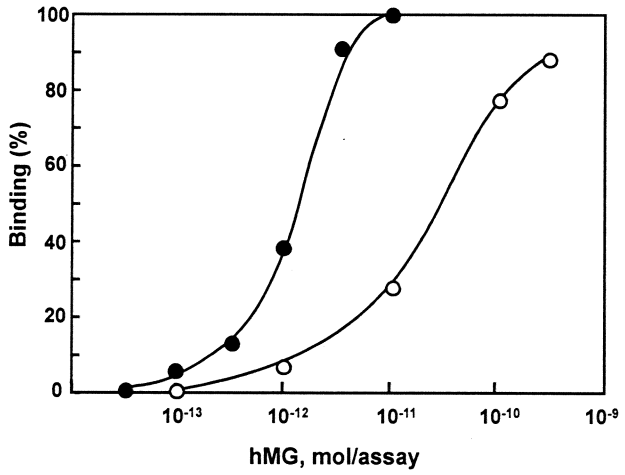


Fig. (5). Standard curves for hMG with EtBr (open circle) and SYBR Green II (closed circle).

posed aptamer-based binding assays, 50 pmol/assay RNA was used with SYBR Green II compared with the assay with EtBr in which 200 pmol/assay RNA was used. Finally, the proposed assay was applied to hMG in pharmaceutical preparations for injection. Since protein (hormonal) activities alone were found in their package insert irrespective of the hMG concentration level, their dilution curves were evaluated. As a result, linear curves were obtained without matrix effects from two samples (data not shown). It was demonstrated that G11 RNA could exhibit a level of performance in the binding assay equal to that of antibody.

In conclusion, by the 12 successive rounds of selection and the binding assay on ME, G11 RNA was obtained as an hMG-specific aptamer. ME is a rapid and simple platform for a binding assay compared with conventional assays such as filter binding assay and affinity chromatography. The electrophoretic separation appears to be an effective technique for oligonucleotide molecules, and it could be a useful approach for efficient aptamer development to fractionate DNA and RNA molecules on the basis of conformational differences. We have been conducting further studies on the potential use of capillary electrophoresis and ME for aptamer development.

ACKNOWLEDGEMENT

None Declared.

CONFLICTS OF INTEREST

None Declared.

REFERENCES

[1] Soelberg SD, Stevens RC, Limaye AP, Furlong CE. Surface plasmon resonance detection using antibody-linked magnetic nanoparticles for analyte capture, purification, concentration, and signal amplification. Anal Chem 2009; 81: 2357-63.

[2] Shen Z, Mernaugh RL, Yan H, Yu L, Zhang Y, Zeng X. Engineered recombinant single-chain fragment variable antibody for immunosensors. Anal Chem 2005; 77: 6834-42.

[3] Enomoto K, Araki A, Nakajima T, *et al.* High-throughput miniaturized immunoassay for human interleukin-13 secreted from NK3.3 cells using homogenous time-resolved fluorescence. J Pharm Biomed Anal 2002; 28: 73-9.

[4] Tuerk C, Gold L. Systematic evolution of ligands by exponential enrichment : RNA ligands to Bacteriophage T4 DNA polymerase. Science 1990; 249: 505-10.

[5] Ellington AD, Szostak JW. *In vitro* selection of RNA molecules that bind specific ligands. Nature 1990; 346: 818-22.

[6] Stoltenburg R, Reinemann C, Strehlitz B. SELEX-a (r)evolutionary method to generate high-affinity nucleic acid ligands. Biomol Eng 2007; 24: 381-403.

[7] Nishikawa F, Arakawa H, Nishikawa S. Application of microchip electrophoresis in the analysis of RNA aptamer-protein interactions. Nucleosides Nucleotides Nucleic Acids 2006; 25: 369-82.

[8] Arakawa H, Shiokawa M, Imamura O, Maeda M. Novel bioluminescent assay of alkaline phosphatase using adenosine-3'-phosphate-5'phosphosulfate as substrate and the luciferin-luciferase reaction and its application. Anal Biochem 2003; 314: 206-11.

[9] Arakawa H, Nakashiro S, Maeda M, Tsuji A. Analysis of single-strand DNA conformation polymorphism by capillary electrophoresis. J Chromatogr A 1996; 722: 359-68.

[10] Arakawa H, Igarashi H, Kashiwazaki H, Maeda M, Tokita A, Yamashiro Y. Single-stranded conformation polymorphism analysis of Vitamin D recepter gene by capillary electrophoresis with laser-induced fluorescence detection. Anal Chim Acta 2001; 445: 197-204.

Received: July 13, 2011 Revised: December 19, 2011 Accepted: December 23, 2011

© Ohno *et al.*; Licensee *Bentham Open.*

This is an open access article licensed under the terms of the Creative Commons Attribution Non-Commercial License (http://creativecommons.org/licenses/by-nc/3.0/) which permits unrestricted, non-commercial use, distribution and reproduction in any medium, provided the work is properly cited.

Bioorganic & Medicinal Chemistry 19 (2011) 3558–3568

Contents lists available at ScienceDirect

Bioorganic & Medicinal Chemistry

journal homepage: www.elsevier.com/locate/bmc

Docking and SAR studies of D- and L-isofagomine isomers as human β-glucocerebrosidase inhibitors

Atsushi Kato [a,*], Saori Miyauchi [a], Noriko Kato [a], Robert J. Nash [b], Yuichi Yoshimura [c], Izumi Nakagome [d], Shuichi Hirono [d], Hiroki Takahata [c], Isao Adachi [a]

[a] Department of Hospital Pharmacy, University of Toyama, Toyama 930-0194, Japan
[b] Institute of Biological, Environmental and Rural Sciences/Phytoquest Limited, Plas Gogerddan, Aberystwyth, Ceredigion SY23 3EB, United Kingdom
[c] Faculty of Pharmaceutical Sciences, Tohoku Pharmaceutical University, Sendai 981-8558, Japan
[d] School of Pharmaceutical Sciences, Kitasato University, Tokyo 108-8641, Japan

ARTICLE INFO

Article history:
Received 16 March 2011
Revised 5 April 2011
Accepted 7 April 2011
Available online 13 April 2011

Keywords:
Isofagomine
Fagomine
Structure–activity relationships
Molecular docking study
β-Glucocerebrosidase
Glycosidase inhibitor
Pharmacological chaperone

ABSTRACT

We report the structure–activity relationship of a series of D-, and L-isofagomine and fagomine isomers as glycosidase inhibitors. Our study revealed that a positive charge at the anomeric position of D-isofagomines enhanced the potency toward β-glycosidases, while the epimerization at the C3 OH group drastically reduced their inhibitory potency by over three orders of magnitude. Furthermore, D-3,4-di-*epi*-isofagomine abolished their inhibition activities against all enzymes. L-Isofagomine was also a fairly potent inhibitor of human β-glucocerebrosidase, with an IC_{50} value of 8.7 μM. A molecular docking study revealed that the positions and orientations of the piperidine ring of D-3-*epi*-isofagomine in the binding site was similar to that of D-isofagomine, while D-3-*epi*-isofagomine missed the hydrogen bond interactions between Asp127 and the 3-OH group and between Trp179 and the 3-OH group. Furthermore, the top 10 docking models ranked by IFDscore suggested that D-3,4-di-*epi*-isofagomine can not bind to β-glucocerebrosidase at a stable interaction mode. These results provide an insight into the structural requirements of isofagomine isomers for developing a new type of pharmacological chaperone for Gaucher disease.

© 2011 Elsevier Ltd. All rights reserved.

1. Introduction

Iminosugars are sugar mimics with a nitrogen atom in place of the ring oxygen of monosaccharides. The biological properties can be explained by their structural resemblance to the terminal sugar moiety in the natural substrates. Glycosidases are involved in several important biological processes, such as intestinal digestion, post-translational processing of the glycoproteins, lysosomal catabolism of glycoconjugates, and quality-control systems in the endoplasmic reticulum (ER) and the ER-associated degradation (ERAD) mechanism. Furthermore, the scope of their biological activity has been extended to the inhibition of a number of enzymes such as glycosyltransferases and glycogen phosphorylases. Hence, there is great interest in utilizing these inhibitors to discover novel therapeutic agents. To date, around 200 natural products are known that may be described as carbohydrate mimics in which the ring oxygen of a sugar is replaced by nitrogen.[1] Recently, modifications of the core naturally-occurring iminosugars have been developed to give sub-nanomolar inhibition of α-L-fucosidases,[2] α-L-rhamnosidases,[3] α-*N*-acetyl-galactosaminidases.[4] These designed inhibitors are mainly focused on the enantiomers of the natural D-iminosugars. We have previously reported that these synthetic enantiomers were frequently powerful glycosidase inhibitors.[5,6] For example, the unnatural enantiomer 1,4-dideoxy-1,4-imino-L-arabinitol (LAB) is a more potent and more specific inhibitor of α-glucosidases than the natural product 1,4-dideoxy-1,4-imino-D-arabinitol (DAB). Furthermore, in the course of designing unnatural iminosugars, we found 1,4-dideoxy-2-hydroxymethyl-1,4-imino-D-threitol (isoDAB), which is a pyrrolidine bearing a branched carbon chain, is a potent and specific inhibitor of rice α-glucosidase and rat intestinal maltase, with K_i value of 4 and 6 μM, respectively.[7] It is therefore necessary to elucidate the structural requirements for the design of selective glycosidase inhibitors involving both enantiomers.

In this paper, we focused on the 1-*N*-iminosugar isofagomine in which a nitrogen atom is at the anomeric position of a monosaccharide. There are some reports and reviews on in vitro glycosidase inhibition by D-isofagomine and its derivatives.[8–10] D-Isofagomine was reported as the most potent inhibitor of β-glucocerebrosidase in vitro and the most effective pharmacological chaperone capable of increasing residual β-glucocerebrosidase activity in N370S fibroblasts. Intracellular β-glucocerebrosidase activity increased approximately twofold when cells were incubated with D-isofagomine. D-Isofagomine (Plicera) has proceeded to Phase II clinical tri-

* Corresponding author.
E-mail address: kato@med.u-toyama.ac.jp (A. Kato).

0968-0896/$ - see front matter © 2011 Elsevier Ltd. All rights reserved.
doi:10.1016/j.bmc.2011.04.011

als for the treatment of Gaucher disease but it has been finally withdrawn from clinical trials due to lack of efficacy. To get closer to therapeutic application, we decided to further systematically study the biological properties of the enantiomers of isofagomine and other diastereomers of isofagomine. Herein, we report the syntheses of both enantiomers of isofagomine, 3-*epi*-isofagomine, 4-*epi*-isofagomine, 3,4-di-*epi*-isofagomine and systematic studies of their glycosidase inhibitory activities. An additional aim of ours was to synthesize both enantiomers of fagomine isomers and investigated the structure–activity relationships of isofagomine and fagomine isomers from the viewpoint of the position of the nitrogen atom and different configurations of OH groups. Furthermore, we investigate the molecular docking properties of all D-isofagomine isomers toward β-glucocerebrosidase by using Induced Fit Docking score.

2. Results and discussion

2.1. Preparation of D- and L-isofagomine isomers

In general, most syntheses of iminosugars are performed by transforming carbohydrate derivatives as the chiral starting materials. However, this procedure is not always suited for obtaining all stereoisomers. Accordingly, our synthesis began with an appropriate common chiral building block readily available from starting materials.

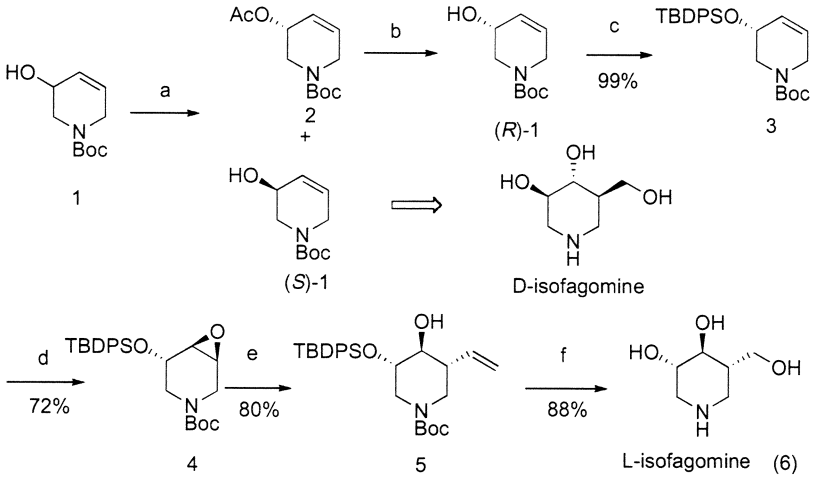
Both enantiomers of isofagomine (**6**) were synthesized in a highly stereocontrolled mode from *N*-Boc-5-hydroxy-3-piperidene **1** as a common chiral building block according to our previous report.[11] The lipase-catalyzed trans-esterification of **1** with vinyl acetate gave the acetate **2** along with the unreacted alcohol (*S*)-**1**, The enzymatic hydrolysis of the acetate **2** with the same lipase in 0.1 M phosphate buffer afforded the enantiometic alcohol (*R*)-**1**. With both enantiomers **1** in hand, (*R*)-**1** was transformed to L-isofagomine (**6**) via stereoselective epoxidation and regioselective ring-cleavage with higher ordered cuprates in a highly stereocontrolled manner as shown in Scheme 1. Other isomers L-3-*epi*-isofagomine (**10**), L-4-*epi*-isofagomine (**11**), and L-3,4-di-*epi*-isofagomine (**14**) were prepared from 5-hydroxymethyl-3-piperidene (**8**), which was obtained by [2,3]-Stille–Wittig rearrangement of *O*-tributylstannylmethyl-3-piperidene **7** derived from readily available (*R*)-**1**. This rearrangement of **7** by transmetallation using *n*-BuLi proceeded smoothly in a nonpolar solvent such as *n*-pentane with no racemization. Thus, the prepared hydroxymethylpiperidine **8** was transformed by dihydroxylation, and epoxidation into stereoisomers **10**, **11**, and **14** of isofagomine as exhibited in Scheme 2.[12] D-Forms of **6**, **10**, **11**, and **14** were prepared from (*S*)-**1** according to procedures similar to those described above.

2.2. Inhibition effects of D- and L-isofagomine isomers on various glycosidases

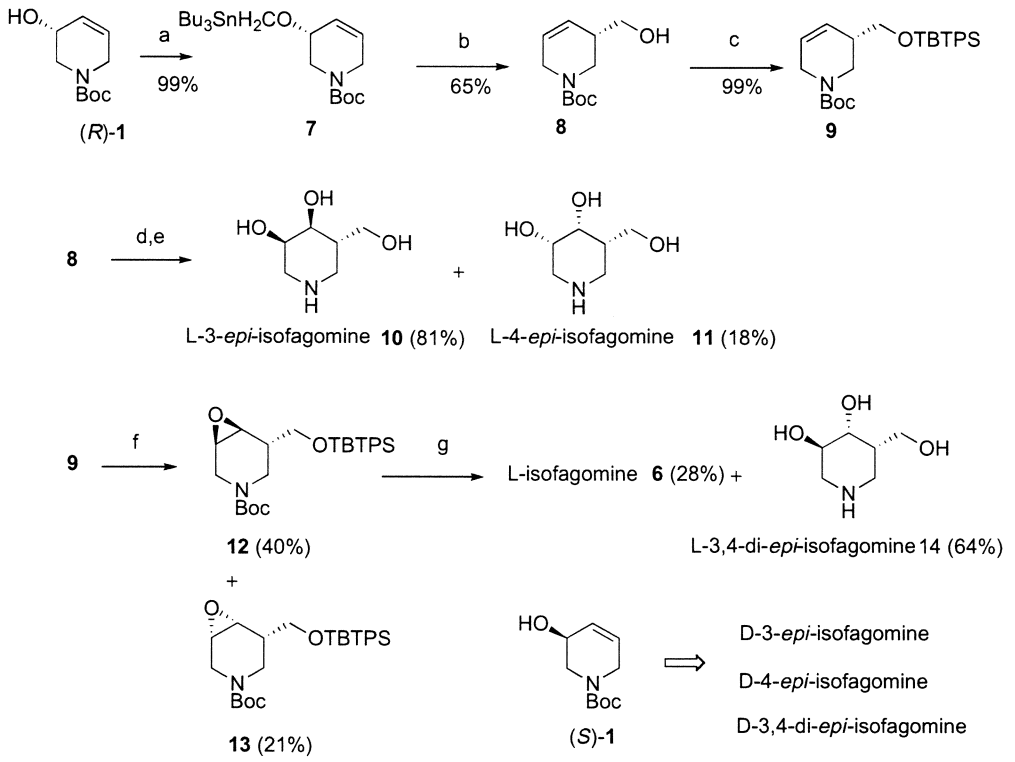
The IC_{50} values of the D- and L-enantiomers of isofagomine isomers toward a variety of glycosidases are shown in Table 1. D-Isofagomine is known to be a potent inhibitor of all types of β-glucosidases. Especially, D-isofagomine was an extremely powerful inhibitor of human lysosomal β-glucosidase (β-glucocerebrosidase), with an IC_{50} value of 0.063 μM. Furthermore, its enantiomer L-isofagomine was also a fairly potent inhibitor of this enzyme, with IC_{50} value of 8.7 μM. L-Isofagomine is a better inhibitor than D-isofagomine of rat intestinal sucrase. In the present study, D-isofagomine was also found to be a potent inhibitor of bovine liver β-galactosidase and rat intestinal lactase, with IC_{50} values of 3.6 and 0.12 μM, respectively. In addition, D-4-*epi*-isofagomine as a D-galactose-type 1-*N*-iminosugar was a potent inhibitor of both rat intestinal cellobiase and lactase, with IC_{50} values of 4.5 and 0.51 μM, respectively. These results suggested that the stereochemistry at the C4 OH group of 1-*N*-iminosugars was not strictly distinguished by β-glucosidases and β-galactosidases. To date, around 200 natural products are known that may be described as carbohydrate mimics. While these naturally-occurring iminosugars are analogues of monosaccharides in which the ring oxygen has been replaced by nitrogen atom, synthesized 1-*N*-iminosugars have a nitrogen atom at the anomeric position of a monosaccharide ring. Therefore, we compared the inhibition spectrum and potency of isofagomine and fagomine isomers against various glycosidases from the viewpoint of the position of the nitrogen atom and different configurations of OH groups (Fig. 1).

2.3. Preparation of D- and L-fagomine isomers

Fagomine was first isolated from buckwheat seeds (*Fagopyrum esulentum* Moenchi) and subsequently isolated from seeds of *Castanospermum australe* (Leguminosae).[13,14] We have previously



Scheme 1. Reagents and conditions: (a) vinyl acetate, lipase PS (immobilized on ceramic particles), *t*-BuOMe; (b) lipase PS (immobilized on ceramic particles), 0.1 M phosphate buffer (pH 7), acetone; (c) TBDPSCl, imidazole, cat. DMAP, CH_2Cl_2; (d) Oxone, aq Na_2EDTA, $NaHCO_3$, CF_3COCH_3, CH_3CN; (e) $(CH_2{=}CH)_2CuCNLi_2$), BF_3, OEt_2, Et_2O; (f) (1) cat. OsO_4, $NaIO_4$, 50% EtOH; (2) $NaBH_4$, 50% EtOH; (3) 10% HCl, dioxane; (4) NH_4OH.



Scheme 2. Reagents and conditions: (a) Bu_3SnCH_2Cl, KH, THF; (b) *n*-BuLi, *n*-pentane; (c) TBDPSCl, imidazole, cat. DMAP, CH_2Cl_2; (d) cat. OsO_4, NMO; (e) (1) concd HCl, CH_3OH, H; (2) NH_4OH; (f) Oxone, CF_3COCH_3, Na_2EDTA, $NaHCO_3$, CH_3CN; (g) (1) 0.3 M KOH, 1,4-dioxane; (2) 6 N HCl; (3) NH_4OH.

Table 1
Concentration of D- and L-isofagomine isomers giving 50% inhibition of various glycosidases

Enzyme	IC_{50} (μM)							
	Isofagomine		3-*epi*-Isofagomine		3,4-di-*epi*-Isofagomine		4-*epi*-Isofagomine	
	D	L	D	L	D	L	D	L
α-Glucosidase								
Rice	NI[a]	NI	NI	NI	NI	NI	NI	NI
Rat intestinal maltase	653	NI	NI	NI	NI	NI	NI	NI
Rat intestinal isomaltase	290	NI	NI	NI	NI	NI	NI	NI
Rat intestinal sucrase	531	34	NI	NI	NI	NI	NI	NI
β-Glucosidase								
Almond	0.98	236	443	NI	NI	NI	3.2	983
Rat intestinal cellobiase	0.30	110	334	NI	912	NI	4.5	607
Bovine liver	31	611	NI	NI	NI	676	63	NI
Human lysosome	0.063	8.7	113	NI	NI	NI	54	NI
α-Galactosidase								
Coffee beans	NI	NI	NI	NI	NI	NI	144	450
β-Galactosidase								
Bovine liver	3.6	821	NI	NI	NI	389	21	NI
Rat intestinal lactase	0.12	20	52	469	211	646	0.51	90
α-Mannosidase								
Jack beans	NI	NI	NI	NI	NI	NI	NI	NI
β-Mannosidase								
snail	NI	NI	NI	NI	NI	NI	NI	NI
α-L-Fucosidase								
Bovine epididymis	NI	NI	NI	NI	NI	NI	NI	NI
α-L-Rhamnosidase								
P. decumbens	NI	NI	NI	NI	NI	NI	NI	NI

[a] NI: no inhibition (less than 50% inhibition at 1000 μM).

reported that fagomine and its 3-OH epimer occurs abundantly in the leaves and roots of *Xanthocercis zambesiaca*, growing in dry forest and woodland of southern Africa.[15] Fagomine and its 4-*O*-β-D-glucopyranoside were found to have a potent antihyperglycemic

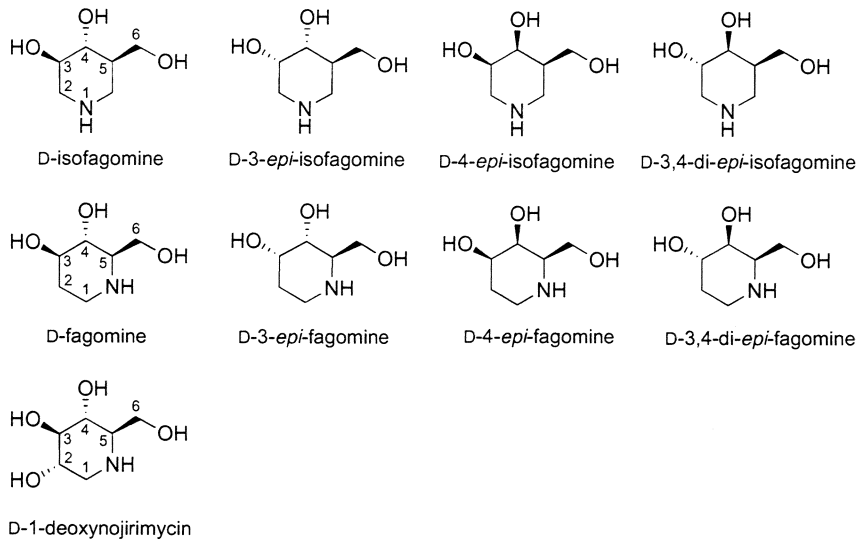


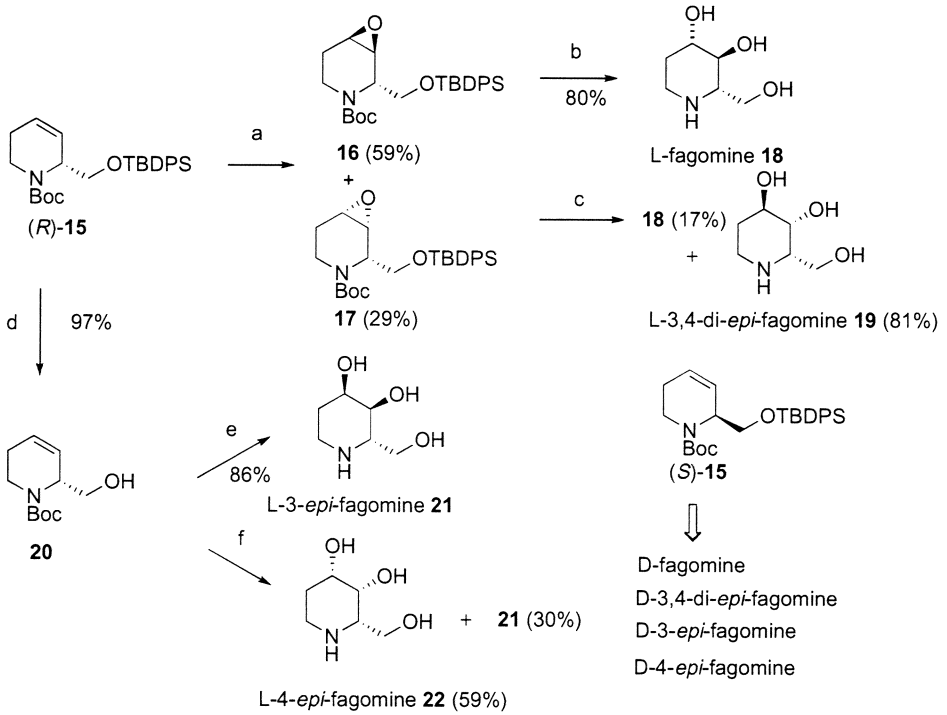
Figure 1. Structural relationship of D-isofagomine isomers, D-fagomine isomers, and D-1-deoxynojirimycin.

effect in streptozotocin-induced diabetic mice and to potentiate markedly insulin release.[16]

The synthesis of D-forms of fagomine and its stereoisomers from 6-silyloxymethylpiperidines (*S*)-**15** as Garner aldehyde-derived chiral building blocks was reported by us.[17] The preparation of L-forms was conducted by almost the same procedure as that reported as shown in Scheme 3. Epoxidation of (*R*)-**15** gave two stereoisomers **16** and **17**. *trans*-Epoxide **16** was hydrolyzed with acid to provide L-fagomine (**18**) as a single product. On the other hand, hydrolysis of *cis*-epoxide **17** with base provided L-3,4-di-*epi*-fagomine **19** as a major product together with a small amount of **18**. Desilylation of **15** afforded hydroxymethylpiperidine **20**. Dihydroxylation of **20** with a modified Upjohn condition gave L-3-*epi*-fagomine **21** as a single diastereomer, while the homoallylic alcohol-directed of **20** with OsO_4–TMEDA complex[18] provided L-4-*epi*-fagomine **22** as a major diastereomer accompanied by **21**.

2.4. Inhibition effects of D- and L-fagomine isomers on various glycosidases

As shown in Table 2, D-fagomine is a moderate inhibitor of rat intestinal isomaltase and sucrase with IC_{50} values of 37 and 34 μM, respectively. However, the potency of inhibition against



Scheme 3. Reagents and conditions: (a) Oxone, CF_3COCH_3, $NaHCO_3$, aq Na_2, EDTA, CH_3CN; (b) (1) H_2SO_4, 1,4-dioxane, H_2O; (2) Amberlite IRA-410; (c) KOH, 1,4-dioxane, H_2O; (2) HCl, CH_3OH; (3) Amberlite IRA-410;(d) TBAF, THF; (e) (1) cat. $K_2OsO_4{\cdot}2H_2O$, NMO, H_2O; (2) 10% HCl; (3) Amberlite IRA-410; (f) (1) OsO_4, TMEDA, CH_2Cl_2; (2) 35% HCl, MeOH; (3) Amberlite IRA-410.

these enzymes was much weaker than the conventional glucose-type iminosugar D-1-deoxynojirimycin, which showed IC_{50} values of 0.65 and 0.51 μM. This behavior is similar to that of D-4-*epi*-fagomine which was found to be a potent and selective inhibitor of coffee bean α-galactosidase with IC_{50} values of 8 μM but this value is over three orders of magnitude weaker than the galactose-type iminosugar D-1-deoxygalactonojirimycin. We have previously reported that L-1-deoxygalactonojirimycin, which can be regarded as the C6 hydroxylated derivative of L-1-deoxyfuconojirimycin, was a potent competitive inhibitor of bovine epididymis α-L-fucosidase with IC_{50} and K_i values of 0.63 and 0.080 μM, respectively.[6] However, this study revealed that L-4-*epi*-fagomine, which can be regarded as the 2-deoxy derivative of L-1-deoxygalactonojirimycin was completely inactive against this enzyme. These results suggested that the presence of the C2 OH group in the iminosugar piperidine ring is an essential feature for recognition and strong binding by the active site of glycosidases. Interestingly, while the structure of the 1-*N*-iminosugars does not have a C2 OH group, isofagomine showed potent inhibition against β-glucosidases and β-galactosidases. However, the epimerization at the C3 OH group in D-isofagomine drastically reduced its inhibitory potency by over three orders of magnitude against β-glucosidases and β-galactosidases (Table 1). In contrast, the epimerization at the C3 OH group in D-fagomine enhanced the inhibitory potency toward these enzymes and abolished inhibition toward α-glucosidases. From the results of these structure–activity relationships, we concluded that a positive charge at the anomeric position shifts the inhibition spectrum from α-glycosidases to β-glycosidases. Stereochemistry at the C4 OH group of 1-*N*-iminosugars was not strictly distinguished by β-glucosidases and β-galactosidases. Moreover, the C3 OH group in isofagomine is a dominant factor for the inhibition of these enzymes. In addition, 3,4-di-*epi*-isofagomine abolished their inhibition activities against all enzymes.

2.5. Induced Fit Docking study of D-isofagomine isomers against human β-glucocerebrosidase

Docking models generated from Induced Fit Docking (Schrödinger Suite 2009, Schrödinger, LLC) were ranked using IFDscore. The top 10 docking models ranked by IFDscore were examined. Interestingly, the variety of poses of ligands, which were extracted from the top 10 ranked docking models for D-isofagomine and D-isofagomine isomers, became increased as the activities of those compounds became weaker. The averaged value of RMSD (Root Mean Square Deviation) between top 1 pose and the other pose was 0.54 Å for D-isofagomine, 1.07 Å for D-4-*epi*-isofagomine, 1.26 Å for D-3-*epi*-isofagomine, and 2.23 Å for D-3,4-di-*epi*-isofagomine) (Fig. 2). The variety of poses for D-3,4-di-*epi*-isofagomine was very large so that a definite binding mode could not be decided. This result suggests that D-3,4-di-*epi*-isofagomine can not bind to β-glucocerebrosidase in a stable interaction mode so that D-3, 4-di-*epi*-isofagomine hardly remains in the binding site of β-glucocerebrosidase.

Top 10 ranked docking models of D-isofagomine, D-4-*epi*-isofagomine and D-3-*epi*-isofagomine were minimized by an OPLS2005 force field and then interaction energies between β-glucocerebrosidase and the ligand were calculated. The best docking model of D-isofagomine was selected based on the interaction energy and was compared with the crystal structure of the β-glucocerebrosidase–D-isofagomine complex. The binding pose in the best docking model of D-isofagomine was almost identical to the binding conformation in the crystal structure of β-glucocerebrosidase–D-isofagomine complex (PDB code: 2NSX) (RMSD: 0.36 Å). In the crystal structure of β-glucocerebrosidase–D-isofagomine complex, the hydroxyl groups of D-isofagomine interact with Asp127, Trp179, Trp381, and Asn396 and the imino group is stabilized by Glu235 and Glu340.[19] The hydrogen bonds formed in the crystal structure of β-glucocerebrosidase–D-isofagomine complex were reproduced successfully in our docking model. These results showed that the

Table 2
Concentration of D- and L-fagomine isomers giving 50% inhibition of various glycosidases

Enzyme	IC_{50} (μM)									
	Fagomine		3-*epi*-Fagomine		3,4-di-*epi*-Fagomine		4-*epi*-Fagomine		1-Deoxynojirimycin	
	D	L	D	L	D	L	D	L	D	L
α-Glucosidase										
Rice	320	NI[a]	120	188	NI	980	NI	NI	0.03	4.3
Rat intestinal maltase	113	NI	NI	357	NI	668	NI	NI	0.65	28
Rat intestinal isomaltase	37	NI	NI	NI	NI	NI	NI	NI	0.65	150
Rat intestinal sucrase	34	NI	NI	225	NI	NI	NI	NI	0.51	18
β-Glucosidase										
Almond	NI	NI	120	NI	NI	NI	NI	NI	80	980
Rat intestinal cellobiase	NI	NI	39	809	NI	NI	NI	NI	327	NI
Bovine liver	250	NI	5.6	NI	NI	NI	NI	NI	NI	NI
Human lysosome	NI	NI	NI	NI	NI	NI	NI	NI	NI	NI
α-Galactosidase										
Coffee beans	NI	NI	NI	NI	NI	NI	8.0	NI	880	NI
β-Galactosidase										
Bovine liver	38	NI	3.0	960	NI	NI	NI	NI	NI	560
Rat intestinal lactase	NI	NI	4.3	122	NI	NI	NI	NI	49	317
α-Mannosidase										
Jack beans	NI	NI	NI	NI	NI	NI	NI	NI	NI	NI
β-Mannosidase										
Snail	NI	NI	NI	NI	NI	NI	NI	NI	NI	NI
α-L-Fucosidase										
Bovine epididymis	NI	NI	NI	260	NI	NI	NI	NI	NI	NI
α-L-Rhamnosidase										
P. decumbens	NI	NI	NI	NI	NI	NI	NI	NI	NI	NI

[a] NI: no inhibition (less than 50% inhibition at 1000 μM).

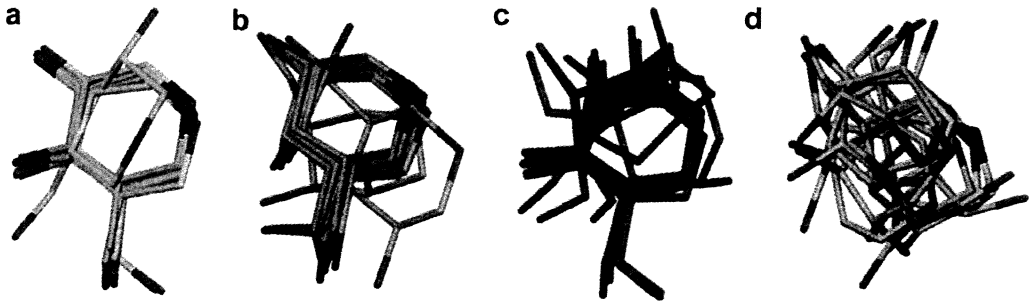


Figure 2. Ligand poses extracted from top 10 docking models ranked by IFDscore. (a) D-isofagomine; (b) D-4-*epi*-isofagomine; (c) D-3-*epi*-isofagomine; (d) D-3,4-di-*epi*-isofagomine.

method using Induced Fit Docking could reproduce the native structure of the β-glucocerebrosidase–ligand complex.

The best docking models for D-3-*epi*-isofagomine and D-4-*epi*-isofagomine were selected and decided as the native docking models that are close to the crystal structures based on the interaction energy. The binding poses were compared between D-isofagomine, D-3-*epi*-isofagomine, and D-4-*epi*-isofagomine. Positions and orientations of the piperidine rings of D-3-*epi*-isofagomine and D-4-*epi*-isofagomine in the binding site were similar to that of D-isofagomine. Orientations of the hydroxyl group of the chiral inversions were only different between D-isofagomine, D-3-*epi*-isofagomine, and D-4-*epi*-isofagomine (Fig. 3). Hydrogen bonds interactions of D-3-*epi*-isofagomine and D-4-*epi*-isofagomine with β-glucocerebrosidase were observed. For D-4-*epi*-isofagomine, one of seven hydrogen bonds, that is, a hydrogen bond interaction between Trp381 of β-glucocerebrosidase and 4-OH group of D-4-*epi*-isofagomine, was absent. For D-3-*epi*-isofagomine, two of seven hydrogen bonds, that is, the hydrogen bond interactions between Asp127 and 3-OH group and between Trp179 and 3-OH group, were missed (Fig. 4). It is likely that one of the reasons for the low activities of D-3-*epi*-isofagomine and D-3,4-di-*epi*-isofagomine is due to a lack of the hydrogen bond interaction between the 3-OH group of each compound and β-glucocerebrosidase (Asp127 and Trp179) caused by the chirality inversion. These results suggested the importance of interactions between the 3-OH group of D-isofagomine and β-glucocerebrosidase.

3. Conclusion

A large number of iminosugars have been isolated from plants and microorganisms.[1] Such sugar mimics have attracted considerable interest because of their ability to effectively and specifically inhibit various glycosidases that are integral to a wide range of important biological processes.[20] Consequently, extensive efforts have been made in recent years to developing methodologies for the asymmetric syntheses of iminosugars. However, the focus of many of these syntheses has been on D-type iminosugar derivatives. On the other hand, there are few reports of systematic studies of the biological properties of the L-enantiomers of iminosugars. In this study, we have synthesized both enantiomers of isofagomine and fagomine isomers in a highly stereocontrolled manner. D-Isofagomine was an extremely powerful inhibitor of human lysosomal β-glucocerebrosidase, with an IC_{50} value of 0.063 μM. Interestingly, its enantiomer L-isofagomine was also a fairly potent inhibitor of this enzyme, with IC_{50} value of 8.7 μM. However, the inhibition potency of the L-form was 10–100 times weaker than its miller image D-form. This behavior is similar to that observed for D-, and L-1-deoxynojirimycin isomers.[6] From the structure–activity relationships of D-isofagomine isomers, the stereochemistry at the C4 OH group was not strictly distinguished by β-glucosidases and β-galactosidases. In contrast, the epimerization at the C3 OH group in D-isofagomine drastically reduced its inhibitory potency over three orders of magnitude on these enzymes (Table 1). Furthermore, D-3,4-di-*epi*-isofagomine abolished their inhibition activities against all enzymes. To understand the structural basis of the interaction of D-isofagomine isomers with β-glucocerebrosidase, we built a docking model generated from Induced Fit Docking by using IFDscore. As a result, we found the averaged values of RMSD between top 1 poses and the other poses for D-3,4-di-*epi*-isofagomine (2.23 Å) was four times larger than for D-isofagomine (0.54 Å) (Fig. 2). Positions and orientations of the piperidine rings of D-3-*epi*-isofagomine in the binding site were similar to that of D-isofagomine. However, D-3-*epi*-isofagomine missed the hydrogen bond interaction between 3-OH group and β-glucocerebrosidase (Asp127 and Trp179) (Figs. 3 and 4). These results support that the C3 OH group in the isofagomine is a dominant factor for the inhibition of β-glucocerebrosidase. Gaucher disease is caused by mutations in the gene encoding β-glucocerebrosidase, the lysosomal enzyme responsible for the metabolism of glucosylceramide into D-glucose and ceramide.[21] Deficiency of the enzyme activity results in the progressive accumulation of glucosylceramide in the macrophages, leading to various clinical manifestations that include hepatosplenomegaly, secondary hypersplenism, anemia, skeletal abnormality, neurologic dysfunctions and Type II and III patients have central nervous system impairment.[22] Recently, pharmacological chaperone therapy has been attempted as a new potential treatment for Gaucher disease. These pharmacological chaperones appear to act as a template that stabilizes the native folding state in the endoplasmic reticulum (ER) by occupying the active site of the mutant β-glucocerebrosidase, thereby facilitating correct folding and trafficking to

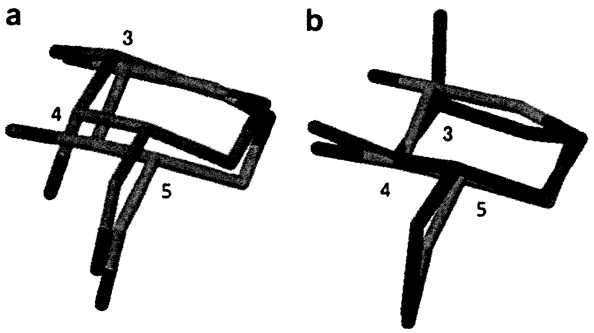


Figure 3. The comparison of the best docking pose of D-isofagomine isomers with the binding conformation of D-isofagomine determined by X-ray crystallography. (a) D-Isofagomine (green) and D-4-*epi*-isofagomine (light purple); (b) D-isofagomine (green) and D-3-*epi*-isofagomine (magenta).

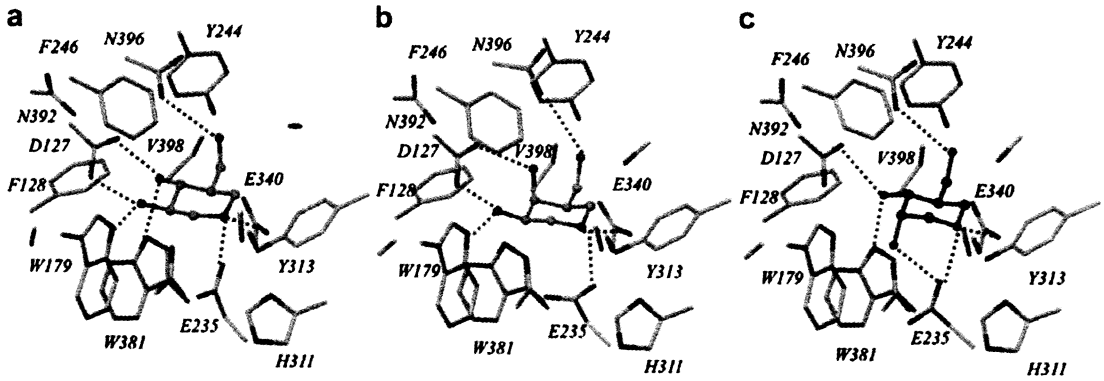


Figure 4. The hydrogen bonds between β-glucocerebrosidase and D-isofagomine isomers. (a) D-Isofagomine; (b) D-4-*epi*-isofagomine; (c) D-3-*epi*-isofagomine.

lysosomes, and increasing total cellular β-glucocerebrosidase activity.[23–25] D-Isofagomine has proceeded to Phase II clinical trials for the treatment of Gaucher disease but it has been finally withdrawn from clinical trials due to lack of efficacy. We expect that the results reported here could help to guide further structural modifications of isofagomines and 1-*N*-iminosugars to improve the permeability and chaperone effects.

4. Experimental

4.1. Chemistry

Infrared (IR) spectra were recorded on a Perkin–Elmer 1600 series FT-IR spectrometer. Mass spectra (MS) were recorded on a JEOL JMN-DX 303/JMA-DA 5000 spectrometer. Microanalyses were performed on a Perkin–Elmer CHN 2400 Elemental Analyzer. Optical rotations were measured with a JASCO DIP-360 or JASCO P-1020 digital polarimeter. Proton nuclear magnetic resonance (^{1}H NMR) spectra were recorded on JEOL JNM-EX 270 (270 MHz) or 300 MHz on a Varian Gemini-300 or JEOL JNM-AL 400 (400 MHz) 500 MHz on a Varian Unity-500 or JNM-LA (600 MHz) spectrometer, using tetramethylsilane as an internal standard. The following abbreviations are used: s = singlet, d = doublet, t = triplet, q = quartet, m = multiplet, br = broad. Column chromatography was carried out on Merck Silica Gel 60 (230–400 mesh) or KANTO Silica Gel 60N (40–50 μm) for flash chromatography. Purification of products via ion-exchange resin chromatography was performed with Dowex 1×2 OH^- form, using water as eluent. D-forms of isofagomine, 3-*epi*-isofagomine, 4-*epi*-isofagomine, and 3,4-di-*epi*-isofagomine were prepared according to our previous reports[11,12] and their spectral data were described in their literatures.[11,12] In addition, D-forms of fagomine, 3,4-di-*epi*-fagomine, 3-*epi*-fagomine, and 4-*epi*-fagomine were available from D-serine-derived Garner aldehyde with the same procedures as previously described.[17]

4.1.1. (*R*)-*N*-*tert*-Butoxycarbonyl-5-(*tert*-butyldiphenylsilyloxy)-3-piperidene (3)

To a solution of (*R*)-**1**[11] (897 mg, 4.5 mmol) in CH_2Cl_2 (10 mL) was added imidazole (511 mg, 7.5 mmol), DMAP (122 mg, 1 mmol), and *tert*-butylchlorodiphenylsilane (1.374 g, 5.0 mmol). The mixture was stirred at room temperature for 3 h. The reaction mixture was filtered through a Celite pad. The filtrate was washed with brine (10 mL), dried over $MgSO_4$, and concentrated under reduced pressure. The residue was purified by flash column chromatography on silica gel (*n*-hexane/AcOEt = 8:1) to give **3** (1.96 g, 99%) as a colorless oil. $[\alpha]_D^{29}$ −22.3 (*c* 1.40, $CHCl_3$). [lit.[11] $[\alpha]_D^{27}$ +22.6 (*c* 1.80, $CHCl_3$) for *ent*-**3**]. ^{1}H NMR (600 MHz, $CDCl_3$) δ: 1.08 (s, 9H), 1.40 (s, 9H), 3.21 (br s, 1H), 3.62–3.96 (m, 3H), 4.25 (br s, 1H), 5.58–5.72 (m, 2H), 7.36–7.44 (m, 6H), 7.67–7.70 (m, 4H). ^{13}C NMR (67.8 MHz, $CDCl_3$) δ: 19.2, 26.9, 28.4, 42.7, 47.9, 65.1, 79.5, 126.0, 127.4, 129.2, 129.5, 133.7, 135.5, 154.4. IR (neat) (cm^{-1}) 1703. EI-MS (*m*/*z*) 438 (M^++1).

4.1.2. (3*S*,4*S*,5*S*)-*N*-*tert*-Butoxycarbonyl-3-(*tert*-butyldiphenylsilyloxy)-4,5-epoxypiperidine (4)

To a cooled (0 °C) solution of **3** (1400 mg, 3.2 mmol) in CH_3CN (35 mL) was added 4 mmol/L of aq Na_2EDTA (17.5 mL, 0.07 mmol) and 1,1,1-trifluoroacetone (3.5 mL). The mixture of $NaHCO_3$ (2.21 g, 26.3 mmol) and Oxone (10.73 g, 17.5 mmol) as a solid was added slowly over a period of 1 h at 0 °C. After being stirred at 0 °C overnight, the solution was quenched by adding water (100 mL) and extracted with $CHCl_3$ (3 × 100 mL). The organic extracts were combined, dried over $MgSO_4$, filtered, and concentrated under reduced pressure. The residue was purified by flash column chromatography on silica gel (*n*-hexane/AcOEt = 8:1) to give **4** (1040 mg, 72%) as colorless prisms and (3*S*,4*R*,5*R*)-*N*-*tert*-butoxycarbonyl-3-(*tert*-butyldiphenylsilyloxy)-4,5-epoxypiperidine (272 mg, 19%) as colorless needles. Mp 70–72 °C (*n*-pentane). $[\alpha]_D^{31}$ −29.7 (*c* 1.82, $CHCl_3$). [lit.[11] $[\alpha]_D^{30}$ +29.2 (*c* 1.11, $CHCl_3$) for *ent*-**4**]. ^{1}H NMR (400 MHz, $CDCl_3$) δ: 1.10 (s, 9H), 1.37 and 1.46 (2s, 9H), 3.07–3.41 (m, 4H), 3.07–3.88 (m, 2H), 4.09–4.15 (m, 1H), 7.36–7.45 (m, 6H), 7.63–7.69 (m, 4H). ^{13}C NMR (67.8 MHz, $CDCl_3$) δ: 19.3, 27.0, 28.4, 41.4, 45.3, 50.6, 53.7, 65.2, 79.8, 127.7, 129.8, 133.1, 135.5, 154.9. IR (KBr) (cm^{-1}) 1701. EI-MS (*m*/*z*) 453 (M^+).

4.1.3. (3*S*,4*S*,5*R*)-*N*-*tert*-Butoxycarbonyl-3-(*tert*-butyldiphenylsilyloxy)-4-hydroxy-5-vinylpiperidine (5)

A solution of *n*-BuLi (3.125 mL, 1.6 M in *n*-hexane, 5 mmol) was added to a solution of tetravinyltin (1.14 g, 5 mmol) in Et_2O (7 mL) at room temperature and the mixture was stirred for 1 h at the same temperature. The solution was added to a suspension of CuCN (224 mg, 2.5 mmol) in dry Et_2O (20 mL) at −78 °C and the mixture was stirred under argon atmosphere at −78 °C for 10 min. The resulting solution was warmed to −10 °C and stirred for 30 min. The reaction mixture was cooled to −78 °C and a solution of **4** (454 mg, 1 mmol) in dry Et_2O (20 mL) was added to the reaction mixture dropwise via syringe at −78 °C. The mixture was stirred at −78 °C for 10 min. $BF_3{\cdot}OEt_2$ (4 mol/L in Et_2O, 5 mL, 2 mmol) was added to the reaction mixture at −78 °C and the solution was stirred for 2 h. The reaction mixture was quenched with 28% NH_4OH/satd NH_4Cl (1:9) solution (50 mL) and stirred overnight at room temperature. The organic layer was separated and the aqueous layer was extracted with Et_2O (2 × 20 mL). The combined organic phases were washed with brine (20 mL), dried over $MgSO_4$, filtered, and concentrated under reduced pressure. The residue was purified by flash column chromatography on silica

gel (*n*-hexane/AcOEt = 8:1) to give **5** (383 mg, 80%) as a colorless oil. $[\alpha]_D^{30}$ +10.6 (*c* 1.00, $CHCl_3$). [lit.[11] $[\alpha]_D^{24}$ −10.5 (*c* 1.16, $CHCl_3$) for *ent*-**5**]. ^1H NMR (600 MHz, $CDCl_3$) δ: 1.09 (s, 9H), 1.31 (s, 9H), 2.12 (br s, 1H), 2.23 (br s, 1H), 2.50 (br s, 1H), 2.65 (dd, *J* = 11.0, 12.5 Hz, 1H), 3.42 (t, *J* = 9.0 Hz, 1H), 3.51–3.55 (m, 1H), 3.82–4.23 (m, 2H), 5.16–5.20 (m, 2H), 5.66–5.72 (m, 1H), 7.38–7.45 (m, 6H), 7.68–7.71 (m, 4H). ^{13}C NMR (67.8 MHz, $CDCl_3$) δ: 19.4, 27.0, 28.3, 45.8, 46.5, 48.7, 73.6, 77.7, 79.8, 117.7, 127.7, 129.8, 133.3, 135.7, 135.9, 154.0. IR (neat) (cm^{-1}) 3472, 1698. EI-MS (*m*/*z*) 482 (M^++1).

4.1.4. (3*S*,4*S*,5*S*)-3,4-Dihydroxy-5-hydroxymethylpiperidine (L-isofagomine) (6)

To a solution of **5** (145 mg, 0.3 mmol) in EtOH (3 mL) and H_2O (3 mL) was added an aqueous solution of 4% OsO_4 (98 μL, 0.015 mmol) and the solution was stirred at room temperature for 10 min. $NaIO_4$ (142 mg, 0.66 mmol) as a powder was added slowly over a period of 30 min, and the mixture was stirred at room temperature for 24 h. $NaBH_4$ (57 mg, 0.15 mmol) as a powder was added, and the reaction mixture was stirred at room temperature for 1 h. The solvent was removed in vacuo. The residue was diluted with $CHCl_3$ (60 mL) and successively washed with 10% $Na_2S_2O_3$ (15 mL), satd $NaHCO_3$ (15 mL), and brine (7 mL). The organic solution was dried over $MgSO_4$, filtered, and concentrated under reduced pressure. The residue was purified by flash column chromatography on silica gel (*n*-hexane/AcOEt = 1:1) to give triol as a colorless oil. To a solution of the prepared triol (122 mg) in dioxane (2.0 mL) was added a solution of 10% HCl (10 mL), and the solution was refluxed for 1 h. After the reaction mixture was cooled to room temperature and diluted with H_2O (40 mL), the resulting dilute solution was washed with Et_2O. The aqueous layer was concentrated under reduced pressure. The residue was dissolved in 28% NH_4OH and concentrated in vacuo. The residue was purified by flash column chromatography on silica gel (28% NH_4OH/EtOH = 1:10) to give **6** (30.9 mg, 88%) as a white powder. $[\alpha]_D^{24}$ −23.8 (*c* 1.10, EtOH). [lit.[11] $[\alpha]_D^{27}$ +25.4 (*c* 1.30, EtOH) for *ent*-**6**]. ^1H NMR (600 MHz, D_2O) δ: 1.61–1.68 (m, 1H), 2.33–2.38 (m, 2H), 3.05 (dd, *J* = 13.0, 3.5 Hz, 1H), 3.10 (dd, *J* = 12.1, 4.8 Hz, 1H), 3.27 (t, *J* = 9.9 Hz, 1H), 3.43–3.48 (m, 1H), 3.59 (dd, *J* = 11.4, 7.0 Hz, 1H), 3.78 (dd, *J* = 11.4, 3.3 Hz, 1H). ^{13}C NMR (67.8 MHz, D_2O) δ: 43.9, 45.7, 48.8, 59.8, 71.4, 73.1. EI-MS (*m*/*z*): 147 (M^+).

4.1.5. (*R*)-*N*-*tert*-Butoxycarbonyl-5-(tributylstannyl)methoxy-3-piperidene (7)

A solution of (*R*)-**1** (995 mg, 5 mmol) in THF (5 mL) was added to a suspension of potassium hydride (860 mg, 35 wt % in oil, 7.5 mmol) in THF (20 mL) and DMF (5 mL) at 0 °C and it was stirred for 1 h. A solution of Bu_3SnCH_2I (3.235 g, 7.5 mmol) in THF (5 mL) was added to the reaction mixture at 0 °C and it was stirred overnight. Ice water was added to the reaction mixture and it was extracted with ether (50 mL) three times. The extracts were washed with brine, dried over $MgSO_4$, and evaporated. The residue was purified by flash column chromatography on silica gel (*n*-hexane/AcOEt = 15:1) to give **7** (2.49 g, 99%) as an oil. $[\alpha]_D^{26}$ −43.9 (*c* 1.08, $CHCl_3$). [lit.[11] $[\alpha]_D^{25}$ +45.7 (*c* 5.10, $CHCl_3$) for *ent*-**7**]. ^1H NMR (600 MHz, $CDCl_3$) δ: 0.86–0.94 (m, 15H), 1.25–1.35 (m, 6H), 1.46–1.56 (m, 15H), 3.11 (br s, 0.5H), 3.31 (br s, 0.5H), 3.63–4.00 (m, 6H), 5.71–5.92 (m, 2H). ^{13}C NMR (67.8 MHz, $CDCl_3$) δ: 9.0, 13.7, 27.2, 28.4, 29.1, 43.6, 44.5, 59.4, 74.6, 79.5, 125.8, 126.9, 154.5. IR (neat) (cm^{-1}) 1703, 758. EI-MS (*m*/*z*): 502 (M^+−1).

4.1.6. (*S*)-*N*-*tert*-Butoxycarbonyl-5-(hydroxymethyl)-3-piperidene (8)

A solution of *n*-BuLi (6.3 mL, 1.6 M in *n*-hexane, 9.77 mmol) was added dropwise to a solution of **7** (2.97 g, 5.92 mmol) in dry pentane (120 mL) at −80 °C and stirred for 1 h at the same temperature, and subsequently stirred at −40 °C for 2 h. satd NH_4Cl (30 mL) was added to the reaction mixture and this was then separated. The organic layer was dried over Na_2SO_4, and evaporated. The residue was purified by flash column chromatography on silica gel (*n*-hexane/AcOEt = 15:1–2:1) to give **8** (815 mg, 65%) as an oil. $[\alpha]_D^{22}$ +89.1 (*c* 1.50, $CHCl_3$). [lit.[11] $[\alpha]_D^{24}$ −92.1 (*c* 1.10, $CHCl_3$) for *ent*-**8**]. ^1H NMR (600 MHz, $CDCl_3$) δ: 1.46 (s, 9H), 2.11 (br s, 0.5H), 2.38 (br s, 1H), 2.96 (br s, 0.5H), 3.21–3.83 (m, 5H), 4.03 (d, *J* = 18.3 Hz, 1H), 5.73 (br s, 2H). ^{13}C NMR (67.8 MHz, $CDCl_3$) δ: 28.4, 38.1, 41.3, 44.2, 63.1, 79.9, 125.8, 126.2, 154.9. IR (neat) (cm^{-1}) 3435, 1698. EI-MS (*m*/*z*): 213 (M^+).

4.1.7. (*S*)-*N*-*tert*-Butoxycarbonyl-5-((*tert*-butyldiphenylsilyloxy)methyl)-3-piperidene (9)

To a solution of **8** (608 mg, 2.86 mmol) in CH_2Cl_2 (18 mL) was added imidazole (292 mg, 4.28 mmol), DMAP (7.0 mg, 0.06 mmol), and *tert*-butylchlorodiphenylsilane (864 mg, 3.14 mmol). The mixture was stirred at room temperature for 3 h. The reaction mixture was filtered through a Celite pad. The filtrate was washed with brine (12 mL), dried over $MgSO_4$, and concentrated under reduced pressure. The residue was purified by flash column chromatography on silica gel (*n*-hexane/AcOEt = 15:1) to give **9** (1.28 g, 99%) as a colorless oil. $[\alpha]_D^{21}$ +85.4 (*c* 1.30, $CHCl_3$). [lit.[11] $[\alpha]_D^{21}$ −82.9 (*c* 1.20, $CHCl_3$) for *ent*-**9**]. ^1H NMR (600 MHz, $CDCl_3$) δ: 1.08 (s, 9H), 1.49 (s, 9H), 2.44–2.54 (m, 1H), 3.30– 3.59 (m, 3H), 3.70–3.89 (m, 2H), 3.94 (dd, *J* = 18.7, 2.0 Hz, 1H), 5.61 (br s, 1H), 5.71 (br s, 1H), 7.38–7.45 (m, 6H), 7.67–7.70 (m, 4H). ^{13}C NMR (150 MHz, $CDCl_3$) δ: 19.2, 26.8, 28.4, 38.4, 43.3, 64.9, 79.4, 126.0, 127.6, 129.6, 133.6, 134.8, 135.5, 155.1. IR (KBr) (cm^{-1}) 1699. EI-MS (*m*/*z*): 452 (M+1).

4.1.8. (3*R*,4*S*,5*S*)-3,4-Dihydroxy-5-(hydroxymethyl)piperidine (L-3-*epi*-isofagomine) (10) and (3*S*,4*R*,5*S*)-3,4-dihydroxy-5-(hydroxymethyl)piperidine (L-4-*epi*-isofagomine) (11)

To a solution of (*S*)-**8**[12] (100 mg, 0.47 mmol) in acetone (3 mL) was added an aqueous 4% OsO_4 solution (65 μL, 0.01 mmol). After 10 min, an aqueous 50% NMO solution (176 mg, 0.75 mmol) was added and the mixture was stirred overnight. To the solution were added Na_2SO_3 and Na_2SO_4. The mixture was filtered through a Celite pad and the filtrate was evaporated. The residue was chromatographed on silica gel ($CHCl_3$/MeOH = 10:1) to give a triol. To a solution of the above triol in 1,4-dioxane (3 mL) was added 10% HCl (8 mL). The reaction mixture was refluxed for 1 h and evaporated. NH_4OH (28%) was added to the residue and evaporated. The residue was chromatographed on silica gel (MeOH/10% NH_4OH = 10:1) to give **10** (51 mg, 81%) and **11** (11 mg, 18%) as oils. For **10**: $[\alpha]_D^{25}$ −83.7 (*c* 1.06, EtOH). [lit.[12] $[\alpha]_D^{24}$ +85.2 (*c* 1.04, EtOH) for *ent*-**10**]. ^1H NMR (270 MHz, D_2O) δ: 1.72–1.88 (m, 1H), 2.22 (t, *J* = 12.1 Hz, 1H), 2.54 (d, *J* = 14.2 Hz, 1H), 2.80–2.98 (m, 2H), 3.42–3.54 (m, 2H), 3.61 (dd, *J* = 11.4, 3.8 Hz, 1H), 3.73 (s, 1H). ^{13}C NMR (67.8 MHz, D_2O) δ: 39.0, 44.9, 48.1, 60.3, 66.8, 69.2. EI-MS (*m*/*z*): 147 (M^+). HRMS calcd for $C_6H_{13}NO_3$: 147.0895, found: 147.0894. For **11**: $[\alpha]_D^{25}$ +3.5 (*c* 1.02, EtOH). [lit.[12] $[\alpha]_D^{25}$ −5.1 (*c* 0.98, EtOH) for *ent*-**11**]. ^1H NMR (270 MHz, D_2O) δ: 1.64–1.78 (m, 1H), 2.33 (t, *J* = 12.3 Hz, 1H), 2.53 (t, *J* = 11.6 Hz, 1H), 2.63 (dd, *J* = 12.9, 4.5 Hz, 1H), 2.72 (dd, *J* = 12.1, 4.9 Hz, 1H), 3.36–3.57 (m, 3H), 4.61 (s, 1H). ^{13}C NMR (67.8 MHz, D_2O) δ: 39.9, 41.5, 43.5, 60.1, 67.1, 68.1. EI-MS (*m*/*z*): 147 (M^+).

4.1.9. (3*R*,4*S*,5*R*)-*N*-*tert*-Butoxycarbonyl-3-((*tert*-butyldiphenylsilyloxy)methyl)-4,5-epoxypiperidine (12) and (3*R*,4*R*,5*S*)-*N*-*tert*-butoxycarbonyl-3-((*tert*-butyldiphenylsilyloxy)methyl)-4,5-epoxypiperidine (13)

To a cooled (0 °C) solution of **9** (346 mg, 0.77 mmol) in CH_3CN (8 mL) was added 4 mmol/L aq Na_2EDTA (4 mL, 0.016 mmol) and 1,1,1-trifluoroacetone (0.8 mL). The mixture of $NaHCO_3$ (504 mg,

6 mmol) and Oxone® ((2.46 g, 4.0 mmol) as a solid were added slowly over a period of 1 h at 0 °C. After being stirred at 0 °C overnight, the solution was quenched by adding water (25 mL), and extracted with $CHCl_3$ (25 mL × 3). The organic extracts were combined, dried over Na_2SO_4, filtered, and concentrated under reduced pressure. The residue was purified by flash column chromatography on silica gel (*n*-hexane/AcOEt = 11:1) to give **12** (142 mg, 40%) and **13** (75 mg, 21%) as colorless oils. **12**: $[\alpha]_D^{22}$ +41.3 (*c* 1.26, $CHCl_3$). ^1H NMR (600 MHz, $CDCl_3$) δ: 1.06 (s, 9H), 1.41 (br d, *J* = 28.9 Hz, 9H), 2.33 (br d, *J* = 25.0 Hz, 1H), 3.06–3.28 (m, 3H), 3.37–3.77 (m, 4H), 3.93 (dd, *J* = 52.4, 14.5 Hz, 1H), 7.30–7.45 (m, 6H), 7.65 (d, *J* = 7.7 Hz, 4H). ^1H NMR (400 MHz, C_6D_6, 60 °C) δ: 1.17 (s, 9H), 1.45 (s, 9H), 2.31 (t, *J* = 5.9 Hz, 1H), 2.68 (t, *J* = 3.2 Hz, 1H), 2.96 (s, 1H), 3.10 (dd, *J* = 13.4, 6.8 Hz, 1H), 3.35 (br s, 1H), 3.57–3.67 (m, 3H), 3.89 (d, *J* = 15.1 Hz, 1H), 7.26–7.30 (m, 6H), 7.72–7.75 (m, 4H). ^{13}C NMR (100 MHz, C_6D_6, 60 °C) δ: 19.5, 27.1, 28.5, 37.1, 40.9, 42.9, 49.8, 52.3, 63.9, 79.2, 127.8, 128.1, 128.3, 128.5, 130.1, 133.9, 133.9, 135.9, 136.0, 155.1. IR (neat) cm^{-1}: 2962, 2931, 2859, 1696, 1473, 1461, 1428, 1392, 1366, 1248, 1174, 1113. EI-MS (*m*/*z*): 468 (M^++1). HRMS calcd for $C_{27}H_{37}NO_4Si$: 467.2492, found: 467.2465.

Compound **13**: $[\alpha]_D^{22}$ +30.5 (*c* 1.33, $CHCl_3$). ^1H NMR (400 MHz, $CDCl_3$) δ: 1.07 (s, 9H), 1.44 (s, 9H), 2.27–2.32 (m, 1H), 2.70–2.72 (m, 1H), 3.25 (br s, 1H), 3.25–3.30 (m, 2H), 3.43–3.51 (m, 1H), 3.64–3.80 (m, 3H), 3.92–4.06 (m, 1H), 7.38–7.45 (m, 6H), 7.66–7.69 (m, 4H). ^{13}C NMR (150 MHz, $CDCl_3$) δ: 19.2, 26.8, 28.4, 38.2, 40.1, 40.7, 41.7, 50.7, 51.9, 63.7, 79.8, 127.7, 129.7, 133.4, 133.4, 135.5, 135.6, 154.7. IR (neat) cm^{-1}: 2962, 2932, 2859, 1695, 1473, 1462, 1428, 1392, 1366, 1247, 1174, 1152, 1113, 1083. EI-MS (*m*/*z*): 468 (M^++1). HRMS calcd for $C_{27}H_{37}NO_4Si$: 467.2492, found: 467.2580.

4.1.10. (3*R*,4*R*,5*S*)-3,4-Dihydroxy-5-hydroxymethylpiperidine (L-3,4-di-*epi*-isofagomine) (14)

A mixture of **12**[12] (140 mg, 0.30 mmol), 1,4-dioxane (7.6 mL), and 3 M KOH (15.3 mL) was refluxed overnight. After evaporation, methanol (3 mL) and 6 N HCl (9.1 mL) were added to the residue. The mixture was heated at 60 °C for 1 h and evaporated. The residue was treated with 28% NH_4OH and evaporated. The residue was chromatographed on silica gel (MeOH/10% NH_4OH = 10:1) to give **6** (12 mg, 28%) and **14** (28 mg, 64%). $[\alpha]_D^{24}$ −18.7 (*c* 1.28, EtOH). [lit.[12] $[\alpha]_D^{19}$ +18.4 (*c* 0.96, EtOH) for *ent*-**14**]. ^1H NMR (270 MHz, D_2O) δ: 1.90–2.02 (m, 1H), 2.47–2.65 (m, 3H), 2.84 (dd, *J* = 13.8, 2.9 Hz, 1H), 3.42 (dd, *J* = 11.1, 8.0 Hz, 1H), 3.48–3.68 (m, 2H), 3.69 (dd, *J* = 5.6, 3.6 Hz, 1H). ^{13}C NMR (67.8 MHz, D_2O) δ: 38.2, 41.4, 45.7, 59.3, 66.8, 68.7. EI-MS (*m*/*z*): 147 (M^+).

4.1.11. (2*S*,6*R*,7*S*)-2-(*tert*-Butyldiphenylsilanyloxymethyl)-7-oxa-3-azabicyclo[4.1.0]heptane-3-carboxylic acid *tert*-butyl ester (17) and (2*S*,6*S*,7*R*)-2-(*tert*-butyldiphenylsilanyloxymethyl)-7-oxa-3-azabicyclo[4.1.0]heptane-3-carboxylic acid *tert*-butyl ester (16)

To a solution of (*R*)-**15**[17] (377 mg, 0.83 mmol) in CH_3CN (6.4 mL) was successively added 4×10^{-4} M Na_2·EDTA (4.2 mL) and CF_3COCH_3 (0.78 mL) at 0 °C. A mixture of $NaHCO_3$ (545 mg) and Oxone (2.56 g) was added to the reaction mixture over 1 h at 0 °C and the whole mixture was stirred at the same temperature for 30 min. H_2O (7 mL) was added to the reaction mixture and the mixture was extracted with CH_2Cl_2. The extract was dried and evaporated. The residue was purified by chromatography (hexane/AcOEt = 5:1) to yield a diastereomeric mixture. The mixture was purified by medium-pressure chromatography (hexane/AcOEt = 15:1) to yield **17** (115 mg, 29%) and **16** (231 mg, 59%) as oils. **17**: $[\alpha]_D^{24}$ +79.8 (*c* 2.41, $CHCl_3$). [lit.[17] $[\alpha]_D^{24}$ −71.2 (*c* 1.27, $CHCl_3$) for *ent*-**17**]. ^1H NMR (500 MHz, $CDCl_3$) δ: 1.07 (s, 9H), 1.38 (s, 6H), 1.44 (s, 3H), 1.86–2.01 (m, 2H), 2.63–2.67 (m, 1H), 3.34–3.71 (m, 3H), 3.79–3.83 (m, 2H), 4.44–4.45 (m, 0.75H), 4.75 (br s, 0.25H), 7.36–7.41 (m, 6H), 7.69–7.73 (m, 4H). ^{13}C NMR (125 MHz, $CDCl_3$) δ: 19.4, 25.3, 26.9, 28.4, 33.6, 51.5, 51.6, 51.9, 61.6, 80.4, 127.8, 129.8, 133.6, 135.6, 135.7, 135.8, 154.3; IR (neat) 2931.7, 1696.0, 1416.1, 1110.8, 1003.5 cm^{-1}; HRMS calcd for $C_{27}H_{37}NO_4Si$ (M^+) 467.2422, found 467.2399. Compound **16**: $[\alpha]_D^{26}$ +57.8 (*c* 1.75, $CHCl_3$); [lit.[17] $[\alpha]_D^{26}$ −50.3 (*c* 1.42, $CHCl_3$) for *ent*-**16**]. ^1H NMR (500 MHz, $CDCl_3$) δ: 1.06 (s, 9H), 1.40 (s, 9H), 1.88–1.93 (m, 1H), 1.99 (br s, 1H), 3.00 (br s, 1H), 3.28 (br s, 1H), 3.31 (br s, 1H), 3.40–3.88 (m, 3H), 4.50 (br s, 1H), 7.36–7.45 (m, 6H), 7.63–7.67 (m, 4H); ^{13}C NMR (125 MHz, $CDCl_3$) δ: 19.3, 22.8, 26.9, 28.5, 50.5, 51.8, 63.8, 80.3, 127.95, 127.96, 129.9, 130.0, 133.109, 135.6, 135.7, 155.3; IR (neat) (cm^{-1}) 2932.3, 1695.4, 1421.5, 1172.1, 1109.9; HRMS calcd for $C_{27}H_{37}NO_4Si$ (M^+) 467.2422, found 467.2452.

4.1.12. (2*S*,3*S*,4*S*)-2-Hydroxymethylpiperidine-3,4-diol (L-fagomine) (18)

A mixture of **16** (136 mg, 0.285 mmol), 1,4-dioxane (1.8 mL), H_2O (1.17 mL), and H_2SO_4 (0.12 mL) was heated at 95 °C for 3 h. After evaporation of the reaction mixture, the residue was treated with ion-exchange resin (Amberlite IRA-410) to yield L-fagomine (**18**) (34 mg, 80%) as a solid. MP 184–185 °C; $[\alpha]_D^{26}$ −20.8 (*c* 1.13, H_2O). [lit.[17] $[\alpha]_D^{24}$ +18.0 (*c* 0.92, H_2O) for *ent*-**18**]. ^1H NMR (500 MHz, D_2O) δ: 1.31 (ddd, *J* = 20.0, 12.8, 4.2 Hz, 1H), 1.83–1.87 (m, 1H), 2.36–2.40 (m, 1H), 2.46 (td, *J* = 12.8, 2.56 Hz, 1H), 2.84–2.88 (m, 1H), 3.02 (t, *J* = 9.4 Hz, 1H), 3.47–3.43 (m, 1H), 3.50 (dd, *J* = 11.5, 6.4 Hz, 1H), 3.72 (dd, *J* = 11.5, 2.9 Hz, 1H). ^{13}C NMR (125 MHz, D_2O) δ: 33.5, 43.4, 61.7, 62.5, 74.0, 74.0.

4.1.13. (2*S*,3*R*,4*R*)-2-Hydroxymethylpiperidine-3,4-diol (L-3,4-di-*epi*-fagomine) (19)

A mixture of **17** (200 mg, 0.42 mmol), 1,4-dioxane (10.7 mL), and 0.3 M KOH (21.5 mL) was refluxed overnight. After evaporation, MeOH (4.1 mL) and 6 N HCl (11.7 mL) were added to the residue. The mixture was heated at 60 °C for 1 h and then evaporated to give an oil. The residue was separated by ion-exchange resin chromatography to give L-fagomine (**18**) (10.5 mg, 17%) and L-3,4-di-*epi*-fagomine (**19**) (51.2 mg, 81%). For **19**. $[\alpha]_D^{25}$ −14.0 (*c* 1.96, H_2O). [lit.[17] $[\alpha]_D^{25}$ +13.4 (*c* 0.32, H_2O) for *ent*-**19**]. ^1H NMR (500 MHz, D_2O) δ: 1.43–1.50 (m, 1H), 1.86 (m, 1H), 2.78 (m, 2H), 3.02–3.06 (m, 1H), 3.56–3.57 (m, 2H), 3.61 (br s, 1H), 3.80 (br s, 1H). ^{13}C NMR (125 MHz, D_2O) δ: 28.2, 39.3, 56.0, 61.3, 68.2, 69.1.

4.1.14. (*R*)-6-Hydroxymethyl-3,6-dihydro-2*H*-pyridine-1-carboxylic acid *tert*-butyl ester (20)

A solution of TBAF (1.59 mL, 1.59 mmol) was added to a solution of **15** (597 mg, 1.32 mmol) in THF (15 mL) with ice cooling and the mixture was stirred at room temperature for 2.5 h. After being diluted with H_2O, the mixture was extracted with AcOEt three times. The extracts were washed with brine, dried, and evaporated. The residue was purified by chromatography (hexane/AcOEt = 3:1) to yield **20** (274 mg, 97%) as an oil. $[\alpha]_D^{24}$ +230.7 (*c* 1.75, $CHCl_3$). [lit.[17] $[\alpha]_D^{24}$ −227.5 (*c* 1.02, $CHCl_3$) for *ent*-**20**]. ^1H NMR (300 MHz, $CDCl_3$) δ: 1.42 (s, 9H), 1.91–1.99 (m, 1H), 2.12–2.21 (m, 1H), 2.52 (br s, 0.5H), 2.83–2.90 (m, 1H), 3.17 (br s, 0.5H), 3.57–3.63 (m, 2H), 4.05 (br s, 1H), 4.49 (br s, 1H), 5.57–5.63 (m, 1H), 5.88–5.93 (1H, m). ^{13}C NMR (75 MHz, $CDCl_3$) δ: 25.0, 26.7, 28.6, 39.3, 54.2, 64.8, 80.2, 124.7, 127.5, 134.7; IR (neat) (cm^{-1}) 3440.0, 2975.8, 2930.1, 1693.0, 1674.3, 1423.6. HRMS calcd for $C_{11}H_{19}NO_3$ (M^+) 213.1652, found 213.1638.

4.1.15. (2*S*,3*S*,4*R*)-2-Hydroxymethylpiperidine-3,4-diol (L-3-*epi*-fagomine) (21)

A solution of NMO (559 mg, 2.39 mmol) and a solution of K_2OsO_4·$2H_2O$ (14.7 mg, 39.7 μmol) in water (0.7 mL) were succes-

sively added to a solution of **20** (170 mg, 0.80 mmol) in acetone (7 mL) and the mixture was stirred at room temperature overnight. Na_2SO_3 was added to the mixture and the mixture was stirred. The insoluble materials were filtered off and the filtrate was evaporated. The residue was dissolved in 1,4-dioxane (4.8 mL), 10% HCl (13.9 mL) was added, and the mixture was heated at 60 °C for 1 h, and then evaporated. The residue was washed with ether and then purified by ion-exchange resin chromatography to give L-3-*epi*-fagomine (**21**) (100 mg, 86%) as a white solid. Mp 220–222 °C. $[\alpha]_D^{26}$ −72.0 (*c* 1.19, H_2O). [lit.[17] $[\alpha]_D^{26}$ +74.4 (*c* 0.95, H_2O)]. ^1H NMR (500 MHz, D_2O) δ:1.56–1.63 (m, 1H), 1.69–1.73 (m, 1H), 2.61–2.68 (m, 2H), 2.70–2.75 (m, 1H), 3.33 (dd, J = 10.2, 2.9 Hz, 1H), 3.49 (dd, J = 11.63, 6.5 Hz, 1H), 3.69 (dd, J = 11.5, 2.9 Hz, 1H), 3.95 (q, J = 2.9 Hz, 1H). ^{13}C NMR (125 MHz, D_2O) δ: 31.8, 39.1, 56.5, 62.9, 68.7, 70.3.

4.1.16. (2*S*,3*R*,4*S*)-2-Hydroxymethylpiperidine-3,4-diol (L-4-*epi*-fagomine) (22)

A solution of OsO_4 (120 mg, 0.47 mmol) in CH_2Cl_2 (1.2 mL) was added to a solution of **20** (98.5 mg, 0.46 mmol) and TMEDA (58.6 mg, 0.50 mmol) in CH_2Cl_2 (12 mL) at −78 °C. The mixture was stirred at the same temperature for 2 h, warmed to room temperature, and stirred for 1 h. The reaction mixture was evaporated. The residue was dissolved in MeOH (12 mL), 35% HCl (four drops) was added, and the mixture was stirred at room temperature for 2 h, and then evaporated. The residue was treated with ion-exchange resin (Amberlite IRA-410) and then separated by ion-exchange resin chromatography to give L-4-*epi*-fagomine (**22**) (39.7 mg, 59%) and L-3-*epi*-fagomine (**21**) (20.2 mg, 30%) as solids. **22**: mp 220–222 °C. $[\alpha]_D^{23}$ −10.4 (*c* 1.02, H_2O). [lit.[17] $[\alpha]_D^{22}$ +10.2 (*c* 1.42, H_2O)]. ^1H NMR (300 MHz, D_2O) δ: 1.49–1.56 (m, 2H), 2.39–2.49 (m, 1H), 2.57 (td, J = 6.9, 5.2 Hz, 1H), 2.91 (td, J = 12.9, 3.3 Hz, 1H), 3.47 (dd, J = 6.7, 3.4 Hz, 2H), 3.50–3.60 (m, 1H), 3.74 (br s, 1H). ^{13}C NMR (75 MHz, D_2O) δ: 28.4, 43.6, 59.7, 62.5, 68.5, 70.7.

4.2. Biological assays

The enzymes α-glucosidase (from rice, assayed at pH 5.0), β-glucosidases (from almond, pH 5.0; from bovine liver, pH 6.8), α-galactosidase (from coffee bean, pH 6.5), β-galactosidase (from bovine liver, pH 6.8), α-mannosidase (from jack beans, pH 4.5), β-mannosidase (from snail, pH 4.5), α-L-fucosidase (from bovine epididymis, pH 5.5), α-L-rhamnosidase (from *Penicillium decumbens*, pH 4.0), *p*-nitrophenyl glycosides, and various disaccharides were purchased from Sigma–Aldrich Co. Brush border membranes were prepared from the rat small intestine according to the method of Kessler et al,[26] and were assayed at pH 5.8 for rat intestinal maltase, isomaltase, sucrase, cellobiase, and lactase using the appropriate disaccharides as substrates. For rice α-glucosidase and rat intestinal maltase activities, the reaction mixture contained 25 mM maltose and the appropriate amount of enzyme, and the incubations were performed for 10–30 min at 37 °C. The reaction was stopped by heating at 100 °C for 3 min. After centrifugation (600g; 10 min), 0.05 mL of the resulting reaction mixture were added to 3 mL of the Glucose CII-test Wako (Wako Pure Chemical Ind., Osaka, Japan). The absorbance at 505 nm was measured to determine the amount of the released D-glucose. Other glycosidase activities were determined using an appropriate *p*-nitrophenyl glycoside as substrate at the optimum pH of each enzyme. The reaction mixture contained 2 mM of the substrate and the appropriate amount of enzyme. The reaction was stopped by adding 2 mL of 400 mM Na_2CO_3. The released *p*-nitrophenol was measured spectrometrically at 400 nm. Human lysosomal α-galactosidase and β-glucosidase were obtained from Genzyme (Boston, MA) and their activities were determined using 4-methylumbelliferyl α-D-galactoside and β-D-glucoside (Sigma–Aldrich Co.), respectively, as substrates. Liberated 4-methylumbelliferone was measured (excitation 362 nm, emission 450 nm) with a F-4500 fluorescence spectrophotometer (Hitachi, Tokyo, Japan).

4.3. Docking studies

We modeled the three-dimensional structures of human β-glucocerebrosidase complexed with D-isofagomine and three D-isofagomine isomers using Induced Fit Docking protocol[27] in Schrödinger software package. The three-dimensional coordinate of the crystal structure of human β-glucocerebrosidase–D-isofagomine complex (PDB code: 2NSX B chain) was used in the docking analyses, because this crystal structure was determined at pH 5.5 (an acidic-pH reflective of the lysosome environment). Water molecules were removed from the structure and H atoms were added using the Protein Preparation Wizard in Maestro 9.0. The docking site was defined as an enclosing box 26 × 26 × 26 Å centered at the centroid of the co-crystallized ligand. First, the docking of D-isofagomine to β-glucocerebrosidase was performed for the purpose of showing that the ligand docking by Induced Fit Docking protocol could reproduce the crystal structure of β-glucocerebrosidase–D-isofagomine complex. In addition the result of the docking analysis for D-isofagomine was used to compare with the results of the docking analyses for D-isofagomine isomers.

The chemical structures of D-isofagomine and D-isofagomine isomers were sketched with ChemDraw (ChemDraw Ultra, Versions 8.0.3, Cambridge Soft Corporation, Cambridge, MA) and were imported into Chem3D (Chem3D Ultra, Versions 8.0.3, Cambridge Soft Corporation, Cambridge, MA) to generate reasonable 3D structures. Then, the conformational analyses using CAMDAS (Conformational Analyzer with Molecular Dynamics and Sampling) program[28] were carried out to generate initial conformers for the docking analyses.

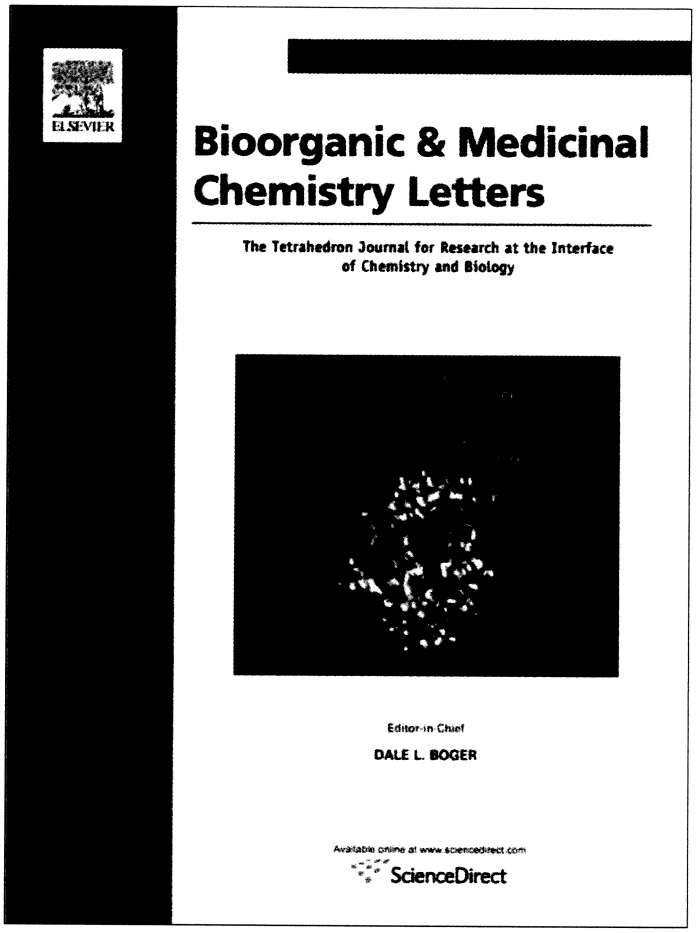
Standard-precision (SP) mode was used in the docking analysis. For the initial docking process of the Induced Fit Docking protocol, the van der Waals radii of both the ligand and the receptor were scaled to 0.5 to reduce the effect of steric clashes and to soften the surfaces of both the protein and the ligand so that a wider variety of poses could be generated. Observation of more than one crystal structure of human β-glucocerebrosidase obtained from the Protein Data Bank database presented that the side chain of Asn396 within the binding site could rotate. Therefore, Asn396 was mutated to alanine temporarily to generate more than one binding mode in the initial docking process. In the final docking process, the original residue type for Asn396 mutated to alanine was restored and ligands were redocked back into all new receptor conformations using the default vdW radii scaling (1.0 receptor, 0.8 ligand).

References and notes

1. Watson, A. A.; Fleet, G. W. J.; Asano, N.; Molyneux, R. J.; Nash, R. J. *Phytochemistry* **2001**, *56*, 265.
2. Chang, C. F.; Ho, C. W.; Wu, C. Y.; Chao, T. A.; Wong, C. H.; Lin, C. H. *Chem. Biol.* **2004**, *11*, 1301.
3. Hakansson, A. E.; Ameijde, J.; Horne, G.; Nash, R. J.; Wormald, M. R.; Kato, A.; Besra, G. S.; Gurchad, S.; Fleet, G. W. J. *Tetrahedron Lett.* **2008**, *49*, 179.
4. Best, D.; Chairatana, P.; Glawar, A. F. G.; Crabtree, E.; Butters, T. D.; Wilson, F. X.; Yu, C.-Y.; Wang, W.-B.; Jia, Y.-M.; Adachi, I.; Kato, A.; Fleet, G. W. J. *Tetrahedron Lett.* **2010**, *51*, 2222.
5. Asano, N.; Ikeda, K.; Yu, L.; Kato, A.; Takebayashi, K.; Adachi, I.; Kato, I.; Ouchi, H.; Takahata, H.; Fleet, G. W. J. *Tetrahedron: Asymmetry* **2005**, *16*, 223.
6. Kato, A.; Kato, N.; Kano, E.; Adachi, I.; Ikeda, K.; Yu, L.; Okamoto, T.; Banba, Y.; Ouchi, H.; Takahata, H.; Asano, N. *J. Med. Chem.* **2005**, *48*, 2036.
7. Best, D.; Jenkinson, S. F.; Savill, A. W.; Alonzi, D. S.; Wormald, M. R.; Butters, T. D.; Norez, C.; Becq, F.; Bleriot, Y.; Adachi, I.; Kato, A.; Fleet, G. W. J. *Tetrahedron Lett.* **2010**, *51*, 4170.
8. Zhu, X.; Sheth, K. A.; Li, S.; Chang, H. H.; Fan, J.-Q. *Amgew. Chem., Int. Ed.* **2005**, *44*, 7450.

9. Chang, H. H.; Asano, N.; Ishii, S.; Ichikawa, Y.; Fan, J.-Q. *FEBS J.* **2006**, *273*, 4082.
10. Yu, Z.; Sawkar, A. R.; Whalen, L. J.; Wong, C. H.; Kelly, J. W. *J. Med. Chem.* **2007**, *50*, 94.
11. Ouchi, H.; Mihara, Y.; Takahata, H. *J. Org. Chem.* **2005**, *70*, 5207.
12. Mihara, Y.; Ojima, H.; Imahori, T.; Yoshimura, Y.; Ouchi, H.; Takahata, H. *Heterocycles* **2007**, *72*, 633.
13. Koyama, M.; Sakamura, S. *Agric. Biol. Chem.* **1974**, *38*, 1111.
14. Molyneux, R. J.; Benson, M.; Wong, R. Y.; Tropea, J. E.; Elbein, A. D. *J. Nat. Prod.* **1988**, *51*, 1198.
15. Kato, A.; Asano, N.; Kizu, H.; Matsui, K. *J. Nat. Prod.* **1997**, *60*, 312.
16. Nojima, H.; Kimura, I.; Chen, F.-J.; Sugihara, Y.; Haruno, M. *J. Nat. Prod.* **1998**, *61*, 397.
17. Takahata, H.; Banba, Y.; Ouchi, H.; Nemoto, H.; Kato, A.; Adachi, I. *J. Org. Chem.* **2003**, *68*, 3603.
18. Donohoe, T. J. *Synlett* **2002**, 1223.
19. Lieberman, R. L.; Wustman, B. A.; Huertas, P.; Powe, A. C., Jr.; Pine, C. W.; Khanna, R.; Schlossmacher, M. G.; Ringe, D.; Petsko, G. A. *Nat. Chem. Biol.* **2007**, *3*, 101.
20. Asano, N. *Cell Mol. Life Sci.* **2009**, *66*, 1479.
21. Brady, R. O.; Kanfer, J. N.; Shapiro, D. *Biochem. Biophys. Res. Commun.* **1965**, *18*, 221.
22. Butters, T. D. *Curr. Opin. Chem. Biol.* **2007**, *11*, 412.
23. Yu, L.; Ikeda, K.; Kato, A.; Adachi, I.; Godin, G.; Compain, P.; Maryin, O.; Asano, N. *Bioorg. Med. Chem.* **2006**, *14*, 7736.
24. Lei, K.; Ninomiya, H.; Suzuki, M.; Inoue, T.; Sawa, M.; Iida, M.; Ida, H.; Eto, Y.; Ogawa, S.; Ohno, K.; Suzuki, Y. *Biochim. Biophys. Acta* **2007**, *1772*, 587.
25. Khanna, R.; Benjamin, E. R.; Pellegrino, L.; Schilling, A.; Rigat, B. A.; Soska, R.; Nafar, H.; Ranes, B. E.; Feng, J.; Lun, Y.; Powe, A. C.; Palling, D. J.; Wustman, B. A.; Schiffmann, R.; Mahuran, D. J.; Lockhart, D. J.; Valenzano, K. J. *FEBS J.* **2010**, *277*, 1618.
26. Kessler, M.; Acuto, O.; Strelli, C.; Murer, H.; Semenza, G. A. *Biochem. Biophys. Acta* **1978**, *506*, 136.
27. Sherman, W.; Day, T.; Jacobson, M. P.; Friesner, R. A.; Farid, R. *J. Med. Chem.* **2006**, *49*, 534.
28. Tsujishita, H.; Hirono, S. *J. Comput. Aided Mol. Des.* **1997**, *11*, 305.

Provided for non-commercial research and education use.
Not for reproduction, distribution or commercial use.



This article appeared in a journal published by Elsevier. The attached copy is furnished to the author for internal non-commercial research and education use, including for instruction at the authors institution and sharing with colleagues.

Other uses, including reproduction and distribution, or selling or licensing copies, or posting to personal, institutional or third party websites are prohibited.

In most cases authors are permitted to post their version of the article (e.g. in Word or Tex form) to their personal website or institutional repository. Authors requiring further information regarding Elsevier's archiving and manuscript policies are encouraged to visit:

http://www.elsevier.com/copyright

Bioorganic & Medicinal Chemistry Letters 21 (2011) 3313–3316

Contents lists available at ScienceDirect

Bioorganic & Medicinal Chemistry Letters

journal homepage: www.elsevier.com/locate/bmcl

Synthesis of 5-thiodidehydropyranylcytosine derivatives as potential anti-HIV agents

Yuichi Yoshimura [a,*], Yoshiko Yamazaki [a,b], Yukako Saito [a], Yoshihiro Natori [a], Tomozumi Imamichi [c], Hiroki Takahata [a,*]

[a] Faculty of Pharmaceutical Sciences, Tohoku Pharmaceutical University, 4-4-1 Komatsushima, Aoba-ku, Sendai 981-8558, Japan
[b] Research and Development Department, SEED CO. Ltd, 1030-7 Fukuro, Kounosu, Saitama 369-0131, Japan
[c] Laboratory of Human Retrovirology, Applied and Development Research Program, National Institute of Allergy and Infectious Diseases at Frederick, Science Applications International Corporation-Frederick, Inc., Frederick, MD 21702, USA

ARTICLE INFO

Article history:
Received 19 February 2011
Revised 2 April 2011
Accepted 5 April 2011
Available online 9 April 2011

Keywords:
Nucleoside
4′-Thionucleoside
Anti-HIV
Antiviral
Pummerer reaction

ABSTRACT

As a part of our ongoing efforts to identify new anti-HIV agents, a 5′-thiopyrano-nucleoside derivative **4**, designed based on 4′-thioD4C **1** and cyclohexenylnucleoside **3**, was synthesized. The dihydrothiopyran skeleton of **4** was constructed by the ring closing metathesis of **21** which was synthesized from but-2-yne-1,4-diol. After converting the protecting group from MOM to TBS followed by oxidation, a Pummerer-type thioglycosylation reaction of **24** with persilylated uracil gave the desired 5-thiodihydrothiopyranyluracils **25** and **26** as a mixture of anomers. The conversion of **25** to a cytosine derivative and subsequent deprotection gave a 5-thiodidehydropyranosylcytosine derivative **4** in good yield. The anti-HIV activity of **4** was also evaluated.

© 2011 Elsevier Ltd. All rights reserved.

HAART (Highly Active Anti-Retroviral Therapy) is the most successful AIDS treatment to date for controlling HIV replication and has greatly improved the lifespan of AIDS patients.[1] However, the emergence of drug resistant viruses during the course of chemotherapy for AIDS continues to be a serious problem even after the establishment of HAART.[2] The HAART protocol involves the use of a cocktail of anti-HIV drugs including nucleoside reverse transcriptase inhibitors (NRTIs), non-nucleoside reverse transcriptase inhibitors (NNRTIs), and protease inhibitors (PIs).[1] Since NRTIs play an important role in HAART,[2] the development of an effective NRTI for HIV, which is also effective for a drug-resistant AIDS virus, would be highly desirable. As a result, a number of nucleoside analogues that are effective for treating HIV have been reported to date.[3] Our efforts in this area have involved attempts to prepare new antiviral nucleoside derivatives that have the potential for use in HIV therapy. Our strategy involved the construction of a novel pseudosugar skeleton that could serve as a structurally novel NRTI. Such a compound could then be used in place of currently used NRTIs that are ineffective against viruses that are resistant to the NRTIs now in use.[4] We previously reported on the synthesis of dihydrothiopyrano-nucleoside **2**[4c,c] which was designed based on the known anti-HIV L-4′-thioD4C **1**.[5] Unfortunately, dihydrothiopyrano-nucleoside **2** did not show anti-HIV activity. Cyclohexenylcytosine **3**, however, was found to have weak anti-HIV activity.[4d] Although these results were insufficient to obtain antiviral nucleosides, we hypothesized that the transformation of the carbocyclic derivative **3** into its 5′-thio counterpart might potentiate anti-HIV activity. To confirm this, we envisioned synthesizing a dihydrothiopyranocytosine derivative **4** as a potential HIV-nucleoside. In this Letter, we report on the synthesis of a racemic mixture of 5-thio-2,3-didehydropyranosylcytosine **4** starting

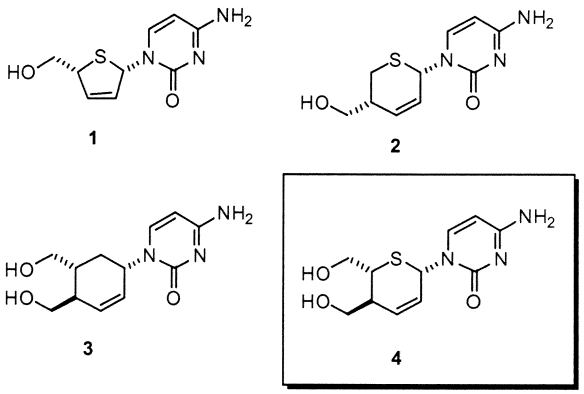


Chart 1.

* Corresponding authors.
E-mail address: yoshimura@tohoku-pharm.ac.jp (Y. Yoshimura).

0960-894X/$ - see front matter © 2011 Elsevier Ltd. All rights reserved.
doi:10.1016/j.bmcl.2011.04.006

from but-2-yne-1,4-diol and a preliminary evaluation of its anti-HIV activity (Chart 1).

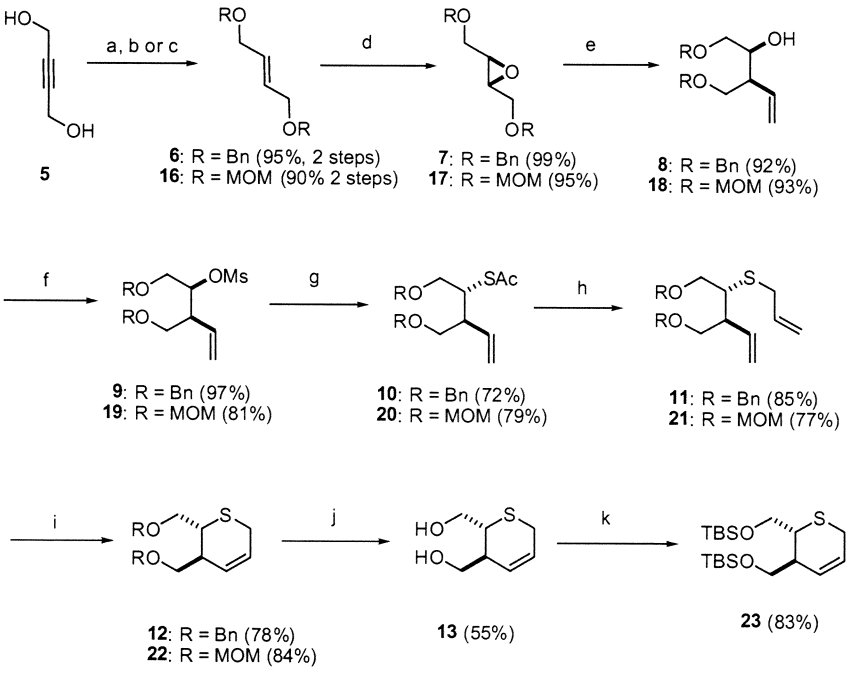
As discussed above, we previously reported on the synthesis of dihydrothiopyrano-nucleoside **2**,[4c,e] which involves two key reactions: (1) the construction of a dihydrothiopyran skeleton by ring-closing metathesis (RCM) and (2) a Pummerer-type thioglycosylation reaction. It should be possible to apply this basic synthetic concept to the synthesis of 5-thio-2,3-didehydropyranosylcytosine **4**. Thus, we started the synthesis from but-2-yne-1,4-diol to construct a dihydrothiopyran skeleton as a pseudosugar. The synthesis of the homoallyl alcohol derivative **8** was accomplished in four steps: (1) the conversion of but-2-yne-1,4-diol **5** to *trans*-but-2-ene-1,4-diol by hydroaluminamtion, (2) benzylation of the hydroxyl groups, (3) epoxidation by *m*CPBA treatment, and (4) cleavage of the resulting oxirane ring by an organocopper reagent.[6] To obtain the intermediate for the RCM reaction, it is necessary to introduce an allyl sulfide unit at the 2-position of **8**. This was achieved as follows. After mesylation of the secondary hydroxyl group of **8**, a nucleophilic substitution reaction by treatment with potassium thioacetate in the presence of crown ether gave the thioacetate **10** in good yield. The acetyl group of **10** was removed by treatment with NaOMe and the resulting thiol derivative was subsequently treated with allyl bromide to give the diene **11** in 85% yield. The diene **11** was then subjected to the RCM reaction. From our previous results, it appeared possible that the use of the Grubbs 1st catalyst might not be efficient in RCM reactions for compounds containing a sulfur atom in their structure.[4c,e] Therefore, the Grubbs 2nd catalyst was used for the RCM reaction of **11**. As expected, when **11** was reacted in the presence of 10 mol % of 2nd Grubbs catalyst in refluxing benzene, the dihydrothiopyran **12** was produced in 78% yield (Scheme 1).

Prior to carrying out the Pummerer-type thioglycosylation reaction,[4c,e,7] the dihydrothiopyran derivative **12** was converted into the corresponding sulfoxide by treatment with $NaIO_4$. The reaction gave sulfoxide **14** in excellent yield as an inseparable 1:1 mixture of diastereomers. The resulting sulfoxide **14**, in hand, was treated with bis(TMS)uracil in the presence of TMSOTf and excess iPr_2NEt to give the desired 5′-thionucleoside **15** in 55% yield as an inseparable mixture of α- and β-anomers (Scheme 2).

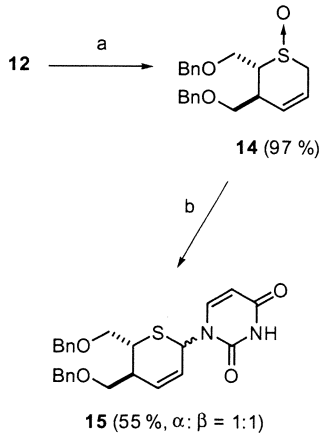
Although attempts were made to remove benzyl groups of **15**, the free nucleosides could not be obtained.[8] Alternatively, deprotection of the dihydrothiopyran derivative **12** was also attempted, which gave the deprotected products, but in poor yields. Failure to obtain free nucleosides or pseudosugar derivatives can be attributed to the instability of **15** and **12** under the reductive or Lewis acid conditions used (data not shown). These results prompted us to synthesize the target compound using other protecting groups.

After serious consideration, we re-examed the entire synthesis starting from the MOM protected derivative **16**. As can be seen in Scheme 1, all reactions starting from **5** to **12** were reproducible using a series of the MOM protected compounds and gave the desired products **16–22** in good yields. It was necessary to convert the MOM group of **22** into another protecting group that tolerates the conditions for the Pummerer-type thioglycosylation reaction.[4c,e,7] To accomplish this, we attempted to convert **22** into a TBS-protected derivative. Since the pseudosugar skeleton, as described above, was assumed to be unstable under acidic conditions, we used Fujioka's method[9] to deprotect the MOM group, since conditions close to neutral are used for this method. Compound **22** was reacted with TMSOTf in the presence of 2,2′-bipyridyl and was subsequently treated with H_2O to give the desired diol **13** in 55% yield.[9] Protection of **13** with a TBS group using standard methodology (TBSCl, imidazole) resulted in the predominant formation of the monosilylated product (data not shown). Instead of TBSCl and imidazole, the use of TBSOTf and 2,6-lutidine resulted in an improved yield, giving the bis(TBS) derivative **23** in 83% yield (Scheme 1).

By the method described above, compound **23** was oxidized to the corresponding sulfoxide **24**, which was subjected to the



Scheme 1. Reagents and conditions: (a) $LiAlH_4$, THF, reflux; (b) BnCl, NaH, THF, DMF, rt; or (c) MOMCl, iPr_2NEt, CH_2Cl_2, 40 °C; (d) *m*CPBA, CH_2Cl_2, rt; (e) $H_2C{=}CHMgCl$, CuI, Et_2O, −40 °C; (f) MsCl, Et_3N, CH_2Cl_2, rt; (g) KSAc, 18-crown-6, CH_3CN, reflux; (h) NaOMe, allyl bromide, CH_3CN, rt; (i) 2nd Grubbs cat., benzene, reflux; (j) TMSOTf, 2,2′-bipyridyl, CH_2Cl_2, 0 °C, then H_2O, Et_2O, rt; (k) TBSOTf, 2,6-lutidine, CH_2Cl_2, rt.



Scheme 2. Reagents and conditions: (a) $NaIO_4$, CH_3CN, rt; (b) bis(TMS)uracil, TMSOTf, iPr_2NEt, $PhCH_3/CH_2Cl_2$.

Pummerer-type thioglycosylation reaction.[4c,e,7] The reaction of **24** with bis(TMS)uracil, TMSOTf and iPr_2NEt afforded an anomeric mixture of the 5′-thionucleosides **25** and **26** in 63% yields. After careful separation by silica gel column chromatography, the stereochemistry at the 1′-position of the isolated **25** and **26** was determined in NOE experiments as depicted in Figure 1.[10]

The uracil ring of the β-5′-thionucleoside **25** was converted into cytosine by treatment with triisopropylbenzenesulfonyl chloride (TPSCl) and triethylamine in the presence of DMAP followed by treatment with ammonium hydroxide[11] to give **27** which contained inseparable impurities. Finally, the TBS groups of **27** were deprotected by treatment with TBAF to furnish the desired 5-thiodidehydropyranosylcytosine **4**[12] in 72% yield from **25**. The α-anomer of **29**[13] was prepared from **26** following the same sequence of reactions (Scheme 3).

Anti-HIV-1 activities of 5-thiodidehydropyranosylcytosine **4** and its anomer **29** were evaluated by the inhibition of HIV replication in peripheral blood mononuclear cells (PBMC), which was determined by a p24 HIV antigen capture assay.[14] The results are summarized in Figure 2. As expected, the β-5-thiodidehydropyranosylcytosine derivative **4** showed significant anti-HIV-1 activity at concentrations of 10 and 100 nM. It is noteworthy that the inhibitory activity of **4** at a concentration of 10 nM suppressed HIV replication to a level of 65% of the control while Lamivudine suppressed it to 37% at the same concentration. Unexpectedly, the suppression of HIV replication for **4** at a concentration of 100 nM was reduced to the level of 75% of the control. Although the reason for this is not clear at this time, the assay was performed using a racemic mixture of the 5′-thiopyrano-nucleoside and the inactive enantiomer of **4** might have had an influence on the anti-HIV activity of the mixture.[15] The α-anomer **29**, on the other hand, showed only weak activity compared with **4**. This result is consistent with the fact that the nucleosides having antiviral and antitumor activities generally possess β-configurations, analogous to naturally occurring nucleosides.

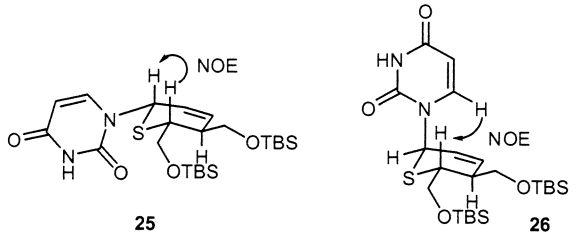
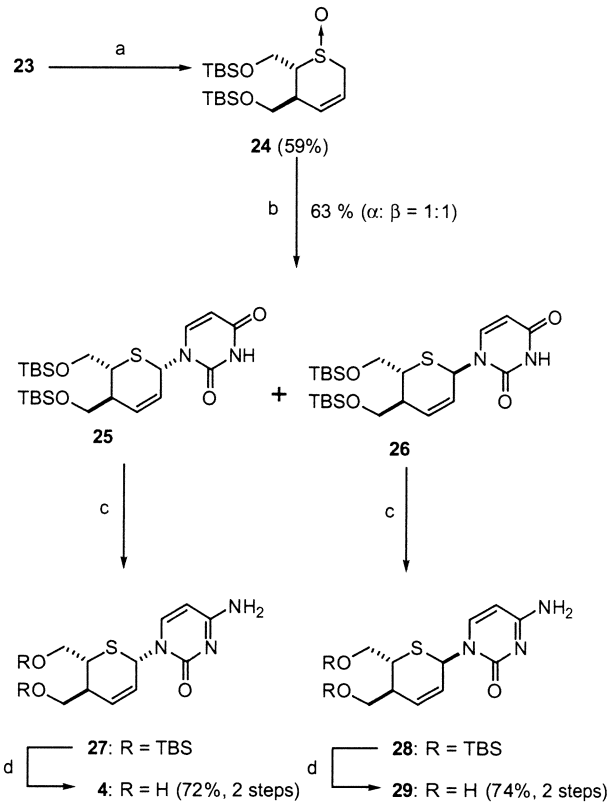


Figure 1. NOE experiments of **25** and **26**.



Scheme 3. Reagents and conditions: (a) $NaIO_4$, CH_3CN, rt (recovery of **23**: 20%); (b) bis(TMS)uracil, TMSOTf, iPr_2NEt, $PhCH_3/CH_2Cl_2$; (c) TPSCl, DMAP Et_3N, CH_3CN, rt, then NH_4OH; (d) TBAF, THF.

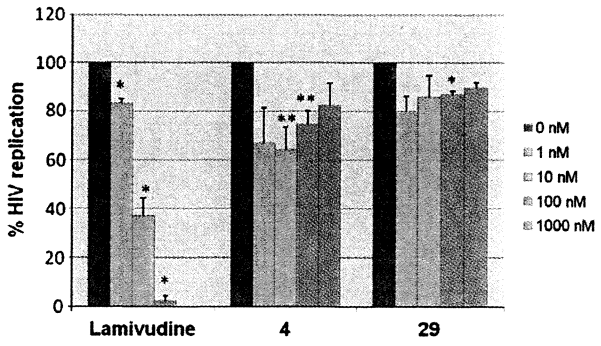


Figure 2. Summary of anti-HIV-1 activities of **4** and **29**. Anti-HIV-1 activity was evaluated by the inhibition of HIV replication in peripheral blood mononuclear cells (PBMC) from healthy volunteers, which was determined by a p24 HIV antigen capture assay (Perkin–Elmer)[14] using Lamivudine as a positive control (*p <0.01, **p <0.05). Statistical analyses were performed using the Student's t-test.

In conclusion, we report on the design and synthesis of the novel 5′-thiodidehydropyrano-nucleosides **4** and **29**. The findings indicate that **4** has significant anti-HIV activity. To obtain more potent analogues for inhibiting HIV replication, investigations on structure–activity relationships including the enantioselective synthesis of both enantiomers of **4** will be needed. These studies are currently underway and the results will be reported in future reports.

Acknowledgments

This work was supported in part by a Grant-in-Aid for Scientific Research (No. 21590119), JSPS (Y.Y.) and by High Technology Research Program from Ministry of Education, Culture, Sports, Science and Technology of Japan.

References and notes

1. Esté, J. A.; Cihlar, T. *Antiviral Res.* **2010**, *85*, 25.
2. (a) Meadows, D. C.; Gervey-Hague, J. *ChemMedChem* **2006**, *1*, 16; (b) Imamichi, T. *Curr. Pharm. Des.* **2004**, *10*, 4039.
3. (a) Mehellou, Y.; De Clercq, E. *J. Med. Chem.* **2010**, *53*, 521. and references cited therein; (b) Cihlar, T.; Ray, A. S. *Antiviral Res.* **2010**, *85*, 39. and references cited therein; (c) Wang, Q.; Li, Y.; Song, C.; Qian, K.; Chen, C.-H.; Lee, K.-H.; Chang, J. *Bioorg. Med. Chem. Lett.* **2010**, *20*, 4053; (d) Boyer, P. L.; Vu, B. C.; Ambrose, Z.; Julias, J. G.; Warnecke, S.; Liao, C.; Meier, C.; Marquez, V. E.; Hughes, S. H. *J. Med. Chem.* **2009**, *52*, 5356.
4. (a) Yamada, K.; Hayakawa, H.; Sakata, S.; Ashida, N.; Yoshimura, Y. *Bioorg. Med. Chem. Lett.* **2010**, *20*, 6013; (b) Yoshimura, Y.; Asami, K.; Imamichi, T.; Kuroda, T.; Shiraki, K.; Tanaka, H.; Takahata, H. *J. Org. Chem.* **2010**, *75*, 4161; (c) Yoshimura, Y.; Yamazaki, Y.; Saito, Y.; Takahata, H. *Tetrahedron* **2009**, *65*, 9091; (d) Yoshimura, Y.; Ohta, M.; Imahori, T.; Imamichi, T.; Takahata, H. *Org. Lett.* **2008**, *10*, 3449; (e) Yoshimura, Y.; Yamazaki, Y.; Kawahata, M.; Yamaguchi, K.; Takahata, H. *Tetrahedron Lett.* **2007**, *48*, 4519; (f) Yoshimura, Y.; Asami, K.; Matsui, H.; Tanaka, H.; Takahata, H. *Org. Lett.* **2006**, *8*, 6015.
5. Young, R. J.; Saw-Ponter, S.; Thomson, J. B.; Miller, J. A.; Cumming, J. G.; Pugh, A. W.; Rider, P. *Bioorg. Med. Chem. Lett.* **1995**, *5*, 2599.
6. Hanazawa, T.; Koiwa, M.; Hareau, G. P.-J.; Sato, F. *Tetrahedron Lett.* **2000**, *41*, 2659.
7. (a) Yoshimura, Y.; Kuze, T.; Ueno, M.; Komiya, F.; Haraguchi, K.; Tanaka, H.; Kano, F.; Yamada, K.; Asami, K.; Kaneko, N.; Takahata, H. *Tetrahedron Lett.* **2006**, *47*, 591; (b) Yoshimura, Y.; Kitano, K.; Yamada, K.; Satoh, H.; Watanabe, M.; Miura, S.; Sakata, S.; Sasaki, T.; Matsuda, A. *J. Org. Chem.* **1997**, *62*, 3140; (c) Yoshimura, Y.; Kitano, K.; Satoh, H.; Watanabe, M.; Miura, S.; Sakata, S.; Sasaki, T.; Matsuda, A. *J. Org. Chem.* **1996**, *61*, 822.
8. Attempts to remove the benzyl group involved the use of a Lewis acidic (BCl_3 in CH_2Cl_2) as well as reductive conditions (Li, NH_3 and Na, naphthalene). The reactions resulted in the formation of a complex mixture.
9. (a) Fujioka, H.; Kubo, O.; Senami, K.; Minamitsuji, Y.; Maegawa, T. *Chem. Commun.* **2009**, 4429; (b) Fujioka, H.; Okitsu, T.; Ohnaka, T.; Li, R.; Kubo, O.; Okamoto, K.; Sawama, Y.; Kita, Y. *J. Org. Chem.* **2007**, *72*, 7898; (c) Fujioka, H.; Sawama, Y.; Murata, N.; Okitsu, T.; Kubo, O.; Matsuda, S.; Kita, Y. *J. Am. Chem. Soc.* **2004**, *126*, 11800.
10. Compound **25** showed a 4.0% NOE at H-1′ when irradiated at H-5′ and compound **26** a 7.7% NOE at H-5′ when H-6 of the pyrimidine ring was irradiated.
11. Sekine, M.; Matsuzaki, J.; Satoh, M.; Hata, T. *J. Org. Chem.* **1982**, *47*, 571.
12. Data for **4**: ^{1}H NMR (400 MHz, CD_3OD) δ 2.69–2.73 (m, 1H), 2.98–3.04 (m, 1H), 3.45–3.59 (m, 4H), 5.78 (ddd, J = 1.4, 3.4, 11.1 Hz, 1H), 5.81 (d, J = 7.7 Hz, 1H), 5.89–5.90 (m, 1H), 6.14 (ddd, J = 2.4, 5.8, 11.1 Hz, 1H), 7.52 (d, J = 7.7 Hz, 1H). ^{13}C NMR (100 MHz, CD_3OD) δ 38.8, 41.3, 52.1, 63.6, 66.2, 96.6, 124.8, 134.9, 143.5, 158.3, 167.5. EI-MS m/z 269 (M^+). HRMS Calcd for $C_{11}H_{15}N_3O_3S$: 269.0834, Found 269.0829.
13. Data for **29**: ^{1}H NMR (400 MHz, CD_3OD) δ 2.25–2.42 (m, 1H), 3.00 (dd, J = 5.8, 13.0 Hz, 1H), 3.65–3.75 (m, 4H), 5.75 (ddd, J = 1.9, 4.3, 10.6 Hz, 1H), 5.79 (d, J = 7.7 Hz, 1H), 6.09–6.14 (m, 2H), 7.61 (d, J = 7.7 Hz, 1H). ^{13}C NMR (100 MHz, CD_3OD) δ 40.5, 41.1, 52.9, 63.8, 63.9, 96.5, 125.3, 137.6, 143.8, 158.2, 167.5. EI-MS: m/z 269 (M^+). HRMS Calcd for $C_{11}H_{15}N_3O_3S$: 269.0834, Found 269.0830.
14. Brann, T. W.; Dewar, R. L.; Jiang, M.-K.; Shah, A.; Nagashima, K.; Metcalf, J. A.; Falloon, J.; Lane, H. C.; Imamichi, T. *J. Virol.* **2006**, *80*, 6136.
15. To clarify an active enantiomer of **4** and influence to anti-HIV activity by the inactive enantiomer, the study on the enantioselective synthesis of **4** is currently under way.

Journal of Steroid Biochemistry & Molecular Biology 121 (2010) 556–564

Contents lists available at ScienceDirect

Journal of Steroid Biochemistry and Molecular Biology

journal homepage: www.elsevier.com/locate/jsbmb

Highly sensitive and specific analysis of sterol profiles in biological samples by HPLC–ESI–MS/MS☆

Akira Honda[a,b], Teruo Miyazaki[a,b], Tadashi Ikegami[c], Junichi Iwamoto[c], Kouwa Yamashita[d], Mitsuteru Numazawa[d], Yasushi Matsuzaki[b,c,*]

[a] Center for Collaborative Research, Tokyo Medical University Ibaraki Medical Center, Ami, Ibaraki 300-0395, Japan
[b] Department of Development for Community Medicine, Tokyo Medical University Ibaraki Medical Center, Ami, Ibaraki 300-0395, Japan
[c] Department of Gastroenterology, Tokyo Medical University Ibaraki Medical Center, Ami, Ibaraki 300-0395, Japan
[d] Faculty of Pharmaceutical Science, Tohoku Pharmaceutical University, Sendai, Miyagi 981-8558, Japan

ARTICLE INFO

Article history:
Received 27 September 2009
Received in revised form 27 January 2010
Accepted 2 March 2010

Keywords:
Review
Analysis
Cholesterol
Sterol
Oxysterol
GC–MS
HPLC–MS/MS
Derivatization

ABSTRACT

High-performance liquid chromatography–tandem mass spectrometry (HPLC–MS/MS) is a powerful method for the microanalysis of compounds in biological samples. Compared with gas chromatography–mass spectrometry (GC–MS), this method is more broadly applicable to various compounds and usually does not require a derivatization step before analysis. However, when neutral sterols are analyzed, the sensitivities of usual HPLC–MS/MS method are not superior to those of GC–MS because the sterols are relatively resistant to ionization. In this review, we introduce the recent development of HPLC–MS/MS analysis for the quantification of non-cholesterol sterols. By adding an effective derivatization step to the conventional procedure, sterol analysis by HPLC–MS/MS surpassed that obtained by GC–MS in sensitivity. In addition, sufficient specificity of this method was achieved by selected reaction monitoring (SRM) and thorough chromatographic separation of each sterol.

© 2010 Elsevier Ltd. All rights reserved.

1. Introduction

Some cholesterol precursors and oxidized cholesterol (oxysterols) are important molecules in the regulation of lipid homeostasis in the body [1]. In addition, they have been used as serum biomarkers for whole body cholesterol synthesis [2,3], intestinal cholesterol absorption [4], hepatic bile acid synthesis [5,6] and the diagnosis of inherited disorders in cholesterol metabolism [7–12]. Therefore, quantification of non-cholesterol sterols in biological samples is a very important technique in studies of lipid metabolism.

Gas chromatography (GC) with flame ionization detection [2,13], high-performance liquid chromatography (HPLC) with ultraviolet (UV) detection [14–16] or HPLC with refractive index (RI) detection [16] are the most generally used methods for the analyses of sterols. However, these methods cannot quantify minor components of endogenous sterols with sufficient sensitivity and specificity.

Mass spectrometry (MS) and tandem mass spectrometry (MS/MS) are powerful detection methods, which are suitable for GC and HPLC systems. These detectors are not only superior in terms of sensitivity but are also highly specific compared with flame ionization, UV and RI detectors. GC–MS has been widely accepted as a reliable analytical method for the determination of sterols in biological samples [17–19]. However, during the last decade, HPLC–MS or HPLC–MS/MS has also come to be used conveniently because these methods do not always require deconjugation and derivatization steps before analysis [20,21]. In addition, while HPLC methods do not cause decomposition of some labile sterols, such as 24S,25-epoxycholesterol, the high temperatures achieved during GC methods can cause degradation of unstable sterols [22,23].

In this review, we introduce the recent development of HPLC–MS/MS methods for the quantification of sterols in biological samples. An effective derivatization step, thorough chromatographic separation and selected reaction monitoring (SRM) by MS/MS have achieved excellent sensitivity and specificity for this method. The method has become a central approach for the simultaneous quantification of sterols in small amounts of biological samples.

☆ Article from special issue on "Steroid profiling and analytics: going towards Sterome".

* Corresponding author at: Department of Gastroenterology, Tokyo Medical University Ibaraki Medical Center, 3-20-1 Chuoh, Ami, Inashiki, Ibaraki 300-0395, Japan. Tel.: +81 29 887 1161; fax: +81 29 887 9113.
E-mail address: ymatsuzaki-gi@umin.ac.jp (Y. Matsuzaki).

0960-0760/$ – see front matter © 2010 Elsevier Ltd. All rights reserved.
doi:10.1016/j.jsbmb.2010.03.030

2. Methods to increase the sensitivity of sterols

2.1. Ionization

Advances in ionization techniques have greatly contributed to the development of LC–MS. Electron impact ionization (EI) is the most commonly used approach for GC–MS analysis of sterols. This ionization method was applied to HPLC–MS by using a particle beam (PB) interface. In 1995 Sattler et al. [24] analyzed plasma 7-dehydrocholesterol and in 1998 Careri et al. [25] quantified oxysterols by HPLC–PB-EI–MS, with detection limits of 10 ng (about 26 pmol) and 2–3 ng (about 5–7.5 pmol), respectively.

While EI is not applicable to polar or high molecular weight compounds, electrospray ionization (ESI) is broadly applicable method for polar compounds in a wide range of molecular weights (Fig. 1). In addition, this ionization source is generally exchangeable in the same mass spectrometer with atmospheric pressure chemical ionization (APCI) or atmospheric pressure photoionization (APPI) sources that are applicable to less polar and low molecular weight compounds. Thus, ESI and the complementary use of APCI or APPI have recently become the standard ionization methods for HPLC–MS.

Since sterols are less polar and relatively low molecular weight compounds, APCI [26–33] or APPI [20,34] have been preferentially used for analysis by HPLC–MS. The detection limits of cholesterol precursors and sitosterol by HPLC-APCI–MS were well below 1 pmol [31], that of cholesterol by HPLC-APCI–MS/MS was 2.2 pmol [32], and those of oxysterols by HPLC-APCI–MS were in the range of 0.2–0.8 ng (about 0.5–2.0 pmol) [26] or 0.1–0.75 ng (about 0.25–1.9 pmol) [27].

While it had previously been considered that ESI was not suitable for the analysis of neutral sterols, in 2007 McDonald et al. reported that sterols were sufficiently ionized when HPLC–ESI–MS/MS was employed using the Applied Biosystems 4000 QTrap triple quadrupole system [21]. According to this report, detection limits of dihydroxy- or epoxysterols were 5–60 fmol while those of monohydroxysterols were 175–2000 fmol on-column. These sensitivities are not inferior to those of APCI, but one weak point is that the sensitivity depends greatly on the instruments.

2.2. Derivatization

As shown in Table 1, conventional HPLC-APCI–MS for the detection of one of the representative oxysterols, 7α-hydroxycholesterol (1.2 pmol) [27], is not as sensitive as GC–MS (4–120 fmol) [35,36] because sterols are relatively resistant to ionization. On the other hand, this oxysterol may be quantified by HPLC–ESI–MS/MS [21] with sensitivity (60 fmol) equivalent to GC–MS, but not all HPLC–ESI–MS/MS instruments are applicable to this sensitive analysis of sterols.

To overcome these problems, sterols have been derivatized to more polar structures. The charged moieties were introduced into the hydroxyl group of the sterols as an *N*-methylpyridyl ether [37], a ferrocenecarbamate ester [38], a sulfate [39], a mono-(dimethylaminoethyl) succinyl ester [40], a dimethylglycine ester [41], and a picolinyl ester [42–44]. Furthermore, the native carbonyl group of oxysterols or the 3-oxo structure, converted from 3β-hydroxysterols by cholesterol oxidase, was derivatized to Girard P hydrazone [45–47]. Each of these derivatizations enhanced the ionization efficiency of the sterols in the ESI process and markedly increased the sensitivity.

As for ionization polarity, the sulfate derivatives are easily deprotonated and exhibit a high ionization efficiency in the negative ESI mode [39]. In contrast, the other derivatives are positively charged permanently or easily protonated, so that they are suitable for the positive ESI mode. Generally speaking, the negative mode exhibits lower background noise compared with that in positive mode. However, the positive mode provides much abundant ions than negative one [48].

It may be noted here that derivatizations are useful to increase the ionization of steroids, not only in ESI, but also in the APCI processes [49,50]. However, derivatized sterols have been preferably analyzed by ESI because ESI is broadly applicable to various deriva-

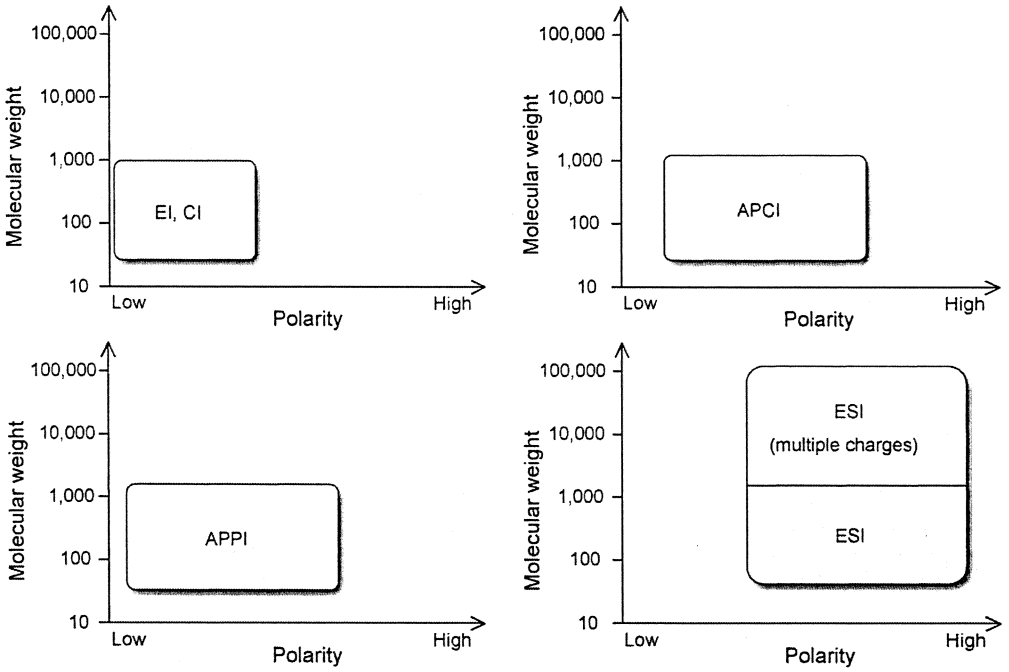


Fig. 1. Applications of various ionization methods to LC–MS. EI, electron impact ionization; CI, chemical ionization; APCI, atmospheric pressure chemical ionization; APPI, atmospheric pressure photoionization; ESI, electrospray ionization.

Table 1
Detection limits of cholesterol and representative oxysterols by different analytical methods.

Author	Year	Reference	Method (ionization mode)	Derivatization	Lower limit of detection	
					Cholesterol	Oxysterol[a]
Sanghvi et al.	1981	[36]	GC–MS (P-EI)	TMS ether	NA	120 fmol (7αOH)
Hylemon et al.	1989	[14]	HPLC-UV	C4	NA	20 pmol (7αOH)
Honda et al.	1991	[35]	GC–HR-MS (P-EI)	DMES ether	NA	4 fmol (7αOH)
Careri et al.	1998	[25]	HPLC–PB-MS (P-EI)	–[b]	5 pmol	5 pmol (7βOH)
Manini et al.	1998	[26]	HPLC–MS (P-APCI)	–	NA	500 fmol (7βOH)
Van Berkel et al.	1998	[38]	HPLC–MS/MS (P-ESI)	FC ester	41 amol	NA
Razzazi-Fazeli et al.	2000	[27]	HPLC–MS (P-APCI)	–	NA	1.2 pmol (7αOH)
Nagy et al.	2006	[31]	HPLC–MS (P-APCI)	–	<1 pmol	NA
Tian et al.	2006	[32]	HPLC–MS/MS (P-APCI)	–	2.2 pmol	NA
Griffiths et al.	2006	[46]	HPLC–MS/MS (P-ESI)	Girard P hydrazone	NA	<2.5 fmol
McDonald et al.	2007	[21]	HPLC–MS/MS (P-ESI)	–	1 pmol	60 fmol (7αOH)
Honda et al.	2008	[43]	HPLC–MS/MS (P-ESI)	picolinyl ester	260 amol	NA
Honda et al.	2009	[44]	HPLC–MS/MS (P-ESI)	picolinyl ester	NA	10 amol (7αOH)

Abbreviations: P-EI, positive electron impact ionization; TMS, trimethylsilyl; NA, not available; 7αOH, 7α-hydroxycholesterol; HPLC-UV, HPLC equipped with an ultraviolet detector; C4, 7α-hydroxy-4-cholesten-3-one; GC–HR-MS, high-resolution GC–MS; DMES, dimethylethylsilyl; HPLC–PB-MS, HPLC–MS with particle beam interface; 7βOH, 7β-hydroxycholesterol; P-APCI, positive atmospheric pressure chemical ionization; P-ESI, positive electrospray ionization; FC, ferrocenecarbamate.
[a] Data of 7α-hydroxycholesterol or other oxysterols with the structures similar to 7α-hydroxycholesterol.
[b] Without derivatization.

tives. In the positive APCI mode, the introduction of moieties with proton affinity increases ionization, while those with highly polar functional groups inhibit ionization and decrease the sensitivity [50]. Thus, the selection of effective derivatives for positive APCI is not as easy as that for ESI. Negative APCI is also used after the addition of electron affinity moieties to sterols. This electron-capturing derivatization in negative APCI mode was first reported by Singh et al. [51] and has been applied to the determination of tissue cholesterol by Kuo et al. [52].

3. Methods to increase the selectivity of each sterol

3.1. Use of appropriate internal standards

Deuterium-labeled sterols are ideal internal standards for quantification by HPLC–MS. The addition of internal standards compensates for the loss of target sterols during clean-up procedures and for the variation in injection volume onto the HPLC column. Thus, internal standards are necessary for accurate quantification by chromatographic methods. In addition, internal standards are used to determine the variation in the retention time of each sterol among samples. When peaks of target sterols are very small or they are not completely separated from interfering peaks, the retention time of the internal standard gives additional information to identify the target peaks. Several deuterated standards are commercially available, as reported by McDonald et al. [21]. Although deuterated analogs are not available for all sterols, deuterated sterol with a structure similar to the target sterol can be used as a surrogate [21,44]. Alternatively, we can use coprostanol as a convenient internal standard for monohydroxysterols in human serum [43]. Coprostanol is synthesized from cholesterol by intestinal bacteria but is not absorbed from the intestine and is not detected in human serum.

3.2. Sample clean-up

The structures of non-cholesterol sterols are similar to native cholesterol, which usually exists at least 100–10,000 times greater than the target sterols in bulk-lipid extracts from biological samples. Therefore, good separation from cholesterol is necessary for reliable quantification of the non-cholesterol sterols. Because oxysterols and epoxysterols are more polar than cholesterol, most of them can be separated from cholesterol by a solid-phase extraction cartridge [18,53]. However, the complete separation of some less polar oxysterols and non-cholesterol monohydroxysterols from cholesterol by using such a cartridge is difficult. Thus, for the analysis of whole sterol profiles in biological samples, the role of solid-phase extraction is limited to the elimination of nonpolar compounds, such as fatty acyl esters of cholesterol [53], that are strongly retained on reversed-phase HPLC columns.

3.3. Separation by HPLC

Since we have not achieved selective elimination of cholesterol from bulk-lipid extracts using solid-phase extraction cartridges, non-cholesterol sterols must be separated from cholesterol by the final HPLC–MS or HPLC–MS/MS analyses. In addition, the separation between non-cholesterol sterols is also important to quantify each sterol. However, isobaric sterol isomers, e.g. cholesterol and lathosterol [43] or 24S-hydroxycholesterol and 25-hydroxycholesterol [21,44], often exhibit similar precursor to product ion fragmentations, so that even SRM cannot always differentiate these sterols. Therefore, careful HPLC separation of each sterol is crucially important to quantify these isomers by selected ion monitoring (SIM) or SRM [33,43].

Although normal phase columns can be used for the separation of sterols by HPLC-PB–MS [24,25] and HPLC–APCI-MS [16], reversed-phase columns are preferably used in HPLC–PB-MS [25], most of the HPLC–APCI-MS [26–31,33], HPLC–APPI-MS [20,34], and virtually all HPLC–ESI–MS methods with [42–44,47] and without derivatization [21]. Normal phase HPLC sometimes achieves better separation of each sterol compared with reversed-phase HPLC [16], but the latter is preferred for HPLC–MS because it displays higher reproducibility than normal phase and the polar mobile phase favors ionization.

Our experiences show that there are many minor unidentified sterols in biological samples and complete chromatographic or mass spectrometric separation of all sterols by a single analysis is impossible at present. We need to select the best column and mobile phase according to the target sterols in which we are interested.

3.4. Selection by MS/MS

Although MS/MS is not an almighty method for the differentiation of each sterol, it is much more specific and sensitive than UV and RI detectors [16]. The triple quadrupole mass spectrometer is the most suitable instrument for the highly sensitive

quantification of sterols. SRM obtained by MS/MS can eliminate interfering peaks with different precursor to product ion fragmentations at specific collision energies. In addition, the monitoring of multiple SRM pairs for a single sterol adds confidence to the identification of the compound and provides further information regarding compound identification based on their relative intensities [21].

Another way to improve the selectivity of SRM is to increase the resolution of the triple quadrupole mass spectrometer. Although the resolution depends on the capacity of the mass spectrometer, analysis with higher resolution reduces interfering peaks and improves S/N ratio of the chromatogram. Furthermore, Griffiths et al. have reported high-resolution MS by a hybrid quadrupole/time of flight (TOF) mass spectrometer [46] or high-resolution MS^n by a hybrid linear ion-trap/Fourier transform mass spectrometer [54]. These mass spectrometers exhibit excellent selectivity, but sensitivity and dynamic range for quantification do not reach those achieved by the triple quadrupole mass spectrometer.

4. Characteristics of picolinyl ester derivative of sterols

4.1. Sensitivity

We have successfully introduced a picolinyl moiety into the hydroxyl group of various sterols and have demonstrated that the picolinyl ester derivatization is a simple and versatile method for sensitive and specific quantification using positive HPLC–ESI–MS/MS [42–44]. The idea originated from a report by Yamashita et al. [55] in which they compared HPLC–ESI–MS/MS behaviors among the picolinyl, 6-methylpicolinyl, nicotinyl, 2-methyoxynicotinyl and isonicotinyl derivatives of estrone, estradiol, dehydroepiandrosterone and testosterone. The picolinyl derivatives showed the best HPLC–ESI–MS/MS behavior and 100-fold higher detection response by SRM compared with underivatized steroid molecules [55,56]. In addition, they have successfully applied the picolinyl derivatization to corticosteroids [57,58] and aldosterone [59,60].

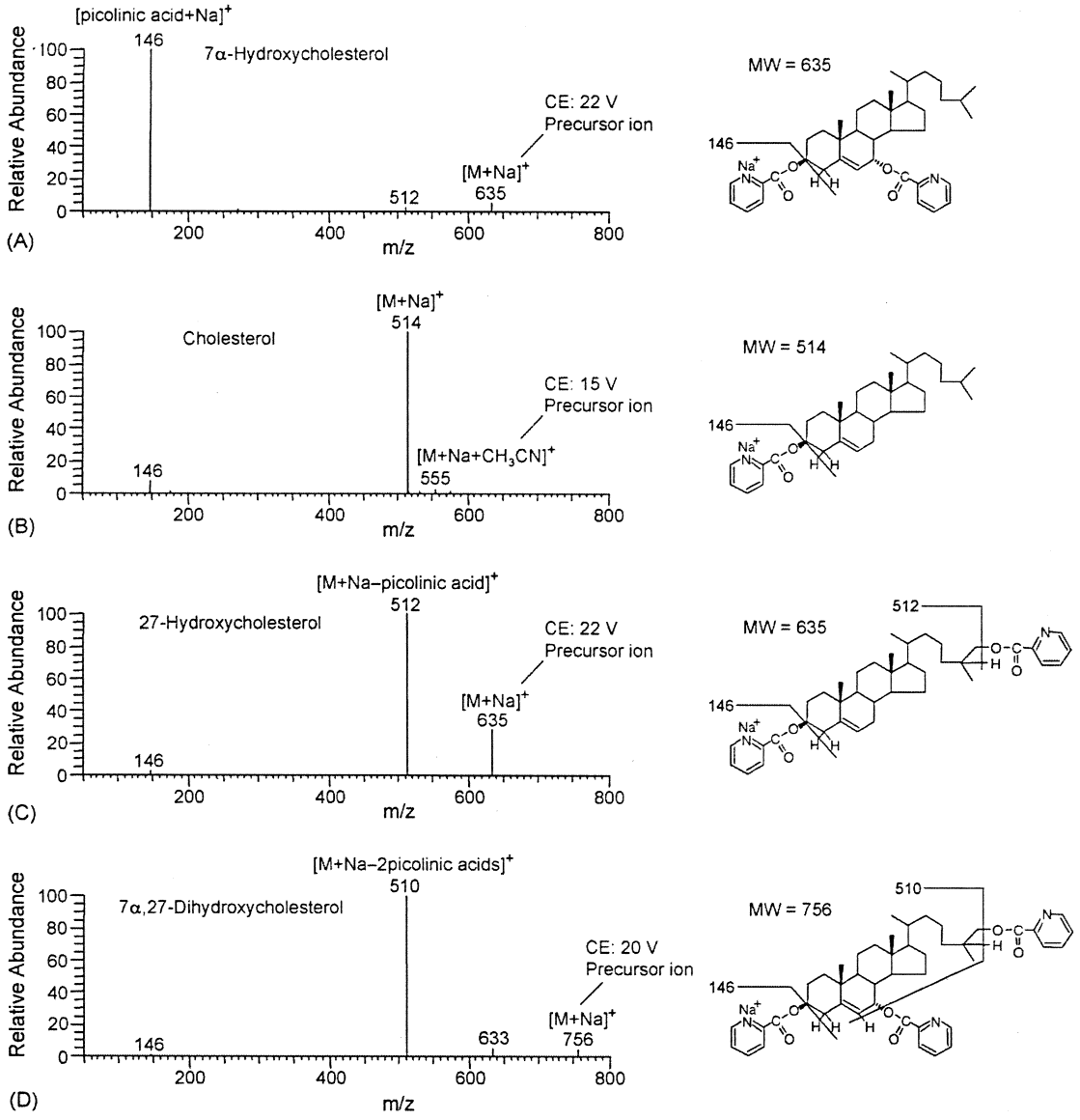


Fig. 2. Representative positive ESI–MS/MS fragmentation patterns of the picolinyl ester derivatives of sterols. (A) 7α-hydroxycholesterol, (B) cholesterol, (C) 27-hydroxycholesterol, (D) 7α,27-dihydroxycholesterol. $[M+Na]^+$ was used as precursor ions for A, C and D, while $[M+Na+CH_3CN]^+$ was used as a precursor ion for B. Fragmentation patterns of A, B, C and D correspond to those in Table 2. The general LC–MS/MS conditions were as follows: introducing solvent, acetonitrile–methanol–water (45:45:10, v/v/v) containing 0.1% acetic acid; flow rate, 300 μl/min; spray voltage, 1000 V. CE, collision energy. In the case of oxysterols with multiple hydroxyl groups (A, C and D), the position of sodium in the picolinyl derivatives has not been determined. In structural formulae, sodium ion was tentatively added to picolinyl group at the C-3β position.

As for sterols, the detection limits (S/N = 3) of cholesterol picolinate and oxysterol dipicolinates by HPLC–ESI–MS/MS (SRM) analysis were about 260 amol and 5–25 amol on-column, respectively [43,44], which was about 3860-fold and 1000-fold, respectively, more sensitive than those with underivatized HPLC–ESI–MS/MS analysis [21]. On the other hand, the detection limits of native cholesterol and oxysterols by HPLC-APCI–MS/MS analysis were about 100 fmol and 10 fmol, respectively [43,44].

4.2. Mass spectra

All picolinyl ester derivatives of 3β-monohydroxysterols exhibited adduct ions of $[M + Na + CH_3CN]^+$ as the base peaks [43], while those of di-, tri- and tetra-hydroxysterols and 3-ketosterols showed $[M + Na]^+$ ions as the base peaks under our HPLC–ESI–MS conditions [44]. However, it should be noted here that the base peaks would change depending on the composition of mobile phase. In contrast to other derived moieties, the picolinyl group is not permanently charged, so that even in the case of oxysterols with multiple hydroxyl groups, a single charged ion was predominant in the positive ESI mass spectra.

Collision of $[M + Na + CH_3CN]^+$ of the picolinyl derivatives of 3β-monohydroxysterols at a relatively low collision energy (10–15 V) resulted in the predominant formation of $[M + Na]^+$ as product ions, while the use of higher collision energies (25–30 V) resulted in the [picolinic acid + Na]$^+$ (m/z = 146) ion as the most abundant product ion. In contrast, collision of $[M + Na]^+$ of the picolinyl derivatives of di-, tri- and tetra-hydroxysterols and 3-ketosterols resulted in the formation of [M + Na–picolinic acid]$^+$ or [picolinic acid + Na]$^+$ ions at any specific collision energy depending on the sterols (10–30 V). Representative MS/MS fragmentation patterns of the picolinyl derivatives are shown in Fig. 2, and the most suitable collision energies and precursor to product ions of each sterol for SRM are listed in Table 2.

4.3. Synthesis of derivatives

The derivatization and purification steps are very simple [44]. As shown in Fig. 3, the reagent mixture, consisting of 2-methyl-6-nitrobenzoic anhydride, 4-dimethylaminopyridine, picolinic acid, pyridine and triethylamine, is added to the sterol extract, and incubated at 80 °C for 60 min. Excess reagents are then precipitated by the addition of *n*-hexane, and the clear supernatant containing picolinyl ester derivatives is collected and evaporated at 80 °C under nitrogen. The residue is redissolved in 50 μl of acetonitrile and an aliquot is used for HPLC–ESI–MS/MS analysis. The

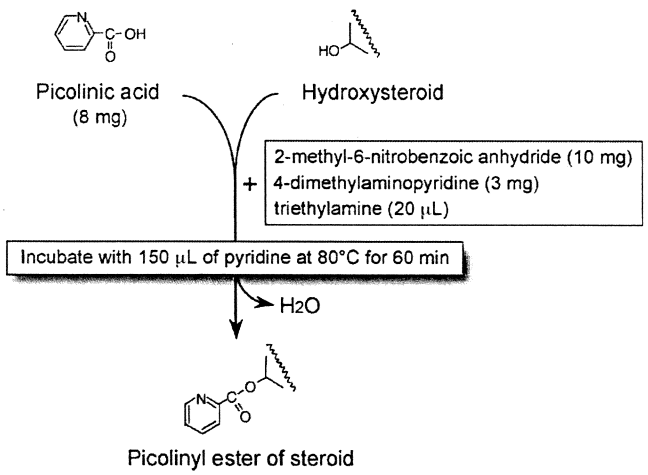


Fig. 3. The formation of picolinyl ester derivative and the conditions of the reaction.

derivatives are stable for at least 6 months in the acetonitrile solution.

In general, this esterification progresses easily at room temperature, but the hydroxyl groups at the C-5α, C-20α and C-25 positions of oxysterols are resistant to picolinyl ester formation at room temperature. In these resistant positions, C-25 is completely esterified by heating at 80 °C for 60 min, but the C-5α and C-20α positions are not esterified at all even if the reaction mixture is heated at 80 °C.

It has been pointed out that cholesterol can be autoxidized during sample preparation [61]. However, to analyze whole sterol profiles in biological samples, it is difficult to remove cholesterol selectively before derivatization. Therefore, we determined the formation of oxysterols from pure cholesterol in the derivatizing conditions, and no significant amounts of oxysterols were detected. The results suggest that the autoxidation of cholesterol during the derivatization step is negligible.

Transesterification of fatty acyl esters during the formation of picolinyl esters is another possibility for the overestimation of sterols. However, the incubation of pure cholesteryl stearate in the reaction mixture showed that the transesterification was not probable.

4.4. Chromatographic separation

HPLC is performed using a reversed-phase Hypersil GOLD column (150 mm × 2.1 mm I.D., 3 μm, Thermo Fisher Scientific, San Jose, CA, USA). In our previous reports, monohydroxysterols [43] and oxysterols [44] were measured separately, but both sterols can be analyzed simultaneously because the HPLC column and gradient conditions are the same. Initially, the mobile phase is comprised of acetonitrile–methanol–water (40:40:20, v/v/v) containing 0.1% acetic acid, and it is then programmed in a linear manner to acetonitrile–methanol–water (45:45:10, v/v/v) containing 0.1% acetic acid over 20 min. The final mobile phase is maintained constant for an additional 20 min. The flow rate is 300 μl/min, and the column is maintained at 40 °C using a column oven.

Relative retention times (RRTs), expressed relative to the retention time of cholesterol, are listed in Table 2. The RRTs show that the separation of sterols by the Hypersil GOLD column is excellent, but several weak points are also indicated. First, 7β-hydroxycholesterol gives a peak just before 7α-hydroxycholesterol, and reliable quantification of each hydroxycholesterol can occasionally be difficult. Second, the retention times of 7α-hydroxy-4-cholesten-3-one and 24S,25-epoxycholesterol are very close to each other, and these sterols show similar MS and MS/MS spectra. However, because 7α-hydroxy-4-cholesten-3-one does not survive alkaline hydrolysis, the peak detected after alkaline hydrolysis is 24S,25-epoxycholesterol alone. Third, lanosterol gives a peak just after cholesterol. Although the monitoring ion for lanosterol is different from that for cholesterol, a huge cholesterol peak in biological samples can sometimes interfere with the lanosterol peak.

These problems are resolved by using another reversed-phase column, Hypersil GOLD aQ (150 mm × 2.1 mm I.D., 3 μm, Thermo Fisher Scientific). This column is usually used for separations employing highly aqueous mobile phases, but we use it as follows: initially, the mobile phase is comprised of acetonitrile–methanol–water (40:40:20, v/v/v) containing 0.1% acetic acid; it is then programmed in a linear manner to acetonitrile–methanol (50:50, v/v) containing 0.1% acetic acid over 40 min. The final mobile phase is maintained constant for an additional 2 min. The flow rate is 300 μl/min, and the column is maintained at 40 °C using a column oven.

The RRTs by the Hypersil GOLD aQ column are also shown in Table 2. Compared with the Hypersil GOLD column, the width of each peak tends to be wide, and the order of elution from the column is very different. Good chromato-

Table 2
Positive ESI-SRM and HPLC data of the picolinyl ester derivative of each sterol[a].

Picolinyl ester derivatives	SRM condition			HPLC data (RRT[c])	
	Precursor to product (*m/z*)	Collision energy (*V*)	Pattern[b]	C18[d]	C18 aQ[e]
24S-Hydroxy-4-cholesten-3-one	528 → 146	24	A	0.34	0.30
25-Hydroxy-4-cholesten-3-one	528 → 146	24	A	0.36	0.37
27-Hydroxy-4-cholesten-3-one	528 → 146	24	A	0.40	0.42
7α-Hydroxy-4-cholesten-3-one	528 → 146	24	A	0.42	0.33
7β-Hydroxy-4-cholesten-3-one	528 → 146	24	A	0.44	0.36
5α-Cholesta-8(9),14,24-trien-3β-ol	551 → 510	12	B	0.71	0.71
Cholesta-5,7,24-trien-3β-ol	551 → 510	12	B	0.73	0.79
Cholesta-5,8,24-trien-3β-ol	551 → 510	12	B	0.75	0.78
5α-Cholesta-7,24-dien-3β-ol	553 → 512	12	B	0.81	0.87
Zymosterol	553 → 512	12	B	0.82	0.86
Desmosterol	553 → 512	12	B	0.83	0.88
5α-Cholesta-8(9),14-dien-3β-ol	553 → 512	12	B	0.84	0.87
5α-Cholesta-6,8(9)-dien-3β-ol	553 → 512	12	B	0.85	0.83
7-Dehydrocholesterol	553 → 512	12	B	0.87	0.92
8-Dehydrocholesterol	553 → 512	12	B	0.89	0.91
Lathosterol	555 → 514	15	B	0.97	0.98
8-Lathosterol	555 → 514	15	B	0.98	0.98
Cholesterol	555 → 514	15	B	1.00	1.00
Coprostanol	557 → 516	14	B	1.05	0.91
Cholestanol	557 → 516	14	B	1.10	1.04
4-Methyl-5α-cholesta-8(9),24-dien-3β-ol	567 → 526	12	B	0.89	0.89
4-Methyl-5α-cholesta-8(9),14-dien-3β-ol	567 → 526	12	B	0.90	0.92
24S,25-Epoxycholesterol	569 → 528	12	B	0.42	0.53
7-Ketocholesterol	569 → 528	12	B	0.53	0.48
4-Methyl-5α-cholest-8(9)-en-3β-ol	569 → 528	12	B	1.07	1.01
Campesterol	569 → 528	12	B	1.10	1.03
20α-Hydroxycholesterol[f]	571 → 530	14	B	0.40	0.43
5β,6β-Epoxycholestanol	571 → 530	14	B	0.68	0.64
5α,6α-Epoxycholestanol	571 → 530	14	B	0.70	0.68
4,4′-Dimethyl-5α-cholesta-8(9),14,24-trien-3β-ol	579 → 538	14	B	0.84	0.78
4,4′-Dimethyl-5α-cholesta-8(9),24-dien-3β-ol	581 → 540	14	B	0.97	0.93
4,4′-Dimethyl-5α-cholesta-8(9),14-dien-3β-ol	581 → 540	14	B	1.01	0.99
4,4′-Dimethyl-5α-cholest-8(9)-en-3β-ol	583 → 542	14	B	1.19	1.04
Sitosterol	583 → 542	14	B	1.22	1.07
Sitostanol	585 → 544	14	B	1.36	1.11
Lanosterol	595 → 554	12	B	1.01	0.90
Dihydrolanosterol	597 → 556	15	B	1.24	1.01
27-Hydroxy-7-dehydrocholesterol	633 → 510	22	C	0.49	0.62
7β-Hydroxycholesterol	635 → 146	22	A	0.61	0.53
7α-Hydroxycholesterol	635 → 146	22	A	0.62	0.51
6-Hydroxycholesterol	635 → 146	22	A	0.69	0.63
4β-Hydroxycholesterol	635 → 146	22	A	0.78	0.76
22R-Hydroxycholesterol	635 → 512	22	C	0.47	0.55
22S-Hydroxycholesterol	635 → 512	22	C	0.50	0.48
24R-Hydroxycholesterol	635 → 512	22	C	0.50	0.56
24S-Hydroxycholesterol	635 → 512	22	C	0.50	0.57
25-Hydroxycholesterol	635 → 512	22	C	0.53	0.66
27-Hydroxycholesterol	635 → 512	22	C	0.58	0.71
5β-Cholestane-3α,7α-diol	637 → 514	22	C	0.64	0.49
7α,27-Dihydroxy-4-cholesten-3-one	649 → 146	28	A	0.18	0.17
7α,12α-Dihydroxy-4-cholesten-3-one	649 → 146	28	A	0.19	0.14
Cholestan-3β,5α,6β-triol[f]	653 → 146	28	A	0.60	0.50
7α,27-Dihydroxycholesterol	756 → 510	20	D	0.33	0.31
5β-Cholestane-3α,7α,12α-triol	758 → 635	28	C	0.32	0.24
5β-Cholestane-3α,7α,12α,25-tetrol	879 → 756	20	C	0.15	0.12

Abbreviations: ESI, electrospray ionization; SRM, selected reaction monitoring; RRT, relative retention time.

[a] Some data in this table have been reported in our previous paper [43,44].

[b] Patterns of precursor to product ions. A: $[M+Na]^+ \rightarrow$ [picolinic acid + Na]$^+$; B: $[M+Na+CH_3CN]^+ \rightarrow [M+Na]^+$; C: $[M+Na]^+ \rightarrow$ [M + Na−picolinic acid]$^+$; D: $[M+Na]^+ \rightarrow$ [M + Na−2 picolinic acids]$^+$. A, B, C and D correspond to those in Fig. 2.

[c] RRTs are expressed relative to the retention time of cholesterol 3β-picolinate.

[d] A reversed-phase C18 column, Hypersil GOLD (150 mm × 2.1 mm I.D., 3 μm, Thermo Fisher Scientific) was employed. Initially, the mobile phase was comprised of acetonitrile–methanol–water (40:40:20, v/v/v) containing 0.1% acetic acid, then it was programmed in a linear manner to acetonitrile–methanol–water (45:45:10, v/v/v) containing 0.1% acetic acid over 20 min. The final mobile phase was kept constant for an additional 20 min. The flow rate was 300 μl/min, and the column was maintained at 40 °C using a column oven. The retention time of cholesterol 3β-picolinate by this condition was around 28.5 min.

[e] Polar endcapped C18 column, Hypersil GOLD aQ (150 mm × 2.1 mm I.D., 3 μm, Thermo Fisher Scientific) was used. Initially, the mobile phase was comprised of acetonitrile–methanol–water (40:40:20, v/v/v) containing 0.1% acetic acid; then it is programmed in a linear manner to acetonitrile–methanol (50:50, v/v) containing 0.1% acetic acid over 40 min. The final mobile phase was kept constant for an additional 2 min. The flow rate was 300 μl/min, and the column was maintained at 40 °C. The retention time of cholesterol 3β-picolinate by this condition was around 36.5 min.

[f] Hydroxyl groups at the C-5α and C-20α positions of oxysterols are not derivatized.

graphic separations are achieved between 7α-hydroxycholesterol and 7β-hydroxycholesterol, 7α-hydroxy-4-cholesten-3-one and 24S,25-epoxycholesterol, and cholesterol and lanosterol. However, the lathosterol and 8-lathosterol peaks are not differentiated.

The separations of picolinylated sterols by these reversed-phase columns are not at all inferior to the separation of free sterols by reversed-phase HPLC [15,21]. For example, the separation of 24-hydroxycholesterol and 25-hydroxycholesterol was difficult, but DeBarber et al. achieved the chromatographic separation and quantification by using a mobile phase consisted of acetonitrile–methanol–water and APCI-MS/MS detector [33]. In contrast, McDonald et al. failed to quantify these sterol isomers separately by using an eluent of methanol–water and ESI–MS/MS detector [21]. They did not use acetonitrile because the presence of acetonitrile significantly reduced signal intensity of sterols analyzed by this detector. As for picolinylated 24- and 25-hydroxycholesterols, they were well separated each other by using acetonitrile–methanol–water as a mobile phase, and excellent sensitivities were achieved by ESI–MS/MS detector.

4.5. Sample preparation

Long term storage or repeated freeze and thaw of biological samples should be avoided because it stimulates cholesterol autoxidation [61]. Addition of the antioxidant, butylated hydroxytoluene, to the sample before sample preparation produced only a modest decrease in oxidation. Therefore, minimizing oxidation by using good lab practices is important [21].

To analyze the unesterified fraction of sterols, serum (1–5 μl), subcellular fraction of tissue (0.1–1.0 mg protein), or cell homogenate (1×10^4–1×10^5 cells) is dried with the added internal standards, and directly derivatized to the picolinyl esters [43]. To analyze the total (unesterified + esterified) fraction, saponification is carried out in 1 N ethanolic KOH at 37 °C for 1 h, and sterols are extracted with *n*-hexane before derivatization [44]. It may be mentioned here that some sterols occur as conjugates with sulfuric or glucuronic acid [62–64]. Negative ESI mode without derivatization is suitable for the analyses of these conjugated sterols, and the conjugated sterols are much more polar than picolinyl esters of unconjugated sterols.

Because this assay method is very sensitive, we can minimize the loading of derivatized sample on the HPLC column. Although the solid-phase extraction/purification step is omitted, target sterols are successfully separated by the HPLC–MS/MS step. In case of human serum analysis, less than 1 ng of picolinyl esters of non-cholesterol sterols are injected onto the column with approximately 200 ng of cholesterol picolinate. Under our HPLC conditions, this amount of cholesterol picolinate is easily trapped in the Hypersil GOLD and Hypersil GOLD aQ columns and eluted at around 28.5 min and 36.5 min, respectively, which is well separated from the picolinyl esters of most non-cholesterol sterols.

While picolinyl esters of sterols are very soluble in acetonitrile, nonpolar compounds, such as fatty acyl esters of cholesterol, remain underivatized and do not dissolve in the final acetonitrile solution. Nonpolar compounds are strongly retained on reversed-phase HPLC columns, but in this method, loading of the nonpolar compounds on the column is minimized.

4.6. Precision and accuracy

The linearity of the standard curves, as determined by simple linear regression, was excellent, as reported in our previous papers [43,44]. Reproducibilities and recoveries of some sterols were validated according to a one-way layout and polynomial equation, respectively [43,44]. The variances between sample preparations and between measurements by this method were calculated to be 1.6–12.7% and 2.5–16.5%, respectively. In these results, higher values of the variances (over 10%) were obtained by the quantification of sterols that showed extremely low concentrations in the samples. To test matrix effects, the recovery experiments were performed using human serum or rat liver microsomes spiked with 0.05–12 ng of sterols. Recoveries of the sterols ranged from 86.7% to 107.3% with a mean recovery of 99.3%, which suggests that matrix effects are not significant in this assay. This method provides reproducible and reliable results for the quantification of sterols in small amounts of biological samples.

5. Perspectives

HPLC–MS or HPLC–MS/MS does not require a derivatization step before the analysis of sterols, which is advantageous for a high-throughput assay. However, the addition of the derivatization step has markedly improved the sensitivities of the neutral sterols. Thus, simple and rapid procedures do not always produce good results for the microanalysis of biological samples. In addition, since many sterols have the same molecular weight and similar structures, a thorough chromatographic separation is essential to maintain the selectivity even if the latest model of mass spectrometer is operated in a high-resolution mode.

The recent development of steroid biochemistry has demonstrated that there are considerable bioactive or biomarker sterols among intermediates and their derivatives in the biosynthetic pathways of cholesterol, bile acids and steroid hormones. Moreover, there are still many unidentified sterols in biological samples. Therefore, not only sensitive and specific quantification of targeted sterols but also metabolomic analysis of whole sterol profiles will become an important methodology for steroid biochemistry and its clinical applications.

References

[1] S. Gill, R. Chow, A.J. Brown, Sterol regulators of cholesterol homeostasis and beyond: the oxysterol hypothesis revisited and revised, Prog. Lipid Res. 47 (2008) 391–404.
[2] I. Björkhem, T. Miettinen, E. Reihner, S. Ewerth, B. Angelin, K. Einarsson, Correlation between serum levels of some cholesterol precursors and activity of HMG-CoA reductase in human liver, J. Lipid Res. 28 (1987) 1137–1143.
[3] H.J. Kempen, J.F. Glatz, J.A. Gevers Leuven, H.A. van der Voort, M.B. Katan, Serum lathosterol concentration is an indicator of whole-body cholesterol synthesis in humans, J. Lipid Res. 29 (1988) 1149–1155.
[4] T.A. Miettinen, R.S. Tilvis, Y.A. Kesäniemi, Serum plant sterols and cholesterol precursors reflect cholesterol absorption and synthesis in volunteers of a randomly selected male population, Am. J. Epidemiol. 131 (1990) 20–31.
[5] I. Björkhem, E. Reihnér, B. Angelin, S. Ewerth, J.-E. Åkerlund, K. Einarsson, On the possible use of the serum level of 7α-hydroxycholesterol as a marker for increased activity of the cholesterol 7α-hydroxylase in humans, J. Lipid Res. 28 (1987) 889–894.
[6] T. Yoshida, A. Honda, N. Tanaka, Y. Matsuzaki, B. He, T. Osuga, N. Kobayashi, K. Ozawa, H. Miyazaki, Simultaneous determination of mevalonate and 7α-hydroxycholesterol in human plasma by gas chromatography–mass spectrometry as indices of cholesterol and bile acid biosynthesis, J. Chromatogr. 613 (1993) 185–193.
[7] G.S. Tint, M. Irons, E.R. Elias, A.K. Batta, R. Frieden, T.S. Chen, G. Salen, Defective cholesterol biosynthesis associated with the Smith–Lemli–Opitz syndrome, N. Engl. J. Med. 330 (1994) 107–113.
[8] D.R. FitzPatrick, J.W. Keeling, M.J. Evans, A.E. Kan, J.E. Bell, M.E. Porteous, K. Mills, R.M. Winter, P.T. Clayton, Clinical phenotype of desmosterolosis, Am. J. Med. Genet. 75 (1998) 145–152.
[9] R.I. Kelley, W.G. Wilcox, M. Smith, L.E. Kratz, A. Moser, D.S. Rimoin, Abnormal sterol metabolism in patients with Conradi–Hunermann–Happle syndrome and sporadic lethal chondrodysplasia punctata, Am. J. Med. Genet. 83 (1999) 213–219.
[10] P.A. Krakowiak, C.A. Wassif, L. Kratz, D. Cozma, M. Kovarova, G. Harris, A. Grinberg, Y. Yang, A.G. Hunter, M. Tsokos, R.I. Kelley, F.D. Porter, Lathosterolosis: an inborn error of human and murine cholesterol synthesis due to lathosterol 5-desaturase deficiency, Hum. Mol. Genet. 12 (2003) 1631–1641.
[11] G. Salen, S. Shefer, L. Nguyen, G.C. Ness, G.S. Tint, V. Shore, Sitosterolemia, J. Lipid Res. 33 (1992) 945–955.
[12] G. Halperin, M. Elisaf, E. Leitersdorf, D. Harats, A new method for determination of serum cholestanol by high-performance liquid chromatography with ultraviolet detection, J. Chromatogr. B Biomed. Sci. Appl. 742 (2000) 345–352.

[13] B.J. Koopman, J.C. van der Molen, B.G. Wolthers, J.B. Vanderpas, Determination of some hydroxycholesterols in human serum samples, J. Chromatogr. 416 (1987) 1–13.
[14] P.B. Hylemon, E.J. Studer, W.M. Pandak, D.M. Heuman, Z.R. Vlahcevic, Y.L. Chiang, Simultaneous measurement of cholesterol 7α-hydroxylase activity by reverse-phase high-performance liquid chromatography using both endogenous and exogenous [4-^{14}C]cholesterol as substrate, Anal. Biochem. 182 (1989) 212–216.
[15] B. Ruan, N. Gerst, G.T. Emmons, J. Shey, G.J. Schroepfer Jr., Sterol synthesis. A timely look at the capabilities of conventional and silver ion high performance liquid chromatography for the separation of C27 sterols related to cholesterol biosynthesis, J. Lipid Res. 38 (1997) 2615–2626.
[16] T. Saldanha, A.C. Sawaya, M.N. Eberlin, N. Bragagnolo, HPLC separation and determination of 12 cholesterol oxidation products in fish: comparative study of RI, UV, and APCI-MS detectors, J. Agric. Food Chem. 54 (2006) 4107–4113.
[17] A. Cohen, H.S. Hertz, J. Mandel, R.C. Paule, R. Schaffer, L.T. Sniegoski, T. Sun, M.J. Welch, V.E. White, Total serum cholesterol by isotope dilution/mass spectrometry: a candidate definitive method, Clin. Chem. 26 (1980) 854–860.
[18] S. Dzeletovic, O. Breuer, E. Lund, U. Diczfalusy, Determination of cholesterol oxidation products in human plasma by isotope dilution-mass spectrometry, Anal. Biochem. 225 (1995) 73–80.
[19] H.S. Ahmida, P. Bertucci, L. Franzo, R. Massoud, C. Cortese, A. Lala, G. Federici, Simultaneous determination of plasmatic phytosterols and cholesterol precursors using gas chromatography–mass spectrometry (GC–MS) with selective ion monitoring (SIM), J. Chromatogr. B Analyt. Technol. Biomed. Life Sci. 842 (2006) 43–47.
[20] J. Lembcke, U. Ceglarek, G.M. Fiedler, S. Baumann, A. Leichtle, J. Thiery, Rapid quantification of free and esterified phytosterols in human serum using APPI-LC–MS/MS, J. Lipid Res. 46 (2005) 21–26.
[21] J.G. McDonald, B.M. Thompson, E.C. McCrum, D.W. Russell, Extraction and analysis of sterols in biological matrices by high performance liquid chromatography electrospray ionization mass spectrometry, Methods Enzymol. 432 (2007) 145–170.
[22] Z. Zhang, D. Li, D.E. Blanchard, S.R. Lear, S.K. Erickson, T.A. Spencer, Key regulatory oxysterols in liver: analysis as Δ^4-3-ketone derivatives by HPLC and response to physiological perturbations, J. Lipid Res. 42 (2001) 649–658.
[23] B. Ruan, W.K. Wilson, J. Pang, N. Gerst, F.D. Pinkerton, J. Tsai, R.I. Kelley, F.G. Whitby, D.M. Milewicz, J. Garbern, G.J. Schroepfer Jr., Sterols in blood of normal and Smith–Lemli–Opitz subjects, J. Lipid Res. 42 (2001) 799–812.
[24] W. Sattler, H.J. Leis, G.M. Kostner, E. Malle, Quantification of 7-dehydrocholesterol in plasma and amniotic fluid by liquid chromatography/particle beam-mass spectrometry as a biochemical diagnostic marker for the Smith–Lemli–Opitz syndrome, Rapid Commun. Mass Spectrom. 9 (1995) 1288–1292.
[25] M. Careri, P. Ferretti, P. Manini, M. Musci, Evaluation of particle beam high-performance liquid chromatography–mass spectrometry for analysis of cholesterol oxides, J. Chromatogr. A 794 (1998) 253–262.
[26] P. Manini, R. Andreoli, M. Careri, L. Elviri, M. Musci, Atmospheric pressure chemical ionization liquid chromatography/mass spectrometry in cholesterol oxide determination and characterization, Rapid Commun. Mass Spectrom. 12 (1998) 883–889.
[27] E. Razzazi-Fazeli, S. Kleineisen, W. Luf, Determination of cholesterol oxides in processed food using high-performance liquid chromatography–mass spectrometry with atmospheric pressure chemical ionization, J. Chromatogr. A 896 (2000) 321–334.
[28] I. Burkard, K.M. Rentsch, A. von Eckardstein, Determination of 24S- and 27-hydroxycholesterol in plasma by high-performance liquid chromatography–mass spectrometry, J. Lipid Res. 45 (2004) 776–781.
[29] J.J. Palmgren, A. Toyras, T. Mauriala, J. Monkkonen, S. Auriola, Quantitative determination of cholesterol, sitosterol, and sitostanol in cultured Caco-2 cells by liquid chromatography-atmospheric pressure chemical ionization mass spectrometry, J. Chromatogr. B Analyt. Technol. Biomed. Life Sci. 821 (2005) 144–152.
[30] K. Raith, C. Brenner, H. Farwanah, G. Müller, K. Eder, R.H.H. Neubert, A new LC/APCI-MS method for the determination of cholesterol oxidation products in food, J. Chromatogr. A 1067 (2005) 207–211.
[31] K. Nagy, A. Jakab, F. Pollreisz, D. Bongiorno, L. Ceraulo, M.R. Averna, D. Noto, K. Vekey, Analysis of sterols by high-performance liquid chromatography/mass spectrometry combined with chemometrics, Rapid Commun. Mass Spectrom. 20 (2006) 2433–2440.
[32] Q. Tian, M.L. Failla, T. Bohn, S.J. Schwartz, High-performance liquid chromatography/atmospheric pressure chemical ionization tandem mass spectrometry determination of cholesterol uptake by Caco-2 cells, Rapid Commun. Mass Spectrom. 20 (2006) 3056–3060.
[33] A.E. DeBarber, D. Lutjohann, L. Merkens, R.D. Steiner, Liquid chromatography-tandem mass spectrometry determination of plasma 24S-hydroxycholesterol with chromatographic separation of 25-hydroxycholesterol, Anal. Biochem. 381 (2008) 151–153.
[34] R. Karuna, A. von Eckardstein, K.M. Rentsch, Dopant assisted-atmospheric pressure photoionization (DA-APPI) liquid chromatography–mass spectrometry for the quantification of 27-hydroxycholesterol in plasma, J. Chromatogr. B Analyt. Technol. Biomed. Life Sci. 877 (2009) 261–268.
[35] A. Honda, J. Shoda, N. Tanaka, Y. Matsuzaki, T. Osuga, N. Shigematsu, M. Tohma, H. Miyazaki, Simultaneous assay of the activities of two key enzymes in cholesterol metabolism by gas chromatography–mass spectrometry, J. Chromatogr. 565 (1991) 53–66.
[36] A. Sanghvi, E. Grassi, C. Bartman, R. Lester, M. Galli Kienle, G. Galli, Measurement of cholesterol 7α-hydroxylase activity with selected ion monitoring, J. Lipid Res. 22 (1981) 720–724.
[37] J.M.E. Quirke, C.L. Adams, G.J. Van Berkel, Chemical derivatization for electrospray ionization mass spectrometry. 1. Alkyl halides, alcohols, phenols, thiols, and amines, Anal. Chem. 66 (1994) 1302–1315.
[38] G.J. Van Berkel, J.M. Quirke, R.A. Tigani, A.S. Dilley, T.R. Covey, Derivatization for electrospray ionization mass spectrometry. 3. Electrochemically ionizable derivatives, Anal. Chem. 70 (1998) 1544–1554.
[39] R. Sandhoff, B. Brugger, D. Jeckel, W.D. Lehmann, F.T. Wieland, Determination of cholesterol at the low picomole level by nano-electrospray ionization tandem mass spectrometry, J. Lipid Res. 40 (1999) 126–132.
[40] D.W. Johnson, H.J. ten Brink, C. Jakobs, A rapid screening procedure for cholesterol and dehydrocholesterol by electrospray ionization tandem mass spectrometry, J. Lipid Res. 42 (2001) 1699–1705.
[41] X. Jiang, D.S. Ory, X. Han, Characterization of oxysterols by electrospray ionization tandem mass spectrometry after one-step derivatization with dimethylglycine, Rapid Commun. Mass Spectrom. 21 (2007) 141–152.
[42] A. Honda, K. Yamashita, M. Numazawa, T. Ikegami, M. Doy, Y. Matsuzaki, H. Miyazaki, Highly sensitive quantification of 7α-hydroxy-4-cholesten-3-one in human serum by LC–ESI–MS/MS, J. Lipid Res. 48 (2007) 458–464.
[43] A. Honda, K. Yamashita, H. Miyazaki, M. Shirai, T. Ikegami, G. Xu, M. Numazawa, T. Hara, Y. Matsuzaki, Highly sensitive analysis of sterol profiles in human serum by LC–ESI–MS/MS, J. Lipid Res. 49 (2008) 2063–2073.
[44] A. Honda, K. Yamashita, T. Hara, T. Ikegami, T. Miyazaki, M. Shirai, G. Xu, M. Numazawa, Y. Matsuzaki, Highly sensitive quantification of key regulatory oxysterols in biological samples by LC–ESI–MS/MS, J. Lipid Res. 50 (2009) 350–357.
[45] W.J. Griffiths, S. Liu, G. Alvelius, J. Sjövall, Derivatisation for the characterisation of neutral oxosteroids by electrospray and matrix-assisted laser desorption/ionisation tandem mass spectrometry: the Girard P derivative, Rapid Commun. Mass Spectrom. 17 (2003) 924–935.
[46] W.J. Griffiths, Y. Wang, G. Alvelius, S. Liu, K. Bodin, J. Sjövall, Analysis of oxysterols by electrospray tandem mass spectrometry, J. Am. Soc. Mass Spectrom. 17 (2006) 341–362.
[47] K. Karu, M. Hornshaw, G. Woffendin, K. Bodin, M. Hamberg, G. Alvelius, J. Sjovall, J. Turton, Y. Wang, W.J. Griffiths, Liquid chromatography-mass spectrometry utilizing multi-stage fragmentation for the identification of oxysterols, J. Lipid Res. 48 (2007) 976–987.
[48] K. Hiraoka, I. Kudaka, Negative-mode electrospray-mass spectrometry using nonaqueous solvents, Rapid Commun. Mass Spectrom. 6 (1992) 265–268.
[49] T. Higashi, K. Shimada, Derivatization of neutral steroids to enhance their detection characteristics in liquid chromatography–mass spectrometry, Anal. Bioanal. Chem. 378 (2004) 875–882.
[50] T. Higashi, N. Takayama, T. Nishio, E. Taniguchi, K. Shimada, Procedure for increasing the detection responses of estrogens in LC–MS based on introduction of a nitrobenzene moiety followed by electron capture atmospheric pressure chemical ionization, Anal. Bioanal. Chem. 386 (2006) 658–665.
[51] G. Singh, A. Gutierrez, K. Xu, I.A. Blair, Liquid chromatography/electron capture atmospheric pressure chemical ionization/mass spectrometry: analysis of pentafluorobenzyl derivatives of biomolecules and drugs in the attomole range, Anal. Chem. 72 (2000) 3007–3013.
[52] M.S. Kuo, J.M. Kalbfleisch, P. Rutherford, D. Gifford-Moore, X.D. Huang, R. Christie, K. Hui, K. Gould, M. Rekhter, Chemical analysis of atherosclerotic plaque cholesterol combined with histology of the same tissue, J. Lipid Res. 49 (2008) 1353–1363.
[53] E.G. Lund, U. Diczfalusy, Quantitation of receptor ligands by mass spectrometry, Methods Enzymol. 364 (2003) 24–37.
[54] W.J. Griffiths, M. Hornshaw, G. Woffendin, S.F. Baker, A. Lockhart, S. Heidelberger, M. Gustafsson, J. Sjövall, Y. Wang, Discovering oxysterols in plasma: a window on the metabolome, J. Proteome Res. 7 (2008) 3602–3612.
[55] K. Yamashita, S. Kobayashi, S. Tsukamoto, M. Numazawa, Synthesis of pyridine-carboxylate derivatives of hydroxysteroids for liquid chromatography–electrospray ionization–mass spectrometry, Steroids 72 (2007) 50–59.
[56] K. Yamashita, M. Okuyama, Y. Watanabe, S. Honma, S. Kobayashi, M. Numazawa, Highly sensitive determination of estrone and estradiol in human serum by liquid chromatography–electrospray ionization tandem mass spectrometry, Steroids 72 (2007) 819–827.
[57] K. Yamashita, M. Takahashi, S. Tsukamoto, M. Numazawa, M. Okuyama, S. Honma, Use of novel picolinoyl derivatization for simultaneous quantification of six corticosteroids by liquid chromatography–electrospray ionization tandem mass spectrometry, J. Chromatogr. A 1173 (2007) 120–128.
[58] K. Yamashita, R. Nakagawa, M. Okuyama, S. Honma, M. Takahashi, M. Numazawa, Simultaneous determination of tetrahydrocortisol, allotetrahydrocortisol and tetrahydrocortisone in human urine by liquid chromatography–electrospray ionization tandem mass spectrometry, Steroids 73 (2008) 727–737.
[59] K. Yamashita, Y. Tadokoro, M. Takahashi, M. Numazawa, Preparation and structural elucidation of the picolinyl ester of aldosterone for liquid chromatography–electrospray ionization tandem mass spectrometry, Chem. Pharm. Bull. 56 (2008) 873–877.
[60] K. Yamashita, M. Okuyama, R. Nakagawa, S. Honma, F. Satoh, R. Morimoto, S. Ito, M. Takahashi, M. Numazawa, Development of sensitive derivatization method for aldosterone in liquid chromatography–electrospray ionization

tandem mass spectrometry of corticosteroids, J. Chromatogr. A 1200 (2008) 114–121.
[61] L.L. Smith, Cholesterol Autoxidation, Plenum Press, New York, 1981.
[62] A.K. Batta, G. Salen, S. Shefer, G.S. Tint, M. Batta, Increased plasma bile alcohol glucuronides in patients with cerebrotendinous xanthomatosis: effect of chenodeoxycholic acid, J. Lipid Res. 28 (1987) 1006–1012.
[63] L.J. Meng, W.J. Griffiths, H. Nazer, Y. Yang, J. Sjövall, High levels of (24S)-24-hydroxycholesterol 3-sulfate, 24-glucuronide in the serum and urine of children with severe cholestatic liver disease, J. Lipid Res. 38 (1997) 926–934.
[64] X. Li, W.M. Pandak, S.K. Erickson, Y. Ma, L. Yin, P. Hylemon, S. Ren, Biosynthesis of the regulatory oxysterol, 5-cholesten-3β,25-diol 3-sulfate, in hepatocytes, J. Lipid Res. 48 (2007) 2587–2596.

Journal of Steroid Biochemistry & Molecular Biology 119 (2010) 141–148

Contents lists available at ScienceDirect

Journal of Steroid Biochemistry and Molecular Biology

journal homepage: www.elsevier.com/locate/jsbmb

Assay of labile estrogen *o*-quinones, potent carcinogenic molecular species, by high performance liquid chromatography–electrospray ionization tandem mass spectrometry with phenazine derivatization

Kouwa Yamashita*, Akina Masuda, Yuka Hoshino, Sachiko Komatsu, Mitsuteru Numazawa

Faculty of Pharmaceutical Sciences, Tohoku Pharmaceutical University, 4-1 Komatsushima 4-Chome, Aoba-ku, Sendai, Miyagi 981-8558, Japan

ARTICLE INFO

Article history:
Received 7 October 2009
Received in revised form 12 February 2010
Accepted 18 February 2010

Keywords:
Liquid chromatography–electrospray ionization tandem mass spectrometry
o-Quinone
Immobilized iodoxybenzoic acid
Phenazine derivative
Tyrosinase
Rat liver microsomes

ABSTRACT

A sensitive and selective assay method for labile estrogen *o*-quinones, estrone (E_1)-2,3-quinone (Q), E_1-3,4-Q, estradiol (E_2)-2,3-Q and E_2-3,4-Q, based on the use of phenazine (Phz) derivatization with *o*-phenylenediamine and high performance liquid chromatography–electrospray ionization tandem mass spectrometry (HPLC–ESI-MS/MS) was described. The Phz derivatives of four estrogen *o*-quinones were purified by solid phase extraction and analyzed by HPLC–ESI-MS/MS. The protonated molecule was observed as a base peak for all Phz derivatives in their ESI-mass spectra (positive mode). In multiple reaction monitoring, the transition from $[M+H]^+$ to *m/z* 231 was chosen for quantification. Calibration curves for the *o*-quinones were obtained using standard catechol estrogens after sodium metaperiodate treatment and Phz derivatization. Using this method, these four estrogen *o*-quinones were analyzed with the limit of quantification of 5 ng/ml in acetonitrile (MeCN)–blank matrix (1:4, v/v), respectively, on a basis of the weight of catechol estrogens. Assay accuracy and precision for four estrogen *o*-quinones were 89.6–113.0% and 3.1–12.6% (5, 125 and 2000 ng/ml in MeCN–blank matrix). Applications of this method enabled to determine the catalytic activities on hydroxylation and subsequent oxidation of E_1 and E_2 of Mushroom tyrosinase and rat liver microsomal fraction. It was confirmed by this method that tyrosinase exhibited 2- and 4-hydroxylation and further oxidation activities for catechols in the ring-A of estrogens. Whereas rat liver microsomal fraction possessed only 2- and 4-hydroxylation activities, and further oxidation activity for catechol estrogens was low.

© 2010 Elsevier Ltd. All rights reserved.

1. Introduction

It is known that estrogens exert inherent carcinogenic activities by generating electrophilic molecular species such as *o*-quinones or semiquinones that can covalently bind to DNA in addition to its hormonal action to stimulate proliferation in receptor-mediated cancer initiation [1–4]. In estrogen metabolism, hydroxylation of aromatic A-ring with CYPs enzymes and subsequent oxidation of catechols to the corresponding *o*-quinones have been hypothesized to be leading cause of generation of electrophilic molecules [5,6] (Fig. 1). Catechol estrogens are typically methylated by catechol O-methyl-transferase to afford monomethyl ethers, however non-methylated 2,3- and 3,4-catechols are transformed with peroxidase or tyrosinase to the reactive *o*-quinones that are proposed to attack nucleophilic groups on DNA via Michael addition [7–9]. It was also demonstrated that tyrosinase was responsible for the direct transformation of estrogens to *o*-quinone and further oxidized products [10]. 2,3-Quinones and 3,4-quinones provided different species of adducts [4,9,11], and these facts were another interest in relation to the existence of the difference in carcinogenic activity between these *o*-quinones.

Most of studies in this field were focused on the investigation with the purpose of obtaining insight into the possible mode of binding mechanism of such *o*-quinones to DNA or glutathione by analyzing the formed adduct qualitatively [3,4,7,12–16]. Synthesis and characterization of estrogen *o*-quinones in a preparative scale was investigated by Abul-Hajji and Dwivedy et al using ^1H nuclear magnetic resonance (NMR) spectroscopy and high performance liquid chromatography (HPLC) with ultraviolet (UV) detection [3,17]. In those reports, it was demonstrated that 3,4-quinones were more stable than 2,3-quinones by the measurement of their half-lives in the solution. Gelbke and Knuppen demonstrated the specific conversion of 2-hydroxyestrogens to the corresponding 2,3-quinones under various conditions and its stability, and investigated further transformation to phenazine (Phz) derivatives to stabilize *o*-quinones [18]. And it was also confirmed that prepared estrogen 2,3-quinone was relatively unstable and not obtained

* Corresponding author. Tel.: +81 22 727 0079; fax: +81 22 727 0137.
E-mail address: kyama@tohoku-pharm.ac.jp (K. Yamashita).

0960-0760/$ – see front matter © 2010 Elsevier Ltd. All rights reserved.
doi:10.1016/j.jsbmb.2010.02.016

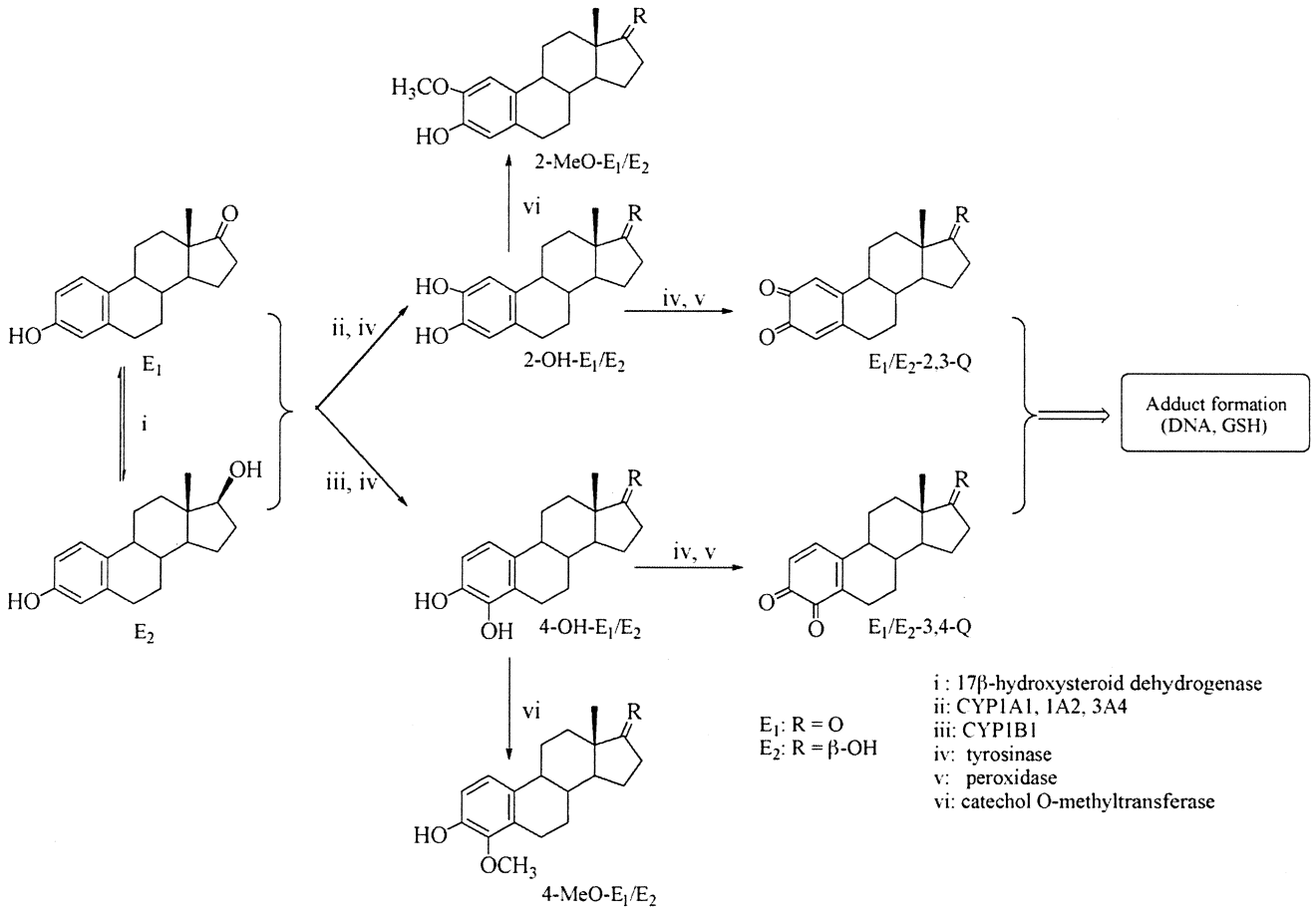


Fig. 1. Possible metabolic pathway of estrone and estradiol with various enzymic systems involving *o*-quinone formation E_1 (estrone), E_2 (estradiol), 2-OH-E_1/E_2 (2-hydroxyestrone/estradiol), 4-OH-E_1/E_2 (4-hydroxyestrone/estradiol), 2-MeO-E_1/E_2 (2-methoxyestrone/estradiol), 4-OH-E_1/E_2 (4-methoxyestrone/estradiol), E_1/E_2-2, 3-Q (estrone/estradiol-2,3-quinones) and E_1/E_2-3,4-Q (estrone/estradiol-3,4-quinones).

by crystalline form, however 2,3-quinones survive in chloroform solution for several hours [18]. The Phz derivatization was also used to the identification of 2-hydroxyestrone in human urine after oxidation [19] and other natural product [20]. However, the feasibility and selectivity of this derivatization reaction in the discriminative determination between *o*-quinone and hydroquinone, especially in a microscale, have been unclear. In this report, we described an assay method for the selective quantification of estrogen *o*-quinones in a microscale based on the use of high performance liquid chromatography–electrospray ionization tandem mass spectrometry (HPLC–ESI-MS/MS) involving *in situ* generation of *o*-quinones from catechols and its trapping by derivatization with *o*-phenylenediamine. A Phz derivative of deuterated estrogen was synthesized and used as an internal standard for quantification. The present method was applied to the determination of the catalytic activities of Mushroom tyrosinase and rat liver microsomal fraction in the conversion of estrone and estradiol to their corresponding *o*-quinones.

2. Experimental

2.1. Materials and reagents

3-Hydroxyestra-1,3,5 (10)-trien-17-one (E_1: estrone, **1**), estra-1,3,5(10)-triene-3,17β-diol (E_2: estradiol, **2a**), estra-1,3,5(10)-triene-3,17β-diol 17-acetate (E_2-17-OAc: estradiol 17-acetate, **2b**), Mushroom tyrosinase (EC 1.18.14.1, 5500 U/mg protein) and β-nicotineamide adenine dinucleotide phosphate (reduced form) (NADPH) were purchased from Sigma–Aldrich (St. Louis, MO, USA). 2,3-Dihydroxyestra-1,3,5(10)-trien-17-one (2-OH-E_1: 2-hydroxyestrone, **3**), estra-1,3,5(10)-triene-2,3,17β-triol (2-OH-E_2: 2-hydroxyestradiol, **4**), 3,4-dihydroxy-estra-1,3,5(10)-trien-17-one (4-OH-E_1: 4-hydroxyestrone, **5**), estra-1,3,5(10)-triene-3,4,17β-triol (4-OH-E_2: 4-hydroxyestradiol, **6**) were obtained from Steraloids (Newport, RI, USA). *o*-Phenylenediamine, sodium metaperiodate ($NaIO_4$), N, N-dimethylformamide (DMF), dimethylsulfoxide (DMSO), 36% hydrochloric acid (HCl), ethyl acetate (EtOAc), hexane, 95% ethanol (EtOH) and $NaIO_4$ were obtained from Nacalai Tesque (Kyoto, Japan). These solvents and reagents were of analytical grade. HPLC grade methanol (MeOH), acetonitrile (MeCN), acetic acid (AcOH) and ultra-pure water were purchased from Wako (Osaka, Japan). Immobilized iodoxybenzoic acid (IBX-polystyrene beads) was obtained from Nova Chemicals (Calgary, Canada). Bond Elut C_{18} (200 mg, 3 ml) and Bond Elut SI (100 mg, 1 ml) cartridges were obtained from Varian (Palo Alto, CA, USA). Pre-coated plate for thin layer chromatography (TLC) (Kiesel Gel 60 F254, 20 cm × 20 cm, 0.5 mm thickness) was obtained from Merck KGaA (Darmstadt, Germany). Freshly prepared solutions of catechol estrogens were used for each experiment. Rat liver microsomal fraction (Four weeks old, male, Wistar strain, 20 mg protein/ml) used in this study was prepared [21] and donated by Dr. Yorihisa Tanaka (Department of Drug Metabolism and Pharmacokinetics, Tohoku Pharmaceutical University).

2.2. Preparation of phenazine (Phz) derivatives (**11**, **12a**, **13**, **14a**) (Fig. 2)

Phz derivatives of four estrogen *o*-quinones, E_1-2,3-Q-Phz (**11**), E_2-2,3-Q-Phz (**12a**), E_1-3,4-Q-Phz (**13**) and E_2-3,4-Q-Phz (**14a**), were prepared from the corresponding catechol estrogens by treatment with $NaIO_4$ in DMF followed by the cyclization with *o*-phenylenediamine as described by Gelbke [18,19]. Derivatives **11** and **13** were also prepared by the direct oxidation of **1** with immobilized IBX-polystyrene beads [22–24] followed by the treatment of crude *o*-quinones with DMF solution of *o*-phenylenediamine. Derivatives **12a** and **14a** were prepared from **2b** in the similar manner as **11** and **13**. In the preparation of these derivatives, **12b** and **14b** were initially prepared as intermediates from **2b**. Treatment of **12b** or **14b** with 5% KOH/MeOH gave **12a** or **14a**. Each Phz derivative was purified by preparative TLC using EtOAc–hexane (1:2, v/v) as a developing solvent. Structures of each Phz derivative were confirmed by the measurement of ^1H NMR spectra (JEOL JNM-400 spectrometer; 400 MHz; $CDCl_3$ solution, Tokyo, Japan), UV spectra (Shimadzu MPS-2450 UV–vis spectrophotometer, Kyoto, Japan) and high resolution mass spectra (HR-MS) (JEOL JMS-700 double focusing mass spectrometer) in an electron ionization mode.

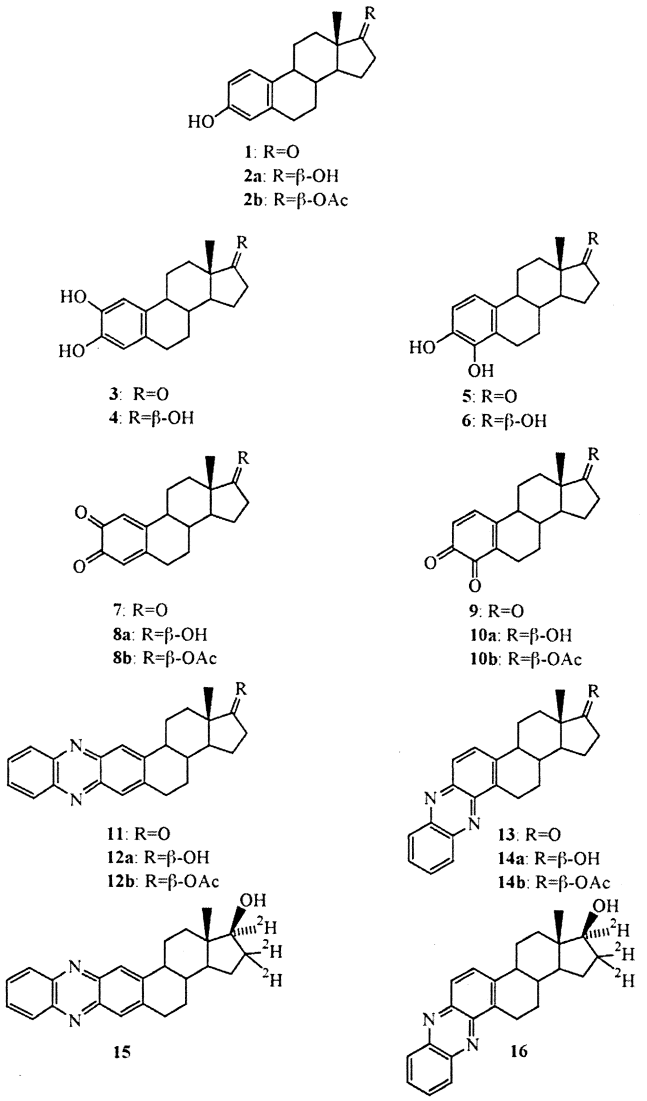


Fig. 2. Chemical structures of estrogens and phenazine derivatives used in this study.

2.3. Synthesis of internal standard (IS)

[16,16,17α-$^2H_3$] E_2-17β-OAc (15 mg) was prepared in our laboratory from [16,16,17α-$^2H_3$] E_2 by two steps of acetylation with acetic anhydride and pyridine, and partial hydrolysis of 3-acetate with $NaHCO_3$ in MeOH. [16,16,17α-$^2H_3$] E_2-17β-OAc was subsequently treated with IBX-polystyrene beads, *o*-phenylenediamine and 5% KOH in methanol to afford deuterium labeled compounds **15** (1.5 mg) and **16** (1.3 mg), after preparative TLC purification using EtOAc–hexane (1:2, v/v) as a developing solvent. Deuterium distributions were as follows: **15**: d_0; 0.5%, d_1; 3.7%, d_2; 22.5%, d_3; 70.0%, d_4; 3.3%, **16**: d_0; 0.2%, d_1; 2.8%, d_2; 22.9%, d_3; 70.9%, d_4; 3.2%. Compound **16** was used as an IS for the simultaneous determination of four estrogen *o*-quinones.

2.4. Preparation of blank matrix

Rat liver microsome suspension (20 mg protein/ml) was treated at 100 °C for 15 min. Denaturated microsome suspension was diluted with 50 mM phosphate buffer (pH 7.4, 40 ml) and then resuspended. The diluted microsome suspension was used as blank matrix.

2.5. High performance liquid chromatography (HPLC)

HPLC was run on a Waters 2695 separation module equipped with a Waters 2487 UV detector (Waters, Milford, MA, USA). The column was an X-Bridge C_{18} (150 mm × 4.6 mm I.D., 5 μm, Waters) and used at an ambient temperature. The mobile phases consisted of MeOH–H_2O–AcOH (45:55:0.1, v/v/v) for *o*-quinones or catechols and MeCN–H_2O–AcOH (70:30:0.1, v/v/v) for Phz derivatives were used at a flow rate of 1 ml/min with an isocratic elution. Wavelength of an UV detector was set at 257 nm for the detection of Phz derivatives and 280 nm for *o*-quinones and catechols, respectively.

2.6. HPLC–electrospray ionization tandem mass spectrometry (ESI-MS/MS)

HPLC–ESI-MS/MS was run on a Finnigan TSQ Quantum triple-stage quadrupole mass spectrometer (Thermo Fischer Scientific, San Jose, CA, USA) equipped with an ESI ion source and a Surveyor auto-sampler and a MS-pump (Thermo Fischer Scientific). The columns was an X-Bridge C_{18} (100 mm × 2.1 mm I.D., 5 μm, Waters) connected to a guard cartridge (C_{18}, 10 mm × 2 mm I.D., 5 μm) in a guard-cartridge holder with the mobile phase consisted of MeCN–H_2O–AcOH (70:30:0.1, v/v/v) at a flow rate of 200 μl/min. Elution was performed with an isocratic mode and at an ambient temperature. The general ESI/MS conditions were as follows: spray voltage, 4500 V (positive); sheath gas, nitrogen, 35 arbitrary unit (gas pressure); auxiliary gas, nitrogen, 15 arbitrary unit (gas pressure); ion transfer capillary temperature, 350 °C; collision gas argon, 1.5 mTorr (gas pressure). Transitions of Phz derivatives for each *o*-quinone in multiple reaction monitoring (MRM) were as follows: E_1-2,3-Q-Phz (**11**) and E_1-3,4-Q-Phz (**13**); m/z 357 → m/z 231 (collision energy, 60 V), E_2-2,3-Q-Phz (**12a**) and E_2-3,4-Q-Phz (**14a**); m/z 359 → m/z 231 (collision energy, 60 V), IS (**16**): m/z 362 → m/z 231 (collision energy, 60 V).

2.7. Generation of *o*-quinones (**7**, **9**, **8a** and **10a**) from 2- and 4-hydroxyestrogens (**3**, **5**, **4** and **6**) with $NaIO_4$ in a microscale

To a mixed solution of catechol estrogens (50 μl) (**3**, **4**, **5** and **6**: 50 μg each/ml) in MeCN–blank matrix (1:4, v/v) was added 10% $NaIO_4$ (20 μl) and AcOH (5 μl), and the resulting mixture was

allowed to stand at room temperature for 2 min. The reaction mixture was immediately analyzed by HPLC (λ 280 nm). A mixture of catechol estrogens (50 μl) (**3**, **4**, **5** and **6**) at two different concentrations (200 ng and 2000 ng/ml: MeCN–blank matrix, 1:4, v/v) were prepared and oxidized with 10% $NaIO_4$, and then submitted to LC–ESI-MS/MS analyses.

2.8. Trapping of o-quinones with o-phenylenediamine

To a solution of estrogen *o*-quinone generated as described above (Section 2.7) was added *o*-phenylenediamine (15 mg/200 μl in DMF, w/v), and the resulting mixture was allowed to stand at room temperature for 30 min. The reaction mixture was diluted 5% HCl (2 ml) and then the transferred onto Bond Elut C_{18} (200 mg, pre-conditioned with 3 ml EtOAc, 3 ml MeOH and 3 ml water). The cartridge was subsequently washed with 5% HCl (3 ml × 3), H_2O (3 ml × 3) and 35% MeCN (3 ml × 3) and the Phz derivative was eluted with EtOAc (2 ml). To this eluate was added hexane (4 ml) and the resulting mixture was passed through Bond Elut SI (100 mg, 1 ml). Eluate was evaporated to dryness and the residue was dissolved in EtOAc (100 μl) and then subjected to LC–ESI-MS/MS.

Absolute recovery rates in the processes of *o*-quinone generation from catechol estrogen followed by the Phz derivatization were assessed by comparing the peak area of the prepared Phz derivative to that of peak area obtained from the corresponding synthetic standards of each Phz derivative using **16** as an internal standard.

2.9. Calibration curves

The mixed solution of four catechol estrogens (50 μl) (**3**, **4**, **5** and **6**: 0, 2.5, 5.0, 12.5, 50, 125, 625, 2500 ng each/ml: MeCN–blank matrix, 1: 4, v/v) was subsequently treated with 10% $NaIO_4$ (20 μl) and AcOH (5 μl) at room temperature for 2 min, and then with *o*-phenylenediamine (15 mg/200 μl in DMF, v/v) at room temperature for 30 min. After addition of IS (**16**, 200 ng/20 μl MeCN), the reaction mixture was diluted 5% HCl, purified by solid phase extraction and then analyzed as mentioned above. Calibration curve for each *o*-quinone was obtained by assigning the catechol-equivalent weight to *x* and the peak area ratio of the Phz derivatives to the corresponding IS to *y*. Subsequently, a linear regression was performed for constructing calibration curve for each component.

2.10. Assay specificity

The mixed solution of four catechol estrogens (**3**, **4**, **5** and **6**: 500 ng each/50 μl: MeCN–blank matrix, 1:1, v/v) was directly treated with *o*-phenylenediamine (15 mg/200 μl DMF, w/v) and AcOH (5 μl) at room temperature for 30 min. The mixture was purified and analyzed in the similar manner as mentioned above. The peak areas corresponding to the retention time (t_R) of each Phz derivative of *o*-quinone were recorded by LC–ESI-MS/MS and compared to those of peak areas obtained for the samples by pretreatment of catechols (500 ng each) with $NaIO_4$, and then data were expressed as relative peak area.

2.11. Assay accuracy and precision

To determine the assay accuracy and precision, the mixed solution known amounts of catechol estrogens (**3**, **4**, **5** and **6**: 5, 125 and 2000 ng each/ml: MeCN–blank matrix, 1:1, v/v) was prepared and a portion of solution (50 μl) was subsequently treated with 10% $NaIO_4$ (20 μl) and AcOH (5 μl) at room temperature for 2 min, and then with *o*-phenylenediamine (15 mg/200 μl in DMF, v/v) at room temperature for 30 min. After addition of IS (200 ng/20 μl MeCN), the reaction mixture was purified as mentioned above. Within assay precision was expressed as relative standard deviation of analytical results for each concentration of sample. Accuracy was determined and expressed as a percentage of analytical as recovery rates of the measured concentrations against the spiked-concentration for each *o*-quinone (catechol estrogen-equivalent weight).

2.12. Determination of o-quinone formation from estrone and estradiol by tyrosinase and rat liver microsomes

The substrate solution (E_1 and E_2: 10 μg each in DMSO 10 μl) was added to the tyrosinase solution (500 μg in 50 mM phosphate buffer, pH 7.4) (1 ml), and the resulting mixture was incubated at 37 °C. At 30 min after starting incubation, a portion of sample (50 μl) was taken out and the sample was treated with *o*-phenylenediamine (15 mg/200 μl DMF, v/v) and AcOH (5 μl) at room temperature for 30 min. After addition of IS (**16**, 200 ng/20 μl MeCN), the reaction mixture was diluted with 5% HCl (2 ml) and the Phz derivative was extracted, purified and analyzed as mentioned above. Pre-treatment samples of incubation mixture (50 μl) with 15% $NaIO_4$ (15 μl) was prepared to estimate the formation of catechol estrogens in the medium.

Similarly, the substrate solution (E_1 and E_2: 10 μg each in DMSO 10 μl) was added to the mixture of rat liver microsomes (500 μg) and NADPH (10 μg) in 50 mM phosphate buffer (pH 7.4) (1 ml), and the resulting mixture was incubated at 37 °C. At 30 min after starting incubation, a portion of sample (50 μl) was taken out and the sample was treated and analyzed as mentioned above.

3. Results and discussion

3.1. Preparation of Phz derivatives of estrogen o-quinones

Phz derivatives of four estrogen *o*-quinones (**11**, **12a**, **13**, **14a**) were prepared as standards. *o*-Quinones have been generally obtained by oxidation of catechol estrogens using various oxidants such as activated manganese dioxide, sodium iodate or $NaIO_4$ as described by Gelke et al. [18,19]. In this study, we employed direct oxidation of E_1 or E_2 with IBX-polystyrene beads [22–24]. Treatment of E_1 with IBX-polystyrene beads in DMF solution resulted in the formation of **7** and **9** as a mixture. IBX-polystyrene beads were easily removed by filtration and *o*-quinone intermediates thus obtained were then treated with *o*-phenylenediamine in DMF solution. Preparative TLC purification of crude product gave the Phz derivatives **11** and **13** as pure materials using EtOAc–hexane (1:2, v/v) as a developing solvent.

Direct oxidation of E_2 with IBX-polystyrene beads resulted in the formation of the mixture of **8a** and **10a**. In addition to the formation of **8a** and **10a**, the production of **7** and **9** as by-products was inevitable by further oxidation at 17β-OH by this reagent showing complicated HPLC and TLC patterns. Then **12a** and **14a** were prepared using **2b** as a starting material. Oxidation of **2b** with IBX-polystyrene beads followed by the treatment with *o*-phenylenediamine resulted in the formation of **12b** and **14b**. Alkaline hydrolysis of **12b** and **14b** followed by the purification with TLC using EtOAc–hexane (1:2, v/v) as a developing solvent gave **12a** and **14a** as pure materials. ^1H NMR, HR-MS and UV spectral measurement supported the structures of **11**, **12a**, **12b**, **13**, **14a** and **14b**, respectively.

3.2. HPLC–ESI-MS/MS

In ESI-MS, the Phz derivatives of these estrogen *o*-quinones gave protonated molecule ($[M+H]^+$) as the base peaks accompanying the appearance of adduct ion of $[M+H+MeCN]^+$ in each derivative. The ESI-mass spectra and product ion spectra of the Phz

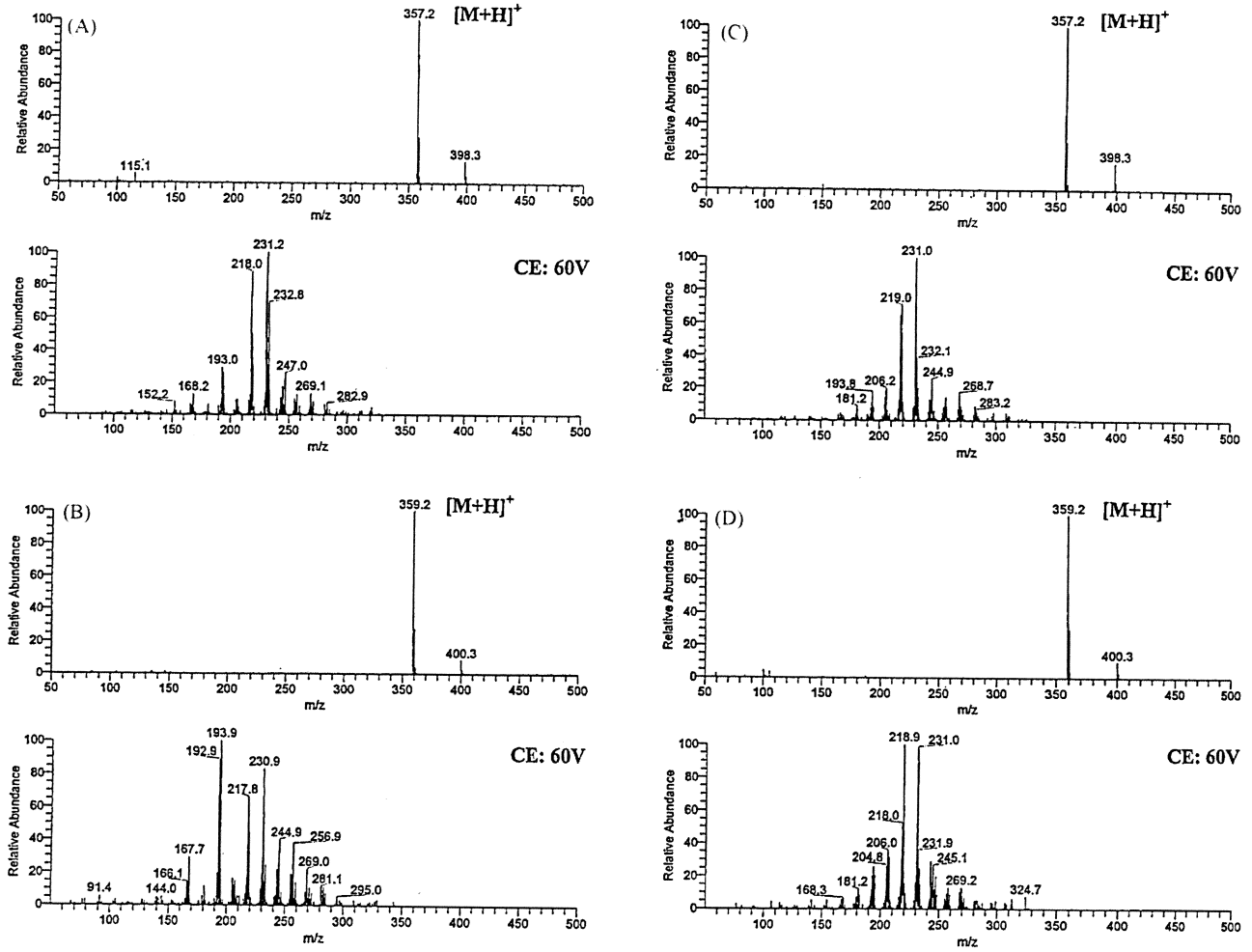


Fig. 3. Representative ESI-mass spectra (upper) and product ion mass spectra (bottom) of the Phz derivatives of estrogen *o*-quinones. (A) E_1-2,3-Q-Phz (**11**), (B) E_2-2,3-Q-Phz (**12a**), (C) E_1-3,4-Q-Phz (**13**) and (D) E_2-3,4-Q (**14a**). Spray voltage: 4500 V, polarity: positive.

derivatives E_1-2,3-Q-Phz (**11**), E_2-2,3-Q-Phz (**12a**), E_1-3,4-Q-Phz (**13**) and E_2-3,4-Q-Phz (**14a**) were shown in Fig. 3A–D. The fragmentation pattern of the base peak ion of each derivative under various levels of collision energy was examined and the ion at *m/z* 231 (formed by cleavage of both C_9–C_{11} and C_8–C_{14} bonds) was observed as common product ion for each Phz derivative of *o*-quinone with relatively high intensity. Then the transition from $[M+H]^+$ to *m/z* 231 was selected for quantification of each Phz derivative in MRM. Using reversed phase ODS-column (X-Bridge C_{18}, 100 mm × 2.1 mm I.D., 5 μm), the Phz derivative of estrogen *o*-quinones were eluted in the order **12a**, **11**, **14a** and **13**, respectively. Retention times for each of the Phz derivatives were as follows (mobile phase; MeCN–H_2O–AcOH = 70:30:0.1, v/v/v, flow rate; 0.2 ml/min): E_2-2,3-Q-Phz (**12a**, t_R = 3.4–3.5 min), E_1-2,3-Q-Phz (**11**, t_R = 3.7–3.8 min), E_2-3,4-Q-Phz (**14a**, t_R = 5.4–5.5 min) and E_1-3,4-Q-Phz (**13**, t_R = 6.0–6.1 min). All Phz derivatives of estrogen *o*-quinones were successfully separated using this mobile phase constitution.

3.3. Generation and derivatization of *o*-quinones in a microscale

o-Quinone generation and derivatization with *o*-phenylenediamine in a microscale was examined using catechol estrogens, **3**, **4**, **5** and **6**. In order to optimize these processes, we investigated the reaction conditions with some variations of constituents (AcOH: 1, 2, 5 and 10 μl, 10% $NaIO_4$: 10, 20 and 30 μl, *o*-phenylenediamine: 5, 10, 15, 30 mg in DMF 200 μl). The highest yields of the Phz derivatives from each catechol estrogen were obtained using the following reagent mixture; AcOH: 5 μl, 10% $NaIO_4$ 20 μl and *o*-phenylenediamine: 15 mg

Table 1
Absolute recovery rates in the processes of *o*-quinone formation and phenazine derivatization from catechol estrogens.

Concentration[a]	Absolute recovery rate[b] (%)			
	E_1-2,3-Q-Phz(**11**)	E_2-2,3-Q-Phz(**12a**)	E_1-3,4-Q-Phz(**13**)	E_2-3,4-Q-Phz(**14a**)
200 ng/ml	60.6 ± 16.2	70.7 ± 9.1	36.3 ± 8.0	55.7 ± 7.7
2000 ng/ml	66.3 ± 6.3	76.0 ± 2.9	34.5 ± 2.5	54.4 ± 0.8

Reaction conditions were as follows:
o-Quinone formation; steroids (50 μl), AcOH (5 μl), 10% $NaIO_4$ (20 μl), 2 min.
Phenazine derivatization: *o*-phenylenediamine 15 mg/200 μl DMF, 30 min.
[a] Concentrations of catechol estrogens in MeCN–blank matrix (1:4, v/v).
[b] Data were calculated on a basis of catechol estrogen-equivalent weight and expressed as the mean value of three experiments.

Table 2
Relative peak area of the generated *o*-quinones from catechols with or without $NaIO_4$ after phenazine derivatization by LC–ESI-MS/MS.

Analytes	Spiked (ng)[a]	$NaIO_4$ treatment	Relative peak area[b,c]
E_1-2,3-Q (**7**)	500	+	1.0
		–	0.0035
E_2-2,3-Q (**8a**)	500	+	1.0
		–	0.0052
E_1-3,4-Q (**9**)	500	+	1.0
		–	0.0053
E_2-3,4-Q (**10a**)	500	+	1.0
		–	0.0079

[a] Spiked amount was expressed on a basis of the weight of catechol estrogens.
[b] Peak areas were determined as their Phz derivatives.
[c] Data were presented as the mean values of three experiments.

Table 3
Assay accuracy and precision.

Analytes	Amount[a] (ng/ml)		Accuracy (%)	RSD (%)
	Added	Found (mean ± SD)[b,c]		
E_1-2,3-Q (**7**)	5	5.0 ± 0.5	100.0	10.0
	125	115.5 ± 14.5	92.4	12.6
	2000	2260.0 ± 108.5	113.0	4.8
E_2-2,3-Q (**8a**)	5	5.5 ± 0.5	110.0	9.1
	125	126.0 ± 15.1	100.8	11.9
	2000	2019.5 ± 103.5	101.0	5.1
E_1-3,4-Q (**9**)	5	5.5 ± 0.6	110.0	10.9
	125	112.0 ± 10.0	89.6	8.9
	2000	2084.0 ± 126.0	104.2	6.0
E_2-3,4-Q (**10a**)	5	5.5 ± 0.5	110.0	9.1
	125	116.5 ± 12.0	93.2	10.3
	2000	2152.5 ± 65.5	107.6	3.1

[a] Added and found values were expressed on a basis of the weight of catechol estrogens.
[b] Data were obtained from four experiments.
[c] *o*-Quinone concentrations were determined as their Phz derivatives.

in 200 μl DMF. The absolute recovery rates of each catechol estrogen were summarized in Table 1. The absolute recovery rates of **11**, **12a**, **13** and **14a** from **3**, **4**, **5** and **6** (2000 ng/ml) were 66.3 ± 6.3%, 76.0 ± 2.9%, 34.5 ± 2.5% and 54.4 ± 0.8%, respectively. Similar recovery rates were obtained for the samples with lower concentration (200 ng/ml). The absolute recovery rates in the processes with the optimized condition were varied from 35% to 76%, however, the overall yields in these processes for each catechol estrogen were reproducible in these concentrations.

3.4. Calibration curves

Calibration curves were constructed for each derivative (**11**, **13**, **12a** and **14a**) by means of catechol estrogens (**3**, **4**, **5** and **6**) after $NaIO_4$ oxidation and Phz derivatization using **16** as an internal standard. Each calibration curve, as determined by sim-

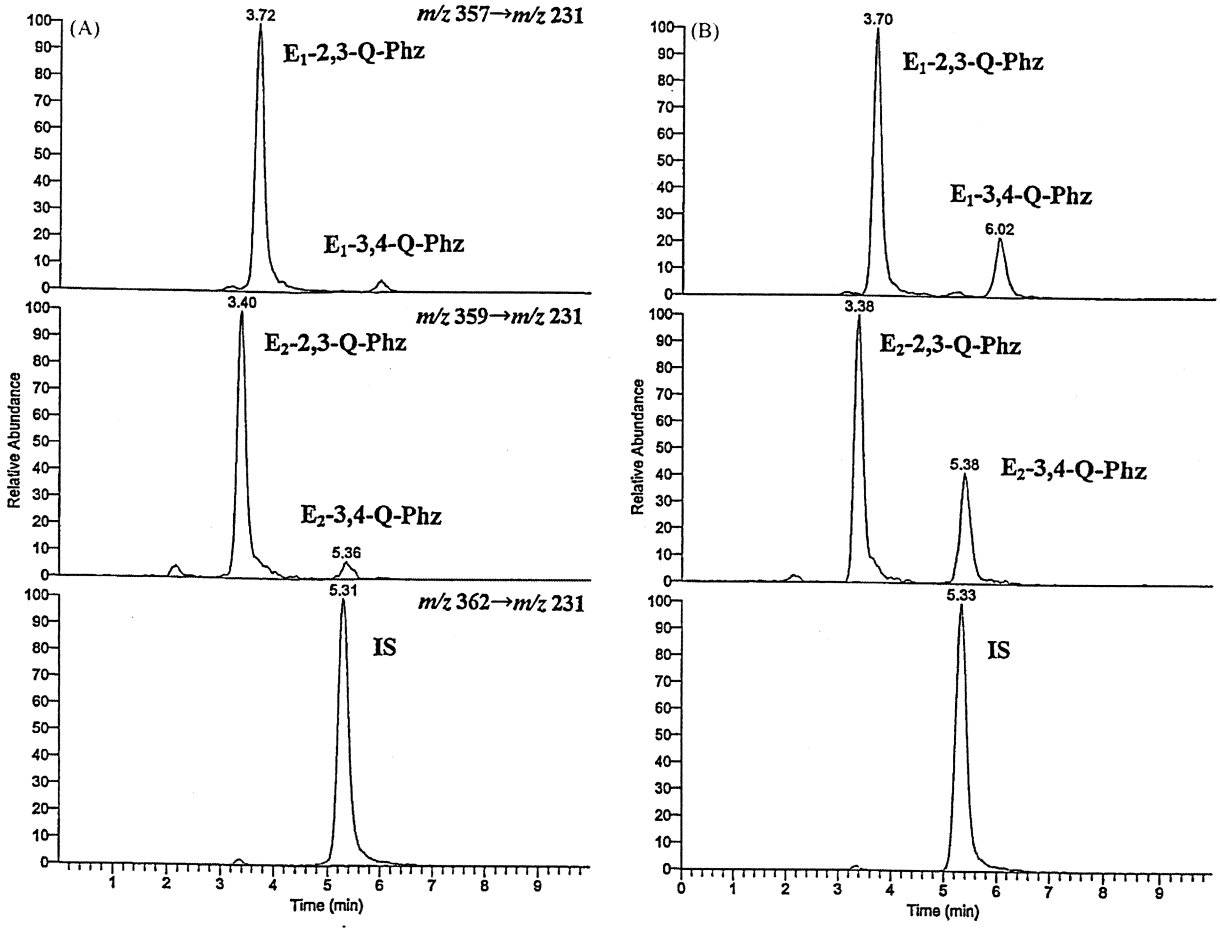


Fig. 4. Typical MRM chromatograms of *o*-quinones formed from E_1 and E_2 after incubation with tyrosinase (500 μg/ml in 50 mM phosphate buffer, pH 7.4, 37 °C for 30 min, substrate concentration: 10 μg each/ml) as their Phz derivatives. (A) Direct derivatization, (B) pre-treatment with 10% $NaIO_4$ at room temperature for 2 min. Spray voltage: 4500 V, collision energy: 60 eV. MRM transitions for each component were as follows: E_1-2,3-Q-Phz (**11**) and E_1-3,4-Q-Phz (**13**); *m/z* 357 → *m/z* 231, E_2-2,3-Q-Phz (**12a**) and E_2-3,4-Q-Phz (**14a**); *m/z* 359 → *m/z* 231 and IS (**16**): *m/z* 362 → *m/z* 231.

ple linear regression analysis, exhibited excellent linearity for the weight range of 2.5–2500 ng/ml (each catechol estrogen-equivalent weight/ml in MeCN–blank matrix, 1:4, v/v) with regression coefficient of more than 0.999 and small *y*-intercept.

3.5. Assay specificity

A degree of Phz derivatives formation from catechol estrogens (hydroquinones) with *o*-phenylenediamine without oxidation process by $NaIO_4$ was assessed by LC–ESI-MS/MS. Results were shown in Table 2. The relative peak areas corresponding to the retention times for **11**, **13**, **12a** and **14a** in the samples obtained from catechol estrogens (500 ng) were 0.0035–0.0079 when compared to those of the peak area of the same samples pre-treated with $NaIO_4$. This result suggested that the Phz derivatization was specific for estrogen *o*-quinones and enabled to determine *o*-quinones selectively even in the presence of hydroquinones.

3.6. Assay accuracy and precision

Results were given in Table 3. Assay accuracy and precision (relative standard deviation, RSD) ranged from 89.6 to 113.0% and 3.1 to 12.6%, respectively. These results indicated that the assay accuracy and reproducibility of this study were found to be satisfactory. The pure Phz derivatives (**11**, **12a**, **13**, **14a**) were detected with injected amount of 500 fg (signal-to-noise ratio of >5), however, the limit of quantifications (LOQs) for each estrogen *o*-quinone as Phz derivatives in the real sample (MeCN–blank matrix; 1:4, v/v) were estimated to be 5 ng/ml with acceptable accuracy and precision (>15%). The LOQ of this method enabled to analyze spontaneously generated estrogen *o*-quinones in the medium obtained by the incubation of E_1 and E_2 with Mushroom tyrosinase or rat liver microsomal fraction at a protein concentration of 0.5 mg/ml.

The Phz derivatives of estrogen *o*-quinones were detected by HPLC–UV method with high sensitivity (10 pg on-column, synthetic standard, data not shown) because of the large ε value of inherent Phz moiety. However, the LOQ in the real sample (MeCN–blank matrix; 1:4, v/v) was limited to be approximately 25 ng/ml due to the co-existing impurities originated from the excess derivatizing agent even after the use of solid phase purification. The typical HPLC–UV chromatogram of the Phz derivatives of generated *o*-quinones from catechol estrogens in the blank matrix was shown in Supplementary materials, which can be found in the electronic version of this article.

3.7. Catalytic activities of tyrosinase and rat liver microsomes on *o*-quinones formation from estrone and/or estradiol

Fig. 4 showed the typical MRM chromatograms of estrogen *o*-quinones formed in the medium after incubation of E_1 or E_2 with Mushroom tyrosinase after Phz derivatization. As

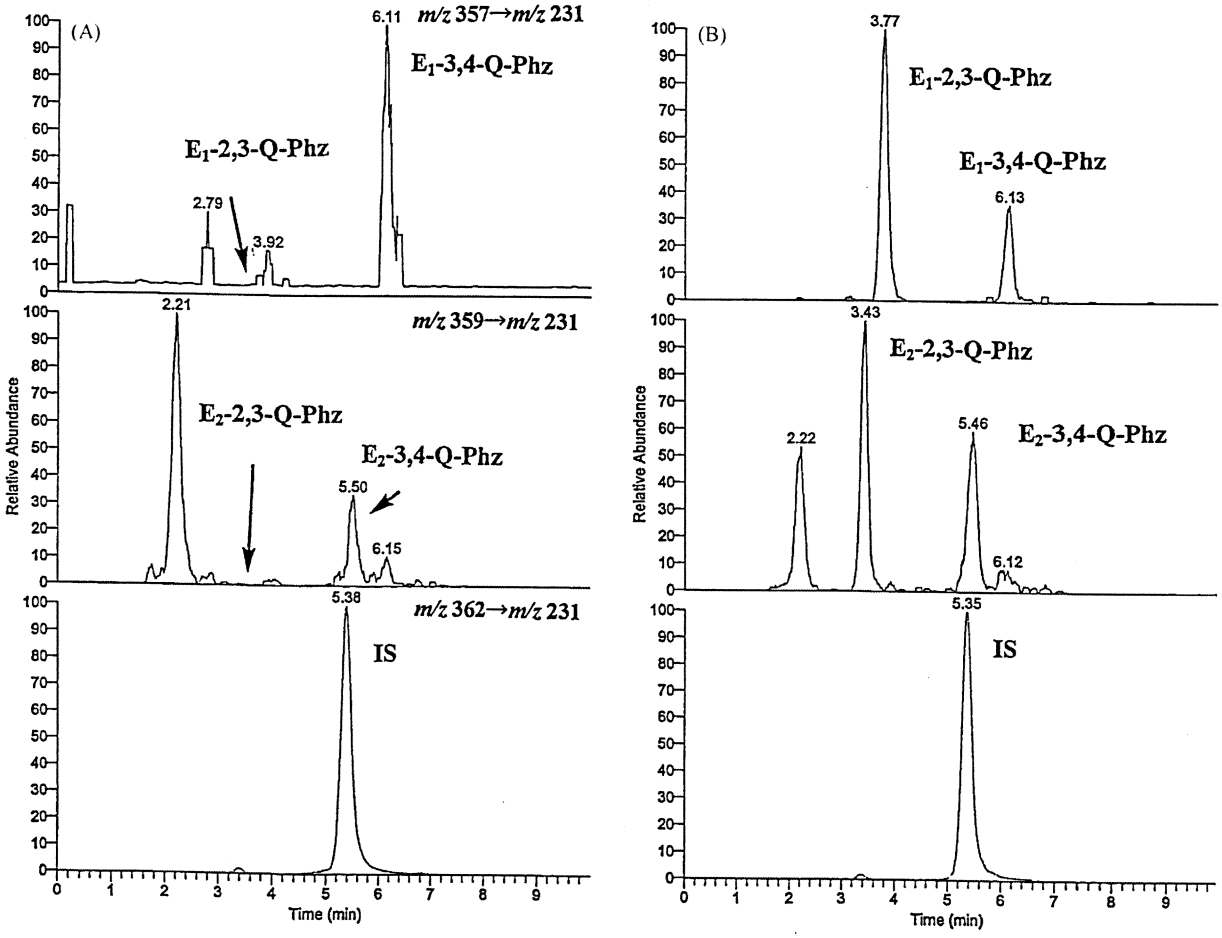


Fig. 5. Typical SRM chromatograms of *o*-quinones formed from E_1 and E_2 after incubation with rat liver microsomes (500 μg/ml in 50 mM phosphate buffer, pH 7.4, 37 °C for 30 min, substrate concentration: 10 μg each/ml) as their Phz derivatives. (A) Direct derivatization, (B) pre-treatment with 10% $NaIO_4$ at room temperature for 2 min. Spray voltage: 4500 V, collision energy: 60 eV. MRM transitions for each component were as follows: E_1-2,3-Q-Phz (**11**) and E_1-3,4-Q-Phz (**13**); *m/z* 357 → *m/z* 231, E_2-2, 3-Q-Phz (**12a**) and E_2-3, 4-Q-Phz (**14a**); *m/z* 359 → *m/z* 231 and IS (**16**): *m/z* 362 → *m/z* 231.

shown in Fig. 4A, the direct derivatization of the incubation mixture of E_1 and E_2 with tyrosinase resulted in the formation of the Phz derivatives E_1-2,3-Q-Phz (**11**) and E_2-2,3-Q-Phz (**12a**) as major products accompanying the production of E_1-3,4-Q-Phz (**13**) and E_2-3,4-Q-Phz (**14a**) in a small quantity (3.8–6.2%, w/w, of **11** and **12a**). Pre-treatment of the incubation mixture with $NaIO_4$ prior to Phz derivatization resulted in the slight increase of **11** and **12a** formation (119–137% of direct derivatization) but the tremendous increase of **13** and **14a** formations (890–913% of direct analysis) (Fig. 4B). These results indicated that tyrosinase possessed the catalytic activities for both 2- and 4-hydroxylation of the ring-A of estrogens and subsequent oxidation of catechols to 2,3-quinones. The catalytic activities of tyrosinase for 4-hydroxylation were 25–50% in comparison with those of 2-hydroxylation activities. The catalytic activity for the oxidation of 3,4-catechols to the corresponding 3,4-quinones was low in contrast to the corresponding oxidation activity for 2,3-catechols. As shown in these results, the high regio-specificities of this enzyme were observed in the oxidation processes between 2,3-catechols and 3,4-catechols to their corresponding *o*-quinones.

On the other hand, the direct derivatization of the incubation mixture of E_1 and E_2 with rat liver microsomes resulted in the detection of **11**, **12a**, **13** and **14a** with only trace levels (Fig. 5A), however the significant increases in the formations of 2,3-quinones and 3,4-quinones were observed after pre-treatment of the incubation mixture with $NaIO_4$ (Fig. 5B). These results indicated that rat liver microsomal fraction possessed mainly the catalytic activities of 2- and 4-hydroxylation of the ring-A of estrogens, which might be attributable to CYP1A1, CYP1A2, CYP3A4 and CYP1B1 activities [25], and further oxidation activities of catechols to the corresponding *o*-quinones were estimated to be low in this enzyme system. These results also suggested that rat hepatic microsomal enzymes seem not to convert primarily produced catechol estrogens to the corresponding *o*-quinones inherently.

In both enzyme systems, the difference in the specificity for hydroxylation and further oxidation of the ring-A of estrogens was not recognized between E_1 and E_2.

4. Conclusion

A sensitive and selective assay method of estrogen *o*-quinones by HPLC–ESI-MS/MS combined with the Phz derivatization was developed in a microscale. The stock solutions of standards of *o*-quinones were not available because of their instabilities, and the generation of *o*-quinones from catechol estrogens was performed *in situ* using $NaIO_4$. Generation of *o*-quinones and Phz derivatization were reproducible even in a microscale, and the Phz derivatives of *o*-quinones were sensitive toward LC–ESI-MS/MS (MRM) detection in a positive mode. Studies on the formation mechanism of such potent carcinogenic estrogen *o*-quinones in biological systems seems to be important to assess the hazard risk of endogenous/exogenous estrogens under various physiological and artificial conditions in relation to the exposures to acceleration/inhibition factors for *o*-quinone formation. The assessment of the robustness of this method and the application of this method to human serum, urine and saliva, are currently being evaluated in our laboratory.

Acknowledgement

This work was supported in part by a High Technology Research Center Project from the Ministry of Education, Culture, Sports, Science and Technology of Japan.

Appendix A. Supplementary data

Supplementary data associated with this article can be found, in the online version, at doi:10.1016/j.jsbmb.2010.02.016.

References

[1] J.D. Yager, N.E. Davidson, Estrogen carcinogenesis in breast cancer, N. Engl. J. Med. 354 (2006) 270–282.
[2] J.G. Liehr, Genotoxic effects of estrogens, Mutat. Res. 238 (1990) 269–276.
[3] I. Dwivedy, P. Devanesan, P. Cremonesi, E. Rogan, E. Cavalieri, Synthesis and characterization of estrogen 2,3- and 3,4-quinones. Comparison of DNA adducts formed by the quinones versus horseradish peroxidase-activated catechol estrogens, Chem. Res. Toxicol. 5 (1992) 828–833.
[4] D.E. Stack, J. Byun, M.L. Gross, E.G. Rogan, E.L. Cavalieri, Molecular characterization of catechol estrogen quinones in reactions with deoxyribonucleosides, Chem. Res. Toxicol. 9 (1996) 851–859.
[5] E.L. Cavalieri, K.-M. Li, N. Balu, M. Saeed, P. Devanesan, S. Higginbotham, J. Zao, M.L. Gross, E.G. Rogan, Catechol ortho-quinones: the electrophilic compound that form depurinating DNA adducts and could initiate cancer and other disease, Carcinogenesis 23 (2002) 1071–1077.
[6] Y. Tsuchiya, M. Nakajima, T. Yokoi, Cytochrome P450-mediated metabolism of estrogens and its regulation in human, Cancer Lett. 227 (2005) 115–124.
[7] J.L. Bolton, G.R.J. Thatcher, Potential mechanisms of estrogen quinone carcinogenesis, Chem. Res. Toxicol. 21 (2008) 93–101.
[8] E. Cavalieri, D. Chakravarti, J. Guttenplan, E. Hart, J. Ingel, R. Jankowiak, P. Muti, E. Rogan, J. Russo, R. Santen, T. Sutter, Catechol estrogen quinones as initiators of breast cancer and other human cancers: implications for biomarkers of susceptibility and cancer prevention, Biochem. Biophys. Acta 1766 (2006) 63–78.
[9] O. Convert, C.V. Aerden, L. Debrauwer, E. Rathahao, H. Molines, F. Fournier, J.-C. Tabet, A. Paris, Reaction of estradiol-2,3-quinones with deoxyribonucleosides: possible insights in the reactivity of estrogen quinones with DNA, Chem. Res. Toxicol. 15 (2002) 754–764.
[10] A. Pezzella, L. Lista, A. Napolitano, M. d'Ischia, Tyrosinase-catalyzed oxidation of 17β-estradiol: structure elucidation of the product formed beyond catechol estrogen quinones, Chem. Res. Toxicol. 18 (2005) 1413–1419.
[11] E.L. Cavalieri, D.E. Stack, P.D. Devanesane, R. Todorovic, I. Dwivedy, S. Haginbotham, S.I. Johansson, K.D. Patil, M.L. Gross, J.K. Gooden, R. Ramanathan, R.L. Cerny, E.G. Rogan, Molecular origin of cancer: catechol estrogens-3,4-quinones as endogenous tumor initiators, Proc. Natl. Acad. Sci. U.S.A. 94 (1997) 10937–10942.
[12] E. Rathahao, A. Page, I. Jouanin, A. Parism, L. Debrauwer, Liquid chromatography coupled to negative electrospray/ion trap mass spectrometry for the identification of isomeric glutathione conjugates of catechol estrogens, Int. J. Mass Spectrom. 231 (2004) 119–129.
[13] K. Cao, D. Stack, R. Ramanathan, M.L. Gross, E.G. Rogan, E.L. Cavalieri, Synthesis and structure elucidation of estrogen quinones conjugated with cystein, N-acetylcysteine, and glutathione, Chem. Res. Toxicol. 11 (1998) 909–916.
[14] A. Akanni, K. Tabakovic, Y.J. Abul-Hajj, Estrogen-nucleic acid adducts: reaction of 3,4-estrone o-quinone with nucleic acid bases, Chem. Res. Toxicol. 10 (1997) 477–481.
[15] D.L. Hachey, S. Dawling, N. Roodi, F. Parl, Sequential action of phase I and II enzymes cytochrome P450 1B1 and glutathione S-transferase P1 in mammary estrogen metabolism, Cancer Res. 63 (2003) 8492–8499.
[16] M. Numazawa, T. Nambara, A new mechanism of in vitro formation of catechol estrogen glutathione conjugate by rat liver microsomes, J. Steroid Biochem. 8 (1977) 835–840.
[17] Y.J. Abul-Hajji, Synthesis of 3, 4-estrogen-o-quinone, J. Steroid Biochem. 21 (1984) 621–622.
[18] H.P. Gelbke, R. Knuppen, Synthesis of specific phenazine derivatives of 2-hydroxyestrogens, Steroids 21 (1973) 689–702.
[19] H.P. Gelbke, M. Kreth, R. Knuppen, A chemical method for quantitative determination of 2-hydroxyestrone in human urine, Steroids 21 (1973) 665–687.
[20] G.R. Pettit, A.J. Thornhill, B.R. Moser, F. Hogan, Antineoplastic agents. 552. Oxidation of combretastatin A-1: trapping the o-quinone intermediate considered the metabolic product of the corresponding phosphate prodrug, J. Nat. Prod. 71 (2008) 1561–1563.
[21] K. Itoh, M. Adachi, J. Sato, K. Shouji, K. Fukiya, K. Fujii, Y. Tanaka, Effect of selenium deficiency on aldehyde oxidase 1 in rats, Biol. Pharm. Bull. 32 (2009) 190–194.
[22] G. Sorg, A. Mengel, G. Jung, J. Rademann, Oxidizing, Polymers:, A polymer-supported recyclable hypervalent iodine (V) reagent for the efficient conversion of alcohols, carbonyl compounds, and unsaturated carbamates in solution, Angew. Chim. Int. Ed. 40 (2001) 4395–4397.
[23] M. Saeed, M. Zahid, E. Rogan, E. Cavalieri, Synthesis of the catechols of natural and synthetic estrogens by using 2-iodoxybenzoic acid (IBX) as the oxidizing agent, Steroids 70 (2005) 173–178.
[24] M. Frigerio, M. Santagostino, S. Sputore, A user-friendly entry to 2-iodoxybenzoic acid (IBX), J. Org. Chem. 64 (1999) 4537–4538.
[25] A.J. Lee, M.X. Cai, P.E. Thomas, A.H. Conney, B.T. Zhu, Characterization of the oxidative metabolites of 17β-estradiol and estrone formed by 15 selectively expressed human cytochrome P450 isoforms, Endocrinology 144 (2003) 3382–3398.

Steroids 75 (2010) 330–337

Contents lists available at ScienceDirect

Steroids

journal homepage: www.elsevier.com/locate/steroids

Probing the binding pocket of the active site of aromatase with 2-phenylaliphatic androsta-1,4-diene-3,17-dione steroids

Madoka Takahashi, Kouwa Yamashita, Mitsuteru Numazawa*

Tohoku Pharmaceutical University, 4-1 Komatsushima-4-chome, Aobaku, Sendai 981-8558, Japan

ARTICLE INFO

Article history:
Received 18 November 2009
Received in revised form 7 January 2010
Accepted 14 January 2010
Available online 22 January 2010

Keywords:
Aromatase
Competitive inhibitor
Androsta-1,4-diene-3,17-dione
2-Phenylaliphatic substituent
Suicide substrate
Breast cancer

ABSTRACT

A series of 2-phenylaliphatic-substituted androsta-1,4-diene-3,17-diones (**6**) as well as their androstenedione derivatives (**5**) were synthesized as aromatase inhibitors to gain insights of structure–activity relationships of varying the alkyl moiety (C_1 to C_4) of the 2-phenylaliphatic substituents as well as introducing a methyl- or trifluoromethyl function to *p*-position of a phenethyl moiety to the inhibitory activity. The inhibitors examined showed a competitive type inhibition. The 2-phenpropylandrosta-1,4-diene **6c** was the most powerful inhibitor (K_i: 16.1 nM) among them. Compounds **6c** along with the phenethyl derivative **6b** caused a time-dependent inactivation of aromatase (k_{inact}: 0.0293 and 0.0454 min^{-1} for **6b** and **6c**, respectively). The inactivation was prevented by the substrate androstenedione, and no significant effect of L-cysteine on the inactivation was observed in each case. Molecular docking of the phenpropyl compound **6c** to aromatase was conducted to demonstrate that the phenpropyl group orients to a hydrophobic binding pocket in the active site to result in the formation of thermodynamically stable enzyme–inhibitor complex.

© 2010 Elsevier Inc. All rights reserved.

1. Introduction

Aromatase is a cytochrome P-450 enzyme that catalyzes the conversion of the androgens, androstenedione (AD) and testosterone, to the estrogens, estrone and estradiol, respectively [1–3]. The aromatase reaction is thought to proceed through three sequential oxygenations at C-19 of the androgens [4–7] (Fig. 1). Aromatase is a potential therapeutic target for the lowering of estrogen levels in patients with advanced estrogen-dependent breast cancer [8–11]. The specific blockade of estrogen biosynthesis has been pursued intensely with the goal of developing practical clinical drugs. For this reason, a number of powerful aromatase inhibitors, which are analogs of the natural substrate AD, have been described by various laboratories.

Androsta-1,4-diene-3,17-dione (Δ^1-AD, **1**), which is the 1-ene derivative of AD, is one of the prototypical mechanism-based inhibitors (suicide substrates); the C(1)=C(2) double bond is the structural feature responsible for aromatase inactivation, although the inactivation mechanism is currently unknown [5,12–21]. Several analogs of compound **1**, having a D-ring lactone (testolactone) [22,23], 1-methyl (atamestane) [24] or 6-methylene (exemestane) [25,26] structure, are clinically evaluated as orally active suicide substrates for aromatase (Fig. 2). We have studied the structure–activity relationships of 6-substituted (alkyl, phenylaliphatic, alkoxy, and ester) Δ^1-AD analogs [27–29] as well as 19-substituted ones [30] as aromatase inhibitors, some of which are among the most potent competitive inhibitors and mechanism-based inhibitors reported so far. The length (bulkiness) and the stereochemistry of the 6-substituents as well as the electronic effects of the 19-substituents play a critical role not only in the binding of inhibitors to the active site of aromatase, but also in the cause of the mechanism-based inactivation of aromatase by the 1,4-dien-3-one steroid **1**. Recently, we have also reported the structure–activity relationships of the 2-alkyl or alkoxy substituted Δ^1-ADs as aromatase inhibitors [31]. Among the 2-substituted derivatives, the 2-hexyl compound is the most powerful competitive inhibitor and inactivates aromatase with the lowest K_I value in a time-dependent manner.

In the cause of our studies on aromatase inhibition by Δ^1-AD analog, we were interest in C-2 substitution of the Δ^1-AD **1** by a phenylaliphatic group. Thus, we synthesized 2-substituted ($C_6H_5CH_n$, $n = 1–4$) Δ^1-AD derivatives **6a–6d** along with *p*-methyl and *p*-trifluoromethylphenethyl analogs **6e** and **6f**, and tested their ability to inhibit aromatase activity as well as their ability to inactivate aromatase in a suicide manner. Furthermore, molecular docking studies of the phenpropyl derivative **6c**, the most powerful inhibitor among them, with human placental aromatase protein were performed.

* Corresponding author. Tel.: +81 22 727 0138; fax: +81 22 727 0137.
E-mail address: numazawa@tohoku-pharm.ac.jp (M. Numazawa).

0039-128X/$ – see front matter © 2010 Elsevier Inc. All rights reserved.
doi:10.1016/j.steroids.2010.01.008

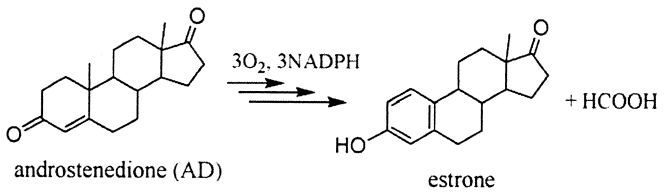


Fig. 1. Aromatization sequence of AD with human placental aromatase.

2. Experimental

2.1. Materials and general methods

17β-*tert*-Butyldimethylsiloxyandrost-4-en-3-one (**2**) [32] was synthesized according to the previous method. [1β-^{3}H]AD (specific activity 27.5 Ci/mmol; ^{3}H-distribution 74–79%) was obtained from New England Nuclear (Boston, MA, USA). NADPH was purchased from Sigma–Aldrich (St. Louise, MO, USA).

Melting points were measured on a Yanagimoto melting point apparatus (Kyoto, Japan) and are uncorrected. Infra red (IR) spectra were recorded on a Perkin-Elmer FT-IR 1725X spectrophotometer in a KBr pellet or nujol form, and ultra violet (UV) spectra were determined in 95% EtOH on a Hitachi 150-20 spectrophotometer (Tokyo, Japan). ^{1}H nuclear magnetic resonance (NMR) spectra were obtained in $CDCl_3$ solution with a JEOL LA 400 (400 MHz) and JEOL LA 600 (600 MHz) spectrometers (Tokyo, Japan) using tetramethylsilane as an internal standard, and mass (MS) spectra (electron impact, EI mode) and high resolution (HR)-MS with a JEOL JMS-DX 303 spectrometer. Thin-layer chromatography (TLC) was performed on E. Merck precoated silica gel plates (silica gel 60F-254, Darmstadt, Germany). Column chromatography was conducted with silica gel 60, 70–230 mesh (E. Merck). High-performance liquid chromatography (HPLC) was carried out using a Waters 600 pump and a UV detector (240 nm) (Milford, MA, USA) where Symmetry column (300 mm × 7.8 mm i.d., Waters) was employed for preparative use and Puresil column (150 mm × 4.6 mm i.d., Waters) for purity determination of compounds.

2.2. 2α-Phenalkyl-17β-tert-butyldimethylsiloxyandrost-4-en-3-ones (3)

Phenbutyl bromide, *p*-methylphenethyl bromide and *p*-trifluoromethyl bromide (Sigma–Aldrich. Co.) (5.84 mmol) was refluxed in acetone (15.6 ml) containing NaI (2.3 g) for 6 h [33], and the solvent removed in a vacuum. Hexane was added, and the resulting solutions washed with water, dilute H_2SO_4 and water, and dried with Na_2SO_4. Evaporation of the solvent gave phenbutyl iodide, *p*-methylphenethyl iodide and *p*-trifluoromethyl iodide.

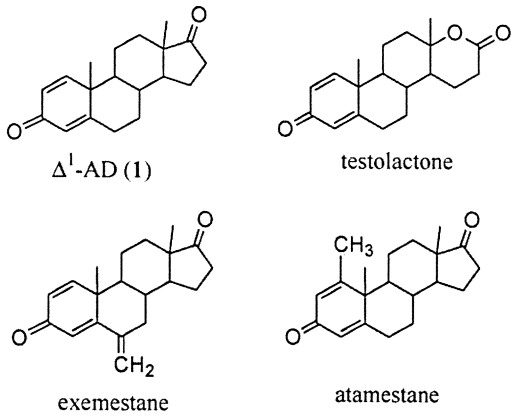


Fig. 2. Structures of suicide substrates of aromatase having a 1,4-dien-3-one structure.

(A) To a stirring solution of 160 μl (1.13 mmol) of diisopropylamine in 1.6 ml of THF, cooled to 0 °C, was added BuLi (690 μL of 1.6 M in hexane). After 20 min, the solution was cooled to −20 °C and 200 mg (0.50 mmol) of compound **2** in 1.6 ml THF was added via cannula to the solution. After an additional 15 min, 170 μl (0.98 mmol) of hexamethylphosphoric triamide (HMPA) was added all at once and the mixture was allowed to stir for another 20 min, and then 2.02 mmol of benzyl bromide or phenbutyl iodide was added dropwise to the mixture [34]. After 1 h at −20 °C reaction, the reaction mixture was quenched with 1 M aqueous HCl and diluted with EtOAc. The organic phase was washed with brine and dried with Na_2SO_4. Evaporation of the solvent gave an oil which was purified by silica gel (20 g) column chromatography with hexane–EtOAc (60:1) to yield an oily substance. Then, the oil was subjected to preparative TLC (hexane–EtOAc, 8:1, multiple developments) to give 2α-benzyl steroid **3a** (64%) or 2α-phenbutyl steroid **3d** (22%).

(B) LDA (1.13 mmol) was prepared similar to the above at 0 °C. A solution of 1 g (2.48 mmol) of compound **2** in 8.00 ml THF was added via cannula to the LDA solution at 0 °C. After the same work-up as the above (78 mmol of HMPA), 13.79 mmol of phenethyl iodide, *p*-methylphenethyl iodide or *p*-trifluoromethyl iodide was added dropwise at 0 °C. After 1.5 h reaction, the reaction mixture was quenched with 1 M aqueous HCl and diluted with EtOAc. The organic phase was washed with brine and dried with Na_2SO_4. Evaporation of the solvent gave an oil which was purified by silica gel (100 g) column chromatography with hexane–EtOAc (30:1) to yield an oily substance. Then, the oil was subjected to preparative TLC (hexane–EtOAc, 5:1) to give 2α-phenethyl steroid **3b**, 2α-*p*-methylphenethyl steroid **3e** or 2α-*p*-trifluoromethyl steroid **3f** (11–22%).

(C) A mixture of 17β-*tert*-butyldimethylsiloxyandrost-4-en-3-one (**2**) (700 mg, 1.74 mmol), 1-iodo-3-phenyl propane (3.6 ml, 23.16 mmol), THF (1.5 ml) and HMPA (0.28 ml) was cooled −60 °C and then *tert*-BuOK (390 mg, 3.48 mmol) in THF (1.5 ml)–HMPA (0.28 ml) was added to this solution [35]. The reaction mixture was stirred at −60 °C for 1.5 h and the temperature was gradually elevated to room temperature. The mixture was extracted of with EtOAc, washed with saturated $NaHCO_3$ solution and saturated NaCl, and dried with Na_2SO_4. Evaporation of the solvent gave an oil which was purified by silica gel (70 g) column chromatography with hexane–EtOAc (60:1) to yield an oily substance. Then, the oil was subjected to preparative TLC (hexane–EtOAc, 20:1, multiple developments) to give 2α-phenpropyl steroid **3c** (193 mg, 22%).

The purities of the oily substances were determined by analytical HPLC (CH_3CN:H_2O = 100:0, v/v; flow rate, 1.0 ml/min) to be more than 98%.

3a: oil; t_R = 19.4 min; IR (KBr): 1672 cm^{-1} (C=O); UV λ_{max} 242 nm (ε = 14,700); ^{1}H NMR δ: 0.01 (6H, s, Si-$(CH_3)_2$), 0.71 (3H, s, 18-Me), 0.88 (9H, s, Si-C$(CH_3)_3$), 1.10 (3H, s, 19-Me), 2.45 (1H, dd, J = 9.2 and 13.9 Hz, phenyl-CH_a), 3.48 (1H, dd, J = 3.8 and 14.0 Hz, phenyl-CH_b), 3.55 (1H, t, J = 8.2 Hz, 17α-H), 5.76 (1H d, J = 1.5 Hz, 4-H), 7.18–7.31 (5H, m, aromatic protons); MS *m/z*: 492 (M$^+$, 14), 435 (100), 359 (12), 91 (16). HR-MS for $C_{32}H_{48}O_2Si$ (M$^+$): calcd 492.3424, found 492.3436.

3b: oil; t_R = 24.9 min; IR (KBr): 1672 cm^{-1} (C=O); UV λ_{max} 242 nm (ε = 14,400); ^{1}H NMR δ: 0.01 (6H, s, Si-$(CH_3)_2$), 0.75 (3H, s, 18-Me), 0.88 (9H, s, Si-C$(CH_3)_3$), 1.16 (3H, s, 19-Me), 2.68 (2H, m, phenyl-CH_2), 3.56 (1H, m, 17α-H), 5.69 (1H, d, J = 1.2 Hz, 4-H), 7.17–7.29 (5H, m, aromatic protons); MS *m/z*: 506 (M$^+$, 1), 499 (68),

402 (100), 373 (9). HR-MS for $C_{33}H_{50}O_2Si$ (M^+): calcd 506.3580, found 506.3576.

3c: oil; t_R = 24.2 min; IR (neat): 1669 cm^{-1} (C=O); UV λ_{max} 242 nm (ε = 8200); ^1H NMR δ: 0.01 (6H, s, Si-$(CH_3)_2$), 0.74 (3H, s, 18-Me), 0.88 (9H, s, Si-C$(CH_3)_3$), 1.17 (3H, s, 19-Me), 2.63 (2H, m, phenyl-CH_2), 3.54 (1H, t, J = 8.3 Hz, 17α-H), 5.69 (1H, d, J = 1.5 Hz, 4-H), 7.16–7.32 (5H, m, aromatic protons); MS *m/z*: 520 (M^+, 86), 463 (100), 402 (20), 387 (14). HR-MS for $C_{34}H_{52}O_2Si$ (M^+): calcd 520.3737, found 520.3748.

3d: oil; t_R = 24.1 min; IR (KBr): 1675 cm^{-1} (C=O); UV λ_{max} 242 nm (ε = 13,200); ^1H NMR δ: 0.01 (6H, s, Si-$(CH_3)_2$), 0.74 (3H, s, 18-Me), 0.88 (9H, s, Si-C$(CH_3)_3$), 1.18 (3H, s, 19-Me), 2.62 (2H, m, phenyl-CH_2), 3.55 (1H, t, J = 8.4 Hz, 17α-H), 5.69 (1H, s, 4-H), 7.16–7.29 (5H, m, aromatic protons); MS *m/z*: 534 (M^+, 48), 477 (100), 402 (35), 75 (41). HR-MS for $C_{35}H_{54}O_2Si$ (M^+): calcd 534.3893, found 534.3885.

3e: oil; t_R = 25.3 min; IR (neat): 1675 cm^{-1} (C=O); UV λ_{max} 242 nm (ε = 11,000); ^1H NMR δ: 0.01 (6H, s, Si-$(CH_3)_2$), 0.75 (3H, s, 18-Me), 0.88 (9H, s, Si-C$(CH_3)_3$), 1.16 (3H, s, 19-Me), 2.31 (3H, m, *p-Me*-phenethyl), 2.63 (2H, m, *p*-Me-phenyl-CH_2), 3.55 (1H, t, J = 8.3 Hz, 17α-H), 5.69 (1H, d, J = 1.5 Hz, 4-H), 7.05–7.11 (4H, m, aromatic protons); MS *m/z*: 520 (M^+, 2), 463 (18), 402 (100), 345 (32). HR-MS for $C_{34}H_{52}O_2Si$ (M^+): calcd 520.3737, found 520.3732.

3f: oil; t_R = 22.4 min; IR (neat): 1672 cm^{-1} (C=O); UV λ_{max} 242 nm (ε = 10,700); ^1H NMR δ: 0.01 (6H, s, Si-$(CH_3)_2$), 0.75 (3H, s, 18-Me), 0.88 (9H, s, Si-C$(CH_3)_3$), 1.17 (3H, s, 19-Me), 2.75 (2H, t, J = 7.8 Hz, *p*-CF_3-phenyl-CH_2), 3.55 (1H, m, 17α-H), 5.70 (1H, d, J = 1.2 Hz, 4-H), 7.32 and 7.53 (2H each, d, J = 8.1 Hz, aromatic protons); MS *m/z*: 574 (M^+, 1), 517 (18), 161 (54), 153 (100). HR-MS for $C_{34}H_{49}F_3O_2Si$ (M^+): calcd 574.3453, found 574.3435.

2.3. 2α-Phenalkyl-17β-hydroxyandrost-4-en-3-ones (4)

5% HCl (1.1 ml) was added to a solution of the 17β-siloxy compounds **3** (0.26 mmol) in THF (2 ml) and 2-propanol (2 ml) and the reaction mixture was stand at room temperature for 6 h. After adding $NaHCO_3$, the mixture was extracted with EtOAc (50 ml), washed with 5% $NaHCO_3$ solution and water, and dried with Na_2SO_4. Evaporation of the solvent gave a 17β-hydroxy product which was purified by silica gel (10 g) column chromatography (hexane–EtOAc = 5:1) followed by recrystallization from acetone or trituration from ether to yield 17-hydroxy compounds **4a–4d** (35–68%). The purities of the oily substances (**4e** and **4f**) were determined by analytical HPLC (CH_3CN:H_2O = 80:20, v/v; flow rate, 1.0 ml/min) to be more than 98%.

4a: mp 252–254 °C. IR (KBr): 1672 cm^{-1} (C=O); UV λ_{max}: 242 nm (ε = 10,300); ^1H NMR δ: 0.74 (3H, s, 18-Me), 1.10 (3H, s, 19-Me), 2.43 (1H, dd, J = 9.3 and 14.1 Hz, phenyl-CH_a), 3.47 (1H, dd, J = 3.8 and 14.0 Hz, phenyl-CH_b), 3.63 (1H, m, 17α-H), 5.75 (1H, d, J = 1.5 Hz, 4-H), 7.16–7.30 (5H, m, aromatic protons); MS *m/z*: 378 (M^+, 100), 363 (5), 121 (31), 91 (50). Anal. Calcd for $C_{26}H_{34}O_2$: C, 82.49; H, 9.05. Found C, 82.60; H, 9.27.

4b: mp 143–145 °C. IR (KBr): 1668 cm^{-1} (C=O); UV λ_{max}: 242 nm (ε = 11,200); ^1H NMR δ: 0.80 (3H, s, 18-Me), 1.17 (3H, s, 19-Me), 2.69 (2H, m, phenyl-CH_2), 3.65 (1H, m, 17α-H), 5.70 (1H, d, J = 1.5 Hz, 4-H), 7.16–7.29 (5H, m, aromatic protons); MS *m/z*: 392 (M^+, 2), 288 (100), 273 (8), 122 (25). Anal. Calcd for $C_{27}H_{36}O_2$: C, 82.61; H, 9.24. Found C, 82.70; H, 9.37.

4c: mp 199–201 °C. IR (KBr): 1667 cm^{-1} (C=O); UV λ_{max}: 241 nm (ε = 9000); ^1H NMR δ: 0.79 (3H, s, 18-Me), 1.18 (3H, s, 19-Me), 2.63 (2H, m, phenyl-CH_2), 3.64 (1H, m, 17α-H), 5.69 (1H, d, J = 1.4 Hz, 4-H), 7.15–7.29 (5H, m, aromatic protons); MS *m/z*: 406 (M^+, 100), 301 (30), 288 (53), 273 (6). Anal. Calcd for $C_{28}H_{38}O_2$: C, 82.71; H, 9.42. Found C, 82.55; H, 9.54.

4d: semi-crystalline; mp 87–89 °C. IR (KBr): 1669 cm^{-1} (C=O); UV λ_{max}: 242 nm (ε = 15,300); ^1H NMR δ: 0.80 (3H, s, 18-Me), 1.19 (3H, s, 19-Me), 2.63 (2H, m, phenyl-CH_2), 3.65 (1H, m, 17α-H), 5.70 (1H, d, J = 1.5 Hz, 4-H), 7.15–7.29 (5H, m, aromatic protons); MS *m/z*: 420 (M^+, 100), 301 (38), 288 (98), 91 (55). HR-MS for $C_{29}H_{40}O_2$: (M^+): calcd 420.3028, found 420.3044.

4e: oil; t_R = 7.0 min; IR (KBr): 1668 cm^{-1} (C=O); UV λ_{max}: 242 nm (ε = 10,600); ^1H NMR δ: 0.80 (3H, s, 18-Me), 1.17 (3H, s, 19-Me), 2.31 (3H, s, *p-Me*-phenethyl), 2.63 (2H, m, *p*-Me-phenyl-CH_2), 3.66 (1H, m, 17α-H), 5.69 (1H, d, J = 1.5 Hz, 4-H), 7.07–7.11 (4H, m, aromatic protons); MS *m/z*: 406 (M^+, 2), 288 (100), 273 (13), 122 (28). HR-MS for $C_{28}H_{38}O_2$ (M^+): calcd 406.2872, found 406.2883.

4f: oil; t_R = 6.8 min; IR (KBr): 1665 cm^{-1} (C=O); UV λ_{max}: 242 nm (ε = 9800); ^1H NMR δ: 0.80 (3H, s, 18-Me), 1.22 (3H, s, 19-Me), 2.75 (2H, t, J = 8.0 Hz, *p*-CF_3-phenyl-CH_2), 3.64 (1H, m, 17α-H), 5.71 (1H, d, J = 1.5 Hz, 4-H), 7.32 and 7.53 (2H each, d, J = 8.1 Hz, aromatic protons); MS *m/z*: 460 (M^+, 1), 345 (7), 288 (100), 273 (11). HR-MS for $C_{28}H_{35}F_3O_2$ (M^+): calcd 460.2589, found 460.2596.

2.4. 2α-phenalkylandrost-4-ene-3,17-diones (5)

Jones reagent (11 drops) was added to a solution of the 17β-hydroxide **4** (0.13 mmol) in acetone (20 ml) under ice-cooling and the mixture was stirred for 3 min. After this time, MeOH (0.1 ml) was added to the mixture and then extracted with EtOAc (10 ml), washed with 5% $NaHCO_3$ solution and water, dried with Na_2SO_4. Evaporation of the solvent gave an oil which was purified by silica gel (5 g) column chromatography (hexane–EtOAc = 7:1) to yield an oily substance. Then, the oily substance was subjected to preparative TLC (hexane–EtOAc, 4:1, multiple developments) or preparative HPLC (CH_3CN:H_2O = 60:40, v/v; flow rate 5 ml/min) to obtained compound **5a–5f** (49–61%). The purities of oil substances were obtained by analytical HPLC as described for those of compounds **4** were more than 97%.

5a: mp 164–166 °C. IR (KBr): 1664 and 1733 cm^{-1} (C=O); UV λ_{max}: 241 nm (ε = 13,300); ^1H NMR δ: 0.87 (3H, s, 18-Me), 1.11 (3H, s, 19-Me), 2.45 (1H, m, phenyl-CH_a), 3.48 (1H, dd, J = 3.8 and 14.1 Hz, phenyl-CH_b), 5.78 (1H, d, J = 1.8 Hz, 4-H), 7.17–7.30 (5H, m, aromatic protons); MS *m/z*: 376 (M^+, 100), 361 (7), 121 (40), 91 (78). Anal. Calcd for $C_{26}H_{32}O_2$: C, 82.94; H, 8.57. Found C, 83.01; H, 8.80.

5b: mp 129–131 °C. IR (KBr): 1670 and 1742 cm^{-1} (C=O); UV λ_{max}: 240 nm (ε = 15,200); ^1H NMR δ: 0.93 (3H, s, 18-Me), 1.18 (3H, s, 19-Me), 2.70 (2H, m, phenyl-CH_2), 5.72 (1H, d, J = 1.5 Hz, 4-H), 7.17–7.29 (5H, m, aromatic protons); ^{13}C NMR δ: 13.7, 17.4, 20.2, 21.7, 30.4, 30.7, 31.3, 32.1, 33.0, 35.0, 35.7, 39.2, 41.1, 42.0, 47.5, 50.8, 54.2, 124.0, 125.8, 128.3, 128.4, 142.0, 168.6, 200.8, 220.4; MS *m/z*: 390 (M^+, 2), 286 (100), 271 (16), 122 (27). Anal. Calcd for $C_{27}H_{34}O_2$: C, 83.03; H, 8.77. Found C, 83.34 H, 8.58.

5c: oil; t_R = 7.2 min; IR (neat): 1671 and 1739 cm^{-1} (C=O); UV λ_{max}: 241 nm (ε = 15,100); ^1H NMR δ: 0.91 (3H, s, 18-Me), 1.20 (3H, s, 19-Me), 2.63 (2H, m, phenyl-CH_2), 5.72 (1H, d, J = 1.5 Hz, 4-H), 7.16–7.29 (5H, m, aromatic protons); ^{13}C NMR δ: 13.7, 17.4, 20.2, 21.7, 28.7, 29.0, 30.7, 31.2, 32.1, 35.0, 35.7, 36.3, 39.1, 41.8, 41.9, 47.5, 50.8, 54.2, 124.0, 125.7, 128.3, 128.4, 142.5, 168.7, 200.8, 220.5; MS *m/z*: 404 (M^+, 100), 300 (72), 286 (85), 271 (18). HR-MS for $C_{28}H_{36}O_2$ (M^+): calcd 404.2715, found 404.2715.

5d: semi-crystalline; mp 117–119 °C. IR (KBr): 1665 and 1743 cm^{-1} (C=O); UV λ_{max}: 241 nm (ε = 13,800); ^1H NMR δ: 0.92 (3H, s, 18-Me), 1.21 (3H, s, 19-Me), 2.63 (2H, m, phenyl-CH_2), 5.72 (1H, d, J = 1.5 Hz, 4-H), 7.15–7.29 (5H, m, aromatic protons); MS *m/z*: 418 (M^+, 100), 299 (30), 286 (85), 271 (13). HR-MS for $C_{29}H_{38}O_2$ (M^+): calcd 418.2872, found 418.2859.

5e: oil; t_R = 7.7 min; IR (KBr): 1671 and 1739 cm^{-1} (C=O); UV λ_{max}: 241 nm (ε = 12,000); ^1H NMR δ: 0.93 (3H, s, 18-Me), 1.19 (3H, s, 19-Me), 2.31 (3H, s, *p-Me*-phenethyl), 2.65 (2H, m, *p*-Me-phenyl-CH_2), 5.72 (1H, d, J = 1.5 Hz, 4-H), 7.07–7.11 (4H, m, aromatic protons). ^{13}C NMR δ: 13.7, 17.4, 20.2, 21.0, 21.7, 30.5, 31.3, 32.0, 32.5, 35.0, 35.7, 39.2, 41.1, 42.0, 47.5, 50.8, 54.2, 124.0, 128.3, 129.0,

135.2, 138.9, 168.5, 200.8, 220.4; MS *m/z*: 404 (M^+, 2), 286 (100), 271 (14), 122 (21). HR-MS for $C_{28}H_{36}O_2$ (M^+): calcd 404.2715, found 404.2722.

5f: oil; t_R = 7.4 min; IR (KBr): 1669 and 1739 cm^{-1} (C=O); UV λ_{max}: 241 nm (ε = 11,000); ^1H NMR δ: 0.93 (3H, s, 18-Me), 1.20 (3H, s, 19-Me), 2.75 (2H, t, J = 8.0 Hz, *p*-CF_3-phenyl-CH_2), 5.74 (1H, d, J = 1.2 Hz, 4-H), 7.32 and 7.53 (2H each, d, J = 7.8 Hz, aromatic protons). ^{13}C NMR δ: 13.7, 17.4, 20.2, 21.7, 30.4, 30.7, 31.3, 32.1, 32.9, 35.0, 35.7, 39.3, 41.1, 42.1, 47.5, 50.8, 54.2, 124.0, 125.21, 125.24, 125.3, 128.7, 146.3, 168.8, 200.4, 220.3; MS *m/z*: 458 (M^+, 1), 439 (4), 286 (100), 271 (48). HR-MS for $C_{28}H_{33}F_3O_2$ (M^+): calcd 458.2433, found 458.2430.

2.5. 2-Alkylandrosta-1,4-diene-3,17-diones (6)

DDQ (0.15 mmol) was added to a solution of the 4-ene-3,17-diones **5** (0.10 mmol) in dioxane (2 ml) and the mixture was heated under reflux for 19 h. After this time, the mixture was treated with Al_2O_3 (1 g) column (EtOAc) and the steroidal material was submitted to purification with preparative TLC (hexane–EtOAc = 4:1, multiple developments) or preparative HPLC (CH_3CN:H_2O = 60:40 (v/v); flow rate 5 ml/min) to obtained compound **6a–6f** (29–49%). The purities of oil substances were obtained by analytical HPLC as described for those of compounds **4** to be more than 98%.

6a: mp 165–168 °C. IR (KBr): 1633 cm^{-1} (C=C), 1662 and 1739 cm^{-1} (C=O); UV λ_{max}: 250 nm (ε = 15,200); ^1H NMR δ: 0.91 (3H, s, 18-Me), 1.19 (3H, s, 19-Me), 3.65 (2H, m, phenyl-CH_2), 6.10 (1H, d, J = 1.1 Hz, 4-H), 6.60 (1H, s, 1-H), 7.18–7.30 (5H, m, aromatic protons); ^{13}C NMR δ: 13.8, 18.8, 22.0, 22.2, 31.2, 32.1, 32.4, 35.1, 35.2, 35.7, 43.3, 47.7, 50.4, 52.6, 124.0, 126.2, 128.4, 129.1, 137.5, 139.5, 151.6, 167.7, 185.8, 220.0; MS *m/z*: 374 (M^+, 80), 359 (36), 223 (19), 210 (100). Anal. Calcd for $C_{26}H_{30}O_2$: C, 83.38; H, 8.07. Found C, 83,13; H, 8.28.

6b: mp 197–199 °C; IR (KBr): 1629 cm^{-1} (C=C), 1664 and 1739 cm^{-1} (C=O); UV λ_{max}: 250 nm (ε = 14,300); ^1H NMR δ: 0.89 (3H, s, 18-Me), 1.09 (3H, s, 19-Me), 2.77 (2H, m, phenyl-CH_2), 6.08 (1H, d, J = 1.0 Hz, 4-H), 6.40 (1H, s, 1-H), 7.08–7.24 (5H, m, aromatic protons); ^{13}C NMR δ: 13.7, 18.6, 21.8, 21.9, 31.1, 31.4, 32.1, 32.4, 34.2, 35.0, 35.6, 43.0, 47.7, 50.4, 52.6, 124.0, 125.7, 128.1, 128.9, 135.8, 141.5, 151.8, 167.6, 186.1, 220.2; MS *m/z*: 388 (M^+, 73), 371 (16), 297 (73), 284 (100). Anal. Calcd for $C_{27}H_{32}O_2$: C, 83.46; H, 8.30. Found: C, 83.43: H, 8.32.

6c: oil; t_R = 5.5 min; IR (neat): 1635 cm^{-1} (C=C), 1665 and 1733 cm^{-1} (C=O); UV λ_{max}: 250 nm (ε = 14,400); ^1H NMR δ: 0.94 (3H, s, 18-Me), 1.21 (3H, s, 19-Me), 2.64 (2H, t, J = 7.9 Hz, phenyl-CH_2), 6.08 (1H, d, J = 1.5 Hz, 4-H), 6.75 (1H, s, 1-H), 7.16–7.29 (5H, m, aromatic protons); ^{13}C NMR δ: 13.8, 19.0, 21.9, 22.2, 29.0, 30.1, 31.2, 32.1, 32.4, 35.1, 35.7, 43.1, 47.7, 50.5, 52.6, 124.1, 125.7, 128.3, 128.4, 128.6, 137.4, 142.3, 150.3, 167.5, 186.2, 220.1; MS *m/z*: 402 (M^+, 94), 298 (100), 283 (15), 134 (96). HR-MS for $C_{28}H_{34}O_2$ (M^+): calcd 402.2559, found 402.2567.

6d: mp 140–142 °C; IR (KBr): 1626 cm^{-1} (C=C), 1661 and 1742 cm^{-1} (C=O); UV λ_{max}: 249 nm (ε = 14,900); ^1H NMR δ: 0.94 (3H, s, 18-Me), 1.21 (3H, s, 19-Me), 2.62 (2H, t, J = 8.0 Hz, phenyl-CH_2), 6.07 (1H, d, J = 1.2 Hz, 4-H), 6.73 (1H, s, 1-H), 7.15–7.29 (5H, m, aromatic protons); ^{13}C NMR δ: 13.8, 18.9, 21.9, 22.2, 27.9, 29.0, 31.1, 31.2, 32.1, 32.4, 35.1, 35.6, 35.7, 43.1, 47.7, 50.4, 52.6, 124.1, 125.6, 128.2, 128.4, 137.5, 142.6, 150.2, 167.4, 186.2, 220.0; MS *m/z*: 416 (M^+, 100), 299 (79), 297 (31), 91 (71). Anal. Calcd for $C_{29}H_{36}O_2$: C, 83.61; H, 8.71. Found C, 83.75 H, 8.80.

6e: mp 181–182 °C; IR (KBr): 1631 cm^{-1} (C=C), 1664 and 1738 cm^{-1} (C=O); UV λ_{max}: 250 nm (ε = 13,800); ^1H NMR δ: 0.90 (3H, s, 18-Me), 1.10 (3H, s, 19-Me), 2.29 (3H, s, *p*-*Me*-phenethyl), 2.71 (2H, m, *p*-Me-phenyl-CH_2), 6.08 (1H, d, J = 1.1 Hz, 4-H), 6.43 (1H, s, 1-H), 6.98–7.04 (4H, m, aromatic protons). MS *m/z*: 402 (M^+, 55), 297 (73), 284 (64), 105 (100). HR-MS for $C_{28}H_{34}O_2$ (M^+): calcd 402.2559, found 402.2556.

6f: oil; t_R = 5.2 min; IR (KBr): 1630 cm^{-1} (C=C), 1664 and 1740 cm^{-1} (C=O); UV λ_{max}: 250 nm (ε = 11,000); ^1H NMR δ: 0.90 (3H, s, 18-Me), 1.08 (3H, s, 19-Me), 2.87 (2H, m, *p*-CF_3-phenyl-CH_2), 6.09 (1H, d, J = 1.0 Hz, 4-H), 6.49 (1H, s, 1-H), 7.23 and 7.50 (2H each, d, J = 8.1 Hz, aromatic protons). ^{13}C NMR δ: 13.7, 18.7, 21.9, 22.0, 31.1, 31.4, 32.1, 32.4, 34.2, 35.0, 35.6, 43.1, 47.6, 50.4, 52.6, 123.9, 125.00, 125.03, 125.1, 129.1, 135.7 145.8, 151.8, 167.9, 186.0, 219.8; MS *m/z*: 456 (M^+, 62), 438 (6), 297 (57), 284 (100). HR-MS for $C_{28}H_{31}F_3O_2$ (M^+): calcd 456.2276, found 456.2278.

2.6. Enzyme preparation

Human placental microsomes (particles sedimenting at 105,000 × *g* for 60 min) were obtained using the method reported by Ryan [12]. They were washed once with 0.05 mM dithiothreitol solution, lyophilized, and stored at −80 °C. No significant loss of activity occurred during this study (2 months).

2.7. Aromatase assay procedure

Aromatase activity was measured according to the procedure of Siiteri and Thompson [36]. The screening assay for determination of IC_{50} value, the kinetic assay, and the time-dependent assay were carried out essentially according to the assay methods described in our previous work. Briefly, 20 μg of protein of the lyophilized microsomes and 20-min incubation time for the screening assay, and 20 μg of protein of the microsomes and 5-min incubation time for the kinetic assay, respectively, were employed in this study, and the assays were carried out in 67 mM phosphate buffer in the presence of NADPH in air [27]. In the time-dependent inactivation experiment, 1/10 of the incubation mixture was used for assays of the remaining aromatase activity.

2.8. Molecular modeling

The crystal structure of human placental aromatase was downloaded from the Protein Data Bank (Accession Code, 3EQM). Molecular modelings, 3D structures, of ligands were built by Spartan'08 software (Wavefunction, Inc., Irvine, CA, USA) using Hartree-Fock 6-31G* calculations. Molecular docking was performed by AutoDock Vina (The Scripps Research Institute, CA, USA) [37]. Docking to aromatase was carried out to propose docked structures with similar calculated affinities (−3.1 to −5.7 kcal/mol). The primary criterion used in choosing best docked structure was the position of the Δ^1-AD derivative relative to the active site aspartate (Asp 309), arginine (Arg 115) and methionine (Met 374), with reference to the bound conformation of AD. The program was able to reproduce the docked conformation of compound **6c** in aromatase with a reasonable rmsd. Graphics were generated with PyMOL software (DeLano Scientific LLC, Palo Alto, CA, USA).

3. Results

3.1. Chemistry

2-Phenyaliphatic-substituted Δ^1-ADs (**6**) were synthesized principally according to reaction sequence of the preparation of 2-alkyl-substituted Δ^1-AD derivatives. Various phenylaliphatic iodide (alkyl: methyl to butyl) and *p*-methyl- and *p*-trifluoromethyl-phenethyl iodide subjected to reaction with testosterone *tert*-butyldimethylsilyl ether (**2**) in presence of *tert*-BuOK or lithium diisopropylamide (LDA) as a base under cooling as a key reaction (Fig. 3). Conditions using *tert*-BuOK at −60 °C was effective only for the formation of 2α-phenpropyl compound

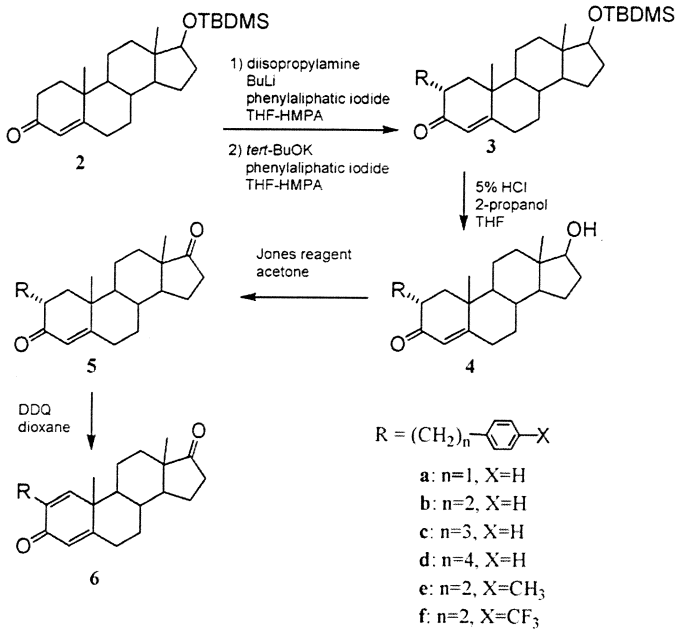


Fig. 3. Synthesis of 2-phenylaliphatic-substituted Δ^1-ADs (**6**).

3c (22% yield). Conditions using LDA at −20 °C were used for the productions of 2α-benzyl- and 2α-phenbutyl- compound **3a** and **3d** (64% for **3a** and 22% for **3d**), whereas 2α-phenethyl- (**3b**), 2α-*p*-methylphenethyl- (**3e**) and 2α-*p*-trifluoromethylphenethyl- (**3f**) compounds were produced under conditions employing LDA at 0 °C (yields: 11–22%). In the reactions, 2α-phenylaliphatic 4-en-3-ones **3** were produced as major products while the 2β-phenyaliphatic isomers, minor products were not isolated. After the purification with silica gel column chromatography or preparative TLC of compounds **3**, these compounds were subjected sequentially to deprotection of the 17β-silyl ethers **3** with diluted HCl in a mixture of THF and 2-propanol and oxidation of the deprotected product 17β-ols **4** with Jones reagent in acetone, giving the 2α-phenylaliphatic 17-keto compounds **5**. Finally, an introduction of a double bond at C-1 of the 17-keto compounds **5**, the AD derivatives with DDQ in dioxane gave 2-phenylaliphatic Δ^1-AD analogs **6**.

The structures of the compounds synthesized were confirmed by the spectrometric analysis and HR-MS, elemental analysis or HPLC analysis.

3.2. Aromatase inhibition

Reversible inhibition of aromatase activity in human placental microsomes by 2-aliphatic-substituted ADs **5** and their Δ^1-AD derivatives **6** was initially studied in vitro by enzyme kinetics. The amount of aromatase activity was measured by determinating the amount of ^3H_2O released from [1β-^{3}H] androstenedione, which is an index of estrogen formation [36]. IC_{50} values were first obtained, and then, to characterize the nature of their binding to the active site of aromatase, aromatization was measured in the presence of several concentrations of the inhibitors and androstenedione. The results of these studies were plotted on typical Lineweaver–Burk plots. All of the steroids examined exhibited clear-cut competitive inhibition. The Lineweaver–Burk plots for the phenpropyl-1,4-dien-3-one **6c** are shown in Fig. 4. The apparent inhibition constants (K_i) were determined by analysis of the Dixon plot and shown in Table 1. In these studies, the apparent K_m and V_{max} for androstenedione was about 40 nM and 120 pmol/min/mg protein, respectively. All the AD derivatives **5** were poor inhibitors of aromatase (IC_{50}: more than 50 μM). In series of the Δ^1-AD

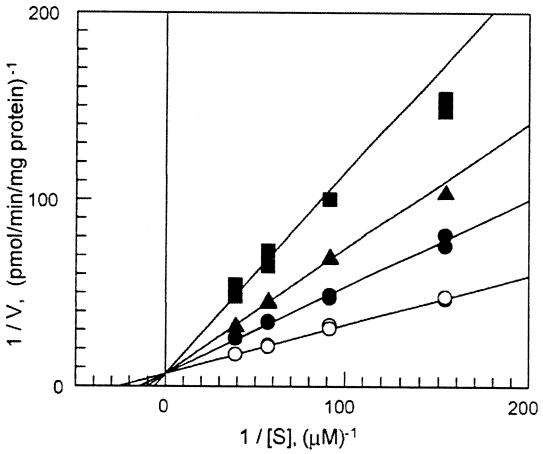


Fig. 4. Lineweaver–Burk plots of inhibition of human placental aromatase by 2-phenpropyl-Δ^1-AD (**6c**) with AD as the substrate. Concentrations of inhibitor: (○) control (0 nM); (●) 12.5 nM; (▲) 25 nM; (■) 50 nM. The inhibition experiments with all the other steroids examined gave essentially similar plots to Fig. 4 (data not shown).

steroids, the inhibitory activities of the phenethyl derivative **6b** and its *p*-methyl compound **6e** and the phenpropyl derivative **6c** were relatively high (apparent K_i: 206 nM for **6b**, 16.1 nM for **6c**, and 348 nM for **6e**) whereas the other compounds were poor inhibitors (K_i: more than 2600 nM).

Compounds **6b**, **6c**, and **6e** with the high affinity for aromatase were then tested for their ability to cause a time-dependent inactivation of aromatase. The phenethyl and phenpropyl compounds **6b** and **6c** showed the time-dependent inactivation only in the presence of NADPH under aerobic conditions. Pseudo-first-order kinetics were obtained during the first 12 min of inactivation with the inhibitors, and the kinetic data were analyzed according to the method of Kitz and Wilson [38] (Fig. 5). Double-reciprocal plots of K_{obs} vs. inhibitor concentration gave k_{inact} and K_I values, respectively (Table 2). The K_I and k_{inact} values for compound **6b** and **6c**

Table 1
In vitro aromatase inhibition by 2α-phenylaliphatic-ADs (**5**) and 2-phenylaliphatic-Δ^1-ADs (**6**).

Compound	IC_{50}, μM[a]	Apparent K_i, nM[b]
2α-phenylaliphatic-ADs (**5**)		
5a, benzyl	466	–
5b, phenethyl	126	–
5c, phenpropyl	50.2	5110 ± 260
5d, phenbutyl	222	–
5e, *p*-methylphenethyl	38.8	4095 ± 191
5f, *p*-trifluoromethylphenethyl	46.6	5142 ± 288
2-phenylaliphatic-Δ^1-ADs (**6**)		
6a, benzyl	86.4	4500 ± 290
6b, phenethyl	2.57	206 ± 8.2
6c, phenpropyl	0.145	16.1 ± 0.58
6d, phenbutyl	34.2	2690 ± 190
6e, *p*-methylphenethyl	6.36	348 ± 21.7
6f, *p*-trifluoromethylphenethyl	34.12	4002 ± 354
For comparison		
Δ^1-AD[c]	0.830	90 ± 6.4

[a] 300 nM of [1β-^{3}H]androstenedione and 20 μg of protein from human placental microsomes were used.

[b] Apparent inhibition constant (K_i) was obtained by Dixon plot. 20 μg of protein from human placental microsomes and 5 min of incubation were employed. All of the inhibitors examined showed a competitive type of inhibition based on analysis of the Lineweaver–Burk plot. The results were means ± S.E. Apparent K_m and V_{max} values for AD were about 40 nM and 120 pmol/min/mg protein, respectively, in this study.

[c] The K_i values of Δ^1-AD were previously obtained to be 43 ± 3.0 nM [27] and 65 ± 3.5 nM [28].

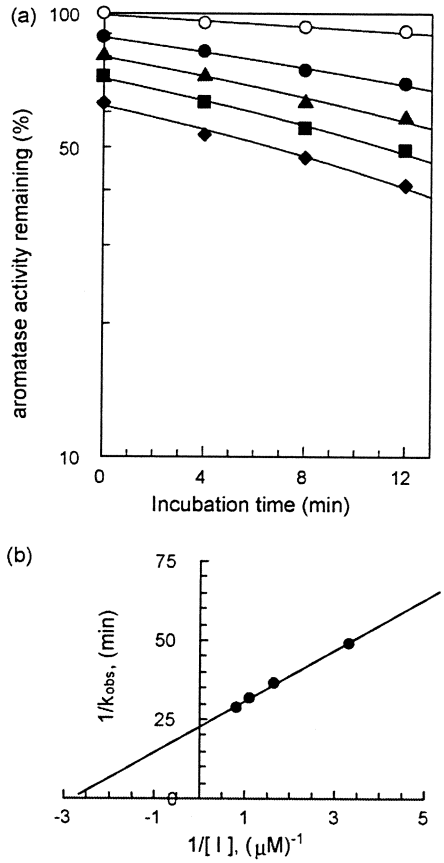


Fig. 5. Time-dependence (a) and concentration-dependence (b) of inactivation of human placental aromatase by 2-phenpropyl-Δ^1-AD (**6c**) in the presence of NADPH in air. Concentrations of the inhibitor: (○) control (0 nM); (●) 300 nM; (▲) 600 nM; (■) 900 nM; (ϑ) 1200 nM. The time-dependent inactivation experiments with 2-phenethyl-Δ^1-AD (**6b**) gave essentially similar plots to Fig. 5 (data not shown).

Table 2
Kinetic analysis of time-dependent inactivation of aromatase caused by 2-phenylaliphatic-Δ^1-ADs[a] (**6**).

Compound	K_I, nM	k_{inact}, min^{-1}
6b, phenethyl	8124	0.0293
6c, phenpropyl	370	0.0454
6e, *p*-methylphenethyl	NT[b]	–
For comparison		
Δ^1-AD [27]	952	0.059

[a] The time-dependent inactivation of compound **6a**, **6d** and **6f** were not determined because of their poor affinity for aromatase. Apparent K_I and k_{inact} were obtained by Kitz–Wilson plot [38].
[b] The time-dependent inactivation was not observed.

were 8124 nM and 0.0293 min^{-1} for compound **6b** and 370 nM and 0.0454 min^{-1} for compound **6c**. The *p*-methylphenethyl compound **6e** did not cause the time-dependent inactivation.

The substrate AD significantly blocked the inactivation by the 1,4-diene inhibitors, while a nucleophile, L-cysteine, had no significant effect (Fig. 6).

3.3. Molecular docking

Phenpropyl-Δ^1-AD steroid (**6c**) was selected for docking to the active site of human placental aromatase. As shown in Fig. 7, the compound **6c** positions in the active site of the enzyme with hydrogen bondings of the C-3 and C-17 carbonyl groups with polar amino acid residues Asp 309 and Arg 115 or Met 374, respectively, similarly to the natural substrate AD. Interestingly, accessible volume,

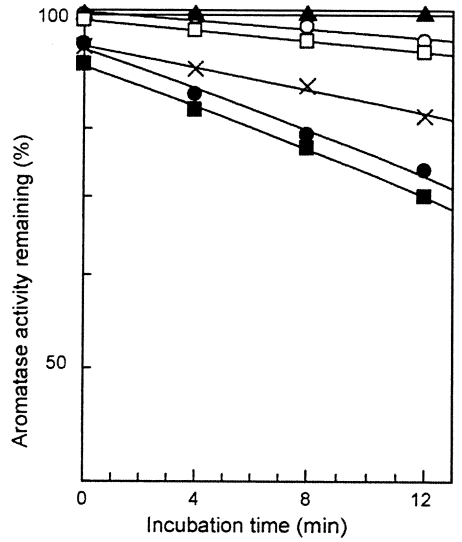


Fig. 6. Inactivation of human placental aromatase by 2-phenpropyl-Δ^1-AD (**6c**) under various conditions: (○) control; (●) inhibitor (600 nM); (▲) control + AD (5.4 μM) or inhibitor (600 nM) + AD (5.4 μM); (□) control + L-cystein (0.5 mM); (■) inhibitor (600 nM) + L-cystein (0.5 mM); (×) inhibitor (600 nM) in the absence NADPH.

hydrophobic binding pocket, extends to towards the C-2 position of compound **6c** and a bulky phenyl group of the phenpropyl group orients to the accessible volume of the binging pocket. The hydrophilic amino acids such as Ile 132, Ile 133, Ile 305, Phe 148, Met 303, and Ala 306 are involved in the binding pocket and may play a critical role in the binding to the active site (Fig. 7).

4. Discussion

The 2-phenylaliphatic Δ^1-ADs (**6a–6d**), which have various lengths of methylene units from a methyl to a butyl as well as the *p*-methylphenyl- and *p*-trifluoromethylphenylethyl derivatives **6e** and **6f** were synthesized. The effect of introducing the phenylalkyl chain at the 2-position of Δ^1-AD were examined with respect to affinity for aromatase and rate of inactivation of the enzyme. The 2-phenpropyl derivative **6c** was very powerful competitive inhibitor of aromatase in human placental microsomes with apparent K_i value of 16.1 ± 0.58 nM where the K_m/K_i ratio of compound **6c** is about 2.5. This corresponds well to those obtained for 6β-alkyl- and 6β-phenylaliphatic-Δ^1-ADs which are among the most powerful inhibitors of aromatase [27,28]. Compound **6c** inactivated aromatase in a mechanism-based manner. The rate of inactivation decreased when the substrate AD was included in the incubation mixture while L-cysteine, a nucleophile, failed to protect aromatase significantly from the inactivation by the inactivator. Thus, covalent-bound formation between aromatase and the reactive intermediate appears to occur at the active site, therefore, preventing diffusion of the active inhibitor, a reactive electrophile, in the surrounding media [39]. Recently, we suggested that the mechanism-based inactivator Δ^1-AD, a parent compound of the phenpropyl steroid **6c**, may inactivate aromatase through oxygenation of 19-oxo function derived from two sequential oxygenations at the C-19 position of the parent compound [30,40]. The aromatase-bound metabolite may be produce during the cleavage of the 19-oxo group, although the exact mechanism is clear so far. Covey [5] has suggested previously that aromatase inactivates itself because the mechanism-based aromatase inhibitor induces the enzyme to autoxidize itself. Since we have no evidence for covalent modification of aromatase by the compound **6c**, a substrate analog-induced autoxidation mechanism for inactiva-

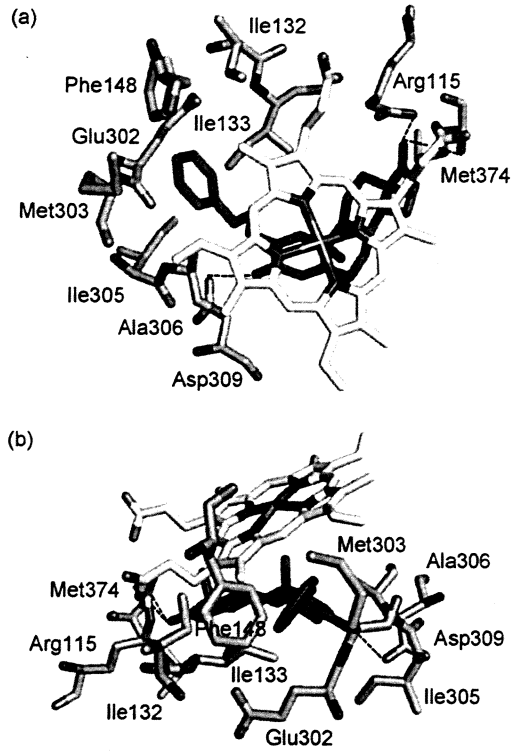


Fig. 7. 2-Phenpropyl-Δ^1-AD (**6c**) is docked into the active site of the human placental aromatase. Views from the heme iron (a) and from the C-2 phenpropyl group (b) are shown in selected active site residues of amino acids which are displayed for gray or white for carbon, blue for nitrogen, red for oxygen and yellow for sulfur. Compound **6c** is colored magenta. The C-3 and C-17 carbonyl groups of compound **6c** positions to hydrogen bonding with Asp 309 and Arg 115 or Met 137, respectively, and the phenpropyl group is oriented in the lipophilic binding pocket of the active site to produce thermodynamically stable enzyme–steroid complex. (For interpretation of the references to color in this figure legend, the reader is referred to the web version of the article.)

tion may be considered as an alternate explanation for the observed time-dependent inactivation.

The aromatase inhibitory activities of the phenethyl and *p*-methylphenethyl compounds **6b** and **6e** were less powerful than the phenpropyl derivative **6c** but still good inhibitors for the enzyme. The other compounds, the benzyl, phenbutyl, and *p*-trifluoromethylphenethyl-1,4-dienes **6a**, **6d**, and **6f**, showed poor activities of the aromatase inhibition. Only the phenethyl compound **6b** among them caused the time-dependent inactivation of aromatase. Compound **6e** has a *p*-methylphenethyl moiety at the 2-position of Δ^1-AD (**1**), which is similar length of the C-2 substituent to a phenpropyl moiety. This suggests that the terminal phenyl group would play a critical role in the suicide inactivation of aromatase and a steric reason would be operative in the aromatase-catalyzed activation reaction of the phenethyl derivative **6e**. All of the time-dependent activators **6b** and **6c** showed that the K_I values obtained from the inactivation experiments are more than 20 times higher than the corresponding apparent K_i values from the competitive inhibition experiments. The similar tendency has previously been reported in the inactivation experiments using other Δ^1-AD steroid derivatives [27–31]. When the observed inactivation is based on the aromatase reaction *per se*, this relation of the K_I value to the K_i value suggests that binding of the activated inhibitor to the nucleophilic residue of the active site rather than activation of the inhibitor becomes rate determining or partial rate determining [39].

All of the AD derivatives **5** were poor inhibitors of aromatase (K_i: more than 4 μM). The previous findings demonstrated that 2-alkyl-substituted ADs have high affinity to the binding site of aromatase; the 2α-methyl- and 2α-ethyl compounds were powerful inhibitors of the enzyme and elongation of the 2α-subsituent up to the hexyl derivative still showed high affinity to the enzyme [31]. The results implied that the binding geometry of the 2-phenylaliphatic steroids **5** in the active site of aromatase would be different from those of the alkyl steroids. The phenyl moiety would prevent the formation of thermodynamically stable inhibitor–enzyme complex.

The crystal structure of human placental aromatase has recently been reported by Ghosh et al. [41]. A molecule of exemestane, one of Δ^1-AD analogs, is build into the active site by using the AD backbone. AD and exemestane superimposed quite well accepts the difference in puckering of the A-ring. Thus exemestane remains tightly bound in the pocket through hydrogen bondings of the C-3 and C-17 carbonyl groups to Asp 309 and Arg 115 or Met 374, respectively, and van der Waals interaction between C-6 methylidene and The 310 is observed. Docking experiment of phenpropyl-Δ^1-AD (**6c**), the most powerful aromatase inhibitor and inactivator, to the crystal structure of the enzyme showed that this compound was bound to the active site in the anchoring effect of hydrogen bondings of the C-3 and C-17 carbonyl groups, as observed in a exemestane molecule, and the lipophilic amino acid residues, Ile 132, Ile 133, Ile 305, Phe 148, Met 303, and Ala 306, in the vicinity of the 2-phenpropyl moiety would also play a critical role in binding of the active site.

5. Conclusion

2-Phenylaliphtic Δ^1-AD (**6**) were synthesized from testosterone 17-*tert*-butyldimethylsilyl ether (**2**) using phenylaliphatic halides in the presence of LDA or $KOC(CH_3)_3$ as a key reaction as the aromatase inhibitors. The phenpropyl compound **6c** was the most powerful inhibitor and this inhibitor inactivated aromatase in a mechanism-based manner. Docking experiments demonstrate that compound **6c** is oriented to the active site of aromatase, binding pocket, though the hydrogen bondings of the 3- and 17-carbonyl groups and the lipophilic interactions of the phenpropyl group to produce thermodynamically stable enzyme–steroid complex.

Acknowledgments

This work was supported in part by a High Technology Research Center Project from the Ministry of Education, Culture, Sports, and Technology of Japan. Human term placenta was kindly donated by Dr. Michihiro Yuki of Yuki Lady's Clinic.

References

[1] Thompson Jr EA, Siiteri PK. The involvement of human placental microsomal cytochrome P-450 in aromatization. J Biol Chem 1974;249:5373–8.
[2] Kellis Jr J, Vickery LE. Purification and characterization of human placental aromatase cytochrome P-450. J Biol Chem 1987;262:4413–20.
[3] Yoshida N, Osawa Y. Purification of human placental aromatase cytochrome P-450 with monoclonal antibody and its characterization. Biochemistry 1991;30:3003–10.
[4] Thompson Jr EA, Siiteri PK. Utilization of oxygen and reduced nicotinamide adenine dinucleotide phosphate by human placental microsomes during aromatization of androstenedione. J Biol Chem 1974;249:5364–72.
[5] Covey DF. Aromatase inhibitors: specific inhibitors of estrogen biosynthesis. In: Berg D, Plempel M, editors. Sterol biosynthesis inhibitors: pharmaceutical and agrochemical aspects. Chichester: Eliss Horwood Ltd.; 1988. p. 534–71.
[6] Oh SS, Robinson CH. Mechanism of human placental aromatase: a new active site model. J Steroid Biochem Mol Biol 1993;44:389–97.
[7] Akhtar M, Lee-Robichaud P, Akhtar ME, Wright JN. The impact of aromatase mechanism on other P450s. J Steroid Biochem Mol Biol 1997;61:127–32.
[8] Bossche HV. Inhibitors of P450-dependent steroid biosynthesis: from research to medical treatment. J Steroid Biochem Mol Biol 1992;43:1003–21.
[9] Brodie AM, Santen RJ. Aromatase and its inhibitors in breast cancer treatment—overview and perspective. Breast Cancer Res Treat 1994;30:1–6.
[10] Johnston JO. Aromatase inhibitors. Crit Rev Biochem Mol Biol 1998;33:375–405.

[11] Harper-Wynne C, Dowsett M. Recent advances in the clinical application of aromatase inhibitors. J Steroid Biochem Mol Biol 2001;76:179–86.
[12] Ryan KJ. Biological aromatization of steroids. J Biol Chem 1959;234:268–72.
[13] Gual C, Morato T, Hayano M, Gut M, Dorfman RI. Biosynthesis of estrogens. Endocrinology 1962;71:920–5.
[14] Meigs RA, Ryan KJ. Enzymatic aromatization of steroids. I. Effects of oxygen and carbon monoxide on the intermediate steps of estrogen biosynthesis. J Biol Chem 1971;246:83–7.
[15] Milewich L, Bradfield DJ, Coe LD, Masters BSS, MacDonald P. Metabolism of 1,4-androstadiene-3,17-dione by human placental microsomes. Enzyme properties and kinetic parameters in the formation of estrogens and 17β-hydroxy-1,4-androstadien-3-one. J Steroid Biochem 1981;14:1115–25.
[16] Numazawa M, Yoshimura A, Oshibe M. Enzymic aromatization of 6-alkyl-substituted androgens, potent competitive and mechanism-based inhibitors of aromatase. Biochem J 1998;329:151–6.
[17] Numazawa M, Yoshimura A. Biological aromatization of $\Delta^{4,6}$- and $\Delta^{1,4,6}$-androgens and their 6-alkyl analogs, potent inhibitors of aromatase. J Steroid Biochem Mol Biol 1999;70:189–96.
[18] Schwarzel WC, Kruggel WG, Brodie HJ. Studies on the mechanism of estrogen biosynthesis. VIII. The development of inhibitors of the enzyme system in human placenta. Endocrinology 1973;92:866–80.
[19] Covey DF, Hood WF. Enzyme-generated intermediates derived from 4-androstene-3,6,17-trione and 1,4,6-androstatriene-3,17-dione cause a time-dependent decrease in human placental aromatase activity. Endocrinology 1981;108:1597–9.
[20] Covey DF, Hood WF. A new hypothesis based on suicide substrate inhibitor studies for the mechanism of action of aromatase. Cancer Res 1982;42(Suppl.):3327s–33s.
[21] Marsh DA, Brodie HJ, Garrett W, Tsai-Morris CH, Brodie AMH. Aromatase inhibitors. Synthesis and biological activity of androstenedione derivatives. J Med Chem 1985;28:788–95.
[22] Segaloff A, Weeth JB, Rongone EL, Murison PJ, Bowers CY. Hormonal therapy in cancer of the breast. XVI. The effect of Δ^1-testololactone on clinical course and hormonal excretion. Cancer 1960;13:1017–20.
[23] Lerner LJ, Bianchi A, Borman A. Δ^1-Testololactone, a nonadrogenic augmentor and inhibitor of androgens. Cancer 1960;13:1201–5.
[24] Henderson D, Norbisrath G, Kerb U. 1-Methyl-1,4-androstadiene-3,17-dione (SH 489): characterization of an irreversible inhibitor of estrogen biosynthesis. J Steroid Biochem 1986;24:303–6.
[25] Salle ED, Briatico G, Giudici D, Ornati G, Zaccheo T. Aromatase inhibition and experimental antitumor activity of FCE 24304, MDL 18962 and SH 489. J Steroid Biochem 1989;34:431–4.
[26] Salle ED, Ornati G, Giudici D, Lassus M, Evans RJ, Coombes RC. Exemestane (FCE 24304) a new steroidal aromatase inhibitor. J Steroid Biochem Mol Biol 1992;43:137–43.
[27] Numazawa M, Oshibe M, Yamaguchi S, Tachibana M. Time-dependent inactivation of aromatase by 6-alkylandrosta-1,4-diene-3,17-diones. Effects of length and configuration of 6-alkyl group. J Med Chem 1996;39:1033–8.
[28] Numazawa M, Yamaguchi S. Synthesis and structure–activity relationships of 6-phenylaliphatic-substituted C_{19} steroids having a 1,4-diene, 4,6-diene, or 1,4,6-triene structure as aromatase inhibitors. Steroids 1999;64:187–96.
[29] Numazawa M, Shelangouski M, Nagasaka M. Probing the binding pocket of the active site of aromatase with 6-ether or 6-ester substituted androst-4-ene-3,17-diones and their diene and triene analogs. Steroids 2000;65:871–82.
[30] Numazawa M, Nagaoka M, Handa W, Ogawa Y, Matsuoka S. Studies directed towards a mechanistic evaluation of inactivation of aromatase by the suicide substrates androta-1,4-diene-3,17-diones and its 6-ene derivatives. Aromatase inactivation by the 19-substituted derivatives and their enzymic aromatization. J Steroid Biochem Mol Biol 2007;107:211–9.
[31] Takahashi M, Handa W, Umeta H, Ishikawa S, Yamashita K, Numazawa M. Aromatase inactivation by 2-substituted derivatives of the suicide substrate androsta-1,4-diene-3,17-dione. J Steroid Biochem Mol Biol 2009;116:191–9.
[32] Hosoda H, Yamashita K, Sagae H, Nambara T, Steroids CI. Dimethyl-*tert*-butylsilyl ethers of steroids. Chem Pharm Bull 1975;23:2118–22.
[33] Abraham EP, Smith JC. Addition of hydrogen chloride and iodide to olefins. Undecenoic acid. J Chem Soc 1936:1605–7.
[34] Roel B, Joannes W, Aede G. A novel route to the marasmane skeleton via a tandem rearrangement-cyclopropanation reaction. Total synthesis of (+)-isovelleral. J Org Chem 2001;66:2350–7.
[35] Nedelec L, Gasc JC, Bucourt R. The kinetically controlled methylation of conjugated polycyclic ketones. Tetrahedron 1974;30:3263–8.
[36] Siiteri PK, Thompson EA. Human placental aromatase. J Steroid Biochem 1975;6:317–22.
[37] Trott A, Olson J. Autodock Vina: improving the speed and accuracy of docking with a new scoring function, efficient optimization and multithreading. J Comput Chem 2009, available online.
[38] Kitz R, Wilson IB. Effects of methanesulfonic acid as irreversible inhibitors of acetylcholine esterase. J Biol Chem 1962;237:3245–9.
[39] Silverman RB. Mechanism-based enzyme inactivation, vol. 1. Boca Raton, FL: CRC press; 1988. Chapter 1, p. 3–30.
[40] Numazawa M, Yamashita K, Kimura N, Takahashi M. Chemical aromatization of 19-hydroxyandrosta-1,4-diene-3,17-dione with acid or alkaline: elimination of the 19-hydroxy methyl group as formaldehyde. Steroids 2009;74:208–11.
[41] Ghosh D, Griswold J, Erman M, Pangborn W. Structural basis for androgen specificity and oestrogen synthesis in human aromatase. Nature 2009;457:219–23.

Fusaric Acid as a Novel Proton-Affinitive Derivatizing Reagent for Highly Sensitive Quantification of Hydroxysteroids by LC-ESI-MS/MS

Kouwa Yamashita, Keiko Yamazaki, Sachiko Komatsu, and Mitsuteru Numazawa

Faculty of Pharmaceutical Sciences, Tohoku Pharmaceutical University, Sendai, Japan

A highly sensitive derivatization method for liquid chromatography (LC)-electrospray ionization (ESI) tandem mass spectrometry of dehydroepiandrosterone (DHEA), testosterone (T), pregnenolone (P5), and 17α-OH-pregnenolone (17-OHP5) was developed based on the use of fusaric acid as a reagent. DHEA, P5, and 17-OHP5 were rapidly and quantitatively converted to the 3-fusarate esters by treatment with fusaric acid and 2-methyl-6-nitrobenzoic anhydride. The positive ESI-mass spectra of the fusarate esters of each steroid were dominated by the appearance of $[M + H]^+$ as base peaks. The fusarate derivatization of these steroids showed 17.6-fold (DHEA), 11.9-fold (P5), 3.3-fold (17-OHP5), and 1.8-fold (T) higher sensitivity to those of the corresponding picolinate derivatives in LC-selected reaction monitoring. (J Am Soc Mass Spectrom 2010, 21, 249–253) © 2010 American Society for Mass Spectrometry

In the recent development of analytical methodology for hydroxysteroids that were generally insensitive to liquid chromatography-electrospray ionization tandem mass spectrometry (LC-ESI-MS/MS), two types of derivatization designs have been proposed to provide high sensitivity to such kind of steroid molecules. The introduction of permanently charged moieties into steroid molecules was proven to be a promising method [1–4]. The use of 1-methylpyridinium for hydroxy group [2] and 2-hydrazino-1-methylpyridine for carbonyl group [4] as derivatizing reagents showed higher sensitivity in analyses of testosterone (T), 5α-dihydrotestosterone (DHT), and dehydroepiandrosterone (DHEA) by LC-ESI-MS/MS. However, the application of these permanently charged derivatives to steroids possessing more than two hydroxy and/or carbonyl groups in one molecule seemed to be inconvenient and failed to obtain simple ESI-mass spectra with the appearance of protonated molecule ($[M + H]^+$) due to the formation of multiple ions of $[M - H]^-$ and $[M]^{2+}$ [4].

The introduction of high proton-affinitive moiety into steroid molecules was the alternative choice to obtain simple ESI mass spectra characterized by the formation of $[M + H]^+$ with high intensity [5–8]. The use of dimethylaminoaphthalene-sulfonate [5, 6], pyridine-sulfonate [7], pyridine-dicarboxylate [8] derivatives for steroidal hydroxyl group, and hydroxime [9, 10] and 2-pyridine-hydrazone [11] derivatives for steroidal ketones have been investigated. However, the introduction of sulfonate moieties was limited to the phenolic hydroxy group of estrogens. Derivatization of T and DHT with pyridine-2,3-dicarboxylic anhydride resulted in the formation of the mixture consisted of two regio-isomers of half esters in their chromatograms [8]. Generation of *syn*- and *ant*-isomeric peaks might also be inevitable in the analyses of T and DHT using hydroxime and pyridine-hydrazone derivatizations [9, 11].

Recently, we have demonstrated that the introduction of picolinate moiety into hydroxysteroids provided some advantages to LC-ESI-MS/MS analyses of these compounds in a positive mode, involving the production of simple $[M + H]^+$ with high intensity, the simplicity of the derivatization and purification process [12–14], and the excellence for liquid chromatographic behaviors in the profile analyses of corticosteroids [15–17] and sterols [18–20]. In our preliminary results, the picolinate derivatives of Δ^5-3β-hydroxysteroids, such as DHEA and pregnenolone (P5), seemed to be less sensitive in ESI compared with those of T and estradiol by selected reaction monitoring (SRM). This report describes the characteristics of fusaric acid derivative, as a novel and sensitive proton-affinitive tag for hydroxysteroids in LC-ESI-MS/MS, and presents some possible explanations to the enhancement of detection sensitivity by this derivative in LC-ESI-MS/MS compared with the picolinic acid derivative.

Address reprint requests to Dr. K. Yamashita, Faculty of Pharmaceutical Sciences, Tohoku Pharmaceutical University, 4-1 Komatsushima 4-chome, Aoba-ku, Sendai-shi, Miyagi-ken 981-8558, Japan. E-mail: kyama@tohoku-pharm.ac.jp

© 2010 American Society for Mass Spectrometry. Published by Elsevier Inc.
1044-0305/10/$32.00
doi:10.1016/j.jasms.2009.10.008

Published online November 14, 2009
Received June 24, 2009
Revised October 2, 2009
Accepted October 10, 2009

Experimental

Materials and Reagents

Dehydroepiandrosterone (DHEA, **1a**), testosterone (T, **2a**), pregnenolone (P5, **3a**), and 17α-hydroxypregnenolone (17-OHP5, **4a**) were purchased from Steraloids (Newport, RI, USA). Fusaric acid was obtained from Sigma-Aldrich (St. Louis, MO, USA), and 2-methyl-6-nitrobenzoic anhydride, 4-dimethylaminopyridne, and triethylamine were obtained from Tokyo Kasei Kogyo (Tokyo, Japan). LC-MS grade ultra pure water, acetonitrile (MeCN), and methanol (MeOH) were purchased from Wako Pure Chemicals (Osaka, Japan). Oasis HLB cartridge (30 mg, 1 mL) was obtained from Waters (Milford, MA, USA).

LC-ESI-MS/MS

LC-ESI-MS/MS was run on a Finnigan TSQ Quantum triple-stage quadrupole mass spectrometer (Thermo Fischer Scientific, San Jose, CA, USA) equipped with an ESI ion source and a Surveyor auto-sampler and a MS-pump (Thermo Fischer Scientific). The columns was a Puresil 5-C_{18} (150 mm × 2.1 mm i.d., 5 μm, Waters) connected to a guard cartridge (C_{18}, 10 mm × 2 mm i.d., 5 μm) in a guard-cartridge holder with the mobile phase consisted of MeCN-ultrapure water-acetic acid (AcOH) (85:15:0.1, vol/vol/vol) at a flow rate of 200 μL/min. Elution was performed with an isocratic mode and at an ambient temperature. The general ESI-MS conditions were as follows: spray voltage, 4500 V (positive); sheath gas, nitrogen, 30 arbitrary unit (gas pressure); auxiliary gas, nitrogen, 15 arbitrary unit (gas pressure); ion transfer capillary temperature, 350 °C; collision gas argon, 1.5 mTorr (gas pressure).

Synthesis of Standard Derivatives

To a solution of DHEA (**1a**, 50 mg; 0.17 mmol in tetrahydrofuran (THF) 1 mL) was added the premixed reagent solution (fusaric acid; 40 mg, 2-methyl-6-nitrobenzoic anhydride: 50 mg, 4-dimethylaminopyridine; 10 mg, triethylamine; 50 μL, THF 1 mL), and the reaction mixture was stirred at room temperature for 1 h. After dilution of the reaction mixture with 5% $NaHCO_3$ (20 mL), the product was then extracted with ethyl acetate EtOAc (20 mL). The organic layer was washed with sat. NaCl (20 mL), 5% HCl (20 mL), and then with sat. NaCl (20 mL × 2), and dried over anhydrous Na_2SO_4. Evaporation of the solvent and re-crystallization of the crude product from EtOAc afforded compound **1c** as colorless leaflets. Similarly, **2c** (colorless prisms), **3c** (colorless needles), and **4c** (colorless prisms) were prepared from **2a**, **3a**, and **4a**, respectively. Picolinate derivatives (**3b**: colorless needles and **4b**: colorless needles) were synthesized in the same manner as **1b** and **2b**, and the structures of all derivatives were confirmed by the measurement of ^1H nuclear magnetic resonance spectra, ultra violet spectra, and elemental analyses as previously described [12].

Microscale Derivatization [13, 14]

To a solution of steroid (**1a**, **2a**, **3a**, or **4a**:1 ng or 1 μg in THF 50 μL) were added the premixed reagent solution (20 μL) (fusaric acid; 40 mg, 2-methyl-6-nitrobenzoic anhydride; 50 mg, 4-dimethylaminopyridine; 10 mg, triethylamine; 100 μL in THF 1 mL), and the resulting mixture was allowed to stand at room temperature for 30 min. After dilution of the reaction mixture with 5% $NaHCO_3$ (1 mL), the resulting sample was transferred onto Oasis HLB cartridge (30 mg-1 mL, preconditioned with MeOH 1 mL and ultra pure water 1 mL). The cartridge was washed with ultra pure water (3 mL), 5% HCl (3 mL), and ultra pure water (3 mL), and the derivative was eluted with 90% MeCN (1 mL). The eluate was evaporated to dryness under reduced pressure and the residue was dissolved in mobile phase (100 μL) and then submitted to LC-ESI-MS/MS. Reaction yield was calculated by comparing the peak intensity prepared in this section with that of the sample obtained and purified in the former section (*Synthesis of standard*) by SRM.

Results and Discussion

As shown in Figure 1, the fusaric acid moiety was incorporated into the steroid molecule via 3β-hydroxy

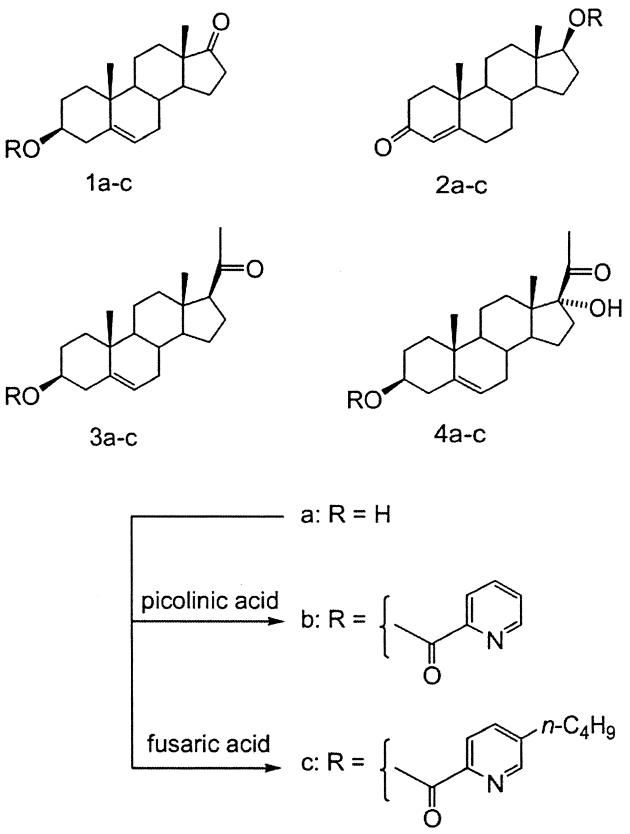


Figure 1. Schematic presentation of the derivatization of DHEA (**1a**), T (**2a**), P5 (**3a**) and 17-OHP5 (**4a**) with picolinic acid and fusaric acid by mixed anhydride method using 2-methyl-6-nitrobenzoic anhydride.

group (**1a**, **3a**, **4a**) or 17β-hydroxy group (**2a**) by ester formation with mixed anhydride method using 2-methyl-6-nitrobenzoic anhydride [21] and 4-dimethylaminopyridine. Fusarate formation by this method underwent quantitatively under mild condition with reaction yield of >85% for **1c**, **2c**, **3c**, and **4c** in the levels of 1 ng and 1 μg as was observed in the pocolinate derivatization [13, 14].

Figure 2 shows the positive ESI mass spectrum (a) and the product ion spectrum (b) of the fusarate derivative of DHEA (**1c**). Positive-ESI-mass spectrum of **1c** was dominated by the appearance of protonated molecule ($[M + H]^+$) at *m/z* 450 as a base peak, and the formation of adduct ions ($[M + Na + CH_3CN]^+$) was observed at *m/z* 513. Collison of $[M + H]^+$ with argon (collision energy: 21 V) resulted in the formation of product ions at *m/z* 271 and 253, these ions were assigned to be formed by the elimination of fusaric acid ($C_{10}H_{13}NO_2$) moiety followed by the additional dehydration from $[M + H]^+$ in **1c**. The formation of these kinds of product ions is not specific to the fusarate derivatives, and is commonly observed in the picolinate derivatives and other pyridine-carboxylate derivatives of **1a** and **2a** as previously reported [12, 14]. Table 1 summarizes the positive-ESI mass and product ion spectral data of these four fusarate derivatives (**1c**, **2c**, **3c**, and **4c**). The same product ion species were observed at *m/z* 271 and 253 in **2c**, *m/z* 299 and 281 in **3c**, and *m/z* 315 and 297 in **4c**, respectively. The formation of product ion at *m/z* 180 originated from the fusaric acid moiety was also observed in all cases, and dominated particularly in **2c**.

In SRM, the transitions of *m/z* 450 → *m/z* 271 (or *m/z* 253) for **1c** and **2c**, *m/z* 478 → *m/z* 281 for **3c** and *m/z* 494 → *m/z* 297 for **4c**, were chosen, respectively, and detection sensitivities were compared with those of the picolinate derivatives (**1b**, **2b**, **3b**, and **4b**). The results are shown in Table 1 (right column). When the detection sensitivity was evaluated by measuring the signal-to-noise (SN) ratios for each peak of 20 fg (injected amount), the values of **1c**, **2c**, **3c**, and **4c** were >60, 2, 15, and 8, respectively. These SN ratios were higher to those of the corresponding picolinate derivatives. The increase of SN ratio was remarkable in **1c**, **3c**, and **4c** rather than **2c**. When absolute detection responses of the fusarate derivatives were compared with those of the corresponding picolinate derivatives by SRM (0.1 pmol; injected amount), the fusarate derivatives of each steroid exhibited higher responses than those of the picolinate derivatives. The fusarate derivative of T (**2c**) showed 1.8 ± 0.2 (mean ± standard deviation; n = 3)-fold higher response to that of **2b**, whereas, the fusarate derivatives of DHEA (**1c**), P5 (**3c**), and 17-OHP5 (**4c**) showed 17.6 ± 3.0-fold, 11.9 ± 2.4-fold, and 3.3 ± 1.0-fold higher responses when compared with those of **1b**, **3b**, and **4b**, respectively. The typical SRM chromatograms of these steroids in matrices is explained in the Supplementary Material, which can be found in the electronic version of this article.

As judged from these results, the derivatization of steroidal hydroxy group by fusaric acid must be a promising technique to afford an excellent sensitivity to the assay of DHEA, P5, and 17-OHP5 by LC-ESI-MS/MS. Appearance of the differences in SRM sensitivity

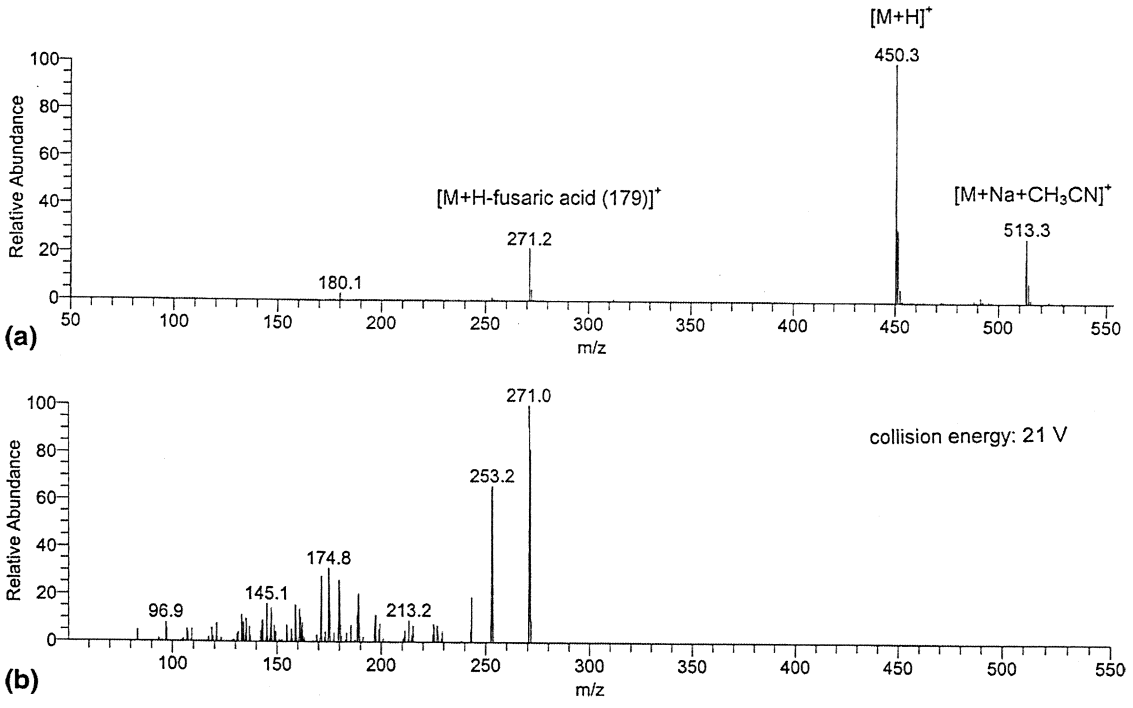


Figure 2. Positive ESI mass spectrum (**a**) and product ion spectrum (**b**) of the fusarate derivative of DHEA (**1c**). Spray voltage: 4500 V.

Table 1. ESI-mass spectral, tandem mass spectral data and signal-to-noise (SN) ratios in SRM of the fusarate derivatives of DHEA (1c), T (2c), P5 (3c), and 17-OHP5 (4c)

Derivatives	ESI-MS data: *m/z* (intensity, %)		MS/MS data: product ions *m/z* (collision energy; V)			SN ratios (20 fg/on column)[a]
	$[M + H]^+$	Other ions				
1c	450 (100)	513[b] (35), 271[c] (28)	271 (21)	253 (28)	180 (21)	>20[d], >60[e]
2c	450 (100)	513[b] (16), 271[c] (1)[c]	180 (20)	253 (27)	271 (22)	2[d]
3c	478 (100)	541[b] (21), 299[c] (22)	299 (16)	281 (21)	180 (18)	15[f]
4c	494 (100)	557[b] (18), 315[c] (50)	297 (21)	315 (19)	180 (19)	8[g]

[a]Values were expressed as injected amounts.
[b]$[M + Na + CH_3CN]^+$.
[c]$[M + H - C_{10}H_{13}O_2N(\text{fusaric acid}) - H_2O]^+$.
[d]*m/z* 450 → *m/z* 253 (27 V).
[e]*m/z* 450 → *m/z* 271 (21 V).
[f]*m/z* 478 → *m/z* 281 (21 V).
[g]*m/z* 494 → *m/z* 297 (21 V).

between the fusarate derivatives and picolinate derivatives for these hydroxysteroid partially are supposed to be attributed to the theoretically higher value of the proton-affinity of 5-butylpyridine (fusarate) moiety (ca 229-230 kcal/mol, estimated value from the database; http://webbook.nist.gov/chemistry/ of National Institute of Standard and Technology (NIST)) than that of pyridine moiety (ca 222.4 kcal/mol). The reason for the observation of difference in the enhancement of sensitivity between T and DHEA was not made clear at this moment.

Conclusions

Derivatization of hydroxysteroids with fusaric acid and the characterization of the prepared derivatives in LC-ESI-MS/MS (positive mode) were described. The use of fusarate derivatization for Δ^5-3β-hydroxysteroids provided robustness and enhanced sensitivity to the assay, and enabled to determine these steroids with the levels of less than sub-femtogram on column. Improvement of sensitivity of fusarate derivative in LC-ESI-MS/MS might partially be attributed to the inherent high proton-affinity of fusarate moiety than that of the picolinate moiety.

Acknowledgments

The authors acknowledge support in part for this work by a High Technology Research Center Project from the Ministry of Education, Culture, Sports, Science, and Technology of Japan.

Appendix A Supplementary Material

Supplementary material associated with this article may be found in the online version at doi:10.1016/j.jasms.2009.10.008.

References

1. Quirke, J. M. E.; Adam, C. L.; Van Berkel, G. J. Chemical Derivatization for Electrospray Ionization Mass Spectrometry. 1. Alkyl halides, Alcohols, Phenols, Thiols, and Amines. *Anal. Chem.* **1994,** *66,* 1302–1305.
2. Nishiyama, T.; Hashimoto, Y.; Takahashi, K. The Influence of Androgen Deprivation Therapy on Dihydrotestosterone Levels in the Prostatic Tissue of Patients with Prostate Cancer. *Cancer. Res.* **2004,** *10,* 7121–7126.
3. Griffith, W. J.; Liu, S.; Alvelius, G.; Sjvöll, J. Derivatization for the Characterization of Neutral Oxosteroids by Electrospray and Matrix-Assisted Laser Desorption/Ionization Mass Spectrometry. *Rapid Commun. Mass Spectrom.* **2003,** *17,* 924–935.
4. Higashi, T.; Yamauchi, A.; Shimada, K. 2-Hydradino-1-Methylpyridine: A Highly Sensitive Derivatization Reagent for Oxosteroids in Liquid Chromatography-Electrospray Ionization Mass Spectrometry. *J. Chromatogr. B* **2005,** *825,* 214–222.
5. Xu, X.; Veenstra, T. D.; Fox, S. D.; Roman, J. M.; Issaq, H. J.; Falk, R.; Saavedra, J. E.; Keefer, L. K.; Ziegler, R. G. Measuring Fifteen Endogenous Estrogens Simultaneously in Human Urine by High-Performance Liquid Chromatography-Mass Spectrometry. *Anal. Chem.* **2005,** *77,* 6646–6654.
6. Salvador, A.; Moretton, C.; Piram, A.; Faure, R. On-Line Solid Phase Extraction with On-Support Derivatization for High-Sensitivity Liquid Chromatography Tandem Mass Spectrometry of Estrogens in Influent/Effluent of Wastewater Treatment Plants. *J. Chromatogr. A* **2007,** *1145,* 102–109.
7. Xu, L.; Spink, D. C. Analysis of Steroidal Estrogens as Pyridine-3-Sulfonyl Derivatives by Electrospray Tandem Mass Spectrometry. *Anal. Biochem.* **2008,** *375,* 105–114.
8. Licea-Perez, H.; Wang, S.; Szapacs, M. E.; Yang, E. Development of a Highly Sensitive and Selective UPLC/MS/MS Method for the Simultaneous Determination of Testosterone and 5α-Dihydrotestosterone in Human Serum to Support Testosterone Replacement Therapy for Hypogonadism. *Steroids* **2008,** *73,* 601–610.
9. Kalhorn, T. F.; Page, S. T.; Howald, W. N.; Mostaghel, E. A.; Nelson, P. S. Analysis of Testosterone and Dihydrotestosterone from Biological Fluids as the Oxime Derivatives Using High-Performance Liquid Chromatography/Tandem Mass Spectrometry. *Rapid Commun. Mass Spectrom.* **2007,** *21,* 3200–3206.
10. Kushnir, M. M.; Rockwood, A. L.; Roberts, W. L.; Pattison, E. G.; Bunker, A. M.; Fitzgerald, R. L.; Meikle, A. W. Performance Characteristics of a Novel Tandem Mass Spectrometry Assay for Serum Testosterone. *Clin. Chem.* **2006,** *52,* 120–128.
11. Shibayama, Y.; Higashi, T.; Shimada, K.; Kashimada, K.; Onishi, T.; Ono, M.; Miyai, K.; Mizutani, S. Liquid Chromatography-Tandem Mass Spectrometric Method for Determination of Salivary 17&;α-Hydroxyprogesterone: A Noninvasive Tool for Evaluating Efficacy of Hormone Replacement Therapy in Congenital Adrenal Hyperplasia. *J. Chromatogr. B* **2008,** *867,* 49–56.
12. Yamashita, K.; Kobayashi, S.; Tsukamoto, S.; Numazawa, M. Synthesis of Pyridine-Carboxylate Derivatives of Hydroxysteroids for Liquid Chromatography-Electrospray Ionization-Mass Spectrometry. *Steroids* **2007,** *72,* 50–59.
13. Yamashita, K.; Okuyama, M.; Watanabe, Y.; Honma, S.; Kobayashi, S.; Numazawa, M. Highly Sensitive Determination of Estrone and Estradiol in Human Serum by Liquid Chromatography-Electrospray Ionization Tandem Mass Spectrometry. *Steroids* **2007,** *72,* 819–827.
14. Yamashita, K.; Yoshimichi, M.; Maekubo, H.; Okuyama, M.; Honma, S.; Takahashi, M.; Numazawa, M. Development of Highly Sensitive Quantification Method for Testosterone and Dihydrotestosterone in Human Serum and Prostate Tissue by Liquid Chromatography-Electrospray Ionization Tandem Mass Spectrometry. *Steroids* **2009,** *74,* 920–926.
15. Yamashita, K.; Takahashi, M.; Tsukamoto, S.; Numazawa, M.; Okuyama, M.; Honma, S. Use of Novel Derivatization for Simultaneous Quantification of Six Corticosteroids by Liquid Chromatography-Electrospray Ionization Tandem Mass Spectrometry. *J. Chromatogr. A* **2007,** *1173,* 120–128.
16. Yamashita, K.; Nakagawa, R.; Okuyama, M.; Honma, S.; Takahashi, M.; Numazawa, M. Simultaneous Determination of Tetrahydrocortisol,

Allotetrahydrocortisol, and Tetrahydrocortisone in Human Urine by Liquid Chromatography-Electrospray Ionization Mass Spectrometry. *Steroids* **2008,** *73,* 727–737.
17. Yamashita, K.; Okuyama, M.; Nakagawa, R.; Honma, S.; Satoh, F.; Morimoto, R.; Ito, S.; Takahashi, M.; Numazawa, M. Development of Sensitive Derivatization Method for Aldosterone in Liquid Chromatography-Electrospray Ionization Mass Spectrometry of Corticosteroids. *J. Chromatogr. A* **2008,** *1200,* 115–121.
18. Honda, A.; Yamashita, K.; Numazawa, M.; Ikegami, T.; Doy, M.; Matsuzaki, Y.; Miyazaki, H. Highly Sensitive Quantification of 7α-Hydroxy-4-Cholesten-3-one in Human Serum by LC-ESI-MS/MS. *J. Lipid Res.* **2007,** *48,* 459–464.
19. Honda, A.; Yamashita, K.; Miyazaki, H.; Shirai, M.; Ikegami, T.; Xu, G.; Numazawa, M.; Hara, T.; Matsuzaki, Y. Highly Sensitive Analysis of Sterol Profiles in Human Serum by LC-ESI-MS/MS. *J. Lipid Res.* **2008,** *49,* 2063–2073.
20. Honda, A.; Yamashita, K.; Hara, T.; Ikegami, T.; Miyazaki, T.; Shirai, M.; Xu, G.; Numazawa, M.; Matsuzaki, Y. Highly Sensitive Quantification of Key Regulatory Oxysterols in Biological Samples by LC-ESI-MS/MS. *J. Lipid Res.* **2008,** *50,* 350–357.
21. Shiina, I.; Ibuka, R.; Kubota, M. A New Condensation Reaction for the Synthesis of Carboxylic Esters from Nearly Equimolar Amounts of Carboxylic Acids and Alcohols Using 2-Methyl-6-Nitrobenzoic Anhydride. *Chem. Lett.* **2002,** *31,* 286–287.

研究テーマ②

エストロゲン受容体制御による加齢性疾患（骨粗鬆症、認知障害）改善薬の創製

Bioorganic & Medicinal Chemistry 22 (2014) 3508–3514

Contents lists available at ScienceDirect

Bioorganic & Medicinal Chemistry

journal homepage: www.elsevier.com/locate/bmc

Novel estrogen receptor (ER) modulators containing various hydrophobic bent-core structures

Kiminori Ohta, Takumi Ogawa, Asako Kaise, Yasuyuki Endo *

Faculty of Pharmaceutical Sciences, Tohoku Pharmaceutical University, 4-4-1 Komatsushima, Aoba-ku, Sendai 981-8558, Japan

ARTICLE INFO

Article history:
Received 26 March 2014
Revised 11 April 2014
Accepted 12 April 2014
Available online 20 April 2014

Keywords:
Bent-core structure
Hydrophobic
Estrogen
Carborane
SERM

ABSTRACT

We previously discovered *m*-carborane-containing estrogen receptor (ER) modulator **4**, which exhibits weak ER-agonistic and antagonistic activities in transactivation assays. With the aim of developing novel ER partial agonists, we designed and synthesized various analogues of **4** with a bent-core structure, that is, pseudo cyclic structure (**5**), tetrahydropyrimidinone (**6**), *m*-benzene (**7**), adamantane (**8**), and 9,10-dimethyl-*m*-carborane (**9**), in place of the *m*-carborane moiety. Compound **9** showed greater binding affinity than **4** in ER-binding assay using [6,7-^{3}H]-17β-estradiol and was a more effective partial agonist than **4** in MCF-7 cell proliferation assay. It appears to be a promising candidate as a selective ER modulator (SERM).

© 2014 Elsevier Ltd. All rights reserved.

1. Introduction

We have shown that the carborane cage is a novel hydrophobic pharmacophore with potential for drug development,[1] and since then, various carborane-containing bioactive compounds have been reported.[2] Prior to that, carboranes had been used only as boron carriers for boron neutron capture therapy (BNCT), based on their high boron content.[3] We also designed and synthesized various carborane-containing bioactive compounds as candidate nuclear receptor ligands.[4] One derivative, 1-(4-hydroxyphenyl)-12-hydroxymethyl-*p*-carborane (BE120, **1**), shows more potent estrogenic activity than the endogenous female hormone estrogen, estradiol (E2, **2**, Fig. 1).[1,5] Subsequently, many carboranyl phenol derivatives were synthesized and their estrogen-related biological activities examined.[6]

Estrogens are known to play important roles in the development and maintenance of reproductive and non-reproductive tissues in both women and men.[7] However, while estrogens have essential functions in the reproductive, skeletal, cardiovascular, and central nervous systems, the proliferative effect of estrogens can be pathological, promoting cancer of the breast and uterus.[7] These multiple functions result in remarkable tissue-selective effects of estrogens, and have led to interest in for the feasibility of using selective estrogen receptor modulators (SERMs), to treat breast cancer, osteoporosis, and female postmenopausal syndrome.[8] However, these drugs involve some risk of cancer of the female reproductive organs.[8] Therefore, researchers are seeking to develop third- or fourth-generation SERMs to circumvent this risk.[8] The most noteworthy feature of these SERMs is the *N,N*-dialkylaminoethyl substituent, which serves to inhibit the binding of co-activators by moving helix-12 of the receptor to an unfavorable position.[9] Tamoxifen (**3a**), which is metabolized in vivo to an active derivative, 4-hydroxytamoxifen (**3b**), is a first-generation SERM

During our studies of carborane-containing ER modulators, we found that *m*-carborane derivative (**4**) showed ER partial agonistic activity in ERα transactivation assays,[10] and we suggested that the central core structure of **4** might play an important role in expressing partial agonistic activity, as well as in the hydrophobic interaction between the ERα ligand-binding domain (LBD) and **4**. (Fig. 2) Therefore, to investigate the role of the hydrophobic core structure of in the partial agonistic activity, we designed various derivatives with a bent-core structure, that is, pseudo cyclic structure

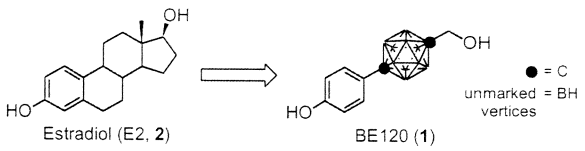


Figure 1. Development of potent ER agonist **1** based on the concept of a spherical hydrophobic pharmacophore.

* Corresponding author. Tel.: +81 22 727 0142; fax: +81 22 275 2013.
E-mail address: yendo@tohoku-pharm.ac.jp (Y. Endo).

http://dx.doi.org/10.1016/j.bmc.2014.04.022
0968-0896/© 2014 Elsevier Ltd. All rights reserved.

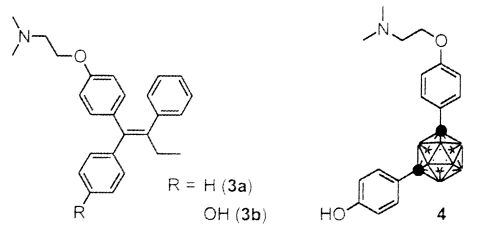


Figure 2. Structures of clinically used tamoxifen (**3a**), its metabolite (**3b**), and carborane-containing ER partial agonist **4**.

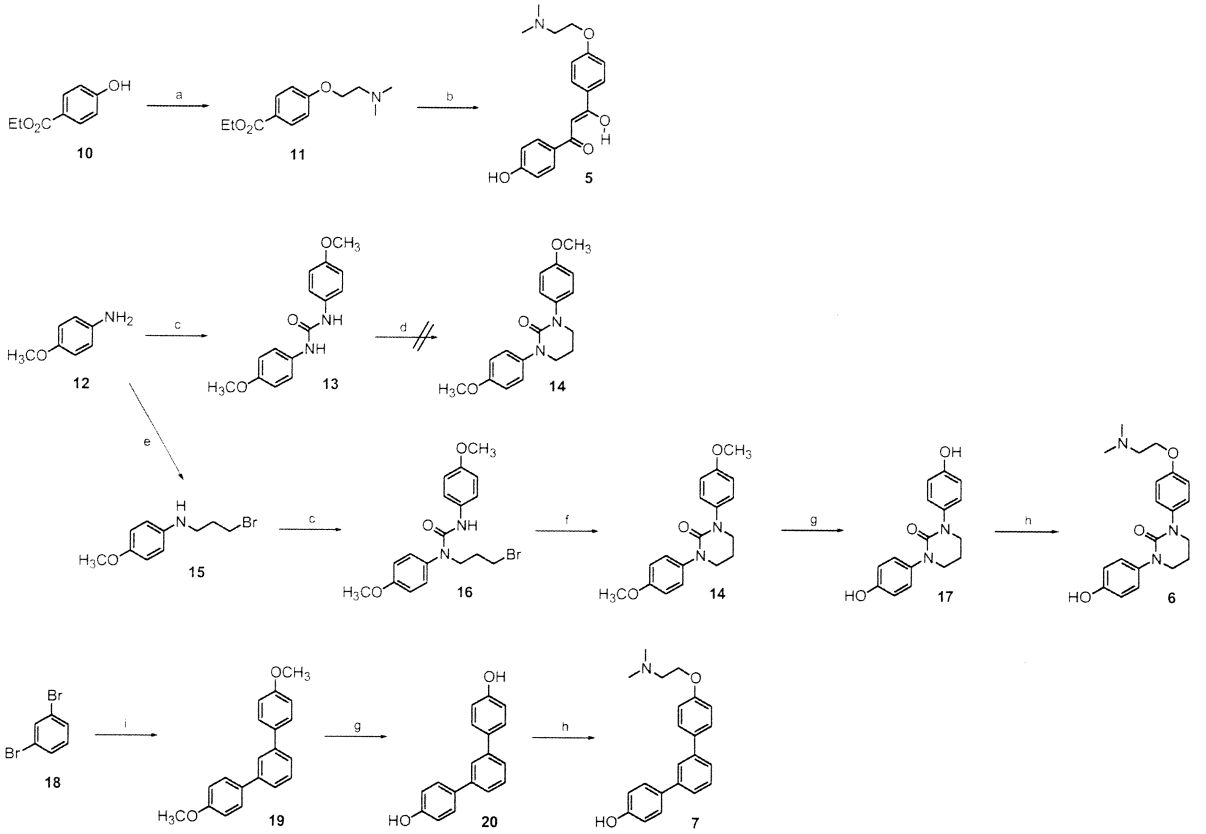
containing an intramolecular hydrogen bond (**5**), tetrahydropyrimidinone ring (**6**), benzene (**7**), adamantane (**8**), and 9,10-dimethyl-*m*-carborane cage (**9**), in place of the *m*-carborane cage of **4** and we measured their activity in ERα transactivation assays (Fig. 3).

2. Results and discussion

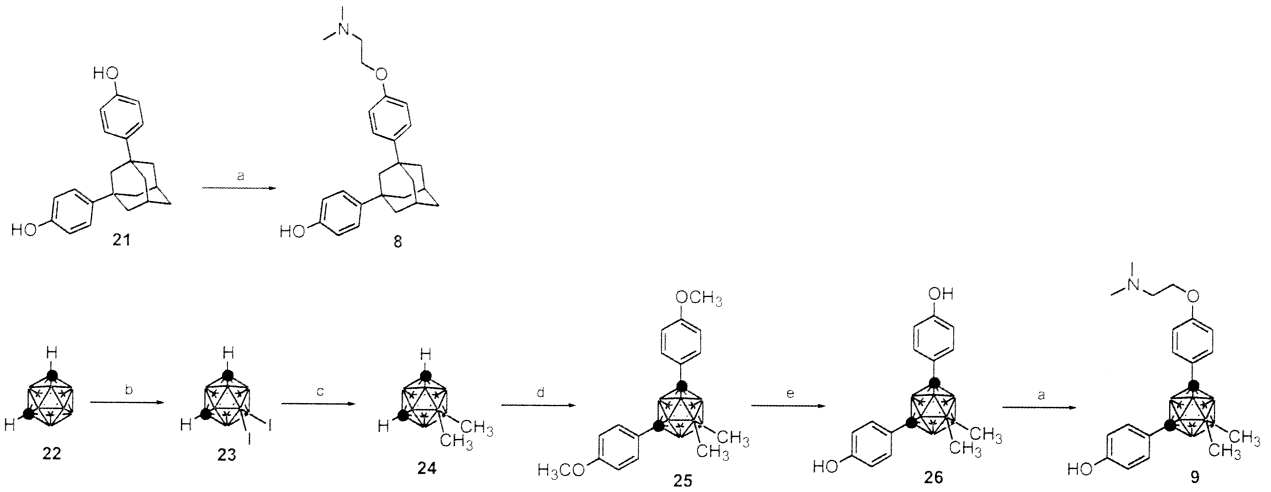
2.1. Synthesis of bisphenol derivatives

Scheme 1 summarizes the synthesis of non-spherical hydrophobic bent-structure derivatives **5–7**. Ethyl 4-hydroxybenzoate **10** was reacted with *N*,*N*-dimethylaminoethanol under Mitsunobu reaction conditions to afford the corresponding alkylated compound **11**. Claisen condensation of **11** with *tert*-butyldimethylsilyl (TBDMS)-protected 4-hydroxyacetophenone afforded 1,3-diketone **5** in 6% yield over 2 steps. We tried to synthesize tetrahydropyrimidinone derivative **6** from *p*-anisidine **12**, which was first reacted with 4-methoxyphenyl isocyanate to afford symmetric urea **13**. Cyclization reaction of **13** with 1,3-dibromopropane, however, gave a complex mixture, which did not contain the desired compound. Therefore, the propane unit was incorporated first into *p*-anisidine **12**, followed by reaction with 4-methoxyphenyl isocyanate, and intramolecular N-alkylation to afford cyclic urea derivative **14**. Demethylation of both methoxy groups of **14** afforded the corresponding bisphenol **17**, which was alkylated with *N*,*N*-dimethylaminoethyl chloride on one side to afford tetrahydropyrimidinone derivative **6** in 5% yield over 5 steps. 1,3-Dibromobenzene was reacted with 4-methoxyphenyl boronic acid under Suzuki–Miyaura cross-coupling conditions to afford *m*-terphenyl derivative **19**.[11] Deprotection of the methoxy group with BBr_3 was followed by O-alkylation with *N*,*N*-dimethylaminoethyl chloride to give terphenyl derivative **7** in 5% yield over 3 steps.

Compound **8** was obtained through alkylation of one phenol group of commercially available **21** in 24% yield. Compound **23**, which was prepared from **22** by treat with iodine in the presence of $AlCl_3$, was transformed into 9,10-dimethyl-*m*-carborane **24** by reaction with methylmagnesium chloride under Pd-catalyzed coupling conditions.[12] Compound **24** was treated with 2 equiv of *n*-BuLi, followed by CuCl to afford the di-Cu salt, which was reacted with 4-iodoanisole in the presence of pyridine as a ligand of Cu to afford diaryl-*m*-carborane intermediate **25**.[13] Deprotection of the methoxy group with BBr_3, followed by O-alkylation with *N*,*N*-dimethylaminoethyl chloride, afforded *m*-carborane-containing derivative **9** in 0.3% yield over 5 steps (Scheme 2).



Scheme 1. Syntheses of target compounds **5–7** with a non-spherical hydrophobic bent core structure. Reagents and conditions: (a) *N*,*N*-dimethylaminoethanol, diethyl azodicarboxylate Ph_3P, THF; (b) NaH, DME; (c) 4-methoxyphenyl isocyanate, triethylamine, toluene; (d) NaH, 1,3-dibromopropane, DMF; (e) 1,3-dibromopropane, CH_3CN; (f) NaH, THF; (g) BBr_3, CH_2Cl_2; (h) *N*,*N*-dimethylaminoethyl chloride hydrochloride, K_2CO_3, DMF/acetone; (i) 4-methoxyphenylboronic acid, $Pd(PPh_3)_4$, 1 M Na_2CO_3 aq, toluene.



Scheme 2. Syntheses of compounds **8** and **9** with a bulky hydrophobic core structure. Reagents and conditions: (a) *N,N*-dimethylaminoethyl chloride hydrochloride; (b) I_2, $AlCl_3$, CH_2Cl_2; (c) CH_3MgBr, $PdCl_2(PPh_3)_2$, DME; (d) *n*-BuLi, CuCl, DME, then pyridine, 4-iodoanisole, DME; (e) BBr_3, CH_2Cl_2.

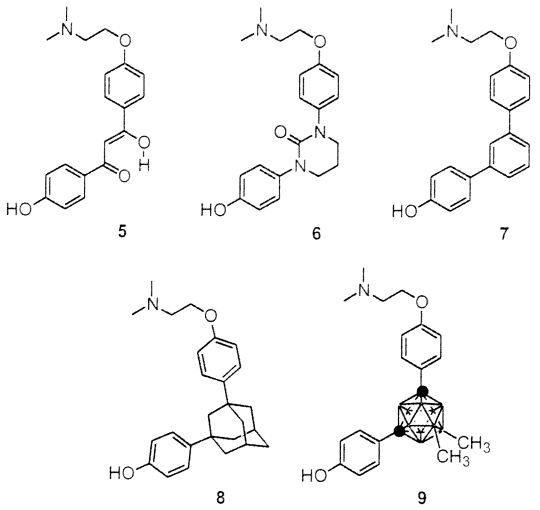


Figure 3. Target compounds **5–9**.

2.2. ERα binding

Binding affinity of compounds **5–9** for ERα was evaluated by means of a competitive binding assay using [6,7-^{3}H]17β-estradiol and human recombinant ERα.[14] The binding affinity data are summarized in Figure 4. Although compounds **5**, **6**, and **7** with non-spherical central core structure showed little binding affinity for ERα, compounds **4**, **8**, and **9**, which have three-dimensional hydrophobic core structure, bound to ERα in a dose-dependent manner. The hydrophobic ER LBD could not accept the benzene ring of **5** as a core structure, or the polar functional groups of **6** and **7**. Compound **8** with adamantane core structure showed about 10 times weaker binding affinity than **4**. We previously reported that the hydrophobic parameter π values of 4-(*m*-carboran-1-yl)phenol and 4-(1-adamantyl)phenol were 4.26 and 4.04, respectively.[15] Thus, adamantane is a less hydrophobic structure than the *m*-carborane cage and interacts less efficiently with the hydrophobic ER LBD. This idea is strongly supported by the binding affinity of **9**. Compound **9**, containing 9,10-dimethyl-*m*-carborane cage as a hydrophobic core structure, showed a greater ER-binding affinity than **4**. This result is consistent with the hydrophobicity of the central core structure, because introduction of two methyl groups into the *m*-carborane cage causes an increase of π value.

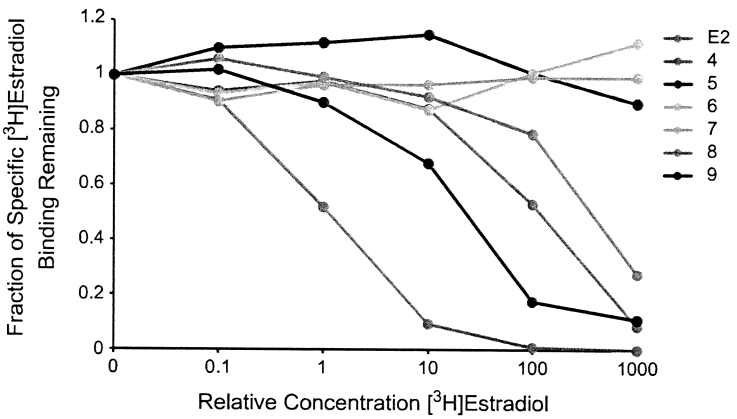


Figure 4. Competitive binding assay of compounds **4–9** with [^{3}H]E2 (4 nM) at ERα. Binding assays were conducted with the test compounds (0.4–4 μM) in the presence of [6,7-^{3}H]17β-estradiol (4 nM) and performed in duplicate (n = 2).

Table 1
Biological activities of **4**, **8**, and, **9** on MCF-7 cell proliferation

Compound	EC_{50}[a] (μM)	E_{max}[b] (%)	IC_{50}[a] (μM)
4	0.039	100	Inactive
8	0.016	17	1.06
9	0.015	23	0.88

[a] MCF-7 cells were treated with the test compounds (1×10^{-13} to 1×10^{-5} M) alone or in the presence of 0.1 nM E2. EC_{50} and IC_{50} values were estimated from the sigmoidal dose–response curves using GraphPad Prism 4 software.
[b] E_{max} values indicate the efficacy for cell proliferation, based on the value for E2 taken as 100.

2.3. MCF-7. cell proliferation assay

The biological activities of selected compounds, **4**, **8** and **9**, were evaluated by means of cell proliferation assay using human breast cancer MCF-7 cells.[14] EC_{50} or IC_{50} values of the test compounds were estimated from dose-response curves of MCF-7 cell proliferation in the absence or presence of 0.1 nM estradiol, respectively. The E_{max} value is the maximal efficacy of each compound in cell proliferation and is an index of ER partial agonistic activity. This value was estimated based on that of estradiol taken as 100 (Table 1). Compound **4** showed an EC_{50} value of 39 nM and its E_{max} value (100%) was equal to that of E2, but it did not show ER-antagonistic activity.[10] Unexpectedly, **4** was not an ER partial agonist in MCF-7 cell proliferation assay. Compounds **8** and **9** showed more potent estrogenic activity than that of E2, with the EC_{50} values of 16 and 15 nM, respectively. Interestingly, they showed low E_{max} values of 17% and 23%, respectively, and acted as ER partial agonists, in spite of containing spherical hydrophobic core structures similar to that of **4**. The difference of ER-agonistic activity among them might be caused by subtle differences of their binding forms in the ERα LBD. It is noteworthy that the biological activities of **4** and **9** are dramatically different, in spite of the very similar geometry. The two methyl substituents of **9** play a significant role in the expression of ER partial agonistic activity. The IC_{50} values of **8** and **9** were estimated to be 1.06 and 0.88 μM, respectively. These compounds effectively inhibit the estrogenic activity of estradiol, and appear to be promising SERM candidates.

3. Conclusion

In conclusion, we have designed and synthesized estrogen receptor modulators with various bent-core structures and examined their biological activities. Compounds **5**, **6**, and **7**, which contain non-spherical bent-core structures, did not bind to ERα. In contrast, spherical hydrophobic bent-core derivatives **4**, **8**, and **9** bound to the ERα LBD. Compounds **8** and **9** showed ERα-agonistic activity with very low E_{max} values of 17% and 23%, respectively, and partial agonistic activity, inhibiting MCF-7 cell proliferation at the concentrations of 1.06 and 0.88 μM, respectively. The two methyl groups of compound **9** have an important role in the expression of ER partial agonistic activity. Thus, as observed in the case of **4** and **9**, modification at the carborane cage causes marked changes of biological activities as well as chemical properties. These findings should be helpful in the molecular design of novel carborane-containing bioactive compounds, as well as ER partial agonists and SERMs.

4. Experimental

4.1. General considerations

Melting points were determined with a Yanaco micro melting point apparatus and were not corrected. ^{1}H NMR and ^{13}C NMR spectra were recorded with JEOL JNM-EX-270 and JNM-LA-400 spectrometers. Chemical shifts for ^{1}H NMR spectra were referenced to tetramethylsilane (0.0 ppm) as an internal standard. Chemical shifts for ^{13}C NMR spectra were referenced to residual ^{13}C present in deuterated solvents. The splitting patterns are designed as follows: s (singlet), d (doublet), t (triplet), q (quartet) and m (multiplet). Mass spectra were recorded on a JEOL JMS-DX-303 spectrometer. Elemental analyses were performed with a Perkin Elmer 2400 CHN spectrometer. Column chromatography was carried out using Fuji Silysia silica gel BW-80S and TLC was performed on Merck silica gel F_{254}. *p*-Carborane was purchased from Katchem s.r.o. (Prague, Czech Republic). Other reagents were purchased from Wako Pure Chemical Industries, Ltd., Sigma–Aldrich Co., and Tokyo Chemical Industry, Ltd. (TCI). All solvents were of reagent quality, purchased commercially, and were used without further purification.

4.1.1. Ethyl 4-(dimethylaminoethoxy)benzoate (11)

To a mixture of ethyl 4-hydroxybenzoate **10** (2.0 g, 12.0 mmol), dimethylaminoethanol (1.33 mL, 13.2 mmol), and triphenylphosphine (3.47 g, 13.2 mmol) in 20 mL of THF was added a 40% solution of DEAD in toluene (5.76 mL, 13.2 mmol) at room temperature. The mixture was stirred at room temperature for 24 h, then concentrated, and the residue was purified by silica gel column chromatography (AcOEt/*n*-hexane = 1:1) to give the title compound as a colorless oil; ^{1}H NMR (270 MHz, $CDCl_3$) δ (ppm) 1.37 (t, *J* = 7.1 Hz, 3H), 2.34 (s, 6H), 2.74 (t, *J* = 5.8 Hz, 2H), 4.11 (t, *J* = 5.6 Hz, 2H), 4.34 (q, *J* = 7.1 Hz, 2H), 6.93 (dd, *J* = 2.1 Hz, 6.9 Hz, 2H), 7.99 (dd, *J* = 2.0 Hz, 6.8 Hz, 2H); MS (EI) *m/z* 237 (M^+, 100%).

4.1.2. 1-[4-(2-Dimethylaminoethoxy)phenyl]-3-(4-hydroxyphenyl)propane-1,3-dione (5)

To a solution of **11** (500 mg, 2.0 mmol) and 4-(*tert*-butyldimethylsilyloxy)acetophenone (580 mg, 2.20 mmol) in 5 mL of dry DME was added sodium hydride (50%, 121 mg, 2.34 mmol) at 0 °C, and the mixture was refluxed for 4 h. A further amount of sodium hydride (50%, 121 mg, 2.34 mmol) was added, and the mixture was refluxed for an additional 1 h, then poured onto ice and extracted with AcOEt. The organic layer was washed with brine, dried over Na_2SO_4, and concentrated. The residue was purified by silica gel column chromatography (AcOEt/*n*-hexane = 1:7–1:5) to give 183 mg (27%) of the title compound as yellow needles; mp 169.5–170.5 °C (MeOH–AcOEt); ^{1}H NMR (270 MHz, $CDCl_3$) δ (ppm) 2,41 (s, 6H), 2.83 (t, *J* = 5.4 Hz, 2H), 4.15 (t, *J* = 5.4 Hz, 2H), 6.65 (s, 1H), 6.83 (d, *J* = 8.7 Hz, 2H), 6.87 (d, *J* = 8.9 Hz, 2H), 7.83 (d, *J* = 8.7 Hz, 2H), 7.88 (d, *J* = 8.9 Hz, 2H); MS (EI) *m/z* 327 (M^+, 100%); HRMS Calcd for $C_{19}H_{21}NO_4$: 327.1471, Found: 327.1477.

4.1.3. *N*-(3-Bromopropyl)anisidine (15)

A solution of anisidine **12** (1.0 g, 8.1 mmol) and 1,3-dibromopropane (1.25 mL, 12.2 mmol) in 10 mL of acetonitrile was stirred at 85 °C for 5 h. Saturated $NaHCO_3$ aqueous solution was added to it, and the mixture was extracted with AcOEt. The organic layer was washed with brine, dried over Na_2SO_4, and concentrated. The residue was purified by silica gel column chromatography (AcOEt/*n*-hexane = 1:7–1:5) to give 470 mg (24%) of the title compound as a colorless oil; ^{1}H NMR (270 MHz, $CDCl_3$) δ (ppm) 2.10 (quint, *J* = 6.6 Hz, 2H), 3.25 (t, *J* = 6.6 Hz, 2H), 3.48 (t, *J* = 6.4 Hz, 2H), 3.54 (br s, 1H), 3.73 (s, 3H), 6.59 (dd, *J* = 2.3 Hz, 6.6 Hz, 2H), 6.78 (dd, *J* = 2.3 Hz, 6.6 Hz, 2H); MS (EI) *m/z* 243:245 (1:1, M^+), 136 (100%).

4.1.4. *N'*-(4-Methoxyphenyl)-*N*-(4-methoxyphenyl)-*N*-(3-bromopropyl)urea (16)

A solution of **15** (470 mg, 1.93 mmol), 4-methoxyphenyl isocyanate (299 μg, 2.31 mmol), and triethylamine (5 mg) in 10 mL of toluene was refluxed for 3 h at room temperature, and then

concentrated. The residue was purified by silica gel column chromatography with 1:2 AcOEt/*n*-hexane to give 598 mg (79%) of the title compound as a colorless oil; ^{1}H NMR (270 MHz, $CDCl_3$) δ (ppm) 2.16 (quint, J = 6.9 Hz, 2H), 3.45 (t, J = 6.9 Hz, 2H), 3.75 (s, 3H), 3.81 (t, J = 6.9 Hz, 2H), 3.86 (s, 3H), 6.00 (brs, 1H), 6.78 (d, J = 9.1 Hz, 2H), 6.99 (d, J = 8.9 Hz, 2H), 7.17 (d, J = 9.1 Hz, 2H), 7.23 (d, J = 8.9 Hz, 2H); MS (EI) m/z 392:394 (1:1, M^+), 136 (100%).

4.1.5. 1,3-Bis(4-methoxyphenyl)tetrahydro-pyrimidinone (14)

To a solution of **16** (70 mg, 188 μmol) in 10 mL of THF was added sodium hydride (50%, 26 mg, 534 μmol) at 0°C. The mixture was stirred for 1.5 h at room temperature, then poured into water and extracted with AcOEt. The organic layer was washed with brine, dried over Na_2SO_4, and concentrated. The residue was purified by silica gel column chromatography (AcOEt/*n*-hexane = 1:1) to give 51 mg (91%) of the title compound as a colorless solid; ^{1}H NMR (270 MHz, $CDCl_3$) δ (ppm) 2.24 (quint, J = 5.9 Hz, 2H), 3.77 (t, J = 5.8 Hz, 4H), 3.78 (s, 6H), 6.86 (dd, J = 2.3 Hz, 6.8 Hz, 4H), 7.24 (dd, J = 2.1 Hz, 6.6 Hz, 4H); MS (EI) m/z 312 (M^+, 100%).

4.1.6. 1,3-Bis(4-hydroxyphenyl)tetrahydro-pyrimidinone (17)

To a solution of **14** (25 mg, 80 μmol) in 2 mL of CH_2Cl_2 was added 1 M BBr_3 in CH_2Cl_2 (0.18 mL, 180 μmol) at −78 °C. The mixture was stirred for 3 h at room temperature, then poured onto ice and extracted with AcOEt. The organic layer was washed with brine, dried over Na_2SO_4, and concentrated. The residue was purified by silica gel column chromatography (AcOEt) to give 19 mg (83%) of the title compound as a colorless solid; ^{1}H NMR (270 MHz, CD_3OD) δ (ppm) 2.13 (quint, J = 5.9 Hz, 2H), 3.63 (t, J = 5.9 Hz, 4H), 6.66 (dd, J = 8.9 Hz, 4H), 7.00 (d, J = 8.9 Hz, 4H); MS (EI) m/z 284 (M^+, 100%).

4.1.7. 1-[4-(2-Dimethylaminoethoxy)phenyl]-3-(4-hydroxyphenyl)tetrahydropyrimidinone (6)

To a solution of **17** (65 mg, 0.22 mmol) and 2-dimethylaminoethylchloride hydrochloride (42.8 mg, 0.3 mmol) in 1 mL of DMF and 1 mL of acetone was added K_2CO_3 (94.8 mg, 0.69 mmol), and the mixture was heated at 80 °C for 5 h. Saturated $NaHCO_3$ aqueous solution was added, and the mixture was extracted with AcOEt. The organic layer was washed with brine, dried over Na_2SO_4, and concentrated. The residue was purified by silica gel column chromatography ($MeOH/CHCl_3$ = 1:3–1:1) to give 25 mg (31%) of the title compound as colorless needles; mp 198.0–200.0 °C (MeOH); ^{1}H NMR (270 MHz, CD_3OD) δ (ppm) 2.14 (quint, J = 5.9 Hz, 2H), 2.32 (s, 6H), 2.77 (t, J = 5.4 Hz, 2H), 3.65 (q, J = 5.4 Hz, 4H), 4.02 (t, J = 5.4 Hz, 2H), 6.66 (d, J = 8.9 Hz, 2H), 6.84 (d, J = 8.9 Hz, 2H), 7.00 (d, J = 8.9 Hz, 2H), 7.12 (d, J = 8.9 Hz, 2H); MS (EI) m/z 355 (M^+, 100%); HRMS Calcd for $C_{20}H_{25}N_3O_3$: 355.1896, Found: 355.1904.

4.1.8. 1,3-Bis(4-methoxyphenyl)benzene (19)

A solution of 1,3-dibromobenzene **18** (110 mg, 0.47 mmol), 4-methoxyphenylboronic acid (156 mg, 1.03 mmol) and $Pd(PPh_3)_4$ (54 mg, 47 μmol) in 5 mL of toluene and 3 mL of saturated Na_2CO_3 aqueous solution was refluxed for 30 h. The mixture was extracted with AcOEt, washed with brine, dried over Na_2SO_4, and then concentrated. The residue was purified by silica gel column chromatography (AcOEt/*n*-hexane = 1:30–1:20) to give 22 mg (16%) of the title compound as a colorless solid; ^{1}H NMR (270 MHz, $CDCl_3$) δ (ppm) 3.86 (s, 6H), 7.00 (dd, J = 2.0 Hz, 6.6 Hz, 4H), 7.45–7.51 (m, 3H), 7.58 (dd, J = 2.0 Hz, 6.6 Hz, 4H), 7.71–7.74 (m, 1H).

4.1.9. 1,3-Bis(4-hydroxyphenyl)benzene (20)

To a solution of **19** (22 mg, 76 μmol) in 2 mL of CH_2Cl_2 was added 1 M BBr_3 in CH_2Cl_2 (0.17 mL, 170 μmol) at −78 °C. The mixture was stirred for 3 h at room temperature, then poured onto ice and extracted with AcOEt. The organic layer was washed with brine, dried over Na_2SO_4, and concentrated. The residue was purified by silica gel column chromatography (AcOEt/*n*-hexane = 1:2) to give 19 mg (95%) of the title compound as a colorless solid; ^{1}H NMR (270 MHz, CD_3OD) δ (ppm) 4.85 (br s, 2H), 6.92 (dd, J = 2.1 Hz, 6.6 Hz, 4H), 7.45–7.50 (m, 3H), 7.53 (dd, J = 2.1 Hz, 6.6 Hz, 4H), 7.68–7.72 (m, 1H); MS (EI) m/z 284 (M^+, 100%).

4.1.10. 1-[4-(2-Dimethylaminoethoxy)phenyl]-3-(4-hydroxyphenyl)benzene (7)

To a solution of **20** (19 mg, 72 μmol) and 2-dimethylaminoethylchloride hydrochloride (14 mg, 94.2 μmol) in 1 mL of DMF and 1 mL of acetone was added K_2CO_3 (30 mg, 0.22 mmol), and the mixture was heated at 80 °C for 8 h. Saturated $NaHCO_3$ aqueous solution was added, and the mixture was extracted with Et_2O. The organic layer was washed with brine, dried over Na_2SO_4, and concentrated. The residue was purified by silica gel column chromatography ($MeOH/CHCl_3$ = 1:15) to give 8 mg (35%) of the title compound as a colorless powder; mp 154.0–155.0 °C (AcOEt–*n*-hexane); ^{1}H NMR (270 MHz, $CDCl_3$) δ (ppm) 2.46 (s, 6H), 2.90 (t, J = 5.4 Hz, 2H), 4.16 (t, J = 5.5 Hz, 2H), 5.53 (br s, 1H), 6.90 (d, J = 8.2 Hz, 2H), 6.92 (d, J = 8.7 Hz, 2H), 7.40–7.55 (m, 7H), 7.65–7.68 (m, 1H); MS (EI) m/z 333 (M^+, 100%); HRMS Calcd for $C_{22}H_{23}NO_2$: 333.1729, Found: 333.1729.

4.1.11. 1-[4-(2-Dimethylaminoethoxy)phenyl]-3-(4-hydroxyphenyl)-1,3-adamantane (8)

To a solution of 1,3-bis(4-hydroxyphenyl)-1,3-adamantane **21** (200 mg, 0.64 mmol) and 2-dimethylaminoethylchloride hydrochloride (117 mg, 0.81 mmol) in 2 mL of DMF was added K_2CO_3 (259 mg, 1.87 mmol), and the mixture was heated at 80 °C for 15 h. Saturated $NaHCO_3$ aqueous solution was added, and the mixture was extracted with Et_2O. The organic layer was washed with brine, dried over Na_2SO_4, and concentrated. The residue was purified by silica gel column chromatography ($MeOH/CHCl_3$ = 1:15–1:10) to give 58 mg (24%) of the title compound as colorless cubes; mp 172.0–173.0 °C (THF–*n*-hexane); ^{1}H NMR (400 MHz, CD_3OD) δ (ppm) 1.80 (br s, 2H), 1.91–1.93 (m, 10H), 2.26 (br s, 2H), 2.35 (s, 6H), 2.78 (t, J = 5.6 Hz, 2H), 4.08 (t, J = 5.6 Hz, 2H), 6.72 (t, J = 8.8 Hz, 1H), 6.88 (d, J = 8.8 Hz, 2H), 7.20 (d, J = 8.8 Hz, 2H), 7.31 (d, J = 9.0 Hz, 2H); MS (EI) m/z 391 (M^+, 100%); HRMS Calcd for $C_{26}H_{33}NO_2$: 391.2511, Found: 391.2504.

4.1.12. 9,10-Diiodo-m-carborane (23)

To a solution of 1,7-dicarba-*closo*-dodecaborane 22 (3.0 g, 20.8 mmol) in 50 mL of CH_2Cl_2 was added iodine (2.64 g, 20.8 mmol) and aluminum trichloride (277 mg, 2.1 mmol) and the mixture was refluxed under an Ar atmosphere. After 1 h, a second portion of iodine (2.64 g, 20.8 mmol) was added and refluxing was continued for 27 h. After cooling, the resultant mixture was poured into water with ice. The organic phase was separated and the aqueous phase was extracted with AcOEt. The combined organic phase was washed with brine, dried over anhydrous sodium sulfate and concentrated. The residue was recrystallized from CH_2Cl_2 to afford 3.89 g (47%) of the title compound as a colorless solid; ^{1}H NMR (270 MHz, acetone-d_6) δ (ppm) 1.50–3.80 (br m, 8H), 4.08 (br s, 2H), MS (EI) m/z 396 (M^+, 100%).

4.1.13. 9,10-Dimethyl-m-carborane (24)

A solution of 3 M methyl magnesium bromide in diethyl ether (6.3 mL, 19.0 mmol) was added dropwise to 10 mL of a dry 1,2-dimethoxyethane solution of **23** (1.0 g, 2.53 mmol) cooled with ice under an Ar atmosphere, and the slurry was stirred at room temperature for 30 min. Bis(triphenylphosphine)palladium(II) dichloride (178 mg, 0.25 mmol) and cupper(I) iodide (48 mg, 0.25 mmol) were added, and the mixture was refluxed for 24 h.

After removal of the solvent, diethyl ether was added to the residue and the excess Grignard reagent was destroyed by slow addition of 10% HCl. The organic layer was separated from the mixture, and the aqueous layer was extracted with diethyl ether. The combined organic layer was washed with water and brine, dried over Na_2SO_4, and concentrated. The residue was purified by column chromatography on silica gel with *n*-hexane to afford 427 mg (98%) as a white solid; ^{1}H NMR (270 MHz, $CDCl_3$) δ (ppm) 0.29 (s, 6 H), 1.50–3.80 (br m, 8H), 2.79 (br s, 2H); MS (EI) *m/z* 172 (M^+), 157 (100%).

4.1.14. 1,7-Bis(4-methoxyphenyl)-9,10-dimethyl-m-carborane (25)

To a solution of **24** (394 mg, 2.29 mmol) in 3 mL of DME was added dropwise 1.56 M *n*-BuLi in hexane (3.2 mL, 5.0 mmol) under an Ar atmosphere at 0 °C. The reaction mixture was stirred for 30 min at room temperature, then CuCl (498 mg, 5.0 mmol) was added in one portion, and the mixture was stirred at room temperature for 1.5 h. Pyridine (2.8 mL, 34.3 mmol) and *p*-iodoanisole (1.18 g, 5.0 mmol) were added in one portion, and the resulting mixture was heated at 110°C for 34 h. After cooling, the mixture was washed with 10% HCl aqueous solution, 10% $Na_2S_2O_3$ aqueous solution, water, and brine, dried over Na_2SO_4, and concentrated. The residue was purified by silica gel column chromatography (Et_2O/*n*-hexane = 1:15–1:10) to give 42 mg (5%) of the title compound as a colorless solid; ^{1}H NMR (270 MHz, $CDCl_3$) δ (ppm) 0.38 (s, 6H), 1.50–3.80 (br m, 8H), 3.77 (s, 6H), 6.75 (d, J = 9.1 Hz, 4H), 7.36 (d, J = 9.1 Hz, 4H); MS (EI) *m/z* 384 (M^+, 100%).

4.1.15. 1,7-Bis(4-hydroxyphenyl)-9,10-dimethyl-m-carborane (26)

To a solution of **25** (42 mg, 0.11 mmol) in 5 mL of CH_2Cl_2 was added 1 M BBr_3 in CH_2Cl_2 (0.24 mL, 240 μmol) at −78 °C, and the mixture was stirred for 6 h at room temperature. The mixture was poured onto ice and extracted with AcOEt. The organic layer was washed with brine, dried over Na_2SO_4, and concentrated. The residue was purified by silica gel column chromatography (AcOEt/*n*-hexane = 1:2) to give 36 mg (92%) of the title compound as a colorless solid; ^{1}H NMR (270 MHz, $CDCl_3$) δ (ppm) 0.40 (s, 6H), 1.50–3.80 (br m, 8H), 5.15 (br s, 2H), 6.69 (d, J = 8.9 Hz, 4H), 7.31 (d, J = 8.9 Hz, 4H); MS (EI) *m/z* 356 (M^+, 100%).

4.1.16. 1-[4-(2-Dimethylaminoethoxy)phenyl]-7-(4-hydroxyphenyl)-9,10-dimethyl-m-carborane (9)

To a solution of **26** (27 mg, 76 μmol) and 2-dimethylaminoethylchloride hydrochloride (14 mg, 99 μmol) in 0.5 mL of DMF and 0.5 mL of acetone was added K_2CO_3 (31 mg, 0.23 mmol), and the mixture was heated at 60 °C for 5 h. Saturated $NaHCO_3$ aqueous solution was added, and the mixture was extracted with Et_2O. The organic layer was washed with brine, dried over Na_2SO_4, and concentrated. The residue was purified by silica gel column chromatography (MeOH/$CHCl_3$ = 1:20–1:10) to give 4 mg (13%) of the title compound as a colorless needles; mp 155.0–156.0 °C (ether); ^{1}H NMR (270 MHz, $CDCl_3$) δ (ppm) 0.37 (s, 6H), 1.40–3.80 (br m, 8H), 2.39 (s, 6H), 2.80 (t, J = 5.4 Hz, 2H), 4.03 (t, J = 5.4 Hz, 2H), 6.56 (d, J = 8.9 Hz, 2H), 6.61 (d, J = 8.7 Hz, 2H), 7.22 (d, J = 8.9 Hz, 2H), 7.30 (d, J = 8.9 Hz, 2H); MS (EI) *m/z* 427 (M^+), 59 (100%); HRMS Calcd for $C_{20}H_{33}B_{10}NO_2$: 427.3514, Found: 427.3507.

4.2. Biological evaluations

4.2.1. ERα-binding assay

Ligand-binding activity to estrogen receptor α (ERα) was determined by means of the nitrocellulose filter binding assay method. ERα (0.5 μg/tube, Invitrogen) was diluted with binding assay buffer (20 mM Tris–HCl pH 8.0, 0.3 M NaCl, 1 mM EDTA pH 8.0, 10 mM 2-mercaptoethanol, 0.2 mM phenylmethylsulfonyl fluoride) and incubated with 4 nM [6,7-^{3}H]17β-estradiol in the presence or absence of an unlabeled competitor at 4 °C for 18 h. The incubation mixture was absorbed by suction onto a nitrocellulose membrane that had been soaked in binding assay buffer. The membrane was washed twice with buffer (20 mM Tris–HCl pH 8.0, 0.15 M NaCl) and then with 25% ethanol in distilled water. Radioactivity that remained on the membrane was measured in Atomlight (Perkin Elmer) by using a liquid scintillation counter.

4.2.2. MCF-7. cell proliferation assay

Human breast adenocarcinoma cell line MCF-7 was routinely cultivated in DMEM supplemented with 10% FBS and 100 IU/mL penicillin and 100 μg/mL streptomycin at 37 °C in a 5% CO_2 humidified incubator. On the day before an assay, MCF-7 cells were switched to DMEM (low glucose, phenol red-free) supplemented with 5% dextran-coated charcoal-stripped FBS (sFBS), 100 IU/mL penicillin, and 100 μg/mL streptomycin. Cells were trypsinized from the maintenance dish with phenol red-free 0.25% trypsin-EDTA and seeded in a 96-well plate at a density of 2000 cells per final volume of 100 μL DMEM (low glucose, phenol red-free) supplemented with 5% sFBS, 100 IU/mL penicillin, and 100 μg/mL streptomycin. After 24 h, the medium was replaced with 90 μL of fresh DMEM (Low glucose, phenol red free) supplemented with 5% sFBS, 100 IU/mL penicillin, and 100 μg/mL streptomycin, and 10 μL aliquots of serial dilutions of test compounds or DMSO (dilution control), were added to triplicate microcultures in the presence or absence of 1×10^{-10} M estradiol. The cells were incubated for 5 days, with one change of the medium after 3 days. Finally, the number of cells was counted by adding WST-8 (10 μL) to the microcultures followed by incubation for 2 h. The absorbance at 450 nm of each well was then determined as a measure of the number of living cells in the culture. EC_{50} and IC_{50} values were estimated with GraphPad Prism 4.

Acknowledgments

This research was supported by a Grant-in-Aid for High Technology Research Program, a Grant-in-Aid for Scientific Research (B) (No. 20390035), and a Grant-in-Aid for Young Scientists (B) (No. 21790116) from the Ministry of Education, Culture, Sports, Science and Technology, Japan.

References and notes

1. Iijima, T.; Endo, Y.; Tsuji, M.; Kawachi, E.; Kagechika, H.; Shudo, K. *Chem. Pharm. Bull.* **1999**, *47*, 398.
2. (a) Ban, H. S.; Minegishi, H.; Shimizu, K.; Maruyama, M.; Yasui, Y.; Nakamura, H. *ChemMedChem* **2010**, *5*, 1236; (b) Michael, F. Z.; Jalisatgi, S. S.; Maderna, A.; Hawthorne, M. F. *Synthesis* **2008**, 555.
3. Soloway, A. H.; Tjarks, W.; Barnum, B. A.; Rong, F.-G.; Barth, R. F.; Codogni, I. M.; Wilson, J. G. *Chem. Rev.* **1998**, *98*, 1515.
4. (a) Goto, T.; Ohta, K.; Fujii, S.; Ohta, S.; Endo, Y. *J. Med. Chem.* **2010**, *53*, 4917; (b) Fujii, S.; Goto, T.; Ohta, K.; Hashimoto, Y.; Suzuki, T.; Ohta, S.; Endo, Y. *J. Med. Chem.* **2005**, *48*, 4654; (c) Endo, Y.; Iijima, T.; Kagechika, H.; Ohta, K.; Kawachi, E.; Shudo, K. *Chem. Pharm. Bull.* **1999**, *47*, 585; (d) Endo, Y.; Yoshimi, T.; Kimura, K.; Itai, A. *Bioorg. Med. Chem. Lett.* **1999**, *9*, 2561.
5. (a) Endo, Y.; Iijima, T.; Yamakoshi, Y.; Yamaguchi, M.; Fukasawa, H.; Shudo, K. *J. Med. Chem.* **1999**, *42*, 1501; (b) Endo, Y.; Iijima, T.; Yamakoshi, Y.; Fukasawa, H.; Miyaura, C.; Inada, M.; Kubo, A.; Itai, A. *Chem. Biol.* **2001**, *8*, 341.
6. (a) Endo, Y.; Iijima, T.; Ogawa, T.; Yamakoshi, Y.; Kubo, A.; Itai, A. *Bioorg. Med. Chem. Lett.* **1999**, *9*, 3313; (b) Endo, Y.; Yoshimi, T.; Iijima, T.; Yamakoshi, Y. *Bioorg. Med. Chem. Lett.* **1999**, *9*, 3387; (c) Endo, Y.; Yoshimi, T.; Yamakoshi, Y. *Chem. Pharm. Bull.* **2000**, *48*, 312; (d) Endo, Y.; Yoshimi, T.; Miyaura, C. *Pure Appl. Chem.* **2003**, *75*, 1197; (e) Endo, Y.; Yoshimi, T.; Ohta, K.; Suzuki, T.; Ohta, S. *J. Med. Chem.* **2005**, *48*, 3941; (f) Ogawa, T.; Ohta, K.; Iijima, T.; Suzuki, T.; Ohta, S.; Endo, Y. *Bioorg. Med. Chem.* **2009**, *17*, 1109; (g) Ohta, K.; Ogawa, T.; Suzuki, T.; Ohta, S.; Endo, Y. *Bioorg. Med. Chem.* **2009**, *17*, 7958; (h) Ohta, K.; Ogawa, T.; Endo, Y. *Bioorg. Med. Chem. Lett.* **2012**, *22*, 4728.
7. (a) Green, S.; Walter, P.; Kumar, V.; Krust, A.; Bornert, J. M.; Argos, P.; Chambon, P. *Nature* **1986**, *320*, 134; (b) Kuiper, G. G. M. J.; Enmark, E.; Pelto-Huikko, M.; Nilsson, S.; Gustafsson, J. A. *Proc. Natl. Acad. Sci. U.S.A.* **1996**, *93*, 5925.

8. Labrie, F.; Labrie, C.; Belanger, A.; Simard, J. In *Selective Estrogen Receptor Modulators*; Manni, A., Verderame, M., Eds.; Humana Press: Totowa, NJ, 2002.
9. Brzozowski, A. M.; Pike, A. C.; Dauter, Z.; Hubbard, R. E.; Bonn, T.; Engstrom, O.; Ohman, L.; Greene, G. L.; Gustafsson, J. A.; Carlquist, M. *Nature* **1997**, *389*, 753.
10. Ogawa, T.; Ohta, K.; Yoshimi, T.; Yamazaki, H.; Suzuki, T.; Ohta, S.; Endo, Y. *Bioorg. Med. Chem. Lett.* **2006**, *16*, 3943.
11. Bey, E.; Marchais-Oberwinkler, S.; Werth, R.; Negri, M.; Al-Soud, Y. A.; Kruchten, P.; Oster, A.; Frotscher, M.; Birk, B.; Hartmann, R. W. *J. Med. Chem.* **2008**, *51*, 6725.
12. Kovredov, A. I.; Shaugumbekova, Zh. S.; Petrovskii, P. V.; Zakharkin, L. I. *Zh. Obshch. Khim.* **1989**, *59*, 607.
13. (a) Coult, R.; Fox, M. A.; Gill, W. R.; Herbertson, P. L.; MacBride, J. A. H.; Wade, K. *J. Organomet. Chem.* **1993**, *462*, 19; (b) Ohta, K.; Goto, T.; Endo, Y. *Inorg. Chem.* **2005**, *44*, 8569.
14. Ohta, K.; Chiba, Y.; Ogawa, T.; Endo, Y. *Bioorg. Med. Chem. Lett.* **2008**, *18*, 5050.
15. (a) Yamamoto, K.; Endo, Y. *Bioorg. Med. Chem. Lett.* **2001**, *11*, 2389; (b) Endo, Y.; Yamamoto, K.; Kagechika, H. *Bioorg. Med. Chem. Lett.* **2003**, *13*, 4089.

医療薬学
40(9) 488—499 (2014)

調剤薬局来局者を対象とした健康食品の使用実態調査とその情報に基づいたCYP2D6活性阻害評価

佐々木崇光[1]，熊谷 健[1]，佐々木瞳[1]，稲見敬太[1]，佐藤 裕[1]，高橋昌悟[1]
松永民秀[2]，頭金正博[3]，細川正清[4]，大森 栄[5,6]，永田 清[*1]
東北薬科大学環境衛生学教室[1]，名古屋市立大学大学院薬学研究科臨床薬学[2]
名古屋市立大学大学院薬学研究科医薬品安全性評価学[3]，千葉科学大学薬学部薬物動態学研究室[4]
信州大学医学部附属病院薬剤部[5]，信州大学大学院医学系研究科分子薬理学[6]

A Questionnaire Survey of Health Food Utilization by Patients and Consumers Visiting Pharmacies and Assessment of Whether the Health Foods Noted in This Survey Inhibit CYP2D6

Takamitsu Sasaki[1], Takeshi Kumagai[1], Hitomi Sasaki[1], Keita Inami[1], Yu Sato[1], Shogo Takahashi[1], Tamihide Matsunaga[2], Masahiro Tohkin[3], Masakiyo Hosokawa[4], Shigeru Ohmori[5,6] and Kiyoshi Nagata[*1]
Department of Environmental and Health Science, Tohoku Pharmaceutical University[1],
Department of Clinical Pharmacy, Graduate School of Pharmaceutical Sciences, Nagoya City University[2],
Department of Medicinal Safety Science, Graduate School of Pharmaceutical Sciences, Nagoya City University[3],
Laboratory of Drug Metabolism and Biopharmaceutics, Faculty of Pharmaceutical Sciences, Chiba Institute of Science[4],
Department of Pharmacy, Shinshu University Hospital[5],
Department of Molecular Pharmacology, Shinshu University Graduate School of Medicine[6]

(Received May 6, 2014
Accepted July 27, 2014)

Owing to the popularity of health food consumption for improving health or beauty, the health food market has been steadily growing in Japan in recent years. Accordingly, harmful interactions between health foods and prescription drugs are predicted to increase because patients who are administered prescription drugs are reported to consume more health foods. We aimed to determine the status of health food consumption in patients and consumers visiting pharmacies, and we investigated whether health foods inhibit cytochrome P450 2D6 (CYP2D6) activity *in vitro*. We conducted a questionnaire survey in pharmacies on the current use of health foods. We received 1,041 responses, and of these respondents, 69.3% consumed health foods, over-the-counter drugs, or foods with health claims, and the use of 249 health foods was confirmed. In addition, a CYP2D6-expressing cell model was constructed using the human hepatoma cell line and the CYP2D6-expressing adenovirus; this model was used to assess the *in vitro* inhibitory effects of 172 of the 249 products, which were available at drug stores or on the Internet, on CYP2D6 activity by using high performance liquid chromatography and liquid chromatography/tandem mass spectrometry. CYP2D6 activity was inhibited by 6 products, including turmeric-, a component having diet effect-, garlic-, and collagen-containing health foods. This study revealed the status of health food utilization and identified the health foods that are currently consumed. Furthermore, we found that 6 products found in these health foods have the potential to inhibit CYP2D6 activity. Our results may provide helpful information to avoid health food-drug interactions during medication use.

Key words —— questionnaire, health food, health food utilization, health food-drug interaction, CYP2D6, inhibition

* 〒981-8558 宮城県仙台市青葉区小松島4-4-1

緒　言

健康志向が高い現代において，「いわゆる健康食品」（健康食品）は，自身の健康保持や美容等の目的から積極的に服用する人が急増している（http://research.goo.ne.jp/database/data/000368/，2013年11月11日）．しかしながら，健康食品は，健康の保持増進に役立つ食品として販売・利用される食品全般を示し，健康増進法に定めている保健機能食品を除いて，法律上の明確な定義および規制はない（http://www.mhlw.go.jp/stf/seisakunitsuite/bunya/kenkou_iryou/shokuhin/hokenkinou/index.html，2013年11月11日）．そのため，市場に流通している大部分の健康食品は，安全性や有効性に関する情報が乏しく，健康食品の摂取による健康被害は，近年増加傾向にある．[1] また，健康食品は，過剰な広告などにより特定の疾患や健康状態に対して，あたかも十分な効果が得られるような印象を消費者に与えている．その結果，健康食品は，有効かつ副作用がないとの先入観から，毎日一定量，場合によっては過剰に摂取することがある．また，近年の健康食品は，濃縮された成分を含むものが多く，食事として摂取する食物中の化学物質よりも，常に多量の化学物質が体内に取り込まれていることになり，医薬品と相互作用を起こす可能性が懸念される．[2] しかしながら，健康食品と医薬品との相互作用は，医薬品間の相互作用と比較して，科学的根拠に基づく情報が乏しく，健康食品の安全使用の観点から情報の蓄積は必要不可欠である．

一般に医薬品間の相互作用は，その機序から薬力学的相互作用と薬物動態学的相互作用の2つに大きく分類される．このうち，薬物動態的相互作用は，医薬品の吸収・分布・代謝・排泄の過程において起こる相互作用であり，なかでも薬物の代謝過程における相互作用の発生頻度が最も高い．この代謝には様々な薬物代謝酵素が関与しているが，臨床上問題となる相互作用の約9割以上において，シトクロムP450（CYP）の関与が報告されている．[3] そのため，健康食品と医薬品との相互作用は，その多くの場合，医薬品間の相互作用と同様に，CYPを介した機構が存在していると推測される．実際，医薬品代謝への関与が最も大きいcytochrome P450 3A4（CYP3A4）は，国内外において健康食品との相互作用が数多く報告されている．なかでも，CYP3A4の代表的な基質薬物である免疫抑制剤シクロスポリンとセントジョーンズワート含有健康食品の相互作用は，シクロスポリンの血中濃度を減弱させる結果，治療効果に大きな影響を及ぼすことは特に重要な事例の1つである．[4] また，グレープフルーツジュースや健康食品の主要成分として汎用されているイチョウ葉エキスは，カルシウム拮抗薬や催眠鎮静剤ミダゾラムのCYP3A4による代謝阻害を介して，その血中濃度を著しく上昇させることが報告されている．さらにCYP3A4に次いで，医薬品代謝への寄与が大きいCYP2C9においても，イチョウ葉エキス含有健康食品がCYP2C9による抗血液凝固薬ワルファリンや抗糖尿病薬トルブタミドの代謝に影響を及ぼすことが報告されており，CYP3A4と同様に健康食品との相互作用情報は蓄積されつつある．[5] しかしながら，抗うつ薬パロキセチン，乳がん治療薬タモキシフェン，そして鎮咳薬デキストロメトルファン等，臨床上，主要な医薬品の代謝に関与しているCYP2D6については，CYP3A4やCYP2C9と比較して，その医薬品代謝における健康食品の影響に関する科学的根拠の伴った情報は十分とは言えない状況にある．[6-8]

そこで，本研究においては，CYP2D6の酵素活性に及ぼす健康食品の影響を明らかにすることを目的に，CYP2D6活性阻害評価系の構築およびその評価を行った．また，健康食品は，多種多様な製品が流通していることから，より正確且つ利用価値の高い評価を行うためには，現在市場に流通し，実際に服用されている健康食品を対象に検討する必要があると考え，アンケート調査による健康食品の使用状況調査も併せて行った．

方　法

1．アンケート調査

アンケート調査は，日本薬剤師会の会員薬剤師に協力を依頼後，調査に対して承諾が得られた全国83店舗の調剤薬局へアンケート用紙を郵送し，

2010年11月～2011年3月にかけて来局した患者および一般消費者を対象とした自記式アンケート調査を行った．また，(株)アイセイ薬局205店舗および日本調剤薬局(株)東北支店35店舗においても，それぞれ2011年10月～2011年11月および2011年11月～2012年2月にかけて同様のアンケート調査を依頼した．アンケート調査は，東北薬科大学薬学部・大学院薬学研究科倫理委員会において承認された同意書に基づき，本研究の趣旨やアンケートに協力しない場合においても最善の医療を提供する旨を薬剤師が説明後，アンケート用紙を配布し本人の自由意志の下に回答を依頼した．この調査依頼に際し，健康食品に関しては，医療用医薬品を除き，自身の健康管理や治療中の疾患の改善のために服用しているものとして説明を行った．なお，アンケート用紙は，調査実施薬局で回収後，各薬局から東北薬科大学に郵送された．調査項目は，年齢，性別，服用中の医薬品の有無とその医薬品名，疾患あるいは医薬品の服用意図，健康食品に関しては，服用経験（現在服用している健康食品）の有無とその製品名およびメーカー名，形状，使用期間，服用頻度，自覚症状による効果および健康被害の有無，そして購入先とした（表1）．複数の健康食品を服用している場合は，製品毎に回答を依頼した．

表1　アンケート調査項目一覧

調査項目
A）一般情報
1. 年齢
2. 性別
3. 服用中の医薬品の有無とその医薬品名
4. 疾患あるいは医薬品の服用意図
B）健康食品に関する情報
1. 服用経験の有無とその製品名およびメーカー名
2. 形状
3. 使用期間
4. 服用頻度
5. 自覚症状による効果および健康被害の有無
6. 購入先

2. 試薬

Dextromethorphan および dextrorphan は，Sigma-Aldrich（St Louis, MO）から購入した．Quinidine は，東京化成工業(株)(東京）を使用した．その他のすべての試薬および溶媒は和光純薬工業(株)(大阪）の特級以上のものを使用した．

3. CYP2D6発現アデノウイルスの作製

cDNA は，ヒト凍結肝細胞（lot HEP187170, 26歳白人女性，Biopredic International, Rennes, France）からTRI Reagent®（Molecular Research Center Inc, Cincinnati, OH）を使用して抽出した total RNA を Moloney murine virus reverse transcriptase（プロメガ(株)，東京）を用いて逆転写反応を行い合成した．これを鋳型として，CYP2D6特異的なプライマー（フォワード：5'-CACCATGGGGCTAGAAGCACTGGTGCCCCTGGCCG-3'，リバース：5'-CTAGCGGGGCACAGCACAAAGCTCA-3'）および KOD-plus-neo（東洋紡，大阪）を用いて増幅後，pENTR™/SD/D-TOPO®（ライフテクノロジー・ジャパン(株)，東京）にクローニングを行った．次に，得られたクローンは，Virapower adenoviral expression system（ライフテクノロジー・ジャパン(株)）を用いて pAd/CMV/V5-DEST Gateway® Vector に載せ替えた後，ヒト胎児腎由来細胞（293細胞，理化学研究所 cell bank，筑波）に導入し，CYP2D6発現アデノウイルス（Ad-CYP2D6）を作製した．この Ad-CYP2D6 は，50% Tissue culture infectious dose（$TCID_{50}$）法を用いて力価測定を行い，以後の実験に使用した．

4. CYP2D6発現アデノウイルス感染細胞の作製

細胞は，ヒト肝がん由来細胞（HepG2細胞，理化学研究所 cell bank）を用い，10%ウシ胎児血清（Biowest, Miami, FL），非必須アミノ酸（ライフテクノロジー・ジャパン(株)），抗生物質－抗菌薬（ライフテクノロジー・ジャパン(株)）を含むダルベッコ変法イーグル培地（和光純薬(株)）を使用して培養を行った．HepG2細胞を48-well plate に 1.0×10^5 cells/well で播種し，24時間後に Ad-CYP2D6 を 1 multiplicity of infection（MOI），3 MOI，10 MOI，あるいは30 MOI で感染させた．その後，24時間培養した細胞を Ad-CYP2D6 感染細胞とした．

5. CYP2D6活性および阻害の評価

CYP2D6活性は，Ad-CYP2D6感染細胞に

dextromethorphan（0.5～80 μM）含有培地を添加し，3時間反応させ，そのO-脱メチル化活性を指標として算出した．CYP2D6活性の阻害評価については，20 μM dextromethorphan含有培地を添加後，直ちにCYP2D6の代表的な阻害剤quinidine（0.005 μM～5.0 μM）含有培地を添加した．これらの培地を回収し，60%過塩素酸を添加後，high performance liquid chromatography（HPLC）分析用試料とした．また，回収した培地に12.5 μM testosterone（内標準物質）を含む酢酸エチルを加え，激しく振とう後，2,500 × g，10分間，遠心分離を行い，その酢酸エチル層を回収した．これを60℃のブロックインキュベーター上で蒸発乾固させ，得られた残渣を0.1%酢酸含有アセトニトリル1.0 mLで溶解し，liquid chromatography/tandem mass spectrometry（LC/MS/MS）分析用試料とした．

HPLCによる分析は，Prominence（島津製作所，京都）を装置として用い，分析用カラムはCAPCELL PAK C18 UG 120（4.6 mm × 250 mm, 5 μm）（資生堂，東京）を使用した．移動相は，5 mMヘキサンスルホン酸ナトリウム含有20 mMリン酸ナトリウム（pH 4.0）：メタノール（58：42，v/v）を用い，流速は1.0 mL/min，カラム温度は40℃，検出波長は励起波長280 nm，蛍光波長310 nmとした．この条件下，dextromethorphanの代謝物であるdextrorphanは，保持時間8 minで検出した．LC/MS/MSによる分析は，Suveyor HPLC systemとFinnigan TSQ Quantum（サーモフィッシャーサンエンティフィック(株)，横浜）を装置として用い，エレクトロンスプレーイオン化法による，selected reaction monitoring（SRM）モードにて行った．分析用カラムはXterra MS C18（2.1 mm × 100 mm, 5 μm）（日本ウォーターズ(株)，東京），移動相は0.1%酢酸含有アセトニトリル：超純水（85：15，v/v），流速は200 μL/min，カラム温度は40℃とした．質量分析計の主な設定は，sheath gas pressure：25 psi，auxiliary gas pressure：15 psi，capillary temperature：350℃，Q1 and Q3 peak widths：0.7 Th，scan time for each analyte：0.2 sとした．dextrorphanおよびtestosteroneのSRMモードで検出した質量電荷比は，それぞれ258.10 > 157.10および289.20 > 109.20とし，そのcllision energyは46 eVおよび32 eVの条件下で分析を行った．

6．試験液の調製

健康食品は，各製品の推奨1日用量に対して，剤形が錠剤，ソフトカプセルまたは散剤の製品では，70%エタノール10 mLを添加し，37℃で2時間加温後，3,500 × gで15分間遠心分離し，その上清を試験液とした．また，液剤に関しては，原液をそのまま使用した．

7．CYP2D6活性に対する各種健康食品の阻害作用評価

CYP2D6活性に対する各種健康食品の阻害作用は，まず，健康食品の試験液のみを0.5%含む培地を前述と同様の条件でHPLC分析を行い，ここで夾雑ピークが認められなかった試験液については，HPLCを用いてCYP2D6活性阻害評価を行った．夾雑ピークが認められた試験液に関しては，その評価をLC/MS/MSを用いて行った．

Ad-CYP2D6感染細胞に20 μM dextromethorphan含有培地添加後，ただちに健康食品の試験液を添加培地量の0.5%となるように加え，前述と同様の条件で反応を行った．ここでCYP2D6活性を阻害する可能性が示唆された試験液に関しては，その試験液を添加培地量の0.5%，0.2%，0.1%となるように加え，添加量依存的な阻害作用を確認し，各試験液の阻害作用の評価を行った．なお，CYP2D6活性に対する各種健康食品の阻害作用は，試験液を添加していないコントロールとの比較により評価を行った．

結　果

1．アンケート調査の総回答者数および調査対象地域

全国83店舗の調剤薬局に送付したアンケートは，28店舗から回答が得られ，その店舗回収率は33.7%であり，アンケート回答者数は350名であった．また，健康食品の利用状況に関する情報をより多く収集するため，(株)アイセイ薬局205店舗および日本調剤薬局(株)東北支店35店舗に

調査を依頼した結果，それぞれ218名および473名の回答が得られ，本アンケート調査の総回答者数は，1,041名となった．回収したアンケートは，すべて解析対象とし，回答が得られなかった項目に関しては，無回答とした．アンケート調査の実施地域は，北海道，東北地区（青森，秋田，山形，岩手，宮城，福島），関東地区（栃木，群馬，埼玉，茨城，千葉，東京，神奈川），中部地区（新潟，石川，長野，岐阜，静岡，愛知），近畿地区（滋賀，京都，大阪，奈良，三重，兵庫），中国地区（島根，山口），四国地区（高知），九州地区（福岡，佐賀）であった．

2. 健康食品等の使用実態調査のためのアンケート調査

アンケート調査の結果を図1に示した．本アンケート調査に回答した来局者は，男性38.2%，女性61.4%であり，年齢は，20歳代9.3%，30歳代19.6%，40歳代12.6%，50歳代15.8%，60歳代15.6%，70歳代17.9%，80歳代8.0%と各世代が均等に分布した集団であった（図1A）．アンケートを解析した結果，健康食品を服用していると回答した回答者は69.3%（721名）おり，このうち20.7%（149名）が保健機能食品，あるいは第1～3類医薬品等のover-the-counter（OTC）医薬品を使用していた．その健康食品等の製品剤形は，錠剤が半数以上を占め，次いでカプセル剤（18.8%），粉剤（11.1%），ドリンク剤（9.7%）の順であった（図1B）．また，服用頻度は，毎日服用が65.9%と最も多く，次いで週に3～4回服用が19.0%であり，その使用期間については，健康食品等服用回答者の約半数が1年以上であった．購入先に関しては，薬局・薬店が36.7%，ドラッグストアが28.7%，雑誌，テレビの通販が13.8%，インターネットが9.0%という結果になった．さらに，健康食品等の服用による効果は，一定の効果を自覚している回答者が58.3%であるのに対し，効果不明あるいは効果なしと感じている

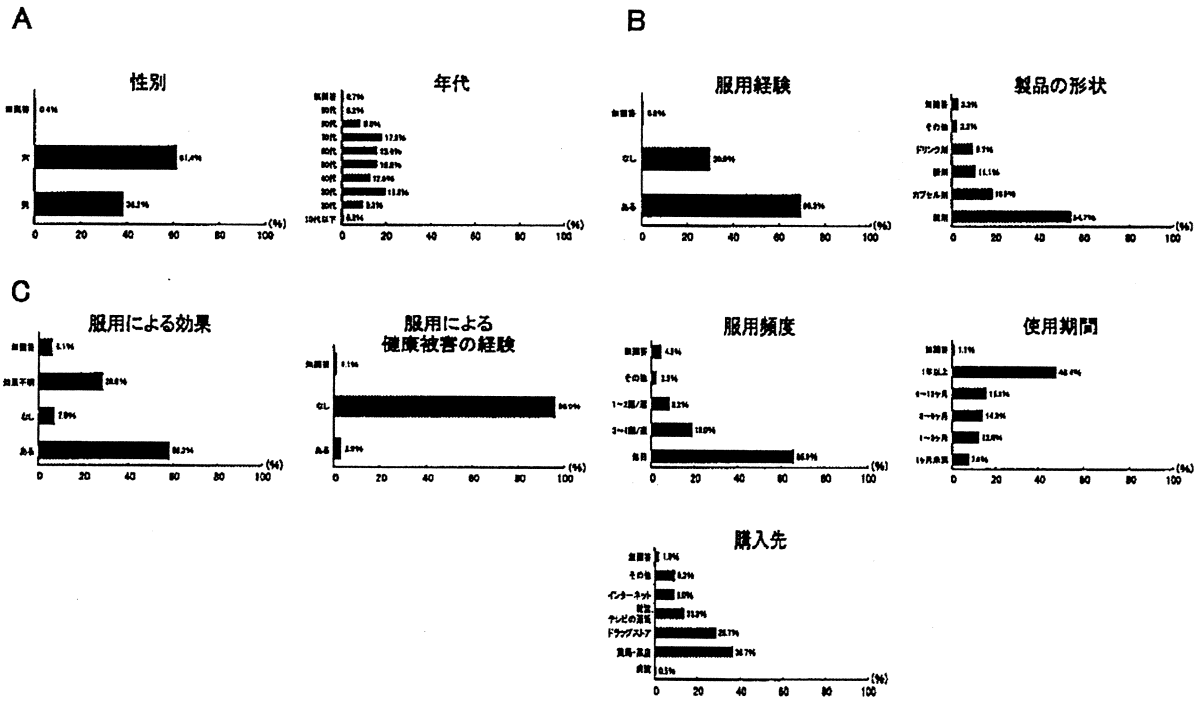


図1　健康食品等の使用実態調査のためのアンケート調査

A：回答者の背景（性別，年齢），B：摂取状況（服用経験，製品の形状，服用頻度，使用期間，購入先），C：自覚症状（服用による効果，服用による健康被害の経験）．本調査は，調剤薬局に来局した患者および一般消費者1,041名を対象とした自記式アンケート調査として行った．年齢（n＝1,041），性別（n＝1,041），健康食品等の服用経験の有無（n＝1,041），製品の形状（n＝908），服用頻度（n＝895），使用期間（n＝892），購入先（n＝825），自覚症状による効果の有無（n＝900）および健康被害の経験（n＝896）の結果についてここに示す．年齢，性別，健康食品等の服用経験の有無の項目以外は，複数回答とした．なお，本調査は，健康食品に加え，保健機能食品，OTCを含む結果となっている．

回答者がそれぞれ28.6%および7.0%であった(図1C)．また，健康食品等の服用に起因した回答者本人による自覚症状として健康被害を経験した方は，2.9%（26名）であった．この26名中，21名は，健康食品を服用しており，さらに19名については，医療用医薬品も服用していた．残りの5名については，第2類医薬品の服用もしくは無回答であった．

3．健康食品の使用状況

本アンケート調査において，保健機能食品やOTC医薬品等を除く健康食品の服用者は572名おり，このうち製品名あるいはメーカー名が不明であった回答者は，健康食品服用者の33.7%（193名)であった．実際に健康食品の製品名およびメーカー名がアンケート調査によって同定された回答者は66.3%（379名）おり，その製品総数（重複製品は除く）は249製品に及んだ．各製品は，その主たる成分あるいは期待される効果に基づき分類し，その製品数について表2に示した．ビタミン系健康食品は，26製品と最も多くの製品の使用が確認され，グルコサミン系，コラーゲン系，ミネラル系についても，それぞれ20製品以上の使用が認められた．次に，植物系，イソフラボン系，ダイエット系，ニンニク系，ルテイン・ベリー系，青汁系は，いずれも10種類以上の製品が服用されていた．

表2　健康食品の製品分類

製品分類	製品数
ビタミン系	26
グルコサミン系（コラーゲン含有も含む）	23
コラーゲン系（サメ軟骨も含む）	23
ミネラル系	20
植物系	18
イソフラボン系	11
ダイエット系	11
ニンニク系（セサミン含有も含む）	11
ルテイン・ベリー系	11
青汁系	10
アミノ酸系	9
クロレラ・スピリルナ系（藻類系も含む）	9
乳酸菌系（微生物系も含む）	7
その他	7
牡蠣系（甲殻類含む）	6
酢系	6
コエンザイムQ10（CoQ10）系	5
ウコン系	5
ドコサヘキサエン酸（DHA）系	4
ビタミン・ミネラル系	4
酵素系	4
セサミン系	3
野菜系	3
ローヤルゼリー系	3
動物系	3
茶系	3
セントジョーンズワート（SJW）系	2
α-リポ酸系	2

4．CYP2D6活性および阻害の評価

CYP2D6活性の評価は，ヒト肝がん由来細胞（HepG2細胞）およびCYP2D6発現アデノウイルス（Ad-CYP2D6）を使用して作製したAd-CYP2D6感染細胞を用いて行った．このAd-CYP2D6感染細胞は，HPLCを用いてCYP2D6活性の測定を行ったところ，Ad-CYP2D6の感染量依存的なCYP2D6活性の上昇が認められた（図2）．次に，十分な酵素活性が認められたAd-CYP2D6を3 MOI感染させたAd-CYP2D6感染細胞を用いて，dextromethorphan代謝の酵素速度論的解析とCYP2D6の代表的な阻害剤であるquinidineによる活性阻害の検討を行った（図3，4）．その結果，CYP2D6によるdextromethorphanの代謝速度は，Michaelis-Mentenの式に従うことが示され，そのKmおよびVmaxは，それぞれ6.23 μM，13.10 pmol//h/wellであった．また，quinidineによるCYP2D6活性の阻害は，quinidine濃度依存的に低

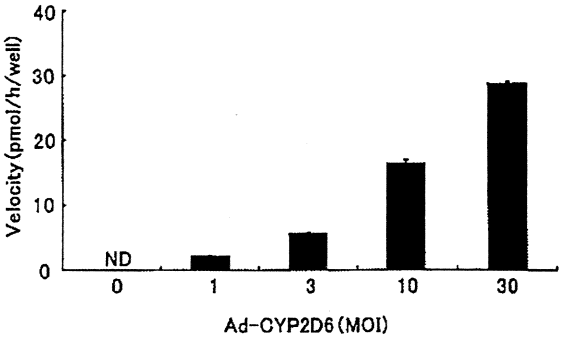


図2　Ad-CYP2D6感染HepG2細胞におけるCYP2D6活性

HepG2細胞を48-well plateに1.0 × 10^5 cells/wellで播種し，24時間後にAd-CYP2D6を1，3，10あるいは30 MOIで感染させた．24時間培養した後，20 μM dextromethorphan含有培地を添加し，3時間反応させた．その後，培地を回収し，HPLCを用いて活性測定を行った．結果は，平均±標準偏差として示した（n = 3）．ND: not detected

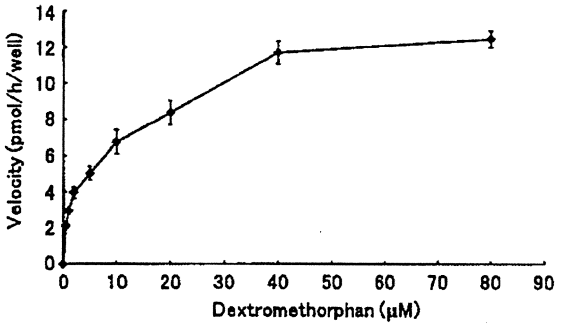


図3　Ad-CYP2D6 感染 HepG2 細胞における dextromethorphan 代謝の Michaelis-Menten プロット

HepG2 細胞を 48-well plate に 1.0 × 10^5 cells/well で播種し，24 時間後に Ad-CYP2D6 を 3 MOI で感染させた．24 時間培養した後，dextromethorphan を 0.5，1.0，2.0，5.0，10，20，40 あるいは 80 μM 含有する培地を添加し，3 時間反応させた．その後，培地を回収し，HPLC を用いて活性測定を行った．結果は，平均 ± 標準偏差として示した（n = 3）．

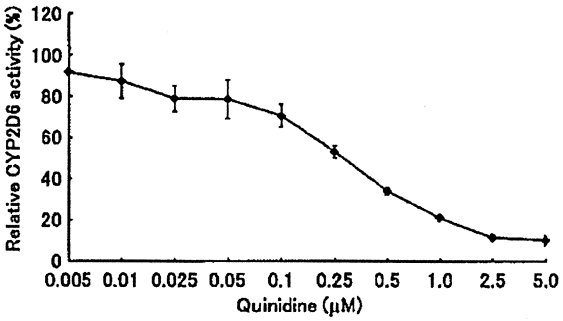


図4　Ad-CYP2D6 感染 HepG2 細胞における CYP2D6 活性に対する quinidine の影響

HepG2 細胞を 48-well plate に 1.0 × 10^5 cells/well で播種し，24 時間後に Ad-CYP2D6 を 3 MOI で感染させた．24 時間培養した後，20 μM dextromethorphan 含有培地を添加した．その後，ただちに quinidine を 0.005，0.01，0.025，0.05，0.1，0.25，0.5，1.0，2.5 あるいは 5.0 μM となるように添加し，3 時間反応させた．この培地を回収し，HPLC を用いて活性測定を行った．結果は，quinidine 未添加時の活性を 100% とし，平均 ± 標準偏差として示した（n = 3）．

下し，その測定値から算出した IC_{50} 値は 0.28 μM とこれまでの報告と同程度の値となった．[9]

5. CYP2D6 活性に対する各種健康食品の阻害作用評価

本評価系を用いて，図5の手順に従い，健康食品による CYP2D6 活性の阻害作用について検討を行った．評価の対象とした健康食品は，調剤薬局の来局者に対して行ったアンケート調査に基づき，実際に使用が確認された 249 製品のうち，今

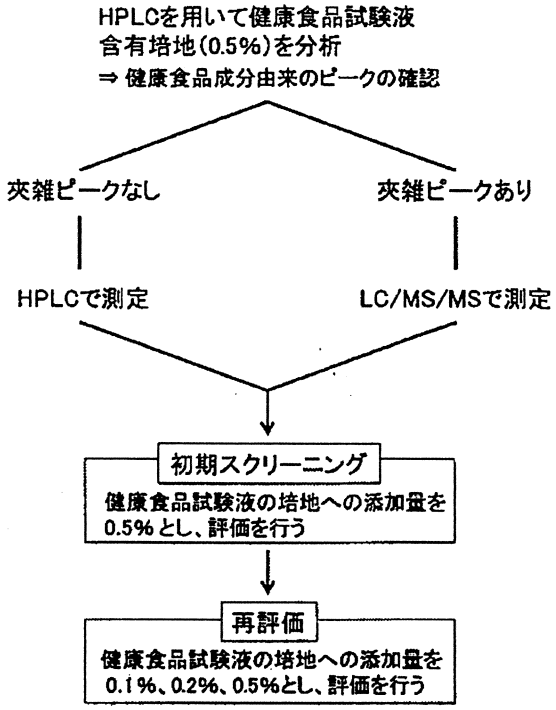


図5　健康食品による CYP2D6 活性阻害評価のストラテジー

回入手できた 172 製品を用いた．本評価を行うにあたり，まず，健康食品 172 製品の試験液を 0.5% 含む培地について，HPLC を用いた CYP2D6 活性測定条件下，夾雑ピークが検出されるかを検証したところ，24 製品の試験液において夾雑ピークが確認された．次に，この 24 製品を除く健康食品 148 製品の試験液を 0.5% 含む培地を Ad-CYP2D6 感染細胞に添加し，独立した実験を 2 回行うことで CYP2D6 活性を阻害する健康食品のスクリーニングを行った（図6）．また，夾雑ピークが認められた 24 製品については，同様の条件下で反応を行い，LC/MS/MS を用いて CYP2D6 活性阻害の評価を実施した（n = 2）（図7）．なお，LC/MS/MS を用いて dextromethorphan 代謝の酵素速度論的解析および quinidine による CYP2D6 活性阻害の検討を行ったところ，Km（4.03 μM）および Vmax（14.45 pmol//h/well），そして IC_{50} 値（0.28 μM）は HPLC で算出した値とほぼ同様であった．これら 2 つ評価系を用いて阻害評価を行った結果，ダイエット系健康食品 2 製品（ダイエット-65，ダイエット-66），ウコン系健康食品 1

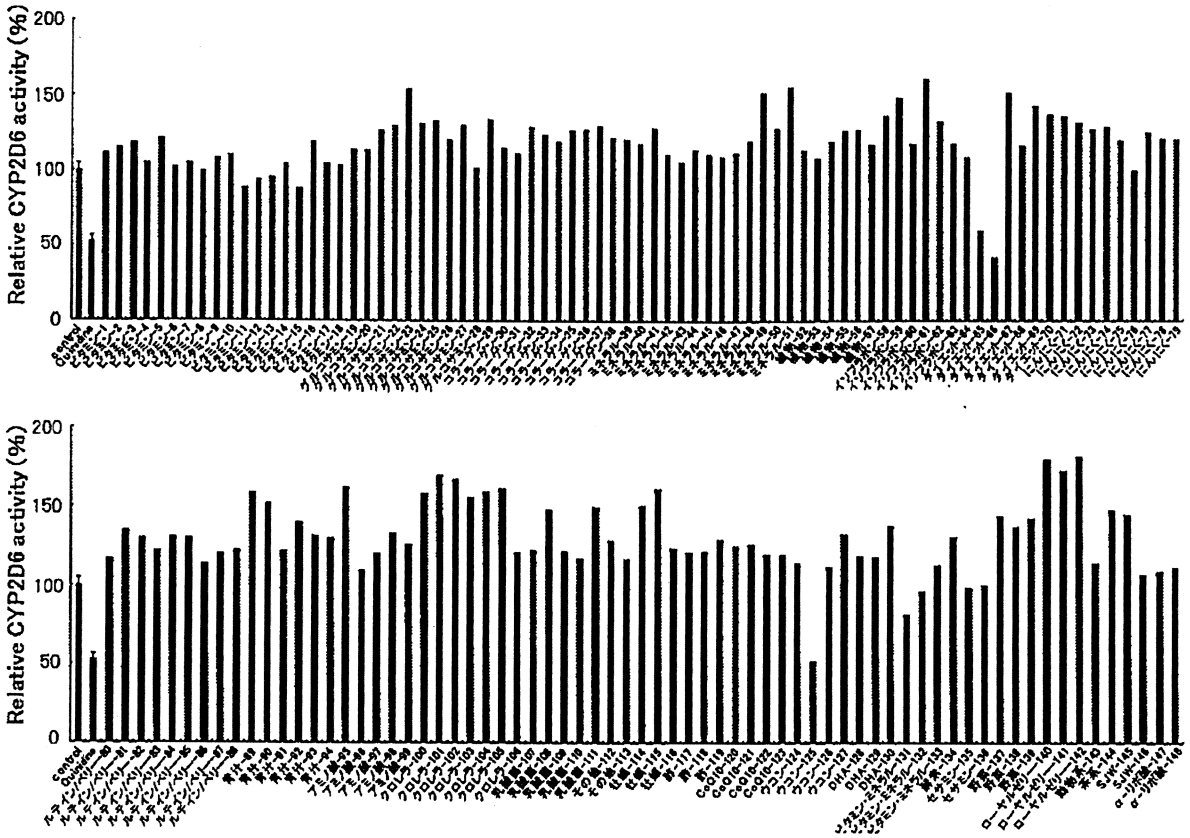


図6　HPLCを用いた健康食品によるCYP2D6活性阻害評価スクリーニング

HepG2細胞を48-well plateに1.0 × 10^5 cells/wellで播種し，24時間後にAd-CYP2D6を3 MOIで感染させた．24時間培養した後，20 μM dextromethorphan含有培地を添加した．その後，ただちに健康食品の試験液（148製品）を添加培地量の0.5%となるように添加し，3時間反応させた．この培地を回収し，HPLCを用いて活性測定を行った．結果は，試験液未添加時の活性を100%とし，平均値を示した（n = 2）．

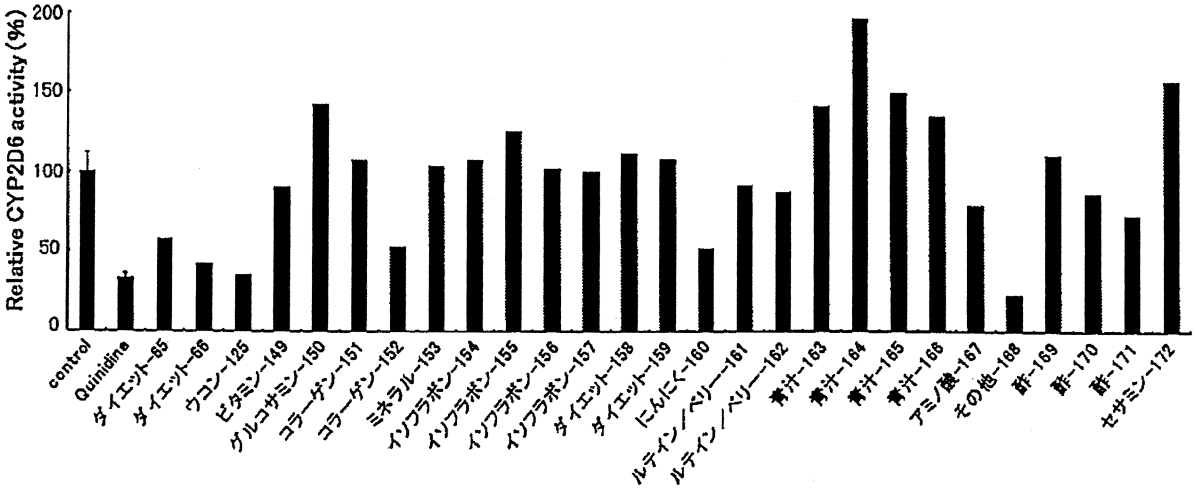


図7　LC/MS/MSを用いた健康食品によるCYP2D6活性阻害評価スクリーニング

HepG2細胞を48-well plateに1.0 × 10^5 cells/wellで播種し，24時間後にAd-CYP2D6を3 MOIで感染させた．24時間培養した後，20 μM dextromethorphan含有培地を添加した．その後，ただちに健康食品の試験液（24製品）を添加培地量の0.5%となるように添加し，3時間反応させた．この培地を回収し，LC/MS/MSを用いて活性測定を行った．結果は，試験液未添加時の活性を100%とし，平均値を示した（n = 2）．

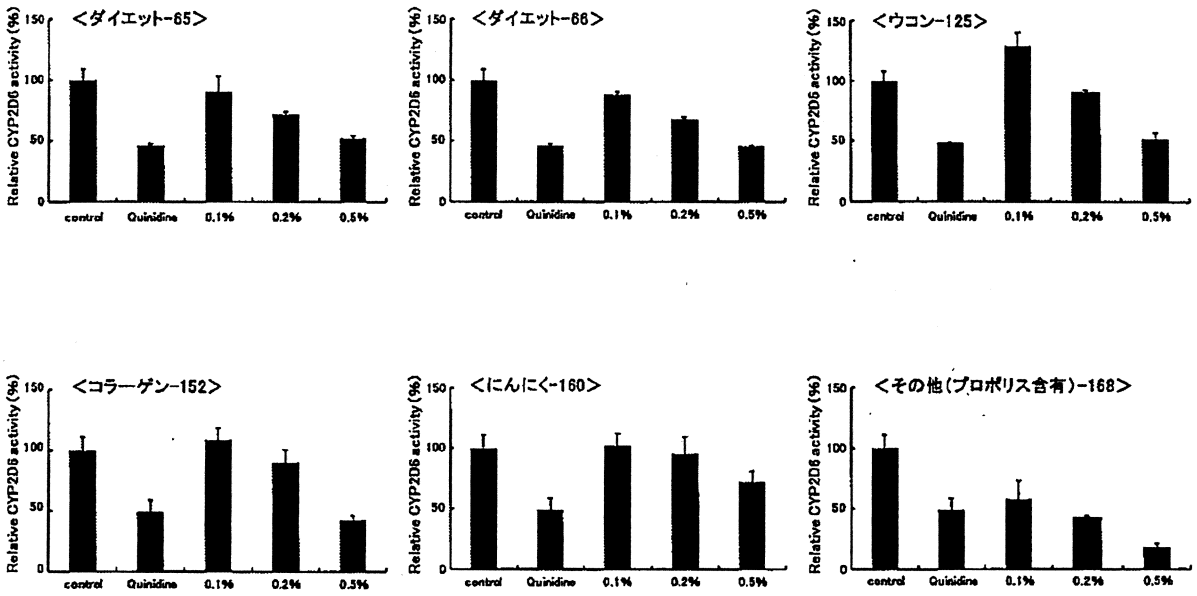


図8　健康食品によるCYP2D6活性阻害作用の再評価

HepG2細胞を48-well plateに1.0 × 10^5 cells/wellで播種し，24時間後にAd-CYP2D6を3 MOIで感染させた．24時間培養した後，20 μM dextromethorphan含有培地を添加した．その後，ただちに健康食品の試験液を添加培地量の0.1%，0.2%，0.5%となるように添加し，3時間反応させた．この培地を回収し，HPLC（ダイエット-65，ダイエット-66，ウコン-125）あるいはLC/MS/MS（コラーゲン-152，にんにく-160，その他（プロポリス含有）-168）を用いて活性測定を行った．結果は，試験液未添加時の活性を100%とし，平均 ± 標準偏差として示した（n = 3）．

製品（ウコン-125），コラーゲン系健康食品1製品（コラーゲン-152），にんにく系健康食品1製品（にんにく-160），その他1製品（その他（プロポリス含有）-168）の6製品において，試験液未添加の細胞と比較して約50%のCYP2D6活性の低下が認められた．なお，HPLCを用いた検討でCYP2D6活性の阻害が確認された健康食品の試験液（ダイエット-65，ダイエット-66，ウコン-125）は，LC/MS/MSを使用した評価系においても同様に阻害が確認された．これらのスクリーニングで同定された製品については，試験液の培地への添加量を0.1%，0.2%あるいは0.5%とし，再評価を行ったところ，添加量依存的な酵素活性の低下が確認された（図8）．

考　察

今回，我々は，CYP2D6を介した健康食品と医薬品における相互作用を解明することを目的に，まず，市場に流通し，且つ服用されている健康食品を明らかにするため，全国の調剤薬局の来局者を対象としたアンケート調査を行った．その結果，保健機能食品やOTC医薬品等を除き，実際に使用されている健康食品を249製品同定した．次に，この健康食品情報に基づき，本研究で確立したCYP2D6活性評価系を用いて172製品の健康食品について評価を行ったところ，6製品がCYP2D6活性を阻害する可能性を見出した．

現在，健康食品は，多種多様な製品が市場に溢れ，その安全使用の観点から様々な調査研究が進められている．[10-12] そのなかでも「健康食品の利用に関する3万人調査」（http://research.goo.ne.jp/database/data/000368/，2013年11月11日）および「消費者の「健康食品」の利用に関する実態調査」（http://www.cao.go.jp/consumer/iinkai/2012/088/doc/088_120518_shiryou1-2.pdf, 2013年11月11日）の両調査は，インターネットを利用した数万人規模の大規模な調査を行っている．これらの調査によると，健康食品の利用者は，前者および後者とも約80%の消費者が健康食品を服用もしくは服用経験があるという結果が得られている．本調査においても約70%の来局者が健康食品等（OTCも含む）を利用していることが明らかになっており，両大規模調査と同程度であった．また本調査

における「健康食品等（OTCも含む）の服用による満足感や効果」や「健康食品等（OTCも含む）の服用に伴う体調不良」に関する質問については「消費者の「健康食品」の利用に関する実態調査」と同様の結果（それぞれ約60%，2%程度）が得られた．一方，「健康食品の利用頻度」に関しては本調査結果（66%）の方が大規模調査（26%）より高い値を示した．これは，本調査が調剤薬局の来局者と限られた集団を対象とした検討であることから，一部バイアスが存在している可能性が考えられた．その理由としては，調剤薬局の来局者は，何らかの疾患を抱えているため，健常人と比較した場合，健康状態あるいは疾患改善に対する意識が高いことが示唆され，これが健康食品等（OTCも含む）を利用する頻度が高い結果に繋がったと推測される．また，回答者が高齢者あるいは服用している医薬品や健康食品が多い場合，調査を依頼した薬剤師がアンケート調査に介入した可能性もあるため，これもバイアスが生じる原因の1つと考えられる．しかしながら，大規模調査と同様の傾向が認められている点も多いため，調査研究としては良好な結果が得られていると考えられる．さらに，本研究においては，上記の大規模調査やその他の調査研究では得られていない，実際に使用されている健康食品の製品情報を収集していることから，この点においても有益な情報が得られたと言える．

次に我々は，健康食品がCYP2D6活性に及ぼす影響を明らかにするため，CYP2D6活性評価系の構築を行った．今回作製したAd-CYP2D6感染細胞は，CYP2D6が代謝に関与する医薬品dextromethorphanを用いた酵素速度論的解析やquinidineよる活性阻害評価を行ったところ，そのKm値やIC_{50}値はこれまでの報告とほぼ同様の値となったことから，CYP2D6活性の評価系として十分使用できると考えられた.[9] 次に，本評価系を使用して健康食品によるCYP2D6活性の阻害効果に対する検討を行った．本研究の計画当初は，Ad-CYP2D6感染細胞の反応後の培地を回収し，その後の処理工程を最小限にして分析を可能としたHPLCのみで評価を行う予定であったが，一部の健康食品において，HPLC分析条件下で夾雑ピークが認められたことから，LC/MS/MSを用いた評価も併せて行うこととした．本検討においては，多検体を正確且つ迅速に評価する必要があることから，まず，独立した実験を2回行うことで，初期スクリーニングを行った．その結果，ダイエット系健康食品2製品（ダイエット-65，ダイエット-66），ウコン系健康食品1製品（ウコン-125），コラーゲン系健康食品1製品（コラーゲン-152），にんにく系健康食品1製品（にんにく-160），その他1製品（その他（プロポリス含有)-168）の6製品において，CYP2D6活性を阻害する可能性を見出した．次に，これらについては，スクリーニング結果の確認を目的に，各試験液の添加量依存的なCYP2D6活性に対する阻害作用について検証を行った．その結果，いずれの製品においても添加量依存的なCYP2D6活性の阻害が認められ，スクリーニングの結果を支持するものであった．これらの製品の主要成分は，ダイエット系健康食品が2製品ともフォルスコリン，ウコン系健康食品がクルクミン，コラーゲン系健康食品はコラーゲン，にんにく系健康食品はアリシンやスコルジニン，そして，その他（プロポリス含有）はプロポリスである．これらの成分のうち，クルクミンは，*in vivo*あるいは*in vitro*試験においてCYP活性を阻害することがすでに報告されており，CYP2D6活性も阻害されることが明らかになっている.[13,14] 本検討においても，阻害が認められたウコン系健康食品は，今回検討を行った5製品のなかでもクルクミン含量が多い秋ウコンの配合量が高いことから，その主たる成分であるクルクミンによってCYP2D6活性が阻害された可能性が高いと考えられた．一方，ダイエット系健康食品に含まれるコレウス・フォルスコリエキス末（10%フォルスコリン含有）は，マウスおよびヒトの*in vitro*試験においてCYP2C活性を阻害することや，マウスを用いた*in vivo*試験においてCYP2C活性を誘導することが報告されているが，CYP2D6活性に関しては明らかとなってない.[15] にんにく系健康食品については，それに含まれるにんにく末が，ヒトを対象とした検討において，CYP2C9活性を阻害することや，CYP3A4およびCYP2D6活性には影響を及ぼさないことが報告さ

れている.[16,17] 本検討では，にんにく系健康食品はCYP2D6活性を阻害していることから，これまでの報告と一部一致しないものとなった．一方，コラーゲン系健康食品やその他(プロポリス含有)については，CYP活性に対する影響を検討した例がほとんどない．しかしながら，コラーゲン系健康食品には，主要成分であるコラーゲン以外にマリアアザミエキスが含まれており，この成分がCYP2D6活性を阻害することが報告されている[8]ことから，本製品については主成分以外の成分による活性阻害の可能性が考えられた．今回の検討において，ウコン系健康食品を除くこれらの健康食品に関してはCYP2D6活性を阻害する可能性を新たに見出したことから，主要成分のみならずその他の含有成分についても今後更なる検討が必要であると考えられる．また，阻害が認められなかった製品のうち，一部において，CYP2D6活性の上昇が認められた．これまでの同様な検討によると，ハーブ類のエタノール抽出液がCYP2D6活性を上昇させることが報告されており，その要因は一部のハーブ含有成分によるアロステリックな効果が示唆されている.[18] しかしながら，その成分や活性上昇機構に関しては，明らかになっていないことから，さらに詳細な検討が必要であると考える．

現在，国内で流通している健康食品の多くは，様々な成分が配合されていることに加え，ハーブ等の植物を抽出あるいは粉末状にした成分も含有している．特に，植物の抽出エキス等が含まれる製品は，産地や収穫時期が異なる場合，含有される成分量が変動するため，同様の植物加工成分を含む製品であっても製品間でCYPに対する影響の程度が異なる可能性がある．また，健康食品には医薬品のような規制がないため，製造業者によって原材料や製品に含まれる添加物の純度などが大きく異なることも推測される．今回の検討においても，CYP2D6活性の阻害効果を有する健康食品が見出されたが，これらの製品と類似した他の製品においては阻害効果が認められていない．従って，現時点では，現在流通している健康食品について，その主成分や添加物等にとらわれず各製品自体がCYP活性に影響を及ぼすか検討する必要があると考えられる．これらの情報を蓄積することで，CYP2D6活性の阻害を介した健康食品と医薬品との相互作用を未然に防ぐことが可能となり，さらには，阻害成分の同定に繋がると考えられる．

謝　辞

本調査研究を行うにあたり，アンケート調査にご協力下さった薬剤師およびアンケートにご回答いただいた皆様に深く感謝申し上げます．また，本調査研究は，厚生労働科学研究費補助金「食品の安全確保推進研究事業」の補助を受けて実施した研究成果の一部であり，ここに謝意を表します．

引用文献

1) 小池麻由, 大津史子, 榊原甚作, 後藤伸之, 健康食品・サプリメントによる健康被害の現状と患者背景の特徴, 医薬品情報学, 2013, **14**, 134-143.
2) 萩本真美, 植松洋子, 樺島順一郎, 鈴木公美, 安野哲子, 鴻丸裕一, 齋藤哲夫, 中村理奈, 伊藤弘一, ミネラル補給用サプリメントのミネラル含有量調査, 東京都健康安全研究センター研究年報, 2006, **57**, 267-271.
3) 千葉　寛, チトクロームP450を介した薬物相互作用, ファルマシア, 1995, **31**, 992-996.
4) Ruschitzka F, Meier PJ, Turina M, Luscher TF, Noll G, Acute heart transplant rejection due to Saint John's wort, *Lancet*, 2000, **355**, 548-549.
5) 内田信也, 山田静雄, 食品・サプリメントと医薬品との相互作用, ぶんせき, 2007, **393**, 454-460.
6) Tanaka E, Hisawa S, Clinically significant pharmacokinetic drug interactions with psychoactive drugs: antidepressants and antipsychotics and the cytochrome P450 system, *J Clin Pharm Ther*, 1999, **24**, 7-16.
7) Desta Z, Ward BA, Soukhova NV, Flockhart DA, Comprehensive evaluation of tamoxifen sequential biotransformation by the human cytochrome P450 system in vitro: prominent roles for CYP3A and CYP2D6, *J Pharmacol Exp Ther*, 2004, **310**, 1062-1075.
8) Choi YH, Chin YW, Kim YG, Herb-drug interactions: focus on metabolic enzymes and transporters,

Arch Pharm Res, 2011, **34**, 1843-1863.

9) Lin T, Pan K, Mordenti J, Pan L, In vitro assessment of cytochrome P450 inhibition: strategies for increasing LC/MS-based assay throughput using a one-point IC_{50} method and multiplexing high-performance liquid chromatography, *J Pharm Sci*, 2007, **96**, 2485-2493.

10) 朝比奈泰子, 本間秀彰, 堀　里子, 大谷壽一, 三木晶子, 後藤輝明, 河野弘之, 澤田康文, 青汁をはじめとする健康食品の使用実態・意識調査, 医療薬学, 2008, **34**, 644-650.

11) 清水るみ子, 藤田圭子, 村井美香, 井口　伸, 山岡由美子, ドラッグストア来局者を対象にしたサプリメントに関する要望の実態調査, 医薬品情報学, 2012, **13**, 173-182.

12) 齋藤百枝美, 加賀睦子, 渡部多真紀, 丸山桂司, 土屋雅勇, 渡邊真知子, 柳川幸重, 井上圭三, 帝京大学病院小児科外来における小児患者のサプリメント・健康食品の使用状況, 医薬品情報学, 2010, **11**, 156-162.

13) Appiah-Opong R, Commandeur JN, van Vugt-Lussenburg B, Vermeulen NP, Inhibition of human recombinant cytochrome P450s by curcumin and curcumin decomposition products, *Toxicology*, 2007, **235**, 83-91.

14) Lee CK, Ki SH, Choi JS, Effects of oral curcumin on the pharmacokinetics of intravenous and oral etoposide in rats: possible role of intestinal CYP3A and P-gp inhibition by curcumin, *Biopharm Drug Dispos*, 2011, **32**, 245-251.

15) Yokotani K, Chiba T, Sato Y, Taki Y, Yamada S, Shinozuka K, Murata M, Umegaki K, Hepatic cytochrome P450 mediates interaction between warfarin and Coleus forskohlii extract in vivo and in vitro, *J Pharm Pharmacol*, 2012, **64**, 1793-1801.

16) Ho BE, Shen DD, McCune JS, Bui T, Risler L, Yang Z, Ho RJ, Effects of Garlic on Cytochromes P450 2C9- and 3A4-Mediated Drug Metabolism in Human Hepatocytes, *Sci Pharm*, 2010, **78**, 473-481.

17) Markowitz JS, Devane CL, Chavin KD, Taylor RM, Ruan Y, Donovan JL, Effects of garlic (Allium sativum L) supplementation on cytochrome P450 2D6 and 3A4 activity in healthy volunteers, *Clin Pharmacol Ther*, 2003, **74**, 170-177.

18) Hellum BH, Hu Z, Nilsen OG, The induction of CYP1A2, CYP2D6 and CYP3A4 by six trade herbal products in cultured primary human hepatocytes, *Basic Clin Pharmacol Toxicol*, 2007, **100**, 23-30.

Drug Metab. Pharmacokinet. 29 (3): 237–243 (2014). Copyright © 2014 by the Japanese Society for the Study of Xenobiotics (JSSX)

Regular Article

An Efficient Method for Differentiation of Human Induced Pluripotent Stem Cells into Hepatocyte-like Cells Retaining Drug Metabolizing Activity

Yuki KONDO[1], Takahiro IWAO[1], Katsunori NAKAMURA[1], Takamitsu SASAKI[2], Shogo TAKAHASHI[2], Noboru KAMADA[3], Tsutomu MATSUBARA[4,5], Frank J. GONZALEZ[4], Hidenori AKUTSU[6], Yoshitaka MIYAGAWA[7], Hajime OKITA[7], Nobutaka KIYOKAWA[7], Masashi TOYODA[6], Akihiro UMEZAWA[6], Kiyoshi NAGATA[2], Tamihide MATSUNAGA[1,*] and Shigeru OHMORI[8]

[1]*Department of Clinical Pharmacy, Graduate School of Pharmaceutical Sciences, Nagoya City University, Nagoya, Japan*
[2]*Department of Environmental Health Science, Tohoku Pharmaceutical University, Sendai, Japan*
[3]*Kissei Pharmaceutical Co. Ltd., Matsumoto, Japan*
[4]*Laboratory of Metabolism, Center for Cancer Research, National Cancer Institute, National Institutes of Health, Bethesda, MD, USA*
[5]*Department of Anatomy and Regenerative Biology, Graduate School of Medicine, Osaka City University, Osaka, Japan*
[6]*Department of Reproductive Biology, National Institute for Child Health and Development, Tokyo, Japan*
[7]*Department of Developmental Biology, National Institute for Child Health and Development, Tokyo, Japan*
[8]*Division of Pharmacy, Shinshu University Hospital, Matsumoto, Japan*

Full text of this paper is available at http://www.jstage.jst.go.jp/browse/dmpk

Summary: The use of human induced pluripotent stem (iPS) cells would be of great value for a variety of applications involving drug development studies. Several reports have been published on the differentiation of human iPS cells into hepatocyte-like cells; however, the cells were insufficient for application in drug metabolism studies. In this study, we aimed to establish effective methods for differentiation of human iPS cells into hepatocytes. Two human iPS cell lines were differentiated by addition of activin A, dimethyl sulfoxide, hepatocyte growth factor, oncostatin M, and dexamethasone. The differentiated cells expressed hepatocyte markers and drug-metabolizing enzymes, revealing that the human iPS cells were differentiated into hepatocyte-like cells. Expression of CYP3A4 and UGT1A1 mRNAs increased with treatment with typical inducers of the enzymes, and the response of the cells against the inducers was similar to that of human hepatocytes. Furthermore, the drug-metabolizing activity of CYP3A4, as monitored by testosterone 6β-hydroxylase activity, was elevated by these inducers. In conclusion, we established methods for differentiation of hepatocyte-like cells expressing drug metabolizing activity from human iPS cells. The hepatocyte-like cells derived from human iPS cells will be useful for drug metabolism studies.

Keywords: iPS; differentiation; hepatocyte; drug-metabolizing enzyme; CYP

Introduction

Induced pluripotent stem (iPS) cells have been generated directly from fibroblast cells by the expression of defined reprogramming factors (OCT3/4, SOX2, KLF4, and c-MYC).[1–4] Recent studies have shown that iPS cells are comparable to embryonic stem (ES) cells including multilineage differentiation potential and intensive proliferation *in vitro*.[5] iPS cell-derived

Received September 26, 2013; Accepted November 25, 2013
J-STAGE Advance Published Date: December 10, 2013, doi:10.2133/dmpk.DMPK-13-RG-104
**To whom correspondence should be addressed:* Tamihide MATSUNAGA, Ph.D., *Department of Clinical Pharmacy, Graduate School of Pharmaceutical Sciences, Nagoya City University, 3-1 Tanabe-dori, Mizuho-ku, Nagoya 467-8603, Japan. Tel. +81-52-836-3791, Fax. +81-52-836-3792, E-mail: tmatsu@phar.nagoya-cu.ac.jp*
This work was supported, in part, by Grants-in-Aid from the Japan Society for the Promotion of Science (23390036), by Research on Publicly Essential Drugs and Medical Devices from Japan Health Sciences Foundation (KHB1011 and KHB1208), and by a National Grant-in-Aid from Japanese Ministry of Health, Labour and Welfare (H22-003).

hepatocytes could provide a valuable model system for novel pharmaceutical drug discovery assays, investigation of drug metabolism, and prediction of liver toxicity.[5,6] However, efficient generation of highly differentiated hepatocytes from iPS cells has not yet been established without transduction of transcription factors in addition to treatment with optimal growth factors.

Cytochrome P450 (CYP) proteins display differential expression levels according to the developmental stages of the liver. CYP3A7 is a major enzyme in the human fetal and newborn liver,[7,8] whereas CYP3A4 is expressed throughout development and finally accounts for about 30% of the amount of total CYP in the human adult liver.[9,10] The human fetal and adult liver expression levels of CYP3A enzymes are increased by exposure to a variety of drugs,[11–13] which in turn leads to accelerated metabolism and concomitant use of the drugs. Several studies have examined the differentiation of ES or iPS cells into hepatocyte-like cells,[14–21] and these cells expressed hepatic markers such as albumin (ALB), α-1 antitrypsin, and hepatocyte nuclear factor (HNF) 4α. However, the activities of drug-metabolizing enzymes have not been detected in the ES or iPS cell-derived hepatocytes using simple methods. Thus, the ES or iPS cell-derived hepatocytes do not entirely recapitulate mature liver function.

We recently established an efficient method to differentiate ES cells into hepatocyte-like cells.[22,23] In the present study, iPS cell-derived hepatocyte-like cells exhibited a sequential pattern of expression of hepatic markers and drug-metabolizing enzymes. Furthermore, drug-metabolizing activity was induced by treatment with drugs, similar to what is observed in human liver and hepatocytes.

Materials and Methods

Materials: Umezawa *et al.* established 2 human iPS cell lines (Fetch, NIHS0604 and Lollipop, JCRB1336), derived from the embryonic human lung fibroblast cell line MCR-5. HepG2 cells were obtained from the RIKEN Cell Bank (Tsukuba, Japan). Mouse embryonic fibroblasts (MEF) were obtained from Oriental Yeast (Tokyo, Japan). BD Matrigel Matrix Growth Factor Reduced (Matrigel) was obtained from BD Biosciences (Bedford, MA). Dulbecco's modified Eagle's medium (DMEM), and DMEM and Ham's nutrient mixture F-12 (DMEM/F12) were obtained from Sigma-Aldrich (St. Louis, MO). KnockOut Serum Replacement (KSR), KnockOut DMEM (KO-DMEM), Roswell Park Memorial Institute (RPMI) + GlutaMax medium, GlutaMax, minimal essential medium nonessential amino acids (MEM NEAA), and SuperScript III were obtained from Invitrogen Life Technologies (Carlsbad, CA). Fetal bovine serum (FBS) was obtained from Hyclone (Waltham, MA). Basic fibroblast growth factor (bFGF) and activin A were obtained from PeproTech (Rocky Hill, NJ). Modified Lanford medium was obtained from Charles River (Tokyo, Japan). Accutase was obtained from MS TechnoSystems (Osaka, Japan). Hepatocyte growth factor (HGF) was obtained from R&D Systems (Minneapolis, MN). RNeasy Mini Kit was obtained from Qiagen (Valencia, CA). Oncostatin M (OSM), dexamethasone (DEX), omeprazole (OME), rifampicin (RIF), dimethyl sulfoxide (DMSO), and human normal adult liver total RNA, derived from a 64-year-old male donor, were obtained from Wako Pure Chemicals (Osaka, Japan). SYBR Green real-time polymerase chain reaction (PCR) Master Mix was obtained from Takara Bio (Otsu, Japan). Collagen Type I (collagen I)-coated microplate was obtained from Asahi Glass (Chiba, Japan). Dissociation solution for human ES/iPS cells was obtained from ReproCELL Incorporated (Tokyo, Japan). All other reagents used were of the highest quality available.

Human iPS cell culture: Undifferentiated human iPS cells were maintained on a feeder layer of mitomycin C-treated MEF on a gelatin-coated dish in a human iPS medium at 37°C in humidified air with 5% CO_2. The human iPS medium consisted of DMEM/F12 supplemented with 20% KSR, 2 mM L-glutamine, 1% MEM NEAA, 0.1 mM 2-mercaptoethanol, and 5 ng/mL bFGF. The medium was changed daily. Human iPS cell colonies composed of closely packed cells were split approximately every 3 to 4 days by incubation in a dissociation solution for 5 min at 37°C and passaged onto new mitomycin C-treated MEF.

Differentiation of human iPS cells into hepatocyte-like cells: Differentiation was initiated when the human iPS cells reached a confluence level of approximately 70%. The human iPS cells were cultured with RPMI + GlutaMax medium containing 0.5% inactivated FBS and 100 ng/mL activin A. Three days later, the culture medium was switched to the RPMI + GlutaMax medium containing 2% KSR and 100 ng/mL activin A for 2 days. After induction of differentiation, the cells were dissociated by the addition of Accutase for 5 min at 37°C and passaged onto 24-well plates coated with collagen I or a thin layer Matrigel (dilute Matrigel 1:30 with cold human iPS medium) and cultured in KO-DMEM containing 20% KSR, 1% GlutaMax, 1% MEM NEAA, 0.1 mM 2-mercaptoethanol, and 1% DMSO for 7 days. The cells were subsequently cultured in modified Lanford medium containing 10 ng/mL HGF, 20 ng/mL OSM, and 100 nM DEX for 9 days. The cells were then cultured in modified Lanford medium for 4 days (**Fig. 1**).

Drug treatments: To clarify the effects of inducers on the expression of CYPs, the cells were treated with 40 μM RIF, 50 μM OME, or 100 μM DEX as described previously[22–25] for the final 72 h of the differentiation protocol. The compounds were dissolved in DMSO, which was added to the culture medium at a final concentration of 0.1%.

RNA extraction and reverse transcription reaction: An RNeasy Mini Kit was used to extract total RNA from the cells according to the manufacturer's instructions. First-strand cDNA was generated from 2–4 μg of total RNA. Reverse transcription (RT) reaction was performed using SuperScript III, according to the manufacturer's instructions.

Real-time RT-PCR analysis: For determination of expression levels, mRNAs were analyzed using SYBR Green real-time quantitative RT-PCR. Relative mRNA expression levels in each sample were normalized to glyceraldehyde-3-phosphate dehydrogenase (GAPDH) expression levels. All PCR procedures were performed using the ABI 7300 Fast System SDS software version 1.3.1 (Applied Biosystems, Foster City, CA), according to each

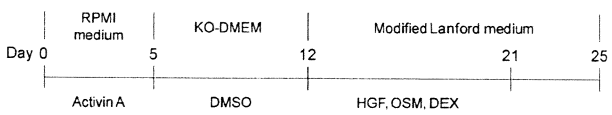


Fig. 1. Differentiation into hepatocytes from 2 human iPS cell lines
Two human iPS cell lines (Fetch and Lollipop) were differentiated into endoderm cells by addition of 100 ng/mL activin A for 5 days, and then into hepatocytes by the addition of 1% DMSO for 7 days. The hepatocytes were then matured by the addition of 10 ng/mL HGF, 20 ng/mL OSM, and 10^{-7} M DEX for 9 days. For the final 4 days, the cells were cultured in modified Lanford medium alone, without HGF, OSM, or DEX.

Copyright © 2014 by the Japanese Society for the Study of Xenobiotics (JSSX)

Table 1. Sequences of primers for real-time RT-PCR analysis

Gene names	Forward primer sequences (5′- -3′)	Reverse primer sequences (5′- -3′)
HNF4α	GAGCTGCAGATCGATGACAA	TACTGGCGGTCGTTGATGTA
ALB	GAGCTTTTTGAGCAGCTTGG	GGTTCAGGACCACGGATAGA
AFP	AGCTTGGTGGTGGATGAAAC	TCTGCAATGACAGCCTCAAG
CYP1A2	CTTTGACAAGAACAGTGTCCG	AGTGTCCAGCTCCTTCTGGAT
CYP1B1	ACCAGGTATCCTGATGTGCAGAC	AGGTGTTGGCAGTGGTGGCATGAG
CYP2C9	GAACACCAAGAATCGATGGACA	TCAGCAGGAGAAGGAGAGCATA
CYP3A4	CTGTGTGTTTCCAAGAGAAGTTAC	TGCATCAATTTCCTCCTGCAG
CYP3A5	CTCTCTGTTTCCAAAAGATACC	TGAAGATTATTGACTGGGCTG
CYP3A7	AGATTTAATCCATTAGATCCATTCG	AGGCGACCTTCTTTTATCTG
UGT1A1	CAGCAGAGGGGACATGAAAT	ACGCTGCAGGAAAGAATCAT
GAPDH	GAGTCAACGGATTTGGTCGT	GACAAGCTTCCCGTTCTCAG

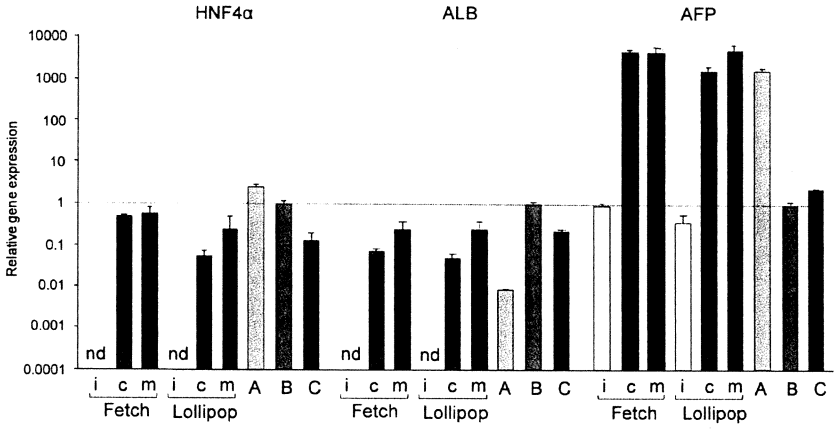


Fig. 2. Expression levels of liver marker protein mRNAs
The expression levels of HNF4α, ALB, and AFP mRNAs in undifferentiated human iPS cells (i) and hepatocyte-like cells differentiated from two human iPS cell lines (Fetch and Lollipop) were analyzed using real-time PCR. Collagen I (c) or Matrigel (m) was used for the differentiation as the extracellular matrix. A, B, and C represent HepG2 cells, human adult liver, and hepatocytes, respectively, as positive controls. Each bar represents the mean ± SD from triplicate experiments. Values were normalized to the level of GAPDH mRNA. The graph represents the relative gene expression level when the level in the liver was taken as 1. nd, not detected.

manufacturer's instructions. PCR was performed using diluted cDNA template in a 25-μL reaction mixture containing 0.3 μM of each primer and 12.5 μL of SYBR Green real-time PCR Master Mix. The primers used are summarized in **Table 1**.

Assay for testosterone 6β-hydroxylase activity: Human iPS cell-derived hepatocyte-like cells were cultured with modified Lanford medium containing 100 μM testosterone for 6 h at 37°C. After incubation, the reaction medium was collected into the tubes with 1.25 mL of ethyl acetate, and 10 μL of 1 μM ethoxyresorufin was added to the medium as an internal standard. The tube was vortexed and centrifuged. Organic phase aliquots (1 mL) were transferred to microcentrifuge tubes. Ethyl acetate was evaporated under nitrogen gas, and the samples were dissolved with 100 μL of a mixture of 10 mM ammonium acetate (98%) and methanol (2%) containing 0.1% formic acid. Metabolites were analyzed using liquid chromatography coupled with tandem mass spectrometry according to the method reported previously.[26]

cDNA microarray analysis: An RNeasy Mini column (Qiagen) was used to extract and purify RNA (10 μg). The RNA was labeled using a SuperScript Indirect cDNA Labeling Kit (Invitrogen) and Cy™3 or Cy™5 Mono-Reactive Dye (GE Healthcare, Little Chalfont, UK). The dye-coupled cDNAs were purified using a MiniElute PCR purification kit (Qiagen) and hybridized to an Agilent 44 K human 60-mer oligo microarray (Agilent Technologies, Santa Clara, CA) according to Agilent instructions. An Agilent microarray scanner (Agilent Technologies) was used to wash, dry, and scan the slides. A Genespring GX software package (Agilent Technologies) was used to process and analyze the data. Ingenuity IPA software (Ingenuity Systems Redwood City, CA) was used to perform pathway analysis.

Results

Expression of hepatic marker gene: In the present study, we succeeded in differentiating human iPS cells into hepatocyte-like cells that exhibited drug metabolizing activity. Activin A was used to differentiate two human iPS cell lines, Fetch and Lollipop, into endoderm cells.[27] The endoderm cells were then induced to hepatocytes by the addition of DMSO.[28] The hepatocytes were subsequently matured by the addition of HGF, OSM, and DEX (**Fig. 1**).[29–31] Collagen I or Matrigel was used as extracellular matrix in the hepatic differentiation of the human iPS cells. The expression of mRNAs encoding typical hepatic marker proteins in the cells differentiated from both human iPS cell lines was compared with those in HepG2 cells, human adult liver, and primary hepatocytes (**Fig. 2**). HNF4α, ALB, and α-fetoprotein (AFP) mRNAs were detected in the cells differentiated from human iPS cells. The expression levels of these mRNAs in the cells differentiated from the two iPS cell lines were similar and the cells cultured on Matrigel were relatively higher than those cultured on collagen I. The expression levels of HNF4α and ALB mRNAs

Copyright © 2014 by the Japanese Society for the Study of Xenobiotics (JSSX)

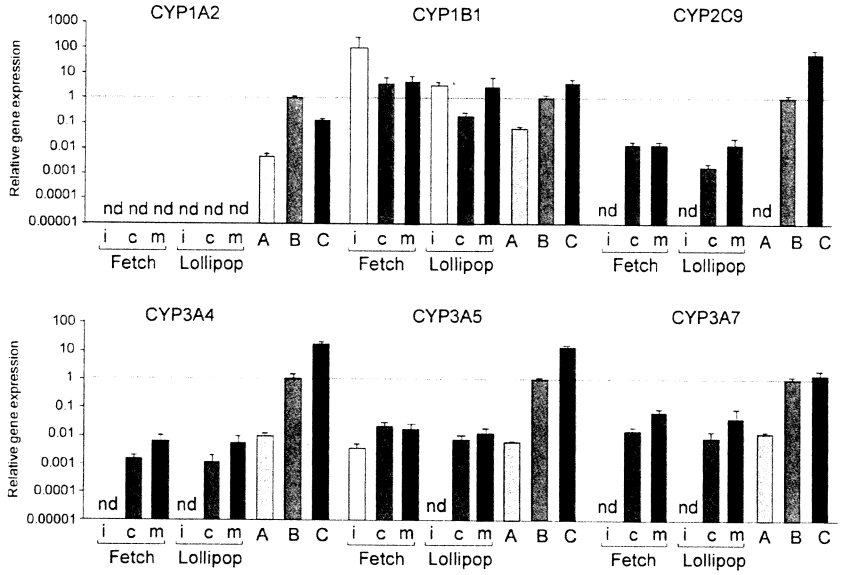


Fig. 3. Expression levels of CYP mRNAs
The expression levels of CYP1A2, CYP1B1, CYP2C9, CYP3A4, CYP3A5, and CYP3A7 mRNAs in undifferentiated human iPS cells (i) and hepatocyte-like cells differentiated from 2 human iPS cell lines (Fetch and Lollipop) were analyzed using real-time PCR. Collagen I (c) or Matrigel (m) was used for the differentiation as the extracellular matrix. A, B, and C represent HepG2 cells, human adult liver, and hepatocytes, respectively, as positive controls. Each bar represents the mean ± SD from triplicate experiments. Values were normalized to the levels of GAPDH mRNA. The graphs represent the relative gene expression level when the level in the liver was taken as 1. nd, not detected.

in the cells differentiated from iPS cells were similar to those in hepatocytes. However, the expression of AFP mRNA, a marker protein for an immature liver,[32] in the cells was almost identical to that of the HepG2 cells, and was markedly higher than the expression in human adult liver and hepatocytes.

Expression of CYP and UGT gene: **Figure 3** shows the expression of CYP mRNAs in the cells differentiated into hepatocytes from iPS cells. The majority of the CYPs involved in drug metabolism display tissue-specific expression in the liver and small intestine.[33] Of these, the mRNA encoding CYP1A2, a liver-specific CYP,[34] was not detected in the cells differentiated into hepatocytes. On the other hand, three CYP3A mRNAs were detected in the cells, but their expression levels were approximately 100–1,000 times lower in the cells differentiated into hepatocytes than in liver and hepatocytes, and were similar to that in HepG2 cells. It is of interest that CYP2C9 mRNA was detected in the cells differentiated into hepatocytes but not in HepG2 cells, although the expression level was lower than that of the liver and hepatocytes. The expression of CYP1B1 mRNA, which is not a liver-specific CYP, was observed in all cells used in this experiment at similar levels. The expression profiles for these CYPs were not largely different between the two cell lines; however, the expression levels of CYP mRNAs tended to be higher in the cells cultured on Matrigel than in those cultured on collagen I. To determine the expression of phase I and II enzymes, the differentiated cells were compared with adult or fetal hepatocytes using microarray analysis. The expression levels of mRNAs encoding the phase II enzymes, uridine diphosphate glucuronosyltransferase (UGT) 2A3, UGT2B4, and UGT2B7, were high in the differentiated cells. In contrast, the expression levels of majority of the phase I enzymes in the differentiated cells were lower than those in adult hepatocytes (**Fig. 4**).

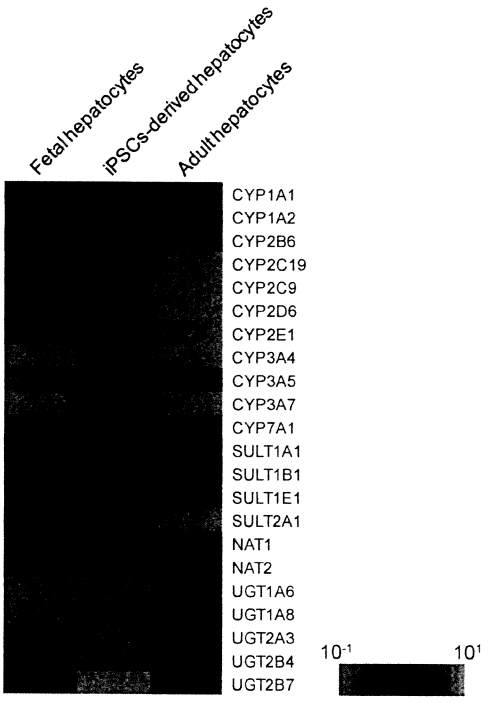


Fig. 4. Microarray analysis of phase I and II enzymes
Human iPS cells (Fetch) were differentiated into hepatocyte-like cells. After differentiation, total mRNA was extracted from the cells. The expression levels of phase I and II enzymes were analyzed by microarray analysis as described in Materials and Methods. The expression levels of fetal liver cells, hepatocyte-like cells differentiated from human iPS cells, and adult hepatocytes are presented in the left, center, and right columns, respectively.

Copyright © 2014 by the Japanese Society for the Study of Xenobiotics (JSSX)

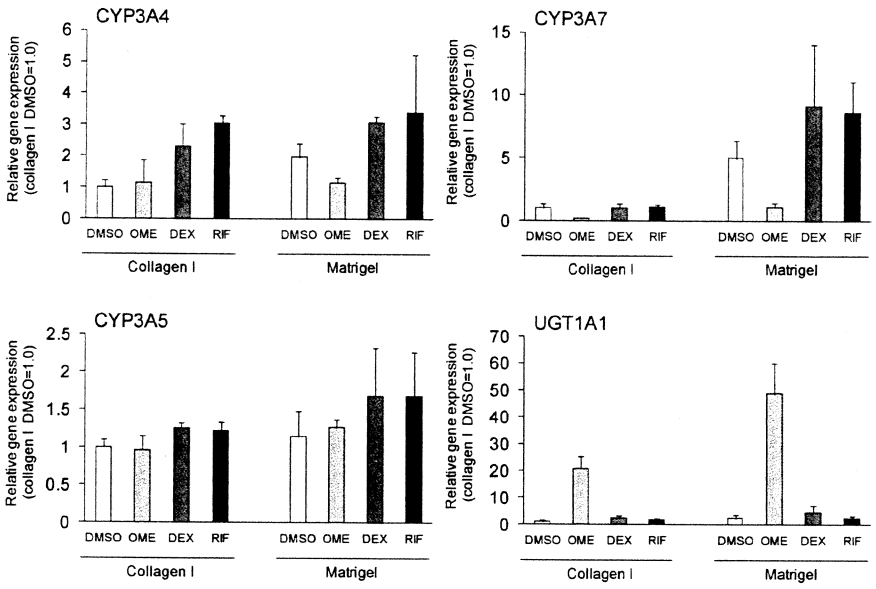


Fig. 5. Effects of drugs on expression of CYP3A enzymes and UGT1A1 mRNAs in the hepatocyte-like cells
The cells differentiated from human iPS cells (Fetch) were treated with OME, DEX, and RIF for 72 h. The total mRNA was extracted from the cells. The expression of CYP3A and UGT1A1 mRNAs were analyzed by microarray analysis as described in Materials and Methods. Each bar represents the mean ± SD from triplicate experiments. Values were normalized to the levels of GAPDH mRNA. The graphs represent the relative gene expression level when the levels in the hepatocyte-like cells using collagen I and DMSO were assigned a value of 1.

Inducibility of CYP3A enzymes and drug metabolizing activity: A specific property of some drug-metabolizing enzymes is the induction of their expression by treatment with drugs. **Figure 5** presents the effects of inducers on expression of CYP3A enzymes and UGT1A1. In the cells differentiated into hepatocytes from human iPS cells on collagen I, expression of CYP3A4 mRNA increased 2.5- and 3-fold with treatment with DEX and RIF, respectively, although expressions of CYP3A5 and CYP3A7 mRNAs were not markedly increased. When the human iPS cells were cultured on Matrigel, marked induction of CYP3A enzymes was not observed. On the other hand, UGT1A1 mRNA was strongly induced by treatment with OME in the cells differentiated into hepatocytes. The induced level was higher in the cells cultured on Matrigel (50-fold induction) than on collagen I (22-fold induction). UGT1A1 is a typical drug-metabolizing enzyme that is strongly induced by polycyclic aromatic hydrocarbons and 2,3,7,8-tetrachlorodibenzo-*p*-dioxin (TCDD) through activation of aryl hydrocarbon receptor (AhR).[35] OME is also known as an AhR activator.[36]

Based on the induction of CYP3A4 mRNA expression, we measured testosterone 6β-hydroxylase activity, which is catalyzed by CYP3A enzymes. As shown in **Figure 6**, testosterone 6β-hydroxylase activity was induced 2.3- and 2.7-fold by treatment with DEX and RIF, respectively, in the cells cultured on collagen I. The activity in the cells cultured on Matrigel was approximately 2.5-fold higher than that of the cells cultured on collagen I in the control (DMSO) and was markedly induced by treatment with RIF.

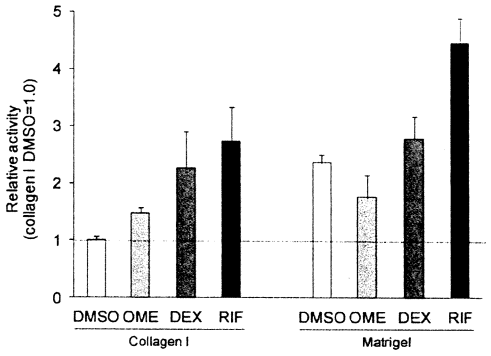


Fig. 6. Effects of drugs on testosterone 6β-hydroxylase activity in hepatocyte-like cells
The cells differentiated from human iPS cells (Fetch) were treated with OME, DEX, and RIF for 72 h and then cultured with the medium containing testosterone for 6 h. 6β-Hydroxytestosterone was analyzed using liquid chromatography coupled with tandem mass spectrometry as described in Materials and Methods. Each bar represents the mean ± SD from triplicate experiments. The graphs represent the relative activity ratios when the value in the hepatocyte-like cells using collagen I and DMSO were assigned a value of 1.

Discussion

In the present study, we established methods for the differentiation of human iPS cells into functional hepatocytes as determined by constitutive and induced expression of CYP3A4 mRNA. Several groups have previously reported the differentiation of human iPS cells into hepatocytes. Song *et al.* reported that human iPS cells can be induced to differentiate into hepatocyte-like cells by using six growth factors and supplements.[17] In addition, Si-Tayeb *et al.* reported that human iPS cells can be induced to efficiently differentiate into hepatocytes by using five growth factors and supplements under hypoxic conditions.[15] Another study by Takayama *et al.* described the use of a highly efficient method for the generation of functional hepatocytes from human iPS cells by sequential transduction of the sex determining region Y box 17 (SOX17), hematopoietically expressed homeobox (HHEX) and HNF4α or forkhead box A2 (FOXA2), and

Copyright © 2014 by the Japanese Society for the Study of Xenobiotics (JSSX)

HNF1α.[18,19] Hepatic differentiation methods (*e.g.*, 3D coculture[20] and hollow fiber[21]) have also been used. However, highly efficient methods are complicated and extremely expensive. Because of the facile approaches that utilized only humoral factors, the responsiveness including CYP activity of differentiated human iPS cells-derived hepatocytes to inducers was unclear.

In the present study, a three-step protocol using three growth factors and two small-molecule compounds was used to differentiate human iPS cells into hepatocytes. The human iPS cells were differentiated into endoderm cells by the addition of 100 ng/mL activin A[27] and were subsequently differentiated into hepatocytes by the addition of 1% DMSO.[28] The hepatocytes were matured by the addition of 10 ng/mL HGF,[28] 20 ng/mL OSM,[28] and 10^{-7} M DEX.[30] Activin A is necessary for the differentiation of human iPS cells into endoderm cells.[27] Few studies have used DMSO, bone morphogenetic protein 4 (BMP4), FGF2, FGF7 or FGF10 for differentiation of human iPS cells into hepatic progenitor cells from human stem cells.[15,17,28] In addition, we used these single factors alone or in combinations, but no increase in differentiation efficiency was observed (data not shown). Further, we selected DMSO, which is structurally stable and inexpensive compared with recombinant proteins such as the cytokines described above. DMSO has been known to maintain the functions of adult hepatocytes *in vitro*[37] and was used to differentiate HepaRG cells.[38] The hepatic progenitor cells were matured by addition of HGF, OSM, and DEX, necessary for maturation of hepatocytes.[29–31]

After 25 days of differentiation, the mRNAs encoding hepatocyte markers, such as ALB, AFP, and drug-metabolizing enzymes, were expressed in the cells differentiated from human iPS cells; the expression of these mRNA were increased using Matrigel. In a previous report, Matrigel led to high expression of liver-enriched transcription factors such as HNF4α[39] and laminin, a main component of Matrigel, increased ALB mRNA level and ALB secretion.[40] The result in the present study is consistent with these findings. The expression level of CYP2C9 mRNA in the cells differentiated from human iPS cells was higher than that in HepG2 cells, although lower than that in hepatocytes. This result suggested that the cells are similar to hepatocytes rather than HepG2 cells, a hepatocellular carcinoma cell line. In addition, mRNA expression levels of CYP3A4 and UGT1A1 in the cells were increased by each inducer and presented responsiveness similar to that of the hepatocytes. These results indicate that human iPS cells were differentiated into hepatocyte-like cells under the present conditions. Furthermore, the cells showed testosterone 6β-hydroxylase activity that was mediated by CYP3A4, and the activity increased with addition of RIF or DEX. CYP3As, in particular CYP3A4, are strongly induced by treatment with RIF and DEX in livers.[41] These data indicated that functional hepatocyte-like cells had been differentiated from human iPS cells. Induction of the *CYP3A4* and *UGT1A1* genes is mediated through the activation of pregnane X receptor (PXR)/constitutive androstane receptor (CAR) and AhR, respectively.[42] AhR and CAR were clearly detected, but PXR was not detected in the hepatocyte-like cells (data not shown). Thus, the CYP3A4 induction observed in this study may have been dependent on CAR and glucocorticoid receptor activation by RIF and DEX, respectively. Furthermore, induction of mRNAs encoding CYP1A2 as well as CYP1A1 was observed in hepatocyte-like cells treated with TCDD, although CYP1A2 mRNA was not detected in untreated hepatocyte-like cells (data not shown). The expression level of CYP3A7 mRNA was reduced when the cells were treated with OME. However, the reason for this remains unknown. Krusekopf *et al.* reported that CYP3A4 in HepG2 cells was induced by OME, whereas CYP3A5, CYP3A7, and CYP3A43 were unaffected or even slightly downregulated by OME.[43] They suggested that the expression of CYP3A4 is differently regulated from that of CYP3A5, CYP3A7, and CYP3A43 depending on the inducer. Expression of the CYP3A subfamily might be differently regulated by OME.

In fetal liver, it is known that the expression level of CYPs is extremely low compared with that in a mature liver.[44] In the hepatocyte-like cells differentiated from human iPS cells, the expression levels of HNF6 and CCAAT-enhancer-binding protein alpha (CEBPα), transcriptional factors involved in the differentiation into mature liver cells, were low (data not shown). From the results of microarrays, the expression levels of phase II enzymes were relatively high in the differentiated cells. In contrast, the expression levels of the phase I enzymes were low, which demonstrated that the human iPS cell-derived hepatocyte-like cells were still immature. These results may suggest that the hepatocyte-like cells from human iPS cells were differentiated at least in part to fetal liver-like cells. Therefore, the differentiated cells may be useful for evaluation in a human fetal liver model.

Multiple iPS cell lines were differentiated into hepatocytes using this method, although there were differences in the differentiation ability. There is a variation of differentiation propensity among multiple human ES/iPS cell lines[45,46] because of the method of stem cell generation, culture conditions, and genetic backgrounds of the donor cells. In future, it is necessary to optimize a differentiation method adapted to each cell line, and to select a cell line that is easy to differentiate into cells of interest.

In conclusion, the three-step protocol and the limited number of differentiation factors used in this study constituted an efficient method for differentiation of human iPS cells into hepatocyte-like cells that showed drug metabolizing activity and induction of CYP3A4 by RIF. However, the expression levels of drug-metabolizing enzymes were very low compared with those in mature livers. Further studies are needed to increase the expression of drug-metabolizing enzymes produced under the conditions of our method.

References

1) Park, I. H., Zhao, R., West, J. A., Yabuuchi, A., Huo, H., Ince, T. A., Lerou, P. H., Lensch, M. W. and Daley, G. Q.: Reprogramming of human somatic cells to pluripotency with defined factors. *Nature*, **451**: 141–146 (2008).
2) Lowry, W. E., Richter, L., Yachechko, R., Pyle, A. D., Tchieu, J., Sridharan, R., Clark, A. T. and Plath, K.: Generation of human induced pluripotent stem cells from dermal fibroblasts. *Proc. Natl. Acad. Sci. USA*, **105**: 2883–2888 (2008).
3) Takahashi, K., Tanabe, K., Ohnuki, M., Narita, M., Ichisaka, T., Tomoda, K. and Yamanaka, S.: Induction of pluripotent stem cells from adult human fibroblasts by defined factors. *Cell*, **131**: 861–872 (2007).
4) Takahashi, K. and Yamanaka, S.: Induction of pluripotent stem cells from mouse embryonic and adult fibroblast cultures by defined factors. *Cell*, **126**: 663–676 (2006).
5) Ochiya, T., Yamamoto, Y. and Banas, A.: Commitment of stem cells into functional hepatocytes. *Differentiation*, **79**: 65–73 (2010).
6) Hannoun, Z., Filippi, C., Sullivan, G., Hay, D. C. and Iredale, J. P.: Hepatic endoderm differentiation from human embryonic stem cells. *Curr. Stem Cell Res. Ther.*, **5**: 233–244 (2010).
7) Lacroix, D., Sonnier, M., Moncion, A., Cheron, G. and Cresteil, T.: Expression of CYP3A in the human liver—Evidence that the shift between CYP3A7 and CYP3A4 occurs immediately after birth. *Eur. J. Biochem.*, **247**: 625–634 (1997).
8) Stevens, J. C., Hines, R. N., Gu, C., Koukouritaki, S. B., Manro, J. R.,

Copyright © 2014 by the Japanese Society for the Study of Xenobiotics (JSSX)

Tandler, P. J. and Zaya, M. J.: Developmental Expression of the Major Human Hepatic CYP3A Enzymes. *J. Pharmacol. Exp. Ther.*, **307**: 573–582 (2003).
9) Shimada, T., Yamazaki, H., Mimura, M., Inui, Y. and Guengerich, F. P.: Interindividual variations in human liver cytochrome P-450 enzymes involved in the oxidation of drugs, carcinogens and toxic chemicals: studies with liver microsomes of 30 Japanese and 30 Caucasians. *J. Pharmacol. Exp. Ther.*, **270**: 414–423 (1994).
10) Wienkers, L. C. and Health, T. G.: Predicting in vivo drug interactions from in vitro drug discovery data. *Nat. Rev. Drug Discov.*, **4**: 825–833 (2005).
11) Li, A. P., Rasmussen, A., Xu, L. and Kaminski, D. L.: Rifampicin induction of lidocaine metabolism in cultured human hepatocytes. *J. Pharmacol. Exp. Ther.*, **274**: 673–677 (1995).
12) Kocarek, T. A., Schuetz, E. G., Strom, S. C., Fisher, R. A. and Guzelian, P. S.: Comparative analysis of cytochrome P4503A induction in primary cultures of rat, rabbit, and human hepatocytes. *Drug Metab. Dispos.*, **23**: 415–421 (1995).
13) Silva, J. M., Morin, P. E., Day, S. H., Kennedy, B. P., Payette, P., Rushmore, T., Yergey, J. A. and Nicoll-Griffith, D. A.: Refinement of an *in vitro* cell model for cytochrome P450 induction. *Drug Metab. Dispos.*, **26**: 490–496 (1998).
14) Cai, J., Zhao, Y., Liu, Y., Ye, F., Song, Z., Qin, H., Meng, S., Chen, Y., Zhou, R., *et al.*: Directed differentiation of human embryonic stem cells into functional hepatic cells. *Hepatology*, **45**: 1229–1239 (2007).
15) Si-Tayeb, K., Noto, F. K., Nagaoka, M., Li, J., Battle, M. A., Duris, C., North, P. E., Dalton, S. and Duncan, S. A.: Highly efficient generation of human hepatocyte-like cells from induced pluripotent stem cells. *Hepatology*, **51**: 297–305 (2010).
16) Touboul, T., Hannan, N. R., Corbineau, S., Martinez, A., Martinet, C., Branchereau, S., Mainot, S., Strick-Marchand, H., Pedersen, R., *et al.*: Generation of functional hepatocytes from human embryonic stem cells under chemically defined conditions that recapitulate liver development. *Hepatology*, **51**: 1754–1765 (2010).
17) Song, Z., Cai, J., Liu, Y., Zhao, D., Yong, J., Duo, S., Song, X., Guo, Y., Zhao, Y., *et al.*: Efficient generation of hepatocyte-like cells from human induced pluripotent stem cells. *Cell Res.*, **19**: 1233–1242 (2009).
18) Takayama, K., Inamura, M., Kawabata, K., Katayama, K., Higuchi, M., Tashiro, K., Nonaka, A., Sakurai, F., Hayakawa, T., *et al.*: Efficient generation of functional hepatocytes from human embryonic stem cells and induced pluripotent stem cells by HNF4α transduction. *Mol. Ther.*, **20**: 127–137 (2012).
19) Takayama, K., Inamura, M., Kawabata, K., Sugawara, M., Kikuchi, K., Higuchi, M., Nagamoto, Y., Watanabe, H., Tashiro, K., *et al.*: Generation of metabolically functioning hepatocytes from human pluripotent stem cells by FOXA2 and HNF1α transduction. *J. Hepatol.*, **57**: 628–636 (2012).
20) Nagamoto, Y., Tashiro, K., Takayama, K., Ohashi, K., Kawabata, K., Sakurai, F., Tachibana, M., Hayakawa, T., Furue, M. K., *et al.*: The promotion of hepatic maturation of human pluripotent stem cells in 3D co-culture using type I collagen and Swiss 3T3 cell sheets. *Biomaterials*, **33**: 4526–4534 (2012).
21) Amimoto, N., Mizumoto, H., Nakazawa, K., Ijima, H., Funatsu, K. and Kajiwara, T.: Hepatic differentiation of mouse embryonic stem cells and induced pluripotent stem cells during organoid formation in hollow fibers. *Tissue Eng. Part A*, **2011**(17): 2071–2078 (2011).
22) Tsuchiya, H., Matsunaga, T., Aikawa, K., Kamada, N., Nakamura, K., Ichikawa, H., Sasaki, K. and Ohmori, S.: Evaluation of human embryonic stem cell-derived hepatocyte-like cells for detection of CYP1A inducers. *Drug Metab. Pharmacokinet.*, **27**: 598–604 (2012).
23) Momose, Y., Matsunaga, T., Murai, K., Takezawa, T. and Ohmori, S.: Differentiation of monkey embryonic stem cells into hepatocytes and mRNA expression of cytochrome P450 enzymes responsible for drug metabolism: comparison of embryoid body formation conditions and matrices. *Biol. Pharm. Bull.*, **32**: 619–626 (2009).
24) Maruyama, M., Matsunaga, T., Harada, E. and Ohmori, S.: Comparison of basal gene expression and induction of CYP3As in HepG2 and human fetal liver cells. *Biol. Pharm. Bull.*, **30**: 2091–2097 (2007).
25) Nishimura, M., Koeda, A., Suganuma, Y., Suzuki, E., Shimizu, T., Nakayama, M., Satoh, T., Narimatsu, S. and Naito, S.: Comparison of inducibility of CYP1A and CYP3A mRNAs by prototypical inducers in primary cultures of human, cynomolgus monkey, and rat hepatocytes. *Drug Metab. Pharmacokinet.*, **22**: 178–186 (2007).
26) Maezawa, K., Matsunaga, T., Takezawa, T., Kanai, M., Ohira, S. and Ohmori, S.: Cytochrome P450 3As gene expression and testosterone 6β-hydroxylase activity in human fetal membranes and placenta at full term. *Biol. Pharm. Bull.*, **33**: 249–254 (2010).
27) D'Amour, K. A., Agulnick, A. D., Eliazer, S., Kelly, O. G., Kroon, E. and Baetge, E. E.: Efficient differentiation of human embryonic stem cells to definitive endoderm. *Nat. Biotechnol.*, **23**: 1534–1541 (2005).
28) Hay, D. C., Zhao, D., Fletcher, J., Hewitt, Z. A., McLean, D., Urruticoechea-Uriguen, A., Black, J. R., Elcombe, C., Ross, J. A., *et al.*: Efficient differentiation of hepatocytes from human embryonic stem cells exhibiting markers recapitulating liver development *in vivo*. *Stem Cells*, **26**: 894–902 (2008).
29) Kamiya, A., Kinoshita, T., Ito, Y., Matsui, T., Morikawa, Y., Senba, E., Nakashima, K., Taga, T., Yoshida, K., *et al.*: Fetal liver development requires a paracrine action of oncostatin M through the gp130 signal transducer. *EMBO J.*, **18**: 2127–2136 (1999).
30) Kamiya, A., Kinoshita, T. and Miyajima, A.: Oncostatin M and hepatocyte growth factor induce hepatic maturation via distinct signaling pathways. *FEBS Lett.*, **492**: 90–94 (2001).
31) Suzuki, A., Iwama, A., Miyashita, H., Nakauchi, H. and Taniguchi, H.: Role for growth factors and extracellular matrix in controlling differentiation of prospectively isolated hepatic stem cells. *Development*, **130**: 2513–2524 (2003).
32) Chou, J. Y.: Regulators of fetal liver differentiation *in vitro*. *Arch. Biochem. Biophys.*, **263**: 378–386 (1988).
33) Jochheim, A., Hillemann, T., Kania, G., Scharf, J., Attaran, M., Manns, M. P., Wobus, A. M. and Ott, M.: Quantitative gene expression profiling reveals a fetal hepatic phenotype of murine ES-derived hepatocytes. *Int. J. Dev. Biol.*, **48**: 23–29 (2004).
34) Kondraganti, S. R., Jiang, W. and Moorthy, B.: Differential regulation of expression of hepatic and pulmonary cytochrome P4501A enzymes by 3-methylcholanthrene in mice lacking the CYP1A2 gene. *J. Pharmacol. Exp. Ther.*, **303**: 945–951 (2002).
35) Bock, K. W.: Functions and transcriptional regulation of adult human hepatic UDP-glucuronosyl-transferases (UGTs): mechanisms responsible for interindividual variation of UGT levels. *Biochem. Pharmacol.*, **80**: 771–777 (2010).
36) Quattrochi, L. C. and Tukey, R. H.: Nuclear uptake of the Ah (dioxin) receptor in response to omeprazole: transcriptional activation of the human CYP1A1 gene. *Mol. Pharmacol.*, **43**: 504–508 (1993).
37) Kamiya, A., Kojima, N., Kinoshita, T., Sakai, Y. and Miyaijma, A.: Maturation of fetal hepatocytes in vitro by extracellular matrices and oncostatin M: induction of tryptophan oxygenase. *Hepatology*, **35**: 1351–1359 (2002).
38) Cerec, V., Glaise, D., Garnier, D., Morosan, S., Turlin, B., Drenou, B., Gripon, P., Kremsdorf, D., Guguen-Guillouzo, C., *et al.*: Transdifferentiation of hepatocyte-like cells from the human hepatoma HepaRG cell line through bipotent progenitor. *Hepatology*, **45**: 957–967 (2007).
39) Oda, H., Nozawa, K., Hitomi, Y. and Kakinuma, A.: Laminin-rich extracellular matrix maintains high level of hepatocyte nuclear factor 4 in rat hepatocyte culture. *Biochem. Biophys. Res. Commun.*, **212**: 800–805 (1995).
40) Caron, J. M.: Induction of albumin gene transcription in hepatocytes by extracellular matrix proteins. *Mol. Cell. Biol.*, **10**: 1239–1243 (1990).
41) Gibson, G. G., Plant, N. J., Swales, K. E., Ayrton, A. and El-Sankary, W.: Receptor-dependent transcriptional activation of cytochrome P4503A genes: induction mechanisms, species differences and interindividual variation in man. *Xenobiotica*, **32**: 165–206 (2002).
42) Sinz, M., Wallace, G. and Sahi, J.: Current industrial practices in assessing CYP450 enzyme induction: preclinical and clinical. *AAPS J.*, **10**: 391–400 (2008).
43) Krusekopf, S., Roots, I. and Kleeberg, U.: Differential drug-induced mRNA expression of human CYP3A4 compared to CYP3A5, CYP3A7 and CYP3A43. *Eur. J. Pharmacol.*, **466**: 7–12 (2003).
44) Ring, J. A., Ghabrial, H., Ching, M. S., Smallwood, R. A. and Morgan, D. J.: Fetal hepatic drug elimination. *Pharmacol. Ther.*, **84**: 429–445 (1999).
45) Osafune, K., Caron, L., Borowiak, M., Martinez, R. J., Fitz-Gerald, C. S., Sato, Y., Cowan, C. A., Chien, K. R. and Melton, D. A.: Marked differences in differentiation propensity among human embryonic stem cell lines. *Nat. Biotechnol.*, **26**: 313–315 (2008).
46) Kajiwara, M., Aoi, T., Okita, K., Takahashi, R., Inoue, H., Takayama, N., Endo, H., Eto, K., Toguchida, J., *et al.*: Donor-dependent variations in hepatic differentiation from human-induced pluripotent stem cells. *Proc. Natl. Acad. Sci. USA*, **109**: 12538–12543 (2012).

Copyright © 2014 by the Japanese Society for the Study of Xenobiotics (JSSX)

Drug Metab. Pharmacokinet. 29 (1): 44–51 (2014). Copyright © 2014 by the Japanese Society for the Study of Xenobiotics (JSSX)

Regular Article

Differentiation of Human Induced Pluripotent Stem Cells into Functional Enterocyte-like Cells Using a Simple Method

Takahiro Iwao[1], Masashi Toyota[2], Yoshitaka Miyagawa[3], Hajime Okita[3], Nobutaka Kiyokawa[3], Hidenori Akutsu[2], Akihiro Umezawa[2], Kiyoshi Nagata[4] and Tamihide Matsunaga[1,*]

[1]*Department of Clinical Pharmacy, Graduate School of Pharmaceutical Sciences, Nagoya City University, Nagoya, Japan*

[2]*Department of Reproductive Biology, National Research Institute for Child Health and Development, Tokyo, Japan*

[3]*Department of Hematology and Oncology Research, National Research Institute for Child Health and Development, Tokyo, Japan*

[4]*Department of Environmental and Health Science, Tohoku Pharmaceutical University, Sendai, Japan*

Full text of this paper is available at http://www.jstage.jst.go.jp/browse/dmpk

Summary: Human induced pluripotent stem (iPS) cells were differentiated into the endoderm using activin A and were then treated with fibroblast growth factor 2 (FGF2) for differentiation into intestinal stem cell-like cells. These immature cells were then differentiated into enterocyte-like cells using epidermal growth factor (EGF) in 2% fetal bovine serum (FBS). At the early stage of differentiation, mRNA expression of caudal type homeobox 2 (CDX2), a major transcription factor related to intestinal development and differentiation, and leucine-rich repeat-containing G-protein-coupled receptor 5 (LGR5), an intestinal stem cell marker, was markedly increased by treatment with FGF2. When cells were cultured in medium containing EGF and a low concentration of FBS, mRNAs of specific markers of intestinal epithelial cells, including sucrase–isomaltase, the intestinal oligopeptide transporter SLC15A1/peptide transporter 1 (PEPT1), and the major metabolizing enzyme CYP3A4, were expressed. In addition, sucrase–isomaltase protein expression and uptake of β-Ala-Lys-N-7-amino-4-methylcoumarin-3-acetic acid (β-Ala-Lys-AMCA), a fluorescence-labeled substrate of the oligopeptide transporter, were detected. These results demonstrate a simple and direct method for differentiating human iPS cells into functional enterocyte-like cells.

Keywords: human iPS cells; intestinal differentiation; enterocytes; pharmacokinetics; drug metabolizing enzymes; drug transporters

Introduction

The small intestine and liver play important roles in all aspects of pharmacokinetics, including drug disposition, drug metabolism, drug transport, drug interactions, and bioavailability. Because drug-metabolizing enzymes such as cytochrome P450 (CYP) and UDP-glucuronyltransferase (UGT) and drug transporters such as ATP-binding cassette (ABC) and solute carrier (SLC) transporters are appreciably expressed in the small intestinal epithelia,[1,2] it is necessary to estimate intestinal metabolism and absorption during the early stages of drug development. To this end, various *in vivo* and *in vitro* systems have been employed to assess the intestinal first-pass effect. However, extrapolation of experimental animal data to humans is often hampered by species differences, and primary human intestinal cells are rarely available. Therefore, a system that accurately and easily estimates intestinal membrane permeability and metabolism is urgently required.

Human induced pluripotent stem (iPS) cells can be generated by transducing reprogramming factors (OCT3/4, SOX2, KLF4, c-MYC) into somatic cells[3] and these cells share many characteristics of embryonic stem (ES) cells.[4] Human iPS cells are expected to be useful not only in regenerative medicine but also in pharmacokinetic and toxicokinetic drug development studies because their use is not as ethically regulated as that of human ES cells.

Received January 25, 2013; Accepted June 21, 2013
J-STAGE Advance Published Date: July 2, 2013, doi:10.2133/dmpk.DMPK-13-RG-005
**To whom correspondence should be addressed:* Tamihide Matsunaga, Ph.D., *Department of Clinical Pharmacy, Graduate School of Pharmaceutical Sciences, Nagoya City University, 3-1 Tanabe-dori, Mizuho-ku, Nagoya 467-8603, Japan. Tel. +81-52-836-3751, Fax. +81-52-836-3751, E-mail: tmatsu@phar.nagoya-cu.ac.jp.*
This work was supported, in part, by Grants-in-Aid from the Japan Society for the Promotion of Science (23390036), by a National Grant-in-Aid from Japanese Ministry of Health, Labor, and Welfare (H22-003), and by a Grant-in-Aid for Research in Nagoya City University.

Therefore, human iPS cells have been differentiated into various cell types, including pancreatic cells,[5,6] neuron cells,[7] cardiomyocytes,[8] and hepatocytes.[9–13]

A few studies report the differentiation of iPS cells into enterocytes. In particular, mouse iPS cells were differentiated into a gut-like organ following the formation of embryoid bodies (EBs),[14] and human iPS cells were differentiated into intestinal tissue using a culture method for intestinal crypt stem cells.[15] However, functional characteristics of drug transporters and drug-metabolizing enzymes of differentiated cells are almost entirely unexplored in these reports. Thus, whether differentiated intestinal tissue or organoids can be used in drug development studies, particularly studies of the absorbability and metabolic capacity of drugs, remains unclear.

The small intestinal epithelium comprises absorptive cells, goblet cells, endocrine cells, and Paneth cells. Several signaling pathways such as Notch, Wnt, phosphoinositide 3-kinase, and bone morphogenic protein signaling are associated with intestinal development.[16] Leucine-rich repeat-containing G-protein-coupled receptor 5 (LGR5) has been identified as an intestinal stem cell marker.[17] Indeed, this was also observed in mouse LGR5-positive cells that formed a crypt–villus structure *in vitro*.[18] Improvements in this technique have enabled long-term culture of human epithelial cells isolated from the small intestine,[19] leading to advances in intestinal stem cell research. However, mechanisms of intestinal development are not sufficiently understood, and it is difficult to control differentiation into all four cell types.

In this study, we established a functional enterocyte-like cell line from human iPS cells for use in drug development studies. We propose a simple and direct differentiation method by two-dimensional culture. Our data may facilitate the development of an intestinal pharmacokinetic analysis system to identify safe drugs with favorable pharmacokinetic characteristics.

Materials and Methods

Materials: FGF2, FGF4, activin A, and epidermal growth factor (EGF) were purchased from PeproTech Inc. (Rocky Hill, NJ). Wnt3a was purchased from R&D Systems, Inc. (Minneapolis, MN). BD Matrigel matrix Growth Factor Reduced (Matrigel) was purchased from BD Biosciences (Bedford, MA). Affinity-isolated rabbit polyclonal antihuman sucrase–isomaltase antibody and intestinal recombinant protein epitope signature tags were purchased from Sigma-Aldrich Co. (St. Louis, MO). The purified IgG fraction of polyclonal goat antiserum against rabbit IgG conjugated with Alexa Fluor 568 and KnockOut Serum Replacement (KSR) were purchased from Invitrogen Life Technologies Co. (Carlsbad, CA). β-Ala-Lys-N-7-amino-4-methylcoumarin-3-acetic acid (β-Ala-Lys-AMCA) was purchased from BIOTREND Chemicals (Destin, FL), and (+)-(*R*)-*trans*-4-(1-aminoethyl)-*N*-(4-pyridyl)cyclohexanecarboxamide dihydrochloride (Y-27632) was purchased from Wako Pure Chemical Industries (Osaka, Japan). Human adult small intestine total RNA from a 66-year-old male donor was purchased from BioChain Institute Inc. (Newark, CA). Murine embryonic fibroblasts (MEFs) were obtained from Oriental Yeast Co. (Tokyo, Japan). The RNeasy Mini Kit was purchased from Qiagen (Valencia, CA). The PrimeScript RT Reagent Kit and TaKaRa SYBR Premix EX Taq II were purchased from Takara Bio Inc. (Otsu, Japan). All other reagents were of the highest quality available.

Human iPS cell cultures: A human iPS cell line (Windy) was provided by Dr. Akihiro Umezawa of the National Center for Child Health and Development. Human iPS cells were maintained in a 1:1 mixture of Dulbecco's modified Eagle's medium and Ham's nutrient mixture F-12 (DMEM/F12) containing 20% KSR, 2 mM L-glutamine, 1% MEM nonessential amino acid solution (NEAA), 0.1 mM 2-mercaptoethanol, and 5 ng/ml FGF2 at 37°C in humidified air with 5% CO_2. The human iPS cells were cultured on a feeder layer of mitomycin C-treated MEFs, and the medium was changed every day.

Differentiation into enterocyte-like cells: The human iPS cells were used for differentiation studies between passages 30 and 50. When the cells reached approximately 70% confluence, differentiation was initiated by replacing the medium with Rosewell Park Memorial Institute (RPMI) 1640 medium containing 2 mM GlutaMAX, 0.5% fetal bovine serum (FBS), 100 ng/ml activin A (a member of the transforming growth factor-β family that is known to efficiently induce differentiation into the definitive endoderm),[20,21] 100 units/ml penicillin, and 100 μg/ml streptomycin. After 48 h, the medium was replaced with RPMI 1640 containing 2 mM GlutaMAX, 2% FBS, 100 ng/ml activin A, 100 units/ml penicillin, and 100 μg/ml streptomycin, and the cells were cultured for 24 h. Subsequently, the culture medium was replaced with DMEM/F12 containing 2% FBS, 2 mM GlutaMAX, and 250 ng/ml FGF2 or FGF4 with or without 50 ng/ml Wnt3a for 96 h. The cells were then treated for 1 h with the selective Rho-associated kinase inhibitor Y-27632 at 10 μM.[22,23] The cells were then passaged on Matrigel-coated 24-well plates and cultured in DMEM/F12 containing 2% or 10% FBS, 2% B-27 supplement, 1% N2 supplement, 1% NEAA, 2 mM L-glutamine, antibiotics (100 units/ml penicillin and 100 μg/ml streptomycin), and 20 ng/ml EGF for 1, 4, 13, or 19 days. Y-27632 was added at 10 μM during the initial 24 h of culture. The medium was changed every 3 days (**Fig. 1**).

RNA extraction and reverse transcription reaction: Total RNA was isolated from differentiated iPS cells using the RNeasy Mini Kit. First-strand cDNA was prepared from 500 ng of total RNA. The reverse transcription reaction was performed using the PrimeScript RT Reagent Kit according to the manufacturer's instructions.

Real-time polymerase chain reaction (PCR) analysis: Relative mRNA expression levels were determined using SYBR Green real-time quantitative reverse transcription-PCR (RT-PCR). Real-time PCR analysis was performed on the Applied Biosystems 7300 Real Time PCR System using 7300 System SDS software version 1.4 (Applied Biosystems, Carlsbad, CA). PCR was performed with the primer pairs listed in **Table 1** using SYBR Premix EX Taq II. mRNA expression levels were normalized relative to that of the housekeeping gene glyceraldehyde-3-phosphate dehydrogenase (GAPDH).

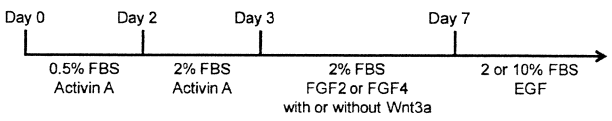


Fig. 1. Schematic of the protocol for the differentiation of human iPS cells into enterocytes
Human iPS cells were cultured in the presence of activin A (100 ng/ml) for 3 days. The cells were further cultured in medium containing FGF2 (250 ng/ml) or FGF4 (250 ng/ml) with or without Wnt3a (50 ng/ml) for 4 days. After 7 days of differentiation, the cells were treated with Y-27632 (10 μM), passaged, and subsequently cultured in the presence of 2% or 10% FBS and EGF (20 ng/ml) for 19 days.

Copyright © 2014 by the Japanese Society for the Study of Xenobiotics (JSSX)

Table 1. Sequences of primers for real-time PCR analysis

Gene name	Sense (5′→3′)	Antisense (5′→3′)	Product length (bp)
CDX2	ACCTGTGCGAGTGGATGC	TCCTTTGCTCTGCGGTTCT	232
LGR5	TGCTCTTCACCAACTGCATC	CTCAGGCTCACCAGATCCTC	193
DPP4	CAAATTGAAGCAGCCAGACA	GGAGTTGGGAGACCCATGTA	212
Sucrase–isomaltase	GGTAAGGAGAAACCGGGAAG	GCACGTCGACCTATGGAAAT	195
Villin 1	AGCCAGATCACTGCTGAGGT	TGGACAGGTGTTCCTCCTTC	169
ISX	CAGGAAGGAAGGAAGAGCAA	TGGGTAGTGGGTAAAGTGGAA	96
CYP3A4	CTGTGTGTTTCCAAGAGAAGTTAC	TGCATCAATTTCCTCCTGCAG	298
SLC15A1/PEPT1	CACCTCCTTGAAGAAGATGGCA	GGGAAGACTGGAAGAGTTTTATCG	105
SLC46A1/PCFT	GGTCTTTGCCTTTGCCACTA	AGAGTTTAGCCCGGATGACA	98
GAPDH	GAGTCAACGGATTTGGTCGT	GACAAGCTTCCCGTTCTCAG	185

Immunofluorescence staining: The cells differentiated with FGF2 and 2% FBS were washed three times with phosphate-buffered saline (PBS) without calcium or magnesium, fixed for 30 min at room temperature in 4% paraformaldehyde, and permeabilized in PBS containing 0.1% Triton X-100 for 5 min at room temperature. After being washed three times with PBS, the cells were blocked in PBS with 2% skim milk for 20 min at room temperature and were incubated with antisucrase–isomaltase antibody diluted at 1:200 for 60 min at room temperature. Rabbit serum was used as a negative control. The cells were washed three times with PBS and incubated with a 1:500 dilution of Alexa Fluor 568-labeled secondary antibody for 60 min at room temperature. After being washed three times with PBS, the cells were incubated with 1 μg/ml 4′,6-diamidino-2-phenylindole (DAPI) for 5 min at room temperature and washed with PBS. The cells were mounted on a glass slide using a 9:1 mixture of glycerol and PBS and viewed using an LSM 510Meta confocal microscope (Carl Zeiss Inc., Oberkochen, Germany).

Uptake study of β-Ala-Lys-AMCA: The cells differentiated with FGF2 and 2% FBS were rinsed several times with PBS and incubated with DMEM/F12 containing 25 μM β-Ala-Lys-AMCA for 4 h at 37°C. After incubation, uptake of β-Ala-Lys-AMCA was stopped by washing with ice-cold PBS. The cells were fixed for 30 min at room temperature in 4% paraformaldehyde, and immunofluorescence staining was performed using the primary and secondary antibodies as described above. The cells were then mounted using a 9:1 mixture of glycerol and PBS and viewed using an LSM 510Meta confocal microscope.

Statistical analysis: Levels of statistical significance were assessed using Student's *t*-test, and multiple comparisons were performed using analysis of variance (ANOVA) followed by Tukey's test.

Results

Early stages of differentiation into intestinal cells: For efficient, selective, and direct differentiation, a protocol designed to mimic intestinal development is desirable. We attempted differentiation into enterocytes that mediate the formation of the definitive endoderm. Because the intestine is an endoderm-derived organ, the human iPS cells were initially differentiated into the endoderm using a high concentration of activin A (100 ng/ml). Subsequently, we investigated the effects of FGF2, FGF4, and Wnt3a, which promote the development of mid- and hindgut lineages,[24,25] during differentiation from the definitive endoderm to intestinal stem cells. In these experiments, mRNA expression of caudal type homeobox 2 (CDX2), a major transcription factor of intestinal development and cell differentiation,[26,27] was slightly higher in FGF4-treated cells than that in FGF2-treated cells (**Fig. 2A**). In contrast, mRNA expression of LGR5 in FGF4-treated cells was significantly lower than that in FGF2-treated cells (**Fig. 2B**). Under all conditions, these mRNA expression levels were higher than those in undifferentiated human iPS cells. No effects of Wnt3a were observed on mRNA expression of CDX2 or LGR5 during the early stages of differentiation.

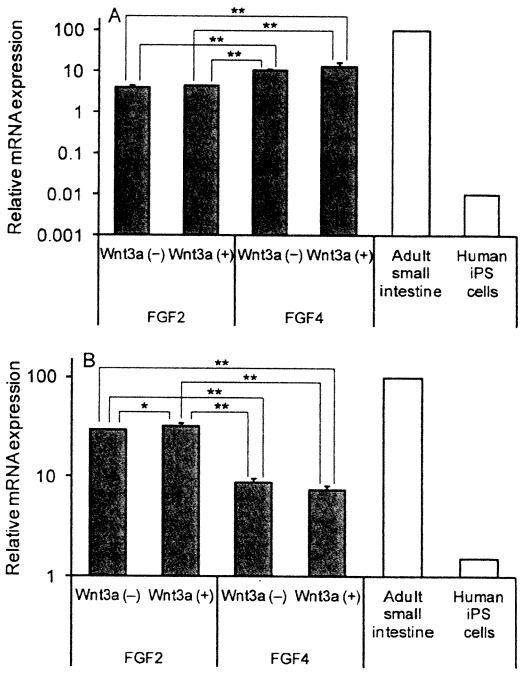


Fig. 2. Relative mRNA expression levels of CDX2 (A) and LGR5 (B) in differentiated intestinal stem cell-like cells
Human iPS cells were cultured in the presence of activin A for 3 days. The cells were further cultured in medium containing FGF2 or FGF4 with or without Wnt3a for 4 days and then in the presence of EGF for 1 day. After 8 days of differentiation, total RNA was extracted and mRNAs were analyzed by SYBR Green real-time RT-PCR. mRNA expression levels were normalized relative to that of GAPDH. Gene expression levels are represented relative to the level in the adult small intestine, which is set as 100. The adult small intestine and undifferentiated human iPS cells (shown as open columns) were used as positive and negative controls, respectively. Data are presented as the mean ± S.D. ($n = 3$), except for the adult small intestine and human iPS cells. Levels of statistical significance were compared among all groups: $^{**}p < 0.01$, $^{*}p < 0.05$.

Differentiation into enterocyte-like cells: To effectively differentiate human iPS cells into enterocyte-like cells, we examined

Copyright © 2014 by the Japanese Society for the Study of Xenobiotics (JSSX)

the effects of FBS concentration in the differentiation medium. Expression of LGR5 in differentiated human iPS cells did not differ in the presence of 2% or 10% FBS (**Fig. 3A**). However, mRNA expression of sucrase–isomaltase was 3.5-fold higher in 2% FBS than that in 10% FBS (**Fig. 3B**). In addition, mRNA expression levels of SLC15A1/peptide transporter 1 (PEPT1) and CYP3A4 were higher in the presence of 2% FBS (**Figs. 3C** and **3D**). In differentiated enterocyte-like cells, sucrase–isomaltase and CYP3A4, which were not detected in undifferentiated human iPS cells, were expressed, and mRNA expression levels of LGR5 and SLC15A1/PEPT1 were 30–40-fold higher than those in undifferentiated human iPS cells. Morphological changes in differentiating human iPS cells are shown in **Figure 4**. Similar to ES cells, undifferentiated human iPS cells had little cytoplasm and were small in size (**Fig. 4A**). When human iPS cells were cultured in the presence of activin A and FGF2, the cells gradually exhibited morphological changes such as enlargement and acquisition of spiky shapes (**Fig. 4B**). At the final stage of differentiation with EGF and 2% FBS, a number of dome-like structures formed and were assumed to contain liquids and cells (**Figs. 4C** and **4D**). In cells differentiated with activin A, FGF2, EGF, and 2% FBS, villin 1[28,29] and intestine specific homeobox (ISX)[30] were expressed, whereas intestinal fatty acid-binding protein (IFABP) was not expressed. Interestingly, mRNA expression levels of CDX2, dipeptidyl peptidase 4 (DPP4), and SLC46A1/proton-coupled folate transporter (PCFT) were similar to those in the adult small intestine, which was used as a positive control (**Fig. 5**). However, gene expression levels of UGT1A1 and ABCB1/multidrug resistance 1 (MDR1) were similar to those in undifferentiated human iPS cells (data not shown).

To determine the optimal duration of differentiation, we examined time-dependent variations in expression levels of specific small intestine genes such as LGR5, sucrase–isomaltase, and SLC15A1/PEPT1. After short-term culture (11 days), mRNA expression levels of sucrase–isomaltase and SLC15A1/PEPT1 were very low but gradually increased with differentiation until day 26. Similarly, CYP3A4 mRNA was not expressed after 11 days of differentiation but was expressed after 20 days (**Fig. 6**). LGR5 mRNA did not change with the duration of differentiation.

Immunofluorescence staining of sucrase–isomaltase in enterocyte-like cells: Sucrase–isomaltase is an essential carbohydrate digestion enzyme that is specifically expressed in brush border membranes of mature enterocytes. Therefore, sucrase–isomaltase expression is thought to be an indicator of differentiation into enterocytes. Indeed, protein expression of sucrase–isomaltase was confirmed in differentiated cells using immunofluorescence staining, in particular, in dense clusters of cells (**Fig. 7**).

Uptake of β-Ala-Lys-AMCA in enterocyte-like cells: Oligopeptide transporters are expressed in the brush border membrane and participate in peptide absorption from the intestinal lumen.[2] As shown in **Figure 3C**, expression of SLC15A1/PEPT1 mRNA in differentiated enterocyte-like cells was more than 30-fold higher than that in undifferentiated human iPS cells. To determine whether this leads to active peptide transport in differentiated cells, we performed peptide uptake assays using β-Ala-Lys-AMCA, a fluorescence-labeled substrate of the oligopeptide transporter.[31] As shown in **Figure 8**, intracellular uptake of β-Ala-Lys-AMCA was observed in cells expressing the sucrase–isomaltase proteins. However, uptake of β-Ala-Lys-AMCA at 4°C was low compared with that at 37°C (data not shown).

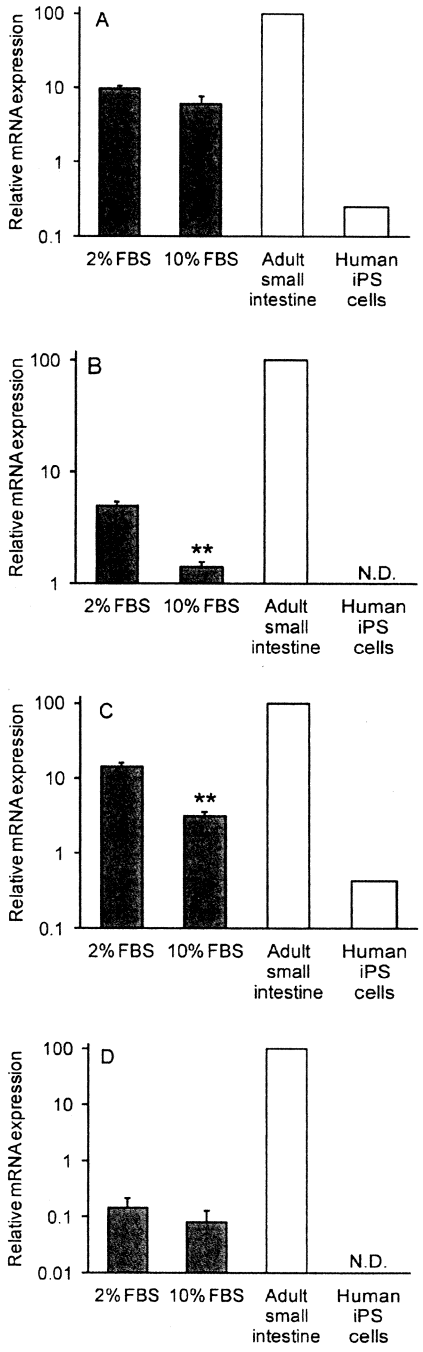


Fig. 3. Relative mRNA expression levels of LGR5 (A), sucrase–isomaltase (B), SLC15A1/PEPT1 (C), and CYP3A4 (D) in differentiated enterocyte-like cells cultured in 2% or 10% FBS

Human iPS cells were cultured in the presence of activin A for 3 days. The cells were further cultured in medium containing FGF2 for 4 days and then in the presence of 2% or 10% FBS and EGF for 17 days. After 24 days of differentiation, total RNA was extracted and mRNAs were analyzed by SYBR Green real-time RT-PCR. mRNA expression levels were normalized relative to that of GAPDH. Gene expression levels are represented relative to the level in the adult small intestine, which is set as 100. The adult small intestine and undifferentiated human iPS cells (shown as open columns) were used as positive and negative controls, respectively. Data are presented as the mean ± S.D. ($n = 3$), except for the adult small intestine and human iPS cells. N.D., not detected. Levels of statistical significance were compared with the 2% FBS group: $^{**}p < 0.01$.

Copyright © 2014 by the Japanese Society for the Study of Xenobiotics (JSSX)

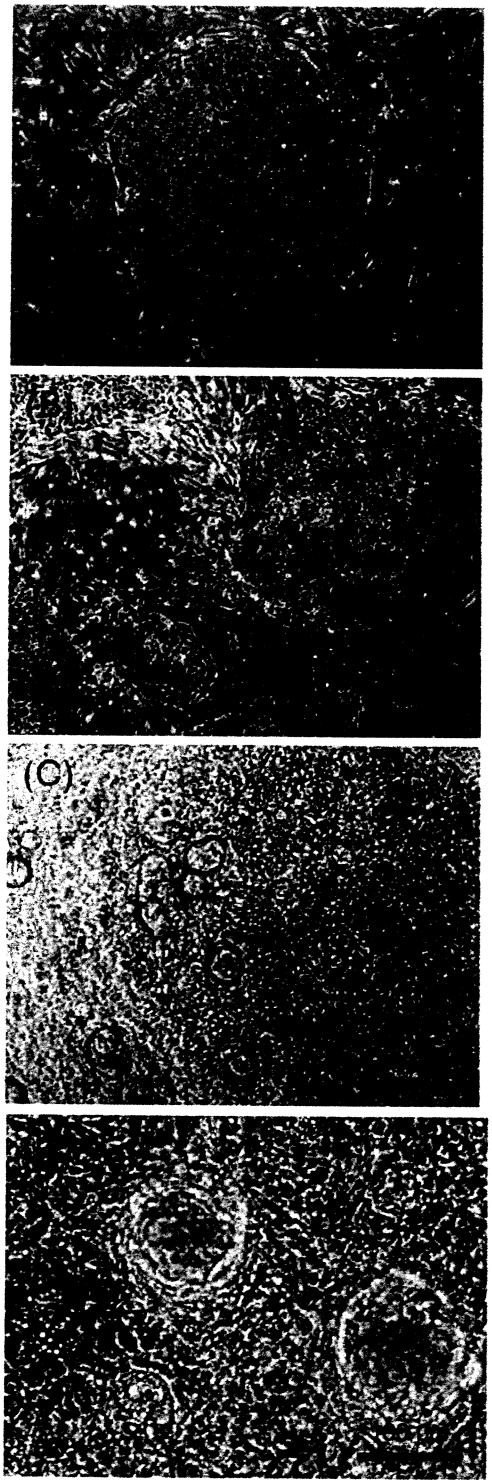


Fig. 4. Morphological changes in human iPS cells during differentiation into enterocyte-like cells
Human iPS cells were cultured in medium containing activin A for 3 days, FGF2 for 4 days, and 2% FBS and EGF for 17 days. (A) Undifferentiated human iPS cells; (B) midgut lineage cell-like cells after 7 days of differentiation; (C, D) enterocyte-like cells after 24 days of differentiation. Scale bar, 500 μm (A–C), 100 μm (D).

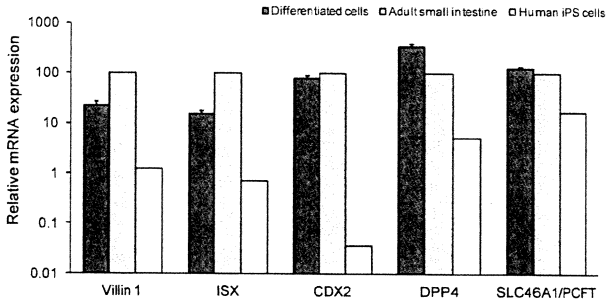


Fig. 5. Relative mRNA expression levels of the intestinal markers villin 1, ISX, CDX2, DPP4, and SLC46A1/PCFT in differentiated enterocyte-like cells
Human iPS cells were cultured in the presence of activin A for 3 days. The cells were further cultured in medium containing FGF2 for 4 days and then in the presence of 2% FBS and EGF for 19 days. After 26 days of differentiation, total RNA was extracted and mRNAs were analyzed by SYBR Green real-time RT-PCR. mRNA expression levels were normalized relative to that of GAPDH. Gene expression levels are represented relative to the level in the adult small intestine, which is set as 100. The adult small intestine and undifferentiated human iPS cells (shown as open columns) were used as positive and negative controls, respectively. Data are presented as the mean ± S.D. ($n = 3$), except for the adult small intestine and human iPS cells.

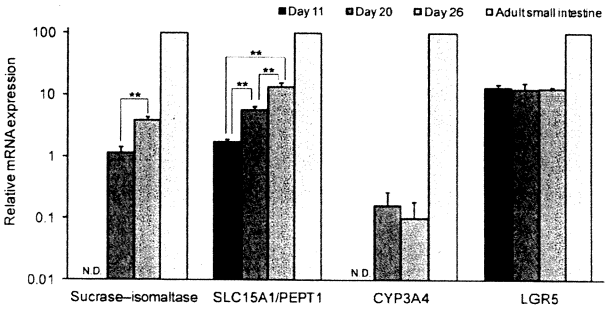


Fig. 6. Time-dependent variation in mRNA expression levels of sucrase–isomaltase, SLC15A1/PEPT1, CYP3A4, and LGR5 in differentiated enterocyte-like cells
Human iPS cells were cultured in the presence of activin A for 3 days. The cells were further cultured in medium containing FGF2 for 4 days and then in the presence of 2% FBS and EGF for 4, 13, or 19 days. After 11, 20, or 26 days of differentiation, total RNA was extracted and mRNAs were analyzed by SYBR Green real-time RT-PCR. mRNA expression levels were normalized relative to that of GAPDH. Gene expression levels are represented relative to the level in the adult small intestine, which is set as 100. The adult small intestine was used as a positive control. Data are presented as the mean ± S.D. ($n = 4$) except for the adult small intestine. N.D., not detected. Levels of statistical significance were compared among all groups: $^{**}p < 0.01$.

Discussion

Ueda *et al.*[14] reported the synthesis of gut-like organs from mouse iPS cells using the EB formulation technique with mouse ES cells. However, this hanging drop culture technique is hampered by its high requirement of skill, low EB formulation efficiency, unstable EB quality, and differing differentiation efficiencies between EBs. Spence *et al.*[15] reported the direct differentiation of human iPS cells into three-dimensional intestinal organoids. These organoids contained various cell types, including enterocytes, endocrine cells, goblet cells, and Paneth cells, although expression of drug-metabolizing enzymes and transporters, which are central to drug absorption and metabolism, was not examined. In their study, the intestinal crypt culture system, in which spheroids

Copyright © 2014 by the Japanese Society for the Study of Xenobiotics (JSSX)

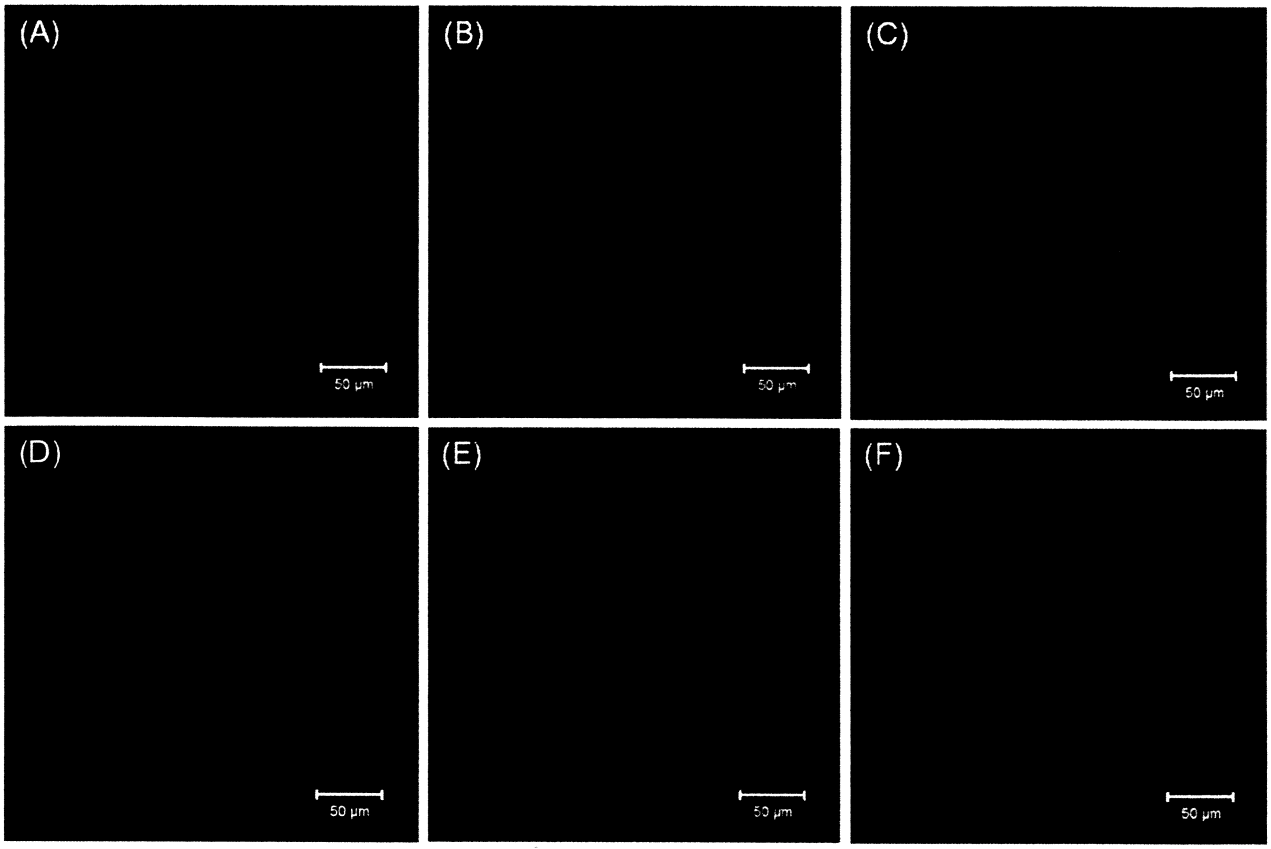


Fig. 7. Immunofluorescence analysis of sucrase–isomaltase in differentiated enterocyte-like cells
Human iPS cells were cultured in the presence of activin A for 3 days. The cells were further cultured in medium containing FGF2 for 4 days and then in the presence of 2% FBS and EGF for 19 days. After 26 days of differentiation, differentiated cells were stained with antisucrase–isomaltase antibody (A–C) or nonimmune rabbit serum as a negative control (D–F). Nuclei were counterstained with DAPI. (A) Immunofluorescence staining of sucrase–isomaltase (red); (D) immunofluorescence staining of rabbit serum as a negative control; (B, E) DAPI-stained DNA (blue); (C, F) overlay (Merge) image of sucrase–isomaltase and DAPI. Scale bar, 50 μm.

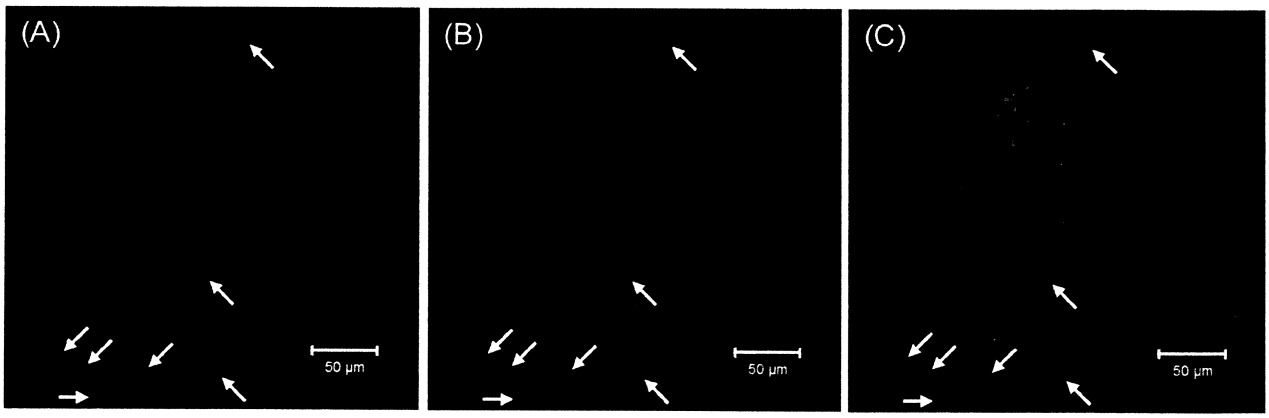


Fig. 8. Uptake of β-Ala-Lys-AMCA into differentiated enterocyte-like cells
Human iPS cells were cultured in the presence of activin A for 3 days. The cells were further cultured in medium containing FGF2 for 4 days and then in the presence of 2% FBS and EGF for 19 days. After 26 days of differentiation, the differentiated cells were incubated with β-Ala-Lys-AMCA (25 μM) for 4 h at 37°C. After uptake was stopped, the differentiated cells were fixed and stained with antisucrase–isomaltase antibody. Typical images from β-Ala-Lys-AMCA uptake experiments. Arrows indicate co-localization of β-Ala-Lys-AMCA and sucrase–isomaltase protein. (A) Intracellular uptake of β-Ala-Lys-AMCA (blue); (B) immunofluorescence staining of sucrase–isomaltase (red); (C) overlay (Merge) image of β-Ala-Lys-AMCA and sucrase–isomaltase. Scale bar, 50 μm.

Copyright © 2014 by the Japanese Society for the Study of Xenobiotics (JSSX)

are formed by three-dimensional culture, was applied during differentiation from the endoderm to intestinal organoids, and several factors were added in large quantities to induce differentiation. This method may be suitable for the culture of intestinal stem cells but not for selective differentiation into enterocytes, and it is complicated and costly. Therefore, we generated enterocyte-like cells using a simple two-dimensional culture method.

Spence *et al.*[15] also reported that the combination of FGF4 (500 ng/ml) and Wnt3a (500 ng/ml) effectively posteriorized the endoderm. Ameri *et al.*[32] reported the induction of CDX2 with FGF2 (256 ng/ml) in a concentration-dependent manner in the human ES cell-derived endoderm. In the present study, we examined the effects of FGF2, FGF4, and Wnt3a on the induction of the midgut endoderm lineage. Our results showed that the expression level of CDX2 was comparable in the FGF2 and FGF4 treatment groups, whereas no effect of Wnt3a was observed. These results were inconsistent with those of Spence *et al.*,[15] possibly because of the lower concentrations of Wnt3a used in our study (50 ng/ml). Sherwood *et al.*[33] demonstrated that β-catenin-dependent Wnt signaling, activated by the glycogen synthase kinase-3 (GSK3) inhibitor, induced the expression of the intestinal master regulator Cdx2 and induced intestinal differentiation of the ES cell-derived endoderm and large intestinal gene expression. They also indicated that because of poor bioactivity, the induction level of Cdx2 expression by Wnt3a was lower than that by the GSK3 inhibitor. Therefore, superior stability and bioactivity of small-molecule compounds may lead to more effective experimental regulation of these signaling pathways. However, the striking activation of Wnt signaling also induced large intestinal gene expression, and further investigations of the extent of activation of Wnt signaling during small intestinal differentiation may be required. The expression of LGR5[17] was higher in the FGF2 treatment group than that in the FGF4 treatment group. Therefore, subsequent differentiation experiments were performed using FGF2.

We have demonstrated that enterocyte-like cells, which express the specific intestinal markers sucrase–isomaltase,[34,35] villin 1, ISX, and pharmacokinetics-related genes, were differentiated from an intestinal stem cell-like cell population by two-dimensional culture with EGF and a low serum concentration. Sucrase–isomaltase and SLC15A1/PEPT1 mRNA gradually increased with the duration of differentiation, indicating that longer duration may be necessary to efficiently obtain mature enterocytes. In contrast, LGR5 mRNA expression remained unchanged, suggesting that enterocytes matured during intestinal stem cell proliferation. DPP4 (serine protease) and SLC46A1/PCFT (folate transporter) are known to be abundantly expressed in epithelial cells of the small intestine.[36,37] Expression of DPP4 and SLC46A1/PCFT in differentiated cells was higher than that in adult small intestine samples. Intestinal differentiation was promoted by low FBS concentrations in this study. Potentially, the growth of extra-enterocytic cells such as fibroblasts may be suppressed with decreasing FBS concentrations, and some differentiation and growth-inhibiting factors may be present in FBS, although the mechanisms underlying these effects remain unclear.

At present, human intestinal epithelial cells are difficult to obtain, and no appropriate model cell system exists. Instead, other tissue cell-derived cell lines, including Caco-2 cells (human colon carcinoma cell line) and Madin–Darby canine kidney (MDCK) cells, have been used as intestinal models in drug absorption studies.[2,38] However, drug transporter expression patterns in these cells considerably differ from those in enterocytes. In particular, CYP3A4 is expressed at very low levels in these cell lines. In the present study, cells expressing the sucrase–isomaltase protein showed uptake of β-Ala-Lys-AMCA, the substrate of the oligopeptide transporter (**Fig. 8**). Differentiated cells also expressed CYP3A4 mRNA, albeit at levels lower than those in the adult small intestine (**Fig. 3**), suggesting that enterocyte-like cells differentiated from human iPS cells have peptide-transporting activity and may be useful in the study of drug absorbability.

In this study, we used a human iPS cell line, which is easily differentiated into hepatocytes of an endodermal lineage, because the intestine is also an endoderm-derived tissue. Differentiation propensity is known to be markedly different among human ES and iPS cell lines.[39,40] Thus, there may be a difference in the degree of intestinal differentiation depending on the human iPS cell line being tested. Regarding this point, we believe it is necessary to perform studies comparing intestinal differentiation among human iPS cell lines in the future.

In conclusion, because the intestine is an endoderm-derived tissue, human iPS cells were directly differentiated into the endoderm using activin A. Subsequently, we devised a simple method for differentiation into enterocyte-like cells with functional peptide transport by two-dimensional culture and the addition of several growth factors. These data suggest that human iPS-derived enterocytes may facilitate future drug development studies. If enterocyte-like cells, which have functional features similar to those of enterocytes, can be generated from human iPS cells, it may be possible to construct systems for easy estimation of overall intestinal function, including absorption and metabolism.

References

1) Paine, M. F., Hart, H. L., Ludington, S. S., Haining, R. L., Rettie, A. E. and Zeldin, D. C.: The human intestinal cytochrome P450 'pie'. *Drug Metab. Dispos.*, **34**: 880–886 (2006).
2) Giacomini, K. M., Huang, S.-M., Tweedie, D. J., Benet, L. Z., Brouwer, K. L. R., Chu, X., Dahlin, A., Evers, R., Fischer, V., *et al.*: Membrane transporters in drug development. *Nat. Rev. Drug Discov.*, **9**: 215–236 (2010).
3) Takahashi, K., Tanabe, K., Ohnuki, M., Narita, M., Ichisaka, T., Tomoda, K. and Yamanaka, S.: Induction of pluripotent stem cells from adult human fibroblasts by defined factors. *Cell*, **131**: 861–872 (2007).
4) Ochiya, T., Yamamoto, Y. and Banas, A.: Commitment of stem cells into functional hepatocytes. *Differentiation*, **79**: 65–73 (2010).
5) Tateishi, K., He, J., Taranova, O., Liang, G., D'Alessio, A. C. and Zhang, Y.: Generation of insulin-secreting islet-like clusters from human skin fibroblasts. *J. Biol. Chem.*, **283**: 31601–31607 (2008).
6) Zhang, D., Jiang, W., Liu, M., Sui, X., Yin, X., Chen, S., Shi, Y. and Deng, H.: Highly efficient differentiation of human ES cells and iPS cells into mature pancreatic insulin-producing cells. *Cell Res.*, **19**: 429–438 (2009).
7) Chambers, S. M., Fasano, C. A., Papapetrou, E. P., Tomishima, M., Sadelain, M. and Studer, L.: Highly efficient neural conversion of human ES and iPS cells by dual inhibition of SMAD signaling. *Nat. Biotechnol.*, **27**: 275–280 (2009).
8) Zhang, J., Wilson, G. F., Soerens, A. G., Koonce, C. H., Yu, J., Palecek, S. P., Thomson, J. A. and Kamp, T. J.: Functional cardiomyocytes derived from human induced pluripotent stem cells. *Circ. Res.*, **104**: e30–e41 (2009).
9) Song, Z., Cai, J., Liu, Y., Zhao, D., Yong, J., Duo, S., Song, X., Guo, Y., Zhao, Y., *et al.*: Efficient generation of hepatocyte-like cells from human induced pluripotent stem cells. *Cell Res.*, **19**: 1233–1242 (2009).
10) Sullivan, G. J., Hay, D. C., Park, I.-H., Fletcher, J., Hannoun, Z., Payne, C. M., Dalgetty, D., Black, J. R., Ross, J. A., *et al.*: Generation of functional human hepatic endoderm from human induced pluripotent stem cells. *Hepatology*, **51**: 329–335 (2010).
11) Si-Tayeb, K., Noto, F. K., Nagaoka, M., Li, J., Battle, M. A., Duris, C., North, P. E., Dalton, S. and Duncan, S. A.: Highly efficient generation of human hepatocyte-like cells from induced pluripotent stem cells.

Copyright © 2014 by the Japanese Society for the Study of Xenobiotics (JSSX)

Hepatology, **51**: 297–305 (2010).
12) Touboul, T., Hannan, N. R. F., Corbineau, S., Martinez, A., Martinet, C., Branchereau, S., Mainot, S., Strick-Marchand, H., Pedersen, R., *et al.*: Generation of functional hepatocytes from human embryonic stem cells under chemically defined conditions that recapitulate liver development. *Hepatology*, **51**: 1754–1765 (2010).
13) Takayama, K., Inamura, M., Kawabata, K., Tashiro, K., Katayama, K., Sakurai, F., Hayakawa, T., Furue, M. K. and Mizuguchi, H.: Efficient and directive generation of two distinct endoderm lineages from human ESCs and iPSCs by differentiation stage-specific SOX17 transduction. *PLoS ONE*, **6**: e21780 (2011).
14) Ueda, T., Yamada, T., Hokuto, D., Koyama, F., Kasuda, S., Kanehiro, H. and Nakajima, Y.: Generation of functional gut-like organ from mouse induced pluripotent stem cells. *Biochem. Biophys. Res. Commun.*, **391**: 38–42 (2010).
15) Spence, J. R., Mayhew, C. N., Rankin, S. A., Kuhar, M. F., Vallance, J. E., Tolle, K., Hoskins, E. E., Kalinichenko, V. V., Wells, S. I., *et al.*: Directed differentiation of human pluripotent stem cells into intestinal tissue in vitro. *Nature*, **470**: 105–109 (2011).
16) Scoville, D. H., Sato, T., He, X. C. and Li, L.: Current view: intestinal stem cells and signaling. *Gastroenterology*, **134**: 849–864 (2008).
17) Barker, N., van Es, J. H., Kuipers, J., Kujala, P., van den Born, M., Cozijnsen, M., Haegebarth, A., Korving, J., Begthel, H., *et al.*: Identification of stem cells in small intestine and colon by marker gene Lgr5. *Nature*, **449**: 1003–1007 (2007).
18) Sato, T., Vries, R. G., Snippert, H. J., van de Wetering, M., Barker, N., Stange, D. E., van Es, J. H., Abo, A., Kujala, P., *et al.*: Single Lgr5 stem cells build crypt-villus structures in vitro without a mesenchymal niche. *Nature*, **459**: 262–265 (2009).
19) Sato, T., Stange, D. E., Ferrante, M., Vries, R. G. J., van Es, J. H., van den Brink, S., van Houdt, W. J., Pronk, A., van Gorp, J., *et al.*: Long-term expansion of epithelial organoids from human colon, adenoma, adenocarcinoma, and Barrett's epithelium. *Gastroenterology*, **141**: 1762–1772 (2011).
20) D'Amour, K. A., Agulnick, A. D., Eliazer, S., Kelly, O. G., Kroon, E. and Baetge, E. E.: Efficient differentiation of human embryonic stem cells to definitive endoderm. *Nat. Biotechnol.*, **23**: 1534–1541 (2005).
21) McLean, A. B., D'Amour, K. A., Jones, K. L., Krishnamoorthy, M., Kulik, M. J., Reynolds, D. M., Sheppard, A. M., Liu, H., Xu, Y., *et al.*: Activin A efficiently specifies definitive endoderm from human embryonic stem cells only when phosphatidylinositol 3-kinase signaling is suppressed. *Stem Cells*, **25**: 29–38 (2007).
22) Ishizaki, T., Uehata, M., Tamechika, I., Keel, J., Nonomura, K., Maekawa, M. and Narumiya, S.: Pharmacological properties of Y-27632, a specific inhibitor of rho-associated kinases. *Mol. Pharmacol.*, **57**: 976–983 (2000).
23) Watanabe, K., Ueno, M., Kamiya, D., Nishiyama, A., Matsumura, M., Wataya, T., Takahashi, J. B., Nishikawa, S., Nishikawa, S., *et al.*: A ROCK inhibitor permits survival of dissociated human embryonic stem cells. *Nat. Biotechnol.*, **25**: 681–686 (2007).
24) Dessimoz, J., Opoka, R., Kordich, J. J., Grapin-Botton, A. and Wells, J. M.: FGF signaling is necessary for establishing gut tube domains along the anterior–posterior axis in vivo. *Mech. Dev.*, **123**: 42–55 (2006).
25) McLin, V. A., Rankin, S. A. and Zorn, A. M.: Repression of Wnt/β-catenin signaling in the anterior endoderm is essential for liver and pancreas development. *Development*, **134**: 2207–2217 (2007).
26) Escaffit, F., Paré, F., Gauthier, R., Rivard, N., Boudreau, F. and Beaulieu, J.-F.: Cdx2 modulates proliferation in normal human intestinal epithelial crypt cells. *Biochem. Biophys. Res. Commun.*, **342**: 66–72 (2006).
27) Gao, N., White, P. and Kaestner, K. H.: Establishment of intestinal identity and epithelial-mesenchymal signaling by Cdx2. *Dev. Cell*, **16**: 588–599 (2009).
28) Robine, S., Huet, C., Moll, R., Sahuquillo-Merino, C., Coudrier, E., Zweibaum, A. and Louvard, D.: Can villin be used to identify malignant and undifferentiated normal digestive epithelial cells? *Proc. Natl. Acad. Sci. USA*, **82**: 8488–8492 (1985).
29) Boller, K., Arpin, M., Pringault, E., Mangeat, P. and Reggio, H.: Differential distribution of villin and villin mRNA in mouse intestinal epithelial cells. *Differentiation*, **39**: 51–57 (1988).
30) Seino, Y., Miki, T., Kiyonari, H., Abe, T., Fujimoto, W., Kimura, K., Takeuchi, A., Takahashi, Y., Oiso, Y., *et al.*: Isx participates in the maintenance of vitamin A metabolism by regulation of beta-carotene 15,15'-monooxygenase (Bcmo1) expression. *J. Biol. Chem.*, **283**: 4905–4911 (2008).
31) Groneberg, D. A., Döring, F., Eynott, P. R., Fischer, A. and Daniel, H.: Intestinal peptide transport: ex vivo uptake studies and localization of peptide carrier PEPT1. *Am. J. Physiol. Gastrointest. Liver Physiol.*, **281**: G697–G704 (2001).
32) Ameri, J., Ståhlberg, A., Pedersen, J., Johansson, J. K., Johannesson, M. M., Artner, I. and Semb, H.: FGF2 specifies hESC-derived definitive endoderm into foregut/midgut cell lineages in a concentration-dependent manner. *Stem Cells*, **28**: 45–56 (2010).
33) Sherwood, R. I., Maehr, R., Mazzoni, E. O. and Melton, D. A.: Wnt signaling specifies and patterns intestinal endoderm. *Mech. Dev.*, **128**: 387–400 (2011).
34) Boudreau, F., Rings, E. H. H. M., van Wering, H. M., Kim, R. K., Swain, G. P., Krasinski, S. D., Moffett, J., Grand, R. J., Suh, E. R., *et al.*: Hepatocyte nuclear factor-1α, GATA-4, and caudal related homeodomain protein Cdx2 interact functionally to modulate intestinal gene transcription. *J. Biol. Chem.*, **277**: 31909–31917 (2002).
35) Gu, N., Adachi, T., Matsunaga, T., Tsujimoto, G., Ishihara, A., Yasuda, K. and Tsuda, K.: HNF-1α participates in glucose regulation of sucrase-isomaltase gene expression in epithelial intestinal cells. *Biochem. Biophys. Res. Commun.*, **353**: 617–622 (2007).
36) Qiu, A., Jansen, M., Sakaris, A., Min, S. H., Chattopadhyay, S., Tsai, E., Sandoval, C., Zhao, R., Akabas, M. H., *et al.*: Identification of an intestinal folate transporter and the molecular basis for hereditary folate malabsorption. *Cell*, **127**: 917–928 (2006).
37) Darmoul, D., Voisin, T., Couvineau, A., Rouyer-Fessard, C., Salomon, R., Wang, Y., Swallow, D. M. and Laburthe, M.: Regional expression of epithelial dipeptidyl peptidase IV in the human intestines. *Biochem. Biophys. Res. Commun.*, **203**: 1224–1229 (1994).
38) Volpe, D. A.: Drug-permeability and transporter assays in Caco-2 and MDCK cell lines. *Future Med. Chem.*, **3**: 2063–2077 (2011).
39) Osafune, K., Caron, L., Borowiak, M., Martinez, R. J., Fitz-Gerald, C. S., Sato, Y., Cowan, C. A., Chien, K. R. and Melton, D. A.: Marked differences in differentiation propensity among human embryonic stem cell lines. *Nat. Biotechnol.*, **26**: 313–315 (2008).
40) Kajiwara, M., Aoi, T., Okita, K., Takahashi, R., Inoue, H., Takayama, N., Endo, H., Eto, K., Toguchida, J., *et al.*: Donor-dependent variations in hepatic differentiation from human-induced pluripotent stem cells. *Proc. Natl. Acad. Sci. USA*, **109**: 12538–12543 (2012).

Copyright © 2014 by the Japanese Society for the Study of Xenobiotics (JSSX)

Supplemental material to this article can be found at:
http://dmd.aspetjournals.org/content/suppl/2013/11/19/dmd.113.054833.DC1.html

1521-009X/42/2/229–238$25.00
DRUG METABOLISM AND DISPOSITION
Copyright © 2013 by The American Society for Pharmacology and Experimental Therapeutics
http://dx.doi.org/10.1124/dmd.113.054833
Drug Metab Dispos 42:229–238, February 2014

Alteration of the Function of the UDP-Glucuronosyltransferase 1A Subfamily by Cytochrome P450 3A4: Different Susceptibility for UGT Isoforms and UGT1A1/7 Variants[S]

Yuji Ishii, Hiroki Koba, Kousuke Kinoshita, Toshiya Oizaki, Yuki Iwamoto, Shuso Takeda,[1] Yuu Miyauchi, Yoshio Nishimura, Natsuki Egoshi, Futoshi Taura,[2] Satoshi Morimoto, Shin'ichi Ikushiro, Kiyoshi Nagata, Yasushi Yamazoe, Peter I. Mackenzie, and Hideyuki Yamada

Laboratory of Molecular Life Sciences (Y.Is., H.K., K.K., T.O., Y.Iw., S.T., Y.M., Y.N., N.E., H.Y.) and Laboratory of Medicinal Resource Regulation (F.T., S.M.), Graduate School of Pharmaceutical Sciences, Kyushu University, Fukuoka, Japan; Biotechnology Research Center, Faculty of Engineering, Toyama Prefectural University, Imizu, Toyama, Japan (S.I.); Tohoku Pharmaceutical University, Sendai, Japan (K.N.); Graduate School of Pharmaceutical Sciences, Tohoku University, Sendai, Japan (Y.Y.); and Department of Clinical Pharmacology, Flinders Medical Centre and Flinders University, Adelaide, Australia (P.I.M.).

Received September 24, 2013; accepted November 19, 2013

ABSTRACT

Functional protein-protein interactions between UDP-glucuronosyltransferase (UGT)1A isoforms and cytochrome P450 (CYP)3A4 were studied. To this end, UGT1A-catalyzed glucuronidation was assayed in Sf-9 cells that simultaneously expressed UGT and CYP3A4. In the kinetics of UGT1A6-catalyzed glucuronidation of serotonin, both Michaelis constant (K_m) and maximal velocity (V_{max}) were increased by CYP3A4. When CYP3A4 was coexpressed with either UGT1A1 or 1A7, the V_{max} for the glucuronidation of the irinotecan metabolite (SN-38) was significantly increased. S_{50} and K_m both which are the substrate concentration giving 0.5 V_{max} were little affected by simultaneous expression of CYP3A4. This study also examined the catalytic properties of the allelic variants of UGT1A1 and 1A7 and their effects on the interaction with CYP3A4. Although the UGT1A1-catalyzing activity of 4-methylumbelliferone glucuronidation was reduced in its variant, UGT1A1*6, the coexpression of CYP3A4 restored the impaired function to a level comparable with the wild type. Similarly, simultaneous expression of CYP3A4 increased the V_{max} of UGT1A7*1 (wild type) and *2 (N129K and R131K), whereas the same was not observed in UGT1A7*3 (N129K, R131K, and W208R). In the kinetics involving different concentrations of UDP-glucuronic acid (UDP-GlcUA), the K_m for UDP-GlcUA was significantly higher for UGT1A7*2 and *3 than *1. The K_m of UGT1A7*1 and *3 was increased by CYP3A4, whereas *2 did not exhibit any such change. These results suggest that (1) CYP3A4 changes the catalytic function of the UGT1A subfamily in a UGT isoform-specific manner and (2) nonsynonymous mutations in UGT1A7*3 reduce not only the ability of UGT to use UDP-GlcUA but also CYP3A4-mediated enhancement of catalytic activity, whereas CYP3A4 is able to restore the UGT1A1*6 function.

Downloaded from dmd.aspetjournals.org at ASPET Journals on April 23, 2015

Introduction

Glucuronidation is one of the major pathways contributing to the elimination of many exogenous and endogenous compounds. This step is catalyzed by UDP-glucuronosyltransferases (UGTs). The UGT isoforms are classified into two families (UGT1 and UGT2) based on sequence identity (Mackenzie et al., 1997, 2005). These UGTs exhibit an overlapping but distinct substrate specificity (Tukey and Strassburg, 2000). For example, human UGT1A1 is the predominant enzyme for bilirubin conjugation (Ritter et al., 1991), and this UGT also plays an important role in the hepatic glucuronidation of SN-38, an active metabolite of irinotecan (Camptosar; Pfizer, New York, NY) (Guillemette, 2003; Rosner et al., 2008). A partial reduction in UGT1A1 activity is believed to cause moderate hyperbilirubinemia, so called Gilbert syndrome (Iyanagi et al., 1998). Of the allelic variants reported thus far, UGT1A1*6 (G71R) and *28 (wild-type protein incapable of being highly expressed due to promoter mutation) are reported to exhibit only

This work was supported in part by the Japan Society for Promotion of Science [Grants-in-Aid for Scientific Research (B) Research No. 25293039 and Grants-in-Aid for Scientific Research (C) Research No. 21590164 to Y. I.].

Presented in part at the 25th Annual Meeting of the Japanese Society for the Study of Xenobiotics, Ohmiya, Japan October, 2010 (Koba et al.); the 27th Kyushu Regional Meeting for the Pharmaceutical Society of Japan, Nagasaki, Japan, December 2010 (Koba et al.); the 19th Microsomes and Drug Oxidations (MDO) and 12th European International Society for the Study of Xenobiotics (ISSX) Meeting, Noordwijk aan Zee, The Netherlands, June 2012 (Ishii et al.); the 28th Annual Meeting of the Japanese Society for the Study of Xenobiotics, Tokyo, Japan, October 2013 (Kinoshita et al.)

[1]Current affiliation: Faculty of Pharmaceutical Sciences, Hiroshima International University, Kure, Hiroshima, Japan.

[2]Current affiliation; Faculty of Pharmaceutical Sciences, Toyama University, Toyama, Japan.

dx.doi.org/10.1124/dmd.113.054833.

[S]This article has supplemental material available at dmd.aspetjournals.org.

ABBREVIATIONS: bp, base pair; ER, endoplasmic reticulum; GST, glutathione S-transferase; HPLC, high-performance liquid chromatography; 5-HT, serotonin; K_m, Michaelis constant; 4-MU, 4-methylumbelliferone; 4-OHBP, 4-hydroxybiphenyl; P450 or CYP, cytochrome P450; PCR, polymerase chain reaction; S_{50}, substrate concentration giving 0.5 V_{max}; SDS-PAGE, sodium dodecylsulfate-polyacrylamide gel electrophoresis; UDP-GlcUA, UDP-glucuronic acid; UGT, UDP-glucuronosyltransferase; V_{max}, maximum velocity.

reduced SN-38 glucuronidation (Gagné et al., 2002; Jinno et al., 2003). However, interindividual differences in UGT1A1 activity seem unable to be explained fully by these polymorphisms. UGT1A6 catalyzes the glucuronidation of phenolic compounds such as serotonin (5-HT) (Basu et al., 2004; Hanioka et al., 2006), and UGT1A7 is involved in the conjugation of compounds such as mycophenolic acid and SN-38 (Basu et al., 2004; Emi et al., 2007; Rosner et al., 2008; Joy et al., 2010). Although UGT1A1 and 1A6 are mainly expressed in the liver, UGT1A7 is expressed in extrahepatic tissues especially in the gastrointestinal tract (Tukey and Strassburg, 2000). There are several polymorphisms of UGT1A7 (Vogel et al., 2001) and, of the allelic variants, the frequency of UGT1A7*3 is approximately 35% and 26% in Caucasian and Japanese populations, respectively (Guillemette, 2003; Huang et al., 2005). A previous study demonstrated that UGT1A7*3 lacks activity toward phenolic compounds that are typical UGT substrates, such as 4-methylumbelliferone (4-MU) (Strassburg et al., 2002). If this is true, UGT1A7*3 may be a risk factor for cancer because of the reduced ability to detoxify carcinogenic phenols (Vogel et al., 2001; Strassburg et al., 2002; Ockenga et al., 2003; Chen et al., 2006). Indeed, epidemiologic studies have provided evidence of a significant association between an allelic variant UGT1A7*3 and carcinogenesis (Ockenga et al., 2003; Chen et al., 2006). However, controversial results showing no relationship between UGT1A7*3 and cancer risk have also been reported (Verlaan et al., 2005; te Morsche et al., 2008).

Some research groups claim that UGT1A7*3 exhibits substantial activity toward SN-38, although it is significantly lower than that of the wild type (Gagne et al., 2002; Villeneuve et al., 2003). In addition, Uchaipichat et al. (2004) investigated the activity of UGT1A7*3-catalyzed 4-MU glucuronidation. We obtained the same cDNA from that laboratory and confirmed its sequence to be UGT1A7*3. Therefore, there remains a discrepancy concerning the catalytic activity of UGT1A7*3 among researchers. Thus, the risk for cancer and irinotecan toxicity associated with poorly active UGT1A7 variants is still an important hypothesis that needs detailed investigation (Gagne et al., 2002; Vogel et al., 2011, references therein).

Cytochromes P450 (P450s, CYPs) are very important drug metabolizing enzymes because they are involved in the metabolism of most drugs (Evans and Relling, 1999). Of these P450s, CYP3A4 is the most abundant and involved in the metabolism of many drugs (Shimada et al., 1994). After our first report of interactions between P450 and UGT (Taura et al., 2000), we demonstrated that the regioselectivity of UGT2B7-catalyzed morphine glucuronidation is altered by CYP3A4, and the *J*-helix of this P450 may contribute to the interaction with the UGT (Takeda et al., 2005, 2009). In these studies, the interaction between CYP3A4 and UGT2B7 was proven by overlay assay, coimmunoprecipitation, and crosslinking. Another group also showed that UGT1A1, UGT1A6, as well as UGT2B7 in solubilized human liver microsomes can be coimmunoprecipitated with CYP3A4 coupled to its antibody (Fremont et al., 2005). Furthermore, our preliminary evidence suggested that CYP3A4 interacts with UGT1A7. Thus, CYP3A4 appears to interact with UGT1A1, 1A6, and 1A7. However, to the best of our knowledge, it remains unknown whether CYP3A4 is able to modify the functions of the UGT1A subfamily. Therefore, this study examined the effect of CYP3A4 on the activity of UGT1A1, 1A6, and 1A7. To this end, we established baculovirus-Sf-9 cells coexpressing UGT1A1, 1A6, and UGT1A7 as well as CYP3A4. Expression systems for UGT allelic variants, UGT1A1 (*6) and UGT1A7 (*2 and *3), were also established to examine the effect of the mutations on the P450-UGT interaction.

Materials and Methods

4-MU and 4-MU glucuronide were purchased from Sigma-Aldrich Co. Ltd. (St. Louis, MO) and Nacalai Tesque Co. Ltd. (Kyoto, Japan), respectively. SN-38 and its glucuronide were generous gifts from Yakult Honsha Co. Ltd (Tokyo, Japan). 4-Hydroxybiphenyl (4-OHBP) was purchased from Wako Pure Chemical Co. Ltd (Tokyo, Japan). 4-OHBP glucuronide was purified in this laboratory from urine obtained from rabbits given 4-OHBP, according to Dodgson et al. (1948). UGT1A7 supersome and pooled human intestinal microsomes were purchased from BD Gentest (BD Bioscience, Franklin Lakes, NJ). All other reagents were of the highest quality commercially available.

Construction of Expression Plasmids. The open reading frame of UGT1A7 (1.6 kbp) was amplified by polymerase chain reaction (PCR) using pIRES-UGT1A7 (Uchaipichat et al., 2004) as a template and the following primers: [BamHI-G-UGT1A7 (-2,17): 5′-CGG GAT CCG TGA TGG CTC GTG CAG GGT G-3′ and BamHI-UGT1A7 (1599,1580): 5′-CGG GAT CCC ACT TCT CAA TGG GTC TTG G-3′]. The numbers in parentheses represent the position of the first and last bases counted from the initiation codon (+1ATG), and underlines represent the *BamHI* restriction sites introduced. *Pfu* turbo DNA-polymerase (Stratagene, Agilent Technologies, Santa Clara, CA) was used for the PCR amplification. The PCR products were then digested with BamHI and cloned into the pFastBac1 vector. The sequence was confirmed to be UGT1A7*3, although it carries a synonymous base change at C33A. Then, UGT1A7*1 and *2 cDNAs (-2nd and 1599th) were prepared by the mega-primer method using pFastBac1-UGT1A7*3 as a template. To obtain the mega-primer, UGT1A7-Meg#1 (249 bp) covering a range between the 385th and 633rd base was used, and PCR was performed using the following primers: UGT1A7F (385-408): 5′-AAT GAC CGA AAA TTA GTA GAA TAC-3′ and UGT1A7R (633-613): 5′-GAT GTG GTT CCA TAC TCT CTC-3′. Another mega-primer pFastBac1-UGT1A7 Meg#2 (689 bp) having a sequence coupling a vector region (3979–4032) and the *2 region (-2–633) was prepared by PCR amplification using the following primers: pFastBacF (3979–4002) 5′-TAA AAA AAC CTA TAA ATA TTC CGG-3′ and mega-primer UGT1A7 Meg#1. Then, to prepare the full-length cDNA, pFastBac1-UGT1A7*2, PCR was carried out using the following primers: pFastBacR(4167-4139) 5′-TTA GGA TCC TCT AGT ACT TCT CGA CAA GC-3′ and pFastBac1-UGT1A7-Meg#2. The full-length cDNA obtained was restricted with *BamHI* and inserted into the *BamHI* site of the pFastBac1 vector. The expressing vector for UGT1A7*1 was prepared as above, using pFastBac1-UGT1A7*2 as a template. The vectors for the expression of UGT1A1*1 and 1A6 were constructed by the methods described below. The *XhoI*/*SalI* fragment of UGT1A1*1 cDNA from pTargeT-UGT1A1 (Nishimura et al., 2007) was inserted into the XhoI/SalI site of pFastBac1 vector. The UGT1A6 cDNA introduced with *BamHI* sites was amplified with *pfu* DNA polymerase from pIRES-UGT1A6 (Uchaipichat et al., 2004), and subcloned into the *BamHI* site of the pFastBac1-vector. pFastBac1-UGT1A1*6 (G211A) was engineered by a site-directed mutagenesis procedure (Agilent Technology, Santa Clara, CA) using the following primers: [UGT1A1F (192,230): 5′-CTC GTT GTA CAT CAG AGA CAG AGC ATT TTA CAC CTT GAA-3′ and UGT1A1R (230,192): 5′-TTC AAG GTG TAA AAT GCT CTG TCT CTG ATG TAC AAC GAG-3′]. The cDNA of CYP3A4 inserted with SalI and KpnI restriction sites was amplified with *pfu* DNA polymerase from pCMV4-CYP3A4 (Takeda et al., 2005). This was digested with *SalI*/*Kpn*I and then inserted into the *SalI*/*Kpn*I sites of the pFastBac1-vector. All sequences of the expression plasmids were verified by DNA sequencing using an ABI 3130xl Genetic analyzer [Applied Biosystems, Life Technologies (NASDAQ: LIFE), Carlsbad, CA].

Expression of CYP3A4 and UGT1As in Sf-9 Cells. The expression of UGT and CYP3A4 was carried out in a Bac-to-Bac system (Invitrogen). Briefly, a recombinant pFastBac1 clone carrying UGT/P450 cDNA(s) with the right orientation was transfected into the competent *Escherichia coli* of the MAX Efficiency DH10Bac strain. Then, Sf-9 cells (2×10^6) were transfected with Bacumid produced by the *E. coli* using Cellfection reagent (Invitrogen). Primary virus was collected 48 hours after transfection. To obtain a high titer of recombinant baculovirus for UGTs and CYP3A4, several rounds of amplification were repeated. For protein expression, baculovirus-infected Sf-9 cells were collected 60 hours after infection and washed with phosphate-buffered saline. The phosphate-buffered saline was prepared according to the manual (Sambrook et al., 1989). We routinely cultured Sf-9 cells transfected with baculovirus in a volume of 200 ml (2.0×10^6 cells/ml). Cellular microsomes were prepared according to the protocols described previously (Ishii et al., 2001) and suspended in phosphate-buffered saline containing 20% glycerol. The above scale of cultivation gave us a sufficient quantity of microsomal protein for all assays and experiments.

Downloaded from dmd.aspetjournals.org at ASPET Journals on April 23, 2015

Glucuronidation Assay. Glucuronidation of 4-MU was assayed according to Nishimura et al. (2007). Unless otherwise stated, the incubation mixture (300 μl) consisted of 50 mM potassium phosphate buffer (pH 7.4), 5 mM $MgCl_2$, 2 mM UDP-GlcUA, recombinant UGT1A1 and 1A7 baculosomes, and 4-MU (see legends to figures for the amount of protein added and substrate concentration). Microsomes were pretreated with alamethicin (50 μg/mg protein; 4°C, 30 minutes) before assay. 4-MU was dissolved in methanol, and the final concentration of methanol in the incubation medium was 0.5%. Incubation was performed at 37°C for 1 hour. The linearity of the time-dependent increase in 4-MU glucuronide was confirmed up to an incubation period of 4 hours. In the kinetics for UGT1A7 catalysis by varying cofactor concentration, the UDP-GlcUA concentration ranged from 31.25 to 4000 μM. The 4-MU glucuronide produced was analyzed by high-performance liquid chromatography (HPLC) coupled to a fluorescence detector (Nishimura et al., 2007). Chromatographic analysis was carried out using a LaChrome Elite HPLC system equipped with an automatic sampler (model L-2200), pump (L-2130 HTA), and fluorescence detector (L-2485) (Hitachi High-Technologies Co., Tokyo, Japan). Data were stored and processed using D-7000 HPLC System Manager software (version 3.1; Hitachi High-Technologies Co.). Separation was achieved using a μBondaspher Phenyl column (5 μm, 150 × 3.9 mm, Waters Co., Milford, MA) housed in an oven (HITACHI L-2300) that was set at 25°C. The column was stepwise eluted by changing the acetonitrile concentration in 100 mM sodium phosphate, pH 2.4 as follows: 5% for 9.9 minutes, raised to 95% over 0.1 minute and holding it for the next 10 minutes, then reducing it to 5% over 0.1 minute and maintaining the starting condition for 10 minutes for the next sample. The flow rate was set at 0.8 ml/min. 4-MU glucuronide was quantified by fluorescence detection (excitation wavelength 315 nm and emission wavelength 375 nm). The retention time of 4-MU glucuronide was 4.1 minutes under the above conditions.

Glucuronidation of SN-38 was determined by HPLC using the procedure reported by Hanioka et al. (2001). Unless otherwise stated, the incubation conditions were the same as those for 4-MU described above, except that the substrate was SN-38 and incubation was performed at 37°C for 2 hours. A time-dependent increase in SN-38 glucuronide was confirmed for an incubation period up to 4 hours. The column was eluted with a linear gradient solution prepared by mixing eluent A (100 mM sodium phosphate, pH 2.4) and eluent B (acetonitrile): the concentration of acetonitrile was increased from 5 to 50% for 0 to 18 minutes and then increased from 50 to 90% over the period 18 to 23 minutes. Finally, it was reduced from 90 to 5% over the period 23 to 30 minutes. The flow rate was set at 0.8 ml/min. SN-38 glucuronide was quantified by fluorescence detection (excitation 370 nm and emission 425 nm), and the retention time of SN-38 glucuronide was 9.2 minutes.

Determination of 4-OHBP glucuronide was carried out by HPLC. Unless otherwise stated, the assay conditions were the same as those for the assay of 4-MU glucuronidation, except that the substrate was 4-OHBP ranging from 50 to 1500 μM. Incubations were performed at 37°C for 1 hour. The reaction was stopped with 100 μl cold 1 M trichloroacetic acid. Samples were chilled on ice for 30 minutes and then transferred to 1.5-ml plastic tubes. The samples were then centrifuged at 12,000 rpm for 10 minutes, and the supernatants were subjected to HPLC analysis. The linearity of the time-dependent increase in 4-OHBP glucuronide was confirmed for incubation periods up to 2 hours. Chromatographic analysis was performed using the apparatus described above. The operating conditions were the same as those for the analysis of 4-MU glucuronide, and 4-OHBP glucuronide was quantified by fluorescence detection (excitation 269 nm and emission 323 nm). The retention time of 4-OHBP glucuronide was 9.3 minutes.

Glucuronidation of 5-HT by UGT1A6 baculosomes was determined according to Hanioka et al. (2006). Glucuronidation at the 3-hydroxy group of 17β-estradiol by UGT1A1 baculosomes was assayed by a method described elsewhere (Nishimura et al., 2007).

Immunoblotting. Proteins separated by 7.5% or 9% SDS-PAGE were electroblotted on to polyvinylidene difluoride membranes (Millipore, Bedford, MA). UGT1A1, UGT1A6, and UGT1A7 were detected using rabbit anti-rat UGT1A com (Ikushiro et al., 1995). Polyclonal rabbit anti-CYP3A4 (epitope Leu331 to Lys342), which was a custom-made sample obtained from Scrum Inc. (Tokyo, Japan), or monoclonal mouse anti-CYP3A antibody (BD Gentest) was used as a primary antibody. Immunochemical staining was performed with alkaline phosphatase-labeled secondary antibody. The band intensity of UGT was quantified using Image-J software (version 1.61). After several transfection trials, Sf-9 cell microsomes expressing UGT1A7 allozymes with a similar glycosylation pattern were selected and subjected to further investigation of their enzymatic properties. The amount of UGT1A7 protein was determined and UGT1A7*2 and *3 proteins, the levels of which were equivalent to that of *1, were used for kinetic experiments. Similarly, UGT1A1*6 was used for kinetic assay at a protein level equivalent to that of *1.

Overlay Assay with GST-CYP3A4 Fusion Protein. The microsomes of insect cells transformed with baculovirus carrying UGT1A7 cDNA (Supersomes, BD Gentest) were used as the source of UGT1A7. The procedures were described previously (Takeda et al., 2005).

Other Methods. Protein concentrations were determined according to Lowry et al. (1951). The kinetic parameters with standard errors were calculated using GraphPad Prism 5J (GraphPad software, La Jolla, CA), and the statistical significances of the kinetic parameters were also determined. In this procedure, the data were fitted to a Michaelis-Menten eq. 1 or a Hill eq. 2. For UGT1A6, the data were also fitted to the substrate inhibition model (eq. 3).

The Michaelis-Menten model

$$V = V_{max} \cdot S/(K_m + S) \quad (1)$$

where V is the rate of reaction, S is the substrate concentration, V_{max} is the maximum enzyme velocity, and K_m is the Michaelis constant (substrate concentration needed to achieve a half-maximum enzyme velocity).

The sigmoidal model

$$V = V_{max} \cdot S^n/(S_{50}^n + S^n) \quad (2)$$

where S_{50} is the substrate concentration giving 0.5 V_{max} and n is the Hill coefficient.

The substrate inhibition model

$$V = V_{max} \cdot S/(K_m \pm S \cdot (1 + S/Ki) \quad (3)$$

where V_{max} is the maximum enzyme velocity if the substrate does not also inhibit enzyme activity and K_i is the substrate inhibition constant.

The significance of differences between two groups was examined by Student's t test using STATview software (ver. J 4.02, SAS Institute, Cary, NC). The differences among more than three groups were examined by one-way ANOVA followed by Scheffe's F test. The statistical significance of the estimated kinetic parameter of repeated kinetics was determined by ANOVA followed by Dunnett's test. A value of $P < 0.05$ was considered statistically significant.

Results

Effect of CYP3A4 on UGT1A6 Function. UGT1A6 was expressed in Sf-9 cells, and the protein bands immunoreactive toward anti-UGT1A antibody and absent in control microsomes was judged to be UGT1A6 having different sugar chains (Fig. 1). CYP3A4 was coexpressed in Sf-9 cells with UGT1A6. Sf-9 cells, the microsomes of which express UGT1A6 with a similar glycosylation pattern to that in the single expression system, were selected and subjected to further investigation of their enzymatic properties (Fig. 1). In addition to the glycosylation pattern, the amount of UGT1A6 and microsomal protein used for the assay was also unified between the single and dual expression systems. For this, we rendered the protein level uniform with baculosomes obtained from Sf-9 cells infected with control baculovirus. When CYP3A4 was expressed together with UGT1A6, the K_m of UGT1A6-catalyzed 5-HT glucuronidation was significantly increased (Fig. 2, Table 1). Although kinetic profiles for both the single and double expression could be fitted to a Michaelis-Menten equation, substrate inhibition or its trend was observed in UGT1A6 single expression at higher substrate concentrations. However, the same was not seen in a system coexpressing CYP3A4 and UGT1A6. This suggests that coexpressed CYP3A4 eliminates the substrate inhibition that occurred

Downloaded from dmd.aspetjournals.org at ASPET Journals on April 23, 2015

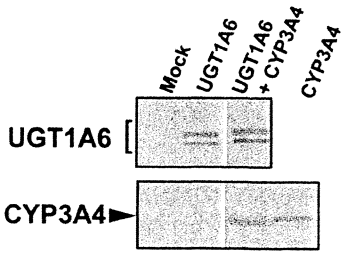


Fig. 1. Immunoblots of the expression of UGT1A6 and CYP3A4 in Sf-9 cells. To obtain microsomes simultaneously expressing CYP3A4 and UGT1A6, Sf-9 cells were transfected with recombinant baculovirus for CYP3A4 and UGT1A6. The lane labeled UGT1A6 shows microsomal samples of single transfected cells. The lane labeled UGT1A6+CYP3A4 shows double transfected cells. Baculosomes (10 μg protein) from UGT1A6 single-expressing Sf-9 cells were electrophoresed (SDS-PAGE). For baculosomes of CYP3A4-UGT1A coexpression systems, protein amounts equivalent to UGT1A6 for the single-expressing system were used. Mock represents the baculosomes (10 μg protein) from Sf-9 cells infected with the baculovirus without passenger DNA, which served as controls. The proteins in the gel were electrically transferred to polyvinilidene difluoride membranes, and blotted with anti-UGT1A common and monoclonal mouse anti-CYP3A, antibodies, respectively.

in UGT1A6-catalyzed 5-HT glucuronidation. Furthermore, the V_{max} was significantly increased by CYP3A4.

Interaction between CYP3A4 and UGT1A1*1/*6. To examine whether CYP3A4 also modifies UGT1A1 function, UGT1A1*1 (wild type) and *6 (an allelic variant) were expressed together with CYP3A4 in Sf-9 cells. Just like the experiments for a UGT1A6/CYP3A4 system, the Sf-9 cell microsomes expressing UGT1A1 with a similar glycosylation pattern to that in the CYP3A4 coexpression system were selected (Fig. 3). Also, the amount of expressed UGT1A1 used for kinetic assay was the same between the single and dual expression systems (Fig. 3). Under the expression conditions used, the level of expressed CYP3A4 did not differ greatly from that in human liver microsomes.

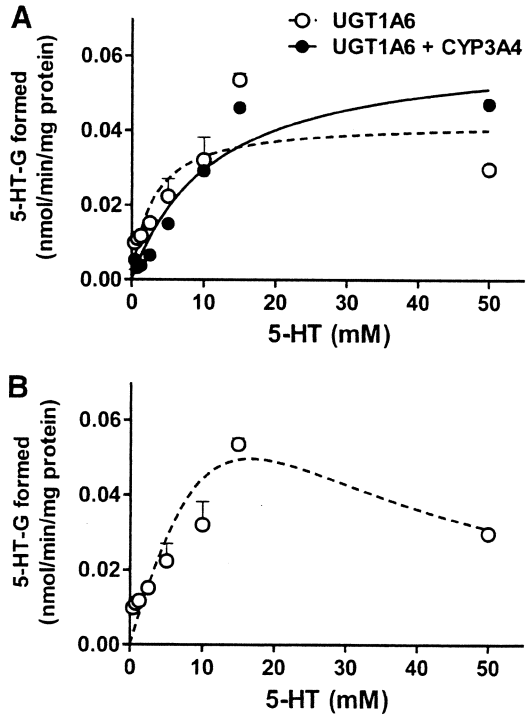


Fig. 2. Michaelis-Menten plots of 5-HT glucuronidation in the UGT1A6 single expression system and CYP3A4/UGT1A6 coexpression system. The 5-HT concentration ranged from 0.4 to 50 mM. Baculosomes (330 μg protein) from UGT1A6 single-expressing Sf-9 cells were used. For microsomes coexpressing CYP3A4, protein amounts equivalent to the single-expressing UGT1A6 were used. Total protein was unified to 700 μg by adding control baculosomes. Kinetic parameters were calculated by curve fitting of Michaelis-Menten (A) and substrate inhibition (B) equations are listed in Table 2.

Figure 4 shows the Michaelis-Menten plotting of 4-MU glucuronidation catalyzed by UGT1A1*1 and *6 and the effect of CYP3A4 coexpression on the profiles. The kinetic parameters together with those for other substrates (SN-38 and 17β-estradiol) are summarized in Table 2. As expected, the V_{max} of UGT1A1*6 was significantly lower than the wild-type *1 and almost half that of *1. Conversely, the S_{50} of UGT1A1*6 was significantly higher than *1. The cotransfection of CYP3A4 with UGT1A1*1 and *6 affected their kinetic parameters. More specifically, CYP3A4 markedly increased the V_{max} values of UGT1A1*1 and *6, whereas their S_{50} values were little affected (Fig. 4 and Table 2). Consequently, CYP3A4 coexpression rendered UGT1A1*6 function comparable with that of wild-type *1.

A similar picture was seen for SN-38 glucuronidation (Table 2). For example, the V_{max} was significantly lower in UGT1A1*6 than in wild-type *1, and the S_{50} of UGT1A1*6 was higher compared with the wild-type *1. Like 4-MU glucuronidation, the V_{max} of SN-38 glucuronidation of both *1 and *6 was significantly enhanced by CYP3A4. Thus, simultaneous expression of CYP3A4 with UGT1A1*6 caused an ~2-fold increase in V_{max}, and the value recovered to approximately 70% of that specific to *1. The same difference between UGT1A1*1 and *6 and the same effect of CYP3A4 coexpression on *1 function were also observed for 17β-estradiol glucuronidation (Table 2).

Protein-Protein Interaction between CYP3A4 and UGT1A7. To examine whether CYP3A4 interacts with UGT1A7, an overlay assay using GST-tagged CYP3A4 was performed. As a positive control, an overlay assay of UGT2B7 was carried out. As we reported previously (Takeda et al., 2005), UGT2B7 was recognized by GST-tagged CYP3A4 (Fig. 5). Like UGT2B7, UGT1A7 was also recognized by GST-tagged CYP3A4. This was supported by the observation that the same was not true for control baculosomes. No reacting band was observed when the overlay assay was performed with GST. These data suggest that CYP3A4 interacts with UGT1A7 as well as UGT2B7.

Comparison of Catalytic Properties among UGT1A7*1, *2, and *3. UGT1A7 allozymes *1, *2, and *3 were expressed in Sf-9 cells by the baculovirus-based expression system. The protein immunoreactive toward anti-UGT1A antibody and not present in control microsomes was judged to be UGT1A7 protein (Fig. 6). Incubation mixtures contained equivalent amounts of UGT protein, as assessed by Western blotting, and equivalent amounts of total protein. The latter was achieved by the addition of baculosome protein from Sf-9 cells infected with control baculovirus. Then, the catalytic properties of UGT1A7 allozymes *1, *2, and *3 were compared using 4-MU as a substrate. At a constant 4-MU concentration (100 μM), the formation of 4-MU glucuronide by UGT1A7*1 was dependent on the amount of microsomal protein over the range 0.5 to 10 μg. Linear 4-MU glucuronide formation was confirmed up to 4 hours (data not shown). The amount of UGT1A7*1 microsomes was set at 5 μg protein, and the incubation was carried out for 1 hour When the 4-MU glucuronidation activity was compared among UGT1A7*1, *2, and *3, the activity was highest in *3, followed by *1 and, finally, *2 (Supplemental Fig. 1A). The pH-dependence of all the allozymes was similar with an optimum pH of 8.0 (Supplemental Fig. 2). Their thermostabilities were also similar (data not shown). Thus, although the differences between them were significant, they were subtle.

Next, we compared the glucuronidation of SN-38, an active metabolite of irinotecan, by UGT1A7 allozymes. Referring to a previous

Downloaded from dmd.aspetjournals.org at ASPET Journals on April 23, 2015

TABLE 1

Kinetic parameters for 5-HT glucuronidation catalyzed by UGT1A6: effect of CYP3A4 cotransfection

Data were fitted to a Michaelis-Menten equation (Fig. 2A). For UGT1A6 single expression, data were also fitted to a substrate inhibition model (Fig. 2B). Results are the estimated value ± S.E.

	K_m (mM)	V_{max} (pmol/min/mg protein)	V_{max}/K_m	Ki
	mM	*pmol/min/mg protein*		*mM*
Michaelis-Menten				
UGT1A6	2.84 ± 1.94	42.3 ± 8.4	14.9	—
UGT1A6 + CYP3A4	11.2 ± 4.4$^{\$\$\$}$	62.6 ± 9.9$^{\$\$}$	5.6	—
Substrate inhibition				
UGT1A6	146 ± 717 (0.0 to 1637)[a]	0.792 ± 3.716 (−6.939 to 8.522)	—	2.37 ± 11.7 (0.0 to 26.79)

UGT activity was determined with 10 substrate concentrations ranging from 0.4 to 50 mM in the presence of 2 mM UDP-GlcUA.
[a]Value in parentheses represents the 95% confidential interval.
$^{\$\$}P = 0.0100$; $^{\$\$\$}P = 0.0015$ from single expression.

report (Gagne et al., 2002), the SN-38 concentration was set at 2 μM. The formation of SN-38 glucuronide was dependent on the amount of UGT1A7*1 microsomal protein within the range 5 to 50 μg (data not shown). The amount of UGT1A7*1 microsomes was set at 10 μg protein, and the incubation was performed for 1 hour. The SN-38 glucuronidation activity in UGT1A7 allozymes *2 and *3 was significantly lower than in wild-type *1, being 65% and 70% of *1, respectively (Supplemental Fig. 1B).

It is known that rabbit UGT1A7 is capable of glucuronidating 4-OHBP (Bruck et al., 1997), so we next examined whether human UGT1A7 also catalyzes 4-OHBP glucuronidation. As shown in Supplemental Fig. 1C, UGT1A7 allozymes *1, *2, and *3 were capable of glucuronidating 4-OHBP. Thus, in this study, it was shown for the first time that 4-OHBP is a substrate of human UGT1A7. When the substrate concentration was set at 400 μM, the formation of 4-OHBP glucuronide was dependent on the amount of UGT1A7*1 microsomal protein ranging from 10 to 100 μg (data not shown). The formation of 4-OHBP glucuronide was linear up to 3 hour (data not shown). The amount of microsomal UGT1A7*1 was set at 20 μg protein, and the incubation was performed for 1 hour. When the 4-OHBP glucuronidation activity was compared among UGT1A7 allozymes *1, *2, and *3, the activity was highest in *3, followed by *1 and, finally, *2 (Supplemental Fig. 1C). Although the difference was significant, it was not very marked.

Comparison of Kinetic Parameters among UGT1A7*1, *2, and *3: Effect of CYP3A4. When UGT1A7 allozymes *1, *2, and *3 were compared, the differences in 4-MU glucuronidation activity between them was significant but subtle. Kinetic studies were carried out to better understand the differences in the catalytic properties of UGT1A7 allozymes and the effect of CYP3A4. Keeping the UDP-GlcUA concentration constant, the concentration of each substrate was varied. Figure 7 shows the Michaelis-Menten plot of 4-MU glucuronidation catalyzed by UGT1A7 allozymes. The fitted kinetic parameters are summarized in Table 3. Although the V_{max} of UGT1A7*2 was smaller than that of the wild-type *1, the intrinsic clearance (V_{max}/K_m) of UGT1A7 allozymes *1, *2, and *3 was not markedly different. However, cotransfection of CYP3A4 with each UGT1A7 allozyme affected their kinetic parameters. As shown in Fig. 7, 4-MU glucuronidation in *1 and *2 was enhanced by CYP3A4

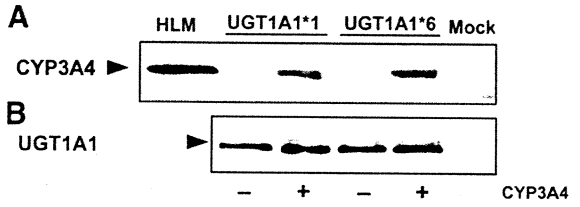


Fig. 3. Western blot analysis of UGT1A1 and CYP3A4 in Sf-9 microsomes expressing UGT1A1 alone and the UGT plus CYP3A4. A, Western blotting was performed with a monoclonal anti-CYP3A antibody, WB-MAB-3A. All microsomal samples applied to wells were adjusted in advance so that they contain comparable amounts of UGT1A1. Human liver microsomes (HLM) (5 μg protein) were used as a positive control. Lane 1, microsomes expressing wild-type UGT1A1 (2.5 μg protein); lane 2, microsomes expressing wild-type UGT1A1 and CYP3A4 (4 μg protein); lane 3, microsomes expressing UGT1A1*6 (2 μg protein); lane 4, microsomes expressing UGT1A1*6 and CYP3A4 (4 μg protein). Mock represents microsomes (20 μg protein) obtained from Sf-9 cells transfected with control baculovirus. B, Western blotting was performed with nonspecific anti-UGT1A antibody as a primary antibody. Lanes 1–4 represent the same samples as those of (A).

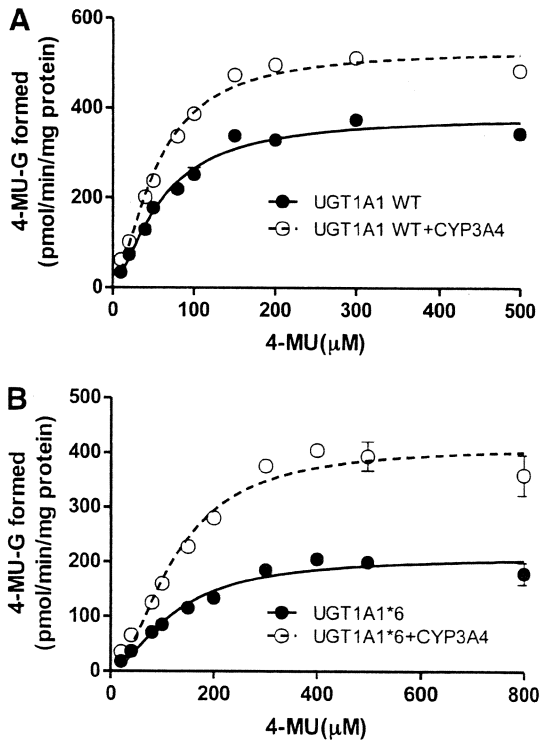


Fig. 4. Michaelis-Menten plots of 4-MU glucuronidation catalyzed by UGT1A1 in the absence and presence of CYP3A4 coexpression. The plots for wild-type UGT1A1*1 (A) and its allelic variant *6 (B) are shown. The 4-MU concentration was varied over the range 10–500 μM (UGT1A*1) and 20–800 μM (UGT1A1*6). The total amount of proteins added to the assay mixture was standardized at 40 μg. For this, when necessary, control baculosomes were added to the reaction mixture. Kinetic parameters were calculated by fitting the curve to a sigmoidal equation, and they are listed in Table 2.

Downloaded from dmd.aspetjournals.org at ASPET Journals on April 23, 2015

TABLE 2

Kinetic parameters for 4-methylumbelliferone, SN-38, and 17β-estradiol (3-hydroxy group) glucuronidation catalyzed by UGT1A1*1 and its allelic variant *6: effect of CYP3A4 cotransfection

Data were fitted to a Michaelis-Menten equation. Results are the estimated value ± S.E.

UGT1A1 and a variant	S_{50}	V_{max}	Hill coefficient
	μM	*pmol/min/mg protein*	*n*
4-MU[a]			
*1	58.8 ± 4.1	385 ± 13	1.5 ± 0.1
*1+CYP3A4	53.6 ± 2.7	534 ± 13$^{\$\$\$}$	1.6 ± 0.1
*6	122 ± 13¶¶¶	211 ± 12¶¶	1.7 ± 0.3
*6+CYP3A4	124 ± 11	413 ± 20$^{\$\$\$}$	1.9 ± 0.3
SN-38[b]			
*1	14.0 ± 0.3	28.6 ± 0.2	1.35 ± 0.03
*1+CYP3A4	16.6 ± 0.3$^{\$\$\$}$	51.1 ± 0.4$^{\$\$\$}$	1.25 ± 0.02$^{\$\$}$
*6	18.1 ± 0.6¶¶	7.1 ± 0.1¶¶¶	1.48 ± 0.06
*6+CYP3A4	30.4 ± 1.1$^{\$\$\$}$	18.9 ± 0.4$^{\$\$\$}$	1.34 ± 0.03
17β-estradiol[c]			
*1	60.0 ± 1.4	150 ± 2	3.8 ± 0.3
*1+CYP3A4	65.9 ± 1.9	231 ± 4$^{\$\$\$}$	3.6 ± 0.3
*6	102 ± 2¶¶¶	35.1 ± 0.6¶¶¶	5.2 ± 0.5
*6+CYP3A4	106 ± 1	66.3 ± 0.7$^{\$\$\$}$	5.4 ± 0.3

[a]UGT activity was determined in the presence of 2 mM UDP-GlcUA with 10 substrate concentrations ranging from 10 to 500 μM (UGT1A*1) and from 20 to 800 μM (UGT1A1*6);
[b]Ranging from 2 to 100 μM;
[c]Ranging from 8 to 500 μM (UGT1A*1) and from 10 to 500 μM (UGT1A1*6).
$^{¶¶}P < 0.001$, $^{¶¶¶}P < 0.0001$ from *1; $^{\$}P = 0.018$, $^{\$\$}P < 0.001$, $^{\$\$\$}P < 0.0001$ from single expression.

whereas that of *3 was reduced. In particular, the effect of CYP3A4 on V_{max} was marked, with the V_{max} of UGT1A7*1 and *2 being significantly increased whereas that of *3 was significantly reduced. Consequently, when CYP3A4 was cotransfected, the intrinsic clearance was increased ~3-fold in *2 followed by *1 (1.5 times) whereas that of *3 was reduced one-half by CYP3A4.

Kinetic experiments were carried out for SN-38 glucuronidation catalyzed by UGT1A7 allozymes, and the fitted kinetic parameters are summarized in Table 3. Although the V_{max} of UGT1A7*2 was smaller than that of the wild-type *1, the intrinsic clearance of UGT1A7 allozymes *1, *2, and *3 was not markedly different. However, like 4-MU, cotransfection of CYP3A4 with each UGT1A7 allozyme affected their kinetic parameters. SN-38 glucuronidation of *2 was significantly enhanced by CYP3A4 whereas that of *3 was reduced. In particular, the effect of CYP3A4 on the V_{max} of *2 was marked, with the V_{max} of UGT1A7 *1 and *2 being increased whereas that of *3 was reduced. Consequently, when CYP3A4 was cotransfected, the intrinsic clearance was increased ~3-fold in *2 whereas that of *3 was reduced to 80% by CYP3A4.

Kinetic studies for 4-OHBP glucuronidation catalyzed by UGT1A7 allozymes were also performed. The fitted kinetic parameters are summarized in Table 3. The intrinsic clearance of UGT1A7 allozymes *1, *2, and *3 was not markedly different. However, cotransfection of CYP3A4 with each UGT1A7 allozyme affected their kinetic parameters. Like 4-MU and SN-38, 4-OHBP glucuronidation involving *1 and *2 was enhanced by CYP3A4 whereas that of *3 was reduced. The effect of CYP3A4 on V_{max} was significant, with the V_{max} of UGT1A7*1 and *2 being increased whereas that of *3 was reduced. Consequently, when CYP3A4 was cotransfected, the intrinsic clearance was increased ~2- to 6-fold in *2 followed by *1 (1.4-fold) whereas that of *3 was reduced one-half by CYP3A4.

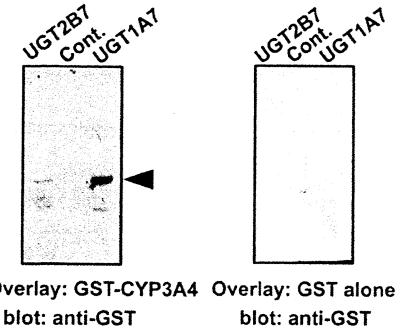


Fig. 5. Detection of interaction between CYP3A4 and UGT1A7 by overlay assay. Proteins in solubilized UGT1A7 supersome (5 μg) were separated by SDS-PAGE (10% gel) and transferred to a polyvinilidene difluoride membrane. The membrane was overlaid with either GST-CYP3A4 fusion protein (left) or GST (right) and then treated with anti-GST antibody. The lanes of "UGT1A7,", "UGT2B7," and "control" mean baculosomes containing UGT1A7, UGT2B7, and those lacking the UGT, respectively. The arrowhead indicates the UGT1A7 position.

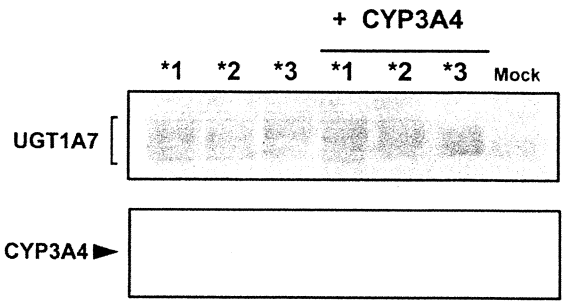


Fig. 6. Immunoblots of the expression of each UGT1A7 allozyme and CYP3A4 in Sf-9 cells. To obtain microsomes simultaneously expressing CYP3A4 and UGT1A7, Sf-9 cells were transfected with recombinant baculovirus for CYP3A4 and UGT1A7. The lanes labeled "*1," "*2," "3," and "+CYP3A4" show microsome samples of the single and double transfect cells. Baculosomes (5 μg protein) from UGT1A7*1 single-expressing Sf-9 cells were electrophoresed (SDS-PAGE). For other baculosomes, amounts of protein were used that were equivalent to the UGT1A7 content in the single-expressing UGT1A7*1. Mock represents the baculosomes (20 μg protein) from Sf-9 cells infected with the baculovirus without passenger DNA and served as controls. The proteins in the gel were electrically transferred to polyvinilidene difluoride membranes, and blotted with anti-UGT1A common (top) and polyclonal anti-CYP3A4 (bottom), antibodies, respectively.

Downloaded from dmd.aspetjournals.org at ASPET Journals on April 23, 2015

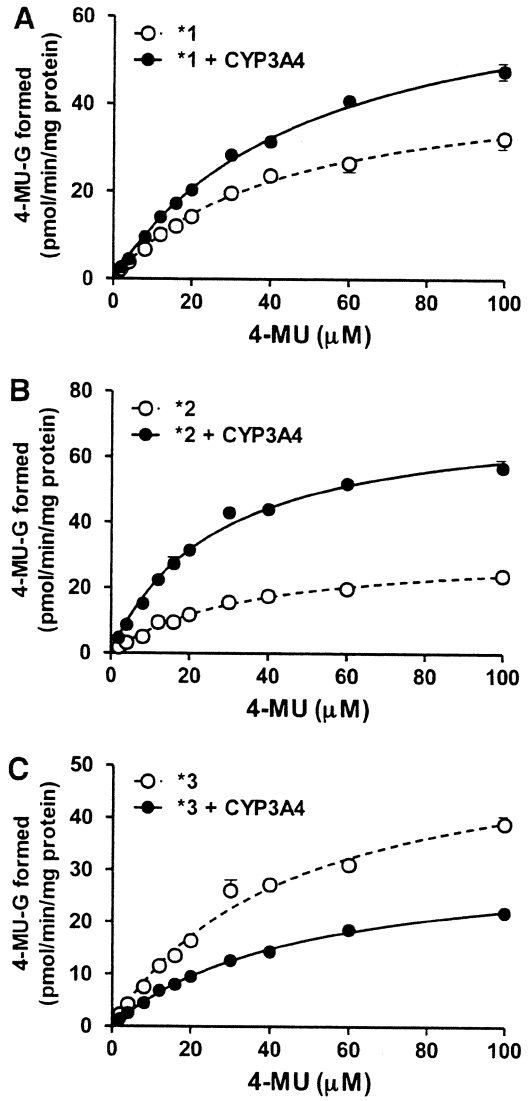


Fig. 7. Michaelis-Menten plots of 4-MU glucuronidation in the UGT1A7 single expression system and CYP3A4/UGT1A7 coexpression system. The plots for allozymes UGT1A7*1 (A), *2 (B), and *3 (C) are shown. The 4-MU concentration ranged from 2 to 100 μM. The amount of protein used is described in the legend to Fig. 5. Kinetic parameters were calculated by curve fitting of a Michaelis-Menten equation and are listed in Table 3.

TABLE 3

Kinetic parameters for 4-methylumbelliferone, SN-38, and 4-hydroxybiphenyl glucuronidation catalyzed by UGT1A7 allozymes *1, *2, and *3: effect of CYP3A4 cotransfection

Data were fitted to a Michaelis-Menten equation. Results are the estimated value ± S.E.

UGT1A7 allozymes	K_m	V_{max}	V_{max}/K_m
	μM	*pmol/min/mg protein*	
4-MU[a]			
*1	43.2 ± 3.0	46.5 ± 1.6	1.08
*1+CYP3A4	50.3 ± 3.2	72.6 ± 2.4[$$]	1.44
*2	34.1 ± 3.5[¶]	31.8 ± 1.5[¶¶]	0.93
*2+CYP3A4	26.8 ± 2.5	74.2 ± 3.0[$$]	2.76
*3	45.5 ± 6.4	56.8 ± 4.0[¶¶]	1.25
*3+CYP3A4	47.9 ± 2.2	32.5 ± 0.8[$$]	0.68
SN-38[b]			
*1	9.72 ± 2.37	1.52 ± 0.13	0.157
*1+CYP3A4	13.81 ± 0.94	1.85 ± 0.05[$]	0.134
*2	7.95 ± 2.08	0.97 ± 0.08[¶¶¶]	0.123
*2+CYP3A4	6.13 ± 1.04	2.37 ± 0.12[$$$]	0.386
*3	9.80 ± 2.03	1.30 ± 0.10	0.133
*3+CYP3A4	8.68 ± 1.03	0.93 ± 0.04[$$$]	0.107
4-OHBP[c]			
*1	679 ± 46	11.6 ± 0.4	0.017
*1+CYP3A4	613 ± 42	14.9 ± 0.5[$$$]	0.024
*2	784 ± 102	10.9 ± 0.7	0.014
*2+CYP3A4	642 ± 70	23.9 ± 1.2[$$$]	0.037
*3	638 ± 45	12.5 ± 0.4[¶¶]	0.020
*3+CYP3A4	716 ± 75	7.0 ± 0.3[$$$]	0.010

[a] UGT activity was determined in the presence of 2 mM UDP-GlcUA with 10 substrate concentrations ranging from 2 to 100 μM;
[b] Ranging from 1 to 50 μM;
[c] Ranging from 50 to 1500 μM.
[¶] $P = 0.0197$, [¶¶] $P < 0.001$, [¶¶¶] $P < 0.0001$ from *1; [$] $P = 0.018$, [$$] $P < 0.001$, [$$$] $P < 0.0001$ from single expression.

Comparison of Kinetic Parameters among UGT1A7*1, *2, and *3: Effect of CYP3A4 at Different UDP-GlcUA Concentrations. Like 4-MU, SN-38, and 4-OHBP as substrates, CYP3A4 similarly alters the V_{max} of UGT1A7 allozymes *1, *2, and *3 in kinetic studies. Thus, the affinity for UDP-GlcUA, a common cofactor of the reactions, was determined using 4-MU as a substrate. The cofactor kinetics were examined for UGT1A7 allozymes *1, *2, and *3. Keeping the 4-MU concentration at 100 μM, the UDP-GlcUA concentration was varied. Compared with the wild-type UGT1A7*1, the K_m for UDP-GlcUA was significantly increased in allozymes *2 and *3 (Table 4). Therefore, it appears that N129K and R131K, which are common mutations in UGT1A7*2 and *3, have an effect on the recognition of UDP-GlcUA. However, the V_{max} of *2 was not significantly different from *1, whereas the V_{max} of *3 was significantly higher than that of *1 (Table 4). When CYP3A4 was coexpressed with each UGT1A7 allozyme, the K_m (UDP-GlcUA) for *1 and *3 was significantly increased whereas that of *2 was not affected. In addition, the V_{max} for *1 and *2 was significantly increased whereas that of *3 remained unchanged. The cofactor kinetics for each UGT1A7 allozyme was investigated in two additional experiments. Then, the statistical significance of the estimated kinetic parameters was analyzed. Consequently, the intrinsic clearance of UGT1A7*2 was increased whereas that of *3 was reduced (Supplemental Fig. 3). The intrinsic clearance of the wild-type *1 remained unchanged, because both K_m (UDP-GlcUA) and V_{max} were increased by CYP3A4. It appears that N129K, R131K, and W208R of UGT1A7*3 affect not only its recognition of UDP-GlcUA but also the modulation by CYP3A4.

Comparison of UGT1A and CYP3A4 Levels between Human Intestinal Microsomes and UGT1A7-CYP3A4 in the Dual Expression System. Although CYP3A4 alters UGT1A7-catalyzed glucuronidation in vitro, it is not known whether the dual expression system used mimics the situation of human intestinal microsomes. Figure 8 compares the level of CYP3A4 and UGT1As in human intestinal microsomes with a UGT1A7-CYP3A4 dual expression system (Fig. 8). Compared with baculosomes for the CYP3A4-UGT1A7 dual expression system, the level of UGT1As was lower in pooled human intestinal microsomes, whereas the level of CYP3A4 was comparable. Thus, it is likely that the ratio of CYP3A4 to UGT1A is somewhat higher in human intestinal microsomes.

Discussion

CYP3A4 alters the function of UGT1A1, 1A6, and 1A7. Although CYP3A4 markedly activated UGT1A1*1- and UGT1A7*1-catalyzed glucuronidation, the effect of CYP3A4 on UGT1A6-catalyzed 5-HT glucuronidation was different. UGT1A1 is major isoform involved in SN-38 glucuronidation. To date, 113 allelic variants of UGT1A1 have

Downloaded from dmd.aspetjournals.org at ASPET Journals on April 23, 2015

TABLE 4

Kinetic parameters for 4-methylumbelliferone glucuronidation catalyzed by UGT1A7 allozymes: kinetics by varying UDP-GlcUA concentration

UGT activity was determined with 10 UDP-GlcUA concentrations ranging from 31.25 to 4000 μM in the presence of 100 μM 4-MU. Data were fitted to a Michaelis-Menten equation. Results are the estimated value ± S.E.

Variants	K_m	V_{max}	V_{max}/K_m
	μM	*pmol/min/mg protein*	
*1	317 ± 10	33.7 ± 0.3	0.106
*1+CYP3A4	455 ± 22$^{\$\$\$}$	56.8 ± 0.9$^{\$\$\$}$	0.125
*2	461 ± 32†††	33.6 ± 0.7	0.073
*2+CYP3A4	512 ± 45	85.2 ± 2.4$^{\$\$\$}$	0.166
*3	480 ± 36†††	42.5 ± 1.0†††	0.088
*3+CYP3A4	725 ± 60$^{\$\$}$	34.8 ± 1.0$^{\$\$\$}$	0.048

$^{\dagger\dagger\dagger}P < 0.0001$ from *1; $^{\$\$\$}P < 0.0001$ from single expression.

been reported (UGT home page: http://www.flinders.edu.au/medicine/sites/clinical-pharmacology/ugt-homepage.cfm). Of these variants, UGT1A1*6, resulting in reduced catalytic activity, seems to be one of the causes of Gilbert syndrome (Aono et al., 1993). It is well known that UGT1A1*28, which is another candidate for the genomic defect explaining Gilbert syndrome, has polymorphic (TA) repeats in the promoter that cause reduced expression of UGT1A1 wild-type protein (Rosner et al., 2008; Sugatani, 2013). Although both UGT1A1*6 and *28 are important, the former is more frequent (15.5%) in the Japanese population than the latter (11%) (Akaba et al., 1998; Huang et al., 2000; Kurose et al., 2012). UGT1A1*28 is considered to be an index that allows effective prediction in terms of the tolerability to irinotecan, an anticancer drug (Ando et al., 2007). However, it should be noted that there are patients showing a normal ability to glucuronidate SN-38 despite carrying the mutant genotypes (Sai et al., 2004). It is, therefore, controversial whether the sensitivity to irinotecan can be predicted only by analyzing the UGT1A1*28 genotype (Deeken et al., 2008). In addition, the allelic frequency (15%) of UGT1A1*6 is higher than that (5%) of Gilbert syndrome in Japanese subjects. In summary, more work is still needed to obtain a better understanding of interindividual differences in UGT1A1 activity. As reported here, CYP3A4 has the potential to enhance the activity of wild-type UGT1A1*1 and a variant UGT1A1*6 with low activity. This observation suggests that a change in CYP3A4 level is involved, at least in part, in interindividual differences in UGT1A1-catalyzed SN-38 glucuronidation. For instance, the observation that CYP3A4 restored the lowered activity of UGT1A1*6 to the level comparable with * 1(Fig. 4, Table 2) suggests a mechanism explaining the reason why some patients exhibit a normal activity although they carry the defect-type UGT1A1 gene.

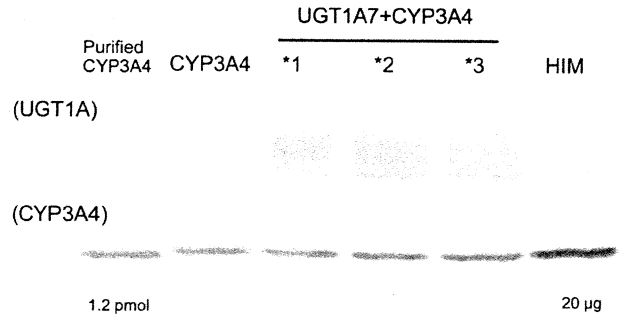


Fig. 8. Immunoblots of the expression of UGT1As and CYP3A4 in pooled human intestinal microsomes and comparison with UGT1A7 and CYP3A4 dual expressed microsomes. The lane "HIM" represents human intestinal microsomes pooled from five donors (20 μg protein). The lanes "*1", "*2," "3," and "UGT1A7+CYP3A4" show microsome samples of double transfected cells from UGT1A7*1, *2, and *3, respectively. Baculosomes (20 μg protein) coexpressing UGT1A7*1 and CYP3A4 were electrophoresed (SDS-PAGE). For other baculosomes, amounts of protein equivalent to the UGT1A7 content in the UGT1A7*1 + CYP3A4 were used. CYP3A4 represents the baculosomes (20 μg protein) from Sf-9 cells infected with the recombinant baculovirus for CYP3A4. Recombinant purified CYP3A4 (1.2 pmol) was on the lane at the extreme left. The proteins in the gel were electrically transferred to polyvinilidene difluoride membranes and blotted with anti-UGT1A common (top) and monoclonal anti-CYP3A (bottom) antibodies, respectively.

The function of UGT1A7 allozymes *1, *2, and *3 was virtually identical when substrate and cosubstrate are present in excess concentrations. Although UGT1A7*3 has been reported to be catalytically inactive toward 4-MU (Strassburg et al., 2002), in our tests, *3 exhibited comparable activity with the wild-type *1. This is also supported by the work of Uchaipichat et al. (2004) who reported UGT1A7-catalyzed 4-MU glucuronidation that was determined using the same cDNA as the UGT1A7*3 of this study. The difference is unclear but the former study used transient expression, whereas the latter used stable expression in HEK293 cells. The assay systems were also different. In the former study, 4-MU glucuronide was detected by thin-layer chromatography, whereas in the latter it was assayed by the fluorescence produced from 4-MU glucuronide in alkaline solution. In the present study, we used a baculovirus-Sf-9 cell system for expressing UGT1A7*3 and detected the 4-MU glucuronide formed by HPLC. Probably other factors that we have not considered also contributed to the difference. Alternatively, it has been reported that UGT1A7*3 exhibited SN-38 glucuronidation activity of ~60% of the wild-type *1 (substrate concentration 1.5 μM) (Villeneuve et al., 2003). UGT1A7*3 that exhibited SN-38 UGT activity of 70% of the wild type (substrate concentration 2 μM) (Supplemental Fig. 1B) corresponded well to that in a previous report (Villeneuve et al., 2003). Taking these factors into consideration, UGT1A7*3 is catalytically active toward 4-MU, SN-38, and 4-OHBP, at least under the assay conditions we used.

The activity of UGT1A7 allozymes *1, *2, and *3 was significantly reduced to ~80% by a 60-minute preincubation at 37°C (data not shown). The addition of UDP-GlcUA during the preincubation step did not prevent this inhibition. Thus, the interaction with UDP-GlcUA does not help to stabilize the UGT1A7 allozymes tested in this study. Without stabilization, the activity should be reduced to 40% by a 4-hour incubation at 37°C. However, the linearity of 4-MU glucuronidation of UGT1A7 was confirmed up to 4 hours in our preliminary experiments (data not shown). Therefore, there are mechanism(s) to stabilize UGT1A7 during incubation at 37°C. Interaction with substrate or other factors during catalysis is likely to be involved in maintaining UGT1A7 stability. In the kinetic study with different 4-MU, SN-38, and 4-OHBP concentrations, the intrinsic clearance of UGT1A7 allozymes *1, *2, and *3 was comparable. However, when the kinetics of 4-MU glucuronidation were investigated using different UDP-GlcUA concentrations, the K_m for UDP-GlcUA was significantly higher in UGT1A7*2 and *3 than in the wild-type *1, whereas their V_{max} values were comparable. This suggests that N129K and R131K of UGT1A7*2 and *3 are involved in the recognition of UDP-GlcUA. It is known that the UDP-GlcUA binding site is present in the carboxy-terminal domain of UGT (Mackenzie et al., 2005). The residues from Trp356 to Gln399 in UGT2B7 have been identified as the UDP-GlcUA-binding site on the basis of crystallographic data (Miley et al., 2007). This forms the signature sequence of UDP-glycosyltransferase (Mackenzie et al., 2005) that binds the UDP-moiety. Photo-affinity labeling experiments showed that the glucuronic acid moiety of UDP-GlcUA interacts with positively charged residue(s) in the N-terminal domain of UGT2B4 (Pillot et al., 1993). It is reasonable to suppose that these should be the site(s) interacting with the glucuronic acid moiety in the N-terminal domain of

Downloaded from dmd.aspetjournals.org at ASPET Journals on April 23, 2015

other UGT isoforms. In UGT1A7*2 and *3, the affinity for UDP-GlcUA is altered by N129K and R131K. These are located in the N-terminal domain and distinct from the above mentioned UDP-binding site. Taking these factors into consideration, it appears that the amino acid substitutions at residues 129 and 131 of UGT1A7 alter its recognition of the glucuronic acid moiety of UDP-GlcUA. However, it remains unclear whether either residue 129 or 131 or both are important.

CYP3A4 interacts with UGT1A7 as well as UGT2B7 (Fig. 4). In the present study, the glucuronidation activity of UGT1A7 allozymes *1, *2, and *3 was altered by cotransfection of CYP3A4. However, the effect differed among the three allozymes. The effects of CYP3A4 on UGT activity toward the three different substrates were similar, except that the effect on UGT1A7*1 in SN-38 glucuronidation was not very marked. The K_m for UDP-GlcUA was significantly increased in *3 and the wild-type *1 whereas that of *2 remained unchanged. The resulting affinity for UDP-GlcUA was further reduced in *3, whereas it was comparable between *2 and the wild-type *1. However the V_{max} of UGT1A7*1 and *2 increased. Therefore, it appears that CYP3A4 interacts with all the UGT1A7 allozymes tested to alter their function. Consequently, the intrinsic clearance of *3 was reduced by CYP3A4 whereas that of *2 was increased. Furthermore, it is reasonable to consider that V_{max} represents the activity with the substrate and cosubstrate at maximum concentrations. To the best of our knowledge, the concentration of UDP-GlcUA in the lumen of the endoplasmic reticulum (ER) has yet to be measured. Because UGT exhibits latency in intact microsomes, it is reasonable to consider that the luminal concentration of UDP-GlcUA is limited to a lowered concentration under in vivo conditions. Thus, the reduced affinity for UDP-GlcUA probably results in an insufficient glucuronidation ability. It is well known that there is large interindividual variability in the level of CYP3A4 (Shimada et al., 1994). It is assumed that the role of UGT1A7*3 in epidemiologic studies is evaluated in terms of the influence of CYP3A4. Taking these factors into consideration, it is likely that UGT1A7*3, but not *2, is a risk factor for carcinogenesis due to the reduced glucuronidation activity toward phenolic compounds.

The coexpression of UGT1A7 and CYP3A4 alters the K_m for the UDP-GlcUA of UGT1A7*3 but not *2. The W208R of UGT1A7*3 is the sole difference from *2. However, it is curious that the K_m for the UDP-GlcUA of wild-type *1 is affected similar to *3. This reason remains to be clarified. As has been established, the main bodies of UGT and P450 are situated on opposite sides of the ER membrane (Ishii et al., 2005). Thus, the respective interaction domains of UGT1A7 and CYP3A4 may meet together in the ER membrane. It is clear that there is another ER retention signal in UGT2B1 other than the carboxy terminal double-lysine motif (Meech and Mackenzie, 1998). Interestingly, an ER retention signal of UGT1A6 has been suggested to be present between residues 140 and 240 (Ouzzine et al., 1999). On the other hand, CYP3A4 is thought to bind to the ER membrane via the N-terminal helix and other hydrophobic surface regions (Nath et al., 2007). Furthermore, it has been reported that the membrane environment has some effects on P450 conformation and activity (Ahn et al., 1998). Therefore, the residues 129, 131, and 208 of UGT1A7 or the surrounding region are candidates for involvement in the CYP3A4-UGT1A7 interaction. We suggested that the *J*-helix region of CYP3A4 may interact with UGT2B7 (Takeda et al., 2009). However, there is no information about the region of UGT involved in the interaction. We believe that our study provides important information about the region of UGT involved in the protein-protein interaction with CYP3A4. Further studies are necessary to clarify the detailed mechanism of the modulation of UGT1A7 activity by CYP3A4.

Acknowledgment

We are grateful for technical support from the Research Support Center, Graduate School of Medical Sciences, Kyushu University.

Authorship Contributions

Participated in research design: Ishii, Koba, Kinoshita, Oizaki, Iwamoto, Takeda, Nishimura, Egoshi, Nagata, Yamazoe, Mackenzie, Yamada.

Conducted experiments: Ishii, Koba, Kinoshita, Oizaki, Iwamoto, Takeda, Egoshi.

Contributed new reagents and analytical tools: Koba, Kinoshita, Nishimura, Taura, Morimoto, Nagata, Yamazoe, Ikushiro, Mackenzie.

Performed data analysis: Ishii, Koba, Kinoshita, Oizaki, Iwamoto, Takeda, Miyauchi, Yamada.

Wrote or contributed to the writing of the manuscript: Ishii, Koba, Kinoshita, Oizaki, Mackenzie, Yamada.

References

Ahn T, Guengerich FP, and Yun CH (1998) Membrane insertion of cytochrome P450 1A2 promoted by anionic phospholipids. *Biochemistry* **37**:12860–12866.

Ando Y, Fujita K, Sasaki Y, and Hasegawa Y (2007) UGT1AI*6 and UGT1A1*27 for individualized irinotecan chemotherapy. *Curr Opin Mol Ther* **9**:258–262.

Akaba K, Kimura T, Sasaki A, Tanabe S, Ikegami T, Hashimoto M, Umeda H, Yoshida H, Umetsu K, and Chiba H, et al. (1998) Neonatal hyperbilirubinemia and mutation of the bilirubin uridine diphosphate-glucuronosyltransferase gene: a common missense mutation among Japanese, Koreans and Chinese. *Biochem Mol Biol Int* **46**:21–26.

Aono S, Yamada Y, Keino H, Hanada N, Nakagawa T, Sasaoka Y, Yazawa T, Sato H, and Koiwai O (1993) Identification of defect in the genes for bilirubin UDP-glucuronosyltransferase in a patient with Crigler-Najjar syndrome type II. *Biochem Biophys Res Commun* **197**:1239–1244.

Basu NK, Ciotti M, Hwang MS, Kole L, Mitra PS, Cho JW, and Owens IS (2004) Differential and special properties of the major human UGT1-encoded gastrointestinal UDP-glucuronosyltransferases enhance potential to control chemical uptake. *J Biol Chem* **279**:1429–1441.

Bruck M, Li Q, Lamb JG, and Tukey RH (1997) Characterization of rabbit UDP-glucuronosyltransferase UGT1A7: tertiary amine glucuronidation is catalyzed by UGT1A7 and UGT1A4. *Arch Biochem Biophys* **348**:357–364.

Chen K, Jin M, Zhu Y, Jiang Q, Yu W, Ma X, and Yao K (2006) Genetic polymorphisms of the uridine diphosphate glucuronosyltransferase 1A7 and colorectal cancer risk in relation to cigarette smoking and alcohol drinking in a Chinese population. *J Gastroenterol Hepatol* **21**: 1036–1041.

Deeken JF, Slack R, and Marshall JL (2008) Irinotecan and uridine diphosphate glucuronosyltransferase 1A1 pharmacogenetics: to test or not to test, that is the question. *Cancer* **113**: 1502–1510.

Dodgson KS, Garton GA, Stubbs AL, and Williams RT (1948) Studies in detoxication: 15. On the glucuronides of stilboestrol, hexoestrol and dienoestrol. *Biochem J* **42**:357–365.

Emi Y, Ikushiro S, and Kato Y (2007) Thyroxine-metabolizing rat uridine diphosphate-glucuronosyltransferase 1A7 is regulated by thyroid hormone receptor. *Endocrinology* **148**: 6124–6133.

Evans WE and Relling MV (1999) Pharmacogenomics: translating functional genomics into rational therapeutics. *Science* **286**:487–491.

Fremont JJ, Wang RW, and King CD (2005) Coimmunoprecipitation of UDP-glucuronosyltransferase isoforms and cytochrome P450 3A4. *Mol Pharmacol* **67**:260–262.

Gagné JF, Montminy V, Bélanger P, Journault K, Gaucher G, and Guillemette C (2002) Common human UGT1A polymorphisms and the altered metabolism of irinotecan active metabolite 7-ethyl-10-hydroxycamptothecin (SN-38). *Mol Pharmacol* **62**:608–617.

Guillemette C (2003) Pharmacogenomics of human UDP-glucuronosyltransferase enzymes. *Pharmacogenomics J* **3**:136–158.

Hanioka N, Ozawa S, Jinno H, Ando M, Saito Y, and Sawada J (2001) Human liver UDP-glucuronosyltransferase isoforms involved in the glucuronidation of 7-ethyl-10-hydroxycamptothecin. *Xenobiotica* **31**:687–699.

Hanioka N, Takeda Y, Jinno H, Tanaka-Kagawa T, Naito S, Koeda A, Shimizu T, Nomura M, and Narimatsu S (2006) Functional characterization of human and cynomolgus monkey UDP-glucuronosyltransferase 1A6 enzymes. *Chem Biol Interact* **164**:136–145.

Huang CS, Luo GA, Huang ML, Yu SC, and Yang SS (2000) Variations of the bilirubin uridine-diphosphoglucuronosyl transferase 1A1 gene in healthy Taiwanese. *Pharmacogenetics* **10**: 539–544.

Huang MJ, Yang SS, Lin MS, and Huang CS (2005) Polymorphisms of uridine-diphosphoglucuronosyltransferase 1A7 gene in Taiwan Chinese. *World J Gastroenterol* **11**:797–802.

Ikushiro S, Emi Y, and Iyanagi T (1995) Identification and analysis of drug-responsive expression of UDP-glucuronosyltransferase family 1 (UGT1) isozyme in rat hepatic microsomes using anti-peptide antibodies. *Arch Biochem Biophys* **324**:267–272.

Ishii Y, Miyoshi A, Watanabe R, Tsuruda K, Tsuda M, Yamaguchi-Nagamatsu Y, Yoshisue K, Tanaka M, Maji D, and Ohgiya S, et al. (2001) Simultaneous expression of guinea pig UDP-glucuronosyltransferase 2B21 and 2B22 in COS-7 cells enhances UDP-glucuronosyltransferase 2B21-catalyzed morphine-6-glucuronide formation. *Mol Pharmacol* **60**:1040–1048.

Ishii Y, Takeda S, Yamada H, and Oguri K (2005) Functional protein-protein interaction of drug metabolizing enzymes. *Front Biosci* **10**:887–895.

Iyanagi T, Emi Y, and Ikushiro S (1998) Biochemical and molecular aspects of genetic disorders of bilirubin metabolism. *Biochim Biophys Acta* **1407**:173–184.

Jinno H, Tanaka-Kagawa T, Hanioka N, Saeki M, Ishida S, Nishimura T, Ando M, Saito Y, Ozawa S, and Sawada J (2003) Glucuronidation of 7-ethyl-10-hydroxycamptothecin (SN-38), an active metabolite of irinotecan (CPT-11), by human UGT1A1 variants, G71R, P229Q, and Y486D. *Drug Metab Dispos* **31**:108–113.

Downloaded from dmd.aspetjournals.org at ASPET Journals on April 23, 2015

Joy MS, Boyette T, Hu Y, Wang J, La M, Hogan SL, Stewart PW, Falk RJ, Dooley MA, and Smith PC (2010) Effects of uridine diphosphate glucuronosyltransferase 2B7 and 1A7 pharmacogenomics and patient clinical parameters on steady-state mycophenolic acid pharmacokinetics in glomerulonephritis. *Eur J Clin Pharmacol* **66**:1119–1130.

Kurose K, Sugiyama E, and Saito Y (2012) Population differences in major functional polymorphisms of pharmacokinetics/pharmacodynamics-related genes in Eastern Asians and Europeans: implications in the clinical trials for novel drug development. *Drug Metab Pharmacokinet* **27**:9–54.

Lowry OH, Rosebrough NJ, Farr AL, and Randall RJ (1951) Protein measurement with the Folin phenol reagent. *J Biol Chem* **193**:265–275.

Mackenzie PI, Owens IS, Burchell B, Bock KW, Bairoch A, Bélanger A, Fournel-Gigleux S, Green M, Hum DW, and Iyanagi T, et al. (1997) The UDP glycosyltransferase gene superfamily: recommended nomenclature update based on evolutionary divergence. *Pharmacogenetics* **7**:255–269.

Mackenzie PI, Bock KW, Burchell B, Guillemette C, Ikushiro S, Iyanagi T, Miners JO, Owens IS, and Nebert DW (2005) Nomenclature update for the mammalian UDP glycosyltransferase (UGT) gene superfamily. *Pharmacogenet Genomics* **15**:677–685.

Meech R and Mackenzie PI (1998) Determinants of UDP glucuronosyltransferase membrane association and residency in the endoplasmic reticulum. *Arch Biochem Biophys* **356**:77–85.

Miley MJ, Zielinska AK, Keenan JE, Bratton SM, Radominska-Pandya A, and Redinbo MR (2007) Crystal structure of the cofactor-binding domain of the human phase II drug-metabolism enzyme UDP-glucuronosyltransferase 2B7. *J Mol Biol* **369**:498–511.

Nath A, Grinkova YV, Sligar SG, and Atkins WM (2007) Ligand binding to cytochrome P450 3A4 in phospholipid bilayer nanodiscs: the effect of model membranes. *J Biol Chem* **282**:28309–28320.

Nishimura Y, Maeda S, Ikushiro S, Mackenzie PI, Ishii Y, and Yamada H (2007) Inhibitory effects of adenine nucleotides and related substances on UDP-glucuronosyltransferase: structure-effect relationships and evidence for an allosteric mechanism. *Biochim Biophys Acta* **1770**:1557–1566.

Ockenga J, Vogel A, Teich N, Keim V, Manns MP, and Strassburg CP (2003) UDP glucuronosyltransferase (UGT1A7) gene polymorphisms increase the risk of chronic pancreatitis and pancreatic cancer. *Gastroenterology* **124**:1802–1808.

Ouzzine M, Magdalou J, Burchell B, and Fournel-Gigleux S (1999) An internal signal sequence mediates the targeting and retention of the human UDP-glucuronosyltransferase 1A6 to the endoplasmic reticulum. *J Biol Chem* **274**:31401–31409.

Pillot T, Ouzzine M, Fournel-Gigleux S, Lafaurie C, Tebbi D, Treat S, Radominska A, Lester R, Siest G, and Magdalou J (1993) Determination of the human liver UDP-glucuronosyltransferase 2B4 domains involved in the binding of UDP-glucuronic acid using photoaffinity labeling of fusion proteins. *Biochem Biophys Res Commun* **197**:785–791.

Ritter JK, Crawford JM, and Owens IS (1991) Cloning of two human liver bilirubin UDP-glucuronosyltransferase cDNAs with expression in COS-1 cells. *J Biol Chem* **266**:1043–1047.

Rosner GL, Panetta JC, Innocenti F, and Ratain MJ (2008) Pharmacogenetic pathway analysis of irinotecan. *Clin Pharmacol Ther* **84**:393–402.

Sai K, Saeki M, Saito Y, Ozawa S, Katori N, Jinno H, Hasegawa R, Kaniwa N, Sawada J, and Komamura K, et al. (2004) UGT1A1 haplotypes associated with reduced glucuronidation and increased serum bilirubin in irinotecan-administered Japanese patients with cancer. *Clin Pharmacol Ther* **75**:501–515.

Sambrook J, Fritsch EF, and Maniatis T(1989) Preparation of reagents and buffers used in molecular cloning, in *Molecular Cloning: A Laboratory Manual, 2nd edition* (Sambrook J, Fritsch EF, and Maniatis T eds), Cold Spring Harbor Laboratory Press, New York.

Shimada T, Yamazaki H, Mimura M, Inui Y, and Guengerich FP (1994) Interindividual variations in human liver cytochrome P-450 enzymes involved in the oxidation of drugs, carcinogens and toxic chemicals: studies with liver microsomes of 30 Japanese and 30 Caucasians. *J Pharmacol Exp Ther* **270**:414–423.

Strassburg CP, Vogel A, Kneip S, Tukey RH, and Manns MP (2002) Polymorphisms of the human UDP-glucuronosyltransferase (UGT) 1A7 gene in colorectal cancer. *Gut* **50**:851–856.

Sugatani J (2013) Function, genetic polymorphism, and transcriptional regulation of human UDP-glucuronosyltransferase (UGT) 1A1. *Drug Metab Pharmacokinet* **28**:83–92.

Takeda S, Ishii Y, Iwanaga M, Mackenzie PI, Nagata K, Yamazoe Y, Oguri K, and Yamada H (2005) Modulation of UDP-glucuronosyltransferase function by cytochrome P450: evidence for the alteration of UGT2B7-catalyzed glucuronidation of morphine by CYP3A4. *Mol Pharmacol* **67**:665–672.

Takeda S, Ishii Y, Iwanaga M, Nurrochmad A, Ito Y, Mackenzie PI, Nagata K, Yamazoe Y, Oguri K, and Yamada H (2009) Interaction of cytochrome P450 3A4 and UDP-glucuronosyltransferase 2B7: evidence for protein-protein association and possible involvement of CYP3A4 J-helix in the interaction. *Mol Pharmacol* **75**:956–964.

Taura KI, Yamada H, Hagino Y, Ishii Y, Mori MA, and Oguri K (2000) Interaction between cytochrome P450 and other drug-metabolizing enzymes: evidence for an association of CYP1A1 with microsomal epoxide hydrolase and UDP-glucuronosyltransferase. *Biochem Biophys Res Commun* **273**:1048–1052.

te Morsche RH, Drenth JP, Truninger K, Schulz HU, Kage A, Landt O, Verlaan M, Rosendahl J, Macek M, Jr, and Jansen JB, et al. (2008) UGT1A7 polymorphisms in chronic pancreatitis: an example of genotyping pitfalls. *Pharmacogenomics J* **8**:34–41.

Tukey RH and Strassburg CP (2000) Human UDP-glucuronosyltransferases: metabolism, expression, and disease. *Annu Rev Pharmacol Toxicol* **40**:581–616.

Uchaipichat V, Mackenzie PI, Guo XH, Gardner-Stephen D, Galetin A, Houston JB, and Miners JO (2004) Human udp-glucuronosyltransferases: isoform selectivity and kinetics of 4-methylumbelliferone and 1-naphthol glucuronidation, effects of organic solvents, and inhibition by diclofenac and probenecid. *Drug Metab Dispos* **32**:413–423.

Verlaan M, Drenth JP, Truninger K, Koudova M, Schulz HU, Bargetzi M, Künzli B, Friess H, Cerny M, and Kage A, et al. (2005) Polymorphisms of UDP-glucuronosyltransferase 1A7 are not involved in pancreatic diseases. *J Med Genet* **42**:e62.

Villeneuve L, Girard H, Fortier LC, Gagné JF, and Guillemette C (2003) Novel functional polymorphisms in the UGT1A7 and UGT1A9 glucuronidating enzymes in Caucasian and African-American subjects and their impact on the metabolism of 7-ethyl-10-hydroxycamptothecin and flavopiridol anticancer drugs. *J Pharmacol Exp Ther* **307**:117–128.

Vogel A, Kneip S, Barut A, Ehmer U, Tukey RH, Manns MP, and Strassburg CP (2001) Genetic link of hepatocellular carcinoma with polymorphisms of the UDP-glucuronosyltransferase UGT1A7 gene. *Gastroenterology* **121**:1136–1144.

Vogel A, Ockenga J, Tukey RH, Manns MP, and Strassburg CP (2011) Genotyping of the UDP-glucuronosyltransferase (UGT) 1A7 gene revisited. *Gastroenterology* **140**:1692–1693.

Address correspondence to: Dr. Yuji Ishii, Graduate School of Pharmaceutical Sciences, Kyushu University, 3-1-1 Maidashi, Higashi-ku, Fukuoka 812-8582, Japan. E-mail: ishii@phar.kyushu-u.ac.jp

Downloaded from dmd.aspetjournals.org at ASPET Journals on April 23, 2015

Bioorganic & Medicinal Chemistry Letters 23 (2013) 6555–6558

Contents lists available at ScienceDirect

Bioorganic & Medicinal Chemistry Letters

journal homepage: www.elsevier.com/locate/bmcl

Enhanced estrogen receptor beta (ERβ) selectivity of fluorinated carborane-containing ER modulators

Kiminori Ohta, Takumi Ogawa, Asako Kaise, Yasuyuki Endo *

Faculty of Pharmaceutical Sciences, Tohoku Pharmaceutical University, 4-4-1 Komatsushima, Aoba-ku, Sendai 981-8558, Japan

ARTICLE INFO

Article history:
Received 1 October 2013
Revised 26 October 2013
Accepted 30 October 2013
Available online 7 November 2013

Keywords:
Carborane
Estrogen receptor
Fluorine
Subtype selectivity

ABSTRACT

We previously showed that fluorination of the carborane-containing selective estrogen receptor modulator (SERM) BE360 altered the agonist/antagonist activity balance and the estrogen receptor (ER) α/β subtype selectivity. Here, we designed and synthesized a series of fluorinated carboranyl phenols as candidate ERβ-selective ligands. Introduction of a fluorine atom onto the carborane cage commonly reduced the binding affinity for ERα, to an extent that depended on the other substituents present. The B-fluorinated *m*-carboranyl phenol **4a** showed fourfold more potent ERβ-binding affinity than the parent non-fluorinated compound **7**. 1-Iodo-9-fluoro-*m*-carboranyl phenol **4f** showed high ERβ-binding affinity with an ERβ/ERα selectivity ratio of 8.2. Among the compounds tested, **6** showed the highest ERβ selectivity (10.1-fold) and the highest ER-agonistic activity (EC_{50}: 5.1×10^{-10} M) in MCF-7 cell proliferation assay.

© 2013 Elsevier Ltd. All rights reserved.

Estrogen receptor (ER), a member of the nuclear receptor superfamily, mediates the activity of estrogens in the regulation of a number of important physiological processes, including the development and function of the female reproductive system and the maintenance of bone mineral density and cardiovascular health.[1] Later, a second form of ER, ERβ, was unexpectedly discovered during a search for novel androgen receptors in a rat prostate cDNA library.[1b,2] Since ERβ, unlike ERα, is expressed in bone, colon, endothelial cells, bladder, and areas of the brain important for cognition, ERβ-selective ligands are proposed to be third-generation selective ER modulators (SERMs).[3] For example, Harris et al. showed that ERβ-selective ligands may be therapeutically useful agents to treat chronic intestinal and joint inflammation by modulation of immune response.[4] Thus, ERβ-selective ligands are of interest as potential clinical candidates and also as probes for ERβ-related molecular biology.

X-ray crystal structures of receptor-ligand complexes of ERα and ERβ show that their binding pockets are quite similar.[2,5] Binding of endogenous estrogen, estradiol (E2, **1**), to the ligand binding domains (LBDs) of the two ERs is illustrated in Figure 1.[2,5] The same amino acid residues are involved in hydrogen bonding with the two hydroxyl groups of E2 in the LBDs of ERα and ERβ. However, in the hydrophobic pocket of the LBDs, Leu384 and Met421 of ERα are substituted by Met336 and Ile373 in ERβ, respectively (Fig. 1). E2 is accommodated equally well by the two LBDs, and most ERβ-selective ligands have been designed based the idea of decreasing the affinity for ERα by introducing ligand substituents that interfere sterically with Met421 of ERα, although decreased ERβ-binding affinity is sometimes also observed.

Several carboranyl phenol derivatives show more potent ER-binding affinity than E2 because the high hydrophobicity and spherical structure of carborane result in effective hydrophobic interaction with the hydrophobic pocket of the ER LBD.[6] Moreover, we have found that the hydrophobicity of the carborane cage is significantly correlated with ERα-binding affinity through QSAR studies using various carboranyl phenol derivatives, which have potent estrogenic activity despite being structurally very simple compounds.[7] In other words, carboranyl phenol appears to be a privileged structure as an ER ligand. We therefore hypothesized that appropriate chemical modification of the carborane ring of carboranyl phenols might be an efficient strategy for weakening the ERα-binding affinity while retaining high ERβ-binding affinity.

Recently, fluorine substitution of drug candidates has been adopted as a means of improving their bioactivity and the absorption, distribution, metabolism, and excretion (ADME) characteristics.[8] Fluorine can effectively replace either hydrogen or oxygen, while altering the biological characteristics of the parent compound.[9] We reported the first fluorinated carborane-containing ER modulator, BE310 (**2**), which is an ER partial agonist with a more antagonistic activity balance than BE360 (**3**) in MCF-7 cell proliferation assay (Figure 2).[10] It may therefore serve as a less risky SERM than **3** for in vivo application. The two compounds also showed different binding affinities for ERα and ERβ. These significant biological differences presumably arise from a difference in the interaction of the compounds with Met421 of ERα due to the replacement of hydrogen with fluorine at the 9 position of the *o*-carborane cage. In the structures of **2** and **3**, one phenol moiety

* Corresponding author.
E-mail address: yendo@tohoku-pharm.ac.jp (Y. Endo).

0960-894X/$ - see front matter © 2013 Elsevier Ltd. All rights reserved.
http://dx.doi.org/10.1016/j.bmcl.2013.10.067

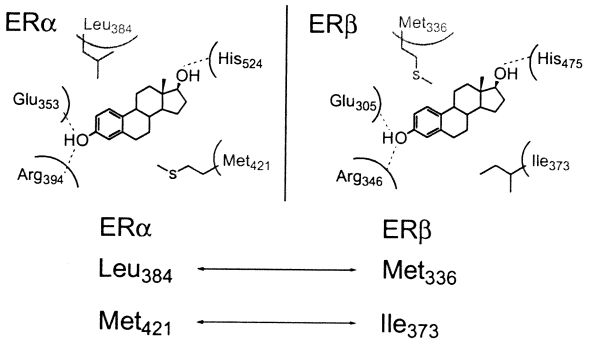
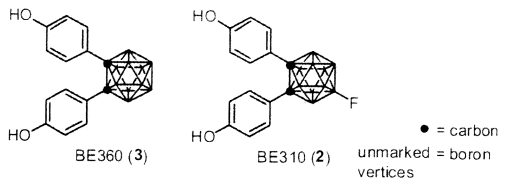


Figure 1. Differences of amino acid residues between ERα and ERβ.



	IC_{50} (nM)	EC_{50} (nM)	E_{max} (%)	RBA (%)		Selectivity (β / α)
				ERα	ERβ	
BE360 (**3**)	0.58	0.024	40	68	46	0.68
BE310 (**2**)	0.63	0.85	26	15	16	1.1

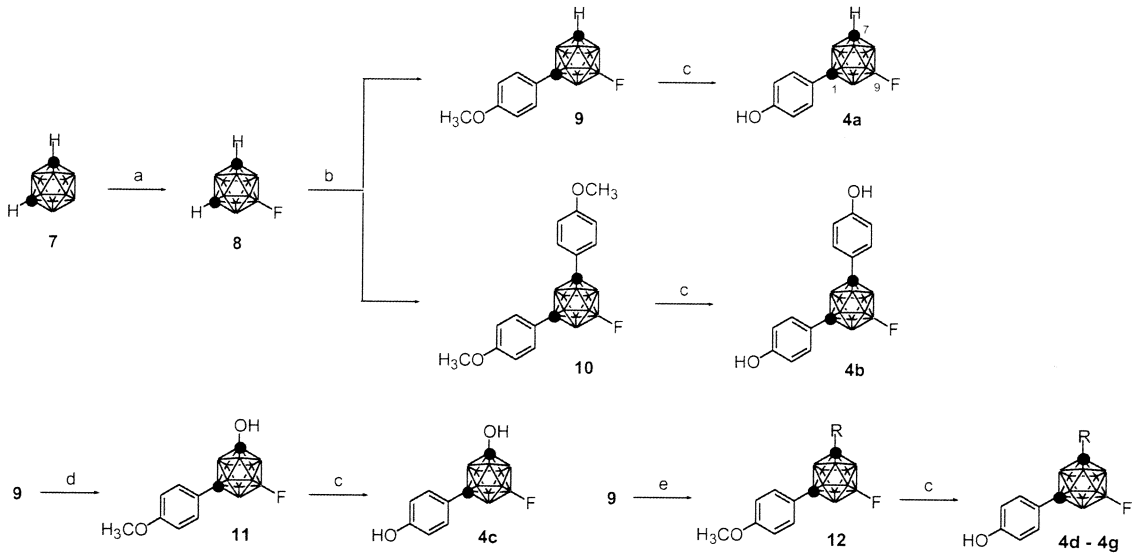
Figure 2. Structures and biological profiles of BE360 (**3**) and BE310 (**2**). RBA: Relative binding affinity with respect to that of E2 taken as 100%. EC_{50} and IC_{50} values were estimated from the sigmoidal dose–response curves. E_{max} values indicate the efficacy for cell proliferation with the value for E2 taken as 100.

is required for ER-binding and another phenol is associated with the expression of partial agonistic activity. We suggested that a weak repulsive interaction between the fluorine atom and Met421 in ERα is efficiently reflected in ER-binding affinity using simple phenol structure. Therefore, in this work, aiming at the development of ER subtype-selective compounds with a fluorinated carboranyl phenol structure, we designed 9-fluorinated *m*-carboranyl phenol derivatives **4**, *C*-fluorinated *m*-carboranyl *B*-phenol derivative **5**, and fluorinated *p*-carboranyl phenol **6**. Since some fluorinated *o*-carboranyl phenols have regioisomers and their synthesis is more difficult, we selected *m*-carborane and *p*-carborane cages as hydrophobic pharmacophores for the ER LBD (Fig. 2).

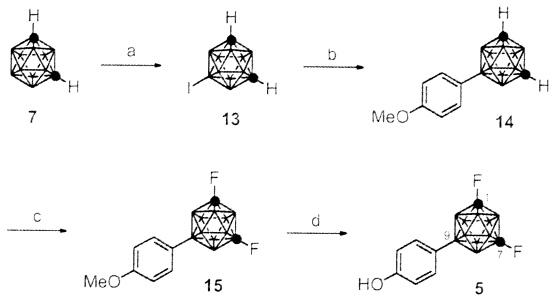
In this Letter, we describe the syntheses of several fluorinated carboranyl phenols **4**, **5**, and **6** and evaluations of their ER-related biological activities and selectivity.

Synthesis of 9-fluorinated *C*-substituted *m*-carboranyl phenols **4a–4g** is summarized in Scheme 1. *m*-Carborane (**7**) was treated with antimony pentafluoride in perfluoronaphthalene at 70 °C for 1 h to afford 9-fluoro-*m*-carborane (**8**) in 48% yield.[11] After treatment of compound **8** with *n*-BuLi, the resultant *C*-lithio-*m*-carborane was transformed into *C*-copper-*m*-carborane, which was reacted with 4-iodoanisole in the presence of pyridine as a ligand of copper to afford monoarylated *m*-carborane (**9**) and diarylated *m*-carborane (**10**) in 31% and 42% yields, respectively.[12] Methoxy groups of compounds **9** and **10** were deprotected with BBr_3 to afford the corresponding phenol derivatives **4a** and **4b** in quantitative and 89% yields, respectively. Compound **9** was treated with *n*-BuLi, and then reacted with trimethoxyborane, followed by oxidative rearrangement to afford the *C*-hydroxy-*m*-carborane derivative **11** in 58% yield.[13] Compound **11** was treated with BBr_3 to afford the corresponding phenol **4c** in quantitative yield. Alternatively, before demethylation with BBr_3, the lithium salt prepared from **9** was reacted with paraformaldehyde, BrI, CF_3CH_2I, or allyl iodide to afford the corresponding *C*-substituted *m*-carboranyl phenols, *C*-hydroxymethyl derivative **4d**, *C*-bromo derivative **4e**, *C*-iodo derivative **4f**, and *C*-allyl derivative **4g** in 97%, 31%, 73%, and 72% yields, respectively.

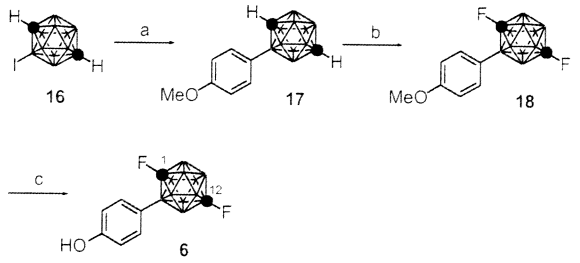
Scheme 2 summarizes the synthesis of *C,C'*-difluoro-*m*-carboranyl phenol **5**. 9-Iodo-*m*-carborane **13**, which was prepared from the reaction of *m*-carborane with iodine monochloride, was reacted with 4-methoxyphenylmagnesium bromide in the presence of catalytic amounts of palladium bis(triphenylphosphine) dichloride and copper(I) iodide to afford **14** in 73% yield.[14] The *m*-carborane C-Hs of **14** were reacted with 2 equimolar of *n*-BuLi and then



Scheme 1. Synthesis of B-fluorinated carborane-containing phenol derivatives. Reagents and conditions: (a) SbF_5, $C_{10}F_{18}$, 70 °C, 1 h, 48%; (b) *n*-BuLi, DME, then CuCl, pyridine, 4-iodoanisole, 100 °C, 24 h, 31% (**9**) and 42% (**10**); (c) BBr_3, CH_2Cl_2, rt, 31–97%; (d) *n*-BuLi, Et_2O, $B(OCH_3)_3$, then H_2O_2, AcOH, 58%; (e) *n*-BuLi, Et_2O, paraformaldehyde, BrI, CF_3CH_2I, or allyl iodide, rt, 1 h, 89%-quant.



Scheme 2. Synthesis of *C,C'*-difluoro-*m*-carboranyl phenol **5**. Reagents and conditions: (a) ICl, $AlCl_3$, CH_2Cl_2, 65%; (b) 4-MeOPhMgBr, CuI, $Pd(PPh_3)_2Cl_2$, THF, reflux, 73%; (c) *n*-BuLi, ether, then NFBS, 15%; (d) BBr_3, CH_2Cl_2, 76%.



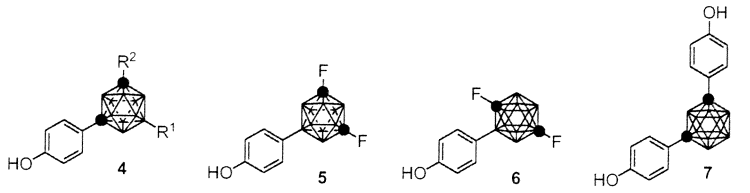
Scheme 3. Synthesis of fluorinated *p*-carborane derivative **6**. Reagents and conditions: (a) 4-methoxyphenylmagnesium bromide, CuI, $Pd(PPh_3)_2Cl_2$, THF, 97%; (b) *n*-BuLi, ether, then NFBS, 47%; (c) BBr_3, CH_2Cl_2, 81%.

fluorinated with *N*-fluorobenzenesulfonimide (NFBS), followed by demethylation of **15** with BBr_3 to give the corresponding phenol **5** in 76% yield in two steps.

Scheme 3 summarizes the synthesis of *C,C'*-difluoro-*p*-carboranyl phenol **6**. Palladium-catalyzed coupling reaction of 2-iodo-*p*-carborane **16**[15] with 4-methoxyphenylmagnesium bromide afforded the corresponding anisole derivative **17** in 97% yield. Dual *C*-fluorination of *p*-carborane C-Hs with NFBS followed by deprotection of methoxy group with BBr_3 afforded the corresponding *p*-carboranyl phenol **6** in 38% yield over the 2 steps.

The biological activity was evaluated by means of competitive ER binding assay using [2,4,6,7-^{3}H]17β-estradiol and human recombinant ERα and ERβ.[16] The binding affinity data are summarized in Table 1. Non-fluorinated *m*-carboranyl phenol (**7**) used as a control compound showed slight ERβ selectivity. Introduction of a fluorine atom at the 9 position of *m*-carborane cage greatly reduced the ERα binding affinity. Based on the relative binding affinity (RBA) values (see footnote to Table 1), compound **4a** showed 8.5-fold selectivity for ERβ. Bisphenol **4b**, although it had a higher ERβ-binding affinity than E2, showed little selectivity. This may suggest that the other phenol group also interacts with the ER LBD. Our previous study showed that non-substituted *m*-carborane bisphenol had a high binding affinity for ER, while introduction of an alkylamino group into the second phenol group greatly decreased the binding affinity and changed the functional activity from ER agonist to ER antagonist.[17] The phenol group may be accommodated in a secondary hydrophobic pocket and form other hydrogen bonds in the ER LBD. The binding affinity of compounds **4c** and **4d** having a polar substituent was greatly decreased for both ERs. Hydrophilic hydroxyl and hydroxymethyl groups are highly disfavored in a hydrophobic environment, and seem to be unable to fit into either the main or secondary hydrophobic pocket. Compounds **4e–4g** showed more potent ERβ-binding affinity than **4a**, presumably because of their hydrophobic substituent, and the fluorine atom resulted in marked subtype selectivity of **4f** and **4g**. Compound **4f** showed a high RBA value, with 8.2-fold selectivity for ERβ. *C,C'*-Difluoro-*m*-carboranyl phenol **5** showed similar ERβ-binding affinity to **4f**, but the selectivity was slightly decreased. It seems that introduction of fluorine atom at the 7 position of the carborane cage of *m*-carboranyl phenol derivatives generally reduces the ERα binding affinity, though the magnitude of the effect depends upon on the other substituents. It suggested that *p*-carboranyl phenol **6**, which was designed to examine the effect of adding another fluorine atom, showed the highest ERβ selectivity of over 10-fold among the test compounds. However, since the binding profiles for ERα and ERβ were quite similar to those of **4a**, it seems that introduction of the additional fluorine atom at the 1 position does not directly affect the interaction of the compound with key amino acid residues of the ER LBD. Further syntheses and structure–activity relationship studies, focusing on fluorinated *p*-carboranyl phenol derivatives, are in progress.

Table 1
Binding affinity for ERα and ERβ and subtype selectivity of the fluorinated compounds **4–7**



Compound	R^1	R^2	RBA[a] (%)		Selectivity ERβ/ERα
			ERα	ERβ	
4a	F	H	4.8	40.5	8.5
4b	F	4-OH-Ph	97.7	142.2	1.5
4c	F	OH	1.1	2.4	2.2
4d	F	CH_2OH	6.4	6.1	1.0
4e	F	Br	25.9	72.3	2.8
4f	F	I	7.8	61.1	8.2
4g	F	CH2—CH=CH_2	7.9	48.8	6.2
5			10.7	61.4	5.7
6			4.9	49.9	10.1
7			3.6	86.5	2.7
E2 (**1**)			100	100	1.0

[a] All binding assays were treated with the test compounds (0.4 nM–4 μM) in the presence of [2,4,6,7-^{3}H]17β-estradiol (4 nM) and performed in triplicate (n = 3). IC_{50} value of estradiol for ERα and ERβ is each 4 nM. RBA values are calculated from the IC_{50} values of E2 and test compounds taking that of E2 as 100%.

Next, we evaluated the agonist and antagonist activities of the test compounds by means of cell proliferation assay using the MCF-7 cell line, which shows estrogen-dependent growth.[16] Compounds with agonistic activity were classified into three groups, normal agonist, partial agonist,[18] or super-agonist,[19] based on their maximum efficacy (E_{max}) of cell proliferation. Compounds **4f** and **6** promoted cell proliferation in a dose-dependent manner. When E_{max} of E2 was taken as 100%, those of **4f** and **6** were 115% and 113%, respectively. The EC_{50} values of **4f** and **6** were 9.2×10^{-10} M and 5.1×10^{-10} M, respectively, so that these compounds showed weaker ER-agonistic activity than E2.

In conclusion, several fluorinated carboranyl phenols were designed and synthesized as ERβ-selective ligands, and their biological activities were evaluated by means of ER binding assay and MCF-7 cell proliferation assay. Introduction of a fluorine atom onto the carborane cage commonly reduced the binding affinity for ERα, to an extent that depended on the other substituents present possibly due to a weak repulsive interaction between the fluorine atom and Met421 in ERα. Compound **6** showed the highest ERβ selectivity and ER-agonistic activity in MCF-7 cell proliferation assay. These findings should be helpful the molecular design of even more highly selective ERβ ligands, which would be useful as tools for elucidation of ERβ functions.

Acknowledgments

This research was supported by a Grant-in-Aid for High Technology Research Program, a Grant-in-Aid for Scientific Research (B) (No. 20390035) and a Grant-in-Aid for Young Scientists (B) (No. 21790116) from the Ministry of Education, Culture, Sports, Science and Technology, Japan.

Supplementary data

Supplementary data associated with this article can be found, in the online version, at http://dx.doi.org/10.1016/j.bmcl.2013.10.067.

References and notes

1. (a) Green, S.; Walter, P.; Kumar, V.; Krust, A.; Bornert, J. M.; Argos, P.; Chambon, P. *Nature* **1986**, *320*, 134; (b) Kuiper, G. G. J. M.; Enmark, E.; Pelto-Huikko, M.; Nilsson, S.; Gustafsson, J. *Proc. Natl. Acad. Sci. U.S.A.* **1996**, *93*, 5925.
2. Paech, K.; Webb, P.; Kuiper, G. G. J. M.; Nilsson, S.; Gustafsson, J.; Kushner, P. J.; Scanlan, T. S. *Science* **1997**, *277*, 1439.
3. (a) Minutolo, F.; Maccbia, M.; Katzenellenbogen, B. S.; Katzenellenbogen, J. A. *Med. Res. Rev.* **2011**, *31*, 364; (b) Kuiper, G. G. J. M.; Carlsson, B.; Grandian, K.; Enmark, E.; Haggblad, J.; Nilsson, S.; Gustafsson, J. *Endocrinology* **1997**, *138*, 863.
4. Harris, H. A.; Albert, L. M.; Leathurby, Y.; Malamas, M. S.; Mewshaw, R. E.; Miller, C. P.; Kharode, Y. P.; Marzolf, K. J.; Komm, B. S.; Winneker, R. C.; Frail, D. E.; Henderson, R. A.; Zhu, Y.; Keith, J. C., Jr. *Endocrinology* **2003**, *144*, 4241.
5. Brzozowski, A. M.; Pike, A. C.; Dauter, Z.; Hubbard, R. E.; Bonn, T.; Engstrom, O.; Ohman, L.; Greene, G. L.; Gustafsson, J. A.; Carlquist, M. *Nature* **1997**, *389*, 753.
6. (a) Endo, Y.; Iijima, T.; Yamakoshi, Y.; Yamaguchi, M.; Fukasawa, H.; Shudo, K. *J. Med. Chem.* **1999**, *42*, 1501; (b) Endo, Y.; Iijima, T.; Yamakoshi, Y.; Fukasawa, H.; Miyaura, C.; Inada, M.; Kubo, A.; Itai, A. *Chem. Biol.* **2001**, *8*, 341; (c) Ogawa, T.; Ohta, K.; Iijima, T.; Suzuki, T.; Ohta, S.; Endo, Y. *Bioorg. Med. Chem.* **2009**, *17*, 1109; (d) Endo, Y.; Yoshimi, T.; Miyaura, C. *Pure Appl. Chem.* **2003**, *75*, 1197.
7. (a) Yamamoto, K.; Endo, Y. *Bioorg. Med. Chem. Lett.* **2001**, *11*, 2389; (b) Endo, Y.; Yamamoto, K.; Kagechika, H. *Bioorg. Med. Chem. Lett.* **2003**, *13*, 4089.
8. (a) Kirk, K. L. *J. Fluorine Chem.* **2006**, *127*, 1013; (b) Kirk, K. L. *Curr. Top. Med. Chem.* **2006**, *6*, 1445.
9. (a) Bondi, A. *J. Phys. Chem.* **1964**, *68*, 441; (b) Hagmann, W. K. *J. Med. Chem.* **2008**, *51*, 4359.
10. Ohta, K.; Ogawa, T.; Endo, Y. *Bioorg. Med. Chem. Lett.* **2012**, *22*, 4728.
11. Lebedev, V. N.; Balagurova, E. V.; Polyakov, A. V.; Yanovsky, A. I.; Struchkov, Yu. T.; Zakharkin, L. I. *J. Organomet. Chem* **1990**, *385*, 307.
12. Coult, R.; Fox, M. A.; Gill, W. R.; Herbertson, P. L.; MacBride, J. A. H.; Wade, K. *J. Organomet. Chem.* **1993**, *462*, 19.
13. Ohta, K.; Goto, T.; Yamazaki, H.; Pichierri, F.; Endo, Y. *Inorg. Chem.* **2007**, *46*, 3966.
14. Zheng, Z.; Jiang, W.; Zinn, A. A.; Knobler, C. B.; Hawthorne, M. F. *Inorg. Chem.* **1995**, *34*, 2095.
15. Ohta, K.; Yamazaki, H.; Kawahata, M.; Yamaguchi, K.; Pichierri, F.; Endo, Y. *Tetrahedron Lett.* **2007**, *48*, 5231.
16. Ohta, K.; Chiba, Y.; Ogawa, T.; Endo, Y. *Bioorg. Med. Chem. Lett.* **2008**, *18*, 5050.
17. Ogawa, T.; Ohta, K.; Yoshimi, T.; Yamazaki, H.; Suzuki, T.; Ohta, S.; Endo, Y. *Bioorg. Med. Chem. Lett.* **2006**, *16*, 3943.
18. Fernand, L.; Claude, L.; Alain, B.; Jacques, S. In *Selective Estrogen Receptor Modulators*; Andrea, M., Michael, V., Eds.; Humana Press, 2002; p 167.
19. Min, J.; Wang, P.; Srinivasan, S.; Nwachukwu, J. C.; Guo, P.; Huang, M.; Carlson, K. E.; Katzenellenbogen, J. A.; Nettles, K. W.; Zhou, H.-B. *J. Med. Chem.* **2013**, *56*, 3346.

Drug Metab. Pharmacokinet. 28 (3): 250–259 (2013). Copyright © 2013 by the Japanese Society for the Study of Xenobiotics (JSSX)

Regular Article

Hepatocyte Nuclear Factor 6 Activates the Transcription of *CYP3A4* in Hepatocyte-like Cells Differentiated from Human Induced Pluripotent Stem Cells

Takamitsu SASAKI[1], Shogo TAKAHASHI[1], Yoshihiro NUMATA[1], Masayo NARITA[1], Yutaka TANAKA[1], Takeshi KUMAGAI[1], Yuki KONDO[2], Tamihide MATSUNAGA[2], Shigeru OHMORI[3,4] and Kiyoshi NAGATA[1,*]

[1]*Department of Environmental and Health Science, Tohoku Pharmaceutical University, Sendai, Japan*
[2]*Department of Clinical Pharmacy, Graduate School of Pharmaceutical Sciences, Nagoya City University, Nagoya, Japan*
[3]*Department of Molecular Pharmacology, Shinshu University Graduate School of Medicine, Matsumoto, Japan*
[4]*Department of Pharmacy, Shinshu University Hospital, Matsumoto, Japan*

Full text of this paper is available at http://www.jstage.jst.go.jp/browse/dmpk

Summary: Human induced pluripotent stem cells (iPSCs) are a valuable source of hepatocytes for applications in drug metabolism studies. However, the current protocols for generating iPSC-derived hepatocyte-like cells (iPSHCs) are still very inefficient, and iPSHCs do not have sufficient hepatocyte-specific features, which include expression of a series of hepatocyte-specific genes, such as those encoding cytochrome P450 (*CYP*). In this study, we investigated whether introduction of human hepatocyte nuclear factor 6 (HNF6) could modulate the expression of *CYP3A4* and other *CYP* genes in iPSHCs as well as in HepG2 cells, a fetal liver cell line (HFL cells), and in hepatocytes. *CYP3A4* mRNA could be detected in iPSHCs, but the expression level was very low compared with those in HepG2 cells and hepatocytes. However, the *CYP3A4* mRNA levels markedly increased on introduction of HNF6 and reached one-tenth of those in hepatocytes. We also found that HNF6 introduction increased *CYP3A4* gene transcription in HFL cells and HepG2 cells, which have features similar to those of fetal hepatocyte-like cells; however, it did not affect *CYP3A4* mRNA expression in hepatocytes. These results suggest that HNF6 plays an important role in the gene regulation of *CYP3A4* during development from the fetal period to the postnatal period.

Keywords: CYP3A4; differentiation; hepatocytes; HNF6; induced pluripotent stem cells; liver-enriched transcription factors

Introduction

Human primary hepatocytes and HepG2 cells are often used to study transcriptional activation of genes implicated in cytochrome P450 (*CYP*) expression.[1] Human hepatocytes that retain liver-specific functions have an entire repertoire of hepatic drug-metabolizing enzymes. However, these cells show a large donor-to-donor variability in drug metabolizing activity and induction response, resulting in difficulties in interpreting data from different sources.[2] Cell lines, such as HepG2 cells, are available and can easily be standardized among laboratories, but have low expression levels of *CYP* genes and liver-enriched transcription factors (LETFs).[3,4]

Recently, human induced pluripotent stem cells (iPSCs) were established from fibroblast cells by introducing Oct3/4, Sox2, Klf4, and c-Myc; these cells can differentiate into most body cell types and may serve as an ideal renewable source of functional human hepatocytes.[5] Several studies have demonstrated the capacity of iPSCs to differentiate into hepatocyte-like cells under chemically defined conditions.[6–8] However, the current protocols for generating iPSC-derived hepatocyte-like cells (iPSHCs) are inefficient, and these cells do not possess a range of hepatocyte-specific fea-

Received November 17, 2012; Accepted December 7, 2012
J-STAGE Advance Published Date: January 1, 2013, doi:10.2133/dmpk.DMPK-12-RG-132
**To whom correspondence should be addressed:* Kiyoshi NAGATA, *Department of Environmental and Health Science, Tohoku Pharmaceutical University, 4-4-1, Komatsushima, Aoba-ku, Sendai 981-8558, Japan. Tel. +81-22-727-0133, Fax. +81-275-2013, E-mail: nagataki@tohoku-pharm.ac.jp*
This work was supported by a Health and Labour Sciences Research Grant for Research on Food Safety (No. 22230301) from the Ministry of Health, Labour and Welfare of Japan; by a Grant-in-Aid for Scientific Research (B) (No. 23790193); and by the Japanese Ministry of Education, Culture, Sports, Science and Technology (MEXT)-Supported Program for the Strategic Research Foundation at Private Universities.

tures, including expression of *CYP*. Thus, the current protocols still require the use of multiple growth factors, cytokines, and low molecular weight compounds, as well as the introduction of hepatic lineage stage-specific genes, such as those encoding LETFs, to modify these cells appropriately.

The expression of many hepatocyte-specific genes in the adult liver is regulated by LETFs, including hepatocyte nuclear factor 1 (HNF1), HNF3, HNF4, HNF6, and CCAAT/enhancer binding protein (c/EBP); these are all key components in the differentiation process in the adult liver.[9] Many studies have identified HNF4α as a direct transactivator of *CYP* genes.[10,11] Kamiyama *et al.* reported that knocking down HNF4α affects the expression of the major drug metabolizing CYPs.[12] Other LETFs, HNF1α, HNF3, and c/EBP, also play an important role in the regulation of many *CYP*s.[13–18] In addition to directly acting as transcriptional regulators of *CYP* genes, these LETFs control each other's expression and the expression of *CYP* genes through a network of cooperative and synergistic effects.

HNF6, a member of the Onecut family of transcription factors, controls the expression of other LETFs.[19–23] It is expressed in the liver, pancreas, and nervous system during embryonic development.[24] In the liver, HNF6 is detected in hepatoblasts and then later in the cholangiocytes and hepatocytes, where it is continually expressed in adults.[24–27] Fetuses of *HNF6*-knockout mice exhibit delayed expression of glucose-6-phosphatase, which catalyzes the final step of gluconeogenesis and is a late marker of hepatocyte maturation.[28] HNF6 also regulates *in vivo* hepatic expression of cholesterol 7α-hydroxylase (CYP7A1), which is only marginally expressed in fetal livers, but is strongly expressed in the liver postnatally.[29] Thus, HNF6 may play an important role in regulation of hepatocyte-specific genes during liver maturation.

As with CYP7A1, CYP3A4 expression significantly changes during ontogeny; CYP3A4 is the most abundant of CYP enzymes in adult human livers.[30,31] Thus, the expression level of CYP3A4 is highly correlated with LETF-mediated hepatocyte differentiation. Therefore, the mechanism regulating *CYP3A4* expression needs to be elucidated to understand the process of generating mature hepatocyte-like cells differentiated from iPSCs. Moreover, the precise role of HNF6 in the regulation of *CYP3A4* and other drug-metabolizing *CYP* genes during liver maturation remains unclear.

In this study, we aimed to determine whether HNF6 could modulate the expression of *CYP3A4* and other *CYP* genes in iPSHCs, by comparing gene expression in immature hepatocytes (HepG2 cells and fetal liver cell line [HFL] cells) and hepatocytes after HNF6 introduction. Our results indicated that HNF6 is strongly involved in *CYP3A4* expression in iPSHCs and immature hepatocytes, suggesting that HNF6 plays an important role in *CYP3A4* regulation during the maturation of liver cells from the fetal to the postnatal stage.

Materials and Methods

Materials: *Bgl*II and *Sal*I were purchased from Nippon Gene Co., Ltd. (Tokyo, Japan). Dexamethasone (DEX), 2-mercaptoethanol (2-ME), oncostatin M (OSM), and Y-27632 were purchased from Wako Pure Chemicals (Osaka, Japan). Mitomycin C and sodium butyrate were purchased from Sigma (St. Louis, MO). Activin, basic fibroblast growth factor (bFGF), and hepatocyte growth factor (HGF) were purchased from Peprotech (Rocky Hill, NJ). Testosterone was purchased from Tokyo Chemical Industry Co., Ltd. (Tokyo, Japan). 6β-Hydroxytestosterone was purchased from BD Biosciences (Heidelberg, Germany). Dimethyl sulfoxide (DMSO) was obtained from Nacalai Tesque (Kyoto, Japan), and other reagents used in the study were commercial products of analytical grade. Oligonucleotides were commercially synthesized by Fasmac (Atsugi, Japan).

Construction of recombinant adenovirus: The open reading frame of *HNF6* was PCR amplified from cDNA obtained from HepG2 cells using the forward primer 5′-ccgagatctCGATGAACGCGCAGCTGACC-3′ and the reverse primer 5′-ccggtcgacTTCATGCTTTGGTACAAGTGC-3′, in which lower case letters represent *Bgl*II and *Sal*I restriction sites, respectively. The amplified fragments were subcloned into the pCR4-TOPO vector (Invitrogen Co., Carlsbad, CA). The plasmid was then digested with *Bgl*II and *Sal*I and was ligated into the corresponding sites of pShuttle-CMV (MP Biomedicals, Solon, OH). Human HNF6-expressing adenovirus (AdhHNF6) was prepared using the AdEasy™ System (Quantum Biotechnologies, Montreal, Canada) as reported previously.[32] Control adenovirus, *i.e.*, a β-galactosidase-expressing adenovirus (AdLacZ), was provided by Dr. Izumi Saito (The University of Tokyo, Tokyo, Japan). The titer of recombinant adenoviruses, 50% tissue culture infectious dose (TCID50), was determined as reported previously.[32] Multiplicity of infection (MOI) was calculated by dividing the TCID50 by the number of cells.

Cell line and cell culture: HepG2 cells were purchased from the RIKEN cell bank (Tsukuba, Japan). Cells were cultured in Dulbecco's modified Eagle's medium (DMEM; Wako Pure Chemicals) supplemented with 10% fetal bovine serum (FBS; Biowest, Miami, FL), minimum essential medium nonessential amino acids (MEM NEAA; Invitrogen), and Antibiotic-Antimycotic (Invitrogen), under 5% CO_2 at 37°C. The cells were seeded in 24-well tissue culture plates (BD Biosciences) at 1.0×10^5 cells per well at 1 d before adenovirus infection. After 72 h, these cells were harvested and total RNA was extracted. Whole cell lysates and total RNA were used for immunoblot analysis and real-time PCR, respectively.

Human primary hepatocyte cells and cell culture: Human fetal hepatocytes were obtained from Applied Cell Biology Research Institute (Kirkland, WA) and cultured in Williams' medium E (Sigma) containing 10% FBS (Biowest), 2 mM L-glutamine (Invitrogen), and antibiotics (Sigma) under 5% CO_2 at 37°C.[33] Human cryopreserved primary hepatocytes (lot HEP187170, 26-year-old Caucasian woman) were purchased from Biopredic International (Rennes, France). The hepatocytes were thawed and cultured using the medium kit according to the manufacturer's protocol. Fetal and adult hepatocytes were seeded in type I collagen-coated 24-well tissue culture plates (Sumitomo Bakelite Co. Ltd., Tokyo, Japan) at 5.0×10^4 and 1.0×10^5 cells per well, respectively, at 1 d before adenovirus infection. After 72 h, total RNA was extracted and used for real-time PCR.

Dual-reporter assays: The luciferase reporter plasmids, pGL3-basic and pGL4.82, were purchased from Promega (Madison, WI). Construction of the *CYP3A4* luciferase reporter plasmid, pCYP3A4-362-7.7k, has been described previously.[34]

HepG2 cells were plated into 48-well tissue culture plates (BD Biosciences) at a density of 6.0×10^4 cells and were then transfected with pCYP3A4-362-7.7k (0.4 μg) and pGL4.82 (0.1 μg), as an internal control, using Targefect F-1 (Nacalai Tesque). The next day, the cell medium was exchanged for culture medium and the cells were infected with the respective recombinant adenoviruses.

Copyright © 2013 by the Japanese Society for the Study of Xenobiotics (JSSX)

Table 1. Primers used for real-time PCR

Genes	Forward primers (5′–3′)	Reverse primers (5′–3′)	Reference
CYP1A1	CATCCCCCACACACAACA	CAGGGGTGAGAAACCGTTCA	35)
CYP1A2	AGTCCAGGAGCAGTATCAGG	CCTGCTCCAAAGATGTCATT	—
CYP2C9	CCTCTGGGGCATTATCCATC	ATATTTGCACAGTGAAACATAGGA	36)
CYP2C19	TTCATGCCTTTCTCAGCAGG	ACAGATAGTGAAATTTGGACC	36)
CYP2D6	GCCTTCCTGCCTTTCTCAGCAG	ATGGGTCACCAGGAAAGCAAA	37)
CYP3A4	CTGTGTGTTTCCAAGAGAAGTTAC	TGCATCAATTTCCTCCTGCAG	38)
CYP3A7	AGATTTAATCCATTAGATCCATTCG	AGGCGACCTTCTTTTATCTG	38)
CYP7A1	CAGAACTGAATGACCTGCCA	GGTGCAAAGTGAAATCCTCC	39)
AFP	AGCTTGGTGGTGGATGAAAC	CCCTCTTCAGCAAAGCAGAC	40)
ALB	TGGCACAATGAAGTGGGTAA	CTGAGCAAAGGCAATCAACA	41)
HNF6	GAAGGATAGAGGCAACACA	AGTTGCTGACAGTGCTCAG	—
GAPDH	CATGGGTGTGAACCATGAGAA	GGTCATGAGTCCTTCCACGAT	42)

After 72 h, cells were suspended in 0.1 mL passive lysis buffer (Promega). Reporter activities were determined using the Dual-Luciferase® Reporter Assay system (Promega). Luminescence derived from reactions using the reporter assay was monitored using a Glomax™ 96 Microplate Luminometer (Promega).

Human induced pluripotent stem cell culture: Human iPSCs, #51 Windy, were provided by Dr. Akihiro Umezawa, National Research Institute for Child Health and Development. The iPSCs were maintained in DMEM/F12 (Sigma) with 20% knockout serum replacement (KSR, Invitrogen), 2 mM L-glutamine (Invitrogen), 0.08 mM MEM NEAA (Invitrogen), 0.1 mM 2-ME, and 5 ng/mL bFGF, on mitomycin C-treated mouse embryonic fibroblasts (Oriental Yeast Co., Ltd., Tokyo, Japan). Cells were cultured under 5% CO_2 at 37°C.

Differentiation of human iPSCs: For induction of definitive endoderm, iPSCs were cultured for 3 d with Roswell Park Memorial Institute 1640 medium (RPMI 1640, Invitrogen) supplemented with 0.5% FBS, GlutaMAX (Invitrogen), 1 mM sodium butyrate, antibiotics (Sigma), and 100 ng/mL activin. Medium was refreshed on the second day. Subsequently, the differentiated cells were incubated in RPMI 1640 containing 2% KSR, GlutaMAX, 0.5 mM sodium butyrate, antibiotics (Sigma), and 100 ng/mL activin for 2 d.

For induction of hepatoblasts, the iPSC-derived definitive endoderms were treated with 10 nM Y-27632 for 1 h and were then passaged with Accutase (Innovative Cell Technologies, Inc., San Diego, CA). Cells were plated onto Matrigel™-coated (BD Matrigel™ Basement Membrane Matrix Growth Factor-Reduced, BD Biosciences) 24-well tissue culture plates (Sumitomo Bakelite Co., Ltd.) in KnockOut™ DMEM (Invitrogen), which was supplemented with 20% KSR, GlutaMAX, 0.1 mM NEAA, 0.1 mM 2-ME, antibiotics, and 1% DMSO. Medium was replaced every other day, and hepatoblast differentiation was continued for a further 7 d.

The iPSC-derived hepatoblasts were induced to differentiate into hepatocytes by switching to modified Lanford medium (Primary Cell Co., Ltd., Sapporo, Japan) supplemented with 10 ng/mL HGF, 20 ng/mL OSM, and 100 nM DEX. Cells were cultured for 14 d, and hepatic differentiation medium was refreshed every 2–3 d. In this hepatic maturation period, the cells were cultured and infected with AdhHNF6 (100 MOI) using 4 conditions (described below). Cells were then incubated with 0.2 mL of the recombinant adenovirus-containing medium for 1 h, followed by the addition of 0.8 mL medium.

For condition 1, the cells were infected with AdhHNF6 on day 15. After 3 d, the cells were recovered; thus, under condition 1, the culture period was 18 d. Under condition 2, the cells were infected with AdhHNF6 on day 19. After 3 d, the cells were recovered, totaling a culture period of 22 d. Under condition 3, the cells were infected with AdhHNF6 on day 22. After 3 d, the cells were recovered, resulting in a culture period of 25 d. Under condition 4, the cells were infected with AdhHNF6 on both days 19 and 22. Six days after the first infection, the cells were recovered, resulting in a culture period of 25 d. After these cells were harvested, total RNA extracted and whole cell lysates prepared were used to carry out real-time PCR and immunoblot analyses, respectively.

RNA purification and real-time PCR: Total RNA was extracted using TRI Reagent® (Molecular Research Center, Cincinnati, OH). First-strand cDNA was synthesized from 2 μg total RNA in a 25-μL reaction mixture using Moloney Murine Virus Reverse Transcriptase (Promega), oligo$(dT)_{20}$ primer, and a ribonuclease inhibitor (TaKaRa Bio, Kyoto, Japan). The cDNA was used for real-time PCR with SYBR Premix ExTaq (TaKaRa Bio) to measure mRNA levels of liver-specific genes, *CYPs*, and *glyceraldehyde-3-phosphate dehydrogenase* (*GAPDH*). Amplification reactions were performed with specific primers (**Table 1**).[35–42] Quantitative values were obtained above the threshold PCR cycle number (Ct) at which the increase in signal associated with an exponential growth in PCR products was detected using Thermal Cycler Dice™ TP800 (TaKaRa Bio). Relative mRNA expression levels in each sample were normalized to *GAPDH* expression levels.

Immunoblot analysis: Immunoblot analysis was performed to detect the expression of HNF6 proteins in HepG2 cells and iPSC-derived hepatocyte-like cells (iPSHCs). Whole cell lysate from these cells that had been infected with AdhHNF6 were size-fractionated by gel electrophoresis on a 10% polyacrylamide/0.1% sodium dodecyl sulfate gel, after being denatured by heating in a 2-ME-containing loading buffer. The proteins were electrotransferred to Immobilon®-P membranes (Millipore, Billerica, MA), which were then incubated for 1 h with polyclonal goat anti-human HNF6 antibody (Santa Cruz Biotechnology, Inc., Santa Cruz, CA) that had been diluted in Tris-buffered saline (1:1,000). The membranes were subsequently incubated for 1 h with a horseradish peroxidase-conjugated secondary antibody diluted in Tris-buffered saline (1:10,000; Santa Cruz Biotechnology, Inc.). After development with SuperSignal West Pico chemiluminescent substrate (Thermo Fisher Scientific Inc., Waltham, MA), the membrane was scanned using a Lumino Imaging Analyzer FAS-1000 (Toyobo, Osaka, Japan).

Determination of testosterone 6β-hydroxylase activity: Testosterone 6β-hydroxylase activity was determined as described previously with minor modification.[43] All iPSCs, iPSHCs,

Copyright © 2013 by the Japanese Society for the Study of Xenobiotics (JSSX)

AdhHNF6-infected iPSHCs (condition 4; see above differentiation of human iPSCs), HepG2 cells, and hepatocytes were incubated in culture medium containing 300 μM testosterone for 6 h. To terminate the 6β-hydroxylase activity, a double volume of 0.05% phosphoric acid containing acetonitrile was mixed with collected medium. The mixtures were centrifuged at 15,000 rpm for 15 min and the supernatants were subjected to HPLC analysis. A HPLC system (Shimadzu Corporation, Kyoto, Japan) equipped with Capcell Pak C18 UG120 column (4.6 × 250; particle size 5.0; Shiseido, Tokyo, Japan) was used. The flow rate was set at 1.0 mL/min and analyses were performed at 40°C. The mobile phase was solvent A (distilled water) and solvent B (0.05% phosphoric acid/acetonitrile). Typical conditions for elution were as follows: 25% B (0–15 min); 25–50% B (15–17 min); 50% B (17–21 min); 50–25% B (21–22 min); and 25% B (22–35 min). A linear gradient was used for all solvent changes. UV absorption intensity was monitored at 254 nm.

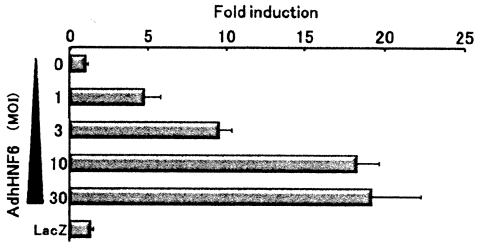


Fig. 1. Effect of HNF6 on CYP3A4 reporter activity in HepG2 cells
(A) HepG2 cells were seeded in 48-well tissue culture plates at 6.0×10^4 cells per well and were then transfected with pCYP3A4-362-7.7k (0.4 μg) and pGL4.82 (0.1 μg) as an internal control. The next day, the cell medium was exchanged for culture medium and cells were infected with recombinant adenovirus AdLacZ (MOI of 30) or AdhHNF6 (MOI of 1, 3, 10, or 30). After 72 h, reporter activities were measured. The reporter activity in non-infected HepG2 cells was set equal to 1.0. The data represent mean ± SD ($n = 3$).

Results

Transcriptional activation of the *CYP3A4* reporter gene by HNF6: To investigate the effect of HNF6 on *CYP3A4* transcriptional activation, a reporter assay was performed in HepG2 cells using a *CYP3A4*-luciferase reporter plasmid, pCYP3A4-362-7.7k, which contained a proximal promoter (+11 bp to 362 bp) and a distal xenobiotic-responsive enhancer module (XREM; −7.2 kb to −7.8 kb). HepG2 cells that had been infected with various amounts (1, 3, 10, and 30 MOI) of AdhHNF6 showed an increase in luciferase activity in an MOI-dependent manner, with an approximately 20-fold increase compared with the activity in non-infected cells (**Fig. 1**).

Expression of *CYP* and liver-specific genes in HNF6-overexpressed HepG2 cells: To confirm bioavailability of AdhHNF6 on the expression of *CYP* and liver-specific genes in HepG2 cells, cells were infected with AdhHNF6. *HNF6* mRNA levels showed a significant increase in an AdhHNF6 MOI-dependent manner. Protein expression of HNF6 was also confirmed in the cells (data not shown). The mRNA levels of *CYPs*, albumin (*ALB*), and α-fetoprotein (*AFP*) in AdhHNF6-infected HepG2 cells were measured by real-time PCR (**Fig. 2**). A previous study has shown that increase in hepatic HNF6 expression, caused by infection with AdHNF6, led to marked upregulation of *CYP7A1* mRNA.[29] In this study, HNF6 overexpression also resulted in an increase in *CYP7A1* mRNA expression. Of all the *CYPs*, the mRNA levels of *CYP3A4* and *CYP3A7* were significantly upregulated in HepG2 cells in an AdhHNF6 MOI-dependent manner, with an approximately 20-fold and 30-fold increase, respectively, as compared with the levels of these mRNAs in non-infected HepG2 cells. Similar increases were also observed for *CYP2C9* and *CYP2C19*, but not for *CYP1A1*, *CYP1A2*, or *CYP2D6*. A typical mature liver-specific gene, *ALB*, was significantly transactivated by the AdhHNF6 infection; however, a typical immature liver-specific gene, *AFP*, was not activated.

Expression of *CYP* and liver-specific genes in HNF6-overexpressed HFL cells and hepatocytes: To confirm the effect of HNF6 overexpression on the expression of *CYP* and liver-specific genes in HFL cells, cells were infected with AdhHNF6. *CYP3A4* mRNA levels showed the greater increase (120-fold increase compared to the levels in non-infected HFL cells) among the *CYPs* tested (**Fig. 3A**). mRNA levels of *CYP1A1*, *CYP1A2*, *CYP2C19*, and *CYP3A7* also significantly increased in HFL cells in an AdhHNF6 MOI-dependent manner, while the AdhHNF6-mediated induction of *AFP* and *ALB* gene transcription reached a peak at 10 MOI, above which the levels decreased. *CYP7A1* mRNA expression was below the detection limit of quantitative analysis by real-time PCR.

A developmental switch occurs between *CYP3A4* and *CYP3A7*, wherein hepatic *CYP3A7* expression dominates in the fetus, and hepatic *CYP3A4* expression dominates in the adult.[31] In contrast, *HNF6* is expressed in both fetal and adult hepatocytes.[44] To confirm the effect of HNF6 on human adult hepatocytes, we infected hepatocytes with AdhHNF6. Consequently, we found that AdhHNF6 infection increased *CYP3A7* mRNA expression, while *CYP3A4* mRNA expression did not change much (**Fig. 3B**). The increase in *CYP3A7* mRNA expression in hepatocytes peaked at 30 MOI, and the levels decreased thereafter in an AdhHNF6 MOI-dependent manner.

Effects of HNF6 on expression of *CYP* and liver-specific genes in iPSC-derived hepatocyte-like cells: Our protocol for differentiating iPSCs into iPSHCs is illustrated in **Figure 4**. This protocol comprised 3 stages: endoderm induction, hepatic specification, and hepatic maturation. In the hepatic maturation stage, we investigated whether HNF6 overexpression affects the expression of *CYP*, *ALB*, and *AFP*. iPSHCs were infected with AdhHNF6 at 3 or 6 d before the end of the hepatic differentiation process and were collected after a total culture period of 18, 22, or 25 d (see Materials and Methods for details). Similar to HepG2 cells, these cells demonstrated a significant increase in *HNF6* mRNA and protein expression after AdhHNF6 infection (**Figs. 5A** and **5B**). AdLacZ infection had no effect on *HNF6* mRNA or on other targeted transcripts in this study (data not shown).

CYP7A1 mRNA levels in iPSHCs at day 18 was similar to those in hepatocytes, but decreased depending on the culture period. However, *CYP7A1* mRNA levels in AdhHNF6-infected iPSHCs under condition 2 (14-fold), 3 (4-fold), or 4 (3-fold) were higher than those in non-infected iPSHCs after each culture period (22 d or 25 d; **Fig. 6A**).

Although *CYP3A4* mRNA was observed in iPSHCs, the expression level was very low as compared with that in HepG2 cells or hepatocytes. However, these levels increased markedly upon AdhHNF6 infection and were enhanced in a culture period-dependent manner (**Fig. 6A**). Maximum expression was observed in iPSHCs infected with AdhHNF6 for 5 d. The *CYP3A4* mRNA level was 1,450-fold higher than that in non-infected iPSHCs, and

Copyright © 2013 by the Japanese Society for the Study of Xenobiotics (JSSX)

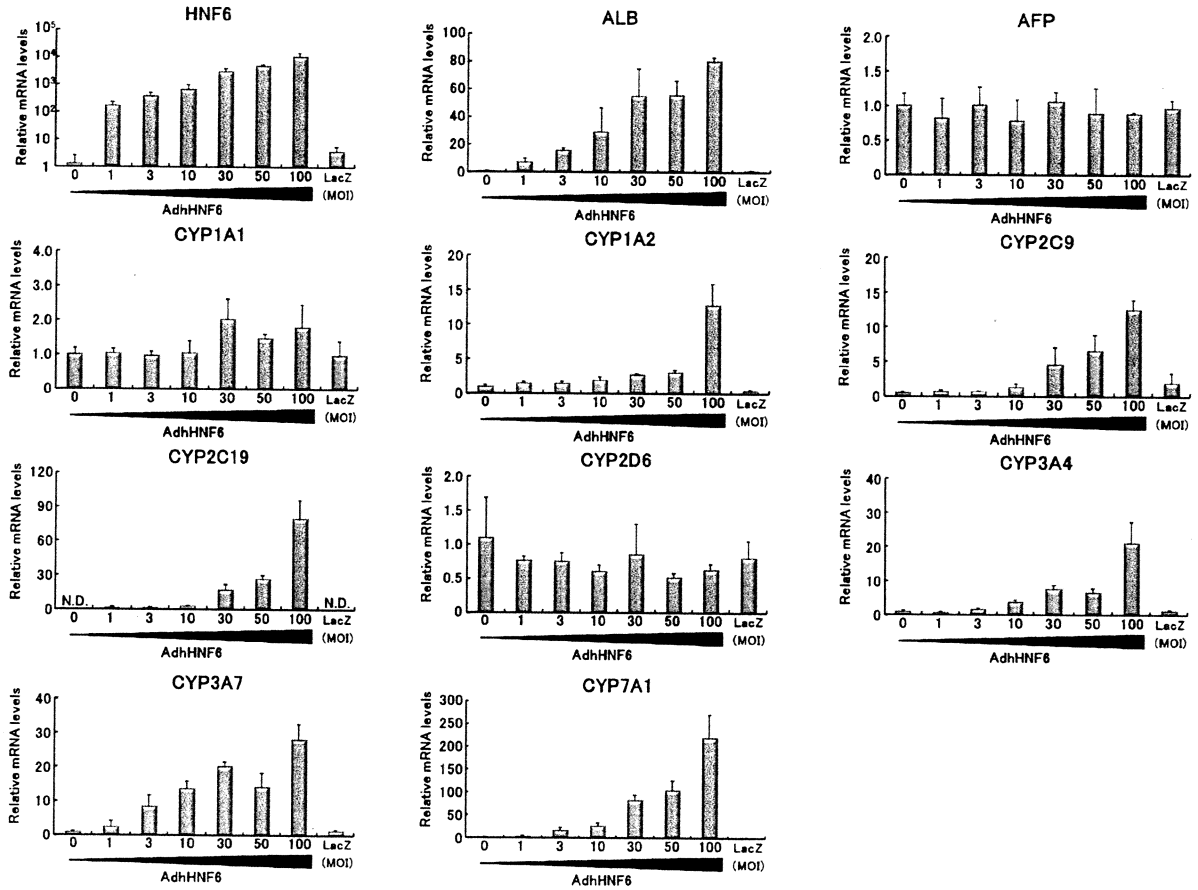


Fig. 2. Effect of HNF6 on *CYP*, *ALB*, and *AFP* mRNA levels in HepG2 cells
HepG2 cells were seeded in 24-well tissue culture plates at 1.0×10^5 cells per well a day before adenovirus infection. The cells were infected with AdLacZ (MOI of 100) or AdhHNF6 (MOI of 1, 3, 10, 30, 50, or 100). After 72 h, total RNA was extracted and real-time PCR was carried out as described in Materials and Methods. *CYP*, *ALB*, and *AFP* mRNA levels were normalized to those of *GAPDH*; the values for each of these mRNAs in non-infected HepG2 cells were set equal to 1.0. The data represent mean ± SD ($n = 3$).

nearly one-tenth of that in hepatocytes. Testosterone 6β-hydroxylase activity in AdhHNF6-infected iPSHCs was also measured. This metabolite was detected in AdhHNF6-infected iPSHCs and hepatocytes, but not in iPSCs, AdLacZ-infected iPSHCs, or HepG2 cells (**Fig. 6B**). Its activity in AdhHNF6-infected iPSHCs was equal to nearly one-fiftieth of that in hepatocytes.

We also observed some increase in *CYP1A2* and *CYP3A7* mRNA levels, but not in those of *CYP1A1*, *CYP2C9*, or *CYP2D6*. In contrast, *CYP2C19* mRNA levels in iPSHCs significantly increased in a culture period-dependent manner, but decreased upon AdhHNF6 infection.

AFP mRNA levels in iPSHCs reached the same levels as those in HepG2 cells and were significantly higher than those in hepatocytes. The *ALB* mRNA levels in iPSHCs at days 22 and 25 were 16-fold higher than those in HepG2 cells. Introducing AdhHNF6 did not affect the *ALB* or *AFP* mRNA levels in iPSHCs.

Discussion

In this study, we investigated whether HNF6 could modulate *CYP* gene transactivation in hepatocyte-like cells differentiated from iPSCs (**Fig. 6A**). Expression levels of the *CYP3A4* gene in iPSHCs were extremely low as compared with those in hepatocytes. Other *CYP* genes, excluding *CYP1A1*, were also expressed at levels significantly lower than those in hepatocytes. Furthermore, *AFP* mRNA levels in iPSHCs were similar to those in HepG2 cells, and were significantly higher than those in hepatocytes. Thus, iPSHCs differentiate into more fetal, rather than adult, hepatocyte-like cells. However, when HNF6 was introduced into iPSHCs, *CYP3A4* expression markedly increased and the cells gained the ability to metabolize testosterone (**Fig. 6B**). To our knowledge, our study is the first to show that HNF6 transactivates *CYP3A4* in iPSHCs.

CYP gene expression changes markedly during liver development, which is regulated by a dynamic network of LETFs. In particular, *CYP3A* genes show unique expression changes, influenced by development, and this developmental switch in gene expression between *CYP3A4* and *CYP3A7* occurs during the first 1–2 years after birth.[45] Previous studies have shown that c/EBPα, HNF3α, HNF3β, HNF3γ, and NF I interact with nucleotide sequences in the *CYP3A4* and *CYP3A7* proximal promoter regions, resulting in their transcriptional activation.[17,18,46] Saito *et al.*[47] indicated that NF I and HNF3β control the basal expression of *CYP3A7*, but not of *CYP3A4*. Conversely, c/EBPα and HNF3γ cooperatively enhance the transcription of *CYP3A4*. These tran-

Copyright © 2013 by the Japanese Society for the Study of Xenobiotics (JSSX)

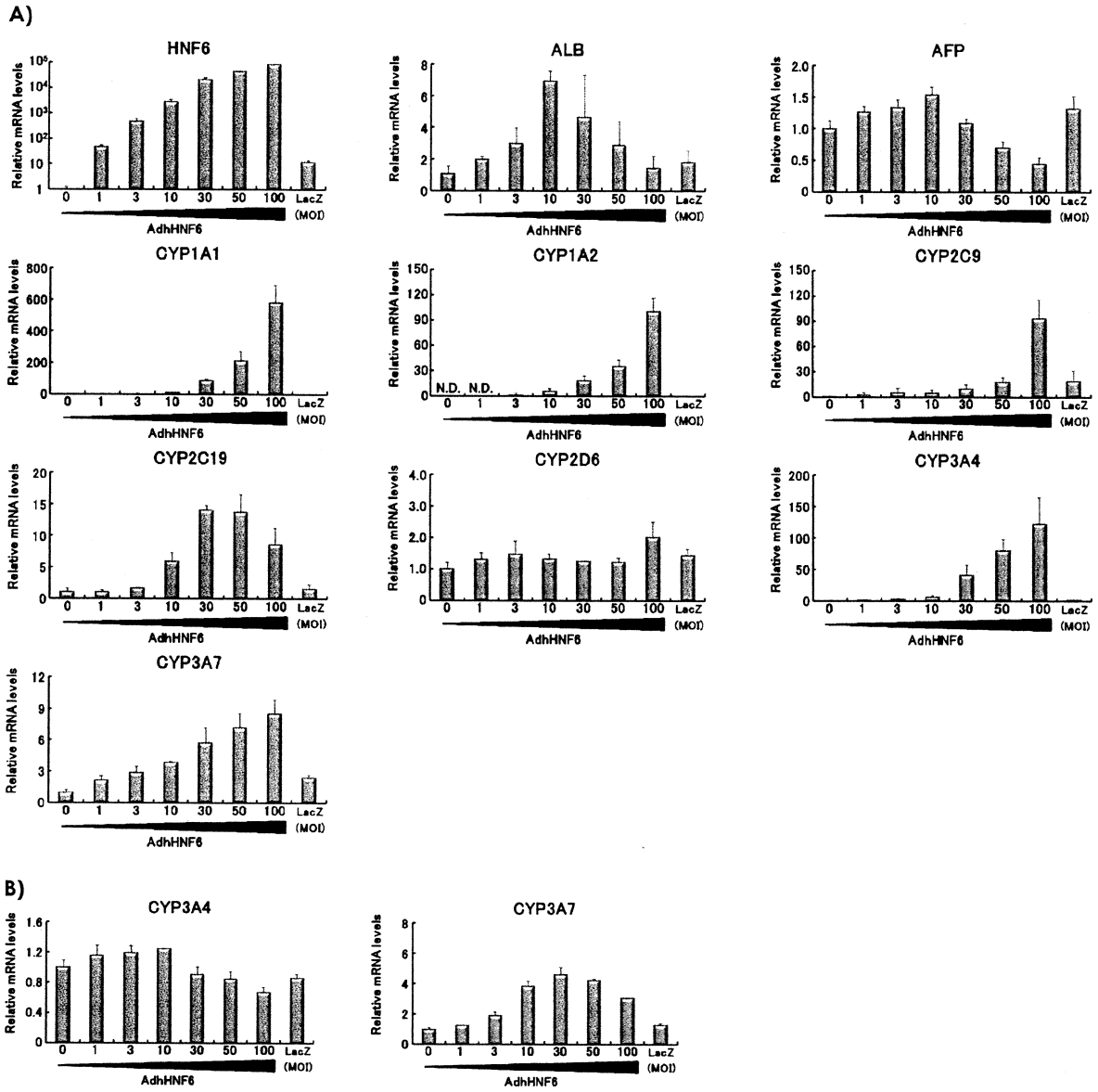


Fig. 3. Effect of HNF6 on *CYP*, *ALB*, and *AFP* mRNA levels in HFL cells and hepatocytes
HFL cells and hepatocytes were seeded in type I collagen-coated 24-well tissue culture plates at 5.0×10^4 and 1.0×10^5 cells per well, respectively, at 1 d before adenovirus infection. These cells were infected with AdLacZ (MOI of 100) or AdhHNF6 (MOI of 1, 3, 10, 30, 50, or 100). After 72 h, total RNA was extracted and real-time PCR was carried out as described in Materials and Methods (A: HFL cells, B: hepatocytes). *CYP3A4* and *CYP3A7* mRNA levels were normalized to those of *GAPDH*; the values for each of these mRNAs in non-infected hepatocytes or HFL cells were set equal to 1.0. The data represent mean ± SD ($n = 3$).

scription factors also upregulate transcription of *CYP3A7*, but to a lesser extent than that of *CYP3A4*. Although the 5′-flanking regions of these 2 genes are more than 90% identical over approximately 9 kb, distinct transcription factor complexes may contribute to developmental regulation by binding to *CYP3A4* and *CYP3A7* proximal promoters. Odom *et al.* showed that HNF6 binds to the promoter region of the genes encoding multidrug resistance-associated protein 2, CYP3A43, CYP51, and uridine diphosphate glucuronosyltransferase, as well as nuclear receptor genes, such as those encoding the pregnane X receptor and HNF4α.[48] These findings support the theory that HNF6 plays important roles in the regulation of pharmacokinetics-related genes. We demonstrated that HNF6 introduction resulted in increased *CYP3A4* gene transactivation in HFL cells and HepG2 cells, which have features similar to those of fetal hepatocyte-like cells, in terms of expressing *CYP3A7* and *AFP* (**Figs. 2** and **3A**). Our results also indicated that HNF6 significantly increased *CYP3A4* transcription in the iPSHCs generated, which showed features similar to those of fetal hepatocyte-like cells (**Fig. 6A**). In contrast, in hepatocytes, HNF6 introduction did not affect *CYP3A4* mRNA expression (**Fig. 3B**). These results suggest that HNF6 may play an important role in the transcriptional regulation of *CYP3A4* during hepatocyte maturation. This concept was supported by the observed changes in *HNF6* mRNA levels between fetal and adult hepatocytes.[49]

Copyright © 2013 by the Japanese Society for the Study of Xenobiotics (JSSX)

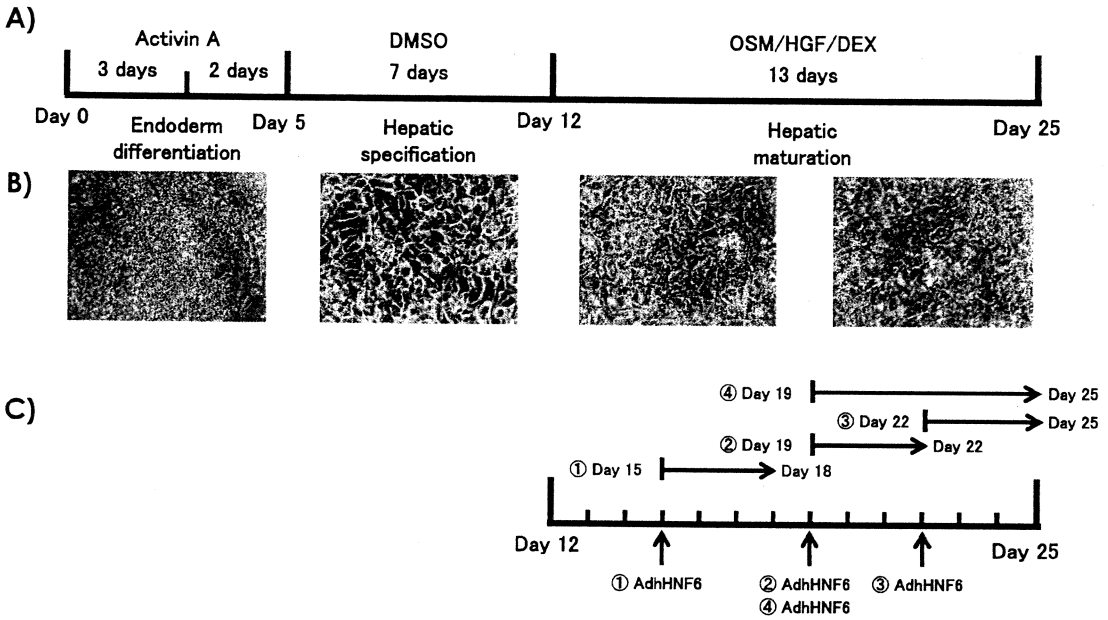


Fig. 4. (Color online) Strategy for the differentiation of iPSCs into hepatocyte-like cells
(A) iPSCs were cultured in RPMI 1640 supplemented with 0.5% FBS, GlutaMAX, 1 mM sodium butyrate, and 100 ng/mL activin for 3 d, and in RPMI 1640 supplemented with 2% KSR, GlutaMAX, 0.5 mM sodium butyrate, and 100 ng/mL activin for 2 d, to induce definitive endoderm formation. Next, the cells were plated onto Matrigel™-coated 24-well tissue culture plates in KnockOut™ DMEM supplemented with 20% KSR, GlutaMAX, 0.1 mM NEAA, 0.1 mM 2-ME, and 1% dimethyl sulfoxide for 7 d to induce hepatoblast formation. Subsequently, the iPSC-derived hepatoblasts were induced to differentiate into hepatocytes by switching to modified Lanford medium supplemented with 10 ng/mL HGF, 20 ng/mL OSM, and 100 nM DEX; these cells were then cultured for a further 14 d. (B) Morphological changes in iPSCs at different stages of differentiation. (C) A schematic representation of the AdhHNF6 infection schedule. Cells were cultured and infected with AdhHNF6 (100 MOI) using 4 conditions. For condition 1, the cells were infected with AdhHNF6 on day 15. After 3 d, the cells were recovered; thus, under condition 1, the culture period was 18 d. Under condition 2, the cells were infected with AdhHNF6 on day 19. After 3 d, the cells were recovered, totaling a culture period of 22 d. Under condition 3, the cells were infected with AdhHNF6 on day 22. After 3 d, the cells were recovered, resulting in a culture period of 25 d. Under condition 4, the cells were infected with AdhHNF6 on both days 19 and 22. Six days after the first infection, the cells were recovered, resulting in a culture period of 25 d.

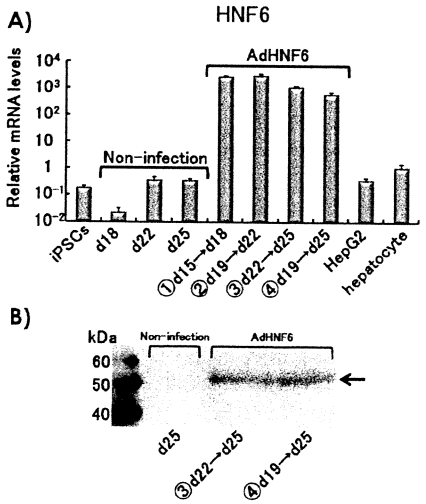


Fig. 5. *HNF6* mRNA and protein expression levels in iPSHCs infected with AdhHNF6
iPSHCs were infected with AdhHNF6 (100 MOI) at days 15, 19, and 22 or at days 19 and 22 (conditions 1, 2, 3, and 4, respectively). The cells were recovered after another 3 or 6 d, that is, following a total culture period of 18 d, 22 d, 25 d, and 25 d, respectively. After these cells were harvested, total RNA extracted and whole cell lysates prepared were used for real-time PCR (A) and immunoblot analyses (B), respectively, as described in Materials and Methods. Hepatocytes were cultured 48 h after plating the cells. *HNF6* mRNA levels were normalized to those of *GAPDH*; the value for HNF6 mRNA in hepatocytes, which had been cultured for 48 h, were set equal to 1.0. The data represent mean ± SD ($n = 3$).

Several studies have reported the successful differentiation of human iPSCs into hepatocyte-like cells. However, Song *et al.* [6] have shown that liver-specific genes such as *CYP2A6*, *CYP3A4*, *A1AT* (encoding α1-antitrypsin), and *ALB* were expressed at a lower level in differentiated iPSCs than in hepatocytes. Another study has also demonstrated that mRNA levels of most phase I and phase II enzymes were lower in iPSCs than in adult liver.[7] However, Takayama *et al.*[50] established a method to induce efficient hepatic differentiation of iPSCs by *HEX*, *SOX17*, and *HNF4α* transduction. *CYP3A4* mRNA levels in these hepatocyte-like cells were similar to those observed in primary hepatocytes. A previous study also showed that HNF1α, HNF4α, and HNF6 form part of a core transcriptional regulatory circuitry in hepatocytes.[51] Thus, HNF6, like HNF4α, may play a relatively important role in hepatic differentiation of iPSCs.

In this study, we observed transcriptional activation of the *CYP3A4* reporter gene, constructed with a proximal promoter and XREM regions, by introduction of HNF6 in HepG2 cells (**Fig. 1**). This result raises the possibility that HNF6 activates *CYP3A4* transcription through the proximal promoter and/or XREM regions. Previous studies have indicated that HNF6 directly controls *HNF1β* expression, cooperates with HNF1α to regulate *HNF4α* expression, and interacts with HNF3β without binding to DNA to stimulate *HNF3β*.[21,52,53] Several researchers have also reported that HNF6 participates in the recruitment of a coactivator, such as peroxisome proliferator-activated receptor gamma coactivator-1α,

Copyright © 2013 by the Japanese Society for the Study of Xenobiotics (JSSX)

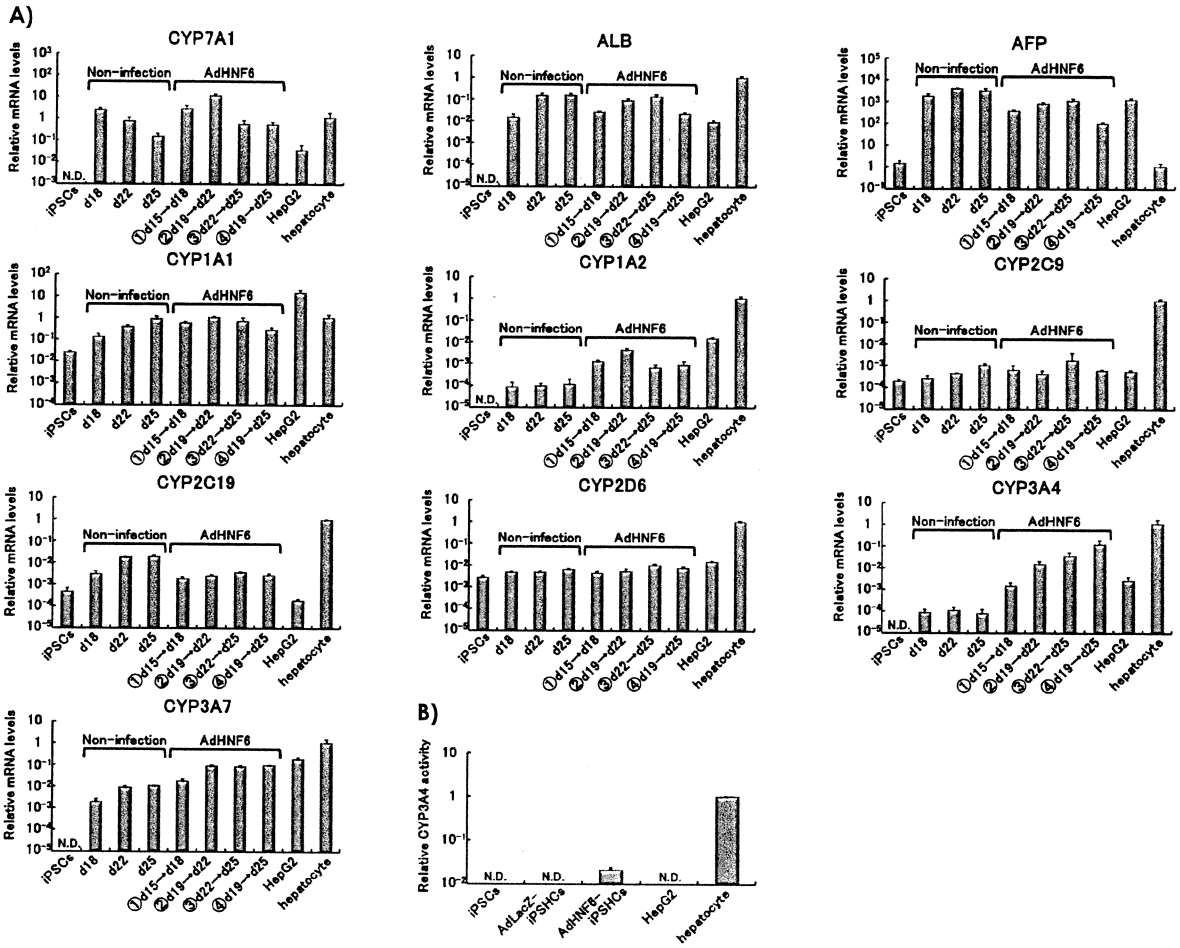


Fig. 6. Effect of HNF6 overexpression on *CYP*, *ALB*, and *AFP* mRNA levels and CYP3A4 activity in iPSHCs
(A) iPSHCs were infected with AdhHNF6 (100 MOI) on days 15, 19, and 22 or on days 19 and 22 (conditions 1, 2, 3, and 4, respectively). The cells were recovered after another 3 or 6 d, that is, following a total culture period of 18 d, 22 d, 25 d, and 25 d, respectively. After these cells were harvested, total RNA was extracted, and real-time PCR was carried out as described in Materials and Methods. *CYP*, *ALB*, and *AFP* mRNA levels were normalized to those of *GAPDH*; the values for each of these mRNAs in hepatocytes, which had been cultured for 48 h, were set equal to 1.0. The data represent mean ± SD ($n = 3$). (B) 6β-Hydroxytestosterone was measured with HPLC as described in Materials and Methods. The amounts of 6β-hydroxytestosterone in hepatocytes, which had been cultured for 48 h, were set equal to 1.0. The data represent mean ± SD ($n = 3$).

CREB-binding protein, and p300/CBP-associated factor, which is involved in *CYP* gene expression.[20,28] Thus, cross-regulatory cascades between HNF6 and other LETFs may be involved in the expression of *CYP3A4* in fetal hepatocyte-like cells, iPSHCs, HepG2 cells, and HFL cells. Further studies are needed to clarify whether the HNF6 directly or indirectly controls the expression of *CYP3A4* gene. Expression of other *CYP* genes was different in the effect of HNF6 introduction among HepG2 cells, HFL cells, and iPSHCs. This phenomenon may be caused by the different pattern of individual LETF expression relating to *CYP* gene expression in these cells.

In this study, we examined the role of HNF6 in the transactivation of *CYP* and liver-specific genes in iPSHCs. Our results showed that HNF6 strongly increases *CYP3A4* mRNA levels in iPSHCs, as well as in HepG2 cells and HFL cells. Furthermore, these cells had the ability to metabolize testosterone. The hepatic differentiation method using AdhHNF6 may contribute to the efficient development of hepatocytes from iPSCs. However, our AdhHNF6-infected iPSHCs still retained characteristics of immature hepatocytes. Future studies are required to further investigate the combinatorial effects of HNF6 and other transcriptional factors.

Acknowledgments: The authors are most grateful to Dr. Akihiro Umezawa (Department of Reproductive Biology and Pathology, National Research Institute for Child Health and Development) who provided the human iPSCs.

References

1) Donato, M. T., Lahoz, A., Castell, J. V. and Gomez-Lechon, M. J.: Cell lines: a tool for in vitro drug metabolism studies. *Curr. Drug Metab.*, **9**: 1–11 (2008).
2) LeCluyse, E., Madan, A., Hamilton, G., Carroll, K., Dehaan, R. and Parkinson, A.: Expression and regulation of cytochrome P450 enzymes in primary cultures of human hepatocytes. *J. Biochem. Mol. Toxicol.*, **14**: 177–188 (2000).
3) Aninat, C., Piton, A., Glaise, D., Le Charpentier, T., Langouet, S., Morel, F., Guguen-Guillouzo, C. and Guillouzo, A.: Expression of cytochromes P450, conjugating enzymes and nuclear receptors in human hepatoma HepaRG cells. *Drug Metab. Dispos.*, **34**: 75–83 (2006).
4) Funakoshi, N., Duret, C., Pascussi, J. M., Blanc, P., Maurel, P., Daujat-

Copyright © 2013 by the Japanese Society for the Study of Xenobiotics (JSSX)

Chavanieu, M. and Gerbal-Chaloin, S.: Comparison of hepatic-like cell production from human embryonic stem cells and adult liver progenitor cells: CAR transduction activates a battery of detoxification genes. *Stem Cell Rev.*, **7**: 518–531 (2011).
5) Takahashi, K., Tanabe, K., Ohnuki, M., Narita, M., Ichisaka, T., Tomoda, K. and Yamanaka, S.: Induction of pluripotent stem cells from adult human fibroblasts by defined factors. *Cell*, **131**: 861–872 (2007).
6) Song, Z., Cai, J., Liu, Y., Zhao, D., Yong, J., Duo, S., Song, X., Guo, Y., Zhao, Y., *et al.*: Efficient generation of hepatocyte-like cells from human induced pluripotent stem cells. *Cell Res.*, **19**: 1233–1242 (2009).
7) Si-Tayeb, K., Noto, F. K., Nagaoka, M., Li, J., Battle, M. A., Duris, C., North, P. E., Dalton, S. and Duncan, S. A.: Highly efficient generation of human hepatocyte-like cells from induced pluripotent stem cells. *Hepatology*, **51**: 297–305 (2010).
8) Takata, A., Otsuka, M., Kogiso, T., Kojima, K., Yoshikawa, T., Tateishi, R., Kato, N., Shiina, S., Yoshida, H., *et al.*: Direct differentiation of hepatic cells from human induced pluripotent stem cells using a limited number of cytokines. *Hepatol. Int.*, **5**: 890–898 (2011).
9) Schrem, H., Klempnauer, J. and Borlak, J.: Liver-enriched transcription factors in liver function and development. Part I: the hepatocyte nuclear factor network and liver-specific gene expression. *Pharmacol. Rev.*, **54**: 129–158 (2002).
10) Gonzalez, F. J.: Regulation of hepatocyte nuclear factor 4 alpha-mediated transcription. *Drug Metab. Pharmacokinet.*, **23**: 2–7 (2008).
11) Jover, R., Moya, M. and Gomez-Lechon, M. J.: Transcriptional regulation of cytochrome p450 genes by the nuclear receptor hepatocyte nuclear factor 4-alpha. *Curr. Drug Metab.*, **10**: 508–519 (2009).
12) Kamiyama, Y., Matsubara, T., Yoshinari, K., Nagata, K., Kamimura, H. and Yamazoe, Y.: Role of human hepatocyte nuclear factor 4alpha in the expression of drug-metabolizing enzymes and transporters in human hepatocytes assessed by use of small interfering RNA. *Drug Metab. Pharmacokinet.*, **22**: 287–298 (2007).
13) Chung, I. and Bresnick, E.: Regulation of the constitutive expression of the human CYP1A2 gene: cis elements and their interactions with proteins. *Mol. Pharmacol.*, **47**: 677–685 (1995).
14) Gonzalez, F. J. and Lee, Y. H.: Constitutive expression of hepatic cytochrome P450 genes. *FASEB J.*, **10**: 1112–1117 (1996).
15) Shintani, M., Ieiri, I., Inoue, K., Mamiya, K., Ninomiya, H., Tashiro, N., Higuchi, S. and Otsubo, K.: Genetic polymorphisms and functional characterization of the 5′-flanking region of the human CYP2C9 gene: in vitro and in vivo studies. *Clin. Pharmacol. Ther.*, **70**: 175–182 (2001).
16) Cheung, C., Akiyama, T. E., Kudo, G. and Gonzalez, F. J.: Hepatic expression of cytochrome P450s in hepatocyte nuclear factor 1-alpha (HNF1alpha)-deficient mice. *Biochem. Pharmacol.*, **66**: 2011–2020 (2003).
17) Rodríguez-Antona, C., Bort, R., Jover, R., Tindberg, N., Ingelman-Sundberg, M., Gomez-Lechon, M. J. and Castell, J. V.: Transcriptional regulation of human CYP3A4 basal expression by CCAAT enhancer-binding protein alpha and hepatocyte nuclear factor-3 gamma. *Mol. Pharmacol.*, **63**: 1180–1189 (2003).
18) Bombail, V., Taylor, K., Gibson, G. G. and Plant, N.: Role of Sp1, C/EBP alpha, HNF3, and PXR in the basal- and xenobiotic-mediated regulation of the CYP3A4 gene. *Drug Metab. Dispos.*, **32**: 525–535 (2004).
19) Lannoy, V. J., Burglin, T. R., Rousseau, G. G. and Lemaigre, F. P.: Isoforms of hepatocyte nuclear factor-6 differ in DNA-binding properties, contain a bifunctional homeodomain, and define the new ONECUT class of homeodomain proteins. *J. Biol. Chem.*, **273**: 13552–13562 (1998).
20) Lannoy, V. J., Rodolosse, A., Pierreux, C. E., Rousseau, G. G. and Lemaigre, F. P.: Transcriptional stimulation by hepatocyte nuclear factor-6. Target-specific recruitment of either CREB-binding protein (CBP) or p300/CBP-associated factor (p/CAF). *J. Biol. Chem.*, **275**: 22098–22103 (2000).
21) Rausa, F. M., Tan, Y. and Costa, R. H.: Association between hepatocyte nuclear factor 6 (HNF-6) and FoxA2 DNA binding domains stimulates FoxA2 transcriptional activity but inhibits HNF-6 DNA binding. *Mol. Cell. Biol.*, **23**: 437–449 (2003).
22) Briançon, N., Bailly, A., Clotman, F., Jacquemin, P., Lemaigre, F. P. and Weiss, M. C.: Expression of the alpha7 isoform of hepatocyte nuclear factor (HNF) 4 is activated by HNF6/OC-2 and HNF1 and repressed by HNF4alpha1 in the liver. *J. Biol. Chem.*, **279**: 33398–33408 (2004).
23) Plumb-Rudewiez, N., Clotman, F., Strick-Marchand, H., Pierreux, C. E., Weiss, M. C., Rousseau, G. G. and Lemaigre, F. P.: Transcription factor HNF-6/OC-1 inhibits the stimulation of the HNF-3alpha/Foxa1 gene by TGF-beta in mouse liver. *Hepatology*, **40**: 1266–1274 (2004).
24) Landry, C., Clotman, F., Hioki, T., Oda, H., Picard, J. J., Lemaigre, F. P. and Rousseau, G. G.: HNF-6 is expressed in endoderm derivatives and nervous system of the mouse embryo and participates to the cross-regulatory network of liver-enriched transcription factors. *Dev. Biol.*, **192**: 247–257 (1997).
25) Jochheim, A., Hillemann, T., Kania, G., Scharf, J., Attaran, M., Manns, M. P., Wobus, A. M. and Ott, M.: Quantitative gene expression profiling reveals a fetal hepatic phenotype of murine ES-derived hepatocytes. *Int. J. Dev. Biol.*, **48**: 23–29 (2004).
26) Clotman, F., Jacquemin, P., Plumb-Rudewiez, N., Pierreux, C. E., Van Der Smissen, P., Dietz, H. C., Courtoy, P. J., Rousseau, G. G. and Lemaigre, F. P.: Control of liver cell fate decision by a gradient of TGF beta signaling modulated by Onecut transcription factors. *Genes Dev.*, **19**: 1849–1854 (2005).
27) Margagliotti, S., Clotman, F., Pierreux, C. E., Beaudry, J. B., Jacquemin, P., Rousseau, G. G. and Lemaigre, F. P.: The Onecut transcription factors HNF-6/OC-1 and OC-2 regulate early liver expansion by controlling hepatoblast migration. *Dev. Biol.*, **311**: 579–589 (2007).
28) Beaudry, J. B., Pierreux, C. E., Hayhurst, G. P., Plumb-Rudewiez, N., Weiss, M. C., Rousseau, G. G. and Lemaigre, F. P.: Threshold levels of hepatocyte nuclear factor 6 (HNF-6) acting in synergy with HNF-4 and PGC-1alpha are required for time-specific gene expression during liver development. *Mol. Cell. Biol.*, **26**: 6037–6046 (2006).
29) Wang, M., Tan, Y., Costa, R. H. and Holterman, A. X.: In vivo regulation of murine CYP7A1 by HNF-6: a novel mechanism for diminished CYP7A1 expression in biliary obstruction. *Hepatology*, **40**: 600–608 (2004).
30) Stevens, J. C., Hines, R. N., Gu, C., Koukouritaki, S. B., Manro, J. R., Tandler, P. J. and Zaya, M. J.: Developmental expression of the major human hepatic CYP3A enzymes. *J. Pharmacol. Exp. Ther.*, **307**: 573–582 (2003).
31) Hines, R. N.: Ontogeny of human hepatic cytochromes P450. *J. Biochem. Mol. Toxicol.*, **21**: 169–175 (2007).
32) Matsubara, T., Noracharttiyapot, W., Toriyabe, T., Yoshinari, K., Nagata, K. and Yamazoe, Y.: Assessment of human pregnane X receptor involvement in pesticide-mediated activation of CYP3A4 gene. *Drug Metab. Dispos.*, **35**: 728–733 (2007).
33) Matsunaga, T., Maruyama, M., Harada, E., Katsuyama, Y., Sugihara, N., Ise, H., Negishi, N., Ikeda, U. and Ohmori, S.: Expression and induction of CYP3As in human fetal hepatocytes. *Biochem. Biophys. Res. Commun.*, **318**: 428–434 (2004).
34) Takada, T., Ogino, M., Miyata, M., Shimada, M., Nagata, K. and Yamazoe, Y.: Differences in transactivation between rat CYP3A1 and human CYP3A4 genes by human pregnane X receptor. *Drug Metab. Pharmacokinet.*, **19**: 103–113 (2004).
35) Berge, G., Mollerup, S., ØVrebø, S., Hewer, A., Phillips, D. H., Eilertsen, E. and Haugen, A.: Role of estrogen receptor in regulation of polycyclic aromatic hydrocarbon metabolic activation in lung. *Lung Cancer*, **45**: 289–297 (2004).
36) Pérez, G., Tabares, B., Jover, R., Gomez-Lechon, M. J. and Castell, J. V.: Semi-automatic quantitative RT-PCR to measure CYP induction by drugs in human hepatocytes. *Toxicol. In Vitro*, **17**: 643–649 (2003).
37) Endrizzi, K., Fischer, J., Klein, K., Schwab, M., Nussler, A., Neuhaus, P., Eichelbaum, M. and Zanger, U. M.: Discriminative quantification of cytochrome P4502D6 and 2D7/8 pseudogene expression by TaqMan real-time reverse transcriptase polymerase chain reaction. *Anal. Biochem.*, **300**: 121–131 (2002).
38) Maezawa, K., Matsunaga, T., Takezawa, T., Kanai, M., Ohira, S. and Ohmori, S.: Cytochrome P450 3As gene expression and testosterone 6 beta-hydroxylase activity in human fetal membranes and placenta at full term. *Biol. Pharm. Bull.*, **33**: 249–254 (2010).
39) Field, F. J., Watt, K. and Mathur, S. N.: TNF-alpha decreases ABCA1 expression and attenuates HDL cholesterol efflux in the human intestinal cell line Caco-2. *J. Lipid. Res.*, **51**: 1407–1415 (2010).
40) Mou, X., Wu, Y., Cao, H., Meng, Q., Wang, Q., Sun, C., Hu, S., Ma, Y. and Zhang, H.: Generation of disease-specific induced pluripotent stem cells from patients with different karyotypes of Down syndrome. *Stem Cell Res. Ther.*, **3**: 14 (2012).
41) Roelandt, P., Pauwelyn, K. A., Sancho-Bru, P., Subramanian, K., Bose, B., Ordovas, L., Vanuytsel, K., Geraerts, M., Firpo, M., *et al.*: Human embryonic and rat adult stem cells with primitive endoderm-like phenotype can be fated to definitive endoderm, and finally hepatocyte-like cells. *PLoS ONE*, **5**: e12101 (2010).
42) Nishimura, M. and Naito, S.: Tissue-specific mRNA expression profiles of human toll-like receptors and related genes. *Biol. Pharm. Bull.*, **28**: 886–892 (2005).
43) Aoyama, K., Yoshinari, K., Kim, H. J., Nagata, K. and Yamazoe, Y.: Simultaneous expression of plural forms of human cytochrome P450 at desired ratios in HepG2 cells: adenovirus-mediated tool for cytochrome P450 reconstitution. *Drug Metab. Pharmacokinet.*, **24**: 209–217 (2009).

Copyright © 2013 by the Japanese Society for the Study of Xenobiotics (JSSX)

44) Limaye, P. B., Alarcon, G., Walls, A. L., Nalesnik, M. A., Michalopoulos, G. K., Demetris, A. J. and Ochoa, E. R.: Expression of specific hepatocyte and cholangiocyte transcription factors in human liver disease and embryonic development. *Lab. Invest.*, **88**: 865–872 (2008).
45) Lacroix, D., Sonnier, M., Moncion, A., Cheron, G. and Cresteil, T.: Expression of CYP3A in the human liver—evidence that the shift between CYP3A7 and CYP3A4 occurs immediately after birth. *Eur. J. Biochem.*, **247**: 625–634 (1997).
46) Riffel, A. K., Schuenemann, E. and Vyhlidal, C. A.: Regulation of the CYP3A4 and CYP3A7 promoters by members of the nuclear factor I transcription factor family. *Mol. Pharmacol.*, **76**: 1104–1114 (2009).
47) Saito, T., Takahashi, Y., Hashimoto, H. and Kamataki, T.: Novel transcriptional regulation of the human CYP3A7 gene by Sp1 and Sp3 through nuclear factor kappa B-like element. *J. Biol. Chem.*, **276**: 38010–38022 (2001).
48) Odom, D. T., Zizlsperger, N., Gordon, D. B., Bell, G. W., Rinaldi, N. J., Murray, H. L., Volkert, T. L., Schreiber, J., Rolfe, P. A., *et al.*: Control of pancreas and liver gene expression by HNF transcription factors. *Science*, **303**: 1378–1381 (2004).
49) Kyrmizi, I., Hatzis, P., Katrakili, N., Tronche, F., Gonzalez, F. J. and Talianidis, I.: Plasticity and expanding complexity of the hepatic transcription factor network during liver development. *Genes Dev.*, **20**: 2293–2305 (2006).
50) Takayama, K., Inamura, M., Kawabata, K., Katayama, K., Higuchi, M., Tashiro, K., Nonaka, A., Sakurai, F., Hayakawa, T., *et al.*: Efficient generation of functional hepatocytes from human embryonic stem cells and induced pluripotent stem cells by HNF4alpha transduction. *Mol. Ther.*, **20**: 127–137 (2012).
51) Odom, D. T., Dowell, R. D., Jacobsen, E. S., Nekludova, L., Rolfe, P. A., Danford, T. W., Gifford, D. K., Fraenkel, E., Bell, G. I., *et al.*: Core transcriptional regulatory circuitry in human hepatocytes. *Mol. Syst. Biol.*, **2**: 2006. 0017 (2006).
52) Hatzis, P. and Talianidis, I.: Regulatory mechanisms controlling human hepatocyte nuclear factor 4alpha gene expression. *Mol. Cell. Biol.*, **21**: 7320–7330 (2001).
53) Clotman, F., Lannoy, V. J., Reber, M., Cereghini, S., Cassiman, D., Jacquemin, P., Roskams, T., Rousseau, G. G. and Lemaigre, F. P.: The onecut transcription factor HNF6 is required for normal development of the biliary tract. *Development*, **129**: 1819–1828 (2002).

Copyright © 2013 by the Japanese Society for the Study of Xenobiotics (JSSX)

Bioorganic & Medicinal Chemistry Letters 22 (2012) 4728–4730

Contents lists available at SciVerse ScienceDirect

Bioorganic & Medicinal Chemistry Letters

journal homepage: www.elsevier.com/locate/bmcl

Estrogenic activity of *B*-fluorinated *o*-carborane-1,2-bisphenol synthesized via S_NAr reaction

Kiminori Ohta, Takumi Ogawa, Yasuyuki Endo *

Faculty of Pharmaceutical Sciences, Tohoku Pharmaceutical University, 4-4-1 Komatsushima, Aoba-ku, Sendai 981-8558, Japan

ARTICLE INFO

Article history:
Received 6 April 2012
Revised 17 May 2012
Accepted 18 May 2012
Available online 30 May 2012

Keywords:
Estrogen
Estrogen receptors
SERMs
Carboranes

ABSTRACT

We previously identified *o*-carborane bisphenol BE360 (**4**) as a selective estrogen receptor modulator (SERM), which ameliorated bone loss without inducing estrogenic action in uterus of OVX and ORX mice. Here, we synthesized a fluorinated derivative, *B*-fluorinated *o*-carborane bisphenol BE310 (**5**) by means of S_NAr reaction. Compound **5** was a partial ER agonist, like **4**, with little change of ERα and ERβ selectivity as compared with **4**. However, its agonistic activity was 40 times weaker than that of **4**. Thus, **5** is a novel SERM candidate with potential for reduced estrogenic side effects, and in vivo evaluation as an anti-osteoporosis agent seems warranted.

© 2012 Elsevier Ltd. All rights reserved.

The estrogen receptor (ER) is a member of the nuclear receptor superfamily. Endogenous estrogen, 17β-estradiol (**1**), plays important roles in regulation of the female and male reproductive systems, as well as in bone metabolism, the cardiovascular system, and the central nervous system.[1] The first step in the appearance of estrogenic activity is binding of agonist ligands to ERα and ERβ, resulting in conformational change of the receptors. The ligand-bound ERs dimerize and form huge complexes with various cofactors, then bind to specific promoter elements of DNA to initiate gene transcription.[2] Compounds that either induce or inhibit cellular estrogenic responses are potential biochemical tools and drug candidates.[3] For example, 4-hydroxytamoxifen (**2**) has potent antagonistic activity for ER and acts as a selective estrogen receptor modulator (SERM).[4] Currently, various third- or fourth-generation SERMs are under development. One of them is compound (**3**), which is a potent antiestrogen, but lacks the alkylamino residue found in typical SERMs[5] (Fig. 1).

During our studies of carborane-containing ER modulators,[6] we found that the simple 1,2-bis(4-hydroxyphenyl)-*o*-carborane BE360 (**4**) exhibited a high binding affinity to ERs and showed partial agonistic activity in vitro (Fig. 2).[7] Furthermore, in an in vivo study, compound **4** exhibited estrogenic action in bone, ameliorating bone loss without showing estrogenic action in uterus of OVX and ORX mice. Thus, it is a candidate for application as a new type of SERM to treat osteoporosis.[8] Development of ERα and ERβ subtype-selective ligands is also of interest to medicinal chemists because they show quite different biological actions in vivo. In several cases, ERβ-selective ligands have been obtained by the introduction of electron-rich substituents, such as halogens, nitrogen, oxygen, or a cyano group, which interact unfavorably with the sulfur atom of the amino acid residue Met421 of ERα.[9]

In recent decades, increasing numbers of fluorine-containing drug candidates have been reported.[10] Fluorine can effectively replace either hydrogen or oxygen, while altering the biological characteristics of the parent molecule. So, we considered that introduction of fluorine on the carborane skeleton of bisphenol **4** might modify the ER subtype selectivity and partial agonistic activity. Therefore, we set out to synthesize *B*-fluorinated *o*-carborane bisphenol BE310 (**5**) as a novel ER modulator candidate (Fig. 2).

Two synthetic methods are available for *o*-carborane bisphenol derivatives (Scheme 1). One is condensation of the corresponding diaryl acetylenes with decaborane (**14**) in the presence of Lewis bases.[11] However, since *B*-fluorinated decaborane is difficult to prepare, this condensation reaction seemed unsuitable to synthesize **5**. The other method is C-arylation by direct coupling reaction of *C*-copper *o*-carborane with aryl iodides.[12] This reaction can afford *C*-monoaryl-*o*-carboranes in moderate yield, but not *C,C'*-diaryl-*o*-carboranes, irrespective of the ratio of reagent to substrate. To overcome this problem, we have recently reported a novel synthetic method for 1,2-diaryl-*o*-carboranes employing S_NAr reaction (Scheme 2).[13] This reaction proceeds smoothly under mild conditions and is a powerful tool for the synthesis of 1,2-diaryl-*o*-carboranes from the monoaryl-*o*-carboranes.

In this Letter, we describe the synthesis of **5** by means of S_NAr reaction and an evaluation of its biological activities. This is the first report of application of the S_NAr reaction to synthesis of *B*-substituted aryl-*o*-carborane.

* Corresponding author.
E-mail address: yendo@tohoku-pharm.ac.jp (Y. Endo).

0960-894X/$ - see front matter © 2012 Elsevier Ltd. All rights reserved.
http://dx.doi.org/10.1016/j.bmcl.2012.05.068

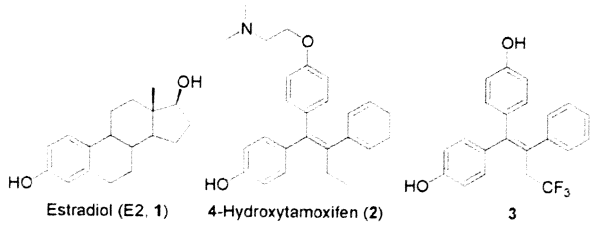


Figure 1. Structures of endogenous ligand and SERMs.

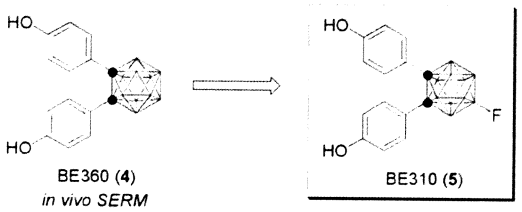
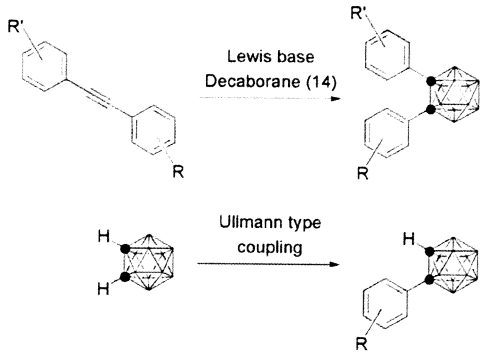
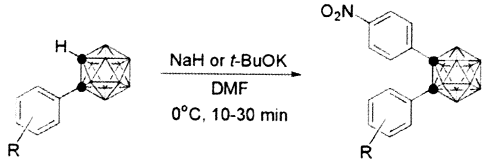


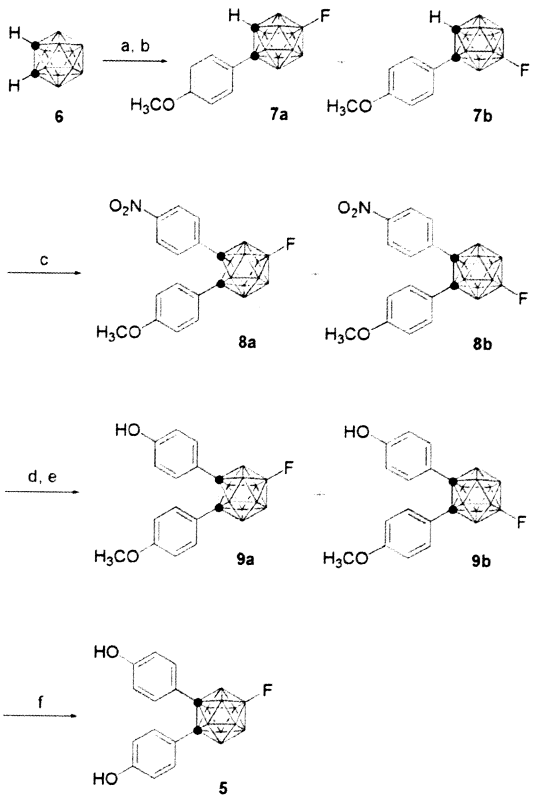
Figure 2. Structures of BE360 (**4**) and the newly synthesized *B*-fluorinated *o*-carborane bisphenol BE310 (**5**).



Scheme 1. Classical synthetic methods for *C*-aryl *o*-carborane derivatives.



Scheme 2. Diaryl *o*-carborane synthesis using S_NAr reaction.



Scheme 3. Synthesis of *B*-fluorinated *o*-carborane bisphenol **5**. Reagents and conditions: (a) SbF_5, $C_{10}F_{18}$, 120 °C, 7 h; (b) *n*-BuLi, DME, then Cu(I)Cl, pyridine, 4-iodoanisole, 110 °C, 24 h; (c) potassium *tert*-butoxide, 4-fluoronitrobenzene, DMF, 0 °C, 30 min; (d) Pd/C, H_2, AcOEt/EtOH = 1/1, rt, 30 min; (e) c.HCl and $NaNO_2$, then H_2SO_4, reflux, 1 h; (f) BBr_3, CH_2Cl_2, rt, 8 h.

Table 1
Comparison of relative binding affinity (RBA) of *o*-carborane bisphenol derivatives for human recombinant ERα and ERβ

Compound	RBA		Selectivity ERβ/ERα
	ERα	ERβ	
E2	100	100	1.0
BE360 (**1**)	68	46	0.68
BE310 (**5**)	15	16	1.1

All binding assays were performed in duplicate ($n = 2$). Values are average of percentage displacement of [^{3}H]estradiol (4 nM) specific binding to human recombinant ERs by each compound at 4 nM. The binding affinity of E2 is taken as 100.

Scheme 3 summarizes the synthesis of compound **5**. *o*-Carborane (**6**) was treated with antimony pentafluoride in perfluorodecalin at 120 °C for 7 h to afford 9-fluorinated *o*-carborane in 69% yield.[14] The *B*-fluorinated position of the *o*-carborane cage was assigned on the basis of the ^{11}B NMR spectrum. After treatment of *B*-fluorinated *o*-carborane with *n*-BuLi, the resultant *C*-lithio-*o*-carborane was transformed into *C*-copper-*o*-carborane, which was reacted with 4-iodoanisole in the presence of pyridine as a ligand of copper to afford a 1:1 mixture of **7a** and **7b** in 28% yield.[12] These compounds could not be separated by silica gel column chromatography under any of the conditions examined. A mixture of **7a** and **7b** was reacted with 4-fluoronitrobenzene in the presence of potassium *tert*-butoxide as a base in DMF at 0 °C for 30 min to afford a 1:1 mixture of diaryl-*o*-carboranes **8a** and **8b** in 73% yield.[13]

This result means that the reactivity of the fluorinated aryl-*o*-carboranes **7** is the same regardless of the position of the fluorine atom. The nitro group of the mixture of **8a** and **8b** was reduced by means of catalytic hydrogenation to afford a mixture of aniline derivatives in 82% yield. The B–F bond remained intact under the catalytic hydrogenation conditions. After diazotization of the mixture of aniline derivatives with concentrated HCl aqueous solution and $NaNO_2$, the mixture was refluxed with 0.5 M aqueous sulfuric acid to afford the corresponding phenol derivatives **9a** and **9b** in 14% yield. The methoxy group was deprotected with BBr_3 to afford the target compound **5** in 87% yield.

The biological activities of **5** were evaluated by means of competitive ER binding assay and MCF-7 cell proliferation assay.[6b,15] Competitive binding assays using [2,4,6,7-^{3}H]17β-estradiol and human recombinant ERα and ERβ were employed. The binding affinity data are summarized in Table 1.

Table 2
IC_{50} and EC_{50} values of *o*-carborane bisphenols in cell proliferation assay using MCF-7 cells

Compound	IC_{50} (μM)	EC_{50} (nM)	Efficacy (%)
BE360 (**4**)	0.58	0.024	40
BE310 (**5**)	0.63	0.85	26

MCF-7 cells were treated with test compounds (1×10–13 to 1×10^{-5} M) alone or in the presence of 0.1 nM E2. EC_{50} and IC_{50} values of the test compounds were estimated from the sigmoidal dose–response curves using GraphPad Prism 4 software.
Efficacy mean the maximal efficacy of each compound based on that of estradiol taken as 100.

The binding affinities of compound **5** for ERα and ERβ were decreased from those of the parent compound **4**. The strongly electron-withdrawing nature of the fluorine atom, due to its high electronegativity, is evident in its effect on the acidity of neighboring functional groups.[10] Whereas fluorination of alkanes decreases lipophilicity, the addition of fluorine on an aromatic ring or adjacent to a π-system or heteroatom-containing functional group increases lipophilicity and can strongly polarize the parent molecule.[16] The decrease of RBA of **5** presumably results from increase of hydrophilicity and polarity of the *o*-carborane cage, which is accommodated in the hydrophobic pocket of ERs, or from changes in the pK_a value of the phenol groups. The selectivity between ERα and ERβ was slightly changed, compared to that of compound **4**. The van der Waals radius of fluorine is 1.47 Å, being larger than that of hydrogen at 1.2 Å.[17] We suggest that the size and high electronegativity of the fluorine atom caused a slight change of the selectivity through weak repulsive interaction with the amino acid residue Met421 of ERα. The effect of the fluorine atom at this position of **5** might offer a clue for the development of ERβ-selective ligands.

Next, we evaluated the agonist and antagonist activities of compound **5** by means of cell proliferation assay using MCF-7 cell lines, which overexpress ERα and proliferate in an estrogen-dependent manner (Table 2). Compound **5** showed anti-estrogenic activity and its IC_{50} value was 0.63 μM, which is similar to that of **4** (IC_{50} = 0.58 μM). Moreover, compound **5** showed ER-agonistic activity and supported MCF-7 cell proliferation in a dose-dependent manner, like **4**. The EC_{50} values of **4** and **5** were 0.024 nM and 0.85 nM, respectively. Interestingly, the agonistic activity of **5** was 40 times weaker than that of **4**, and the efficacy of **5** was also lower than that of **4**. Thus, although **4** and **5** are both partial agonists, they show a different agonist/antagonist balance. Activation of most nuclear receptors is controlled by the location of helix-12.[18] We suggest that the presence of fluorine in compound **5** moved helix-12 towards the antagonistic location, even though the binding affinity was reduced, as a result of electrostatic repulsion between the introduced fluorine atom and an amino acid of the ER LBD. Since compound **5** is a more antagonistic partial agonist than **4**, it may act as SERM with lower risk of adverse effects on the reproductive system than **4**. Further, if it could be used to treat breast cancer, its weak estrogenic activity might improve the side effect of hot flushes, caused by the inhibition of estrogenic action. Thus, we believe that further biological evaluation of compound **5**, including in vivo studies, would be worthwhile.

In conclusion, we applied our diaryl *o*-carborane synthesis using S_NAr reaction to the synthesis of *B*-fluorinated monoaryl-*o*-carborane, and subsequent transformations afforded diaryl-*o*-carborane derivative BE310, which is an ER partial agonist with a more antagonistic balance of activity than BE360. Syntheses of other *B*-substituted BE360 analogues, such as *B*-halogenated and *B*-alkylated derivatives, using the S_NAr reaction are in progress, aiming at the development of novel selective estrogen receptor modulators (SERMs) and ERα- and β-subtype selective ligands.

Acknowledgements

This research was supported by a Grant-in-Aid of Strategic Research Program for Private Universities (2010–2014), a Grant-in-Aid for Scientific Research (B) (No. 20390035) and a Grant-in-Aid for Young Scientists (B) (No. 21790116) from the Ministry of Education, Culture, Sports, Science and Technology, Japan.

Supplementary data

Supplementary data (synthesis, biological assays, and compound characterization) associated with this article can be found, in the online version, at http://dx.doi.org/10.1016/j.bmcl.2012.05.068.

References and notes

1. (a) Green, S.; Walter, P.; Kumar, V.; Krust, A.; Bornert, J. M.; Argos, P.; Chambon, P. *Nature* **1986**, *320*, 134; (b) Kuiper, G. G. J. M.; Enmark, E.; Pelto-Huikko, M.; Nilsson, S.; Gustafsson, J. A. *Proc. Natl. Acad. Sci. U.S.A.* **1996**, *93*, 5925.
2. Brzozowski, A. M.; Pike, A. C.; Dauter, Z.; Hubbard, R. E.; Bonn, T.; Engstrom, O.; Ohman, L.; Greene, G. L.; Gustafsson, J. A.; Carlquist, M. *Nature* **1997**, *389*, 753.
3. (a) Constantine, G. D.; Pickar, J. H. *Curr. Opin. Pharmacol.* **2003**, 3, 626; (b) Leng, X.-H.; Bray, P. F. *Drug Discovery Today* **2005**, *2*, 85; (c) Motivala, A.; Pitt, B. *Drugs* **2007**, *67*, 647.
4. Fernand, L.; Claude, L.; Alain, B.; Jacques, S. In Selective Estrogen Receptor Modulators; Andrea, M.; Michael, V., Eds.; Humana Press, 2002, p. 167.
5. Lubczyk, V.; Bachmann, H.; Gust, R. *J. Med. Chem.* **2002**, *45*, 5358.
6. (a) Endo, Y.; Iijima, T.; Yamakoshi, Y.; Yamaguchi, M.; Fukasawa, H.; Shudo, K. *J. Med. Chem.* **1999**, *42*, 1501; (b) Endo, Y.; Iijima, T.; Yamakoshi, Y.; Fukasawa, H.; Miyaura, C.; Inada, M.; Kubo, A.; Itai, A. *Chem. Biol.* **2001**, *8*, 341; (c) Endo, Y.; Yoshimi, T.; Ohta, K.; Suzuki, T.; Ohta, S. *J. Med. Chem.* **2005**, *48*, 3941; (d) Ogawa, T.; Ohta, K.; Yoshimi, T.; Yamazaki, H.; Suzuki, T.; Ohta, S.; Endo, Y. *Bioorg. Med. Chem. Lett.* **2006**, *16*, 3943; (e) Ogawa, T.; Ohta, K.; Iijima, T.; Suzuki, T.; Ohta, S.; Endo, Y. *Bioorg. Med. Chem.* **2009**, *17*, 1109; (f) Ohta, K.; Ogawa, T.; Suzuki, T.; Ohta, S.; Endo, Y. *Bioorg. Med. Chem.* **2009**, *17*, 7958.
7. Endo, Y.; Yoshimi, T.; Miyaura, C. *Pure Appl. Chem.* **2003**, *75*, 1197.
8. Hirata, M.; Inada, M.; Matsumoto, C.; Takita, M.; Ogawa, T.; Endo, Y.; Miyaura, C. *Biochem. Biophys. Res. Commun.* **2009**, *380*, 218.
9. (a) Stauffer, S. R.; Coletta, C. J.; Tedesco, R.; Nishiguchi, G.; Carlson, K. E.; Sun, J.; Katzenellenbogen, B. S.; Katzenellenbogen, J. A. *J. Med. Chem.* **2000**, *43*, 4934; (b) Meyers, M. J.; Sun, J.; Carlson, K. E.; Marriner, G. A.; Katzenellenbogen, B. S.; Katzenellenbogen, J. A. *J. Med. Chem.* **2001**, *44*, 4230.
10. Hagmann, W. K. *J. Med. Chem.* **2008**, *51*, 4359.
11. Heying, T. L.; Ager, Jr. J. W.; Clark, S. L.; Mangold, D. J.; Goldstein, H. L.; Hillman, M.; Polak, R. J.; Szymanski, J. W. *Inorg. Chem.* **1963**, *2*, 1089.
12. Coult, R.; Fox, M. A.; Gill, W. R.; Herbertson, P. L.; MacBride, J. A. H.; Wade, K. *J. Organomet. Chem.* **1993**, *462*, 19.
13. (a) Ohta, K.; Goto, T.; Endo, Y. *Tetrahedron Lett.* **2005**, *46*, 483; (b) Ohta, K.; Goto, T.; Endo, Y. *Inorg. Chem.* **2005**, *44*, 8569.
14. Lebedev, V. N.; Balagurova, E. V.; Polyakov, A. V.; Yanovsky, A. I.; Struchkov, Yu. T.; Zakharkin, L. I. *J. Organomet. Chem.* **1990**, *385*, 307.
15. Ohta, K.; Chiba, Y.; Ogawa, T.; Endo, Y. *Bioorg. Med. Chem. Lett.* **2008**, *18*, 5050.
16. Smart, B. E. in: Organofluorine Chemistry, Principles and Commercial Applications, Banks, R. E., Smart, B. E.; Tatlow, J. C., Eds.; Plenum Press, 1994, p. 57.
17. Bondi, A. *J. Phys. Chem.* **1964**, *68*, 441.
18. Hashimoto, Y.; Miyachi, H. *Bioorg. Med. Chem.* **2005**, *13*, 5080.

MedChemComm

Dynamic Article Links

Cite this: *Med. Chem. Commun.*, 2012, **3**, 680

www.rsc.org/medchemcomm

CONCISE ARTICLE

Development of androgen receptor ligands by application of ten-vertex *para*-carborane as a novel hydrophobic core structure†

Shinya Fujii,[a] Kiminori Ohta,[b] Tokuhito Goto,[b] Akifumi Oda,[b] Hiroyuki Masuno,[a] Yasuyuki Endo[b] and Hiroyuki Kagechika*[a]

Received 28th November 2011, Accepted 1st April 2012
DOI: 10.1039/c2md00294a

We report here the design, synthesis, androgenic activity and anti-androgenic activity of novel derivatives of hexadecahedral 1,10-dicarba-*closo*-decaborane, which is generally called ten-vertex *para*-carborane. The synthesized compounds exhibited very high binding affinity for the androgen receptor and showed anti-androgenic activity toward the androgen-dependent SC-3 cell line. Two compounds also exhibited partial agonistic activity in SC-3 assay. The docking studies of carborane derivatives to AR demonstrate that ten-vertex carborane is useful for development of novel bioactive compounds as well as twelve-vertex carboranes that are well known to be versatile pharmacophores. Ten-vertex carborane, which has not previously been applied in the field of medicinal chemistry, appears to have potential as a hydrophobic pharmacophore with characteristic properties.

Introduction

Closo boranes ($[B_nH_n]^{2-}$,where n is the number of vertices)[1] have characteristic properties, such as closed three-dimensional structures and unusual stability, unlike other classes of boranes. Dicarba-*closo*-boranes ($C_2B_{n-2}H_n$),[1,2] a class of *closo* boranes bearing two carbon atoms in place of boron atoms, are among the most stable boron clusters because of their electrically neutral nature and symmetrical, closed structure. Although there has been extensive investigation of dicarba-*closo*-boranes as components of functional molecules and materials, almost all studies have focused on the twelve-vertex dicarba-*closo*-dodecaboranes (n = 12, $C_2B_{10}H_{12}$; **1a–c**) (Fig. 1).[3] Twelve-vertex dicarba-*closo*-dodecaboranes, which are usually called twelve-vertex carboranes or more simply carboranes, have a highly symmetrical icosahedral geometry, and remarkable thermal and chemical stability. Focusing on the hydrophobic character of twelve-vertex carboranes, we have investigated their application as hydrophobic building blocks of biological active molecules. We have demonstrated that they are versatile hydrophobic core structures of ligands for nuclear receptors, such as androgen receptor,[4,5] estrogen receptor,[6] retinoid receptors,[7] and vitamin D receptor.[8] Since hydrophobicity of the molecular surface is essential for nuclear receptor ligand function, these results demonstrated that the hydrophobic twelve-vertex carboranes can interact effectively with the hydrophobic surface of the receptor proteins.

Hundreds of twelve-vertex carborane derivatives have been synthesized and investigated. However, there have been only a few investigations of smaller dicarba-*closo*-boranes[9] for liquid crystal applications[10] and electronic materials,[11] and they have not been utilized in the field of medicinal chemistry. We considered that smaller dicarba-*closo*-boranes might have different characteristics as hydrophobic pharmacophores from twelve-vertex carboranes, and the present study was designed to test this idea.

Here, we focused on 1,10-dicarba-*closo*-decaborane (n = 10, $C_2B_8H_{10}$; **2**), also called ten-vertex *para*-carborane. Like

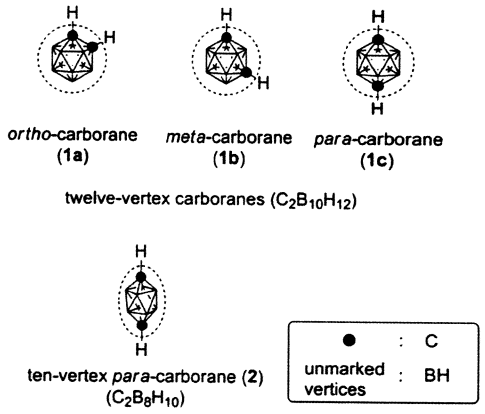


Fig. 1 Structures of carboranes. Hashed circles indicate the overall geometry of the boron clusters.

[a]*Graduate School of Biomedical Science, Institute of Biomaterials and Bioengineering, Tokyo Medical and Dental University, 2-3-10, Kanda-Surugadai, Chiyoda-ku, Tokyo, 101-0062 Japan. E-mail: kage.omc@tmd.ac.jp; Fax: +81-3-5280-8127; Tel: +81-3-5280-8032*
[b]*Faculty of Pharmaceutical Sciences, Tohoku Pharmaceutical University, 4-4-1, Komatsushima, Aoba-ku, Sendai 981-8558, Japan*

† Electronic supplementary information (ESI) available. See DOI: 10.1039/c2md00294a

This journal is © The Royal Society of Chemistry 2012

twelve-vertex carboranes, ten-vertex *para*-carborane has a hydrophobic surface, and so is expected to have potential to serve as the hydrophobic core of nuclear receptor ligands. On the other hand, ten-vertex *para*-carborane has an overall ellipsoidal geometry that is quite different from that of the highly symmetrical twelve-vertex carboranes. Therefore, derivatives of ten-vertex *para*-carborane may have activities distinct from those of the corresponding twelve-vertex carborane derivatives. On the basis of these considerations, we designed and synthesized a series of ten-vertex *para*-carborane derivatives as candidate nuclear receptor ligands.

As the biological target, we selected the androgen receptor (AR).[12] AR is a member of the nuclear receptor superfamily of ligand-regulated transcriptional factors[13] specific for testosterone (**3**) or dihydrotestosterone (DHT; **4**), and regulates numerous physiological functions, such as maintenance of the male reproductive system, and bone and muscle homeostasis. AR is also closely related to prostate cancer, and therefore AR antagonists such as flutamide (**5**) and bicalutamide (**7**) are used clinically for treatment of prostate cancer (Fig. 2).[14] Previously we reported the development of two types of potent AR antagonists bearing twelve-vertex carborane as a hydrophobic pharmacophore, *i.e.*, the phenylcarborane derivatives **8–11** (ref. 4) and the carboranylcyclohexenone **12**.[5] In these compounds, the spatial volume of the twelve-vertex carborane cage is essential for antagonistic activity.[15] Therefore, the difference in shape and bulkiness of **2**, compared to **1**, may influence the biological activities. To see whether this is indeed the case, we synthesized ten-vertex *para*-carborane derivatives **13–17** (Fig. 3).

Results and discussion

The crystal structure of AR bound to testosterone shows that the 3-carbonyl group of steroidal ligands interacts with Gln711 and Arg752 of AR.[16] The cyclohexenone ring of twelve-vertex carborane (**12**) corresponds to the hydrophilic pharmacophore of testosterone (**3**). Further, a docking study revealed that the nitro- and cyano groups of **8–11** interact effectively with the same residues through hydrogen bonding.[15] Thus, we designed ten-vertex *para*-carborane derivatives bearing a nitro- or cyanophenyl group (**13–16**) and a cyclohexenone group (**17**) as candidate AR ligands based on our previously developed twelve-vertex carborane-based AR ligands.

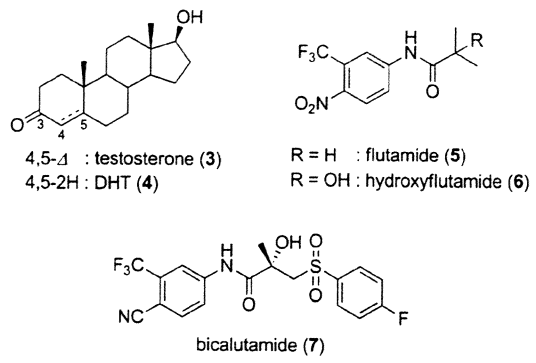


Fig. 2 Structures of endogenous and synthetic AR ligands.

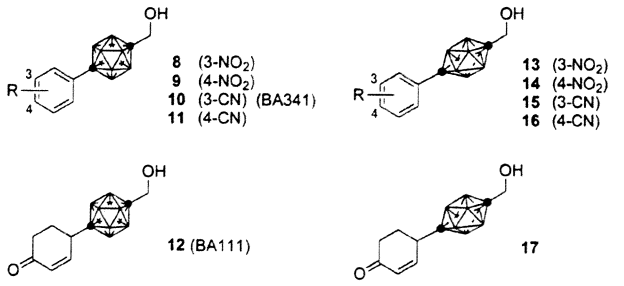


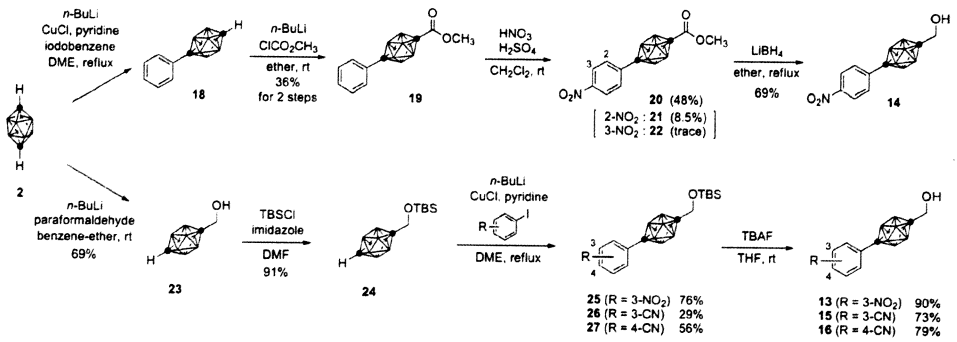
Fig. 3 Structures of the designed ten-vertex carborane derivatives (right) and the corresponding twelve-vertex carborane derivatives (left).

We first examined synthetic methods similar to those used for the twelve-vertex carborane derivatives. The synthetic routes to the phenyl-ten-vertex *para*-carborane derivatives **13–16** are illustrated in Scheme 1. The coupling reaction between *C*-lithiated **2** and iodobenzene using copper(I) chloride[17] gave 1-phenyl-ten-vertex *para*-carborane **18**, and introduction of a methoxycarbonyl group afforded ester **19**. Nitration of **19** yielded the 4-nitrophenyl compound **20** as the main product. However, 3-nitrated derivative **22** was not obtained, and 2-nitrated derivative **21** was obtained as a minor product. In the case of twelve-vertex carborane, nitration of phenylcarborane yielded the 4-nitrophenylcarborane derivative as the major product (*ca.* 60%) and the 3-nitrated derivative as a minor product (*ca.* 20%), while the 2-nitrated compound was not obtained. The difference in orientation of nitration could be attributed to the difference of bulkiness between ten-vertex carborane and twelve-vertex carborane. Reduction of ester **20** with lithium borohydride gave **14**. The 3-nitrophenyl and cyanophenyl derivatives were synthesized by another method. Reaction of **2** and paraformaldehyde gave alcohol **23**, and the hydroxyl group of **23** was protected with TBS to afford **24**. A copper(I)-mediated coupling reaction between *C*-lithiated **24** and iodobenzenes afforded the corresponding phenylcarborane derivatives **25–27**. Finally, removal of the TBS group afforded **13**, **15** and **16** (Scheme 1).

Scheme 2 illustrates the synthesis of cyclohexenone **17**. Reaction of **2** with 1,4-cyclohexanedione-mono-ethyleneketal gave tertiary alcohol **28**. Deprotection of the ketal, followed by dehydration and isomerization of the olefinic double bond with concentrated sulfuric acid, afforded the α,β-unsaturated ketone **29** in one pot. The unsaturated ketone **29** was converted to allyl alcohol **30** by reduction, and protection of the alcohol gave **31**. Reaction of **31** with *n*-butyl lithium and paraformaldehyde afforded alcohol **32**, and deprotection of the MOM group with hydrochloric acid gave diol **33**. Finally, selective oxidation of allyl alcohol using manganese oxide afforded the desired enone **17** (Scheme 2).

The androgenic and anti-androgenic activities of the synthesized molecules were assessed by assay of growth promotion/inhibition potency toward androgen-dependent SC-3 cells (Fig. 4).[18] Fig. 4A shows the cell growth-promoting activity of the carborane derivatives. As we had previously reported, none of the twelve-vertex carborane derivatives **8–12** showed growth-promoting activity, which means these twelve-vertex carborane derivatives do not have AR agonistic activity.[4,5] On the other hand, the cyclohexanone derivative of ten-vertex *para*-carborane

This journal is © The Royal Society of Chemistry 2012



Scheme 1 Synthesis of phenyl-ten-vertex *para*-carborane derivatives.

17 showed significant SC-3 cell growth-promoting activity, and the 3-cyanophenyl derivative **15** also promoted SC-3 cell growth. The other compounds did not exhibit agonistic activity. Fig. 4B shows the antagonistic activity toward SC-3 cell growth promoted by 1 nM testosterone (**3**). All the synthesized molecules exhibited cell growth-inhibitory activity toward SC-3 cells, that is, these compounds have AR antagonistic activity. The nitrophenyl and cyanophenyl derivatives exhibited significant antagonistic potency, and the 3-nitro derivative **13** and the 3-cyano derivative **15** showed the greatest activity, being more potent than hydroxyflutamide **6**, the metabolically activated form of flutamide **5**. The cyclohexenone derivative **17** also exhibited androgen antagonistic activity. There was no significant difference in antagonistic potency between ten-vertex *para*-carborane derivatives and twelve-vertex carborane derivatives, except for the agonistic activity of **15** and **17** at the concentration of 1×10^{-5} M. These results suggest that ten-vertex *para*-carborane derivatives **15** and **17** are partial agonists for AR.

Next, the AR-binding affinity of the ten-vertex *para*-carborane derivatives was examined by a competitive binding assay using ^{3}H-labeled dihydrotestosterone ([^{3}H]DHT) and human AR ligand-binding domain (hAR-LBD),[19] and compared with that of the twelve-vertex derivatives. Fig. 5 shows the dose–response relationship of cyanophenylcarborane derivatives and cyclohexanone derivatives in competitive binding over the concentration range 1×10^{-7} to 1×10^{-4} M. The binding potencies of these ten-vertex derivatives were comparable to those of the twelve-vertex derivatives, and the most potent ten-vertex derivative **15** with the 3-cyano group exhibited higher affinity ($IC_{50} = 7.6 \times 10^{-7}$ M) than the corresponding twelve-vertex derivative **10** ($IC_{50} = 1.9 \times 10^{-6}$ M). With regard to cyclohexanone

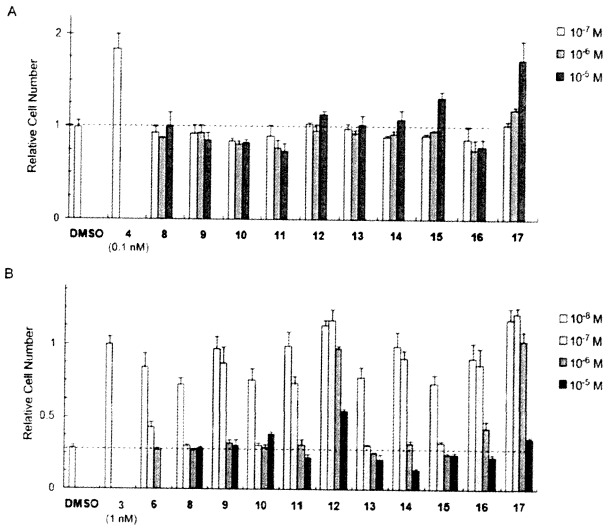
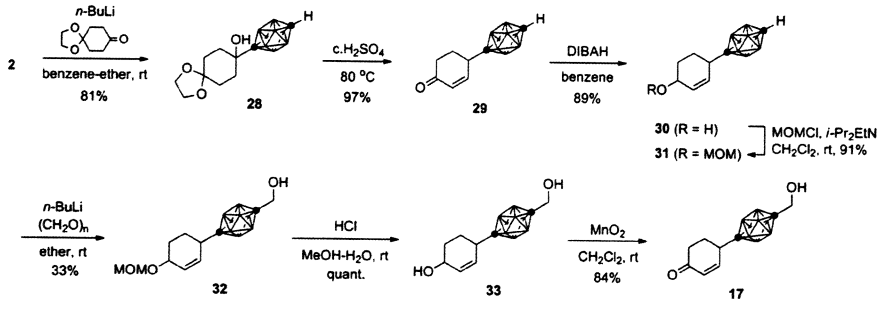


Fig. 4 SC-3 cell proliferation promotion/inhibition assay. (A) SC-3 cell proliferation-promoting activity of test compound only. (B) Inhibitory activity towards testosterone-induced SC-3 cell proliferation. The concentration of testosterone was 1 nM. Cell number was normalized to that in the absence of test compounds, taken as 1.

derivatives, the ten-vertex derivative **17** also exhibited higher affinity for hAR ($IC_{50} = 6.1 \times 10^{-6}$ M) than the twelve-vertex derivative **12** ($IC_{50} = 9.7 \times 10^{-6}$ M). On the other hand, the ten-vertex derivative **16** with the 4-cyano group exhibited lower affinity ($IC_{50} = 1.6 \times 10^{-5}$ M) than the corresponding twelve-vertex derivative **11** ($IC_{50} = 1.0 \times 10^{-5}$ M). It is interesting that



Scheme 2 Synthesis of cyclohexenone derivative **17**.

This journal is © The Royal Society of Chemistry 2012

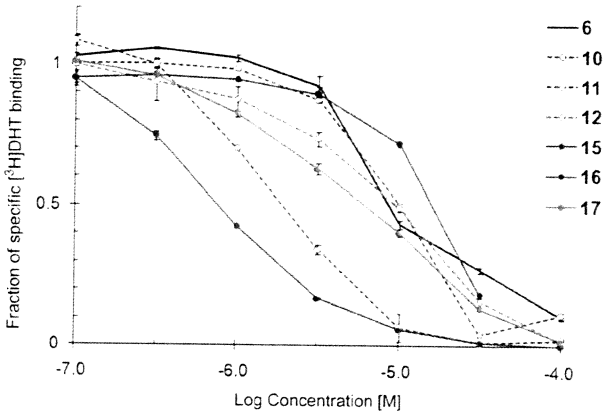


Fig. 5 Competitive binding assay of synthesized ten-vertex carborane derivatives and twelve-vertex carborane derivatives. Solid lines indicate ten-vertex carborane derivatives, and hashed lines indicate twelve-vertex carborane derivatives. The concentration of [^{3}H]DHT was 4 nM.

compounds **15** and **17**, which exhibited partial agonistic activity, showed higher binding affinity than the corresponding twelve-vertex carborane derivatives (Fig. 5). These results suggest that the ten-vertex cage is more favorable as a hydrophobic core of AR ligands than twelve-vertex carborane for exerting androgen-dependent transcriptional activity.

We conducted docking studies of carborane derivatives to AR in order to investigate the difference between the ten-vertex carborane derivative **15** and the corresponding twelve-vertex carborane derivative **10**. Fig. 6 shows the docking simulation of these compounds with AR-LBD by using the co-crystal structure of hAR-LBD with metribolone (PDB:1E3G), by a docking program GOLD.[20] In the calculated binding mode, the ten-vertex carborane derivative **15** is embedded in the ligand-binding pocket of AR in a manner similar to that of **10**. However, the locations of cyano groups, that form key hydrogen-bonds with Gln711 and Arg752, are considerably different from each other. The differences can be attributed to the shape of the clusters. X-ray crystallographic studies reported that ten-vertex *para*-carborane has not only narrower structure than twelve-vertex *para*-carborane but also longer C–C distance (3.39 Å) than twelve-vertex (3.13 Å).[21] We also calculated the molecular volume difference between compounds **10** and **15**; and compound **15** occupies a smaller volume (239 Å^3) than compound **10** (263 Å^3). These results are consistent with our prediction that the spatial volume of the twelve-vertex carborane cage and direction of the cyano

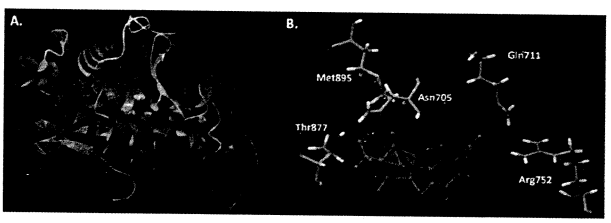


Fig. 6 Docking models of **10** and **15** to hAR-LBD. Compounds **10** and **15** are colored in green and brown, respectively. (A) Overall structure of AR-LBD bound to ligands. (B) Amino acid residue of hAR-LBD around the ligands.

group are essential for full-antagonistic activity of **10**.[15] The difference of cluster geometry can cause the different binding modes of these two compounds, and also induce partial agonistic activity of compound **15**.

Conclusions

We have designed and synthesized derivatives of ten-vertex carborane, which has never previously been used in medicinal chemical applications, and studied their activity as novel AR ligands in comparison with the corresponding twelve-vertex carborane derivatives. The synthesized molecules exhibited potent androgen antagonistic activity, as did the corresponding twelve-vertex carborane derivatives, but the ten-vertex carboranes showed higher AR binding affinity. Among the synthesized molecules, compounds **15** and **17** exhibited partial agonistic activity, in marked contrast to the corresponding twelve-vertex carborane derivatives. Introduction of the ten-vertex cage in place of the twelve-vertex cage may reduce steric interference with the ligand-binding pocket of AR, resulting in partial agonistic activity. Docking simulation suggested that ten-vertex carborane functions as a hydrophobic anchor, and that the characteristic ellipsoidal structure of ten-vertex carborane induces binding modes of the derivatives different from the corresponding twelve-vertex carborane derivatives. Thus, we have shown for the first time that ten-vertex *para*-carborane can function as a hydrophobic core structure of biologically active molecules as well as twelve-vertex carboranes, and may generate a unique profile of biological activities. Structural development studies with ten-vertex and twelve-vertex carboranes may be fruitful approaches to uncover key hydrophobic interactions of other ligand–receptor combinations.

Acknowledgements

This study was partially supported by Grants-in-Aid for Scientific Research from the Ministry of Education, Culture, Sports, Science and Technology, Japan (no. 21790110). We also thank Sasagawa Scientific Research Grant by the Japan Science Society (no. 20-605).

Notes and references

1 *The Borane, Carborane, Carbocation Continuum*, ed. J. Casanova, Wiley Interscience, New York, 1998.
2 *Carboranes*, ed. R. N. Grimes, Academic Press, Elsevier, 2nd ed, 2011.
3 (*a*) V. I. Bregadze, *Chem. Rev.*, 1992, **92**, 209–223; (*b*) M. F. Hawthorne, *Angew. Chem., Int. Ed. Engl.*, 1993, **32**, 950–984; (*c*) A. H. Soloway, W. Tjarks and J. G. Barnum, *Chem. Rev.*, 1998, **98**, 1515–1562; (*d*) F. Issa, M. Kassiou and L. M. Rendina, *Chem. Rev.*, 2011, **111**, 5701–5722.
4 (*a*) S. Fujii, T. Goto, K. Ohta, Y. Hashimoto, T. Suzuki, S. Ohta and Y. Endo, *J. Med. Chem.*, 2005, **48**, 4654–4662; (*b*) S. Fujii, A. Yamada, K. Tomita, M. Nagano, T. Goto, K. Ohta, T. Harayama, Y. Endo and H. Kagechika, *Med. Chem. Commun.*, 2011, **2**, 877–880.
5 S. Fujii, Y. Hashimoto, T. Suzuki, S. Ohta and Y. Endo, *Bioorg. Med. Chem. Lett.*, 2005, **15**, 227–230.
6 (*a*) Y. Endo, T. Iijima, Y. Yamakoshi, M. Yamaguchi, H. Fukasawa and K. Shudo, *J. Med. Chem.*, 1999, **42**, 1501–1504; (*b*) Y. Endo, T. Iijima, Y. Yamakoshi, H. Fukasawa, C. Miyaura, M. Inada, A. Kubo and A. Itai, *Chem. Biol.*, 2001, **8**, 341–355.
7 (*a*) T. Iijima, Y. Endo, M. Tsuji, E. Kawachi, H. Kagechika and K. Shudo, *Chem. Pharm. Bull.*, 1999, **47**, 398–404; (*b*) Y. Endo,

This journal is © The Royal Society of Chemistry 2012

K. Yaguchi, E. Kawachi and H. Kagechika, *Bioorg. Med. Chem. Lett.*, 2000, **10**, 1733–1736; (*c*) K. Ohta, T. Iijima, E. Kawachi, H. Kagechika and Y. Endo, *Bioorg. Med. Chem. Lett.*, 2004, **14**, 5913–5918.
8 (*a*) S. Fujii, H. Masuno, Y. Taoda, A. Kano, A. Wongmayura, M. Nakabayashi, N. Ito, M. Shimizu, E. Kawachi, T. Hirano, Y. Endo, A. Tanatani and H. Kagechika, *J. Am. Chem. Soc.*, 2011, **133**, 20933–20941; (*b*) A. Wongmayura, S. Fujii, S. Ito, A. Kano, Y. Taoda, E. Kawachi, H. Kagechika and A. Tanatani, *Bioorg. Med. Chem. Lett.*, 2012, **22**, 1756–1760.
9 B. Stibr, *Chem. Rev.*, 1992, **92**, 225–250.
10 (*a*) B. Ringstrand and P. Kaszynski, *J. Mater. Chem.*, 2010, **20**, 9613–9615; (*b*) P. Kaszynski, S. Pakhomov, K. F. Tesh and V. G. Yong, Jr, *Inorg. Chem.*, 2001, **40**, 6622–6631.
11 S. Pakhomov, P. Kaszynski and V. G. Yong, Jr, *Inorg. Chem.*, 2000, **39**, 2243–2245.
12 (*a*) A. D. Mooradian, J. E. Morley and S. G. Korenman, *Endocr. Rev.*, 1987, **8**, 1–28; (*b*) C. J. Bagatell and W. J. Bremner, *N. Engl. J. Med.*, 1996, **334**, 707–714; (*c*) J. M. Kaufman and A. Vermeulen, *Endocr. Rev.*, 2005, **26**, 833–876.
13 (*a*) R. M. Evans, *Science*, 1988, **240**, 889–894; (*b*) H. E. MacLean, G. L. Warne and J. D. Zajac, *J. Steroid Biochem. Mol. Biol.*, 1997, **62**, 233–242; (*c*) I. J. McEwan, *Biochem. Soc. Trans.*, 2000, **28**, 369–373; (*d*) M. E. Taplin, *Expert Rev. Anti-Infect. Ther.*, 2008, **8**, 1495–1508.
14 R. K. Ross, M. C. Pike, G. A. Coetzee, J. K. Reichardt, M. C. Yu, H. Feigelson, F. Z. Stanczyk, L. N. Kolonel and B. E. Henderson, *Cancer Res.*, 1998, **58**, 4497–4504.
15 K. Ohta, T. Goto, S. Fujii, M. Kawahata, A. Oda, S. Ohta, K. Yamaguchi, S. Hirono and Y. Endo, *Bioorg. Med. Chem.*, 2011, **19**, 3540–3548.
16 (*a*) P. M. Matias, P. Donner, R. Coelho, M. Thomaz, C. Peixoto, S. Macedo, N. Otto, S. Joschko, P. Scholz, A. Wegg, S. Bäsler, M. Schäfer, U. Egner and M. A. Carrondo, *J. Biol. Chem.*, 2000, **275**, 26164–26171; (*b*) J. S. Sack, K. F. Kish, C. Wang, R. M. Attar, S. E. Kiefer, Y. An, G. Y. Wu, J. E. Scheffler, M. E. Salvati, S. R. Krystek, Jr, R. Weinmann and H. M. Einspahr, *Proc. Natl. Acad. Sci. U. S. A.*, 2001, **98**, 4904–4909.
17 R. Coult, M. A. Fox, W. R. Gill, P. L. Herbertson, J. A. H. MacBride and K. Wade, *J. Organomet. Chem.*, 1993, **462**, 19–29.
18 D. Hiraoka, N. Nakamura, Y. Nishizawa, N. Uchida, S. Noguchi, K. Matsumoto and B. Sato, *Cancer Res.*, 1987, **47**, 6560–6564.
19 T. Ishioka, A. Kubo, Y. Koiso, K. Nagasawa, A. Itai and Y. Hashimoto, *Bioorg. Med. Chem.*, 2002, **10**, 1555–1566.
20 G. Jones, P. Willett and R. C. Glen, *J. Mol. Biol.*, 1995, **245**, 43–53.
21 M. A. Fox, T. E. Baines, D. Albesa-Jove, J. A. K. Howard and P. J. Low, *J. Organomet. Chem.*, 2006, **691**, 3889–3894.

This journal is © The Royal Society of Chemistry 2012

Drug Metab. Pharmacokinet. 27 (2): 200–206 (2012). Copyright © 2012 by the Japanese Society for the Study of Xenobiotics (JSSX)

Regular Article

Polycyclic Aromatic Hydrocarbons Activate CYP3A4 Gene Transcription through Human Pregnane X Receptor

Takeshi KUMAGAI[1,*], Hiroyuki SUZUKI[1], Takamitsu SASAKI[1], Shuhei SAKAGUCHI[1], Shinichi MIYAIRI[2], Yasushi YAMAZOE[3] and Kiyoshi NAGATA[1]

[1]*Department of Environmental Health Science, Tohoku Pharmaceutical University, Sendai, Japan*

[2]*Laboratory of Organic Chemistry, School of Pharmacy, Nihon University, Funabashi, Japan*

[3]*Division of Drug Metabolism and Molecular Toxicology, Graduate School of Pharmaceutical Sciences, Tohoku University, Sendai, Japan*

Full text of this paper is available at http://www.jstage.jst.go.jp/browse/dmpk

Summary: Aryl hydrocarbon receptor (AhR) activators have been shown to induce members of the cytochrome P450 (P450) 1 family. Here we demonstrate that the AhR activators induce CYP3A4 through human pregnane X receptor (PXR). AhR activators, polycyclic aromatic hydrocarbons (PAHs) and 2,3,7,8-tetrachlorodibenzo-*p*-dioxin (TCDD) increased CYP3A4 reporter activity and CYP3A4 mRNA expression in HepG2 cells. The CYP3A4 reporter activity was also increased by treatment with cigarette tar. The increased CYP3A4 reporter activity was clearly knocked down by the introduction of human PXR-small interfering RNA, but not by that of human AhR-small interfering RNA. The CYP3A4 reporter activity enhanced by overexpression of human PXR was further increased by treatment with PAHs and TCDD as well as by treatment with rifampicin. These results suggest that PAHs contained in cigarette smoke induce CYP3A4 in human liver.

Keywords: AhR activator; polycyclic aromatic hydrocarbons; TCDD; CYP3A4 induction; PXR

Introduction

Members of the cytochrome P450 (CYP) supergene family of monooxygenases play an important role in efficient detoxification, by converting pollutants, plant toxins, carcinogens, and drugs to products that can be excreted in urine or bile.[1,2] Human CYP3A4 is of particular significance in this respect because it is involved in the metabolism of approximately two-thirds of clinically relevant drugs.[3] A number of compounds, including pesticides, herbal supplements, vitamins, and drugs, activate *CYP3A4* gene transcription both in the liver and in the small intestine.[4,5] This process of induction constitutes the molecular basis for a number of important drug interactions in patients taking multiple medications.

Pregnane X receptor (PXR; NR1I2) is the principal regulator of *CYP3A4* gene expression and binds as a heterodimer with retinoid X receptor α (RXRα) to regulatory DNA sequences. These sequences include AG(G/T)TCA-like direct repeats spaced by 3 bases (DR3) located at −8 kb upstream from the transcription start point and identified as distal nuclear receptor-binding element 1 (dNR1) and the everted repeats separated by 6 bases (ER6) located in the CYP3A4 proximal promoter (prER6).[6] Recently, we identified a distinct PXR response element as an essential distal nuclear receptor-binding element (eNR3A4) for CYP3A4 induction.[7] PXR is activated by a number of structurally and chemically diverse ligands such as various xenobiotics [rifampicin (RIF) and clotrimazole],[8] pesticides (pyributicarb and endosulfan),[9,10] natural and synthetic

Received August 22, 2011; Accepted October 20, 2011

J-STAGE Advance Published Date: November 10, 2011, doi:10.2133/dmpk.DMPK-11-RG-094

*To whom correspondence should be addressed: Takeshi KUMAGAI, Ph.D., *Department of Environmental Health Science, Tohoku Pharmaceutical University, 4-4-1 Komatsushima, Aoba-ku, Sendai 981-8558, Japan. Tel. +81-22-727-0134, Fax. +81-22-275-2013, E-mail: ta-kuma@tohoku-pharm.ac.jp*

This work was supported in part by a Grant-in Aid for Scientific Research (C) from the Japan Society for the Promotion Science, by the High-Tech Research Center Program from the Ministry of Education, Culture, Sports, Science and Technology of Japan, and by the Program for the Promotion of Studies in Health Sciences of the Ministry of Health, Labor and Welfare of Japan.

steroids (dexamethasone),[8] bile acids (lithocholic acid)[11] and herbal medicines (St. John's wort, *Ginkgo biloba*, and *Sophora flavescens*).[12–14] As a result, CYP3A4 induction by these PXR activators leads to the accelerated metabolism of the drugs themselves and the efficacy of concomitant drugs is decreased. Interestingly, there are significant species differences in the activation by PXR ligands between humans and rodents.[15] Drugs such as RIF and clotrimazole activate human PXR but are weak activators of rodent PXR. In contrast, dexamethasone and pregnenolone 16α-carbonitrile activate rodent PXR but are weak activators of human PXR.

Cigarette smoke contains thousands of chemical compounds including a number of carcinogenic polycyclic aromatic hydrocarbons (PAHs) and is known to affect drug therapy in both pharmacokinetic and pharmacodynamic events.[16,17] PAHs induce CYP1A1 and CYP1A2, which mediate the rate-limiting step in the metabolism of many drugs, including theophylline and clozapine, as well as in the bioactivation of procarcinogens. These P450 inductions are also expected to cause drug interaction in this respect. In fact, it was reported that cigarette smoking reduced the therapeutic efficacy of theopylline.[18] The molecular mechanisms by which PAHs or 2,3,7,8-tetrachlorodibenzo-*p*-dioxin (TCDD) transcriptionally activates the *CYP1A1* and *CYP1A2* genes involve the binding of the ligand to aryl hydrocarbon receptor (AhR).[19]

Diazepam (DZ) is a drug that relieves anxiety and controls agitation; it has long been controversial whether cigarette smoking reduces its therapeutic efficacy. Norman *et al.* reported that cigarette smoking strongly decreased the elimination half-life and AUC of DZ, but Klots *et al.* reported no effect.[20,21] DZ is mainly metabolized to 3-hydroxydiazepam and *N*-desmethyldiazepam by CYP3A4 and CYP2C19, respectively. However, there have been no reports about the induction of CYP3A4 and/or CYP2C19 by AhR activators, PAHs or TCDD. Recently, we found a novel event in CYP3A4 induction by AhR activators.

In the present study, we investigated the effect of the AhR activators on transcriptional activation of the *CYP3A4* gene and clearly demonstrated that the AhR activators induced CYP3A4 through PXR pathways in HepG2 cells.

Materials and Methods

Materials: 3-Methylcholanthrene (3-MC) and RIF were purchased from Sigma-Aldrich (St. Louis, MO). Benzo[*a*]-pyrene (B[*a*]P) was purchased from Tokyo Chemical Industry Co., Ltd. (Tokyo, Japan). TCDD was purchased from Wako Pure Chemicals (Osaka, Japan). Tar was provided from Japan Tobacco Inc. (Tokyo, Japan). The chemicals used for this study were dissolved in dimethylsulfoxide (DMSO). All other reagents used were of the highest quality available. Dulbecco's modified Eagle's medium (DMEM) and fetal bovine serum were obtained from Wako Pure Chemical Industries, Ltd. (Osaka, Japan) and Hyclone Laboratories (Logan, UT). MEM Non-Essential Amino Acids and Antibiotic-Antimycotic were purchased from Invitrogen (Paisley, UK).

Cell culture: HepG2 human hepatoma cells and Huh7 human hepatoma cells were obtained from American Type Culture Collection (Manassas, VA). LS174T human colon adenocarcinoma cells were obtained from the Institute of Development, Aging, and Cancer, Tohoku University (Sendai, Japan). HepG2-derived cell lines stably expressing the *CYP3A4*-luciferase reporter gene, 3-1-20 cells, were as reported previously.[22] These cells were cultured in DMEM supplemented with 10% fetal bovine serum, MEM Non-Essential Amino Acids, and Antibiotic-Antimycotic. The cells were seeded at the appropriate cell density for each experimental condition. The next day, the cell medium was exchanged for the medium containing chemicals (0.1% DMSO) and cultured for 48 h. Adenovirus infection and small interfering RNA (siRNA) transfection were carried out as described previously.[23]

Construction of recombinant adenovirus: Construction of the *CYP3A4* gene reporter adenovirus (AdCYP3A4-362-7.7k) and human PXR-expressing adenovirus (AdhPXR) was performed previously.[9] Control adenovirus, β-galactosidase-expressing adenovirus (AdCont; AxCALacZ), was provided by Dr. Izumi Saito (Tokyo University, Tokyo, Japan). The titer of adenoviruses, 50% titer culture infectious dose (TCID50), was determined as reported previously.[9] Multiplicity of infection (MOI) was calculated by dividing the $TCID_{50}$ by the number of cells.

Small interfering RNA-mediated protein knockdown: Double-stranded siRNAs (25-mer) targeting human AhR (hAhR), human PXR (hPXR), and control siRNA were obtained from Invitrogen (Carlsbad, CA). The corresponding target mRNA sequences for the siRNAs were as follows: hAhR-siRNA, 5′-uuaagucggucucuaugccgcuugg-3′; hPXR-siRNA, 5′-uuucaucugagcguccaucagcucc-3′; control siRNA 5′-uagucauugcacacugcacaguagc-3′. Cells were transfected with each siRNA using Lipofectamine RNAiMAX (Invitrogen) according to the manufacturer's instructions.

Luciferase gene reporter assay: The cells were washed with Dulbecco's phosphate buffered saline (D-PBS) obtained from Wako Pure Chemical Industries, Ltd. (Osaka, Japan) and suspended in Passive Lysis Buffer from Promega (Madison, WI) in a microcentrifuge tube. The cell suspension was centrifuged at 12,000 × *g* for 5 min at 4°C, and the cell extract was used for luciferase assay. Luciferase assay was performed according to the manufacturer's instructions using the Luciferase Assay System and GloMax™ 96 Microplate Luminometer (Promega). Resulting data are presented as ratio of luminescence of treated cell samples to that of control. Luminescence of each sample was normalized by its protein concentration determined with the Protein Assay Kit from Bio-Rad Laboratories (Hercules, CA).

Copyright © 2012 by the Japanese Society for the Study of Xenobiotics (JSSX)

Table 1. Sequences of the oligonucleotide primers used for PCR amplification

	Primer sequence
Human CYP3A4	
sense	5′-GATTGACTCTCAGAATTCAAAAGAAACTGA-3′
antisense	5′-GGTGAGTGGCCAGTTCATACATAATG-3′
Human CYP1A1	
sense	5′-ACTGCTTAGCCTAGTCAACCTG-3′
antisense	5′-CAATCAGGCTGTCTGTGATGTC-3′
Human GAPDH	
sense	5′-GAGTCAACGGATTTGGTCGT-3′
antisense	5′-TTGATTTTGGAGGGATCTCG-3′

RNA isolation and quantitative real-time polymerase chain reaction analysis: Total RNA was isolated from 3-1-20 cells using TRI Reagent (Molecular Research Center, Inc., Cincinnati, OH) according to the manufacturer's protocol. cDNA was prepared from 0.5 μg of total RNA with MMLV reverse transcriptase (Promega) using oligo (dT) primer (Greiner Japan, Tokyo, Japan) and porcine RNase inhibitor (Takara Bio, Shiga, Japan). Quantitative real-time polymerase chain reaction (PCR) was performed using Permix Ex Taq (Perfect Real Time, Takara Bio) in a Thermal Cycler Dice Real Time System (Takara Bio). All samples were quantified using a comparative Ct method for relative quantification of gene expression, normalized to glyceraldehyde-3-phosphate dehydrogenase (GAPDH). The sequences of primers are shown in **Table 1**.

Statistical analysis: Data were evaluated by the paired Student's *t*-test. When the p value was less than 0.05, the difference was considered to be significant.

Results

Transcriptional activation of the CYP3A4 reporter gene by tar: We investigated whether tar as a major component of cigarette smoke activates the CYP3A4 transcription using HepG2-derived cells stably expressing the *CYP3A4* gene reporter (3-1-20 cells) as reported previously.[22] The cells were treated with 1 to 200 μg/ml tar for 48 h and reporter activities were determined. As shown in **Figure 1**, tar increased *CYP3A4* gene reporter activity in a dose-dependent manner. In contrast, nicotine, which is one of the major components of cigarette smoke, had no effect (data not shown).

Transcriptional activation of the CYP3A4 reporter gene by PAHs: Tar, a by-product of the gasification process, is a complex mixture consisting of a wide range of different compounds in which PAH is one of the major compounds.[24] Therefore, we examined the effect of typical PAHs and TCDD on CYP3A4 reporter activity, which are known as ligands for AhR. RIF was used as a positive control. 3-1-20 cells were treated with RIF (10 μM), 3-MC (1 μM), B[*a*]P (1 μM), and TCDD (10 nM) for 48 h. As shown in **Figure 2**, RIF, 3-MC, B[*a*]P, and TCDD increased CYP3A4 reporter activity by 18.6 ± 2.5-fold,

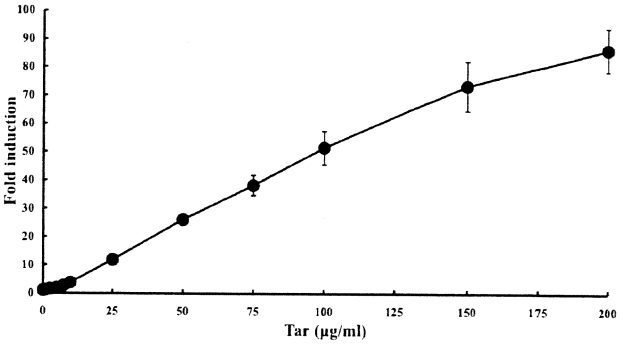


Fig. 1. Effect of tar on CYP3A4 reporter activity in 3-1-20 cells
Clone 3-1-20 was seeded at 1 × 10^4 cells in 96-well tissue culture plates with 0.1 ml of DMEM 1 day before tar treatment. The cells were treated with 1–200 μg/ml tar for 2 days and the reporter activity was measured by luciferase assay. Reporter activities are expressed as fold increase compared with that in the vehicle-treated cells. Results represent the mean ± S.D. of three separate experiments.

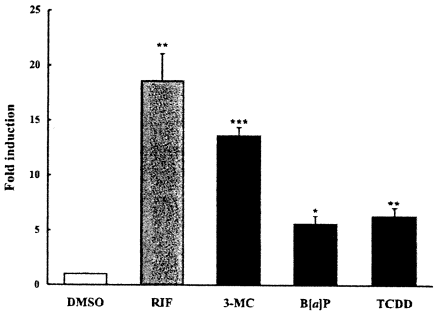


Fig. 2. Effects of 3-MC, B[*a*]P and TCDD on CYP3A4 reporter activity in 3-1-20 cells
Clone 3-1-20 was seeded at 3 × 10^4 cells in 48-well tissue culture plates with 0.2 ml of DMEM 24 h before RIF, 3-MC, B[*a*]P, or TCDD treatment. The cells were treated with 10 μM RIF, 1 μM 3-MC, 1 μM B[*a*]P, or 10 nM TCDD for 48 h and the reporter activity was measured by luciferase assay. Reporter activities are expressed as fold increase compared with that in the vehicle-treated cells. Results represent the mean ± S.D. of three separate experiments. *, $p < 0.05$, **, $p < 0.01$, ***, $p < 0.005$, difference from the vehicle-treated cells based on unpaired Student's *t*-test.

13.6 ± 0.8-fold, 5.57 ± 0.8-fold, and 6.3 ± 0.8-fold, respectively. Furthermore, we investigated the effect of PAHs on endogenous CYP3A4 mRNA expression in 3-1-20 cells. As a result, all chemicals used in this study increased CYP3A4 mRNA expression (**Fig. 3A**). The CYP3A4 mRNA expressions of 3-MC and B[*a*]P were higher than that of RIF. On the other hand, CYP3A4 mRNA expression induced by TCDD was equivalent to that by RIF. In addition, 3-MC, B[*a*]P, and TCDD strongly increased endogenous CYP1A1 mRNA expression, whereas RIF had no effect (**Fig. 3B**). In particular, 3-MC and TCDD increased CYP1A1 mRNA expression by 365.7 ± 39.3-fold and 378.3 ± 37.0-fold, respectively. These results suggest that PAHs induce

Copyright © 2012 by the Japanese Society for the Study of Xenobiotics (JSSX)

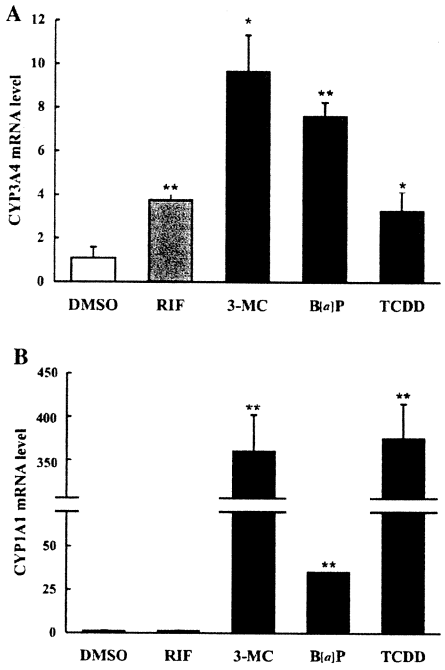


Fig. 3. Effects of 3-MC, B[a]P and TCDD on CYP mRNA expression in 3-1-20 cells

Clone 3-1-20 was seeded at 3×10^4 cells in 48-well tissue culture plates with 0.2 ml of DMEM 24 h before RIF, 3-MC, B[a]P, and TCDD treatment. The cells were treated with 10 μM RIF, 1 μM 3-MC, 1 μM B[a]P, or 10 nM TCDD for 48 h and then assayed using real-time RT-PCR. CYP3A4 mRNA or CYP1A1 mRNA expression was normalized by expression of the GAPDH housekeeping gene and presented as fold increase compared with that of vehicle-treated cells. Results represent the mean ± S.D. of three separate experiments. (A) CYP3A4 mRNA level, (B) CYP1A1 mRNA level. *, $p < 0.05$, **, $p < 0.005$, difference from the vehicle-treated cells based on unpaired Student's *t*-test.

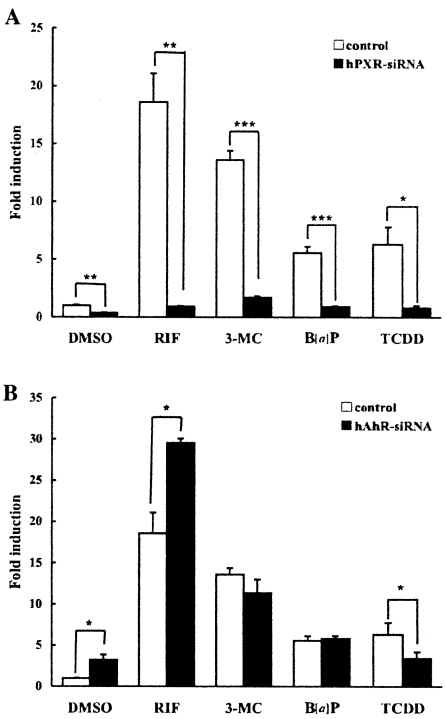


Fig. 4. Effects of hPXR-siRNA and hAhR-siRNA on CYP3A4 reporter activity in 3-1-20 cells

Clone 3-1-20 was seeded at 3×10^4 cells in 48-well tissue culture plates and the cells were treated with hPXR-siRNA (A) or hAhR-siRNA (B). After 48 h, the cells were treated with 10 μM RIF, 1 μM 3-MC, 1 μM B[a]P, or 10 nM TCDD for 48 h and the reporter activity was measured by luciferase assay. Reporter activities are expressed as fold increase compared with that in the vehicle-treated cells transfected with the control siRNA. Results represent the mean ± S.D. of three separate experiments. *, $p < 0.05$, **, $p < 0.01$, ***, $p < 0.005$, difference from the control siRNA-transfected cells based on unpaired Student's *t*-test.

CYP3A4 expression in 3-1-20 cells. In addition, these compounds also increased CYP3A4 mRNA expression in HepG2 cells (data not shown).

Effects of PXR and AhR on activation of CYP3A4 reporter gene by PAHs: PXR is widely known as a major transcription factor mediating CYP3A4 induction, whereas AhR is well known as a transcription factor mediating CYP1A1 induction by PAHs. Therefore, to clarify whether PXR or AhR mediates the CYP3A4 activation by PAHs, we utilized knockdown of PXR or AhR using hPXR-siRNA or hAhR-siRNA and overexpression of PXR using AdhPXR, hPXR-expressing adenovirus. CYP3A4 reporter activities induced by 3-MC, B[*a*]P, and TCDD were significantly decreased by the introduction of hPXR-siRNA (**Fig. 4A**). In contrast, knockdown of the AhR using hAhR-siRNA did not affect the CYP3A4 reporter activity induced by 3-MC or B[*a*]P, whereas CYP3A4 reporter activities induced by TCDD were slightly decreased by the introduction of hAhR-siRNA (**Fig. 4B**). Then, we examined the effect of overexpression of PXR using AdhPXR on CYP3A4 reporter activity induced by PAHs in 3-1-20 cells. As shown in **Figure 5**, we found that the CYP3A4 reporter activation treated with 3-MC, B[*a*]P, and TCDD as well as RIF was increased by the introduction of AdhPXR in 3-1-20 cells.

Effect of PAHs on CYP3A4 reporter activity in Huh7 cells and LS174T cells: Next, we investigated whether the PAHs induce CYP3A4 reporter activity in different cell lines. Huh7 cells and LS174T cells were used, which are *in vitro* models of hepatic and intestinal cells, respectively. As shown in **Figure 6**, the CYP3A4 reporter activation upon treatment with 3-MC, B[*a*]P, and TCDD as well as RIF was increased by the introduction of AdhPXR in Huh7 cells. On the other hand, RIF increased CYP3A4 reporter activity, whereas 3-MC, B[*a*]P, and TCDD had no effect on the activity in LS174T cells.

Discussion

In this study, we investigated the effect of PAHs on transactivation of the *CYP3A4* gene using 3-1-20 cells. 3-MC

Copyright © 2012 by the Japanese Society for the Study of Xenobiotics (JSSX)

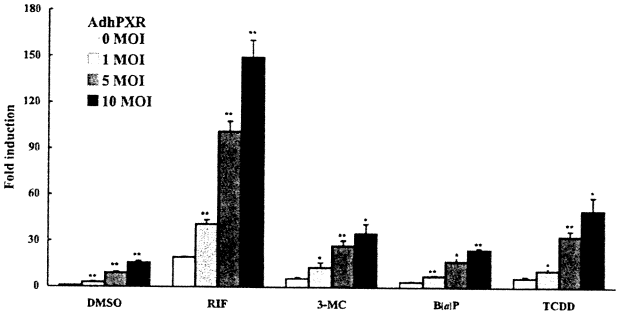


Fig. 5. Effect of AdhPXR on CYP3A4 reporter activity in 3-1-20 cells

Clone 3-1-20 was seeded at 3 × 10^4 cells in 48-well tissue culture plates pre-incubated for 24 h and then treated with AdhPXR (MOI of 0, 1, 5, 10). Forty-eight hours after infection, these cells were treated with 10 μM RIF, 1 μM 3-MC, 1 μM B[*a*]P, or 10 nM TCDD for 48 h and the reporter activity was measured by luciferase assay. Reporter activities are expressed as fold increase compared with that in the vehicle-treated cells uninfected with AdhPXR. Results represent the mean ± S.D. of three separate experiments. *, $p < 0.05$, **, $p < 0.005$, difference from the uninfected cells based on unpaired Student's *t*-test.

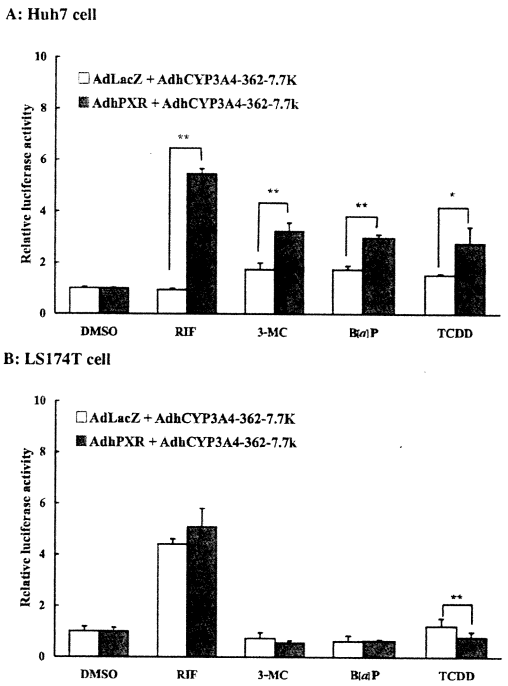


Fig. 6. Effect of AdhPXR on CYP3A4 reporter activity in Huh7 cells and LS174T cells

Huh7 cells (A) and LS174T cells (B) were seeded at 2 × 10^4 cells in 24-well tissue culture plates pre-incubated for 24 h and then were treated with AdLacZ (10 MOI) or AdhPXR (10 MOI) and Ad-CYP3A4-362-7.7k (5 MOI). Forty-eight hours after infection, these cells were treated with 10 μM RIF, 1 μM 3-MC, 1 μM B[*a*]P, or 10 nM TCDD for 48 h and the reporter activity was measured by luciferase assay. Reporter activities are expressed as fold change compared with that in the vehicle-treated cells. Results represent the mean ± S.D. of three separate experiments. *, $p < 0.05$, **, $p < 0.005$, difference from the corresponding AdLacZ-infected cells based on unpaired Student's *t*-test.

and B[*a*]P, which are typical PAHs, activated the *CYP3A4* reporter gene (**Fig. 2**). The expression of endogenous CYP3A4 mRNA was also induced by PAHs in 3-1-20 cells (**Fig. 3**). These results indicate that PAHs are potent inducers of CYP3A4. However, the CYP3A4 induction profiles by RIF and PAHs were different between CYP3A4 reporter activity and CYP3A4 mRNA expression level. It is reported that the distal promoter region, from −7836 nt to −7200 nt, and the proximal promoter region, from −362 nt to +11 nt, of the *CYP3A4* gene play important roles for CYP3A4 induction.[25] Recently, Matsumura *et al.* discovered that a novel enhancer region from −11.4 to −10.5 kb, designated the constitutive liver enhancer module of CYP3A4 (CLEM4), is involved in the constitutive activation of the *CYP3A4* gene in HepG2 cells.[26] Furthermore, Liu *et al.* identified a functional nuclear receptor responsive element (F-ER6 at −11368 to −11351) in Huh7 cells.[27] Taking these reports together, for intrinsic CYP3A4 induction, all these *cis*-elements might be required in human liver. However, the cell line 3-1-20 was established by Noracharttiyapot *et al.* by insertion of the luciferase reporter plasmid, pGL3-CYP3A4-362-7.7k, which includes both −7836 to −7200 of the distal promoter region and −362 to +11 of the proximal promoter region of the *CYP3A4* gene, the elements reported to be necessary for high response to RIF, into HepG2 cell chromosome.[22] Therefore, the differences of these CYP3A4 activation patterns by RIF and PAHs might be attributable to other enhancer regions not included in pGL3-CYP3A4-362-7.7k. In addition, CYP1A1 plays critical roles in the metabolism of PAHs.[28] Thus, 3-MC and B[*a*]P were initially metabolized by CYP1A1 induced through AhR activation in this culture condition. Subsequently, the metabolites of 3-MC and B[*a*]P might cause CYP3A4 induction. On the other hand, the induction profile was different among AhR ligands. Although CYP3A4 induction potency is similar between 3-MC and B[*a*]P, the CYP1A1 induction potency of B[*a*]P was far lower than that of 3-MC. This result may suggest that AhR is not directly involved in the *CYP3A4* gene activation by 3-MC and B[*a*]P.

CYP3A4 induction by xenobiotics and hormones is mediated by PXR,[29–31] constitutive androstane receptor (CAR, NR1I3),[32] vitamin D receptor (VDR, NR1I1),[33] and glucocorticoid receptor-α (GRα, NR3C1)[34] in the liver. In particular, chemical-induced activation of the *CYP3A4* gene is mainly mediated by PXR through binding to the *CYP3A4* 5′-flanking region,[29,31,35] whereas PAHs cause transactivation of *CYP1A1* and *1A2* genes *via* AhR.[19] Therefore, we knocked down hPXR expression using hPXR-siRNA. When hPXR-siRNA was introduced into the 3-1-20 cells, the activation of the *CYP3A4* reporter gene by PAHs as well as RIF was significantly decreased (**Fig. 4A**), whereas the knockdown of AhR by hAhR-siRNA had no effect on the activation of the *CYP3A4* reporter gene by RIF and PAHs (**Fig. 4B**). The same results were observed when hPXR-

Copyright © 2012 by the Japanese Society for the Study of Xenobiotics (JSSX)

siRNA was introduced by adenovirus (data not shown). Furthermore, the overexpression of PXR using AdhPXR increased CYP3A4 reporter activity by PAHs as well as RIF in an infection dose-dependent manner (**Fig. 5**). Therefore, these results strongly suggest that 3-MC and B[*a*]P enhance the transactivation of the *CYP3A4* gene through PXR activation but not through AhR activation. On the other hand, knockdown of AhR by hAhR-siRNA decreased the CYP3A4 reporter activity by TCDD (**Fig. 4**). This reason for this is unclear. The *CYP3A4* gene might be transactivated partially by TCDD through the AhR pathway owing to its strong AhR activation potency. Further studies are needed to resolve this issue.

It is known that the drug-induced expression of the *CYP3A4* gene in the liver is predominantly regulated through PXR.[36] In contrast, VDR controls the CYP3A4 transactivation with the secondary bile acid, lithocholic acid (LCA), in the intestine.[37,38] In addition, recently, a novel PXR functional *cis*-acting PXR-binding element designated eNR3A4 has been discovered to be an essential element for RIF-inducible CYP3A4 transactivation in human liver.[7] This element is located approximately 7.6 kb upstream from the transcription initiation site of the *CYP3A4* gene, to which hPXR binds as a heterodimer with human RXRα. Furthermore, Pavek *et al.* reported that eNR3A4 has negligible or no effect on CYP3A4 transactivation through VDR.[39] Thus, these findings indicate that eNR3A4 is a key regulatory element for the xenobiotic induction of CYP3A4 through hPXR in the liver. In this study, we show that PAHs increased CYP3A4 reporter activity in PXR-overexpressing hepatoma cells, whereas this phenomenon was not observed in PXR-overexpressing intestinal cells (**Fig. 6**). These results indicate that eNR3A4 might have been involved in the activation of the *CYP3A4* gene through hPXR by PAHs in the liver. Since the difference of the HepG2 cells and the LS174T cells in an induction mechanism of the *CYP3A4* gene by PAHs is unknown, further analysis is still in progress.

Numerous studies of induction by treatment with PAHs have been carried out to date. PAHs as well as TCDD have been believed to strongly induce CYP1A1 and CYP1A2 through the AhR pathway. However, there are no data about CYP3A induction by them in experimental animals. Recently, it was reported that 3-MC induces CYP3A4 in HepG2 cells.[40] In addition, when the reporter assay was measured in pGL3-CYP3A4-362-7.7k-transformed rat hepatoma Reuber H35 cells, PAHs and TCDD did not increase the reporter activity (data not shown). Together with these results, it is suggested that PAHs and TCDD activate human PXR, but not rat or mouse PXRs. Further studies are needed to clarify this issue.

In conclusion, we have demonstrated that PAHs activate *CYP3A4* gene transcription through the activation of hPXR in HepG2 cells. Thus, PAHs may contribute to CYP3A4 induction in human liver. More detailed study on the molecular mechanism behind the CYP3A4 induction by PAHs may provide important information on the drug-drug interaction.

Acknowledgments: We thank Mr. Shinpei Kobayashi and Ms. Rie Shoji for excellent technical assistance.

References

1) Gonzalez, F. J.: Human cytochromes P450: problem and prospects. *Trends Pharmacol. Sci.*, **13**: 346–352 (1992).
2) Nebert, D. W. and Russell, D. W.: Clinical importance of cytochromes P450. *Lancet*, **360**: 1155–1162 (2002).
3) Thummel, K. E. and Wilkinson, G. R.: *In vitro* and *in vivo* drug interactiona involving human CYP3A. *Annu. Rev. Pharmacol. Toxicol.*, **38**: 389–430 (1998).
4) Quattrochi, L. C. and Guzelian, P. S.: CYP3A regulation: From pharmacology to nuclear receptors. *Drug Metab. Dispos.*, **29**: 615–622 (2001).
5) Thelen, K. and Dressman, J. B.: Cytochrome P450-mediated metabolism in the human gut wall. *J. Pharm. Pharmacol.*, **61**: 541–558 (2009).
6) Tolson, A. H. and Wang, H.: Regulation of drug-metabolizing enzymes by xenobiotic receptors: PXR and CAR. *Adv. Drug Deliv. Rev.*, **62**: 1238–1249 (2010).
7) Toriyabe, T., Nagata, K., Takada, T., Aratsu, Y., Matsubara, T., Yoshinari, K. and Yamazoe, Y.: Unveiling a new essential cis element for the transactivation of the CYP3A4 gene by xenobiotics. *Mol. Pharmacol.*, **75**: 677–684 (2009).
8) Luo, G., Cunningham, M., Kim, S., Burn, T., Lin, J., Sinz, M., Hamilton, G., Rizzo, C., Jolley, S., Gilbert, D., Downey, A., Mudra, D., Graham, R., Carroll, K., Xie, J., Madan, A., Parkinson, A., Christ, D., Selling, B., LeCluyse, E. and Gan, L. S.: CYP3A4 induction by drugs: correlation between a pregnane X receptor reporter gene assay and CYP3A4 expression in human hepatocytes. *Drug Metab. Dispos.*, **30**: 795–804 (2002).
9) Matsubara, T., Noracharttiyapot, W., Toriyabe, T., Yoshinari, K., Nagata, K. and Yamazoe, Y.: Assessment of human pregnane X receptor involvement in pesticide mediated activation of CYP3A4 gene. *Drug Metab. Dispos.*, **35**: 728–733 (2007).
10) Casabar, R. C., Das, P. C., DeKrey, G. K., Gardiner, C. S., Cao, Y., Rose, R. and Wallace, A. D.: Endosulfan induce CYP2B6 and CYP3A4 by activating the pregnane X receptor. *Toxicol. Appl. Pharmacol.*, **245**: 335–343 (2010).
11) Matsubara, T., Yoshinari, K., Aoyama, K., Sugawara, M., Sekiya, Y., Nagata, K. and Yamazoe, Y.: Role of vitamin D receptor in the lithocholic acid-mediated CYP3A induction in vitro and in vivo. *Drug Metab. Dispos.*, **36**: 2058–2063 (2008).
12) Moore, L. B., Goodwin, B., Jones, S. A., Wisely, G. B., Serabjit-Singh, C. J., Willson, T. M., Collins, J. L. and Kliewer, S. A.: St. John's wort induces hepatic drug metabolism through activation of the pregnane X receptor. *Proc. Natl. Acad. Sci. USA*, **97**: 7500–7502 (2000).
13) Yeung, E. Y., Sueyoshi, T., Negishi, M. and Chang, T. K.: Identification of *Ginkgo biloba* as a novel activator of pregnane X receptor. *Drug Metab. Dispos.*, **36**: 2270–2276 (2008).
14) Wang, L., Li, F., Lu, J., Li, G., Li, D., Zhong, X., Guo, G. L. and Ma, X.: The chinese herbal medicine *Sophora flavescens* activates pregnane X receptor. *Drug Metab. Dispos.*, **38**: 2226–2231 (2010).
15) Jones, S. A., Moore, L. B., Shenk, J. L., Wisely, G. B., Hamilton, G. A., Tomkinson, N. C., LeCluyse, E. L., Lambert, M. H., Willson, T. M., Kliewer, S. A. and Moore, J. T.: The pregnane X receptor: a promiscuous xenobiotic receptor that has diverged during evolution. *Mol. Endocrinol.*, **14**: 27–39 (2000).
16) Kitamura, M. and Kasai, A.: Cigarette smoke as a trigger for the

Copyright © 2012 by the Japanese Society for the Study of Xenobiotics (JSSX)

dioxin receptor-mediated signaling pathway. *Cancer Lett.*, **252**: 184–194 (2007).
17) Kroon, L. A.: Drug interactions with smoking. *Am. J. Health Syst. Pharm.*, **64**: 1917–1921 (2007).
18) Zevin, S. and Benowitz, N. L.: Drug interactions with tobacco smoking, an update. *Clin. Pharmacokinet.*, **36**: 425–438 (1999).
19) Kawajiri, K. and Fujii-Kuriyama, Y.: Cytochrome P450 gene regulation and physiological functions mediated by aryl hydrocarbon receptor. *Arch. Biochem. Biophys.*, **464**: 207–212 (2007).
20) Norman, T. R., Fulton, A., Burrows, G. D. and Maguire, K. P.: Pharmacokinetics of N-desmethyldiazepam after a single oral dose of clorazepate: the effect of smoking. *Eur. J. Clin. Pharmacol.*, **21**: 229–233 (1981).
21) Klotz, U., Avant, G. R., Hoyumpa, A., Schenker, S. and Wilkinson, G. R.: The effects of age and liver disease on the disposition and elimination of diazepam in adult man. *J. Clin. Invest.*, **55**: 347–359 (1975).
22) Noracharttiyapot, W., Nagai, Y., Matsubara, T., Miyata, M., Shimada, M., Nagata, K. and Yamazoe, Y.: Construction of several human-derived stable cell lines displaying distinct profiles of CYP3A4 induction. *Drug Metab. Pharmacokinet.*, **21**: 99–108 (2006).
23) Suzuki, H., Sasaki, T., Kumagai, T., Sakaguchi, S. and Nagata, K.: Malondialdehyde-modified low density lipoprotein-induced cell growth was suppressed by polycyclic aromatic hydrocarbons. *J. Toxicol. Sci.*, **35**: 137–147 (2010).
24) Hittle, D. C. and Stukel, J. J.: Particle size distribution and chemical composition of coal-tar fumes. *Am. Ind. Hyg. Assoc. J.*, **37**: 199–204 (1976).
25) Takada, T., Ogino, M., Miyata, M., Shimada, M., Nagata, K. and Yamazoe, Y.: Differences in transactivation between rat CYP3A1 and human CYP3A4 genes by hyman pregnane X receptor. *Drug Metab. Pharmacokinet.*, **19**: 103–113 (2004).
26) Matsumura, K., Saito, T., Takahashi, Y., Ozeki, T., Kiyotani, K., Fujieda, M., Yamazaki, H., Kunitoh, H. and Kamataki, T.: Identification of a novel polymorphic enhancer of the human CYP3A4 gene. *Mol. Pharmacol.*, **65**: 326–334 (2004).
27) Liu, F. J., Song, X., Yang, D., Deng, R. and Yan, B.: The far and distal enhancers in the CYP3A4 gene co-ordinate the proximal promoter in responding similarly to the pregnane X receptor but differentially to hepatocyte nuclear gactor-4α. *Biochem. J.*, **409**: 243–250 (2008).
28) Ma, Q. and Lu, A. Y.: CYP1A induction and human risk assessment: An evolving tale of in vitro and in vivo studies. *Drug Metab. Dispos.*, **35**: 1009–1016 (2007).
29) Bertilsson, G., Heidrich, J., Svensson, K., Asman, M., Jendeberg, L., Sydow-Backman, M., Ohlsson, R., Postillnd, H., Blomquist, P. and Berkenstam, A.: Identification of a human nuclear receptor defines a new signaling pathway for CYP3A induction. *Proc. Natl. Acad. Sci. USA*, **95**: 12208–12213 (1998).
30) Goodwin, B., Hodgson, E. and Liddle, C.: The orphan human pregnane X receptor mediates the transcriptional activation of CYP3A4 by rifampicin through a distal enhancer module. *Mol. Pharmacol.*, **56**: 1329–1339 (1999).
31) Lehmann, J. M., McKee, D. D., Watson, M. A., Willson, T. M., Moore, J. T. and Kliewer, S. A.: The human orphan nuclear receptor PXR is activated by compounds that regulate CYP3A4 gene expression and cause drug interactions. *J. Clin. Invest.*, **102**: 1016–1023 (1998).
32) Goodwin, B., Hodgson, E., D'Costa, D. J., Roberson, G. R. and Liddle, C.: Transcriptional regulation of the human CYP3A4 gene by the constitutive androstane receptor. *Mol. Pharmacol.*, **62**: 359–365 (2002).
33) Drocourt, L., Ourlin, J. C., Pascussi, J. M., Maurel, P. and Vilarem, M. J.: Expression of CYP3A4, CYP2B6, and CYP2C9 is regulated by the vitamin D receptor pathway in primary human hepatocytes. *J. Biol. Chem.*, **277**: 25125–25132 (2002).
34) Pascussi, J. M., Drocourt, L., Gerbal-Chaloin, S., Fabre, J. M., Maurel, P. and Vilarem, M. J.: Dual effect of dexamethasone on CYP3A4 gene expression in human hepatocytes, Sequential role of glucocorticoid receptor and pregnane X receptor. *Eur. J. Biochem.*, **268**: 6346–6358 (2001).
35) Blumberg, B., Sabbagh, W., Jr., Juguilon, H., Bolado, J., Jr., van Meter, C. M., Ong, E. S. and Evans, R. M.: SXR, a novel steroid and xenobiotic-sensing nuclear receptor. *Genes Dev.*, **12**: 3195–3205 (1998).
36) Lin, J. H.: Cyp induction-mediated drug interactions: in vitro assessment and clinical implications. *Pharm. Res.*, **23**: 1089–1116 (2006).
37) Makishima, M., Okamoto, A. Y., Repa, J. J., Tu, H., Learned, R. M., Luk, A., Hull, M. V., Lustig, K. D., Mangelsdorf, D. J. and Shan, B.: Identification of a nuclear receptor for bile acids. *Science*, **284**: 1362–1365 (1999).
38) Pavek, P. and Dvorak, Z.: Xenobiotic-induced transcriptional regulation of xenobiotic metabolizing enzymes of the cytochrome P450 superfamily in human extrahepatic tissues. *Curr. Drug Metab.*, **9**: 129–143 (2008).
39) Pavek, P., Pospechova, K., Svecova, L., Syrova, Z., Stejkalova, L., Blazkova, J., Dvorak, Z. and Blahos, J.: Intestinal cell-specific vitamin D receptor (VDR)-mediated transcriptional regulation of CYP3A4 gene. *Biochem. Pharmacol.*, **79**: 277–287 (2010).
40) Westerink, W. M. and Schoonen, W. G.: Cytchrome P450 enzyme levels in HepG2 cells and cryopreserved primary human hepatocytes and their induction in HepG2 cells. *Toxicol. In Vitro*, **21**: 1581–1591 (2007).

Copyright © 2012 by the Japanese Society for the Study of Xenobiotics (JSSX)

Bioorganic & Medicinal Chemistry 19 (2011) 3540–3548

Contents lists available at ScienceDirect

Bioorganic & Medicinal Chemistry

journal homepage: www.elsevier.com/locate/bmc

Crystal structure, docking study and structure–activity relationship of carborane-containing androgen receptor antagonist 3-(12-hydroxymethyl-1,12-dicarba-*closo*-dodecaboran-1-yl)benzonitrile

Kiminori Ohta [a], Tokuhito Goto [a], Shinya Fujii [b], Masatoshi Kawahata [c], Akifumi Oda [a], Shigeru Ohta [d], Kentaro Yamaguchi [c], Shuichi Hirono [e], Yasuyuki Endo [a,*]

[a] *Faculty of Pharmaceutical Sciences, Tohoku Pharmaceutical University, 4-4-1 Komatsushima, Aoba-ku, Sendai 981-8558, Japan*
[b] *Graduate School of Biomedical Science, Institute of Biomaterials and Bioengineering, Tokyo Medical and Dental University, 2-3-10 Kanda-Surugadai, Chiyoda-ku, Tokyo 101-0062, Japan*
[c] *Faculty of Pharmaceutical Sciences at Kagawa Campus, Tokushima Bunri University, 1314-1 Shido, Sanuki, Kagawa 769-2193, Japan*
[d] *Graduate School of Medical Sciences, Hiroshima University, 1-2-3, Kasumi, Minami-ku, Hiroshima 734-8551, Japan*
[e] *School of Pharmaceutical Sciences, Kitasato University, 5-9-1 Shirokane, Minato-ku, Tokyo 108-8641, Japan*

ARTICLE INFO

Article history:
Received 3 March 2011
Revised 6 April 2011
Accepted 8 April 2011
Available online 20 April 2011

Keywords:
Androgen receptor
Antagonist
Carborane
X-ray crystallography
Docking study
Structure–activity study

ABSTRACT

A potent androgen receptor (AR) antagonist, 3-(12-hydroxymethyl-1,12 dicarba-*closo*-dodecaboran-1-yl)benzonitrile (**3a**, BA341), contains a *p*-carborane cage as a hydrophobic pharmacophore. We elucidated the structural properties of **3a** by means of single-crystal X-ray diffraction analysis and conducted a docking study of **3a** with hAR LBD. The cyano group of **3a** formed hydrogen bonds with Gln711 and Arg752 and the hydroxymethyl group did so with Asn705 and Thr877 in hAR LBD. The bulky *p*-carborane cage was accommodated in the hydrophobic pocket of hAR LBD. To understand the structure–activity relationship around the hydroxymethyl group of **3a**, we designed, synthesized, and evaluated the biological activities of various novel AR ligands. Since the biological activities of carbonyl compounds **8a**, **8b**, and **8c** were similar to or weaker than those of the parent hydroxyl compounds **3a**, **7a**, and **7b**, it seems to be necessary to have not only a hydrogen bonding acceptor, but also a hydrogen bonding donor adjacent to the hydroxymethyl group of **3a** for efficient interaction with hAR LBD.

© 2011 Elsevier Ltd. All rights reserved.

1. Introduction

Dicarba-*closo*-dodecaboranes (carboranes) are chemical building blocks of remarkable thermal stability and high boron content; they are resistant to attack by most types of reagent, and are generally inactive towards biological systems.[1] One of their most striking features is the ability of the two carbon atoms and ten boron atoms to adopt icosahedral geometry, in which the carbon and boron atoms are hexa-coordinated (Fig. 1a).[2] This feature gives rise to the unusual properties of such molecules and their derivatives. Their properties make them uniquely suitable for various specialized applications, including polymers for high temperature use, neutron shielding, and optical signaling.[3] In the fields of medicinal chemistry and pharmaceutical sciences, incorporation of large numbers of boron atoms into tumor cells for boron neutron capture therapy (BNCT) has become of interest in the last few decades.[4] Most carborane-containing compounds that have so far been synthesized are composed of cellular building blocks (nucleic acids,[5] amino acids,[6] sugars,[7] and so on), to which carborane units have been added. On the other hand, we have focused on the exceptional hydrophobic character and spherical geometry of carboranes to develop novel and useful hydrophobic structures for application as hydrophobic pharmacophores in biologically active molecules that interact with receptors and regulate the function of the receptors.[8] Especially, we have developed carborane-containing ligands for nuclear receptors, such as estrogen receptor, retinoic acid receptor, and retinoid X receptor, and demonstrated by means of computational docking studies that the spherical hydrophobic surface of the carborane cage interacts effectively with the hydrophobic pocket of the nuclear receptor ligand binding domain (LBD).[9]

Androgens regulate diverse physiological processes involving both reproductive and non-reproductive functions.[10] Most of the signaling effects of androgens are mediated through the androgen receptor (AR), a member of the nuclear receptor superfamily of transcription factors.[11] Inadequate circulating levels of the natural AR ligands, testosterone and dihydrotestosterone (DHT), which is the active metabolite of testosterone generated by 5α-reductase, in hypogonadal men can be compensated by administration of

* Corresponding author. Tel.: +81 22 727 0142; fax: +81 22 275 2013.
E-mail address: yendo@tohoku-pharm.ac.jp (Y. Endo).

0968-0896/$ - see front matter © 2011 Elsevier Ltd. All rights reserved.
doi:10.1016/j.bmc.2011.04.017

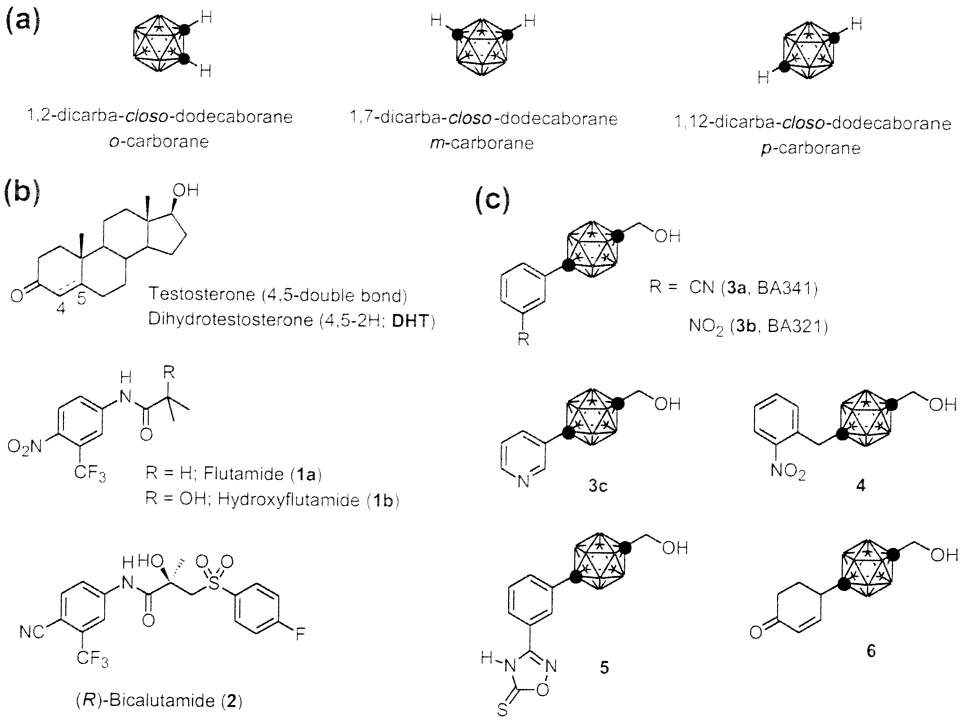


Figure 1. (a) Structures of icosahedral carboranes. (b) Structures of native androgens and androgen receptor antagonists, including pharmaceutical drugs. (c) Structures of carborane-containing inorganic AR antagonists developed in our previous studies.

exogenous androgens (Fig. 1b).[12] For decades, AR has been a target for drug development focused upon the treatment of pathological conditions arising from abnormal androgen levels or altered target tissue responsiveness, including improvement of physical performance, and regulation of male fertility. On the other hand, excessive stimulation of AR is thought to be closely related to prostate cancer.[13] Prostate cancer is the most common type of cancer and the second leading cause of cancer deaths in males.[14] The primary focus for drug discovery in this area is the synthesis of novel ligands to regulate the transcriptional activity of AR based on structural (steroidal or non-steroidal) and functional (androgenic, antiandrogenic, or anabolic) characteristics.[15] A non-steroidal ligand, flutamide (**1a**),[16] which is metabolized to a more potent antiandrogen, hydroxyflutamide (**1b**),[17] and bicalutamide, which is a racemate of a more potent (*R*)-bicalutamide (**2**)[18] and a less potent (*S*)-bicalutamide, are well-known AR antagonists used for the treatment of prostate cancer during its early stage (Fig. 1b).[19]

Binding of ligands to the AR ligand binding domain (LBD) primarily requires a nitro or cyano group, which forms a direct hydrogen bond with Arg752 of the hAR LBD.[20] This group is also hydrogen-bonded to Gln711 and Met745 via one H_2O molecule.[20] An X-ray co-crystal structure analysis of the complex of AR LBD with DHT indicated that the secondary alcohol group of DHT is hydrogen-bonded to Asn705 and Thr877 of hAR.[21] The hydrophobic group should be closely matched to the hydrophobic surface of the AR in order to increase the binding affinity. In the ligand-dependent control of nuclear receptors, a general and important structural feature has been elucidated by means of X-ray crystal analysis of complexes of several nuclear receptor LBDs with agonists and antagonists, that is, it is considered that the orientation of helix-12 is responsible for the agonist/antagonist function of nuclear receptors.[22] Therefore, for efficient design of nuclear receptor ligands, an understanding of the spatial relations between the ligand and helix-12 is absolutely essential.

Recently, we have reported potent AR antagonists bearing a carborane moiety, 3-(12-hydroxymethyl-1,12-dicarba-*closo*-dodecaboran-1-yl)benzonitrile (**3a**, BA341) and 3-(12-hydroxymethyl-1,12-dicarba-*closo*-dodecaboran-1-yl)nitrobenzene (**3b**, BA321), which are more potent than **1b** in AR-binding assay and cell proliferation assay (Fig. 1c).[23] Novel AR antagonists **3c**,[24] **4**,[25] and **5**[26] based on the structure of **3a** were also developed in our medicinal-chemical studies (Fig. 1c). Surprisingly, compound **6** acted as a potent AR antagonist, although it was designed based upon the structure of an AR agonist, testosterone (Fig. 1c).[27] We have not found any carborane-containing ligand that acts as an agonist for wild-type AR. These results support the idea that the bulky carborane cage favors expression of AR antagonistic activity. We have suggested that the carborane structure interacts sterically with Met895 and its surrounding amino acid residues in the hydrophobic pocket of hAR-LBD in such a way that helix-12 is moved away from the location required for agonist activity.[27]

We have been investigating the structure–activity relationships of **3a** around the cyanophenyl moiety and have explored novel bioisosteres of the cyano group. A wide range of the structure–activity relationship studies on **3a** is needed to aid the development of useful carborane-containing ligands, and docking simulation studies of **3a** with hAR LBD are also expected to be helpful for understanding the significance of the carborane cage in AR ligands. Here, we describe X-ray crystal structure analysis, docking studies with hAR LBD, and the structure–activity relationships of a number of novel analogues of **3a**.

2. Results and discussion

2.1. X-ray crystal structure of 3a

The potent AR antagonist, **3a**, was obtained according to the reported procedure.[22] Single crystals of **3a** were grown from a

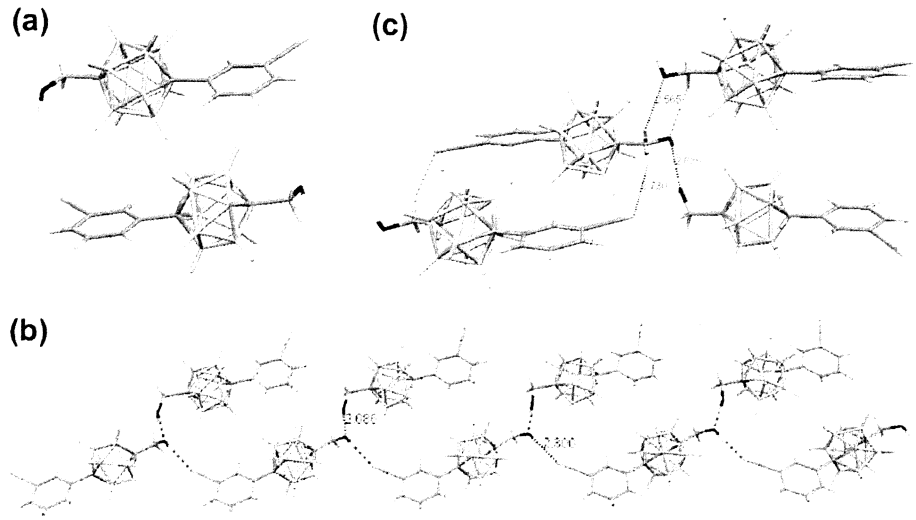


Figure 2. Various views of the X-ray structure of **3a**; Atom colors are C (gray), H (white), B (pink), N (blue), and O (red) (a) Ortep structure of **3a**. (b) Structure of OH···O and OH···N hydrogen bond networks; the distances between hetero atoms, O(H)···O and O(H)···N, are 2.686 and 2.800 Å, respectively. (c) Structure of interaction networks via weak hydrogen bonds, such as C–H···O and C–H···N; the distances of C–H···O and C–H···N, are 2.565 and 2.730 Å, respectively.

solution in $CHCl_3$ by slow evaporation of the solvent, and the solid-state structure was confirmed by single-crystal X-ray diffraction analysis. Compound **3a** crystallizes in the triclinic space group *P*–1. The crystal included two different structures of **3a** (Fig. 2a), which were designated as structure A and structure B (C(1)–C(10) and C(11)–C(20), respectively). Selected geometrical parameters of each structure are shown as Table 4 in Experimental section. All of the bond distances of structure A, except for C(8)–O(1), are shorter than those of structure B. The bond length of C(8)–O(1) of structure A is longer than the corresponding bond length of structure B owing to a more obtuse angle of C(9)–C(10)–O(1). The distance between the two carbon atoms, C(8) and C(9), of the *p*-carborane cage is 3.119 Å, which is 0.3 Å longer than the diameter (2.810 Å) of the benzene ring, C(3)–C(6). The distances between the hydrogen bonding acceptors, N(1)–O(1) and N(2)–O(2), which are essential for ligand-receptor binding, are 11.013 and 11.116 Å, respectively.

In the crystal packing of **3a**, the primary hydroxyl group forms two hydrogen bonds with a hydroxyl group and a cyano group of neighboring **3a** (Fig. 2b). The hydrogen of the hydroxyl group is used for formation of an O(H)···N hydrogen bond with a cyano group, and the oxygen of the hydroxyl group interacts with a hydroxyl group of neighboring **3a**, forming an O···(H)O hydrogen bond. The O···O and O···N distances are 2.686 and 2.800 Å, respectively. The methylene C–H hydrogen is activated by the electron-withdrawing character of the *p*-carborane cage and can behave as a hydrogen-bonding donor. Figure 2c shows a set of hydrogen-bonding networks, including classical and non-classical hydrogen bonds, in the crystal structure of **3a**. Both C–H hydrogens of a methylene group interact with the oxygen atom of the hydroxyl group and the cyano group of a neighboring **3a** via non-classical hydrogen bonds with distances of 2.565 and 2.730 Å, respectively. The steric bulkiness of the *p*-carborane cage has no effect on intermolecular hydrogen bond formation by the cyano and the hydroxymethyl groups of **3a**.

2.2. Docking study of 3a with hAR

Several studies on the three-dimensional structure of the complex formed by AR ligand and the hAR LBD have revealed the structural requirements for the appearance of agonist/antagonist activity. Docking simulation study of the potent AR antagonist **3a** is likely to be of great significance for the development of carborane-containing AR ligands with various biological profiles, such as partial agonists, selective androgen receptor modulators (SARMs), and pure AR antagonists for numerous mutated ARs. However, there is no report of docking simulation studies of carborane-containing AR ligand with hAR LBD. Initially, a docking simulation of wild-type hAR LBD with the carborane-containing ligand, **3a**, using the co-crystal structure of hAR LBD with the AR antagonist, metribolone (PDB: 1E3G), was performed with an automatic docking program (FlexX). Arg752 and Gln711 in hAR LBD, which are essential amino acid residues for receptor-ligand binding, interact directly with the cyano group of **3a**, with N···N distances of 2.49 and 2.86 Å, respectively (Fig. 3). The primary hydroxyl group of **3a** interacts with the carbonyl group of Asn705 and the hydroxyl group of Thr877, with O···O distances of 3.09 and 2.78 Å, respectively. Two C–H hydrogens of the methylene group of **3a** showed no clear interaction with amino acid residues of hAR LBD. The highly hydrophobic *p*-carborane cage is located in the hydrophobic pocket of the receptor. Four hydrogen bonds and the hydrophobic interaction in the ligand-receptor complex appear to be essential for high binding affinity of **3a** to the hAR. The *p*-carborane cage of **3a** is close to Met895, which is a part of helix-12, and it seems that the steric bulkiness of the *p*-carborane cage causes helix-12 to move from the agonist to the antagonist form. In our previous study, compounds with a hydroxyl group and a hydroxyethyl group instead of the hydroxymethyl group of **3a** showed much weaker binding affinity than that of **3a**.[22] It would appear that the spatial arrangement among the hydrogen-bonding functional groups and the *p*-carborane cage of **3a** is the most appropriate for forming the necessary hydrogen bonds and hydrophobic interaction with hAR LBD.

2.3. Design and synthesis of novel AR ligands

It is of great interest to examine the structure–activity relationships around the hydroxymethyl group of **3a** since this group lies near helix-12, according to the result of the docking study. Thus, we designed novel AR ligands, compounds **7a–7d** with a secondary or tertiary hydroxyl group, to examine the role of the region around Asn705, Thr877, and Met895 in hAR LBD (Fig. 4). We also designed

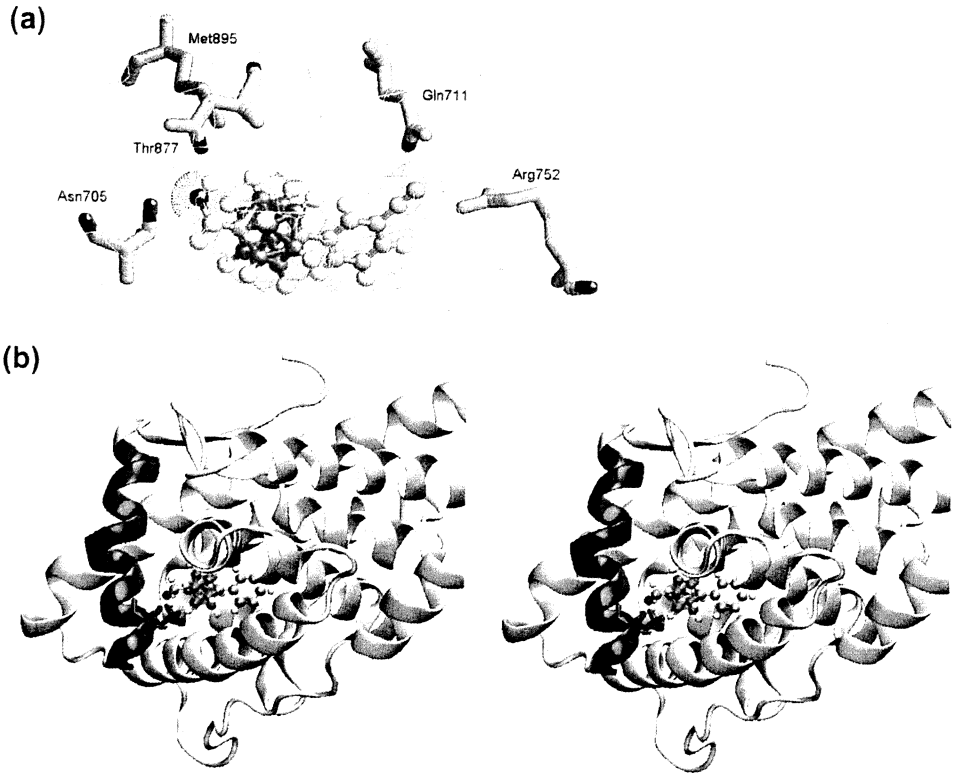
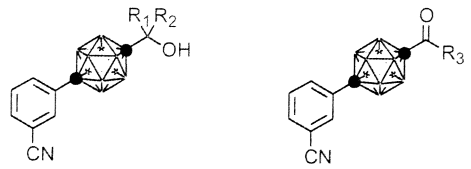
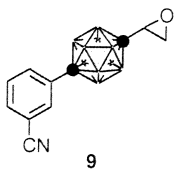


Figure 3. Docking model of **3a** to the hAR LBD. (a) Hydrogen bondings of **3a** with four amino acid residues in hAR LBD and the arrangements of Met895 (gold) and the *p*-carborane cage (green) of **3a**. (b) Stereoview of the overall picture of the docking model. Met895 and helix-12, carbon, and boron atoms are colored red, blue, and green, respectively.



7a (R_1 = H, R_2 = CH_3)
7b (R_1 = H, R_2 = Ph)
7c (R_1 = CH_3, R_2 = CH_3)
7d (R_1 = CH_3, R_2 = Ph)

8a (R_3 = H)
8b (R_3 = CH_3)
8c (R_3 = Ph)



9

Figure 4. Design of new androgen receptor antagonists **7–9**.

carbonyl compounds **8a–8c** and epoxide **9**, with hydrogen-bonding acceptors instead of the primary hydroxyl group of **3a**.

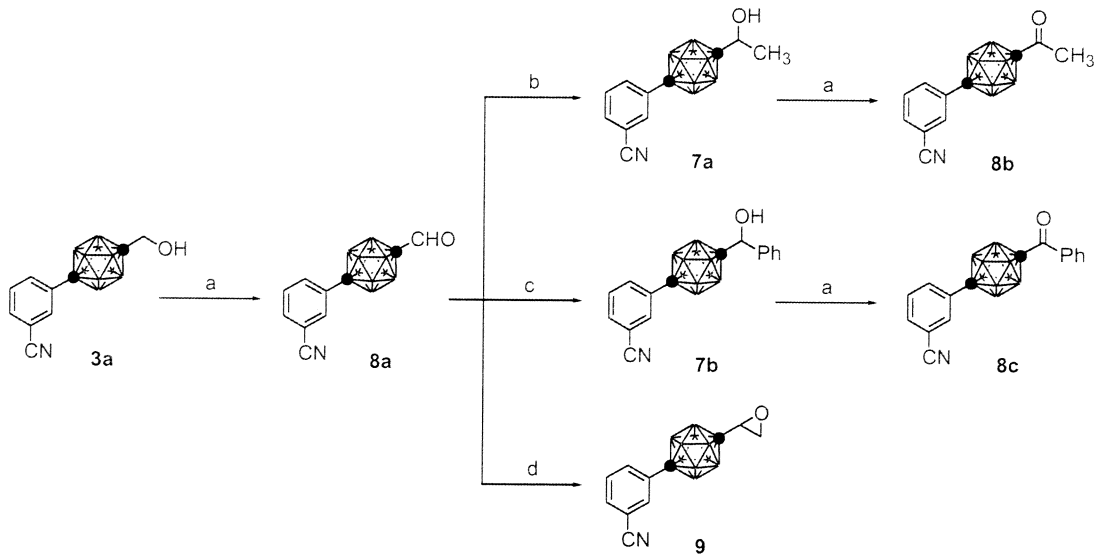
The synthesis of the designed compounds **7–9** is summarized in Scheme 1. The potent AR antagonist, **3a**, was treated with Dess–Martin reagent in CH_2Cl_2 to afford the key intermediate **8a** in 91% yield.[28] Compound **8a** was reacted with Grignard reagents, methylmagnesium bromide (CH_3MgBr) and phenylmagnesium bromide (PhMgBr), in THF at −78 °C to afford the secondary alcohols **7a** and **7b** in 84% and 77% yields, respectively, followed by oxidation reaction with Dess–Martin reagent in CH_2Cl_2 to afford the corresponding carbonyl compounds **8b** and **8c** in 90% and 93% yields, respectively. Transformation of the aldehyde **8a** into epoxide **9** was accomplished by Simmons-Smith reaction using diethylzinc, chloroiodomethane and tetrahydrothiophene in 71% yield.[29]

The synthesis of the tertiary alcohols **7c** and **7d** is summarized in Scheme 2. First, we tried the reaction of ketones **8b** and **8c** with CH_3MgBr but the starting materials were recovered, and the desired products were not obtained. Next, the reactions of **8b** and **8c** with methyllithium (CH_3Li) reagent were performed in THF at −78 °C. The yields of the products **7c** and **7d** in this reaction are summarized in Table 1.

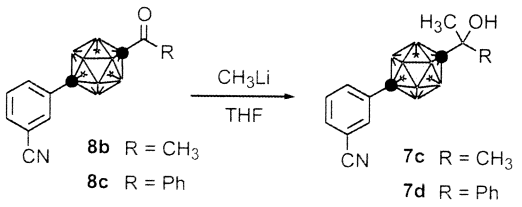
Compound **8b** was treated with 3.0-fold molar excess of CH_3Li to afford only the desired product **7c** in 58% yield (Entry 2). Use of 13.4-fold molar excess of CH_3Li afforded not only the corresponding tertiary alcohol **7c** in 14% yield, but also the 3-acetylphenyl derivatives **10** in 42% yield, which is generated by the reaction of the benzonitrile moiety with CH_3Li (Entry 3, Fig. 5). Since the steric bulkiness of the carborane cage hindered nucleophilic attack of the lithium reagent on the aldehyde, an excess of lithium reagent was necessary to obtain the desired compounds. When the sterically crowded ketone **8c** was used as a starting material, no reaction was occurred with 3.0-fold molar excess of CH_3Li (Entry 4). Finally, the desired product **7b** was obtained by the use of 8.9-fold molar excess of CH_3Li, in 81% yield (Entry 5). The corresponding acetophenone derivative was not observed in this reaction. Compounds **7a**, **7b**, **7d**, and **9** have an asymmetric carbon and were used for biological assays in racemic form.

2.4. Biological evaluations

The binding affinity of the new carborane-containing compounds for AR was evaluated by means of competitive-binding assay using [1,2-^{3}H]dihydrotestosterone ([^{3}H]DHT) and hAR.[30]



Scheme 1. Synthesis of analogues of **3a**. Reagents: (a) Dess–Martin reagent, CH_2Cl_2; (b) CH_3MgBr, THF; (c) PhMgBr, THF; (d) Et_2Zn, $ClCH_2I$, tetrahydrothiophene CH_2Cl_2.



Scheme 2. The reaction of *C*-acylcarborane derivatives **7c** and **7d** with methyllithium.

Table 1
Yields of the desired products **7** in the reaction of **8** with methyl lithium[a]

Entry	Compound	R	CH_3Li (equiv)	Yield (%)
1	**8b**	CH_3	1.0	0 (**7c**)
2	**8b**	CH_3	3.0	58 (**7c**)
3	**8b**	CH_3	13.4	14 (**7c**)[b]
4	**8c**	Ph	3.0	0 (**7d**)
5	**8c**	Ph	8.9	81 (**7d**)

[a] The reactions were performed at -78 °C for 30 min.
[b] 3-Acetylphenyl derivatives **10** was obtained in 42% yield.

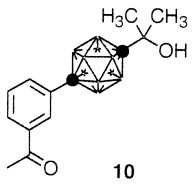


Figure 5. Structure of the by-product **10** obtained from the reaction of **8b** with methyl lithium.

Table 2 summarizes the binding affinity data of the synthesized compounds: the values indicate the percent displacement of specific [^{3}H]DHT binding to hAR by each compounds at the concentration of 10 μM. Compounds **7a**, **7b** and **8a** showed high binding affinity for hAR but were less potent binders than **3a**. The binding affinity of the synthesized compounds was affected by the hydrogen-bonding groups with Asn705 and Thr877 of AR LBD and the size of the substituents R_1, R_2, and R_3.

Table 2
Biological properties of the designed compounds **7–10**

Compound	Binding affinity[a] (%)	IC_{50}[b] (μM)
7a	78	0.32
7b	71	1.80
7c	52	0.33
7d	54	0.61
8a	78	0.17
8b	16	0.48
8c	24	1.67
9	33	nt[c]
10	44	5.39
3a (BA341)	95	0.15

[a] Values are percentage displacement of [^{3}H]DHT (4 nM) specific binding to hAR by each compound at 10 μM. All binding assays were performed in duplicate (n = 2), and the average value is indicated as the binding affinity.
[b] NIH3T3 cells were transiently transfected with hAR-expression plasmid, ARE/Luci (*firefly* luciferase) and pRL/CMV (*Renilla* luciferase) plasmids, and treated with the test compounds in the presence of DHT (1×10^{-10} M). IC_{50} values of the test compounds were estimated from the sigmoidal dose–response curves using GraphPad Prism 4 software.
[c] nt indicates not tested.

To evaluate the functional activity, agonist or antagonist, of the synthesized compounds, except for **9**, transcriptional assay was done with hAR-expression plasmid, ARE/Luci (*firefly* luciferase) and pRL/CMV in NIH3T3 cells.[31] None of the synthesized compounds exhibited AR-agonistic activity at the concentration of 1×10^{-5}–1×10^{-8} M. These compounds dose-dependently inhibited the transcriptional activation induced by 1×10^{-10} M DHT and acted as AR antagonists. Table 2 summarizes the IC_{50} values of **3a** analogues **7–10** in AR transactivation assay. Compounds **7a** and **7c**, which have methyl groups on the methylene carbon, showed potent inhibitory activity for DHT-induced AR transactivation, and their IC_{50} values were 0.32 and 0.33 μM, respectively. Although their inhibitory activities are two-fold weaker than that of the parent compound **3a**, methyl groups seem to be allowed at that position. Meanwhile, introduction of a phenyl group on the methylene carbon led to a marked decrease of DHT-induced AR transactivation (Table 2; **7b** and **7d**).

Carbonyl-containing compounds **8a–8c** showed similar structure–activity relationships to the alcohol derivatives, and their activity was markedly decreased with increasing size of substituents connected with the carbonyl group. Compound **10** with an acetyl

group instead of the cyano group showed weak AR antagonistic activity and the highest IC_{50} value, 5.39 μM, among the evaluated compounds. Compound **8a** exhibited the most potent inhibitory activity for DHT-induced AR transactivation (IC_{50} = 0.17 μM), and its IC_{50} value is similar to that of **3a** (IC_{50} = 0.15 μM). As regards the biological activities of these derivatives, the alcohol derivatives showed better biological profiles than the carbonyl derivatives (**3a** vs **8a** and **7a** vs **8b**). This can be explained in terms of the existence or not of hydrogen bonding between the hydroxyl group of the ligands and the carbonyl group of Asn705 in hAR LBD. From the SAR studies of these compounds, it seems that Asn705 and Thr877 in hAR LBD require hydrogen-bonding donors and acceptors, respectively, in the carborane-containing ligands for receptor-ligand binding. In addition, a large substituent, such as phenyl group, around Thr877 is unfavorable for AR antagonistic activity.

3. Conclusions

We have established the molecular structure of the carborane-containing potent AR ligand **3a** by means of X-ray crystal structure analysis, and examined the binding mode of **3a** with hAR LBD by means of computational docking study using the FlexX program. As expected, the cyano group of **3a** interacts with Arg752 and Gln711, and the hydroxymethyl group forms hydrogen bonds with Thr877 and Asn705. The *p*-carborane cage is located along the hydrophobic surface of hAR LBD and lies close to Met895, which is associated with helix-12. Compound **3a** derivatives designed based upon the docking study showed potent AR-binding affinity and AR antagonistic activity. The hydrogen bonds between the carborane-containing ligands and the four amino acid residues in hAR LBD are important for the receptor-ligand binding, and the steric repulsion of *p*-carborane cage with helix-12 results in the AR antagonistic activity of carborane-containing AR ligands. These findings are expected to be helpful for the development of novel carborane-containing anti-androgens, having a different spectrum of ligand responsiveness from other therapeutic agents.

4. Experimental

4.1. General considerations

Melting points were determined with a Yanagimoto micro melting point apparatus without correction. ^{1}H NMR, ^{13}C NMR and ^{10}B NMR spectra were recorded with JEOL JNM-LA-400 and JNM-FX-400 spectrometers. Chemical shifts for ^{1}H NMR spectra were referenced to tetramethylsilane (0.0 ppm) as an internal standard. Chemical shifts for ^{13}C NMR spectra were referenced to residual ^{13}C present in deuterated solvents. Chemical shift values for ^{11}B spectra were referenced to external BF_3•OEt (0.0 ppm, with negative values upfield). The chemical shifts are reported in ppm (δ scale) and all coupling constant (J) values are given in hertz (Hz). The splitting patterns are designated as follows: s (singlet), d (doublet), t (triplet), q (quartet), m (multiplet) and br (broad). Mass spectra were recorded on a JEOL JMS-DX-303 spectrometer. Elemental analyses were performed with a Perkin Elmer 2400 CHN spectrometer. Unless otherwise noted, the reagents and solvents were purchased from Aldrich Chemical Co., TCI, Kanto Chemicals, or Wako Chemicals, Inc. and were used as received. *p*-Carborane was purchased from Katchem s.r.o. (Prague, Czech Republic). Compound **3a** was prepared according to the literature.[23]

4.2. X-ray crystallography

Details of data collection and structure refinement for **3a** are given in Table 3. Diffraction data were obtained with a Rigaku AFC7S four-circle diffractometer with graphitemonochromated Mo Ka radiation (λ = 0.71073 Å). Generally, indexing was performed from three oscillation images exposed for 4.0 min, and a total of 15 oscillation images within the 2θ value of 50.0° were collected with the imaging plate area detector. The structure was solved by direct methods using SHELXS-97[32] and refined by the full matrix least-squares technique on F2 using SHELXL-97.

4.3. Docking study

The most stable model for **3a** was estimated using the automatic docking program FlexX version 1.2[33] implemented in SYBYL 6.91 (Tripos, Inc., St. Louis, MO). For the docking calculation, the quantum-chemically optimized structure of ligand **3a** was used as the initial structure. The optimization of the crystal structure of **3a** was carried out with B3LYP/6-31G(d,p) using GAUSSIAN 98 (Gaussian, Inc., Wallingford, CT). The structure of the hAR LBD was obtained from the crystal structure of the hAR LBD-metribolone complex (PDB code: 1E3G) by removing the metribolone molecule. All hydrogen atoms that are missing in the crystal structure but should exist in the protein structure were computationally located at appropriate positions by use of the Biopolymer module of SYBYL 6.91. The active site of hAR LBD was defined as the collection of amino acids for which at least one atom was closer than 6.5 Å to any atom of the bound metribolone. For FlexX calculation, the maximum number of generated poses was set to 500 and the parameter MAX_OVERLAP_VOL was expanded to 8.0 Å^3. Default values were used for other parameters, and the treatment of the ligand molecule was the same as in a previous study. [21] The generated docking poses were evaluated by means of a consensus scoring scheme using the CScore module of SYBYL 6.91, and the top-ranked pose which won the highest number of votes was selected.

4.4. Synthesis

4.4.1. 3-(12-Formyl-1,12-dicarba-*closo*-dodecaboran-1-yl)benzonitrile (8a)

To a solution of **3a** (146 mg, 0.53 mmol) in 3 mL of dry CH_2Cl_2 was added Dess–Martin periodinate (450 mg, 1.06 mmol). The reaction mixture was stirred for 8 h at room temperature under

Table 3
Crystal data of **3a**

Compound	**3a**
Formula	$C_{10}H_{17}B_{10}NO$
M_r	275.35
Recryst. solvent	$CHCl_3$
Crystal system	Triclinic
Lattice parameter	
a (A)	11.5045 (13)
b (A)	12.7194 (15)
c (A)	13.1240 (15)
α (°)	107.2910 (10)
β (°)	109.8900 (10)
γ (°)	107.4630 (10)
V (Å^3)	1542.5 (3)
Space group	P−1
Z value	4
P_{calc} (Mg/m^3)	1.186
Absorption coefficient (mm^{-1})	0.063
Crystal size (mm^3)	0.50 × 0.50 × 0.50
Temperature (K)	150
2θ max (°)	56.5
Reflections collected	15282
Independent reflections	6589
Data/restraints/parameters	6589/0/483
Goodness-of-fit on F^2	0.94
Residuals: R, Rw	0.0593, 0.1540
CCDC reference number	787463

Table 4
Comparison of selected geometrical parameters of each structure of **3a**

Distance and angle	Structure A	Structure B
C(1)–C(7)	1.435	1.440
C(3)–C(6)	2.810	2.804
C(3)–C(8)	1.506	1.509
C(8)–C(9)	3.119	3.130
C(9)–C(10)	1.534	1.541
C(8)–O(1)	5.401	5.386
C(10)–O(1)	1.400	1.424
C(7)–N(1)	1.142	1.146
C(10)–N(1)	10.054	10.077
B(1)–B(9)	3.373	3.373
N(1)–O(1)	11.013	11.116
C(9)–C(10)–O(1)	113.43	111.72

an Ar atmosphere, then filtered through Celite and the filtrate was concentrated. The residue was purified by silica gel column chromatography (eluent: *n*-hexane/AcOEt 20:1) to afford 129 mg (89%) of compound **8a** as a colorless solid; Colorless cubes (CH_2Cl_2/*n*-hexane); mp 127.5–128.5 °C; ^{1}H NMR (270 MHz, $CDCl_3$) δ (ppm) 1.0–3.5 (br m, 10H), 7.33 (m, 1H), 7.44 (dt, J = 1.3 Hz, 8.2 Hz, 1H), 7.48 (m, 1H), 7.55 (dt, J = 1.3 Hz, 7.6 Hz, 1H), 8.87 (s, 1H); ^{13}C NMR (68 MHz, $CDCl_3$) δ (ppm) 81.9, 84.1, 112.6, 117.7, 129.1, 130.4, 131.1, 132.1, 137.2, 185.4; MS (EI) *m/z* 273 (M^+, 100%); Anal. Calcd for $C_{10}H_{15}B_{10}NO$: C, 43.94; H, 5.53; N, 5.12. Found: C, 44.19; H, 5.61; N, 5.26.

4.4.2. 3-[12-(1-Hydroxyethyl)-1,12-dicarba-*closo*-dodecaboran-1-yl]benzonitrile (7a)

To a solution of **8a** (100 mg, 0.37 mmol) in 4 mL of dry THF was added CH_3MgBr (2.8 mL, 2.59 mmol) at -78 °C under an Ar atmosphere. The reaction mixture was stirred for 21 h at the same temperature, then quenched with saturated aqueous NH_4Cl solution, and extracted with AcOEt. The organic solution was washed with water and brine, dried over $MgSO_4$, and concentrated. The residue was purified by silica gel column chromatography (eluent: *n*-hexane/CH_2Cl_2 1:2 to *n*-hexane/AcOEt 10:1) to afford 58 mg (54%) of compound **7a** as a colorless solid; Colorless cubes (CH_2Cl_2/*n*-hexane); mp 114–115 °C; ^{1}H NMR (270 MHz, $CDCl_3$) δ (ppm) 1.0–3.5 (br m, 10H), 1.12 (d, J = 6.3 Hz, 3H), 1.73 (br s, 1H), 3.75 (quint, J = 6.3 Hz, 1H), 7.30 (m, 1H), 7.45 (m, 1H), 7.50 (m, 1H), 7.51 (m, 1H); ^{13}C NMR (68 MHz, $CDCl_3$) δ (ppm) 22.9, 69.3, 81.0, 87.7, 112.6, 118.1, 129.1, 130.8, 131.5, 131.9, 137.6; MS (EI) *m/z* 289 (M^+, 100%); Anal. Calcd for $C_{11}H_{19}B_{10}NO$: C, 45.65; H, 6.62; N, 4.84. Found: C, 45.79; H, 6.64; N, 4.93.

4.4.3. 3-[12-(1-Hydroxybenzyl)-1,12-dicarba-*closo*-dodecaboran-1-yl]benzonitrile (7b)

To a solution of **8a** (100 mg, 0.37 mmol) in 4 mL of dry THF was added PhMgBr (0.72 mL, 0.74 mmol) at -78 °C under an Ar atmosphere. The reaction mixture was stirred for 18 h at the same temperature, quenched with saturated aqueous NH_4Cl solution, and extracted with AcOE. The organic solution was washed with water and brine, dried over $MgSO_4$, and concentrated. The residue was purified by silica gel column chromatography (eluent: *n*-hexane/AcOEt 10:1) to afford 100 mg (77%) of compound **7b** as a colorless solid; Colorless prisms (CH_2Cl_2/*n*-hexane); mp 135.5–137.0 °C; ^{1}H NMR (270 MHz, $CDCl_3$) δ (ppm) 1.0–3.5 (br m, 10H), 1.59 (s, 1H), 4.67 (s, 1H), 7.13–7.53 (m, 9H); ^{13}C NMR (68 MHz, $CDCl_3$) δ (ppm) 75.7, 81.5, 86.9, 112.5, 118.1, 126.7, 128.1, 128.8, 129.0, 130.8, 131.5, 131.9, 137.6, 139.9; MS (EI) *m/z* 351 (M^+), 107 (100%); Anal. Calcd for $C_{16}H_{21}B_{10}NO$: C, 54.68; H, 6.02; N, 3.99. Found: C, 54.60; H, 6.10; N, 4.09.

4.4.4. 3-(12-Acetyl-1,12-dicarba-*closo*-dodecaboran-1-yl)benzonitrile (8b)

Compound **8b** was prepared by the same method as described for the synthesis of **8a**; 90% yield; Colorless prisms (CH_2Cl_2/*n*-hexane); mp 108.0–108.5 °C; ^{1}H NMR (270 MHz, $CDCl_3$) δ (ppm) 1.0–3.5 (br m, 10H), 2.12 (s, 3H), 7.30 (dd, J = 7.5 Hz, 8.6 Hz, 1H), 7.45 (ddd, J = 1.2 Hz, 2.0 Hz, 8.1 Hz, 1H), 7.50 (t, J = 1.5 Hz, 1H), 7.54 (ddd, J = 1.3 Hz, 1.5 Hz, 7.6 Hz, 1H); ^{13}C NMR (68 MHz, $CDCl_3$) δ (ppm) 27.3, 83.1, 84.6, 112.6, 117.8, 129.1, 130.4, 131.2, 132.0, 137.2, 192.2; MS (EI) *m/z* 287 (M^+, 100%); Anal. Calcd for $C_{11}H_{17}B_{10}NO$: C, 45.97; H, 5.96; N, 4.87. Found: C, 45.75; H, 5.81; N, 4.78.

4.4.5. 3-(12-Benzoyl-1,12-dicarba-*closo*-dodecaboran-1-yl)benzonitrile (8c)

Compound **8c** was prepared by the same method as described for the synthesis of **8a**; 93% yield; Colorless cotton (CH_2Cl_2/*n*-hexane); mp 143.5–144.0 °C; ^{1}H NMR (270 MHz, $CDCl_3$) δ (ppm) 1.0–3.5 (br m, 10H), 7.29–7.55 (m, 9H); ^{13}C NMR (68 MHz, $CDCl_3$) δ (ppm) 84.3, 112.6, 117.8, 127.8, 128.0, 129.0, 130.4, 130.7, 131.1, 131.9, 132.2, 135.9, 137.2, 189.1; MS (EI) *m/z* 349 (M^+), 105 (100%); Anal. Calcd for $C_{16}H_{19}B_{10}NO$: C, 54.99; H, 5.48; N, 4.01. Found: C, 54.77; H, 5.45; N, 3.90.

4.4.6. 3-[12-(1-Hydroxy-1-methyl)ethyl-1,12-dicarba-*closo*-dodecaboran-1-yl]benzonitrile (7c)

To a solution of **8b** (100 mg, 0.35 mmol) in 5 mL of dry ether was added CH_3Li (1.02 mL, 1.05 mmol) at −78 °C under an Ar atmosphere. The reaction mixture was stirred for 30 min at the same temperature, quenched with saturated aqueous NH_4Cl solution, and extracted with AcOEt. The organic solution was washed with water and brine, dried over $MgSO_4$, and concentrated. The residue was purified by silica gel column chromatography (eluent: *n*-hexane/AcOEt 20:1) to afford 61 mg (58%) of compound **7c** as a colorless solid; Colorless needles (CH_2Cl_2/*n*-hexane); mp 172.5–174.0 °C; ^{1}H NMR (270 MHz, $CDCl_3$) δ (ppm) 1.0–3.5 (br m, 10H), 1.23 (s, 6H), 2.05 (s, 3H), 7.30 (m, 1H), 7.45 (ddd, J = 1.3 Hz, 2.1 Hz, 8.4 Hz, 1H), 7.50 (m, 1H), 7.52 (ddd, J = 1.3 Hz, 1.5 Hz, 7.1 Hz, 1H); ^{13}C NMR (68 MHz, $CDCl_3$) δ (ppm) 31.6, 70.9, 81.6, 92.8, 112.5, 118.0, 128.9, 130.7, 131.4, 131.8, 137.5; MS (EI) *m/z* 305 (M^++2), 288 (100%); Anal. Calcd for $C_{12}H_{21}B_{10}NO$: C, 47.50; H, 6.98; N, 4.62. Found: C, 47.21; H, 6.85; N, 4.48.

4.4.7. 3-[12-(1-Hydroxy-1-phenyl)ethyl-1,12-dicarba-*closo*-dodecaboran-1-yl]benzonitrile (7d)

To a solution of **8c** (50 mg, 0.14 mmol) in 3 mL of dry THF was added CH_3Li (1.2 mL, 1.25 mmol) at −78 °C under an Ar atmosphere. The reaction mixture was stirred for 30 min at the same temperature, quenched with saturated aqueous NH_4Cl solution, and extracted with AcOEt. The organic solution was washed with water and brine, dried over $MgSO_4$, and concentrated. The residue was purified by silica gel column chromatography (eluent: *n*-hexane/AcOEt 10:1) to afford 42 mg (81%) of compound **7d** as a colorless solid; Colorless leaflets (CH_2Cl_2/*n*-hexane); mp 199.5–201.0 °C; ^{1}H NMR (270 MHz, $CDCl_3$) δ (ppm) 1.0–3.5 (br m, 10H), 1.65 (s, 3H), 7.2–7.6 (m, 9H); ^{13}C NMR (68 MHz, $CDCl_3$) δ (ppm) 44.4, 74.0, 82.0, 82.9, 112.4, 118.0, 121.6, 125.5, 127.7, 128.9, 130.6, 131.4, 131.7, 131.8, 137.5; MS (EI) *m/z* 366 (M^++1), 121 (100%); Anal. Calcd for $C_{15}H_{23}B_{10}NO$: C, 55.87; H, 6.34; N, 3.83. Found: C, 55.57; H, 6.36; N, 3.64.

4.4.8. 3-[12-(1,2-Epoxyethane)-1,12-dicarba-*closo*-dodecaboran-1-yl]benzonitrile (9)

To a solution of tetrahydrothiophene (727 mg, 8.24 mmol) in 50 mL of dry CH_2Cl_2 was added chloroiodomethane (0.6 mL, 8.24 mmol), and the mixture was stirred for 30 min at room tem-

perature under an Ar atmosphere. To the reaction mixture was added **8a** (1.13 g, 4.12 mmol), followed by a solution of Et_2Zn (1.0 M in hexane, 4.12 mL, 4.12 mmol). The reaction mixture was stirred for 6.5 h at the same temperature, quenched with water, and extracted with CH_2Cl_2. The organic layer was washed with brine, dried over $MgSO_4$, and concentrated. The residue was purified by silica gel column chromatography (eluent: *n*-hexane/AcOEt 10:1) to afford 843 mg (71%) of compound **9** as a colorless solid; Colorless cotton (CH_2Cl_2/*n*-hexane); mp 124–125 °C; ^{1}H NMR (270 MHz, $CDCl_3$) δ (ppm) 1.0–3.5 (br m, 10H), 2.46 (dd, J = 2.3 Hz, 4.9 Hz, 1H), 2.64 (dd, J = 3.4 Hz, 4.8 Hz, 1H), 2.88 (dd, J = 2.3 Hz, 3.8 Hz, 1H), 7.31 (dt, J = 0.7 Hz, 7.6 Hz, 1H), 7.43 (ddd, J = 1.2 Hz, 2.1 Hz, 8.1 Hz, 1H), 7.48 (t, J = 1.5 Hz, 1H), 7.52 (ddd, J = 1.3 Hz, 1.5 Hz, 7.6 Hz, 1H); ^{13}C NMR (68 MHz, $CDCl_3$) δ (ppm) 48.1, 52.7, 79.3, 81.3, 112.8, 118.0, 129.4, 130.7, 131.6, 132.2, 137.5; MS (EI) *m/z* 287 (M^+, 100%); Anal. Calcd for $C_{11}H_{17}B_{10}NO$: C, 45.97; H, 5.96; N, 4.87. Found: C, 45.81; H, 5.82; N, 4.80.

4.4.9. 3-[12-(1-Hydroxy-1-methyl)ethyl-1,12-dicarba-*closo*-dodecaboran-1-yl]acetophenone (10)

To a solution of **8b** (150 mg, 0.52 mmol) in 7 mL of dry THF was added CH_3Li (6.71 mL, 6.98 mmol) at −78 °C under an Ar atmosphere. The reaction mixture was stirred for 30 min at the same temperature, quenched with saturated aqueous NH_4Cl solution, and extracted with AcOEt. The organic solution was washed with water and brine, dried over $MgSO_4$, and concentrated. The residue was purified by silica gel column chromatography (eluent: *n*-hexane/AcOEt 20:1) to afford 70 mg (42%) of compound **10** as a colorless solid and 19 mg (14%) of compound **7c** as a colorless solid; Colorless cotton (CH_2Cl_2/*n*-hexane); mp 108.5–109.5 °C; ^{1}H NMR (270 MHz, $CDCl_3$) δ (ppm) 1.0–3.5 (br m, 10H), 2.12 (s, 3H), 7.30 (dd, J = 7.5 Hz, 8.6 Hz, 1H), 7.45 (ddd, J = 1.2 Hz, 2.0 Hz, 8.1 Hz, 1H), 7.50 (t, J = 1.5 Hz, 1H), 7.54 (ddd, J = 1.3 Hz, 1.5 Hz, 7.6 Hz, 1H); ^{13}C NMR (68 MHz, $CDCl_3$) δ (ppm) 26.6, 31.5, 70.7, 82.8, 92.1, 126.7, 128.1, 128.2, 131.4, 136.6, 136.7, 196.9; MS (EI) *m/z* 320 (M^+), 305 (100%); Anal. Calcd for $C_{13}H_{24}B_{10}O_2$: C, 48.73; H, 7.55. Found: C, 48.43; H, 7.68.

4.5. Biological evaluation

4.5.1. Competitive-binding assay with hAR[30]

Binding affinities of test compounds for hAR (human androgen receptor) were measured in competition experiments using [^{3}H]DHT and cytosolic fraction of hAR-LBD (hAR ligand-binding domain)-transformed *Escherichia coli*. hAR-LBD expression plasmid vector encoding GST-hARLBD (627–919 aa, EF domain) fusion protein under the *lac* promoter (provided by Prof. S. Kato, University of Tokyo) was transfected into *E. coli* strain *HB-101*. An overnight culture (10 mL) of the bacteria was added to 1 L of LB medium and incubated at 27 °C until its optical density reached 0.6–0.7 at 600 nm. Following the addition of IPTG to a concentration of 1 mM, incubation was continued for an additional 4.5 h. Cells were harvested by centrifugation at 4000*g* at 4 °C for 15 min and stored at −80 °C until use. All subsequent operations were performed at 4 °C. The bacterial pellet obtained from 40 mL of culture was resuspended in 1 mL of ice-cold TEGDM buffer (10 mM Tris–HCl pH 7.4, 1 mM EDTA, 10% glycerol, 10 mM DTT, 10 mM sodium molybdate). This suspension was subjected to sonication (10 × 10 s bursts) on ice, and crude GST-hARLBD fraction was prepared by centrifugation of the suspension at 12,000*g* for 30 min at 4 °C. This crude receptor fraction was diluted with buffer (20 mM Tris–HCl pH 8.0, 0.3 M KCl, 1 mM EDTA) to a protein concentration of 0.3–0.5 mg/mL and used in binding assays as hAR-LBD fraction. Aliquots of the hAR-LBD fraction were incubated in the dark at 4 °C with [^{3}H]DHT (NEN, 4 nM final concentration), triamcinolone acetonide (1 μM final concentration), and reference or test compounds (dissolved in DMSO). Nonspecific binding was assessed by addition of a 200-fold excess of nonradioactive DHT. After 15 h, a Dextran T-70/γ-globulin-coated-charcoal suspension was added to the ligand/protein mixture (1% Norit A, 0.05% γ-globulin, 0.05% Dextran T-70 final concentration each) and the whole was incubated at 4 °C for 10 min. The charcoal was removed by centrifugation for 5 min at 1300*g*, and the radioactivity of the supernatant was measured in Atomlight (NEN) by using a liquid scintillation counter.

4.5.2. Transcriptional activation assays[31]

Assay of androgenic activity was performed by means of ARE-luciferase reporter assay using NIH3T3 cells. Culture was conducted in phenol red-free DMEM (SIGMA), supplemented with dextran-coated charcoal-stripped FBS (sFBS) to deplete internal stores of steroids, penicillin, and streptomycin for 2–3 days. Transient transfections of NIH3T3 cells were performed using Transfast™ (Promega) according to the manufacturer's protocol. Transfections were done in 48-well plates at 2×10^4 cells/well with 50 ng of pSG5-hAR, 300 ng of p(ARE)$_2$-luc and 10 ng of pRL/CMV (Promega) as an internal standard. Twenty-four hours after addition of the sample (final concentration, 10^{-5}–10^{-7} M) and 1×10^{-10} DHT, cells were harvested with 25 μL of cell lysis buffer (Promega), and the *firefly* and *Renilla* luciferase activities were determined with a Dual Luciferase Asaay Kit (Promega) by measuring luminescence with a Wallac Micro-Beta scintillation counter (Perkin-Elmer Life Sciences). *Firefly* luciferase reporter activity was normalized to *Renilla* luciferase activity from pRL/CMV.

Acknowledgments

This research was supported by a Grant-in-Aid for High Technology Research Program, a Grant-in-Aid for Scientific Research (B) (No. 20390035) from the Ministry of Education, Culture, Sports, Science and Technology, Japan.

Supplementary data

Supplementary data associated with this article can be found, in the online version, at doi:10.1016/j.bmc.2011.04.017.

References and notes

1. Hawthorne, M. F.; Zheng, Z. *Acc. Chem. Res.* **1997**, *30*, 267; Kaszynski, P. *Collect Czech. Chem. Commun.* **1999**, *64*, 895; Valliant, J. F.; Guenther, K. J.; King, A. S.; Morel, P.; Schaffer, P.; Sogbein, O. O.; Stephenson, K. A. *Coord. Chem. Rev.* **2002**, *232*, 173; Lesnikowski, Z. J. *Collect Czech. Chem. Commun.* **2007**, *72*, 1646.
2. Bregradze, V. I. *Chem. Rev.* **1992**, *92*, 209; Fox, M. A.; Hughes, A. K. *Coord. Chem. Rev.* **2004**, *248*, 457.
3. Plešek, J. *Chem. Rev.* **1992**, *92*, 269; Peterson, J. J.; Simon, Y. C.; Coughlin, E. B.; Carter, K. R. *Chem. Commun.* **2009**, 4950; Kokado, K.; Tokoro, Y.; Chujo, Y. *Biomacromolecules* **2009**, *42*, 2925.
4. Soloway, A. H.; Tjarks, W.; Barnum, B. A.; Rong, F.-G.; Barth, R. F.; Codogni, I. M.; Wilson, J. G. *Chem. Rev.* **1998**, *98*, 1515; Hawthorne, M. F.; Maderna, A. *Chem. Rev.* **1999**, *99*, 3421; Crossley, E. L.; Ziolkowski, E. J.; Coderre, J. A.; Rendina, L. M. *Mini-Rev. Med. Chem.* **2007**, *7*, 303; Armstrong, A. F.; Valliant, J. F. *Dalton Trans.* **2007**, 4240; Yamamoto, T.; Nakai, K.; Matsumura, A. *Cancer Lett.* **2008**, *262*, 143.
5. Lesnikowski, Z. J.; Shi, J.; Schinazi, R. F. *J. Organomet. Chem.* **1999**, *581*, 156; Todd, J. A.; Rendina, L. M. *Inorg. Chem.* **2002**, *41*, 3331; Lesnikowski, Z. J. *Eur. J. Org. Chem.* **2003**, 4489; Olejniczak, A. B.; Semenuc, A.; Kwiatkowski, M.; Lesnikowski, Z. J. *J. Organomet. Chem.* **2003**, *680*, 124; Tjarks, W.; Tiwari, R.; Byun, Y.; Narayanasamy, S.; Barth, R. F. *Chem. Commun.* **2007**, 4978.
6. Wyzlic, I. M.; Soloway, A.; A.H. *Tetrahedron Lett.* **1992**, *33*, 7489; Kahl, S. B.; Kasar, R. A. *J. Am. Chem. Soc.* **1996**, *118*, 1223; Naeslund, C.; Ghirmal, S.; Sjoeberg, S. *Tetrahedron* **2005**, *61*, 1181.
7. Thimon, C.; Panza, L.; Morin, C. *Synlett* **2003**, 1399; Morandi, S.; Ristori, S.; Berti, D.; Panza, L.; Becciolini, A.; Martini, G. *Biochim. Biophys. Acta* **2004**, *1664*, 53; Bonechi, C.; Ristori, S.; Martini, S.; Panza, L.; Martini, G.; Rossi, C.; Donati, A. *Biophys. Chem.* **2007**, *125*, 320.
8. Endo, Y.; Iijima, T.; Yamakoshi, Y.; Yamaguchi, M.; Fukasawa, H.; Shudo, K. *J. Med. Chem.* **1999**, *42*, 1501; Iijima, T.; Endo, Y.; Tsuji, M.; Kawachi, E.;

Kagechika, H.; Shudo, K. *Chem. Pharm. Bull.* **1999**, *47*, 398; Ohta, K.; Iijima, T.; Kawachi, E.; Kagechika, H.; Endo, Y. *Bioorg. Med. Chem. Lett.* **2004**, *14*, 5913; Endo, Y.; Yoshimi, T.; Ohta, K.; Suzuki, T.; Ohta, S. *J. Med. Chem.* **2005**, *48*, 3941; Calléja, C.; Messaddeq, N.; Chapellier, B.; Yang, H.; Krezel, W.; Li, M.; Metzger, D.; Mascrez, B.; Ohta, K.; Kagechika, H.; Endo, Y.; Mark, M.; Ghyselinck, N. B.; Chambon, P. *Gene Dev.* **2006**, *20*, 1525; Hirata, M.; Inada, M.; Matsumoto, C.; Takita, M.; Ogawa, T.; Endo, Y.; Miyaura, C. *Biochem. Biophys. Res. Commun.* **2009**, *380*, 218.

9. Endo, Y.; Iijima, T.; Yamakoshi, Y.; Fukasawa, H.; Miyaura, C.; Inada, M.; Kubo, A.; Itai, A. *Chem. Biol.* **2001**, *8*, 341; Endo, Y.; Iijima, T.; Yaguchi, K.; Kawachi, E.; Inoue, N.; Kagechika, H.; Kubo, K.; Itai, A. *Bioorg. Med. Chem. Lett.* **2001**, *11*, 1307; Endo, Y.; Yamamoto, K.; Kagechika, H. *Bioorg. Med. Chem. Lett.* **2003**, *13*, 4089; Johnsamuel, J.; Byun, Y.; Jones, T. P.; Endo, Y.; Tjarks, W. *Bioorg. Med. Chem. Lett.* **2003**, *13*, 3213; Johnsamuel, J.; Byun, Y.; Jones, T. P.; Endo, Y.; Tjarks, W. J. *Organomet. Chem.* **2003**, *680*, 223.
10. Mooradian, A. D.; Morley, J. E.; Korenman, S. G. *Endocr. Rev.* **1987**, *8*, 1; Bagatell, C. J.; Bremner, W. J. *N. Engl. J. Med.* **1996**, *334*, 707; Kaufman, J. M.; Vermeulen, A. *Endocr. Rev.* **2005**, *26*, 833.
11. Evans, R. M. *Science* **1988**, *240*, 889; MacLean, H. E.; Warne, G. L.; Zajac, J. D. *J. Steroid Biochem. Mol. Biol.* **1997**, *62*, 233; McEwan, I. J. *Biochem. Soc. Trans.* **2000**, *28*, 369; Taplin, M.-E. *Expert. Rev. Anticancer Ther.* **2008**, *8*, 1495.
12. Liu, P. Y.; Swerdloff, R. S.; Veldhuis, J. D. *J. Clin. Endocrinol. Metab.* **2004**, *89*, 4789.
13. Debes, J. D.; Tindall, D. J. *Cancer Lett.* **2002**, *187*, 1.
14. Visakorpi, T.; Hyytinen, E.; Koivisto, P.; Tanner, M.; Keinanen, R.; Palmberg, C.; Palotie, A.; Tammela, T.; Isola, J.; Kallioniemi, O.-P. *Nat. Genet.* **1995**, *9*, 401; Taplin, M. E.; Bubley, G. J.; Shuster, T. D.; Frantz, M. E.; Spooner, A. E.; Ogata, G. K.; Keer, H. N.; Balk, S. P. *N. Engl. J. Med.* **1995**, *332*, 1393; Brinkmann, A. O.; Trapman, J. *Nat. Med.* **2000**, *6*, 628; Jemal, A.; Thomas, H.; Murray, T.; Thun, M. *CA Cancer J. Clin.* **2002**, *52*, 23; Mohler, J. L.; Gregory, C. W.; Ford, O. H., III; Kim, D.; Weaver, C. M.; Petrusz, P.; Wilson, E. M.; French, F. S. *Clin. Cancer Res.* **2004**, *10*, 440.
15. Chengalvala, M.; Oh, T.; Roy, A. K. *Expert Opin. Ther. Pat.* **2003**, *13*, 59; Gao, W.; Bohl, C. E.; Dalton, J. T. *Chem. Rev.* **2005**, *105*, 3352; Chen, J.; Kim, J.; Dalton, J. T. *Mol. Invest.* **2005**, *5*, 173.
16. Neri, R. O.; Peets, E. A. *J. Steroid Biochem.* **1975**, *6*, 815; Koch, H. *Drugs Today* **1984**, *20*, 561; Neri, R. *Urology* **1989**, *34*, 19.
17. Wakeling, A. E.; Furr, B. J.; Glen, A. T.; Hughes, L. R. *J. Steroid Biochem.* **1981**, *15*, 355; Yeh, S.; Miyamoto, H.; Chang, C. *Lancet* **1997**, *349*, 852; Bohl, C. E.; Miller, D. D.; Chen, J.; Bell, C. E.; Dalton, J. T. *J. Biol. Chem.* **2005**, *280*, 37747.
18. Tucker, H.; Chesterson, G. J. *J. Med. Chem.* **1988**, *31*, 885; Fradet, Y. *Expert. Rev. Anticancer Ther.* **2004**, *4*, 37; Kolvenbag, G. J.; Blackledge, G. R.; Gotting-Smith, K. *Prostate* **1998**, *34*, 61.
19. Boccardo, F. *Crit. Rev. Oncol. Hematol.* **2000**, *35*, 121; Suzuki, H.; Kamiya, N.; Imamoto, T.; Kawamura, K.; Yano, M.; Takano, M.; Utsumi, T.; Naya, Y.; Ichikawa, T. *Int. J. Clin. Oncol.* **2008**, *13*, 401.
20. Bohl, C. E.; Gao, W.; Miller, D. D.; Bell, C. E.; Dalton, J. T. *Proc. Natl. Acad. Sci. U.S.A.* **2005**, *102*, 6201.
21. Sack, J. S.; Kish, K. F.; Wang, C.; Attar, R. M.; Kiefer, S. E.; An, Y.; Wu, G. Y.; Scheffler, J. E.; Salvati, M. E.; Krystek, S. R., Jr.; Weinmann, R.; Einspahr, H. M. *Proc. Natl. Acad. Sci. U.S.A.* **2001**, *98*, 4904; De Jésus-Tran, K. P.; Côté, P.-L.; Cantin, L.; Blanchet, J.; Labrie, F.; Breton, R. *Protein Sci.* **2006**, *15*, 987.
22. Hashimoto, Y.; Miyachi, H. *Bioorg. Med. Chem.* **2005**, *13*, 5080.
23. Fujii, S.; Goto, T.; Ohta, K.; Hashimoto, Y.; Suzuki, T.; Ohta, S.; Endo, Y. *J. Med. Chem.* **2005**, *48*, 4654.
24. Ohta, K.; Goto, T.; Fujii, S.; Suzuki, T.; Ohta, S.; Endo, Y. *Bioorg. Med. Chem.* **2008**, *16*, 8022.
25. Goto, T.; Ohta, K.; Suzuki, T.; Ohta, S.; Endo, Y. *Bioorg. Med. Chem.* **2005**, *13*, 6414.
26. Fujii, S.; Ohta, K.; Goto, T.; Kagechika, H.; Endo, Y. *Bioorg. Med. Chem.* **2009**, *17*, 344.
27. Fujii, S.; Hashimoto, Y.; Suzuki, T.; Ohta, S.; Endo, Y. *Bioorg. Med. Chem. Lett.* **2005**, *15*, 227.
28. Dess, D. B.; Martin, J. C. *J. Org. Chem.* **1983**, *48*, 4155; Dess, D. B.; Martin, J. C. *J. Am. Chem. Soc.* **1991**, *113*, 7277.
29. Aggarwal, V. K.; Ali, A.; Coogan, M. P. *J. Org. Chem.* **1997**, *62*, 8628; Aggarwal, V. K.; Coogan, M. P.; Stenson, R. A.; Jones, R. V. H.; Fieldhouse, R.; Blacker, J. *Eur. J. Org. Chem.* **2002**, 319.
30. Ishioka, T.; Kubo, A.; Koiso, Y.; Nagasawa, K.; Itai, A.; Hashimoto, Y. *Bioorg. Med. Chem.* **2002**, *10*, 1555.
31. Kitamura, S.; Suzuki, T.; Ohta, S.; Fujimoto, N. *Environ. Health Perspect.* **2003**, *111*, 503.
32. Sheldrick, G. M. SHELXS97. Program for the Solution of Crystal Structures, 1997, University of Göttingen, Germany.
33. Rarey, M.; Kramer, B.; Lengauer, T.; Klebe, G. *J. Mol. Biol.* **1996**, *261*, 470.

MedChemComm

View Online / Journal Homepage / Table of Contents for this issue
Dynamic Article Links

Cite this: *Med. Chem. Commun.*, 2011, **2**, 877

www.rsc.org/medchemcomm

CONCISE ARTICLE

p-Carborane-based androgen antagonists active in LNCaP cells with a mutated androgen receptor†

Shinya Fujii,[a] Ayumi Yamada,[a] Keiko Tomita,[b] Mao Nagano,[b] Tokuhito Goto,[c] Kiminori Ohta,[c] Takashi Harayama,[b] Yasuyuki Endo[c] and Hiroyuki Kagechika*[a]

Received 5th January 2011, Accepted 17th June 2011
DOI: 10.1039/c1md00001b

Published on 21 July 2011 on http://pubs.rsc.org | doi:10.1039/C1MD00001B
Downloaded by TOHOKU YAKKA DAIGAKU on 25 November 2011

Development of antagonists for a mutated androgen receptor (AR) is important for treatment of anti-androgen-refractory prostate cancers. We describe here application of the *p*-carborane cage as a hydrophobic core structure for novel anti-androgens active toward LNCaP human prostate cancer cells with mutated AR. These compounds are expected to be versatile lead compounds not only for development of AR pan-antagonists, but also for discovery of mutant-selective anti-androgens.

The androgen receptor (AR) is a member of the nuclear receptor superfamily of ligand-regulated transcriptional factors,[1] and plays critical roles in numerous physiological processes, such as development and regulation of the male reproductive system, and maintenance of muscle and bone mass.[2] AR is closely related to prostate cancer, and transcriptional activation by AR agonist exacerbates the disease in many cases.[3] Prostate cancer is the most common type of cancer and the second leading cause of cancer deaths in males.[4] Since endogenous androgens, testosterone (**1**) and its more active metabolite 5α-dihydrotestosterone (5α-DHT: **2**, Fig. 1), are involved in aggravation of prostate cancer by activation of AR, synthetic androgen antagonists, so-called anti-androgens, are used in the treatment of prostate cancer. However, anti-androgen therapy often leads to hormone-refractory prostate cancer.[5] In some cases, the androgen antagonists, such as flutamide (**3**) and hydroxyflutamide (**4**), function as agonists toward the hormone-refractory cancer cells, and exacerbate the disease. This is known as anti-androgen withdrawal syndrome, since withdrawal of androgen antagonist results in clinical improvement.[6] Although the mechanism is not fully understood, mutation in AR is thought to be a major cause of hormone-refractory prostate cancer.[7,8] Therefore, development of androgen antagonists effective for mutated AR is required for the therapy of prostate cancer.

Several mutated ARs have been found in the course of anti-androgen therapy of prostate cancer. The T877A mutation is the most common AR mutation observed clinically in prostate cancers.[7] Anti-androgens **3** and **4** act as agonists toward T877A AR. Bicalutamide (**5**), the most widely used anti-androgen, acts as an antagonist for T877A AR, but exhibits significant androgenic activity toward W741L or W741C point-mutated AR; this is known as bicalutamide withdrawal syndrome.[9] Other mutations of AR in prostate cancers are also well-documented, and several mutant ARs, such as T877S, H874Y, V715M, and L701H/T877A, have a broadened spectrum of ligand responsiveness.[10] It is therefore of interest to develop a new generation of anti-androgens that would function as antagonists for mutant ARs.

We previously reported development of potent androgen antagonists by using the carborane cage as a novel hydrophobic core structure.[11,12] Carboranes, more specifically dicarba-*closo*-dodecaboranes, members of the class of carbon-containing boron clusters, have characteristic properties including spherical geometry, remarkable thermal and chemical stability, and a hydrophobic molecular surface.[13] We have reported the development of a range of bioactive molecules, including specific ligands for estrogen receptor[14] and retinoid receptors[15] that contain a carborane cage as a hydrophobic pharmacophore, and we have obtained several promising drug candidates. The most

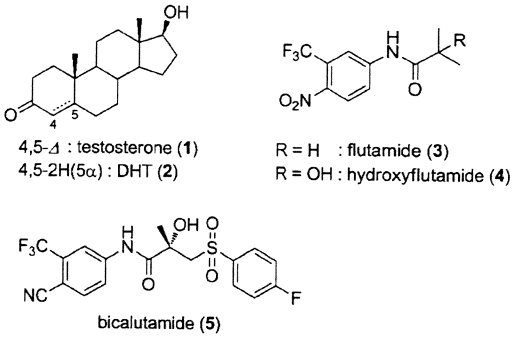


Fig. 1 Structures of endogenous and synthetic AR ligands.

[a]*Graduate School of Biomedical Science, Institute of Biomaterials and Bioengineering, Tokyo Medical and Dental University, 2-3-10, Kanda-Surugadai, Chiyoda-ku, Tokyo, 101-0062, Japan. E-mail: kage.omc@tmd.ac.jp; Fax: +81-3-5280-8127; Tel: +81-3-5280-8032*
[b]*Faculty of Pharmaceutical Sciences at Kagawa Campus, Tokushima Bunri University, 1314-1,Shido, Sanuki, Kagawa, 769-2193, Japan*
[c]*Faculty of Pharmaceutical Sciences, Tohoku Pharmaceutical University, 4-4-1, Komatsushima, Aoba-ku, Sendai, 981-8558, Japan*

† Electronic supplementary information (ESI) available. See DOI: 10.1039/c1md00001b

This journal is © The Royal Society of Chemistry 2011

Published on 21 July 2011 on http://pubs.rsc.org | doi:10.1039/C1MD00001B
Downloaded by TOHOKU YAKKA DAIGAKU on 25 November 2011

potent carborane-containing molecule with androgen antagonist activity so far synthesized is 3-(12-hydroxymethyl-1,12-dicarba-*closo*-dodecaborane-1-yl)benzonitrile (**6**: BA341, Fig. 2),[11] which exhibits remarkable anti-androgenic activity toward androgen-dependent Shionogi carcinoma cells SC-3 bearing wild-type AR.[16] However, compound **6** increased the proliferation of human prostate cancer cell line LNCaP bearing T877A AR, with an EC_{50} value of 6.3×10^{-7} M.

Recently, we have reported novel AR antagonists, such as compound **7**, based on the structural features of both **5** and **6**. These hybrid-type compounds acted as anti-androgens for LNCaP cells.[17] These results suggest that introduction of a bulky substituent near the hydroxyl group of **6** is an effective strategy to develop anti-androgens for mutated ARs. The bulky substituent bound to the carborane core *via* an ether or a thioether linking group is assumed to inhibit proper folding of helix-12 of mutated AR, which is essential to transcriptional activation of nuclear receptors. According to this hypothesis, the rigidity of the linking group and the direction of the substituent would be important determinants of antagonistic potency. The T877A mutation in AR of LNCaP cells is thought to be one of the reasons for the change of **6** from antagonist to agonist. Docking simulation suggested that the T877 residue of wild-type AR interacts with the hydroxyl group of **6**, as it does with the 17-hydroxyl group of **2**.[18] However, considering the antagonist activity of **6**, the interaction of **6** with AR would induce a receptor conformation with slightly different folding of helix12 from that in the active form. In the case of T877A AR, both **2** and **6** will induce essentially the same active conformation of AR, because of the lack of hydrogen bonding with the T877A residue. If this is correct, we anticipated that introduction of a bulky substituent in place of the hydroxyl group would inhibit active folding of the mutated AR and so exert antagonistic activity. On the other hand, the hydroxyl group of **6** would also interact with N705, hence a polar functionality is needed at this position of the ligand structure to form hydrogen-bonding to N705 of both wild-type and T877A ARs. On the basis of these considerations, we designed carboranyl amide compounds **8–11**, which have the required rigidity, hydrogen-bonding hydrophilic moiety and bulky folding-blocker, as candidate compounds with potent anti-androgenic activity toward LNCaP cells (Fig. 3).

Scheme 1 illustrates the synthesis of the designed amide compounds. Compounds with the carboranecarboxamide moiety, **8** and **9**, were synthesized from *p*-carborane (**12**) as a starting material. Ullmann-type coupling using the *C*-copper(I)

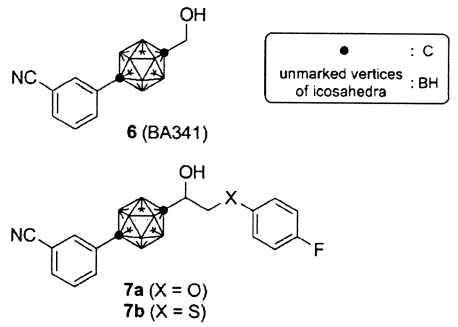


Fig. 2 Structures of carborane derivatives with AR ligand activity.

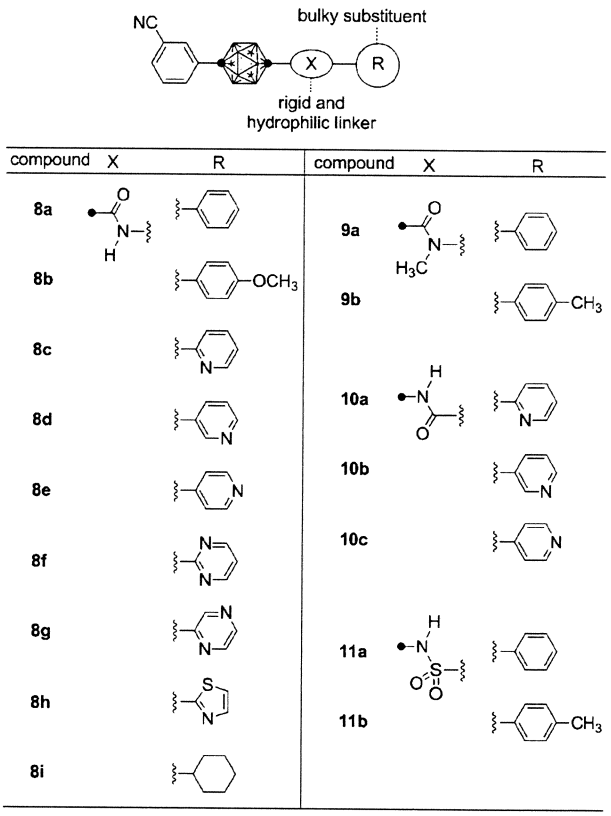
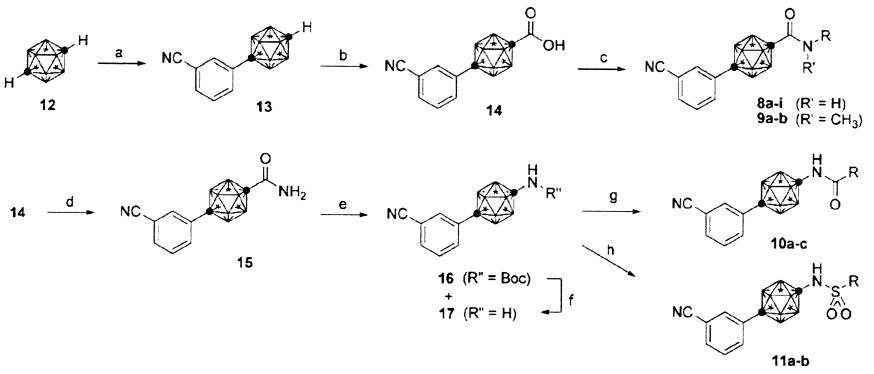


Fig. 3 Structure of designed AR full antagonist candidates toward mutated AR.

derivative of *p*-carborane[19] and 3-iodobenzonitrile gave phenylcarborane **13**. Then a carboxyl moiety was introduced into the contralateral *C*-vertex of the carborane cage of **13** by using LDA and carbon dioxide to afford carboxylic acid **14**. Condensation of **14** and various amines *via* acid chloride using oxalyl chloride gave the desired amide compounds **8a–i** and **9a,b**. Acyl- or sulfonylaminocarborane derivatives **10** and **11** were also synthesized from carboxylic acid **14**. Primary amide **15** was prepared from **14** by amide condensation with ammonium hydroxide. Hofmann rearrangement of **15** using [bis(trifluoroacetoxy)iodo]benzene[20] in *tert*-butyl alcohol gave the *N*-Boc-protected aminocarborane derivative **16** together with the free amine **17** as a minor product. The Boc group of **16** was cleaved with TFA to afford **17**. Amide condensation of **17** with various acyl chlorides or sulfonyl chloride gave the desired molecules **10a–c** and **11a,b**, respectively.

The effects of the synthesized compounds on LNCaP cells were investigated in terms of growth-promoting or inhibitory activity.[17] None of the synthesized compounds promoted cell growth in the absence of any other AR agonist, while some of them inhibited LNCaP cell growth promoted by 1 nM testosterone (Table 1). The anilide **8a** potently inhibited cell growth with a submicromolar IC_{50} value. Heterocyclic amide derivatives also showed LNCaP cell growth-inhibitory activity with similar potency to that of anilide **8a**. Compounds with both electron-deficient heterocycles (pyridine, pyrimidine and pyrazine) and an electron-rich heterocycle (thiazole) exhibited potent activity. Among the synthesized amide compounds, 2-pyridiyl amide **8c** exhibited the most potent anti-androgenic activity toward

This journal is © The Royal Society of Chemistry 2011



Scheme 1 Synthesis of carborane derivatives **8–11**. *Reagents and conditions*: (a) *n*-BuLi, CuCl, pyridine, DME, rt, then 3-iodobenzonitrile, reflux, 75%. (b) LDA, CO_2, −78 °C, 83%. (c) $(COCl)_2$, DMF, CH_2Cl_2, rt, then amine, pyridine, THF, rt. (d) $(COCl)_2$, DMF, CH_2Cl_2, rt, then NH_4OH, THF, rt, quant. (e) $PhI(OCOCF_3)_2$, *tert*-BuOH, 80 °C, 60% (**16**) and 13% (**17**). (f) TFA, CH_2Cl_2, rt, 87%. (g) Acyl chloride, pyridine, rt. (h) Sulfonyl chloride, pyridine, rt.

Downloaded by TOHOKU YAKKA DAIGAKU on 25 November 2011
Published on 21 July 2011 on http://pubs.rsc.org | doi:10.1039/C1MD00001B

LNCaP cells in this assay system. Anti-androgenic activity of cyclohexyl amide **8i** was less potent as compared with aromatic amides, and *N*-methylation of anilide caused loss of inhibitory activity toward LNCaP cell proliferation (compounds **9a** and **9b**). These results suggested that a secondary *N*-heteroaromatic carboranecarboxamide structure is promising for anti-androgenic activity toward LNCaP cells. Compounds **10a–c** bearing an acylaminocarborane moiety, *i.e.* retro-amide derivatives of compound **8**, also exhibited anti-androgenic activity. Alteration of direction of the amide structure did not result in a significant change of anti-androgenic activity toward LNCaP cells. It was interesting that sulfonamides **11a** and **11b** exhibited no inhibitory activity toward LNCaP cell proliferation, whereas the benzenesulfonyl group is an important fragment of **5**. This result can be partly explained by conformational differences. Secondary carboxamide compounds usually take linear *trans* conformation, whereas benzenesulfonamides take a bent *gauche*-like structure. *N*-Methylation of anilide also causes a structural change to folded *cis* conformation.[21] These considerations suggest that linear secondary amide structure is important for novel carborane-based anti-androgens to exert anti-androgenic activity toward LNCaP cells.

The effects of these compounds, which have potent anti-androgenic activity toward LNCaP cells, on wild-type AR were also evaluated in terms of growth-promoting or inhibitory activity toward androgen-dependent SC-3 cells and binding affinity to wild-type human AR ligand-binding domain (hAR-LBD).[22] None of the tested compounds exhibited SC-3 cell growth-promoting activity. Table 2 summarizes the results of SC-3 cell growth-inhibitory activity and competitive binding assay to hAR-LBD. *N*-Heterocyclic amides (**8c–h**) showed SC-3 cell proliferation-inhibitory activity with a submicromolar IC_{50} value, and therefore these compounds were also anti-androgens for androgen-dependent SC-3 cells with wild-type AR. Among the tested compounds, 2-pyrimidinyl amide **8f** and 2-thiazolyl amide **8h** exhibited the most potent antagonistic activity toward SC-3 cells, and their potencies were comparable to that of the lead compound **6**. The high binding affinity of **8f** and **8h** to hAR-LBD is consistent with these remarkable androgen-antagonistic activities. Compound **8c**, the most potent anti-androgen for LNCaP cells, also exhibited considerable inhibitory potency toward DHT-promoted SC-3 cell growth. This result suggests that these *N*-heterocyclic carboranecarboxamides are full antagonists for both wild-type and T877A-mutated AR. Development of AR pan-antagonists which

Table 1 IC_{50} values of carborane derivatives for LNCaP cell proliferation

Compound	IC_{50}[a]/M	Compound	IC_{50}[a]/M
8a	2.0×10^{-7}	**9a**	$>10^{-6}$
8b	5.7×10^{-7}	**9b**	$>10^{-6}$
8c	9.4×10^{-8}	**10a**	3.5×10^{-7}
8d	3.0×10^{-7}	**10b**	3.0×10^{-7}
8e	3.2×10^{-7}	**10c**	1.1×10^{-7}
8f	1.6×10^{-7}	**11a**	$>10^{-6}$
8g	1.2×10^{-7}	**11b**	$>10^{-6}$
8h	1.4×10^{-7}	**5**	5.7×10^{-7}
8i	5.9×10^{-7}	**6**	Agonist[b]

[a] LNCaP cells were incubated with test compounds in the presence of testosterone (1 nM) for 5 days. All assays were performed in triplicate ($n = 3$). [b] Compound **6** promoted LNCaP cell proliferation with an EC_{50} value of 6.3×10^{-7} M (see text).

Table 2 IC_{50} Values for SC-3 cell proliferation and binding affinity to hAR

Compound	SC-3 proliferation IC_{50}[a]/M	Inhibition of [^{3}H]DHT binding to hAR[b]
8c	4.1×10^{-7}	23
8d	2.9×10^{-7}	37
8e	3.6×10^{-7}	56
8f	3.3×10^{-8}	73
8g	2.9×10^{-7}	14
8h	2.6×10^{-8}	77
10a	1.6×10^{-7}	42
10b	1.4×10^{-7}	18
10c	$>10^{-6}$	*NB*[c]
6	1.5×10^{-8}	95

[a] SC-3 cells were incubated with test compounds in the presence of testosterone (1 nM) for 3 days. All assays were performed in triplicate ($n = 3$). [b] Values are percentage displacement of [^{3}H]DHT (4 nM) specific binding to hAR-LBD by each compound at 10 μM. [c] Significant binding was not observed at the concentration of 10 μM.

act as full antagonists for wild-type and any mutated AR is highly desirable for overcoming hormone-refractory prostate cancers, and these compounds should be versatile leads for such AR pan-antagonists. Regarding the acylaminocarborane derivatives, interestingly, isonicotinamide **10c** did not exhibit significant SC-3 cell growth-inhibitory potency or binding affinity toward hAR-LBD. In the structure–anti-androgen activity relationship study for LNCaP cells, the direction of the amide structure was not critical for the activity, and both **10c** and its retro-amide derivative **8e** exhibited considerable anti-androgenic activity toward LNCaP cells. These results suggest that differences in the direction and substituent of the amide moiety are critical for receptor affinity and antagonistic activity toward wild-type AR, but are not important for anti-androgenic activity toward LNCaP cells. Therefore, it may be possible to discover selective antagonists for mutated AR by focusing on the differences in structure–activity relationships between wild-type AR and mutated AR. Mutant-selective AR modulators would have potential for various medicinal applications, and compound **10c** is a potential lead compound for development of mutant-selective androgen receptor modulators.

In conclusion, we have developed novel anti-androgens active toward LNCaP cells, based on a carboranyl amide structure that is expected to inhibit the concise folding of helix-12. *N*-Heterocyclic amide **8c–h** exhibited potent anti-androgenic activity toward both LNCaP cells with T877A-mutated AR and SC-3 cells with wild-type AR, whereas isonicotinamide **10c** exhibited anti-androgenic activity toward only LNCaP cells. These compounds are expected to be versatile lead compounds not only for development of AR pan-antagonists, but also for discovery of mutant selective anti-androgens.

References

1 (*a*) R. M. Evans, *Science*, 1988, **240**, 889–894; (*b*) H. E. MacLean, G. L. Warne and J. D. Zajac, *J. Steroid Biochem. Mol. Biol.*, 1997, **62**, 233–242; (*c*) I. J. McEwan, *Biochem. Soc. Trans.*, 2000, **28**, 369–373; (*d*) M. E. Taplin, *Expert Rev. Anti-Infect. Ther.*, 2008, **8**, 1495–1508.

2 (*a*) A. D. Mooradian, J. E. Morley and S. G. Korenman, *Endocr. Rev.*, 1987, **8**, 1–28; (*b*) C. J. Bagatell and W. J. Bremner, *N. Engl. J. Med.*, 1996, **334**, 707–714; (*c*) J. M. Kaufman and A. Vermeulen, *Endocr. Rev.*, 2005, **26**, 833–876.

3 R. K. Ross, M. C. Pike, G. A. Coetzee, J. K. Reichardt, M. C. Yu, H. Feigelson, F. Z. Stanczyk, L. N. Kolonel and B. E. Henderson, *Cancer Res.*, 1998, **58**, 4497–4504.

4 (*a*) J. L. Mohler, C. W. Gregory, O. H. Ford, III, D. Kim, C. M. Weaver, P. Petrusz, E. M. Wilson and F. S. French, *Clin. Cancer Res.*, 2004, **10**, 440–448; (*b*) A. Jemal, H. Thomas, T. Murray and M. Thun, *Ca-Cancer J. Clin.*, 2002, **52**, 23–47; (*c*) T. Visakorpi, E. Hyytinen, P. Koivisto, M. Tanner, R. Keinanen, C. Palmberg, A. Palotie, T. Tammela, J. Isola and O. P. Kallioniemi, *Nat. Genet.*, 1995, **9**, 401–406; (*d*) M. E. Taplin, G. J. Bubley, T. D. Shuster, M. E. Frantz, A. E. Spooner, G. K. Ogata, H. N. Keer and S. P. Balk, *N. Engl. J. Med.*, 1995, **332**, 1393–1398.

5 H. I. Scher, G. Steineck and W. K. Kelly, *Urology*, 1995, **46**, 142–148.

6 (*a*) H. Suzuki, K. Akakura, A. Komiya, S. Aida, S. Akimoto and J. Shimazaki, *Prostate (N. Y., NY, U. S.)*, 1996, **29**, 153–158; (*b*) M. E. Taplin, B. Rajeshkumar, S. Halabi, C. P. Werner, B. A. Woda, J. Picus, W. Stadler, D. F. Hayes, P. W. Kantoff, N. J. Vogelzang and E. J. Small, *J. Clin. Oncol.*, 2003, **21**, 2673–2678; (*c*) H. Miyamoto, M. M. Rahman and C. Chang, *J. Cell. Biochem.*, 2003, **91**, 3–12.

7 (*a*) J. Veldscholte, C. A. Berrevoets, A. O. Brinkmann, J. A. Grootegoed and E. Mulder, *Biochemistry*, 1992, **31**, 2393–2399; (*b*) J. Zhou, B. Liu, G. Geng and J. H. Wu, *Proteins: Struct., Funct., Bioinf.*, 2010, **78**, 623–637.

8 (*a*) M. A. Fenton, T. D. Shuster, A. M. Fertig, M. E. Taplin, G. Kolvenbag, G. J. Bubley and S. P. Balk, *Clin. Cancer Res.*, 1997, **3**, 1383–1388; (*b*) X. Y. Zhao, P. J. Malloy, A. V. Krishnan, S. Swami, N. M. Navone, D. M. Peehl and D. Feldman, *Nat. Med. (N. Y.)*, 2000, **6**, 703–706.

9 (*a*) T. Hara, J. Miyazaki, H. Araki, M. Yamaoka, N. Kanzaki, M. Kusaka and M. Miyamoto, *Cancer Res.*, 2003, **63**, 149–153; (*b*) T. Yoshida, H. Kinoshita, T. Segawa, E. Nakamura, T. Inoue, Y. Shimizu, T. Kamoto and T. Ogawa, *Cancer Res.*, 2005, **65**, 9611–9616.

10 (*a*) Z. Culig, A. Hobisch, M. V. Cronauer, A. C. B. Cato, A. Hittmair, C. Radmayr, J. Eberle, G. Bartsch and H. Klocker, *Mol. Endocrinol.*, 1993, **7**, 1541–1550; (*b*) M. Marcelli, M. Ittmann, S. Mariani, R. Sutherland, R. Nigam, L. Murthy, Y. Zhao, D. DiConcini, E. Puxeddu, A. Esen, J. Eastham, N. L. Weigel and D. J. Lamb, *Cancer Res.*, 2000, **90**, 944–949.

11 S. Fujii, T. Goto, K. Ohta, Y. Hashimoto, T. Suzuki, S. Ohta and Y. Endo, *J. Med. Chem.*, 2005, **48**, 4654–4662.

12 (*a*) S. Fujii, Y. Hashimoto, T. Suzuki, S. Ohta and Y. Endo, *Bioorg. Med. Chem. Lett.*, 2005, **15**, 227–230; (*b*) T. Goto, K. Ohta, T. Suzuki, S. Ohta and Y. Endo, *Bioorg. Med. Chem.*, 2005, **13**, 6414–6424; (*c*) K. Ohta, T. Goto, S. Fujii, T. Suzuki, S. Ohta and Y. Endo, *Bioorg. Med. Chem.*, 2008, **16**, 8022–8028; (*d*) S. Fujii, K. Ohta, T. Goto, H. Kagechika and Y. Endo, *Bioorg. Med. Chem.*, 2009, **17**, 344–350.

13 (*a*) V. I. Bregadze, *Chem. Rev.*, 1992, **92**, 209–223; (*b*) M. F. Hawthorne, *Angew. Chem., Int. Ed. Engl.*, 1993, **32**, 950–984; (*c*) A. H. Soloway, W. Tjarks and J. G. Barnum, *Chem. Rev.*, 1998, **98**, 1515–1562.

14 (*a*) Y. Endo, T. Iijima, Y. Yamakoshi, M. Yamaguchi, H. Fukasawa and K. Shudo, *J. Med. Chem.*, 1999, **42**, 1501–1504; (*b*) Y. Endo, T. Iijima, Y. Yamakoshi, H. Fukasawa, C. Miyaura, M. Inada, A. Kubo and A. Itai, *Chem. Biol.*, 2001, **8**, 341–355; (*c*) Y. Endo, T. Yoshimi, K. Ohta, T. Suzuki and S. Ohta, *J. Med. Chem.*, 2005, **48**, 3941–3944; (*d*) M. Hirata, M. Inada, C. Matsumoto, M. Takita, T. Ogawa, Y. Endo and C. Miyaura, *Biochem. Biophys. Res. Commun.*, 2009, **380**, 218–222; (*e*) K. Ohta, T. Ogawa, T. Suzuki, S. Ohta and Y. Endo, *Bioorg. Med. Chem.*, 2009, **17**, 7958–7963.

15 For retinoic acid receptor ligands: (*a*) T. Iijima, Y. Endo, M. Tsuji, E. Kawachi, H. Kagechika and K. Shudo, *Chem. Pharm. Bull.*, 1999, **47**, 398–404; (*b*) Y. Endo, K. Yaguchi, E. Kawachi and H. Kagechika, *Bioorg. Med. Chem. Lett.*, 2000, **10**, 1733–1736; (*c*) Y. Endo, T. Iijima, K. Yaguchi, E. Kawachi, N. Inoue, H. Kagechika, A. Kubo and A. Itai, *Bioorg. Med. Chem. Lett.*, 2001, **11**, 1307–1311, For retinoid X receptor ligands: K. Ohta, T. Iijima, E. Kawachi, H. Kagechika and Y. Endo, *Bioorg. Med. Chem. Lett.*, 2004, **14**, 5913–5918.

16 D. Hiraoka, N. Nakamura, Y. Nishizawa, N. Uchida, S. Noguchi, K. Matsumoto and B. Sato, *Cancer Res.*, 1987, **47**, 6560–6564.

17 T. Goto, K. Ohta, S. Fujii, S. Ohta and Y. Endo, *J. Med. Chem.*, 2010, **53**, 4917–4926.

18 K. Ohta, T. Goto, S. Fujii, M. Kawahata, A. Oda, S. Ohta, K. Yamaguchi, S. Hirono and Y. Endo, *Bioorg. Med. Chem.*, 2011, **19**, 3540–3548.

19 R. Coult, M. A. Fox, W. R. Gill, P. L. Herbertson, J. A. H. MacBride and K. Wade, *J. Organomet. Chem.*, 1993, **462**, 19–29.

20 A. S. Radhakrishna, M. E. Parham, R. M. Riggs and G. M. Loudon, *J. Org. Chem.*, 1979, **44**, 1746–1747.

21 (*a*) A. Itai, Y. Toriumi, N. Tomioka, H. Kagechika, I. Azumaya and K. Shudo, *Tetrahedron Lett.*, 1989, **30**, 6177–6180; (*b*) H. Kagechika, E. Kawachi, Y. Hashimoto, K. Shudo and T. Himi, *J. Med. Chem.*, 1988, **31**, 2182–2192.

22 T. Ishioka, T. A. Kubo, Y. Koiso, K. Nagasawa, A. Itai and Y. Hashimoto, *Bioorg. Med. Chem.*, 2002, **10**, 1555–1566.

Published on 21 July 2011 on http://pubs.rsc.org | doi:10.1039/C1MD00001B
Downloaded by TOHOKU YAKKA DAIGAKU on 25 November 2011

This journal is © The Royal Society of Chemistry 2011

Behavioural Brain Research 224 (2011) 159–165

Contents lists available at ScienceDirect

Behavioural Brain Research

journal homepage: www.elsevier.com/locate/bbr

Research report

p-Hydroxyamphetamine causes prepulse inhibition disruption in mice: Contribution of serotonin neurotransmission

Hiroshi Onogi[a,b], Osamu Nakagawasai[a,*], Atsushi Sato[a], Satoru Mitazaki[c], Kota Nakaya[a], Kenya Watanabe[a], Fukie Niijima-Yaoita[a], Koichi Tan-No[a], Yuichiro Arai[d], Tsuneaki Kikuchi[b], Takeshi Tadano[a]

[a] Department of Pharmacology, Tohoku Pharmaceutical University, 4-4-1 Komatsushima, Aoba-ku, Sendai 981-8558, Japan
[b] Faculty of health science, Tohoku Fukushi University, 1-8-1 Kunimi, Aoba-ku, Sendai 981-8522, Japan
[c] Laboratory of Forensic Toxicology, Faculty of Pharmacy, Takasaki University of Health and Welfare, 60 Nakaorui-machi, Takasaki 370-0033, Japan
[d] Tokyo Ariake University of Medical and Health Sciences, Tokyo 135-0063, Japan

ARTICLE INFO

Article history:
Received 15 October 2010
Received in revised form 28 May 2011
Accepted 2 June 2011

Key words:
p-Hydroxyamphetamine
Prepulse inhibition
Serotonin

ABSTRACT

p-Hydroxyamphetamine (p-OHA) has been shown to have a number of pharmacological actions, including causing abnormal behaviors such as increased locomotor activity and head-twitch response in rodents. We have recently reported that intracerebroventricular (i.c.v.) administration of p-OHA dose-dependently induces prepulse inhibition (PPI) disruption in mice, which is attenuated by pretreatment with haloperidol, clozapine or several dopaminergic agents. Haloperidol and clozapine have affinities for serotonergic (especially 5-HT_{2A}) receptors. To investigate the involvement of the central serotonergic systems in p-OHA-induced PPI disruption, herein we tested several serotonergic agents to determine their effects on p-OHA-induced PPI disruption. p-OHA-induced PPI disruption was attenuated by pretreatment with 5,7-dihydroxytryptamine (5,7-DHT, a neurotoxin which targets serotonin-containing neurons) and p-chlorophenylalanine (PCPA, a serotonin synthesis inhibitor). p-OHA-induced PPI disruption was also attenuated by pretreatment with ketanserin (a 5-$HT_{2A/2C}$ receptor antagonist) and MDL100,907 (a selective 5-HT_{2A} receptor antagonist). These data suggest that p-OHA-induced PPI disruption may involve increased serotonin release into the synaptic cleft, which then interacts with the post-synaptic 5-HT_{2A} receptor.

© 2011 Elsevier B.V. All rights reserved.

1. Introduction

p-Hydroxyamphetamine (p-OHA), an amphetamine (AMPH) and methamphetamine (METH) metabolite, has been shown to have a number of pharmacological actions, including causing psychostimulant-induced behaviors such as those induced by drugs of abuse [3,8,17,36]. For example, we have recently reported that intracerebroventricular (i.c.v.) administration of p-OHA induces hyperlocomotion and prepulse inhibition (PPI) disruption in mice, the hyperlocomotion is inhibited by pretreatment with a dopamine (DA)-reuptake inhibitor [30], and the PPI disruption is attenuated by pretreatment with haloperidol, clozapine, L-741,626 (a selective D_2 receptor antagonist), L-745,870 (a selective D_4 receptor antagonist) or 6-hydroxydopamine (a neurotoxin which targets DA-containing neurons) (Table 1, [31]). PPI of the acoustic startle response (ASR) is a form of sensorimotor gating, defined as an inhibition of the startle reflex that occurs when the startling stimulus is preceded by a weak prestimulus [12]. Schizophrenia patients exhibit impairment in PPI of the ASR, which is commonly interpreted as a sensorimotor gating deficit [40]. PPI is also diminished in rodents treated with psychotomimetic drugs such as AMPH, METH and phencyclidine [2,22,23]. PPI has been suggested to be a relevant model for studying the pathophysiology of schizophrenia [12]. Our reports indicate that the central dopaminergic system may be involved in abnormal behaviors induced by p-OHA [30,31]. However, p-OHA has been assumed to induce the release of neurotransmitters from presynaptic monoaminergic neurons. Indeed, previous reports have shown that the release of DA and serotonin (5-HT) can be induced by p-OHA [17,27]. We have previously reported that i.c.v. administration of p-OHA induces a head-twitch response (HTR) in mice, a possible model of hallucination [41]. HTR is markedly reduced by pretreatment with a

Abbreviations: AMPH, amphetamine; ANOVA, analysis of variance; ASR, acoustic startle response; DA, dopamine; 5,7-DHT, 5,7-dihydroxytryptamine; DRN, dorsal raphe nucleus; 5-HT, 5-hydroxytryptamine; HTR, head-twitch response; i.c.v., intracerebroventricular; METH, metamphetamine; MRN, median raphe nucleus; NA, noradrenaline; PCPAp-, chlorophenylalanine; p-OHA, p-hydroxyamphetamine; PPI, prepulse inhibition; SEM, standard errors of the mean; SERT, serotonin transporter.

* Corresponding author. Tel.: +81 22 727 0123; fax: +81 22 727 0123.
E-mail address: osamun@tohoku-pharm.ac.jp (O. Nakagawasai).

0166-4328/$ – see front matter © 2011 Elsevier B.V. All rights reserved.
doi:10.1016/j.bbr.2011.06.002

Table 1
Effects of antipsychotics and dopaminergic agents on *p*-hydroxyamphetamine (*p*-OHA)-induced prepulse inhibition (PPI) disruption [31].

Drug	Classification	Attenuate/ineffective
Haloperidol	A typical antipsychotic	Attenuate
Clozapine	An atypical antipsychotic	Attenuate
SCH 23390	A selective D_1 antagonist	Ineffective
L-741,626	A selective D_2 antagonist	Attenuate
Eticlopride	A D_2/D_3 antagonist	Ineffective
L-745,870	A selective D_4 antagonist	Attenuate
6-Hydroxydopamine	A neurotoxin for DA neurons	Attenuate
GBR 12909	A DA-reuptake inhibitor	Ineffective

Pretreatment with haloperidol, clozapine, SCH 23390, L-741,626, eticlopride, L-745,870, GBR 12909 or their solvents as vehicle was performed by intraperitoneal (i.p.) or subcutaneous (s.c.) administration 30 min before intracerebroventricular (i.c.v.) administration of *p*-OHA (80 μg/mouse) or Ringer's solution. Pretreatment with 6-hydroxydopamine (40 μg/mouse) or vehicle was performed by i.c.v. administration 7 days before i.c.v. administration of *p*-OHA or Ringer's solution; i.c.v. administration of *p*-OHA or Ringer's solution was performed 25 min before the start of PPI testing.

5-HT synthesis inhibitor such as *p*-chlorophenylalanine (PCPA) or pretreatment with 5-HT receptor antagonists such as cyproheptadine and dimethothiazine, indicating the involvement of the central serotonergic system [41].

Thus, to investigate the involvement of the central serotonergic system in *p*-OHA-induced PPI disruption, we investigated the effects of several serotonergic agents on PPI disruption. First, we used presynaptic serotonergic agents i.e., 5,7-dihydroxytriptamine (5,7-DHT, a neurotoxin which targets 5-HT-containing neurons) or PCPA (a 5-HT synthesis inhibitor) on *p*-OHA-induced PPI disruption. Both these agents were shown to reduce 5-HT levels [15,26,38]. If increased 5-HT levels from presynaptic 5-HT nerve terminals are involved in *p*-OHA-induced PPI disruption, then 5,7-DHT or PCPA treatment is expected to attenuate PPI disruption. Next, we tested the effects of ketanserin or MDL100,907, for the purpose of inhibiting the 5-HT_{2A} receptor, which, along with the D_2 receptor, is one of the main targets of antipsychotics.

2. Materials and methods

All experiments were performed with the approval of the Ethics Committee of Animal Experiments in Tohoku Pharmaceutical University and according to the National Institutes of Health Guide for the Care and Use of Laboratory Animals. Efforts were made to minimize suffering and to reduce the number of animals used.

2.1. Animals

Male ddY strain mice (weighing 28–34 g, Japan SLC, Japan) were used for all experiments. Approximately 5–7 mice were housed in cages with free access to food and water under conditions of constant temperature (22 ± 2 °C) and humidity (55 ± 5%), on a 12 h light–dark cycle (lights on: 07:00 to 19:00).

2.2. Drugs and treatments

The following drugs were used: the racemic form of *p*-OHA hydrobromide (Smith-Kline and French, USA), 5,7-DHT, PCPA, ketanserin tartrate salt (Sigma–Aldrich, USA) and MDL100,907 (ABX Advanced Biochemical Compounds, Germany). *p*-OHA was dissolved in Ringer's solution. 5,7-DHT was dissolved in Ringer's solution containing 0.1% ascorbic acid. PCPA and MDL100,907 were dissolved in 0.5% Tween 80 and ketanserin was dissolved in 0.9% saline. For all solutions, pH was adjusted to 7.4 at 37 °C. Doses of all drugs were based on previous studies [4,9,26,31,35,38].

The technique employed herein for i.c.v. injection into mice was the same as that originally described by Brittain and Handley [7]. Briefly, i.c.v. administration of *p*-OHA, 5,7-DHT or Ringer's solution was performed with a disposable 27-G needle attached to a 50 μL Hamilton microsyringe and inserted into the left lateral ventricle of unanesthetized mice. *p*-OHA, 5,7-DHT or Ringer's solution was administered in a total volume of 5 μL at a constant rate of 1 μL/2 s. Administration (i.c.v.) of *p*-OHA or Ringer's solution was performed 25 min before the start of PPI testing. Pretreatment with ketanserin, MDL100,907 or their solvents as vehicle was performed by intraperitoneal (i.p.) administration 30 min before i.c.v. administration of *p*-OHA or Ringer's solution. Pretreatment with PCPA or 0.5% Tween 80 as vehicle was performed by i.p. administration 12 h before i.c.v. administration of *p*-OHA or Ringer's solution (Fig. 1). After the experimental period, brains were removed, snap-frozen, and cut into 20 μm coronal sections using a Cryostat HM560 M (Carl Zeiss, Germany). Accuracy of all i.c.v. injection sites were visually confirmed by examining cresyl violet-stained coronal sections.

2.3. 5,7-DHT lesion

The 5,7-DHT lesioning technique is based on a previous report [38] with minor modifications. Briefly, 20 min prior to 5,7-DHT injection, mice were administered desipramine (25 mg/kg, i.p.) to protect noradrenaline (NA)-containing neurons. 5,7-DHT (50 μg/mouse) or vehicle was injected into the left lateral ventricle of unanesthetized mice. Seven days after i.c.v. administration of 5,7-DHT or vehicle, *p*-OHA or Ringer's solution was administered i.c.v. 25 min before the start of PPI testing (Fig. 1).

2.4. Quantitative autoradiography

To confirm the 5,7-DHT lesion effect, two cohorts of mice were used for autoradiographic labeling of the serotonin transporter (SERT), which is located on serotonergic terminals. After the behavioral experiments, the vehicle (i.c.v.) + Ringer's (i.c.v.) group and 5,7-DHT (i.c.v.) + Ringer's (i.c.v.) group were sacrificed by decapitation. Brains were quickly removed, frozen in isopentane at −40 °C and then stored at −80 °C. Using a Cryostat, 20 μm coronal sections including both the dorsal raphe nucleus (DRN) and median raphe nucleus (MRN) were obtained on gelatin-coated slides and stored at −80 °C until use. SERT binding sites were visualized using [^{3}H]-citalopram (79.0 Ci/mmol) (PerkinElmer Life and Analytical Sciences, USA). The protocol was adapted from previous studies [20] with minor modifications. Briefly, the slides were warmed to room temperature for an hour and preincubated in 50 mM Tris–HCl buffer (NaCl 120 mM, $CaCl_2$ 4 mM, pH 7.4) at room temperature for 15 min. The slides were then incubated in an assay buffer containing 2 nM [^{3}H]-citalopram in the same buffer for 60 min at room temperature to determine total binding. Non-specific binding was determined by incubation of 10 μM fluoxetine (TOCRIS, USA) in the assay buffer, which already contained 2 nM [^{3}H]-citalopram. At the end of incubation, sections were rinsed four times, 2 min each in ice-cold buffer as described above, then dipped in deionized water to remove salts and rapidly dried. All slides were exposed to a tritium sensitive imaging plate (Fuji Film, Japan) together with [^{3}H] microscale standards (GE Healthcare UK Ltd., UK) for 10 days to determine [^{3}H]-citalopram binding. Specific labeling was quantified (nGi/mg wet weight) using a computer-assisted Image Reader BAS 5000 ver. 1. 12 (Fuji Film).

2.5. PPI of the acoustic startle response

Tests were conducted using the SR-LAB system (SR-LAB, San Diego Instruments, USA) that comprised two sound-attenuating chambers each equipped with a cylindrical Plexiglas animal enclosure (length: 6.7 cm; inner diameter: 3.8 cm). Ventilation was provided by a small electric fan that also generated a 70 dB background noise. Tone pulses were presented by a speaker positioned 24 cm directly above the animal enclosure. A piezoelectric accelerometer affixed to the animal enclosure frame was used to detect and transduce motion resulting from the animal's response. Tone pulse parameters were controlled by a computer using a commercial software package (SR-LAB) and interface assembly that also digitized, rectified and recorded stabilimeter readings.

Measures of both ASR and PPI were obtained in a single session as described by Nakagawasai et al. [29]. Twenty-five minutes after i.c.v. administration of *p*-OHA or Ringer's solution, animals were placed in the Plexiglas enclosure and allowed to acclimatize to the environment for 5 min before being tested during 42 discrete trials. On the first two trials, the magnitude of the ASR to a 120 dB tone lasting 50 ms was measured. These first two startle tones were presented in order to habituate the animals to the testing procedure. Therefore, the ASR magnitude of these two trials was omitted from the statistical analysis of the mean ASR amplitude. On the subsequent 40 trials, the startle tone was either presented alone or 100 ms after presentation of 30 ms duration prepulse. Prepulse intensity ranged from 3 to 15 dB above background noise and was varied randomly between trials in 3 dB steps. Measures were taken at each of the five prepulse intensities during five trials; animals were randomly presented with the startle tone alone during another ten trials; null trials (background tone alone) during the other five trials. The same stimulus condition was never presented on more than two consecutive trials. The interval between each trial was programmed to a variable time schedule with an average duration of 15 s (range 5–30 s). A measure of startle response amplitude was derived from the mean of 100 digitized data points collected from stimulus onset at a rate of 1 kHz. Prepulse effectiveness in suppressing the startle response was expressed as a percentage based on the mean amplitude of responses to the startle tone alone (10 startle tones) relative to those recorded under the five prepulse conditions (5 startle tones/condition): PPI = 100 − [(mean startle amplitude for prepulse + pulse trials/mean startle amplitude for pulse-alone trials) × 100]%. PPI data also expressed as average across all prepulse intensities (average PPI).

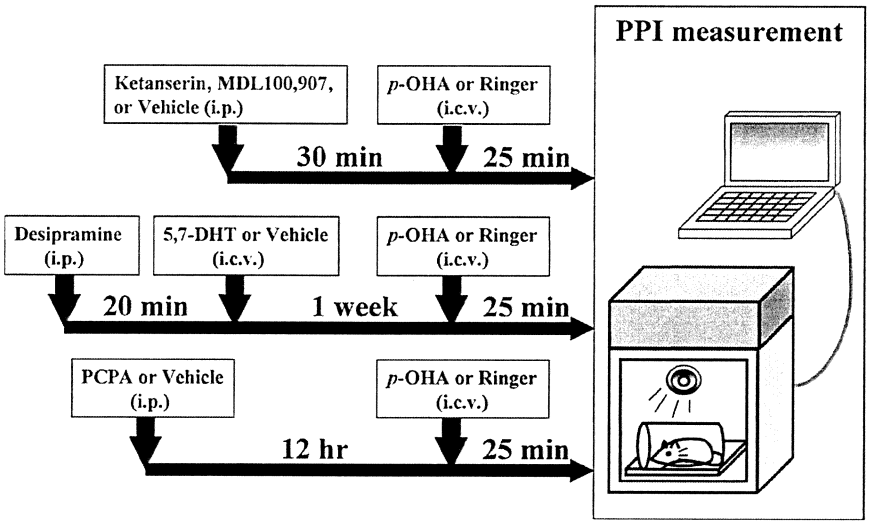


Fig. 1. Time course of drug treatments. *p*-OHA: *p*-hydroxyamphetamine; 5,7-DHT: 5,7-dihydroxytriptamine; PCPA: *p*-chlorophenylalanine; i.p.: intraperitoneal administration; i.c.v.: intracerebroventricular administration; PPI: prepulse inhibition.

2.6. Statistical analyses

Results are expressed as mean ± standard errors of the mean (SEM). A one-way analysis of variance (ANOVA) was used to assess the treatment effects on the magnitude of the ASR and average PPI. The SERT binding data was analyzed by one-way factorial ANOVA with the treatment effect as independent factor and within-subjects ANOVA with the brain region as a within-subject factor. The PPI data were analyzed by two-way repeated measures ANOVA with the treatment as independent factor and prepulse intensity as repeated measures. A post hoc Fisher's PLSD test was conducted when appropriate. The criterion of significance was set at $p < 0.05$.

3. Results

3.1. Effects of serotonergic agents and/or p-OHA on the startle amplitude

There was no significant difference in the startle amplitude between all treatment groups (Table 2).

3.2. Effects of 5,7-DHT lesion on SERT binding and p-OHA-induced PPI disruption

Fig. 2 shows quantitative autoradiography of [^{3}H]-citalopram binding sites in the DRN and MRN of the Ringer- or 5,7-DHT-treated group. A one-way factorial ANOVA of [^{3}H]-citalopram binding sites revealed a significant effect of treatment [$F_{(1,36)} = 21.309$, $p < 0.0001$], but a within-subjects ANOVA revealed no significant difference between brain regions (Fig. 2D). The post hoc test revealed significantly lower [^{3}H]-citalopram binding in the DRN and MRN of 5,7-DHT-treated mice compared with those of Ringer-treated mice (Fig. 2D). Fig. 3 shows the effects of 5,7-DHT (50 μg/mouse, i.c.v.) on *p*-OHA-induced PPI disruption (Fig. 3A and B). A two-way repeated-measures ANOVA of PPI revealed significant effects of treatment [$F_{(3,36)} = 12.313$, $p < 0.0001$] and prepulse intensity [$F_{(4,\ 44)} = 24.466$, $p < 0.0001$], but not their interaction (Fig. 3A). A one-way factorial ANOVA of average PPI revealed a significant effect of treatment [$F_{(3,36)} = 12.313$, $p < 0.0001$] (Fig. 3B). The post hoc test revealed that 5,7-DHT attenuated the extent of PPI disruption induced by *p*-OHA at 79 and 85 dB prepulse intensity (Fig. 3A), but not average PPI (Fig. 3B).

3.3. Effects of PCPA on p-OHA-induced PPI disruption

Fig. 4 shows the effects of PCPA (200 mg/kg, i.p.) on *p*-OHA-induced PPI disruption (Fig. 4A and B). The ANOVA of PPI revealed significant effects of treatment [$F_{(3,36)} = 7.698$, $p = 0.0004$] and prepulse intensity [$F_{(4,144)} = 22.088$, $p < 0.0001$], but not their interaction (Fig. 4A). The ANOVA of average PPI revealed a significant effect of treatment [$F_{(3,36)} = 7.698$, $p = 0.0004$] (Fig. 4B). The post hoc test revealed that PCPA attenuated the extent of PPI disruption induced by *p*-OHA at 73 and 79 dB prepulse intensity and average PPI (Fig. 4A and B).

3.4. Effects of ketanserin on p-OHA-induced PPI disruption

Fig. 5 shows the effects of ketanserin (1, 2 and 4 mg/kg, i.p.) on *p*-OHA-induced PPI disruption (Fig. 5A and B). The ANOVA of PPI

Table 2
Effects of serotonergic agents, control or *p*-OHA on the startle amplitude response in mice.

Pretreatment	i.c.v. Treatment	Mean (SEM)
Ringer (5,7-DHT vehicle)	Ringer	107.07 (7.88)
	p-OHA	115.05 (12.02)
5,7-DHT (50 ng/mouse)	Ringer	82.16 (16.63)
	p-OHA	104.45 (18.70)
0.5% Tween 80 (PCPA vehicle)	Ringer	94.04 (13.81)
	p-OHA	110.46 (19.82)
PCPA (200 mg/kg)	Ringer	133.62 (23.01)
	p-OHA	135.67 (20.34)
0.9% saline (Ketanserin vehicle)	Ringer	114.02 (16.82)
	p-OHA	106.03 (20.55)
Ketanserin (1 mg/kg)	Ringer	86.1 (12.25)
	p-OHA	108.28 (9.08)
Ketanserin (2 mg/kg)	Ringer	71.83 (14.56)
	p-OHA	101.46 (11.02)
Ketanserin (4 mg/kg)	Ringer	107.18 (19.09)
	p-OHA	104.87 (11.58)
0.5% Tween 80 (MDL 100,907 vehicle)	Ringer	113.14 (9.09)
	p-OHA	120.56 (22.33)
MDL100,907 (0.5 mg/kg)	Ringer	76.7 (9.25)
	p-OHA	107.81 (22.12)
MDL 100,907 (1 mg/kg)	Ringer	74.32 (9.76)
	p-OHA	122.77 (13.14)
MDL100,907 (2 mg/kg)	Ringer	79.12 (14.09)
	p-OHA	113.17 (22.78)

Data represent the means ± SEM for 10 animals per group.

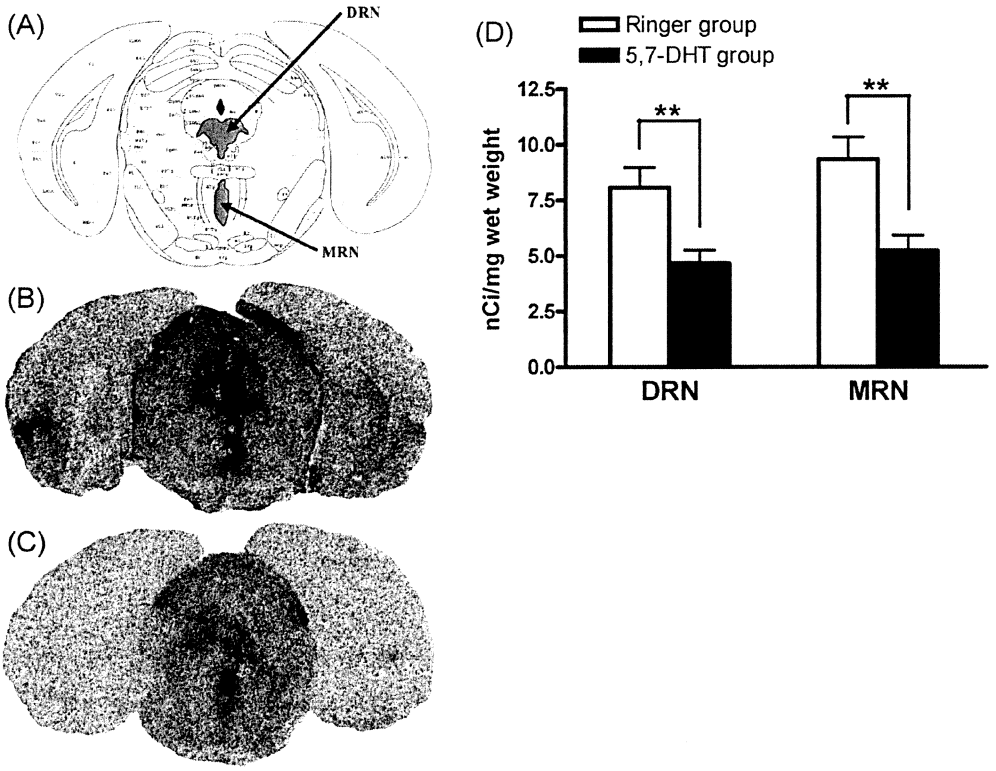


Fig. 2. Serotonin transporter (SERT) binding sites in the dorsal raphe nucleus (DRN) and median raphe nucleus (MRN) of Ringer- or 5,7-DHT-treated mice. (A) Shows a diagram of a section of the mouse brain showing the location of DRN and MRN [11]. Autoradiograms showing the distribution of [^{3}H]-citalopram binding sites in representative coronal sections of Ringer-treated (B) or 5,7-DHT-treated (C) mice. Quantitative autoradiography of [^{3}H]-citalopram binding sites in the DRN and MRN of the Ringer- or 5,7-DHT-treated group (D). Data represent the means ± SEM for 10 animals per group.

revealed significant effects of treatment [$F_{(7,72)} = 11.939, p < 0.0001$] and prepulse intensity [$F_{(4,288)} = 61.854$, $p < 0.0001$], but not their interaction (Fig. 5A). The ANOVA of average PPI revealed a significant effect of treatment [$F_{(7,72)} = 11.939$, $p < 0.0001$] (Fig. 5B). The post hoc test revealed that ketanserin attenuated *p*-OHA-induced PPI disruption at all of prepulse intensities and average PPI (Fig. 5A and B).

3.5. Effects of MDL100,907 on p-OHA-induced PPI disruption

Fig. 6 shows the effects of MDL100,907 (0.5, 1 and 2 mg/kg, i.p.) on *p*-OHA-induced PPI disruption (Fig. 6A and B). The ANOVA of PPI revealed significant effects of treatment [$F_{(7,72)} = 13.571, p < 0.0001$] and prepulse intensity [$F_{(4,288)} = 51.084$, $p < 0.0001$], but not their interaction (Fig. 6A). The ANOVA of average PPI revealed a signif-

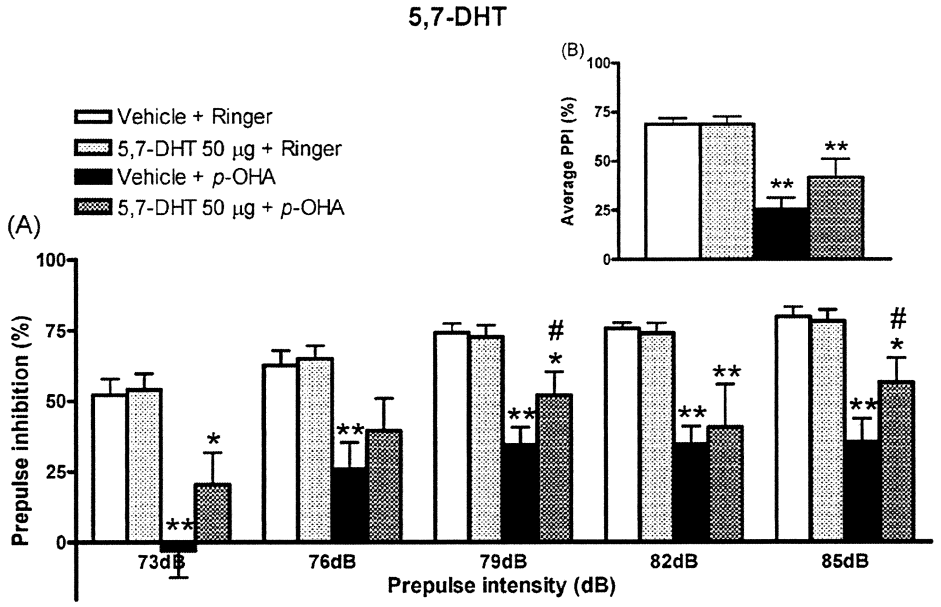


Fig. 3. Effects of 5,7-DHT (50 μg/mouse, i.c.v.) on *p*-OHA-induced PPI disruption in mice. (A) Shows PPI expressed per prepulse intensity level (73, 76, 79, 82 and 85 dB), whereas (B) shows PPI data expressed as an average across all prepulse intensities (average PPI). Data represent the means ± SEM for 10 animals per group. *$P < 0.05$, **$P < 0.01$ vs. vehicle (i.c.v.) + Ringer's (i.c.v.) group. #$P < 0.05$ vs. vehicle (i.c.v.) + *p*-OHA (80 μg/mouse, i.c.v.) group.

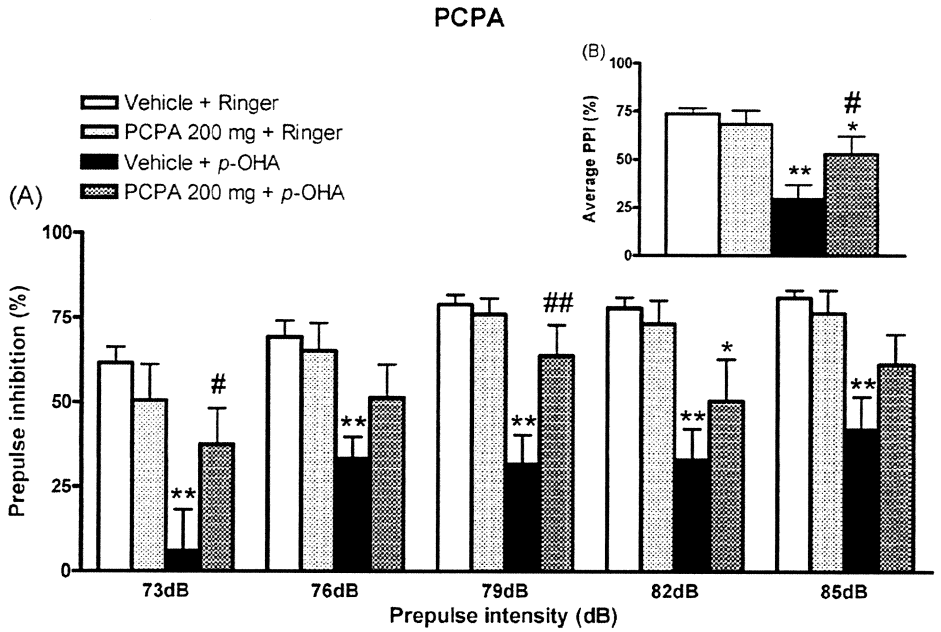


Fig. 4. Effects of PCPA (200 mg/kg, i.p.) on *p*-OHA-induced PPI disruption in mice. (A) Shows PPI expressed per prepulse intensity level (73, 76, 79, 82 and 85 dB), whereas (B) shows PPI data expressed as an average across all prepulse intensities (average PPI). Data represent the means ± SEM for 10 animals per group. $^{*}P < 0.05$, $^{**}P < 0.01$ vs. vehicle (i.p.) + Ringer's (i.c.v.) group. $\#P < 0.05$, $\#\#P < 0.01$ vs. vehicle (i.p.) + *p*-OHA (80 μg/mouse, i.c.v.) group.

icant effect of treatment [$F_{(7,72)} = 13.571$, $p < 0.0001$] (Fig. 6B). The post hoc test revealed that MDL100,907 attenuated *p*-OHA-induced PPI disruption at 73, 79, 82 dB prepulse intensity and average PPI (Fig. 6A and B).

4. Discussion

Our recent findings on *p*-OHA have shown that i.c.v. administration of *p*-OHA induces PPI disruption in mice, which is attenuated by pretreatment with haloperidol (a predominantly D_2-blocking typical antipsychotic), clozapine (a multireceptor-blocking atypical antipsychotic), or several dopaminergic agents (Table 1, [31]). These findings indicate that selective blockade of either the D_2 or D_4 receptor subtype may prevent disruption of PPI induced by *p*-OHA via presynaptic DA release [31]. However, haloperidol and clozapine have affinities for serotonergic (especially 5-HT_{2A}) receptors [34]. Moreover, previous reports have shown that the release of DA and 5-HT are induced by *p*-OHA [17,27]. Therefore, we decided to investigate the involvement of the central serotonergic systems in *p*-OHA-induced PPI disruption.

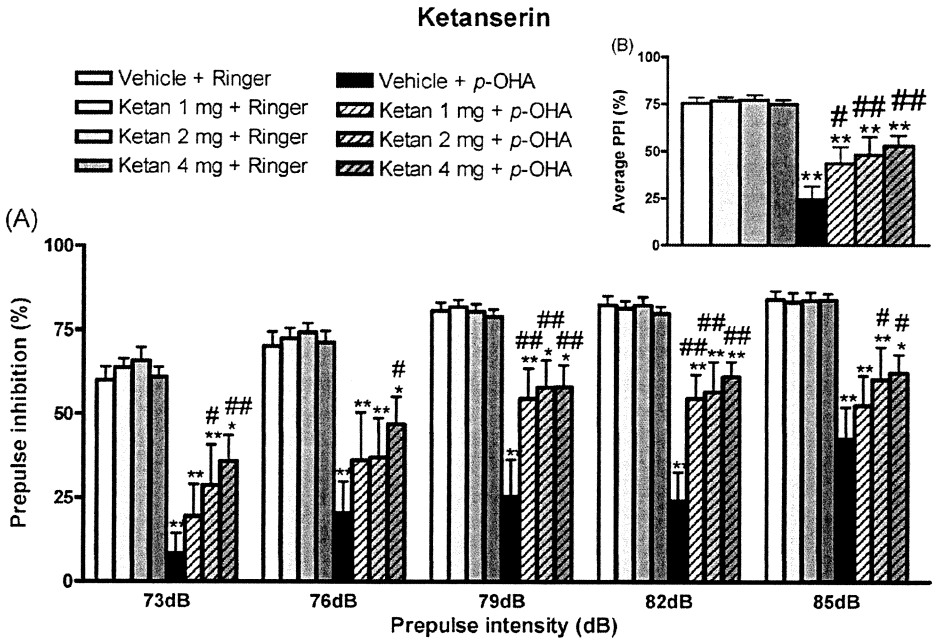


Fig. 5. Effects of ketanserin (1, 2 and 4 mg/kg, i.p.) on *p*-OHA-induced PPI disruption in mice. (A) Shows PPI expressed per prepulse intensity level (73, 76, 79, 82 and 85 dB), whereas (B) shows PPI data expressed as an average across all prepulse intensities (average PPI). Data represent the means ± SEM for 10 animals per group. $^{*}P < 0.05$, $^{**}P < 0.01$ vs. vehicle (i.p.) + Ringer's (i.c.v.) group. $\#P < 0.05$, $\#\#P < 0.01$ vs. vehicle (i.p.) + *p*-OHA (80 μg/mouse, i.c.v.) group.

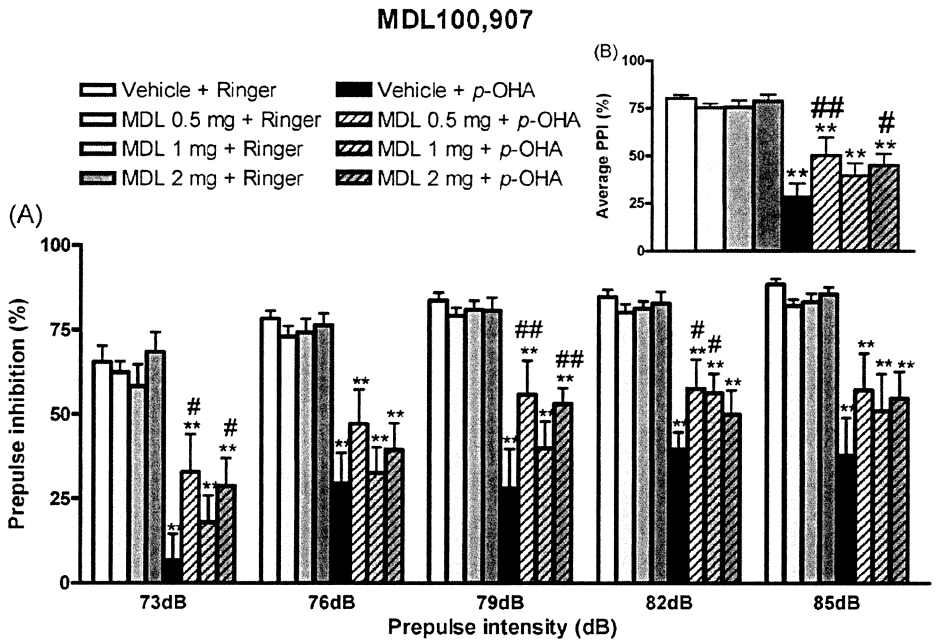


Fig. 6. Effects of MDL100,907 (0.5, 1 and 2 mg/kg, i.p.) on *p*-OHA-induced PPI disruption in mice. (A) Shows PPI expressed per prepulse intensity level (73, 76, 79, 82 and 85 dB), whereas (B) shows PPI data expressed as an average across all prepulse intensities (average PPI). Data represent the means ± SEM for 10 animals per group. $^{*}P < 0.05$, $^{**}P < 0.01$ vs. vehicle (i.p.) + Ringer's (i.c.v.) group. $\#P < 0.05$, $\#\#P < 0.01$ vs. vehicle (i.p.) + *p*-OHA (80 μg/mouse, i.c.v.) group.

AMPH is first metabolized to *p*-OHA in the periphery and brain [13,14], but peripherally metabolized *p*-OHA does not easily cross the blood–brain barrier [21]. In the brain, AMPH is metabolized to *p*-OHA by the enzyme DA-β-hydroxylase [13,14]. Interestingly, despite the rapid disappearance of AMPH after its administration, long-lasting accumulation of *p*-OHA is found in various brain regions [16,18]. Thus, *p*-OHA-induced abnormal behaviors may reflect withdrawal periods following chronic administration of AMPH [31]. As peripherally administered *p*-OHA has difficulty in penetrating the blood–brain barrier [21], we used direct administration of *p*-OHA into the brain in these studies.

p-OHA-induced PPI disruption was attenuated by 5,7-DHT and PCPA. As both 5,7-DHT and PCPA were shown to reduce 5-HT levels [15,26,38], our results concerning the effects of presynaptic agents on *p*-OHA-induced PPI disruption indicate that increased 5-HT levels from presynaptic 5-HT nerve terminals are involved in *p*-OHA-induced PPI disruption. The central serotonergic system is known to modulate PPI. The brain regions that regulate PPI are in the basal forebrain [28] and central serotonergic neurons project to various cortical and limbic structures and innervate almost the entire brain [1]. In addition, as Kusljic et al. [19] have reported that PPI is regulated by serotonergic projections arising from the raphe nuclei, we have measured loss of the 5-HT transporters not only in the raphe nuclei but also in other regions of the brain (i.e., dorsal hippocampus, prefrontal cortex, striatum and nucleus accumbens). 5,7-DHT resulted in a reduction of [^{3}H]-citalopram binding in the raphe nuclei (Fig. 2) and another brain regions (data not shown). A previous report showed that 5-HT releasing agents disrupt PPI via a presynaptic mechanism [25]. Similarly, the hallucinogenic 5-$HT_{2A/2C}$ agonist DOI (2,5-dimethoxy-4-iodoamphetamine) disrupts PPI in rats [10,37]. Antagonism of 5-HT_{2A} receptors can also reverse the behavioral effects of a hyperdopaminergic state induced by the modulation of dopaminergic neural transmission [4,39]. For example, MDL100,907 attenuated PPI deficits in mice with a selective deletion of the gene for the DA transporter (DAT), which exhibit elevated synaptic levels of DA [4]. Barr et al. [4] have shown that these MDL100,907 effects on the hyperdopaminergic state may result from modification of stimulated release of DA in the medial prefrontal cortex [32] and nucleus accumbens shell [24]. Our results concerning the effects of 5-HT_{2A} antagonists on *p*-OHA-induced PPI disruption are supported by these previous reports.

In the present study, ketanserin may have had a greater effect than MDL100,907 (both 5-HT2A antagonists) on *p*-OHA-induced PPI disruption. Similarly, the PCPA may have had a greater effect than 5,7-DHT (both reduce 5-HT levels). There is speculation that these differences in efficacy may be due to the properties of the pretreatment agents with respect to specificity for serotonergic and noradrenergic transmitter systems. Ketanserin has affinity for 5-$HT_{2A/2C}$ receptors, but also binds with less potency to the α_1 receptor [6], whereas MDL100,907 is a more selective 5-HT_{2A} receptor antagonist than ketanserin [5]. Although 5,7-DHT, administered under desipramine protection, selectively depletes 5-HT; PCPA treatment results in a decrease in both 5-HT and NA levels [15,33]. Given that these previous studies suggest that compounds with noradrenergic actions via α_1 receptors as well as compounds with serotonergic actions via 5-HT_{2A} receptors might be effective antipsychotics [34], our results may indicate that compounds which have both serotonergic and noradrenergic actions might be more effective in attenuating *p*-OHA-induced PPI disruption than selective serotonergic compounds such as MDL100,907 or 5,7-DHT. Preliminary data from our laboratory show that prazosin, an α_1 receptor antagonist, attenuates *p*-OHA-induced PPI disruption. Further experiments concerning the effects of noradrenergic agents or the combined effects of 'subthreshold' doses of MDL100907 and prazosin on *p*-OHA-induced PPI disruption will be presented in future studies.

In summary, *p*-OHA-induced PPI disruption was attenuated by pretreatment with 5,7-DHT and PCPA. *p*-OHA-induced PPI disruption was also attenuated by pretreatment with ketanserin and MDL100,907. These data suggest that central serotonergic systems may play important roles in *p*-OHA induced PPI disruption in mice. Taken in conjunction with our recent findings concerning *p*-OHA, our recent series of reports indicate that *p*-OHA induces PPI disruptions via presynaptic DA and 5-HT release. A better understanding

of these unique properties of *p*-OHA may provide new insights into, not only the abuse of drugs, but also into psychiatric disorders such as schizophrenia.

Acknowledgments

This study was supported in part by Grants-in-Aid for Scientific Research (20790309, 22600010) and Matching Fund Subsidy for Private Universities from the Ministry of Education, Culture, Sports, Science and Technology of Japan.

References

[1] Abi-Dargham A, Laruelle M, Aghajanian GK, Charney D, Krystal J. The role of serotonin in the pathophysiology and treatment of schizophrenia. Journal of Neuropsychology and Clinical Neurosciences 1997;9:1–17.
[2] Arai S, Takuma K, Mizoguchi H, Ibi D, Nagai T, Takahashi K, et al. Involvement of pallidotegmental neurons in methamphetamine- and MK-801-induced impairment of prepulse inhibition of the acoustic startle reflex in mice: reversal by GABAB receptor agonist baclofen. Neuropsychopharmacology 2008;33:3164–75.
[3] Arai Y, Kim SK, Kinemuchi H, Tadano T, Satoh SE, Satoh N, et al. Inhibition of brain type A monoamine oxidase and 5-hydroxytryptamine uptake by two amphetamine metabolites, p-hydroxyamphetamine and p-hydroxynorephedrine. Journal of Neurochemistry 1990;55:403–8.
[4] Barr AM, Lehmann-Masten V, Paulus M, Gainetdinov RR, Caron MG, Geyer MA. The selective serotonin-2A receptor antagonist M100907 reverses behavioral deficits in dopamine transporter knockout mice. Neuropsychopharmacology 2004;29:221–8.
[5] Barnes NM, Sharp T. A review of central 5-HT receptors and their function. Neuropharmacology 1999;38:1083–152.
[6] Bøgesø KP, Arnt J, Boeck V, Christensen AV, Hyttel J, Jensen KG. Antihypertensive activity in a series of 1-piperazino-3-phenylindans with potent 5-HT2-antagonistic activity. Journal of Medical Chemistry 1988;31:2247–56.
[7] Brittain RT, Handley SL. Temperature changes produced by the injection of catecholamines and 5-hydroxytryptamine into the cerebral ventricles of the conscious mouse. Journal of Physiology 1967;192:805–13.
[8] Dougan DF, Labrie SL, Paull PD, Duffield PH, Wade DN. Evidence that alpha-methyl-p-tyramine is implicated in behavioural augmentation to amphetamine. General Pharmacology 1986;17:453–6.
[9] Fantegrossi WE, Godlewski T, Karabenick RL, Stephens JM, Ullrich T, Rice KC, et al. Pharmacological characterization of the effects of 3,4-methylenedioxymethamphetamine ("ecstasy") and its enantiomers on lethality, core temperature, and locomotor activity in singly housed and crowded mice. Psychopharmacology (Berlin) 2003;166:202–11.
[10] Feifel D, Melendez G, Shilling PD. A systemically administered neurotensin agonist blocks disruption of prepulse inhibition produced by a serotonin-2A agonist. Neuropsychopharmacology 2003;28:651–3.
[11] Franklin K, Paxinos G. The mouse brain in stereotaxic coordinates. San Diego, CA: Academic Press; 1997.
[12] Geyer MA, Krebs-Thomson K, Braff DL, Swerdlow NR. Pharmacological studies of prepulse inhibition models of sensorimotor gating deficits in schizophrenia: a decade in review. Psychopharmacology (Berlin) 2001;156:117–54.
[13] Goldstein M, Contrera JF. The substrate specificity of phenylamine-beta-hydroxylase. Journal of Biological Chemistry 1962;237:1898–902.
[14] Goldstein M, Anagnoste B. The conversion in vivo of D-amphetamine to (+)-p-hydroxynorephedrine. Biochimica et Biophysica Acta 1965;107:166–8.
[15] Jha S, Rajendran R, Davda J, Vaidya VA. Selective serotonin depletion does not regulate hippocampal neurogenesis in the adult rat brain: differential effects of p-chlorophenylalanine and 5,7-dihydroxytryptamine. Brain Research 2006;1075:48–59.
[16] Jori A, Caccia S. Distribution of amphetamine and its hydroxylated metabolites in various areas of the rat brain. Journal of Pharmacy and Pharmacology 1974;26:746–8.
[17] Kaminskas LM, Irvine RJ, Callaghan PD, White JM, Kirkbride P. The contribution of the metabolite p-hydroxyamphetamine to the central actions of p-methoxyamphetamine. Psychopharmacology (Berlin) 2002;160:155–60.
[18] Kuhn CM, Schanberg SM, Breese GR. Metabolism of amphetamine by rat brain tissue. Biochemical Pharmacology 1978;27:343–51.
[19] Kusljic S, Copolov DL, van den Buuse M. Differential role of serotonergic projections arising from the dorsal and median raphe nuclei in locomotor hyperactivity and prepulse inhibition. Neuropsychopharmacology 2003;28:2138–47.
[20] Kusljic S, van den Buuse M. Differential involvement of 5-HT projections within the amygdala in prepulse inhibition but not in psychotomimetic drug-induced hyperlocomotion. Behavioural Brain Research 2006;168:74–82.
[21] Lindenbaum A, Marcher K, Wepierre J, Cohen Y. Blood–brain barrier. II. Kinetics of distribution of 3H-parahydroxyamphetamine in brain structures after intravenous administration in the rat. Archives Internationales de Pharmacodynamie et de Therapie 1975;215:168–76.
[22] Mansbach RS, Geyer MA, Braff DL. Dopaminergic stimulation disrupts sensorimotor gating in the rat. Psychopharmacology (Berlin) 1988;94:507–14.
[23] Mansbach RS, Geyer MA. Effects of phencyclidine and phencyclidine biologs on sensorimotor gating in the rat. Neuropsychopharmacology 1989;2:299–308.
[24] Marcus MM, Nomikos GG, Svensson TH. Effects of atypical antipsychotic drugs on dopamine output in the shell and core of the nucleus accumbens: role of 5-HT(2A) and alpha(1)-adrenoceptor antagonism. European Neuropsychopharmacology 2000;10:245–53.
[25] Martinez DL, Geyer MA. Characterization of the disruptions of prepulse inhibition and habituation of startle induced by alpha-ethyltryptamine. Neuropsychopharmacology 1997;16:246–55.
[26] Maruyama Y, Hayashi G, Smits SE, Takemori AE. Studies on the relationship between 5-hydroxytryptamine turnover in brain and tolerance and physical dependence in mice. Journal of Pharmacology and Experimental Therapeutics 1971;178:20–9.
[27] Matsuda LA, Hanson GR, Gibb JW. Neurochemical effects of amphetamine metabolites on central dopaminergic and serotonergic systems. Journal of Pharmacology and Experimental Therapeutics 1989;251:901–8.
[28] Moore H, West AR, Grace AA. The regulation of forebrain dopamine transmission: relevance to the pathophysiology and psychopathology of schizophrenia. Biological Psychiatry 1999;46:40–55.
[29] Nakagawasai O, Onogi H, Mitazaki S, Sato A, Watanabe K, Saito H, et al. Behavioral and neurochemical characterization of mice deficient in the N-type Ca(2+) channel alpha(1B) subunit. Behavioural Brain Research 2010;208:224–30.
[30] Onogi H, Hozumi M, Nakagawasai O, Arai Y, Ishigaki S, Sato A, et al. Central administration of p-hydroxyamphetamine produces a behavioral stimulant effect in rodents: evidence for the involvement of dopaminergic systems. Psychopharmacology (Berlin) 2010;208:323–31.
[31] Onogi H, Nakagawasai O, Tan-No K, Mitazaki S, Sato A, Nakaya K, et al. p-Hydroxyamphetamine causes prepulse inhibition disruptions in mice: Contribution of dopamine neurotransmission. Behavioural Brain Research 2010;214:349–56.
[32] Pehek EA, McFarlane HG, Maguschak K, Price B, Pluto CP. M100,907, a selective 5-HT(2A) antagonist, attenuates dopamine release in the rat medial prefrontal cortex. Brain Research 2001;888:51–9.
[33] Reader TA, Gauthier P. Catecholamines and serotonin in the rat central nervous system after 6-OHDA, 5-7-DHT and p-CPA. Journal of Neural Transmission 1984;59:207–27.
[34] Roth BL, Sheffler DJ, Kroeze WK. Magic shotguns versus magic bullets: selectively non-selective drugs for mood disorders and schizophrenia. Nature Reviews Drug Discovery 2004;3:353–9.
[35] Salomon L, Lanteri C, Godeheu G, Blanc G, Gingrich J, Tassin JP. Paradoxical constitutive behavioral sensitization to amphetamine in mice lacking 5-HT2A receptors. Psychopharmacology (Berlin) 2007;194:11–20.
[36] Simpson LL. Blood pressure and heart rate response evoked by p-hydroxyamphetamine and by p-hydroxynorephedrine II. A quantitative assessment of the role of amphetamine metabolites in acute responses evoked by d-amphetamine. Journal of Pharmacology and Experimental Therapeutics 1980;213:504–8.
[37] Sipes TE, Geyer MA. DOI disruption of prepulse inhibition of startle in the rat is mediated by 5-HT(2A) and not by 5-HT(2C) receptors. Behavioural Pharmacology 1995;6:839–42.
[38] Snape MF, Colado MI, Green AR. Chlormethiazole and dizocilpine block the behavioural, but not the neurotoxic effects of 5,7-dihydroxytryptamine in mice. Pharmacology & Toxicology 1994;74:40–2.
[39] Sorensen SM, Kehne JH, Fadayel GM, Humphreys TM, Ketteler HJ, Sullivan CK, et al. Characterization of the 5-HT2 receptor antagonist MDL 100907 as a putative atypical antipsychotic: behavioral, electrophysiological and neurochemical studies. Journal of Pharmacology and Experimental Therapeutics 1993;266:684–91.
[40] Swerdlow NR, Braff DL, Taaid N, Geyer MA. Assessing the validity of an animal model of deficient sensorimotor gating in schizophrenic patients. Archives of General Psychiatry 1994;51:139–54.
[41] Tadano T, Satoh S, Kisara K. Head-twitches induced by p-hydroxyamphetamine. Japanese Journal of Pharmacology 1986;41:519–23.

Behavioural Brain Research 218 (2011) 165–173

Contents lists available at ScienceDirect

Behavioural Brain Research

journal homepage: www.elsevier.com/locate/bbr

Research report

Pharmacological characterizations of memantine-induced disruption of prepulse inhibition of the acoustic startle response in mice: Involvement of dopamine D_2 and 5-HT_{2A} receptors

Kota Nakaya[a], Osamu Nakagawasai[a,*], Yuichiro Arai[b], Hiroshi Onogi[a], Atsushi Sato[a], Fukie Niijima[a], Koichi Tan-No[a], Takeshi Tadano[a]

[a] Department of Pharmacology, Tohoku Pharmaceutical University, 4-4-1 Komatsushima, Aoba-ku, Sendai 981-8558, Japan
[b] Tokyo Ariake University of Medical and Health Sciences, Tokyo 135-0063, Japan

ARTICLE INFO

Article history:
Received 8 July 2010
Received in revised form
22 November 2010
Accepted 28 November 2010

Keywords:
Memantine
Antipsychotics
Dopamine (DA)
Serotonin (5-HT)
Prepulse inhibition

ABSTRACT

It has recently been reported that psychotic symptoms in patients such as those with Parkinson's disease dementia (PDD) and Lewy body dementia (LBD) may worsen following treatment with memantine, a non-competitive NMDA receptor antagonist. Prepulse inhibition (PPI) of the acoustic startle response (ASR) is used as a measure for sensorimotor gating and it has been reported that PPI is disrupted by memantine. However, the mechanism of memantine-induced PPI disruption remains unclear. In the present study, we investigated the effects of memantine on PPI of the ASR in mice. Memantine (1.25–20 mg/kg, intraperitoneally) increased the ASR and dose-dependently decreased PPI for all prepulse intensities tested. This effect of memantine on PPI was attenuated by pretreatment with the antipsychotics clozapine (3 and 6 mg/kg), risperidone (0.3 mg/kg) and haloperidol (0.5 mg/kg), the selective D_2 antagonist sulpiride (40 mg/kg) and 5-$HT_{2A/2C}$ antagonist ketanserin (2 and 4 mg/kg) but not with the selective D_1 antagonist SCH23390 (0.05 and 0.1 mg/kg). Clozapine (6 mg/kg) and risperidone (0.3 mg/kg) significantly attenuated the increased startle amplitude in the memantine-treated groups. These results suggest that involvement of dopaminergic and/or serotonergic neurotransmission may play a crucial role in memantine-induced PPI disruption, and additionally, indicate that blockade of either the D_2 or 5-HT_{2A} receptor may prevent disruption of PPI induced by memantine in mice. Conceivably, memantine may exacerbate psychotic symptoms in patients with PDD and LBD.

© 2010 Elsevier B.V. All rights reserved.

1. Introduction

Memantine, a non-competitive NMDA receptor antagonist, has been used in the treatment of moderate to severe Alzheimer's disease (AD). It has been shown to delay cognitive decline in patients with dementia [28,48,64], an effect hypothesized to arise from its ability to block the excessive influx of calcium ions through the channel of the activated NMDA receptor [44]. Recently, it has been reported that memantine might be a treatment option in patients with Parkinson's disease dementia (PDD) and Lewy body dementia (LBD) (for details see: [1,16]). However, there are few clinical studies in patients with PDD or LBD, with both improvement and worsening with memantine treatment in case reports [17,36,50,52]. Thus, there may or may not be a deleterious effect of memantine in dementia subgroup.

Sensorimotor information gating processes have received much attention in an attempt to better understand the mechanisms involved in the physiopathology of schizophrenia [8,42,47,60]. One well-established method for evaluating sensorimotor gating is prepulse inhibition (PPI), which occurs when a weak prestimulus (prepulse) precedes a startling stimulus (pulse alone) and thus inhibits the startle response. Interestingly, PPI is an unlearned phenomenon [57] and, using virtually identical techniques, is readily demonstrated in a number of species ranging from mice to humans [9,18]. PPI disruption observed in schizophrenic, PDD and LBD patients has been described in detail for several studies [6,7,46,47]. PPI disruption can also be observed in both mice and rats treated with psychomimetic agents. Indeed, dopamine (DA) agonists such as apomorphine or amphetamine and NMDA antagonists such as

Abbreviations: AD, alzheimer's disease; ANOVA, analysis of variance; ASR, acoustic startle response; DA, dopamine; NMDA, N-methyl-D-aspartate; PCP, phencyclidine; PDD, Parkinson's disease dementia; LBD, Lewy body dementia; PPI, prepulse inhibition; SEM, standard error of the mean; 5-HT, serotonin.

* Corresponding author. Tel.: +81 22 727 0123; fax: +81 22 727 0123.
E-mail addresses: 20951124@is.tohoku-pharm.ac.jp (K. Nakaya), osamun@tohoku-pharm.ac.jp (O. Nakagawasai), arai@tau.ac.jp (Y. Arai), hirogle@yahoo.co.jp (H. Onogi), obx0315@yahoo.co.jp (A. Sato), niijima@tohoku-pharm.ac.jp (F. Niijima), koichi@tohoku-pharm.ac.jp (K. Tan-No), tadano@tohoku-pharm.ac.jp (T. Tadano).

0166-4328/$ – see front matter © 2010 Elsevier B.V. All rights reserved.
doi:10.1016/j.bbr.2010.11.053

MK-801 (dizocilpine), phencyclidine (PCP) or ketamine, induce PPI disruption [29,30]. DA agonist-induced PPI disruption can be attenuated by both typical and atypical antipsychotics whereas those induced by NMDA antagonists seem to be attenuated only by atypical antipsychotics [3,4,33,56,65,66]. Recently, it has been reported that memantine produces dose-dependent PPI disruption in rats [63,70]. Memantine has a wide variety of neurochemical effects, in addition to its actions as a NMDA antagonist, memantine has been found to increase DA levels indirectly [43,45,54], and to weakly inhibit reuptake and turnover of serotonin (5-HT) [43]. However, the mechanism of memantine-induced PPI disruption remains unclear.

The purpose of the present study was to determine the neurochemical basis of the effects of memantine on sensorimotor gating by evaluating the ability of various receptor antagonists to attenuate memantine-induced PPI disruption in naïve mice. We initially studied the effects of atypical antipsychotics such as clozapine and risperidone on memantine-induced PPI disruption. The atypical antipsychotics have antagonistic properties at several neurotransmitter systems. For example, risperidone has strong affinity to D_2-like and 5-HT_{2A} receptors [49], whereas clozapine has a multipharmacological profile with the highest affinity to 5-HT_{1A}, 5-$HT_{2A/2C}$ [49] and muscarinic receptors [11]. Finally, in order to determine whether reversal of memantine effects could be attributed to any single property of atypical antipsychotic drugs, we tested the DA antagonist haloperidol, selective D_1 antagonist SCH23390, selective D_2 antagonist sulpiride and the 5-$HT_{2A/2C}$ antagonist ketanserin for their ability to block memantine-induced PPI disruption.

2. Materials and methods

2.1. Animals

Male ddY strain mice (weighing 28–32 g, Japan SLC, Japan) were used in the experiments presented herein. Animals were housed in clear plastic cages and were maintained under controlled conditions (temperature 22 ± 2 °C and humidity 55 ± 5%), on a 12:12 h light–dark cycle (light term: 07:00 to 19:00). Food and water were provided ad libitum throughout the experiments except during behavioral testing. In all experiments, separate groups of naïve mice were used.

All experiments were performed with the approval of the Ethics Committee of Animal Experiments in Tohoku Pharmaceutical University and according to the National Institutes of Health Guide for the Care and Use of Laboratory Animals. Efforts were made to minimize suffering and to reduce the number of animals used.

2.2. Drugs and treatments

The following drugs were used: memantine hydrochloride, haloperidol, clozapine and ketanserin, R-(+)-SCH-23390, (−)-sulpiride (Sigma–Aldrich, USA) and risperidone (Wako Pure Chemical Industries, Ltd, Japan). Memantine hydrochloride, ketanserin and R-(+)-SCH-23390 were dissolved in physiological saline. Haloperidol, risperidone, clozapine and (−)-sulpiride were dissolved in 0.5% Tween80. All drugs were injected intraperitoneally (i.p.) at a volume of 10 ml/kg.

Memantine (1.25, 2.5, 5, 10 and 20 mg/kg) and saline were administered 30 min prior to PPI testing. The higher doses of memantine (5, 10 and 20 mg/kg) were chosen based on their efficacy in decreasing amyloid β plaque deposition in the Tg2576 mouse model of Alzheimer's disease [13]. The other (lower) doses of memantine were chosen based on the paper published by Wiley et al. [70]. Time course experiments were conducted with memantine at 15, 30, 60, 120 and 240 min prior to PPI testing. Pretreatment with clozapine (3 and 6 mg/kg), riperidone (0.3 mg/kg), haloperidol (0.5 mg/kg), R-(+)-SCH23390 (0.05 and 0.1 mg/kg), (−)-sulpiride (40 mg/kg) or ketanserin (2 and 4 mg/kg) was performed 30 min prior to administration of memantine or saline. The doses of clozapine, risperidone and sulpiride were chosen based on their efficacy in attenuating the enhancing effect of PCP on immobility (a negative symptom of schizophrenia) in the forced swimming test [40,41]. The doses of haloperidol and SCH23390 utilized in the present studies were selected because they have been previously reported to effectively attenuate apomorphine-induced PPI disruption [12,21]. However, doses of SCH23390 higher than 0.1 mg/kg were not used because they cause too great a reduction in startle amplitude in the studies presented herein. Previous studies have demonstrated that ketanserin significantly attenuated dizocilpine-induced PPI disruption and hyperactivity in rats [65] at the doses used in this study (2 and 4 mg/kg).

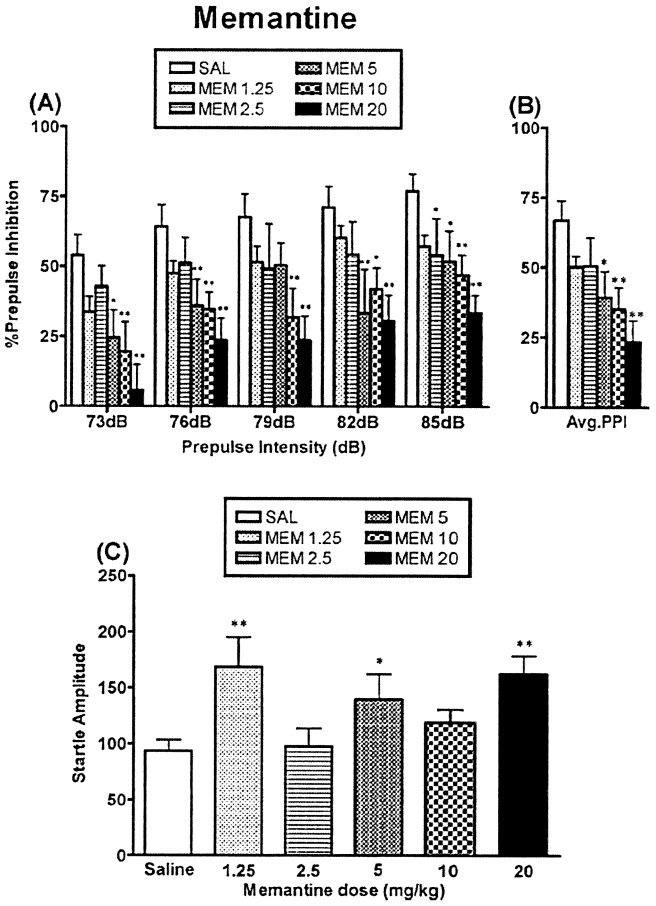


Fig. 1. Effects of memantine on PPI (A), average PPI (B) and startle amplitude (C) in naïve mice. Each column represents the mean ± SEM. *$P < 0.05$, **$P < 0.01$ compared to the saline-treated group; $N = 12$–22 per group. SAL: saline and MEM: memantine.

2.3. Measurement of the startle response and prepulse inhibition

Tests were conducted using a SR-LAB unit (San Diego Instruments, San Diego, California, USA) that comprised of two sound-attenuating chambers each equipped with a cylindrical plexiglass animal enclosure (length, 6.7 cm; inner diameter, 3.8 cm). Ventilation was provided by a small electric fan that also generated a 70 dB background noise. Tone pulses were presented by a speaker positioned 24 cm directly above the animal enclosure. A piezoelectric accelerometer affixed to the animal enclosure frame was used to detect and transduce motion resulting from the animal's response. Tone pulse parameters were controlled by a microcomputer using the SR-LAB software package and interface assembly that also digitized, rectified and recorded stabilimeter readings.

Measures of both acoustic startle response (ASR) and PPI were obtained in a single session as described by Nakagawasai et al. [39] with minor modifications. Mice were placed in the plexiglass enclosure and allowed to acclimatize to the environment for 5 min before being tested in 42 discrete trials. In the first two trials, the magnitude of the ASR to a 120 dB tone of 50 ms duration was measured. These first two startle tones were presented to habituate the animals to the testing procedure. Therefore, the ASR magnitude of these two trials was omitted from the statistical analysis of the mean ASR amplitude. In the subsequent 40 trials, the startle tone was either presented alone or 100 ms after presentation of a 30-ms-duration prepulse. Prepulse intensity ranged from 3 to 15 dB above background noise and was varied randomly between trials in 3 dB steps. Measurements of the magnitude of the ASR were taken at each of the five prepulse intensities in five trials; animals were randomly presented with the startle tone alone during the other ten trials; null trials (background tone alone) during the other five trials. The same stimulus condition was never presented in more than two consecutive trials. The interval between each trial was programmed to a variable time schedule with an average duration of 15 s (range 5–30 s). A measure of startle response amplitude was derived from the mean of 100 digitized data points collected from stimulus onset at a rate 1 kHz. Prepulse effectiveness in suppressing the startle response was expressed as a percentage based on the mean amplitude of responses to the startle alone (10 startle tones) relative to those recorded under the five condition (5 startle tones/condition): %

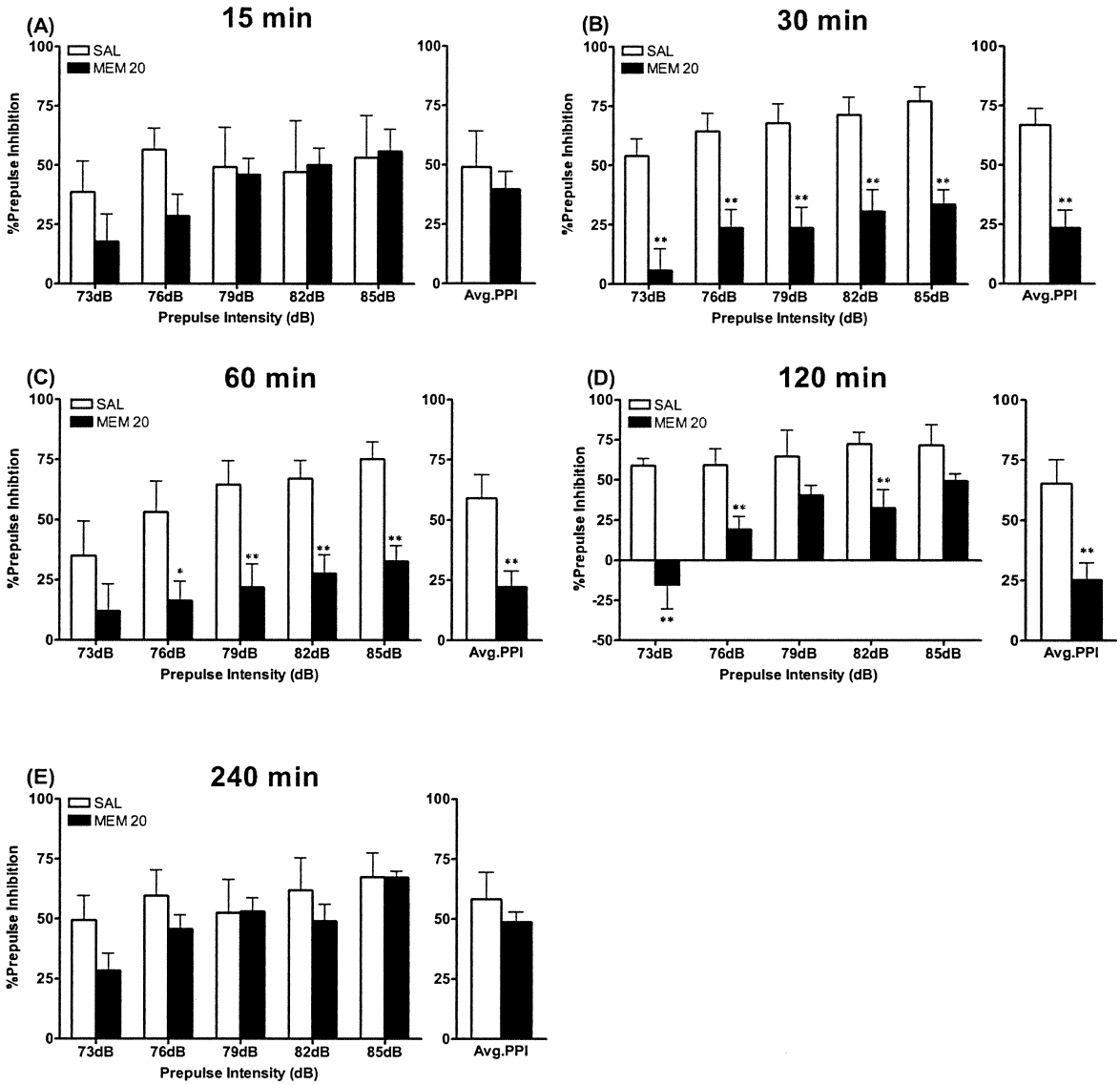


Fig. 2. Time course effects of memantine on PPI and average PPI (A–E) in naïve mice. Each column represents the mean ± SEM. $^{*}P < 0.05$, $^{**}P < 0.01$ compared to the saline-treated group; $N = 10$–22 per group. SAL: saline and MEM: memantine.

PPI = 100 − [(mean startle amplitude for prepulse + pulse trials/mean startle amplitude for pulse − alone trials) × 100] %. Average PPI is expressed as the average across all prepulse intensities proposed by van den Buuse et al. [10].

2.4. Statistical analysis

Results are expressed as mean ± standard errors of the mean (SEM). A one-way analysis of variance (ANOVA) was used to assess the treatment effects on the magnitude of the ASR and average PPI. With respect to assessing the treatment effects on the magnitude of the ASR and average PPI in the time course experiments, the Student's *t*-test for two-group comparison was used. The PPI data were analyzed by two-way repeated-measures ANOVA with the treatment as independent factor and prepulse intensity as repeated measures. A post hoc Fisher's PLSD test was conducted when appropriate. The criterion was set at $P < 0.05$.

3. Results

3.1. Effect of memantine on prepulse inhibition and startle amplitude

Two-way repeated-measures ANOVA of PPI revealed significant effects of the treatment [$F_{(5, 92)} = 4.00$, $P < 0.01$] and prepulse intensity [$F_{(4, 368)} = 20.86$, $P < 0.01$], but not treatment × prepulse intensity interaction [$F_{(20, 368)} = 0.89$, $P = 0.60$] (Fig. 1A). In addition, a one-way ANOVA of average PPI revealed a significant effect of treatment [$F_{(5, 92)} = 4.00$, $P < 0.01$] (Fig. 1A and B). A post hoc test revealed that i.p. administration of memantine dose-dependently induced disruption of PPI and average PPI. We observed that PPI was disrupted most severely by a dose of 20 mg/kg for all prepulse intensities tested ($P < 0.01$) as well as average PPI ($P < 0.01$) (Fig. 1A and B). In all subsequent experiments we employed a dose of 20 mg/kg of memantine to induce disruption of PPI.

A one-way ANOVA of startle amplitude revealed a significant effect of treatment [$F_{(5, 92)} = 3.73$, $P < 0.01$] (Fig. 1C). A post hoc test revealed that the startle amplitude was enhanced at doses of 1.25, 5 and 20 mg/kg of memantine ($P < 0.01$, $P < 0.05$, $P < 0.01$ respectively) (Fig. 1C).

3.2. Time course effects of memantine on prepulse inhibition and startle amplitude.

Time course experiments with memantine (20 mg/kg) indicated that memantine disrupted PPI when administered 30–120 min

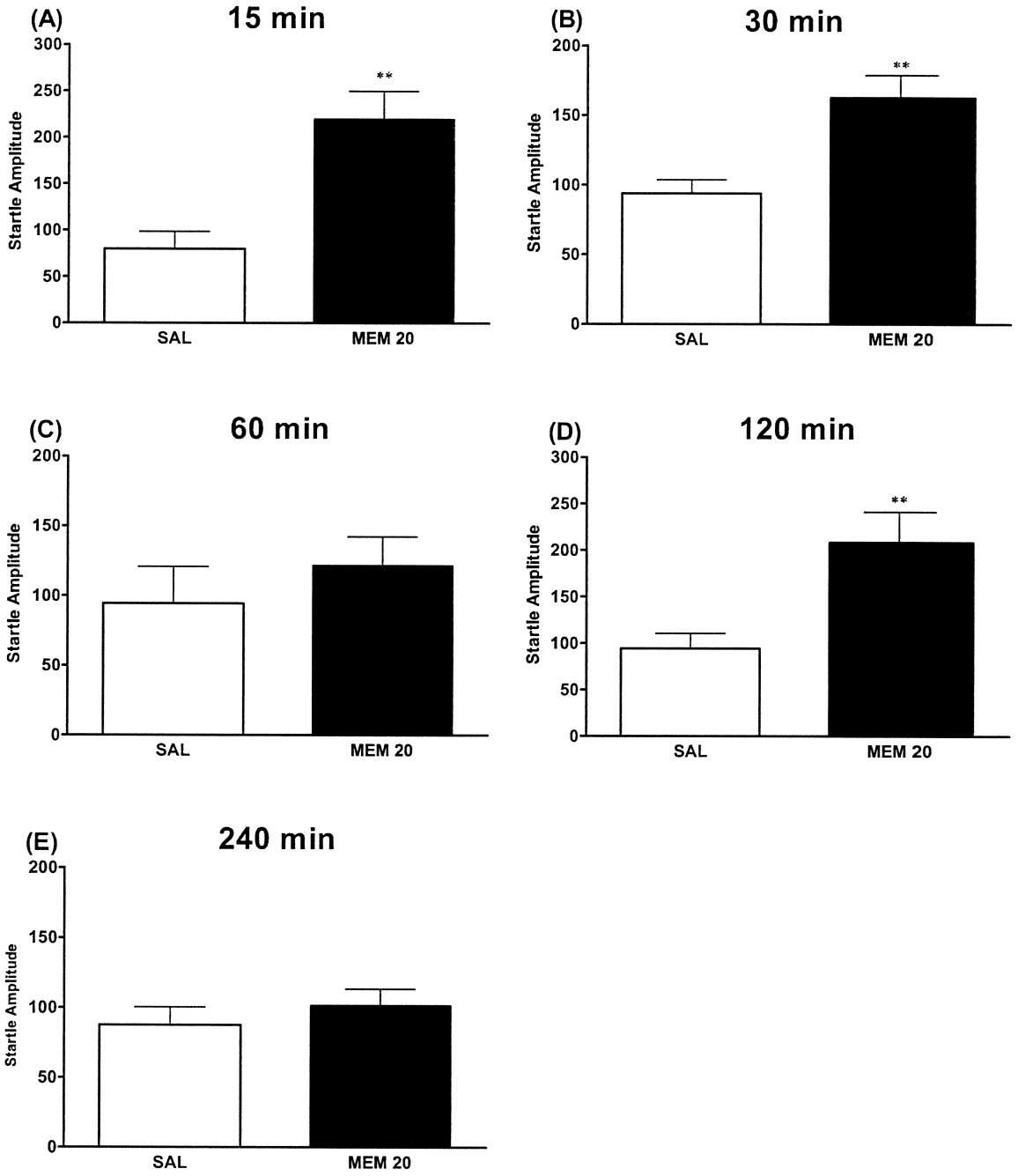


Fig. 3. Time course effects of memantine on startle amplitude (A–E) in naïve mice. Each column represents the mean ± SEM. $^{*}P < 0.05$, $^{**}P < 0.01$ compared to the saline-treated group; $N = 10$–22 per group. SAL: saline and MEM: memantine.

prior to testing (Fig. 2B–D). In Fig. 2B, a two-way repeated-measures ANOVA of PPI revealed significant effects of treatment [$F_{(1,\ 36)} = 17.28$, $P < 0.01$] and prepulse intensity [$F_{(4,\ 144)} = 17.37$, $P < 0.01$], but not treatment × prepulse intensity interaction [$F_{(4,\ 144)} = 0.45$, $P = 0.77$]. In Fig. 2C, a two-way repeated-measures ANOVA of PPI revealed significant effects of treatment [$F_{(1,\ 18)} = 9.57$, $P < 0.01$] and prepulse intensity [$F_{(4,\ 72)} = 8.12$, $P < 0.01$], but not treatment × prepulse intensity interaction [$F_{(4,\ 72)} = 0.96$, $P = 0.43$]. In Fig. 2D, a two-way repeated-measures ANOVA of PPI revealed significant effects of treatment [$F_{(1,\ 18)} = 10.63$, $P < 0.01$] and prepulse intensity [$F_{(4,\ 72)} = 10.35$, $P < 0.01$] and treatment × prepulse intensity interaction [$F_{(4,\ 72)} = 4.85$, $P < 0.01$]. In addition, a Student's t-test revealed that average PPI was also disrupted by memantine [$t = 4.157$, $P < 0.01$ (B); $t = 3.09$, $P < 0.01$ (C); $t = 3.26$, $P < 0.01$ (D) respectively]. A post hoc test revealed that administration of memantine 30 min prior to testing produced disruption of PPI for all prepulse intensities tested ($P < 0.01$) as well as average PPI ($P < 0.01$) (B) whereas administration of memantine 60 prior to testing disrupted PPI at PP 73 dB ($P < 0.05$) and PP 79–85 dB ($P < 0.01$) and average PPI ($P < 0.01$) (C), and administration of memantine 120 prior to testing disrupted PPI at PP 73, 76 and 82 dB ($P < 0.01$) and average PPI ($P < 0.01$) (D). Administration of memantine 60 and 120 min prior to testing only partially disrupted PPI.

Time course effects of memantine on startle amplitude are shown in Fig. 3. Experiments performed 15, 30, 60, 120 and 240 min after memantine administration are shown in panels A, B, C, D and E respectively. A Student's *t*-test revealed that memantine significantly enhanced startle amplitude 15, 30 and 120 min after administration [$t=-3.95$, $P<0.01$ (A); $t=-3.84$, $P<0.01$ (B); $t=-3.13$, $P<0.01$ (D) respectively], but not at 60 or 240 min (C and E).

3.3. Effects of drugs on memantine-induced PPI disruption

3.3.1. Clozapine

A two-way repeated-measures ANOVA of PPI revealed a significant effect of treatment [$F_{(5, 60)}=21.51$, $P<0.01$] and prepulse intensity [$F_{(4, 240)}=41.64$, $P<0.01$], but not treatment × prepulse intensity interaction [$F_{(20, 240)}=0.75$, $P=0.77$] (Fig. 4A). In addition, a one-way ANOVA of average PPI revealed a significant effect of treatment [$F_{(5, 60)}=21.51$, $P<0.01$] (Fig. 4A). A post hoc test revealed that clozapine (3 and 6 mg/kg) attenuated memantine-induced PPI disruption for all prepulse intensities tested ($P<0.01$) as well as average PPI ($P<0.01$) (Fig. 4A).

3.3.2. Risperidone

A two-way repeated-measures ANOVA of PPI revealed a significant effect of treatment [$F_{(3, 48)}=26.69$, $P<0.01$] and prepulse intensity [$F_{(4, 192)}=39.72$, $P<0.01$], but not treatment × prepulse intensity interaction [$F_{(12, 192)}=1.20$, $P=0.29$] (Fig. 4B). In addition, a one-way ANOVA of average PPI revealed a significant effect of treatment [$F_{(3, 48)}=26.69$, $P<0.01$] (Fig. 4B). A post hoc test revealed no significant effect of risperidone on PPI in saline-treated groups. In contrast, risperidone attenuated memantine-induced PPI disruption for all prepulse intensities tested ($P<0.01$) as well as average PPI ($P<0.01$) (Fig. 4B).

3.3.3. Haloperidol

A two-way repeated-measures ANOVA of PPI revealed a significant effect of treatment [$F_{(3, 52)}=31.57$, $P<0.01$] and prepulse intensity [$F_{(4, 208)}=38.29$, $P<0.01$], but not treatment × prepulse intensity interaction [$F_{(12, 208)}=0.98$, $P=0.47$] (Fig. 5A). In addition, a one-way ANOVA of average PPI revealed a significant effect of treatment [$F_{(3, 52)}=32.62$, $P<0.01$] (Fig. 5A). A post hoc test revealed that haloperidol attenuated memantine-induced PPI disruption for all prepulse intensities tested ($P<0.01$) as well as average PPI ($P<0.01$), but it had no effect in the saline-treated group (Fig. 5A).

3.3.4. SCH23390

A two-way repeated-measures ANOVA of PPI revealed a significant effect of treatment [$F_{(5, 70)}=11.73$, $P<0.01$] and prepulse intensity [$F_{(4, 280)}=22.45$, $P<0.01$], but not treatment × prepulse intensity interaction [$F_{(20, 280)}=0.91$, $P=0.58$] (Fig. 5B). In addition, a one-way ANOVA of average PPI revealed a significant effect of treatment [$F_{(5, 70)}=11.73$, $P<0.01$] (Fig. 5B). A post hoc test revealed that SCH 23390 (0.05 and 0.1 mg/kg) did not attenuate memantine-induced PPI disruption or average PPI (Fig. 5B).

3.3.5. Sulpiride

A two-way repeated-measures ANOVA of PPI revealed a significant effect of treatment [$F_{(3, 52)}=12.94$, $P<0.01$] and prepulse intensity [$F_{(4, 208)}=43.95$, $P<0.01$], but not treatment × prepulse intensity interaction [$F_{(12, 208)}=0.77$, $P=0.68$] (Fig. 5C). In addition, a one-way ANOVA of average PPI revealed a significant effect of treatment [$F_{(3, 52)}=12.94$, $P<0.01$] (Fig. 5C). A post hoc test revealed that sulpiride attenuated memantine-induced PPI disruption for all prepulse intensities tested ($P<0.01$ respectively) excluding PP 73 dB ($P<0.05$) and average PPI ($P<0.01$) (Fig. 5C).

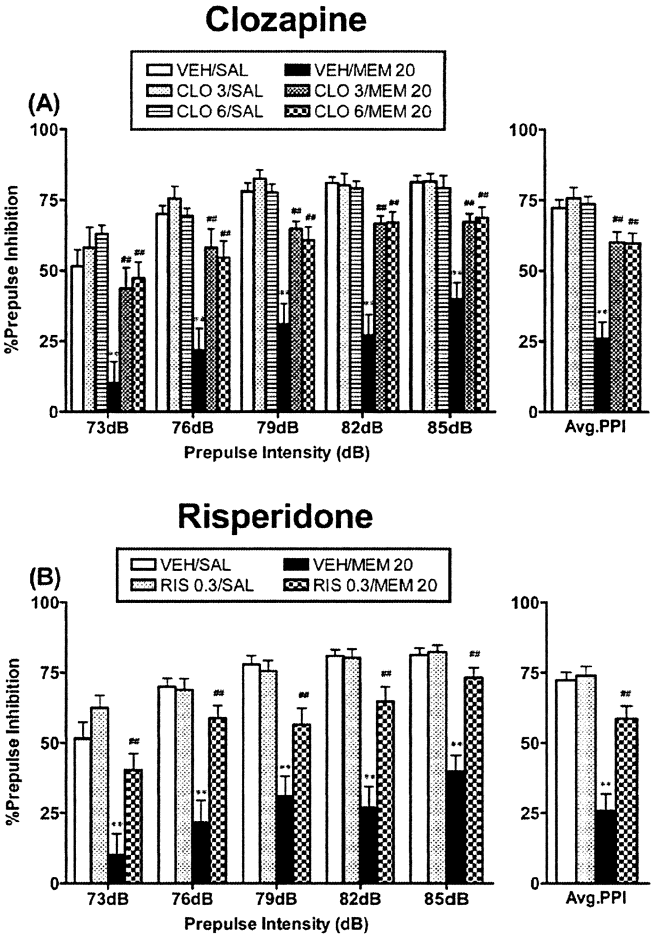


Fig. 4. Effects of clozapine (A) and risperidone (B) on PPI and average PPI in saline- and memantine-treated groups. Each column represents the mean ± SEM. $^{*}P<0.05$, $^{**}P<0.01$ compared to VEH/SAL; $^{\#}P<0.05$, $^{\#\#}P<0.01$ compared to VEH/MEM; $N=9$–16 per group. SAL: saline; MEM: memantine; CLO: clozapine; RIS: risperidone.

3.3.6. Ketanserin

A two-way repeated-measures ANOVA of PPI revealed a significant effect of treatment [$F_{(5, 63)}=21.68$, $P<0.01$] and prepulse intensity [$F_{(4, 252)}=47.45$, $P<0.01$], but not treatment × prepulse intensity interaction [$F_{(20, 252)}=1.50$, $P=0.08$] (Fig. 6). In addition, a one-way ANOVA of average PPI revealed a significant effect of treatment [$F_{(5, 63)}=21.68$, $P<0.01$] (Fig. 6). A post hoc test revealed that ketanserin (2 and 4 mg/kg) attenuated memantine-induced PPI disruption for all prepulse intensities tested ($P<0.01$) excluding PP 73 and 76 dB with the dose of 2 mg/kg ($P<0.05$ and $P=0.05$, respectively) as well as average PPI ($P<0.01$) (Fig. 6).

3.3.7. Startle amplitude

Drug effects on startle amplitude (pulse alone) are shown in Fig. 7. In the clozapine, rispridone, haloperidol, SCH23390, sulpiride and ketanserin experiments (Fig. 7, panels A, B, C, D, E and F respectively), a one-way ANOVA of startle amplitude revealed significant effects of treatment [$F_{(5, 60)}=4.00$, $P<0.01$] (A), [$F_{(3, 48)}=2.78$, $P=0.05$] (B), [$F_{(3, 52)}=2.71$, $P=0.05$] (C), [$F_{(5, 70)}=3.65$, $P<0.01$] (D), [$F_{(3, 52)}=7.30$, $P<0.01$] (E) and [$F_{(5, 63)}=2.86$, $P<0.05$] (F) respectively. A post hoc test revealed that clozapine (6 mg/kg) and risperidone (0.3 mg/kg) reduced startle amplitude in the memantine-treated group ($P<0.05$). Doses of SCH23390 higher than 0.1 mg/kg were not used because they cause too great a reduction in startle amplitude in the studies presented herein.

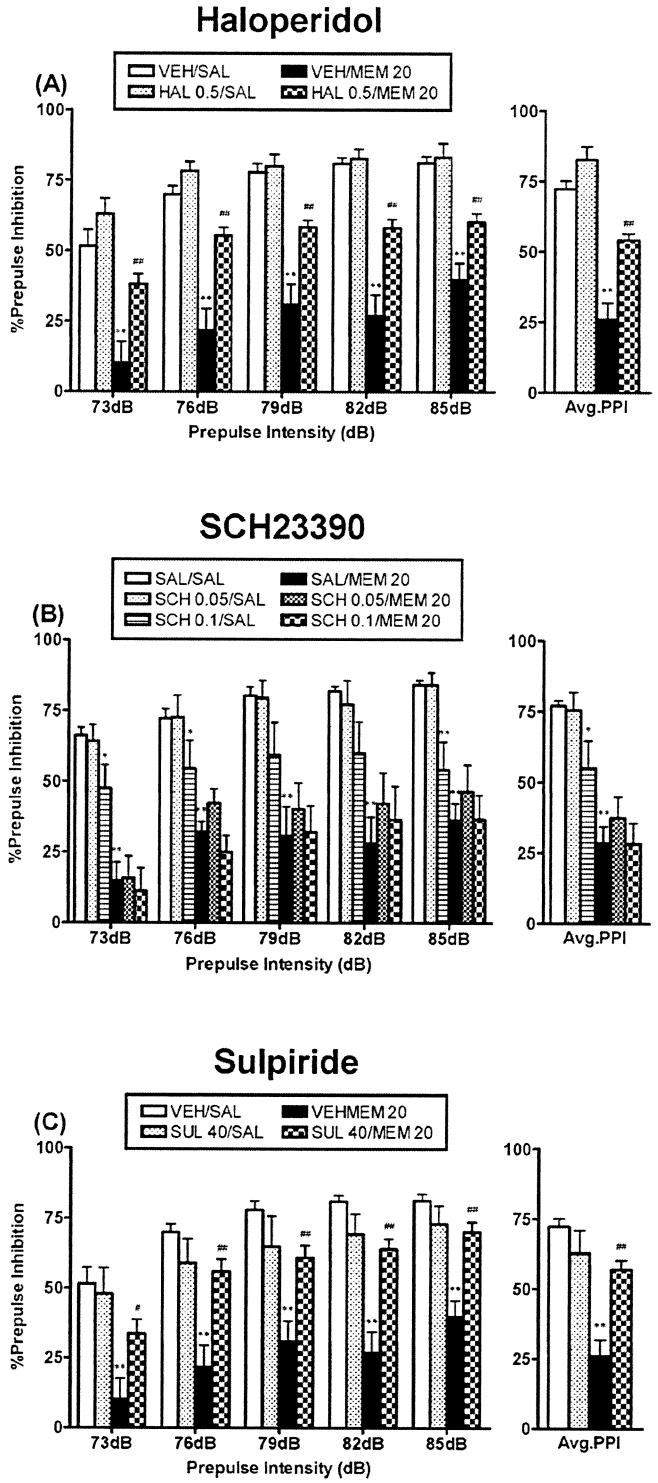


Fig. 5. Effects of haloperidol (A), SCH 23390 (B) and sulpiride (C) on PPI and average PPI in saline- and memantine-treated groups. Each column represents the mean ± SEM. $^{*}P<0.05$, $^{**}P<0.01$ compared to VEH (or SAL)/SAL; $^{\#}P<0.05$, $^{\#\#}P<0.01$ compared to VEH (or SAL)/MEM; $N=12$–16 per group. SAL: saline; MEM: memantine; HAL: haloperidol; SCH: SCH23390; SUL: sulpiride.

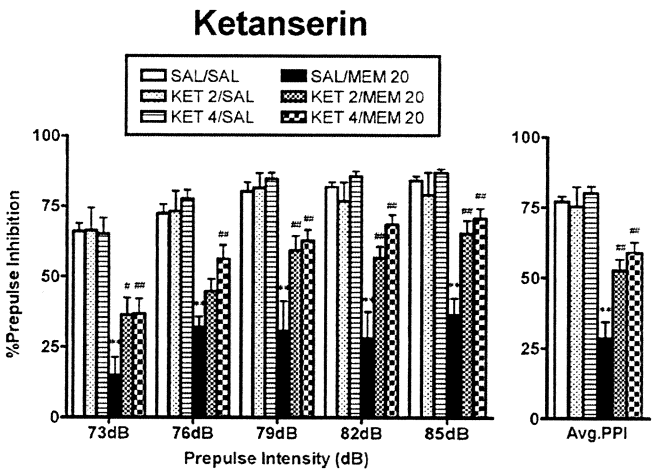


Fig. 6. Effects of ketanserin on PPI and average PPI in saline- and memantine-treated groups. Each column represents the mean ± SEM. $^{*}P<0.05$, $^{**}P<0.01$ compared to SAL/SAL; $^{\#}P<0.05$, $^{\#\#}P<0.01$ compared to SAL/MEM; $N=10$–14 per group. SAL: saline; MEM: memantine; KET: ketanserin.

4. Discussion

Herein, we have shown that memantine significantly increased the acoustic startle response and dose-dependently disrupted PPI in mice for all prepulse intensities tested (Fig. 1A–C). Memantine increased startle response during pulse-alone trials. Increases in startle amplitude have also been previously observed following administration of NMDA receptor antagonists and DA agonists [29,30]. As memantine did not decrease startle amplitude, it is unlikely that the PPI disruption is merely an artifact of a decrease in reactivity. It appears that memantine administration does, in fact, produce disruption of sensorimotor gating. This effect was observed from 30 to 120 min after memantine administration (Fig. 2) and was attenuated by pretreatment with clozapine, risperidone, haloperidol, sulpiride and ketanserin but not SCH23390 (Figs. 4–7). These results suggest that the PPI-disruptive effects of memantine may result from interactions between multiple neurotransmitter systems. The results of the present tests with memantine in mice are consistent with previous reports of memantine-induced PPI disruption in rats [63,70]. We and Wiley et al. [70] demonstrated, in mice and rats, that memantine produced a dose-dependent reduction in PPI using 100 ms prepulse intervals. The findings at 100 ms prepulse intervals are consistent across reports. For example, other NMDA receptor antagonists such as PCP and dizocilpine also reliably disrupt PPI in rodents using by 100 ms prepulse intervals [22,30]. However, memantine is known to have both PPI-increasing and PPI-decreasing effects in rats and humans, using different (short- or long-) prepulse-pulse intervals [63] and, additionally, there is evidence of cross-species differences in the NMDA regulation of PPI [63]. Swerdlow et al. used a range (10–120 ms) of prepulse intervals in naïve rats and normal humans. They showed that, in rats, memantine caused either an increase in PPI at short prepulse intervals (10–20 ms), or a decrease in PPI at long prepulse intervals (120 ms) whereas humans exhibit an increase in PPI [63]. Some researchers also reported that acute treatment of NMDA receptor antagonists such as ketamine [2,14] and amantadine [5,62] in normal humans increases PPI at long prepulse intervals where schizophrenic patients exhibit PPI disruption. Recently, memantine has been studied as an adjunctive treatment for schizophrenia in numerous studies and case reports [23,26,27]. It had significant beneficial effects on their mental status [23,27] whereas it has shown little clinical benefits effects in other studies [26]. Additionally, none of these studies have documented that memantine worsened the psychotic symptoms of schizophrenic patients. These results suggested that memantine may not cause schizophrenia-like symptoms in normal humans or exacerbate psychotic symptoms in schizophrenic patients although memantine dose-dependently produced PPI disruption in rodents

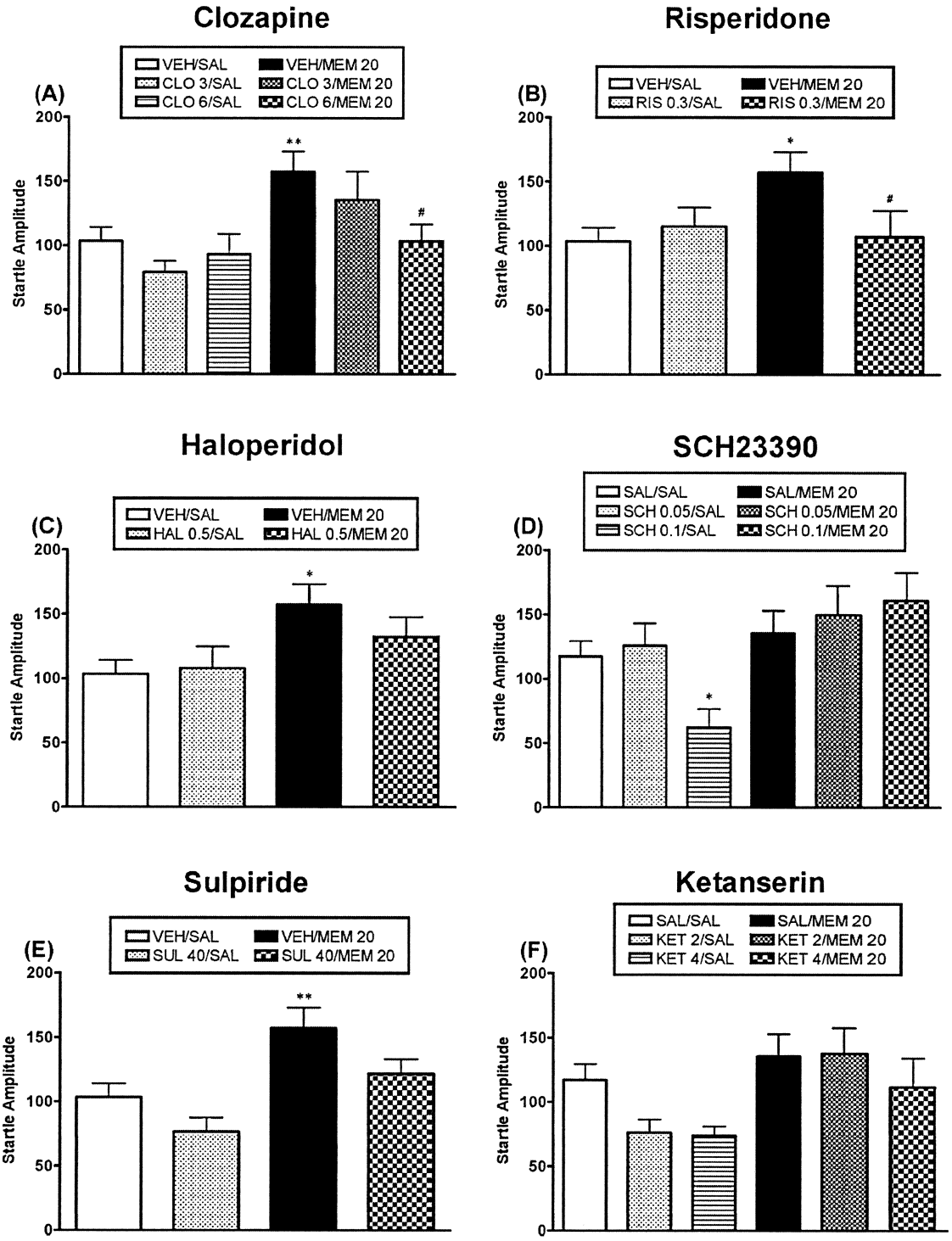


Fig. 7. Effects of clozapine (A), risperidone (B), haloperidol (C), SCH 23390 (D), sulpiride (E) and ketanserin (F) on startle amplitude in saline- and memantine-treated groups. Each column represents the mean ± SEM. $^{*}P < 0.05$, $^{**}P < 0.01$ compared to VEH (or SAL)/SAL; $^{\#}P < 0.05$, $^{\#\#}P < 0.01$ compared to VEH (or SAL)/MEM. SAL: saline; MEM: memantine; CLO: clozapine; RIS: risperidone; HAL: haloperidol; SCH: SCH23390; SUL: sulpiride; KET: ketanserin.

and, conceivably, may worsen the psychotic symptoms of patients such as PDD and LBD [36,50]. However, we think that the effects of chronic memantine administration should be assessed clinically in the future because our present experiments addressed only the effects of acute administration on PPI.

In the present study, it was found that the atypical antipsychotics clozapine and risperidone attenuated the memantine-induced PPI disruption in mice. The atypical antipsychotic clozapine has multipharmacological properties but higher affinity to 5-$HT_{2A/2C}$ receptors over D_2 receptors [49]. It has been reported that PCP-induced PPI disruption was attenuated by pretreatment with clozapine [3]. In addition, risperidone, a high affinity D_2 and 5-HT_{2A} receptor antagonist, has been reported to attenuate dizocilpine-induced PPI disruption [65]. Given the reports cited

above, our results indicate that the DA and 5-HT_{2A} receptors may be predominantly involved in memantine-induced PPI disruption in mice (Fig. 4A and B).

Haloperidol has a much higher affinity for D_2-like receptors than for D_1 receptors [51], and memantine-induced PPI disruption was inhibited by haloperidol (Fig. 5A). In contrast, PPI disruption in rats and mice induced by high-affinity NMDA receptor antagonists PCP and dizocilpine were unaffected by pretreatment with haloperidol [20,22]. This discrepancy may be explained by the action of memantine on the dopaminergic system. Memantine has been shown to increase DA levels in the prefrontal cortex [54] and it is well known that DA receptors in the prefrontal cortex play an important role in PPI. The memantine and amantadine compounds are based on the chemical structure of amino-adamantane derivations. Amantadine also increases DA release by antagonism at NMDA receptors [68]. Swerdlow et al. [61] have shown that 100 mg/kg amantadine produced a moderate disruption of PPI. Our previous report has shown that memantine has a weak MAO (monoamine oxidase) inhibitory effect and inhibits DA reuptake [43]. Interestingly, a previous study reported that PCP and ketamine have direct effects on the DA D_2 receptor [25]. Recently, it has been reported that memantine also has a strong DA D_2 agonist action at rat striatal D_2 receptors [53]. Considering the two studies cited above, it seems that memantine and ketamine have a higher affinity for the D_2 receptor than PCP has. Ketamine is also known to produce schizophrenia-like symptoms in humans [24] and to disrupt PPI [31,59]. Although only partial, these effects of ketamine were attenuated by haloperidol [32]. This previous study is consistent with the memantine results presented herein. These characteristic effects of memantine may explain why haloperidol attenuates memantine-induced PPI disruption. Therefore, we further investigated the involvement of the central dopaminergic system in memantine-induced PPI disruption and investigated the effects of selective D_1 and D_2 antagonists. Memantine-induced PPI disruption was attenuated by pretreatment with the D_2 selective antagonist sulpiride but not by the D_1 selective antagonist SCH23390 (Fig. 5B and C). Several studies have reported the inability of SCH23390 to attenuate PPI disruption induced by dizocilpine and PCP [3,67]. Furthermore, sulpiride and haloperidol reduce dizocilpine-induced hyperlocomotion whereas no effect is observed with SCH23390 [35]. In our previous study, administration of haloperidol inhibited memantine-induced hyperlocomotion [43]. Haloperidol completely attenuated PPI disruption in rodents treated with the DA agonist apomorphine [58]. These results suggest that D_2 receptors, but not D_1 receptors, could be involved in the memantine-induced PPI disruption in mice.

Risperidone has higher affinity (Ki values) for the 5-HT_{2A} receptor than clozapine [51]. Thus, the capacity of ketanserin to attenuate the memantine-induced PPI disruption was investigated. We observed that the memantine-induced PPI disruption was attenuated by the administration of ketanserin (Fig. 6). Some groups have shown that the ability of drugs to attenuate PCP- or dizocilpine-induced PPI disruption is correlated to their affinities for the 5-HT_{2A} receptor [65,72]. The systemic administration of DOI, a 5-HT_{2A} agonist, was reported to disrupt PPI in rats, which in turn was antagonized by the microinfusion of MDL100907, a specific 5-HT_{2A} antagonist [55]. It has been reported that 5-HT_{2A} receptor antagonists reversed PCP-induced hyperlocomotor activity [19,34], head-twitch response (HTR) and head-waving [37,38,73]. In our previous study, i.c.v. administration of memantine did not induce the HTR. However, the 5-HT-induced HTR was potentiated by combined administration of 5-HT and memantine. The enhanced HTR was inhibited by i.p. administration of haloperidol or ketanserin [43]. Previous studies have demonstrated that haloperidol significantly attenuates 5-HT_{2A} agonist DOI-induced HTR in mice [15,69]. It has been reported that haloperidol may act as an antagonist at 5-HT_2 receptors [15,71]. Our previous study has demonstrated that memantine has a weak effect on inhibition of 5-HT reuptake [43]. The 5-HT_{2A} receptors might also contribute to the PPI disruption of memantine in mice. However, ketanserin binding affinity is not only to 5-$HT_{2A/2C}$ receptors but also α receptors. It is reported the memantine-induces an increase in prefrontal cortex noradrenaline levels [54]. Therefore, further studies are needed to investigate the effects of selective 5-HT_{2A} antagonists on memantine-induced PPI disruption in mice.

In summary, the moderate-affinity NMDA receptor antagonist memantine disrupted PPI in naïve mice. These results suggest that involvement of dopaminergic and/or serotonergic neurotransmission may play a crucial role in memantine-induced PPI disruption, and additionally, indicated that blockade of either the D_2 or 5-HT_{2A} receptors may prevent disruption of PPI by memantine. Finally, the effect of memantine treatment to improve cognition in patients with LBD and PDD, has not only the possibility of becoming a remarkable, promising medicine treatment, but also the potential for adverse events because the number of clinical study reports is currently still few. Therefore, future studies into cognition other than AD, such as LBD and PDD, are needed to determine the safety and efficacy of memantine in treatment with these disorders.

Acknowledgements

This study was supported in part by Grants-in-Aid for Scientific Research (20790309) and Matching Fund Subsidy for Private Universities from the Ministry of Education, Culture, Sports, Science and Technology of Japan.

References

[1] Aarsland D, Ballard C, Walker Z, Bostrom F, Alves G, Kossakowski K, et al. Memantine in patients with parkinson's disease dementia or dementia with lewy bodies: a double-blind, placebo-controlled, multicentre trial. Lancet Neurol 2009;7:613–8.
[2] Abel KM, Allin MP, Hemsley DR, Geyer MA. Low dose ketamine increases prepulse inhibition in healthy men. Neuropharmacology 2003;6:729–37.
[3] Bakshi VP, Swerdlow NR, Geyer MA. Clozapine antagonizes phencyclidine-induced deficits in sensorimotor gating of the startle response. J Pharmacol Exp Ther 1994;271:787–94.
[4] Bakshi VP, Geyer MA. Antagonism of phencyclidine-induced deficits in prepulse inhibition by the putative atypical antipsychotic olanzapine. Psychopharmacology (Berl) 1995;122:198–201.
[5] Bitsios P, Giakoumaki SG, Frangou S. The effects of dopamine agonists on prepulse inhibition in healthy men depended on baseline PPI values. Psychopharmacology (Berl) 2005;182:144–52.
[6] Bolino F, Michele V, Di Cicco L, Manna V, Daneluzzo E, Casacchia M. Sensorimotor gating and habituation evoked by electro-cutaneous stimulation in schizophrenia. Biol Psychiatry 1994;36:670–9.
[7] Braff DL, Grillon C, Geyer MA. Gating and habituation of the startle reflex in schizophrenic patients. Arch Gen Psychiatry 1992;49:206–15.
[8] Braff DL. Information processing and attention dysfunctions in schizophrenia. Schizophr Bull 1993;19:233–59.
[9] Braff DL, Geyer MA, Swerdlow NR. Human studies of prepulse inhibition of startle; normal subject, patient groups, and pharmacological studies. Psychopharmacology (Berl) 2001;156:234–58.
[10] Van den Buuse M, Gogos A. Differential effects of antipsychotic drugs on serotonin-1A receptor-mediated disruption of prepulse inhibition. J Pharmacol Exp Ther 2007;320:1224–36.
[11] Bymaster FP, Feleder CC, Tzavara E, Nomikos GG, Calligaro DO, Mckinzie DL. Muscarinic mechanisms of antipsychotic atypicality. Prog Neuropsychopharmacol Biol Psychiatry 2003;27:1125–43.
[12] Depoortere R, Perrault G, Sanger DJ. Potentiation of prepulse inhibition of the startle reflex in rats: pharmacological evaluation of the procedure as a model for detecting antipsychotic activity. Psychopharmacology (Berl) 1997;132:366–74.
[13] Dong H, Yuede CM, Coughlan C, Csernansky JG. Effects of memantine on neuronal structure and conditioned fear in the Tg2576 mouse model of Alzheimer's disease. Neuropsychopharmacology 2008;33:3226–36.
[14] Duncan EJ, Madonick SH, Parwani A, Angrist B, Rajan R, Chakravorty S, et al. Clinical and sensorimotor gating effects of ketamine in normals. Neuropsychopharmacology 2001;1:72–83.
[15] Dursun SM, Handley SL. Similarities in the pharmacology of spontaneous and DOI-induced head-shakes suggests 5HT2A receptors are active under physiological conditions. Psychopharmacology (Berl) 1996;128:198–205.
[16] Emre M, Tsolaki M, Bonuccelli U, Destee A, Tolosa E, Kutzelnigg A, et al. Memantine for patients with parkinson's disease dementia or dementia with lewy

bodies: a randomized, double-blind, placebo-controlled trial. Lancet Neurol 2010;10:969–77.
[17] Fox CG, Umoh G, Samuel M, Barbara B, Nil M. Memantine in parkinson's disease dementia: clinical experience. Mov Disord 2005;20:P418.
[18] Geyer MA, Mcllwain KL, Paylor R. Mouse genetic models for prepulse inhibition: an early review. Mol Psychiatry 2002;7:1039–53.
[19] Gleason SD, Shannon HE. Blockade of phencyclidine-induced hyperlocomotion by olanzapine, clozapine and serotonin receptor subtype selective antagonists in mice. Psychopharmacology (Berl) 1997;129:79–84.
[20] Hoffman DC, Donovan H, Cassella JV. The effects of haloperidol and clozapine on disruption of sensorimotor gating induced by the noncompetitive glutamate antagonist MK-801. Psychopharmacology (Berl) 1993;111:339–44.
[21] Hoffman DC, Donovan H. D1 and D2 dopamine receptor antagonists reverse prepulse inhibition deficits in an animal model of schizophrenia. Psychopharmacology (Berl) 1994;115:447–53.
[22] Keith VA, Mansbach RS, Geyer MA. Failure to haloperidol to block the effects of phencyclidine and dizocilpine on prepulse inhibition of startle. Biol Psychiarty 1991;30:557–66.
[23] Krivoy A, Weizman A, Laor L, Hellinger N, Zemishlany Z, Fischel T. Addition of memantine to antipsychotic treatment in schizophrenia inpatients with residual symptoms: a preliminary study. Eur Neuropsychopharmacol 2008;2:117–21.
[24] Krystal JH, Karper LP, Freeman GK, Delaney R, Bremmer JD, Heninger GR, et al. Subanesthetic effects of the noncompetitive NMDA antagonist, ketamine, in humans. Psychomimetic, perceptual, cognitive, and neuroendocrine responses. Arch Gen Psychiatry 1994;51:199–214.
[25] Kupar S, Seeman P. NMDA receptor antagonists ketamine and PCP have direct effects on the dopamine D2 and serotonin 5-HT2 receptors implications for models of schizophrenia. Mol Psychiatry 2002;7:837–44.
[26] Lieberman JA, Papadakis K, Csernansky J, Litman R, Volavka J, Jia XD, et al. A randomized, placebo-controlled study of memantine as adjunctive treatment in patients with schizophrenia. Neuropsychopharmacology 2009;34:1322–9.
[27] de Lucena D, Fernandes BS, Berk M, Dodd S, Medeiros DW, Pedrini M, et al. Improvement of negative and positive symptoms in treatment-refractory schizophrenia: a double-blind, randomized, placebo-controlled trial with memantine as add-on therapy to clozapine. J Clin Psychiatry 2009;10:1416–23.
[28] Mcshane R, Areosa Sastre A, Minakaran N. Memantine for dementia. Cochrane Database Syst Rev 2006;CD003154.
[29] Mansbach RS, Geyer MA, Braff DL. Dopaminergic stimulation disrupts sensorimotor gating in the rat. Psychopharmacology (Berl) 1988;94:507–14.
[30] Mansbach RS, Geyer MA. Effects of phencyclidine and phencyclidine biologs on sensorimotor gating in the rat. Neuropsychopharmacology 1998;2:299–308.
[31] Mansbach RS, Geyer MA. Parametric determinations in pre-stimulus modification of acoustic startle: interaction with ketamine. Psychopharmacology (Berl) 1991;105:162–8.
[32] Manbach RS, Carver J, Zorn SH. Blockade of drug-induced deficits in prepulse inhibition of acoustic startle by ziprasidone. Pharmacol Biochem Behav 2001;69:535–42.
[33] Martinez ZA, Oostwegel J, Geyer MA, Ellison GD, Swerdlow NR. 'Early' and 'late' effects of sustained haloperidol on apomorphine- and phencyclidine-induced sensorimotor gating deficits. Neuropsychopharmacology 2000;23:513–27.
[34] Maurel RS, Bervoets K, Millan MJ. Blockade of phencyclidine-induced hyperlocomotion by clozapine and MDL100,907 in rats reflects antagonism of 5-HT2A receptors. Eur J Pharmacol 1995;280:R9–11.
[35] Mele A, Castellano C, Felici A, Cabib S, Caccia S, Oliverio A. Dopamine-N-methyl-D-aspartate interactions in the modulation of locomotor activity and memory consolidation in mice. Eur J Pharmacol 1996;308:1–12.
[36] Menendez-Gonzalez M, Calatayud MT, Blazquez-Menes B. Exacerbation of lewy bodies dementia due to memantine. J Alzheimers Dis 2005;8:289–91.
[37] Nabeshima T, Yamaguchi K, Hiramatsu M, Amano M, Furukawa H, Kameyama T. Serotonergic involvement in phencyclidine-induced behaviors. Pharmacol Biochem Behav 1984;21:401–8.
[38] Nabeshima T, Ishibashi K, Yamaguchi K, Furukawa H, Kameyama T. Phencyclidine-induced head-twitch response as 5-HT2 receptor-mediated behavior in rats. Neurosci Lett 1987;76:335–8.
[39] Nakagawasai O, Onogi H, Mitazaki S, Sato A, Watanabe K, Saito H, et al. Behavioral and neurochemical characterization of mice deficient in the N-type Ca(2+) channel alpha(1B) subunit. Behav Brain Res 2010;208:224–30.
[40] Noda Y, Yamada K, Furukawa H, Nabeshima T. Enhancement of immobility in a forced swimming test by subacute or repeated treatment with phencyclidine: a new model of schizophrenia. Br J Pharmacol 1995;116:2531–7.
[41] Noda Y, Kamei H, Mamiya T, Furukawa H, Nabeshima T. Repeated phencyclidine treatment induces negative symptom-like behavior in forced swimming test in mice: imbalance of prefrontal serotonergic and dopaminergic functions. Neuropsychopharmacology 2000;23:375–87.
[42] Nuechterlein KH, Dawson ME, Green MF. Information-processing abnormalities as neuropsychological vulnerability indicators for schizophrenia. Acta Psychiatr Scand Suppl 1994;384:71–9.
[43] Onogi H, Ishigaki S, Nakagawasai O, Arai-Kato Y, Arai Y, Watanabe H, et al. Influence of memantine on brain monoaminergic neurotransmission parameters in mice: neurochemical and behavioral study. Biol Pharm Bull 2009;32:850–5.
[44] Parsons CG, Stoffler A, Danysz W. Memantine: a NMDA receptor antagonist that improves memory by restoration of homeostasis in the glutamatergic system-too little activation is bad, too much is even worse. Neuropharmacology 2007;53:699–723.
[45] Peeters M, Maloteaux JM, Hermans E. Distinct effects of amantadine and memantine on dopaminergic transmission in the rat striatum. Neurosci Lett 2003;343:205–9.
[46] Perriol MP, Dujardin K, Derambure P, Marcq A, Bourriez JL, Laureau E, et al. Disturbance of sensory filtering in dementia with lewy bodies: comparison with parkinson's disease dementia and alzheimer's disease. J Neurol Neurosurg Psychiatry 2005;76:106–8.
[47] Perry W, Braff DL. Information-processing deficits and thought disorder in schizophrenia. Am J Psychiatry 1994;151:363–7.
[48] Reisberg B, Doody R, Stoffler A, Schmitt F, Ferris S, Mobius HJ. Memantine in moderate-to-severe Alzheimer's disease. N Engl Med 2003;348:1333–41.
[49] Richelson E, Sounder T. Binding of antipsychotic drugs to human brain receptors focus on newer generation compounds. Life Sci 2000;68:29–39.
[50] Ridha BH, Josephs KA, Rossor MN. Delusions and hallucinations in dementia with Lewy bodies: worsening with memantine. Neurology 2005;65:481–2.
[51] Roth BL, Sheffler DJ, Kroeze WK. Magic shotguns versus magic bullets: selectively non-selective drugs for mood disorders and schizophrenia. Nat Rev Drug Discov 2004;3:353–9.
[52] Sabbagh M, Hake A, Ahmed S, Farlow M. The use of memantine in dementia with lewy bodies. J Alzheimers Dis 2005;7:285–9.
[53] Seeman P, Caruso C, Lasaga M. Memantine agonist action at dopamine D2High receptors. Synapse 2008;62:149–53.
[54] Shearman E, Rossi S, Szasz B, Juranyi Z, Fallon S, Pomara N, et al. Changes in cerebral neurotransmitters and metabolites induced by acute donepezil and memantine administrations: a microdialysis study. Brain Res Bull 2006;69:204–13.
[55] Sipes TA, Geyer MA. DOI disrupts prepulse inhibition of startle in rats via 5-HT2A receptors in the ventral pallidum. Brain Res 1997;761:97–104.
[56] Swerdlow NR, Geyer MA. Clozapine and haloperidol in an animal model of sensorimotor gating deficits in schizophrenia. Pharmacol Biochem Behav 1993;44:741–4.
[57] Swerdlow NR, Braff DL, Taaid N, Geyer MA. Assesing the validity of an animal model of deficit sensorimotor gating in schizophrenic patients. Arch Gen Psychiatry 1994;51:139–54.
[58] Swerdlow NR, Bakshi V, Geyer MA. Seroquel restores sensorimotor gating in phencyclidine-treated rats. J Pharmacol Exp Ther 1996;279:1290–9.
[59] Swerdlow NR, Bakshi V, Geyer MA. Seroquel, clozapine and chlorpromazine restore sensorimotor gating in ketamine-treated rats. Psychophamacology (Berl) 1998;140:75–80.
[60] Swerdlow NR, Geyer MA. Using an animal model of deficient sensorimotor gating to study the pathophysiology and new treatments of schizophrenia. Schizophr Bull 1998;24:285–301.
[61] Swerdlow NR, Taaid N, Oostwegel JL, Randolph E, Geyer MA. Towards a cross-species pharmacology of sensorimotor gating: effects of amantadine, bromocriptine, pergolide and ropinirole on prepulse inhibition of acoustic startle in rats. Behav Pharmacol 1998;9:389–96.
[62] Swerdlow NR, Stephany N, Shoemaker JM, Ross L, Wasserman LC, Talledo J, et al. Effects of amantadine and bromocriptine on startle and sensorimotor gating: parametric studies and cross-species comparisons. Psychopharmacology (Berl) 2002;164:82–92.
[63] Swerdlow NR, Van Bergeijk DP, Bergsma F, Weber E, Talledo J. The effects of memantine on prepulse inhibition. Neuropsychopharmacology 2009;34:1854–64.
[64] Tariot PN, Farlow MR, Grossberg GT, Graham SM, McDonald S, Gergel I. Memantine treatment in patients with moderate to severe Alzheimer disease already receiving donepezil: a randomized controlled trial. JAMA 2004;291:317–24.
[65] Varty GB, Higgins GA. Reversal of dizocilpine-induced disruption of prepulse inhibition of acoustic startle response by the 5-HT2 receptor antagonist ketanserin. Eur J Pharmacol 1995;287:201–5.
[66] Varty GB, Walters N, Cohen-Williams M, Carey GJ. Comparison of apomorphine, amphetamine and dizocilpine disruption of prepulse inhibiton in inbred and outbred mice strains. Eur J Pharmacol 2001;424:27–36.
[67] Wedzony K, Golembiowska K, Zazuka M. Differential effects of CGP 37849 and MK-801, competitive and noncompetitive NMDA antagonists, with respect to the modulation of sensorimotor gating and dopamine outflow in the prefrontal cortex of rats. Naunyn Schmiedebergs Arch Pharmacol 1994;350:555–62.
[68] Weseman W, Ekkna O. Effect of 1-aminoadamantanes on the MAO activity in brain, liver, and kidney of the rat. Arzneimittelforschung 1982;32:1241–3.
[69] Wettstein JG, Host M, Hiychcock JM. Selectivity of action of typical and atypical anti-psychotic drugs as antagonists of the behavioral effects of 1-[2,5-dimethoxy-4-iodophenyl]-2-aminopropane (DOI). Prog Neuropsychopharmacol Biol Psychiatry 1999;23:533–44.
[70] Wiley JL, Harvey SA, Balster RL, Nicholson KL. Affinity and specificity of N-methyl-D-aspartate channel blockers affect their ability to disrupt prepulse inhibition of acoustic startle in rats. Psychopharmacology (Berl) 2003;165:378–85.
[71] Yamada J, Sugimoto Y, Horisaka K, Serotonin2. (5-HT2) receptor agonist 1-(2, 5-dimethoxy-4-iodophenyl)-2-aminopropane (DOI) inhibits chlorpromazine- and haloperidol-induced hypothermia in mice. Biol Pharm Bull 1995;18:1580–3.
[72] Yamada S, Harano M, Annoh N, Nakamura K, Tanaka M. Involvement of serotonin 2A receptors in phencyclidine-induced disruption of prepulse inhibition of acoustic startle in rats. Biol Psychiatry 1999;46:832–8.
[73] Yamaguchi K, Nabeshima T, Ishibashi K, Yoshida S, Kameyama T. Phencyclidine-induced head-twitch through interaction with 5-HT1 and 5-HT2 receptors in reserpinized rats. Neuropharmacology 1987;26:1489–97.

Journal of
Medicinal
Chemistry
Article

J. Med. Chem. **2010**, *53*, 4917–4926 **4917**
DOI: 10.1021/jm100316f

Design and Synthesis of Androgen Receptor Full Antagonists Bearing a *p*-Carborane Cage: Promising Ligands for Anti-Androgen Withdrawal Syndrome

Tokuhito Goto,[†] Kiminori Ohta,[†] Shinya Fujii,[‡] Shigeru Ohta,[§] and Yasuyuki Endo*[,†]

[†]*Faculty of Pharmaceutical Sciences, Tohoku Pharmaceutical University, 4-4-1, Komatsushima, Aoba-ku, Sendai 981-8558, Japan,* [‡]*School of Medical Science, Institute of Biomaterials and Bioengineering, Tokyo Medical and Dental University, 2-3-10, Kanda-Surugadai, Chiyoda-ku, Tokyo 101-0062, Japan, and* [§]*Graduate School of Medical Sciences, Hiroshima University, 1-2-3 Kasumi, Minami-ku, Hiroshima 734-8551, Japan*

Received March 10, 2010

Pure androgen receptor (AR) full antagonists are candidates to treat anti-androgen refractory prostate cancers. We previously developed a carborane-containing AR antagonist, 3-(12-hydroxymethyl-1,12-dicarba-*closo*-dodecaborane-1-yl)benzonitrile (BA341), which was more potent than hydroxyflutamide (**4**) but acted as an agonist toward LNCaP prostate cancer cells expressing T877A AR mutant. Here, we designed and synthesized novel AR full antagonists structurally based upon the clinically used AR full antagonist (*R*)-bicalutamide (**5**) to test our hypothesis that the carborane cage is suitable as a hydrophobic pharmacophore for AR ligands. Compounds **7b** and **8b** showed good biological profiles in AR binding and transactivation assays and dose-dependently inhibited the testosterone-induced proliferation of LNCaP cells, as well as SC-3 cells. The IC_{50} values of compounds **7b** and **8b** were 3.8×10^{-7} and 4.2×10^{-7} M, respectively [**5**, 8.7×10^{-7} M]. Since compounds **7b** and **8b** did not show any agonistic activity in functional assays, they seem to be pure AR full antagonists and are therefore candidates for treatment of anti-androgen withdrawal syndrome.

Introduction

Androgens play a key role of the development and maintenance of the male reproductive system.[1] A native androgen, testosterone (**1**), or its more potent tissue metabolite dihydrotestosterone (DHT,[a] **2**), binds to androgen receptor (AR), which is a member of the nuclear receptor superfamily, and mediates specific gene transcriptions.[2] Synthetic AR modulators can be structurally classified as either steroidal or nonsteroidal and may have various functional (androgenic, antiandrogenic, or anabolic) activities.[3] A nonsteroidal ligand, flutamide (**3**),[4] which is metabolized to the more potent AR antagonist hydroxyflutamide (**4**),[5] is a well-known AR antagonist used for the treatment of prostate cancer. On the other hand, (*R*)-bicalutamide (**5**) is used for the treatment of D2 stage metastatic prostate cancer.[6] These typical nonsteroidal AR antagonists have high selectivity for AR, in contrast to steroidal ligands (Figure 1).

Ligands containing a nitro or cyano group can form a direct hydrogen bond with R752 of the human AR ligand-binding domain (hAR-LBD)[7] and can also hydrogen-bond to Q711 and M745 via one H_2O molecule.[7] An X-ray cocrystal structure analysis of the complex of hAR-LBD with **2** indicated that the secondary alcohol group of **2** is hydrogen-bonded to T877.[8] The hydrophobic moiety of the ligand should possess sufficient affinity for the hydrophobic surface of the AR in order to increase the binding affinity. The hydrophobic structure also plays a role as a scaffold, fixing the spatial positions of hydrogen-bonding functional groups.

AR antagonists, that is to say anti-androgens, are particularly useful for the treatment of prostate cancer during its early stages.[9] However, prostate cancer often advances to a hormone-refractory state in which the disease progresses despite continued androgen ablation or anti-androgen therapy, owing to the appearance of androgen-independent prostate cancer cells or the ability of adrenal androgens to support tumor growth.[10] Instances of anti-androgen withdrawal syndrome, i.e., where withdrawal of antiandrogen therapy results in clinical improvement, have also been reported after prolonged treatment with anti-androgens.[11] Thus, development of pure AR full antagonists is one of the goals of drug discovery for AR. Although the molecular mechanism is not fully understood, one hypothesis is that mutation of AR occurs.[12] Indeed, such mutation has been found in patients treated with **3**.[13] AR mutations that result in receptor promiscuity and the ability of anti-androgens to exhibit agonist activity might at least partially account for this phenomenon. In particular, T877 point mutation has been found in the AR LBD in anti-androgen withdrawal syndrome patients and has been considered as a hotspot for the critical pathology.[14] Compound **5**, which is the most widely used pure anti-androgen, acts as an anti-androgen for T877A mutant AR but exhibits significant androgenic activity toward W741L or W741C point mutated AR; this is known as bicalutamide withdrawal syndrome.[15] Therefore, it is of interest to develop a new generation of pure anti-androgens that would work with both wild-type and mutant ARs.

Carborane (dicarba-*closo*-dodecaborane, $C_2B_{10}H_{12}$) is an icosahedral boron cluster, has a bulky spherical structure,

*To whom correspondence should be addressed. Phone: +81-22-234-4181. Fax: +81-22-275-2013. E-mail: yendo@tohoku-pharm.ac.jp.

[a] Abbreviations: DHT, dihydrotestosterone; AR, androgen receptor; LBD, ligand binding domain; NaH, sodium hydride; K_2CO_3, potassium carbonate; *m*CPBA, *m*-chloroperbenzoic acid; [^{3}H]DHT, [1,2-^{3}H]-dihydrotestosterone; SO_2, sulfone; SARM, selective androgen receptor modulator.

© 2010 American Chemical Society

Published on Web 06/03/2010

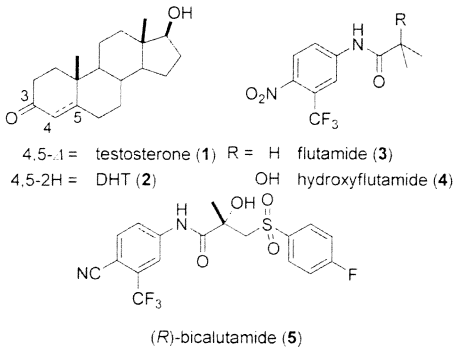


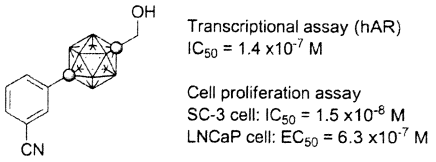
Figure 1. Structures of native and synthetic ligands for AR.

exhibits remarkable thermal stability, and has high hydrophobicity.[16] Carborane-containing ligands are of interest in medicinal chemistry, since they have a different spectrum of ligand responsiveness from other therapeutic agents owing to their unique chemical and structural features.[17] We have reported the development of bioactive molecules, including estrogen receptor modulators,[18] retinoic acid receptor modulators,[19] and retinoid X receptor antagonists,[20] that contain a carborane cage as a hydrophobic pharmacophore, and we have obtained several promising drug candidates. We also developed a carborane-containing AR antagonist, 3-(12-hydroxymethyl-1,12-dicarba-*closo*-dodecaborane-1-yl)benzonitrile (BA341, **6**),[21] which shows more potent AR-binding and AR-antagonistic activity than **4** and its analogues.[22] Our strategy for the development of novel anti-androgens is direct control of helix-12 by using steric repulsion between the bulky carborane cage and several amino acid residues, mainly M895 and F876, in the hydrophobic pocket of the hAR-LBD. In the present work, we first evaluated the biological potential of **6** focusing on its cell proliferation−inhibitory activity toward LNCaP cells, which express the point-mutated receptor, T877A AR. Unfortunately, compound **6** acted as an agonist, showing an EC_{50} value of 6.3×10^{-7} M in a LNCaP cell proliferation assay (Figure 2).

Thus, we next focused upon the development of novel AR full antagonists and designed novel pure anti-androgen candidates **7**−**10** based upon the structure of **5** with a carborane moiety as a hydrophobic pharmacophore (Figure 3). The designed molecules consisted of a linker part X and two aromatic rings A and B, of which ring A is fixed as a 3-cyanophenyl group and ring B contains various substituents at the para position to the linker group. In addition, compound **7g** containing two *p*-carborane cages was also designed to examine whether or not a carborane cage could replace ring B (Figure 3). In this paper, we describe the synthesis of these designed molecules and their biological activities, i.e., AR binding, AR transcriptional activation, and effect on AR-dependent proliferation of SC-3 and LNCaP cells, as well as the structure−activity relationships at the linker X and the B ring for AR full antagonistic activity.

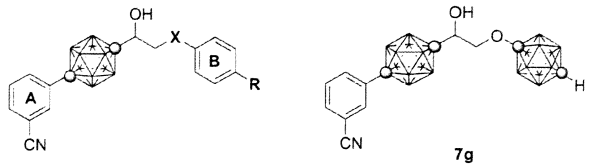
Chemistry

To obtain the designed molecules, we devised an effective synthetic strategy of compounds **7**−**10**. The outline and key intermediate are summarized in Scheme 1. An epoxide **11** is a suitable intermediate for synthesis of the target molecules because the oxirane ring of **11** is availabe for a nucleophilic



6 (BA341)

Figure 2. Structure and biological activities of **6**.



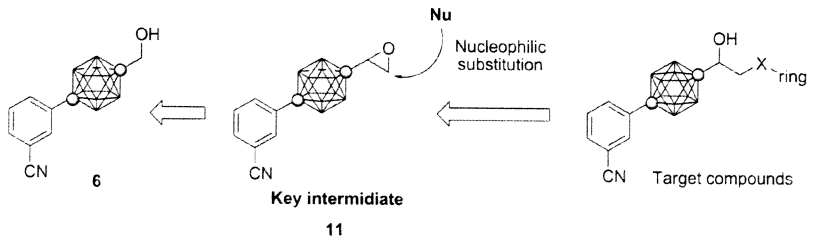
7g

Compound	X	R
7a	O	H
7b		F
7c		OCH_3
7d		$NHCOCH_3$
7e		NO_2
7f		Br
8a	S	H
8b		F
8c		OCH_3
8d		$NHCOCH_3$
8e		CF_3
9a	SO_2	H
9b		F
9c		OCH_3
9d		$NHCOCH_3$
9e		CF_3
10	NH	H

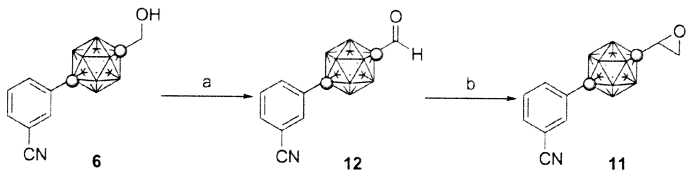
Figure 3. Pure AR antagonist candidates with a *p*-carborane cage as the hydrophobic pharmacophore.

substitution reaction. In addition, compound **11** can be obtained by oxidation reaction of the primary hydroxyl group of **6**, followed by transformation to the epoxide.[21] Therefore, we attempted to synthesize the key intermediate **11** using **6** as a starting material (Scheme 2). The primary hydroxyl group of **6** was oxidized to aldehyde with Dess−Martin periodinate to afford the corresponding compound **12** in 91% yield.[23] We tried to prepare compound **11** by means of Corey−Chaykovsky reaction, which is a good method for the transformation of aldehyde to epoxide.[24] However, the reaction of **12** with trimethylsulfonium iodide in the presence of sodium hydride (NaH) as a base did not give the desired compound **11** but provided the deformylated compound as the main product. Finally, the key intermediate **11** was prepared by the reaction of **12** with zinc carbenoid, which was prepared from diethylzinc and chloroiodomethane in the presence of tetrahydrothiophene, in 71% yield.[25] The general method employed for preparation of the designed compounds **7**−**10** is illustrated in Scheme 3. Nucleophilic attack of several phenols and *p*-carboranol on the oxirane ring of **11** in the presence of potassium carbonate (K_2CO_3) gave the desired molecules **7a**−**g** in 30−90% yields. The key intermediate **11** was reacted with various thiophenols in the presence of NaH to give the corresponding thioether derivatives **8a**−**e** in 67−77% yields, which were easily transformed into the corresponding sulfone derivatives **9a**−**e** by oxidation of the sulfide group with *m*-chloroperbenzoic acid (*m*CPBA) in 75% quantitative yields. The reaction of aniline with **11**

Scheme 1. Synthetic Strategy for Target Compounds

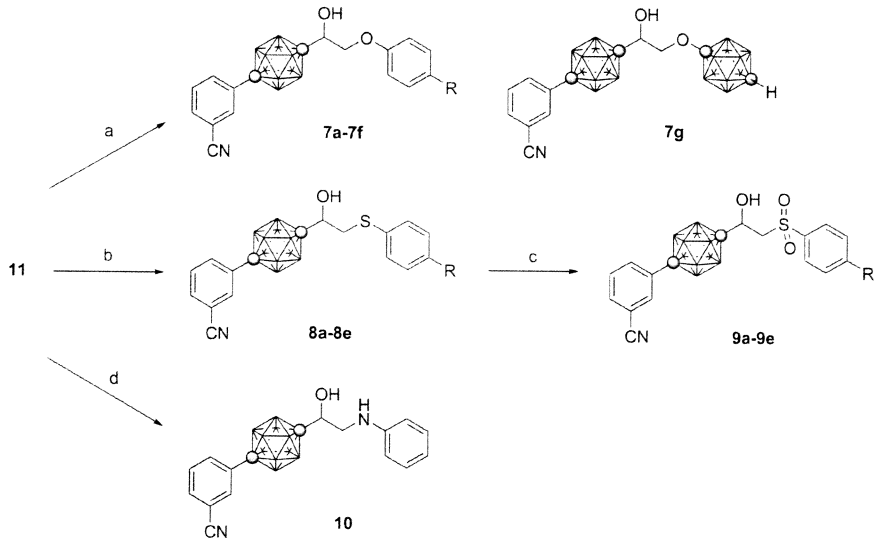


Scheme 2. Synthesis of the Key Intermediate **11**[a]



[a] Reagents and conditions: (a) Dess–Martin periodinate, CH_2Cl_2, 91%; (b) Et_2Zn, $ClCH_2I$, tetrahydrothiophene, CH_2Cl_2, 71%.

Scheme 3. Synthesis of the Designed Compounds **7**–**10**[a]



[a] Reagents and conditions: (a) phenols or *p*-carboranol, K_2CO_3, 2-propanol, 30–90%; (b) thiophenols, NaH, THF, 67–77%; (c) *m*CPBA, CH_2Cl_2, 75% quant; (d) aniline, methanol, 65%.

gave the corresponding derivative **10** in 65% yield. Compounds **7**–**10** all have an asymmetric carbon bearing a secondary alcohol and were used for biological assays in racemic form.

Binding Assay and Biological Studies

The binding affinity of the new carborane-containing compounds for AR was evaluated by means of competitive binding assay using [1,2-^{3}H]dihydrotestosterone ([^{3}H]DHT) and hAR.[26] Table 1 summarizes the binding affinity data of the synthesized compounds. The values indicate the percent displacement of specific [^{3}H]DHT binding to hAR by each compound at 10 μM. The binding of the synthesized compounds to AR is influenced more by the substituents on the B ring than by the linking group X. Compounds bearing phenyl, *p*-fluorophenyl, and *p*-methoxyphenyl rings at the position of the B ring, **7a**–**c**, **8a**–**c**, and **9a**–**c**, showed moderate binding affinity (40–60% displacement of [^{3}H]DHT), regardless of the chemical properties of the linking group. The *p*-bromophenyl derivative, **7f**, also has moderate binding affinity. Compounds **7d** and **8d** containing an acetamide group on the B ring exhibited potent binding affinity for AR (84% and 80% displacement, respectively), although they are less potent than **5** and **6**. On the other hand, another acetamide-containing compound **9d** with a sulfone (SO_2) linker showed very weak binding affinity for AR (12% displacement) despite containing the acetamide group on the B ring. Either the SO_2 linking group or the acetamide group of **9d** seems to work negatively for binding to AR. Compounds **7e**, **8e**, and **9e** bearing a nitro or a trifluoromethyl group on the B ring showed weak binding affinity for AR (around 20% displacement). Introduction of a *p*-carborane cage at the position of the B ring in place of a benzene ring led to a marked decrease of AR-binding affinity, suggesting that the *p*-carborane cage is too bulky to be accommodated at that position in the AR LBD (Table 1, **7g**). Compound **10**, with an amino

Table 1. Binding Affinity of Compounds **7**–**10** versus Specific [1,2-^{3}H]DHT (4 nM) Binding with hAR and Inhibition Percentages of Transactivation Induced by **2**

compd	X	R	binding affinity[a] displacement (%)	transactivation[b] inhibition (%)
7a	O	H	52	37
7b		F	60	51
7c		OCH_3	46	42
7d		$NHCOCH_3$	84	65
7e		NO_2	17	19
7f		Br	46	21
7g			3	nt[c]
8a	S	H	47	27
8b		F	51	38
8c		OCH_3	40	48
8d		$NHCOCH_3$	80	67
8e		CF_3	22	19
9a	SO_2	H	63	54
9b		F	54	23
9c		OCH3	47	19
9d		$NHCOCH_3$	12	44
9e		CF_3	26	21
10	NH	H	32	20
3			12	62
5			90	nt[c]
6			95	88

[a] Values are percentage displacement of [^{3}H]DHT (4 nM) specific binding to hAR by each compound at 10 μM, and the relative binding affinity of **2** is taken as 100. All binding assays were performed in duplicate experiments (n = 2), and the average value is indicated as the binding affinity. [b] NIH3T3 cells were transiently transfected with hAR-expression plasmid, ARE/Luci (firefly luciferase) and pRL/CMV (*Renilla* luciferase) plasmids and were treated with the test compounds at 1 μM in the presence of 0.1 nM **2**. All transactivation assays were performed in triplicate (n = 3). [c] nt indicates not tested.

group as a linker, exhibited a weaker AR-binding affinity than **7a**, **8a**, and **9a** with different linking groups. All the evaluated compounds **7**–**9**, except for the acetamide-containing compounds **7b**, **8b**, and **9b**, exhibited similar structure–activity relationships for the substituents on the B ring, regardless of the chemical and electronic properties of the linking groups. Electronic properties, such as electron-donating or -withdrawing character, of the substituents on the B ring also had no effect on the AR-binding affinity so that a change of electron density on the B ring is not important for the AR-ligand binding. Thus, the main driving forces for the receptor–ligand binding appear to be the formation of hydrogen bonds and van der Waals interactions between the substituents on the B ring, as well as the basic structure of **6**, and amino acid residues of the AR LBD.

The functional activities, agonist or antagonist, of the synthesized compounds were evaluated by means of transient transcriptional assay using NIH3T3 cells co-transfected with hAR expression plasmid, ARE/Luci (firefly luciferase) and pRL/CMV (*Renilla* luciferase) plasmids.[27] All the test compounds dose-dependently inhibited the transcriptional activation in the presence of 0.1 nM **2**. None of the synthesized compounds exhibited androgen agonistic activity. Table 1 summarizes the transactivation data for the synthesized compounds. The values indicate the percent inhibition of 0.1 nM **2**-induced transcriptional activation by each compound at 1 μM. Compounds **7a**–**c**, **8a**–**c**, and **9a** showed moderate AR-antagonistic activity, and the results correlated well with those of binding assay. On the other hand, compounds **7f**, **9b**, and **9c** inhibited **2**-induced AR transactivation by only around 20%, in spite of showing moderate binding to AR. Introductions of a trifluoromethyl group and a nitro group on the B ring and an amino group as a linking group led to a remarkable decrease of the activity, as observed in the results of binding assay (Table 1; **7e**, **8e**, **9e**, and **10**). The high-affinity AR-binding compounds **7d** and **8d** with the acetamide group on the B ring exhibited potent transactivation inhibitory activity (65% and 67%, respectively), being as potent as **3** but less potent than **6**. Unexpectedly, compound **9d**, with weak AR-binding affinity, exhibited moderate AR-antagonistic activity. This kind of biological profile is also observed with the clinically used AR antagonist **3**. These results appear to correlate well with those of binding assay. Among the test compounds, **7a**–**d**, **8a**–**d**, **9a**, and **9d** showed promising biological profiles, and their IC_{50} values were estimated from dose–response curves obtained in this assay (Table 2). The IC_{50} values of **7d**, **8d**, and **9a** were lower than those of the other test compounds (0.80, 0.87, and 0.84 μM, respectively) but are still around 6 times higher than that of the parent AR antagonist **6**.

Table 2. IC_{50} Values of Selected Compounds in AR Transactivation Assay

compd	IC_{50} (M)[a]
7a	2.3×10^{-6}
7b	1.3×10^{-6}
7c	1.0×10^{-6}
7d	8.0×10^{-7}
8a	2.5×10^{-6}
8b	1.3×10^{-6}
8c	1.6×10^{-6}
8d	8.7×10^{-7}
9a	8.4×10^{-7}
9d	1.1×10^{-6}
6	1.4×10^{-7}

[a] NIH3T3 cells were treated with test compounds (1×10^{-8} to 1×10^{-5} M) in the presence of 0.1 nM **2**. All transactivation assays were performed in triplicate (n = 3). IC_{50} values of the test compounds were estimated from the sigmoidal dose–response curves using GraphPad Prism 4 software.

Next, the effects of selected compounds on proliferation of SC-3 and LNCaP cells, which show androgen-dependent growth, were evaluated.[28] Human prostate cancer LNCaP cells express T877A point-mutated AR, toward which compound **4** shows androgenic action, and the evaluation of LNCaP cell proliferation–inhibitory activity is absolutely imperative for the development of pure AR full antagonists and anti-androgen withdrawal syndrome therapeutic agents. The anti-androgenic activity of the selected compounds is summarized in Table 3. In the evaluation using SC-3 cells, none of the test compounds showed growth-promoting activity, suggesting that none was an androgen agonist. All the test compounds, except for **7g**, dose-dependently inhibited SC-3 cell proliferation induced by 1 nM testosterone in the concentration range of 1 nM to 10 μM, although their IC_{50} values are higher than those of **6** and **4**, which showed potent cell growth-inhibitory activity with IC_{50} values of 15 and 24 nM, respectively. Compounds **8d** and **9d** showed similar IC_{50} values, 0.17 and 0.16 μM, to that of **5**, 0.14 μM.

The biological activity of these compounds toward LNCaP cells was examined in terms of the ability to induce cell proliferation alone or to inhibit cell proliferation induced by 1 nM testosterone. As shown in Table 3, compounds **3** and **4** induced cell proliferation alone, as did compound **6**, and did not show antagonistic activity, as expected. In contrast, a clinically used AR full antagonist, **5**, effectively inhibited LNCaP cell proliferation induced by 1 nM testosterone.

Table 3. IC_{50} Values of Selected Compounds for SC-3 and LNCaP Cell Growth

compd	R	X	growth-inhibitory activities IC_{50} (M)[a] SC-3[b]	LNCaP[b]
7a	O	H	2.9×10^{-7}	4.2×10^{-7}
7b		F	2.8×10^{-7}	3.8×10^{-7}
7c		OCH_3	2.5×10^{-7}	7.9×10^{-7}
7d		$NHCOCH_3$	2.6×10^{-7}	$> 10^{-5}$
8a	S	H	3.6×10^{-7}	7.5×10^{-7}
8b		F	2.6×10^{-7}	4.2×10^{-7}
8c		OCH_3	3.6×10^{-7}	nt[c]
8d		$NHCOCH_3$	1.7×10^{-7}	1.3×10^{-6}
9a	SO_2	H	7.1×10^{-7}	$> 10^{-5}$
9d		$NHCOCH_3$	1.6×10^{-7}	$> 10^{-5}$
3			7.2×10^{-7}	agonist
4			2.4×10^{-8}	agonist
5			1.4×10^{-7}	8.7×10^{-7}
6			1.5×10^{-8}	agonist

[a] IC_{50} values of the test compounds were estimated from the sigmoidal dose–response curves using GraphPad Prism 4 software. [b] SC-3 and LNCaP cells were incubated with test compounds (1×10^{-10} to 1×10^{-5} M) in the presence of testosterone (1×10^{-9} M) for 3 and 5 days, respectively. All transactivation assays were performed in triplicate ($n = 3$). [c] nt indicates not tested.

Compounds **7a–c**, **8a**, and **8b** showed more potent cell proliferation–inhibitory activity than **5**. Unfortunately, compounds **7d** and **8d** with an acetamide group on the B ring showed no activity and weak activity as inhibitors of cell proliferation, respectively, although they had shown good biological profiles in AR-binding assay, transactivation assay, and SC-3 cell proliferation assay. Compounds **9a** and **9d** containing a SO_2 linking group were also inactive, and the SO_2 linking group negatively affected LNCaP cell proliferation–inhibitory activity, in contrast to **5**. The negative results obtained with **7d**, **8d**, and **9d** indicate that an acetylamide group is impermissible to interact with the T877A point-mutated AR LBD. Compounds **7b** and **8b** showed the best biological profiles and appear to be candidates for anti-androgen withdrawal syndrome therapeutic agents.

Discussion

Some combination of the structure of **6** and **5** appears to be optimal for the design of AR full antagonists. Our structure–activity relationship study of the designed compounds showed that the linking group and the substituent on the B ring play important roles in AR-binding, Ar transactivation, and cell proliferation–inhibitory activity, at least for SC-3 and LNCaP cells. It is particularly noteworthy that the hybrid compounds **7a–c**, **8a**, and **8b** showed more potent inhibitory activity than **5** in LNCaP cell proliferation assay.

Mutation of AR in prostate cancers has been well-documented, and several mutant ARs, such as T877A, T877S, H874Y, V715M, and L701H/T877A, have a broadened spectrum of ligand responsiveness; compound **4** works as an agonist for these mutants.[29] Compound **5** does not work as an agonist for these mutant ARs in prostate cancer, but it has recently been reported that it does work as an agonist for prostate cancers with W741C and W741L mutated AR.[15] The X-ray crystal structure of the mutant W741L AR LBD bound to **5** has been reported by Bohl et.al.[7] From the viewpoint of bicalutamide withdrawal syndrome and anti-androgen withdrawal syndrome in prostate cancer patients, it seems that T877 and W741 are hot spots of AR mutation selected by treatment with **3** and **5**, respectively.

Generally, carborane-containing ligands are expected to show a different spectrum of ligand responsiveness to known therapeutic agents because a carborane cage has a bulky spherical structure and a highly hydrophobic surface.[17] We previously designed a cyclohexenone–carborane hybrid AR ligand based upon the structure of **1**, a native AR ligand, and reported its AR-antagonistic activity.[22a] The results indicated that the C and D rings of the natural hormone, **1**, play an important role in determining whether a compound's activity is agonistic or antagonistic. The size of the carborane cage seems to be too big to be accommodated in place of the C and D rings of testosterone in the hydrophobic pocket of hAR LBD. These results confirmed the idea that the carborane ring would be a suitable moiety for the expression of AR-antagonistic activity because the bulky carborane structure interacts sterically with M895 and its surrounding amino acid residues in the hydrophobic pocket of wild-type hAR-LBD in such a way that helix-12 is moved away from the location required for expression of agonist activity. Since the hydrophobic structure of these carborane-containing compounds is bulkier than those of **3**, **4**, and **5**, there is greater potential to express AR-antagonistic activity, including a direct repulsion between helix-12 of AR LBD and the carborane cage. Thus, these carborane-containing compounds, especially **7b** and **8b**, might work as AR full antagonists and be candidates for treating anti-androgen withdrawal syndrome.

Miller and co-workers have reported selective androgen receptor modulators (SARMs), which is another goal of the AR ligand discovery, with an ether linking group designed based upon the structure of **5**.[30] It is anticipated that various SARMs could act as antagonists or weak agonists in the prostate, with reduced potential to stimulate nascent prostate cancer, and as agonists in the pituitary and muscle, with potential to treat muscle wasting conditions, hypogonadism, or age-related frailty.[31] The (*R*)-bicalutamide-based SARM candidates reported by Miller and co-workers showed moderate AR-binding affinity and acted as a potent AR agonists.[30] Their compounds exhibited agonistic, weak agonistic, and antagonistic activities in transactivation assay, and there was no correlation between binding affinity and in vitro functional activity. Unlike their SARMs, our carborane-containing compounds exhibited AR-antagonistic activity and showed no agonistic activity in transactivation and cell proliferation assays using SC-3 and LNCaP cells; there was a good correlation between binding affinity and in vitro functional activity. Although the structures of our carborane-containing compounds are similar to those of SARMs, we consider that they can act as pure AR full antagonists owing to the bulkiness of the carborane cage.

In conclusion, we have designed and synthesized novel carboran-containing AR full antagonists based upon the structures of **5** and **6**, examined their structure–activity relationships for AR-antagonistic activity, and found promising candidate AR ligands for the treatment of anti-androgen withdrawal syndrome. Compounds **7d** and **8d** with an acetamide group showed potent AR-biding and AR-transactivation inhibitory activities but were ineffective in LNCaP cells. In contrast, compounds **7b** and **8b** with a fluoro substituent on the B ring showed moderate binding affinities for hAR, better IC_{50} values in AR transactivation assay, and more potent inhibitory activity than **5** for **2**-induced LNCaP cell proliferation. The SO_2 linking group in these compounds seems to be

unfavorable for proliferation of LNCaP cells, regardless of the substituents on the B ring. Since the carborane cage has a bulky spherical structure and a hydrophobic surface, these carborane-containing AR ligands might have a different spectrum of ligand responsiveness from that of **5** and are candidate AR full antagonists for treatment of anti-androgen withdrawal syndromes.

Experimental Section

Chemistry. *p*-Carborane was purchased from Katchem s.r.o. Other chemicals were purchased from Aldrich or Tokyo Kasei Ltd. and used without further purification in the reactions or were prepared according to procedures described in the literature. Reactions were monitored with thin layer chromatography (TLC) conducted on Merck DC-platten Kieselgel $60F_{254}$ with UV detection. The structures of the compounds were confirmed by melting points, NMR spectra (^1H and ^{13}C), and MS spectra. The purities of the compounds (≥95%) were determined by elemental analyses. Melting points were determined with a Yanaco micro-melting point apparatus and were not corrected. ^1H NMR and ^{13}C NMR were recorded with JEOL JNM-EX-270 and JNM-LA-400 spectrometers. The chemical shifts are reported in parts per million (δ scale), and all coupling constants (J) are in hertz (Hz). The splitting patterns are designed as follows: s (singlet), d (doublet), t (triplet), q (quartet), m (multiplet), and br (broad). Chemical shifts for ^1H NMR spectra were referenced to tetramethylsilane (0.0 ppm) as an internal standard. Chemical shifts for ^{13}C NMR spectra were referenced to residual ^{13}C present in deuterated solvent. Mass spectra were recorded on a JEOL JMS-DX-303 spectrometer. Elemental analyses were performed on a Perkin-Elmer 2400 CHN spectrometer.

3-(12-Formyl-1,12-dicarba-*closo*-dodecaborane-1-yl)benzonitrile (11). To a solution of **6** (146 mg, 0.53 mmol) in 3 mL of CH_2Cl_2 was added Dess–Martin periodinate (450 mg, 1.06 mmol), and the mixture was stirred at room temperature for 8 h under an argon (Ar) atmosphere. The reaction mixture was filtered through Celite, and the filtrate was concentrated. The crude residue was purified by silica gel column chromatography with 20:1 *n*-hexane/EtOAc to give 129 mg (89%) of the title compound as a colorless solid: colorless cubes (CH_2Cl_2–*n*-hexane); mp 127.5–128.5 °C; ^1H NMR (270 MHz, $CDCl_3$) 1.0–3.5 (brm, 10H), 7.33 (m, 1H), 7.44 (dd, J = 1.3, 8.2 Hz, 1H), 7.48 (m, 1H), 7.55 (dd, J = 1.3, 7.6 Hz, 1H), 8.87 (s, 1H); ^{13}C NMR (68 MHz, $CDCl_3$) 81.85, 84.07, 112.63, 117.70, 129.05, 130.38, 131.07, 132.05, 137.19, 185.35. MS (EI) *m/z*: 273 (M^+, 100). Anal. Calcd for $C_{10}H_{15}B_{10}NO$: C, 43.94; H, 5.53; N, 5.12. Found: C, 44.19; H, 5.61; N, 5.26.

3-(12-Oxiranyl-1,12-dicarba-*closo*-dodecaborane-1-yl)benzonitrile (12). Chloroiodomethane (0.6 mL, 8.24 mmol) was added to a stirred solution of tetrahydrothiophene (727 μL, 8.24 mmol) in 50 mL of CH_2Cl_2 at room temperature under an Ar atmosphere. After 30 min, aldehyde (1.13 g, 4.12 mmol) was added, follwed by 1 M Et_2Zn in hexane (4.12 mL, 4.12 mmol). After 6.5 h, the reaction mixture was poured into water, extracted with CH_2Cl_2, dried over $MgSO_4$, and then concentrated. The crude residue was purified by silica gel column chromatography with 10:1 *n*-hexane/EtOAc to give 843 mg (71%) of the title compound as a colorless solid: colorless cotton (CH_2Cl_2–*n*-hexane); mp 124–125 °C; ^1H NMR (270 MHz, $CDCl_3$) 1.0–3.5 (brm, 10H), 2.46 (dd, J = 2.3, 4.9 Hz, 1H), 2.64 (dd, J = 3.4, 4.8 Hz, 1H), 2.88 (dd, J = 2.3, 3.8 Hz, 1H), 7.31 (dd, J = 0.7, 7.6 Hz, 1H), 7.43 (ddd, J = 1.2, 2.1, 8.1 Hz, 1H), 7.48 (d, J = 1.5 Hz, 1H), 7.52 (ddd, J = 1.3, 1.5, 7.6 Hz, 1H); ^{13}C NMR (68 MHz, $CDCl_3$) 48.11, 52.66, 79.25, 81.29, 112.76, 117.96, 129.37, 130.74, 131.57, 132.19, 137.51. MS (EI) *m/z* 287 (M^+, 100). Anal. Calcd for $C_{11}H_{17}B_{10}NO$: C, 45.97; H, 5.96; N, 4.87. Found: C, 45.81; H, 5.82; N, 4.80.

General Procedure for Preparation of Ether Derivatives (7). To a solution of compound **11** (100 mg, 0.35 mmol) and the corresponding phenol (0.53 mmol) in 2 mL of 2-propanol was added K_2CO_3 (73 mg, 0.53 mmol), and the mixture was refluxed for 29 h to 6 days under an Ar atmosphere. The mixture was poured into water and extracted with Et_2O. The organic layer was washed with 10% NaOH aqueous solution, water, and brine, dried over $MgSO_4$, and then concentrated. The crude residue was purified by silica gel column chromatography to give the corresponding ether derivative.

3-[12-(1-Hydroxy-2-phenoxyethyl)-1,12-dicarba-*closo*-dodecaborane-1-yl]benzonitrile (7a). Reaction time, 29 h; 90% yield; colorless cubes (methanol); mp 147–149 °C; ^1H NMR (270 MHz, $CDCl_3$) 1.0–3.5 (brm, 10H), 2.63 (d, J = 4.9 Hz, 1H), 3.65 (dd, J = 8.1, 10.2 Hz, 1H), 3.85–3.92 (m, 2H), 6.85 (d, J = 7.7 Hz, 2H), 6.99 (dd, J = 7.3, 7.4 Hz, 1H), 7.26–7.34 (m, 3H), 7.54 (ddd, J = 1.2, 2.0, 8.2 Hz, 2H), 7.50–7.54 (m, 2H); ^{13}C NMR (68 MHz, $CDCl_3$) 70.15, 70.36, 81.91, 82.77, 112.46, 114.46, 117.95, 121.60, 129.02, 129.52, 130.64, 131.41, 131.89, 137.46, 157.59. MS (EI) *m/z*: 381 (M^+), 94 (100%). Anal. Calcd for $C_{17}H_{23}B_{10}NO_2$: C, 53.52; H, 6.08; N, 3.67. Found: C, 53.32; H, 6.17; N, 3.61.

3-{12-[1-Hydroxy-2-(4-fluorophenoxy)ethyl]-1,12-dicarba-*closo*-dodecaborane-1-yl}benzonitrile (7b). Reaction time, 37 h; 89% yield; colorless cubes (*n*-hexane–CH_2Cl_2); mp 130–131 °C; ^1H NMR (270 MHz, $CDCl_3$) 1.0–3.5 (brm, 10H), 2.85 (brs, 1H), 3.62 (dd, J = 7.1, 9.2 Hz, 1H), 3.82–3.90 (m, 2H), 6.79 (dd, J = 4.3, 9.1 Hz, 2H), 6.96 (dd, J = 8.2, 9.1 Hz, 2H), 7.31 (dd, J = 7.4, 8.2 Hz, 1H), 7.45 (dd, J = 1.3, 8.2 Hz, 1H), 7.49–7.52 (m, 2H); ^{13}C NMR (68 MHz, $CDCl_3$) 70.36, 70.91, 81.93, 82.72, 112.45, 115.55, 115.66, 115.74, 116.08, 117.95, 129.05, 130.64, 131.42, 131.90, 137.43, 153.75, 153.77, 155.85, 158.37. MS (EI) *m/z*: 399 (M^+), 112 (100%). Anal. Calcd for $C_{17}H_{22}B_{10}FNO_2$: C, 51.11; H, 5.55; N, 3.51. Found: C, 51.10; H, 5.74; N, 3.34.

3-{12-[1-Hydroxy-2-(4-methoxyphenoxy)ethyl]-1,12-dicarba-*closo*-dodecaborane-1-yl}benzonitrile (7c). Reaction time, 74 h; 30% yield; colorless cubes (*n*-hexane-CH_2Cl_2); mp 111–113 °C; ^1H NMR (270 MHz, $CDCl_3$) 1.0–3.5 (brm, 10H), 2.60 (d, J = 4.8 Hz, 1H), 3.60 (dd, J = 7.3, 9.6 Hz, 1H), 3.77 (s, 3H), 3.75–3.86 (s, 2H), 6.77–6.85 (m, 4H), 7.30 (dd, J = 7.6, 8.1 Hz, 1H), 7.45 (dd, J = 8.1, 8.3 Hz, 2H), 7.50–7.53 (m, 2H); ^{13}C NMR (68 MHz, $CDCl_3$) 55.67, 70.45, 71.05, 81.98, 82.75, 112.53, 114.71, 115.62, 118.01, 129.07, 130.72, 131.60, 131.93, 137.54, 151.75, 154.46. MS (EI) *m/z*: 411 (M^+), 124 (100%). Anal. Calcd for $C_{18}H_{25}B_{10}NO_3$: C, 52.54; H, 6.12; N, 3.40. Found: C, 52.41; H, 6.22; N, 3.32.

3-{12-[1-Hydroxy-2-(4-acetamidephenoxy)ethyl]-1,12-dicarba-*closo*-dodecaborane-1-yl}benzonitrile (7d). Reaction time, 37 h; 71% yield; colorless needles (AcOEt); mp 170–171 °C; ^1H NMR (270 MHz, $CDCl_3$) 1.0–3.5 (brm, 10H), 2.10 (s, 3H), 3.61 (dd, J = 7.3, 9.4 Hz, 1H), 3.79–3.88 (m, 2H), 6.73 (d, J = 8.9 Hz, 2H), 7.28–7.38 (m, 3H), 7.46 (dd, J = 1.2, 8.1 Hz, 1H), 7.49–7.53 (m, 2H), 8.05 (s, 1H); ^{13}C NMR (68 MHz, $CDCl_3$) 24.01, 70.29, 70.62, 81.84, 83.11, 112.35, 114.72, 118.00, 121.99, 129.06, 130.62, 131.48, 131.75, 131.88, 137.49, 154.46, 168.89. MS (EI) *m/z*: 438 (M^+), 109 (100%). Anal. Calcd for $C_{19}H_{26}B_{10}N_2O_3$: C, 52.04; H, 5.98; N, 6.39. Found: C, 51.92; H, 6.18; N, 6.35.

3-{12-[1-Hydroxy-2-(4-nitrophenoxy)ethyl]-1,12-dicarba-*closo*-dodecaborane-1-yl}benzonitrile (7e). Reaction time, 6 days; 61% yield; colorless cubes (*n*-hexane–CH_2Cl_2); mp 191–192 °C; ^1H NMR (270 MHz, $CDCl_3$) 1.0–3.5 (brm, 10H), 3.79 (dd, J = 7.9, 10.2 Hz, 1H), 3.94–4.01 (m, 2H), 6.94 (d, J = 9.2 Hz, 2H), 7.33 (dd, J = 7.6, 9.1 Hz, 1H), 7.44–7.50 (m, 2H), 7.54 (d, J = 7.6 Hz, 1H), 8.20 (d, J = 9.2 Hz, 2H); ^{13}C NMR (68 MHz, $CDCl_3$) 70.22, 70.82, 82.13, 82.49, 112.49, 114.50, 117.94, 125.88, 129.12, 130.63, 131.43, 131.99, 137.31, 142.01, 162.63. MS (EI) *m/z*: 426 (M^+), 140 (100%). Anal. Calcd for $C_{19}H_{26}B_{10}N_2O_3$: C, 52.04; H, 5.98; N, 6.39. Found: C, 51.92; H, 6.18; N, 6.35.

3-{12-[1-Hydroxy-2-(4-bromophenoxy)ethyl]-1,12-dicarba-*closo*-dodecaborane-1-yl}benzonitrile (7f). Reaction time, 48 h; 82% yield; colorless cotton (AcOEt); mp 178–179 °C; ^1H NMR (270 MHz, $CDCl_3$) 1.0–3.5 (brm, 10H), 3.62 (dd, J = 7.1, 9.2 Hz, 1H), 3.82–3.91 (m, 2H), 6.73 (d, J = 9.1 Hz, 2H), 7.31 (dd, J = 7.6, 8.2 Hz, 1H), 7.37 (d, J = 8.9 Hz, 2H), 7.45 (ddd, J = 1.2, 2.0, 8.2 Hz, 1H), 7.49–7.53 (m, 2H); ^{13}C NMR (68 MHz, $CDCl_3$) 70.35, 70.46,

82.01, 82.60, 112.51, 113.88, 116.26, 117.96, 129.07, 130.67, 131.43, 131.94, 132.38, 137.43, 156.76. MS (EI) *m/z*: 460 (M^+), 172 (100%). Anal. Calcd for $C_{17}H_{22}B_{10}BrNO_2$: C, 44.35; H, 4.82; N, 3.04. Found: C, 44.36; H, 5.12; N, 2.96.

General Procedure for Preparation of Thioether Derivatives (8). A thiophenol (0.7 mmol) was added dropwise to a stirred suspension of NaH (60% in oil, 29 mg, 0.73 mmol) in 5 mL of THF at 0 °C under Ar atmosphere. After 20 min, compound **5** (200 mg, 0.7 mmol) was added to the mixture at 0 °C, and the mixture was stirred at room temperature for 6.5 h to 8 days. The reaction mixture was quenched by addition of water, and the mixture was extracted with Et_2O. The organic layer was washed with water and brine, dried over $MgSO_4$, and then concentrated. The crude residue was purified by silica gel column chromatography to give the corresponding thioether.

3-[12-(1-Hydroxy-2-phenylsulfanylethyl)-1,12-dicarba-*closo*-dodecaborane-1-yl]benzonitrile (8a). Reaction time, 75 h; 76% yield; colorless needles (methanol); mp 144−145 °C; ^{1}H NMR (270 MHz, $CDCl_3$) 1.0−3.5 (brm, 10H), 2.60 (dd, J = 10.4, 13.8 Hz, 1H), 2.74 (d, J = 3.8 Hz, 1H), 3.07 (dd, J = 2.5, 13.8 Hz, 1H), 3.54 (ddd, J = 2.5, 3.8, 10.4 Hz, 1H), 7.20−7.33 (m, 6H), 7.43 (ddd, J = 1.2, 2.0, 8.1 Hz, 1H), 7.48−7.53 (m, 2H); ^{13}C NMR (68 MHz, $CDCl_3$) 41.51, 70.07, 81.72, 84.69, 112.49, 117.95, 127.04, 129.03, 129.19, 129.95, 130.68, 131.43, 131.89, 133.93, 137.46. MS (EI) *m/z*: 397 (M^+), 124 (100%). Anal. Calcd for $C_{17}H_{23}B_{10}NOS$: C, 51.36; H, 5.83; N, 3.52. Found: C, 51.43; H, 6.11; N, 3.40.

3-{12-[1-Hydroxy-2-(4-fluorophenylsulfanyl)ethyl]-1,12-dicarba-*closo*-dodecaborane-1-yl}benzonitrile (8b). Reaction time, 73 h; 77% yield; colorless cubes (methanol); mp 104−105 °C; ^{1}H NMR (270 MHz, $CDCl_3$) 1.0−3.5 (brm, 10H), 2.61 (dd, J = 10.4, 13.7 Hz, 1H), 2.97 (dd, J = 2.3, 13.7 Hz, 1H), 3.05 (m, 1H), 3.53 (d, J = 10.1 Hz, 1H), 6.99 (dd, J = 8.6, 8.7 Hz, 2H), 7.27−7.35 (m, 3H), 7.44 (d, J = 8.7 Hz, 1H), 7.49−7.52 (m, 2H); ^{13}C NMR (68 MHz, $CDCl_3$) 42.53, 70.19, 81.61, 84.84, 112.37, 116.05, 116.38, 117.85, 128.97, 129.10, 129.15, 130.55, 131.35, 131.82, 132.80, 132.91, 137.34. MS (EI) *m/z*: 415 (M^+), 141 (100%). Anal. Calcd for $C_{17}H_{22}B_{10}FNOS$: C, 49.14; H, 5.34; N, 3.37. Found: C, 49.15; H, 5.44; N, 3.36.

3-{12-[1-Hydroxy-2-(4-methoxyphenylsulfanyl)ethyl]-1,12-dicarba-*closo*-dodecaborane-1-yl}benzonitrile (8c). Reaction time, 6.5 h; 84% yield; colorless cotton (methanol); mp 133−134 °C; ^{1}H NMR (270 MHz, $CDCl_3$) 1.0−3.5 (brm, 10H), 2.51 (dd, J = 10.6, 13.7 Hz, 1H), 2.89−2.95 (m, 2H), 3.45 (m, 1H), 3.79 (s, 3H), 7.28−7.32 (m, 3H), 7.43 (dd, J = 1.2, 8.1 Hz, 1H), 7.48−7.52 (m, 2H), 7.84 (d, J = 8.7 Hz, 2H); ^{13}C NMR (68 MHz, $CDCl_3$) 43.49, 55.26, 69.88, 81.65, 84.64, 112.44, 114.85, 117.96, 123.69, 129.01, 130.65, 131.42, 131.86, 133.69, 137.47, 158.51. MS (EI) *m/z*: 427 (M^+), 153 (100%). Anal. Calcd for $C_{18}H_{25}B_{10}NO_2S$: C, 50.56; H, 5.89; N, 3.28. Found: C, 50.73; H, 6.10; N, 3.13.

3-{12-[1-Hydroxy-2-(4-acetamidephenylsulfanyl)ethyl]-1,12-dicarba-*closo*-dodecaborane-1-yl}benzonitrile (8d). Reaction time, 36 h; 71% yield; colorless leaflets (*n*-hexane−CH_2Cl_2); mp 142−143 °C; ^{1}H NMR (270 MHz, $CDCl_3$) 1.0−3.5 (brm, 10H), 2.19 (s, 3H), 2.55 (dd, J = 10.4, 13.8 Hz, 1H), 3.00 (dd, J = 2.5, 13.8 Hz, 1H), 3.48 (m, 1H), 7.16 (brs, 1H), 7.27−7.33 (m, 3H), 7.42−7.48 (m, 4H), 7.52 (d, J = 7.6 Hz, 1H); ^{13}C NMR (68 MHz, $CDCl_3$) 24.47, 42.34, 70.09, 81.66, 84.86, 112.41, 118.05, 120.58, 128.73, 129.07, 130.70, 131.52, 131.62, 131.91, 137.35, 137.50, 168.73. MS (EI) *m/z*: 454 (M^+), 43 (100%). Anal. Calcd for $C_{19}H_{26}B_{10}N_2O_2S$: C, 50.20; H, 5.76; N, 6.16. Found: C, 50.27; H, 5.78; N, 6.04.

3-{12-[1-Hydroxy-2-(4-trifluoromethylphenylsulfanyl)ethyl]-1,12-dicarba-*closo*-dodecaborane-1-yl}benzonitrile (8e). Reaction time, 8 days; 67% yield; colorless leaflets (*n*-hexane−CH_2Cl_2); mp 142−143 °C; ^{1}H NMR (270 MHz, $CDCl_3$) 1.0−3.5 (brm, 10H), 2.50 (d, J = 4.3 Hz, 1H), 2.72 (dd, J = 10.2, 14.0 Hz, 1H), 3.13 (dd, J = 2.5, 14.0 Hz, 1H), 3.64 (ddd, J = 2.5, 4.3, 10.2 Hz, 1H), 7.28−7.36 (m, 3H), 7.46 (d, J = 8.2 Hz, 1H), 7.51−7.55 (m, 4H); ^{13}C NMR (68 MHz, $CDCl_3$) 40.01, 70.48, 81.93, 84.66, 112.57, 117.99, 123.89 (J = 272.1 Hz), 125.94 (J = 3.9 Hz), 128.19, 128.70, 129.11, 129.18, 130.72, 131.73 (J = 36.9 Hz), 137.37, 139.98 (J = 1.7 Hz). MS (EI) *m/z*: 465 (M^+), 192 (100%). Anal. Calcd for $C_{18}H_{22}B_{10}F_3NOS$: C, 46.44; H, 4.76; N, 3.01. Found: C, 46.63; H, 4.98; N, 2.90.

General Procedure for Preparation of Sulfone Derivatives (9). To a stirred solution of the appropriate thioether **8** (1 mmol) in 2 mL of CH_2Cl_2 was added *m*CPBA (2.6 mmol) in portions. The reaction mixture was stirred at room temperature for 7−45 h. An excess of *m*CPBA was decomposed with saturated $NaHSO_3$ aqueous solution. The organic layer was separated, washed with saturated $NaHCO_3$ aqueous solution and brine, dried over $MgSO_4$, and then concentrated. The crude residue was purified by silica gel column chromatography to give the corresponding sulfone derivative.

3-[12-(1-Hydroxy-2-phenylsulfonylethyl)-1,12-dicarba-*closo*-dodecaborane-1-yl]benzonitrile (9a). Reaction time, 7 h; 95% yield; colorless prisms (methanol); mp 182−184 °C; ^{1}H NMR (270 MHz, $CDCl_3$) 1.0−3.5 (brm, 10H), 3.02 (dd, J = 10.1, 14.0 Hz, 1H), 3.13 (dd, J = 1.8, 14.0 Hz, 1H), 3.33 (d, J = 3.3 Hz, 1H), 4.08−4.12 (m, 1H), 7.30 (m, 1H), 7.41 (ddd, J = 1.2, 2.1, 8.1 Hz, 1H), 7.45 (ddd, J = 1.3, 1.5, 7.4 Hz, 1H), 7.46 (dd, J = 1.4, 1.5 Hz, 2H), 7.71 (tt, J = 2.1, 7.5 Hz, 1H), 7.88 (dd, J = 1.5, 8.4 Hz, 2H); ^{13}C NMR (68 MHz, $CDCl_3$) 61.50, 67.30, 81.91, 83.83, 112.52, 127.91, 129.11, 129.45, 130.61, 131.38, 131.99, 134.27, 137.22, 138.72. MS (EI) *m/z*: 429 (M^+), 77 (100%). Anal. Calcd for $C_{17}H_{23}B_{10}NO_3S$: C, 47.53; H, 5.40; N, 3.26. Found: C, 47.65; H, 5.38; N, 3.19.

3-{12-[1-Hydroxy-2-(4-fluorophenylsulfonyl)ethyl]-1,12-dicarba-*closo*-dodecaborane-1-yl}benzonitrile (9b). Reaction time, 14 h; 100% yield; colorless cotton (methanol); mp 171.5−172.5 °C; ^{1}H NMR (270 MHz, $CDCl_3$) 1.0−3.5 (brm, 10H), 3.01 (dd, J = 10.1, 14.2 Hz, 1H), 3.10−3.15 (m, 2H), 4.11 (m, 1H), 7.23−7.33 (m, 3H), 7.41 (d, J = 8.1 Hz, 1H), 7.46 (s, 1H), 7.52 (d, J = 7.6 Hz, 1H), 7.89 (dd, J = 4.9, 8.7 Hz, 2H); ^{13}C NMR (68 MHz, $CDCl_3$) 61.64, 67.39, 81.83, 84.03, 112.39, 116.45, 116.79, 117.84, 129.09, 130.53, 130.88, 131.03, 131.36, 131.97, 134.99, 135.03, 137.12, 164.01, 167.79. MS (EI) *m/z*: 447 (M^+), 143 (100%). Anal. Calcd for $C_{17}H_{22}B_{10}FNO_3S$: C, 45.62; H, 4.95; N, 3.13. Found: C, 45.66; H, 4.96; N, 3.11.

3-{12-[1-Hydroxy-2-(4-methoxyphenylsulfonyl)ethyl]-1,12-dicarba-*closo*-dodecaborane-1-yl}benzonitrile (9c). Reaction time, 16 h; 94% yield; colorless prisms (methanol); mp 186−187 °C; ^{1}H NMR (270 MHz, $CDCl_3$) 1.0−3.5 (brm, 10H), 2.97 (dd, J = 10.4, 14.1 Hz, 1H), 3.09 (dd, J = 1.6, 14.1 Hz, 1H), 3.42 (d, J = 3.0 Hz, 1H), 4.04−4.08 (m, 1H), 7.04 (d, J = 9.1 Hz, 2H), 7.26−7.33 (m, 1H), 7.41 (dd, J = 1.3, 8.2 Hz, 1H), 7.46 (s, 1H), 7.52 (dd, J = 1.3, 7.6 Hz, 1H), 7.79 (d, J = 9.1 Hz, 2H); ^{13}C NMR (68 MHz, $CDCl_3$) 55.77, 61.72, 67.38, 81.96, 83.62, 112.60, 114.72, 117.97, 129.12, 129.90, 130.22, 130.68, 131.41, 132.03, 137.29, 164.24. MS (EI) *m/z*: 459 (M^+), 108 (100%). Anal. Calcd for $C_{18}H_{25}B_{10}NO_4S$: C, 47.04; H, 5.48; N, 3.05. Found: C, 47.02; H, 5.42; N, 3.00.

3-{12-[1-Hydroxy-2-(4-acetamidephenylsulfonyl)ethyl]-1,12-dicarba-*closo*-dodecaborane-1-yl}benzonitrile (9d). Reaction time, 45 h; 75% yield; colorless leaflets (methanol−AcOEt); mp 274−276 °C; ^{1}H NMR (270 MHz, CD_3OD) 1.0−3.5 (brm, 10H), 2.15 (s, 3H), 3.10 (dd, J = 2.8, 14.3 Hz, 1H), 3.19 (dd, J = 9.6, 14.3 Hz, 1H), 4.01 (m, 1H), 7.40 (dd, J = 7.6, 9.1 Hz, 1H), 7.51−7.53 (m, 2H), 7.63 (d, J = 7.6 Hz, 1H), 7.78 (s, 4H); ^{13}C NMR (68 MHz, DMSO-d_6) 24.15, 61.12, 67.17, 81.30, 86.76, 111.85, 117.85, 118.34, 129.16, 129.95, 130.05, 131.65, 132.78, 133.23, 136.45, 143.86, 169.11. MS (EI) *m/z*: 486 (M^+), 135 (100%). Anal. Calcd for $C_{19}H_{26}B_{10}N_2O_4S$: C, 46.90; H, 5.39; N, 5.76. Found: C, 47.06; H, 5.46; N, 5.68.

3-{12-[1-Hydroxy-2-(4-trifluoromethylphenylsulfonyl)ethyl]-1,12-dicarba-*closo*-dodecaborane-1-yl}benzonitrile (9e). Reaction time, 23 h; 100% yield; colorless cubes (*n*-hexane−CH_2Cl_2); mp 196−197.5 °C; ^{1}H NMR (270 MHz, $CDCl_3$) 1.0−3.5 (brm, 10H),

2.92 (d, J = 3.8 Hz, 1H), 3.07 (dd, J = 9.8, 14.4 Hz, 1H), 3.16 (dd, J = 2.3, 14.4 Hz, 1H), 4.19 (ddd, J = 2.3, 3.8, 9.8 Hz, 1H), 7.30 (dd, J = 7.6, 8.2 Hz, 1H), 7.43 (dd, J = 1.3, 8.2 Hz, 1H), 7.46 (s, 1H), 7.52 (dd, J = 1.3, 7.6 Hz, 1H), 7.85 (d, J = 8.7 Hz, 2H), 8.01 (d, J = 8.4 Hz, 2H); ^{13}C NMR (68 MHz, $CDCl_3$) 61.56, 67.52, 82.04, 83.88, 112.57, 117.90, 120.96, 124.98, 126.44, 126.50, 128.74, 129.16, 130.64, 131.40, 132.08, 135.50, 135.99, 137.17, 142.76. MS (EI) m/z: 497 (M^+), 193 (100%). Anal. Calcd for $C_{18}H_{22}B_{10}F_3NO_3S$: C, 43.45; H, 4.46; N, 2.82. Found: C, 43.64; H, 4.53; N, 2.78.

3-{12-[1-Hydroxy-2-anilinoethyl]-1,12-dicarba-*closo*-dodecaborane-1-yl}benzonitrile (10). A solution of **11** (97 mg, 0.34 mmol) and aniline (37 μL, 0.41 mmol) in 4 mL of methanol was refluxed for 84 h. The mixture was poured into water and extracted with Et_2O. The organic layer was washed with water and brine, dried over $MgSO_4$, and then concentrated. The crude residue was purified by silica gel column chromatography with 10:1 to 3:1 *n*-hexane/AcOEt to methanol to give 84 mg (65%) of the title compound as a colorless solid: colorless cubes (AcOEt); mp 171 °C; ^{1}H NMR (270 MHz, $CDCl_3$) 1.0−3.5 (brm, 10H), 3.48 (dd, J = 2.8, 13.4 Hz, 1H), 3.71 (dd, J = 2.8, 9.6 Hz, 1H), 3.79 (dd, J = 9.6, 13.4 Hz, 1H), 6.57 (d, J = 7.6 Hz, 2H), 6.75 (t, J = 7.4 Hz, 2H), 7.18 (dd, J = 7.4 Hz, 2H), 7.31 (dd, J = 7.4, 8.1 Hz, 1H), 7.46 (dd, J = 1.2, 8.1 Hz, 1H), 7.50−7.54 (m, 2H); ^{13}C NMR (68 MHz, $CDCl_3$) 49.20, 70.22, 81.86, 84.48, 112.59, 113.46, 118.06, 118.60, 129.14, 129.42, 130.79, 131.53, 132.01, 137.54, 147.17. MS (EI) m/z: 380 (M^+), 106 (100%). Anal. Calcd for $C_{17}H_{24}B_{10}N_2O$: C, 53.66; H, 6.36; N, 7.36. Found: C, 53.49; H, 6.44; N, 7.22.

Receptor Binding Assay. Binding affinities of test compounds for hAR (human androgen receptor) were measured in competition experiments using [^{3}H]testosterone and cytosolic fraction of hAR-LBD (hAR ligand-binding domain)-transformed *E. coli* as described previously. A hAR-LBD expression plasmid vector that encodes GST-hARLBD (627−919 aa, EF domain) fusion protein under the *lac* promoter (provided by Prof. S. Kato, University of Tokyo) was transfected into *E. coli* strain *HB-101*. An overnight culture (10 mL) of the bacteria was added to 1 L of LB medium and incubated at 27 °C until its optical density reached 0.6−0.7 at 600 nm. Following the addition of IPTG to 1 mM, incubation was continued for an additional 4.5 h. Cells were harvested by centrifugation at 4000*g* at 4 °C for 15 min and stored at −80 °C until use. All subsequent operations were performed at 4 °C. The bacterial pellet obtained from 40 mL of culture was resuspended in 1 mL of ice-cold TEGDM buffer (10 mM Tris-HCl, pH 7.4, 1 mM EDTA, 10% glycerol, 10 mM DTT, 10 mM sodium molybdate). This suspension was subjected to sonication using 10 × 10 s bursts on ice, and crude GST-hARLBD fraction was prepared by centrifugation of the suspension at 12000*g* for 30 min at 4 °C. This crude receptor fraction was diluted with buffer (20 mM Tris-HCl, pH 8.0, 0.3 M KCl, 1 mM EDTA) to a protein concentration of 0.3−0.5 mg/mL and used in binding assays as hAR-LBD fraction. Aliquots of the hAR-LBD fraction were incubated in the dark at 4 °C with [^{3}H]DHT (NEN, 4 nM final concentration), triamcinolone acetonide (1 μM final concentration), and reference or test compounds (dissolved in DMSO). Nonspecific binding was assessed by addition of a 200-fold excess of nonradioactive **2**. After 15 h, a dextran T-70/γ-globulin-coated-charcoal suspension was added to the ligand/protein mixture (1% Norit A, 0.05% γ-globulin, 0.05% dextran T-70 final concentration each) and the whole was incubated at 4 °C for 10 min. The charcoal was removed by centrifugation for 5 min at 1300*g*, and the radioactivity of the supernatant was measured in Atomlight (NEN) by using a liquid scintillation counter.

ARE-Luciferase Reporter Assay. Assay of androgenic activity was performed by means of ARE-luciferase reporter assay using NIH3T3 cells. Culture was conducted in phenol red-free DMEM (Sigma), supplemented with dextran-coated charcoal-stripped FBS (sFBS) to deplete internal stores of steroids, penicillin, and streptomycin for 2−3 days. Transient transfections of NIH3T3 cells were performed using Transfast (Promega) according to the manufacture's protocol. Transfections were done in 48-well plates at 2 × 10^4 cells/well with 50 ng of pSG5-hAR, 300 ng of p(ARE)$_2$-luc, and 10 ng of pRL/CMV (Promega) as an internal standard. Twenty-four hours after addition of the sample (final concentration, 10^{-5}−10^{-7} M) and 1 × 10^{-10} M **2**, cells were harvested with 25 μL of cell lysis buffer (Promega), and the firefly and Renilla luciferase activities were determined with a dual luciferase assay kit (Promega) by measuring luminescence with a Wallac Micro-Beta scintillation counter (PerkinElmer Life Sciences). Firely luciferase reporter activity was normalized to Renilla luciferase activity from pRL/CMV.

SC-3 Cell Proliferation Assay. SC-3 cells were cultured in the presence of MEMα (Wako Co.) supplemented with 2% FBS and 10 nM testosterone at 37 °C under 5% CO_2. All experiments were performed in triplicate or more. Cells were trypsinized and diluted to 2 × 10^{-4} cell/mL with MEMα supplemented with 2% stripped FBS. This cell suspension was seeded in 96-well plates at a volume of 100 μL and incubated at 24 h. After removal of 10 μL of medium from each well, 10 μL of the drug solution, which was supplemented with serial dilutions of the test compounds or DMSO as a dilution control in the presence or absence of 1 nM testosterone, was added. Then the plates were incubated at 37 °C under 5% CO_2 for 3 days, and the cell number was determined using a Cell Counting Kit-8 (DOJINDO). A 10 μL aliquot of WST-8 was added to each well of microcultures, and the cells were incubated for 4 h. The absorbance at 450 nm was measured with a model 680 microplate reader (BIO-RAD). This parameter is related to the number of living cells in the culture.

LNCap Cell Proliferation Assay. The human prostate adenocarcinoma cell line LNCap was cultured in the presence of RPMI-1640 (Wako Co.) supplemented with 10% FBS at 37 °C under 5% CO_2. Cells were trypsinized and diluted to 3 × 10^{-4} cell/mL with RPMI-1640 supplemented with 10% stripped-FBS. This cell suspension was seeded in 96-well plates (100 μL/well) and incubated for 24 h. After removal of 10 μL of medium from each well, 10 μL of drug solution, which was supplemented with serial dilutions of the test compounds or DMSO as a dilution control in the presence or absence of 1 nM testosterone, was added. Then the plates were incubated at 37 °C under 5% CO_2 for 6 days. During this period, half of the medium was removed and medium with the test compounds or DMSO as a dilution control in the presence or absence of 1 nM testosterone was replaced once after 3 days. The cell number was determined using a Cell Counting Kit-8 (CCK-8, DOJINDO). A 10 μL aliquot of CCK-8 was added to each well of microcultures, and the cells were incubated for 4 h. The absorbance at 450 nm was measured with a model 680 microplate reader (BIO-RAD). This parameter is related to the number of living cells in the culture.

Acknowledgment. This research was supported by Grant-in-Aid for High Technology Research Program, Grant-in-Aid for Scientific Research (B) (Grant No. 20390035), and Grant-in-Aid for Young Scientist (B) (Grant No. 21790116) from the Ministry of Education, Culture, Sport, Science and Technology, Japan.

References

(1) (a) Mooradian, A. D.; Morley, J. E.; Korenman, S. G. Biological actions of androgens. *Endocr. Rev.* **1987**, *8*, 1–28. (b) Bagatell, C. J.; Bremner, W. J. Androgens in men—uses and abuses. *N. Engl. J. Med.* **1996**, *334*, 707–714. (c) Kaufman, J. M.; Vermeulen, A. The decline of androgen levels in elderly men and its clinical and therapeutic implications. *Endocr. Rev.* **2005**, *26*, 833–876.

(2) (a) Evans, R. M. The steroid and thyroid hormone receptor superfamily. *Science* **1988**, *240*, 889–894. (b) MacLean, H. E.; Warne, G. L.; Zajac, J. D. Localization of functional domains in the androgen receptor. *J. Steroid Biochem. Mol. Biol.* **1997**, *62*, 233–242. (c) McEwan, I. J. Gene regulation through chromatin remodeling by members of the nuclear receptor superfamily. *Biochem. Soc. Trans.*

2000, *28*, 369–373. (d) Taplin, M.-E. Androgen receptor: role and novel therapeutic prospects in prostate cancer. *Expert. Rev. Anticancer Ther.* **2008**, *8*, 1495–1508.

(3) (a) Chengalvala, M.; Oh, T.; Roy, A. K. Selective androgen receptor modulators. *Expert Opin. Ther. Pat.* **2003**, *13*, 59–66. (b) Gao, W.; Bohl, C. E.; Dalton, J. T. Chemistry and structural biology of androgen receptor. *Chem. Rev.* **2005**, *105*, 3352–3370. (c) Chen, J.; Kim, J.; Dalton, J. T. Discovery and therapeutic promise selective androgen receptor modulators. *Mol. Invest.* **2005**, *5*, 173–188.

(4) (a) Neri, R. O.; Peets, E. A. Biological aspects of antiandrogens. *J. Steroid Biochem.* **1975**, *6*, 815–819. (b) Koch, H. Flutamide—a new non-steroidal anti-androgen. *Drugs Today* **1984**, *20*, 561–574. (c) Neri, R. Pharmacology and pharmacokinetics of flutamide. *Urology* **1989**, *34*, 19–21.

(5) (a) Wakeling, A. E.; Furr, B. J.; Glen, A. T.; Hughes, L. R. Receptor binding and biological activity of steroidal and nonsteroidal antiandrogens. *J. Steroid Biochem.* **1981**, *15*, 355–359. (b) Yeh, S.; Miyamoto, H.; Chang, C. Hydroxyflutamide may not always be a pure antiandrogen. *Lancet* **1997**, *349*, 852–853. (c) Bohl, C. E.; Miller, D. D.; Chen, J.; Bell, C. E.; Dalton, J. T. Structural basis for accommodation of nonsteroid ligands in the androgen receptor. *J. Biol. Chem.* **2005**, *280*, 37747–37754.

(6) (a) Tucker, H.; Chesterson, G. J. Resolution of the nonsteroidal antiandrogen 4′-cyano-3-[(4-fluorophenyl)sulfonyl]-2-hydroxy-2-methyl-3′-(trifluoromethyl)-propionanilide and the determination of the absolute configuration of the active enantiomer. *J. Med. Chem.* **1988**, *31*, 885–887. (b) Fradet, Y. Bicalutamide (Casodex) in the treatment of prostate cancer. *Expert Rev. Anticancer Ther.* **2004**, *4*, 37–48. (c) Kolvenbag, G. J.; Blackledge, G. R.; Gotting-Smith, K. Bicalutamide (Casodex) in the treatment of prostate cancer: history of clinical development. *Prostate* **1998**, *34*, 61–72.

(7) Bohl, C. E.; Gao, W.; Miller, D. D.; Bell, C. E.; Dalton, J. T. Structural basis for antagonism and resistance of bicalutamide in prostate cancer. *Proc. Natl. Acad. Sci. U.S.A.* **2005**, *102*, 6201–6206.

(8) (a) Sack, J. S.; Kish, K. F.; Wang, C.; Attar, R. M.; Kiefer, S. E.; An, Y.; Wu, G. Y.; Scheffler, J. E.; Salvati, M. E.; Krystek, S. R., Jr.; Weinmann, R.; Einspahr, H. M. Crystallographic structures of the ligand-binding domains of the androgen receptor and its T877A mutant complexed with the natural agonist dihydrotestosterone. *Proc. Natl. Acad. Sci. U.S.A.* **2001**, *98*, 4904–4909. (b) De Jésus-Tran, K. P.; Côté, P.-L.; Cantin, L.; Blanchet, J.; Labrie, F.; Breton, R. Comparison of crystal structures of human androgen receptor ligand-binding domain complexed with various agonists reveals molecular determinants responsible for binding affinity. *Protein Sci.* **2006**, *15*, 987–999.

(9) (a) Boccardo, F. Hormone therapy of prostate cancer: Is there a role for antiandrogen monotherapy? *Crit. Rev. Oncol. Hematol.* **2000**, *35*, 121–132. (b) Suzuki, H.; Kamiya, N.; Imamoto, T.; Kawamura, K.; Yano, M.; Takano, M.; Utsumi, T.; Naya, Y.; Ichikawa, T. Current topics and perspectives relating to hormone therapy for prostate cancer. *Int. J. Clin. Oncol.* **2008**, *13*, 401–410.

(10) Scher, H. I.; Steineck, G.; Kelly, W. K. Hormone-refractory (D3) prostate cancer: refining the concept. *Urology* **1995**, *46*, 142–148.

(11) (a) Taplin, M. E.; Rajeshkumar, B.; Halabi, S.; Werner, C. P.; Woda, B. A.; Picus, J.; Stadler, W.; Hayes, D. F.; Kantoff, P. W.; Vogelzang, N. J.; Small, E. J. Androgen receptor mutation in androgen-independent prostate cancer: cancer and leukemia group B study 9663. *J. Clin. Oncol.* **2003**, *21*, 2673–2678. (b) Miyamoto, H.; Rahman, M. M.; Chang, C. Molecular basis for the antiandrogen withdrawal syndrome. *J. Cell. Biochem.* **2003**, *91*, 3–12.

(12) (a) Veldscholte, J.; Berrevoets, C. A.; Brinkmann, A. O.; Grootegoed, J. A.; Mulder, E. Anti-androgens and the mutated androgen receptor LNCaP cells: differential effects on binding affinity, heat-shock protein interaction, and transcription activation. *Biochemistry* **1992**, *31*, 2393–2399. (b) Fenton, M. A.; Shuster, T. D.; Fertig, A. M.; Taplin, M. E.; Kolvenbag, G.; Bubley, G. J.; Balk, S. P. Functional characterization of mutant androgen receptors from androgen-independent prostate cancer. *Clin. Cancer Res.* **1997**, *3*, 1383–1388. (c) Zhao, X. Y.; Malloy, P. J.; Krishnan, A. V.; Swami, S.; Navone, N. M.; Peehl, D. M.; Feldman, D. Glucocorticoids can promote androgen-independent growth of prostate cancer cells through a mutated androgen receptor. *Nat. Med.* **2000**, *6*, 703–706.

(13) Taplin, M. E.; Bubley, G. J.; Ko, Y. J.; Small, E. J.; Upton, M.; Rajeshkumar, B.; Balk, S. P. Selection for androgen receptor mutations in prostate cancers treated with androgen antagonist. *Cancer Res.* **1999**, *59*, 2511–2515.

(14) (a) Suzuki, H.; Akakura, K.; Komiya, A.; Aida, S.; Akimoto, S.; Shimazaki, J. Codon 877 mutation in the androgen receptor gene in advanced prostate cancer: relation to antiandrogen withdrawal syndrome. *Prostate* **1996**, *29*, 153–158. (b) Zhou, J.; Liu, B.; Geng, G.; Wu, J. H. Study of the impact of the T877A mutation on ligand induced helix-12 positioning of the androgen receptor resulted in design and synthesis of novel antiandrogens. *Proteins* **2010**, *78*, 623–637.

(15) (a) Hara, T.; Miyazaki, J.; Araki, H.; Yamaoka, M.; Kanzaki, N.; Kusaka, M.; Miyamoto, M. Novel mutations of androgen receptor: a possible mechanism of bicalutamide withdrawal syndrome. *Cancer Res.* **2003**, *63*, 149–153. (b) Yoshida, T.; Kinoshita, H.; Segawa, T.; Nakamura, E.; Inoue, T.; Shimizu, Y.; Kamoto, T.; Ogawa, T. Antiandrogen bicalutamide promotes tumor growth in a novel androgen-dependent prostate cancer xenograft model derived from a bicalutamide-treated patients. *Cancer Res.* **2005**, *65*, 9611–9616.

(16) (a) Bregadze, V. I. Dicarba-*closo*-dodecaboranes $C_2B_{10}H_{12}$ and their derivatives. *Chem. Rev.* **1992**, *92*, 209–223. (b) Soloway, A. H.; Tjarks, W.; Barnum, B. A.; Rong, F.-G.; Barth, R. F.; Codogni, I. M.; Wilson, J. G. The chemistry of neutron capture therapy. *Chem. Rev.* **1998**, *98*, 1515–1562.

(17) (a) Valliant, J. F.; Guenther, K. J.; King, A. S.; Morel, P.; Schaffer, P.; Sogbein, O. O.; Stephenson, K. A. The medicinal chemistry of carboranes. *Coord. Chem. Rev.* **2002**, *232*, 173–230. (b) Armstrong, A. F.; Valliant, J. F. The bioinorganic and medicinal chemistry of carboranes: from new drug discovery to molecular imaging and therapy. *Dalton Trans.* **2007**, 4240–4251.

(18) (a) Endo, Y.; Iijima, T.; Yamakoshi, Y.; Yamaguchi, M.; Fukasawa, H.; Shudo, K. Potent estrogenic agonists bearing dicarba-*closo*-dodecaborane as a hydrophobic pharmacophore. *J. Med. Chem.* **1999**, *42*, 1501–1504. (b) Endo, Y.; Iijima, T.; Yamakoshi, Y.; Fukasawa, H.; Miyaura, C.; Inada, M.; Kubo, A.; Itai, A. Potent agonists based on carborane as a hydrophobic skeletal structure: a new medicinal application of boron clusters. *Chem. Biol.* **2001**, *8*, 341–355. (c) Endo, Y.; Yoshimi, T.; Ohta, K.; Suzuki, T.; Ohta, S. Potent estrogen receptor ligands based on bisphenols with a globular hydrophobic core. *J. Med. Chem.* **2005**, *48*, 3941–3944. (d) Hirata, M.; Inada, M.; Matsumoto, C.; Takita, M.; Ogawa, T.; Endo, Y.; Miyaura, C. A novel carborane analogue, BE360, with a carbon-containing polyhedral boron-cluster is a new selective estrogen receptor modulator for bone. *Biochem. Biophys. Res. Commun.* **2009**, *380*, 218–222. (e) Ohta, K.; Ogawa, T.; Suzuki, T.; Ohta, S.; Endo, Y. Novel estrogen receptor (ER) modulators: carbamate and thiocarbamate derivatives with m-carborane bisphenol structure. *Bioorg. Med. Chem.* **2009**, *17*, 7958–7963.

(19) (a) Iijima, T.; Endo, Y.; Tsuji, M.; Kawachi, E.; Kagechika, H.; Shudo, K. Dicarba-*closo*-dodecaboranes as a pharmacophore. Retinoidal antagonists and potential agonists. *Chem. Pharm. Bull.* **1999**, *47*, 398–404. (b) Endo, Y.; Yaguchi, K.; Kawachi, E.; Kagechika, H. Polymethylcarborane as a novel bioactive moiety: derivatives with potent retinoid antagonistic activity. *Bioorg. Med. Chem. Lett.* **2000**, *10*, 1733–1736. (c) Endo, Y.; Iijima, T.; Yaguchi, K.; Kawachi, E.; Inoue, N.; Kagechika, H.; Kubo, K.; Itai, A. Structure—activity study of retinoid agonists bearing substituted dicarba-closo-dodecaborane. Relation between retinoidal activity and conformation of two aromatic nuclei. *Bioorg. Med. Chem. Lett.* **2001**, *11*, 1307–1311.

(20) (a) Ohta, K.; Iijima, T.; Kawachi, E.; Kagechika, H.; Endo, Y. Novel retinoid X receptor (RXR) antagonists having a dicarba-*closo*-dodecaborane as a hydrophobic moiety. *Bioorg. Med. Chem. Lett.* **2004**, *14*, 5913–5918. (b) Calléja, C.; Messaddeq, N.; Chapellier, B.; Yang, H.; Krezel, W.; Li, M.; Metzger, D.; Mascrez, B.; Ohta, K.; Kagechika, H.; Endo, Y.; Mark, M.; Ghyselinck, N. B.; Chambon, P. Genetic and pharmacological evidence that a retinoic acid cannot be the RXR-activating ligand in mouse epidermis keratinocytes. *Gene Dev.* **2006**, *20*, 1525–1538.

(21) Fujii, S.; Goto, T.; Ohta, K.; Hashimoto, Y.; Suzuki, T.; Ohta, S.; Endo, Y. Potent androgen antagonists based on carborane as a hydrophobic core structure. *J. Med. Chem.* **2005**, *48*, 4654–4662.

(22) (a) Fujii, S.; Hashimoto, Y.; Suzuki, T.; Ohta, S.; Endo, Y. A new class of androgen receptor antagonists bearing carborane in place of a steroidal skeleton. *Bioorg. Med. Chem. Lett.* **2005**, *15*, 227–230. (b) Goto, T.; Ohta, K.; Suzuki, T.; Ohta, S.; Endo, Y. Design and synthesis of novel androgen receptor antagonists with sterically bulky icosahedral carborane. *Bioorg. Med. Chem.* **2005**, *13*, 6414–6424. (c) Ohta, K.; Goto, T.; Fujii, S.; Suzuki, T.; Ohta, S.; Endo, Y. Design and synthesis of carborane-containing androgen receptor (AR) antagonist bearing a pyridine ring. *Bioorg. Med. Chem.* **2008**, *16*, 8022–8028. (d) Fujii, S.; Ohta, K.; Goto, T.; Kagechika, H.; Endo, Y. Acidic heterocycles as novel hydrophilic pharmacophore of androgen receptor ligands with a carborane core structure. *Bioorg. Med. Chem.* **2009**, *17*, 344–350.

(23) (a) Dess, D. B.; Martin, J. C. Readily accessible 12-I-5 oxidant for the conversion of primary and secondary alcohols to aldehydes and ketones. *J. Org. Chem.* **1983**, *48*, 4155–4156. (b) Dess, D. B.; Martin, J. C. A useful 12-I-5 triacetoxyperiodinane (the Dess—Martin periodinane) for the selective oxidation of primary or secondary alcohols and a variety of related 12-I-5 species. *J. Am. Chem. Soc.* **1991**, *113*, 7277–7287.

(24) (a) Corey, E. J.; Chaykovsky, M. Dimethylsulfonium methylide, a reagent for selective oxirane synthesis from aldehydes and ketones. *J. Am. Chem. Soc.* **1962**, *84*, 3782–3783. (b) Corey, E. J.; Chaykovsky, M.

Dimethyloxosulfonium methylide and dimethylsulfonium methylide. Formation and application to organic synthesis. *J. Am. Chem. Soc.* **1965**, *87*, 1353–1364.

(25) (a) Aggarwal, V. K.; Ali, A.; Coogan, M. P. A novel procedure for the synthesis of epoxides: Application of Simmons–Smith reagents toward epoxidation. *J. Org. Chem.* **1997**, *62*, 8628–8629. (b) Aggarwal, V. K.; Coogan, M. P.; Stenson, R. A.; Jones, R. V. H.; Fieldhouse, R.; Blacker, J. Developments in the Simmons–Smith-mediated epoxidation reaction. *Eur. J. Org. Chem.* **2002**, 319–326.

(26) Ishioka, T.; Kubo, A.; Koiso, Y.; Nagasawa, K.; Itai, A.; Hashimoto, Y. Novel non-steroidal/non-anilide type androgen antagonists with an isoxazolone moiety. *Bioorg. Med. Chem.* **2002**, *10*, 1555–1566.

(27) Kitamura, S.; Suzuki, T.; Ohta, S.; Fujimoto, N. Antiandrogenic activity and metabolism of the organophosphorus pesticide fenthion and related compounds. *Environ. Health Perspect.* **2003**, *111*, 503–508.

(28) (a) Hiraoka, D.; Nakamura, N.; Nishizawa, Y.; Uchida, N.; Noguchi, S.; Matsumoto, K.; Sato, B. Inhibitory and stimulatory effects of glucocorticoid on androgen-induced growth of murine Shionogi carcinoma 115 in vivo and in cell culture. *Cancer Res.* **1987**, *47*, 6560–6564. (b) Kasayama, S.; Saito, H.; Kouhara, H.; Sumitani, S.; Sato, B. Suramin interrupts androgen-inducible autocrine loop involving heparin binding growth factor in mouse mammary cancer (Shionogi carcinoma 115) cells. *J. Cell. Physiol.* **1993**, *154*, 254–261.

(29) (a) Culig, Z.; Hobisch, A.; Cronauer, M. V.; Cato, A. C. B.; Hittmair, A.; Radmayr, C.; Eberle, J.; Bartsch, G.; Klocker, H. Mutant androgen receptor detected in an advanced-stage prostatic carcinoma is activated by adrenal androgens and progesterone. *Mol. Endocrinol.* **1993**, *7*, 1541–1550. (b) Taplin, M. E.; Bubley, G. J.; Shuster, T. D.; Frantz, M. E.; Spooner, A. E.; Ogata, G. K.; Keer, H. N.; Balk, S. P. Mutation of the androgen receptor gene in metastatic androgen-independent prostate cancer. *N. Engl. J. Med.* **1995**, *332*, 1393–1398. (c) Marcelli, M.; Ittmann, M.; Mariani, S.; Sutherland, R.; Nigam, R.; Murthy, L.; Zhao, Y.; DiConcini, D.; Puxeddu, E.; Esen, A.; Eastham, J.; Weigel, N. L.; Lamb, D. J. Androgen receptor mutations in prostate cancer. *Cancer Res.* **2000**, *90*, 944–949.

(30) (a) Yin, D.; Gao, W.; Kearbey, J. D.; Xu, H.; Chung, K.; He, Y.; Marhefka, C. A.; Veverka, K. A.; Miller, D. D.; Dalton, J. T. Pharmacodynamics of selective androgen receptor modulators. *J. Pharmacol. Exp. Ther.* **2003**, *304*, 1334–1340. (b) Marhefka, C. A.; Gao, W.; Chung, K.; Kim, J.; He, Y.; Yin, D.; Bohl, C.; Dalton, J. T.; Miller, D. D. Design, synthesis and biological characterization of metabolically stable selective androgen receptor modulators. *J. Med. Chem.* **2004**, *47*, 993–998. (c) Kearbey, J. D.; Gao, W.; Narayanan, R.; Fisher, S. J.; Wu, D.; Miller, D. D.; Dalton, J. T. Selective androgen receptor modulator (SARM) treatment prevents bone loss and reduces body fat in ovariectomized rats. *Pharm. Res.* **2007**, *24*, 328–335.

(31) (a) Zhi, L.; Martinborough, E. *Annu. Rep. Med. Chem.* **2001**, *36*, 169–180. (b) Brown, T. R. Nonsteroidal selective androgen receptor modulators (SARMs): designer androgens with flexible structures provide clinical promise. *Endocrinology* **2004**, *145*, 5417–5419.

Behavioural Brain Research 215 (2010) 141–145

Contents lists available at ScienceDirect

Behavioural Brain Research

journal homepage: www.elsevier.com/locate/bbr

Research report

Influence of olfactory bulbectomy on maternal behavior and dopaminergic function in nucleus accumbens in mice

Atsushi Sato, Osamu Nakagawasai*, Koichi Tan-No, Hiroshi Onogi, Fukie Niijima, Takeshi Tadano

Department of Pharmacology, Tohoku Pharmaceutical University, 4-4-1 Komatsushima, Aoba-ku, Sendai 981-8558, Japan

ARTICLE INFO

Article history:
Received 7 June 2010
Received in revised form 9 July 2010
Accepted 10 July 2010
Available online 16 July 2010

Keywords:
Olfactory bulbectomy
Maternal behavior
Dopamine
Tyrosine hydroxylase
Depression
Autoradiography

ABSTRACT

Olfactory bulbectomy (OBX) induces behavioral, physiological, and neurochemical alterations resembling clinical depression and is widely used as an animal model of depression. It has been reported that depression is a critical cause of child abuse and neglect and that maternal behavior involves dopaminergic neurons of the mesolimbic pathway. In a previous study we found that OBX mice show maternal behavior deficits which are improved by administration of apomorphine, a non-selective dopamine agonist. Therefore, in this study, we investigated the effect of L-3,4-dihydroxyphenylalanine (L-DOPA) on maternal behavior deficits to examine the influence of pre-synaptic dopaminergic function in OBX mice. Furthermore, we measured tyrosine hydroxylase (TH) levels using microphotometry and quantified dopamine D1- and D2-like receptors using autoradiography in the nucleus accumbens (NAc). As a result, 25 mg/kg L-DOPA with 12.5 mg/kg benserazide improved disrupted maternal behavior in OBX mice and there are no changes in TH levels or number of D1- and D2-like receptors between sham and OBX mothers. The behavioral data support the hypothesis that changed dopaminergic function may contribute to maternal behavior deficits in OBX mice. However, our findings concerning dopaminergic function suggest that the deficits in OBX mice are not simply due to changes in TH levels or dopamine receptor number in the NAc.

© 2010 Elsevier B.V. All rights reserved.

1. Introduction

Bilateral olfactory bulbectomized (OBX) rodents are one of the most commonly used animal models of depression. They express behavioral, physiological and neurochemical alterations similar to clinical depression symptoms and these changes are reversed by chronic, but not acute, antidepressant treatment (for review, see [38]). Specifically, OBX produces neurodegeneration in the locus coeruleus or dorsal raphe that causes dysfunction of the noradrenergic or serotonergic system, respectively [16,17]. In addition, OBX animals show varied behavioral changes including impairment of cognitive function and an increase in nocturnal locomotor activity and exploratory behavior [11,13,25,26,41,46]. Recently, it has been reported that abnormal maternal behavior is expressed in various animal models of depression. Flinders Sensitive Line rats, a genetic animal model of depression, show reduced nursing and licking behaviors compared with Sprague–Dawley control rats [4,23]. Furthermore, rat mothers that have acquired learned helplessness display decreased licking and arched back nursing behavior [21]. In addition, OBX has been reported to induce deficits in maternal responding in mice [9,10], and we observed maternal behavior deficits in OBX mice in a previous study [35].

Maternal behavior is strongly related to the mesolimbic dopaminergic system which is a major component of the brain reward system (for review, see [20,31]). Dysfunction of the reward system causes anhedonia [24] which is one of the core symptoms of major depression, and it is also observed in OBX animals [5,34,35,39]. It is known that disruption of the mesolimbic dopaminergic system leads to maternal behavior deficits, for example, destruction of the ventral tegmental area (VTA) which projects dopaminergic nerves to the mesolimbic area or by administration of a dopamine antagonist or 6-hydroxydopamine to the nucleus accumbens (NAc) disrupted maternal behavior [8,12,19,29,37]. Furthermore, it has been reported that maternal interaction with their pups increases dopamine release into the mother's NAc [6,22]. Previously, we found that disruption of maternal behavior in OBX mice was ameliorated by administration of apomorphine, a non-

Abbreviations: ANOVA, analysis of variance; L-DOPA, L-3,4-dihydroxyphenylalanine; MPOA, medial preoptic area; NAc, nucleus accumbens; NAcC, nucleus accumbens core; NAcSh, nucleus accumbens shell; NGS, normal goat serum; OB, olfactory bulb; OBX, olfactory bulbectomy; PBS, phosphate-buffered saline; PND, postnatal day; SEM, standard error of the mean; SSRI, selective serotonin reuptake inhibitor; TH, tyrosine hydroxylase; vBST, ventral bed nucleus of the stria terminalis; VP, ventral pallidum; VTA, ventral tegmental area.

* Corresponding author. Tel.: +81 22 727 0123; fax: +81 22 727 0123.
E-mail addresses: obx0315@yahoo.co.jp (A. Sato), osamun@tohoku-pharm.ac.jp (O. Nakagawasai), koichi@tohoku-pharm.ac.jp (K. Tan-No), hirogle@yahoo.co.jp (H. Onogi), niijima@tohoku-pharm.ac.jp (F. Niijima), tadano@tohoku-pharm.ac.jp (T. Tadano).

0166-4328/$ – see front matter © 2010 Elsevier B.V. All rights reserved.
doi:10.1016/j.bbr.2010.07.012

selective dopamine agonist [35]. This result suggests that the disruption of maternal behavior in OBX mice is related to dopaminergic function in the central nervous system.

Therefore, we examined the effect of L-3,4-dihydroxyphenylalanine (L-DOPA) on maternal behavior and tyrosine hydroxylase (TH) levels, the biosynthetic rate-controlling enzyme of catecholamines such as dopamine, in the NAc to investigate pre-synaptic function of dopaminergic nerves in OBX mothers in present study. We quantified D1- and D2-like dopamine receptors in the NAc using autoradiography, because it is reported that roles of dopamine receptors in maternal behavior vary according to subtype [29]. As OBX mice have depressive symptoms this study also investigated whether the antidepressive effect of a selective serotonin reuptake inhibitor (SSRI) can improve the maternal behavior deficits in OBX mice. In this study, we selected fluvoxamine as a SSRI, because it has been reported that the drug has a relatively low reproductive toxicity compared to other SSRIs [42].

2. Materials and methods

2.1. Animals

Eight-week-old ddY virgin female mice were obtained from Nippon SLC (Hamamatsu, Japan). Animals were housed in polypropylene cages (13 cm height × 21 cm width × 31 cm length) with a stainless steel wire lid and wood shavings as bedding material (Beta chip, Charles River Laboratory International, Inc., USA). The animals had free access to food and water. Temperature (22 ± 2 °C) and humidity (55 ± 10%) were maintained within a narrow range and the animals were on a 12-h light/dark cycle (light phase; 7:00–19:00 h). In the behavioral study, 45 sham and 36 OBX mice were used. A further 12 (sham, $n = 6$; OBX, $n = 6$) and 10 mice (sham, $n = 5$; OBX, $n = 5$) were used to examine TH levels and dopamine receptors in the NAc, respectively. All experiments were performed according to the Guide for Care and Use of Laboratory Animals at Tohoku Pharmaceutical University.

2.2. Drugs

L-DOPA (12.5 and 25 mg/kg, Sigma–Aldrich, Inc., St. Louis, MO, USA) was dissolved in physiological saline and benserazide (12.5 mg/kg, Sigma–Aldrich, Inc.) was suspended in 0.5% Tween 80. L-DOPA was intraperitoneally administered 15 min before and benserazide was administered 45 min before maternal behavior observation began to prevent peripheral metabolism of L-DOPA. The time of administration of these drugs was based on a previous report by Tayarani-Binazir et al. [40]. Fluvoxamine dissolved in distilled water (60 mg/kg) was administered perorally from the end of mating until delivery (14–21 days). On the day of testing fluvoxamine was administered 60 min before behavior observation began. The dosage of fluvoxamine was determined accorded to the report of Ichimaru et al. [14]. Drugs were administered at a dose of 0.1 mL/10 g of mouse body weight.

2.3. Surgery

Mice anesthetized with pentobarbital Na (50 mg/kg, i.p.; Dainippon Sumitomo Pharma, Osaka, Japan) were placed in a stereotaxic frame. The scalp was incised, two holes were drilled to expose the olfactory bulb (OB), which was then bilaterally aspirated using a suction pump. All animals were sacrificed at the end of the experiment and the lesions were verified visually. It was confirmed that at least two thirds of the OB had been removed and that some parts of the olfactory nuclei also had also been lesioned. If the lesion was either not extensive enough or extended to the cortex, data from these animals were excluded. Sham operations were performed in the same manner but without the removal of the OB.

2.4. Mating and maternal behavior observation

Two or three females were allowed to mate with a male of the same strain for 7 days, 2 weeks post surgery. Pregnant mice were transferred to another cage of the same type and housed individually and were checked daily for parturition. Postnatal day (PND) 0 is defined as the day when delivery is complete by 12:00. Based on the report of Champagne et al. [7], maternal behavior observation was conducted for 75 min on PND 0 and 4 between 12:00 and 17:00. The observed maternal behaviors comprise one of the following two types that were shown to improve following administration of apomorphine in a previous study [35]: (1) Mother off pups (duration when mother was apart from her pups) and (2) arched back posture (mother is arching her back with rigid limbs and blankets the pups attached to her nipples).

2.5. Immunohistochemical procedure

The preparation of brains for the measurement of TH levels was conducted within 24 h following delivery. Lactating female mice were anesthetized with pentobarbital Na (50 mg/kg, i.p.) and perfused through the heart with ice-cold phosphate-buffered saline (PBS, pH 7.4), immediately followed by a fixative containing 4% paraformaldehyde (Sigma–Aldrich, Inc., St. Louis, MO, USA) and 0.2% glutaraldehyde (Nacalai Tesque, Osaka, Japan) in PBS. The brain was then postfixed with the same fixative solution at 4 °C for 1 h and then placed in a 10% sucrose-buffered solution at 4 °C for 12 h. The tissue was frozen on dry ice and cut into 20 μm-thick coronal sections (NAc; Bregma, 1.10 mm) on a cryostat (Leitz, Stuttgart, Germany). The immunohistochemical staining procedure was carried out as previously described [27]. Briefly, the rabbit anti-TH antibody (diluted 1:100 with PBS including 0.1% Triton X-100 and 0.05% normal goat serum (NGS); Millipore corporation, Billerica, MA, USA) was applied to each brain slice, which was then incubated at 4 °C for 12 h. The polyclonal antibody to bovine brain TH was produced in rabbit. This TH antibody cross-reacted immunohistochemically with TH from the brains of several species including mice, rats, ferrets and feline. The secondary antibody consisted of FITC-labeled anti-rabbit IgG goat serum (diluted 1:200 with PBS; Millipore corporation), and was allowed to react in the dark at room temperature for 3 h. The stained sections were mounted in 10% glycerin-PBS, and kept at 4 °C in a dark room until measurements were carried out. The distribution of TH immunofluorescence intensities was quantitatively analyzed using a modified brain mapping analyzer system (Yamato Scientific Co., Inc., Tokyo, Japan). The background value, including non-specific fluorescence originating from glutaraldehyde, was subtracted photometrically from the total fluorescence intensity value at each point measured. Immunohistochemical fluorescence intensities obtained for the various regions are relative to that of standard 1 mM quinine sulphate.

2.6. Quantitative receptor autoradiography

Sham and OBX mice were sacrificed by decapitation within 24 h after delivery and their brains were removed and frozen in isopentane at −40 °C and stored at −80 °C. Using a cryostat (Leitz, Stuttgart, Germany), 20 μm-thick coronal sections from the NAc were collected on gelatin-coated slides and stored at −80 °C until use. Dopamine D1- and D2-like receptor binding sites were visualized using [^{3}H]SCH23390 (85.0 Ci/mmol) and [^{3}H]raclopride (62.2 Ci/mmol) respectively (PerkinElmer Life and Analytical Sciences, Boston, MA, USA). The protocol was carried out as previously described [1] with minor modifications. Briefly, sections were preincubated for 15 min in Tris–HCl buffer [Tris 50 (for D1) or 170 (for D2) mM, NaCl 120 mM, KCl 5 mM, $CaCl_2$ 2 mM, $MgCl_2$ 1 mM, pH 7.4] at room temperature prior to a 60 min incubation in the same buffer containing either 1 nM [^{3}H]SCH23390 or 3 nM [^{3}H]raclopride. Non-specific binding was determined by inclusion of 1 μM SCH23390 (Sigma–Aldrich, Inc.) or 300 μM sulpiride (Sigma–Aldrich, Inc.) in the assay buffer containing 1 nM [^{3}H]SCH23390 or 3 nM [^{3}H]raclopride, respectively. At the end of the incubation, sections were rinsed four times, 2 min each in ice-cold buffer, then dipped in deionized water to remove salts and rapidly dried. All slides were exposed to a tritium sensitive imaging plate (Fujifilm Corporation, Tokyo, Japan) together with [^{3}H]microscale standards (GE Healthcare UK Ltd., Buckinghamshire, UK) for 10 days for both bindings. Specific labeling was quantified (nCi/mg wet weight) using a computer-assisted Image Reader BAS 5000 ver. 1.12 (Fujifilm Corporation).

2.7. Data analysis

The significance of differences was determined using the Student's t-test for two-group comparison of TH levels and dopamine D1 and D2 receptor on PND 0. Two-way analysis of variance (ANOVA) was used for comparison of the effect of L-DOPA or fluvoxamine on maternal behavior. Post hoc analysis was performed using the Fisher's PLSD test. The criterion of significance was set at $p < 0.05$. All results are expressed as mean ± standard error of the mean (SEM).

3. Results

3.1. Effect of L-DOPA on maternal behavior

A two-way ANOVA revealed a significant effect of group in time mothers spent off pups [group: $F_{(1,60)} = 7.359$, $p = 0.0087$; treatment: $F_{(2,60)} = 2.096$, $p = 0.1318$; group × treatment: $F_{(2,60)} = 2.242$, $p = 0.1151$]. A post hoc test revealed that the duration of time mothers spent off pups in OBX mice was significantly increased compared with the sham group ($p = 0.0022$) and it was reduced following administration of L-DOPA 0.25 mg/kg ($p = 0.0070$) (Fig. 1A). Regarding arched back posture, an ANOVA revealed a significant effect of group and group × treatment [group: $F_{(1,60)} = 9.882$, $p = 0.0026$; treatment: $F_{(2,60)} = 0.831$, $p = 0.4404$;

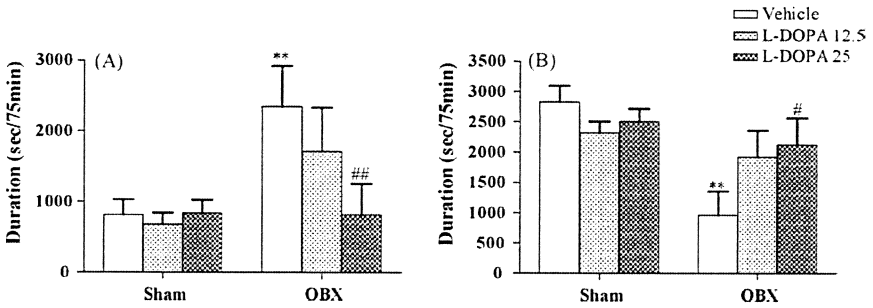


Fig. 1. Changes in maternal behaviors: mother off pups (A) and arched back posture (B) in sham control and OBX groups after administration of L-DOPA on PND 0. Vertical bars represent S.E.M. $^{**}P<0.01$ compared with sham + vehicle group. $^{\#}P<0.05$ and $^{\#\#}P<0.01$ compared with OBX + vehicle group ($n=8$–19 per group).

group × treatment: $F_{(2,60)}=3.483$, $p=0.0370$] and a post hoc test revealed a reduction in the time OBX mothers spent in the arched back posture ($p<0.0001$) and an improvement in the disrupted maternal behavior with administration of 0.25 mg/kg L-DOPA ($p=0.0206$) (Fig. 1B).

3.2. Effect of fluvoxamine on maternal behavior

An ANOVA revealed a significant effect of group, but not treatment or group × treatment, in the time mothers spent off pups [group: $F_{(1,40)}=19.606$, $p<0.0001$; treatment: $F_{(1,40)}=2.838$, $p=0.0998$; group × treatment: $F_{(1,40)}=1.257$, $p=0.2690$] and time spent in the arched back posture [group: $F_{(1,40)}=20.194$, $p<0.0001$; treatment: $F_{(1,40)}=1.658$, $p=0.2052$; group × treatment: $F_{(1,40)}=0.089$, $p=0.7671$]. A post hoc test revealed that the duration of time mothers spent off pups in OBX mice was significantly increased compared with the sham vehicle group (vehicle: $p=0.0090$, fluvoxamine 60 mg/kg: $p<0.0001$). Similar results are found in the duration spent in the arched back posture (sham vehicle × OBX vehicle: $p=0.0003$, sham vehicle × OBX fluvoxamine 60 mg/kg: $p<0.0001$) (Fig. 2).

3.3. Distribution of TH

The distribution of TH fluorescence intensity in each mouse brain section was determined by microphotometry and classified into 16 levels (shown as different colors in Fig. 3, with the lowest concentration shown as black and the highest concentration represented by white). There were no changes in TH levels in either the nucleus accumbens core (NAcC) ($t=0.497$, $p=0.6301$) or in the nucleus accumbens shell (NAcSh) ($t=0.515$, $p=0.6175$) between sham and OBX mothers (Fig. 3C).

3.4. Quantitative receptor autoradiography

We conducted the autoradiography to investigate the bindings of dopamine receptors in the NAc. As a result, levels of D1- (NAcC: $t=1.381$, $p=0.1834$; NAcSh: $t=1.344$, $p=0.1948$) and D2-like receptor binding (NAcC: $t=0.377$, $p=0.7134$; NAcSh: $t=0.963$, $p=0.3490$) were not different between sham and OBX mice on PND0 (Fig. 4).

4. Discussion

In this study, we found that increased time mothers spent off pups and decreased time spent in the arched back posture in OBX mice were improved by administration of 0.25 mg/kg L-DOPA (Fig. 1). The improvement effects of L-DOPA on maternal behavior deficits in OBX mice was similar to the results obtained in a previous study using apomorphine [35] and suggest that increased dopamine release into the synaptic cleft by the dopamine precursor replacement may be able to promote improved maternal behavior.

The additional study using chronic administration of fluvoxamine did not show an ameliorating effect on maternal behavior deficits in OBX mothers (Fig. 2). It has been reported that changes in serotonergic function induced by OBX contribute to the expression of depressive symptoms in OBX animals [38]. The abnormal behavior in OBX animals is improved by chronic administration of antidepressants which affect serotonergic function [38]. These reports suggest that maternal behavior deficits may also be ameliorated by chronic administration of antidepressants but this was not observed in the current study. The reports which investigated serotonergic function and maternal behavior are mostly concerned with maternal aggression and it has been reported that maternal aggression is decreased by administration of a precursor of serotonin, 5-HT_1 or 5-HT_2 receptor agonists and SSRIs [15,32]. On the other hand, it has been reported that chronic administration of fluoxetine only increased frequency of touching and sniffing of pups [18]. However, we cannot determine that chronic administration of SSRIs can improve maternal behavior deficits because the improvement effect of fluoxetine affects only a small part of maternal behavior and we did not observe this aspect of maternal behavior in current study. Therefore, we consider that dopaminergic agonists or dopamine reuptake inhibitors are more effective

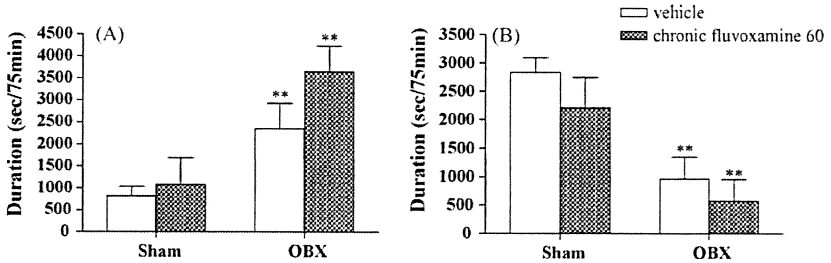


Fig. 2. Changes in maternal behaviors: mother off pups (A) and arched back posture (B) in sham control and OBX groups after chronic administration of fluvoxamine on PND 0. Vertical bars represent S.E.M. $^{**}P<0.01$ compared with sham + vehicle group ($n=7$–19 per group).

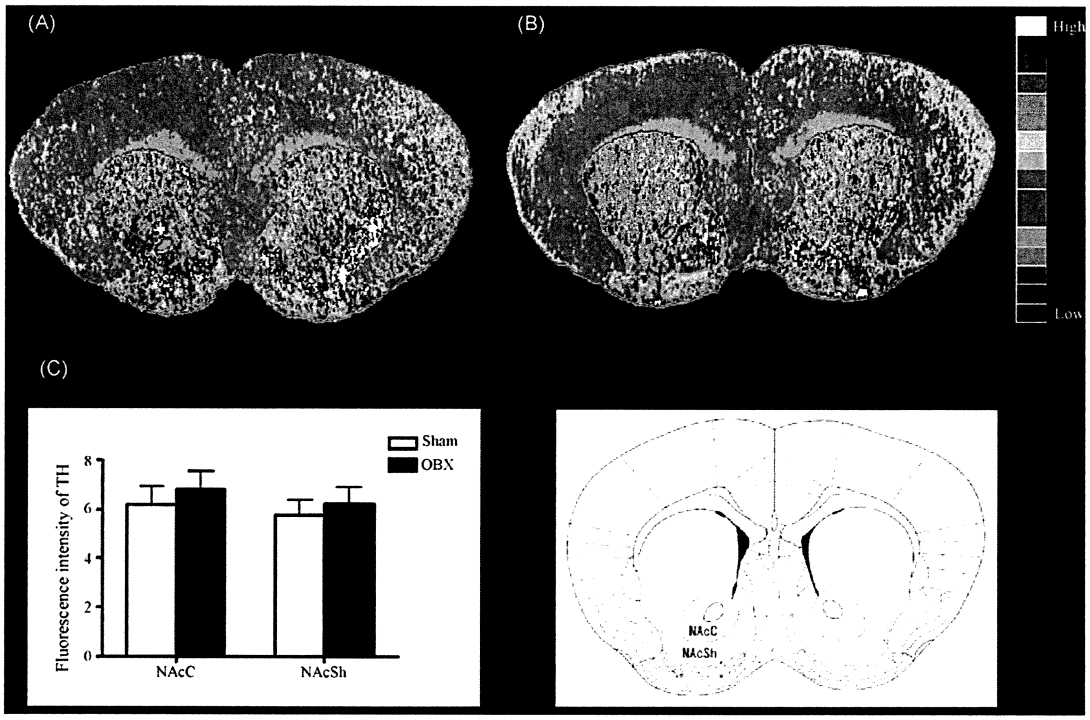


Fig. 3. Distribution of the immunohistochemical fluorescence intensity for TH in mice brain (Bregma, mm), including NAcC and NAcSh on PND0. (A) Sham mouse; (B) OBX mouse; (C) Values for the immunofluorescence intensity of TH in NAcC and NAcSh of the mouse brain on PND0.

than antidepressants such as SSRIs on maternal behavior deficits in OBX mice.

Numan and Stolzenberg [31] suggested that the hypothetic neural circuit regulates maternal behavior and consists of the reward circuit [VTA, NAc and ventral pallidum (VP)], medial preoptic area and ventral bed nucleus of the stria terminalis (MPOA/vBST) [28,31]. According to their report, MPOA/vBST is the center of maternal behavior that facilitates expression of maternal behavior by regulating the VTA-NAc-VP axis. The VTA has dopaminergic projection neurons to the NAc, in turn the NAc projects GABAergic neurons to the VP. Dopaminergic inputs from the VTA to the NAc inhibit GABAergic output from the NAc to the VP which disinhibits the VP allowing it to respond to inputs from the prefrontal cortex or basolateral amygdale, areas which receive pup-related stimuli. As a result, expression of maternal behavior is enhanced by an activated VP. Furthermore, the input of dopamine from the VTA to the NAc is stimulated by the MPOA/vBST which itself is activated by hormones or pup-related stimuli. In this study, the immunohistochemical study revealed that the levels of TH in the NAc was not different between sham and OBX mothers (Fig. 3), and L-DOPA improved maternal behavior deficits in OBX mice. Furthermore, we demonstrated that OBX did not affect dopamine D1- and D2-like receptors in the NAc (Fig. 4), and in a previous study, apomorphine recovered disruption of maternal behavior in OBX mice [35]. These results suggest that disruption of maternal behavior in OBX mice is not induced by alteration of pre-synaptic function of dopaminergic nervous or expression of dopamine D1- and D2-like receptors in the NAc and can be improved by administration of dopaminergic agonists. Considering all the various factors together, it is very possible that maternal behavior deficits in OBX mice are related to dysfunction or absence of activation of the MPOA/vBST which is a higher center in the maternal behavior circuit. In addition, because MPOA has various hormonal receptors such as estrogen [36], progesterone [30], prolactin [2] and oxytocin [3], changes in secretion of these hormones or sensibility to hormones in the MPOA may relate to the maternal behavior deficits in OBX mice. In fact, some studies concerning hormonal changes in OBX animals have been published [33,43–45], and these suggest that MPOA activation by hormones may be altered in OBX mothers. Furthermore, as the MPOA is also activated by pup-related stimuli, including pup odor, the MPOA of OBX animals may not be able to be activated by pup odor stimuli as these animals have lost olfaction because of the extraction of

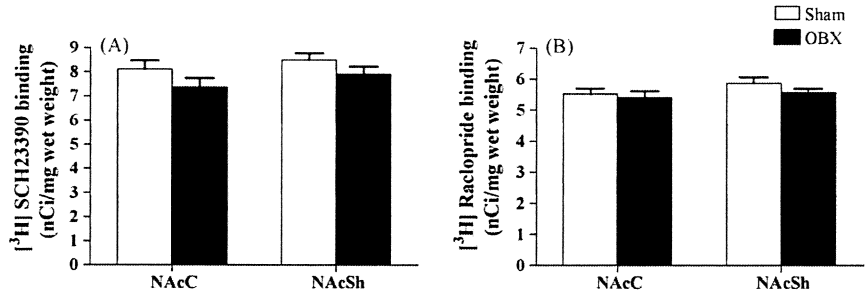


Fig. 4. Quantitative autoradiography of (A) [^{3}H]SCH23390 and (B) [^{3}H]raclopride binding sites in the NAc of sham and OBX mice on PND0. Specific binding is expressed as nCi/mg wet weight. Vertical bars represent SEM.

OB (the center of olfaction). Thus, we should examine the responsiveness of the MPOA to hormones and pup-related stimuli in OBX mice.

In conclusion, maternal behavior deficits in OBX mice were improved by administration of L-DOPA, but not chronic administration of fluvoxamine. Furthermore, microphotometry and autoradiography revealed no changes in the levels of TH or dopamine receptor binding in the NAc of sham and OBX groups. The behavioral data suggest that changes in dopaminergic function may contribute to the maternal behavior deficits in OBX mice. However, our findings concerning dopaminergic function indicate that maternal disruption in OBX mice is not simply due to changes in TH levels or dopamine receptors in the NAc.

Acknowledgements

This study was supported in part by a Grant-in-Aid for Scientific Research (C) (KAKENHI 21610019) from the Japan Society for the Promotion of Science to TT and ON, and Matching Fund Subsidy for Private Universities from the Ministry of Education, Culture, Sports, Science and Technology, Japan. The authors acknowledge the editorial support of ProSciEd's professional editor.

References

[1] Araki T, Tanji H, Kato H, Imai Y, Mizugaki M, Itoyama Y. Temporal changes of dopaminergic and glutamatergic receptors in 6-hydroxydopamine-treated rat brain. Eur Neuropsychopharmacol 2000;10:365–75.
[2] Bakowska JC, Morrell JI. Atlas of the neurons that express mRNA for the long form of the prolactin receptor in the forebrain of the female rat. J Comp Neurol 1997;386:161–77.
[3] Bealer SL, Lipschitz DL, Ramoz G, Crowley WR. Oxytocin receptor binding in the hypothalamus during gestation in rats. Am J Physiol Regul Integr Comp Physiol 2006;291:R53–8.
[4] Braw Y, Malkesman O, Merenlender A, Dagan M, Bercovich A, Lavi-Avnon Y, et al. Divergent maternal behavioral patterns in two genetic animal models of depression. Physiol Behav 2009;96:209–17.
[5] Calcagnetti DJ, Quatrella LA, Schechter MD. Olfactory bulbectomy disrupts the expression of cocaine-induced conditioned place preference. Physiol Behav 1996;59:597–604.
[6] Champagne FA, Chretien P, Stevenson CW, Zhang TY, Gratton A, Meaney MJ. Variations in nucleus accumbens dopamine associated with individual differences in maternal behavior in the rat. J Neurosci 2004;24:4113–23.
[7] Champagne FA, Francis DD, Mar A, Meaney MJ. Variations in maternal care in the rat as a mediating influence for the effects of environment on development. Physiol Behav 2003;79:359–71.
[8] Gaffori O, Le Moal M. Disruption of maternal behavior and appearance of cannibalism after ventral mesencephalic tegmentum lesions. Physiol Behav 1979;23:317–23.
[9] Gandelman R, Zarrow MX, Denenberg VH. Reproductive and maternal performance in the mouse following removal of the olfactory bulbs. J Reprod Fert 1972;28:453–6.
[10] Gandelman R, Zarrow MX, Denenberg VH, Myers M. Olfactory bulb removal eliminates maternal behavior in the mouse. Science 1971;171:210–1.
[11] Giardina WJ, Radek RJ. Effects of imipramine on the nocturnal behavior of bilateral olfactory bulbectomized rats. Biol Psychiatry 1991;29:1200–8.
[12] Hansen S, Harthon C, Wallin E, Lofberg L, Svensson K. The effects of 6-OHDA-induced dopamine depletions in the ventral or dorsal striatum on maternal and sexual behavior in the female rat. Pharmacol Biochem Behav 1991;39:71–7.
[13] Hozumi S, Nakagawasai O, Tan-No K, Niijima F, Yamadera F, Murata A, et al. Characteristics of changes in cholinergic function and impairment of learning and memory-related behavior induced by olfactory bulbectomy. Behav Brain Res 2003;138:9–15.
[14] Ichimaru Y, Egawa T, Sawa A. 5-HT_{1A}-receptor subtype mediates the effect of fluvoxamine, a selective serotonin reuptake inhibitor, on marble-burying behavior in mice. Jpn J Pharmacol 1995;68:65–70.
[15] Ieni JR, Thurmond JB. Maternal aggression in mice: effects of treatments with PCPA, 5-HTP and 5-HT receptor antagonists. Eur J Pharmacol 1985;111:211–20.
[16] Jancsár SM, Leonard BE. Behavioural and neurochemical interactions between chronic reserpine and chronic antidepressants. A possible model for the detection of atypical antidepressants. Biochem Pharmacol 1983;32:1569–71.
[17] Jancsár SM, Leonard BE. Changes in neurotransmitter metabolism following olfactory bulbectomy in the rat. Prog Neuropsychopharmacol Biol Psychiatry 1984;8:263–9.
[18] Johns JM, Joyner PW, McMurray MS, Elliott DL, Hofler VE, Middleton CL, et al. The effects of dopaminergic/serotonergic reuptake inhibition on maternal behavior, maternal aggression, and oxytocin in the rat. Pharmacol Biochem Behav 2005;81:769–85.
[19] Keer SE, Stern JM. Dopamine receptor blockade in the nucleus accumbens inhibits maternal retrieval and licking, but enhances nursing behavior in lactating rats. Physiol Behav 1999;67:659–69.
[20] Kornetsky C. Brain-stimulation reward, morphine-induced oral stereotypy, and sensitization: implications for abuse. Neurosci Biobehav Rev 2004;27:777–86.
[21] Kurata A, Morinobu S, Fuchikami M, Yamamoto S, Yamawaki S. Maternal postpartum learned helplessness (LH) affects maternal care by dams and responses to the LH test in adolescent offspring. Horm Behav 2009;56:112–20.
[22] Lavi-Avnon Y, Weller A, Finberg JP, Gispan-Herman I, Kinor N, Stern Y, et al. The reward system and maternal behavior in an animal model of depression: a microdialysis study. Psychopharmacology (Berl) 2008;196:281–91.
[23] Lavi-Avnon Y, Yadid G, Overstreet DH, Weller A. Abnormal patterns of maternal behavior in a genetic animal model of depression. Physiol Behav 2005;84:607–15.
[24] Markou A, Kosten TR, Koob GF. Neurobiological similarities in depression and drug dependence: a self-medication hypothesis. Neuropsychopharmacology 1998;18:135–74.
[25] Moriguchi S, Han F, Nakagawasai O, Tadano T, Fukunaga K. Decreased calcium/calmodulin-dependent protein kinase II and protein kinase C activities mediate impairment of hippocampal long-term potentiation in the olfactory bulbectomized mice. J Neurochem 2006;97:22–9.
[26] Nakagawasai O, Hozumi S, Tan-No K, Niijima F, Arai Y, Yasuhara H, et al. Immunohistochemical fluorescence intensity reduction of brain somatostatin in the impairment of learning and memory-related behaviour induced by olfactory bulbectomy. Behav Brain Res 2003;142:63–7.
[27] Nakagawasai O, Yamadera F, Iwasaki K, Asao T, Tan-No K, Niijima F, et al. Preventive effect of kami-untan-to on performance in the forced swimming test in thiamine-deficient mice: relationship to functions of catecholaminergic neurons. Behav Brain Res 2007;177:315–21.
[28] Numan M, Insel TR. The neurobiology of parental behavior. New York: Springer-Verlag; 2003.
[29] Numan M, Numan MJ, Pliakou N, Stolzenberg DS, Mullins OJ, Murphy JM, et al. The effects of D1 or D2 dopamine receptor antagonism in the medial preoptic area, ventral pallidum, or nucleus accumbens on the maternal retrieval response and other aspects of maternal behavior in rats. Behav Neurosci 2005;119:1588–604.
[30] Numan M, Roach JK, del Cerro MC, Guillamón A, Segovia S, Sheehan TP, et al. Expression of intracellular progesterone receptors in rat brain during different reproductive states, and involvement in maternal behavior. Brain Res 1999;830:358–71.
[31] Numan M, Stolzenberg DS. Medial preoptic area interactions with dopamine neural systems in the control of the onset and maintenance of maternal behavior in rats. Front Neuroendocrinol 2009;30:46–64.
[32] Olivier B, Mos J, van Oorschot R, Hen R. Serotonin receptors and animal models of aggressive behavior. Pharmacopsychiatry 1995;(Suppl. 2):80–90.
[33] Pieper DR, Gala RR. Influence of the pineal gland, olfactory bulbs and photoperiod on surges of plasma prolactin in the female rat. J Endocrinol 1979;82:279–85.
[34] Romeas T, Morissette MC, Mnie-Filali O, Piñeyro G, Boye SM. Simultaneous anhedonia and exaggerated locomotor activation in an animal model of depression. Psychopharmacology 2009;205:293–303.
[35] Sato A, Nakagawasai O, Tan-No K, Onogi H, Niijima F, Tadano T. Effect of non-selective dopaminergic receptor agonist on disrupted maternal behavior in olfactory bulbectomized mice. Behav Brain Res 2010;210:251–6.
[36] Shughrue PJ, Lane MV, Merchenthaler I. Comparative distribution of estrogen receptor-alpha and -beta mRNA in the rat central nervous system. J Comp Neurol 1997;388:507–25.
[37] Silva MR, Bernardi MM, Cruz-Casallas PE, Felicio LF. Pimozide injections into the nucleus accumbens disrupt maternal behaviour in lactating rats. Pharmacol Toxicol 2003;93:42–7.
[38] Song C, Leonard BE. The olfactory bulbectomized rat as a model of depression. Neurosci Biobehav Rev 2005;29:627–47.
[39] Stock HS, Ford K, Wilson MA. Gender and gonadal hormone effects in the olfactory bulbectomy animal model of depression. Pharmacol Biochem Behav 2000;67:183–91.
[40] Tayarani-Binazir KA, Jackson MJ, Fisher R, Zoubiane G, Rose S, Jenner P. The timing of administration, dose dependence and efficacy of dopa decarboxylase inhibitors on the reversal of motor disability produced by L-DOPA in the MPTP-treated common marmoset. Eur J Pharmacol 2010;635:109–16.
[41] Thorne BM, Aaron M, Latham EE. Effects of olfactory bulb ablation upon emotionality and muricidal behavior in four rat strains. J Comp Physiol Psychol 1973;84:339–44.
[42] Tuccori M, Testi A, Antonioli L, Fornai M, Montagnani S, Ghisu N, et al. Safety concerns associated with the use of serotonin reuptake inhibitors and other serotonergic/noradrenergic antidepressants during pregnancy: a review. Clin Ther 2009;31:1426–53.
[43] Tyler JL, Gorski RA. Bulbectomy and sensitivity to estrogen: anatomical and functional specificity. Physiol Behav 1980;24:593–600.
[44] Vandenbergh JG. Effects of central and peripheral anosmia on reproduction of female mice. Physiol Behav 1973;10:257–61.
[45] Williams GW, Goldman J, McGinnis MY, Possidente B, Lumia AR. Effects of ovarian hormones on sexual receptivity, proceptivity, and motivation in olfactory bulbectomized female rats. Physiol Behav 1991;50:751–5.
[46] Zueger M, Urani A, Chourbaji S, Zacher C, Roche M, Harkin A, et al. Olfactory bulbectomy in mice induces alterations in exploratory behavior. Neurosci Lett 2005;374:142–6.

Behavioural Brain Research 214 (2010) 349–356

Contents lists available at ScienceDirect

Behavioural Brain Research

journal homepage: www.elsevier.com/locate/bbr

Research report

p-Hydroxyamphetamine causes prepulse inhibition disruptions in mice: Contribution of dopamine neurotransmission

Hiroshi Onogi[a], Osamu Nakagawasai[a,*], Koichi Tan-No[a], Satoru Mitazaki[b], Atsushi Sato[a], Kota Nakaya[a], Fukie Niijima[a], Yuichiro Arai[c], Tsuneaki Kikuchi[d], Takeshi Tadano[a]

[a] Department of Pharmacology, Tohoku Pharmaceutical University, 4-4-1 Komatsushima, Aoba-ku, Sendai 981-8558, Japan
[b] Laboratory of Forensic Toxicology, Faculty of Pharmacy, Takasaki University of Health and Welfare, 60 Nakaorui-machi, Takasaki 370-0033, Japan
[c] Tokyo Ariake University of Medical and Health Sciences, Tokyo 135-0063, Japan
[d] Faculty of Health Science, Tohoku Fukushi University, 1-8-1 Kunimi, Aoba-ku, Sendai 981-8522, Japan

ARTICLE INFO

Article history:
Received 9 April 2010
Received in revised form 22 May 2010
Accepted 1 June 2010
Available online 9 June 2010

Keywords:
p-Hydroxyamphetamine
Prepulse inhibition
Dopamine
Schizophrenia

ABSTRACT

It is well known that amphetamine induces disrupted prepulse inhibition (PPI) in humans and rodents. We have previously reported that intracerebroventricular (i.c.v.) administration of p-hydroxyamphetamine (p-OHA) induces multiple behavioral responses, such as increased locomotor activity and head-twitch response in rodents. To reveal the characteristics of p-OHA on sensorimotor function in rodents, herein we tested the effects of p-OHA on PPI in mice. i.c.v. administration of p-OHA dose-dependently induced PPI disruptions for all prepulse intervals tested. This effect of p-OHA on PPI was attenuated by pretreatment with haloperidol or clozapine. p-OHA-induced PPI disruptions were also attenuated by pretreatment with L-741,626 (a selective D_2 receptor antagonist), L-745,870 (a selective D_4 receptor antagonist) or 6-hydroxydopamine (a neurotoxin which targets DA-containing neurons), but not by SCH 23390 (a selective D_1 receptor antagonist), eticlopride (a D_2/D_3 receptor antagonist) or GBR 12909 (a DA-reuptake inhibitor). These results indicate that selective blockade of either the D_2 or D_4 receptor subtype may prevent disruption of PPI induced by p-OHA via presynaptic DA release.

© 2010 Elsevier B.V. All rights reserved.

1. Introduction

Prepulse inhibition (PPI) of the acoustic startle response (ASR) is a form of sensorimotor gating, defined as an inhibition of the startle response when a low intensity stimulus, the prepulse, precedes the startling stimulus [21]. Schizophrenia patients exhibit impairment in PPI of the ASR, which is commonly interpreted as a sensorimotor gating deficit [44]. PPI is also diminished in rodents treated with psychotomimetic drugs such as amphetamine (AMPH), methamphetamine (METH) and phencyclidine [1,30,31]. PPI has been suggested as a relevant model for studying the pathophysiology of schizophrenia [16].

p-Hydroxyamphetamine (p-OHA), an AMPH and METH metabolite, has been shown to have a number of pharmacological actions, including causing abnormal behaviors such as those induced by drugs of abuse [2,13,24,42]. For example, we have previously reported that intracerebroventricular (i.c.v.) administration of p-OHA induces a head-twitch response (HTR) in mice as a model of hallucination, furthermore the HTR is markedly reduced by pretreatment with a 5-HT synthesis inhibitor, such as p-chlorophenylalanine [46], or pretreatment with 5-HT receptor antagonists such as cyproheptadine or dimethothiazine [46], indicating involvement of the central serotonergic system [47]. i.c.v. administration of p-OHA also induced hyperlocomotion in mice and this p-OHA-induced hyperlocomotion is inhibited by pretreatment with a dopamine (DA)-reuptake inhibitor, indicating involvement of the central dopaminergic system [35].

There are many reports concerning AMPH-induced PPI disruptions [36,37,41], however, to our knowledge, no research has yet been carried out on the effects of p-OHA on the PPI of ASR. To reveal the characteristics of p-OHA on sensorimotor function in rodents, in the present study we investigated the influence of p-OHA on the PPI of ASR in mice and the mechanisms of action of p-OHA using pharmacological tools. In a preliminary study, i.c.v. administration of p-OHA induced PPI disruptions in mice. As several antipsychotic drugs are known to attenuate AMPH-induced PPI disruptions [15,48], we investigated the effects of haloperidol (a typical antipsychotic) and clozapine (an atypical antipsychotic) on p-OHA-induced PPI disruptions in mice. The central dopamin-

Abbreviations: AMPH, amphetamine; ANOVA, analysis of variance; ASR, acoustic startle response; Avg., average; DA, dopamine; HTR, head-twitch response; 5-HT, 5-hydroxytryptamine; i.c.v., intracerebroventricular; METH, methamphetamine; 6-OHDA, 6-hydroxydopamine; p-OHA, p-hydroxyamphetamine; PPI, prepulse inhibition.

* Corresponding author. Tel.: +81 22 727 0123; fax: +81 22 727 0123.
E-mail address: osamun@tohoku-pharm.ac.jp (O. Nakagawasai).

0166-4328/$ – see front matter © 2010 Elsevier B.V. All rights reserved.
doi:10.1016/j.bbr.2010.06.005

ergic system, especially the D_2 receptor, is one of the main targets of antipsychotics. Therefore, we focused on the involvement of the central dopaminergic system in *p*-OHA-induced PPI disruptions and investigated the effects of pretreatment with several dopaminergic agents. Briefly, we used SCH 23390 (a selective D_1 receptor antagonist), L-741,626 (a selective D_2 receptor antagonist), eticlopride (a D_2/D_3 receptor antagonist), or L-745,870 (a selective D_4 receptor antagonist) as DA receptor antagonists on *p*-OHA-induced PPI disruptions in mice. Moreover, as *p*-OHA is also assumed to induce the release of neurotransmitters from presynaptic monoaminergic neurons [2,24], we also tested the effect of presynaptic dopaminergic agents i.e., 6-hydroxydopamine (6-OHDA, a neurotoxin which targets DA-containing neurons) or GBR 12909 (a DA-reuptake inhibitor) on *p*-OHA induced PPI disruptions in mice.

2. Materials and methods

All experiments were performed following the approval of the Ethics Committee of Animal Experiment in Tohoku Pharmaceutical University and according to the National Institutes of Health Guide for the Care and Use of Laboratory Animals. Efforts were made to minimize suffering and to reduce the number of animals used.

2.1. Animals

Male ddY strain mice (weighing 28–32 g, Japan SLC, Japan) were used for all experiments. Mice were housed in cages with free access to food and water under conditions of constant temperature (22 ± 2 °C) and humidity (55 ± 5%), on a 12 h light–dark cycle (lights on: 07:00 to 19:00).

2.2. Drugs and treatments

The following drugs were used: the racemic form of *p*-OHA hydrobromide (Smith-Kline and French, USA), L-745,870 (Tocris Cookson, UK), desipramine (Wako Pure Chemical Industries, Ltd., Japan), haloperidol, clozapine, SCH 23390, L-741,626, eticlopride, GBR 12909 and 6-OHDA (Sigma–Aldrich, USA). *p*-OHA was dissolved in Ringer's solution. 6-OHDA was dissolved in Ringer's solution containing 0.1% ascorbic acid. Haloperidol, clozapine and L-741,626 were dissolved in 0.5% Tween 80 and all other drugs were dissolved in 0.9% saline. For all solutions, pH was adjusted to 7.4 at 37 °C. Doses of all drugs were based on previous studies [3,4,10,11,14,19,23,27,29,46].

The technique employed herein for i.c.v. injection into mice was the same as that originally described by Brittain and Handley [6]. Briefly, i.c.v. administration of *p*-OHA, 6-OHDA or Ringer's solution was performed with a disposable 27-G needle attached to a 50 μL Hamilton microsyringe and inserted into the left lateral ventricle of unanesthetized mice. *p*-OHA, 6-OHDA or Ringer's solution was administered in a total volume of 5 μL at a constant rate of 1 μL/2 s. i.c.v. administration of *p*-OHA or Ringer's solution was performed 25 min before the start of PPI testing. Pretreatment with L-741,626 or 0.5% Tween 80 as vehicle was performed by subcutaneous (s.c.) administration 30 min before i.c.v. administration of *p*-OHA or Ringer's solution. Pretreatment with haloperidol, clozapine, SCH 23390, eticlopride, L-745,870, GBR 12909 or their solvents as vehicle was performed by intraperitoneal (i.p.) administration 30 min before i.c.v. administration of *p*-OHA or Ringer's solution.

2.3. 6-OHDA lesion

The 6-OHDA lesioning technique is based on a previous report [4] with minor modifications. Briefly, 20 min prior to 6-OHDA injection, mice were administered desipramine (25 mg/kg, i.p.) to protect noradrenaline-containing neurons. i.c.v. administration of 6-OHDA (40 μg/mouse) or vehicle was injected into the left lateral ventricle of unanesthetized mice. On day 7, following i.c.v. administration of 6-OHDA or vehicle, *p*-OHA or Ringer's solution was administered i.c.v. 25 min before the start of PPI testing.

2.4. PPI of the acoustic startle response

Tests were conducted using the SR-LAB system (SR-LAB, San Diego Instruments, USA) that comprised two sound-attenuating chambers each equipped with a cylindrical Plexiglas animal enclosure (length: 6.7 cm; inner diameter: 3.8 cm). Ventilation was provided by a small electric fan that also generated a 70 dB background noise. Tone pulses were presented by a speaker positioned 24 cm directly above the animal enclosure. A piezoelectric accelerometer affixed to the animal enclosure frame was used to detect and transduce motion resulting from the animal's response. Tone pulse parameters were controlled by a computer using a commercial software package (SR-LAB) and interface assembly that also digitized, rectified and recorded stabilimeter readings.

Measures of both ASR and PPI were obtained in a single session as described by Nakagawasai et al. [34]. Twenty-five minutes after i.c.v. administration of *p*-OHA or Ringer's solution, animals were placed in the Plexiglas enclosure and allowed to acclimatize to the environment for 5 min before being tested during 42 discrete trials. On the first two trials, the magnitude of the ASR to a 50 ms duration of 120 dB tone was measured. These first two startle tones were presented in order to habituate the animals to the testing procedure. Therefore, the ASR magnitude of these two trials was omitted from the statistical analysis of the mean ASR amplitude. On the subsequent 40 trials, the startle tone was either presented alone or 100 ms after presentation of 30 ms duration prepulse. Prepulse intensity ranged from 3 to 15 dB above background noise and was varied randomly between trials in 3 dB steps. Measures were taken at each of the five prepulse intensities on 5 trials; animals were randomly presented with the startle tone alone during the other 10 trials; null trials (background tone alone) during the other 5 trials. The same stimulus condition was never presented on more than two consecutive trials. The interval between each trial was programmed to a variable time schedule with an average duration of 15 s (range 5–30 s). A measure of startle response amplitude was derived from the mean of 100 digitized data points collected from stimulus onset at a rate of 1 kHz. Prepulse effectiveness in suppressing the startle response was expressed as a percentage based on the mean amplitude of responses to the startle tone alone (10 startle tones) relative to those recorded under the five prepulse conditions (5 startle tones/condition): PPI = 100 − [(mean startle amplitude for prepulse + pulse trials/mean startle amplitude for pulse-alone trials) × 100]%. PPI data also expressed as average across all prepulse intensities (Average PPI).

2.5. Statistical analysis

Results are expressed as mean ± standard errors of the mean (SEM). A one-way analysis of variance (ANOVA) was used to assess the treatment effects on the magnitude of the ASR and the Average PPI. The PPI data were analyzed by two-way repeated-measures ANOVA with the treatment as independent factor and prepulse intensity as repeated measures. Post hoc Fisher's PLSD test was conducted when appropriate. The criterion of significance was set at $p < 0.05$.

3. Results

3.1. Effects of p-OHA on PPI

p-OHA had no effect on the startle amplitude in mice (Tables 1 and 2). Fig. 1 shows the effects of *p*-OHA (5, 20 and 80 μg/mouse, i.c.v.) on PPI (Fig. 1A and B). Two-way repeated-measures ANOVA of PPI revealed significant effects of treatment [$F_{(3, 36)} = 13.715$, $p < 0.0001$] and prepulse intensity [$F_{(4, 144)} = 43.955$, $p < 0.0001$], but not their interaction (Fig. 1A). One-way ANOVA of Average PPI revealed a significant effect of the treatment [$F_{(3, 36)} = 13.715$, $p < 0.0001$] (Fig. 1B). The post hoc test revealed that i.c.v. administration of *p*-OHA dose-dependently induced PPI disruptions for all prepulse intervals tested and Average PPI (Fig. 1A and B). In subsequent experiments, we employed a dose of 80 μg/mouse of *p*-OHA to induce PPI disruptions.

Table 1
Effects of *p*-hydroxyamphetamine (*p*-OHA) on the acoustic startle response in mice.

Compound	Dose (μg/mouse)	Startle amplitude ± SEM
p-OHA	0 (vehicle)	133.3 ± 13.3
	5	128.4 ± 18.1
	20	135.9 ± 19.9
	80	131.8 ± 12.7

Startle data are expressed as mean startle amplitude for pulse-alone trials.

Table 2
Comparison of "vehicle + vehicle" vs. "vehicle + *p*-OHA" on the acoustic startle response in mice.

Pretreatment	Startle amplitude ± SEM	
	p-OHA vehicle	*p*-OHA (80 μg/mouse)
Saline	87.5 ± 9.4	102.2 ± 20.7
0.5% Tween 80	99.9 ± 7.3	93.0 ± 10.3
Ringer	108.5 ± 20.5	120.5 ± 19.2

Saline was used as a solvent of SCH 23390, eticlopride or L-745,870. 0.5% Tween 80 was used as a solvent of haloperidol, clozapine or L-741,626. Ringer's solution, containing 0.1% ascorbic acid, was used as a solvent of 6-OHDA.

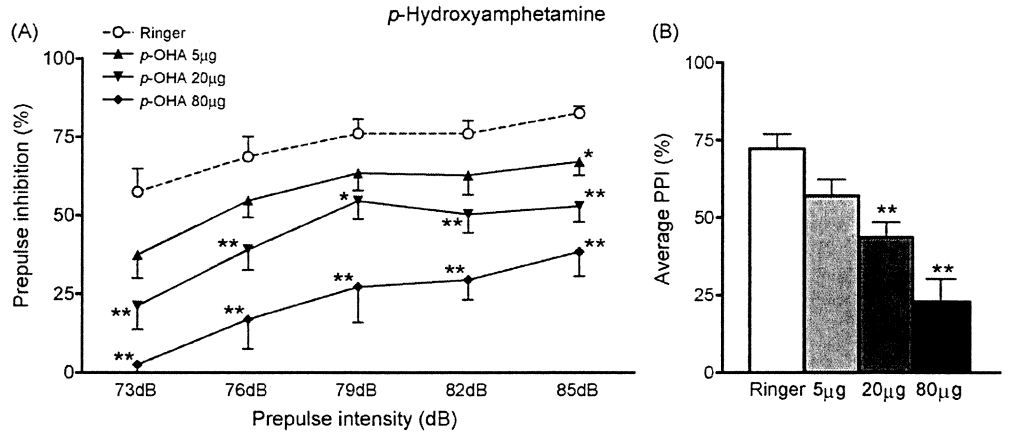


Fig. 1. Effects of *p*-hydroxyamphetamine (*p*-OHA) on prepulse inhibition (PPI). The left panel (A) shows PPI expressed per prepulse intensity level (73, 76, 79, 82 and 85 dB), and the right panel (B) shows PPI data expressed as an average across all prepulse intensities (Average PPI). Data represent the means ± SEM for 10 animals per group. $^{*}P < 0.05$, $^{**}P < 0.01$ vs. Ringer's only (i.c.v.) group.

3.2. Effects of haloperidol or clozapine on p-OHA-induced PPI disruptions

Fig. 2 shows the effects of haloperidol (0.25 and 0.5 mg/kg, i.p.) or clozapine (3 and 6 mg/kg, i.p.) on *p*-OHA-induced PPI disruptions (Fig. 2A–D). Haloperidol had no effect on the startle amplitude (Table 3). Two-way repeated-measures ANOVA of PPI revealed significant effects of treatment [$F_{(3, 36)} = 9.511$, $p < 0.0001$], prepulse intensity [$F_{(4, 144)} = 23.013$, $p < 0.0001$] and their interaction [$F_{(12, 144)} = 2.509$, $p = 0.0051$] (Fig. 2A). One-way ANOVA of Average PPI also revealed a significant effect of treatment [$F_{(3, 36)} = 9.511$, $p < 0.0001$] (Fig. 2B). The post hoc test revealed that haloperidol attenuated *p*-OHA-induced PPI disruptions for all prepulse intensities and Average PPI (Fig. 2A and B). As shown in Table 3, clozapine had also no effect on the startle amplitude. Two-way repeated-measures ANOVA of PPI revealed significant

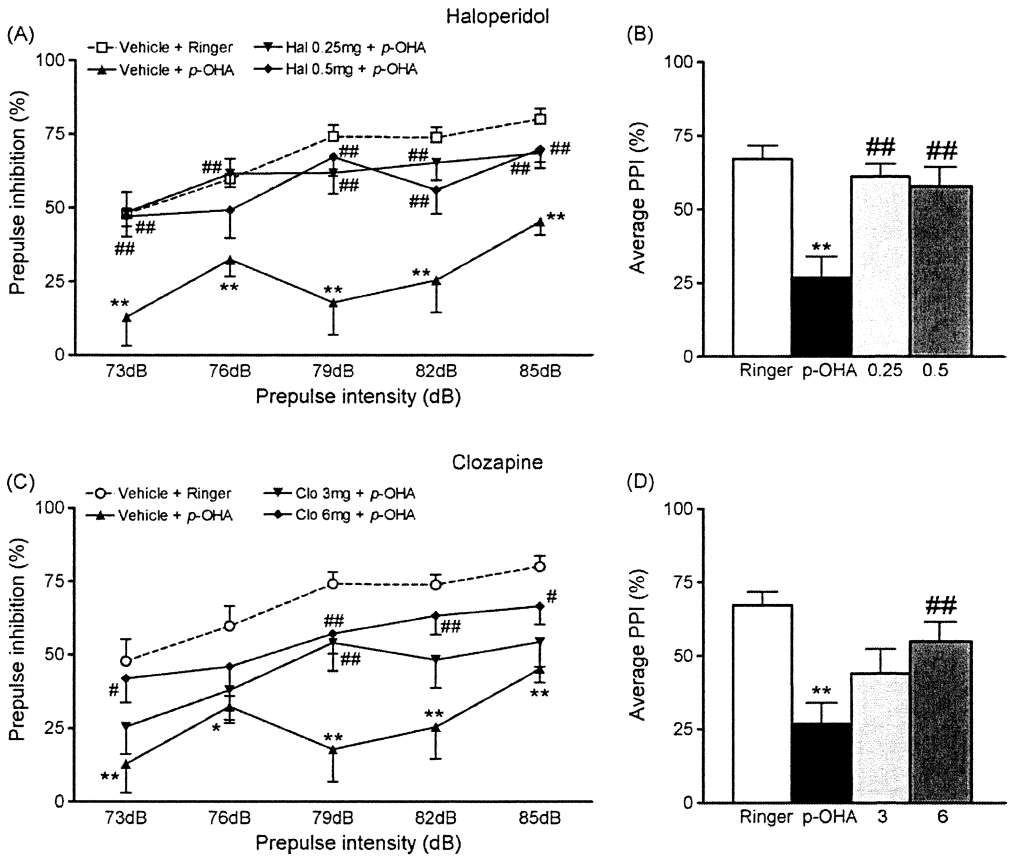


Fig. 2. Effects of haloperidol (A and B) or clozapine (C and D) on *p*-OHA-induced PPI disruptions in mice. Left panels (A and C) show PPI expressed per prepulse intensity level (73, 76, 79, 82 and 85 dB), and right panels (B and D) show PPI data expressed as an average across all prepulse intensities (Average PPI). Data represent the means ± SEM for 10 animals per group. $^{*}P < 0.05$, $^{**}P < 0.01$ vs. the vehicle (i.p.) + Ringer's (i.c.v.) group. $\#P < 0.05$, $\#\#P < 0.01$ vs. vehicle (i.p.) + *p*-OHA (80 μg/mouse, i.c.v.) group.

Table 3
Effects of haloperidol, clozapine or vehicle + *p*-OHA (80 μg/mouse) on the acoustic startle response in mice.

Compound	Dose (mg/kg)	Startle amplitude ± SEM
Haloperidol	Vehicle	93.0 ± 10.3
	0.25	85.5 ± 11.6
	0.5	100.7 ± 11.7
Clozapine	Vehicle	93.0 ± 10.3
	3	101.7 ± 8.4
	6	90.9 ± 25.8

effects of treatment [$F_{(3, 36)} = 6.245$, $p = 0.0016$], prepulse intensity [$F_{(4, 144)} = 24.275$, $p < 0.0001$] and their interaction [$F_{(12, 144)} = 1.948$, $p = 0.0332$] (Fig. 2C). One-way ANOVA of Average PPI also revealed a significant effect of the treatment [$F_{(3, 36)} = 6.245$, $p = 0.0016$] (Fig. 2D). The post hoc test revealed that clozapine attenuated *p*-OHA-induced PPI disruptions at 73, 79, 82 and 85 dB prepulse intensity and Average PPI (Fig. 2C and D).

3.3. Effects of DA receptor antagonists on p-OHA-induced PPI disruptions

One-way ANOVA of startle amplitude revealed that all of the DA receptor antagonists had no effect on the startle amplitude (Table 4). The effects of SCH 23390 (0.025, 0.05 and 0.1 mg/kg, i.p.) on *p*-OHA-induced PPI disruptions are shown in Fig. 3A and B. There were significant effects of treatment [$F_{(4, 45)} = 13.358$, $p < 0.0001$] and prepulse intensity [$F_{(4, 180)} = 21.216$, $p < 0.0001$] but not their interaction (Fig. 3A). One-way ANOVA of Average PPI revealed a significant effect of treatment [$F_{(4, 45)} = 13.358$, $p < 0.0001$] (Fig. 3B). The post hoc test revealed that SCH 23390 did not influence *p*-OHA-induced PPI disruptions and Average PPI (Fig. 3A and B). The effects of L-741,626 (2 and 4 mg/kg, s.c.) on *p*-OHA-induced PPI disruptions are shown in Fig. 3C and D. There were significant effects of treatment [$F_{(3, 36)} = 5.306$, $p = 0.0039$], prepulse intensity [$F_{(4, 144)} = 25.178$, $p < 0.0001$] and their interaction [$F_{(12, 144)} = 1.960$, $p = 0.0321$] (Fig. 3C). One-way ANOVA of Average PPI also revealed a significant effect of treatment [$F_{(3, 36)} = 5.306$, $p = 0.0039$] (Fig. 3D). The post hoc test revealed that L-741,626 attenuated *p*-OHA-induced PPI disruptions at 79 dB prepulse intensity (Fig. 3C), but not Average PPI (Fig. 3D). The effects of eticlopride (0.05, 0.1 and 1 mg/kg, i.p.) on *p*-OHA-induced PPI disruptions are shown in Fig. 3E and F. There were significant effects of treatment [$F_{(4, 45)} = 3.141$, $p = 0.0232$] and prepulse intensity [$F_{(4, 180)} = 13.909$, $p < 0.0001$] but not their interaction (Fig. 3E). One-way ANOVA of Average PPI revealed a significant effect of treatment [$F_{(4, 45)} = 3.141$, $p = 0.0232$] (Fig. 3F). The post hoc test revealed that eticlopride did not influence *p*-OHA-induced PPI disruptions and Average PPI (Fig. 3E and F). The effects of L-745,870 (0.5, 1, 3 and 9 mg/kg, i.p.) are shown in Fig. 3G and H. The ANOVA revealed significant effects of treatment [$F_{(5, 54)} = 5.552$, $p = 0.0003$] and prepulse intensity [$F_{(4, 216)} = 23.501$, $p < 0.0001$], but not their interaction (Fig. 3G). One-way ANOVA of Average PPI revealed a significant effect of treatment [$F_{(5, 54)} = 5.552$, $p = 0.0003$] (Fig. 3H). The post hoc test revealed that L-745,870 attenuated *p*-OHA-induced PPI disruptions at a dose of 9 mg/kg at 79 and 85 dB prepulse intensity and Average PPI (Fig. 3G and H).

Table 4
Effects of DA receptor antagonists or vehicle + *p*-OHA (80 μg/mouse) on the acoustic startle response in mice.

Compound	Dose (mg/kg)	Startle amplitude ± SEM
SCH 23390	Vehicle	102.2 ± 20.7
	0.025	106.8 ± 17.2
	0.05	109.2 ± 11.0
	0.1	117.2 ± 18.7
L-741,626	Vehicle	93.0 ± 10.3
	2	116.7 ± 15.7
	4	91.5 ± 14.4
Eticlopride	Vehicle	102.2 ± 20.7
	0.05	105.0 ± 9.8
	0.1	84.9 ± 13.7
	1	80.8 ± 16.8
L-745,870	Vehicle	102.2 ± 20.7
	0.5	109.6 ± 17.1
	1	90.0 ± 12.5
	3	112.9 ± 18.5
	9	97.1 ± 12.3

Table 5
Effects of 6-hydroxydopamine (6-OHDA), GBR 12909 or vehicle + *p*-OHA (80 μg/mouse) or vehicle on the acoustic startle response in mice.

Compound	Dose	Startle amplitude ± SEM	
		p-OHA vehicle	*p*-OHA (80 μg/mouse)
6-OHDA	Vehicle	108.5 ± 20.5	120.5 ± 19.2
	40 μg/mouse	100.1 ± 20.1	117.4 ± 11.2
GBR 12909	Vehicle	87.5 ± 9.4	102.2 ± 20.7
	5 mg/kg	84.1 ± 12.7	93.9 ± 18.4

3.4. Effects of 6-OHDA lesion or DA-reuptake inhibitor on p-OHA-induced PPI disruptions

Fig. 4 shows the effects of 6-OHDA (40 μg/mouse, i.c.v.) or GBR 12909 (5 mg/kg, i.p.) on *p*-OHA-induced PPI disruptions (Fig. 4A–D). 6-OHDA had no effect on the startle amplitude (Table 5). The ANOVA of PPI revealed significant effects of treatment [$F_{(3, 36)} = 4.623$, $p = 0.0078$] and prepulse intensity [$F_{(4, 144)} = 20.945$, $p < 0.0001$], but not their interaction (Fig. 4A). One-way ANOVA of Average PPI revealed a significant effect of treatment [$F_{(3, 36)} = 4.623$, $p = 0.0078$] (Fig. 4B). The post hoc test revealed that 6-OHDA attenuated the extent of PPI disruptions induced by *p*-OHA at 85 dB prepulse intensity (Fig. 4A), but not Average PPI (Fig. 4B). As shown in Table 5, GBR 12909 had also no effect on the startle amplitude. The ANOVA of PPI revealed significant effects of treatment [$F_{(3, 36)} = 13.814$, $p < 0.0001$] and prepulse intensity [$F_{(4, 144)} = 7.324$, $p < 0.0001$], but not their interaction (Fig. 4C). One-way ANOVA of Average PPI revealed a significant effect of treatment [$F_{(3, 36)} = 13.814$, $p < 0.0001$] (Fig. 4D). The post hoc test revealed that GBR 12909 did not attenuate *p*-OHA-induced PPI disruptions and Average PPI (Fig. 4C and D).

4. Discussion

There are many reports concerning AMPH-induced PPI disruptions in rodents [36,37,41], however, this is the first report that *p*-OHA, an AMPH and METH metabolite, induced PPI disruptions. AMPH is first metabolized to *p*-OHA in the periphery and brain [17,18], but peripherally metabolized *p*-OHA does not easily cross the blood–brain barrier [28]. In the brain, AMPH is metabolized to *p*-OHA by the enzyme dopamine-β-hydroxylase [17,18]. Interestingly, despite the rapid disappearance of AMPH after its administration, long-lasting accumulation of *p*-OHA is found in various brain regions [22,26]. As peripherally administered *p*-OHA hardly penetrates the blood–brain barrier [28], we used direct administration of *p*-OHA into the brain. i.c.v. administration of *p*-OHA dose-dependently induced PPI disruptions for all prepulse intervals tested (3–15 dB above background) and average PPI. Interestingly, a previous report has demonstrated that in rats repeatedly exposed to AMPH, PPI was disrupted during the withdrawal period [36]. Peleg-Raibstein et al. [36] have also reported post-mortem neurochemistry obtained following withdrawal peri-

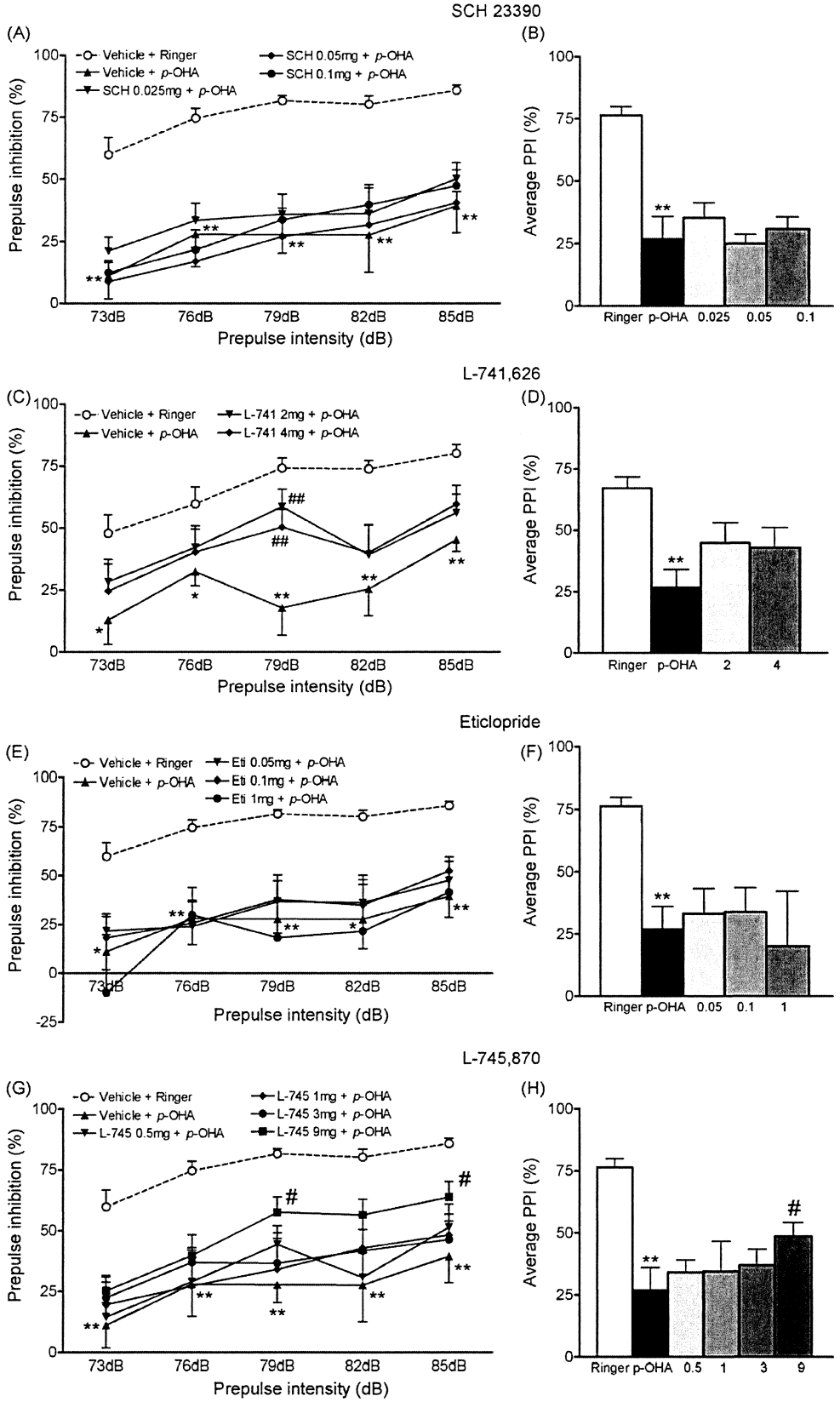


Fig. 3. Effects of SCH 23390 (A and B), L-741,626 (C and D), eticlopride (E and F) or L-745,870 (G and H) on *p*-OHA-induced PPI disruptions in mice. Left panels (A, C, E, and G) show PPI expressed per prepulse intensity level (73, 76, 79, 82 and 85 dB), whereas right panels (B, D, F and H) show PPI data expressed as an average across all prepulse intensities (Average PPI). Data represent the means ± SEM for 10 animals per group. $^{*}P < 0.05$, $^{**}P < 0.01$ vs. vehicle (i.p. or s.c.) + Ringer's (i.c.v.) group. $\#P < 0.05$, $\#\#P < 0.01$ vs. vehicle (i.p. or s.c.) + *p*-OHA (80 μg/mouse, i.c.v.) group.

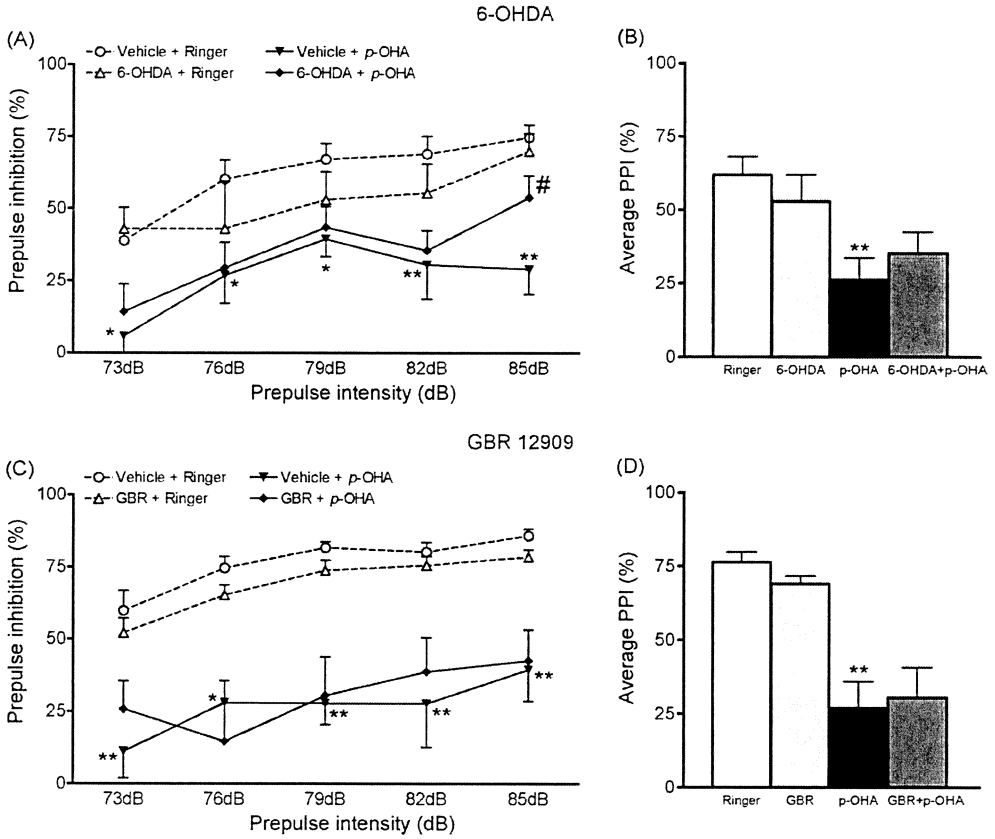


Fig. 4. Effects of 6-hydroxydopamine (6-OHDA) (A and B) or GBR 12909 (C and D) on *p*-OHA-induced PPI disruptions in mice. Left panels (A and C) show PPI expressed per prepulse intensity level (73, 76, 79, 82 and 85 dB), whereas right panels (B and D) show PPI data expressed as average across all prepulse intensities (Average PPI). Data represent the means ± SEM for 10 animals per group. $^{*}P < 0.05$, $^{**}P < 0.01$ vs. vehicle + Ringer's (i.c.v.) group. $\#P < 0.05$ vs. vehicle + *p*-OHA (80 μg/mouse, i.c.v.).

ods that revealed reduced DA levels in the rat caudate putamen and nucleus accumbens. This report is similar to our previous finding that i.c.v. administration of *p*-OHA in mice significantly reduced striatal DA levels [3]. As *p*-OHA has been found in the brain after systemic administration of AMPH [12], the chronic administration of AMPH by Peleg-Raibstein et al. [36] may have caused *p*-OHA accumulation in rat brain, resulting in PPI disruptions and reduced DA levels. Thus, *p*-OHA-induced PPI disruptions may reflect the withdrawal periods after chronic administration of AMPH.

p-OHA-induced PPI disruptions were attenuated by pretreatment with both haloperidol (a predominantly D_2-blocking typical antipsychotic) and clozapine (a multi-receptor-blocking atypical antipsychotic). Haloperidol effects extended to all prepulse intensities and average PPI. Clozapine also attenuated the PPI disruptions over a wide range of prepulse intensities, however, clozapine effects were relatively weak compared to those of haloperidol. Clozapine has a highly complex pharmacological profile, with high affinity for a number of serotonin ($5\text{-}HT_{2A}$, $5\text{-}HT_{2C}$, $5\text{-}HT_6$, $5\text{-}HT_7$), dopamine (D_4), muscarinic (M_1, M_2, M_3, M_4, M_5), adrenergic (α_1- and α_2-subtypes) and other biogenic amine receptors [38]. Yamada [49] has shown that the ED50 value of the drugs used to reverse the apomorphine (a D_1 and D_2 agonist)-induced PPI disruption was significantly correlated with affinity for the D_2 receptor, but not for the D_1 receptor of each drug (including typical antipsychotics). As there is a difference in D_2 receptor affinity between haloperidol and clozapine, our results demonstrating the effects of haloperidol or clozapine indicate that the D_2 receptor may be involved in the *p*-OHA-induced PPI disruptions in mice. However, haloperidol also has affinity for the D_1, D_3 and D_4 receptors [38], therefore we have to consider possible involvement of these receptors in the *p*-OHA-induced PPI disruptions in mice. Furthermore, as it has been suggested that *p*-OHA can be taken up into dopaminergic nerve terminals, followed by DA release into the synaptic cleft [3] and as we have previously reported that *p*-OHA-induced hyperlocomotion is inhibited by a DA-reuptake inhibitor [35], we focused on the involvement of the central presynaptic or postsynaptic dopaminergic system on *p*-OHA-induced PPI disruptions and investigated the effects of pretreatment with several dopaminergic agents. Regarding the effects of these DA receptor antagonists, *p*-OHA-induced PPI disruptions were attenuated by pretreatment with L-741,626 (a selective D_2 receptor antagonist) and L-745,870 (a selective D_4 receptor antagonist), but not by SCH 23390 (a selective D_1 receptor antagonist) or eticlopride (a D_2/D_3 receptor antagonist). As described above, anti-DA agonist effects have been positively correlated with affinity for D_2 but not D_1 receptors [49]. Moreover, Swerdlow et al. [45] have reported that both systemic and intramedial prefrontal cortical D_1 blockade reduces PPI in rats. It has been proposed that DA dysfunction in schizophrenia includes both hyperfunction of subcortical D_2 and hypofunction of cortical D_1 systems [40]. In a previous study using knock-out mice lacking D_2, D_3 or D_4 receptors, AMPH significantly disrupted PPI in both the D_3 (−/−) and D_4 (−/−) mice, but not in the D_2 (−/−) mice [37]. Our results concerning the effects of a D_2 antagonist (L-741,626) on *p*-OHA-induced PPI disruptions are supported by the previous report concerning AMPH effects in D_2 (−/−) mice, although our D_4 antagonist (L-745,870) results were not supported by AMPH effects in D_4 (−/−) mice. However, Ralph et al. [37] have described gender differences in AMPH effects in D_4 (−/−) and wild-type mice. Our results relating to D_4 antagonist effects were supported by another report that the three D_4-selective compounds (CP-293,019,

U-101,387 and L-745,870) significantly attenuated PPI disruptions produced by apomorphine [32]. *p*-OHA-induced PPI disruptions were not attenuated by 0.01–1.0 mg/kg of eticlopride, a selective D_2/D_3 antagonist (Ki values are 0.50 nM and 0.16 nM respectively [33]). Eticlopride may attenuate *p*-OHA-induced PPI disruptions at other doses, especially at a high dose. However, effects of a high dose of eticlopride may be due to the D_2-blocking effect. This theory is supported by a previous report showing that low doses of nafadotride, a preferential D_3 antagonist (Ki values of 0.3 nM at D_3, 3.0 nM at D_2), increases spontaneous locomotion in habituated rats and climbing behavior in mice, however, a high dose of nafadotride, like haloperidol, produces catalepsy and antagonizes apomorphine-induced climbing, indicating that D_3 receptor blockade results in motor activation, which contrasts with the motor sedation caused by D_2 receptor blockade [39]. Differences in the signaling of D_2 and D_3 receptors have also been reported and it appears that the D_3 receptor has a greatly reduced ability to translocate β-arrestin to the plasma membrane and sequesters much less than the D_2 receptor does [25]. The specific role of the D_3 receptor in the effects of DA agonists remains unclear because of limited availability of selective ligands [37]. For example, Caine et al. [9] have reported that the preferential D_3 antagonist UH 232 failed to attenuate an apomorphine-induced disruption of PPI. On the other hand, previous studies have reported that 0.01–0.1 mg/kg of eticlopride attenuated PPI disruption induced by apomorphine [20] and 0.01–0.06 mg/kg of eticlopride attenuated AMPH-induced task-performance disruption [50]. Our result with eticlopride does not match with the D_2 antagonist results or previous reports using eticlopride. However, unlike apomorphine or AMPH, *p*-OHA has been shown to have unique properties (described in Section 1) and plays a distinct role in central neural transmission, affecting not only dopamine but also serotonin and noradrenaline. These differences may explain our finding that eticlopride failed to attenuate *p*-OHA-induced PPI disruptions. Our results demonstrating the effects of several DA receptor antagonists indicate that at least D_2 and D_4 receptors may be involved in the *p*-OHA-induced PPI disruptions in mice.

As AMPH induces the release of monoamines, *p*-OHA has also been assumed to induce the release of neurotransmitters from presynaptic monoaminergic neurons. Indeed, it has been suggested that *p*-OHA is taken up into serotonergic as well as dopaminergic nerve terminals, followed by DA release into the synaptic cleft [3]. Moreover, *p*-OHA-induced hyperlocomotion was inhibited by pretreatment with a DA-reuptake inhibitor [35]. Therefore, we used 6-OHDA (a neurotoxin which targets DA-containing neurons) or GBR 12909 (a DA-reuptake inhibitor) to determine whether *p*-OHA-induced PPI disruptions are due to DA release into the synaptic cleft. Although it has been reported that 6-OHDA impaired PPI in rodents [7], we used 40 μg/mouse of 6-OHDA which did not induce any PPI disruptions. As a result, 6-OHDA lesions attenuated the extent of PPI disruptions induced by *p*-OHA. This is supported by a previous report that 6-OHDA lesions of the nucleus accumbens in rats attenuated the ability of AMPH to disrupt PPI [43]. In contrast to 6-OHDA, GBR 12909 did not attenuate *p*-OHA-induced PPI disruptions. We used GBR 12909 at a dose of 5.0 mg/kg because 10 mg/kg of GBR 12909 induced PPI disruptions (data not shown). However, in the *p*-OHA-induced hyperlocomotion experiment, 5.0 mg/kg of nomifensine (a DA-reuptake inhibitor), which when given alone induced hyperlocomotion in rats, inhibited *p*-OHA-induced hyperlocomotion more strongly than 2.5 mg/kg of nomifensine with no changes in mice ambulation, indicating that 5.0 mg/kg of nomifensine is a more effective dose for DA-reuptake inhibition [35]. In fact, Baumann et al. [5] have reported that GBR 12909 blocked AMPH-induced elevation of dialysate DA levels in the nucleus accumbens of rats. In a previous study using knock-out mice lacking the DA transporter (DAT) gene (DAT-KO mice), infusion of AMPH directly into the NAc did not produce an increase in DA levels in DAT-KO mice, although there were robust drug-induced increases in wild-type controls [8]. Further studies are needed to investigate the effects of GBR 12909 on *p*-OHA-induced PPI disruptions, focusing on dose–response or time-course of administration.

In summary, *p*-OHA, an AMPH and METH metabolite, dose-dependently induced PPI disruptions in mice. *p*-OHA-induced PPI disruptions were attenuated by haloperidol and clozapine. *p*-OHA-induced PPI disruptions were also attenuated by L-741,626 (a selective D_2 receptor antagonist), L-745,870 (a selective D_4 receptor antagonist) and 6-OHDA (a neurotoxin which targets DA-containing neurons), but not by SCH 23390 (a selective D_1 receptor antagonist), eticlopride (a D_2/D_3 receptor antagonist) or GBR 12909 (a DA-reuptake inhibitor). Our results indicate that selective blockade of either the D_2 or D_4 receptor subtype may prevent disruption of PPI induced by *p*-OHA via presynaptic DA release. This approach to explore the unique properties of *p*-OHA may help to elucidate psychostimulant action in the central nervous system and to ultimately clarify schizophrenia-relevant pathogenesis.

Acknowledgments

This study was supported in part by Grants-in-Aid for Scientific Research (20790309) and Matching Fund Subsidy for Private Universities from the Ministry of Education, Culture, Sports, Science and Technology of Japan. The authors acknowledge the editorial support of ProSciEd's professional editor.

References

[1] Arai S, Takuma K, Mizoguchi H, Ibi D, Nagai T, Takahashi K, et al. Involvement of pallidotegmental neurons in methamphetamine- and MK-801-induced impairment of prepulse inhibition of the acoustic startle reflex in mice: reversal by GABAB receptor agonist baclofen. Neuropsychopharmacology 2008;33:3164–75.
[2] Arai Y, Kim SK, Kinemuchi H, Tadano T, Satoh SE, Satoh N, et al. Inhibition of brain type A monoamine oxidase and 5-hydroxytryptamine uptake by two amphetamine metabolites, *p*-hydroxyamphetamine and *p*-hydroxynorephedrine. J Neurochem 1990;55:403–8.
[3] Arai Y, Kim SK, Kinemuchi H, Tadano T, Oyama K, Satoh N, et al. Inhibition of brain MAO-A and animal behaviour induced by *p*-hydroxyamphetamine. Brain Res Bull 1991;27:81–4.
[4] Asanuma M, Hirata H, Cadet JL. Attenuation of 6-hydroxydopamine-induced dopaminergic nigrostriatal lesions in superoxide dismutase transgenic mice. Neuroscience 1998;85:907–17.
[5] Baumann MH, Char GU, De Costa BR, Rice KC, Rothman RB. GBR12909 attenuates cocaine-induced activation of mesolimbic dopamine neurons in the rat. J Pharmacol Exp Ther 1994;271:1216–22.
[6] Brittain RT, Handley SL. Temperature changes produced by the injection of catecholamines and 5-hydroxytryptamine into the cerebral ventricles of the conscious mouse. J Physiol 1967;192:805–13.
[7] Bubser M, Koch M. Prepulse inhibition of the acoustic startle response of rats is reduced by 6-hydroxydopamine lesions of the medial prefrontal cortex. Psychopharmacology (Berl) 1994;113:487–92.
[8] Budygin EA, Brodie MS, Sotnikova TD, Mateo Y, John CE, Cyr M, et al. Dissociation of rewarding and dopamine transporter-mediated properties of amphetamine. Proc Natl Acad Sci USA 2004;101:7781–6.
[9] Caine SB, Geyer MA, Swerdlow NR. Effects of D_3/D_2 dopamine receptor agonists and antagonists on prepulse inhibition of acoustic startle in the rat. Neuropsychopharmacology 1995;12:139–45.
[10] Caine SB, Negus SS, Mello NK, Patel S, Bristow L, Kulagowski J, et al. Role of dopamine D_2-like receptors in cocaine self-administration: studies with D_2 receptor mutant mice and novel D_2 receptor antagonists. J Neurosci 2002;22:2977–88.
[11] Caine SB, Thomsen M, Gabriel KI, Berkowitz JS, Gold LH, Koob GF, et al. Lack of self-administration of cocaine in dopamine D_1 receptor knock-out mice. J Neurosci 2007;27:13140–50.
[12] Cho AK, Fischer JF, Schaeffer JC. The accumulation of *p*-hydroxyamphetamine by brain homogenates and its role in the release of catecholamines. Biochem Pharmacol 1977;26:1367–72.
[13] Dougan DF, Labrie SL, Paull PD, Duffield PH, Wade DN. Evidence that alpha-methyl-*p*-tyramine is implicated in behavioural augmentation to amphetamine. Gen Pharmacol 1986;17:453–6.
[14] Duncan GE, Moy SS, Lieberman JA, Koller BH. Effects of haloperidol, clozapine, and quetiapine on sensorimotor gating in a genetic model of reduced NMDA receptor function. Psychopharmacology (Berl) 2006;184:190–200.

[15] Feifel D, Reza T, Robeck S. Antipsychotic potential of CCK-based treatments: an assessment using the prepulse inhibition model of psychosis. Neuropsychopharmacology 1999;20:141–9.
[16] Geyer MA, Krebs-Thomson K, Braff DL, Swerdlow NR. Pharmacological studies of prepulse inhibition models of sensorimotor gating deficits in schizophrenia: a decade in review. Psychopharmacology (Berl) 2001;156:117–54.
[17] Goldstein M, Contrera JF. The substrate specificity of phenylamine-β-hydroxylase. J Biol Chem 1962;237:1898–902.
[18] Goldstein M, Anagnoste B. The conversion in vivo of D-amphetamine to (+)*p*-hydroxynorephedrine. Biochim Biophys Acta 1965;107:166–8.
[19] Hattori K, Uchino S, Isosaka T, Maekawa M, Iyo M, Sato T, et al. Fyn is required for haloperidol-induced catalepsy in mice. J Biol Chem 2006;281:7129–35.
[20] Hoffman DC, Donovan H. D_1 and D_2 dopamine receptor antagonists reverse prepulse inhibition deficits in an animal model of schizophrenia. Psychopharmacology (Berl) 1994;115:447–53.
[21] Joober R, Zarate JM, Rouleau GA, Skamene E, Boksa P. Provisional mapping of quantitative trait loci modulating the acoustic startle response and prepulse inhibition of acoustic startle. Neuropsychopharmacology 2002;27:765–81.
[22] Jori A, Caccia S. Distribution of amphetamine and its hydroxylated metabolites in various areas of the rat brain. J Pharm Pharmacol 1974;26:746–8.
[23] Kamdar NK, Miller SA, Syed YM, Bhayana R, Gupta T, Rhodes JS. Acute effects of naltrexone and GBR 12909 on ethanol drinking-in-the-dark in C57BL/6J mice. Psychopharmacology (Berl) 2007;192:207–17.
[24] Kaminskas LM, Irvine RJ, Callaghan PD, White JM, Kirkbride P. The contribution of the metabolite *p*-hydroxyamphetamine to the central actions of *p*-methoxyamphetamine. Psychopharmacology (Berl) 2002;160:155–60.
[25] Kim KM, Valenzano KJ, Robinson SR, Yao WD, Barak LS, Caron MG. Differential regulation of the dopamine D_2 and D_3 receptors by G protein-coupled receptor kinases and beta-arrestins. J Biol Chem 2001;276:37409–14.
[26] Kuhn CM, Schanberg SM, Breese GR. Metabolism of amphetamine by rat brain tissue. Biochem Pharmacol 1978;27:343–51.
[27] Laloux C, Derambure P, Jacquesson JM, Bordet R, Destée A, Monaca C. The effects of serotoninergic, noradrenergic, cholinergic and dopaminergic drugs on vigilance states in MPTP-treated mice. Brain Res 2007;1161:79–87.
[28] Lindenbaum A, Marcher K, Wepierre J, Cohen Y. Blood–brain barrier. II. Kinetics of distribution of ^{3}H-parahydroxyamphetamine in brain structures after intravenous administration in the rat. Arch Int Pharmacodyn Ther 1975;215:168–76.
[29] Mamiya T, Matsumura T, Ukai M. Effects of L-745,870, a dopamine D_4 receptor antagonist, on naloxone-induced morphine dependence in mice. Ann N Y Acad Sci 2004;1025:424–9.
[30] Mansbach RS, Geyer MA, Braff DL. Dopaminergic stimulation disrupts sensorimotor gating in the rat. Psychopharmacology (Berl) 1988;94:507–14.
[31] Mansbach RS, Geyer MA. Effects of phencyclidine and phencyclidine biologs on sensorimotor gating in the rat. Neuropsychopharmacology 1989;2: 299–308.
[32] Mansbach RS, Brooks EW, Sanner MA, Zorn SH. Selective dopamine D_4 receptor antagonists reverse apomorphine-induced blockade of prepulse inhibition. Psychopharmacology (Berl) 1998;135:194–200.
[33] Nader MA, Green KL, Luedtke RR, Mach RH. The effects of benzamide analogues on cocaine self-administration in rhesus monkeys. Psychopharmacology (Berl) 1999;147:143–52.
[34] Nakagawasai O, Onogi H, Mitazaki S, Sato A, Watanabe K, Saito H, et al. Behavioral and neurochemical characterization of mice deficient in the N-type Ca(2+) channel alpha(1B) subunit. Behav Brain Res 2010;208:224–30.
[35] Onogi H, Hozumi M, Nakagawasai O, Arai Y, Ishigaki S, Sato A, et al. Central administration of *p*-hydroxyamphetamine produces a behavioral stimulant effect in rodents: evidence for the involvement of dopaminergic systems. Psychopharmacology (Berl) 2010;208:323–31.
[36] Peleg-Raibstein D, Knuesel I, Feldon J. Amphetamine sensitization in rats as an animal model of schizophrenia. Behav Brain Res 2008;191:190–201.
[37] Ralph RJ, Varty GB, Kelly MA, Wang YM, Caron MG, Rubinstein M, et al. The dopamine D_2, but not D_3 or D_4, receptor subtype is essential for the disruption of prepulse inhibition produced by amphetamine in mice. J Neurosci 1999;19:4627–33.
[38] Roth BL, Sheffler DJ, Kroeze WK. Magic shotguns versus magic bullets: selectively non-selective drugs for mood disorders and schizophrenia. Nat Rev Drug Discov 2004;3:353–9.
[39] Sautel F, Griffon N, Sokoloff P, Schwartz JC, Launay C, Simon P, et al. Nafadotride, a potent preferential dopamine D_3 receptor antagonist, activates locomotion in rodents. J Pharmacol Exp Ther 1995;275:1239–46.
[40] Seamans JK, Yang CR. The principal features and mechanisms of dopamine modulation in the prefrontal cortex. Prog Neurobiol 2004;74:1–58.
[41] Sills TL. Amphetamine dose dependently disrupts prepulse inhibition of the acoustic startle response in rats within a narrow time window. Brain Res Bull 1999;48:445–8.
[42] Simpson LL. Blood pressure and heart rate response evoked by *p*-hydroxyamphetamine and by *p*-hydroxynorephedrine. II. A quantitative assessment of the role of amphetamine metabolites in acute responses evoked by D-amphetamine. J Pharmacol Exp Ther 1980;213:504–8.
[43] Swerdlow NR, Mansbach RS, Geyer MA, Pulvirenti L, Koob GF, Braff DL. Amphetamine disruption of prepulse inhibition of acoustic startle is reversed by depletion of mesolimbic dopamine. Psychopharmacology (Berl) 1990;100:413–6.
[44] Swerdlow NR, Braff DL, Taaid N, Geyer MA. Assessing the validity of an animal model of deficient sensorimotor gating in schizophrenic patients. Arch Gen Psychiatry 1994;51:139–54.
[45] Swerdlow NR, Shoemaker JM, Bongiovanni MJ, Neary AC, Tochen LS, Saint Marie RL. Reduced startle gating after D_1 blockade: effects of concurrent D_2 blockade. Pharmacol Biochem Behav 2005;82:293–9.
[46] Tadano T, Satoh S, Kisara K. Head-twitches induced by *p*-hydroxyamphetamine. Jpn J Pharmacol 1986;41:519–23.
[47] Tadano T, Satoh S, Satoh N, Kisara K, Arai Y, Kim SK, et al. Potentiation of para-hydroxyamphetamine-induced head-twitch response by inhibition of monoamine oxidase type A in the brain. J Pharmacol Exp Ther 1989;250:254–60.
[48] Tenn CC, Fletcher PJ, Kapur S. A putative animal model of the "prodromal" state of schizophrenia. Biol Psychiatry 2005;57:586–93.
[49] Yamada S. Disruption of prepulse inhibition of acoustic startle as an animal model for schizophrenia. Nihon Shinkei Seishin Yakurigaku Zasshi 2000;20:131–9.
[50] Zeeb FD, Robbins TW, Winstanley CA. Serotonergic and dopaminergic modulation of gambling behavior as assessed using a novel rat gambling task. Neuropsychopharmacology 2009;34:2329–43.

Behavioural Brain Research 210 (2010) 251–256

Contents lists available at ScienceDirect

Behavioural Brain Research

journal homepage: www.elsevier.com/locate/bbr

Research report

Effect of non-selective dopaminergic receptor agonist on disrupted maternal behavior in olfactory bulbectomized mice

Atsushi Sato, Osamu Nakagawasai*, Koichi Tan-No, Hiroshi Onogi, Fukie Niijima, Takeshi Tadano

Department of Pharmacology, Tohoku Pharmaceutical University, 4-4-1 Komatsushima, Aoba-ku, Sendai 981-8558, Japan

ARTICLE INFO

Article history:
Received 29 December 2009
Received in revised form 16 February 2010
Accepted 20 February 2010
Available online 26 February 2010

Keywords:
Olfactory bulbectomy
Maternal behavior
Reward
Dopamine
Sucrose preference
Depression

ABSTRACT

Olfactory bulbectomy (OBX) animals are considered a putative model of depression that produces behavioral, physiological, and neurochemical alterations resembling clinical depression. Depression is a critical cause of child abuse and neglect, and it has been reported that maternal behavior involves dopaminergic neurons of the mesolimbic pathway. In this study, we investigated the effect of apomorphine, a non-selective dopaminergic receptor agonist, on maternal behavior to examine the influence of activated brain dopaminergic function in OBX mice. In addition, we conducted the sucrose preference test to examine the reward system which has a critical relationship to mesolimbic dopaminergic function and maternal behavior. Maternal behavior was observed on postnatal day (PND) 0 and 4. OBX female mice showed a reduction in sucrose preference 2 weeks post surgery. OBX dams showed maternal behavior deficits on PND 0, and these deficits were ameliorated by administration of apomorphine. These results suggest that maternal behavior deficits in OBX dams may involve brain hypodopaminergic function in the central nervous system induced by OBX.

© 2010 Elsevier B.V. All rights reserved.

1. Introduction

Bilateral olfactory bulbectomized (OBX) rodents have been widely used as an animal model of depression because OBX induces behavioral, physiological and neurochemical alterations similar to clinical depression symptoms. Furthermore, these effects are reversed by chronic, but not acute, antidepressant treatment (for review, see [37]). The olfactory bulbectomy produces far-reaching neurodegeneration in many brain regions, in particular structural alterations in the locus coeruleus or dorsal raphe causes dysfunction of the noradrenergic or serotonergic system of the other [26,37]. OBX rodents also display varied behavioral changes including impairment of cognitive function and an increase in nocturnal locomotor activity and exploratory behaviors [11,13,24,25,41,45]. Thus, OBX rodents meet accepted validity criteria for an animal model of depression, including face, construct and predictive validity.

Recently, a search for animal models that can be used to investigate the possible mechanisms underlying the relationship between maternal behavior and depression has received the attention of researchers. Abnormal maternal behavior has been observed in Flinders Sensitive Line (FSL) rats, a genetic animal model of depression [3,20]. Furthermore, rat mothers that have acquired learned helplessness (an animal model of depression) display decreased licking and grooming and arched back nursing behavior [18]. OBX has also been associated with deficits in maternal responding [9,10], indicating that olfactory bulb (OB) or projections from the OB are critical for maternal behavior.

It is well known that maternal behavior is profoundly associated with the mesolimbic dopaminergic system which is a major component of the brain reward system (for review, see [17,32]). Dysfunction of the reward system causes anhedonia [21], one of the core symptoms of major depression and may lead to disrupted maternal behavior. Some studies have indicated that OBX rats display reward system dysfunction. The OBX rats express a blunted response to amphetamine's rewarding effect, a reduction in sucrose preference and disruption of cocaine-induced conditioned place preference [5,34,38]. On the other hand, it is known that maternal behavior is disrupted by destruction of the ventral tegmental area which projects dopaminergic nerves to the mesolimbic area or by administration of a dopamine antagonist or 6-hydroxydopamine to the nucleus accumbens [8,12,15,28,36]. Furthermore, it has been reported that maternal interaction with their pups increases the dopamine released into the mother's nucleus accumbens [6,19].

Abbreviations: ANOVA, analysis of variance; FSL, flinders sensitive line; HLG, high licking and grooming; LLG, low licking and grooming; MPOA, medial preoptic area; OB, olfactory bulb; OBX, olfactory bulbectomy; PND, postnatal day; SD, Sprague–Dawley; SEM, standard error of the mean; TH, tyrosine hydroxylase.

* Corresponding author. Tel.: +81 22 727 0123; fax: +81 22 727 0123.
E-mail addresses: obx0315@yahoo.co.jp (A. Sato), osamun@tohoku-pharm.ac.jp (O. Nakagawasai), koichi@tohoku-pharm.ac.jp (K. Tan-No), hirogle@yahoo.co.jp (H. Onogi), niijima@tohoku-pharm.ac.jp (F. Niijima), tadano@tohoku-pharm.ac.jp (T. Tadano).

0166-4328/$ – see front matter © 2010 Elsevier B.V. All rights reserved.
doi:10.1016/j.bbr.2010.02.042

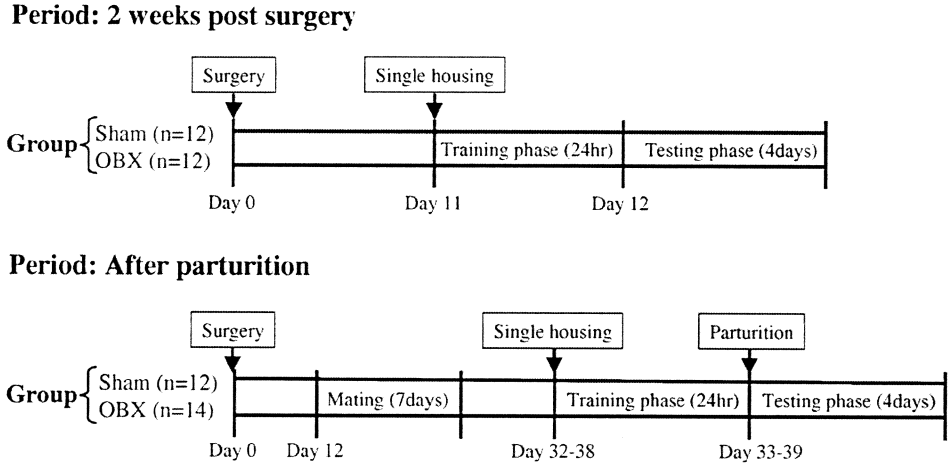


Fig. 1. Time courses of sucrose preference test. Different animals were used in each experimental period.

These studies indicate that the mesolimbic dopaminergic system regulates behavioral responsiveness to biologically significant stimuli and OBX mothers, who have maternal behavior deficits, will respond to pups after dopamine agonist treatment.

Therefore, we observed the effect of apomorphine, a non-selective dopaminergic receptor agonist, on maternal behavior to examine the influence of activated brain dopaminergic function in OBX mice. Furthermore, as OBX and dopamine depletion are associated with anhedonic behavior, the present study also investigated whether OBX is associated with a deficit in sucrose preference. Such a finding would suggest that neglectful mothers may also be anhedonic.

2. Materials and methods

2.1. Animals

Eight-week-old ddY virgin female mice were obtained from Nippon SLC (Hamamatsu, Japan). Animals were housed in polypropylene cages (13 cm height × 21 cm width × 31 cm length) with a stainless steel wire lid and wood shavings were used as bedding materials (Beta chip, Charles River Laboratory International, Inc., USA). The animals had free access to food and water. Temperature (22 ± 2 °C) and humidity (55 ± 10%) were maintained a narrow range and the animals were on a 12-h light/dark cycle (light phase: 7:00–19:00 h). All experiments were performed according to the Guide for Care and Use of Laboratory Animals at Tohoku Pharmaceutical University.

2.2. Drugs

Two different doses (0.125 and 0.25 mg/kg) of apomorphine (Sigma–Aldrich, Inc., St. Louis, MO, U.S.A.) were prepared in 0.5% Tween 80 containing 0.02% ascorbic acid. The drug was subcutaneously administered at a dose of 0.1 mL/10 g of mouse body weight, 15 min before maternal behavior observation began.

2.3. Surgery

Mice anesthetized with pentobarbital Na (50 mg/kg, i.p.; Dainippon Sumitomo Pharma, Osaka, Japan) were placed in a stereotaxic instrument. The scalp was incised, 2 holes were drilled to expose the OB, which was then bilaterally aspirated by a suction pump. All animals were sacrificed at the end of the experiment and the lesions were verified visually. It was confirmed that at least two thirds of the OB had been removed and that some parts of the olfactory nuclei also had been lesioned. If the lesion was either not extensive enough or extended to cortex, data from these animals were excluded. Sham operations were performed in the same manner but without the removal of the OB.

2.4. Mating and maternal behavior observation

Two or three females were mated with a male of the same strain for 7 days, 2 weeks post surgery. Pregnant mice were individually transferred to new cage (same type cage) and were checked daily for parturition. Postnatal day (PND) 0 is defined as the day when delivery is complete by 12:00. Maternal behavior was observed for 75 min on PND 0 and 4 between 12:00 and 17:00. The observed maternal behaviors comprise one of the following three types: (1) Mother off pups (duration when mother was separate from her pups), (2) licking and grooming (mother is licking and grooming pup's body, predominantly the anogenital region to help their excretion) and (3) arched back posture (mother is arching her back with rigid limbs and blankets the pups attached to her nipples). The number of surviving pups was determined by counting the number of pups immediately following the birth of the litter and again at the end of the maternal behavior observation period.

2.5. Sucrose preference

This experiment was conducted for 4 days, starting either 14 days post surgery or from PND 0 (Fig. 1). Different mice used for either of the experimental periods (group 1: 2 weeks post surgery: 12 sham and 12 OBX mice, singly housed, no mating; group 2: after parturition: 12 sham and 14 OBX mice, housed individually with their pups). The training phase lasted at least 24 h and took place before the testing phase to allow the animals to adapt to the novel solution. When starting the training phase, animals were transferred into single housing with free access to food and two bottles, one of which contained 1% sucrose solution and the second bottle contained tap water. To prevent possible effects of side preference in drinking, the position of the bottles was switched twice a day. Bottles were weighed to record the consumption of tap water and sucrose fluid every morning (9:00–11:00). A sucrose preference score was calculated using the following formula and the average of the 4 days was calculated.

$$\%\,\text{preference} = \frac{\text{sucrose intake}}{\text{total intake}} \times 100$$

2.6. Data analysis

The significance of differences was determined using the Student's *t*-test for two-group comparison in maternal behavior on PND 0 and 4. Two-way analysis of variance (ANOVA) was used for comparison of the sucrose preference test and effect of apomorphine on maternal behavior. The changes in number of pups at birth, PND 0 and 4 were examined using a two-way repeated measure ANOVA. Post hoc analysis was performed using the Fisher's PLSD test. The criterion of significance was set at $p < 0.05$. All results are expressed as mean ± standard error of the mean (SEM).

3. Results

3.1. Changes in OBX mothers' pup numbers

As shown in Fig. 2, two-way repeated ANOVA revealed a significant effect of group, day and group × day interaction [group: $F_{(1,21)} = 28.453$, $p < 0.0001$; day: $F_{(2,42)} = 11.154$, $p = 0.0001$; group × day: $F_{(2,42)} = 9.120$, $p = 0.0004$]. A post hoc test revealed that the OBX mothers' pups significantly decreased by day, whereas almost all pups of the sham group survived until weaning (PND0: $p = 0.0008$; PND4: $p < 0.0001$).

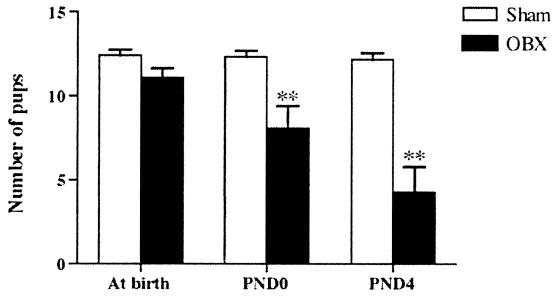


Fig. 2. Influence of OBX on the number of pups. Each column shows the number of pups at birth, PND 0 and PND 4 in sham control ($n = 12$) and OBX ($n = 11$) mice. The mean litter size at birth and the number of pups present when maternal behavior observations are completed on PND 0 and PND 4 are shown. Vertical bars represent standard errors of means (SEM). $^{**}p < 0.01$ significant difference between sham control and OBX group.

3.2. Changes in maternal behavior on PND 0 and 4

When we observed maternal behavior on PND 0 and 4, OBX mothers showed significantly increased time off pups ($t = -2.675$, $p = 0.0160$) and decreased licking and grooming ($t = 2.924$, $p = 0.0099$) and arched back posture ($t = 3.168$, $p = 0.0060$) compared with sham mothers on PND 0, but there were no difference in any of the maternal behaviors on PND 4 (Figs. 3 and 4).

3.3. Sucrose preference

A two-way ANOVA revealed a significant effect of period, but not group or group × period, for tap water consumption [group: $F_{(1,46)} = 0.278$, $p = 0.6008$; period: $F_{(1,46)} = 17.404$, $p = 0.0001$; group × period: $F_{(1,46)} = 0.515$, $p = 0.4766$]. The post hoc test revealed that tap water consumption after parturition in both groups significantly increased compared with 2 weeks post surgery (Fig. 5a). Regarding sucrose fluid consumption, an ANOVA revealed a significant effect of group and period but no significant group × period interaction effect [group: $F_{(1,46)} = 6.285$, $p = 0.0158$; period: $F_{(1,46)} = 137.754$, $p < 0.0001$; group × period: $F_{(1,46)} = 1.461$, $p = 0.2329$]. The post hoc test revealed that the sucrose fluid consumption in the OBX group 2 weeks post surgery significantly decreased compared with the sham group ($p = 0.0131$) (Fig. 5b). For total fluid consumption, an ANOVA revealed a significant effect of group and period but no significant group × period interaction

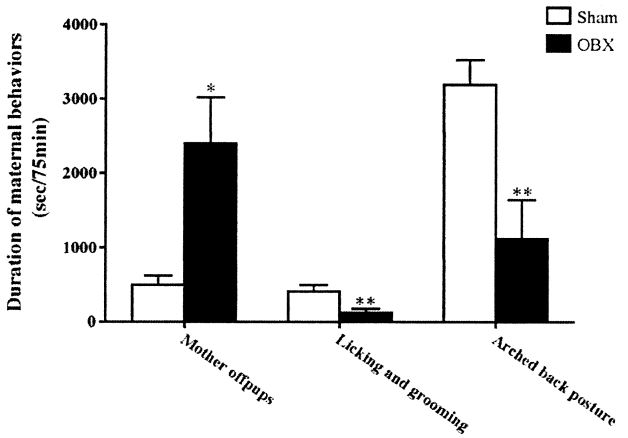


Fig. 3. Mean duration of maternal behaviors (mother off pups, licking and grooming and arched back posture) of sham control and OBX mice on PND 0. Vertical bars represent SEM. $^{*}p < 0.05$ and $^{**}p < 0.01$ significant difference between sham control and OBX groups ($n = 8$–10 per group).

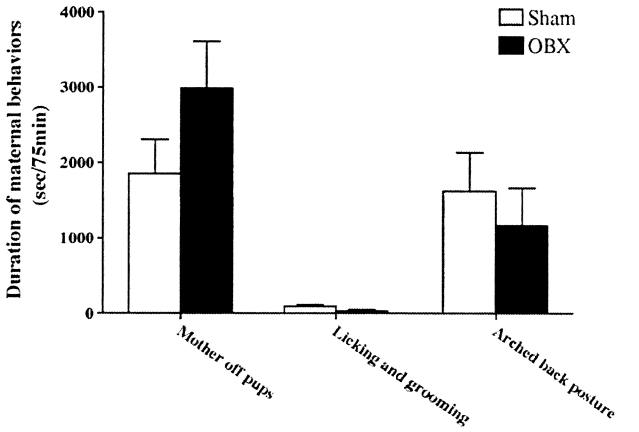


Fig. 4. Mean duration of maternal behaviors in sham control and OBX mice on PND 4. Vertical bars represent SEM ($n = 8$–10 per group).

effect [group: $F_{(1,46)} = 10.459$, $p = 0.0023$; period: $F_{(1,46)} = 264.210$, $p < 0.0001$; group × period: $F_{(1,46)} = 0.849$, $p = 0.3617$]. Total fluid consumption in the sham group was significantly higher than OBX mice 2 weeks post surgery ($p = 0.0059$ by Fisher's PLSD) (Fig. 5c). An ANOVA of sucrose preference revealed a significant effect of group, period and interaction [group: $F_{(1,46)} = 7.380$, $p = 0.0093$; period: $F_{(1,46)} = 16.226$, $p = 0.0002$; group × period: $F_{(1,46)} = 4.468$, $p = 0.0400$]. The post hoc test revealed that sucrose preference in sham mice was higher than OBX mice 2 weeks post surgery ($p = 0.0016$), but produced no effect after parturition (Fig. 5d).

3.4. Effect of apomorphine on maternal behavior

A two-way ANOVA revealed a significant effect of group in time mothers spent off pups [group: $F_{(1,59)} = 10.095$, $p = 0.0024$; treatment: $F_{(2,59)} = 0.789$, $p = 0.4588$; group × treatment: $F_{(2,59)} = 3.285$, $p = 0.0428$]. A post hoc test revealed that the increased duration of time mothers spent off pups observed in OBX mothers was ameliorated by administration of 0.25 mg/kg apomorphine ($p = 0.0381$) (Fig. 6a). Regarding arched back posture, ANOVA revealed a significant effect of group [group: $F_{(1,59)} = 9.479$, $p = 0.0032$; treatment: $F_{(2,59)} = 0.469$, $p = 0.6280$; group × treatment: $F_{(2,59)} = 2.429$, $p = 0.0969$] and the post hoc test revealed that 0.25 mg/kg apomorphine improved, but not significantly, the reduction of arched back posture in OBX mothers ($p = 0.0546$) (Fig. 6c). An ANOVA revealed a significant effect of group in licking and grooming [group: $F_{(1,59)} = 10.283$, $p = 0.0022$; treatment: $F_{(2,59)} = 1.017$, $p = 0.3681$; group × treatment: $F_{(2,59)} = 0.434$, $p = 0.6501$]. The reduced licking and grooming time of OBX mothers failed to respond to the apomorphine treatment (Fig. 6b).

4. Discussion

Herein, we have shown that OBX mothers display significantly different behaviors compared to sham-operated controls. The number of OBX mothers' pups significantly decreased per day (Fig. 2). Observation of maternal behavior in sham and OBX dams on PND 0 and 4 showed that OBX mice spent significantly more time off pups and significantly less time licking and grooming or in arched back posture on PND 0 relative to sham mothers (Figs. 3 and 4). The alteration of maternal behavior in OBX mothers was ameliorated by administration of apomorphine (Fig. 6). Furthermore, the sucrose preference test revealed dysfunction of the reward system in OBX mice 2 weeks post surgery (Fig. 5). These results suggest that OBX disrupted both the onset of maternal behavior and reward function.

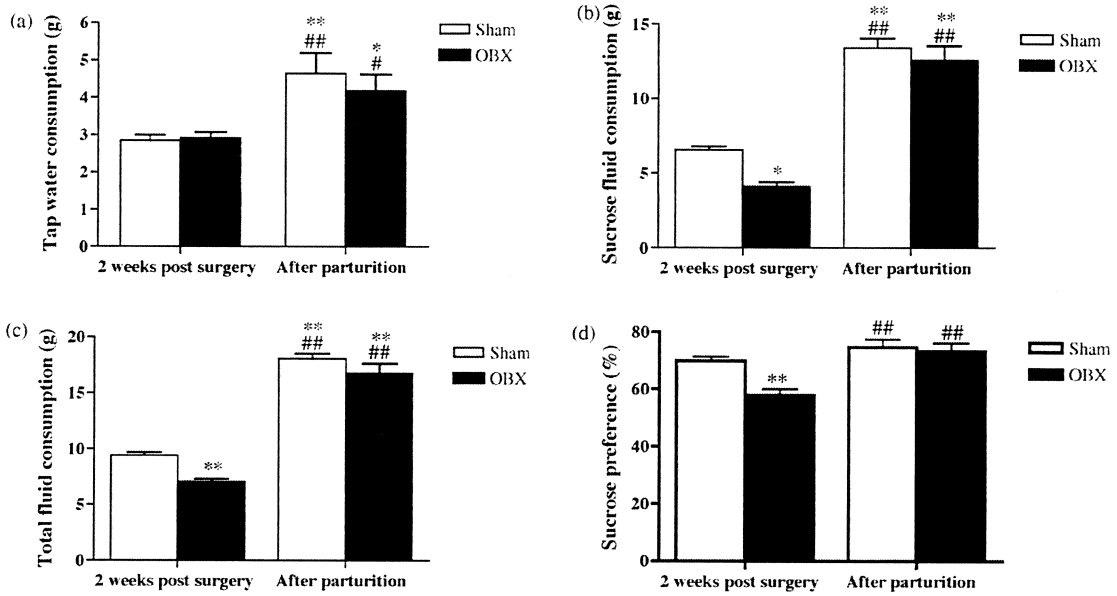


Fig. 5. Effects of OBX on sucrose preference 2 weeks post surgery and after parturition. This figure shows the 4-day average of tap water (a), sucrose fluid (b), total fluid consumption (c) and sucrose preference (d) in sham and OBX group 2 weeks post surgery and after parturition. Vertical bars represent SEM. $^{*}p < 0.05$ and $^{**}p < 0.01$ compared with the sham group 2 weeks post surgery. $^{\#}p < 0.05$ and $^{\#\#}p < 0.01$ compared with the OBX group 2 weeks post surgery ($n = 12$–14).

Many studies have shown that the mesolimbic dopaminergic system plays an important role in maternal behavior [27,29,32]. In the current study, OBX mice showed significantly decreased sucrose preference 2 weeks post surgery (Fig. 5). This result is supported by previous studies describing the alteration of the reward system in OBX rats [5,34,38]. Reduction of sucrose preference indicates impairment of the reward system (i.e., anhedonia) and may relate to disrupted maternal behavior in OBX mice. However, there were no changes in sucrose preference between both groups after parturition. The disappearance of differences in sucrose preference after parturition might be affected by the increased requirement of water and energy by parturition and lactation. In fact, mice in both groups consumed more tap water and sucrose fluid after parturition than 2 weeks post surgery, and it is obvious that lactating mothers need more water and nutrition. Therefore, although sucrose preference level in OBX group after parturition was equal to that of the sham group, their reward system may not necessarily act in the same way as that of the sham group. In addition, sucrose preference may be affected by sweet taste sensitivity. Zukerman et al. have investigated the relationship between olfaction and sweet taste function in C57BL/6 mice that were subject to either sham or OBX surgery [46]. As a result, OBX mice showed decreased sucrose preference with lower concentrations of sucrose fluid (0.5–2%) compared to sham mice, but not at higher concentration (4–32%). They concluded that the decreased sucrose preference sweet taste sensitivity is related to diminished ability of the olfaction system to discriminate dilute sucrose solution from water and changes of motivational function induced by OBX. This report and the results of the sucrose preference test in this study indicate the need to review the reward system in OBX mice by another method which is

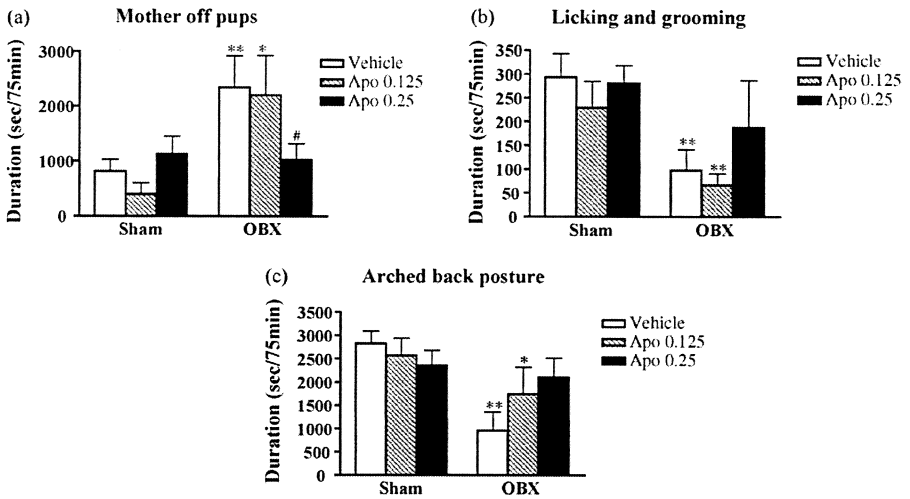


Fig. 6. Changes in maternal behaviors: mother off pups (a), licking and grooming (b) and arched back posture (c) in sham control and OBX groups after administration of apomorphine on PND 0. Vertical bars represent SEM. $^{*}p < 0.05$ and $^{**}p < 0.01$ compared with sham + vehicle group. $^{\#}p < 0.05$ compared with OBX + vehicle group ($n = 8$–19 per group).

unaffected by energy, water demands or gustation, for example, the conditioned place preference test using drugs that have rewarding effects.

It is highly possible that the reduction in dopaminergic function contributes to the dysfunction of the reward system in OBX animals. Thus, to examine whether stimulation of dopaminergic function improves the disruption of maternal behavior in OBX mothers on PND 0, we investigated the effects of apomorphine. Administration of apomorphine at 0.25 mg/kg ameliorated the reduction of arched back posture duration in OBX mice, and time spent off pups was improved at 0.25 mg/kg (Fig. 6). These results suggest that disruption of maternal behavior in OBX mice is associated with dopaminergic function in the central nervous system. Previously, we found a reduction in tyrosine hydroxylase (TH) levels, the biosynthetic rate-controlling enzyme of catecholamines such as dopamine, in the nucleus accumbens core and shell of male OBX mice [40]. In addition, Iwasaki et al. [14] found decreased dopamine levels in the lateral hypothalamus in OBX rats. These findings strongly link the dysfunction of the reward system, caused by degeneration of dopaminergic neurons, and disrupted maternal behavior in OBX mice.

As OBX animals are without the OB, the center of olfaction, there is a possibility that anosmia induced by OBX enhances the level of disruption of maternal behavior. Concerning olfaction, OBX animals have an anosmia to both volatile and non-volatile odors, because OBX eliminates input from both the main and accessory olfactory systems which are thought to be involved in the detection and processing of volatile and non-volatile odors, respectively. It has been reported that OBX rats showed stronger disruption of maternal behavior than other rat groups that have an anosmia to volatile odor induced by intranasal administration of zinc sulfate [16]. On the other hand, vomeronasal organ removal in rats that cannot detect non-volatile odors have shown normal maternal behavior. This report suggests that strong disruption of maternal behavior in OBX rats is induced by multiple effects of an anosmia to both volatile and non-volatile odors and changes in the central nervous system. Therefore, anosmia may have a capacity to potentiate deficits of maternal behavior in OBX animals.

The phenotype of maternal behavior may be changed by differences in stimulated dopamine receptor subtype and administration method. Rat mothers express stable individual differences in the intensity of maternal behavior [7]. Meaney and colleagues have conducted various studies using high licking and grooming (HLG) females and low licking and glooming (LLG) females and they have shown that HLG mothers have more D1 and D3 receptors in the nucleus accumbens shell region than LLG mothers [6]. Furthermore, lactating rats receiving SCH23390, a selective D1 receptor antagonist, into the nucleus accumbens shell showed disruption of retrieval behavior without affecting total nursing duration, whereas selective D2 receptor antagonism had no effect on maternal behavior [28]. Furthermore, microinjection of a D1 receptor agonist, but not D2, into either nucleus accumbens or medial preoptic area (MPOA) promotes maternal responses in pregnancy terminated rats [39]. Miller and Lonstein [23] have reported that D1 antagonism in the preoptic area impaired retrieval and licking behavior, on the other hand, D2 antagonism showed a facilitative effect on nursing behavior without affecting oral maternal behaviors. Peripheral administration of D1 or D2 receptor antagonist disturbs expression of maternal behaviors immediately following parturition [4]. These reports indicate that expression of maternal behavior changes according to site of drug administration and which dopamine receptor subtypes the drug acts on. This requires further research in OBX mice using selective dopaminergic receptor agonists and local administration into specific brain regions related to maternal behavior.

The effect of the dramatic endocrine events associated with pregnancy and parturition is necessary for rapid onset of maternal behavior after parturition [27], and it is well known that the MPOA, which is located in the rostral hypothalamus and interacts with mesolimbic dopaminergic system, is an important brain region for onset and maintenance of maternal behavior [32]. The MPOA contains estrogen receptors [35], oxytocin receptors [2], prolactin receptors [1] and progesterone receptors [30]. It has been reported that implantation of estradiol benzoate into the MPOA facilitated the onset of maternal behavior in pregnancy terminated rats [31]. In OBX animals, there are some findings that OBX induced a decrease in the nocturnal surge of prolactin [33], hypersensitivity to estrogen [22,42,44] and lengthened and made irregular the estrous cycle [43]. Therefore, disruption of the onset of maternal behavior in some OBX mothers may be related with alterations in hormone secretion or hormone receptors in the central nervous system. Additionally, we intend to investigate changes in various functions which can influence maternal behavior such as the mesolimbic dopaminergic system, MPOA neuron activity, the hormonal basis and function in OBX mothers as well as investigate the effects of various antidepressants, especially bupropion, a selective dopamine and noradrenaline reuptake inhibitor, on maternal behavior. Future experiments should consider using different animal models of depression that naturally express the disrupted maternal behavior, such as the FSL rat, because OBX animals have an anosmia which affects maternal behavior.

In conclusion, OBX female mice showed a reduction in sucrose preference 2 weeks post surgery, this finding indicates that OBX induces anhedonia, which is dysfunction of the reward system. Furthermore, serious disruption of maternal behavior was observed in OBX mothers on PND 0 which was ameliorated by administration of apomorphine. These results suggest that disruption of maternal behavior in OBX mothers is related to depressed dopaminergic function in the central nervous system induced by OBX.

Acknowledgements

This study was supported in part by a Grant-in-Aid for Scientific Research (C) (KAKENHI 21610019) from the Japan Society for the Promotion of Science to TT and ON, and a Grant-in-Aid for High Technology Research Program from the Ministry of Education, Culture, Sports, Science and Technology, Japan. The authors acknowledge the editorial support of ProSciEd's professional editor.

References

[1] Bakowska JC, Morrell JI. Atlas of the neurons that express mRNA for the long form of the prolactin receptor in the forebrain of the female rat. J Comp Neurol 1997;386:161–77.
[2] Bealer SL, Lipschitz DL, Ramoz G, Crowley WR. Oxytocin receptor binding in the hypothalamus during gestation in rats. Am J Physiol Regul Integr Comp Physiol 2006;291:R53–8.
[3] Braw Y, Malkesman O, Merenlender A, Dagan M, Bercovich A, Lavi-Avnon Y, et al. Divergent maternal behavioral patterns in two genetic animal models of depression. Physiol Behav 2009;96:209–17.
[4] Byrnes EM, Rigero BA, Bridges RS. Dopamine antagonists during parturition disrupt maternal care and the retention of maternal behavior in rats. Pharmacol Biochem Behav 2002;73:869–75.
[5] Calcagnetti DJ, Quatrella LA, Schechter MD. Olfactory bulbectomy disrupts the expression of cocaine-induced conditioned place preference. Physiol Behav 1996;59:597–604.
[6] Champagne FA, Chretien P, Stevenson CW, Zhang TY, Gratton A, Meaney MJ. Variations in nucleus accumbens dopamine associated with individual differences in maternal behavior in the rat. J Neurosci 2004;24:4113–23.
[7] Champagne FA, Francis DD, Mar A, Meaney MJ. Variations in maternal care in the rat as a mediating influence for the effects of environment on development. Physiol Behav 2003;79:359–71.
[8] Gaffori O, Le Moal M. Disruption of maternal behavior and appearance of cannibalism after ventral mesencephalic tegmentum lesions. Physiol Behav 1979;23:317–23.

[9] Gandelman R, Zarrow MX, Denenberg VH. Reproductive and maternal performance in the mouse following removal of the olfactory bulbs. J Reprod Fertil 1972;28:453–6.
[10] Gandelman R, Zarrow MX, Denenberg VH, Myers M. Olfactory bulb removal eliminates maternal behavior in the mouse. Science 1971;171:210–1.
[11] Giardina WJ, Radek RJ. Effects of imipramine on the nocturnal behavior of bilateral olfactory bulbectomized rats. Biol Psychiatry 1991;29:1200–8.
[12] Hansen S, Harthon C, Wallin E, Lofberg L, Svensson K. The effects of 6-OHDA-induced dopamine depletions in the ventral or dorsal striatum on maternal and sexual behavior in the female rat. Pharmacol Biochem Behav 1991;39:71–7.
[13] Hozumi S, Nakagawasai O, Tan-No K, Niijima F, Yamadera F, Murata A, et al. Characteristics of changes in cholinergic function and impairment of learning and memory-related behavior induced by olfactory bulbectomy. Behav Brain Res 2003;138:9–15.
[14] Iwasaki K, Fujiwara M, Shibata S, Ueki S. Changes in brain catecholamine levels following olfactory bulbectomy and the effect of acute and chronic administration of desipramine in rats. Pharmacol Biochem Behav 1986;24:1715–9.
[15] Keer SE, Stern JM. Dopamine receptor blockade in the nucleus accumbens inhibits maternal retrieval and licking, but enhances nursing behavior in lactating rats. Physiol Behav 1999;67:659–69.
[16] Kolunie JM, Stern JM. Maternal aggression in rats: effects of olfactory bulbectomy, $ZnSO_4$-induced anosmia, and vomeronasal organ removal. Horm Behav 1995;29:492–518.
[17] Kornetsky C. Brain-stimulation reward, morphine-induced oral stereotypy, and sensitization: implications for abuse. Neurosci Biobehav Rev 2004;27:777–86.
[18] Kurata A, Morinobu S, Fuchikami M, Yamamoto S, Yamawaki S. Maternal postpartum learned helplessness (LH) affects maternal care by dams and responses to the LH test in adolescent offspring. Horm Behav 2009;56:112–20.
[19] Lavi-Avnon Y, Weller A, Finberg JP, Gispan-Herman I, Kinor N, Stern Y, et al. The reward system and maternal behavior in an animal model of depression: a microdialysis study. Psychopharmacology (Berl) 2008;196:281–91.
[20] Lavi-Avnon Y, Yadid G, Overstreet DH, Weller A. Abnormal patterns of maternal behavior in a genetic animal model of depression. Physiol Behav 2005;84:607–15.
[21] Markou A, Kosten TR, Koob GF. Neurobiological similarities in depression and drug dependence: a self-medication hypothesis. Neuropsychopharmacology 1998;18:135–74.
[22] McGinnis MY, Lumia AR, McEwen BS. Increased estrogen receptor binding in amygdala correlates with facilitation of feminine sexual behavior induced by olfactory bulbectomy. Brain Res 1985;334:19–25.
[23] Miller SM, Lonstein JS. Dopamine D1 and D2 receptor antagonism in the preoptic area produces different effects on maternal behavior in lactating rats. Behav Neurosci 2005;119:1072–83.
[24] Moriguchi S, Han F, Nakagawasai O, Tadano T, Fukunaga K. Decreased calcium/calmodulin-dependent protein kinase II and protein kinase C activities mediate impairment of hippocampal long-term potentiation in the olfactory bulbectomized mice. J Neurochem 2006;97:22–9.
[25] Nakagawasai O, Hozumi S, Tan-No K, Niijima F, Arai Y, Yasuhara H, et al. Immunohistochemical fluorescence intensity reduction of brain somatostatin in the impairment of learning and memory-related behaviour induced by olfactory bulbectomy. Behav Brain Res 2003;142:63–7.
[26] Nakagawasai O, Tadano T, Arai Y, Hozumi S, Oba A, Tan-No K, et al. Enhancement of 5-hydroxytryptamine-induced head-twitch response after olfactory bulbectomy. Neuroscience 2003;117:1017–23.
[27] Numan M, Insel TR. The neurobiology of parental behavior. New York: Springer-Verlag; 2003.
[28] Numan M, Numan MJ, Pliakou N, Stolzenberg DS, Mullins OJ, Murphy JM, et al. The effects of D1 or D2 dopamine receptor antagonism in the medial preoptic area, ventral pallidum, or nucleus accumbens on the maternal retrieval response and other aspects of maternal behavior in rats. Behav Neurosci 2005;119:1588–604.
[29] Numan M, Numan MJ, Schwarz JM, Neuner CM, Flood TF, Smith CD. Medial preoptic area interactions with the nucleus accumbens-ventral pallidum circuit and maternal behavior in rats. Behav Brain Res 2005;158:53–68.
[30] Numan M, Roach JK, del Cerro MC, Guillamón A, Segovia S, Sheehan TP, et al. Expression of intracellular progesterone receptors in rat brain during different reproductive states, and involvement in maternal behavior. Brain Res 1999;830:358–71.
[31] Numan M, Rosenblatt JS, Komisaruk BR. Medial preoptic area and onset of maternal behavior in the rat. J Comp Physiol Psychol 1977;91:146–64.
[32] Numan M, Stolzenberg DS. Medial preoptic area interactions with dopamine neural systems in the control of the onset and maintenance of maternal behavior in rats. Front Neuroendocrinol 2009;30:46–64.
[33] Pieper DR, Gala RR. Influence of the pineal gland, olfactory bulbs and photoperiod on surges of plasma prolactin in the female rat. J Endocrinol 1979;82:279–85.
[34] Romeas T, Morissette MC, Mnie-Filali O, Piñeyro G, Boye SM. Simultaneous anhedonia and exaggerated locomotor activation in an animal model of depression. Psychopharmacology 2009;205:293–303.
[35] Shughrue PJ, Lane MV, Merchenthaler I. Comparative distribution of estrogen receptor-alpha and -beta mRNA in the rat central nervous system. J Comp Neurol 1997;388:507–25.
[36] Silva MR, Bernardi MM, Cruz-Casallas PE, Felicio LF. Pimozide injections into the nucleus accumbens disrupt maternal behaviour in lactating rats. Pharmacol Toxicol 2003;93:42–7.
[37] Song C, Leonard BE. The olfactory bulbectomized rat as a model of depression. Neurosci Biobehav Rev 2005;29:627–47.
[38] Stock HS, Ford K, Wilson MA. Gender and gonadal hormone effects in the olfactory bulbectomy animal model of depression. Pharmacol Biochem Behav 2000;67:183–91.
[39] Stolzenberg DS, McKenna JB, Keough S, Hancock R, Numan MJ, Numan M. Dopamine D1 receptor stimulation of the nucleus accumbens or the medial preoptic area promotes the onset of maternal behavior in pregnancy-terminated rats. Behav Neurosci 2007;121:907–19.
[40] Sugawara M, Koichi T, Osamu N, Fukie N, Takeshi T. Relationship between impairment of memory-related behavior and dopaminergic function in olfactory bulbectomized mice. J Pharmacol Sci 2005;97:163.
[41] Thorne BM, Aaron M, Latham EE. Effects of olfactory bulb ablation upon emotionality and muricidal behavior in four rat strains. J Comp Physiol Psychol 1973;84:339–44.
[42] Tyler JL, Gorski RA. Bulbectomy and sensitivity to estrogen: anatomical and functional specificity. Physiol Behav 1980;24:593–600.
[43] Vandenbergh JG. Effects of central and peripheral anosmia on reproduction of female mice. Physiol Behav 1973;10:257–61.
[44] Williams GW, Goldman J, McGinnis MY, Possidente B, Lumia AR. Effects of ovarian hormones on sexual receptivity, proceptivity, and motivation in olfactory bulbectomized female rats. Physiol Behav 1991;50:751–5.
[45] Zueger M, Urani A, Chourbaji S, Zacher C, Roche M, Harkin A, et al. Olfactory bulbectomy in mice induces alterations in exploratory behavior. Neurosci Lett 2005;374:142–6.
[46] Zukerman S, Touzani K, Margolskee RF, Sclafani A. Role of olfaction in the conditioned sucrose preference of sweet-ageusic T1R3 knockout mice. Chem Senses 2009;34:685–94.

Psychopharmacology (2010) 208:323–331
DOI 10.1007/s00213-009-1734-x

ORIGINAL INVESTIGATION

Central administration of *p*-hydroxyamphetamine produces a behavioral stimulant effect in rodents: evidence for the involvement of dopaminergic systems

Hiroshi Onogi · Masato Hozumi · Osamu Nakagawasai · Yuichiro Arai · Seiichiro Ishigaki · Atsushi Sato · Seiichi Furuta · Fukie Niijima · Koichi Tan-No · Takeshi Tadano

Received: 3 April 2009 / Accepted: 16 November 2009 / Published online: 4 December 2009
© Springer-Verlag 2009

Abstract
Rationale and objectives It is well-known that amphetamine induces increased locomotor activity in rodents. We previously found that intracerebroventricular (i.c.v.) administration of *p*-hydroxyamphetamine (*p*-OHA), an amphetamine metabolite, increases synaptic dopamine (DA) levels in the striatum. In the present study, we investigated the effect of *p*-OHA on locomotor activity in rodents.
Results In mice, i.c.v. administration of *p*-OHA significantly increased locomotor activity in a dose-dependent manner. *p*-Hydroxynorephedrine, another amphetamine metabolite, did not increase locomotor activity. This effect of *p*-OHA was inhibited by pretreatment with nomifensine, a dopamine-uptake inhibitor, but not by fluoxetine, a serotonin-uptake inhibitor, or diethyldithiocarbamate, a dopamine-β-hydroxylase inhibitor. Furthermore, we tested the effects of microinjections of *p*-OHA into the rat nucleus accumbens (NAc) on locomotor activity. Local infusion of *p*-OHA into the NAc significantly increased locomotor activity. As in mice, the increased locomotor activity induced by *p*-OHA microinjection into the NAc in rats was inhibited by nomifensine.
Conclusions These data suggest that dopaminergic systems in the NAc may play important roles in *p*-OHA-induced locomotor activity in rodents.

Keywords *p*-Hydroxyamphetamine · Dopamine · Nucleus accumbens · Locomotor activity

H. Onogi · M. Hozumi · O. Nakagawasai (✉) · A. Sato · F. Niijima · K. Tan-No · T. Tadano
Department of Pharmacology, Tohoku Pharmaceutical University, 4-4-1 Komatsushima, Aoba-ku, Sendai 981-8558, Japan
e-mail: osamun@tohoku-pharm.ac.jp

Y. Arai
Tokyo Ariake University of Medical and Health Sciences, Tokyo 135-0063, Japan

S. Ishigaki
Department of Neurology, School of Medicine, Showa University, Tokyo 142-8666, Japan

S. Furuta
Division of Pharmaceutical Community Health Care, Hokkaido Pharmaceutical University, 7-1 Katsuraoka, Otaru 047-0264, Japan

Introduction

Amphetamine (AMPH), an indirect sympathomimetic compound, elicits its neurobehavioral effects, including anorexia, stimulation of physical performance, insomnia, and euphoria, by inducing release of dopamine (DA), serotonin (5-HT), and other neurotransmitters within the brain (Pirisino et al. 2006). Release of these neurotransmitters has been suggested to occur via two separate mechanisms: the redistribution of catecholamines from synaptic vesicles to the cytosol and induction of reverse transport of transmitters through their plasma membrane uptake carriers (for a review, see Sulzer et al. 2005). Other effects of AMPH, such as monoamine oxidase inhibition, are also important for regulating extracellular catecholamine levels (Scorza et al. 1997). Substituted amphetamines, including methamphetamine (METH), methylphenidate, methylenedioxymethamphetamine, and *p*-methoxyamphetamine, also play important medical and social roles in many cultures, exert profound effects on mental function and behavior, and can produce neurodegeneration and addiction (Sulzer et al. 2005).

In rodents, it has been reported that administration of drugs of abuse, including AMPH and METH, induces

multiple behavioral responses, such as increased locomotor activity (Porrino et al. 1984; Salahpour et al. 2008), stereotypy (Battisti et al. 2000; Fowler et al. 2007), and disrupted prepulse inhibition of acoustic response (Sills 1999; Peleg-Raibstein et al. 2008). *p*-Hydroxyamphetamine (*p*-OHA), an AMPH and METH metabolite, has been shown to have a number of pharmacological actions, including causing abnormal behaviors such as those induced by drugs of abuse (Simpson 1980; Dougan et al. 1986; Arai et al. 1990; Kaminskas et al. 2002). For example, we have previously reported that intracerebroventricular (i.c.v.) administration of *p*-OHA induces a head-twitch response (HTR) as a model of hallucination, while the HTR is markedly reduced by pretreatment with a 5-HT synthesis inhibitor such as *p*-chlorophenylalanine (Tadano et al. 1986) or pretreatment with 5-HT receptor antagonists such as cyproheptadine and dimethothiazine (Tadano et al. 1986), indicating the involvement of the central serotonergic system (Tadano et al. 1989). In a preliminary study, we examined the effect of *p*-OHA on locomotor activity in rodents. *p*-OHA significantly increased locomotor activity in mice. By contrast, another AMPH metabolite, *p*-hydroxynorephedrine (*p*-OHN), did not. The mesocorticolimbic DA pathways, particularly those projecting from the ventral tegmental area (VTA, a DA cell body area) to the nucleus accumbens (NAc, a DA terminal area), are known to be critical for the production of locomotor behaviors by psychomotor stimulants like AMPH (for a review, see Vezina 2004). For example, locomotor sensitization is produced by infusions of AMPH into the VTA but not by infusions into the NAc (Cador et al. 1995). Other reports have shown that AMPH-induced locomotor activity is in part mediated by DA release in the NAc, a brain region that is also critical for drug reward (Di Chiara and Imperato 1988). Thus, studying the mechanisms underlying *p*-OHA-induced locomotor activity may provide insights into the subjectively rewarding effects of drugs in humans.

In the present study, we investigated the role of DA, noradrenaline (NA) and 5-HT neural transmission in brain in *p*-OHA-induced locomotor activity using pharmacological tools. It was suggested that *p*-OHA is actively taken up into catecholaminergic and serotonergic nerve terminals followed by monoamine oxidase A (MAO_A) inhibition, thereby eliciting an increase in DA, NA, and 5-HT levels. These neurotransmitters are then released into the synaptic cleft and/or neuronal cytosol from its store sites by increasing displacement (for a review, see Nakagawasai et al. 2004). Thus, to investigate the involvement of presynaptic release of DA, NA, and 5-HT in *p*-OHA-induced locomotor activity, first, we used the selective serotonin reuptake inhibitor (SSRI) fluoxetine, previously shown to reduce *p*-OHA-induced HTR (Oyama et al. 1989), for the purpose of inhibiting *p*-OHA uptake into serotonergic nerve terminals. Next, we used the DA-β-hydroxylase inhibitor diethyldithiocarbamate (DDC), which was shown to reduce NA levels (Collins 1965; Chang et al. 1995; Gaval-Cruz et al. 2008). If increased NA levels from presynaptic noradrenergic nerve terminals are involved in *p*-OHA-induced locomotor activity, then DDC treatment is expected to reduce hyperlocomotion. Nomifensine was used to inhibit the uptake of DA, which also resulted in the inhibition of *p*-OHA-induced locomotor activity. Furthermore, to clarify the role of an important brain site in the action of *p*-OHA, we focused on the mesocorticolimbic DA pathways and tested the effects of microinjecting *p*-OHA into the NAc (a DA terminal area) on locomotor activity in rats.

Materials and methods

Animals

Male ddY strain mice (weighing 22–25 g, Japan SLC, Japan) and male Wistar rats (weighing 200–250 g, Japan SLC) were used throughout the experiments. The animals were housed in cages with free access to food and water under conditions of constant temperature (22±2°C) and humidity (55±5%), on a 12:12 h light–dark cycle (light term, 0800–2000 hours).

All experiments were performed following the approval of the Ethics Committee of Animal Experiment in Tohoku Pharmaceutical University and according to the National Institutes of Health Guide for the Care and Use of Laboratory Animals. Efforts were made to minimize suffering and to reduce the number of animals used.

Surgery

Rats anesthetized intraperitoneally (i.p.) with pentobarbital sodium (50 mg/kg; Dainippon Sumitomo Pharma Co., Ltd., Japan) were immobilized in a stereotaxic frame. The scalp was opened to uncover the skull, and two 1-mm diameter holes were drilled to access the brain. Two guide cannulas (stainless steel; outside diameter of shaft, 0.6 mm) were implanted bilaterally in NAc, according to the following coordinates: AP, +1.7 mm; ML, 1.2 mm; DV, −7 mm, relative to the bregma (Paxinos and Watson 1997). The guide cannulas were fixed to the skull with dental cement. The rats were singly housed following surgery and were allowed to recover for at least 7 days before behavioral testing.

Drugs and treatments

The following drugs were used: the racemic form of *p*-OHA hydrobromide (Smith-Kline and French, USA), fluoxetine hydrochloride (Tocris Cookson, UK), diethyldi-

thiocarbamate (DDC; Wako Pure Chemical Industries, Ltd., Japan), the racemic form of *p*-OHN hydrochloride, and nomifensine maleate salt (Sigma-Aldrich, USA). *p*-OHA and *p*-OHN were dissolved in Ringer's solution, and all other drugs were dissolved in 0.9% saline. For all solutions, pH was adjusted to 7.4 at 37°C. Doses of fluoxetine, DDC, and nomifensine were based on previous studies (Oyama et al. 1989; Escarabajal and Aragon 2003; Paulus et al. 1993; Puglisi-Allegra et al. 1994; Yamada et al. 2004).

The technique employed here for i.c.v. injection into mice was the same as that originally described by Brittain and Handley (1967). Briefly, i.c.v. administration of *p*-OHA, *p*-OHN, or Ringer's solution was performed with a disposable 27-G needle attached to a 50-μL Hamilton microsyringe and inserted into the left lateral ventricle of unanesthetized mice. *p*-OHA, *p*-OHN, or Ringer's solution was administered in a total volume of 5 μL at a constant rate of 1 μL/2 s. Microinjections into rats was performed using an infusion pump (Stoelting, USA) and a 10 μL Hamilton microsyringe connected to a needle that was inserted into the NAc via a guide cannula. *p*-OHA was infused bilaterally at a flow rate of 0.5 μL/15 s (total injection volume, 0.5 μL). The needle was withdrawn 2 min after completion of the infusion. Sham-operated animals received the same volume of Ringer's solution. Pretreatment with fluoxetine, nomifensine, or saline as vehicle (Veh) was performed by i.p. administration 30 min before i.c.v. or microinjection of *p*-OHA or Ringer's solution. DDC or Veh was administered i.p. 12 h before i.c.v. injection of *p*-OHA or Ringer's solution (Fig. 1). After the experimental period, brains were removed, snap-frozen, and cut into 20-μm coronal section using a Cryostat HM560M (Carl Zeiss Japan, Inc, Japan). Accuracy of all injection sites were confirmed by cresyl violet-stained coronal sections.

Measurement of locomotor activity in mice and rats

The locomotor activity in mice was measured using a 12-channel Animex-autosystem (Muromachi Kikai Co., Japan). This instrument can monitor even minute movements in all three planes of motion (sagittal, coronal, and horizontal) as one movement, owing to its infrared sensor with multiple Fresnel lenses that can be moved close enough to the cage to capture multidirectional locomotor alterations in a single mouse. The Animex instrument was connected to a behavioral analyzing system (CompACT AMS; Muromachi Kikai), which can interpret each movement as one count. Therefore, vertical movements such as jumping, as well as horizontal movements such as walking and running, could be counted.

After i.p. pretreatment, mice were individually placed in activity cages and allowed to adapt for 15 min before the i.c.v. injection of *p*-OHA, *p*-OHN, or Ringer's solution. The number of activity counts was recorded for the total locomotor activity over a 180-min period after the i.c.v. injection of three solutions as above.

The locomotor activity in rats was determined as a measure of ambulation (the number of blocks traversed in the open-field apparatus) for 3 min at 15-min intervals in an open-field situation, as described previously (Hall 1934; Ueki et al. 1972). The activity was measured for 120 min after microinjection of *p*-OHA or Ringer's solution.

Statistical analysis

The significance of differences was determined by one- or two-way analysis of variance (ANOVA), followed by Fisher's protected least significant difference (PLSD) test for multigroup comparisons. The criterion of significance was set at $p<0.05$. All behavioral data are expressed as means ± standard errors of the mean (SEM).

Results

Effects of *p*-OHA and *p*-OHN on locomotor activity in mice

The i.c.v. administration of *p*-OHA (20, 40, and 80 μg/mouse) significantly increased locomotor activity compared

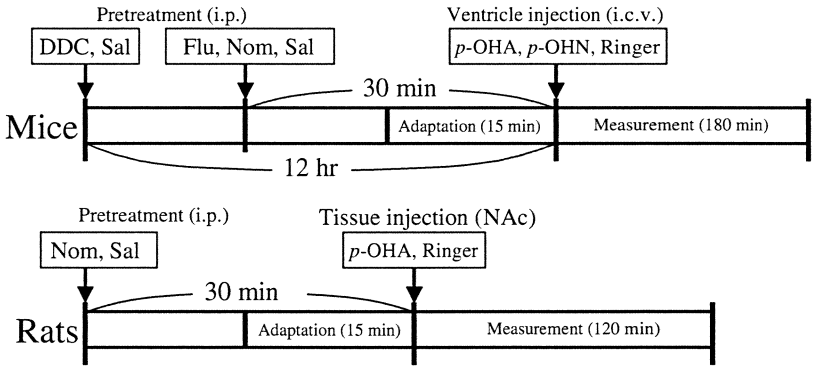


Fig. 1 Time courses of drug treatments. *p-OHA* *p*-hydroxyamphetamine, *p-OHN* *p*-hydroxynorephedrine, *DDC* diethyldithiocarbamate, *Sal* saline, *Flu* fluoxetine hydrochloride, *Nom* nomifensine maleate, *i.p.* intraperitoneal administration, *i.c.v.* intracerebroventricular administration, *NAc* nucleus accumbens

with administration of Ringer's solution [treatment, $F_{(4, 45)}$= 35.854, p<0.0001; time, $F_{(11, 495)}$=34.846, p<0.0001; treatment × time, $F_{(44, 495)}$=6.755, p<0.0001] (Fig. 2a). This effect continued for 120–165 min with a peak about 75–90 min after administration of p-OHA (Fig. 2a). The total counts of locomotor activity for 180 min in the p-OHA group were also significantly increased, in a dose-dependent manner, compared with those in the Ringer's group [$F_{(4, 45)}$= 35.854, p<0.0001] (Fig. 2b). By contrast, there was no difference in the locomotor activity between the Ringer and p-OHN groups [treatment, $F_{(2, 42)}$=0.300, p=0.7425; time, $F_{(11, 462)}$=4.931, p<0.0001; treatment × time, $F_{(22, 462)}$= 1.303, p=0.1629] (Fig. 2c). The total counts of locomotor activity in the p-OHN group also were not significantly different from those in the Ringer's group [$F_{(2, 42)}$=0.300, p=0.7425] (Fig. 2d).

Effects of serotonergic, noradrenergic, and dopaminergic agents on p-OHA-induced locomotor activity in mice

To clarify the involvement of the serotonergic system in p-OHA-induced locomotor activity, we investigated the effects of pretreatment with fluoxetine, a SSRI. As shown in Fig. 3a, fluoxetine failed to affect the time course of p-OHA-induced locomotor activity [treatment, $F_{(3, 36)}$= 63.163, p<0.0001; time, $F_{(5, 180)}$=32.851, p<0.0001; treatment × time, $F_{(15, 180)}$=12.035, p<0.0001; p>0.05 by Fisher's PLSD, compared with Veh + p-OHA group]. There was also no significant difference in the total counts of locomotor activity over 180 min between the fluoxetine + p-OHA group and the vehicle + p-OHA group [$F_{(3, 36)}$= 63.163, p<0.0001; p>0.05 by Fisher's PLSD, compared with the Veh + p-OHA group] (Fig. 3b). Next, we investigated the effects of pretreatment with the DA-β-hydroxylase inhibitor DDC on p-OHA-induced locomotor activity to determine whether the noradrenergic system was involved. As for fluoxetine, DDC did not influence p-OHA-induced locomotor activity in terms of both time course [treatment, $F_{(3, 36)}$=18.411, p<0.0001; time, $F_{(5, 180)}$= 18.521, p<0.0001; treatment × time, $F_{(15, 180)}$=8.492, p< 0.0001; p>0.05 by Fisher's PLSD, compared with the Veh + p-OHA group] and total counts [$F_{(3, 36)}$=18.411, p<0.0001; p>0.05 by Fisher's PLSD, compared with the Veh + p-OHA group] (Fig. 3c, d).

To examine the involvement of the dopaminergic system in p-OHA-induced locomotor activity, we also investigated the effects of pretreatment with the DA uptake inhibitor nomifensine. Compared with the Veh + p-OHA group, the nomifensine + p-OHA group showed significant decreases in locomotor activity 60–90 min after administration of p-OHA [treatment, $F_{(3, 36)}$=37.946, p<0.0001; time, $F_{(5, 180)}$= 22.741, p<0.0001; treatment × time, $F_{(15, 180)}$=11.477, p< 0.0001] (Fig. 3e). Total counts of locomotor activity over 180 min in the nomifensine + p-OHA group were also

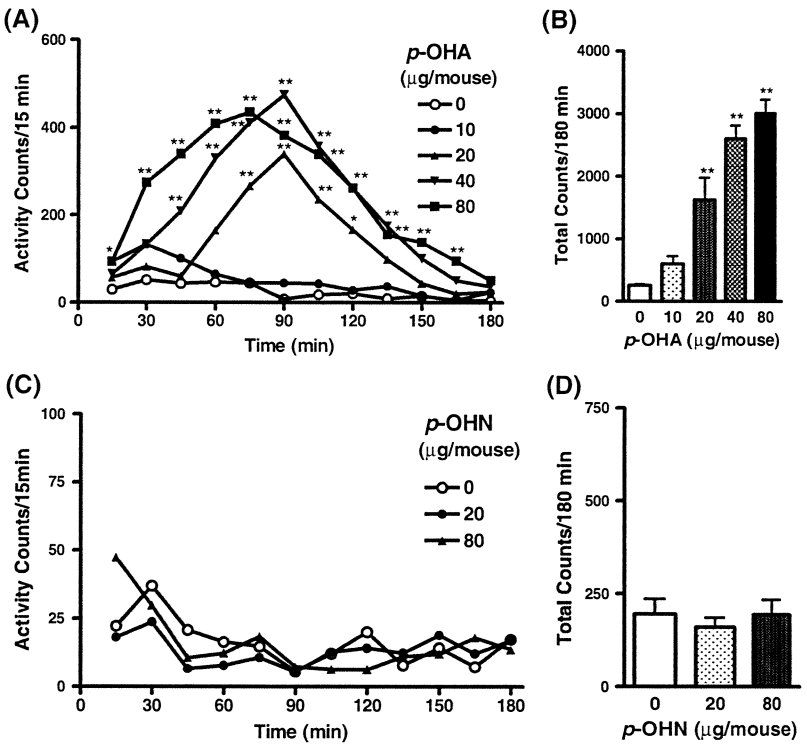


Fig. 2 Effects of intracerebroventricular (i.c.v.) administration of p-OHA (**a**, **b**) and p-OHN (**c**, **d**) on locomotor activity in mice. **a**, **c** Time course of locomotor activity. Ordinates give the mean numbers of photocell counts in 15-min periods. **b**, **d** Total locomotor activity during a 180-min period. Data represent the means ± SEM for 10–15 animals per group. *P<0.05, **P< 0.01 vs the Ringer's only (0 μg/mouse, i.c.v.) group

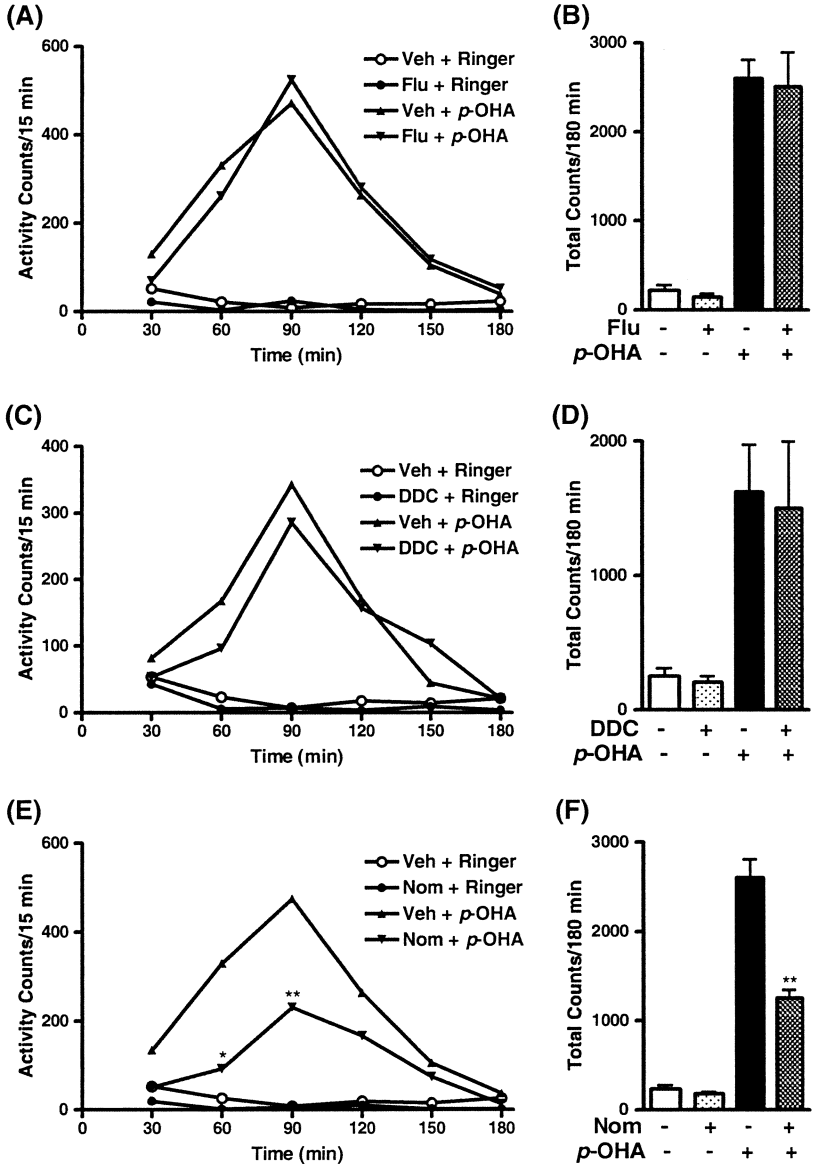


Fig. 3 Effects of fluoxetine (Flu; **a**, **b**), diethyldithiocarbamate (DDC; **c**, **d**), and nomifensine (Nom; **e**, **f**) on *p*-OHA-induced locomotor activity in mice. Animals were pretreated with Flu (10 mg/kg, i.p.), Nom (2.5 mg/kg, i.p.), or saline (Veh; i.p.) 30 min before *p*-OHA (40 μg/mouse, i.c.v.) or Ringer's solution (i.c.v.) treatment. Animals were pretreated with DDC (500 mg/kg, i.p.) or saline (Veh; i.p.) 12 h before *p*-OHA (20 μg/mouse, i.c.v.) or Ringer's solution (i.c.v.) treatment. **a**, **c**, **e** Time course of locomotor activity. *Ordinates* give the mean numbers of photocell counts in 15-min periods. **b**, **d**, **f** Total locomotor activity during a 180-min period. Data represent the means ± SEM for ten animals per group. $^{*}P<0.05$, $^{**}P<0.01$ vs the Veh + *p*-OHA group

significantly lower than those in the Veh + *p*-OHA group [$F_{(3,\ 36)}=37.946$, $p<0.0001$] (Fig. 3f).

Effects of *p*-OHA into NAc on ambulation counts in rats

p-OHA significantly increased locomotor activity in mice. In addition, we tested the effect of local microinfusions of *p*-OHA into the NAc (Fig. 4) on ambulation counts in rats. As shown in Fig. 5a, microinfusions of *p*-OHA (0.5–2.0 μg/rat) into the NAc significantly and dose-dependently increased ambulation counts 15–75 min after the administration of *p*-OHA [treatment, $F_{(3,\ 36)}=38.131$, $p<0.0001$; time, $F_{(7,\ 252)}=5.411$, $p<0.0001$; treatment × time, $F_{(21,\ 252)}=2.740$, $p=0.0001$]. *p*-OHA microinjection into the NAc dose-dependently increased total ambulation counts [$F_{(3,\ 36)}=38.131$, $p<0.0001$] (Fig. 5b).

Effects of nomifensine on the ambulation induced by microinjection of *p*-OHA into the NAc in rats

To verify the involvement of the dopaminergic system in the increased ambulation induced by microinjection of *p*-OHA (2.0 μg/rat) into the NAc, rats were pretreated with nomifensine (5 mg/kg, i.p.) for 30 min before *p*-OHA injection followed by ambulation counts. As shown in Fig. 6a, the nomifensine + *p*-OHA group showed a significant decrease in ambulation counts 15–90 min after *p*-OHA microinfusion compared with the Veh + *p*-OHA group [treatment, $F_{(3,\ 36)}=21.171$, $p<0.0001$; time, $F_{(7,\ 252)}=0.876$, $p=0.5258$; treatment × time, $F_{(21,\ 252)}=1.333$, $p=0.1543$]. Total ambulation counts over a 120-min period were also decreased by nomifensine [$F_{(3,\ 36)}=21.171$, $p<$

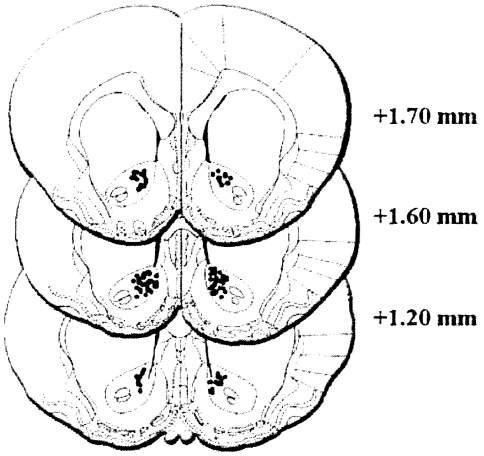


Fig. 4 Schematic illustration showing the locations of the bilateral infusion cannulas in the rat NAc. The coronal sections were adopted from Paxinos and Watson (1997). Distances are in reference to the bregma

0.0001] (Fig. 6b). Post hoc tests also revealed a significant increase in nomifensine + Ringer group compared with Veh + Ringer group (Fig. 6a, b).

Discussion

The present study shows that i.c.v. administration of *p*-OHA significantly increases locomotor activity. This is consistent with a previous finding (Fog and Pakkenberg 1971). However, a few studies have shown that i.p. injection of *p*-OHA does not change or decreases locomotor activity (Bauer 1980; Bushnell 1986). The reason for this discrepancy may be the route of administration. While Bauer (1980) and Bushnell (1986) administered *p*-OHA through the peripheral route, we and other researchers (Fog and Pakkenberg 1971) have used the direct administration into the brain because *p*-OHA hardly penetrates the blood–brain barrier (Lindenbaum et al. 1975). On the other hand, *p*-OHN did not influence locomotor activity in mice. Our early studies revealed that i.c.v. administration of *p*-OHA induces a HTR in contrast to its metabolite *p*-OHN (Sakurada 1975; Satoh et al. 1985; Tadano et al. 1986, 1987). Although both *p*-OHA and *p*-OHN inhibited MAO_A, *p*-OHA was shown to be more potent than *p*-OHN in inhibiting DA and 5-HT uptake from mouse forebrain homogenates (Arai et al. 1990). Thus, the differences in our results with both compounds may be due to differences in their inhibitory effects on MAO_A, as well as DA and 5-HT uptake.

A previous report has shown that an i.c.v. administration of 200 or 400 μg of AMPH induced hyperlocomotion, whereas 0.5–25 μg produced no discernible alterations in the behavior of Swiss albino mice (McCullough et al. 1970). The i.c.v. injection of a similar dose of *p*-OHA (200 μg) was also shown to induce hyperlocomotion, whereas 0.5–25 μg produced no alterations (McCullough et al. 1970). Furthermore, it was shown that the i.c.v. administration of 100 μg of AMPH also induced hyperlocomotion in rats (Beauchamp et al. 2000). In addition, we previously reported that the i.c.v. administration of 80 and 160 μg of *p*-OHA alters the content of DA and its metabolites in mice striatum (Arai et al. 1991). Thus, the dose range of *p*-OHA (10–80 μg) used in the present study was lower than in our previous study and selected in reference to the behavioral and neurochemical reports above. Consistent with these studies using i.c.v. injection of AMPH, we did not observe the induction of hyperlocomotion with 10 μg of *p*-OHA. It is difficult to compare the *p*-OHA doses used in our study (i.c.v. or local injection) with the AMPH doses from other studies using systemic injections, since we did not measure the actual concentration of *p*-OHA in the regions of interest. Furthermore, AMPH is first metabolized to *p*-OHA in the periphery and brain, which is then further hydroxylated to *p*-OHN (Axelod 1970; Goldstein and Contrera 1962; Goldstein and Anagnoste 1965), and *p*-OHA does not easily cross the blood–brain barrier.

Because AMPH induces the release of monoamines, *p*-OHA has also been assumed to induce the release of

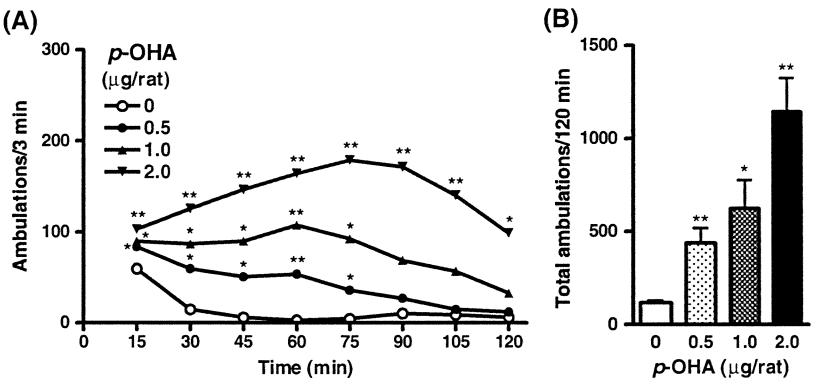


Fig. 5 Effects of microinjections of *p*-OHA into the NAc on ambulation counts in rats (**a**, **b**). The animals received bilateral injections of *p*-OHA (0.5, 1.0, and 2.0 μg/rat) or Ringer's solution (0 μg/rat) into the NAc. **a** Time course of ambulation counts for 3 min at 15-min intervals. **b** Total ambulation counts during a 120-min period. Data represent the means ± SEM for ten animals per group. **P*< 0.05, ***P*<0.01 vs the Ringer's solution (0 μg/rat) group

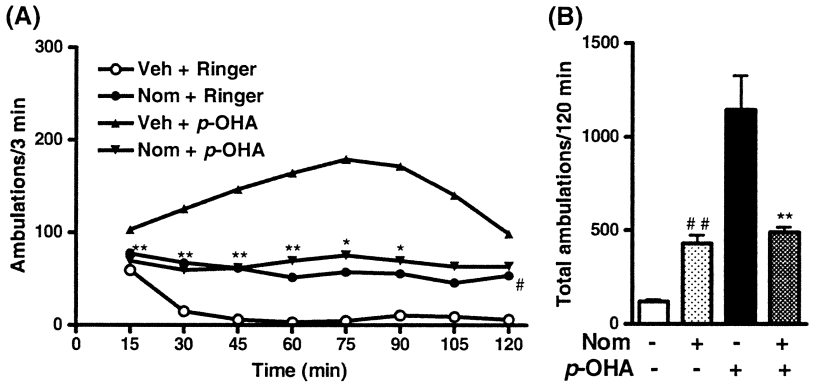


Fig. 6 Effects of nomifensine (Nom) on ambulation induced by intra-NAc infusions of *p*-OHA in rats (**a**, **b**). Rats were pretreated with Nom (5.0 mg/kg, i.p.) or saline (Veh; i.p.) 30 min before intra-NAc infusions of *p*-OHA (2.0 μg/rat) or Ringer's solution. **a** Time course of ambulation counts for 3 min at 15-min intervals. **b** Total ambulation counts during a 120-min period. Data represent the means ± SEM for ten animals per group. $^{\#}P<0.05$, $^{\#\#}P<0.01$ vs the Veh + Ringer group (especially shown in Nom + Ringer group only), $^{*}P<0.05$, $^{**}P<0.01$ vs the Veh + *p*-OHA group

neurotransmitters from presynaptic monoaminergic neurons. Indeed, previous reports have shown that the release of DA, NA, and 5-HT can be induced by *p*-OHA (Cho et al. 1977; Matsuda et al. 1989; Kaminskas et al. 2002). In addition, previous studies have reported that central 5-HT and NA neural transmission is involved in the regulation of locomotor activity. For example, MDL100907, a selective 5-HT_{2A} antagonist, reversed the locomotor stimulant effects of AMPH in rats without having any effect on locomotor activity (Moser et al. 1996), and NA uptake inhibitors antagonized the locomotor-stimulant effect of AMPH (Tyler and Tessel 1980). Furthermore, because the DA-β-hydroxylase inhibitor DDC reduced NA levels (Collins 1965; Chang et al. 1995; Gaval-Cruz et al. 2008), we used nomifensine, fluoxetine, or DDC treatment to determine whether *p*-OHA-induced hyperlocomotion is due to DA, 5-HT, or NA release. In the present study, *p*-OHA-induced locomotor activity was inhibited by pretreatments with nomifensine but not by pretreatments with fluoxetine and DDC. These results indicate that DA neural transmission is one of the main factors involved in *p*-OHA-induced locomotor activity.

Nomifensine blocks NA uptake but also inhibits DA uptake into dopaminergic nerve terminals (Brogden et al. 1979), thereby increasing DA levels in the synaptic cleft. *p*-OHA was suggested to be taken up into serotonergic as well as dopaminergic nerve terminals followed by DA release into the synaptic cleft (Arai et al. 1991). The effects of nomifensine on *p*-OHA-induced hyperlocomotion could be due to its inhibition of *p*-OHA uptake into dopaminergic nerve terminals. Fung and Uretsky (1980) have reported that nomifensine can inhibit AMPH-induced circling and both the stimulation of synthesis and release of DA by AMPH. In addition, DA knockout mice displayed a strong decrease of locomotion after AMPH administration (Spielewoy et al. 2001). In the i.c.v. experiment in mice, 2.5 mg/kg of nomifensine was less effective in locomotion so that the blocking of *p*-OHA-induced hyperlocomotion (Fig. 3), whereas for the NAc infusion experiment, the nomifensine dose was 5.0 mg/kg, which increased locomotion in Ringer-treated control (Fig. 6), indicating that 5.0 mg/kg was a much more effective dose as a DA uptake inhibitor. These results suggest that the inhibition of DA transporter in the NAc is involved in the *p*-OHA-induced hyperlocomotion.

As mentioned above, to confirm the involvement of the dopaminergic system in *p*-OHA-induced locomotor activity, we focused on the mesocorticolimbic DA pathways, particularly those projecting from the VTA (a DA cell body area) to the NAc (a DA terminal area), and tested the effects of microinjection of *p*-OHA into the NAc (a DA terminal area) on ambulation counts in rats. Local infusions of *p*-OHA into the NAc significantly increased ambulation counts. The ambulation induced by microinjection of *p*-OHA into the NAc was inhibited by pretreatments with nomifensine. Our results are consistent with previous findings showing that intra-NAc injections of AMPH produce increased locomotion (Vezina and Stewart 1990). Other reports have shown that AMPH-induced locomotor activity is blocked by DA receptor antagonists or by 6-hydroxydopamine lesions of DA nerve terminals in the NAc (Joyce and Koob 1981; Vezina 1996). Based on previous reports, our results indicate that the NAc may be important for the expression of locomotor activity induced by *p*-OHA.

Our previous experiments revealed that i.c.v. administration of *p*-OHA decreased the levels of striatal DA and its metabolite 3,4-dihydroxyphenylacetic acid, as well as inhibited DA uptake into the nerve endings and MAO activity (Arai et al. 1990, 1991). Cocaine and the DA transporter inhibitor GBR12909 increase locomotor activity

resulting from increased levels of synaptic DA following DA reuptake inhibition (Mcgeehan et al. 2004). In addition, administration of a MAO inhibitor (for example, nialamide) alone to rodents induces little behavioral excitation (Kuribara 1997). It is also suggested that AMPH has inhibitory actions on MAO activity (Kuribara and Tadokoro 1983) and the uptake of catecholamine at presynaptic nerve terminals (McMillen 1983). Thus, *p*-OHA-induced hyperlocomotion could be due to an increase in DA levels in the NAc dopaminergic synaptic cleft owing to the inhibitory effects of *p*-OHA on MAO and DA uptake.

It should be stressed that our findings in mice may not be generalized to rats and vice versa. However, central *p*-OHA administration showed similar findings between both species. Nonetheless, our study indicates that the central dopaminergic system is involved in *p*-OHA-induced locomotor activity in rodents and points to the NAc as an important brain site for the action of *p*-OHA. However, *p*-OHA administration may also affect other NAc neurochemical systems involved in motor function, such as the glutamatergic and acetylcholinergic systems. Further studies are needed to investigate these possibilities.

Acknowledgments This study was supported in part by Grants-in-Aid for Scientific Research (20790309) and a High Technology Research Program from the Ministry of Education, Culture, Sports, Science, and Technology of Japan.

References

Arai Y, Kim SK, Kinemuchi H, Tadano T, Satoh SE, Satoh N, Kisara K (1990) Inhibition of brain type A monoamine oxidase and 5-hydroxytryptamine uptake by two amphetamine metabolites, *p*-hydroxyamphetamine and *p*-hydroxynorephedrine. J Neurochem 55:403–408

Arai Y, Kim SK, Kinemuchi H, Tadano T, Oyama K, Satoh N, Kisara K (1991) Inhibition of brain MAO-A and animal behaviour induced by *p*-hydroxyamphetamine. Brain Res Bull 27:81–84

Axelod J (1970) Amphetamine: metabolism, physiological storage. In: Costa E, Gerattini S (eds) International symposium on amphetamine and related compounds. Raven, New York, pp 207–216

Battisti JJ, Shreffler CB, Uretsky NJ, Wallace LJ (2000) NMDA antagonists block expression of sensitization of amphetamine- and apomorphine-induced stereotypy. Pharmacol Biochem Behav 67:241–246

Bauer RH (1980) The effects of l-, d-, and parahydroxy-amphetamine on locomotor activity and wall climbing in rats of different ages. Pharmacol Biochem Behav 13:155–165

Beauchamp MH, Ormerod BK, Jhamandas K, Boegman RJ, Beninger RJ (2000) Neurosteroids and reward: allopregnanolone produces a conditioned place aversion in rats. Pharmacol Biochem Behav 67:29–35

Brittain RT, Handley SL (1967) Temperature changes produced by the injection of catecholamines and 5-hydroxytryptamine into the cerebral ventricles of the conscious mouse. J Physiol 192:805–813

Brogden RN, Heel RC, Speight TM, Avery GS (1979) Nomifensine: a review of its pharmacological properties and therapeutic efficacy in depressive illness. Drugs 18:1–24

Bushnell PJ (1986) Differential effects of amphetamine and related compounds on locomotor activity and metabolic rate in mice. Pharmacol Biochem Behav 25:161–170

Cador M, Bjijou Y, Stinus L (1995) Evidence of a complete independence of the neurobiological substrates for the induction and expression of behavioral sensitization to amphetamine. Neuroscience 65:385–395

Chang WJ, Barb CR, Kraeling RR, Rampacek GB, Wright JT (1995) Biogenic amines in the hypothalamus of rats after diethyldithiocarbamate or AIMAX treatment, an alternative for norepinephrine depletion. J Anim Sci 73:1147–1151

Cho AK, Fischer JF, Schaeffer JC (1977) The accumulation of *p*-hydroxyamphetamine by brain homogenates and its role in the release of catecholamines. Biochem Pharmacol 26:1367–1372

Collins GG (1965) Inhibition of dopamine-beta-oxidase by diethyldithiocarbamate. J Pharm Pharmacol 17:526–527

Di Chiara G, Imperato A (1988) Drugs abused by humans preferentially increase synaptic dopamine concentrations in the mesolimbic system of freely moving rats. Proc Natl Acad Sci USA 85:5274–5278

Dougan DF, Labrie SL, Paull PD, Duffield PH, Wade DN (1986) Evidence that alpha-methyl-p-tyramine is implicated in behavioural augmentation to amphetamine. Gen Pharmacol 17:453–456

Escarabajal MD, Aragon CM (2003) DDTC, a metabolite of disulfiram, reduces the stimulating effect on ethanol's locomotor activity in mice. Psychopharmacol Bull 37:113–119

Fog R, Pakkenberg H (1971) Behavioral effects of dopamine and *p*-hydroxyamphetamine injected into corpus striatum of rats. Exp Neurol 31:75–86

Fowler SC, Pinkston JW, Vorontsova E (2007) Clozapine and prazosin slow the rhythm of head movements during focused stereotypy induced by d-amphetamine in rats. Psychopharmacology (Berl) 192:219–230

Fung YK, Uretsky NJ (1980) The effect of dopamine uptake blocking agents on the amphetamine-induced circling behavior in mice with unilateral nigro-striatal lesions. J Pharmacol Exp Ther 214:651–656

Gaval-Cruz M, Schroeder JP, Liles LC, Javors MA, Weinshenker D (2008) Effects of disulfiram and dopamine beta-hydroxylase knockout on cocaine-induced seizures. Pharmacol Biochem Behav 89:556–562

Goldstein M, Anagnoste B (1965) The conversion in vivo of D-amphetamine to (+)*p*-hydroxynorephedrine. Biochim Biophys Acta 107:166–168

Goldstein M, Contrera JF (1962) The substrate specificity of phenylamine-β-hydroxylase. J Biol Chem 237:1898–1902

Hall CS (1934) Emotional behavior in the rat. I. Defecation and urination as measures of individual differences in emotionality. J Comp Psychol 18:385–403

Joyce EM, Koob GF (1981) Amphetamine-, scopolamine- and caffeine-induced locomotor activity following 6-hydroxydopamine lesions of the mesolimbic dopamine system. Psychopharmacology (Berl) 73:311–313

Kaminskas LM, Irvine RJ, Callaghan PD, White JM, Kirkbride P (2002) The contribution of the metabolite *p*-hydroxyamphetamine to the central actions of *p*-methoxyamphetamine. Psychopharmacology (Berl) 160:155–160

Kuribara H (1997) Effects of tetrabenazine on methamphetamine-induced hyperactivity in mice are dependent on order and time-course of administration. Pharmacol Biochem Behav 56:9–14

Kuribara H, Tadokoro S (1983) Comparisons of susceptibilities to the effects of antipsychotic drugs on lever-press avoidance response between mice and rats. Jpn J Pharmacol 33:1127–1133

Lindenbaum A, Marcher K, Wepierre J, Cohen Y (1975) Blood-brain barrier. II. Kinetics of distribution of 3H-parahydroxyamphetamine in brain structures after intravenous administration in the rat. Arch Int Pharmacodyn Ther 215:168–176 (article in French)

Matsuda LA, Hanson GR, Gibb JW (1989) Neurochemical effects of amphetamine metabolites on central dopaminergic and serotonergic systems. J Pharmacol Exp Ther 251:901–908

McCullough DO, Milberg JN, Robinson SM (1970) A central site for the hypothermic effects of (+)-amphetamine sulphate and *p*-hydroxyamphetamine hydrobromide in mice. Br J Pharmacol 40:219–226

Mcgeehan AJ, Janak PH, Olive MF (2004) Effect of the mGluR5 antagonist 6-methyl-2-(phenylethynyl)pyridine (MPEP) on the acute locomotor stimulant properties of cocaine, D-amphetamine, and the dopamine reuptake inhibitor GBR12909 in mice. Psychopharmacology 174:266–273

McMillen BA (1983) CNS stimulant: two distinct mechanisms of action for amphetamine-like drugs. Trends Pharmacol Sci 4:429–432

Moser PC, Moran PM, Frank RA, Kehne JH (1996) Reversal of amphetamine-induced behaviours by MDL 100, 907, a selective 5-HT2A antagonist. Behav Brain Res 73:163–167

Nakagawasai O, Arai Y, Satoh SE, Satoh N, Neda M, Hozumi M, Oka R, Hiraga H, Tadano T (2004) Monoamine oxidase and head-twitch response in mice. Mechanisms of alpha-methylated substrate derivatives. Neurotoxicology 25:223–232, Review

Oyama K, Tadano T, Kisara K, Arai Y, Kinemuchi H (1989) Behavioral and biochemical effects of *p*-hydroxyamphetamine on central monoamine neurons. Jpn J Pharmacol 49:335

Paulus MP, Callaway CW, Geyer MA (1993) Quantitative assessment of the microstructure of rat behavior: II. Distinctive effects of dopamine releasers and uptake inhibitors. Psychopharmacology (Berl) 113:187–198

Paxinos G, Watson C (1997) The rat brain in stereotaxic coordinates. Academic, New York

Peleg-Raibstein D, Knuesel I, Feldon J (2008) Amphetamine sensitization in rats as an animal model of schizophrenia. Behav Brain Res 191:190–201

Pirisino R, Galeotti N, Livi S, Raimondi L, Ghelardini C (2006) 4-methyl benzylamine stimulates food consumption and counteracts the hypophagic effects of amphetamine acting on brain *Shaker-like* Kv1.1 channels. Br J Pharmacol 147:218–224

Porrino LJ, Lucignani G, Dow-Edwards D, Sokoloff L (1984) Correlation of dose-dependent effects of acute amphetamine administration on behavior and local cerebral metabolism in rats. Brain Res 307:311–320

Puglisi-Allegra S, Cestari V, Cabib S, Castellano C (1994) Strain-dependent effects of post-training cocaine or nomifensine on memory storage involve both D1 and D2 dopamine receptors. Psychopharmacology (Berl) 115:157–162

Sakurada S (1975) Effects of beta-phenylethylamine derivatives on the central nervous system. (5) The effect of intracerebral administration of tyramine on head twitching in mice pre-treated with isocarboxazid. Nippon Yakurigaku Zasshi 71: 779–787 (article in Japanese)

Salahpour A, Ramsey AJ, Medvedev IO, Kile B, Sotnikova TD, Holmstrand E, Ghisi V, Nicholls PJ, Wong L, Murphy K, Sesack SR, Wightman RM, Gainetdinov RR, Caron MG (2008) Increased amphetamine-induced hyperactivity and reward in mice overexpressing the dopamine transporter. Proc Natl Acad Sci USA 105:4405–4410

Satoh S, Satoh N, Tadano T, Kisara K (1985) Enhancement of para-hydroxyamphetamine induced head-twitch response by central catecholamine depletion. Res Commun Substance Abuse 6:213–219

Scorza MC, Carrau C, Silveira R, Zapata-Torres G, Cassels BK, Reyes-Parada M (1997) Monoamine oxidase inhibitory properties of some methoxylated and alkylthio amphetamine derivatives: structure-activity relationships. Biochem Pharmacol 54:1361–1369

Sills TL (1999) Amphetamine dose dependently disrupts prepulse inhibition of the acoustic startle response in rats within a narrow time window. Brain Res Bull 48:445–448

Simpson LL (1980) Blood pressure and heart rate response evoked by *p*-hydroxyamphetamine and by *p*-hydroxynorephedrine II. A quantitative assessment of the role of amphetamine metabolites in acute responses evoked by d-amphetamine. J Pharmacol Exp Ther 213:504–508

Spielewoy C, Biala G, Roubert C, Hamon M, Betancur C, Giros B (2001) Hyperlocomotor effects of acute and daily *d*-amphetamine in mice lacking the dopamine transporter. Psychopharmacology 159:2–9

Sulzer D, Sonders MS, Poulsen NW, Galli A (2005) Mechanisms of neurotransmitter release by amphetamines: a review. Prog Neurobiol 75: 406–433 (review)

Tadano T, Satoh S, Kisara K (1986) Head-twitches induced by *p*-hydroxyamphetamine. Jpn J Pharmacol 41:519–523

Tadano T, Satoh S, Satoh N, Kisara K, Arai Y, Kinemuchi H (1987) Involvement of alpha-adrenoceptors in para-hydroxyamphetamine-induced head-twitch response. Psychopharmacology 26:1463–1467

Tadano T, Satoh S, Satoh N, Kisara K, Arai Y, Kim SK, Kinemuchi H (1989) Potentiation of para-hydroxyamphetamine-induced head-twitch response by inhibition of monoamine oxidase type A in the brain. J Pharmacol Exp Ther 250:254–260

Tyler TD, Tessel RE (1980) Norepinephrine uptake inhibitors as biochemically and behaviorally selective antagonists of the locomotor stimulation induced by indirectly acting sympathomimetic aminetic amines in mice. Psychopharmacology (Berl) 69:27–34

Ueki S, Nurimoto S, Ogawa N (1972) Effects of psychotropic drugs on emotional behavior in rats with limbic lesions, with special reference to olfactory bulb ablations. Folia Psychiatr Neurol Jpn 26:245–255

Vezina P (1996) D1 dopamine receptor activation is necessary for the induction of sensitization by amphetamine in the ventral tegmental area. J Neurosci 16:2411–2420

Vezina P (2004) Sensitization of midbrain dopamine neuron reactivity and the self-administration of psychomotor stimulant drugs. Neurosci Biobehav Rev 27:827–839 (review)

Vezina P, Stewart J (1990) Amphetamine administered to the ventral tegmental area but not to the nucleus accumbens sensitizes rats to systemic morphine: lack of conditioned effects. Brain Res 516:99–106

Yamada J, Sugimoto Y, Yamada S (2004) Involvement of dopamine receptors in the anti-immobility effects of dopamine re-uptake inhibitors in the forced swimming test. Eur J Pharmacol 504:207–211

Behavioural Brain Research 208 (2010) 224–230

Contents lists available at ScienceDirect

Behavioural Brain Research

journal homepage: www.elsevier.com/locate/bbr

Research report

Behavioral and neurochemical characterization of mice deficient in the N-type Ca^{2+} channel α_{1B} subunit

Osamu Nakagawasai[a,*], Hiroshi Onogi[a], Satoru Mitazaki[a,b,1], Atsushi Sato[a], Kenya Watanabe[a], Hiroko Saito[c], Shigeo Murai[c], Kota Nakaya[a], Manabu Murakami[d], Eiki Takahashi[e], Koichi Tan-No[a], Takeshi Tadano[a]

[a] Department of Pharmacology, Tohoku Pharmaceutical University, 4-4-1 Komatsushima, Aoba-ku, Sendai 981-8558, Japan
[b] Laboratory of Forensic Toxicology, Faculty of Pharmacy, Takasaki University of Health and Welfare, 60 Nakaorui-machi, Takasaki-shi, Gunma 370-0033, Japan
[c] Laboratory of Pharmacology, Aomori University, Aomori 030-0943, Japan
[d] Department of Physiology, Akita University School of Medicine, Akita 010-8543, Japan
[e] Riken Brain Science Institute, Saitama 351-0198, Japan

ARTICLE INFO

Article history:
Received 9 August 2009
Received in revised form
24 November 2009
Accepted 30 November 2009
Available online 4 December 2009

Keywords:
N-type calcium channel
Locomotion
Memory
Prepulse inhibition
Dopamine
Serotonin

ABSTRACT

N-type voltage-dependent calcium channels (VDCCs) play an important role in neurotransmission, synaptic plasticity, and brain development. They are composed of several subunits named α_1, α_2, δ, β and γ. The α_1 subunit is essential for channel functions and determines fundamental channel properties. Since N-type VDCC are critically involved in the release of neurotransmitters and clinical relevance, we predicted that α_1 subunit KO mice would show several alterations in behavior. In the present study, we investigated neuronal functions in mice lacking the α_{1B} ($Ca_V2.2$) subunit of the N-type calcium channels. $Ca_V2.2^{-/-}$ mice exhibited a significant increase in locomotion on an activity wheel during the dark phase. Furthermore, when challenged with apomorphine, mutant mice showed enhanced locomotor activity. Cognitive functions were examined using a Y-maze task for short-term memory and a passive avoidance task for long-term memory. The Y-maze revealed no differences in spontaneous alternation behavior between mutant and wild-type mice. The passive avoidance test revealed that the latency time in mutant mice was significantly decreased. The mutant mice showed prepulse inhibition deficits reminiscent of the sensorimotor gating deficits observed in a large majority of schizophrenic patients. Decreases in baseline levels of dopamine and serotonin within the striata and frontal cortices of mutant mice were also observed. These results suggest that Ca^{2+} in the central nervous system modulates various neurophysiological functions, such as locomotor activity, long-term memory, and sensorimotor gating through the α_{1B} subunit of the N-type calcium channels.

© 2009 Elsevier B.V. All rights reserved.

1. Introduction

Voltage-dependent calcium channels (VDCCs) are key elements of the presynaptic machinery for the vesicular release of neurotransmitters [15]. In the mammalian central nervous system (CNS), fast synaptic transmission is mediated synergistically by multiple types of VDCCs, including P/Q-type, N-type and R-type channels, which are predominantly expressed in neurons [17,51]. N-type calcium channels are critically involved in the release of neurotransmitters, including glutamate [44], GABA [28], acetylcholine [66], dopamine [26,63,69], serotonin [22], and noradrenaline [11], from central neurons. Molecular studies have revealed that the α_{1B} ($Ca_V2.2$) gene encodes a subunit specific for the N-type calcium channel, so mice lacking the α_{1B} subunit could be a useful tool for studying neurotransmitter mechanisms. Such mice have been adopted for modeling disorders attributable to sympathetic nerve dysfunction [31] and for studying pain-related disorders [25,39,53].

Calcium entry via N-type channels plays a critical role in neuronal survival [23,27,46] as well as directing migration of immature neurons [42]. In the cerebral cortex, the number of binding sites and mRNA levels for N-type channels increase gradually during early postnatal life [19,61], when they are required for transmit-

Abbreviations: ANOVA, analysis of variance; ASR, acoustic startle response; CNS, central nervous system; DA, dopamine; DOPAC, 3,4-dihydroxyphenylacetic acid; EEG, electronencephalographic; 5-HIAA, 5-hydroxytryptamine; HPLC, high-performance liquid chromatography; 5-HT, 5-hydroxytryptamine; HVA, homovanillic acid; NE, norepinephrine; PPI, prepulse inhibition; SC, subcutaneous; VDCCs, voltage-dependent calcium channels; VTA, ventral tegmental area.

* Corresponding author. Tel.: +81 22 727 0123; fax: +81 22 727 0123.
E-mail addresses: osamun@tohoku-pharm.ac.jp (O. Nakagawasai), hirogle@yahoo.co.jp (H. Onogi), mitazaki427@yahoo.co.jp (S. Mitazaki), obx0315@yahoo.co.jp (A. Sato), ken5233@fmu.ac.jp (K. Watanabe), hsaito@aomori-u.ac.jp (H. Saito), smurai@aomori-u.ac.jp (S. Murai), mmura0123@hotmail.co.jp (M. Murakami), etakahashi@brain.riken.jp (E. Takahashi), koichi@tohoku-pharm.ac.jp (K. Tan-No), tadano@tohoku-pharm.ac.jp (T. Tadano).
[1] Tel.: +81 27 352 1180; fax: +81 27 352 1118.

0166-4328/$ – see front matter © 2009 Elsevier B.V. All rights reserved.
doi:10.1016/j.bbr.2009.11.042

ter release from terminals in the hippocampus [55,64], cortex [30], and ventral tegmental area (VTA) [6,67] cell populations sending projections to the medial prefrontal cortex. Presynaptic VDCC blockade leads to disruption of synaptic signaling and could affect activity levels in neural circuits, possibly leading to perturbation of activity-dependent development. Activity-dependent development is a cornerstone of numerous developmental processes, such as neuronal survival [18,30], gene expression [1,9,54], and synaptic proliferation [3,47] and refinement [36,70]; thus, these processes may be impaired in animals lacking N-type calcium channels. In a recent report it was suggested that the P/Q-type calcium channel (α_{1A} subunit) seems to have a compensatory role in the cerebral cortex, hippocampus and cerebellum of mutant mice lacking N-type calcium channels (α_{1B} subunit) [59]. Another report has shown a selective elimination of N-type VDCC activity in superior cervical ganglion neurons and sympathetic nerve terminals in these mutant mice, whose sympathetic nerve activity was markedly diminished whereas parasympathetic nerve activity was unaffected [31]. Although Takahashi and Nagasu [59] have indicated that the compensatory mechanisms differ in different brain regions of N-type calcium channel α_{1B} subunit-deficient mice, further studies using transcriptome and proteome analyses, as well as pharmacological analysis of neurotransmitter release, will be necessary to elucidate the mechanisms of the N-type calcium channel. Of clinical relevance, expression levels of the mRNA encoding LIM, which is known to interact with the N-type calcium channel α_{1B} subunit [7], were shown to be significantly increased in the postmortem brain tissues of patients with bipolar disorder, schizophrenia and major depression, whereas it was decreased in the immortalized lymphoblastoid cell lines of patients with bipolar disorder [32,33]. It is also of note that schizophrenia has been strongly associated with genes important for presynaptic signaling [49,50,60].

To better understand the possible roles of N-type calcium channels in the CNS, mutant mice lacking N-type calcium channels were generated by gene targeting. Since N-type calcium channels are critically involved in the release of neurotransmitters and clinical relevance, we predicted that knockout mice for this channel may show several behavioral changes previously reported to occur in animal models of neurodevelopmental disorders such as schizophrenia [62]. Specifically, we assayed the acoustic startle response, prepulse inhibition (PPI) of startle, novelty- and apomorphine (a dopamine agonist)-induced locomotion, and memory-related behavior in the passive avoidance and Y-maze tasks. In addition, the amounts of monoamines and their metabolites in mice brains were measured to demonstrate the relationship between behavioral abnormalities and alterations in monoamine metabolism.

2. Materials and methods

All experiments were performed according to the Guide for Care and Use of Laboratory Animals at Tohoku Pharmaceutical University.

2.1. Animals

The mutant mice lacking the N-type Ca^{2+} channel α_{1B} subunit were generated on a CBA × C57BL/6 background, as previously described [31]. Chimeric male mice were mated with C57BL/6 females, and heterozygous male and female were interbred to generate mice in which the α_{1B} subunit of VDCC was knocked out. Male homozygous mice (−/−) and wild-type mice (+/+) weighing 30–35 g were used. Approximately 5–8 mice were housed as a group in one plastic cage (31 cm × 21 cm × 13 cm). All experiments were performed on mice at the age of 3–5 months. The total numbers of mice used in the study were 16 (+/+) mice and 21 (−/−) mice. The mice were maintained under conditions of constant temperature (23 ± 1 °C) and humidity (55 ± 5%) on a 12-h/12-h light-dark cycle (light from 9 to 21 h; dark from 21 to 9 h). The mice had free access to food and water throughout the experimental period.

The animals were subjected to several basal tests of locomotion, memory tests and acoustic startle response and PPI of the acoustic startle response. The order of the tests followed earlier recommendations ranking the tests from least stressful to more stressful [48,65]. To avoid interferences between the different tests, three clusters of tests were used: (1) one cohort of the three treatment groups was subject to Diurnal rhythm of spontaneous locomotor activity, prepulse inhibition of the startle and step-through passive avoidance task [(+/+, n = 6) and (−/−, n = 8)]; (2) a second cohort performed the Y-maze test and Behavioral responsiveness of dopaminergic agonist [(+/+, n = 6) and (−/−, n = 8)]; (3) a third cohort was assigned to determination of the levels of monoamine and its metabolites in the brain [(+/+, n = 4) and (−/−, n = 5)]. In each cohort, a pause of at least 1 week was kept between the individual tests.

2.2. Diurnal rhythm of spontaneous locomotor activity

Locomotor activity on an activity wheel (Muromachi Kikai Co., Tokyo, Japan) was measured every hour for three consecutive days. During the experimental period, mice had free access to food and water. The mice were placed individually on activity wheels they had not previously experienced under a constant light-dark cycle (lights on 09:00; lights off 21:00).

2.3. Behavioral responsiveness of dopaminergic agonist

The locomotor activities of homozygous and wild-type mice were evaluated using the multichannel activity-counting system SUPERMEX (Muromachi Kikai Co., Tokyo, Japan). This instrument can monitor even minute movements in all three planes of motion (sagittal, coronal and horizontal) as one movement, owing to its infrared sensor with multiple Fresnel lenses that can be moved close enough to the cage to capture multidirectional locomotor alterations in a single mouse. The Supermex instrument was connected to a behavioral analyzing system (CompACT AMS) (Muromachi Kikai), which can interpret each movement as one count. Therefore, vertical movements such as jumping, as well as horizontal movements such as walking and running, could be counted. Measurements of activity were conducted between 11:00 and 15:00 during the light phase.

Mice from each group [(+/+, n = 6) and (−/−, n = 8)] were placed in activity boxes and basal locomotion was recorded for 60 min. Following subcutaneous (s.c.) injection of vehicle (1 ml/kg/0.1% ascorbic acid/0.9% NaCl solution) the mice were placed in locomotor activity boxes for 60 min. Mice were then injected with apomorphine (1.0 mg/kg, s.c.), and locomotor activity was recorded for 60 min.

2.4. Step-through passive avoidance task

Training and retention trials for the passive avoidance task were conducted in a plexiglass box that contained dark (25 cm × 25 cm × 25 cm) and light (14 cm × 10 cm × 25 cm) compartments. The floor was constructed of stainless steel rods. The floor rods in the dark compartment were connected to an electronic stimulator (Nihon Kohden, Tokyo, Japan). As a training trial, a mouse was placed in the light compartment of the box. As soon as the mouse had completely entered the dark compartment, an electric shock (0.5 mA for 500 ms) was supplied to the floor bars. As a retention trial, on the 1st and 3rd days after the training trial, each mouse was repeatedly placed in the light compartment again for a cut-off time of 600 s. Latency time was estimated by measuring the length of time for the mouse to move from the light compartment to the dark compartment. Behavior in the passive avoidance task is generally considered to reflect long-term memory.

2.5. Y-maze test

The Y-maze apparatus consisted of three compartments (3 cm (W) × 40 cm (D) × 25 cm (H)) radiating out from the center. The mice were placed in one of the compartments and allowed to move freely for 8 min. Experiments were performed at a light intensity of 35 lx. An arm entry was defined as three legs entering one of the arms, and the sequence of entries was manually recorded. An alternation was defined as entry into all three arms on consecutive choices. Thus, the maximum number of alterations was the total number of entries minus 2, and the percent alteration was calculated as (actual alterations/maximum alterations) × 100. The percent alteration was designated as the spontaneous alternation behavior of the mouse, and was taken as a measure of spatial short-term memory.

2.6. Prepulse inhibition of the acoustic startle

Tests were conducted using an SR-LAB system (San Diego Instruments, San Diego, California, USA) that comprised four sound-attenuating chambers each equipped with a cylindrical Plexiglass animal enclosure (length, 6.5 cm; inner diameter, 3.8 cm). Ventilation was provided by a small electric fan that also generated a 70-dB background noise. Tone pulses were presented by a speaker positioned 24 cm directly above the animal enclosure. A piezoelectric accelerometer affixed to the animal enclosure frame was used to detect and transduce motion resulting from the animal's response. Tone pulse parameters were controlled by a microcomputer using a software package (SR-LAB) and interface assembly that also digitized, rectified and recorded stabilimeter readings.

Measures of both acoustic startle response (ASR) and PPI were obtained in a single session as described by Brake et al. [4] with minor modifications. Mice were placed in the Plexiglass enclosure and allowed to acclimatize to the environment

for 5 min before being tested in 37 discrete trials. In the first two trials, the magnitude of the ASR to a 120 dB tone of 50 ms duration was measured. These first two startle tones were presented to habituate the animals to the testing procedure. Therefore, the ASR magnitude of these two trials was omitted from the statistical analysis of the mean ASR amplitude. In the subsequent 35 trials, the startle tone was either presented alone or 100 ms after presentation of a 30-ms-duration prepulse. Prepulse intensity ranged from 3 to 15 dB above background noise and was varied randomly between trials in 3-dB steps. Measurements of the magnitude of the ASR were taken at each of the five prepulse intensities in five trials; animals were randomly presented with the startle tone alone during the other ten trials. The same stimulus condition was never presented in more than two consecutive trials. The interval between each trial was programmed to a variable time schedule with an average duration of 15 s (range 5–30 s). A measure of startle response amplitude was derived from the mean of 100 digitized data points collected from stimulus onset at a rate of 1 kHz. Prepulse effectiveness in suppressing the startle response was expressed as a percentage based on the mean amplitude of responses to the startle tone alone ($n = 10$) relative to those recorded under the five prepulse conditions ($n = 5$/condition): % PPI = 100 − [(mean startle amplitude for prepulse + pulse trials/mean startle amplitude for pulse-alone trials) × 100]%.

2.7. Determination of the levels of monoamine and its metabolites in the brain

Animals were killed by focused microwave irradiation, and the brains were rapidly removed. The frontal cortex and striatum were dissected out on an ice-cold plate. Each brain sample was quickly frozen and stored in a deep freezer at −80 °C until assayed. The contents of norepinephrine (NE), dopamine (DA), 3,4-dihydroxyphenylacetic acid (DOPAC), homovanillic acid (HVA), 5-hydroxytryptamine (5-HT), and 5-hydroxyindoleacetic acid (5-HIAA) were determined using high-performance liquid chromatography (HPLC) with electrochemical detection.

2.8. Statistical analysis

Results are expressed as means ± standard errors of the mean (SEM). The significance of differences was determined by the Student's *t*-test for two-group comparison (Total activity, startle amplitude and HPLC data), and by a one-way or two-way analysis of variance (ANOVA), followed by Fisher's PLSD test for multigroup comparisons. $p < 0.05$ represented a significant difference.

3. Results

3.1. Locomotor activity

The locomotor activity on the activity wheel was measured during a 24-h period on the third day for three consecutive days (Fig. 1). A two-way repeated measures ANOVA of the activity wheel data revealed a significant effect of genotype [$F(1,12) = 6.62$, $p < 0.05$], effect of time [$F(24,288) = 9.81$, $p < 0.01$] and a time × genotype interaction [$F(24,288) = 5.72$, $p < 0.01$]. The homozygous mice moved more actively in the dark phase (23:00, $p < 0.05$; 24:00, $p < 0.05$; 7:00, $p < 0.05$; 8:00, $p < 0.05$; Fig. 1).

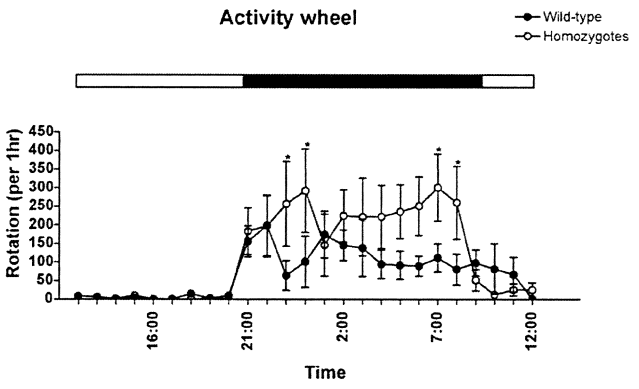


Fig. 1. Chronological distributions of wheel revolutions on the activity wheel. The rotation on the activity wheel was measured during a 24-h period on the third day for three consecutive days. The data are expressed as the means ± SEM for $n = 6$–8 mice/group. Closed circle (●), wild-type mice; open circle (○), the homozygous mice. *$p < 0.05$ vs. wild-type mice.

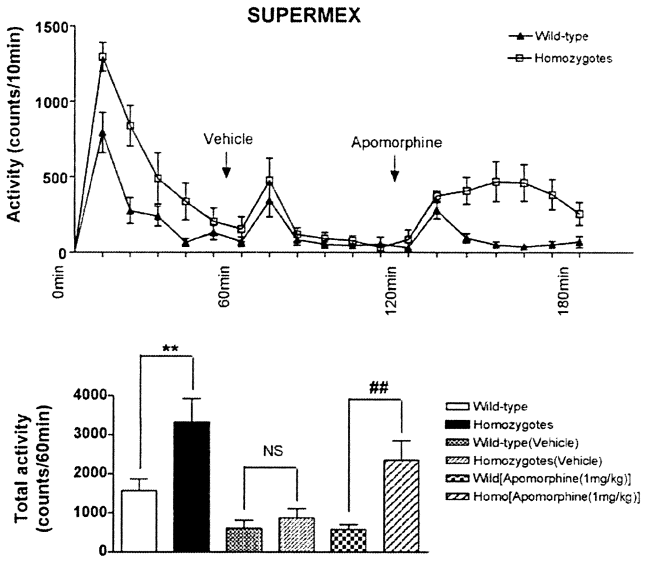


Fig. 2. Locomotor activity induced by apomorphine (1 mg/kg, s.c.) in homozygous mice. (a) Temporal profile of apomorphine-induced locomotion. (b) Analysis of total activity scores following apomorphine treatment reveals that knockout mice are more active than control animals. **$p < 0.01$ vs. wild-type mice.

To estimate changes in behaviors, locomotor activity induced by apomorphine was investigated in wild-type and homozygous mice. In a first step, animals were subjected to a 1-h session of novel conditions (Habituation stage) in the locomotor activity apparatus, followed by another 1-h period of locomotor activity after a saline injection (saline stage). Lastly, the sensitivity to apomorphine was tested for an additional 1-h period (apomorphine stage).

3.1.1. Habituation stage

Two-way ANOVA of activity revealed a significant effect of genotype [$F(1,12) = 10.75$, $p < 0.01$], time [$F(5,60) = 4.52$, $p < 0.01$] and genotype × time interaction [$F(5,60) = 3.70$, $p < 0.01$]. Post-hoc test revealed that under habituation at 10, 20 and 40 min on locomotor activity was higher in homozygous mice than wild-type mice ($p < 0.01$; Fig. 2). Total activity also was higher in homozygous mice than wild-type mice ($p < 0.01$; Fig. 2 bottom panel).

3.1.2. Saline stage

No significant effect of saline injection on the activity and total activity was observed in these groups of mice. ANOVA revealed no significant main effect of genotype [$F(1,12) = 0.52$, $p > 0.05$], time [$F(5,60) = 0.91$, $p > 0.05$] and genotype × time interaction [$F(5,60) = 0.47$, $p > 0.05$].

3.1.3. Apomorphine stage

ANOVA revealed a significant effect of genotype [$F(1,12) = 13.42$, $p < 0.01$], time [$F(5,60) = 19.46$, $p < 0.01$] and genotype × time interaction [$F(5,60) = 5.91$, $p < 0.01$]. Post-hoc test revealed that locomotor activity after apomorphine administration was significantly higher in homozygous mice compared with wild-type mice ($p < 0.01$; Fig. 2), reflecting a hypersensitivity to the locomotor stimulant effect of this DA agonist. Total activity after apomorphine administration also was higher in homozygous mice than wild-type mice ($p < 0.01$; Fig. 2 bottom panel).

3.2. Passive avoidance

On days 1 and 3, a passive avoidance paradigm was used to assess the long-term memory of these mice over time (Fig. 3). On

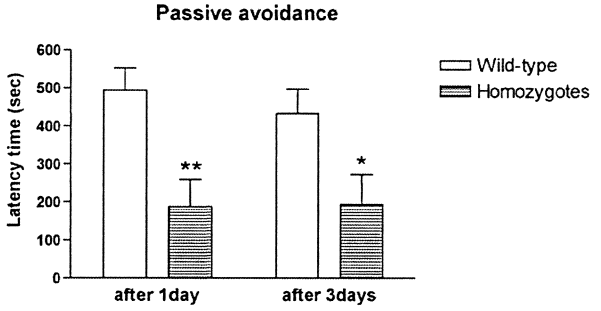


Fig. 3. Passive avoidance test in the homozygous mice. Data are expressed as the means ± SEM for $n = 6$–8 mice/group.

day 0 (training trial day), wild-type and homozygous mice showed similar latency times to enter the dark compartment (data not shown). Test latency time, a measure of retention, was assessed on days 1 and 3 after training. A two-way repeated ANOVA revealed a significant effect of genotype [$F(1,12) = 22.50$, $p < 0.01$], but no significant of genotype × day interaction [$F(1,12) = 3.12$, $p > 0.05$]. The latency time to cross to the dark compartment was lower in homozygous mice than wild-type mice (day 1, $p < 0.05$; day3, $p < 0.01$).

3.3. Y-maze

The Y-maze task was used to assess the short-term memory using both wild-type and homozygous mice (Fig. 4). There were no significant differences in total arm entries [$F(1,12) = 2.02$, $p > 0.05$] and spontaneous alternation behavior [$F(1,12) = 1.98$, $p > 0.05$] between homozygous mice and wild-type mice.

3.4. Acoustic startle and PPI

Fig. 5 shows the mean startle amplitudes of wild-type and homozygous mice. There was no significant difference in startle amplitude between mice with either genotype ($p > 0.05$). Homozygous mice exhibited reductions in sensorimotor gating as measured by the PPI paradigm. A two-way ANOVA revealed a significant effect of genotype [$F(1,12) = 11.50$, $p < 0.01$], an effect of prepulse intensity [$F(4,48) = 3.12$, $p < 0.05$] and a genotype × prepulse intensity interaction [$F(4,48) = 3.02$, $p < 0.05$]. A post-hoc test revealed that homozygous mice displayed significant deficits at three prepulse intensities (79 dB, $p < 0.01$; 82 dB, $p < 0.01$, 85 dB, $p < 0.01$).

3.5. Measurements of the levels of monoamines and their metabolites

The brain amounts of monoamines and their metabolites in wild-type and homozygous mice were measured using HPLC (Tables 1 and 2). The DA content in homozygous mice was significantly decreased in the striatum and frontal cortex compared with that in wild-type mice (Table 1). The turnover rate of DA, defined as the ratio of DOPAC or HVA to DA was significantly increased in the frontal cortices of homozygous mice. There was no difference in the NE content between wild-type and homozygous mice (Table 1). The concentration of 5-HT in homozygous mice was significantly decreased in the striatum and frontal cortex compared with that in wild-type mice (Table 2). The turnover rate of 5-HT, defined as the ratio of 5-HIAA to 5-HT, was significantly increased in the frontal cortices of homozygous mice.

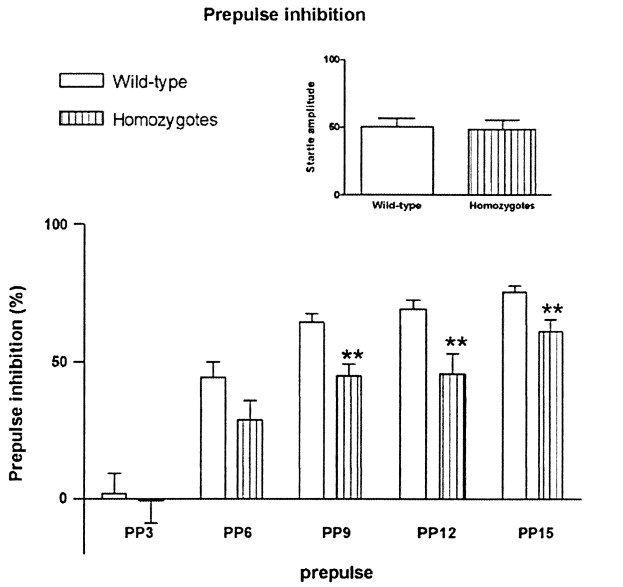


Fig. 5. Mean startle amplitudes (upper) and percent PPI (lower) in the homozygous mice. Data are expressed as the means ± SEM for $n = 6$–8 mice/group. $^{**}p < 0.01$ vs. wild-type mice.

4. Discussion

The present studies represent the first extensive behavioral and neurochemical characterization of mice lacking the α_{1B} subunit of N-type calcium channels. Significant differences between wild-type and knockout mice were found in several behavioral models (increased locomotor activity under the habituated condition during the dark phase, memory impairment, PPI deficit and enhanced locomotor response to apomorphine) and in brain neurochemistry (decreased DA and 5-HT levels in the frontal cortex and striatum).

The activity wheel was used to examine locomotion under habituated conditions. It has been demonstrated that $Ca_V2.2^{-/-}$ mice are more spontaneously active than wild-type mice during the dark phase [2]. Consistent with this finding, increased locomotor activity in the homozygous mice under the habituated condition was

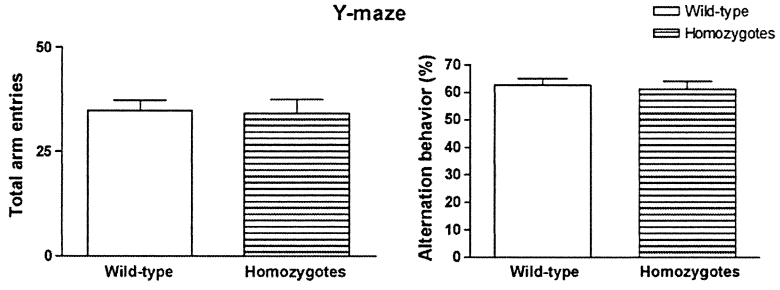


Fig. 4. Y-maze test in the homozygous mice. Data are expressed as the means ± SEM for $n = 6$–8 mice/group.

Table 1
Concentrations of monoamines and their metabolites in wild-type and homozygous mice.

	NE	DA	DOPAC	DOPAC/DA	HVA	HVA/DA
Striatum						
Wild-type	405 ± 11	3398 ± 93	2269 ± 261	0.657 ± 0.078	980 ± 86	0.289 ± 0.027
Homozygotes	368 ± 19	2840 ± 148*	2570 ± 167	0.922 ± 0.111	1020 ± 57	0.365 ± 0.039
Frontal cortex						
Wild-type	332 ± 15	360 ± 20	456 ± 51	1.269 ± 0.127	384 ± 16	1.075 ± 0.057
Homozygotes	296 ± 10	229 ± 61*	529 ± 143	2.309 ± 0.352**	343 ± 48	1.627 ± 0.238*

Data shown are in ng/g of brain tissue for 4–5 mice/group. *$p < 0.05$ and **$p < 0.01$ vs. wild-type mice.

also observed in the present study (Fig. 1). Beuckmann et al. [2] have reported that homozygous mice show a distorted circadian rhythm of locomotor activity under the habituated environment during the dark phase, based on increased electronencephalographic (EEG) spectral power during wakefulness, and decreased EEG spectral power and frequency during non-REM sleep. These findings suggest the possibility that the α_{1B} subunit of N-type calcium channels may participate in the development of systems underlying regulation of intrinsic biological rhythms in the brain.

To our knowledge, $Ca_V2.2^{-/-}$ mice have not been previously tested for passive avoidance or spontaneous alternation in Y-maze tests. Spontaneous alternation tests have been used as relatively rapid procedures to assess spatial working memory in rodents [14,29,43]. These tests are based on the natural tendency of rodents to alternate in their choices of arms visited when they are placed in a multi-arm maze. Importantly, spontaneous alternation behavior is dependent on intact hippocampal function, supported by the cognitive deficits observed in hippocampal-lesioned rodents [12], making it a relevant task for studying the role of the α_{1B} subunit of N-type calcium channels. In the current study, $Ca_V2.2^{-/-}$ mice exhibited no significant deficits in spontaneous alternation behavior in the Y-maze. Although the $Ca_V2.2^{-/-}$ mice showed similar numbers of arm entries in the Y-maze test to wild-type mice while displaying increased locomotor activity [2], it is noteworthy that these findings should not be compared directly. In the Y-maze spontaneous alternation test, mice are tested over a short period (8 min) unlike the locomotor test (which was over 12 min). Furthermore, the narrow Y-maze is a different environment to the large locomotor activity cage, which resembles the mouse cage. Consequently, the spontaneous locomotor activity measured in terms of arm entries in the Y-maze may not reflect the activity measured in Beuckmann et al.'s locomotor activity test [2]. Because the results suggested unaltered spatial working memory (short-term memory), we further investigated the role of the α_{1B} subunit of N-type calcium channels in an additional memory paradigm by testing these mice in a passive avoidance test. This test is considered to be a measure of long-term memory of an aversive experience. The $Ca_V2.2^{-/-}$ mice showed significant deficits in their latency time compared with wild-type mice. Because we observed no obvious difference in time to escape back to the illuminated compartment following the 0.5-s shock duration between wild-type and homozygous mice in the training trial (data not shown), it is unlikely that the difference in latency time is due to an alteration of nociception [53], although the possibility of subtle changes cannot be ruled out by our data. Passive avoidance is also a fear-associated learning test. It is reported that the startle response tends to be stronger with increased anxiety [40]. Our results indicated that the startle response at 120 dB was not different between wild-type and $Ca_V2.2^{-/-}$ mice. However, the results of the passive avoidance test in this study indicate the need to review the cognitive function in $Ca_V2.2^{-/-}$ mice by another method which is unaffected by locomotor activity and foot shock, such as the delayed non match to sample. In support of an involvement of the α_{1B} subunit of N-type calcium channels in avoidance learning, the impairment of long-term potentiation, which is though to be a molecular event underlying learning and memory, has been observed in $Ca_V2.2^{-/-}$ mice [34]. The administration of the $Ca_V2.2$ blocker ω-conotoxin GVIA caused memory impairment in a passive avoidance task in chick [8]. We therefore propose that a lack of the α_{1B} subunit of N-type calcium channels may impair long-term memory, but not short-term memory, because they play a role in the development of required neuronal circuits and/or they regulate associated synaptic plasticity in mouse brain.

Table 2
Concentrations of 5-hydroxytryptamine and its metabolite in the brain.

	5-HT	5-HIAA	5-HIAA/5-HT
Striatum			
Wild-type	2581 ± 46	591 ± 58	0.229 ± 0.019
Homozygotes	2246 ± 82**	490 ± 13	0.218 ± 0.003
Frontal cortex			
Wild-type	749 ± 25	487 ± 29	0.653 ± 0.046
Homozygotes	581 ± 83*	413 ± 9	0.739 ± 0.105**

Data shown are in ng/g of brain tissue for 4–5 mice/group. *$p < 0.05$ and **$p < 0.01$ vs. wild-type mice.

Abnormalities in information processing and attention mechanisms have long been associated with schizophrenia. A well-established method for evaluating sensorimotor gating is PPI, which is a reduction of the startle reflex after exposure to a weak-intensity prepulse administered immediately before the startle stimulus. The disruption of PPI in schizophrenic patients has been reported [24]. In the present studies, we observed PPI deficits in $Ca_V2.2^{-/-}$ mice. In rodents, the disruption of PPI occurs after acute administration of DA agonists [57,58], NMDA antagonists [38], or 5-HT agonists [37,52,56]. Manipulations that decrease DA transmission in the prefrontal cortex disrupt PPI [5,16,41]. Whereas DA level in frontal cortex was significantly decreased, DA turnover was significantly increased in $Ca_V2.2^{-/-}$ mice. The decreased DA content in the frontal cortex may be due to the lack of the α_{1B} subunit of N-type calcium channels, because this channel acts in numerous developmental processes, such as neuronal survival [18,30], gene expression [1,9,54], and synaptic proliferation [3,47] and refinement [36,70]. The apparently increased DA turnover (DOPAC/DA and HVA/DA) in the frontal cortex could be accompanied by decreased DA levels in $Ca_V2.2^{-/-}$ mice. Thus, dopaminergic hypofunction found within the frontal cortical circuitry of $Ca_V2.2^{-/-}$ mice may underlie the observed PPI deficit in the present study.

The serotonergic system is also reported to be involved in the modulation of PPI. In the present study, we observed decreased 5-HT levels in the striata of $Ca_V2.2^{-/-}$ mice. This result is consistent with the results of a previous study, which reported that microinjections of the 5-HT neurotoxin 5,7-dihydroxytryptamine into the dorsal and median raphe nuclei and i.p. injection of the 5-HT synthesis inhibitor para-chlorophenylalanine, depleted striatum 5-HT levels and disrupted PPI [21]. Thus, the decreased striatal 5-HT level also may result in PPI deficits. Table 1 also shows no alterations in the NE content between wild-type and $Ca_V2.2^{-/-}$ mice, indicating

that N-type calcium channels may not contribute as much to the release of NE than to DA and 5-HT release. However, N-type calcium channels also have been shown to be critically involved in the release of other neurotransmitters, including glutamate [44], GABA [28] and acetylcholine [66]. Further studies are needed to investigate these possibilities in our mouse model.

Manipulation of 5-HT activity modulates the expression of DA-mediated neurotransmission and behavior. The interactions between these two systems are complex but, at least under certain circumstances, 5-HT depletion may potentiate DA-mediated behavior [20]. In this context 5-HT depletion enhances the stimulant effect of apomorphine in an open-field [13]. $Ca_V2.2^{-/-}$ mice showed an enhanced locomotor response to apomorphine. High doses of apomorphine produce spontaneous stereotyped behavior in the mouse consisting of repetitive movements of the head, mouth and forelimbs [10,35], or cage-climbing behavior [45,68]. The dose of apomorphine used in the present study was not high enough to cause locomotor activity and stereotyped behavior (data not shown) as no obvious differences were noted between apomorphine and vehicle treated wild-type mice. This altered response to a DA agonist could be accompanied by region-specific alterations in dopaminergic and serotonergic activity, predominantly within the striata of $Ca_V2.2^{-/-}$ mice.

In summary, we have used a genetic approach to begin to investigate the role of the α_{1B} subunit of N-type calcium channels in CNS function. The aim of the present studies was to begin to characterize $Ca_V2.2$ wild-type and knockout mice using a broad spectrum of well-established behavioral tests to gain insight into how disruption of $Ca_V2.2$ affects behavior. Future experiments with $Ca_V2.2^{-/-}$ mice, using modifications of the models, additional animal models, or drug challenges, may reveal additional abnormal phenotypes.

Acknowledgements

This study was supported in part by NISHINOMIYA Basic Research Fund, Grants-in-Aid for Scientific Research (20790309) and for High Technology Research Program from the Ministry of Education, Culture, Sports, Science and Technology of Japan.

References

[1] Alcantara S, Soriano E, Ferrer I. Thalamic and basal forebrain afferents modulate the development of parvalbumin and calbindin D28K immunoreactivity in the barrel cortex of the rat. Eur J Neurosci 1996;8:1522–34.
[2] Beuckmann CT, Sinton CM, Miyamoto N, Ino M, Yanagisawa M. N-type calcium channel α_{1B} subunit ($Ca_V2.2$) knock-out mice display hyperactivity and vigilance state differences. J Neurosci 2003;23:6793–7.
[3] Bouwman J, Maia AS, Camoletto PG, Posthuma G, Roubos EW, Oorschot VM, et al. Quantification of synapse formation and maintenance in vivo in the absence of synaptic release. Neuroscience 2004;126:115–26.
[4] Brake WG, Flores G, Francis D, Meaney MJ, Srivastava LK, Gratton A. Enhanced nucleus accumbens dopamine and plasma corticosterone stress response in adult rats with neonatal excitotoxic lesion of the medial prefrontal cortex. Neuroscience 2000;96:687–95.
[5] Bubser M, Koch M. Prepulse inhibition of the acoustic startle response of rats is reduced by 6-hydroxydopamine lesions of the medial prefrontal cortex. Psychopharmacology 1994;113:487–92.
[6] Cardozo DL, Bean BP. Voltage-dependent calcium channels in rat midbrain dopamine neurons: modulation by dopamine and GABAB receptors. J Neurophysiol 1995;74:1137–48.
[7] Chen Y, Lai M, Maeno-Hikichi Y, Zhang JF. Essential role of the LIM domain in the formation of the PKCepsilon-RNH-N-type Ca^{2+} channel complex. Cell Signal 2006;18:215–24.
[8] Clements MP, Rose SP, Tiunova A. ω-Conotoxin GVIA disrupts memory formation in the day-old chick. Neurobiol Learn Mem 1995;64:276–84.
[9] Colonnese MT, Shi J, Constantine-Paton M. Chronic NMDA receptor blockade from birth delays the maturation of NMDA currents, but does not affect AMPA/kainite currents. J Neurophysiol 2003;89:57–68.
[10] Creese I, Iversen SD. The role of forebrain dopamine systems in amphetamine induced stereotyped behavior in the rat. Psychopharmacologia 1974;39:345–57.
[11] Dooley DJ, Lupp A, Hertting G, Osswald H. ω-Conotoxin GVIA and pharmacological modulation of hippocampal noradrenaline release. Eur J Pharmacol 1988;148:261–7.
[12] Doyle E, Bruce MT, Breen KC, Smith DC, Anderton B, Regan CM. Intraventricular infusions of antibodies to amyloid-beta-protein precursor impair the acquisition of a passive avoidance response in the rat. Neurosci Lett 1990;115:97–102.
[13] Drescher K, Fink H, Langnickel R. Neurochemical and behavioural effects after 5,7-DHT lesion of the median and dorsal raphe nucleus. Biogenic Amines 1985;2:227–33.
[14] Dudchenko PA. An overview of the tasks used to test working memory in rodents. Neurosci Biobehav Rev 2004;28:699–709.
[15] Dunlap K, Luebke JI, Turner TJ. Exocytotic Ca^{2+} channels in mammalian central neurons. Trends Neurosci 1995;18:89–98.
[16] Ellenbroek BA, Budde S, Cools AR. Prepulse inhibition and latent inhibition: the role of dopamine in the medial prefrontal cortex. Neuroscience 1996;75:535–42.
[17] Ertel EA, Campbell KP, Harpold MM, Hofmann F, Mori Y, Perez-Reyes E, et al. Nomenclature of voltage-gated calcium channels. Neuron 2000;25:533–5.
[18] Farber NB, Olney JW. Drugs of abuse that cause developing neurons to commit suicide. Brain Res Dev Brain Res 2003;147:37–45.
[19] Filloux F, Schapper A, Naisbitt SR, Olivera BM, McIntosh JM. Complex patterns of [^{125}I] omega-conotoxin GVIA binding site expression during postnatal rat brain development. Brain Res Dev Brain Res 1994;78:131–6.
[20] Fletcher PJ, Korth KM, Chambers JW. Selective destruction of brain serotonin neurons by 5,7-dihydroxytryptamine increases responding for a conditioned reward. Psychopharmacolgy 1999;147:291–9.
[21] Fletcher PJ, Selhi ZF, Azampanah A, Sills TL. Reduced brain serotonin activity disrupts prepulse inhibition of the acoustic startle reflex: effects of 5,7-dihydroxytryptamine and p-chlorophenylalanine. Neuropsychopharmacology 2001;24:399–409.
[22] Foehring RC. Serotonin modulates N- and P-type calcium currents in neocortical pyramidal neurons via a membrane-delimited pathway. J Neurophysiol 1996;75:648–59.
[23] Fujita R, Takayama N, Ueda H. The cognition-enhancer nefiracetam is protective in BDNF-independent neuronal cell death under the serum-free condition. Neurochem Int 2002;40:139–43.
[24] Geyer MA, Krebs-Thomson K, Braff DL, Swerdlow NR. Pharmacological studies of prepulse inhibition models of sensorimotor gating deficits in schizophrenia: a decade in review. Psychopharmacology 2001;156:117–54.
[25] Hatakeyama S, Wakamori M, Ino M, Miyamoto N, Takahashi E, Yoshinaga T, et al. Differential nociceptive responses in mice lacking the α_{1B} subunit of N-type Ca^{2+} channels. NeuroReport 2001;12:2423–7.
[26] Herdon H, Nahorski SR. Investigations of the roles of dihydropyridine and ω-conotoxin-sensitive calcium channels in mediating depolarization-evoked endogenous dopamine release from striatal slices. Naunyn Schmiedebergs Arch Pharmacol 1989;340:36–40.
[27] Holm NR, Christophersen P, Hounsgaard J, Gammeltoft S, Olesen SP. CNTF inhibits high voltage activated Ca^{2+} currents in fetal mouse cortical neurons. J Neurochem 2002;82:495–503.
[28] Horne AL, Kemp JA. The effect of ω-conotoxin GVIA on synaptic transmission within the nucleus accumbens and hippocampus of the rat in vitro. Br J Pharmacol 1991;103:1733–9.
[29] Hughes RN. The value of spontaneous alternation behavior (SAB) as a test of retention in pharmacological investigations of memory. Neurosci Biobehav Rev 2004;28:497–505.
[30] Ikonomidou C, Bosch F, Miksa M, Bittigau P, Vockler J, Dikranian K, et al. Blockade of NMDA receptors and apoptotic neurodegeneration in the developing brain. Science 1999;283:70–4.
[31] Ino M, Yoshinaga T, Wakamori M, Miyamoto N, Takahashi E, Sonoda J, et al. Functional disorders of the sympathetic nervous system in mice lacking the α_{1B} subunit ($Ca_V2.2$) of N-type calcium channels. Proc Natl Acad Sci U S A 2001;98:5323–8.
[32] Iwamoto K, Bundo M, Washizuka S, Kakiuchi C, Kato T. Expression of HSPF1 and LIM in the lymphoblastoid cells derived from patients with bipolar disorder and schizophrenia. J Hum Genet 2004;49:227–31.
[33] Iwamoto K, Kakiuchi C, Bundo M, Ikeda K, Kato T. Molecular characterization of bipolar disorder by comparing gene expression profiles of postmortem brains of major mental disorders. Mol Psychiatry 2004;9:406–16.
[34] Jeon D, Kim C, Yang YM, Rhim H, Yim E, Oh U, et al. Impaired long-term memory and long-term potentiation in N-type Ca^{2+} channel-deficient mice. Genes Brain Behav 2007;6:375–88.
[35] Joyce EM, Iversen SD. Dissociable effects of 6-OHDA-induced lesions of neostriatum on anorexia, locomotor activity and stereotypy: the role of behavioural competition. Psychopharmacology 1984;83:363–6.
[36] Katz LC, Shatz CJ. Synaptic activity and the construction of cortical circuits. Science 1996;257:806–9.
[37] Kehne JH, Padich RA, McCloskey TC, Taylor VL, Schmidt CJ. 5-HT modulation of auditory and visual sensorimotor gating: I. Effects of 5-HT releasers on sound and light prepulse inhibition in Wistar rats. Psychopharmacology 1996;124:95–106.
[38] Keith VA, Mansbach RS, Geyer MA. Failure of haloperidol to block the effects of phencyclidine and dizocilpine on prepulse inhibition of startle. Biol Psychiatry 1991;30:557–66.
[39] Kim C, Jun K, Lee T, Kim SS, McEnery MW, Chin H, et al. Altered nociceptive response in mice deficient in the α_{1B} subunit of the voltage-dependent calcium channel. Mol Cell Neurosci 2001;18:235–45.
[40] Koch M. The neurobiology of startle. Prog Neurobiol 1999;59:107–28.

[41] Koch M, Bubser M. Deficient sensorimotor gating after 6-hydroxydopamine lesion of the rat medial prefrontal cortex is reversed by haloperidol. Eur J Neurosci 1994;6:1837–45.
[42] Komuro H, Rakic P. Selective role of N-type calcium channels in neuronal migration. Science 1992;257:806–9.
[43] Lalonde R. The neurobiological basis of spontaneous alteration. Neurosci Biobehav Rev 2002;26:91–104.
[44] Luebke JI, Dunlap K, Turner TJ. Multiple calcium channel types control glutamatergic synaptic transmission in the hippocampus. Neuron 1993;11:895–902.
[45] Marcais H, Protais P, Costentin J, Schwartz JC. A gradual score to evaluate the climbing behaviour elicited by apomorphine in mice. Psychopharmacology 1978;56:233–4.
[46] Marshall J, Dolan BM, Garcia EP, Sathe S, Tang X, Mao Z, et al. Calcium channel and NMDA receptor activities differentially regulate nuclear C/EBPbeta levels to control neuronal survival. Neuron 2003;39:625–39.
[47] Marty S, Wehrle R, Sotelo C. Neuronal activity and brain-derived neurotrophic factor regulate the density of inhibitory synapses in organotypic slice cultures of postnatal hippocampus. J Neurosci 2000;20:8087–95.
[48] McIlwain KL, Merriweather MY, Yuva-Paylor LA, Paylor R. The use of behavioral test batteries: effects of training history. Physiol Behav 2001;73:705–17.
[49] Mirnicks K, Middleton FA, Marquez A, Lewis DA, Levitt P. Molecular characterization of schizophrenia viewed by microarray analysis of gene expression in prefrontal cortex. Neuron 2000;28:53–67.
[50] Numakawa T, Yagasaki Y, Ishimoto T, Okada T, Suzuki T, Iwata N, et al. Evidence of novel neuronal functions of dysbindin, a susceptibility gene for schizophrenia. Hum Mol Genet 2004;13:2699–708.
[51] Olivera BM, Gray WR, Zeikus R, McIntosh JM, Varga J, River J, et al. Peptide neurotoxins from fish-hunting cone snails. Science 1985;230:1338–43.
[52] Padich RA, McCloskey TC, Kehne JH. 5-HT modulation of auditory and visual sensorimotor gating: II. Effects of the 5-HT2A antagonist MDL 100,907 on disruption of sound and light prepulse inhibition produced by 5-HT agonists in Wistar rats. Psychopharmacology 1996;124:107–16.
[53] Saegusa H, Kurihara T, Zong S, Kazuno A, Matsuda Y, Nonaka T, et al. Suppression of inflammatory and neuropathic pain symptoms in mice lacking the N-type Ca^{2+} channel. EMBO J 2001;20:2349–56.
[54] Scheetz AJ, Constantine-Paton M. Modulation of NMDA receptor function: implications for vertebrate neural development. FASEB J 1994;8:745–52.
[55] Scholz KP, Miller RJ. Developmental changes in presynaptic calcium channels coupled to glutamate release in cultured rat hippocampal neurons. J Neurosci 1995;15:4612–7.
[56] Sipes TA, Geyer MA. Multiple serotonin receptor subtypes modulate prepulse inhibition of the startle response in rats. Neuropharmacology 1994;33:441–8.
[57] Swerdlow NR, Braff DL, Geyer MA, Koob GF. Central dopamine hyperactivity in rats mimics abnormal acoustic startle response in schizophrenics. Biol Psychiatry 1986;21:23–33.
[58] Swerdlow NR, Shoemaker JM, Kuczenski R, Bongiovanni MJ, Neary AC, Tochen LS, et al. Forebrain D1 function and sensorimotor gating in rats: effects of D1 blockade, frontal lesions and dopamine denervation. Neurosci Lett 2006;402:40–5.
[59] Takahashi E, Nagasu T. Pattern of compensatory expression of voltage-dependent Ca^{2+} channel α_1 and β subunits in brain of N-type Ca^{2+} channel α_{1B} subunit gene-deficient mice with a CBA/JN genetic background. Exp Anim 2005;54:29–36.
[60] Talbot K, Eidem WL, Tinsley CL, Benson MA, Thompson EW, Smith RJ, et al. Dysbindin-1 is reduced in intrinsic, glutamatergic terminals of the hippocampal formation in schizophrenia. J Clin Invest 2004;113:1353–63.
[61] Tanaka O, Sakagami H, Kondo H. Localization of mRNAs of voltage-dependent Ca(2+)-channels: four subtypes of alpha 1- and beta-subunits in developing and mature rat brain. Brain Res Mol Brain Res 1995;30:1–16.
[62] Tseng KY, Chambers RA, Lipska BK. The neonatal ventral hippocampal lesion as a heuristic neurodevelopmental model of schizophrenia. Behav Brain Res 2009;204:295–305.
[63] Turner TJ, Adams ME, Dunlap K. Multiple Ca^{2+} channel types coexist to regulate synaptosomal neurotransmitter release. Proc Natl Acad Sci U S A 1993;90:9518–22.
[64] Verderio C, Coco S, Fumagalli G, Matteoli M. Calcium-dependent glutamate release during neuronal development and synaptogenesis: different involvement of omega-agatoxin IVA- and omega-conotoxin GVIA-sensitive channels. Proc Natl Acad Sci U S A 1995;92:6449–53.
[65] Vogt MA, Chourbaji S, Brandwein C, Dormann C, Sprengel R, Gass P. Suitability of tamoxifen-induced mutagenesis for behavioral phenotyping. Exp Neurol 2008;211:25–33.
[66] Wessler I, Dooley DJ, Werhand J, Schlemmer F. Differential effects of calcium channel antagonists (ω-conotoxin GVIA, nifedipine, verapamil) on the electrically-evoked release of [^{3}H]acetylcholine from the myenteric plexus, phrenic nerve and neocortex of rats. Naunyn Schmiedebergs Arch Pharmacol 1990;341:288–94.
[67] Whyte KA, Greenfield SA. Expression of voltage-dependent calcium channels in the embryonic rat midbrain. Brain Res Dev Brain Res 2002;139:189–97.
[68] Wilcox RE, Smith RV, Anderson JA, Riffee WH. Apomorphine-induced stereotypic cage climbing in mice as a model for studying changes in dopamine receptor sensitivity. Pharmacol Biochem Behav 1980;12:29–33.
[69] Woodward JJ, Rezazadeh SM, Leslie SW. Differential sensitivity of synaptosomal calcium entry and endogenous dopamine release to ω-conotoxin. Brain Res 1988;475:141–5.
[70] Yu CR, Power J, Barnea G, O'Donnell S, Brown HE, Osborne J, et al. Spontaneous neural activity is required for the establishment and maintenance of the olfactory sensory map. Neuron 2004;42:553–66.

The Journal of Toxicological Sciences (J. Toxicol. Sci.)
Vol.35, No.2, 137-147, 2010

Original Article

Malondialdehyde-modified low density lipoprotein (MDA-LDL)-induced cell growth was suppressed by polycyclic aromatic hydrocarbons (PAHs)

Hiroyuki Suzuki, Takamitsu Sasaki, Takeshi Kumagai, Shuhei Sakaguchi and Kiyoshi Nagata

Tohoku Pharmaceutical University, 4-4-1 Komatsushima, Aobaku, Sendai, Miyagi 981-8558, Japan

(Received November 9, 2009; Accepted November 19, 2009)

ABSTRACT — Malondialdehyde-modified low-density lipoprotein (MDA-LDL) and oxidized LDL (Ox-LDL), which accelerate the pathogenesis of arteriosclerosis, are thought to be involved in parthenogenesis caused by smooth muscle cell proliferation. In this study, we investigated the suppression mechanism of polycyclic aromatic hydrocarbons (PAHs) on the growth of an MDA-LDL-induced human acute monocyte leukemia suspension cell line (THP-1 cells). We found that PAHs suppressed MDA-LDL-induced THP-1 cell growth. Cotreatment with benzo[*a*]pyrene (BaP) or 3-methylchoranthrene (3-MC) decreased MDA-LDL-induced THP-1 cell growth, whereas treatment with benzo[*e*]pyrene (BeP) or pyrene, which is not a ligand for the arylhydrocarbon receptor (AhR), did not decrease THP-1 cell growth. Our findings clearly demonstrated that THP-1 cell growth, which was suppressed by PAHs, was restored by the addition of α-naphtoflavone, which is a partial antagonist to AhR. Moreover, it was shown that cotreatment with MDA-LDL and BaP markedly induced the expression of human cytochrome P4501A1 (hCYP1A1) messenger ribonucleic acid (mRNA) and significantly induced the expressions of p53 and p21 mRNAs. In support of these findings, AhR small interfering RNA suppressed the induced level of p21 mRNA and by BaP and the overexpression of hCYP1A1 significantly induced levels of p21 mRNA. On the other hand, the uptake rate of [^{14}C]BaP into cells was increased more significantly by cotreatment with MDA-LDL than by treatment with [^{14}C]BaP alone. These results strongly suggest that the suppression of MDA-LDL-induced THP-1 cell growth is caused by the increased uptake of PAHs, which strongly activate the AhR signal pathway accompanying DNA damage.

Key words: AhR, hCYP1A1, MDA-LDL, PAHs, p21

INTRODUCTION

Polycyclic aromatic hydrocarbons (PAHs) are common environmental pollutants; exposure to PAHs has been suspected to be associated with the occurrence of pulmonary diseases. Benzo[*a*]pyrene (BaP) is a well-studied PAHs found in many environmental complex mixtures, including cigarette smoke and air pollution. BaP is highly mutagenic and must be metabolically activated to exert its carcinogenic potential (Miller and Ramos, 2001). In addition, BaP induces metabolic enzymes such as human cytochrome p4501A1/2 (hCYP1A1/2) and hCYP1B1 via arylhydrocarbon receptor (AhR) (Harrigan *et al.*, 2006; Jonsson *et al.*, 2006; Willett *et al.*, 2006). Thus, these hCYPs are involved in BaP-induced carcinogenesis (Galván *et al.*, 2005; Kim *et al.*, 1998; Harrigan *et al.*, 2004).

The pathogenesis of arteriosclerosis, now generally considered to be an inflammatory disease, is well characterized, but the initiating event is unknown (Ross, 1999). Individuals who smoke are at increased risk for developing arteriosclerosis and associated clinical events (Chouraki *et al.*, 2008; Antoniades *et al.*, 2008; Iribarren *et al.*, 1999; LaCroix *et al.*, 1991). These findings, combined with data from clinical studies, indicate that the pathogenesis of arteriosclerosis is accelerated through a number of different mechanisms, which collectively contribute to increased risk of developing the disease. The subendothelial accumulation of foam cells, which are primarily derived from monocytes and macrophages through

Correspondence: Hiroyuki Suzuki (E-mail: aube@msd.biglobe.ne.jp)

the uptake of oxidized LDL (Ox-LDL), plays a key role in the initiation of arteriosclerosis (Steinberg and Witztum, 1990). It is well known that the LDL receptor, which is down-regulated when intracellular cholesterol levels are increased, is not involved in the intracellular accumulation of cholesterol in foam cells. However, macrophages avidly accumulate Ox-LDL via scavenger receptors that are unresponsive to intracellular cholesterol levels (Goldstein and Brown, 1977; Ylä-Herttuala *et al.*, 1991). Furthermore, Ox-LDL induces proliferation of monocytes and macrophages, smooth muscle cells, and other cells (Heery *et al.*, 1995; Zhao *et al.*, 2005; Matsumura *et al.*, 1997; Martens *et al.*, 1998; Hamilton *et al.*, 1999).

Generally, the pathogenesis of arteriosclerosis is accelerated through MDA-LDL and Ox-LDL. Interestingly, MDA-LDL was reportedly involved in atherogenesis by causing smooth muscle cell proliferation (Ozer *et al.*, 1993), which was generated by the uptake of MDA-LDL in macrophages via scavenger receptors; PAHs have also been reported to induce arteriosclerosis (Iwano *et al.*, 2005). However, the interaction between PAHs and MDA-LDL has not been clarified. Therefore, in this study, we investigated the suppression mechanism of MDA-LDL-induced THP-1 cell growth by PAHs to clarify the association between PAHs and MDA-LDL.

MATERIALS AND METHODS

Chemicals

BaP, β-naphthoflavone (β-NF), benzo[*e*]pyrene (BeP), pyrene, and α-naphthoflavone (α-NF) were purchased from Tokyo Chemical Industry Corporation (Tokyo, Japan). 3-Methylcholanthrene (3-MC) was purchased from Sigma-Aldrich (St. Louis, MO, USA). All other chemicals used were of analytical grade and purchased from commercial sources.

Cell culture

THP-1 (human acute monocytic leukemia) cells were obtained from Japan Human Health Sciences Foundation (Tokyo, Japan) and HepG2 (human hepatoma cell lines) cells were obtained from Riken Bioresource Center (Ibaraki, Japan). THP-1 cells were maintained in Roswell Park Memorial Institute (RPMI) 1640 medium from Invitrogen (Carlsbad, CA, USA) supplemented with 5% fetal bovine serum (FBS), 100 U/ml penicillin, and 100 μg/ml streptomycin. HepG2 cells were cultured in Dulbecco's modified Eagle medium (DMEM) from Wako (Osaka, Japan) containing 10% FBS, 100 U/ml penicillin, 100 μg/ml streptomycin, 0.25 μg/ml amphotericin B, and 0.1 mM nonessential amino acids. THP-1 cells were seeded onto 96-well plates (3×10^4 cells/well) and 24-well plates (1×10^6 cells/well) from Becton Dickinson (Heidelberg, Germany). THP-1 cells were incubated with 0.1 ml (96-well plate for cell proliferation) and 0.5 ml (24-well plate for cell proliferation and incorporation of [^{14}C] BaP) of the medium containing PAHs (BaP, 3-MC, BeP, and pyrene): β-NF, MDA-LDL, 0.1% DMSO, or cotreatment with PAHs and MDA-LDL. The HepG2 cells were seeded onto 24-well plates at 5×10^4 cells/well for 24 hr, and used for a virus infection experiment.

Recombinant adenovirus

Adenovirus-expressing human *CYP1A1* and *CYP1A2* (Ad-hCYP1A1 and Ad-hCYP1A2) were done with the AdEasy™ System (Quantam Biotechnologies, Montreal, Canada) according to a previous report (Aoyama *et al.*, 2009). AdCont (AxCALacZ), which expresses β-galactosidase, was provided by Dr. Izumi Saito (Tokyo University) and used as a control adenovirus. The titer of the recombinant adenovirus, 50% titer culture infection dose ($TCID_{50}$), and multiplicity of infection (MOI) were determined as reported previously (Kamiyama *et al.*, 2007).

Infection of recombinant adenovirus

The HepG2 cells were incubated with 0.1 ml of a medium containing a recombinant adenovirus for 1 hr followed by the addition of 0.9 ml of medium and further culturing for 96 hr. Seventy-two hr after the adenovirus infection, the HepG2 cells were treated with 0.01 μM and 0.1 μM BaP or 0.1% DMSO for 24 hr.

Modification of LDL by malondialdehyde

Malondialdehyde was generated at room temperature by rapid acid hydrolysis (0.2 ml of 12 M HCl) of tetramethoxypropane (Nacalai Tesque, Kyoto, Japan). Then, 4.6 ml of 0.1 M sodium phosphate buffer (pH 6) was added to this reaction medium and the solution was adjusted to pH 6 with 10 M NaOH. Synthesized MDA was subsequently added to freshly prepared LDL (Chemicon, Tokyo, Japan) (2 mg/ml) and incubated at a final concentration of 0.02 mM for 3 hr at 37°C. The reaction was stopped by dialysis against phosphate-buffered saline (PBS) (pH 7.6) for 24 hr at 4°C. The extent of modification was determined by a colorimetric thiobarbituric acid assay (Fogelman *et al.*, 1980; Patton and Kurtz, 1951).

Tritiated thymidine incorporation assay

Proliferation of THP-1 cells was determined by the incorporation of [^{3}H] thymidine into cellular DNA. Briefly, 10 μl of 10 μCi/ml methyl [^{3}H] thymidine (80 Ci/mmol, Amersham Bioscience) was added to each well of

a 24-well plate and incubated for the final 18 hr in each experiment. The medium was then aspirated, cells were washed with ice-cold 10% trichloroacetic acid to precipitate DNA and unincorporated labeled thymidine was removed. Cells were dissolved in 0.1 M NaOH to hydrolyze the acid-insoluble material. Radioactivity was measured using a liquid scintillation counter (Beckman Counter LS 6500 AT, Fullerton, CA, USA).

WST-8 growth assay

THP-1 proliferation was determined by WST-8 [2-(2-methoxy-4-nitrophenyl)-3-(4-nitrophenyl)-5-(2,4-dinitrophenyl)-2H-tetrazolium, monosodium salt] assays using a Cell Counting Kit-8 (Donjindo, Kumamoto, Japan). Briefly, 10 μl of WST-8/1-methoxy-phenazine methosulfate solution was added to each well of a 96-well plate and incubated for 2 hr at 37°C. The absorbance at 450 nm was then measured with a multiwell spectrophotometer (MPR-A4i; Toso, Tokyo, Japan).

[^{14}C]BaP incorporation assay

BaP incorporation into cellular DNA was determined by incorporation of [^{14}C]BaP. Briefly, 2 μl of [^{14}C]BaP (60 mCi/mmol, Amersham Bioscience) was added to each well of a 24-well plate. The medium was then aspirated, cells were washed with ice-cold 10% trichloroacetic acid to precipitate DNA and unincorporated labeled BaP was removed. Cells were dissolved in 0.1 M NaOH to hydrolyze the acid-insoluble material. Radioactivity was measured using a liquid scintillation counter.

Quantitative real-time polymerase chain reaction (PCR)

Total ribonucleic acid (RNA) was extracted from the cells using TRIzol according to the manufacturer's protocol. The cDNA was synthesized from 1 μg of total RNA using an oligo dT-adaptor and avian myeloblastosis virus ExScript reverse transcriptase (Takara, Shiga, Japan). Quantitative real-time PCR was performed using a Thermal Cycler Dice™ TP800 (Takara). The primer sequences used in this study were as follows: hCYP1A1: sense (5′-GGCCACTTTGACCCTTACAA-3′) and anti-sense (5′-CAGGTAACGGAGGACAGGAA-3′); hCYP1A2: sense (5′-GTTCCTGCAGAAAACAGTCCA-3′) and anti-sense (5′-CTGTGCTTGAACAGGGCAC -3′); AhR: sense (5′-GCACGAGAGGCTCAGGTTATCA-3′) and anti-sense (5′-GTGCATTAGACTGGACCCAAGTC-3′); p53: sense (5′-CTGTCCCTTCCCACAAAACC-3′) and anti-sense (5′-CCACTCGGATAAGATGCT-3′); p21: sense (5′-CGACTGTGATGCGCTAATGG-3′) and anti-sense (5′-CCAGTGGTGTCTCGGTGACA-3′); and glyceraldehyde-3-phosphate dehydrogenase (GAPDH): sense (5′-TCGGAGTCAACGGATTTGGTCGTA-3′) and anti-sense (5′-ATGGACTGTGGTCATGAGTCCTTC-3′). PCR was performed using a SYBR® Premix Ex Taq™ (Takara). The reaction was carried out under the following conditions: 50°C for 2 min, 95°C for 2 min, followed by 40 cycles at 95°C for 5 sec, and 60°C for 30 sec. To confirm the amplification specificity, the PCR products were subjected to a melting curve analysis. The mRNA expression levels of the hCYP1A1, hCYP1A2, AhR, p53, and p21 in each sample were normalized to that of GAPDH.

Small interfering RNA

Double-strand siRNAs (25-mer) that target the AhR and control siRNA that target estrogen receptor α (ERα) were designed and synthesized by Invitrogen. The corresponding target mRNA sequences for the siRNAs were as follows: AhR siRNA, UUAAGUCGGUCUCUAUGCCGCUUGG; ERα siRNA, UAGUCAUUGCACACUGCACAGUAGC. HepG2 cells were transfected with siRNA when cells reached 30-50% confluence (48-well plate), according to the manufacturer's protocol. Briefly, gene-specific siRNA oligomers (20 nM) and 0.4 μl/well lipofectamine RNAiMAX were diluted in 40 μl/well DMEM (Invitrogen). After 20-min incubation at room temperature, the complexes were added to the cells in a final volume of 240 μl medium. Forty-eight hr after the siRNA transfection, the HepG2 cells were treated with 0.01 μM and 0.1 μM BaP or 0.1% DMSO for 48 hr.

Preparation of S9 fraction

HepG2 cells were washed with ice-cold PBS (without $CaCl_2$ and $MgCl_2$) and then removed with a cell scraper. The cells were suspended in 0.25 M sucrose/1 mM EDTA/10 mM Tris HCl buffer (pH 7.4). The sonicated cells were then homogenized under ice-cold conditions. After centrifugation of the homogenated cells at 9,000 × *g* for 20 min at 4°C, the supernatant (S9) was collected. Protein content was determined by using a Protein Assay Kit (Bio-Rad, Tokyo, Japan) according to the manufacturer's protocol, with bovine serum albumin as the standard.

7-Ethoxyresorufin O-deethylase (EROD) assays

CYP1A activity was determined using an EROD assay according to the methods of Burke and Mayer (1974) with the following modifications. The reaction mixture contained 1 μM 7-ethoxyresorufin (Sigma), S9 fraction (200 μg of S9 protein), and 0.1 M potassium phosphate buffer (pH 7.4) in a final volume of 0.5 ml. After preincubation of the mixture at 37°C for 5 min, 0.5 mM NADPH

(Wako) was added to initiate the reaction, and the mixture was further incubated for 10 min. The reaction was terminated by the addition of 2 ml of ice-cold methanol, and the samples were then centrifuged at 9,000 × *g* for 10 min. The metabolite, resorufin, was measured using Powerscan®HT (Dainippon Sumitomo Pharma, Osaka, Japan) (excitation and emission wavelengths of 530 nm and 585 nm, respectively).

Statistical analysis

Data are expressed as the mean ± standard (S.D.) error from three determinations. Statistical comparison of two groups was performed using a two-tailed Student's *t*-test. *P*-values less than 0.05 were considered to be statistically significant.

RESULTS

Effects of PAHs on MDA-LDL-induced THP-1 cell growth

We examined the effects of MDA-LDL on THP-1 cells growth. THP-1 cell growth increased nearly 30% compared to the control by treatment with 0.4 mg/ml MDA-LDL. We further investigated whether PAHs had an effect on MDA-LDL-induced THP-1 cell growth. Cotreatment with BaP or 3-MC and MDA-LDL reduced MDA-LDL-induced THP-1 cell growth (Fig. 1-A). On the other hand, cotreatment with BeP or pyrene, which does not activate the AhR, and MDA-LDL did not reduce MDA-LDL-induced THP-1 cell growth (Fig. 1-B). Or, that the experiments with Ox-LDL yielded similar results to those observed in MDA-LDL; however, we examined the role of the MDA-LDL in this study because the results of MDA-LDL were clearer than the results of Ox-LDL.

Effects of α-NF or β-NF on suppression of MDA-LDL-induced THP-1 cell growth by BaP

Among the PAHs, BaP and 3-MC activate AhR-mediated signal transduction, but pyrene and BeP do not. To clarify whether AhR-mediated signal transduction is involved in the suppression of MDA-LDL-induced THP-1 cell growth by BaP, we examined the effect of α-NF, a partial antagonist to AhR, on [^{3}H] thymidine incorporation. Cotreatment with BaP and MDA-LDL reduced [^{3}H] thymidine incorporation. The suppression of [^{3}H] thymidine incorporation into THP-1 cells was clearly restored by the addition of 1 μM α-NF (Fig. 2-A). β-NF is a potent agonist to AhR, but not to PAHs, and does not cause cell damage. To clarify the involvement of AhR in suppression of MDA-LDL-induced THP-1 cell growth, we further examined whether β-NF, as well as BaP, suppresses MDA-LDL-induced THP-1 cell growth. Co-treatment with β-NF and MDA-LDL did not reduce the MDA-LDL-induced THP-1 cell growth (Fig. 2-B).

Effect of MDA-LDL and BaP on hCYP1A1 mRNA expression

To further clarify whether AhR-mediated signal transduction was activated by BaP, we examined the effect of cotreatment with MDA-LDL and BaP on the expression of hCYP1A1 mRNA. hCYP1A1 is a BaP-activating enzyme, and the expression was induced by activation of the AhR pathway. Cotreatment with MDA-LDL and BaP markedly induced the expression of hCYP1A1 mRNA (28-fold). In contrast, BaP treatment also induced the expression, but at a low level (9.8-fold) (Fig. 3).

The role of MDA-LDL in BaP activation in THP-1 cells

Together with the above results, cotreatment with BaP and MDA-LDL was predicted to cause strong BaP activation due to the acceleration of BaP incorporation into the cells. We next examined the incorporation of BaP into THP-1 cells. Incorporation of [^{14}C]BaP with MDA-LDL into THP-1 cells increased 5.6-fold compared to the results from treatment with [^{14}C]BaP alone (Fig. 4).

Analysis of the suppression mechanism of MDA-LDL-induced THP-1 cell growth by BaP

Together with these results, induced hCYP1A1 is predicted to transform BaP to an activated form causing DNA damage and, consequently, increased levels of tumor suppressor proteins such as p53 and p21, the proliferation inhibitor protein. Therefore, we next measured p53 and p21 mRNA levels by cotreatment with MDA-LDL and BaP. As expected, cotreatment with BaP and MDA-LDL significantly induced the expression of p53 (2.6-fold) and p21 (1.9-fold) mRNAs compared to that of the control. Treatment with BaP alone did not induce the expression of mRNAs (Fig. 5).

Effect of knockdown of AhR and overexpression of hCYP1A1 on the expression level of p21 mRNAs

To determine the influence of the AhR pathway or metabolic activation of BaP by hCYP1A1 on the expression level of p21 mRNA, we performed knockdown of the AhR using AhR siRNA and overexpression of hCYP1A1 using an hCYP1A1-expressing adenovirus (Ad-hCYP1A1). It was difficult to overexpress the recombinant protein in THP-1 cells through a cDNA expression vector. Therefore, in this study, we used HepG2 cells and a hCYP1A1-

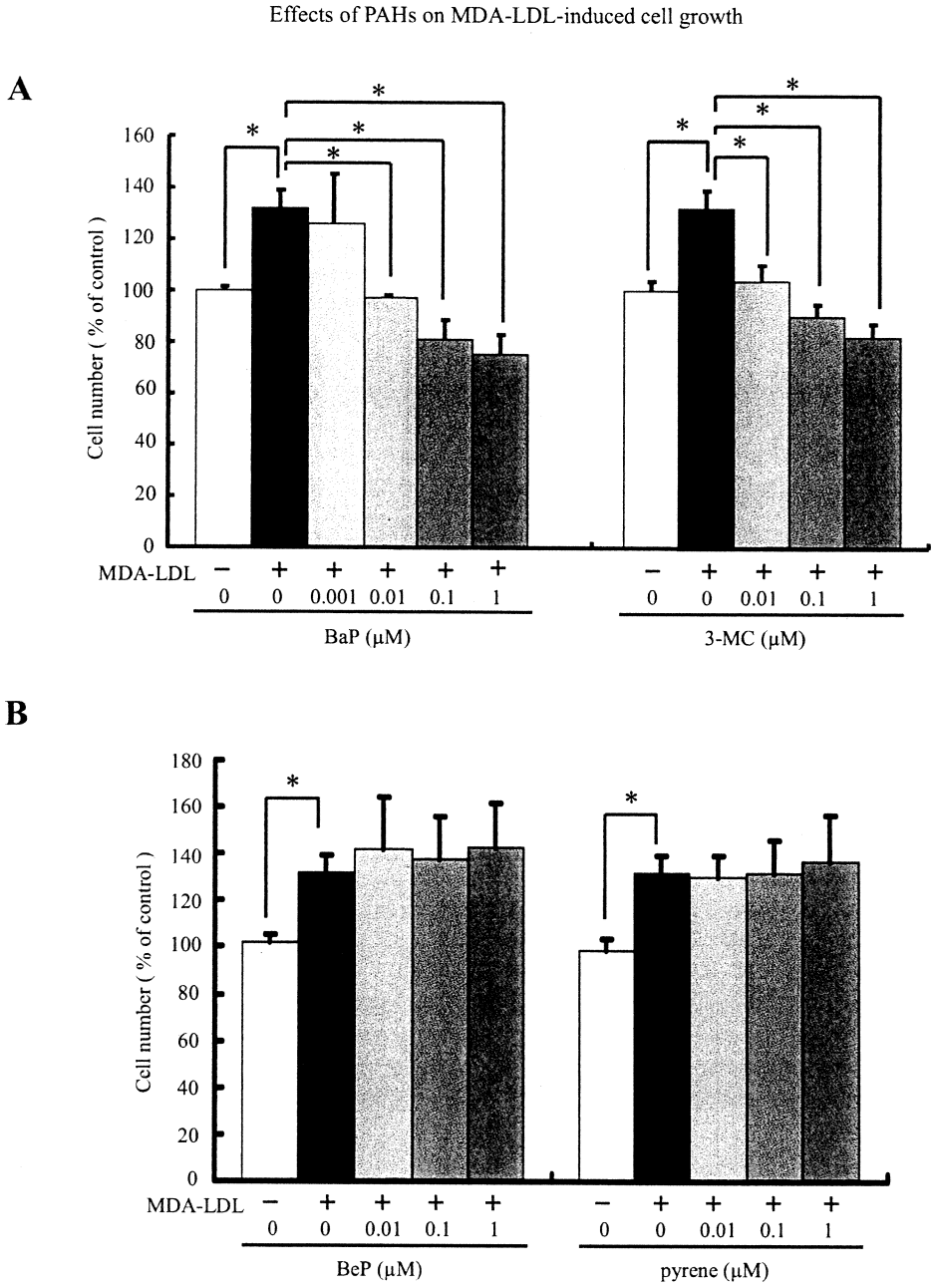


Fig. 1. Effects of BaP and 3-MC (A) and BeP and pyrene (B) on MDA-LDL-induced THP-1 cell growth. THP-1 cell proliferation was assessed by a WST-8 assay. Concentrations of MDA-LDL and PAHs were 0.4 mg/ml and 0.01-1 μM, respectively. Data show the mean ± S.D. of at three independent experiments. $^{*}p < 0.001$.

expressing adenovirus. As a result, the levels of AhR and CYP1A1 mRNA were downregulated by 73% and more than 50%, respectively, compared with the control (Fig. 6-A). The level of p21 mRNA was induced in a dose-dependent manner by the addition of BaP compared with the control (1.7- to 2.0-fold) in 48-hr cultured cells. However, when AhR siRNA was introduced into cells, p21 mRNA was not induced in 48-hr cultured cells (Fig. 6-

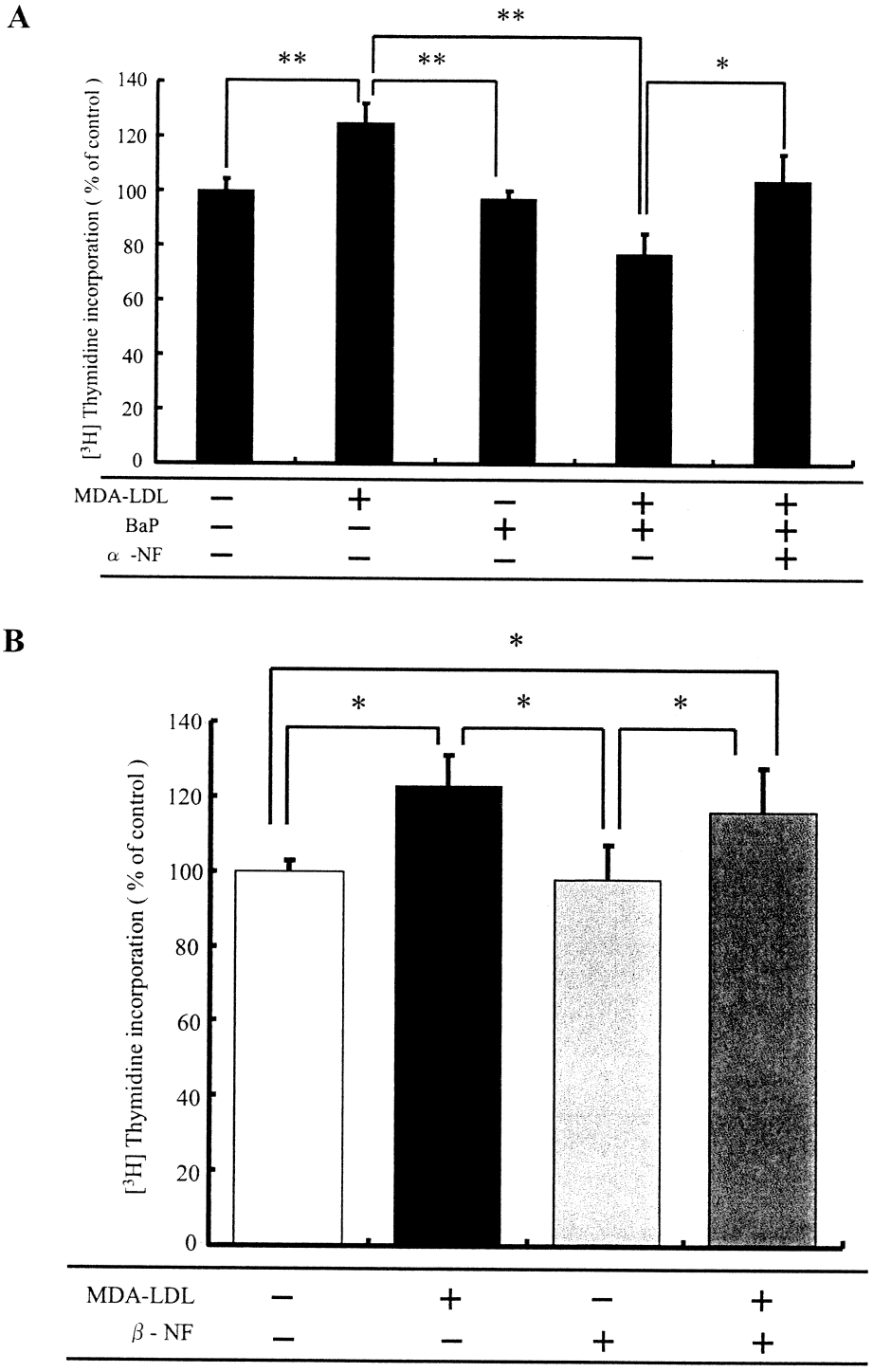


Fig. 2. Effects of α-NF (A) and β-NF (B) on BaP suppression of MDA-LDL-induced THP-1 cell growth. THP-1 cell proliferation was assessed by a [3H] thymidine incorporation assay. Concentrations of BaP, MDA-LDL, α-NF, and β-NF were 0.1 μM, 0.4 mg/ml, 0.1 μM, and 0.1 μM, respectively. Data show the mean ± S.D. of at three independent experiments. $^{*}p < 0.01$; $^{**}p < 0.001$.

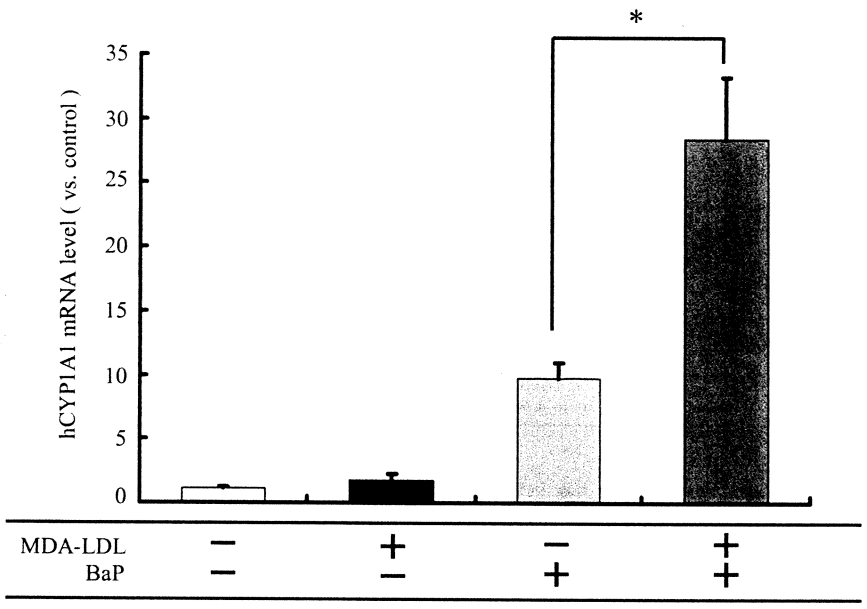


Fig. 3. Expression of hCYP1A1 mRNA in THP-1 cells. THP-1 cells were incubated with DMSO, BaP, MDA-LDL, or MDA-LDL along with BaP for 12 hr. Total RNA was prepared 12 hr later as described in the experimental procedures. The mRNA expression of the target genes was analyzed by real-time RT-PCR, and the mRNA levels of the target gene were normalized to that of GAPDH. Concentrations of MDA-LDL and BaP were 0.4 mg/ml and 0.1 μM, respectively. Data show the mean ± S.D. of at three independent experiments. $^{*}p < 0.01$.

B). Moreover, p21 mRNA was induced in a dose-dependent manner by treatment with Ad-hCYP1A1 and BaP in 24-hr cultured cells (Fig. 6-C) but not with Ad-hCYP1A2 and BaP. Typical catalylic activities for hCYP1A1 and hCYP1A2 were detected with EROD. EROD activities of overexpressed hCYP1A1 and hCYP1A2 were 2.0 and 2.39 times higher, respectively, than that of the control (Fig. 6-D).

DISCUSSION

Macrophage proliferation is recognized as an important factor of pathogenesis in the development of arteriosclerosis. Studies from several research groups have shown that Ox-LDL induced macrophage proliferation (Matsumura *et al.*, 1997; Martens *et al.*, 1998; Hamilton *et al.*, 1999). Interestingly, PAHs have been known to induce arteriosclerosis (Curfs *et al.*, 2005; van Grevenynghe *et al.*, 2004), and several observations support the hypothesis that the aggravation of arteriosclerosis is caused by PAHs coexiting with Ox-LDL such as MDA-LDL. However, it is unclear as to how arteriosclerosis is promoted by PAHs. Therefore, we expected that MDA-LDL-induced cell growth is supported by the presence of PAHs. In the present study, we used THP-1 cells to examine whether MDA-LDL-induced cell growth was caused by PAHs. Contrary to expectations, our results demonstrated that cotreatment of BaP or 3-MC with MDA-LDL decreased MDA-LDL-induced THP-1 cell growth (Fig. 1-A). Interestingly, we found that there were differences between the ligands (BaP or 3-MC) and nonligands (pyrene or BeP) of the AhR (Figs. 1-A and B). In addition, we conducted experiments using an AhR partial antagonist (α-NF) and agonist (β-NF) other than PAHs to determine whether depressed MDA-LDL-induced THP-1 cell growth in the AhR could be found under the same conditions. It is of interest that α-NF clearly restored the synergistic action by the combination of BaP and MDA-LDL (Fig. 2-A), but β-NF did not depress MDA-LDL-induced THP-1 cell growth. It seems that activation of the AhR pathway is involved in the depression of MDA-LDL-induced THP-1 cells growth; however, involvement of another mechanism after activation of the AhR pathway was predicted. Next, we designed an experiment to investigate the expression level of hCYP1A1 mRNA. Higher expression of mRNA was observed after cotreatment of

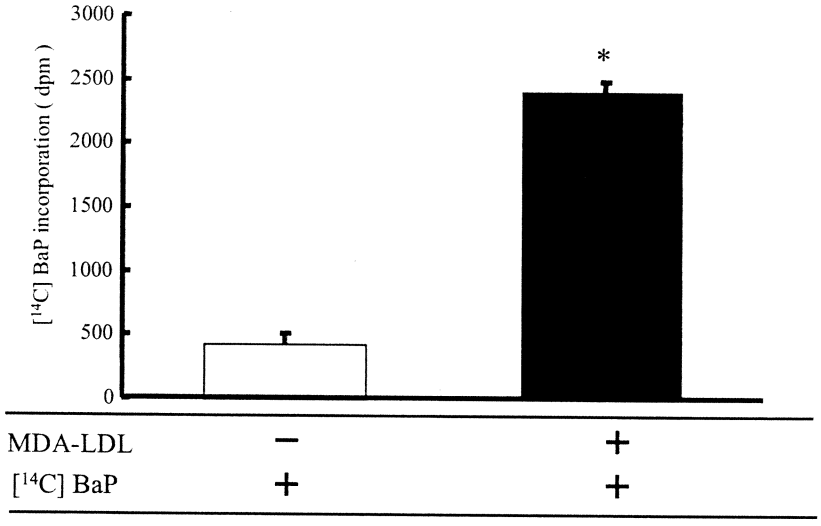


Fig. 4. Effect of MDA-LDL on [^{14}C]BaP incorporation into THP-1 cells. THP-1 cells were incubated with either [^{14}C]BaP or BaP and MDA-LDL for 24 hr. Incorporation of BaP was assessed by a [^{14}C]BaP incorporation assay. Concentrations of [^{14}C]BaP and MDA-LDL were 0.1 μCi/ml and 0.4 mg/ml, respectively. Data show the mean ± S.D. of at three independent experiments. $^{*}p < 0.001$ compared with [^{14}C]BaP alone.

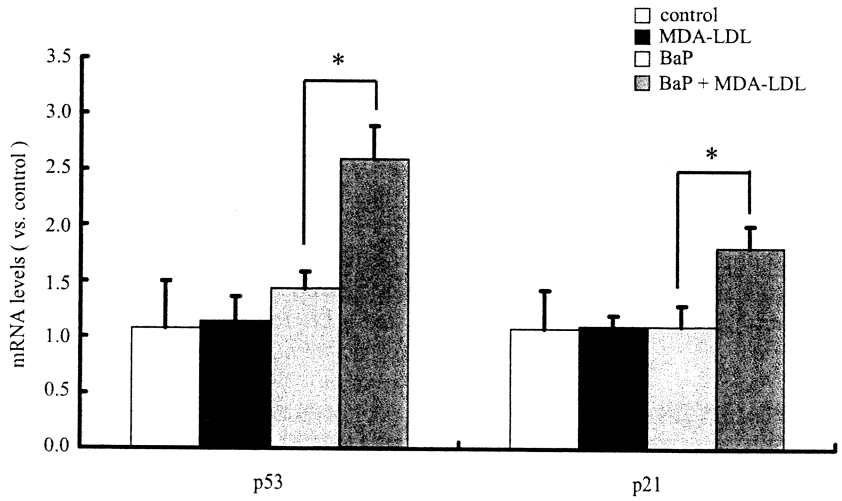


Fig. 5. Expression of p53 and p21 mRNAs in THP-1 cells. THP-1 cells were incubated with DMSO, BaP, MDA-LDL, or MDA-LDL along with BaP for 12 hr. Total RNA was prepared 12 hr later as described in the experimental procedures. The mRNA expression of the target genes was analyzed by real-time RT-PCR, and the mRNA levels of the target gene were normalized to that of GAPDH. Concentrations of MDA-LDL and BaP were 0.4 mg/ml and 0.1 μM, respectively. Data show the mean ± S.D. of at three independent experiments. $^{*}p < 0.001$.

BaP and MDA-LDL than after treatment with BaP alone (Fig. 3). These findings suggest that the influence of PAHs on THP-1 cell growth is likely to be through AhR, and strong BaP activation is predicted to be due to the acceleration of BaP incorporation into cells.

BaP, as well as other PAHs, is poorly soluble in water.

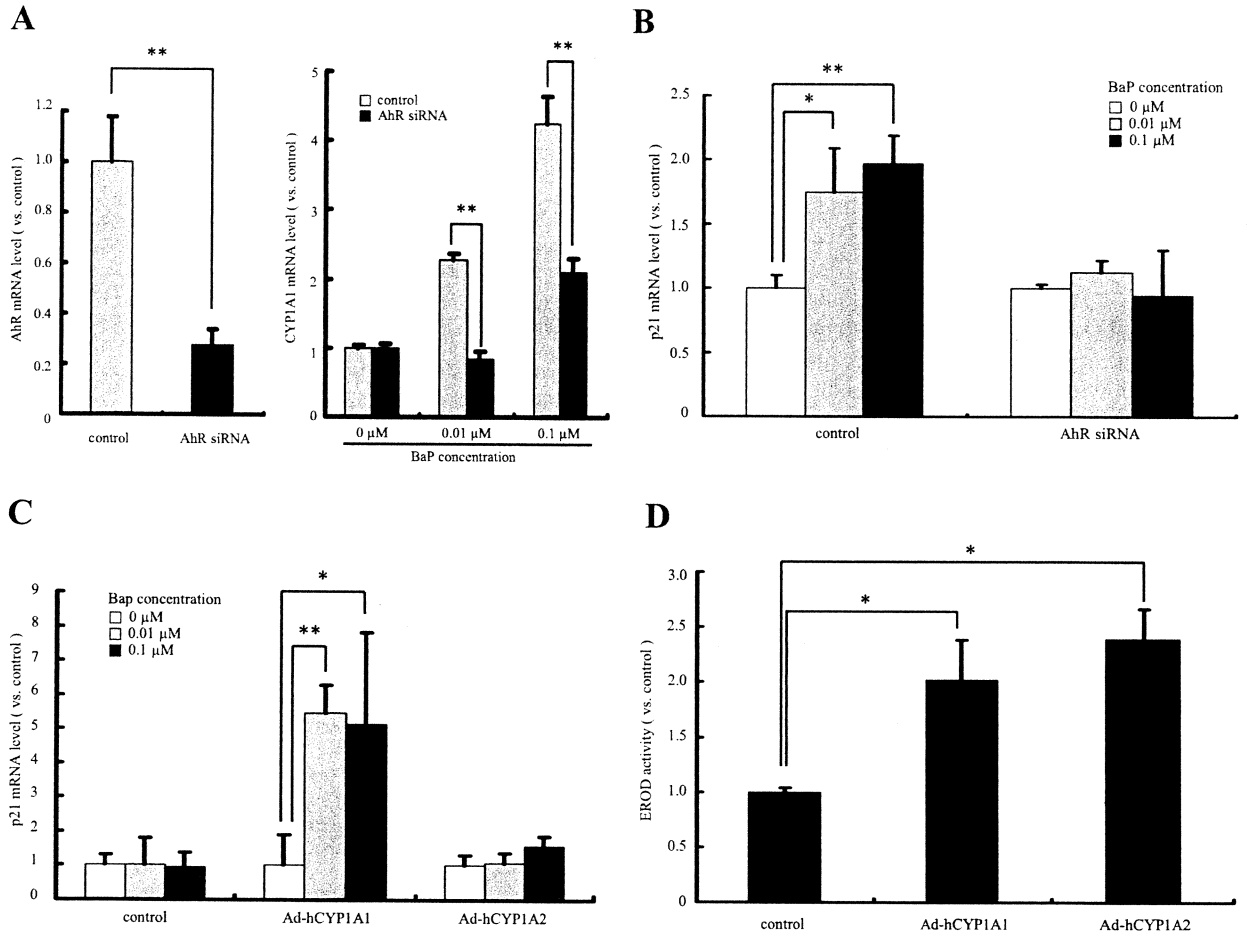


Fig. 6. (A) Effects of AhR siRNA on the expression levels of the AhR and CYP1A1 mRNA in HepG2 cells. Effects of AhR siRNA (B) and overexpression of hCYP1A1 (C) on the expression levels of p21 mRNA in HepG2 cells. (D) EROD activity of hCYP1A1 and hCYP1A2 in HepG2 cells. The mRNA expression of target genes was analyzed by real-time RT-PCR, and the mRNA levels of the target gene were normalized to that of GAPDH. EROD activity compared to the control is shown. Data show the mean ± S.D. of at three independent experiments. $^{*}p < 0.05$; $^{**}p < 0.001$.

In plasma, BaP partitions readily incorporate into plasma lipoproteins (Avigan, 1959; Shu and Nichols, 1979). The entry of BaP into cells from plasma lipoproteins has been shown to be via diffusion and to be nonmediated by a transfer process (Remsen and Shireman, 1981; Plant *et al.*, 1985). Therefore, we investigated the uptake of BaP into THP-1 cell using [^{14}C]BaP. Interestingly, the uptake rate of [^{14}C]BaP was increased by cotreatment with MDA-LDL compared to treatment with [^{14}C]BaP alone (Fig. 4). The relatively slow rate of BaP uptake into cells suggests that the lipophilic properties of PAHs would likely result in extremely slow permeation into the tissues. It is important to understand the mechanism by which PAHs enter cells.

In a recent study, Iseki *et al.* (2005) suggested that the AhR in Leydig cells mediated growth inhibition through p21, which is a major transcriptional target of the tumor suppressor p53. Furthermore, p21 is known to play an important role in cell cycle control by interacting with the cyclin-dependent kinase complexes. Finally, the cell cycle may be arrested after the p53/p21 pathway is induced by DNA damage (Iwano *et al.*, 2006). Therefore, in the next experiment, we measured the expression levels of p53 and p21 mRNAs and found that expression of p53 and p21 mRNAs was significantly increased after cotreatment with BaP and MDA-LDL (Fig. 5). Our findings also indi-

cated that suppression of MDA-LDL-induced THP-1 cells growth by BaP may be attributable to apoptosis (Fig. 5). However, this finding is not compatible with the results of flow cytometry (data not shown). Furthermore, as mentioned previously, β-NF is a typical hCYP1A1 inducer that does not contribute to the suppression of MDA-LDL-induced THP-1 cell growth. These findings suggest that metabolites of BaP by hCYP1A1 induced through AhR activation may cause DNA damage. The cell cycle arrest was caused by p53/p21 activation through DNA damage. These results were strongly supported by the AhR siRNA experiment. AhR siRNA restored p21 mRNA expression level as shown in Fig. 6-B. The metabolic activation of BaP by hCYP1A1 could be a necessary step for suppression of MDA-LDL-induced THP-1 cell growth. Recently, knockout experiments of CYP1A1 have shown that CYP1A1 is not involved in BaP toxicity and was reported to be a detoxication enzyme (Uno *et al.*, 2006; Endo *et al.*, 2008). However, our overexpression experiment of hCYP1A1 using an hCYP1A1-expressing adenovirus further supported our findings. The reason for the discrepancy is not clear at this time but could be attributed to differences in the experimental conditions.

In conclusion, suppression of MDA-LDL-induced THP-1 cell growth by BaP may be due to accelerated incorporation of BaP. Thereafter, the hCYP1A1 gene is strongly induced by activation of the AhR by incorporated BaP. It seems that MDA-LDL may play an important role, at least in part, in that incorporation. In addition, BaP was metabolized to the activated form by strongly induced hCYP1A1. Subsequently, DNA damage was caused by the activated BaP, and the p53/p21 pathway was strongly activated. It is, therefore, possible that MDA-LDL-induced THP-1 cell growth was suppressed by PAHs.

Our findings suggest that compounds involved in arteriosclerosis are easily incorporated into cell via MDA-LDL, and further investigation is needed.

REFERENCES

Antoniades, C., Tousoulis, D. and Stefanadis, C. (2008): Smoking in Asians: it doesn't stop at vascular endothelium. Int. J. Cardiol., **128**, 151-153.

Aoyama, K., Yoshinari, K., Kim, H.J., Nagata, K. and Yamazoe, Y. (2009): Simultaneous expression of plural forms of human cytochrome P450 at desired ratios in HepG2 cells: adenovirus-mediated tool for cytochrome P450 reconstitution. Drug Metab. Pharmacokinet., **24**, 209-217.

Avigan, J. (1959): The interaction between carcinogenic hydrocarbons and serumlipoproteins. Cancer Res., **19**, 831-834.

Burke, M.D. and Mayer, R.T. (1974): Ethoxyresorufin: direct fluorometric assay of a microsomal O-dealkylation which is preferentially inducible by 3-methylcholanthrene. Drug Metab. Dispos., **2**, 583-588.

Chouraki, V., Wagner, A., Ferrieres, J., Kee, F., Bingham, A., Haas, B., Ruidavets, J.B., Evans, A., Ducimetiere, P., Amouyel, P. and Dallongeville, J. (2008): Smoking habits, waist circumference and coronary artery disease risk relationship: the PRIME study. Eur. J. Cardiovasc. Prev. Rehabil., **15**, 625-630.

Curfs, D.M., Knaapen, A.M., Pachen, D.M., Gijbels, M.J., Lutgens, E., Smook, M.L., Kockx, M.M., Daemen, M.J. and van Schooten, F.J. (2005): Polycyclic aromatic hydrocarbons induce an inflammatory atherosclerotic plaque phenotype irrespective of their DNA binding properties. FASEB. J., **19**, 1290-1292.

Endo, K., Uno, S., Seki, T., Ariga, T., Ksumi, Y., Mitsumata, M., Yamada, S. and Makishima, M. (2008): Inhibition of aryl hydrocarbon receptor transactivation and DNA adduct formation by CYP1 isoform-selective metabolic deactivation of benzo[a]pyrene. Toxicol. Appl. Pharmacol., **230**, 135-143.

Fogelman, A.M., Shechter, I., Seager, J., Hokom, M., Child, J.S. and Edwards, P.A. (1980): Malondialdehyde alteration of low density lipoproteins leads to cholesteryl ester accumulation in human monocyte-macrophages. PNAS USA, **77**, 2214-2218.

Galván, N., Teske, D.E., Zhou, G., Moorthy, B., MacWilliams, P.S., Czuprynski, C.J. and Jefcoate, C.R. (2005): Induction of CYP1A1 and CYP1B1 in liver and lung by benzo(a)pyrene and 7,12-dimethylbenz(a)anthracene do not affect distribution of polycyclic hydrocarbons to target tissue: role of AhR and CYP1B1 in bone marrow cytotoxicity. Toxicol. Appl. Pharmacol., **202**, 244-257.

Goldstein, J.L. and Brown, M.S. (1977): The low-density lipoprotein pathway and its relation to atherosclerosis. Annu. Rev. Biochem., **46**, 897-930.

Hamilton, J.A., Myers, D., Jessup, W., Cochrane, F., Byrne, R., Whitty, G. and Moss, S. (1999): Oxidized LDL can induce macrophage survival, DNA synthesis, and enhanced proliferative response to CSF-1 and GM-CSF. Arterioscler. Thromb. Vasc. Biol., **19**, 98-105.

Harrigan, J.A., McGarrigle, B.P., Sutter, T.R. and Olson, J.R. (2006): Tissue specific induction of cytochrome P450 (CYP) 1A1 and 1B1 in rat liver and lung following *in vitro* (tissue slice) and *in vivo* exposure to benzo(a)pyrene. Toxicol. In Vitro, **20**, 426-438.

Harrigan, J.A., Vezina, C.M., McGarrigle, B.P., Ersing, N., Box, H.C., Maccubbin, A.E. and Olson, J.R. (2004): DNA adduct formation in precision-cut rat liver and lung slices exposed to benzo[a]pyrene. Toxicol. Sci., **77**, 307-314.

Heery, J.M., Kozak, M., Stafforini, D.M., Jones, D.A., Zimmerman, G.A., McIntyre, T.M. and Prescott, S.M. (1995): Oxidatively modified LDL contains phospholipids with platelet-activating factor-like activity and stimulates the growth of smooth muscle cells. J. Clin. Invest., **96**, 2322-2330.

Iribarren, C., Tekawa, I.S., Sidney, S. and Friedman, G.D. (1999): Effect of cigar smoking on the risk of cardiovascular disease, chronic obstructive pulmonary disease, and cancer in men. N. Engl. J. Med., **340**, 1773-1780.

Iseki, M., Ikuta, T., Kobayashi, T. and Kawajiri, K. (2005): Growth suppression of Leydig TM3 cells mediated by aryl hydrocarbon receptor. Biochem. Biophys. Res. Commun., **331**, 902-908.

Iwano, S., Asanuma, F., Nukaya, M., Saito, T. and Kamataki, T. (2005): CYP1A1-mediated mechanism for atherosclerosis induced by polycyclic aromatic hydrocarbons. Biochem. Biophys. Res. Commun., **337**, 708-712.

Iwano, S., Shibahara, N., Saito, T. and Kamataki, T. (2006): Activation of p53 as a causal step for atherosclerosis induced by polycyclic aromatic hydrocarbons. FEBS Lett., **580**, 890-893.

Jonsson, E.M., Abrahamson, A., Brunstrom, B. and Brandt, I. (2006): Cytochrome P4501A induction in rainbow trout gills and liver following exposure to waterborne indigo, benzo[a]pyrene and 3,3',4,4',5-pentachlorobiphenyl. Aquat. Toxicol., **79**, 226-232.

Kamiyama, Y., Matsubara, T., Yoshinari, K., Nagata, K., Kamimura, H. and Yamazoe, Y. (2007): Role of human hepatocyte nuclear factor 4alpha in the expression of drug-metabolizing enzymes and transporters in human hepatocytes assessed by use of small interfering RNA. Drug Metab. Pharmacokinet., **22**, 287-298.

Kim, J.H., Stansbury, K.H., Walker, N.J., Trush, M.A., Strickland, P.T. and Sutter, T.R. (1998): Metabolism of benzo[a]pyrene and benzo[a]pyrene-7,8-diol by human cytochrome P450 1B1. Carcinogenesis, **19**, 1847-1853.

LaCroix, A.Z., Lang, J., Scherr, P., Wallace, R.B., Cornoni-Huntley, J., Berkman, L., Curb, J.D., Evans, D. and Hennekens, C.H. (1991): Smoking and mortality among older men and women in three communities. N. Engl. J. Med., **324**, 1619-1625.

Martens, J.S., Reiner, N.E., Herrera-Velit, P. and Steinbrecher, U.P. (1998): Phosphatidylinositol 3-kinase is involved in the induction of macrophage growth by oxidized low density lipoprotein. J. Biol. Chem., **273**, 4915-4920.

Matsumura, T., Sakai, M., Kobori, S., Biwa, T., Takemura, T., Matsuda, H., Hakamata, H., Horiuchi, S. and Shichiri, M. (1997): Two intracellular signaling pathways for activation of protein kinase C are involved in oxidized low-density lipoprotein-induced macrophage growth. Arterioscler. Thromb. Vasc. Biol., **17**, 3013-3020.

Miller, K.P. and Ramos, K.S. (2001): Impact of cellular metabolism on the biological effects of benzo[a]pyrene and related hydrocarbons. Drug Metab. Rev., **33**, 1-35.

Ozer, N.K., Palozza, P., Boscoboinik, D. and Azzi, A. (1993): d-alpha-Tocopherol inhibits low density lipoprotein induced proliferation and protein kinase C activity in vascular smooth muscle cells. FEBS Lett., **322**, 307-310.

Patton, S. and Kurtz, G.W. (1951): 2-Thiobarbituric acid as a reagent for detecting milk fat oxidation. J. Dai. Sci., **34**, 669-674.

Plant, A.L., Benson, D.M. and Smith, L.C. (1985): Cellular uptake and intracellular localization of benzo(a)pyrene by digital fluorescence imaging microscopy. J. Cell Biol., **100**, 1295-1308.

Remsen, J.F. and Shireman, R.B. (1981): Effect of low-density lipoprotein on the incorporation of benzo(a)pyrene by cultured cells. Cancer Res., **41**, 3179-3185.

Ross, R. (1999): Atherosclerosis--an inflammatory disease. N. Engl. J. Med., **340**, 115-126.

Sean, W.K. and Stephanie, P.J. (1994): Simultaneous measurement of cytochrome P4501A catalytic activity and total protein concentration with a fluorescence plate reader. Anal. Biochem., **222**, 217-223.

Shu, H.P. and Nichols, A.V. (1979): Benzo(a)pyrene uptake by human plasma lipoproteins *in vitro*. Cancer Res., **39**, 1224-1230.

Steinberg, D. and Witztum, J.L. (1990): Lipoproteins and atherogenesis. Current. concepts. JAMA, **264**, 3047-3052.

Uno, S., Dalton, T.P., Dragin, N., Curran, C.P., Derkenne, S., Miller, M.L., Shertzer, H.G., Gonzalez, F.J. and Nebert, D.W. (2006): Oral benzo[a]pyrene in cyp1 knockout mouse lines: CYP1A1 important in detoxication, CYP1B1 metabolism required for immune damage independent of total-body burden and clearance rate. Mol. Pharmacol., **69**, 1103-1114.

van Grevenynghe, J., Sparfel, L., Le Vee, M., Gilot, D., Drenou, B., Fauchet, R. and Fardel, O. (2004): Cytochrome P450-dependent toxicity of environmental polycyclic aromatic hydrocarbons towards human macrophages. Biochem. Biophys. Res. Commun., **317**, 708-716.

Willett, K.L., Ganesan, S., Patel, M., Metzger, C., Quiniou, S., Waldbieser, G. and Scheffler, B. (2006): *In vivo* and *in vitro* CYP1B mRNA expression in channel catfish. Mar. Environ. Res., **62 Suppl.**, S332-336.

Ylä-Herttuala, S., Rosenfeld, M.E., Parthasarathy, S., Sigal, E., Särkioja, T., Witztum, J.L. and Steinberg, D. (1991): Gene expression in macrophage-rich human atherosclerotic lesions. 15-lipoxygenase and acetyl low density lipoprotein receptor messenger RNA colocalize with oxidation specific lipid-protein adducts. J. Clin. Invest., **87**, 1146-1152.

Zhao, G.F., Seng, J.J., Zhang, H. and She, M.P. (2005): Effects of oxidized low density lipoprotein on the growth of human artery smooth muscle cells. Chin. Med. J. (Engl.), **118**, 1973-1978.

研究テーマ③
癌および加齢性疾患に対する疼痛制御による QOL 向上の研究

J Pharmacol Sci 124, 258 – 266 (2014)

Journal of Pharmacological Sciences
© *The Japanese Pharmacological Society*

Full Paper

Potential Involvement of μ-Opioid Receptor Dysregulation on the Reduced Antinociception of Morphine in the Inflammatory Pain State in Mice

Yuta Aoki[1], Hirokazu Mizoguchi[1], Chizuko Watanabe[1], Kumiko Takeda[1], Tsukasa Sakurada[2], and Shinobu Sakurada[1,*]

[1]*Department of Physiology and Anatomy, Tohoku Pharmaceutical University, 4-4-1 Komatsushima, Aoba-ku, Sendai 981-8558, Japan*

[2]*First Department of Pharmacology, Daiichi College of Pharmaceutical Sciences, 22-1 Tamagawa-cho, Minami-ku, Fukuoka 815-8511, Japan*

Received November 18, 2013; Accepted December 17, 2013

Abstract. The antinociceptive effect of morphine in the inflammatory pain state was described in the von Frey filament test using the complete Freund's adjuvant (CFA)-induced mouse inflammatory pain model. After an i.pl. injection of CFA, mechanical allodynia was observed in the ipsilateral paw. The antinociceptive effect of morphine injected s.c. and i.t. against mechanical allodynia was reduced bilaterally at 1 day and 4 days after the CFA pretreatment. The expression level of mRNA for μ-opioid receptors at 1 day after the CFA pretreatment was reduced bilaterally in the lumbar spinal cord and dorsal root ganglion (DRG). In contrast, the protein level of μ-opioid receptors at 1 day after CFA pretreatment was decreased in the ipsilateral side in the DRG but not the lumbar spinal cord. Single or repeated i.t. pretreatment with the protein kinase Cα (PKCα) inhibitor Ro-32-0432 completely restored the reduced morphine antinociception in the contralateral paw but only partially restored it in the ipsilateral paw in the inflammatory pain state. In conclusion, reduced morphine antinociception against mechanical allodynia in the inflammatory pain state is mainly mediated via a decrease in μ-opioid receptors in the ipsilateral side and via the desensitization of μ-opioid receptors in the contralateral side by PKCα-induced phosphorylation.

Keywords: antinociception, morphine, inflammatory pain, μ-opioid receptor, protein kinase C

Introduction

Morphine is a μ-opioid receptor agonist and is commonly used in the clinic for the management of various types of pain. Although morphine is very effective against most types of pain, specifically acute pain, there are several pain types that are difficult to control using morphine. These types of pain include neuropathic pain, cancer pain, or a component of inflammatory pain known as morphine-resistant intractable pains. In these pain states, an increased dose of morphine can sometimes retain good analgesia; however, elevated side effects by increased doses of morphine, such as drowsiness, respiratory depression, nausea, and constipation, can seriously affect patient quality of life. Thus, it is important to understand the mechanism of morphine-resistant intractable pain and develop new treatments for such pain.

Among the types of morphine-resistant intractable pain, inflammatory pain exhibits distinct characteristics. Unlike other types of intractable pain, whose expression is restricted to the ipsilateral side, inflammatory pain is observed on both the ipsilateral and contralateral sides (1). Moreover, mechanical allodynia, thermal hyperalgesia, and mechanical hyperalgesia are prominent features of inflammatory pain in addition to edema. Several types of inflammatory pain induced by formalin, carrageenan, and complete Freund's adjuvant (CFA), among others, have been developed in rodents and used as experimental inflammatory pain models. In particular, the CFA-induced inflammatory pain model is widely

*Corresponding author. s-sakura@tohoku-pharm.ac.jp
Published online in J-STAGE
doi: 10.1254/jphs.13242FP

used to describe the mechanisms of the inflammatory pain state and the effectiveness of analgesics against inflammatory pain.

It has been well established that the antinociceptive effect of μ-opioid receptor agonists, including morphine, is enhanced or retained against mechanical hyperalgesia (2, 3) and thermal hyperalgesia (2) in the CFA-induced inflammatory pain rodent model. However, most studies describing the antinociceptive effect of μ-opioid receptor agonists in this inflammatory pain model have focused on their effectiveness against hyperalgesia but not against allodynia. We recently found that the antinociceptive effect of morphine was markedly suppressed against mechanical allodynia in this inflammatory pain model (4). In the present study, using the CFA-induced inflammatory pain model in mice, we characterized the antinociceptive effect of morphine against mechanical allodynia and investigated the mechanism underlying the reduction of its antinociceptive effect on the inflammatory pain state.

Materials and Methods

All experiments were performed with the approval of the Ethics Committee for Animal Experiments at Tohoku Pharmaceutical University and according to the National Institutes of Health Guide for the Care and Use of Laboratory Animals. Every effort was made to minimize the number of animals and animal suffering in the following experiments.

Animals

Male ddY mice (Japan SLC, Hamamatsu) weighing 20 – 24 g were used. The mice were housed in a room with controlled temperature (22°C – 23°C) and humidity (50% – 60%), with an alternating 12-h light/dark (lights on at 7:00 and off at 19:00) cycle. Food and water were provided ad libitum.

Mouse model for inflammatory pain

To generate the inflammatory pain model, mice were injected intraplantarly (i.pl.) with 50 μl of CFA (Sigma-Aldrich, St. Louis, MO, USA) in the left hind paw using a syringe with a 27-gauge needle. Control mice were injected i.pl. with sterile saline.

Measurement of mechanical allodynia and morphine analgesia

Mechanical allodynia and the antinociceptive effect of morphine were measured using the von Frey filament test. Prior to the experiment, mice were placed in a clear plastic compartment (10 cm × 10 cm × 14 cm) for 1 h to habituate to the experimental environment. The presence of the withdrawal response (biting, licking, or flinching) due to stimulation of the plantar surface of the hind paw by the variable strength of the von Frey filament (applied pressure by each filament: 0.041, 0.073, 0.163, 0.400, 0.610, 1.000, 1.430, 2.100, and 4.200 g) within 3 s after the filament application was determined. The up-down method was used to evaluate the withdrawal threshold from the filament. The intensity of the application of the filament was adjusted so that the pre-drug threshold was 0.400 or 0.610 g. Mice demonstrating a threshold of 0.073 or 0.163 g after the CFA injection were used in the inflammatory pain model.

Intrathecal (i.t.) administration

Intrathecal administration was performed according to the procedure described by Hylden and Wilcox (5) using a 50-μl Hamilton microsyringe with a 29-gauge needle. For i.t. injection, drugs were dissolved in sterile artificial cerebrospinal fluid (aCSF) containing 126.6 mM NaCl, 2.5 mM KCl, 2.0 mM $MgCl_2$, and 1.3 mM $CaCl_2$. The injection volume of the drugs was 5 μl.

Drugs

The drugs used included morphine hydrochloride (Takeda, Osaka) and the protein kinase Cα (PKCα) inhibitor Ro-32-0432 (Merck KGaA, Darmstadt, Germany). Morphine hydrochloride and Ro-32-0432 were dissolved in sterile saline and dimethyl sulfoxide (DMSO), respectively.

Semi-quantitative reverse transcription polymerase chain reaction (RT-PCR)

Total RNA in the mouse dorsal root ganglion (DRG: L4 – L6) and lumbar spinal cord was extracted using the RNeasy Lipid Tissue Mini Kit (QIAGEN K.K., Tokyo). The purified total RNA was quantified using a spectrophotometer at A260. RT-PCR amplification was performed using the SuperScript One Step RT-PCR system, Platinum version (Life Technologies, Carlsbad, CA, USA). The synthetic forward primer and reverse primer for the μ-opioid receptor were 5′-CAG CCA GCA TTC AGA ACC ATG G-3′ and 5′-ATG GTG CAG AGG GTG AAG ATA CTG G-3′, respectively. The synthetic forward primer and reverse primer for β-actin were 5′-GCT CGT CGT CGA CAA CGG CTC-3′ and 5′-CAA ACA TGA TCT GGG TCA TCT TCT T-3′, respectively. The samples were heated to 50°C for 30 min for cDNA synthesis and to 94°C for 2 min for pre-denaturation and then cycled 30 times at 94°C for 30 s for denaturation, 55°C for 30 s for annealing, and 72°C for 30 s for extension; the samples were finally heated to 72°C for 7 min for the final extension. The resulting PCR product was electrophoresed on a 0.8%

agarose gel containing ethidium bromide. The agarose gel was imaged using a UV Imaging Analyzer FAS-III (Toyobo, Osaka), and the PCR product for the μ-opioid receptor in agarose gel was semi-quantified against β-actin using Lumino Imaging Analyzer FAS-1000 (Toyobo).

Western blotting analysis

Mouse lumbar spinal cord or DRG (L4 – L6) were homogenized in lysis buffer (50 mM Tris-HCl, 150 mM NaCl, 2.5 mM EGTA, 1 mM Na_3VO_4, 0.5% TritonX-100, 0.5% NP-40) containing 1% Protease Inhibitor Cocktail (Sigma-Aldrich) and centrifuged at 20,000 × g for 10 min at 4°C. The supernatants were collected, and total protein was measured using the Protein Assay Reagent (Bio-Rad, Hercules, CA, USA). The proteins (12 μg) were boiled in sample buffer (31.25 mM Tris-HCl, 1% sodium dodecyl sulfate (SDS), 5% glycerol, 0.00625% bromophenol blue, and 2.5% β-mercaptoethanol: pH 6.8), electrophoresed in a 10% SDS-PAGE gel, and then transferred onto a Hybond-P membrane (GE Healthcare UK Ltd., Buckinghamshire, UK). The blotted membrane was incubated in Blocking One (Nacalai Tesque, Osaka) for 1 h at room temperature to inhibit non-specific binding reactions. After washing, the membranes were incubated for 16 h at 4°C with a rabbit antiserum for the μ-opioid receptor (Abcam plc, Cambridge, UK) at 1:3000 dilution in Can Get Signal solution 1 (Toyobo) or with a rabbit antiserum for β-actin (IMGENEX Corp., San Diego, CA, USA) at 1:1000 dilution in Can Get Signal solution 1. The membranes were extensively washed and then incubated for 1 h with a goat HRP-conjugated anti-rabbit IgG (Santa Cruz Biotechnology, Inc., Dallas, TX, USA) at 1:5000 dilution in Can Get Signal solution 2 (Toyobo). After washing, the proteins were detected using the ECL-Plus Western blotting detection system (GE Healthcare UK, Ltd.) and visualized with the FAS-1000 Lumino Imaging Analyzer (Toyobo).

Statistical analyses

The data are expressed as means ± S.E.Ms for at least 10 mice. The statistical significance of the differences between groups was assessed using one-way analysis of variance (ANOVA) or two-way ANOVA followed by Bonferroni's test.

Results

CFA-induced mechanical allodynia

Groups of mice were injected i.pl. with 50 μl of saline or CFA in the left hind paw, and the withdrawal threshold against mechanical stimulation by a von Frey filament applied to the plantar surface of the each hind paw was measured for 40 days. After the CFA injection, the decrease in mechanical threshold (mechanical allodynia) was observed in the ipsilateral paw but not in the contralateral paw (Fig. 1). The mechanical allodynia in the ipsilateral paw in the CFA-treated mice peaked at 1 day after the CFA treatment and was prolonged to 34 days after CFA treatment. In contrast, the mechanical threshold was not altered in mice treated i.pl. with saline.

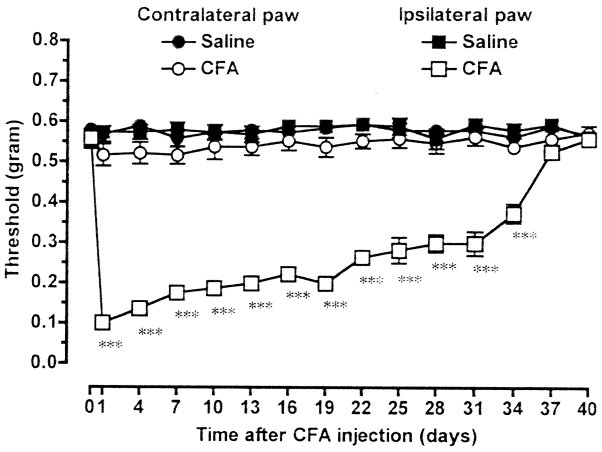


Fig. 1. CFA-induced mechanical allodynia in mice. Groups of mice were injected i.pl. with 50 μl of saline or CFA in the left hind paw, and the withdrawal threshold on the ipsilateral paw and contralateral paw against mechanical stimulation by a von Frey filament applied to the plantar surface of each hind paw was measured for 40 days. Each value represents the mean ± S.E.M. for at least 10 mice. ***$P < 0.001$ vs. control model (saline-i.pl. pretreated) mice.

Antinociceptive effect of morphine injected subcutaneously (s.c.) or i.t. in the inflammatory pain state

Groups of mice pretreated i.pl. with 50 μl of saline or CFA in the left hind paw were injected s.c. with morphine (7.1 mg/kg) at 1 day and 4 days after i.pl. pretreatment, and the withdrawal threshold against mechanical stimulation by a von Frey filament applied to the plantar surface of the each hind paw was measured for 180 min. The potent increase of the mechanical threshold (antinociceptive effect) by morphine was observed bilaterally in saline-pretreated mice (Fig. 2: A and B). However, the antinociceptive effect of morphine was significantly suppressed bilaterally at 1 day and 4 days after CFA pretreatment. More potent suppression of morphine antinociception was observed in the ipsilateral paw (Fig. 2B) compared to the contralateral paw (Fig. 2A). Moreover, in the contralateral paw, the suppression of morphine antinociception tended to increase its intensity at 4 days after the pretreatment

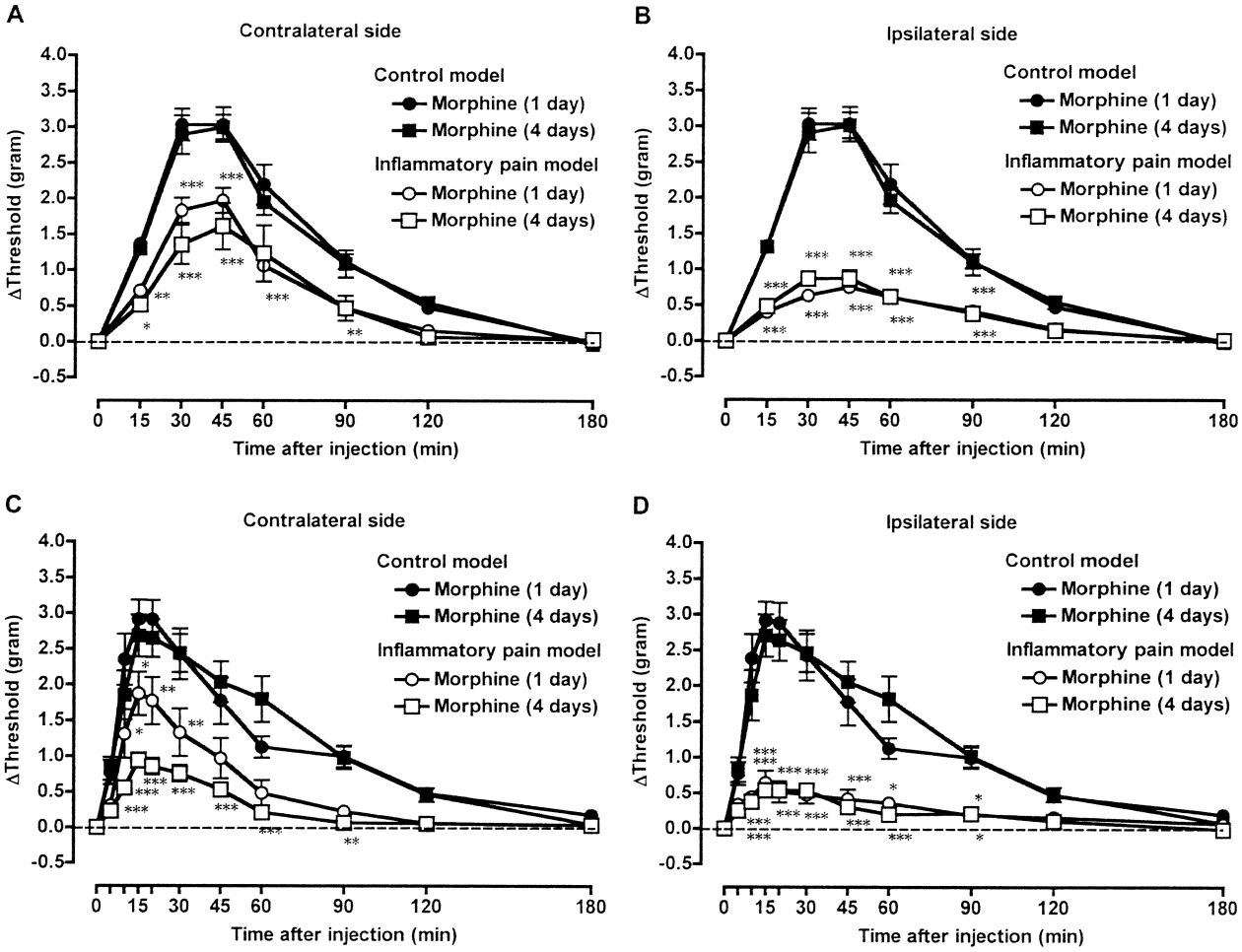


Fig. 2. The peripheral antinociceptive effect (A and B) and spinal antinociceptive effect (C and D) of morphine in the inflammatory pain state in mice. Groups of mice pretreated i.pl. with 50 μl of saline or CFA in the left hind paw were injected s.c. with morphine (7.1 mg/kg) (A and B) or injected i.t. with morphine (5.0 nmol) (C and D) at 1 day and 4 days after the i.pl. pretreatment, and the withdrawal threshold on the contralateral paw (A and C) and ipsilateral paw (B and D) against mechanical stimulation by a von Frey filament applied to the plantar surface of each hind paw was measured for 180 min. Each value represents the mean ± S.E.M. for at least 10 mice. $*P < 0.05$, $**P < 0.01$, $***P < 0.001$ vs. control model (saline-i.pl. pretreated) mice.

compared to 1 day after pretreatment (Fig. 2A).

Other groups of mice pretreated i.pl. with 50 μl of saline or CFA in the left hind paw were injected i.t. with morphine (5.0 nmol) at 1 day and 4 days after i.pl. pretreatment, and the withdrawal threshold against mechanical stimulation by a von Frey filament applied to the plantar surface of the each hind paw was measured for 180 min. The potent antinociceptive effect of morphine was observed bilaterally in saline-pretreated mice (Fig. 2: C and D). However, the antinociceptive effect of morphine was significantly suppressed bilaterally at 1 day and 4 days after CFA pretreatment. More potent suppression of morphine antinociception was observed in the ipsilateral paw (Fig. 2D) compared to the contralateral paw (Fig. 2C). Moreover, in the contralateral paw, the magnitude of suppression for morphine antinociception was significantly increased at 4 days after pretreatment compared to 1 day after pretreatment (Fig. 2C).

mRNA expression and protein levels of μ-opioid receptors in the inflammatory pain state

Groups of mice were injected i.pl. with 50 μl of saline or CFA in the left hind paw, and the mRNA expression levels of μ-opioid receptors in the DRG (L4 – L6) and lumbar spinal cord in the ipsilateral and contralateral sides were measured using semi-quantitative RT-PCR. In the lumbar spinal cord, the mRNA expression levels

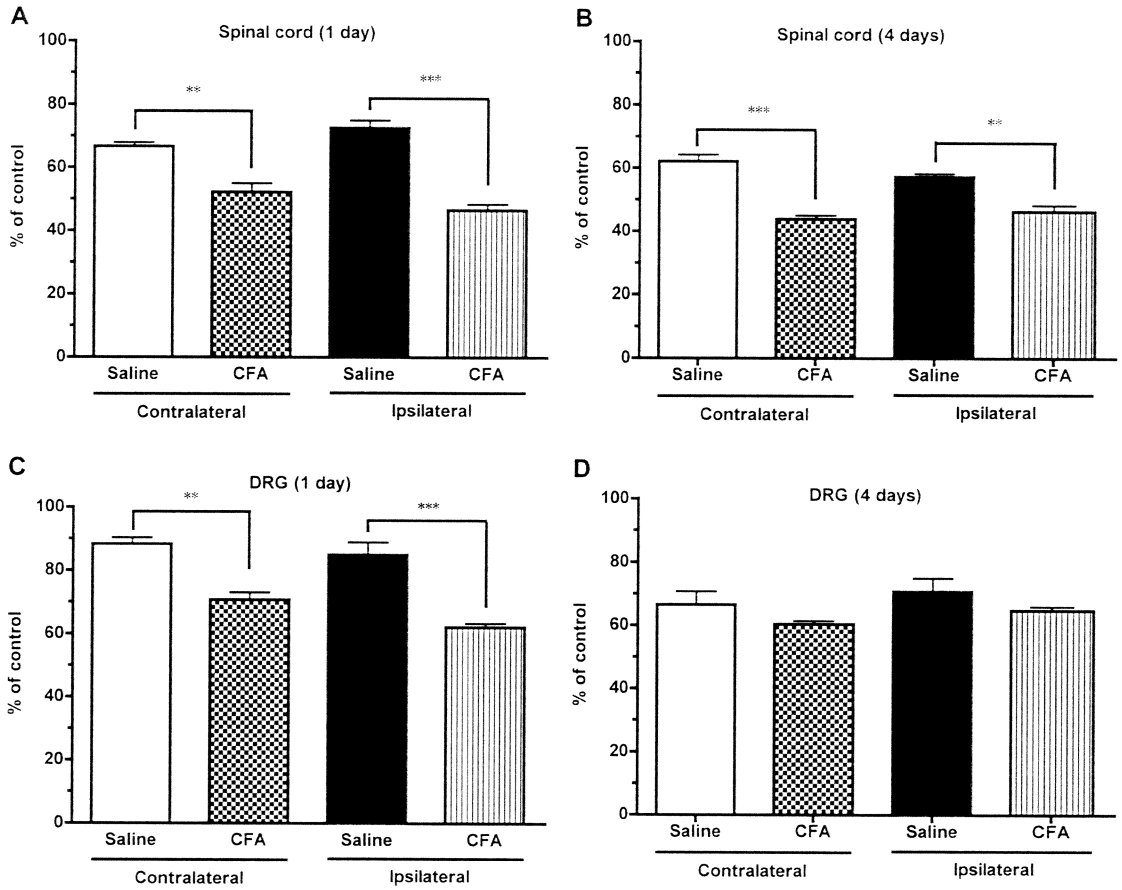


Fig. 3. The mRNA expression levels of μ-opioid receptors in the lumbar spinal cord (A and B) and DRG (L4 – L6) (C and D) in the inflammatory pain state in mice. Groups of mice were injected i.pl. with 50 μl of saline or CFA in the left hind paw, and the mRNA expression levels of μ-opioid receptors in the lumbar spinal cord (A and B) and DRG (L4 – L6) (C and D) on the ipsilateral side and contralateral side at 1 day (A and C) and 4 days (B and D) after CFA pretreatment were measured using semi-quantitative RT-PCR. Data are expressed as the % of the mRNA level for μ-opioid receptors normalized against β-actin. Each value represents the mean ± S.E.M. for 3 independent sets of experiments. $^{**}P < 0.01$, $^{***}P < 0.001$ vs. saline-i.pl. pretreated mice.

of μ-opioid receptors were significantly decreased bilaterally at 1 day and 4 days after CFA pretreatment (Fig. 3: A and B). Bilateral reduction of the mRNA expression levels of μ-opioid receptor was also observed in the DRG at 1 day after CFA pretreatment (Fig. 3C) but disappeared at 4 days after CFA pretreatment (Fig. 3D).

Other groups of mice were injected i.pl. with 50 μl of saline or CFA in the left hind paw, and the protein levels of μ-opioid receptors in the DRG (L4 – L6) and lumbar spinal cord in the ipsilateral and contralateral sides were measured using western blotting analysis. In the DRG, the protein levels of μ-opioid receptors were significantly reduced only on the ipsilateral side at 1 day after CFA pretreatment (Fig. 4C), not at 4 days after CFA pretreatment (Fig. 4D). In contrast, the protein levels of μ-opioid receptors in the lumbar spinal cord was not altered at either 1 day or 4 days after CFA pretreatment (Fig. 4: A and B).

Involvement of the phosphorylation of μ-opioid receptors in the reduction of morphine analgesia in the inflammatory pain state

Groups of mice pretreated i.t. with the PKCα inhibitor Ro-32-0432 (1 nmol) or DMSO along with i.pl. pretreatment with CFA (50 μl) or saline in the left hind paw were injected s.c. with morphine (7.1 mg/kg) at 1 day after pretreatment. The increase in the withdrawal threshold (antinociception) induced by morphine against mechanical stimulation by a von Frey filament applied to the plantar surface of the each hind paw was then measured at 45 min after morphine treatment. The antinociceptive effect of morphine was bilaterally reduced

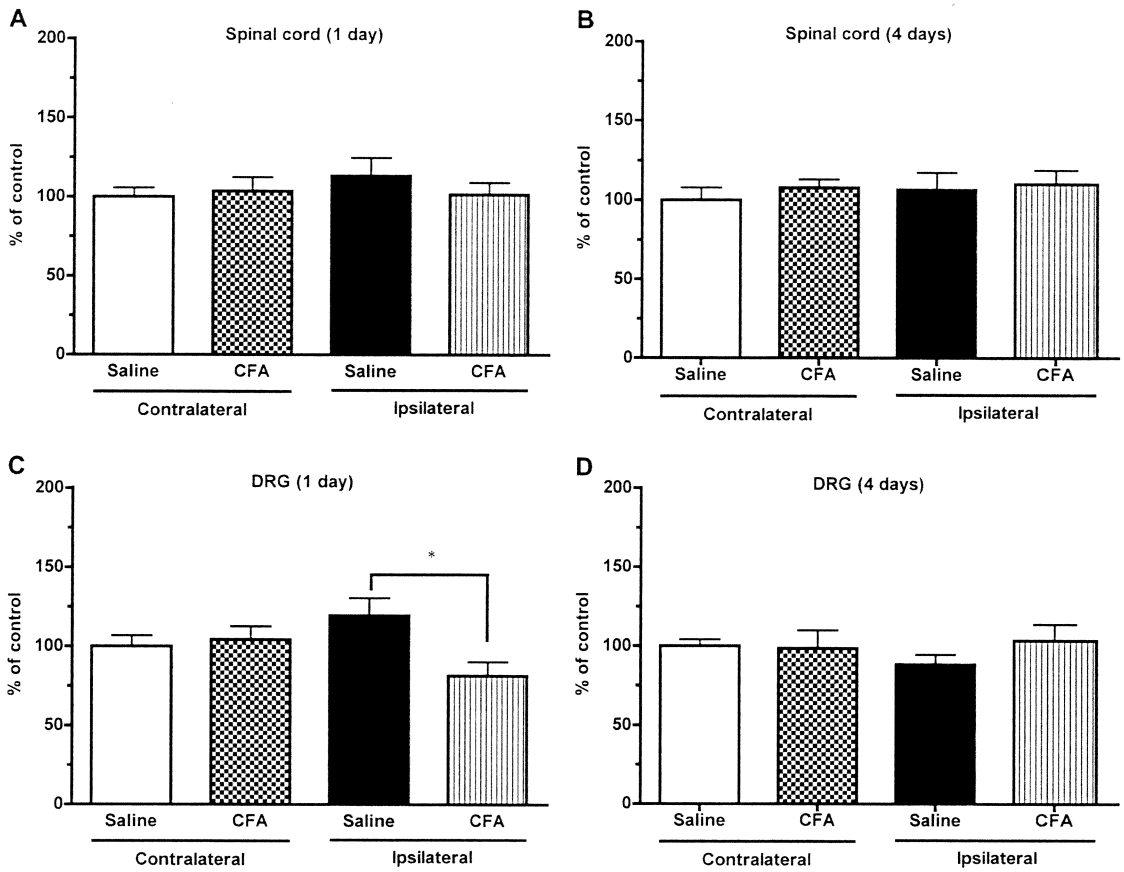


Fig. 4. The protein level of μ-opioid receptors in the lumbar spinal cord (A and B) and DRG (L4 – L6) (C and D) in the inflammatory pain state in mice. Groups of mice were injected i.pl. with 50 μl of saline or CFA in the left hind paw, and the protein level of μ-opioid receptors in lumbar spinal cord (A and B) and DRG (L4 – L6) (C and D) on the ipsilateral side and contralateral side at 1 day (A and C) and 4 days (B and D) after CFA pretreatment was measured using western blotting analysis. Data are expressed as the % of μ-opioid receptor level normalized against β-actin. Each value represents the mean ± S.E.M. for 3 independent sets of experiments. $*P < 0.05$ vs. saline-i.pl. pretreated mice.

at 1 day after CFA pretreatment (Fig. 5A). However, the reduced antinociception of morphine was completely restored in the contralateral paw and was partially restored in the ipsilateral paw by pretreatment with Ro-32-0432. In mice pretreated i.pl. with saline, the morphine antinociception in both the ipsilateral and contralateral paws was not altered by the i.t. pretreatment with Ro-32-0432.

Other groups of mice repeatedly pretreated i.t. with Ro-32-0432 (1 nmol) or DMSO for 4 days along with a single i.pl. pretreatment with CFA (50 μl) or saline in the left hind paw were injected s.c. with morphine (7.1 mg/kg) at 4 days after the i.pl. pretreatment, and the increase in the withdrawal threshold (antinociception) induced by morphine against mechanical stimulation by a von Frey filament applied to the plantar surface of each hind paw was measured at 45 min after morphine treatment. The antinociceptive effect of morphine was bilaterally reduced at 4 days after CFA pretreatment (Fig. 5B). However, the reduced antinociception of morphine was completely restored in the contralateral paw and was partially restored in the ipsilateral paw by repeated pretreatment with Ro-32-0432. In mice pretreated i.pl. with saline, the morphine antinociception in both the ipsilateral and contralateral paws was not altered by the repeated pretreatment with Ro-32-0432.

Discussion

CFA, which is commonly used as an emulsified antigen solution to produce antibodies, consists of mineral oil with inactivated and dried mycobacteria (usually *M. tuberculosis*). It stimulates cell-mediated immunity and potentiates the production of immunoglobulins as

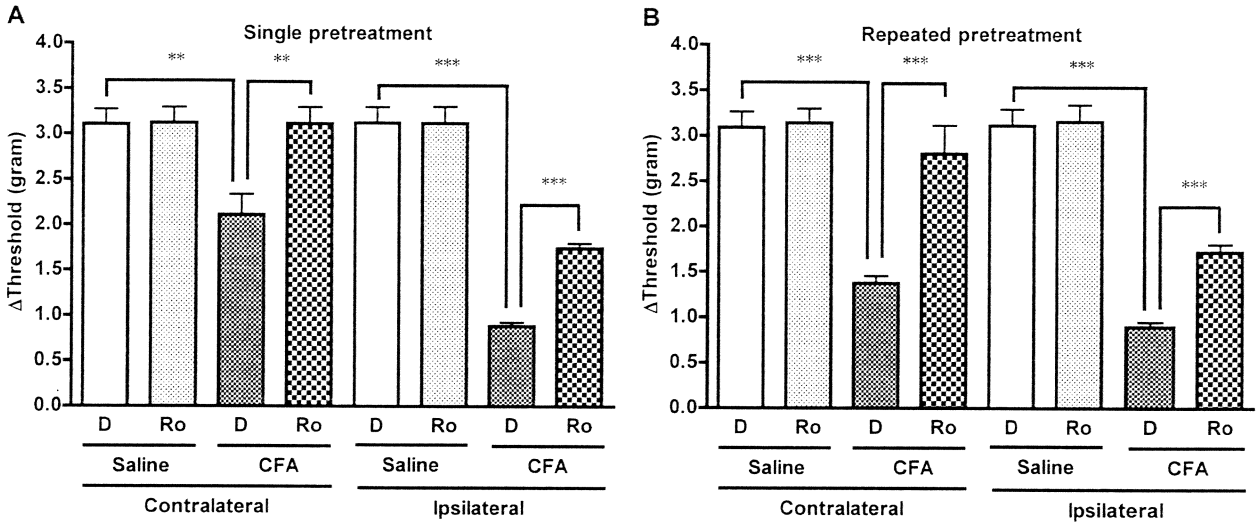


Fig. 5. Effects of single (A) and repeated (B) pretreatment with protein kinase Cα inhibitor on the antinociceptive effect of morphine in the inflammatory pain state in mice. A) Groups of mice pretreated i.t. with protein kinase Cα inhibitor Ro-32-0432 (Ro: 1 nmol) or DMSO (D) along with the i.pl. pretreatment with CFA (50 μl) or saline in the left hind paw were injected s.c. with morphine (7.1 mg/kg) at 1 day after the pretreatment. B) Groups of mice repeatedly pretreated i.t. with the protein kinase Cα inhibitor Ro-32-0432 (Ro: 1 nmol) or DMSO (D) for 4 days combined with the single i.pl. pretreatment with CFA (50 μl) or saline in the left hind paw were injected s.c. with morphine (7.1 mg/kg) at 4 days after the i.pl. pretreatment. The increase in the withdrawal threshold (antinociception) induced by morphine against mechanical stimulation by a von Frey filament applied to the plantar surface of each hind paw was measured at 45 min after the morphine treatment. Each value represents the mean ± S.E.M. for at least 10 mice. $^{**}P < 0.01$, $^{***}P < 0.001$ vs. DMSO + CFA-pretreated mice.

an immunopotentiator (6). These reactions induced by CFA result in tissue inflammation at the site of injection. The administration of CFA into the knee joint in rodents causes knee joint inflammation, which is used as an experimental model for knee arthritis (7). However, inflammation in the hind paw, which is caused by the i.pl. administration of CFA, is used as an experimental model for inflammatory pain (8). In the present study, the i.pl. administration of CFA induced strong edema (an approximately 50% increase in paw volume), thermal hyperalgesia, and mechanical allodynia on the ipsilateral paw, which were apparent at 1 day after CFA injection and retained for 97 days, 16 days, and 34 days, respectively (data not shown). It has been established in rats that CFA-induced inflammation expands from the ipsilateral paw to the contralateral paw and that mechanical allodynia is observed bilaterally, whereas thermal hyperalgesia is observed in only the ipsilateral paw (1). In the present study, mechanical allodynia in mice was only observed in the ipsilateral paw, not in the contralateral paw, after CFA injection. Differences in the animal species used and in the magnitude of the induced inflammation may be involved in this discrepancy.

It is well established that the antinociceptive effect of morphine against thermal hyperalgesia and mechanical hyperalgesia is enhanced or retained in the CFA-induced inflammatory pain state (2, 3). However, in the present study, the antinociceptive effect of morphine injected s.c. against mechanical allodynia in the CFA-induced inflammatory pain state was reduced in the ipsilateral paw. Allodynia is defined as pain perceived in response to non-noxious stimuli after tissue or nerve injury and is considered to be mainly mediated via the Aβ fibers of the primary afferent nerves (9). In contrast, hyperalgesia is a hypersensitivity to noxious stimuli after tissue or nerve injury and is considered to be mainly mediated through the C fibers of the primary afferent nerves (10). The discrepancy in morphine antinociception between hyperalgesia and allodynia in the CFA-induced inflammatory pain state may be correlated to the neurons mediating each pain type. Interestingly, in the present study, the antinociceptive effect of morphine given s.c. against mechanical allodynia in the CFA-induced inflammatory pain state was also reduced in the contralateral paw. It has been reported that mechanical allodynia in the CFA-induced inflammatory pain state is observed bilaterally (1). Although we did not observe mechanical allodynia in the contralateral paw after CFA injection in the present study, inflammation may bilaterally reveal plastic changes in the primary afferent nerves and

may affect the antinociceptive effect of morphine given s.c. against mechanical allodynia in both paws. The bilateral reduction of morphine antinociception against mechanical allodynia in the CFA-induced inflammatory pain state was also observed after the i.t. injection of morphine. The neural plastic changes, which may relate to the bilateral reduction of morphine antinociception against mechanical allodynia after CFA injection, may be present at least in the spinal site.

The most likely neural plastic changes to occur, which result in the bilateral reduction of morphine antinociception against mechanical allodynia after CFA injection, may be the down-regulation of spinal μ-opioid receptors, which is observed in morphine-resistant neuropathic pain (11). Thus, in the present study, the mRNA expression levels of μ-opioid receptors and the protein levels of μ-opioid receptors after CFA injection at the spinal site were quantified using RT-PCR and western blotting analysis, respectively. As a result, the mRNA expression levels of μ-opioid receptors were decreased bilaterally in the DRG at 1 day after CFA injection and in the lumbar spinal cord at 1 day and 4 days after CFA injection. In contrast, the decrease in the protein levels of μ-opioid receptors was only observed in the ipsilateral DRG at 1 day after CFA injection, not in the lumbar spinal cord. These results suggest that the downregulation of μ-opioid receptors in the ipsilateral DRG is at least involved in the reduced morphine antinociception against mechanical allodynia in the ipsilateral paw in the CFA-induced inflammatory pain state. However, the mechanism underlying reduced morphine antinociception against mechanical allodynia in the contralateral paw in the CFA-induced inflammatory pain state remains uncertain because the protein levels of μ-opioid receptors in the contralateral DRG or lumbar spinal cord were not altered after CFA injection. It has been suggested that the phosphorylation of μ-opioid receptors by PKC enhances the desensitization of μ-opioid receptors by retaining the desensitized μ-opioid receptors at the membrane surface (12). Thus, in the present study, involvement of the phosphorylation of μ-opioid receptors by PKC in the reduction of morphine antinociception against mechanical allodynia in the CFA-induced inflammatory pain state was investigated. PKC has several isoforms known as conventional PKC (α, βI, βII, and γ), novel PKC (δ, ε, η, and θ) and atypical PKC (ζ, ι, and λ) (13). Among these isoforms, PKCα has been reported to be distributed in both pre-synaptic and post-synaptic neurons and to play an important role in the desensitization of opioid receptors (14). In the present study, the reduced antinociception of morphine against mechanical allodynia in the CFA-induced inflammatory pain state was completely restored in the contralateral paw but was only partially restored in the ipsilateral paw by i.t. pretreatment with Ro-32-0432, a cell-permeable selective inhibitor for PKCα. These results clearly suggest that the desensitization of spinal μ-opioid receptors by PKCα-induced phosphorylation is involved in the bilateral reduction of morphine antinociception against mechanical allodynia in the CFA-induced inflammatory pain state, particularly in the contralateral paw. In the present study, the phosphorylation levels of μ-opioid receptors at CFA-induced inflammatory pain state were not examined. Therefore, the involvement of other PKCα substrates, as downstream signal transductions activated following the μ-opioid receptor stimulation, in the bilateral reduction of morphine antinociception against mechanical allodynia in the CFA-induced inflammatory pain state can not be completely excluded at this point. To conform this hypothesis, extensive research may be required.

In conclusion, the antinociceptive effect of morphine was markedly reduced bilaterally against mechanical allodynia in the inflammatory pain state. The reduced morphine antinociception might be mainly mediated via a decrease in μ-opioid receptors on the ipsilateral side and via the desensitization of μ-opioid receptors on contralateral side as a result of PKCα-induced phosphorylation.

Acknowledgments

This study was supported by JSPS KAKENHI Grant Numbers 22600009 and 24590731 and the MEXT (Ministry of Education, Culture, Sports, Science and Technology)-Supported Program for the Strategic Research Foundation at Private Universities (2010 – 2014).

References

1 Nagakura Y, Okada M, Kohara A, Kiso T, Toya T, Iwai A, et al. Allodynia and hyperalgesia in adjuvant-induced arthritic rats: time course of progression and efficacy of analgesics. J Pharmacol Exp Ther. 2003;306:490–497.
2 Fernández-Dueñas V, Pol O, García-Nogales P, Hernández L, Planas E, Puig MM. Tolerance to the antinociceptive and anti-exudative effects of morphine in a murine model of peripheral inflammation. J Pharmacol Exp Ther. 2007;322:360–368.
3 Maldonado R, Valverde O, Turcaud S, Fournié-Zaluski MC, Roques BP. Antinociceptive response induced by mixed inhibitors of enkephalin catabolism in peripheral inflammation. Pain. 1994;58:77–83.
4 Aoki Y, Mizoguchi H, Watanabe C, Yonezawa A, Sakurada S. Involvement of altered mu-opioid receptors in spinal cord on the inflammatory pain state. J Pharmacol Sci. 2012;118 (Suppl 1): 194P.
5 Hylden JL, Wilcox GL. Intrathecal morphine in mice: a new technique. Eur J Pharmacol. 1980;67:313–316.
6 Helfgott SM, Kieval RI, Breedveld FC, Brahn E, Young CT, Dynesius-Trentham R, et al. Detection of arthritogenic factor in

adjuvant arthritis. J Immunol. 1988;140:1838–1843.
7 McDougall JJ, Barin AK, McDougall CM. Loss of vasomotor responsiveness to the μ-opioid receptor ligand endomorphin-1 in adjuvant monoarthritic rat knee joints. Am J Physiol Regul Integr Comp Physiol. 2004;286:R634–R641.
8 Ohsawa M, Narita M, Mizoguchi H, Suzuki T, Tseng LF. Involvement of spinal protein kinase C in thermal hyperalgesia evoked by partial sciatic nerve ligation, but not by inflammation in the mouse. Eur J Pharmacol. 2000;403:81–85.
9 Cervero F, Laird JM. Mechanisms of touch-evoked pain (allodynia): a new model. Pain. 1996;68:13–23.
10 Cline MA, Ochoa J, Torebjörk HE. Chronic hyperalgesia and skin warming caused by sensitized C nociceptors. Brain. 1989; 112:621–647.
11 Zhang X, Bao L, Shi TJ, Ju G, Elde R, Hökfelt T. Down-regulation of μ-opioid receptors in rat and monkey dorsal root ganglion neurons and spinal cord after peripheral axotomy. Neuroscience. 1998;82:223–240.
12 Bohn LM, Dykstra LA, Lefkowitz RJ, Caron MG, Barak LS. Relative opioid efficacy is determined by the complements of the G protein-coupled receptor desensitization machinery. Mol Pharmacol. 2004;66:106–112.
13 Breitkreutz D, Braiman-Wiksman L, Daum N, Denning MF, Tennenbaum T. Protein kinase C family: on the crossroads of cell signaling in skin and tumor epithelium. J Cancer Res Clin Oncol. 2007;133:793–808.
14 Bailey CP, Smith FL, Kelly E, Dewey WL, Henderson G. How important is protein kinase C in μ-opioid receptor desensitization and morphine tolerance? Trends Pharmacol Sci. 2006;27:558–565.

Neuroscience Letters 560 (2014) 122–125

Contents lists available at ScienceDirect

Neuroscience Letters

journal homepage: www.elsevier.com/locate/neulet

Differential alternation of the antinociceptive effect of narcotic analgesics on the inflammatory pain state

Yuta Aoki[a], Hirokazu Mizoguchi[a], Chizuko Watanabe[a], Tsukasa Sakurada[b], Shinobu Sakurada[a,*]

[a] Department of Physiology and Anatomy, Tohoku Pharmaceutical University, 4-4-1 Komatsushima, Aoba-ku, Sendai 981-8558, Japan
[b] First Department of Pharmacology, Daiichi College of Pharmaceutical Sciences, 22-1 Tamagawa-cho, Minami-ku, Fukuoka 815-8511, Japan

HIGHLIGHTS

- Mechanical allodynia is observed in adjuvant-induced inflammatory pain state.
- Antinociception of narcotic analgesics against mechanical allodynia was measured.
- Antinociception of fentanyl was reduced bilaterally in inflammatory pain state.
- Antinociception of oxycodone was reduced bilaterally in inflammatory pain state.
- Antinociception of methadone was reduced unilaterally in inflammatory pain state.

ARTICLE INFO

Article history:
Received 4 November 2013
Received in revised form 1 December 2013
Accepted 10 December 2013

Keywords:
Inflammatory pain
Narcotic analgesic
Antinociception
μ-Receptor
Mice

ABSTRACT

Antinociceptive effect of narcotic analgesics, fentanyl, oxycodone and methadone in inflammatory pain state was described in the von Frey filament test using the complete Freund's adjuvant (CFA)-induced mouse inflammatory pain model. After the i.pl. injection of CFA, mechanical allodynia (decrease of mechanical threshold) was observed in ipsilateral paw. The antinociceptive effect of fentanyl and oxycodone injected s.c. against mechanical allodynia in inflammatory pain state was reduced bilaterally at 1 day after CFA pretreatment. However, the antinociceptive effect of methadone injected s.c. against mechanical allodynia in inflammatory pain state was reduced unilaterally at 1 day after CFA pretreatment. Moreover, the reduction of the antinociceptive effect of methadone in ipsilateral paw on inflammatory pain state was smaller than those of fentanyl or oxycodone. In conclusion, the alternation of the antinociceptive effect of narcotic analgesics in inflammatory pain state is variable among the narcotic analgesics used.

© 2013 Elsevier Ireland Ltd. All rights reserved.

1. Introduction

The complete Freund's adjuvant (CFA), which is commonly used as antigen emulsified solution to produce antibody, is composed of mineral oil with inactivated and dried mycobacteria (usually M. tuberculosis). It stimulates cell-mediated immunity and potentiates the production of immunoglobulins as an immunopotentiator [1]. These reactions induced by CFA lead to the tissue inflammation in injected site. The intraplantar (i.pl.) administration of CFA to the mouse hind-paw results in a painful inflammation, which is used as the experimental model for inflammatory pain [2]. With a mechanical allodynia, thermal hyperalgesia and mechanical hyperalgesia as main symptoms of inflammatory pain along with edema, the CFA-induced inflammatory pain model is widely used for describing mechanisms of the inflammatory pain state and effectiveness of analgesics against the inflammatory pain. It is well established that antinociceptive effect of μ-opioid receptor agonists including morphine is enhanced or retained against the mechanical hyperalgesia [3,4] and thermal hyperalgesia [3] on the CFA-induced inflammatory pain model in rodents. However, most of studies describing the antinociceptive effect of μ-opioid receptor agonists in this inflammatory pain model are focused on their effectiveness against hyperalgesia, not against allodynia. We recently found that the antinociceptive effect of morphine was markedly suppressed bilaterally against the mechanical allodynia in this inflammatory pain model [5]. In the present study, using the CFA-induced inflammatory pain model in mice, we characterized the antinociceptive effect of other narcotic analgesics fentanyl, oxycodone and methadone against mechanical allodynia on the inflammatory pain state.

* Corresponding author. Tel.: +81 22 727 0124; fax: +81 22 727 0125.
E-mail address: s-sakura@tohoku-pharm.ac.jp (S. Sakurada).

0304-3940/$ – see front matter © 2013 Elsevier Ireland Ltd. All rights reserved.
http://dx.doi.org/10.1016/j.neulet.2013.12.020

2. Material and methods

All experiments were performed following the approval of the Ethics Committee for Animal Experiments at Tohoku Pharmaceutical University and according to the National Institutes of Health Guide for the Care and Use of Laboratory Animals. Every effort was made to minimize the number and any suffering of the animal used in the following experiments.

2.1. Animals

Male ddY mice (Japan SLC, Hamamatsu, Japan) weighing 20–24 g were used. Mice were housed in a room controlled a temperature (22–23 °C) and humidity (50–60%) with an alternating 12-h light/dark (turn on at 7:00 and off at 19:00) cycle. Food and water were available *ad libitum*.

2.2. Mouse model for inflammatory pain

To produce the inflammatory pain model, mice were injected i.pl. with 50 μl of CFA (Sigma-Aldrich, St. Louis, MO) in the left hind paw using a syringe with a 27-gauge needle. Control mice were injected i.pl. with sterile saline.

2.3. Measurement of mechanical allodynia and morphine analgesia

A mechanical allodynia and antinociceptive effect of narcotic analgesics were measured by von Frey filament test. Before the experiment, mice were placed on a clear plastic compartment (10 cm × 10 cm × 14 cm) for 1 h to habituate to the experimental environment. The presence of the withdrawal response (biting, licking or flinching) from the stimulation to the plantar surface of the hind paw by the variable strength of von Frey filament (applied pressure by each filament: 0.041, 0.073, 0.163, 0.400, 0.610, 1.000, 1.430, 2.100, and 4.200 g) within 3 s after the filament application was observed. The up-down method was used to evaluate the withdrawal threshold from the filament. The intensity of the application of the filament was adjusted so that the pre-drug threshold was 0.400 or 0.610 g. The mice showing threshold 0.073 or 0.163 g after the CFA injection were used as the inflammatory pain model mice.

2.4. Drugs

Fentanyl citrate, oxycodone hydrochloride and methadone hydrochloride (Mallinckrodt Pharmaceuticals, St. Louis, MO) were dissolved in the sterile saline.

2.5. Statistical analysis

The data are expressed as the means ± S.E.M for at least 10 mice. The statistical significance of differences between the groups was assessed with a two-way analysis of variance (ANOVA) followed by Bonferroni's test.

3. Results

3.1. CFA-induced mechanical allodynia

Groups of mice were injected i.pl. with 50 μl of saline or CFA in the left hind paw, and the withdrawal threshold against mechanical stimulation by von Frey filament to the plantar surface of the each hind paw was measured for 40 days. After the CFA injection, the decrease of mechanical threshold (mechanical allodynia) was observed in the ipsilateral paw, but not contralateral paw (data not shown). The mechanical allodynia in the ipsilateral paw in the CFA-treated mice piked at 1 day after the CFA treatment, and prolonged to 34 days after the CFA treatment. In contrast, the mechanical threshold was not altered in mice treated i.pl. with saline. Beside the mechanical allodynia, a strong edema (approximately 50% increase of the paw volume) on the ipsilateral paw was also apparent at 1 day after the CFA injection and retained for 97 days (data not shown).

3.2. Antinociceptive effect of narcotic analgesics in inflammatory pain state

The antinociceptive effect of narcotic analgesics injected subcutaneously (s.c.) in inflammatory pain state was described using a von Frey filament test. Groups of mice pretreated i.pl. with 50 μl of saline or CFA in the left hind paw, were injected s.c. with fentanyl (0.113 mg/kg), oxycodone (2.1 mg/kg) and methadone (2.8 mg/kg) at 1 day after the i.pl. pretreatment, and the withdrawal threshold against mechanical stimulation by von Frey filament to the plantar surface of the each hind paw was measured for 60 min, 90 min and 180 min, respectively. The potent increase of mechanical threshold (antinociceptive effect) by these narcotic analgesics was observed bilaterally in saline-pretreated mice (Figs. 1–3). The peak antinociceptive effect of these narcotic analgesics at the doses used is equipotent (approximately 3.1 g of Δ withdrawal threshold), and is nearly cut-off effect in this experimental paradigm. However, the antinociceptive effect of fentanyl and oxycodone was significantly suppressed bilaterally after the CFA pretreatment (Figs. 1 and 2). The more potent suppression of the antinociceptive effect of fentanyl and oxycodone was observed in the ipsilateral paw than in the contralateral paw. On the other hands, antinociceptive effect of methadone was significantly suppressed in only ipsilateral paw, but not altered in contralateral paw, after the CFA pretreatment (Fig. 3). Moreover, the reduction of the antinociceptive effect of methadone in ipsilateral paw on inflammatory pain state was smaller than those of fentanyl or oxycodone.

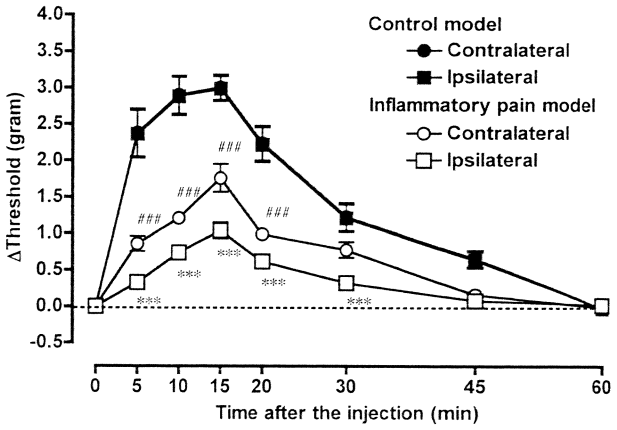


Fig. 1. The antinociceptive effect of fentanyl in the inflammatory pain state in mice. Groups of mice pretreated i.pl. with 50 μl of saline or CFA in the left hind paw, were injected s.c. with fentanyl (0.113 mg/kg) at 1 day after the i.pl. pretreatment, and the withdrawal threshold against mechanical stimulation by von Frey filament to the plantar surface of the each hind paw was measured for 60 min. Each value represents the means ± S.E.M. for at least 10 mice. The statistical significance of the differences between the groups was assessed with a two-way ANOVA followed by Bonferroni's test. The F values of the two-way ANOVA for ipsilateral paw and contralateral paw were $F[1,144] = 237.1$ ($P < 0.001$) and $F[1,144] = 114.2$ ($P < 0.001$). $^{***}P < 0.001$ vs. ipsilateral paw of control model (saline-i.pl. pretreated) mice. $^{###}P < 0.001$ vs. contralateral paw of control model (saline-i.pl. pretreated) mice.

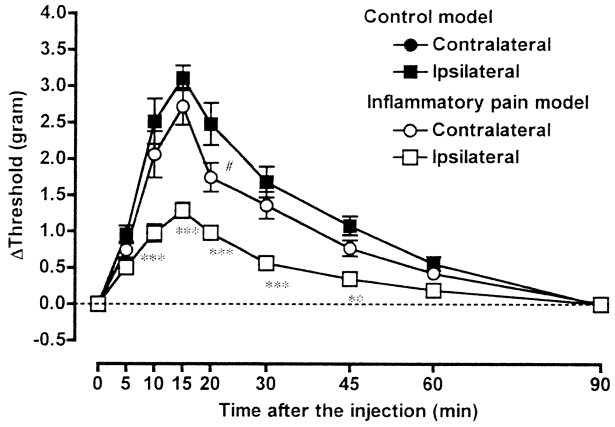


Fig. 2. The antinociceptive effect of oxycodone in the inflammatory pain state in mice. Groups of mice pretreated i.pl. with 50 μl of saline or CFA in the left hind paw, were injected s.c. with oxycodone (2.1 mg/kg) at 1 day after the i.pl. pretreatment, and the withdrawal threshold against mechanical stimulation by von Frey filament to the plantar surface of the each hind paw was measured for 90 min. Each value represents the means ± S.E.M. for at least 10 mice. The statistical significance of the differences between the groups was assessed with a two-way ANOVA followed by Bonferroni's test. The F values of the two-way ANOVA for ipsilateral paw and contralateral paw were $F[1,162] = 162.1$ ($P < 0.001$) and $F[1,162] = 11.22$ ($P < 0.01$). $^{**}P < 0.01$, $^{***}P < 0.001$ vs. ipsilateral paw of control model (saline-i.pl. pretreated) mice. $^{\#}P < 0.05$ vs. contralateral paw of control model (saline-i.pl. pretreated) mice.

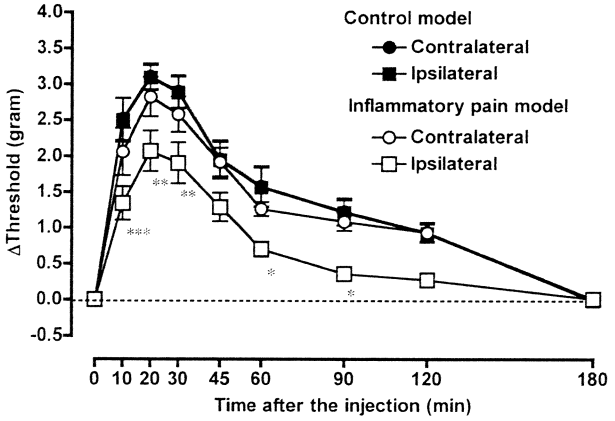


Fig. 3. The antinociceptive effect of methadone in the inflammatory pain state in mice. Groups of mice pretreated i.pl. with 50 μl of saline or CFA in the left hind paw, were injected s.c. with methadone (2.8 mg/kg) at 1 day after the i.pl. pretreatment, and the withdrawal threshold against mechanical stimulation by von Frey filament to the plantar surface of the each hind paw was measured for 180 min. Each value represents the means ± S.E.M. for at least 10 mice. The statistical significance of the differences between the groups was assessed with a two-way ANOVA followed by Bonferroni's test. The F values of the two-way ANOVA for ipsilateral paw and contralateral paw were $F[1,162] = 59.28$ ($P < 0.001$) and $F[1,162] = 3.387$ ($P = 0.0676$). $^{*}P < 0.05$, $^{**}P < 0.01$, $^{***}P < 0.001$ vs. ipsilateral paw of control model (saline-i.pl. pretreated) mice.

4. Discussion

It is well established that the antinociceptive effect of morphine against thermal hyperalgesia and mechanical hyperalgesia is enhanced or retained in the CFA-induced inflammatory pain state [3,4]. However, we recently reported that the antinociceptive effect of morphine injected s.c. or intrathecally against mechanical allodynia was significantly suppressed in CFA-induced inflammatory pain state [5]. It has been considered that the allodynia is mainly mediated through Aβ fibers of primary afferent nerves [6], whereas the hyperalgesia is mainly mediated through C fibers of primary afferent nerves [7]. The discrepancy on morphine antinociception between hyperalgesia and allodynia in CFA-induced inflammatory pain state may relate to the neurons each pain sensation is going through.

In the present study, the antinociceptive effect of fentanyl and oxycodone given s.c. against mechanical allodynia in the CFA-induced inflammatory pain state was suppressed on contralateral paw as well as on ipsilateral paw. We recently found that the antinociceptive effect of morphine given s.c. against mechanical allodynia in the CFA-induced inflammatory pain state was also suppressed bilaterally, and suggested that the suppression of the antinociceptive effect of morphine on ipsilateral paw in the inflammatory pain state was mainly revealed by the down-regulation of spinal μ-opioid receptors, whereas the suppression of the antinociceptive effect of morphine on contralateral paw in the inflammatory pain state was mainly caused by the inactivation of spinal μ-opioid receptors by phosphorylation [5]. The mechanisms underlying the bilateral reduction of morphine antinociception against mechanical allodynia in the CFA-induced inflammatory pain state may also be involved in the bilateral reduction of the antinociceptive effect of fentanyl and oxycodone against mechanical allodynia in the CFA-induced inflammatory pain state that is observed in the present study.

In contrast to fentanyl and oxycodone, the antinociceptive effect of methadone against mechanical allodynia in the CFA-induced inflammatory pain state was significantly suppressed in only ipsilateral paw, but not in contralateral paw. Moreover, the reduction of antinociceptive effect of methadone in ipsilateral paw was smaller than those of fentanyl or oxycodone. Methadone is composed to *l*-methadone that has agonistic activity for μ-opioid receptors and to *d*-methadone that has antagonistic activity for NMDA receptors [8]. It has been well established that the activation of NMDA receptors causes the phosphorylation of μ-opioid receptors co-localized, which results in the desensitization of μ-opioid receptors [9]. Conversely, the blockade of NMDA receptors by antagonist prevents the development of antinociceptive tolerance to μ-opioid receptor agonist [10]. The less suppression of methadone antinociception against mechanical allodynia in inflammatory pain state may be caused by the blockade of NMDA receptors.

5. Conclusion

In conclusion, like morphine, the antinociceptive effect of fentanyl and oxycodone was markedly suppressed bilaterally against mechanical allodynia on inflammatory pain state. On the other hand, antinociceptive effect of methadone was suppressed in only ipsilateral side, but not contralateral side. The alternation of the antinociceptive effect of narcotic analgesics in inflammatory pain state is variable among the narcotic analgesics used.

Acknowledgment

This work was supported by JSPS KAKENHI Grant Numbers 22600009 and 24590731, and a MEXT (Ministry of Education, Culture, Sports, Science and Technology)-Supported Program for the Strategic Research Foundation at Private Universities (2010–2014).

References

[1] S.M. Helfgott, R.I. Kieval, F.C. Breedveld, E. Brahn, C.T. Young, R. Dynesius-Trentham, D.E. Trentham, Detection of arthritogenic factor in adjuvant arthritis, J. Immunol. 140 (1988) 1838–1843.
[2] M. Ohsawa, M. Narita, H. Mizoguchi, T. Suzuki, L.F. Tseng, Involvement of spinal protein kinase C in thermal hyperalgesia evoked by partial sciatic nerve ligation, but not by inflammation in the mouse, Eur. J. Pharmacol. 403 (2000) 81–85.
[3] V. Fernández-Dueñas, O. Pol, P. García-Nogales, L. Hernández, E. Planas, M.M. Puig, Tolerance to the antinociceptive and antiexudative effects of morphine in

a murine model of peripheral inflammation, J. Pharmacol. Exp. Ther. 322 (2007) 360–368.
[4] R. Maldonado, O. Valverde, S. Turcaud, M.C. Fournié-Zaluski, B.P. Roques, Antinociceptive response induced by mixed inhibitors of enkephalin catabolism in peripheral inflammation, Pain 58 (1994) 77–83.
[5] Y. Aoki, H. Mizoguchi, C. Watanabe, A. Yonezawa, S. Sakurada, Involvement of phosphorylation of μ-opioid receptors on the bilateral reduction of morphine analgesia in inflammatory pain state, J. Pharmacol. Sci. 121 (Supp. 1) (2013) 60P.
[6] F. Cervero, J.M. Laird, Mechanisms of touch-evoked pain (allodynia): a new model, Pain 68 (1996) 13–23.
[7] M.A. Cline, J. Ochoa, H.E. Torebjörk, Chronic hyperalgesia and skin warming caused by sensitized C nociceptors, Brain 112 (1989) 621–647.
[8] C.E. Inturrisi, Pharmacology of methadone and its isomers, Minerva Anestesiol. 71 (2005) 435–437.
[9] P. Sánchez-Blázquez, M. Rodríguez-Muñoz, E. Berrocoso, J. Garzón, The plasticity of the association between μ-opioid receptor and glutamate ionotropic receptor N in opioid analgesic tolerance and neuropathic pain, Eur. J. Pharmacol. 716 (2013) 94–105.
[10] J. Mao, D.D. Price, J. Lu, D.J. Mayer, Antinociceptive tolerance to the μ-opioid agonist DAMGO is dose-dependently reduced by MK-801 in rats, Neurosci. Lett. 250 (1998) 193–196.

Original Paper

International Archives of Allergy and Immunology

Int Arch Allergy Immunol 2014;163:297–306
DOI: 10.1159/000360577

Received: June 14, 2013
Accepted after revision: February 12, 2014
Published online: April 26, 2014

The Involvement of Glucocorticoids in Psychological Stress-Induced Exacerbations of Experimental Allergic Asthma

Kaori Okuyama[a] Kazuhisa Dobashi[a] Tomomitsu Miyasaka[a] Naoki Yamazaki[a]
Toshiaki Kikuchi[b] Ichiro Sora[c] Motoaki Takayanagi[a] Hirohito Kita[d] Isao Ohno[a]

[a]Department of Pathophysiology, Tohoku Pharmaceutical University and Departments of [b]Respiratory Medicine and [c]Biological Psychiatry, Tohoku University Graduate School of Medicine, Sendai, Japan; [d]Division of Allergic Diseases, Department of Internal Medicine, Mayo Clinic, Rochester, Minn., USA

Key Words
Asthma exacerbation · Psychological stress · Allergic airway inflammation · Glucocorticoids

Abstract
Background: Psychological stress is associated with the aggravation of asthma symptoms. Glucocorticoids (GC), which are stress hormones released upon exposure to stress, have the potential to shift immune responses towards a predominant Th2 response by priming antigen-presenting cells to produce lower levels of IL-12 as well as reducing the development of regulatory T cells. However, the involvement of GC in psychological stress-induced exacerbations of allergic asthma has not yet been clarified. ***Methods:*** Sensitized mice were exposed to restraint stress followed by forced swimming stress, during which a GC receptor antagonist or a GC synthesis inhibitor was administered, and then antigen was inhaled. Corticosterone levels in the blood were measured in stressed and nonstressed mice. After antigen inhalation, the airway responses to aerosolized methacholine, epithelial mucus secretion and airway inflammation were evaluated, and the IL-13 contents in bronchoalveolar lavage fluid were measured. ***Results:*** The exposure to stress significantly increased corticosterone levels. Allergic airway responses and the increase of IL-13 contents evoked by antigen inhalation were significantly higher in stressed mice than in nonstressed mice. The administration of a GC receptor antagonist and a GC synthesis inhibitor during stress exposure significantly reduced the exacerbation of the airway responses and the increase of IL-13 contents in stressed mice challenged with antigen. ***Conclusions:*** These results indicate that the increased release of GC upon exposure to stress has a priming effect on the aggravation of allergic airway responses following the exposure, suggesting a pathophysiological role for the neuroendocrine axis in linking psychological stress to asthma exacerbations.

© 2014 S. Karger AG, Basel

Introduction

Bronchial asthma is a chronic inflammatory airway disease characterized by a complex interplay between inflammatory cells including eosinophils, mast cells, basophils, dendritic cells and lymphocytes, and structural cells such as epithelial cells, fibroblasts and smooth muscle cells. Inflammatory mediators released from these cells following stimulation such as arachidonic acid metabolites, reactive oxygen species, cytokines and chemokines, induce the narrowing and remodeling of the airways and airway hyperresponsiveness that are cardinal features of

KARGER

E-Mail karger@karger.com
www.karger.com/iaa

© 2014 S. Karger AG, Basel
1018–2438/14/1634–0297$39.50/0

Correspondence to: Prof. Dr. med. Isao Ohno
Department of Pathophysiology, Tohoku Pharmaceutical University
4-4-1 Komatsushima, Aoba-ku
Sendai 981-8558 (Japan)
E-Mail iohno@tohoku-pharm.ac.jp

asthma. Type 2 T helper (Th2) cells and Th2 cytokines such as interleukin (IL)-4, IL-5 and IL-13 play a central role in regulating the behavior of inflammatory cells in asthmatic airways. It has been proposed that interferon-γ-producing Th1 cells inhibit the development of allergic diseases by counterbalancing the proliferation and development of Th2 cells in some stages of inflammation [1–4]. $CD4^+CD25^+$ regulatory T (Treg) cells play a critical role in the balance of the immune network by suppressing or limiting effector immune responses against internal and external insults. Recent studies have demonstrated that the failure of Treg cells to suppress Th2-mediated immune responses to innocuous inhaled antigens leads to an inappropriate balance between Treg cells and effector Th2 responses following allergen activation, resulting in the development and maintenance of asthmatic airway inflammation characterized by uncontrolled Th2-biased immune responses [5–7].

A number of clinical studies have demonstrated an association between psychological stress and the aggravation of asthma symptoms [8, 9]. For example, 20–35% of asthmatics experience an exacerbation of their symptoms during periods of stress [10]. Chronic exposure to high levels of psychosocial stress has been shown to increase the risk of asthma attacks in childhood [11, 12] and adult [13, 14] asthma. It has become increasingly apparent that psychological stress increases the frequency, duration and severity of asthmatics' symptoms by enhancing airway inflammatory responses, characterized by further skewing towards a Th2-dominant cytokine profile [15, 16]. Students with asthma showed an increase in eosinophil counts and IL-5 levels in sputum, enhanced production of Th2 cytokines and reduced production of Th1 cytokines by peripheral blood mononuclear cells during exam periods compared with nonexam periods [17, 18]. Lower socioeconomic status and more stressful life events have been associated with higher levels of Th2 cytokine production and higher eosinophil counts in peripheral blood [19–21]. In addition, the involvement of central nervous system activation in stress-induced asthma exacerbation has been demonstrated using functional magnetic resonance imaging [22]. In animal models of asthma, various types of psychological stress including electric foot shock stress (FS), sound stress, restraint stress (RS) and forced swimming stress (FSS) have been shown to exacerbate allergen-induced airway inflammation [23–25]. However, the precise mechanisms by which psychological stress aggravates Th2 immune responses have still to be clarified.

Recently, we demonstrated that RS was associated with the increased secretion of GC and leads to increased airway inflammation measured by inflammatory cell accumulation and Th2 cytokine expression, following allergen inhalation subsequent to stress in a murine model of allergic asthma [25]. In addition, a Th2 cytokine profile was predominant, and the development of Treg cells was reduced in cultures of draining lymph node cells from stressed mice when compared with nonstressed mice [26]. Therefore, we hypothesized that an increased release of GC during stress periods led to the exacerbation of allergic airway responses in association with the aggravation of Th2 immune responses to inhaled antigen immediately subsequent to stress exposure. To address this hypothesis, we examined the effects of a GC receptor antagonist and a GC synthesis inhibitor on stress-induced exacerbations of asthmatic responses to inhaled antigen in our stress asthma model.

Materials and Methods

Animals

Specific pathogen-free female and male C57BL/6 (B6) mice were purchased from CLEA Japan (Osaka, Japan). Male mice were used only in experiments for figure 8. Animals were housed under a 12-hour light/dark cycle at a constant temperature (22 ± 2°C). Sterilized food and water were available ad libitum. All experiments described below were approved by and conformed to the guidelines of the Committee of Animal Experiments at Tohoku Pharmaceutical University.

Protocols for Sensitization, Challenge and Stress Exposure

Mice (6–8 weeks old) were sensitized and were made to inhale antigen as previously described [25]. Briefly, they were sensitized by i.p. injection of ovalbumin (OVA; Grade V, Sigma, St. Louis, Mo., USA; 8 μg/mouse) adsorbed with aluminum hydroxide (Wako Pure Chemical Industries, Osaka, Japan) on days 0 and 5. On days 17 and 24, mice were challenged with aerosolized OVA for 1 h. For RS, each mouse was placed in a 50-ml conical centrifuge tube with multiple ventilation holes for 6 h per day [25]. For FSS, each mouse was forced to swim in a plastic tank containing 20 cm of deep water (32°C) for 3 min/day [24]. After each swim, the mice were immediately removed from the tank, dried with a towel and returned to their home cages. The RS and FSS are generally regarded as inducing psychological stress in the animal [24, 25]. On day 17, the stressed mice in the 50-ml conical centrifuge tubes were left in plastic chambers for 6 h. For the first hour, OVA flowed through the chambers so that the mice were exposed to it. These stressed mice were further subjected to the RS on 2 consecutive days, i.e. days 18 and 19 (at the same time each day). To avoid habituation to RS, they were then exposed to FSS on 4 consecutive days, i.e. days 20–23 (at the same time each day). Nonstressed mice were deprived of food and water (but were not otherwise stressed) for the same period of time as the stressed mice were exposed to the stress conditions. Deprivation of food and water has been used as a nonstress condition in other rodent experiments that have investigated the effect of stress [27, 28]. Before and immediately after

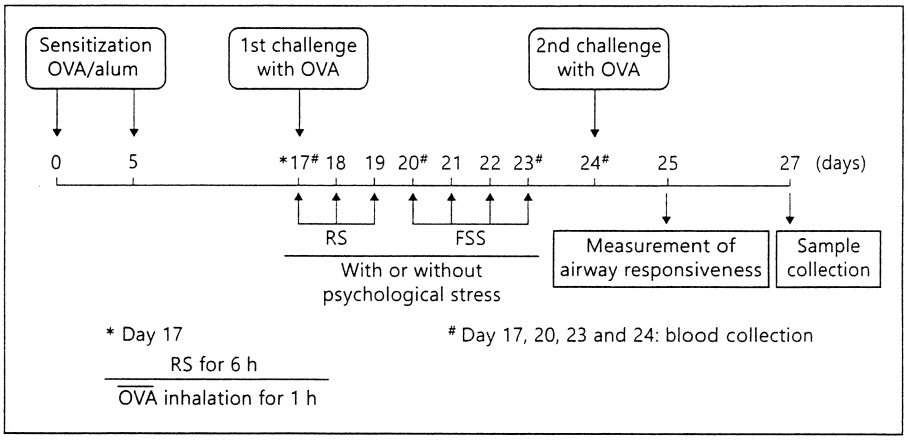


Fig. 1. Diagrammatic representation of the protocols for sensitization, challenge and stress exposure.

the RS on day 17, immediately after the FSS on days 20 and 23 and immediately after the second OVA challenge on day 24, blood samples were taken from the mice as previously described [25]. Blood was collected from the nonstressed mice using the same method. Plasma samples separated from the isolated blood were stored at –80°C until corticosterone concentration measurements were made by enzyme immunoassay. On day 24, the nonstressed and stressed mice were left in plastic chambers for 1 h, during which OVA flowed through the chambers and the mice were exposed to it. In some experiments, dexamethasone (1.25, 2.5 and 5 mg/kg body weight in 0.5 ml calcium- and magnesium-free PBS/mouse; Sigma) or solvent alone (0.5 ml/mouse) was i.p. injected 3 times at 24-hour intervals, beginning 2 h before the OVA exposure on day 24. On day 25, airway responsiveness was measured as described below. On day 27, bronchoalveolar lavage (BAL) fluids and lung tissues were collected as previously described [29]. Lung tissues were processed as described below. BAL fluids were processed to count the total cells, examine the cell differentials and measure the cytokine content (fig. 1). In experiments using the GC receptor antagonist, mifepristone (RU-486; Sigma) in polyethylene glycol 400 (Fluka, Buchs, Switzerland) was subcutaneously administered 1 h before each stress exposure at the dose indicated. In experiments using the GC synthesis inhibitor, metyrapone (Enzo Life Sciences, Plymouth Meeting, Pa., USA) dissolved in calcium- and magnesium-free PBS was i.p. administered 1.5 h before each stress at the dose indicated. The solvents of RU-486 and metyrapone were used as controls for these agents.

Corticosterone Measurement

The corticosterone content in plasma was measured using an enzyme immunoassay kit (Assay Designs Inc., Ann Arbor, Mich., USA) according to the manufacturer's protocol. The limit of detection was 32 pg/ml of corticosterone.

Measurement of Airway Responsiveness

Mice were anesthetized using an i.p. injection of a mixture of xylazine (Bayer Healthcare, Brussels, Belgium) and pentobarbital sodium (Schering-Plough Animal Health Co, Kenilworth, N.J., USA), and their tracheas were cannulated via tracheostomy. The mice were then placed in a whole-body plethysmograph chamber (Buxco Electronics, Troy, N.Y., USA) and mechanically ventilated at a tidal volume of 0.2 ml and a frequency of 150 breaths/min. Lung resistance (R_L) at baseline, in response to aerosolized saline and in response to increasing doses (1.25–20 mg/ml) of aerosolized acetyl β-methylcholine chloride (methacholine; Sigma) was measured for 3 min under each condition [30]. To measure airway reactivity, the highest values of R_L obtained after each dose of methacholine were identified and expressed as a percentage of their respective basal value. To measure airway sensitivity, the concentration of methacholine needed to increase R_L to 200% above baseline (PC_{200}) was also calculated by interpolating the log concentration-lung resistance curve from individual animals.

Lung Histology

Lung tissues were fixed with 10% buffered formaldehyde and embedded in paraffin. Sections (4-μm thick) were stained with periodic acid Schiff (PAS) and counter-stained with hematoxylin for the evaluation of mucus-containing goblet cells in the bronchial epithelium [29]. Levels of airway mucus expression were quantified by counting the total number of PAS-positive and PAS-negative cells in the airway epithelium of random bronchioles in lung sections from each mouse. Slides were examined in a blinded fashion. The percentage of PAS-positive cells was calculated in each of 3 random bronchioles in two lung sections from each mouse, and the results were expressed as the mean percentage of PAS-positive cells per bronchiole. To count the tissue eosinophils, 4-μm-thick sections were stained with hematoxylin and eosin. Eosinophils in the peribronchial area were counted and expressed as the number in 1 mm^2 along the epithelial basement membrane [31].

Cytokine Measurements

The IL-13 concentrations in the BAL fluids were measured using ELISA kits (R&D systems, Minneapolis, Minn., USA) according to the manufacturer's protocol. The limit of detection was 1.5 pg/ml.

Statistical Analysis

Data are expressed as the mean ± SEM. The n values are from multiple independent experiments with 2–4 mice. An unpaired t test was used to determine differences between the 2 groups. For comparisons between multiple groups, a 1-way analysis of variance followed by Bonferroni's correction was performed. These analyses were performed using Prism4 (GraphPad Software, San Diego, Calif., USA). $p < 0.05$ was considered significant.

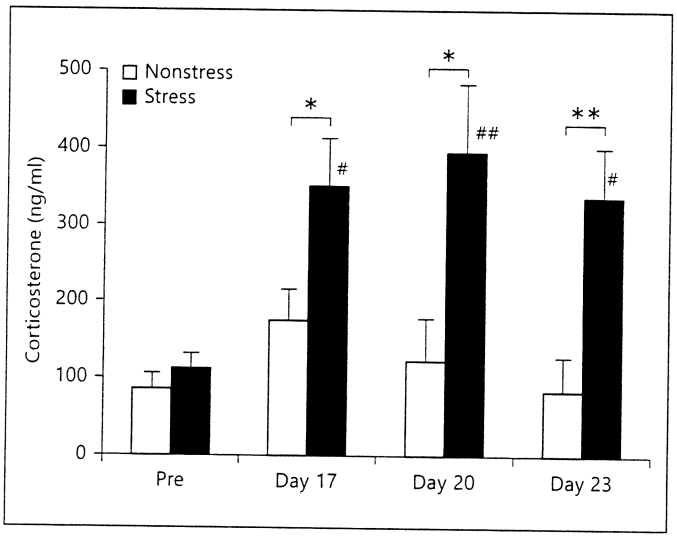


Fig. 2. The effect of psychological stress on plasma corticosterone concentrations. Blood was collected from stressed and nonstressed mice before the 1st stress (Pre) and after the 1st (Day 17), 4th (Day 20) and 7th (Day 23) stress exposures, and the corticosterone levels in plasma were measured by enzyme immunoassay. Data are expressed as the means ± SEM (n = 4–8 from 4 independent experiments). # $p < 0.05$ and ## $p < 0.01$ compared with pre-stress time point. * $p < 0.05$ and ** $p < 0.01$ compared with nonstressed mice on the same day.

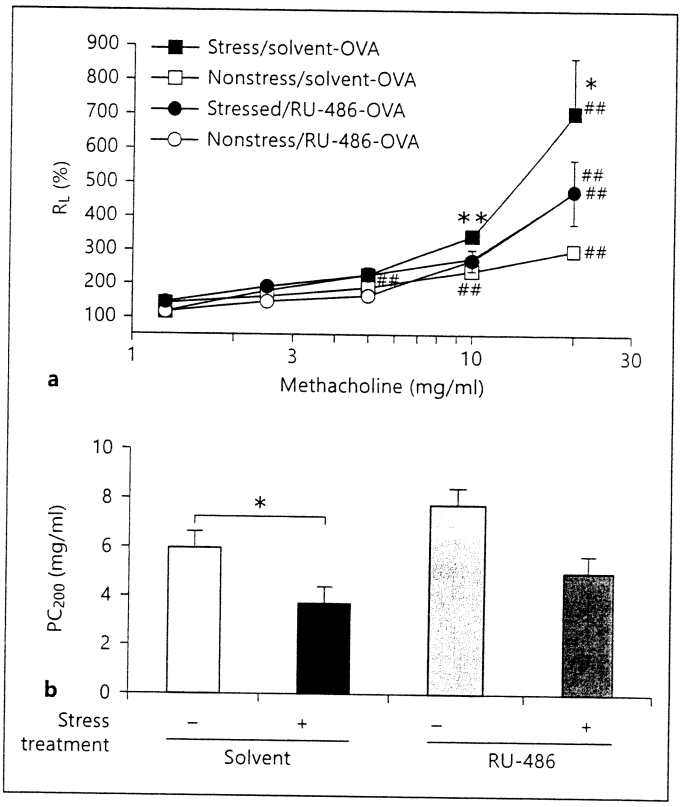


Fig. 3. The effect of a GC receptor antagonist on methacholine-induced hyperresponsiveness. RU-486 (6.25 mg/kg, s.c.), a GC receptor antagonist or solvent was administered before each stress exposure. Airway reactivity (**a**) and airway sensitivity (**b**) were measured as described in Materials and Methods. Data are expressed as the means ± SEM (n = 6–8 from 4 independent experiments). # $p < 0.05$ and ## $p < 0.01$ compared with before methacholine inhalation. * $p < 0.05$ and ** $p < 0.01$ compared with nonstressed mice with solvent.

Results

The Effect of Psychological Stress on Plasma Corticosterone Concentration

The corticosterone concentrations in stressed mice were significantly higher than those in nonstressed mice after the 1st, 4th and 7th stress exposure on days 17, 20 and 23, respectively (1st: 351.3 ± 61.4 (n = 8) vs. 174.7 ± 40.7 (n = 6) ng/ml, $p < 0.05$; 4th: 395.1 ± 88.3 (n = 8) vs. 122.3 ± 55.7 (n = 6) ng/ml, $p < 0.05$; 7th: 336.9 ± 63.9 (n = 8) vs. 83.6 ± 44.0 (n = 6) ng/ml, $p < 0.01$). Before the exposure to stress, there had been no significant difference in corticosterone concentrations between the stressed and the nonstressed mice. Furthermore, the concentrations following stress at any of the measured time points were significantly higher than those before stress exposure in the stressed mice, while no such increases were observed in the nonstressed mice (fig. 2). The concentrations following stress were also not significantly different between the time points measured. No significant differences were observed in the concentrations after the second OVA challenge (day 24) between stressed (245.3 ± 16.7 ng/ml; n = 6) and nonstressed (209.7 ± 10.0 ng/ml; n = 6) mice.

Effects of a GC Receptor Antagonist on Stress-Induced Exacerbations of Airway Responses and Airway Mucus Secretion

In all groups, R_L(%) increased dose-dependently in response to inhaled methacholine. Furthermore, R_L(%) in the solvent-treated stressed mice (n = 7) was significantly higher than that in solvent-treated nonstressed mice (n = 7) at 10 mg/ml (338.5 ± 19.5 vs. 239.0 ± 10.6%, $p < 0.01$) and 30 mg/ml (707.2 ± 157.1 vs. 299.9 ± 23.5%, $p < 0.05$) of methacholine (fig. 3a). Similarly, PC_{200} in the solvent-treated stressed mice was significantly lower than in the solvent-treated nonstressed mice (3.7 ± 0.6 vs. 6.0 ± 0.7 mg/ml, $p < 0.05$; fig. 3b). There were trends towards a decrease in R_L(%) (fig. 3a) and an increase in PC_{200} (fig. 3b) in the RU-486-treated stressed mice compared to the solvent-treated stressed mice, but these dif-

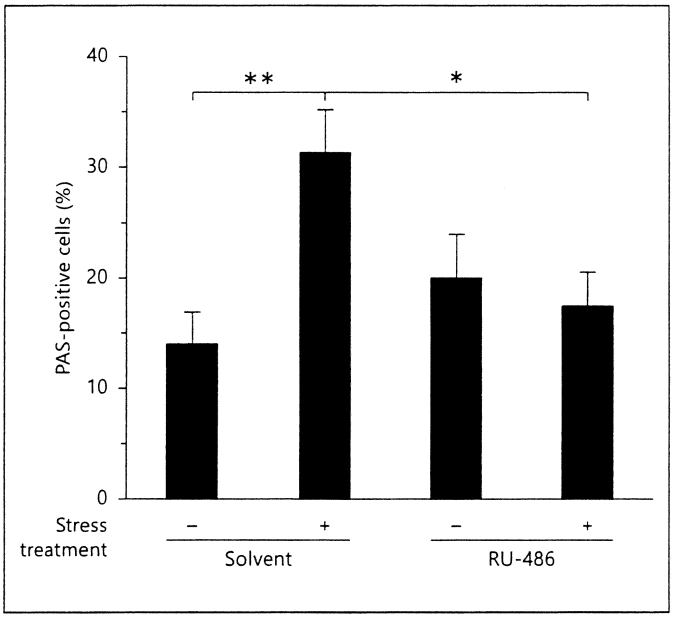


Fig. 4. The effect of a GC receptor antagonist on airway mucus expression. RU-486 (6.25 mg/kg, s.c.) or solvent was administered before each stress exposure. The percentage of PAS-positive cells was measured as described in Materials and Methods. Data are expressed as the means ± SEM (n = 11–12 from 4 independent experiments). * $p < 0.05$ and ** $p < 0.01$.

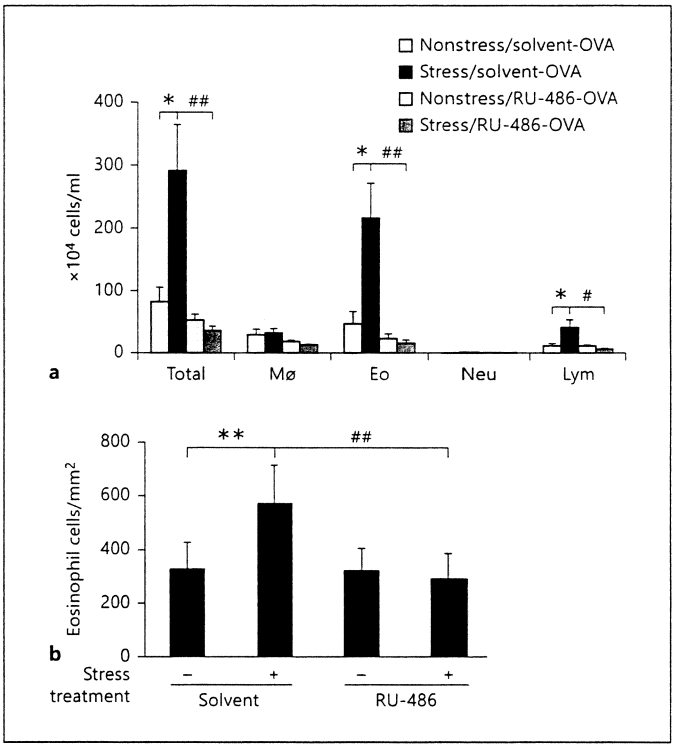


Fig. 5. The effect of a GC receptor antagonist on lung inflammation after OVA challenge. RU-486 (6.25 mg/kg, s.c.) or solvent was administered before each stress exposure. The numbers of total cells (total), macrophages (Mø), eosinophils (Eo), neutrophils (Neu) and lymphocytes (Lym) in the BAL fluid (**a**) and the number of eosinophils in lung tissues (**b**) from stressed and nonstressed mice 3 days after the second OVA challenge were counted. Data are expressed as the means ± SEM (n = 6–10 from 4 independent experiments). * $p < 0.05$ and ** $p < 0.01$ compared with nonstressed mice with solvent. # $p < 0.05$ and ## $p < 0.01$ compared with stressed mice with solvent.

ferences were not significant. The number of PAS-positive cells was significantly higher in the solvent-treated stressed mice than in the solvent-treated nonstressed mice, whereas in RU-486-treated stressed and nonstressed mice, this cell count was similar. The treatment with RU-486 significantly decreased the number of PAS-positive cells compared to the treatment with solvent in the stressed mice, but not in the nonstressed mice (fig. 4). These findings suggest that RU-486 indeed inhibited the exacerbation of airway mucus secretion caused by stress exposure.

Effects of a GC Receptor Antagonist on Stress-Induced Exacerbations of Lung Inflammation

The numbers of total cells, eosinophils and lymphocytes in BAL fluid from the stressed mice treated with solvent (n = 9) were significantly reduced following the treatment with RU-486 (n = 8): 291.2 ± 73.3 vs. 35.7 ± 7.2 × 10^4 cells/ml, $p < 0.01$ (total cells); 216.4 ± 55.4 vs. 15.6 ± 5.3 × 10^4 cells/ml, $p < 0.01$ (eosinophils); 41.2 ± 12.1 vs. 6.3 ± 1.5 × 10^4 cells/ml, $p < 0.05$ (lymphocytes). With regard to the number of inflammatory cells, no significant differences were observed between stressed and nonstressed mice treated with RU-486 or between nonstressed mice treated with solvent and those treated with RU-486 (fig. 5a). The increased number of tissue eosinophils in the stressed mice treated with solvent was significantly reduced by the treatment with RU-486 (fig. 5b). These results indicate that RU-486 inhibited the increased influx of inflammatory cells caused by stress exposure. In addition, treatment with metyrapone, which is a GC synthesis inhibitor, also abolished the increase in the numbers of inflammatory cells in BAL fluid caused by stress [solvent (n = 7) vs. metyrapone (n = 9): 105.1 ± 17.2 vs. 65.2 ± 8.8 × 10^4 cells/ml, $p < 0.05$ (total cells) and 76.1 ± 14.4 vs. 42.3 ± 7.8 × 10^4 cells/ml, $p < 0.05$ (eosinophils); fig. 6]. The increase in IL-13 in BAL fluid caused by stress was abolished by treatment with RU-486 [solvent (n = 9) vs. RU-486 (n = 9): 23.8 ± 3.4 vs. 9.8 ± 1.3 pg/ml, $p < 0.01$; fig. 7].

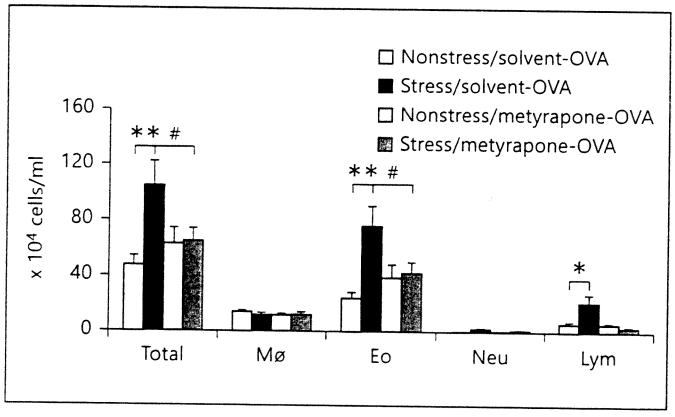


Fig. 6. The effect of a GC synthesis inhibitor on cell number in the BAL fluid after OVA challenge. The GC synthesis inhibitor metyrapone (50 mg/kg, i.p.) or solvent was administered before each stress exposure. The numbers of total cells (total), macrophages (Mø), eosinophils (Eo), neutrophils (Neu) and lymphocytes (Lym) in the BAL fluid from stressed and nonstressed mice 3 days after the second OVA challenge were counted. Data are expressed as the means ± SEM (n = 6–10 from 4 independent experiments). * $p < 0.05$ and ** $p < 0.01$ compared with nonstressed mice with solvent. # $p < 0.05$ compared with stressed mice with solvent.

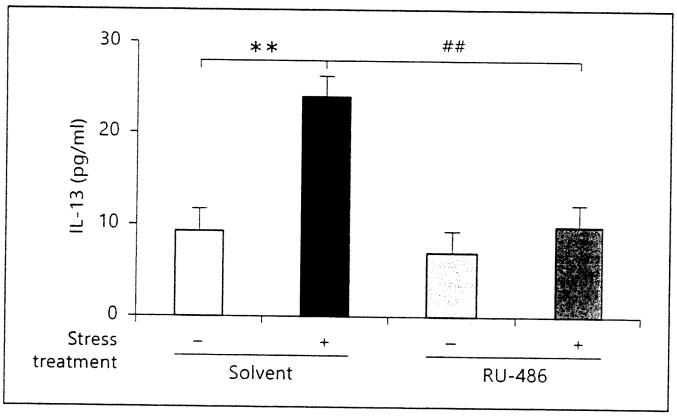


Fig. 7. The effect of a GC receptor antagonist on the IL-13 levels in the BAL fluid. RU-486 (6.25 mg/kg, s.c.) or solvent was administered before each stress exposure. The BAL fluids were obtained from stressed and nonstressed mice 3 days after the second OVA challenge. The levels of IL-13 were measured as described in Materials and Methods. Data are expressed as the means ± SEM (n = 6–10 from 3 independent experiments). ** $p < 0.01$ compared with nonstressed mice with solvent. ## $p < 0.01$ compared with stressed mice with solvent.

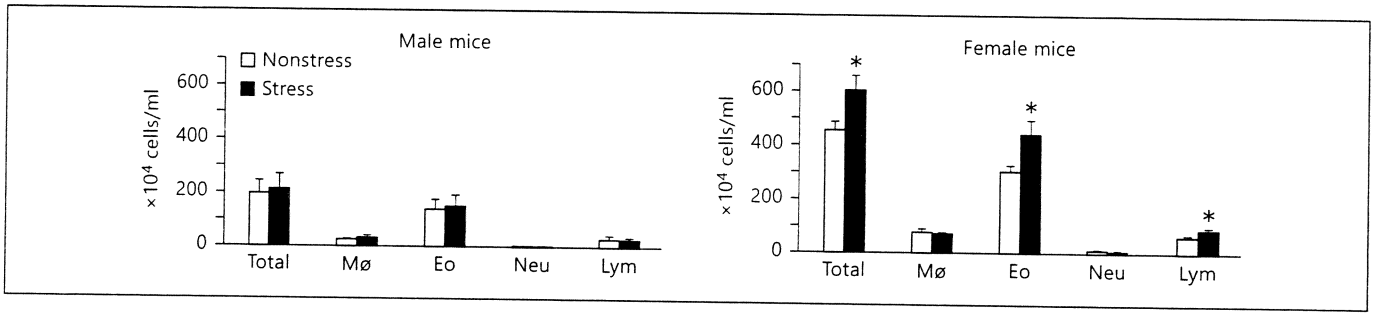


Fig. 8. Sex differences in stress-induced exacerbations of allergic airway inflammation. In male and female mice, the numbers of total cells (total), macrophages (Mø), eosinophils (Eo), neutrophils (Neu) and lymphocytes (Lym) in the BAL fluid from stressed and nonstressed mice 3 days after the second OVA challenge were counted. Data are expressed as the means ± SEM (n = 6–9 from 2 independent experiments). * $p < 0.05$ compared with non-stressed mice.

Sex Differences in Stress-Induced Exacerbations of Allergic Airway Inflammation

Our findings with RU-486 and metyrapone suggested that corticosterone that is released upon exposure to stress could play a critical role in the exacerbation of allergic airway responses subsequent to the stress exposure. Corticosterone release in response to stress exposure has been shown to be higher in female B6 and BALB/c mice than in males [32]. Therefore, we compared the effects of stress exposure on allergic airway inflammation in the females and the males. Stress exposure increased the numbers of total cells, eosinophils and lymphocytes in the BAL fluid in the females but not in the males (fig. 8). The sex differences in allergic airway inflammation in nonstressed mice were also observed as reported previously [31].

Effects of Exogenous GC on Airway Inflammation Caused by the Second OVA Challenge

To examine whether stress-induced exacerbations of allergic airway responses were due to the hyporesponsiveness to anti-inflammatory effects of GC, we examined the effects of exogenous GC on the worsening of airway inflammation evoked by the second antigen challenge subsequent to exposure to stress. The administration of dexa-

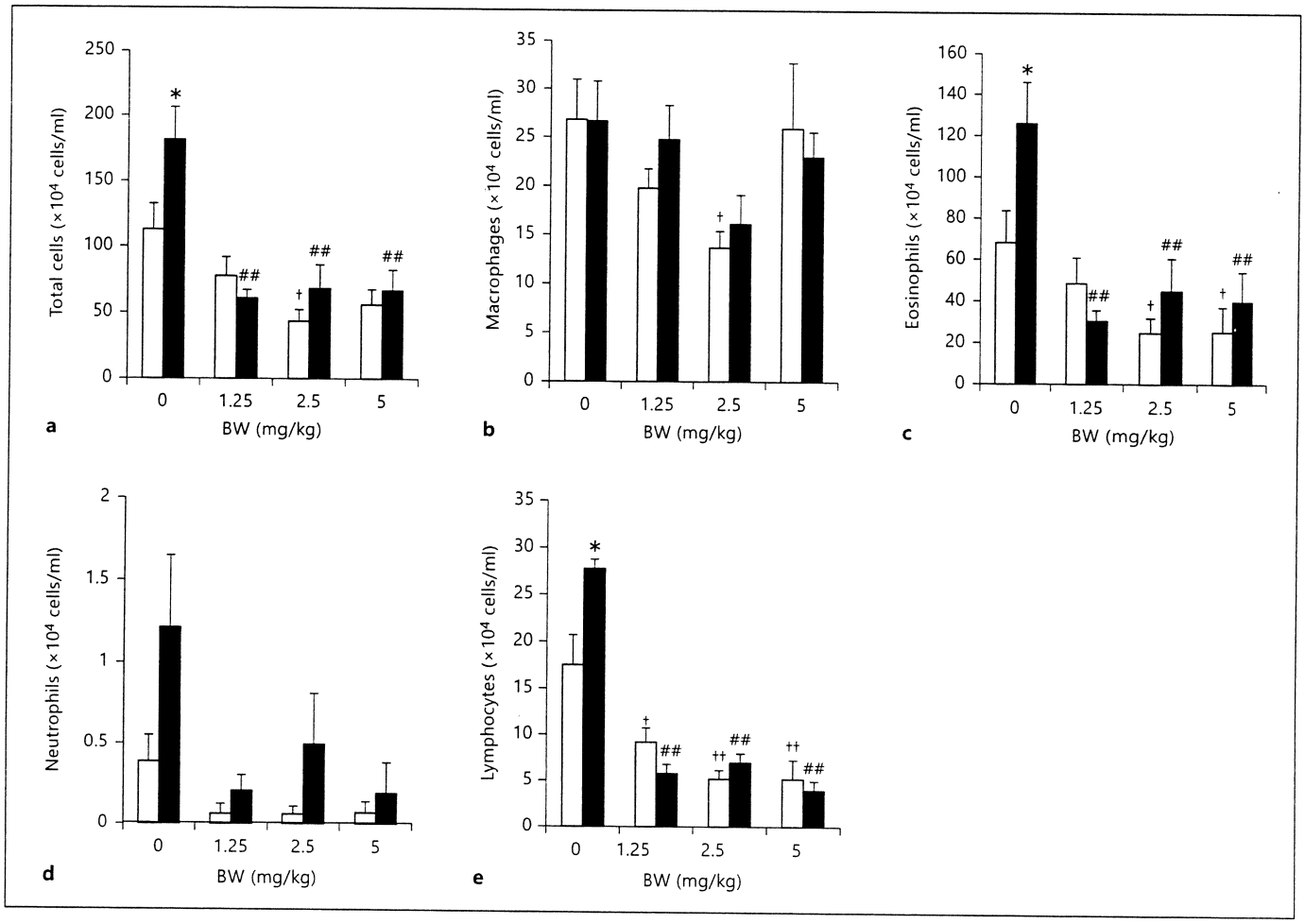


Fig. 9. Effects of dexamethasone on antigen-induced airway inflammation. Dexamethasone [0, 1.25, 2.5 and 5.0 mg/kg body weight (BW)] was administered in stressed (closed columns) and nonstressed (open columns) mice as described in Materials and Methods. The numbers of total cells (**a**), macrophages (**b**), eosinophils (**c**), neutrophils (**d**) and lymphocytes (**e**) in the BAL fluid 3 days after the second OVA challenge were counted. Data are expressed as the means ± SEM (n = 6–14 from 4 independent experiments). * $p < 0.05$ compared with nonstressed mice. ## $p < 0.01$ compared with 0 mg/kg BW in stressed mice. † $p < 0.05$ and †† $p < 0.01$ compared with 0 mg/kg BW in nonstressed mice.

methasone significantly decreased the numbers of total cells, eosinophils and lymphocytes in the BAL fluid in nonstressed and stressed mice, resulting in the abolishment of the differences in these numbers that had been observed without administration of dexamethasone (fig. 9).

Discussion

Using a murine model of stress asthma, we have demonstrated, for the first time, that corticosterone released following stress exposure is involved in the exacerbation of allergic airway responses evoked by allergen inhalation immediately subsequent to exposure to stress.

To investigate the pathological role of this corticosterone release in the aggravation of Th2-driven allergic airway responses, we examined the effect of administering the GC receptor antagonist RU-486 before each stress exposure. RU-486 significantly inhibited the increase in inflammatory cell accumulation and IL-13 levels in the BAL fluid caused by stress exposure. This significant inhibition of the cellular infiltrates caused by stress was also observed following the administration of the GC synthesis inhibitor metyrapone. The data on the effect of RU-486 on proportions of PAS-positive cells also suggest that RU-486 may attenuate the aggravation of mucus secretion caused by stress. These findings strongly suggest that the increased release of corticosterone during the stress

exposure was involved in the stress-induced exacerbation of allergic airway responses in OVA-challenged mice. The reasons why the difference in airway responsiveness between the stress/solvent-OVA and stress/RU-486-OVA groups did not reach statistical significance were not determined in this study. However, it is possible that other stress-related hormones such as catecholamine [33] or neuropeptides such as substance P [23] may be involved in the exacerbation of airway responses, or else the procedure for administering the solvent may in itself be a type of stress that caused the exacerbation of airway responses via pathways other than the activation of the hypothalamic-pituitary-adrenal (HPA) axis.

The contribution of GC to the stress-induced exacerbation of allergic asthma has been investigated in 2 other studies using murine models of stress asthma [24, 34]. In a study by Forsythe et al. [24], animals exposed to long-term stress (RS on 3 consecutive days followed by FSS on 4 consecutive days) followed by antigen challenge showed an increase in inflammatory cell numbers, but cytokine levels had not changed when compared to animals without stress exposure. In their study, in contrast to our results, the administration of RU-486 did not influence the increase in inflammatory cell numbers, even though the same type of stress was applied in both studies. The authors argued that other stress-induced mediators such as corticotropin-releasing hormone and catecholamines augmented airway inflammation via the activation of mast cells and increasing blood granulocytes, respectively. Given the differences in sex and mouse strain between the 2 studies (Forsythe et al. [24]: male BALB/c and our study: female B6 mice), the neuroendocrine mechanisms underlying the exacerbation of allergic airway responses by stress may have been distinct, even with the same methods of stress exposure, because corticosterone release in response to stress exposure differs depending on the sex and genetic background of the mice. For example, in B6 and BALB/c mice, corticosterone release by RS exposure has been shown to be higher in females than in males [32]. The idea of the sex difference influencing the neuroendocrine mechanisms might be supported by our finding that the effects of the stress exposure on the exacerbation of allergic airway inflammation were observed in the female but not the male B6 mice. Although the increase in inflammatory cell numbers in BAL fluid following the OVA challenge was observed in both female BALB/c and B6 mice exposed to stress [35], stress responses in terms of corticosterone levels have been reported to be higher in BALB/c mice than in B6 mice [32, 36, 37].

In another study, by Chida et al. [34], male BALB/c mice were exposed to FS or communication box-induced stress (CS) at the age of 4 weeks and were then sensitized and challenged with antigen as adults at the age of 8–11 weeks. Both FS and CS early in life led to exacerbated airway inflammation and airway responsiveness after antigen challenge as an adult. The CS group, but not the FS group, exhibited a significantly smaller increase in corticosterone levels compared to the control group after antigen challenge, so the authors administered RU-486 before antigen challenge to preclude the influence of the difference in corticosterone levels on the difference in inflammatory cell numbers between the nonstressed and stressed groups. The administration of RU-486 diminished the difference in inflammatory cell numbers between the control and CS groups by augmenting the inflammation in the control group. The authors concluded that the reduced release of corticosterone, which has well-known anti-inflammatory and immunosuppressive properties, resulted in accelerated inflammation in the CS group. The hyporesponsiveness of the HPA axis, which results from long-lasting activation of this axis due to repeated stress exposure, has been proposed as a possible pathway by which stress induces asthma exacerbation [15, 38]. However, the FS group showed similar levels of responsiveness in the HPA axis to the nonstressed group, although corticosterone release was increased following the stress exposure in the FS and CS groups. In our study, responsiveness of the HPA axis in the stressed mice was unlikely to be impaired because corticosterone concentrations in the stressed mice were similar to those in the nonstressed mice after the second OVA challenge following stress exposure. In addition, the administration of RU-486 before each stress exposure, in contrast to the administration of RU-486 long after the stress exposure in the study by Chida et al. [34], abolished the exacerbation of Th2-driven airway inflammation. Accordingly, it is likely that, depending on the strain and sex of the mice as well as the type of stressor and the age of the mice at the time of the exposure to stress, the activation of the HPA axis at this time could play a role other than induction of hyporesponsiveness of this axis in the exacerbation of asthmatic responses caused by stress exposure.

In addition to hyporesponsiveness of the HPA axis, the reduction of the anti-inflammatory effects of corticosteroids has been proposed as being a mechanism which underlies the enhancement of allergic airway inflammation evoked by chronic stress. Chen et al. [19] reported that the peripheral blood mononuclear cells of asthmatic children exposed to more social stress showed a higher po-

tential to express Th2 cytokines in association with a lower expression of GC receptor mRNAs, while such cells from normal subjects did not demonstrate these changes [39]. In a previous study, the inhibitory effects of GC on antigen-stimulated Th2 cytokine production by splenocytes from sensitized and stressed mice was reduced compared to that from sensitized and nonstressed mice. Furthermore, splenocytes from the sensitized and stressed mice expressed lower levels of GC receptor mRNAs [40]. In our study, although the expression of GC receptor mRNAs was not examined, the levels of inflammatory cell accumulation elicited by the second OVA challenge in stressed mice were suppressed to the levels in nonstressed mice by the administration of dexamethasone after the second OVA challenge. Therefore, in our model, hyporesponsiveness to endogenous GC resulting from the repetition of increased release of GC due to chronic stress exposure is likely not an underlying mechanism for the stress-induced exacerbation of allergic airway conditions.

We previously demonstrated that cells isolated from bronchial lymph nodes in stressed mice, in which the stress caused more severe Th2-driven airway inflammation and higher corticosterone concentrations, produced cytokines with a more Th2-dominant profile, and differentiated into a T cell population with a lower proportion of Treg cells than cells from nonstressed mice after stimulation with the antigen in vitro [26]. It has been reported that the induction of Treg cells is impaired in patients with posttraumatic stress disorder [41] and in individuals exposed to a mental stressor [42]. The administration of corticosteroids was reported to inhibit respiratory tolerance [43] and to permanently amplify the Th2 responses [44]. Dendritic cells from corticosteroid-treated mice have been shown to be unable to transfer respiratory tolerance or induce Treg cells [45]. Therefore, GC released upon stress exposure might bias immune regulation preferentially towards a Th2 response in response to a specific antigen, thereby eventually aggravating asthmatic responses to antigen challenges subsequent to stress exposure.

Using μ-opioid receptor (MOR) gene-knockout (MORKO) and MOR-transgenic MORKO mice expressing MOR in the specific regions in the brain, we showed that MORs in the central nervous system are involved in stress-induced exacerbations of allergic airway inflammation and also in the stress-induced increase in plasma corticosterone concentrations [25, 26]. Together, our results suggest a possible pathway linking stress exposure to asthma exacerbations, in which the stress exposure increases corticosteroid release via activation of MORs, leading to the worsening of allergic airway inflammation.

In summary, this is the first report to our knowledge demonstrating that corticosterone release during stress exposure has a priming effect on exacerbations of allergic airway responses following exposure to stress. It will be necessary to further explore the cellular and molecular events linking the corticosterone release to stress-induced immune regulation accelerating Th2-driven adaptive immunity. These investigations would further clarify the pathological role of the neuroendocrine-immune axis in psychological stress-related asthma exacerbation, leading to the development of new strategies for the treatment of specific asthma phenotypes such as psychiatry-related asthma [46, 47].

Acknowledgement

This work was supported in part by a Grant-in-Aid for Scientific Research (No. 22590843) and by the Matching Fund Subsidy for Private Universities from the Ministry of Education, Culture, Sports, Science and Technology (MEXT) of Japan.

References

1 Galli SJ, Tsai M, Piliponaky AM: The development of allergic inflammation. Nature 2008; 454:445–454.
2 Lemanske RF Jr, Busse WW: Asthma: clinical expression and molecular mechanisms. J Allergy Clin Immunol 2010;125:S95–S102.
3 Holgate ST: Pathophysiology of asthma: what has our current understanding taught us about new therapeutic approaches? J Allergy Clin Immunol 2011;128:495–505.
4 Barnes PJ: Pathophysiology of allergic inflammation. Immunol Rev 2011;242:31–50.
5 Robinson DS: Regulatory T cells and asthma. Clin Exp Allergy 2009;39:1314–1323.
6 Lloyd CM, Hawrylowicz CM: Regulatory T cells in asthma. Immunity 2009;31:438–449.
7 Akdis CA, Akdis M: Mechanisms and treatment of allergic disease in the big picture of regulatory T cells. J Allergy Clin Immunol 2009;123:735–746.
8 Chetta A, Foresi A, Marangio E, Olivieri D: Psychological implications of respiratory health and disease. Respiration 2005;72:210–215.
9 Wainwright NW, Surtees PG, Wareham NJ, Harrison BD: Psychosocial factors and incident asthma hospital admissions in the EPIC-Norfolk cohort study. Allergy 2007;62:554–560.
10 Isenberg SA, Lehrer PM, Hochron S: The effects of suggestion and emotional arousal on pulmonary function in asthma: a review and a hypothesis regarding vagal mediation. Psychosom Med 1992;54:192–216.
11 Sandberg S, Paton JY, Ahola S, McCann DC, McGuinness D, Hillary CR, Oja H: The role of acute and chronic stress in asthma attacks in children. Lancet 2000;356:982–987.
12 Lange NE, Bunyavanich S, Silberg JL, Canino G, Rosner BA, Celedón JC: Parental psychosocial stress and asthma morbidity in Puerto Rican twins. J Allergy Clin Immunol 2011; 127:734–740.

13 Oraka E, King ME, Callahan DB: Asthma and serious psychological distress; prevalence and risk factors among US adults, 2001–2007. Chest 2010;137:609–616.
14 Archea C, Yen IH, Chen H, Eisner MD, Katz PP, Masharani U, Yelin EH, Earnest G, Blanc PD: Negative life events and quality of life in adults with asthma. Thorax 2007;62:139–146.
15 Chen E, Miller GE: Stress and inflammation in exacerbations of asthma. Brain Behav Immun 2007;21:993–999.
16 Wright RJ, Cohen RT, Cohen S: The impact of stress on the development and expression of atopy. Cur Opin Allergy Clin Immunol 2005;5:23–29.
17 Liu LY, Coe CL, Swenson CA, Kelly EA, Kita H, Busse WW: School examinations enhance airway inflammation to antigen challenge. Am J Respir Crit Care Med 2002;165:1062–1067.
18 Höglund CO, Axén J, Kemi C, Jernelöv S, Grunewald J, Müller-Suur C, Smith Y, Grönneberg R, Eklund A, Stierna P, Lekander M: Changes in immune regulation in response to examination stress in atopic and healthy individuals. Clin Exp Allergy 2006;36:982–992.
19 Chen E, Hanson MD, Paterson LQ, Griffin MJ, Walker HA, Miller GE: Socioeconomic status and inflammatory processes in childhood asthma: the role of psychological stress. J Allergy Clin Immunol 2006;117:1014–1020.
20 Chen E, Chim LS, Strunk RC, Miller GE: The role of the social environment in children and adolescents with asthma. Am J Respir Crit Care Med 2007;176:644–649.
21 Wolf JM, Miller GE, Chen E: Parent psychological states predict changes in inflammatory markers in children with asthma and healthy children. Brain Behav Immun 2008;22:433–441.
22 Rosenkranz MA, Busse WW, Johnstone T, Swenson CA, Crisafi GM, Jackson MM, Bosch JA, Sheridan JF, Davidson RJ: Neural circuitry underlying the interaction between emotion and asthma symptom exacerbation. Proc Natl Acad Sci USA 2005;102:13319–13324.
23 Joachim RA, Sagach V, Quarcoo D, Dinh QT, Arck PC, Klapp BF: Neurokinin-1 receptor mediates stress-exacerbated allergic airway inflammation and airway hyperresponsiveness in mice. Psychosom Med 2004;66:564–571.
24 Forsythe P, Ebeling C, Gordon JR, Befus AD, Vliagoftis H: Opposing effects of short- and long-term stress on airway inflammation. Am J Respir Crit Care Med 2004;169:220–226.
25 Okuyama K, Wada K, Sakurada S, Mizoguchi H, Komatsu H, Sora I, Tamura G, Ohkawara Y, Takayanagi M, Ohno I: The involvement of μ-opioid receptors in the central nervous system in the worsening of allergic airway inflammation by psychological stress in mice. Int Arch Allergy Immunol 2010;152:342–352.
26 Okuyama K, Ide S, Sakurada S, Sasaki K, Sora I, Tamura G, Ohkawara Y, Takayanagi M, Ohno I: μ-opioid receptor-mediated alterations of allergen-induced immune responses of bronchial lymph node cells in a murine model of stress asthma. Allergol Int 2012;61:245–258.
27 Mercado AM, Padgett DA, Sheridan JF, Marucha PT: Altered kinetics of IL-1 alpha, IL-1 beta, and KGF-1 gene expression in early wounds of restrained mice. Brain Behav Immun 2002;16:150–162.
28 Ashcraft KA, Hunzeker J, Bonneau RH: Psychological stress impairs the local CD8+ T cell response to mucosal HSV-1 infection and allows for increased pathogenicity via a glucocorticoid receptor-mediated mechanism. Psychoneuroendocrinology 2008;33:951–963.
29 Nagafuku M, Okuyama K, Onimaru Y, Suzuki A, Odagiri Y, Yamashita T, Iwasaki K, Fujiwara M, Takayanagi M, Ohno I, Inokuchi J: CD4 and CD8 T cells require different membrane gangliosides for activation. Proc Natl Acad Sci USA 2012;109:E336–E342.
30 Takeda M, Ito W, Tanabe M, Ueki S, Kato H, Kihara J, Tanigai T, Chiba T, Yamaguchi K, Kayaba H, Imai Y, Okuyama K, Ohno I, Sasaki T, Chihara J: Allergic airway hyperresponsiveness, inflammation, and remodeling do not develop in phosphoinositide 3-kinase gamma-deficient mice. J Allergy Clin Immunol 2009;123:805–812.
31 Okuyama K, Wada K, Chihara J, Takayanagi M, Ohno I: Sex-related splenocyte function in a murine model of allergic asthma. Clin Exp Allergy 2008;38:1212–1219.
32 Harizi H, Homo-Delarche F, Amrani A, Coulaud J, Mormède P: Marked genetic differences in the regulation of blood glucose under immune and restraint stress in mice reveals a wide range of corticosensitivity. J Neuroimmunol 2007;189:59–68.
33 Black PH: Stress and the inflammatory response: a review of neurogenic inflammation. Brain Behav Immun 2002;16:622–653.
34 Chida Y, Sudo N, Sonoda J, Hiramoto T, Kubo C: Early-life psychological stress exacerbates adult mouse asthma via the hypothalamus-pituitary-adrenal axis. Am J Respir Crit Care Med 2007;175:316–322.
35 Okuyama K, Ohwada K, Sakurada S, Sato N, Sora I, Tamura G, Takayanagi M, Ohno I: The distinctive effects of acute and chronic psychological stress on airway inflammation in a murine model of allergic asthma. Allergol Int 2007;56:29–35.
36 Anisman H, Hayley S, Kelly O, Borowski T, Merali Z: Psychogenic, neurogenic, and systemic stressor effects on plasma corticosterone and behavior: mouse strain-dependent outcomes. Behav Neurosci 2001;115:443–454.
37 Browne CA, Clarke G, Dinan TG, Cryan JF: Differential stress-induced alterations in tryptophan hydroxylase activity and serotonin turnover in two inbred mouse strains. Neuropharmacol 2011;60:683–691.
38 Buske-Kirschbaum A, Ebrecht M, Hellhammer DH: Blunted HPA axis responsiveness to stress in atopic patients is associated with the acuity and severeness of allergic inflammation. Brain Behav Immun 2010;24:1347–1353.
39 Miller GE, Chen E, Fok AK, Walker H, Lim A, Nicholls EF, Cole S, Kobor MS: Low early-life social class leaves a biological residue manifested by decreased glucocorticoid and increased proinflammatory signaling. Proc Natl Acad Sci USA 2009;106:14716–14721.
40 Bailey MT, Kierstein S, Sharma S, Spaits M, Kinsey SG, Tliba O, Amrani Y, Sheridan JF, Panettieri RA, Haczku A: Social stress enhances allergen-induced airway inflammation in mice and inhibits corticosteroid responsiveness of cytokine production. J Immunol 2009;182:7888–7896.
41 Sommershof A, Aichinger H, Engler H, Adenauer H, Catani C, Boneberg EM, Elbert T, Groettrup M, Kolassa IT: Substantial reduction of naïve and regulatory T cells following traumatic stress. Brain Behav Immun 2009;23:1117–1124.
42 Freier E, Weber CS, Nowottne U, Horn C, Bartels K, Meyer S, Hildebrandt Y, Luetkens T, Cao Y, Pabst C, Muzzulini J, Schnee B, Brunner-Weinzierl MC, Marangolo M, Bokemeyer C, Deter HC, Atanackovic D: Decrease of CD4(+)FOXP3(+) T regulatory cells in the peripheral blood of human subjects undergoing a mental stressor. Pscychoneuroendocrinology 2010;35:663–673.
43 Stock P, Akbari O, DeKruyff RH, Umetsu DT: Respiratory tolerance is inhibited by the administration of corticosteroids. J Immunol 2005;175:7380–7387.
44 Wiley RE, Cwiartka M, Alvarez D, Mackenzie DC, Johnson JR, Goncharova S, Lundblad L, Jordana M: Transient corticosteroid treatment permanently amplifies the Th2 response in a murine model of asthma. J Immunol 2004;172:4995–5005.
45 Kerzerho J, Wunsch D, Szely N, Meyer H-A, Lurz L, Rose L, Wahn U, Akbari O, Stock P: Effects of systemic versus local administration of corticosteroids on mucosal tolerance. J Immunol 2012;188:470–476.
46 Rosenkranz MA, Busse WW, Sheridan JF, Crisafi GM, Davidson RJ: Are there neurophenotypes for asthma? Functional brain imaging of the interaction between emotion and inflammation in asthma. PLoS One 2012;7:e40921.
47 Busse WW: The brain and asthma: what are the linkages? Chem Immunol Allergy 2012;98:14–31.

European Journal of Pharmacology 711 (2013) 80–86

Contents lists available at SciVerse ScienceDirect

European Journal of Pharmacology

journal homepage: www.elsevier.com/locate/ejphar

Neuropharmacology and analgesia

Distinct physiological role of amidino-TAPA-sensitive and DAMGO-insensitive μ-opioid receptor splice variants in the mouse spinal cord

Hirokazu Mizoguchi [a], Chizuko Watanabe [a], Takayuki Higashiya [a], Satoshi Takeda [a], Kaori Moriyama [a], Yuta Aoki [a], Takashi Kon-no [a], Hirokazu Takagi [a], Akihiko Yonezawa [a], Takumi Sato [b], Tsukasa Sakurada [c], Shinobu Sakurada [a,*]

[a] Department of Physiology and Anatomy, Tohoku Pharmaceutical University, 4-4-1 Komatsushima, Aoba-ku, Sendai 981-8558, Japan
[b] Department of Pharmacology, Nihon Pharmaceutical University, 10281 Komuro, Ina-machi, Kitaadachi-gun, Saitama 362-0806, Japan
[c] First Department of Pharmacology, Daiichi College of Pharmaceutical Sciences, 22-1 Tamagawa-cho, Minami-ku, Fukuoka 815-8511, Japan

ARTICLE INFO

Article history:
Received 3 December 2012
Received in revised form
28 March 2013
Accepted 3 April 2013
Available online 23 April 2013

Keywords:
Antinociception
Mu-opioid receptor
Splice variants
Endogenous opioid peptides
Spinal cord

ABSTRACT

The physiological role of the distinct splice variants for cloned mouse μ-opioid receptor (mMOR-1), mMOR-1J, mMOR-1K and mMOR-1L, which are sensitive to N^{α}-amidino-Tyr-D-Arg-Phe-β-Ala (amidino-TAPA) and insensitive to [D-Ala^2,*N*-MePhe^4,Gly-ol^5]enkephalin (DAMGO), was described in the mouse spinal cord. The antinociception induced by intrathecally (i.t.) injected amidino-TAPA was attenuated by i.t. pretreatment with antisera against the endogenous opioid peptides dynorphin A, dynorphin B, α-neo-endorphin, or [Leu^5]enkephalin in naïve mice. However, in mice whose spinal mMOR-1J had been knocked-down using the antisense oligodeoxynucleotide (ODN) for exon-12 of mMOR-1 gene, the inhibiting effect of antiserum against dynorphin A on amidino-TAPA-induced antinociception was eliminated. In contrast, the inhibiting effect of antisera against dynorphin B or α-neo-endorphin on amidino-TAPA-induced antinociception was eliminated in mice whose spinal mMOR-1K had been knocked-down using the antisense ODN for exon-13 of mMOR-1 gene. Moreover, the inhibiting effect of antisera against dynorphin A or [Leu^5]enkephalin on amidino-TAPA-induced antinociception was eliminated in mice whose spinal mMOR-1L had been knocked-down using the antisense ODN for exon-14 of mMOR-1 gene. The present results suggest that the distinct antinociceptive profile of amidino-TAPA, that is the release of endogenous κ- and δ-opioid peptides in spinal cord, is mediated through the activation of mMOR-1J, mMOR-1K or mMOR-1L, which contain the sequence encoded by exon-12, exon-13 or exon-14 of mMOR-1 gene, respectively.

© 2013 Elsevier B.V. All rights reserved.

1. Introduction

N^{α}-amidino-Tyr-D-Arg-Phe-β-Ala (amidino-TAPA) is a N-terminal tetrapeptide derivative of dermorphin, which has a very high affinity and selectivity for μ-opioid receptors and produces an extremely potent and longer-lasting antinociception (Mizoguchi et al., 2007; Ogawa et al., 2002). Unlike the traditional μ-opioid receptor agonist [D-Ala^2,*N*-MePhe^4,Gly-ol^5]enkephalin (DAMGO) or morphine, amidino-TAPA has distinct profile for spinal antinociception. The antinociceptive effect of intrathecally (i.t.) administered amidino-TAPA is mediated through the release of the endogenous κ-opioid peptides dynorphin A, dynorphin B and α-neo-endorphin and the endogenous δ-opioid peptide [Leu^5]enkephalin via activation of μ-opioid receptors in the spinal cord (Mizoguchi et al., 2007). The spinal release of the endogenous opioid peptides via activation of μ-opioid receptors is also observed for the other selective μ-opioid receptor agonists endomorphin-2 (Mizoguchi et al., 2006b; Sakurada et al., 2001), Tyr-D-Arg-Phe-Sar (TAPS) (Mizoguchi et al., 2006a) and $(CH_3)_2$Tyr-D-Arg-Phe-Lys-NH_2 ([Dmt^1]DALDA) (Szeto et al., 2003). The traditional μ-opioid receptor agonists, such as DAMGO and morphine, do not have these effects (Mizoguchi et al., 2007; Szeto et al., 2003). The distinct antinociceptive profiles of these opioid peptides that are the release of the endogenous opioid peptides may be mediated by the activation of distinct μ-opioid receptors that are sensitive to these peptides but insensitive to traditional μ-opioid receptor agonists.

The μ-opioid receptor was firstly cloned on 1993 (Chen et al., 1993; Wang et al., 1993), and then 19 exons have been identified in cloned mouse μ-opioid receptor (mMOR-1) gene. Based on the splicing of the mRNA precursor for mMOR-1, 32 of splice variants for mMOR-1 currently have been identified (Doyle et al., 2007a, 2007b; Kvam et al., 2004; Pan et al., 2001, 2005). The sequence variability of the splice variants is mainly found in the sequences of the *N*-terminal and first transmembrane region, and in the sequence of the intracellular C-terminal region. Most of the splice

* Corresponding author. Tel.: +81 22 727 0124; fax: +81 22 727 0125.
E-mail address: s-sakura@tohoku-pharm.ac.jp (S. Sakurada).

0014-2999/$ - see front matter © 2013 Elsevier B.V. All rights reserved.
http://dx.doi.org/10.1016/j.ejphar.2013.04.014

variants for mMOR-1 identified contain the sequence encoded by exon-1 of mMOR-1 gene (Doyle et al., 2007a, 2007b; Kvam et al., 2004; Pan et al., 2001, 2005), and all μ-opioid receptor agonists examined, including the traditional μ-opioid receptor agonists DAMGO and morphine, have a high affinity and intrinsic activity to the mMOR-1 splice variants containing the sequence encoded by exon-1 of mMOR-1 gene (Pasternak, 2004). However, we recently found that the specific mMOR-1 splice variants containing the sequence encoded by exon-11 of mMOR-1 gene, mMOR-1J, mMOR-1K and mMOR-1L, were amidino-TAPA-sensitive and DAMGO-insensitive splice variants (Mizoguchi et al., 2011). The spinal antinociceptive effect of amidino-TAPA is mediated through the activation of these splice variants, whereas that of DAMGO is not mediated by these splice variants (Mizoguchi et al., 2011). The evidence leads the hypothesis that the DAMGO-insensitive splice variants, mMOR-1J, mMOR-1K and mMOR-1L, may be distinct μ-opioid receptors, which mediate the distinct antinociceptive profile of amidino-TAPA including the release of the endogenous opioid peptides.

The present study was conducted to identify the involvement of distinct mMOR-1 splice variants, mMOR-1J, mMOR-1K and mMOR-1L, on the distinct antinociceptive property of amidino-TAPA that is the release of endogenous κ- and δ-opioid peptides.

2. Materials and methods

All experiments were performed following the approval of the Ethics Committee for Animal Experiments at Tohoku Pharmaceutical University and according to the National Institutes of Health Guide for the Care and Use of Laboratory Animals. Every effort was made to minimize the number and any suffering of the animal used in the following experiments.

2.1. Animals

Male ddY mice (Japan SLC, Hamamatsu, Japan) weighing 22–25 g were used. The animals were housed in a room maintained at 22–23 °C and 50–60% relative humidity with an alternating 12-h light/dark cycle. Food and water were available ad libitum. Mice were used only once.

2.2. Assessment of antinociception

Antinociception was determined with the tail-flick test (D'Amour and Smith, 1941). For measurement of the latency of the tail-flick response, mice were gently held by hand with their tail positioned in an apparatus (Ugo Basile, Italy) for radiant heat stimulation on the ventral surface of the tail. The intensity of the heat stimulus was adjusted so that the animal withdrew its tail after 2.5–3.5 s. The inhibition of the tail-flick response was expressed as the percent maximal possible effect, % MPE, which was calculated as follows: $[(T_1-T_0)/(T_2-T_0)] \times 100$, where T_0 and T_1 are the tail-flick latencies before and after the treatments, respectively, and T_2 is the cutoff time, set at 10 s to avoid injury to the tail.

2.3. Intrathecal injection

The i.t. injection was performed following the method described by Hylden and Wilcox (1980) using a 29-gauge stainless-steel needle attached to a 50-μl Hamilton microsyringe. For i.t. injections, drugs were dissolved in sterile artificial cerebrospinal fluid (aCSF) containing 126.6 mM NaCl, 2.5 mM KCl, 2.0 mM $MgCl_2$, and 1.3 mM $CaCl_2$. The volume for the i.t. injections was 5 μl.

2.4. Exon-specific knock-down for mMOR-1 splice variants

The exon-specific knock-down for mMOR-1 splice variants sensitive to amidino-TAPA in the mouse spinal cord was performed as previously described (Mizoguchi et al., 2011), using the exon-specific antisense oligodeoxynucleotides (ODNs). The single i.t. pretreatment with amidino-TAPA (2 pmol) causes the temporal desensitization of amidino-TAPA-sensitive mMOR-1 splice variants in the spinal cord, which disappears within 3 h by new synthesis of the desensitized splice variants. The concomitant i.t. pretreatment with antisense ODN (5 μg) for each exon of mMOR-1 gene, which codes the sequence contained in the amidino-TAPA-sensitive splice variants, retains the desensitization of exon-specific splice variants over 24 h by suppressing the new synthesis of those splice variants. In this procedure, the mMOR-1 splice variants sensitive to amidino-TAPA can be selectively knocked-down in exon-specific manner by single pretreatment.

2.5. Drugs

The drugs used were amidino-TAPA (Peptides Institute, Osaka, Japan), rabbit antiserum against dynorphin A (A/Dyn A: Phoenix Pharmaceutical Inc., St. Joseph, MO), rabbit antiserum against dynorphin B (A/Dyn B: Bachem, San Carlos, CA), rabbit antiserum against α-neo-endorphin (A/αNeoE: Bachem), and rabbit antiserum against [Leu^5]enkephalin (A/L-Enk: Millipore Co., Billerica, MA). The selectivity of antisera has been guaranteed by the data sheet provided from the commercial source. The lack of cross-reactivity of the antisera to amidino-TAPA has been verified with an enzyme-linked immunosorbent assay (data not shown). Antisense phosphorothioate-linked ODNs for exon-12, exon-13 and exon-14 of mMOR-1 gene, which were purchased from The Midland Certified Reagent Company (Midland, TX), had the following sequences: 5′–GTG AAG CAC TGT CTT CTA AAG GGG-3′ (antisense ODN for exon-12), 5′–TCA GTC TTT ATC AGC TCA CCG CCA-3′ (antisense ODN for exon-13) and 5′–TAT TTT GAT TTT CAG TTG ATT C-3′ (antisense ODN for exon-14).

2.6. Statistical analyses

The data were represented as the mean ± S.E.M. for at least 10 mice. The dose–response curves were calculated by a built-in equation "sigmoidal dose–response (variable slope)" in a computer-assisted curve-fitting program (GraphPad Prism 4; GraphPad Software, Inc., San Diego, CA). The entire dose–response curves were compared using the *F*-test, according to the instructions provided with GraphPad Prism.

3. Results

3.1. Involvement of the spinal release of the endogenous opioid peptides on the spinal antinociception of amidino-TAPA in naïve mice

Effects of antisera against the endogenous opioid peptides on the spinal antinociception induced by amidino-TAPA were determined in naïve mice. Groups of mice pretreated i.t. with aCSF 24 h before, were injected i.t. with aCSF or antisera (1:50 dilution) against dynorphin A, dynorphin B, α-neo-endorphin or [Leu^5]enkephalin 20 min before the i.t. treatment with various doses of amidino-TAPA (0.5, 1, 2, 3 or 4 pmol), and the tail-flick inhibition induced by amidino-TAPA was measured at 10 min after the treatment. The pretreatment with antisera against dynorphin A, dynorphin B, α-neo-endorphin or [Leu^5]enkephalin dramatically suppressed amidino-TAPA-induced antinociception (Fig. 1). The dose–response curve of amidino-TAPA for antinociception was

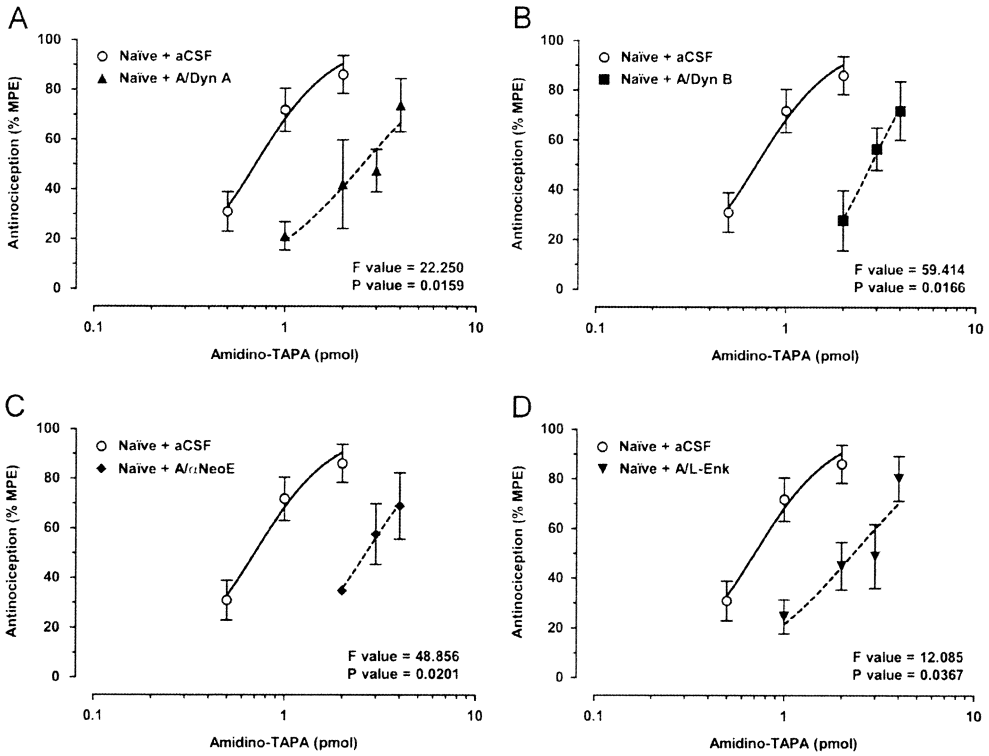


Fig. 1. Effects of antisera against the endogenous opioid peptides on the antinociception induced by amidino-TAPA in naïve mice. Groups of mice pretreated i.t. with aCSF 24 h before, were injected i.t. with aCSF or antisera (1:50 dilution) against dynorphin A (A/Dyn A: A), dynorphin B (A/Dyn B: B), α-neo-endorphin (A/αNeoE: C) or [Leu^5] enkephalin (A/L-Enk: D) 20 min before the i.t. treatment with various doses of amidino-TAPA (0.5, 1, 2, 3 or 4 pmol), and the tail-flick inhibition induced by amidino-TAPA was measured at 10 min after the treatment. The antinociceptive effect was represented as the mean ± S.E.M. for at least 10 mice.

significantly shifted to the right by the pretreatment with antisera against dynorphin A, dynorphin B, α-neo-endorphin or [Leu^5] enkephalin.

3.2. *Involvement of the spinal release of the endogenous opioid peptides on the spinal antinociception of amidino-TAPA in mice, whose spinal mMOR-1J had been knocked-down*

Effects of antisera against the endogenous opioid peptides on the antinociception induced by amidino-TAPA were also determined in mice, whose spinal mMOR-1J had been knocked-down using exon-12-specific antisense ODN. Groups of mice pretreated i.t. with amidino-TAPA (2 pmol) in combination with antisense ODN for exon-12 of mMOR-1 gene (5 μg) 24 h before, were injected i.t. with aCSF or antisera (1:50 dilution) against dynorphin A, dynorphin B, α-neo-endorphin or [Leu^5]enkephalin 20 min before the i.t. treatment with various doses of amidino-TAPA (1, 2, 4 or 8 pmol), and the tail-flick inhibition induced by amidino-TAPA was measured at 10 min after the treatment. In mice whose spinal mMOR-1J had been knocked-down using antisense ODN for exon-12 of mMOR-1 gene, amidino-TAPA-induced antinociception was suppressed by the pretreatment with antisera against dynorphin B, α-neo-endorphin or [Leu^5]enkephalin, but not dynorphin A (Fig. 2). The dose–response curve of amidino-TAPA for antinociception was significantly shifted to the right by the pretreatments with antisera against dynorphin B, α-neo-endorphin or [Leu^5] enkephalin in mice whose spinal mMOR-1J had been knocked-down (Fig. 2B–D). In contrast, the right forward shift of the dose–response curve of amidino-TAPA for antinociception by the pretreatment with antiserum against dynorphin A, which was observed in naïve mice, was eliminated in mice whose spinal mMOR-1J had been knocked-down (Fig. 2A).

3.3. *Involvement of the spinal release of the endogenous opioid peptides on the spinal antinociception of amidino-TAPA in mice, whose spinal mMOR-1K had been knocked-down*

Effects of antisera against the endogenous opioid peptides on the antinociception induced by amidino-TAPA were also determined in mice, whose spinal mMOR-1K had been knocked-down using exon-13-specific antisense ODN. Groups of mice pretreated i.t. with amidino-TAPA (2 pmol) in combination with antisense ODN for exon-13 of mMOR-1 gene (5 μg) 24 h before, were injected i.t. with aCSF or antisera (1:50 dilution) against dynorphin A, dynorphin B, α-neo-endorphin or [Leu^5]enkephalin 20 min before the i.t. treatment with various doses of amidino-TAPA (0.5, 1, 2, 4 or 8 pmol), and the tail-flick inhibition induced by amidino-TAPA was measured at 10 min after the treatment. In mice whose spinal mMOR-1K had been knocked-down using antisense ODN for exon-13 of mMOR-1 gene, amidino-TAPA-induced antinociception was suppressed by the pretreatment with antisera against dynorphin A or [Leu^5]enkephalin, but not dynorphin B or α-neo-endorphin (Fig. 3). The dose–response curve of amidino-TAPA for antinociception was significantly shifted to the right by the pretreatments with antisera against dynorphin A or [Leu^5]enkephalin in mice whose spinal mMOR-1K had been knocked-down (Fig. 3A and D). In contrast, the right forward shift of the dose–response curve of amidino-TAPA for antinociception by the pretreatment with antisera against dynorphin B or α-neo-endorphin, which was observed in naïve mice, was eliminated in

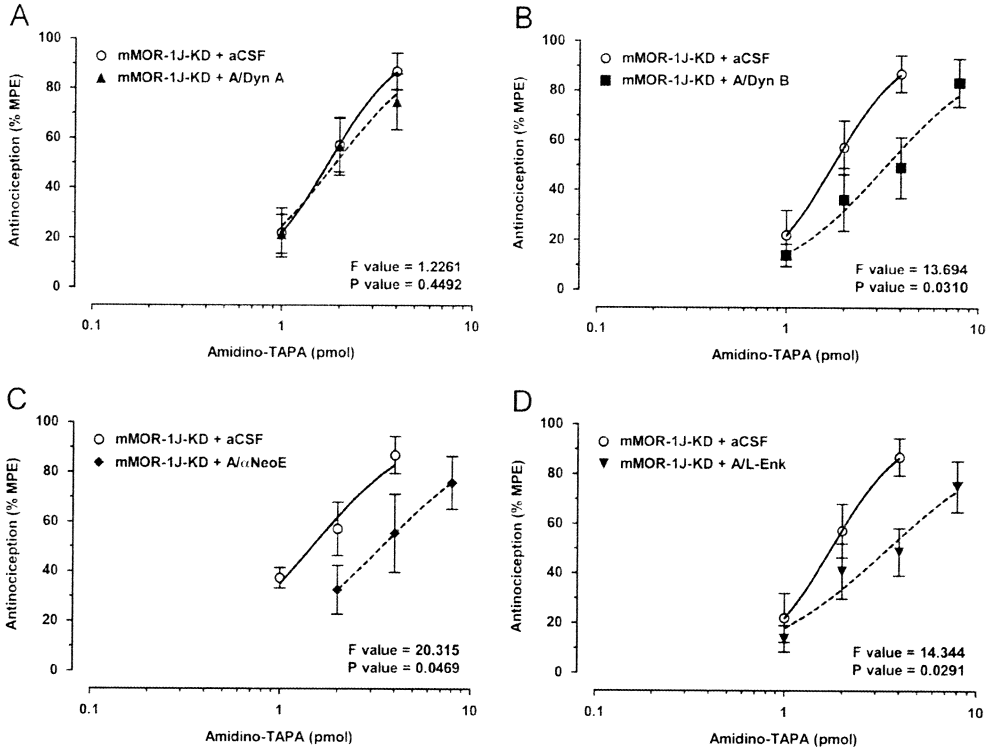


Fig. 2. Effects of antisera against the endogenous opioid peptides on the antinociception induced by amidino-TAPA in mice, whose spinal mMOR-1J (mMOR-1 splice variant containing the sequence encoded by exon-12 of mMOR-1 gene) had been knocked-down (mMOR-1J-KD). Groups of mice pretreated i.t. with amidino-TAPA (2 pmol) in combination with antisense ODN for exon-12 of mMOR-1 gene (5 μg) 24 h before, were injected i.t. with aCSF or antisera (1:50 dilution) against dynorphin A (A/Dyn A: A), dynorphin B (A/Dyn B: B), α-neo-endorphin (A/αNeoE: C) or [Leu^5]enkephalin (A/L-Enk: D) 20 min before the i.t. treatment with various doses of amidino-TAPA (1, 2, 4 or 8 pmol), and the tail-flick inhibition induced by amidino-TAPA was measured at 10 min after the treatment. The antinociceptive effect was represented as the mean ± S.E.M. for at least 10 mice.

mice whose spinal mMOR-1K had been knocked-down (Fig. 3B and C).

3.4. *Involvement of the spinal release of the endogenous opioid peptides on the spinal antinociception of amidino-TAPA in mice, whose spinal mMOR-1L had been knocked-down*

Effects of antisera against the endogenous opioid peptides on the antinociception induced by amidino-TAPA were also determined in mice, whose spinal mMOR-1L had been knocked-down using exon-14-specific antisense ODN. Groups of mice pretreated i.t. with amidino-TAPA (2 pmol) in combination with antisense ODN for exon-14 of mMOR-1 gene (5 μg) 24 h before, were injected i.t. with aCSF or antisera (1:50 dilution) against dynorphin A, dynorphin B, α-neo-endorphin or [Leu^5]enkephalin 20 min before the i.t. treatment with various doses of amidino-TAPA (2, 4, 8 or 16 pmol), and the tail-flick inhibition induced by amidino-TAPA was measured at 10 min after the treatment. In mice whose spinal mMOR-1L had been knocked-down using antisense ODN for exon-14 of mMOR-1 gene, amidino-TAPA-induced antinociception was suppressed by the pretreatment with antisera against dynorphin B or α-neo-endorphin, but not dynorphin A or [Leu^5]enkephalin (Fig. 4). The dose–response curve of amidino-TAPA for antinociception was significantly shifted to the right by the pretreatments with antisera against dynorphin B or α-neo-endorphin in mice whose spinal mMOR-1L had been knocked-down (Fig. 4B and C). In contrast, the right forward shift of the dose–response curve of amidino-TAPA for antinociception by the pretreatment with antisera against dynorphin A or [Leu^5]enkephalin, which was observed in naïve mice, was eliminated in mice whose spinal mMOR-1L had been knocked-down (Fig. 4A and D).

4. Discussion

The μ-opioid receptor is a G-protein coupled receptor and has a lot of variability (splice variants) basing on the splicing of the mRNA precursor for mMOR-1 gene. At present, 19 of exons for mMOR-1 gene and 32 of splice variants (mMOR-1, mMOR-1A, mMOR-1B1, mMOR-1B2, mMOR-1B3, mMOR-1B4, mMOR-1B5, mMOR-1C, mMOR-1D, mMOR-1E1, mMOR-1E2, mMOR-1E3, mMOR-1E4, mMOR-1F, mMOR-1G, mMOR-1H, mMOR-1I, mMOR-1J, mMOR-1K, mMOR-1L, mMOR-1M, mMOR-1N, mMOR-1O, mMOR-1P, mMOR-1Q, mMOR-1R, mMOR-1S, mMOR-1T, mMOR-1U, mMOR-1V1, mMOR-1V2, mMOR-1W) for mMOR-1 have been identified (Doyle et al., 2007a, 2007b; Kvam et al., 2004; Pan et al., 2001, 2005). The most of splice variants for mMOR-1 identified contain the sequence encoded by exon-1 of mMOR-1 gene. Pasternak and his colleagues described the selectivity and intrinsic activity of various μ-opioid receptor agonists for mMOR-1 splice variants (mMOR-1, mMOR-1A, mMOR-1C, mMOR-1D, mMOR-1E and mMOR-1F) containing the sequences encoded by exon-1 of mMOR-1 gene, using the CHO cells expressing each of these splice variants (Bolan et al., 2004; Pan et al., 1999, 2000; Pasternak 2004). However, no remarkable differences in the selectivity and intrinsic activity of any μ-opioid receptor agonist were observed between mMOR-1 splice variants examined. In other splice

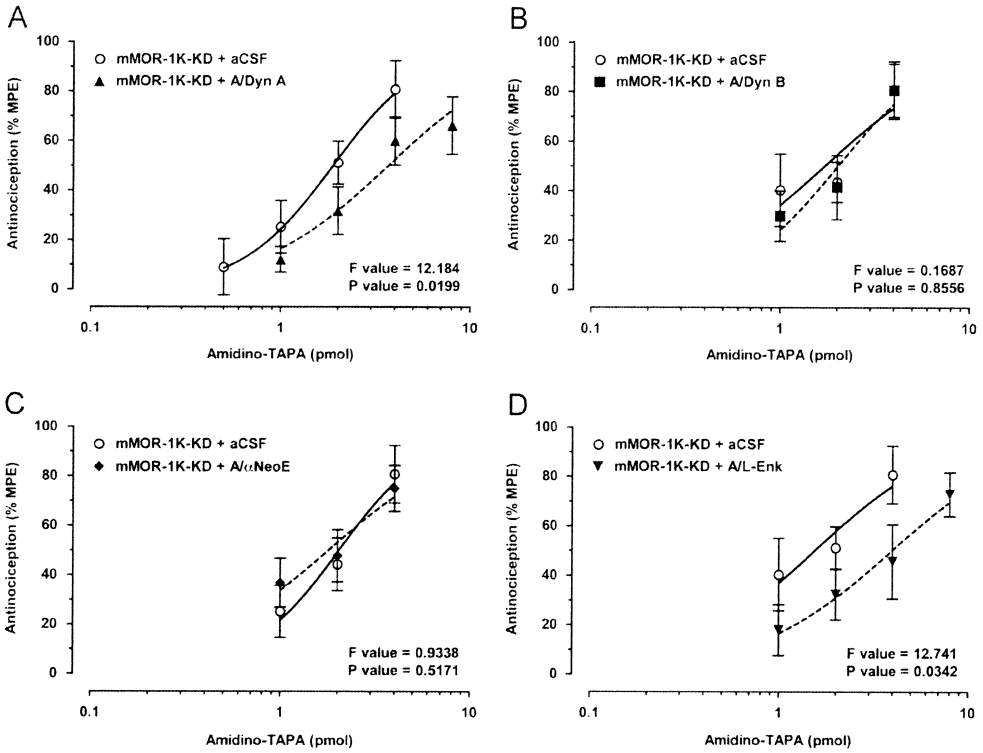


Fig. 3. Effects of antisera against the endogenous opioid peptides on the antinociception induced by amidino-TAPA in mice, whose spinal mMOR-1K (mMOR-1 splice variant containing the sequence encoded by exon-13 of mMOR-1 gene) had been knocked-down (mMOR-1K-KD). Groups of mice pretreated i.t. with amidino-TAPA (2 pmol) in combination with antisense ODN for exon-13 of mMOR-1 gene (5 μg) 24 h before, were injected i.t. with aCSF or antisera (1:50 dilution) against dynorphin A (A/Dyn A: A), dynorphin B (A/Dyn B: B), α-neo-endorphin (A/αNeoE: C) or [Leu^5]enkephalin (A/L-Enk: D) 20 min before the i.t. treatment with various doses of amidino-TAPA (0.5, 1, 2, 4 or 8 pmol), and the tail-flick inhibition induced by amidino-TAPA was measured at 10 min after the treatment. The antinociceptive effect was represented as the mean ± S.E.M. for at least 10 mice.

variants for mMOR-1, the selectivity and intrinsic activity of μ-opioid receptor agonists is still unknown. Moreover, the physiological roles of each splice variants for mMOR-1 and their functional differences are also still unknown, although the distribution for most of splice variants for mMOR-1 have been already described in the rodent central nervous system (Doyle et al., 2007a, 2007b; Pan et al., 1999, 2000, 2001, 2005).

We previously found that amidino-TAPA induces the release of endogenous κ-opioid peptides dynorphin A, dynorphin B and α-neo-endorphin and the endogenous δ-opioid peptide [Leu^5] enkephalin at spinal cord to produce the antinociception via activation of spinal μ-opioid receptors (Mizoguchi et al., 2007). The traditional μ-opioid receptor agonists, such as DAMGO and morphine, do not have these distinct mechanisms for spinal antinociception. Therefore, the distinct antinociceptive profiles of amidino-TAPA that are the release of the endogenous opioid peptides, may be mediated through the activation of distinct μ-opioid receptors that are mMOR-1 splice variants sensitive to amidino-TAPA and insensitive to traditional μ-opioid receptor agonists. Among 32 of splice variants for mMOR-1 identified (Doyle et al., 2007a, 2007b; Kvam et al., 2004; Pan et al., 2001, 2005), we recently found that mMOR-1J, mMOR-1K and mMOR-1L containing the sequence encoded by exon-12, exon-13 and exon-14 of mMOR-1 gene, respectively, are the amidino-TAPA-sensitive and DAMGO-insensitive mMOR-1 splice variants in the spinal cord (Mizoguchi et al., 2011). The spinal antinociception of amidino-TAPA but not DAMGO was suppressed by the exon-specific knock-down of mMOR-1J, mMOR-1K and mMOR-1L using the antisense ODNs for exon-12, exon-13 and exon-14 of mMOR-1 gene, respectively. The release of endogenous opioid peptides by amidino-TAPA may be mediated through the activation of these splice variants for mMOR-1 in the spinal cord. In the present study, to identify the specific mMOR-1 splice variants involved in the release of each endogenous opioid peptides in the spinal cord, which are related to the spinal antinociception of amidino-TAPA, effects of antisera against endogenous opioid peptides on the spinal antinociception induced by amidino-TAPA were determined in mice which spinal mMOR-1J, mMOR-1K or mMOR-1L have been knocked-down, using antisense ODNs for exon-12, exon-13 or exon-14 of mMOR-1 gene, respectively. As we previously reported (Mizoguchi et al., 2007), the amidino-TAPA-induced spinal antinociception was suppressed by the i.t. pretreatment with antisera against dynorphin A, dynorphin B, α-neo-endorphin or [Leu^5] enkephalin in naïve mice. In mice spinal mMOR-1J had been knocked-down, amidino-TAPA-induced spinal antinociception was suppressed by the i.t.-pretreatment with antisera against dynorphin B, α-neo-endorphin or [Leu^5]enkephalin, whereas the suppression of amidino-TAPA-induced antinociception by the antiserum against dynorphin A, which was observed in naïve mice, was disappeared, suggesting that the release of dynorphin A by amidino-TAPA is mediated through the spinal mMOR-1J. In mice spinal mMOR-1K had been knocked-down, amidino-TAPA-induced spinal antinociception was suppressed by the i.t.-pretreatment with antisera against dynorphin A or [Leu^5]enkephalin, whereas the suppression of amidino-TAPA-induced antinociception by the antisera against dynorphin B or α-neo-endorphin was disappeared, suggesting that the release of dynorphin B or α-neo-endorphin by amidino-TAPA is mediated through the spinal mMOR-1K. In mice spinal mMOR-1L had been knocked-down, amidino-TAPA-induced spinal antinociception was suppressed

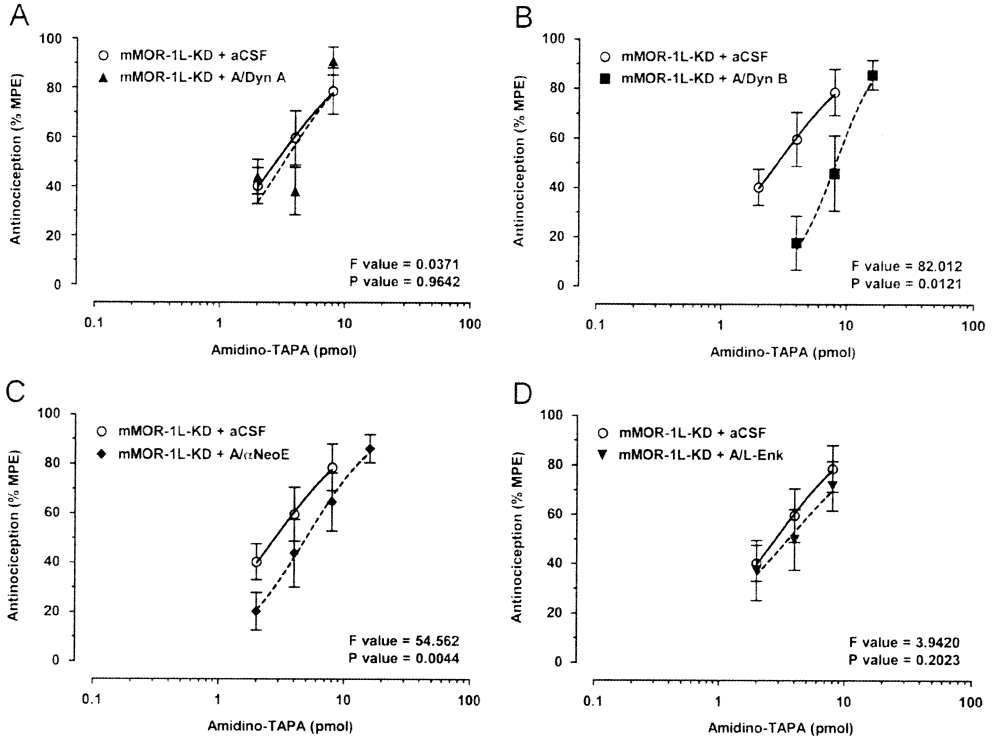


Fig. 4. Effects of antisera against the endogenous opioid peptides on the antinociception induced by amidino-TAPA in mice, whose spinal mMOR-1L (mMOR-1 splice variant containing the sequence encoded by exon-14 of mMOR-1 gene) had been knocked-down (mMOR-1L-KD). Groups of mice pretreated i.t. with amidino-TAPA (2 pmol) in combination with antisense ODN for exon-14 of mMOR-1 gene (5 μg) 24 h before, were injected i.t. with aCSF or antisera (1:50 dilution) against dynorphin A (A/Dyn A: A), dynorphin B (A/Dyn B: B), α-neo-endorphin (A/αNeoE: C) or [Leu^5]enkephalin (A/L-Enk: D) 20 min before the i.t. treatment with various doses of amidino-TAPA (2, 4, 8 or 16 pmol), and the tail-flick inhibition induced by amidino-TAPA was measured at 10 min after the treatment. The antinociceptive effect was represented as the mean ± S.E.M. for at least 10 mice.

by the i.t.-pretreatment with antisera against dynorphin B or α-neo-endorphin, whereas suppression of amidino-TAPA-induced antinociception by the antisera against dynorphin A or [Leu^5]enkephalin was disappeared, suggesting that the release of dynorphin A or [Leu^5]enkephalin by amidino-TAPA is mediated through the spinal mMOR-1L. The present results clearly show that the release of endogenous opioid peptides involved in the distinct antinociceptive property for amidino-TAPA, is mediated through the activation of distinct mMOR-1 splice variants, mMOR-1J, mMOR-1K or mMOR-1L, in spinal cord. Although 32 of splice variants for mMOR-1 have been identified and the distribution for most of splice variants have been described in the rodent central nervous system (Doyle et al., 2007a, 2007b; Pan et al., 1999, 2000, 2001, 2005), the physiological roles of each splice variants have been unclear. The present study firstly identified the distinct physiological roles of specific splice variants for mMOR-1 in spinal cord.

In the present study, we found that the spinal release of endogenous κ-opioid peptides dynorphin A, dynorphin B and α-neo-endorphin and the endogenous δ-opioid peptide [Leu^5]enkephalin were revealed by the activation of different mMOR-1 splice variants. These endogenous opioid peptides are all processed from same precursor, prodynorphin (Kakidani et al., 1982), and the immunoreactivities to these endogenous opioid peptides are co-localized in many brain and spinal regions. Therefore, these endogenous opioid peptides are originally considered to be contained in and to be released from same neurons. However, the distributions and processing ratios of these endogenous opioid peptides are not same. The immunoreactivity to dynorphin B is also found in some neurons in which the immunoreactivities to dynorphin A and α-neo-endorphin are not found (Weber and Barchas, 1983). Moreover, the dynorphin B and dynorphin A (1–8), but not dynorphin A, α-neo-endorphin or [Leu^5]enkephalin, were released from the guinea pig hippocampus by the focal electrical stimulation (Wagner et al., 1991). The evidences clearly suggest that there is a tissue (site)-specific processing involved in the variable distributions and processing ratios of each endogenous opioid peptide, and each endogenous opioid peptide is theoretically possible to be individually released from different neurons. The present result indicating that the spinal release of each endogenous opioid peptide is revealed by the activation of different mMOR-1 splice variants, is another strong evidence to prove this hypothesis.

The spinal antinociception mediated through the release of endogenous opioid peptides is also observed in other selective μ-opioid receptor agonists, endomorphin-2 (Mizoguchi et al., 2006b; Sakurada et al., 2001), TAPS (Mizoguchi et al., 2006a) and [Dmt^1]DALDA (Szeto et al., 2003). Interestingly, released endogenous opioid peptides are variable in above μ-opioid receptor agonists. In contrast with amidino-TAPA, which leads to the release of dynorphin A, dynorphin B, α-neo-endorphin and [Leu^5]enkephalin to produce the antinociception, the spinal antinociceptions of endomorphin-2 and [Dmt^1]DALDA are mediated through the release of dynorphin A and [Met^5]enkephalin (Sakurada et al., 2001, Szeto et al., 2003). On the other hand, the spinal antinociception of TAPS is mediated through the release of dynorphin B only (Mizoguchi et al., 2006a). Like amidino-TAPA, these μ-opioid receptor agonists also may activate distinct mMOR-1 splice variants to reveal the spinal release of endogenous opioid peptides. By conducting the same experiments using these μ-opioid receptor agonists, the physiological roles of other splice variants for mMOR-1 in spinal cord also may be identified.

5. Conclusion

In conclusion, the distinct antinociceptive property of amidino-TAPA, which is a release of the endogenous κ-opioid peptides dynorphin A, dynorphin B and α-neo-endorphin and the endogenous δ-opioid peptide [Leu^5]enkephalin in spinal cord, may be mediated through the activation of mMOR-1J, mMOR-1K and mMOR-1L. The splice variants for mMOR-1 in spinal cord that are insensitive to traditional μ-opioid receptor agonists may have the distinct physiological roles with other splice variants.

Acknowledgements

This work was supported by a Grant-in-Aid for Scientific Research (C) [KAKENHI 22600009 and 24590731] from the Japan Society for the Promotion of Science, and a MEXT (Ministry of Education, Culture, Sports, Science and Technology)-Supported Program for the Strategic Research Foundation at Private Universities (2010–2014).

References

Bolan, E.A., Pan, Y.-X., Pasternak, G.W., 2004. Functional analysis of MOR-1 splice variants of the mouse mu opioid receptor gene *Oprm*. Synapse 51, 11–18.

Chen, Y., Mestek, A., Liu, J., Hurley, A., Yu, L., 1993. Molecular cloning and functional expression of a μ-opioid receptor from rat brain. Mol. Pharmacol. 44, 8–12.

D'Amour, F.E., Smith, D.L., 1941. A method for determining loss of pain sensation. J. Pharmacol. Exp. Ther. 72, 74–79.

Doyle, G.A., Sheng, X.R., Lin, S.S., Press, D.M., Grice, D.E., Buono, R.J., Ferraro, T.N., Berrettini, W.H., 2007a. Identification of three mouse μ-opioid receptor (MOR) gene (Oprm1) splice variants containing a newly identified alternatively spliced exon. Gene 388, 135–147.

Doyle, G.A., Sheng, X.R., Lin, S.S., Press, D.M., Grice, D.E., Buono, R.J., Ferraro, T.N., Berrettini, W.H., 2007b. Identification of five mouse μ-opioid receptor (MOR) gene (Oprm1) splice variants containing a newly identified alternatively spliced exon. Gene 395, 98–107.

Hylden, J.L., Wilcox, G.L., 1980. Intrathecal morphine in mice: a new technique. Eur. J. Pharmacol. 67, 313–316.

Kakidani, H., Furutani, Y., Takahashi, H., Noda, M., Morimoto, Y., Hirose, T., Asai, M., Inayama, S., Nakanishi, S., Numa, S., 1982. Cloning and sequence analysis of cDNA for porcine β-neo-endorphin/dynorphin precursor. Nature 298, 245–249.

Kvam, T.-M., Baar, C., Rakvåg, T.T., Kaasa, S., Krokan, H.E., Skorpen, F., 2004. Genetic analysis of the murine μ opioid receptor: increased complexity of Oprm gene splicing. J. Mol. Med. 82, 250–255.

Mizoguchi, H., Ito, K., Watanabe, H., Watanabe, C., Katsuyama, S., Fujimura, T., Sakurada, T., Sakurada, S., 2006a. Contribution of spinal μ_1-opioid receptors and dynorphin B to the antinociception induced by Tyr-D-Arg-Phe-Sar. Peptides 27, 2786–2793.

Mizoguchi, H., Watanabe, H., Hayashi, T., Sakurada, W., Sawai, T., Fujimura, T., Sakurada, T., Sakurada, S., 2006b. Possible involvement of dynorphin A (1–17) release via μ_1-opioid receptors in spinal antinociception by endomorphin-2. J. Pharmacol. Exp. Ther. 317, 362–368.

Mizoguchi, H., Watanabe, C., Higashiya, T., Takeda, S., Moriyama, K., Yonezawa, A., Sato, T., Komatsu, T., Sakurada, T., Sakurada, S., 2011. Involvement of mouse μ-opioid receptor splice variants in the spinal antinociception induced by the dermorphin tetrapeptide analog amidino-TAPA. Eur. J. Pharmacol. 651, 66–72.

Mizoguchi, H., Watanabe, C., Watanabe, H., Moriyama, K., Sato, B., Ohwada, K., Yonezawa, A., Sakurada, T., Sakurada, S., 2007. Involvement of endogenous opioid peptides in the antinociception induced by the novel dermorphin tetrapeptide analog amidino-TAPA. Eur. J. Pharmacol. 560, 150–159.

Ogawa, T., Miyamae, T., Murayama, K., Okuyama, K., Okayama, T., Hagiwara, M., Sakurada, S., Morikawa, T., 2002. Synthesis and structure-activity relationships of an orally available and long-acting analgesic peptide, N^{ω}-amidino-Tyr-D-Arg-Phe-MeβAla-OH (ADAMB). J. Med. Chem. 45, 5081–5089.

Pan, Y.-X., Xu, J., Bolan, E., Abbadie, C., Chang, A., Zuckerman, A., Rossi, G., Pasternak, G.W., 1999. Identification and characterization of three new alternatively spliced μ-opioid receptor isoforms. Mol. Pharmacol. 56 936-403.

Pan, Y.-X., Xu, J., Bolan, E., Chang, A., Mahurter, L.A., Rossi, G., Pasternak, G.W., 2000. Isolation and expression of a novel alternatively spliced mu opioid receptor isoform, MOR-1F. FEBS Lett. 466, 337–340.

Pan, Y.-X., Xu, J., Bolan, E., Moskowitz, H.S., Xu, M., Pasternak, G.W., 2005. Identification of four novel exon 5 splice variants of the mouse μ-opioid receptor gene: functional consequences of C-terminal splicing. Mol. Pharmacol. 68, 866–875.

Pan, Y.-X., Xu, J., Mahurter, L., Bolan, E., Xu, M., Pasternak, G.W., 2001. Generation of the mu opioid receptor (MOR-1) protein by three new splice variants of the Oprm gene. PNAS 98, 14084–14089.

Pasternak, G.W., 2004. Multiple opiate receptors: déjà vu all over again. Neuropharmacology 47, 312–323.

Sakurada, S., Hayashi, T., Yuhki, M., Orito, T., Zadina, J.E., Kastin, A.J., Fujimura, T., Murayama, K., Sakurada, C., Sakurada, T., Narita, M., Suzuki, T., Tan-no, K., Tseng, L.F., 2001. Differential antinociceptive effects induced by intrathecally administered endomorphin-1 and endomorphin-2 in the mouse. Eur. J. Pharmacol. 427, 203–210.

Szeto, H.H., Soong, Y., Wu, D., Qian, X., Zhao, G.M., 2003. Endogenous opioid peptides contribute to antinociceptive potency of intrathecal [Dmt^1]DALDA. J. Pharmacol. Exp. Ther. 305, 696–702.

Wagner, J.J., Evans, C.J., Chavkin, C., 1991. Focal stimulation of the mossy fibers releases endogenous dynorphins that bind κ_1-opioid receptors in guinea pig hippocampus. J. Neurochem. 57, 333–343.

Wang, J.B., Imai, Y., Eppler, C.M., Gregor, P., Spivak, C.E., Uhl, G.R., 1993. μ Opiate receptor: cDNA cloning and expression. PNAS 90, 10230–10234.

Weber, E., Barchas, J.D., 1983. Immunohistochemical distribution of dynorphin B in rat brain: relation to dynorphin A and α-neo-endorphin systems. PNAS 80, 1125–1129.

Cell. Mol. Life Sci. (2013) 70:3067–3075
DOI 10.1007/s00018-012-1208-x

Cellular and Molecular Life Sciences

REVIEW

Heterogeneity of gangliosides among T cell subsets

Jin-ichi Inokuchi · Masakazu Nagafuku · Isao Ohno · Akemi Suzuki

Received: 26 August 2012 / Revised: 7 October 2012 / Accepted: 5 November 2012 / Published online: 12 December 2012
© Springer Basel 2012

Abstract Gangliosides are major components of highly organized membrane microdomains or rafts, yet little is known about the role of gangliosides in raft organization. This is also the case of gangliosides in TCR-mediated activation. Comprehensive structural analysis of gangliosides in the primary thymocytes and $CD4^+$ T and $CD8^+$ T cells was not achieved due to technical difficulties. We have found that $CD8^+$ T cells express very high levels of o-series gangliosides, but on the other hand, $CD4^+$ T cells preferably express a-series gangliosides. In the TCR-dependent activation, $CD4^+$ T cells selectively require a-series gangliosides, but $CD8^+$ T cells do require only o-series gangliosides but not a-series gangliosides. Ganglioside GM3 synthase-deficient mice lacking a-series gangliosides neither exhibited the TCR-dependent activation of $CD4^+$ T nor developed ovalbumin-induced allergic airway inflammation. These findings imply that the distinct expression pattern of ganglioside species in $CD4^+$ and $CD8^+$ T cells define the immune function of each T cell subset.

J. Inokuchi (✉) · M. Nagafuku
Division of Glycopathology, Institute of Molecular Biomembrane and Glycobiology, Tohoku Pharmaceutical University, 4-4-1 Komatsushima, Aoba-ku, Sendai 981-8558, Japan
e-mail: jin@tohoku-pharm.ac.jp

I. Ohno
Department of Pathophysiology, Tohoku Pharmaceutical University, Sendai 981-8558, Japan

A. Suzuki
Institute of Glycoscience, Tokai University, Hiratsuka, Kanagawa 259-1292, Japan

Keywords Gangliosides · Lipid rafts · T cell activation · Asthma

Abbreviations

GM3S	GM3 synthase
GM2/GD2S	GM2/GD2 synthase
GSLs	Glycosphingolipids
SA	Sialic acid
CTx-B	Cholera toxin B subunit

Introduction

T cells constitute an important component of our immune system and are involved in immune surveillance and antigen recognition. Virtually all mature T cells are either $CD4^+CD8^-$ or $CD4^-CD8^+$, indicating that these surface-phenotype distinctions must be crucial for the entire T cell response. $CD4^+$-expressing helper lineage T cells participate in a wide variety of immune functions including humoral immunity, allergic responses, etc. On the other hand, $CD8^+$-expressing cytotoxic lineage T cells possess killing ability against cancer cells and virus-infected cells. Antigen (Ag)-specific immune responses are elicited when T cells expressing a specific Ag receptor [the T cell receptor (TCR)] interact with Ag-presenting cells (APCs) that bear a cognate Ag peptide–MHC (pMHC). This interaction is responsible for the formation of a unique "immunological synapse" [1].

The membrane fluidity is directly determined by the physicochemical characteristics of lipid molecules composing the lipid bilayer of cell membranes. However, the composition and behavior of lipids in the immunological synapse are still not completely understood. "Lipid rafts"

have long been proposed to be an essential platform for TCR signaling [2]. Several recent studies have detailed the molecular components of both lipid rafts and the immunological synapse, and elegantly described the dynamic nature of molecules participating in these processes during the course of T cell activation [3–7]. However, regulatory mechanisms governing recruitment of molecules to rafts and synapse organization are less well understood.

Major lipid species existing in lipid rafts are glycosphingolipids (GSLs), sphingomyelin, and cholesterol. Involvement of sialic acid (SA)-containing GSLs, gangliosides, in the T cell activation has been demonstrated by a number of observations. For example, it has been demonstrated that the polarization of GM1 ganglioside occurs only in $CD4^+$ T cells but not in $CD8^+$ T cells, when TCR clustering of both T cell subsets was induced by anti-CD3 and anti-CD28 antibodies [8]. Furthermore, GM1 and GM3 gangliosides appear to define different types of rafts, which segregate to the leading pole and the trailing uropod of the polarized human T cells, respectively [9]. Cholera toxin B subunit (CTx-B) has long been utilized for the visualization and functional analysis of rafts, but the raft recognized by CTx-B represents only a part of them, indicating that rafts must be heterogeneous and be grouped into subclasses. In addition, there are big differences in the expression levels of GM1, which depend on the cell types, and cellular development and differentiation. Sometimes GM1 expression on the cell surface is much lower than the other ganglioside species.

Therefore, in order to understand the role of rafts in the course of differentiation and maturation of $CD4^+$ T and $CD8^+$ T cells in vivo, it is prerequisite to know the detailed ganglioside composition in the respective T cell subset. Here we propose that the functional repertoire selection from double-positive to single-positive T cells is accompanied with the selection of ganglioside expression in the individual T cell subsets. This ganglioside selection process is indispensable for the functional microcluster formation and/or lipid rafts for mature T cells.

Structural analyses of ganglioside species in the T cell subsets

Glycosphingolipids are built on a ceramide backbone comprising a long-chain amino alcohol, sphingosine, and an amide-linked fatty acid. Gangliosides are SA-containing GSLs. GM3, the simplest of the "a-series" gangliosides, is synthesized by GM3 synthase (GM3S), which catalyzes the transfer of SA to the nonreducing terminal galactose (Gal) of lactosylceramide (LacCer). GM3 is altered by GM2/GD2 synthase (GM2/GD2S) to form GM2, a downstream a-series ganglioside, or by GD3 synthase (GD3S) to form GD3, the simplest of the "b-series" gangliosides. GM2/GD2S also elongates LacCer to form GA2, the simplest precursor GSL of the "o-series" ganglioside. Each branch of GSL biosynthesis is a committed pathway (Fig. 1), then competition between enzymes at a key branch point determines the relative expression levels of o-, a-, and b-series gangliosides.

Ganglioside expression in primary T cells has previously been studied using biochemical analyses (TLC and HPLC) of whole T cell populations including cloned T cell lines and T cell blastocytes stimulated by concanavalin A. However, whole T cell populations are truly a "mixed population", therefore any such results would be of limited value in terms of studying characteristic features of specific T cell subsets. Previously, FACS analysis with monoclonal antibodies (mAbs) against several ganglioside demonstrated that mature peripheral $CD4^+$ T cells and $CD8^+$ T cells express differential species of gangliosides [10, 11]. These studies mainly demonstrated the predominance of GalNAc–GM1b in CD8T cells [10] and GD1c in CD4T cells [11].

We examined the structures of gangliosides in immature thymocytes, and the primary $CD4^+$ T cells and $CD8^+$ T cells isolated from cell mixtures prepared from lymph nodes and spleen by LC–MS/MS analysis (Table 1) [12]. Thymocytes consisting mainly of $CD4^+$ $CD8^+$ T double-positive (DP) cells expressed the six distinct species, GM1a, GM1b, GD1b, GD1c, GalNAcGM1b, and extended-GM1b, and their relative expression levels (%) were 8.4, 18.9, 29.9, 13.3, 23.0, and 6.5, respectively. The presence of these gangliosides was common in all T cell subsets, but their expression levels are remarkably different in each subset (Table 1). The expression of o-series gangliosides, GalNAcGM1b and extended-GM1b, was greatly enhanced by the differentiation from thymocytes (23.0 and 6.5 %) to $CD4^+$ T (36.6 and 18.9 %) and $CD8^+$ T (49.0 and 37.1 %) cells. On the other hand, the expression of another o-series ganglioside GD1c was enhanced to double in $CD4^+$ T cells (20.3 %) but greatly decreased in $CD8^+$ T cells (3.7 %). GD1b was expressed in a considerable amount (30 %) in thymocytes, but 6 % in $CD4^+$ T and 0.8 % in $CD8^+$ T cells. The expression of GM1b was maintained among T cell subsets, but GM1a was expressed in both thymocytes and $CD4^+$ T cells but only trace amounts in CD8T cells. We examined the expression of *GM3S* and *GM2/GD2S* genes among T cell subsets [12]. *GM2/GD2S* expression was markedly increased more than 100-folds in both $CD4^+$ T and $CD8^+$ T cells compared to thymocytes. *GM3S* expression was increased to 180 % in $CD4^+$ T cells and was decreased to 30 % in $CD8^+$ T cells, compared to the expression in thymocytes. These gene expression patterns could partially explain the above-mentioned distinct expression profile of gangliosides

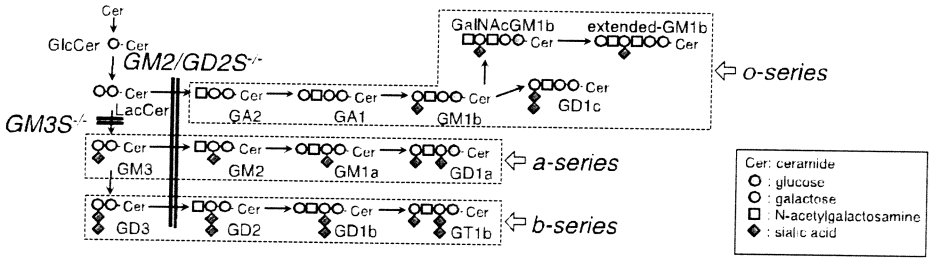


Fig. 1 Ganglio-series glycosphingolipids are synthesized from ceramide and are divided into o-, a-, and b-series species

during the differentiation processes from immature thymocytes to the mature $CD4^+$ T and $CD8^+$ T cells. In the case of GD1c, Nakamura et al. [11] reported that $CD4^+$ T cells can be separated into GD1c-positive IL-2-producing Th1-like cells and GD1c-negative IL-4-producing Th2-like cells. These findings suggest that T cell subsets can be classified into the distinct functional subpopulations based on the differences of gangliosides expression profiles. Wang et al. [13, 14] reported that cross-linking of GM1 on $CD4^+$ and $CD8^+$ effector T cells (Teff) by galactin-1 plays a significant role in autoimmune suppression through the modulation of Ca^{+2} influx via transient receptor potential channel 5 (TRPC5). They showed that resting $CD4^+$ Teff and $CD8^+$ Teff contain GM1 and GD1a as the major gangliosides detected by HPTLC with sialidase treatment and CTx-B binding, $CD8^+$ Teff express higher levels of GD1a than $CD4^+$ Teff and both GM1 and GD1a are upregulated by the activation with anti-CD3 and anti-CD28. They did not discuss the possibility that GD1a assigned in their analysis might contain extended-GM1 but this possibility is supported by the following lines of evidence; extended-GM1 is sialidase-resistant, migrates like GD1a on HPTLC developed with chloroform–methanol-water containing $CaCl_2$ [24], exhibits CTx-B binding activity very similar to GM1 [24] and is detected in a higher amount in $CD8^+$ T cells than $CD4^+$ T cells [12]. GD1a-containing NeuGc of $CD4^+$ and $CD8^+$ T cells was present and was a minor component, compared with GM1 and extended-GM1, in our LC–MS analysis [12]. Another point for requiring ganglioside analysis of primary native cells without any activations is that the downregulation of CMP-NeuAc hydroxylase by an activation was reported in mouse B cells [15]. The change of sialic acid expression from NeuGc to NeuAc even in T cells is possible and this is another future subject for understanding physiological functions of gangliosides in the immunocytes.

We were also interested in the role of fatty acid acyl chain lengths of gangliosides in the organization of ganglioside-dependent rafts in T cell lineages [12]. As shown in Fig. 2, the relative expression levels of ceramide moiety carrying d18:1–16:0 in all gangliosides significantly decreased in $CD4^+$ T and $CD8^+$ T cells compared to those of thymocytes. On the other hand, ceramides with more hydrophobic nature, d18:1–22:0 and d18:1–24:0, in almost all gangliosides tend to increase in $CD4^+$ T and $CD8^+$ T cells. The contribution of the long and saturated acyl chains of glycosphingolipids to raft formation has been appreciated [16]. These glycosphingolipids allow close packing of the lipids resulting in a high melting temperature (Tm). Self-aggregates of sphingolipids form a separate phase that is less fluid (liquid-ordered) than the bulk liquid-disordered phospholipids. These observations suggest that the hydrophobicity of individual ganglioside is increased in peripheral primary T cells to create the rigid raft structure necessary for TCR signaling. It has been demonstrated that lactosylceramide, having a C24 fatty acid chain, is crucial for association of the lyn molecule, which is responsible for GSL-mediated outside-in signal transduction [17].

Distinct selectivity of gangliosides required for $CD4^+$ T and $CD8^+$ T cell activation

The role of gangliosides in TCR signaling and T cell activation has been studied using inhibitors of GSL biosynthesis [18]. We previously demonstrated that the treatment of Jurkat cells with D-threo–1–phenyl–2–decanoylamino–3–morpholino–1–propanol (D-PDMP), an inhibitor of glucosylceramide synthase [19], preferentially reduces the level of GSLs in rafts without affecting SM and cholesterol levels, and the alteration of GSL content neither impairs signal transduction via the T cell receptor nor the protein distribution in lipid rafts. However, D-PDMP treatment resulted in the upregulation of TCR signaling via GPI-anchored protein [19]. On the other hand, it has been reported that the treatment of human peripheral blood lymphocytes with this inhibitor attenuates TCR signaling and T cell activation as indicated by a reduced expression of markers of T cell activation and a reduced secretion of IFN-γ [20].

To investigate functional roles of gangliosides in T cell development and immunity, we utilized two types of gene-targeted mice with interrupted ganglioside biosynthesis (Fig. 1). GM3S null mice lack all a- and b-series

Table 1 Structures of ganglioside species found in mouse primary T cells

Structure	Biosynthetic pathway[a]	Trivial name	Relative expression level (%)		
			Thy	CD4T	CD8T
Galβ1-3GalNAcβ1-4(SAα2-3)Galβ1-4Glcβ1-1'Cer	a-series	GM1a	8.4	4.1	0.8
SAα2-3Galβ1-3GalNAcβ1-4Galβ1-4Glcβ1-1'Cer	o-series	GM1b	18.9	14.4	8.6
Galβ1-3GalNAcβ1-4(SAα2-8SAα2-3)Galβ1-4Glcβ1-1'Cer	b-series	GD1b	29.9	5.7	0.8
SAα2-8SAα2-3Galβ1-3GalNAcβ1-4Galβ1-4Glcβ1-1'Cer	o-series	GD1c	13.3	20.3	3.7
GalNAcβ1-4(SAα2-3)Galβ1-3GalNAcβ1-4Galβ1-4Glcβ1-1'Cer	o-series	GalNAcGM1b	23	36.6	49
Galβ1-4GalNAcβ1-4(SAα2-3)Galβ1-3GalNAcβ1-4Galβ1-4Glcβ1-1'Cer	o-series	extended-GM1b	6.5	18.9	37.1

Structures of gangliosides and their relative distribution among T cell subsets are the summary of Fig. 4b and Fig. S4 in ref [12]

Thy thymocytes

[a] Biosynthetic pathway of each series gangliosides is illustrated in Fig. 1

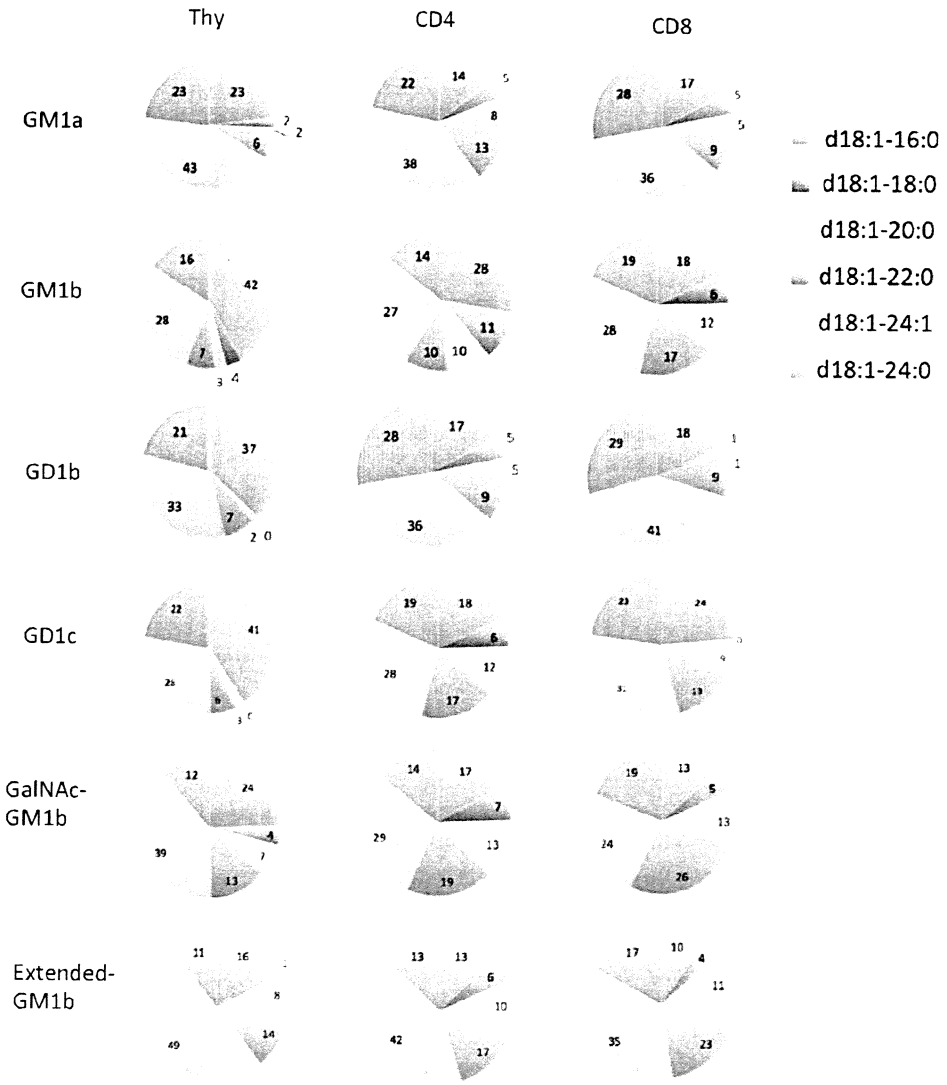


Fig. 2 Alteration of fatty acid moieties of gangliosides in thymocytes (Thy) and primary $CD4^+$ T and $CD8^+$ T cells [12]

gangliosides, resulting in LacCer accumulation and compensatory increase of o-series GSLs [21]. GM2/GD2S null mice lack all o-series GSLs and all elongated a- and b-series gangliosides, then they accumulate LacCer and express only GM3 and GD3 gangliosides [22].

GM3S null and GM2/GD2S null mice did not reveal any obvious alteration in the cellularity of the lymphoid organs, indicating no gross defects in T cell development despite the altered ganglioside expression. However, $CD4^+$ T cells (but not $CD8^+$ T cells) from GM3S null mice exhibited severe defects in their proliferative response to the stimulation with an anti-CD3/anti-CD28 antibody mixture, but maintained a normal response to a phorbol myristate acetate (PMA) plus ionomycin (Io) treatment. Conversely, $CD8^+$ T cells (but not $CD4^+$ T cells) from GM2/GD2S null mice exhibited similar severe defects in TCR-mediated activation when stimulated with the antibody mixture [12]. Following the TCR stimulation, both IL-2 and IFNγ production were severely reduced in both GM3S null $CD4^+$ T cells and GM2/GD2S null $CD8^+$ T cells. Responses to an alloantigen, a superantigen, and a specific antigen peptide were similar to those observed with the anti-CD3/anti-CD28 mixture. In contrast to T cells, splenic B cells isolated from GM3S null and GM2/GD2S null mice exhibited no obvious alterations in proliferative responses to various concentrations of anti-IgM antibody and lipopolysaccharide [12].

Staining with CTx-B, commonly used to detect GM1a and visualize rafts, has demonstrated that $CD8^+$ T cells express higher levels of GM1a in the rafts than $CD4^+$ T cells [23]. However, this toxin also reacts to other gangliosides including fucosylated GM1a and extended-GM1b, both of which have a monosialo–ganglio–triose structure, Galβ1–3GalNAcβ1–4(SAα2–3)Galβ1– [24]. In fact, we were able to detect two CTx-B-reactive gangliosides, GM1a and extended-GM1b, in T cells with different quantities in individual T cell subsets [12]. In WT $CD4^+$ T cells, GM1a was expressed in both thymocytes and $CD4^+$ T cells but only trace amounts in $CD8^+$ T cells. Thus, extended-GM1b was expressed much more than GM1a in WT $CD8^+$ T cells as shown in Table 1. The thymocytes and peripheral $CD4^+$ T and $CD8^+$ T cells of GM3S null mice lacked a-series GM1a and expressed o-series extended-GM1b, while the cells from GM2/GD2S null mice did not express either (Fig. 1). The presence of a variety of rafts with different gangliosides in a single cell has been suggested [8, 9]. It has been reported that cross-linking of gangliosides using CTx-B or a homologue, the heat-labile enterotoxin of *Escherichia coli*, can induce apoptosis in $CD8^+$ T cells but not in $CD4^+$ T cells [25]. The apoptosis is caused by activation of NF-κB and c-Myc via the induction of caspase-dependent signaling [26]. While this process is known to proceed in a Fas- and p55 tumor necrosis factor receptor-independent pathway [27], the events in rafts following the ganglioside cross-linking remain undetermined. Considering the difference in the expression of CTx-B-binding gangliosides between $CD4^+$ T cells and $CD8^+$ T cells, the apoptosis caused by CTx-B cross-linking possibly involve extended-GM1b rafts but not GM1a rafts. This suggests that each T cell subset has unique rafts in the plasma membrane and that these rafts provide distinct functions in different intracellular events following receptor-mediated stimulation.

In the experiments to determine which gangliosides have an essential role in TCR-mediated activation of T cell subsets, $CD4^+$ T cells and $CD8^+$ T cells from WT, GM3S null, and GM2/GD2S null mice were pretreated with gangliosides followed by anti-CD3/anti-CD28 stimulation [12]. Proliferative responses of GM3S null $CD4^+$ T cells were restored by the pretreatment with any of the a-series gangliosides (GM3, GM1, and GD1a), but were not restored with any of o- or b-series gangliosides such as GM1b or GD1b (Fig. 3). Conversely, the proliferative responses of GM2/GD2S null $CD8^+$ T cells were restored by the pretreatment with any of the o-series gangliosides (GA2, GA1, and GM1b), but not with any of a- or b-series gangliosides. Importantly, the gangliosides themselves had no effect without the proliferative stimulation. These results indicate that o-series ganglioside expression is essential for TCR-mediated activation of $CD8^+$ T cells and a-series ganglioside is indispensable for that of $CD4^+$ T cells. These data suggest that different species of gangliosides are essentially required by $CD4^+$ T cells and $CD8^+$ T cells in terms of TCR-mediated activation (Fig. 3) [12].

Why do $CD4^+$ T cells and $CD8^+$ T cells require the expression of distinct gangliosides for proper immune

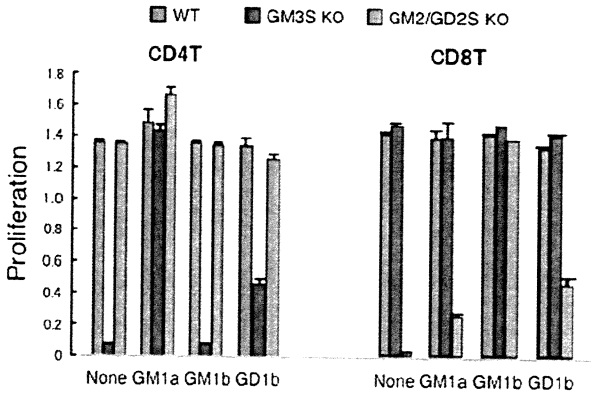


Fig. 3 Activation of $CD4^+$ T and $CD8^+$ T cells upon TCR-mediated stimulation. Purified peripheral $CD4^+$ T and $CD8^+$ T cells from WT, GM3S null, and GM2/GD2S null mice were stimulated with anti-CD3 antibody plus anti-CD28 antibody in the presence or absence of the indicated ganglioside [12]

function? Both cells share a part of molecular mechanisms for TCR-mediated signaling, but certainly do have different cellular and molecular modifications. CD4 and CD8 are considered to localize to lipid rafts by palmitoylation at their juxtamembrane region [28, 29], yet raft localization seems not to be determined by lipid modification alone [29, 30]. To ensure that CD4 and CD8 undergo proper intracellular trafficking and successful localization on the plasma membrane, it might be vital for CD4/CD8 to interact with rafts carrying a specific ganglioside. CD28, a B7 type co-stimulatory molecule, provides functional differences between $CD4^+$ T cells and $CD8^+$ T cells [31, 32]. In human and mouse $CD4^+$ T cells, CD28 promotes the clustering of CTx-B-detectable rafts at the immunological synapse through its downstream signaling molecule protein kinase Cθ [33]. However, $CD8^+$ T cells do not re-orient CTx-B-detectable rafts to the T cell–antigen-presenting cell (APC) interface during TCR activation [8, 34].

Another aspect to consider is the physicochemical properties of sugar residues of gangliosides on plasma membranes. Sonnino and his colleagues [35] proposed that the segregation of one ganglioside with respect to the other in plasma membranes is a spontaneous process explained on the basis of the different geometrical properties of ganglioside headgroup. Based on their assumption, the external galactose of GM1a is quite free. In fact, the disaccharide Galß1–3GalNAcß is characterized by two pairs of torsional angles of +30°, +14°, and +30°, −20°, respectively. Instead, the trisaccharide GalNAcß1–4(Neu5Acα2–3)Galß is a rigid structure in which each linkage is defined by a single pair of torsional angles because of the stabilization by a hydrogen bond between the GalNAc amide portion and the Neu5Ac carboxyl group [36]. In GM1b, the conformational properties should be completely different. All the linkages are free to rotate, each being defined by at least two pairs of torsional angles. This means that the Gal–GalNAc–(Neu5Ac) Gal of GM1a is defined by two conformers, while the Neu5Ac–Gal–GalNAc–Gal of GM1b is defined by eight conformers (Fig. 4). Thus, the volume requested by GM1b to stay in the membrane should be much bigger than that of GM1a. It is expected that

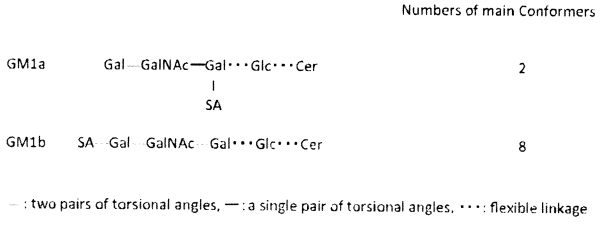


Fig. 4 Dynamic of the ganglioside glycosidic linkages as a function of the primary and secondary structure of gangliosides. Dynamics is reflected as a number of conformers (see details in text)

geometrical properties of GM1a and GM1b are quite different and a bigger influence on a positive membrane curvature is brought by GM1b than by GM1a.

Considering these results and discussion, we speculate that ganglioside compositions in rafts required for the signal transduction mediated by TCR and co-stimulatory molecules are unique and different in $CD4^+$ T cells and $CD8^+$ T cells.

Selective suppression of $CD4^+$ T cell in GM3S null mice resulted in amelioration of experimental asthma

Allergic airway inflammation is tightly regulated by adaptive immunity, in which $CD4^+$ T cells play a crucial role via Th2 cytokine production. We examined allergic airway responses induced by inhalation of ovalbumin (OVA) in OVA-sensitized mice (experimental asthma). OVA challenge induced extensive mucus hypersecretion, a cardinal feature of asthma, in WT but not in the GM3S null mice (Fig. 5) [12]. Although both types of mice challenged with OVA exhibited airway infiltration of inflammatory cells including eosinophils and lymphocytes, the numbers of infiltrating cells were significantly lower in GM3 null mice. Serum OVA-specific IgE levels were greatly increased on days three and five after OVA-challenge in WT mice, but not in GM3S null mice. Decreased levels of Th2 cytokines in the bronchoalveolar lavage (BAL) fluids were also observed in GM3S null mice. In adoptive transfer experiments, $CD4^+$ T cells isolated from OVA-sensitized WT, GM3S, and GM3/GD2S null mice were transferred into naive WT mice, and the recipient mice were challenged with OVA. Infiltration of inflammatory cells, particularly eosinophils and lymphocytes, was suppressed in the recipient mice of $CD4^+$ T cells from GM3S null mice. In the recipient mice of $CD4^+$ T cells from GM2/GD2S null mice, there was no difference in the numbers of infiltrated cells compared to those of recipient mice of $CD4^+$ T cells from WT mice. These results indicate that the immune function of $CD4^+$ T cells in vivo is selectively deficient in GM3S null mice.

Recently, novel $CD4^+$ T cell subsets, in addition to Th1 and Th2 cells, Th17, and regulatory T (Treg), have been described. In allergic airway inflammation, the balance between effector Th2 cells and suppressive Treg cells is skewed towards Th2 predominance [37]. Th17 cells have been suggested to contribute to neutrophilic, steroid-resistant severe asthma and to enhance Th2-mediated airway inflammation, although a role for the cells in asthma remains to be determined [38]. Reportedly, GM3S null mice exhibit a decreased number of Th17 cells skewed by in vitro culture [39]. As the adoptive transfer experiments confirmed the marked reduction of allergic responses in

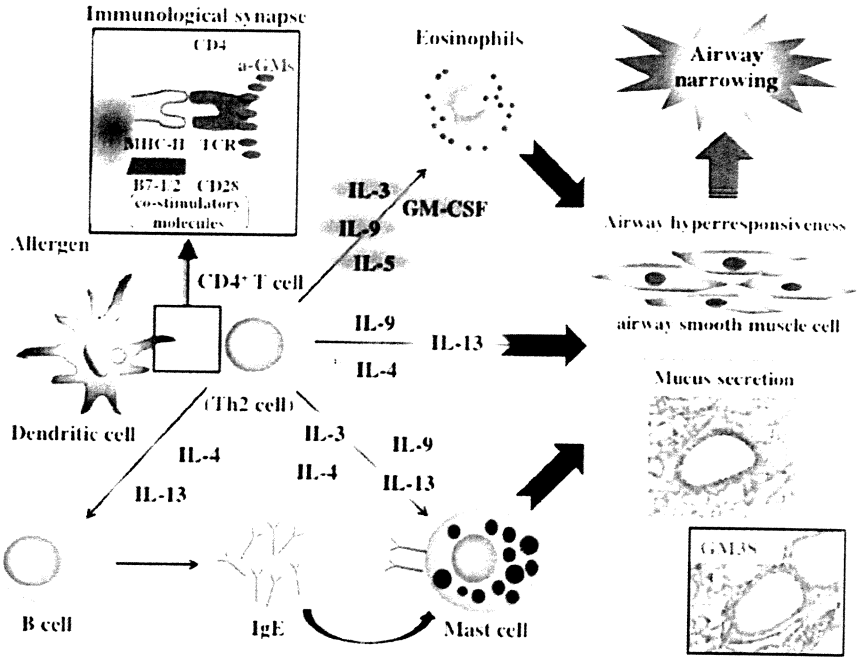


Fig. 5 The role of gangliosides in the pathogenesis of allergic asthma. a-series gangliosides (a-GMs) in $CD4^+$ T cells is critical for the signal transduction through immunological synapse, resulting in the synthesis and release of Th2 cytokines such as IL-4, IL-5, and IL-13. These cytokines play a central role in the development of airway narrowing by activating eosinophils, B cells, and mast cells, which cause mucus secretion and airway hyperresponsiveness

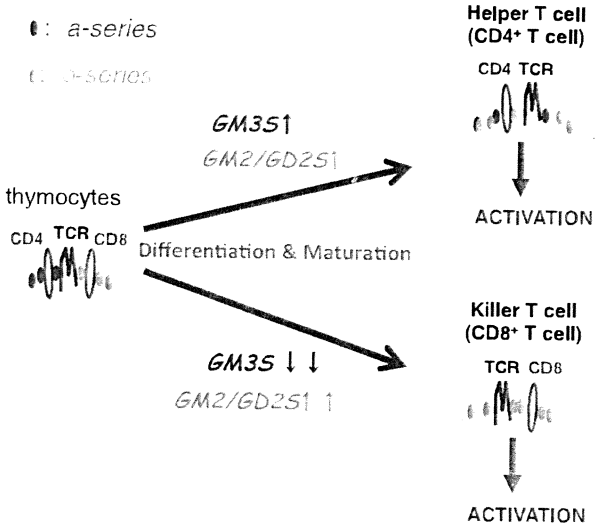


Fig. 6 Distinct difference of lipid rafts in individual T cell subsets. The repertoire selection from immature thymocytes ($CD4^+$ and $CD8^+$ double-positive) to mature single-positive T cell subpopulations is accompanied by selective ganglioside expression. The gene expression patterns together with ganglioside analysis confirm that $CD8^+$ T cells exclusively express o-series gangliosides due to downregulation of *GM3S* and upregulation of *GM2/GD2S* expression. On the other hand, $CD4^+$ T cells maintain the expression of GM1a due to the upregulation of *GM3S*. This suggests that each T cell subset has unique rafts composed of different ganglioside species and that these rafts provide distinct functions in different intracellular events following receptor-mediated stimulation. This ganglioside selection process may be indispensable in the formation of distinct and functional lipid rafts in mature T cells

WT mice transferred a whole of $CD4^+$ T cell population from sensitized GM3S null mice [12], we are underway to identify which $CD4^+$ T cell subset is affected in GM3S null mice in vivo.

Concluding remarks

We determined the ganglioside expression patterns of primary T cells, specifically those of immature thymocytes and mature peripheral $CD4^+$ T cells and $CD8^+$ T cells. Our most important finding was that distinct expression patterns of gangliosides exist in $CD4^+$ T cells and $CD8^+$ T cells, and these define the immune function of each T cell subset. $CD4^+$ T cells preferentially express a-series gangliosides, and cells isolated from GM3S null mice exhibit severe impairments in TCR-mediated cytokine production and clonal expansion, but can be rescued by exogenously added a-series gangliosides. Similarly, $CD8^+$ T cells preferentially express o-series GSLs, and cells isolated from GM2/GD2S null mice exhibit severe impairments in TCR-mediated cytokine production and clonal expansion. They can be rescued by re-introducing o-series gangliosides. These results suggest that $CD4^+$ T cell and $CD8^+$ T cell subsets require a-series and o-series ganglioside expression, respectively, to undergo activation upon TCR ligation [12].

We propose that the repertoire selection from thymocytes to T cell subsets is accompanied by selective GSLs expression in individual T cell subsets. This GSL selection

process may be indispensable for the formation of distinct and functional lipid rafts in mature T cells (Fig. 6). These findings may open up a strategy for targeting helper T cells to treat allergic inflammation including asthma by controlling ganglioside expression in lipid rafts.

References

1. Fooksman DR, Vardhana S, Vasiliver-Shamis G, Liese J, Blair DA, Waite J, Sacristán C, Victora GD, Zanin-Zhorov A, Dustin ML (2010) Functional anatomy of T cell activation and synapse formation. Annu Rev Immunol 28:79–105
2. Dykstra M, Cherukuri A, Won Sohn H, Tzeng A-J, Pierce SK (2003) Location is everything: lipid rafts and immune cell signaling. Annu Rev Immunol 21:457–481
3. Harder T, Rentero C, Zech T, Gaus K (2007) Plasma membrane segregation during T cell activation: probing the order of domains. Curr Opin Immunol 19:470–475
4. Monks CR, Freiberg BA, Kupfer H, Sciaky N, Kupfer A (1998) Three-dimensional segregation of supramolecular activation clusters in T cells. Nature 395:82–86
5. Davis DM, Dustin ML (2004) What is the importance of the immunological synapse? Trends Immunol 25:323–327
6. Saito T, Yokosuka T (2006) Immunological synapse and microclusters: the site for recognition and activation of T cells. Curr Opin Immunol 18:305–313
7. Grakoui A, Bromley S, Sumen C, Davis M, Shaw A, Allen P, Dustin ML (1999) The immunological synapse: a molecular machine controlling T cell activation. Science 285:221–227
8. Kovacs B, Maus MV, Riley JL, Derimanov GS, Koretzky GA, June CH, Finkel TH (2002) Human $CD8^+$ T cells do not require the polarization of lipid rafts for activation and proliferation. Proc Natl Acad Sci USA 99:15006–15011
9. Gómez-Móuton C, Abad JL, Mira E, Lacalle RA, Gallardo E, Jiménez-Baranda S, Illa I, Bernad A, Mañes S, Martínez AC (2001) Segregation of leading-edge and uropod components into specific lipid rafts during T cell polarization. Proc Natl Acad Sci USA 98:9642–9647
10. Marusic A, Markotic A, Kovacic N, Muthing J (2004) Expression of glycosphingolipids in lymph nodes of mice lacking TNF receptor 1: biochemical and flow cytometry analysis. Carbohydr Res 339:77–86
11. Nakamura K, Suzuki H, Hirabayashi Y, Suzuki A (1995) IV3 alpha (NeuGc alpha 2–8NeuGc)-Gg4Cer is restricted to CD4+ T cells producing interleukin-2 and a small population of mature thymocytes in mice. J Biol Chem 270:3876–3881
12. Nagafuku M, Okuyama K, Onimaru Y, Suzuki A, Odagiri Y, Yamashita T, Iwasaki K, Fujiwara M, Takayanagi M, Ohno I, Inokuchi J (2012) CD4 and CD8 T cells require different membrane gangliosides for activation. Proc Natl Acad Sci USA 109:E336–E342
13. Wong J, Lu Z-H, Gabius H-J, Rohowsky-Kochan C, Ledeen RW, Wu G (2009) Cross-linking of GM1 ganglioside by galectin-1 mediates regulatory T cell activity involving TRPC5 channel activation: possible role in suppressing experimental autoimmune encephalomyelitis. J Immunol 182:4036–4045
14. Wu G, Lu Z-H, Gabius H-J, Ledeen RW, Bleich D (2009) Ganglioside GM1 deficiency in effector T cells from NOD mice induces resistance to regulatory T-cell suppression. Diabetes 60:2341–2349
15. Naito Y, Takematsu H, Koyama S, Miyake S, Yamamoto H, Fujinawa R, Sugai M, Okuno Y, Tsujimoto G, Yamaji T, Hashimoto Y, Itohara S, Kawasaki T, Suzuki A, Kozutsumi Y (2007) Germinal center marker GL7 probes activation-dependent repression of N-glycolylneuraminic acid, a sialic acid species involved in the negative modulation of B-cell activation. Mol Cell Biol 27:3008–3022
16. Brown DA, London E (2000) Structure and function of sphingolipid- and cholesterol-rich membrane rafts. J Biol Chem 275:17221–17224
17. Iwabuchi K, Nagaoka I (2000) Lactosylceramide-enriched glycosphingolipid signaling domain mediates superoxide generation from human neutrophils. Blood 100:1454–1464
18. Inokuchi J, Rain NS (1987) Preparation of active isomer of 1-phenyl-2-decanoylamino-3-morpholino-1-propanol, inhibitor of murine glucocerebroside synthetase. J Lipid Res 28:565–571
19. Nagafuku M, Kabayama K, Oka D, Kato A, Tani-ichi S, Shimada Y, Ohno-Iwashita Y, Yamasaki S, Saito T, Iwabuchi K, Hamaoka T, Inokuchi J, Kosugi A (2003) Reduction of glycosphingolipid levels in lipid rafts affects the expression state and function of glycosylphosphatidyl-inositol-anchored proteins but does not impair signal transduction via the T cell receptor. J Biol Chem 278:51920–51927
20. Blank N, Schiller M, Gabler C, Kalden JR, Lorenz HM (2005) Inhibition of sphingolipid synthesis impairs cellular activation, cytokine production and proliferation in human lymphocytes. Biochem Pharmacol 71:126–135
21. Yoshikawa M, Go S, Takasaki K, Kakazu Y, Ohashi M, Nagafuku M, Kabayama K, Sekimoto J, Suzuki S, Takaiwa K, Kimitsuki T, Matsumoto N, Komune S, Kamei D, Saito M, Fujiwara M, Iwasaki K, Inokuchi J (2009) Mice lacking ganglioside GM3 synthase exhibit complete hearing loss due to selective degeneration of the organ of Corti. Proc Natl Acad Sci USA 106:9483–9488
22. Takamiya K, Yamamoto A, Furukawa K, Yamashiro S, Shin M, Okada M, Fukumoto S, Haraguchi M, Takeda N, Fujimura K, Sakae M, Kishikawa M, Shiku H, Furukawa K, Aizawa S (1996) Mice with disrupted GM2/GD2 synthase gene lack complex gangliosides but exhibit only subtle defects in their nervous system. Proc Natl Acad Sci USA 93:10662–10667
23. de Mello Coelho V, Nguyen D, Giri B, Bunbury A, Schaffer E, Taub DD (2004) Quantitative differences in lipid raft components between murine $CD4^+$ and $CD8^+$ T cells. BMC Immunol 5:2
24. Nakamura K, Suzuki M, Inagaki F, Yamakawa T, Suzuki A (1987) A new ganglioside showing choleragenoid-binding activity in mouse spleen. J Biochem 101:825–835
25. Trambley J, Bingaman AW, Lin A, Elwood ET, Waitze SY, Ha J, Durham MM, Corbascio M, Cowan SR, Pearson TC, Larsen CP (1999) Asialo GM1(+) CD8(+) T cells play a critical role in costimulation blockade-resistant allograft rejection. J Clin Invest 104:1715–1722
26. Sorice M, Parolini I, Sansolini T, Garofalo T, Dolo V, Sargiacomo M, Tai T, Peschle C, Torrisi MR, Pavan A (1997) Evidence for the existence of ganglioside-enriched plasma membrane domains in human peripheral lymphocytes. J Lipid Res 38:969–980
27. Salmond RJ, Pitman RS, Jimi E, Soriani M, Hirst TR, Ghosh S, Rincón M, Williams NA (2002) $CD8^+$ T cell apoptosis induced by Escherichia coli heat-labile enterotoxin B subunit occurs via a novel pathway involving NF-kappaB-dependent caspase activation. Eur J Immunol 32:1737–1747
28. Balamuth F, Brogdon JL, Bottomly K (2004) CD4 raft association and signaling regulate molecular clustering at the immunological synapse site. J Immunol 172:5887–5892
29. Pang DJ, Hayday AC, Bijlmakers MJ (2007) CD8 Raft localization is induced by its assembly into CD8alpha beta heterodimers, not CD8alpha alpha homodimers. J Biol Chem 282:13884–13894

30. Popik W, Alce TM (2004) CD4 receptor localized to non-raft membrane microdomains supports HIV-1 entry. Identification of a novel raft localization marker in CD4. J Biol Chem 279:704–712
31. Kroczek RA, Mages HW, Hutloff A (2004) Emerging paradigms of T-cell co-stimulation. Curr Opin Immunol 16:321–327
32. Greenwald RJ, Freeman GJ, Sharpe AH (2005) The B7 family revisited. Annu Rev Immunol 23:515–548
33. Bi K, Tanaka Y, Coudronniere N, Sugie K, Hong S, van Stipdonk MJ, Altman A (2001) Antigen-induced translocation of PKC-theta to membrane rafts is required for T cell activation. Nat Immunol 2:556–563
34. O'Keefe JP, Blaine K, Alegre ML, Gajewski TF (2004) Formation of a central supramolecular activation cluster is not required for activation of naive $CD8^+$ T cells. Proc Natl Acad Sci USA 101:9351–9356
35. Sonnino S, Prinetti A, Mauri L, Chigorno V, Tettamanti G (2006) Dynamic and structural properties of sphingolipids as driving forces for the formation of membrane domains. Chem Rev 106:2111–2125
36. Poppe L, van Halbeek H, Acquotti D, Sonnino S (1994) Carbohydrate dynamics at a micellar surface: GD1a headgroup transformations revealed by NMR spectroscopy. Biophys J 66:1642–1652
37. Shalaby KH, Martin JG (2010) Overview of asthma: the place of the T cell. Curr Opin Pharmacol 10:218–225
38. Lloyd CM, Hessel EM (2010) Functions of T cells in asthma: more than just T(H)2 cells. Nat Rev Immunol 10:838–848
39. Zhu Y, Gumlaw N, Karman J, Zhao H, Zhang J, Jiang JL, Maniatis P, Edling A, Chuang WL, Siegel C, Shayman JA, Kaplan J, Jiang C, Cheng SH (2011) Lowering glycosphingolipid levels in $CD4^+$ T cells attenuates T cell receptor signaling, cytokine production, and differentiation to the Th17 lineage. J Biol Chem 286:14787–14794

Available online at www.sciencedirect.com

SciVerse ScienceDirect

Current Opinion in Pharmacology

New vistas in opioid control of pain

Hirokazu Mizoguchi[1], Chizuko Watanabe[1], Tsukasa Sakurada[2] and Shinobu Sakurada[1]

The μ-opioid receptors mainly contribute to the control of pain transmission, while a number of splice variants may have different physiological roles. In fact, some μ-opioid receptor agonists show distinct antinociceptive properties probably mediated via splice variants insensitive to traditional μ-opioid receptor agonists. These atypical μ-opioid receptor agonists are extremely effective against morphine-resistant interactive pain and lack the psychological dependence liability. μ-Opioid receptor splice variants specific for these atypical agonists may be the target for better analgesics effective against morphine-resistant interactive pain and lacking psychological dependence liability.

Addresses
[1] Department of Physiology and Anatomy, Tohoku Pharmaceutical University, 4-4-1 Komatsushima, Aoba-ku, Sendai 981-8558, Japan
[2] First Department of Pharmacology, Daiichi College of Pharmaceutical Sciences, 22-1 Tamagawa-cho, Minami-ku, Fukuoka 815-8511, Japan

Corresponding author: Sakurada, Shinobu (s-sakura@tohoku-pharm.ac.jp)

Current Opinion in Pharmacology 2012, **12**:87–91

This review comes from a themed issue on Neurosciences
Edited by Giacinto Bagetta and Shinobu Sakurada

Available online 19th November 2011

1471-4892/$ – see front matter
© 2011 Elsevier Ltd. All rights reserved.

DOI 10.1016/j.coph.2011.10.020

Introduction

The opioid receptors are Gi/Go-protein-coupled receptors, and have been classified 4 major subtypes, μ-opioid, δ-opioid and κ-opioid receptors and opioid receptor like-1 (ORL-1) receptor [1]. Among the opioid receptor subtypes, the μ-opioid receptors mainly contribute to the control of pain transmission. Narcotic analgesics used in clinic are all agonists for μ-opioid receptors. The μ-opioid receptors are widely distributed in the central nervous system, including legions involved in pain transmission, for example spinal dorsal horn, medulla, periaqueductal grey matter, thalamus or cortex [2]. Based on the distribution of μ-opioid receptor and on functional studies of μ-opioid receptor agonists, two major mechanisms for producing the analgesic effect of μ-opioid receptor agonists have been proposed [3]. One is suppression of pain transmission on the spinal dorsal horn, thalamus and cortex, and the other is the activation of descending pain control system projected to spinal dorsal horn. To suppress pain transmission, μ-opioid receptor agonists stimulate the μ-opioid receptor on the terminal of primary afferent neuron at spinal dorsal horn or on the terminal of 2nd order neuron in the thalamus to cause presynaptic inhibition of neurotransmitter release; these also stimulate the μ-opioid receptor on the cell-body of 2nd order neuron at spinal dorsal horn and on the cell-body of 3rd order neuron in the thalamus to cause postsynaptic hyperpolarization of excitatory neurons. On the contrary, to activate the descending pain control system, μ-opioid receptor agonists stimulate the μ-opioid receptor located on the GABAnergic neurons in the medulla and periaqueductal grey matter to cause disinhibition of noradrenergic and serotonergic neurons projected to spinal dorsal horn. The released noradrenaline and serotonin by disinhibition of their containing neurons stimulate the α_2 receptor and 5-HT_1 receptor, respectively on the terminal of primary afferent neuron and the cell-body of 2nd order neuron in the spinal dorsal horn to suppress pain transmission. With these common mechanisms, the μ-opioid receptor agonists, including morphine, produce their potent analgesic effect. However, there are differences in the analgesic profiles of diverse μ-opioid receptor agonists [4], supporting the existence of multiple μ-opioid receptors endowed with different physiological roles.

Variability of μ-opioid receptor

The existence of multiple μ-opioid receptors had been originally proposed at early 80s by Pasternak and his colleagues. On the basis of biochemical and pharmacological evidence, μ-opioid receptor had been classically divided into putative μ_1-opioid and μ_2-opioid receptors [4–7]. The putative μ_1-opioid receptor shows a high affinity for both opioid peptides and opioid alkaloids, whereas the putative μ_2-opioid receptor has a higher affinity for opioid alkaloids than for opioid peptides [5,6]. The putative μ_1-opioid and μ_2-opioid receptors have been also identified by the sensitivity for μ-opioid receptor antagonist naloxonazine, which irreversibly binds to putative μ_1-opioid receptor, but reversibly binds to putative μ_2-opioid receptor [6,7]. As a putative μ_1-opioid receptor antagonist, naloxonazine can discriminate the antinociceptive effect of putative μ_1-opioid receptor agonist from that of putative μ_2-opioid receptor agonist [7–9]. At present, more selective antagonists for putative μ_1-opioid or μ_2-opioid receptors have been developed. Tyr-D-Pro-Trp-Gly-NH_2 (D-Pro^2-Tyr-W-MIF-1) [10,11] and Tyr-D-Pro-Trp-Phe-NH_2 (D-Pro^2-endomorphin-1)

[11,12] are selective antagonists for putative μ_2-opioid receptors, and Tyr-D-Pro-Phe-Phe-NH_2 (D-Pro^2-endomorphin-2) [11,12] is selective antagonist for putative μ_1-opioid receptors. However, pharmacological evidence accumulated using these new antagonists suggests the existence of multiple μ-opioid receptors [13,14].

In 1993, the gene for μ-opioid receptor was first cloned and its sequence structure has been identified [15,16]. Identified gene for μ-opioid receptor contains multiple exons and splice variants for its mRNA has been reported soon after cloning of the gene. At present, 19 exons and 33 splice variants have been identified in mouse μ-opioid receptor gene and mRNA, respectively [17–21]. The splice variants have been proposed to be multiple μ-opioid receptors that have been putatively suggested on the basis of pharmacological studies in which antagonists have been used. Although the distributions of most of the splice variants in the rodent central nervous system have been described [17,19–23], the selectivity and intrinsic activity of μ-opioid receptor agonists for each splice variant and the physiological roles of each splice variant are still unknown. However, it has been recently reported that the MOR-1J, MOR-1K and MOR-1L are μ-opioid receptor splice variants insensitive to traditional μ-opioid receptor agonists [D-Ala^2,NMePhe^4,Gly-ol^5]enkephalin (DAMGO) and morphine in the mouse spinal cord [24••,25]. These splice variants are sensitive to μ-opioid receptor agonist $H_2NC(=NH)$-Tyr-D-Arg-Phe-β-Ala-OH (amidino-TAPA), dermorphin tetrapeptide analog containing D-Arg^2, and spinal antinociceptive effect of amidino-TAPA is partially mediated through the activation of these splice variants. This evidence proves the existence of multiple μ-opioid receptors, insensitive to traditional μ-opioid receptor agonists.

Distinct antinociceptive profiles mediated by μ-opioid receptors

The endogenous μ-opioid peptide endomorphin-2 discovered in 1997 [26] displays antinociceptive profiles that are distinct from traditional μ-opioid receptor agonists. The antinociceptive effects of i.t.-injected or i.c.v.-injected endomorphin-2 are potently suppressed by the κ-opioid receptor antagonist nor-binaltorphimine or δ-opioid receptor antagonist naltrindole [14,27–30], although endomorphin-2 is very selective for μ-opioid receptors and does not have significant affinity for κ-opioid or δ-opioid receptors [26]. Activation of μ-opioid receptor by endomorphin-2 leads to the release of the endogenous κ-opioid peptide dynorphin A or the endogenous δ-opioid peptide [Met^5]enkephalin in the supraspinal and spinal sites, which subsequently stimulate κ-opioid or δ-opioid receptor, respectively [27–29]. Traditional μ-opioid receptor agonists, such as morphine, DAMGO or even endomorphin-1, the latter having only one difference in amino acid residue from endomorphin-2 at position 3, do not cause the release of endogenous opioid peptides through the activation of μ-opioid receptors [27–29,31–33]. This phenomenon is also observed with some μ-opioid receptor agonists, especially dermorphin tetrapeptide analogs containing D-Arg^2. The antinociceptive effects of i.t.-administered $(CH_3)_2$Tyr-D-Arg-Phe-Lys-NH_2 ([Dmt^1]DALDA) [31], Tyr-D-Arg-Phe-Sar-OH (TAPS) [32] and amidino-TAPA [33] are potently suppressed by the κ-opioid receptor antagonist nor-binaltorphimine, although those peptides are very selective for μ-opioid receptors and do not have significant affinity for κ-opioid receptors. Like endomorphin-2, these peptides also evoke the spinal release of dynorphins through the activation of μ-opioid receptors; released dynorphins subsequently stimulate κ-opioid receptors. Intriguingly, released dynorphins are variable with these peptides. TAPS causes the release of dynorphin B, whereas [Dmt^1]DALDA, similarly to endomorphin-2, causes the release of dynorphin A [31,32]. Amidino-TAPA causes the release of all three endogenous κ-opioid peptides: dynorphin A, dynorphin B and α-neo-endorphin [33]. In addition, [Dmt^1]DALDA and amidino-TAPA evoke the spinal release of [Met^5]enkephalin and [Leu^5]enkephalin, respectively [31,33]. In fact, their spinal antinociceptive effects are also attenuated by the δ-opioid receptor antagonists naltriben and naltrindole. With a synergistic activation to μ-opioid receptor and κ-opioid or δ-opioid receptors, these μ-opioid receptor agonists show extremely potent and longer-lasting antinociceptive effect than morphine following subcutaneous and intrathecal injections. The distinct antinociceptive profiles of these opioid peptides, which include the release of endogenous opioid peptides, may be mediated by the activation of distinct μ-opioid receptors that are insensitive to traditional μ-opioid receptor agonists, supporting the existence of multiple μ-opioid receptors, probably splice variants endowed with distinct physiological roles.

Analgesics lacking the dependence liability

The psychological dependence is one of the major side effects resulting from chronic treatment with morphine. It is caused by the rewarding effect of morphine revealed by the increased release of dopamine in the nucleus accumbens through the activation of μ-opioid receptor in the ventral tegmental area [34,35]. All narcotic analgesics used in clinic are μ-opioid receptor agonists and therefore they have rewarding effect and develop psychological dependence. In contrast to μ-opioid receptor agonists, κ-opioid receptor agonists suppress the release of dopamine in the nucleus accumbens [35,36]. Therefore, co-administration of κ-opioid receptor agonists with μ-opioid receptor agonists theoretically suppresses the rewarding effect of the latter agonists [37]. Unfortunately, there is no potent μ-opioid receptor agonist with the agonistic property for κ-opioid receptor. However, as described above the selective μ-opioid receptor agonist endomorphin-2 indirectly stimulates κ-opioid receptor by

released dynorphin A via activation of μ-opioid receptor, and, therefore, shows lack of the psychological dependence liability [38,39]. Similarly to endomorphin-2, amidino-TAPA also lacks the psychological dependence liability [40••]. The released dynorphins via activation of μ-opioid receptors by amidino-TAPA activate the κ-opioid receptors and eliminate the psychological dependence liability of amidino-TAPA [33,40••]. In fact, amidino-TAPA shows a remarkable rewarding effect in prodynorphin-deficient mice.

Management of morphine-resistant interactive pain

Traumatic, inflammatory, ischemic, metabolic and neoplastic insults to the peripheral or central nervous system, usually related to direct nerve injury, stroke, chronic inflammation of tissue, cancer, diabetes, or other nerve diseases, leads to abnormal pain, which is characterized by continuous or intermittent spontaneous pain and abnormal sensitivity of the painful site to a variety of noxious (hyperalgesia) or innocuous (allodynia) stimuli [41]. Since morphine treatment is ineffective or extremely less effective against these abnormal forms of pain in the normal therapeutic dose range, they are usually called as the morphine-resistant interactive pain [42–44]. Like morphine, most narcotic analgesics, except oxycodone, are ineffective against the morphine-resistant interactive pain. Oxycodone is the only narcotic analgesic reported to be effective against morphine-resistant interactive pain [45,46]. Although oxycodone is extremely selective to μ-opioid receptor and does not have remarkable affinity to κ-opioid receptor [47], its antinociceptive effect has been suggested to be partially mediated through the activation of κ-opioid receptor, especially under condition of morphine-resistant interactive pain [48,49]. At present, the mechanism underlying the stimulation of the κ-opioid receptor by oxycodone is unclear. However, the morphine-insensitive mechanism (probably indirect stimulation of κ-opioid receptor) for oxycodone may be involved in the anti-allodynic and anti-hyperalgesic effects of oxycodone against morphine-resistant interactive pain.

As described above the endogenous μ-opioid peptide endomorphin-2 indirectly stimulated κ-opioid receptor by releasing dynorphin A [14,27–30]. Endomorphin-2 was also reported to show potent anti-allodynic effect against neuropathic pain, one of the morphine-resistant interactive pains [50,51]. In addition, the gene transfer for endomorphin-2 reverses allodynia in neuropathic pain state [52,53••]. It is more noteworthy that amidino-TAPA, which induces the release of endogenous κ-opioid peptides dynorphin A, dynorphin B and α-neo-endorphin via activation of μ-opioid receptor to produce antinociception [33], is extremely effective against the morphine-resistant interactive pain [54••]. The anti-allodynic effect of amidino-TAPA is not altered at all in the nerve-injured neuropathic pain. Similarly to oxycodone, the indirect stimulation of κ-opioid receptor via released endogenous κ-opioid peptides by amidino-TAPA and endomorphin-2 may be involved in their potent anti-allodynic and anti-hyperalgesic effects against morphine-resistant interactive pain.

Conclusion

Among the 3 major opioid receptor subtypes, μ-opioid receptor is still a dominant receptor for controlling pain transmission. However, traditional μ-opioid receptor agonists used in clinic all develop dependence and are ineffective against morphine-resistant interactive pain. Fortunately, μ-opioid receptor agonists oxycodone, endomorphin-2 and amidino-TAPA, which cause indirect stimulation of κ-opioid receptor via the morphine-insensitive mechanism to produce antinociception, show excellent effectiveness against morphine-resistant interactive pain. Moreover, releasing the endogenous κ-opioid peptides, endomorphin-2 and amidino-TAPA lack the psychological dependence liability. The μ-opioid receptors (probably μ-opioid receptor splice variants) sensitive to oxycodone, endomorphin-2 or amidino-TAPA but insensitive to morphine, may be the target molecule to produce better analgesics effective against morphine-resistant interactive pain devoid psychological dependence liability.

Acknowledgements

This work was supported by a Grant-in-Aid for Scientific Research (C) [KAKENHI 21600013 and 22600009] from the Japan Society for the Promotion of Science, and a Matching Fund Subsidy for Private Universities from the Ministry of Education, Culture, Sports, Science, and Technology Japan (2010–2014).

References and recommended reading

Papers of particular interest, published within the period of review, have been highlighted as:

- • of special interest
- •• of outstanding interest

1. Dietis N, Rowbotham DJ, Lambert DG: **Opioid receptor subtypes: fact or artifact?** *Br J Anaesth* 2011, **107**:8-18.
2. Mansour A, Fox CA, Burke S, Akil H, Watson SJ: **Immunohistochemical localization of the cloned μ opioid receptor in the rat CNS.** *J Chem Neuroanat* 1995, **8**:283-305.
3. Mense S: **Basic neurobiologic mechanisms of pain and analgesia.** *Am J Med* 1983, **75**:4-14.
4. Pasternak GW, Wood PJ: **Multiple μ opiate receptors.** *Life Sci* 1986, **38**:1889-1898.
5. Wolozin BL, Pasternak GW: **Classification of multiple morphine and enkephalin binding sites in the central nervous system.** *Proc Natl Acad Sci USA* 1981, **78**:6181-6185.
6. Hahn EF, Pasternak GW: **Naloxonazine, a potent, long-lasting inhibitor of opiate binding sites.** *Life Sci* 1982, **31**:1385-1388.
7. Pasternak GW, Gintzler AR, Houghten RA, Ling GS, Goodman RR, Spiegel K, Nishimura S, Johnson N, Recht LD: **Biochemical and pharmacological evidence for opioid receptor multiplicity in the central nervous system.** *Life Sci* 1983, **33(Suppl. 1)**:167-173.
8. Sato T, Sakurada S, Takahashi N, Sakurada T, Tan-No K, Wako K, Kisara K: **Contribution of spinal μ_1-opioid receptors to**

morphine-induced antinociception. *Eur J Pharmacol* 1999, **369**:183-187.

9. Sakurada S, Zadina JE, Kastin AJ, Katsuyama S, Fujimura T, Murayama K, Yuki M, Ueda H, Sakurada T: **Differential involvement of μ-opioid receptor subtypes in endomorphin-1- and -2-induced antinociception**. *Eur J Pharmacol* 1999, **372**:25-30.

10. Watanabe H, Nakayama D, Ito K, Watanabe C, Mizoguchi H, Fujimura T, Murayama K, Kawamura S, Sato T, Sakurada C *et al.*: **A Tyr-W-MIF-1 analog containing D-Pro^2 acts as a selective μ_2-opioid receptor antagonist in the mouse**. *J Pharmacol Exp Ther* 2005, **312**:1075-1081.

11. Mizoguchi H, Nakayama D, Watanabe H, Ito K, Sakurada W, Sawai T, Fujimura T, Sato T, Sakurada T, Sakurada S: **Involvement of spinal μ_1-opioid receptors on the Tyr-D-Arg-Phe-sarcosine-induced antinociception**. *Eur J Pharmacol* 2006, **540**:67-72.

12. Sakurada S, Watanabe H, Hayashi T, Yuhki M, Fujimura T, Murayama K, Sakurada C, Sakurada T: **Endomorphin analogues containing D-Pro^2 discriminate different μ-opioid receptor mediated antinociception in mice**. *Br J Pharmacol* 2002, **137**:1143-1146.

13. Nakayama D, Watanabe C, Watanabe H, Mizoguchi H, Sakurada T, Sakurada S: **A Tyr-W-MIF-1 analog containing D-Pro^2 discriminates among antinociception in mice mediated by different classes of μ-opioid receptors**. *Eur J Pharmacol* 2007, **563**:109-116.

14. Mizoguchi H, Watanabe H, Hayashi T, Sakurada W, Sawai T, Fujimura T, Sakurada T, Sakurada S: **Possible involvement of dynorphin A-(1-17) release via μ_1-opioid receptors in spinal antinociception by endomorphin-2**. *J Pharmacol Exp Ther* 2006, **317**:362-368.

15. Chen Y, Mestek A, Liu J, Hurley A, Yu L: **Molecular cloning and functional expression of a μ-opioid receptor from rat brain**. *Mol Pharmacol* 1993, **44**:8-12.

16. Wang JB, Imai Y, Eppler CM, Gregor P, Spivak CE, Uhl GR: **μ Opiate receptor: cDNA cloning and expression**. *Proc Natl Acad Sci USA* 1993, **90**:10230-10234.

17. Pan Y-X, Xu J, Mahurter L, Bolan E, Xu M, Pasternak GW: **Generation of the μ opioid receptor (MOR-1) protein by three new splice variants of the Oprm gene**. *Proc Natl Acad Sci USA* 2001, **98**:14084-14089.

18. Kvam T-M, Baar C, Rakvåg TT, Kaasa S, Krokan HE, Skorpen F: **Genetic analysis of the murine μ opioid receptor: increased complexity of Oprm gene splicing**. *J Mol Med* 2004, **82**:250-255.

19. Pan Y-X, Xu J, Bolan E, Moskowitz HS, Xu M, Pasternak GW: **Identification of four novel exon 5 splice variants of the mouse μ-opioid receptor gene: functional consequences of C-terminal splicing**. *Mol Pharmacol* 2005, **68**:866-875.

20. Doyle GA, Sheng XR, Lin SS, Press DM, Grice DE, Buono RJ, Ferraro TN, Berrettini WH: **Identification of three mouse μ-opioid receptor (MOR) gene (Oprm1) splice variants containing a newly identified alternatively spliced exon**. *Gene* 2007, **388**:135-147.

21. Doyle GA, Sheng XR, Lin SS, Press DM, Grice DE, Buono RJ, Ferraro TN, Berrettini WH: **Identification of five mouse μ-opioid receptor (MOR) gene (Oprm1) splice variants containing a newly identified alternatively spliced exon**. *Gene* 2007, **395**:98-107.

22. Pan Y-X, Xu J, Bolan E, Abbadie C, Chang A, Zuckerman A, Rossi G, Pasternak GW: **Identification and characterization of three new alternatively spliced μ-opioid receptor isoforms**. *Mol Pharmacol* 1999, **56**:396-403.

23. Pan Y-X, Xu J, Bolan E, Chang A, Mahurter LA, Rossi G, Pasternak GW: **Isolation and expression of a novel alternatively spliced μ opioid receptor isoform, MOR-1F**. *FEBS Lett* 2000, **466**:337-340.

24. •• Mizoguchi H, Watanabe C, Higashiya T, Takeda S, Moriyama K, Yonezawa A, Sato T, Komatsu T, Sakurada T, Sakurada S: **Involvement of mouse μ-opioid receptor splice variants in the spinal antinociception induced by the dermorphin tetrapeptide analog amidino-TAPA**. *Eur J Pharmacol* 2011, **651**:66-72.

The article described the μ-opioid receptor splice variants, which have different physiological roles.

25. Mizoguchi H, Bagetta G, Sakurada T, Sakurada S: **Dermorphin tetrapeptide analogs as potent and long-lasting analgesics with pharmacological profiles distinct from morphine**. *Peptides* 2011, **32**:421-427.

26. Zadina JE, Hackler L, Ge LJ, Kastin AJ: **A potent and selective endogenous agonist for the μ-opiate receptor**. *Nature* 1997, **386**:499-502.

27. Tseng LF, Narita M, Suganuma C, Mizoguchi H, Ohsawa M, Nagase H, Kampine JP: **Differential antinociceptive effects of endomorphin-1 and endomorphin-2 in the mouse**. *J Pharmacol Exp Ther* 2000, **292**:576-583.

28. Sakurada S, Hayashi T, Yuhki M, Orito T, Zadina JE, Kastin AJ, Fujimura T, Murayama K, Sakurada C, Sakurada T *et al.*: **Differential antinociceptive effects induced by intrathecally administered endomorphin-1 and endomorphin-2 in the mouse**. *Eur J Pharmacol* 2001, **427**:203-210.

29. Ohsawa M, Mizoguchi H, Narita M, Nagase H, Kampine JP, Tseng LF: **Differential antinociception induced by spinally administered endomorphin-1 and endomorphin-2 in the mouse**. *J Pharmacol Exp Ther* 2001, **298**:592-597.

30. Sakurada S, Sawai T, Mizoguchi H, Watanabe H, Watanabe C, Yonezawa A, Morimoto M, Sato T, Komatsu T, Sakurada T: **Possible involvement of dynorphin A release via μ_1-opioid receptor on supraspinal antinociception of endomorphin-2**. *Peptides* 2008, **29**:1554-1560.

31. Szeto HH, Soong Y, Wu D, Qian X, Zhao GM: **Endogenous opioid peptides contribute to antinociceptive potency of intrathecal [Dmt^1]DALDA**. *J Pharmacol Exp Ther* 2003, **305**:696-702.

32. Mizoguchi H, Ito K, Watanabe H, Watanabe C, Katsuyama S, Fujimura T, Sakurada T, Sakurada S: **Contribution of spinal μ_1-opioid receptors and dynorphin B to the antinociception induced by Tyr-D-Arg-Phe-Sar**. *Peptides* 2006, **27**:2786-2793.

33. Mizoguchi H, Watanabe C, Watanabe H, Moriyama K, Sato B, Ohwada K, Yonezawa A, Sakurada T, Sakurada S: **Involvement of endogenous opioid peptides in the antinociception induced by the novel dermorphin tetrapeptide analog amidino-TAPA**. *Eur J Pharmacol* 2007, **560**:150-159.

34. Herz A, Spanagel R: **Endogenous opioids and addiction**. In *The Pharmacology of Opioid Peptides*. Edited by Tseng LF. Harwood Academic Publishers; 1995:445-462.

35. Spanagel R, Herz A, Shippenberg TS: **Opposing tonically active endogenous opioid systems modulate the mesolimbic dopaminergic pathway**. *Proc Natl Acad Sci USA* 1992, **89**:2046-2050.

36. Spanagel R, Herz A, Shippenberg TS: **The effects of opioid peptides on dopamine release in the nucleus accumbens: an in vivo microdialysis study**. *J Neurochem* 1990, **55**:1734-1740.

37. Funada M, Suzuki T, Narita M, Misawa M, Nagase H: **Blockade of morphine reward through the activation of κ-opioid receptors in mice**. *Neuropharmacology* 1993, **32**:1315-1323.

38. Narita M, Ozaki S, Ioka M, Mizoguchi H, Nagase H, Tseng LF, Suzuki T: **Different motivational effects induced by the endogenous μ-opioid receptor ligands endomorphin-1 and -2 in the mouse**. *Neuroscience* 2001, **105**:213-218.

39. Wu HE, MacDougall RS, Clithero AD, Leitermann RJ, Terashvili M, Tseng LF: **Opposite conditioned place preference responses to endomorphin-1 and endomorphin-2 in the mouse**. *Neurosci Lett* 2004, **365**:157-161.

40. •• Mizoguchi H, Watanabe C, Osada S, Yoshioka M, Aoki Y, Natsui S, Yonezawa A, Kanno S, Ishikawa M, Sakurada T *et al.*: **Lack of a rewarding effect and a locomotor-enhancing effect of the selective μ-opioid receptor agonist amidino-TAPA**. *Psychopharmacology (Berl)* 2010, **212**:215-225.

The article described new analgesic (μ-opioid receptor agonist) lacking dependence liability.

41. Yarnitsky D, Eisenberg E: **Neuropathic pain: between positive and negative ends**. *Pain Forum* 1998, **7**:241-242.

42. Arné S, Meyerson BA: **Lack of analgesic effect of opioids on neuropathic and idiopathic forms of pain**. *Pain* 1988, **33**:11-23.

43. Portenoy RK, Foley KM, Inturrisi CE: **The nature of opioid responsiveness and its implications for neuropathic pain: new hypotheses derived from studies of opioid infusions**. *Pain* 1990, **43**:273-286.

44. Eisenberg E, McNicol ED, Carr DB: **Efficacy of μ-opioid agonists in the treatment of evoked neuropathic pain: systematic review of randomized controlled trials**. *Eur J Pain* 2006, **10**:667-676.

45. Watson CPN, Babul N: **Efficacy of oxycodone in neuropathic pain: a randomized trial in postherpetic neuralgia**. *Neurology* 1998, **50**:1837-1841.

46. Watson CP, Moulin D, Watt-Watson J, Gordon A, Eisenhoffer J: **Controlled-release oxycodone relieves neuropathic pain: a randomized controlled trial in painful diabetic neuropathy**. *Pain* 2003, **105**:71-78.

47. Narita M, Nakamura A, Ozaki M, Imai S, Miyoshi K, Suzuki M, Suzuki T: **Comparative pharmacological profiles of morphine and oxycodone under a neuropathic pain-like state in mice: evidence for less sensitivity to morphine**. *Neuropsychopharmacology* 2008, **33**:1097-1112.

48. Nozaki C, Saitoh A, Tamura N, Kamei J: **Antinociceptive effect of oxycodone in diabetic mice**. *Eur J Pharmacol* 2005, **524**:75-79.

49. Nielsen CK, Ross FB, Lotfipour S, Saini KS, Edwards SR, Smith MT: **Oxycodone and morphine have distinctly different pharmacological profiles: radioligand binding and behavioural studies in two rat models of neuropathic pain**. *Pain* 2007, **132**:289-300.

50. Przewłocka B, Mika J, Labuz D, Toth G, Przewłocki R: **Spinal analgesic action of endomorphins in acute, inflammatory and neuropathic pain in rats**. *Eur J Pharmacol* 1999, **367**:189-196.

51. Przewłocki R, Labuz D, Mika J, Przewłocka B, Tomboly C, Toth G: **Pain inhibition by endomorphins**. *Ann NY Acad Sci* 1999, **897**:154-164.

52. Wolfe D, Hao S, Hu J, Srinivasan R, Goss J, Mata M, Fink DJ, Glorioso JC: **Engineering an endomorphin-2 gene for use in neuropathic pain therapy**. *Pain* 2007, **133**:29-38.

53. •• Wolfe D, Mata M, Fink DJ: **A human trial of HSV-mediated gene transfer for the treatment of chronic pain**. *Gene Ther* 2009, **16**:455-460.
The article described the gene therapy for neuropathic pain.

54. •• Mizoguchi H, Watanabe C, Yonezawa A, Sakurada S: **New therapy for neuropathic pain**. *Int Rev Neurobiol* 2009, **85**:249-460.
The review article described the management of neuropathic pain by analgesics.

Original Paper

International Archives of Allergy and Immunology

Int Arch Allergy Immunol 2012;158(suppl 1):35–41
DOI: 10.1159/000337759

Published online: May 15, 2012

Higher Sensitivity of Male CD4+ T Cells to Suppressive Effects of CD8+ T Cells on IL-5 Production Compared to Female CD4+ T Cells

Kaori Okuyama[a] Tsuyoshi Kashimura[a] Tasuku Kawano[a] Yuichi Ohkawara[a]
Motoaki Takayanagi[a] Toshiaki Kikuchi[b] Isao Ohno[a]

[a]Department of Pathophysiology, Tohoku Pharmaceutical University, and [b]Department of Pulmonary Medicine, Tohoku University Hospital, Sendai, Japan

Key Words
Bronchial asthma · Gender difference · Cytokines · Splenocytes · CD4+ and CD8+ T cells

Abstract
Background: Asthma prevalence and severity are higher in females than in males after puberty. The underlying mechanisms of this gender difference are not fully understood. More severe airway inflammation in female mice has been reported to be associated with higher levels of T helper type 2 (Th2) cytokines in asthma models. The aim of this study was to investigate sex differences in CD4+ and CD8+ T cell functions in Th2 cytokine production. ***Methods:*** Splenocytes from naive mice were stimulated with anti-CD3/CD28 antibodies and the proportions of CD4+ and CD8+ T cells were analyzed. CD4+ T cells were stimulated in the presence of CD8+ T cells. The concentrations of interleukin (IL)-5, IL-10 and interferon (IFN)-γ in the cultures were measured. ***Results:*** The concentration of IL-5, but not IFN-γ, was significantly higher in female splenocytes than in male splenocytes. There were no sex differences in the proportions of CD4+ and CD8+ T cells in the splenocytes. Although the IL-5 production levels in male and female CD4+ T cells were similar, IL-5 production in male CD4+ T cells, but not female CD4+ T cells, was suppressed by both male and female CD8+ T cells. While IL-5 and IL-10 were not detected in the cultures from both male and female CD8+ T cells, IFN-γ concentration in female CD8+ T cells was significantly higher than in male CD8+ T cells. ***Conclusions:*** The sex difference in the sensitivity of CD4+ T cells to CD8+ T cell suppression might contribute to the sex difference in IL-5 production by splenocytes.
Copyright © 2012 S. Karger AG, Basel

Introduction

Allergic asthma is a chronic airway disease characterized by chronic eosinophilic airway inflammation in response to inhaled allergens. The hallmarks of the disease include the infiltration of inflammatory cells (e.g. eosinophils and mast cells) in the airways, mucus production and variable airflow obstruction with airway hyperresponsiveness. CD4+ T helper type 2 (Th2) cells that produce Th2 cytokines, such as interleukin (IL)-4, IL-5 and IL-13, play an important role in these processes [1, 2]. CD8+ T cells, a subset of MHC class I-restricted T cells, form functional Tc1 and Tc2 subsets that exhibit similar cytokine profiles as CD4+ Th1 and Th2 cells, respectively. The numbers of CD8+ T cells within asthmatic lungs are strongly correlated with disease severity. CD8+ T cells

KARGER
Fax +41 61 306 12 34
E-Mail karger@karger.ch
www.karger.com

© 2012 S. Karger AG, Basel
1018–2438/12/1585–0035$38.00/0

Accessible online at:
www.karger.com/iaa

Correspondence to: Dr. Isao Ohno
Department of Pathophysiology, Tohoku Pharmaceutical University
-4-1 Komatsushima, Aoba-ku
Sendai 981-8558 (Japan)
Tel. +81 22 727 0126, E-Mail iohno@tohoku-pharm.ac.jp

isolated from asthmatics have been shown to secrete high levels of type 2 cytokines, such as IL-4, IL-5 and IL-13 [3]. Tc2 cells identified in the lungs of allergic mice have been shown to play influential roles in propagating inflammation in rodent models. In contrast to Tc2 cells, it is suggested that Tc1 cells have suppressive effects on Th2-dominant allergic airway inflammation [4]. In a murine asthma model, allergen-specific Tc1 cells could suppress allergic airway inflammation via the induction of IL-12 by lung dendritic cells [3].

Clinical observations and epidemiological studies have indicated that the prevalence and severity of asthma are higher in females than in males, with a switch occurring at the time of puberty [5–7]; this strongly suggests that sex hormones play a role in the pathogenesis of the disease [8, 9]. Recent studies using murine models of allergic asthma have demonstrated a higher susceptibility to allergic airway inflammation in female mice and an effect of the administration of sex hormones on airway inflammation [10, 11]. However, the underlying mechanisms of gender difference in the prevalence and severity of asthma are not fully understood. It has been shown that the interferon (IFN)-γ:IL-4 ratio was significantly higher in the supernatants of cultures of phytohemagglutinin-stimulated T cells from men than in supernatants from women and that supplementation of these T cell cultures with sex hormones did not modify the secretion of these cytokines [12, 13]. Previously, we have shown that splenocytes from sensitized female mice produce more IL-5 than those from sensitized male mice upon stimulation with ovalbumin, and that allergen-induced airway inflammation in mice transferred with splenocytes from sensitized female mice is more severe than the inflammation in mice with splenocytes from sensitized male mice [14]. In addition, we observe greater antigen-induced Th2 cytokine production and Th2 cell differentiation in association with higher expression levels of a Th2-oriented transcription factor, GATA-3, in bronchial lymph node cells from sensitized female mice compared to cells from sensitized male mice [15]. Recently, we reported that IL-5 production by T cell antigen receptor (TCR)-activated splenocytes is higher in female mice than in male mice; this difference is not observed in either CD4+ or CD8+ T cell-deficient mice [16]. Interestingly, the disappearance of the sex difference in CD8+ T cell-deficient mice was attributable to an increase of IL-5 production in male mice [16]. These results led us to hypothesize that TCR-activated CD8+ T cells from male mice exerted more suppressive effects on IL-5 production by TCR-activated CD4+ T cells than TCR-activated CD8+ T cells from female mice.

To address this hypothesis, in this study, we compared the proportions of T cell subsets (CD4+ and CD8+ T cells) in splenocytes and IL-5 production levels by TCR-activated CD4+ and CD8+ T cells purified from splenocytes from male and female mice. Finally, we investigated whether CD8+ T cells from male mice showed more suppressive activity on IL-5 production by TCR-activated CD4+ T cells than CD8+ T cells from female mice.

Materials and Methods

Animals

Specific pathogen-free 8- to 10-week-old male and female C57BL/6 (B6) mice were purchased from CLEA Japan (Osaka, Japan). Animals were housed under a 12-hour light/dark cycle with a constant temperature (22 ± 2°C). Sterilized food and water were available ad libitum. All experiments described below were approved by and conformed to the guidelines of the Committee of Animal Experiments at Tohoku Pharmaceutical University.

Purification and Culture of CD4+ T and CD8+ T Cells from Splenocytes

Splenocytes were prepared from the mice as previously described [14]. CD4+ and CD8+ T cells in splenocytes were purified by positive selection on an autoMACS Separator (Miltenyi Biotec, Bergisch Gladbach, Germany) using anti-mouse CD4 (L3T4) MicroBeads (Miltenyi Biotec) or anti-mouse CD8a (Ly-2) MicroBeads (Miltenyi Biotec) according to the manufacturer's protocol. The purity of both cell populations after purification exceeded 95%, as assessed by flow cytometry, and viability exceeded 98% by trypan blue dye exclusion. Purified CD4+ and CD8+ T cells were suspended in complete medium consisting of RPMI 1640 (Gibco BRL, Rockville, Md., USA) with 10% fetal bovine serum (ICN Biomedicals, Inc., Aurosa, Ohio, USA), 55 μM 2-mercaptoethanol (Wako Pure Chemical Industries, Osaka, Japan), 2 mg/ml $NaHCO_3$, 50 U/ml penicillin G (Meijiseika, Tokyo, Japan), 50 μg/ml streptomycin sulfate (Meijiseika) and 2 mM L-glutamine (Wako Pure Chemical Industries). The cells (1×10^6 cells/200 μl/well) were stimulated with anti-mouse CD3 Hamster IgG_1 (5 μg/ml) (BD Biosciences Pharmingen, San Diego, Calif., USA) and anti-mouse CD28 Hamster IgG_2 (0.1 μg/ml) (BD Biosciences) antibodies for 3 days as previously described [16]. An isotype-matched antibody (BD Biosciences) was used as a stimulation control. Throughout the coculture experiments, CD4+ T cells (1×10^6 cells/well) were incubated with various numbers of CD8+ T cells (0.5, 0.25, 0.125 and 0.0625 $\times 10^6$ cells/well) in 200 μl of culture medium. The supernatants were stored at −80°C for cytokine measurement using an enzyme-linked immunosorbent assay (ELISA).

Cytokine Measurement

The IL-5, IFN-γ and IL-10 concentrations in the supernatants were measured using ELISA kits (R&D Systems, Minneapolis, Minn., USA) according to the manufacturer's protocol. Complete medium was used as a negative control and for the dilution of the samples. IL-5 and IFN-γ concentrations were calculated using a

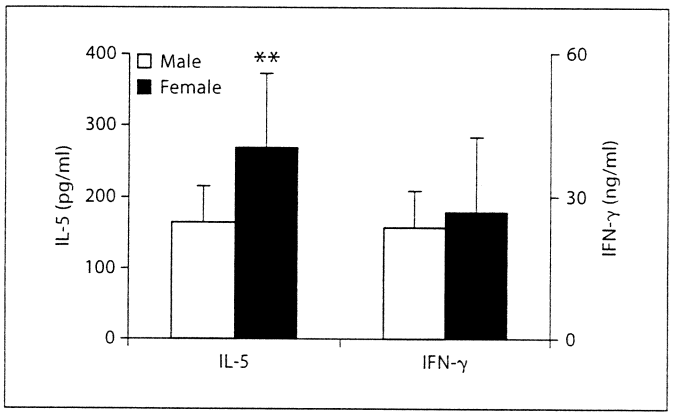


Fig. 1. IL-5 and IFN-γ production by splenocytes stimulated with anti-CD3/CD28. Splenocytes from male (open columns) and female (closed columns) mice were stimulated with anti-CD3 and anti-CD28 antibodies for 3 days. The IL-5 and IFN-γ concentrations in the culture supernatants were measured by ELISA. Data are expressed as means ± SD. ** $p < 0.01$ compared to male mice.

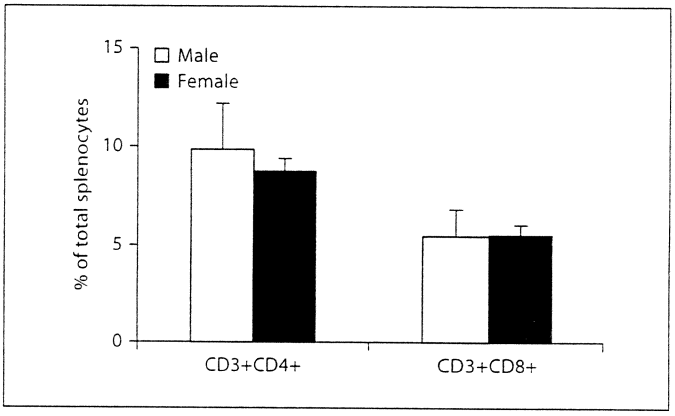


Fig. 2. The proportions of T cell subsets in splenocytes. Splenocytes from male (open columns) and female (closed columns) mice were analyzed for the proportions of CD3+CD4+ and CD3+CD8+ cells, the numbers of which are shown as percentages of total numbers of splenocytes. Data are expressed as means ± SD.

standard curve after subtracting the negative controls. The limits of detection were 7 pg/ml for IL-5, 2 pg/ml for IFN-γ and 4 pg/ml for IL-10.

Flow Cytometric Analysis

CD3+CD4+ and CD3+CD8+ subsets of splenocytes were analyzed as previously described [15]. Briefly, the cells were preincubated with anti-CD16/CD32 (FcγIII/II receptor; BD Biosciences) to reduce nonspecific binding of the following antibodies: anti-CD3e-allophycocynin (clone 145-2C11), anti-CD4-phycoerythrin (clone GK 1.5), anti-CD8a-fluorescein isothiocyanate (clone 53-6.7) or isotype control antibodies (all from BD Biosciences), which were added directly to the cells. Cells were counted on a FACScan instrument (BD Biosciences), and data were analyzed using Cell Quest software (BD Biosciences).

Data Analysis

Data are expressed as the means ± SD. Significant differences between 2 groups were determined using the nonparametric Mann-Whitney U test. In the case of the coculture experiments, the Kruskal-Wallis test with the Dunn's post-test was used. These analyses were performed using Prism4 (GraphPad Software, San Diego, Calif., USA). A p value of less than 0.05 was considered significant.

Results

The Sex Differences in IL-5 Production by TCR-Activated Splenocytes and the Proportions of T Cell Subsets in Splenocytes

As previously reported [16], the concentration of IL-5 in a culture supernatant from female splenocytes stimulated with anti-CD3/CD28 antibodies was significantly higher than a supernatant from male splenocytes (females: 269.2 ± 102.0 pg/ml, n = 10; males: 164.8 ± 49.1 pg/ml, n = 8; $p < 0.05$), although there was no significant difference in the concentrations of IFN-γ between female and male splenocytes (fig. 1). The previous findings that the sex difference was not observed in splenocytes from CD4+ and CD8+ T cell-deficient mice raised the possibility that the proportions of CD4+ and CD8+ T cells in splenocytes were different between the sexes [16]. However, analyses of T cell subsets in splenocytes indicated that female and male mice exhibited similar proportions of CD3+CD4+ and CD3+CD8+ cells (fig. 2).

IL-5 Production by TCR-Activated CD4+ and CD8+ T Cells from Splenocytes

Next, we evaluated IL-5 production by each T cell subset. No difference in IL-5 production was identified between male and female CD4+ T cells. However, the concentrations of IL-5 in TCR-activated CD8+ T cells were lower than the limit of detection in both sexes (fig. 3).

Suppressive Effect of TCR-Activated CD8+ T Cells on IL-5 Production by TCR-Activated CD4+ T Cells

The previous study indicated that the disappearance of the sex difference in CD8+ T cell-deficient mice was attributable to an increase in IL-5 production in male mice [16]. Therefore, to assess whether TCR-activated CD8+ T cells from males exert more suppressive effects on IL-5 production by TCR-activated CD4+ T cells than

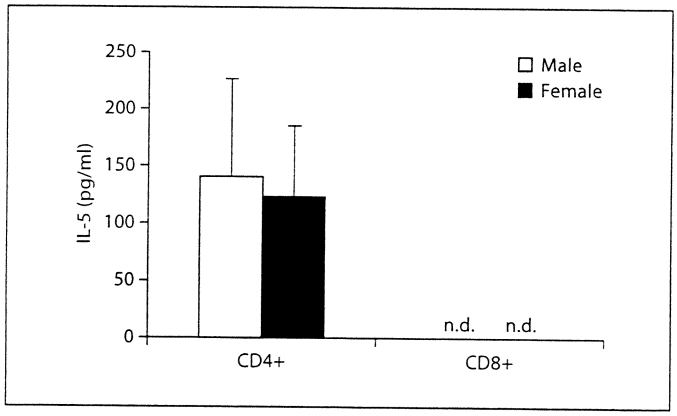


Fig. 3. IL-5 production by CD4+ and CD8+ T cells stimulated with anti-CD3/CD28. Purified CD4+ and CD8+ T cells from splenocytes of male (open columns) and female (closed columns) mice were stimulated, and the IL-5 concentrations in the culture supernatants were measured as in figure 1. Data are expressed as means ± SD. n.d. = Not detected.

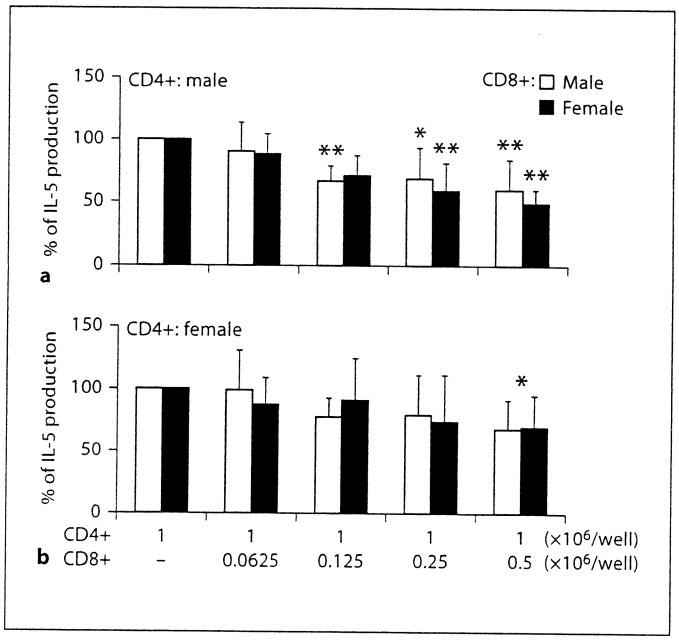


Fig. 4. The suppressive effect of CD8+ T cells on IL-5 production by CD4+ T cells stimulated with anti-CD3/CD28. Purified CD4+ T cells (1×10^6 cells/well) from male (**a**) and female (**b**) mice were cultured with the indicated numbers of purified CD8+ T cells from male (open columns) and female (closed columns) mice in the presence of anti-CD3 and anti-CD28 antibodies. The IL-5 concentrations in the culture supernatants were measured as in figure 1. The IL-5 concentrations are shown as percentages of the concentrations in CD4+ T cells cultured without CD8+ T cells. Data are expressed as means ± SD. * $p < 0.05$ and ** $p < 0.01$ compared to male and female CD4+ T cells in the absence of CD8+ T cells.

do TCR-activated CD8+ T cells from female mice, coculture experiments were performed. The concentrations of IL-5 in the culture supernatants of TCR-activated CD4+ T cells in the presence of increased numbers of TCR-activated CD8+ T cells were compared to the concentrations in the absence of TCR-activated CD8+ T cells. In CD4+ T cells from male mice, the presence of CD8+ T cells from either male or female mice resulted in a dose-dependent reduction in IL-5 production (fig. 4a). In contrast, in the case of CD4+ T cells from female mice, female CD8+ T cells did not exert this suppressive activity at any cell numbers examined; additionally, male CD8+ T cells exhibited a significantly suppressive activity only at the highest cell number (fig. 4b).

The Sex Differences in IFN-γ Production from TCR-Activated CD8+ T Cells

Because IFN-γ and IL-10 have been proposed as mediators for inhibiting Th2 responses, we examined whether there were sex differences in the production of these cytokines by CD4+ and CD8+ T cells.

While no differences in IFN-γ production by TCR-activated CD4+ T cells were identified between the sexes, IFN-γ production by TCR-activated CD8+ T cells from female mice was significantly higher than the production level from male mice (females: 19.9 ± 7.9 ng/ml, n = 7; males: 9.1 ± 2.7 ng/ml, n = 6; $p < 0.01$) (fig. 5a). There was no significant difference in IL-10 production by TCR-activated CD4+ T cells between the sexes. However, the concentrations of IL-10 in TCR-activated CD8+ T cells were lower than the limit of detection in both sexes (fig. 5b).

Discussion

Our main and novel findings in this study are that IL-5 production by TCR-activated CD4+ T cells from female mice was not suppressed by TCR-activated CD8+ T cells, while IL-5 production by TCR-activated CD4+ T cells from male mice was suppressed. The sex difference in the sensitivity of CD4+ T cells to CD8+ T cell suppression might contribute to the higher production levels of Th2 cytokines in splenocytes and bronchial lymph node cells from female mice [14, 15], leading to more severe airway inflammation in female mice [14].

The production of IL-5 by TCR-activated splenocytes from female mice was greater than that from male mice. However, there was no difference in IL-5 production between male and female TCR-activated CD4+ T cells. In

our previous study, the sex difference in IL-5 production was not observed in splenocytes from CD4+ T cell-deficient mice [16]. Together with these findings, we assume that CD4+ T cells are necessary but not sufficient to account for the sex difference in IL-5 production by TCR-activated splenocytes. However, we had also noted the disappearance of this sex difference in CD8+ T cell-deficient mice, which was attributable to an increase of IL-5 production in male mice [16]. From these results, we hypothesized that male CD8+ T cells had more potential to suppress IL-5 production by CD4+ T cells. Unexpectedly, IL-5 production by TCR-activated male CD4+ T cells was significantly inhibited in cultures with both male and female CD8+ T cells. However, IL-5 production by female CD4+ T cells was not reduced in the presence of CD8+ T cells from either male or female mice, except in the presence of male CD8+ T cells at the highest cell number. In addition, IL-5 was not detected in the cultures of CD8+ T cells from splenocytes from both male and female mice. These results suggest that TCR-activated CD4+ T cells from male mice are more sensitive to the suppressive effects of TCR-activated CD8+ T cells on IL-5 production. However, it was not determined whether the suppression of IL-5 production resulted from the decreased number of IL-5-producing CD4+ T cells or the reduced potential of CD4+ T cells to synthesize IL-5. There is increasing evidence demonstrating that sex hormones can influence the development of specific lymphocyte populations and cytokine production profiles. For example, progesterone increases the production of IL-4 and IL-5 [17, 18], and testosterone increases the development of CD8+ cell populations and mitogen-induced IFN-γ-producing CD8+ T cells [19, 20]. However, in this study, there were no sex differences in the production of IL-5 by TCR-activated CD4+ T cells or in the proportions of CD4+ T and CD8+ T cells in splenocytes. Therefore, the greater production of IL-5 in TCR-activated female splenocytes could be due to the sex difference in the sensitivity of CD4+ T cells to the suppressive effects of CD8+ T cells.

CD8+ T cells play a role in both the progression of and protection from allergic diseases, including asthma [3]. Indeed, CD8+ T cells that produce IL-4, IL-5 and IL-13 (Tc2-type CD8+ T cells) were isolated from asthmatic airways [21]. Tc2 cells identified in the lungs of allergic mice have been shown to play an influential role in propagating inflammation in rodent models [3]. In contrast, IFN-γ-producing Tc1-type CD8+ T cells have been reported to exert suppressive effects on Th2-dominant allergic airway inflammation. Adoptive transfer of IFN-γ-producing CD8+ T cells to sensitized mice suppressed the development of airway eosinophilic inflammation, while the adoptive transfer of IFN-γ-deficient CD8+ T cells failed to do so [22]. In a murine asthma model, allergen-specific Tc1 cells could suppress allergic airway inflammation through induction of IL-12 and IL-18 by lung dendritic cells [3]. In addition, CD8+ regulatory T cells have been proposed as a counterpart to CD4+ regulatory T cells. In humans, several CD8+ regulatory T cell subsets, such as TGF-β-producing CD8+ T cells and IL-10-producing CD8+ T cells, have been described, although their functional significance has yet to be fully elucidated [3]. In this study, while IL-10 production in TCR-activated CD8+ T cells was lower than the limit of detection in both sexes, IFN-γ production by TCR-activated CD8+ T cells from male mice was lower than the production from female mice. Nevertheless, CD8+ T cells from both male and female mice reduced IL-5 production by male CD4+ T cells to similar levels; the addition of female CD4+ T cells did not replicate this phenotype. Therefore, although the effect of anti-IFN-γ antibody on IL-5 production and the pathways through which CD8+ T cells suppress IL-5 production were not investigated in this study, sex differences in the density/affinity and signal transduction of

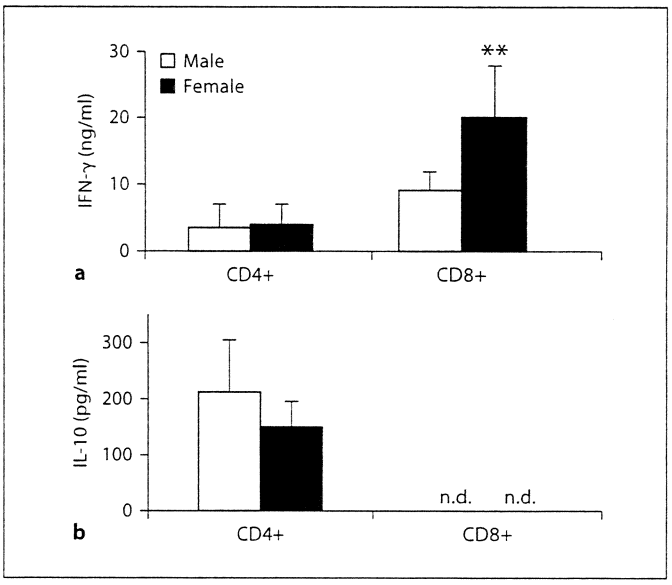


Fig. 5. IFN-γ and IL-10 production by CD4+ and CD8+ T cells stimulated with anti-CD3/CD28. Purified CD4+ and CD8+ T cells from splenocytes from male (open columns) and female (closed columns) mice were stimulated as in figure 1, and the IFN-γ (**a**) and IL-10 (**b**) concentrations in the culture supernatants were measured by ELISA. Data are expressed as means ± SD. ** $p < 0.01$ compared to male mice. n.d. = Not detected.

IFN-γ receptors on CD4+ T cells might be one of the possible mechanisms underlying the greater sensitivity of male CD4+ T cells to CD8+ T cell suppression. In addition, cell-cell interaction between CD8+ and CD4+ T cells needs to be investigated as a possible mechanism of the suppression.

The minor histocompatibility (H) male-specific (Y) antigen (H-Y), which is expressed in male tissues, is derived from a protein encoded by the *Smcy*, *Dby* and *Uty* gene located on the Y chromosome [23]. This antigen is MHC-I and II restricted and has been known as the basis for female mouse rejection of the same-strain male organ grafts which are MHC-matched [24]. It has been also reported that purified CD8+ T cells from H-Y TCR transgenic mice proliferate upon stimulation with specific agonists [25]. Therefore, in our coculture experiments, it could not be excluded that female CD8+ T cells were stimulated by H-Y antigen and MHC-I complexes on male CD4+ T cells, which contributed to the inhibition of IL-5 production from male CD4+ T cells.

Sex differences in Th1/Th2 cytokine production by human lymphocytes have been reported. In healthy adult subjects, Th2-dominant cytokine production by phytohemagglutinin-stimulated peripheral blood mononuclear cells (PBMCs) was significantly higher in women than in men [12]. Furthermore, in atopic asthmatic adults, female PBMCs had a significantly greater proportion of IL-13+ T cells upon stimulation with CD3/CD28 antibodies compared to male PBMCs [26]. In contrast to adult subjects, in preschool children, phytohemagglutinin-induced IFN-γ, IL-5 and IL-13 secretion were significantly increased in PBMCs from wheezing boys compared to wheezing girls [27]. However, the cell types and mechanisms responsible for these sex differences have not yet been determined.

In conclusion, the sex difference in IL-5 production by splenocytes might be due, at least in part, to the sex difference in the sensitivity of CD4+ T cells to suppression by CD8+ T cells. We are attempting to investigate the mechanisms of this sex difference in CD4+ and CD8+ T cell interactions, including expression and/or activation of cytokine receptors and intracellular events following TCR activation in each cell type. Clarification of the mechanisms could lead to further understanding of the pathogenesis of diseases associated with sex differences, such as asthma and collagen diseases.

Acknowledgments

This work was supported in part by Grant-in-Aid for Scientific Research (No. 21590970 to Y.O. and No. 22590843 to I.O.) and by the Matching Fund Subsidy for Private Universities from the Ministry of Education, Culture, Sports, Science and Technology (MEXT) of Japan. This manuscript was checked for proper English usage by American Journal Experts (Certification No.: D516-25C2-0BC3-4076-2BAA).

Disclosure Statement

The authors declare that no financial or other conflict of interest exists in relation to the contents of this article.

References

1 Holgate ST: Pathogenesis of asthma. Clin Exp Allergy 2008;38:872–897.
2 Robinson DS: The role of the T cell in asthma. J Allergy Clin Immunol 2010;126:1081–1091.
3 Betts RJ, Kemeny DM: CD8+ T cells in asthma: friend or foe? Pharmacol Ther 2009;121:123–131.
4 Ishimitsu R, Nishimura H, Yajima T, Watase T, Kawauchi H, Yoshikai Y: Overexpression of IL-15 in vivo enhances Tc1 response, which inhibits allergic inflammation in a murine model of asthma. J Immunol 2001;166:1991–2001.
5 The ENFUMOSA Study Group: The ENFUMOSA cross-sectional European multicentre study of the clinical phenotype of chronic severe asthma. Eur Respir J 2003;22:470–477.
6 Siroux V, Curt F, Oryszczyn MP, Maccario J, Kauffmann F: Role of gender and hormone-related events on IgE, atopy, and eosinophils in the Epidemiological Study on the Genetics and Environment of Asthma, bronchial hyperresponsiveness and atopy. J Allergy Clin Immunol 2004;114:491–498.
7 Almqvist C, Worm M, Leynaert B, Working Group of GA2LEN WP 2.5 Gender: Impact of gender on asthma in childhood and adolescence: a GA2LEN review. Allergy 2008;63:47–57.
8 Chen W, Mempel M, Schober W, Behrendt H, Ring J: Gender difference, sex hormones, and immediate type hypersensitivity reactions. Allergy 2008;63:1418–1427.
9 Balzano G, Fuschillo S, Melillo G, Bonini S: Asthma and sex hormones. Allergy 2001;56:13–20.
10 Melgert BN, Postma DS, Kuipers I, Geerlings M, Luinge MA, van der Strate BW, Kerstjens HA, Timens W, Hylkema MN: Female mice are more susceptible to the development of allergic airway inflammation than male mice. Clin Exp Allergy 2005;35:1496–1503.
11 Riffo-Vasquez Y, Ligeiro de Oliveira AP, Page CP, Spina D, Tavares-de-Lima W: Role of sex hormones in allergic inflammation in mice. Clin Exp Allergy 2007;37:459–470.
12 Girón-González JA, Moral FJ, Elvira J, Garcia-Gil D, Guerrero F, Gavilán I, Escobar L: Consistent production of a higher Th1:Th2 cytokine ratio by stimulated T cells in men compared with women. Eur J Endocrinol 2000;143:31–36.

13 Jarefors S, Bennet L, You E, Forsberg P, Ekerfelt C, Berglund J, Emerudh J: Lyme borreliosis reinfection: might it be explained by a gender difference in immune response? Immunology 2006;118:224–232.
14 Okuyama K, Wada K, Chihara J, Takayanagi M, Ohno I: Sex-related splenocyte function in a murine model of allergic asthma. Clin Exp Allergy 2008;38:1212–1219.
15 Wada K, Okuyama K, Ohkawara Y, Takayanagi M, Ohno I: Sex differences in transcriptional regulation of IL-5 expression by bronchial lymph node cells in a mouse model of asthma. Respirology 2010;15:629–635.
16 Okuyama K, Hamanaka Y, Kawano T, Ohkawara Y, Takayanagi M, Kikuchi T, Ohno I: T cell subsets related with a sex difference in IL-5 production. Int Arch Allergy Immunol 2011;155 (suppl 1):21–26.
17 Hellings PW, Vandekerckhovez P, Claeysz R, Billenz J, Kasran A, Ceuppens JL: Progesterone increases airway eosinophilia and hyper-responsiveness in a murine model of allergic asthma. Clin Exp Allergy 2003;33: 1457–1463.
18 Miyaura H, Iwata M: Direct and indirect inhibition of Th1 development by progesterone and glucocorticoids. J Immunol 2002;168: 1087–1094.
19 Yao G, Liang J, Han X, Hou Y: In vivo modulation of the circulating lymphocyte subsets and monocytes by androgen. Int Immunopharmacol 2003;3:1853–1860.
20 Page ST, Plymate SR, Bremner WJ, Matsumoto AM, Hess DL, Lin DW, Amory JK, Nelson PS, Wu JD: Effect of medical castration on CD4+ CD25+ T cells, CD8+ T cell IFN-gamma expression, and NK cells: a physiological role for testosterone and/or its metabolites. Am J Physiol Endocrinol Metab 2006; 290:E856–E863.
21 Cho SH, Stanciu LA, Holgate ST, Johnston SL: Increased interleukin-4, interleukin-5, and interferon-gamma in airway CD4+ and CD8+ T cells in atopic asthma. Am J Respir Crit Care Med 2005;171:224–230.
22 Marsland BJ, Harris NL, Camberis M, Kopf M, Hook SM, Le Gros G: Bystander suppression of allergic airway inflammation by lung resident memory CD8+ T cells. Proc Natl Acad Sci USA 2004;101:6116–6121.
23 Markiewicz MA, Girao C, Opferman JT, Sun J, Hu Q, Agulnik AA, Bishop CE, Thompson CB, Ashton-Rickardt PG: Long-term T cell memory requires the surface expression of self-peptide/major histocompatibility complex molecules. Proc Natl Acad Sci USA 1998;95:3065–3070.
24 Simpson E, Scott D, Chandler P: The male-specific histocompatibility antigen, H-Y: a history of transplantation, immune response genes, sex determination and expression cloning. Annu Rev Immunol 1997;15:39–61.
25 Maile R, Siler CA, Kerry SE, Midkiff KE, Collins EJ, Frelinger JA: Peripheral 'CD8 tuning' dynamically modulates the size and responsiveness of an antigen-specific T cell pool in vivo. J Immunol 2005;174:619–627.
26 Loza MJ, Foster S, Bleecker ER, Peters SP, Penn RB: Asthma and gender impact accumulation of T cell subtypes. Respir Res 2010; 11:103.
27 Uekert SJ, Akan G, Evans MD, Li Z, Roberg K, Tisler C, Dasilva D, Anderson E, Gangnon R, Allen DB, Gern JE, Lemanske RF Jr: Sex-related differences in immune development and the expression of atopy in early childhood. J Allergy Clin Immunol 2006;118: 1375–1381.

Allergology International. 2012;61:245-258
DOI: 10.2332/allergolint.11-OA-0304

ORIGINAL ARTICLE

μ-opioid Receptor-Mediated Alterations of Allergen-Induced Immune Responses of Bronchial Lymph Node Cells in a Murine Model of Stress Asthma

Kaori Okuyama[1], Soichiro Ide[2], Shinobu Sakurada[3], Kazumasu Sasaki[4], Ichiro Sora[4], Gen Tamura[5], Yuichi Ohkawara[1], Motoaki Takayanagi[1] and Isao Ohno[1]

ABSTRACT

Background: Psychological stress has a recognized association with asthma symptoms. Using a murine model of allergic asthma, we recently demonstrated the involvement of μ-opioid receptors (MORs) in the central nervous system in the stress-induced exacerbation of airway inflammation. However, the involvement of MORs on neurons and immunological alterations in the stress asthma model remain unclear.

Methods: MOR-knockout (MORKO) mice that express MORs only on noradrenergic and adrenergic neurons (MORKO/Tg mice) were produced and characterized for stress responses. Sensitized mice inhaled antigen and were then subjected to restraint stress. After a second antigen inhalation, bronchoalveolar lavage cells were counted. Before the second inhalation, bronchial lymph node (BLN) cells and splenocytes from stressed and non-stressed mice were cultured with antigen, and cytokine levels and the proportions of T cell subsets were measured.

Results: Stress-induced worsening of allergic airway inflammation was observed in wild-type and MORKO/Tg mice but not MORKO mice. In wild-type stressed mice, IFN-γ/IL-4 ratios in cell culture supernatants and the proportion of regulatory T cells in BLN cell populations were significantly lower than those in non-stressed mice. These differences in BLN cells were not observed between the stressed and non-stressed MORKO mice. Restraint stress had no effect on cytokine production or T cell subsets in splenocytes.

Conclusions: Restraint stress aggravated allergic airway inflammation in association with alterations in local immunity characterized by greater Th2-associated cytokine production and a reduced development of regulatory T cells, mediated by MORs.

KEY WORDS

adaptive immune response, allergic asthma, mu opioid receptor, murine model, psychological stress

INTRODUCTION

Bronchial asthma is a chronic airway inflammatory disease characterized by the accumulation and activation of inflammatory cells, such as eosinophils and mast cells, in the bronchial wall and airway lumen. Inflammatory mediators released from these cells upon stimulation, such as arachidonic acid metabolites and reactive oxygen species, induce the airway narrowing and airway hyper-responsiveness observed in asthmatics. Type 2 $CD4^+$ T (Th2) cells and Th2-biased cytokines, such as IL-4, IL-5 and IL-13, play a central

[1]Department of Pathophysiology, [3]Department of Physiology and Anatomy, Tohoku Pharmaceutical University, [4]Department of Biological Psychiatry, Tohoku University Graduate School of Medicine, [5]Division of Respiratory Medicine, Airway Institute in Sendai, Miyagi and [2]Department of Pharmacology, Graduate School of Pharmaceutical Sciences, Hokkaido University, Hokkaido, Japan.
Authors' contributions: KO and SI contributed equally to this work.
Conflict of interest: No potential conflict of interest was disclosed.

Correspondence: Isao Ohno, Department of Pathophysiology, Tohoku Pharmaceutical University, 4–4–1 Komatsushima, Aoba-ku, Sendai, Miyagi 981–8558, Japan.
Email: iohno@tohoku-pharm.ac.jp
Received 20 January 2011. Accepted for publication 25 August 2011.
©2012 Japanese Society of Allergology

role in regulating the behavior of inflammatory cells in asthmatic airways. It has been proposed that interferon-γ (IFN-γ)-producing type 1 $CD4^+$ T (Th1) cells inhibit the development of allergic diseases by counterbalancing the proliferation and development of Th2 cells, depending on the stage of inflammation.[1-4]

$CD4^+CD25^+$ regulatory T (Treg) cells play a critical role in the immune balance network by suppressing or limiting effector immune responses against inner and external insults, for example, preventing organ-specific autoimmunity and allograft rejection as well as maintaining self-tolerance.[5-8] Recent studies have demonstrated that the failure of Treg cells to suppress Th2-mediated immune responses to innocuous inhaled antigens leads to an inappropriate balance between allergen activation of Treg cells and effector Th2 responses, resulting in the development and maintenance of asthmatic airway inflammation characterized by uncontrolled Th2-biased immune responses.[9-11]

A number of clinical studies have demonstrated an association between psychological stress and asthma symptom aggravation.[12,13] For example, 20-35% of asthmatics experience an exacerbation of their symptoms during periods of stress.[14] In childhood asthma, high levels of chronic stress combined with an acutely negative life events have been shown to increase the risk of asthma attacks.[15] Furthermore, psychological stress has effects on the inflammatory and immune responses implicated in asthma, such as Th2 cytokines. For example, chronic stress caused by academic examinations has been shown to increase IL-5 production and eosinophil accumulation after antigen inhalation in college students with mild asthma.[16,17] However, the precise mechanisms by which psychological stress aggravates Th2 immune responses remain to be clarified.

Psychological stress upregulates the production of endogenous opioids, including endorphins, enkephalins and dynorphins. These endogenous opioids exert their effects, such as analgesia, neuroendocrine function and immunoregulation, by binding to opioid receptors consisting of three subtypes, μ, δ and κ.[18,19] We recently established a murine model of psychological stress-induced asthma exacerbation in which allergen-induced airway inflammation in restraint-stressed mice was more severe than in non-stressed mice. This increased airway inflammation in the restraint-stressed mice was associated with higher levels of Th2 cytokines. Using this model, we have demonstrated that μ-opioid receptors (MORs) in the central nervous system (CNS) are involved in psychological stress-induced asthma exacerbation.[20,21] However, MORs are expressed not only on neurons but also on several other cell types, including lymphocytes, and the function of MORs on these cells have been extensively studied.[22-25]

Therefore, we first aimed to confirm the involvement of neuron MORs in the aggravation of allergic airway inflammation evoked by the stress exposure, using mice that express MORs exclusively on neurons. Then we hypothesized that the aggravation of Th2 responses observed in psychological stress-induced asthma exacerbation may result from a failure in the development of Treg cells in airways and that MORs might be involved in these immune alterations. To address this hypothesis, we examined antigen-induced Th1, Th2 and regulatory cytokine production and T cell subset proportions in populations of bronchial lymph node (BLN) cells and splenocytes from wild-type and MOR-gene-knockout (MORKO) mice exposed to restraint stress.

METHODS

ANIMALS

Specific pathogen-free female C57BL/6 (B6) mice were purchased from Japan SLC (Hamamatsu, Japan). MORKO mice were generated and backcrossed with B6 mice as described previously.[26,27] MOR-transgenic MORKO (MORKO/Tg) mice were produced as discussed below. Animals were housed under a 12 h light/dark cycle with a constant temperature (22 ± 2℃). Sterilized food and water were available *ad libitum*. All experiments described below were approved by the Committee of Animal Experiments at Tohoku Pharmaceutical University and Tohoku University and conformed to the committee guidelines of each university.

PLASMID CONSTRUCT AND PRODUCTION OF MORKO/Tg MICE

The plasmid pDIL,[28] which contains the human dopamine β-hydroxylase (DBH) gene promoter connected to a cDNA fragment encoding the human interleukin 2 receptor α subunit (IL-2Rα), was donated by Dr. K. Kobayashi (Fukushima Medical University School of Medicine, Fukushima, Japan). We replaced the cDNA part of pDIL with a cDNA fragment encoding the human μ-opioid receptor gene, which we had previously cloned.[29] Figure 1 shows the transgene construct used in this study. The construct was microinjected into fertilized B6 mouse eggs, which were implanted into pseudopregnant female mice. Microinjections were conducted by Central Laboratories of Experimental Animals (Kawasaki, Japan) and YSNT Inst., Inc. (Shimotsuga, Japan). Successful integration of the transgene was confirmed by Southern blot analysis of tail DNA. The transgenic mice were then crossed with homozygous MORKO mice with a B6 genetic background[23] to obtain the Tg mouse (F1 offspring: heterozygous MORKO/Tg). Homozygous MORKO/Tg mice were produced by crossing the F1 offspring with homozygous MORKO mice.

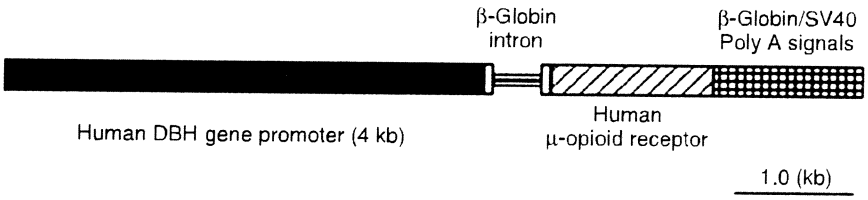


Fig. 1 Human DBH promoter—human MOR cDNA fusion gene in the plasmid. This construct includes the 4 kb DNA fragment of the human DBH promoter in addition to the rabbit β-globin second intron, human MOR cDNA, rabbit β-globin polyadenylation signal, and SV40 early gene polyadenylation signal.

In situ HYBRIDIZATION

Brains were removed quickly and frozen in powdered dry ice. Coronal sections (16 μm) were prepared in a cryostat, thaw-mounted onto gelatin-coated slides and stored at -80℃ until in situ hybridization was conducted. Because the coding regions of human and mouse MOR mRNA are highly homologous, 5'-noncoding regions of MOR cDNA were used as the templates to synthesize the RNA probes. ^{35}S-labeled antisense and sense RNA probes for the in situ hybridization were synthesized in the presence of [α^{35}S] UTP (30 TBq/mmol, Amersham, Buckingham, NY, USA), using a T3 RNA polymerase (Promega, Madison, WI, USA). For the in situ hybridization, sections were fixed in 4% formalin in 10 mM phosphate-buffered saline for 30 min, treated with proteinase K (0.5 μg/ml) for 10 min and immersed in 0.25% acetic anhydride in 0.1 M triethanolamine/saline for 10 min. After dehydration in an ethanol series (70, 85, 95, 100%), prehybridization was carried out at 55℃ for 1 hr in the following buffer: 50% formamide, 4x SSC (1x SSC = 150 mM NaCl, 15 mM tri-sodium citrate, pH 7.0), 5x Denhardt's solution, 10 mM EDTA, 250 μg/ml yeast tRNA, 20 mM dithiothreitol (DTT) and 500 μg/ml heat-denatured salmon sperm DNA, and the sections were then hybridized to the antisense or sense RNA probe at 55℃ for 17 h. For the hybridization, 10% dextran sulfate was added to the buffer. After the hybridization, sections were washed four times in 2x SSC/10 mM DTT for 10 min at 55℃, incubated with RNase A (50 μg/ml in 0.5 M NaCl/10 mM Tris/1 mM EDTA, pH 8.0) for 30 min at 37℃ and then washed twice in 50% formamide/2x SSC/10 mM DTT for 30 min at 55℃. The sections were dehydrated in the ethanol series and dried. The slides were exposed to Hyperfilm-β max (Amersham) and then dipped in autoradiographic emulsion NTB-3 (Kodak, Rochester, NY, USA) diluted 1 : 1 with water. After 3 weeks of exposure, the slides were developed with D-19 (Kodak) and counterstained with cresyl violet.

LIGAND BINDING AND AUTORADIOGRAPHY

Brains and adrenal glands were removed from wild-type, MORKO and MORKO/Tg mice and quickly frozen at -80℃. The brains were cryosectioned at 10 μm and thaw-mounted onto gelatin-coated slides. Tissue sections were preincubated with 50 mM Tris buffer (pH 7.4) containing 10 mM $MgCl_2$ and 1 mM EDTA for 10 min at 25℃. The sections were then incubated with 2 nM [^{3}H]DAMGO (50.5 Ci/mmol) (DuPont-New England Nuclear, Boston, MA, USA) for 60 min at 25℃. DAMGO [D-Ala^2, *N*-MePhe^4, Gly-ol^5] enkephalin is a MOR-selective agonist. After the incubation, sections were washed twice in fresh buffer for 120 min at 25℃ and in deionized water for 5 min at 4℃ and then dried for 60 min at 4℃. Sections were exposed to IP-film for 4 weeks and analyzed using the BAS3100II system (Fujix, Tokyo, Japan).

TAIL SUSPENSION TESTING

For tail suspension testing, mice were taped by their tail to a metal hook in a test chamber (20 × 20 × 25 cm) made of white plastic walls and floor. Each hook was connected to a computerized strain gauge that was adjusted to detect all movements of the animals (Tail suspension system; Neuroscience Inc., Osaka, Japan). The total duration of the immobility testing was 15 min.

STRESS PROCEDURES AND CORTICOSTERONE EIA

First, blood samples were obtained from naive wild-type, MORKO and MORKO/Tg mice tail veins. Next, after a 3-day interval, the 15-minute tail suspension procedure was performed on these mice. Blood samples were obtained again at 30 min after the tail suspension testing. Finally, after a 1-day interval, the physical restraint procedure was performed on these mice. For the restraint stress procedure, mice were placed in a 50 ml conical centrifuge tube with multiple ventilation holes. Mice were restrained vertically in the tube for 12 h, followed by 12 h of rest during which food and water were available *ad libitum*. This restraint allowed the mice to rotate from a supine to prone position but not to turn their heads toward their tails or take food and water. Restraint stress is generally considered to induce psychological stress in animals.[30] Mice were restrained for two cycles as described, and blood samples were then obtained. All

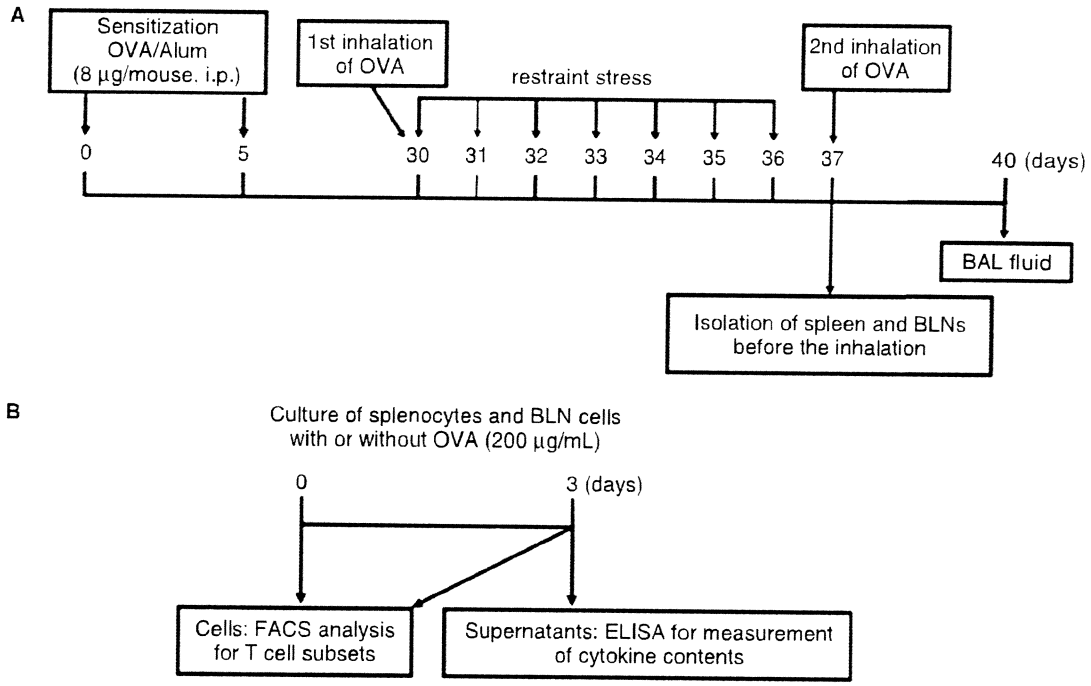


Fig. 2 Diagrammatic representation of the protocols. (**A**) Isolation of spleen, BLNs and BAL fluid. (**B**) Culture of splenocytes and BLN cells.

blood samples were immediately centrifuged for 20 min at 1,000 g, and obtained plasma samples were then stored at -80℃ until the analysis. Plasma corticosterone levels were determined using a Corticosterone Enzyme Immunoassay Kit (Assay Design Inc., Ann Arbor, MI, USA).

PROTOCOLS FOR SENSITIZATION, CHALLENGE AND STRESS EXPOSURE

Our previously published murine model of stress-induced exacerbation of allergic airway inflammation[21] was used in this study. Briefly, mice 6-8 weeks old were sensitized by intraperitoneal injections of chicken ovalbumin (OVA) (Grade V, Sigma, St. Louis, MO, USA) (8 μg/mouse) adsorbed with aluminum hydroxide (Wako Pure Chemical Industries, Osaka, Japan) (4 mg/mouse) on days 0 and 5. For restraint stress, each mouse was placed in a 50-ml conical centrifuge tube as described above for 6 h per day. On day 30, stressed mice in the 50-ml conical centrifuge tubes were left in plastic chambers for 6 h. For the first hour of this period, aerosolized OVA was pumped through the chambers to expose the mice in the tubes to OVA. Stressed mice were subjected to the restraint stress for 6 consecutive days, on days 31 to 36, at the same time each day. Non-stressed mice were only deprived of food and water for the same period as the stressed mice were exposed to stress. Food and water deprivation has been used as a non-stress condition in other rodent experiments investigating the effects of restraint stress.[31,32] On day 37, stressed and non-stressed mice were challenged with aerosolized OVA. On day 40, their lungs were lavaged twice with an injection of 0.25 ml of cold saline through the trachea, as described previously, and the recovered bronchoalveolar lavage (BAL) fluid was pooled. Approximately 0.4 ml of instilled fluid was consistently recovered from each mouse. BAL fluid was processed for counting total cells and cell differentials (Fig. 2A). In other experiments, stressed and non-stressed mice were sacrificed on day 37 to collect spleen and BLNs (Fig. 2A).

PREPARATION AND CULTURE OF SPLENOCYTES AND BLN CELLS

Splenocytes and BLN cells were prepared and cultured as previously described.[33,34] For each experiment, BLN cells were prepared from BLNs collected from 6-8 wild-type mice and 5 MORKO mice, and splenocytes were prepared from the spleen of one mouse. Splenocytes and BLN cells were suspended at 5×10^6 cells/ml in complete media consisting of RPMI 1640 (Gibco BRL, Rockville, MD, USA) supplemented with 10% fetal bovine serum (ICN Biomedicals, Inc., Aurosa, OH, USA), 55 μM 2-mercaptoethanol (Wako Pure Chemical Industries), 2 mg/ml $NaHCO_3$, 50 U/ml penicillin G (Meiji Seika, Tokyo, Japan), 50 μg/ml streptomycin sulphate (Meiji Seika) and 2 mM L-glutamine (Wako Pure Chemical Industries). Cell viability of the suspension was more than

98%, as determined by trypan blue dye exclusion. The cells were cultured at 1 × 10^7 cells/well in 24-well culture plates (MICROPlate, Asahi Techno Glass, Chiba, Japan) in the presence or absence of OVA (200 μg/ml) for 3 days. After the culture, the number of viable cells was counted, and the samples were centrifuged. The supernatants were stored at -80℃ for cytokine measurements using an enzyme-linked immunosorbent assay (ELISA), and the cells were subjected to lymphocyte compartment analysis by flow cytometry before and after the culture (Fig. 2B).

CYTOKINE MEASUREMENTS

IL-4, IL-5, IL-10, IL-13, IFN-γ and TGF-β1 levels in the supernatant were measured using specific ELISA kits (R&D systems, Minneapolis, MN, USA) according to the manufacturer's protocol. The sensitivity of detection was 2 pg/ml for IL-4, 7 pg/ml for IL-5, 4 pg/ml for IL-10, 1.5 pg/ml for IL-13, 2 pg/ml for IFN-γ and 2.9 pg/ml for TGF-β1. Because IFN-γ and IL-4 are classical examples of antagonistic signature cytokines for Th1 and Th2 activity, respectively, the Th1/Th2 balance was monitored by IFN-γ/IL-4 ratio,[35] which was calculated with the values of these two cytokines obtained from the same experiment.

FLOW CYTOMETRIC ANALYSIS

$CD3^+CD4^+$, $CD3^+CD4^+T1/ST2^+$ and Treg compartments of splenocytes and BLN cells were analyzed as previously described.[34] Briefly, the cells were preincubated with anti-CD16/CD32 (FCγIII/II receptor; BD Biosciences PharMingen, San Diego, CA, USA) to reduce nonspecific binding of the subsequent antibodies. Anti-T1/ST2-fluorescein isothiocyanate (clone DJ8, 0.8 μg/10^6 cells) (Morwell Diagnostic, Zurich, Switzerland), anti-CD3e-allophycocyanin (clone 145-2C11, 0.8 μg/10^6 cells) (BD Biosciences PharMingen), anti-CD4-R-phycoerythrin (clone GK1.5, 0.5 μg/10^6 cells) (BD Biosciences PharMingen) or isotype control antibodies were added directly to the cells. T1/ST2 was employed as a surface marker for Th2 cells because it is preferentially expressed on the surface of murine Th2 cells and plays an important role in the activation of Th2 cells, including proliferation and Th2 cytokine production.[36,37] Treg cells were identified as $CD4^+CD25^+$ cells, using a mouse regulatory T cell staining kit (eBioscience, San Diego, CA, USA) according to the manufacturer's protocol. Cells were counted on a FACScan (BD Biosciences PharMingen), and the analyses were performed using Cell Quest (BD Biosciences PharMingen).

DATA ANALYSIS

In the behavior analyses, significant differences were statistically evaluated using an analysis of variance (ANOVA) followed by the Bonferroni *post hoc* test or a paired *t*-test. Significant differences between two groups were determined using the nonparametric Mann-Whitney *U*-test. These analyses were performed using Prism4 (GraphPad Software, San Diego, CA, USA). A p value of less than 0.05 was considered significant.

RESULTS

ANALYSIS OF TRANSGENE mRNA AND FUNCTIONAL MOR PROTEIN EXPRESSION

The expression of the human MOR was investigated in MORKO/Tg mice by *in situ* hybridization with selective probes for mouse and human MOR mRNA. In brainstem sections, the specific expression of human MOR mRNA was found in locus ceruleus (LC) regions in the MORKO/Tg mouse (Fig. 3A, B). Lower expression levels of the human MOR mRNA were found in other brain regions. The lack of detection of the expression signals in both wild-type mouse by the human selective probe and the MORKO/Tg mouse by the mouse selective probe confirmed the expression of human MOR mRNA by the transgene. Next, the functional expression of MOR protein was confirmed in MORKO/Tg mice by [^{3}H]DAMGO binding (Fig. 3C). In MORKO/Tg mice, the [^{3}H]DAMGO binding sites were specifically found in the cortex and thalamus, which were quite different from those in wild-type mice.

TAIL SUSPENSION TEST

Immobility times in the 15-min tail suspension assay were analyzed in wild-type, MORKO, and MORKO/Tg mice (Fig. 4A, B). Although all the studied genotypes showed a time-dependent increase in immobility time, there were significant differences in the manner of this increase among the genotypes (two-way repeated measures ANOVA: $p < 0.05$; $F = 5.13$; $df = 2.560$). MORKO mice showed significantly less immobility compared with wild-type mice from 5 to 10 min after initiation of the tail suspension ($p < 0.05$). Interestingly, this decreased immobility in MORKO mice was not found in MORKO/Tg mice. MORKO/Tg mice showed no difference from wild-type mice but did show a significant difference compared with MORKO mice ($p < 0.05$) in immobility time (Fig. 4B).

STRESS-INDUCED CORTICOSTERONE RELEASE

We analyzed both tail suspension and restrained stress-induced changes in plasma corticosterone concentration in wild-type, MORKO, and MORKO/Tg mice (Fig. 5). Both tail suspension and restraint stress significantly increased plasma corticosterone concentrations in wild-type (paired *t*-test: $p < 0.0005$, $t = -5.68$, $p < 0.0001$, $t = -7.56$, respectively), MORKO (paired *t*-test: $p < 0.0005$, $t = -4.54$, $p < 0.0001$, $t = -9.84$, respectively), and MORKO/Tg mice (paired *t*-test: $p < 0.0001$, $t = -7.39$, $p < 0.0001$, $t = -24.01$, respectively). In addition, the ANOVA showed significant differences among these genotypes in changes in

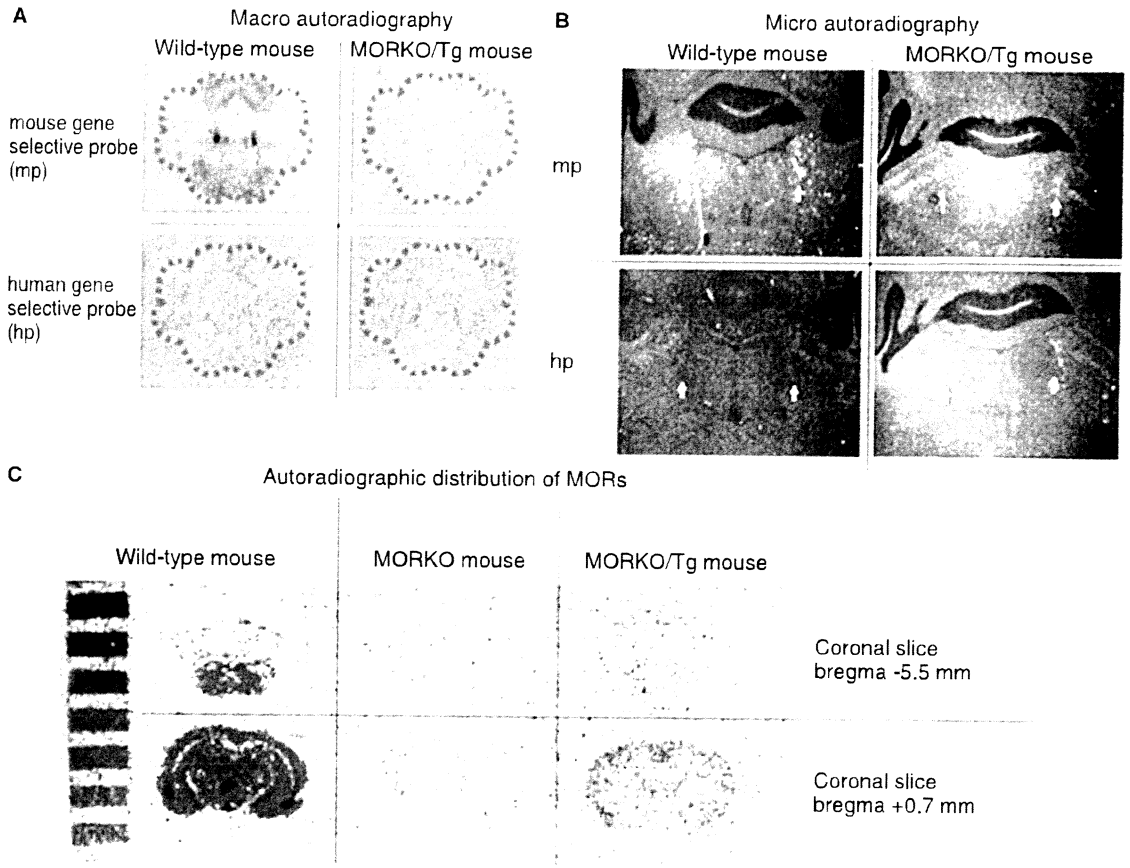


Fig. 3 Autoradiographs of MOR mRNA expression and [3H]DAMGO binding sites. Macro(**A**)- and micro(**B**)-autoradiographs of in situ hybridization for mouse and human MOR mRNA showed the LC region-specific expression of human MOR mRNA in coronal sections (bregma -5.5 mm) of the MORKO/Tg mouse. White arrows indicate the LC regions. (**C**) Autoradiographic distribution of [3H]DAMGO binding sites in coronal brain slices of wild-type, MORKO, and MORKO/Tg mice. Sections were taken through the brainstem: LC (bregma +5.5 mm: upper panel) and thalamus: cortex (bregma -0.7 mm: lower panel).

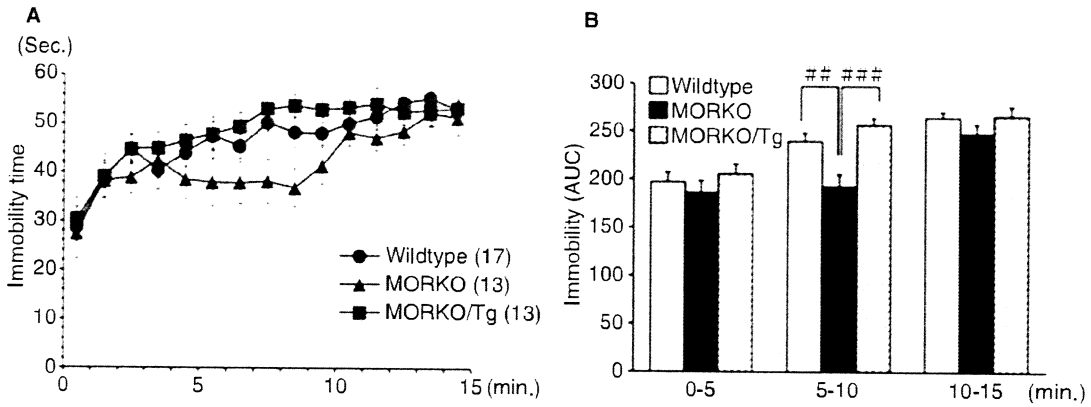


Fig. 4 Immobility in wild-type, MORKO, and MORKO/Tg mice in the 15-min tail suspension test. (**A**) Immobility times were measured in wild-type (n = 17), MORKO (n = 13), and MORKO/Tg (n = 13) mice. (**B**) AUC of the immobility times over 5 min in the tail suspension tests. ##, ### $p < 0.01$, 0.001, indicating a significant difference from the corresponding value in MORKO mice. Data are expressed as the mean ± SEM.

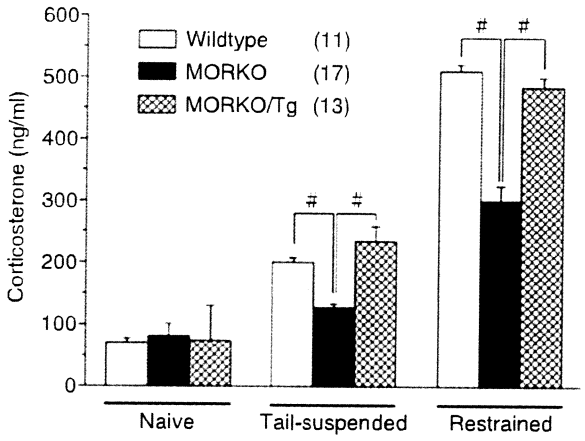


Fig. 5 Stress-induced increase in plasma corticosterone concentrations in wild-type, MORKO, and MORKO/Tg mice. Plasma corticosterone levels were analyzed in wild-type (n = 11), MORKO (n = 17), and MORKO/Tg (n = 13) mice before any test, after the tail suspension test, and after the restraint stress. #$p < 0.05$, showing a significant difference from the corresponding value in MORKO mice. Data are expressed as the mean ± SEM.

plasma corticosterone concentration (tail suspension stress: $p < 0.0005$; F = 11.14; df = 2.38; restrained stress: $p < 0.0001$; F = 14.04; df = 2.38). MORKO mice showed significantly lower plasma corticosterone concentrations compared with wild-type mice after both the tail suspension and restraint stress procedure ($p < 0.05$). Furthermore, MORKO/Tg mice showed the same level of increase in corticosterone concentration compared to wild-type mice, and this change was significantly different from MORKO mice ($p < 0.05$).

RESTRAINT STRESS-INDUCED AGGRAVATION OF ALLERGIC AIRWAY INFLAMMATION IN MORKO/Tg MICE

As previously demonstrated,[21] the stress-induced worsening of allergic airway inflammation observed in wild-type mice (non-stress vs. stress: total cells, 134.5 ± 57.1 vs. 340.6 ± 164.8 × 10^4 cells/ml, $p < 0.01$; eosinophils, 82.0 ± 35.8 vs. 262.4 ± 128.0 × 10^4 cells/ml, $p < 0.01$; lymphocytes, 16.7 ± 7.7 vs. 39.0 ± 30.1 × 10^4 cells/ml, $p < 0.01$) (Fig. 6A) was not observed in the MORKO mice (Fig. 6B). However, as shown in Figure 6C, the numbers of total cells and eosinophils in BAL fluid three days after the second antigen inhalation in stressed MORKO/Tg mice were significantly higher than those in non-stressed MORKO/Tg mice (non-stress vs. stress: total cells, 170.7 ± 67.8 vs. 320.6 ± 62.5 × 10^4 cells/ml, $p < 0.01$; eosinophils, 124.0 ± 43.7 vs. 251.5 ± 57.2 × 10^4 cells/ml, $p < 0.01$), although the difference in the number of lymphocytes did not reach significance (non-stress vs. stress: 27.5 ± 23.4 vs. 41.8 ± 15.5 × 10^4 cells/ml).

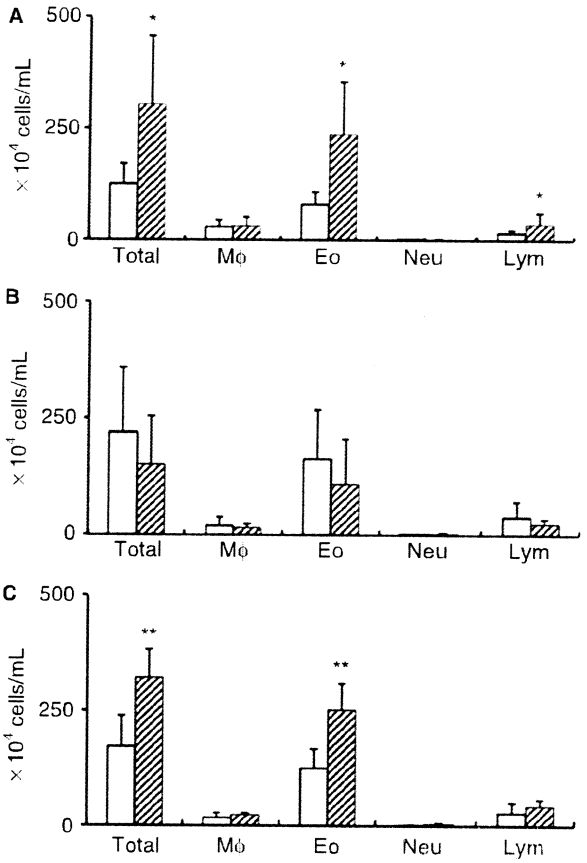


Fig. 6 Comparison of cell numbers in BAL fluids between stressed and non-stressed mice. The numbers of total cells (Total), macrophages (Mϕ), eosinophils (Eo), neutrophils (Neu) and lymphocytes (Lym) in BAL fluids were counted for non-stressed (open bars) and stressed (hatched bars) wild-type (5 and 6, respectively, in **A**), MORKO (7 and 8, respectively, in **B**) and MORKO/Tg (5 and 6, respectively, in **C**) mice three days after the 2nd OVA inhalation (day 40). Data are expressed as the mean ± S.D. *$p < 0.05$ and **$p < 0.01$ compared to non-stressed mice.

THE EFFECT OF RESTRAINT STRESS ON CYTOKINE PRODUCTION BY SPLENOCYTES AND BLN CELLS

The levels of the Th2 cytokines IL-4, IL-5 and IL-13 in splenocyte culture supernatants stimulated with OVA were not significantly different between stressed and non-stressed wild-type mice (n = 8 for IL-4, n = 7 for IL-5 and n = 8 for IL-13). Similarly, the production of the Th1 cytokine IFN-γ and the regulatory cytokines IL-10 and TGF-β1 by OVA-stimulated splenocytes was not significantly influenced by stress exposure (n = 10 for IFN-γ, n = 10 for IL-10 and n = 9 for TGF-β1) (Table 1). IFN-γ/IL-4 ratio, as a measure of the Th1/

Table 1 Cytokine production by splenocytes and BLN cells

	splenocytes		BLN cells	
	OVA (-)	OVA (+)	OVA (-)	OVA (+)
IL-4	9.4 ± 2.6† / 7.9 ± 6.1	49.4 ± 23.8 / 41.7 ± 35.5	8.3 ± 1.0 / 8.6 ± 3.2	74.0 ± 24.6 / 118.2 ± 60.2
IL-5	0.0 ± 0.0 / 2.9 ± 4.6	1504.4 ± 1094.0 / 1430.8 ± 1075.6	244.9 ± 108.4 / 184.1 ± 93.6	3110.4 ± 529.9 / 3645.0 ± 998.6
IL-13	67.0 ± 46.8 / 102.0 ± 73.5	6110.4 ± 3570.7 / 5244.8 ± 2477.4	440.1 ± 230.6 / 584.3 ± 286.1	5512.2 ± 1079.3 / 6885.0 ± 2554.8
IFN-γ	100.0 ± 104.7 / 338.0 ± 303.8	1681.2 ± 629.3 / 1116.0 ± 606.9	8.0 ± 4.7 / 8.8 ± 5.6	125.3 ± 39.0 / 102.1 ± 47.3
IL-10	11.4 ± 4.9 / 15.2 ± 7.1	934.0 ± 540.0 / 730.6 ± 458.5	44.8 ± 27.1 / 46.9 ± 17.6	1065.0 ± 106.9 / 1160.0 ± 255.7
TGF-β1	370.8 ± 169.8 / 391.3 ± 239.9	453.8 ± 222.5 / 411.1 ± 271.8	54.0 ± 59.3 / 0.0 ± 0.0	193.1 ± 121.0 / 148.2 ± 58.1

† mean ± SD (pg/ml) in non-stressed mice / mean ± SD (pg/ml) in stressed mice

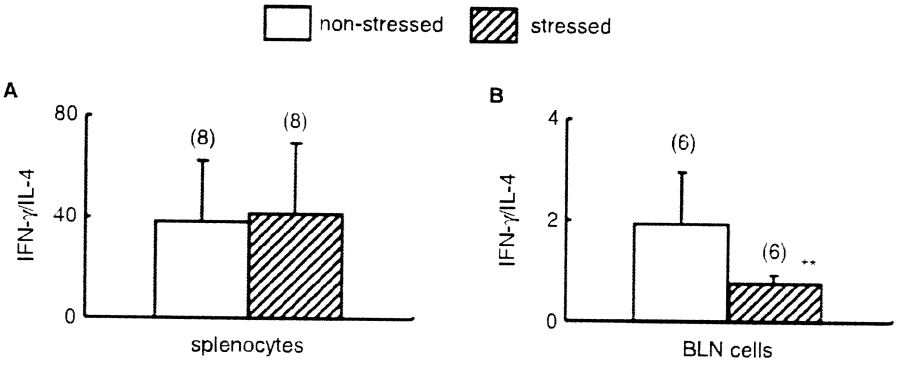


Fig. 7 IFN-γ/IL-4 ratio in splenocytes and BLN cells. The IFN-γ/IL-4 ratio was calculated as described in "Methods" in splenocytes (**A**) and BLN cells (**B**) from non-stressed (open bars) and stressed (hatched bars) wild-type mice. The numbers of samples for each condition are shown in parentheses. Data are expressed as the mean ± S.D. $^{**}p < 0.01$.

Th2 balance, in the culture supernatants was not significantly different between stressed (n = 8) and non-stressed (n = 8) wild-type mice (Fig. 7A). There were no significant differences between non-stressed and stressed wild-type mice in cytokine levels in the culture supernatants without OVA (n = 6 for IL-4, IL-5, IL-13, IFN-γ, IL-10 and TGF-β1) (Table 1).

Similar to the results for cytokine production by splenocytes, stress exposure did not significantly affect cytokine production by BLN cells cultured with (n = 6 for IL-4, n = 5 for IL-5, n = 6 for IL-13, n = 6 for IFN-γ, IL-10 and TGF-β1) or without (n = 6 for IL-4, n = 5 for IL-5, n = 6 for IL-13, n = 6 for IFN-γ, n = 4 for IL-10 and n = 6 for TGF-β1) OVA (Table 1). However, the IFN-γ/IL-4 ratio in the culture supernatants of BLN cells stimulated with OVA from stressed wild-type mice was significantly lower than that from non-stressed wild-type mice (0.7 ± 0.2: n = 6 vs. 1.9 ± 1.0: n = 6, $p < 0.01$) (Fig. 7B).

THE EFFECT OF RESTRAINT STRESS ON T CELL SUBSET PROPORTIONS IN SPLENOCYTES AND BLN CELLS

In splenocytes, there was no significant difference in the numbers of viable cells after culture with OVA between non-stressed and stressed wild-type mice (data not shown). In both non-stressed and stressed wild-type mice, there were significant increases in the proportion of $CD3^+CD4^+$ and $CD3^+CD4^+T1/ST2^+$ cells after culture with OVA. The proportion of these cells in stressed wild-type mice was not significantly different from those in non-stressed wild-type mice, either before (n = 4) or after (n = 5) culture. The proportion of $CD4^+CD25^+$ cells after culture with OVA was not significantly increased compared with the percentage before culture in either non-stressed or stressed wild-type mice, and there were no significant differences in the proportion of these cells between stressed and

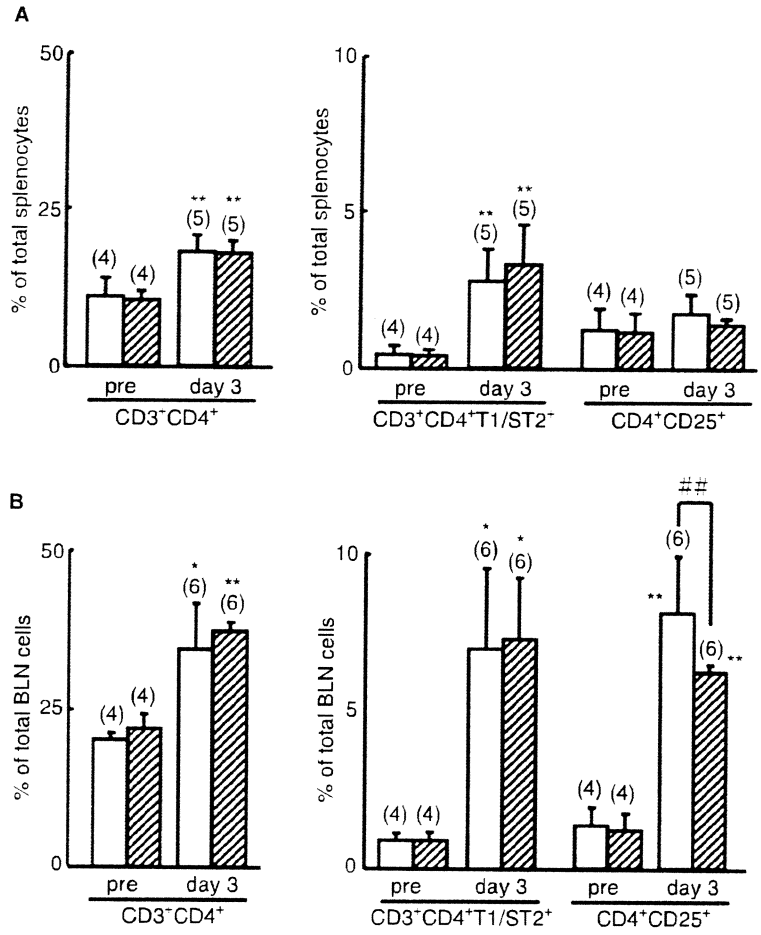


Fig. 8 The proportion of T cell subsets in splenocytes and BLN cells. Splenocytes (**A**) and BLN cells (**B**) from non-stressed (open bars) and stressed (hatched bars) wild-type mice were analyzed for the percentages of $CD3^+CD4^+$, $CD3^-CD4^+T1/ST2^-$ and $CD4^+CD25^-$ cells before (pre) and 3 days after the culture with OVA. The numbers of $CD3^-CD4^+$, $CD3^+CD4^+T1/ST2^-$ and $CD4^+CD25^+$ cells are shown as percentages of the total number of splenocytes and BLN cells. The numbers of mice examined and the experiment numbers are shown in parentheses in **A** and **B**, respectively. Data are expressed as the mean ± S.D. $^*p < 0.05$ and $^{**}p < 0.01$ compared with pre, $\#\#p < 0.01$.

non-stressed wild type mice, either before (n = 4) or after (n = 5) culture (Fig. 8A).

In BLN cells, there was no significant difference in the numbers of viable cells after the culture with OVA between non-stressed and stressed wild-type mice (data not shown). Similar to splenocytes, culturing the cells with OVA significantly increased the proportion of $CD3^+CD4^+$ and $CD3^-CD4^+T1/ST2^+$ cells from both non-stressed and stressed wild-type mice. There were no significant differences in the proportion of these cells between stressed and non-stressed wild-type mice, either before (n = 4) or after (n = 6) culture. Regarding the $CD4^+CD25^+$ population in BLN cells, in both non-stressed and stressed wild-type mice, the proportion of these cells was significantly increased after the culture with OVA (non-stressed: 7.3 ± 1.7: n = 6 vs. 1.2 ± 0.5: n = 4 %, $p < 0.01$, stressed: 5.6 ± 0.2: n = 6 vs. 1.1 ± 0.4: n = 4 %, $p < 0.01$). Although no significant difference was observed between the mice in the proportion of $CD4^+CD25^+$ cells before the culture, this proportion in stressed mice was significantly lower than that from non-stressed mice after the culture (5.6 ± 0.2: n = 6 vs. 7.3 ± 1.7: n = 6 %, $p < 0.01$) (Fig. 8B).

ABOLISHMENT OF THE EFFECT OF RESTRAINT STRESS ON BLN CELLS IN MORKO MICE

The stress-induced aggravation of allergen-mediated

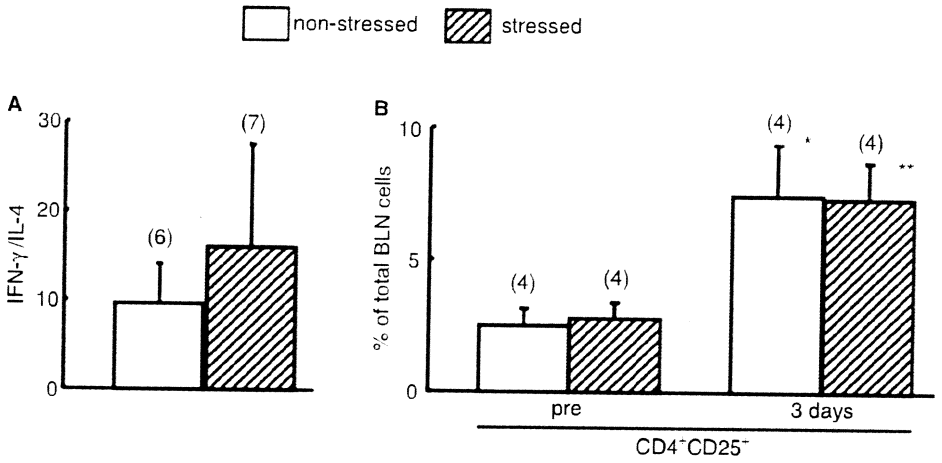


Fig. 9 IFN-γ/IL-4 ratio and the proportion of $CD4^+CD25^+$ cells in BLN cells of MORKO mice. BLN cells from non-stressed (open bars) and stressed (hatched bars) MORKO mice were cultured with OVA for 3 days. The IFN-γ/IL-4 ratio (**A**) was calculated as in Figure 7, and the proportion of $CD4^+CD25^+$ cells was analyzed as in Figure 8. The numbers of experiments for each condition are shown in parentheses. Data are expressed as the mean ± S.D. $^*p < 0.05$ and $^{**}p < 0.01$ compared with pre.

airway inflammation was abolished in MORKO mice, as previously reported.[21] Therefore, we investigated whether MOR was involved in the immunological alterations observed in BLN cells from stressed wild-type mice. In contrast to the case of wild-type mice, the IFN-γ/IL-4 ratio in the culture supernatants of OVA-stimulated BLN cells from stressed MORKO mice (n = 7) was not significantly different from that of the non-stressed MORKO mice (n = 6) (Fig. 9A). Similar to wild-type mice, the proportion of $CD4^+$ $CD25^+$ cells from stressed and non-stressed MORKO mice showed a similar increase after culture with OVA. However, no significant difference was observed in the proportion of $CD4^+CD25^+$ cells between non-stressed (n = 4) and stressed (n = 4) MORKO mice (Fig. 9B).

DISCUSSION

In the present study, we produced Tg mice, in which the expression of MORs is under the control of the human DBH gene promoter. Furthermore, by mating these Tg mice with MORKO mice, we produced MORKO/Tg mice that express MORs only on noradrenergic and adrenergic neurons. This human DBH gene promoter has been previously used for producing transgenic mice, successfully expressing phenylethanolamine-N-methyltransferase[38] or IL-2Rα[28] on noradrenergic and adrenergic neurons. The expression of human MOR mRNA in coronal brainstem sections of MORKO/Tg mice was mostly limited to the LC, in which the cell bodies of noradrenergic neurons are congregated. Furthermore, we confirmed the functional expression of MOR protein on cortex regions, into which many noradrenergic neurons project, in MORKO/Tg mice. Despite these alterations, no abnormalities in growth, fertility, or general activity were detected in MORKO/Tg mice.

MORKO/Tg mice also showed the same level of immobility in the tail suspension test and stress-induced plasma corticosterone concentrations as wild-type mice, and these levels were significantly different from MORKO mice. MORKO mice showed a significantly decreased immobility time in the tail suspension test and a reduced stress-induced change in plasma corticosterone concentration compared with wild-type mice, which is consistent with our previous report.[39] These results indicate that the MORs on noradrenergic and adrenergic neurons has functional roles in stress sensibility or responses.

Next, we compared the effect of restraint stress on allergic airway inflammation between wild-type, MORKO and MORKO/Tg mice. We found that the stress-induced exacerbation of airway inflammation observed in wild-type mice, which was abrogated in MORKO mice, was recovered in MORKO/Tg mice. These results indicate that MORs on neurons in the CNS and periphery, in this case noradrenergic and adrenergic neurons, are involved in the stress-induced aggravation of allergic airway inflammation. MORs are expressed not only on neurons but also on several other types of cells, including lymphocytes, and the functions of these receptors on lymphocytes have been extensively studied, including cell differentiation and the production of pro-inflammatory and Th2 cytokines.[22-25] Previously, we demonstrated that the effect of stress in wild-type mice was completely

abolished by the intracerebroventricular injection of an MOR antagonist, β-funaltrexamine, that selectively inhibits the activation of MORs in the CNS, but this abolishment was not seen by the peritoneal injection of naloxone methiodide, a nonselective opioid receptor antagonist that cannot pass through the blood-brain barrier.[21] The peritoneal injection of naloxone methiodide would inhibit the activation of MORs on immune cells and neurons in the periphery. Therefore, together with our previous findings, the current results strongly suggest that the effect of restraint stress on allergic airway inflammation is mediated by MORs on cells in the CNS, including noradrenergic and adrenergic neurons, although the involvement of MORs on immune cells present in the CNS during the stress exposure cannot be completely excluded.

We have demonstrated for the first time the effects of restraint stress as psychological stress on allergen-specific immune responses at the site of inflammation in a murine model of psychological stress-induced asthma exacerbations and the involvement of MORs in these immunological alterations associated with restraint stress.

To investigate stress-induced allergen-specific immune responses, we compared cytokine production profiles and the proportions of T cell subsets in BLN cell populations from stressed and non-stressed mice. Levels of Th1, Th2 and regulatory cytokines produced by BLN cells upon stimulation with the allergen were not significantly different between stressed and non-stressed mice. However, IFN-γ/IL-4 ratios in stressed mice were significantly lower than those in non-stressed mice, suggesting that restraint stress shifted the allergic immune response towards a Th2 character. Regarding the T cell subset proportions, culturing the cells with OVA increased the proportion of Th2 cells in both groups. However, there was no significant difference in the proportion of Th2 cells either before or after the culture with the allergen between the stressed and non-stressed mice. However, whereas the proportion of Treg cells increased after the culture in both groups, the final Treg percentage in stressed mice was significantly lower than that in non-stressed mice after the culture. The increase in the Treg cell population after the exposure to allergen is consistent with the finding by Thunberg S *et al.* that allergen provocation increased the number of $CD4^+CD25^{bright}$ Treg cells in asthmatic lungs.[40] In the current study, CD4 and CD25 were used as markers to identify the Treg population, as in other murine models of allergic asthma.[41-43] The entire population of $CD4^+CD25^+$ T cells, expressing both low and high CD25 levels, exhibits a regulatory function in mice.[44-46] However, the expression of CD25 after the culture with antigen could also represent activated $CD4^+$ cells. Further characterization of more specific markers, including Foxp3, and inhibitory functions in $CD4^+CD25^+$ cells would be needed to distinguish Tregs from activated $CD4^+$ cells.

Mental stress has been reported to reduce the number of Treg cells in peripheral blood in human subjects. A brief laboratory stressor was shown to cause a decrease of $CD4^+Foxp3^+$ Treg cells in healthy young males.[47] A significant reduction in the proportion of Treg cells was observed in patients with post-traumatic stress disorder (PTSD) compared to individuals without PTSD.[48] Regarding changes in immune regulation in response to stressors in allergic subjects, Höglund *et al.* reported systemic immunological responses to examination stress in healthy and atopic individuals.[49] The ratio of Th1 and Th2 cytokines produced by peripheral blood mononuclear cells stimulated with PHA/PMA was decreased in response to stress in atopic individuals but not in controls, similar to our findings. In contrast to our findings, the proportion of Treg ($CD4^+CD45RO^+$ $CD25^{bright}$) cells in peripheral blood increased in response to stress in atopic subjects. However, this increase of Treg cells was also observed in control subjects. The discrepancy in the change in Treg cell proportion may be attributable to sites investigated (systemic or local) or stimulation (with or without allergen), as well to differences in the subjects examined. The importance of the site and allergen exposure in the effect of stress on immune regulation is discussed below.

Deficiency and dysfunction of Treg cells are observed in asthmatics and are thought to be responsible for Th2-predominant immune responses in asthma.[9-11] The recovery of Treg cell numbers has been shown to ameliorate allergen-induced airway inflammation and hyper-responsiveness in murine models of allergic asthma,[42,43,50] and successful allergen-specific immunotherapy has been correlated with increased numbers and the activation of allergen-specific Treg cells.[51,52] Furthermore, the presence of Treg cells in the lungs has been inversely correlated with eosinophilic airway inflammation in murine models of allergic asthma.[53] Therefore, we assume that the lower number of Treg cells induced by stressors might allow more pronounced Th2 responses in allergen-challenged conditions, resulting in the aggravation of allergic airway inflammation observed in our model. This interpretation is supported by a report showing that the reconstitution of a T cell repertoire with a limited number of Treg cells resulted in severe Th2-associated inflammatory disease upon the subsequent transfer of effector T cells.[41]

Using our stress model, we previously demonstrated that MORs in the central nervous system were involved in the stress-induced aggravation of allergic airway inflammation.[21] In the current study, the effect of stress on the IFN-γ/IL-4 ratio and the number of Treg cells in BLN cell populations cultured with allergen was not observed in MORKO mice. Considering these results, it might be assumed that

restraint stress evokes an alteration of the immune responses to allergen through the activation of MORs, resulting in the exacerbation of allergen-induced airway inflammation. Although the hypothalamic-pituitary-adrenal axis and the sympathetic and adrenomedullary system have been proposed as relevant pathways through which stress modifies inflammatory/immune responses to induce asthma exacerbation,[54] the psycho-neuro-immunological cascade involved in the worsening of asthma symptoms due to psychological stress is not fully understood. In this study, we have reported for the first time potential components, MORs and Treg cells, in neurological and immunological pathways linking stress to asthma exacerbation.

Stress is perceived in the brain, which subsequently activates physiologic systems in the body. Accordingly, immunological alterations would be expected to occur not specifically in BLNs, but also in the spleen. However, a stress effect on immune responses to specific antigen was not observed in splenocytes. Sensitized mice were exposed to allergen by inhalation at the beginning of the stress exposure on day 30; consequently, BLN cells but not splenocytes were in contact with the allergen during the period of stress exposure. In this stress model, when mice were treated with saline by inhalation on day 30, no significant difference was observed between the stressed and non-stressed mice in airway inflammation elicited by the second allergen challenge on day 37 (data not shown). These findings suggest that the simultaneous presence of allergen with immune cells during the stress exposure was required for the development of stress-induced altered immune responses to the subsequent allergen stimulation. Immature dendritic cells, having captured allergens, migrate to regional lymph nodes,[55] where they induce different subsets of T cells, including Treg cells.[56,57] Stress might exert some effects on this induction of Treg cells[7,10,11] such that the proportion of Treg cells in the stressed mice is reduced after the culture with allergen, whereas it is not different in the non-stressed mice.

In conclusion, we produced mice that express MORs only on noradrenergic and adrenergic neurons, and we confirmed the contribution of MORs in the CNS to restraint stress-induced worsening of allergic airway inflammation. We also demonstrated that upon allergen stimulation, the profile of cytokine production was more Th2 dominated and the development of Treg cells was reduced in BLN cells from allergic mice exposed to restraint stress, and that MORs were involved in these immunological alterations induced by stress exposure. The mechanisms by which the activation of MORs induced the alterations of immune responses to allergen were not determined in the current study. Further investigations, including functional analysis and adoptive transfer of BLN cells from wild-type and MORKO mice with or without stress, are needed to clarify the pathways linking psychological stress to asthma exacerbation in terms of a neuro-immunological cascade.

ACKNOWLEDGEMENTS

This manuscript was checked for proper English usage by American Journal Experts (Certification Number: 48E9-1603-8F24-0A92-FACE). This work was supported by a Grant-in-Aid for Scientific Research (No. 16616007 and 19590909, I.O.) and the High Technology Research Program (K.O., S.S. and I.O.) from the Ministry of Education, Culture, Sports, Science and Technology of Japan, the Naito Foundation, the Suzuken Memorial Foundation, and the NIDA-IRP, NIH, and DHSS.

REFERENCES

1. Bousquet J, Jeffery PK, Busse WW, Johnson M, Vignola AM. Asthma: From bronchoconstriction to airways inflammation and remodeling. *Am J Respir Crit Care Med* 2000;**161**:1720-45.
2. Kay AB. The role of T lymphocytes in asthma. *Chem Immunol Allergy* 2006;**91**:59-75.
3. Barnes PJ. Immunology of asthma and chronic obstructive pulmonary disease. *Nat Rev Immunol* 2008;**8**:183-92.
4. Holgate ST. Pathogenesis of asthma. *Clin Exp Allergy* 2008;**38**:872-97.
5. Bacchetta R, Gambineri E, Roncarolo MG. Role of regulatory T cells and Foxp3 in human diseases. *J Allergy Clin Immunol* 2007;**120**:227-35.
6. Tang Q, Bluestone JA. The Foxp3+ regulatory T cell: a jack of all trades, master of regulation. *Nat Immunol* 2008; **9**:239-44.
7. Workman CJ, Szymczak-Workman AL, Collison LW, Pillai MR, Vignali DA. The development and function of regulatory T cells. *Cell Mol Life Sci* 2009;**66**:2603-22.
8. Wing K, Sakaguchi S. Regulatory T cells exert checks and balances on self tolerance and autoimmunity. *Nat Immunol* 2010;**11**:7-13.
9. Robinson DS. Regulatory T cells and asthma. *Clin Exp Allergy* 2009;**39**:1314-23.
10. Lloyd CM, Hawrylowicz CM. Regulatory T cells in asthma. *Immunity* 2009;**31**:438-49.
11. Akdis CA, Akdis M. Mechanisms and treatment of allergic disease in the big picture of regulatory T cells. *J Allergy Clin Immunol* 2009;**123**:735-46.
12. Rietveld S, Everaerd W, Creer TL. Stress-induced asthma: a review of research and potential mechanisms. *Clin Exp Allergy* 2000;**30**:1058-66.
13. Chetta A, Foresi A, Marangio E, Olivieri D. Psychological implications of respiratory health and disease. *Respiration* 2005;**72**:210-5.
14. Isenberg SA, Lehrer PM, Hochron S. The effects of suggestion and emotional arousal on pulmonary function in asthma: a review and a hypothesis regarding vagal mediation. *Psychosom Med* 1992;**54**:192-216.
15. Sandberg S, Paton JY, Ahola S *et al.* The role of acute and chronic stress in asthma attacks in children. *Lancet* 2000; **356**:982-7.
16. Kang DH, Coe CL, McCarthy DO *et al.* Cytokine profiles of stimulated blood lymphocytes in asthmatic and healthy adolescents across the school year. *J Interferon Cytokine*

Res 1997;**17**:481-7.
17. Liu LY, Coe CL, Swenson CA, Kelly EA, Kita H, Busse WW. School examinations enhance airway inflammation to antigen challenge. *Am J Respir Crit Care Med* 2002; **165**:1062-7.
18. Lopez-Carderon A, Arizmavarreta C, Chen CL. Influence of chronic restraint stress on pro-opiomelanocortin mRNA and β-endorphin in the rat hypothalamus. *J Mol Endocrinol* 1991;**7**:197-204.
19. Drolet G, Dumont EC, Gosselin I, Kinkead R, Laforest S, Trottier L-F. Role of endogenous opioid system in the regulation of the stress response. *Prog Neuro-Psychopharmacol Biol Psychiatry* 2001;**25**:729-41.
20. Okuyama K, Ohwada K, Sakurada S *et al.* The distinctive effects of acute and chronic psychological stress on airway inflammation in a murine model of allergic asthma. *Allergol Int* 2007;**56**:29-35.
21. Okuyama K, Wada K, Sakurada S *et al.* The Involvement of μ-opioid receptors in the central nervous system in the worsening of allergic airway inflammation by psychological stress in mice. *Int Arch Allergy Immunol* 2010;**152**: 342-52.
22. Roy S, Cain KJ, Chapin RB, Charboneau RG, Barke RA. Morphine modulates NF kappa B activation in macrophages. *Biochem Biophys Res Commun* 1998;**245**:392-6.
23. Wetzel MA, Steele AD, Eisenstein TK, Adler MW, Henderson EE, Rogers TJ. Mu-opioid induction of monocyte chemoattractant protein-1, RANTES, and IFN-gamma-inducible protein-10 expression in human peripheral blood mononuclear cells. *J Immunol* 2000;**165**:6519-24.
24. Greeneltch KM, Kelly-Welch AE, Shi Y, Keegan AD. Chronic morphine treatment promotes specific Th2 cytokine production by murine T cells in vitro via a Fas/Fas ligand-dependent mechanism. *J Immunol* 2005;**175**:4999-5005.
25. Roy S, Wang J, Charboneau R, Loh HH, Barke RA. Morphine induces CD4+ T cell IL-4 expression through an adenylyl cyclase mechanism independent of the protein kinase A pathway. *J Immunol* 2005;**175**:6361-7.
26. Sora I, Takahashi N, Funada M *et al.* Opiate receptor knockout mice define μ receptor roles in endogenous nociceptive responses and morphine-induced analgesia. *Proc Natl Acad Sci U S A* 1997;**94**:1544-9.
27. Hall FS, Li XF, Goeb M *et al.* Congenic C57BL/6 μ-opiate receptor (MOR) knockout mice: baseline and opiate effects. *Genes Brain Behav* 2003;**2**:114-21.
28. Kobayashi K, Morita S, Sawada H *et al.* Immunotoxin-mediated conditional disruption of specific neurons in transgenic mice. *Proc Natl Acad Sci U S A* 1995;**92**:1132-6.
29. Ide S, Minami M, Satoh M, Uhl GR, Sora I, Ikeda K. Buprenorphine antinociception is abolished, but naloxone-sensitive reward is retained, in μ-opioid receptor knockout mice. *Neuropsychopharmacology* 2004;**29**:1656-63.
30. Posevitz V, Vizler C, Benyhe S, Duda E, Borsodi A. Restraint stress and anti-tumor immune response in mice. *Acta Biologica Hungarica* 2003;**54**:167-76.
31. Mercado AM, Padgett DA, Sheridan JF, Marucha PT. Altered kinetics of IL-1α, IL-1β, and KGF-1 gene expression in early wounds of restrained mice. *Brain Behav Immun* 2002;**16**:150-62.
32. Ashcraft KA, Hunzeker J, Bonneau RH. Psychological stress impairs the local $CD8^+$ T cells response to mucosal HSV-1 infection and allows for increased pathogenicity via a glucocorticoid receptor-mediated mechanism. *Psychoneuroendocrinology* 2008;**33**:951-63.
33. Okuyama K, Wada K, Chihara J, Takayanagi M, Ohno I. Sex-related splenocyte function in a murine model of allergic asthma. *Clin Exp Allergy* 2008;**38**:1212-9.
34. Wada K, Okuyama K, Ohkawara Y, Takayanagi M, Ohno I. Gender differences in transcriptional regulation of IL-5 expression by bronchial lymph node cells in a mouse model of asthma. *Respirology* 2010;**15**:629-35.
35. Barthold SW. Specificity of infection-induced immunity among *Borrelia burgdorferi* sensu lato species. *Infect Immun* 1999;**67**:36-42.
36. Loehning M, Stroehmann A, Coyle AJ *et al.* T1/ST2 is preferentially expressed on murine Th2 cells, independent of interleukin 4, interleukin 5, and interleukin 10, and important for Th2 effector function. *Proc Natl Acad Sci U S A* 1998;**95**:6930-5.
37. Meisel C, Bonhagen K, Loehning M *et al.* Regulation and function of T1 ST2 expression on $CD4^+$ T cells: Induction of type 2 cytokine production by T1/ST2 cross-linking. *J Immunol* 2001;**166**:3143-50.
38. Kobayashi K, Sasaoka T, Morita S *et al.* Genetic alteration of catecholamine specificity in transgenic mice. *Proc Natl Acad Sci U S A* 1992;**89**:1631-5.
39. Ide S, Sora I, Ikeda K *et al.* Reduced emotional and corticosterone responses to stress in mu-opioid receptor knockout mice. *Neuropharmacology* 2010;**58**:241-7.
40. Thunberg S, Gafvelin G, Nord M *et al.* Allergen provocation increases TH2-cytokines and FOXP3 expression in the asthmatic lung. *Allergy* 2010;**65**:311-8.
41. Milner JD, Ward JM, Keane-Myers A, Paul WE. Lymphopenic mice reconstituted with limited repertoire T cells develop severe, multiorgan, Th2-associated inflammatory disease. *Proc Natl Acad Sci U S A* 2007;**104**:576-81.
42. Kearley J, Robinson DS, Lloyd CM. $CD4^+CD25^+$ regulatory T cells reverse established allergic airway inflammation and prevent airway remodeling. *J Allergy Clin Immunol* 2008;**122**:617-24.
43. McGee HS, Agrawal DK. Naturally occurring and inducible T-reguratory cells modulating immune responses in allergic asthma. *Am J Respir Crit Care Med* 2009;**180**:211-25.
44. Sakaguchi S, Sakaguchi N, Asano M, Itoh M, Toda M. Immunologic self-tolerance maintained by activated T cells expressing IL-2 receptor alpha-chains (CD25). Breakdown of a single mechanism of self-tolerance causes various autoimmune diseases. *J Immunol* 1995;**155**:1151-64.
45. Thornton AM, Shevach EM. $CD4^+CD25^+$ immunoregulatory T cells suppress polyclonal T cell activation in vitro by inhibiting interleukin 2 production. *J Exp Med* 1998; **188**:287-96.
46. Itoh M, Takahashi T, Sakaguchi N *et al.* Thymus and autoimmunity: production of $CD25^+CD4^+$ naturally anergic and suppressive T cells as a key function of the thymus in maintaining immunologic self-tolerance. *J Immunol* 1999;**162**:5317-26.
47. Freier E, Weber CS, Nowottne U *et al.* Decrease of $CD4^+$ $FOXP3^+$ T regulatory cells in the peripheral blood of human subjects undergoing a mental stressor. *Psychoneuroendocrinology* 2010;**35**:663-73.
48. Sommershof A, Aichinger H, Engler H *et al.* Substantial reduction of naïve and regulatory T cells following traumatic stress. *Brain Behav Immun* 2009;**23**:1117-24.
49. Hoelund CO, Axen J, Kemi C *et al.* Changes in immune regulation in response to examination stress in atopic and healthy individuals. *Clin Exp Allergy* 2006;**36**:982-92.
50. Kearley J, Barker JE, Robinson DS, Lloyd CM. Resolution

of airway inflammation and hyperreactivity after in vivo transfer of $CD4^+CD25^+$ regulatory T cells is interleukin 10 dependent. *J Exp Med* 2005;**202**:1539-47.
51. Scadding G, Durham S. Mechanisms of sublingual immunotherapy. *J Asthma* 2009;**46**:322-34.
52. Akdis M. Immune tolerance in allergy. *Curr Opin Immunol* 2009;**21**:700-7.
53. Matsumoto K, Inoue H, Fukuyama S *et al.* Frequency of $Foxp3^+CD4^+CD25^+$ T cells is associated with the phenotypes of allergic asthma. *Respirology* 2009;**14**:187-94.
54. Chen E, Miller GE. Stress and inflammation in exacerbations of asthma. *Brain Behav Immun* 2007;**21**:993-9.
55. Xia W, Pinto CE, Kradin RL. The antigen-presenting activities of Ia^+ dendritic cells shift dynamically from lung to lymph node after an airway challenge with soluble antigen. *J Exp Med* 1995;**181**:1275-83.
56. Leech MD, Benson RA, De Vries A, Fitch PM, Howie SE. Resolution of Der p1-induced allergic airway inflammation is dependent on $CD4^+CD25^+Foxp3^+$ regulatory cells. *J Immunol* 2007;**179**:7050-8.
57. Strickland DH, Stumbles PA, Zosky GR *et al.* Reversal of airway hyperresponsiveness by induction of airway mucosal $CD4^+CD25^+$ regulatory T cells. *J Exp Med* 2006;**203**:2649-60.

CD4 and CD8 T cells require different membrane gangliosides for activation

Masakazu Nagafuku[a,b], Kaori Okuyama[c], Yuri Onimaru[d], Akemi Suzuki[e], Yuta Odagiri[a], Tadashi Yamashita[f], Katsunori Iwasaki[d,g], Michihiro Fujiwara[d], Motoaki Takayanagi[c], Isao Ohno[c], and Jin-ichi Inokuchi[a,b,g,1]

[a]Division of Glycopathology, Institute of Molecular Biomembrane and Glycobiology, and [c]Department of Pathophysiology, Tohoku Pharmaceutical University, Sendai 981-8558, Japan; [b]Core Research for Evolutional Science and Technology, Japan Science and Technology Agency, Saitama 332-0012, Japan; [d]Department of Neuropharmacology, Faculty of Pharmaceutical Sciences, and [g]Academic, Industrial and Governmental Institute for Aging and Brain Sciences, Fukuoka University, Fukuoka 814-0180, Japan; [e]Institute of Glycoscience, Tokai University, Kanagawa 259-1292, Japan; and [f]Division of Integrated Life Science, Faculty of Advanced Life Science, Hokkaido University, Sapporo 001-0021, Japan

Edited* by Sen-itiroh Hakomori, Pacific Northwest Research Institute, Seattle, WA, and approved December 19, 2011 (received for review September 17, 2011)

Initial events of T-cell activation involve movement of the T-cell receptor into lipid rafts. Gangliosides are major components of lipid rafts. While investigating T-cell activation in ganglioside-deficient mice, we observed that $CD4^+$ and $CD8^+$ T cells required different ganglioside subsets for activation. Activation of $CD4^+$ T cells from GM3 synthase-null mice, deficient in GM3-derived gangliosides, is severely compromised, whereas $CD8^+$ T-cell activation is normal. Conversely, in cells from GM2/GD2 synthase-null mice, expressing only GM3 and GD3, $CD4^+$ T-cell activation is normal, whereas $CD8^+$ T-cell activation is deficient. Supplementing the cells with the corresponding missing gangliosides restores normal activation. GM3 synthase-null mice do not develop experimental asthma. Distinct expression patterns of ganglioside species in $CD4^+$ T and $CD8^+$ T cells, perhaps in uniquely functional lipid rafts, define immune functions in each T-cell subset. Control of ganglioside expression would offer a strategy targeting for specific T-cell subpopulations to treat immune diseases.

glycosphingolipids | repertoire selection

The initial events of T-cell activation involve movement of the T-cell receptor into specialized membrane microdomains known as lipid rafts. The term "lipid rafts" was introduced by Kai Simons and Elina Ikonen, on the basis of the close association of sphingolipids and cholesterol as the detergent resistant complex of signaling molecules present in the membrane microdomains (1). In T lymphocytes, lipid rafts are implicated in signaling from T-cell antigen receptor (TCR) and in localization and function of proteins residing proximal to the receptor, such as coreceptors CD4 and CD8, Src family kinases Lck and Fyn, transmembrane adaptor linker for activation for T cells (LAT), and protein kinase Cθ (2, 3). Gangliosides, sialic acid (SA)-containing glycosphingolipids (GSLs) associated with lipid rafts, are thought to be involved in T-cell activation. For example, following TCR clustering induced by anti-CD3 and anti-CD28 antibodies, polarization of GM1a ganglioside occurs in $CD4^+$ T cells but not in $CD8^+$ T cells (4). In polarized human T cells, asymmetric redistribution results in ganglioside GM3- and GM1a-enriched raft domains segregating to the leading edge and uropod, respectively (5). Additionally, major differences in GM1a expression levels are apparent among cell types or stages of cellular development (6), and at times GM1a expression in certain cell types is much lower than that of other gangliosides (7). Thus, to understand the role of lipid rafts in the differentiation, maturation, and activation of $CD4^+$ T and $CD8^+$ T cells in vivo, it is necessary to understand the ganglioside composition in each respective T-cell subset. To date, however, there has been no report detailing the ganglioside structures in naive or primary T-cell subsets.

In the present study, we analyzed the expression of gangliosides during T-cell differentiation and investigated whether the activation of individual T-cell subsets requires distinct species of gangliosides (Fig. 1*A*). We used two kinds of gene-targeted mice, one carrying disrupted GM3 synthase (GM3S), and so lacking GM3-derived gangliosides (a- and b-series gangliosides) (8), and the other with an altered GM2/GD2 synthase (GM2/GD2S) and expressing only GM3 and GD3 gangliosides while lacking the o-series (9). We found distinct and dramatic changes in ganglioside profiles between primary thymocytes and resting $CD4^+$ T and $CD8^+$ T cells. In particular, $CD4^+$ T cells preferentially express a-series gangliosides, whereas $CD8^+$ T cells express very high levels of o-series gangliosides. Likewise, TCR-dependent activation of $CD4^+$ T cells selectively requires a-series gangliosides, yet for similar activation of $CD8^+$ T cells, o-series gangliosides and not a-series gangliosides are indispensable. Distinct expression patterns of gangliosides in $CD4^+$ T and $CD8^+$ T cells in unique functional lipid rafts may define immune functions in each T-cell subset.

We propose that the repertoire selection from immature thymocytes to mature T-cell subsets is accompanied by selective GSL expression in individual T-cell subsets. This GSL selection process may be indispensable in the formation of distinct and functional lipid rafts in mature T cells.

Results

Distinct Selectivity of Gangliosides Required for $CD4^+$ T- and $CD8^+$ T-Cell Activation. GSLs are built on a ceramide backbone comprising a long-chain amino alcohol, sphingosine, and an amide-linked fatty acid. Gangliosides are SA-containing GSLs (Fig. 1*A*). GM3, the simplest of the "a-series" gangliosides, is synthesized by GM3S, which catalyzes the transfer of SA to the nonreducing terminal galactose (Gal) of lactosylceramide (LacCer). GM3 is altered by GM2/GD2S to form GM2, a downstream a-series ganglioside, or by GD3 synthase to form GD3, the simplest of the "b-series" gangliosides. GM2/GD2S also elongates LacCer to form GA2, the simplest of the "o-series" ganglio-series GSLs. Each branch of GSL biosynthesis is a committed pathway (Fig. 1*A*), so competition between enzymes at a key branch point determines the relative expression levels of o-, a-, and b-series gangliosides.

To investigate functional roles of gangliosides in T-cell development and immunity, we used two types of gene-targeted mice with interrupted ganglioside biosynthesis (Fig. 1*A*). GM3S null mice presumably lack all a- and b-series gangliosides, resulting in LacCer accumulation and compensatory increase of o-series GSLs (8). GM2/GD2S null mice lack all o-series GSLs and all elongated a- and b-series gangliosides, so they accumu-

Author contributions: M.N., A.S., T.Y., K.I., M.F., M.T., I.O., and J.-i.I. designed research; M.N., K.O., Y. Onimaru, A.S., Y. Odagiri, I.O., and J.-i.I. performed research; M.N., K.O., A.S., I.O., and J.-i.I. analyzed data; and M.N., A.S., I.O., and J.-i.I. wrote the paper.

The authors declare no conflict of interest.

*This Direct Submission article had a prearranged editor.

[1]To whom correspondence should be addressed. E-mail: jin@tohoku-pharm.ac.jp.

See Author Summary on page 1832.

This article contains supporting information online at www.pnas.org/lookup/suppl/doi:10.1073/pnas.1114965109/-/DCSupplemental.

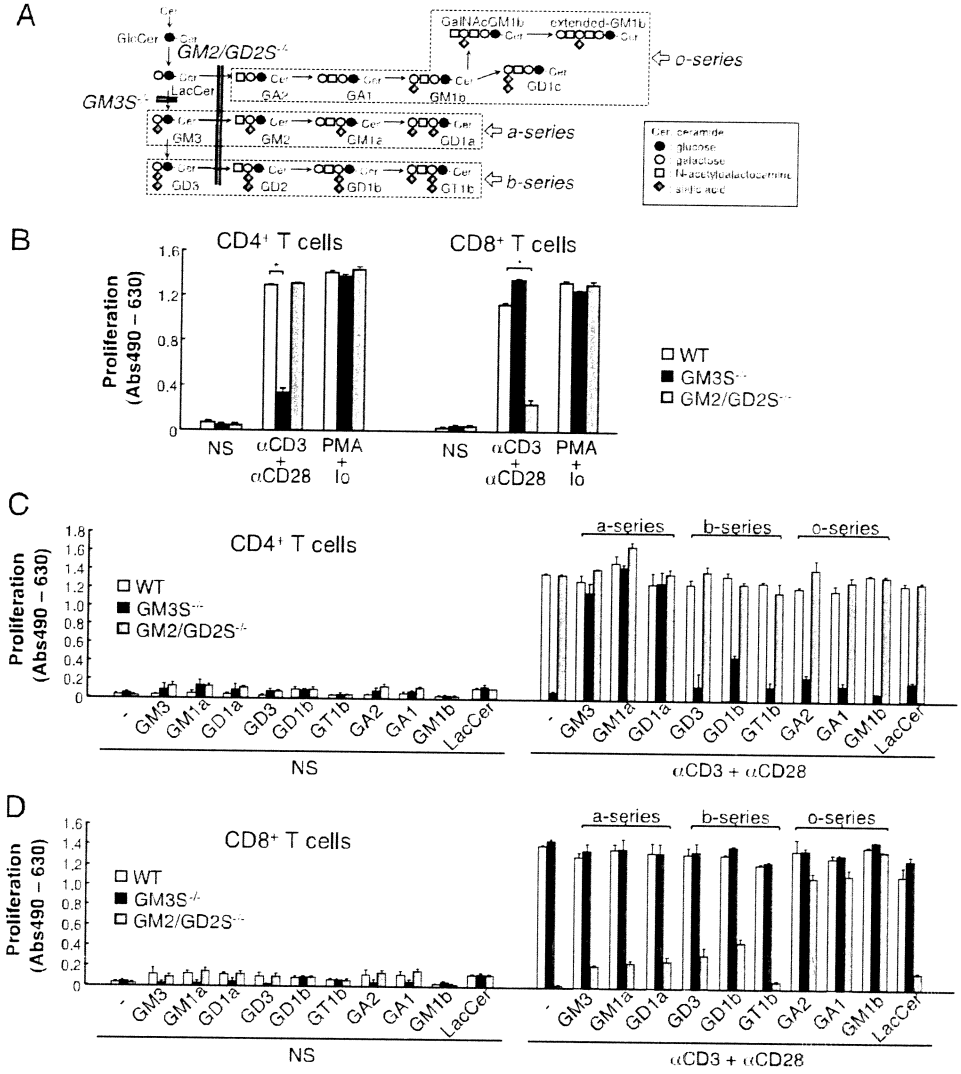


Fig. 1. Distinct selectivity of ganglioside species for CD4+ T and CD8+ T activation. (*A*) Ganglio-series glycosphingolipids are synthesized from ceramide and are divided into o-, a-, and b-series species. (*B*) Activation of CD4+ T and CD8+ T cells upon TCR-mediated stimulation. Purified peripheral CD4+ T and CD8+ T cells from WT, GM3S null, and GM2/GD2S null mice (20–25 mice each) were left unstimulated (NS) or were stimulated for 72 h with anti-CD3 antibody plus anti-CD28 antibody or with PMA plus ionomycin (Io). Proliferative responses were determined after an 8-h pulse with XTT reagent. One representative of three experiments is presented. $*P < 0.01$. (*C* and *D*) Functional rescue experiments by supplementation of gangliosides. Purified peripheral CD4+ T (*C*) and CD8+ T (*D*) cells from WT, GM3S null, and GM2/GD2S null mice were pretreated for 2 h with the indicated GSL (5 μg/mL). The cells were left unstimulated (NS) or were stimulated for 72 h with anti-CD3 antibody plus anti-CD28 antibody. Proliferative responses were determined after an 8-h pulse with XTT reagent. Data are representative of more than three experiments.

late LacCer and express only GM3 and GD3 gangliosides (9), as described later in detail.

Initial analysis of GM3S null and GM2/GD2S null mice did not reveal any obvious alteration in the cellularity of the lymphoid organs (Fig. S1*A*). To assess T-cell development, we performed flow cytometry for CD4 and CD8 on thymocytes and found similar distribution patterns in the thymocyte populations of the null and wild-type (WT) mice (Fig. S1*B*). In the spleen and lymph nodes, there was no obvious alteration in relative distribution within the T-cell and B-cell populations (Fig. S1*C*) and the $CD4^+$ T- and $CD8^+$ T-cell populations (Fig. S1*D*). These data indicate no gross defects in T-cell development despite the altered ganglioside expression. Then we examined the T-cell activation in purified peripheral $CD4^+$ T and $CD8^+$ T cells of the two null mice (Fig. 1*B*). Remarkably, $CD4^+$ T cells (but not $CD8^+$ T cells) from GM3S null mice exhibited severe defects in their proliferative response to the anti-CD3/anti-CD28 antibody mixture, but maintained a normal response to phorbol myristate acetate (PMA) plus ionomycin (Io). Conversely, $CD8^+$ T cells (but not $CD4^+$ T cells) from GM2/GD2S null mice exhibited similar severe defects in TCR-mediated activation when stimulated with the antibody mixture. Following TCR stimulation with the antibody mixture, both IL-2 production and IFN-γ production were severely reduced in both GM3S null $CD4^+$ T cells and GM2/GD2S null $CD8^+$ T cells (Fig. S2). Responses to an alloantigen, a superantigen, and a specific antigen peptide were similar to those observed with the anti-CD3/anti-CD28 mixture (Fig. 2). In contrast to T cells, splenic B cells isolated from GM3S null and GM2/GD2S null mice exhibited no obvious alterations in proliferative responses to various concentrations of anti-IgM antibody and lipopolysaccharide (Fig. S3). In experiments to determine which gangliosides have an essential role in

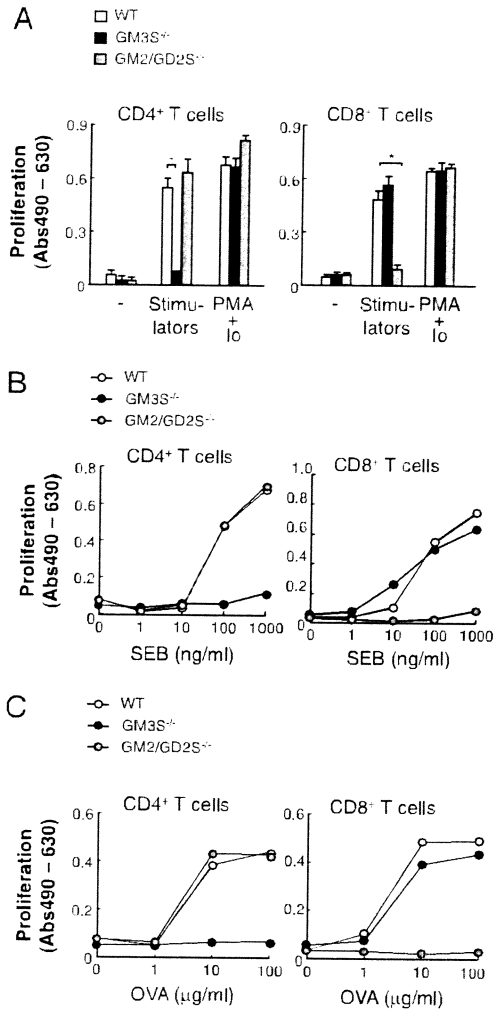


Fig. 2. Antigen-specific responses of CD4+ T and CD8+ T cells of GM3S null and GM2/GD2S null mice. (*A* and *B*) Peripheral CD4+ T and CD8+ T cells were purified from WT, GM3S null, and GM2/GD2S null mice. (*A*) Mixed lymphocyte reaction. The cells were left untreated (–), mixed with MMC-treated MHC-mismatched splenocytes from BALB/c as stimulators, or treated with PMA plus ionomycin (Io) for 72 h. (*B*) Superantigen-induced activation. The indicated cells were stimulated with indicated amounts of *Staphylococcal* enterotoxin B (SEB) and MMC-treated WT splenocytes as APCs. (*C*) Antigen-specific T-cell responses. Purified CD4+T and CD8+T cells from WT, GM3S null and GM2/GD2S null mice were obtained 7 d after immunization with TNP-OVA. The resulting cells were cocultured with MMC-treated WT splenocytes as APCs, together with the indicated amounts of OVA peptide. Proliferative responses were determined after an 8-h pulse with XTT reagent. Data are representative of three experiments. $*P < 0.01$ vs. WT.

TCR-mediated activation of T-cell subsets, CD4+ T cells and CD8+ T cells from WT, GM3S null, or GM2/GD2S null mice were pretreated with gangliosides followed by anti-CD3/anti-CD28 stimulation. Proliferative responses of GM3S null CD4+ T cells were restored following pretreatment with any of the a-series species (GM3, GM1, and GD1a), but were not restored with any o- or b-series species (Fig. 1*C*). Conversely, the proliferative responses of GM2/GD2S null CD8+ T cells were restored following pretreatment with any of the o-series species (GA2, GA1, and GM1b), but not with any of the a- or b-series species (Fig. 1*D*). Importantly, the gangliosides themselves had no effect in the absence of stimulation. These results indicate that o-series ganglioside expression is essential for TCR-mediated activation of CD8+ T cells and a-series ganglioside expression is indispensable for that of CD4+ T cells. Data from these lipid-restoring experiments demonstrate that a different series of gangliosides is necessary in each T-cell subset for proper T-cell activation following TCR stimulation. These data suggest that different species of gangliosides are essential in TCR-mediated activation of CD4+ T cells vs. CD8+ T cells.

We compared ganglioside profiles among thymocytes and peripheral CD4+ T and CD8+ T cells from WT, GM3S null, and GM2/GD2S null mice using TLC (Fig. 3). Acidic lipid fractions from thymocytes and CD4+ T and CD8+ T cells were separated by TLC, and lipids were stained with HRP-conjugated cholera toxin B subunit (CTx-B) (Fig. 3*A*). CTx-B recognizes a monosialo-ganglio-triose moiety, Galβ1-3GalNAcβ1-4 (SAα2-3)Galβ1-, which is found in GM1a, fucosylated GM1a, and GalGalNAcGM1b (extended-GM1b) (6). In WT CD4+ T cells, GM1a was dominantly expressed, but extended-GM1b was expressed much more than GM1a in WT CD8+ T cells. The thymocytes and peripheral CD4+ T and CD8+ T cells of GM3S null mice lacked a-series GM1a and expressed o-series extended GM1b, whereas the cells from GM2/GD2S null mice did not express either one (Fig. 3*A*). GM2/GD2S null cells also did not express complex gangliosides but did express GM3 and GD3 (Fig. 3*B*). None of the cells from GM3S null mice exhibited any accumulation of LacCer (Fig. 3*C*). In contrast, the cells from GM2/GD2S null mice exhibited an absence of GA1 and an accumulation of LacCer (Fig. 3*C*). Taken together, these results indicate that the ganglioside expression patterns of GM3S null mice, compared with those of WT cells, switch from an a-series–rich pattern to an o-series–rich pattern. GM2/GD2S null mice express LacCer, GM3, and GD3 in thymocytes and peripheral CD4+ T cells, but only LacCer in CD8+ T cells.

Differentiation from Thymocytes to Mature T-Cell Subsets Is Accompanied by Selective GSL Expression. We examined the expression of *GM3S* and *GM2/GD2S* genes in thymocytes and peripheral CD4+ T and CD8+ T cells from WT mice. *GM3S* expression was increased to 180% in CD4+ T cells and was decreased to 30% in CD8+ T cells compared with expression in thymocytes (Fig. 4*A*, *Left*). *GM2/GD2S* expression was markedly increased in both CD4+ T and CD8+ T cells compared with thymocytes (Fig. 4*A*, *Right*). These gene expression patterns suggest that CD4+ T cells dominantly express a-series gangliosides due to up-regulation of *GM3S* and CD8+ T cells would carry o-series GSLs due to down-regulation of *GM3S* and up-regulation of *GM2/GD2S* expression.

Liquid chromatography (LC)-MS analysis demonstrated that thymocytes and peripheral CD4+ T and CD8+ T cells predominantly express GM1, GD1, GalNAcGM1b, and extended GM1b. Whereas GM1 and GD1 levels were comparable in all three cell types, GalNAcGM1b and extended-GM1b levels were dramatically increased in the CD8+ T-cell subset (Fig. 4*B*, and Fig. S4 *A* and *B*). MS^2 analysis distinguished positional isomers of GM1 (GM1a and GM1b) and GD1 (GD1b and GD1c) and their ratios (Fig. S4 *C–E*, and Fig. S5). GD1a was not detectable in any of the three cell types. Consistent with CTx-B TLC staining (Fig. 3*A*), LC-MS indicates that the expression pattern of ganglioside species is altered during T-cell development, and o-series and a-series gangliosides are dominantly expressed in CD8+ T and CD4+ T cells, respectively (Fig. 4*B*).

Airway Inflammatory Responses in GM3S Null Mice. Allergic airway inflammation is tightly regulated by adaptive immunity, in which CD4+ T cells play a crucial role via Th2 cytokine production. We examined allergic airway responses induced by inhalation of ovalbumin (OVA) in OVA-sensitized mice (experimental asthma). OVA challenge induced extensive mucus hypersecretion, a cardinal feature of asthma, in WT but not in the GM3S null

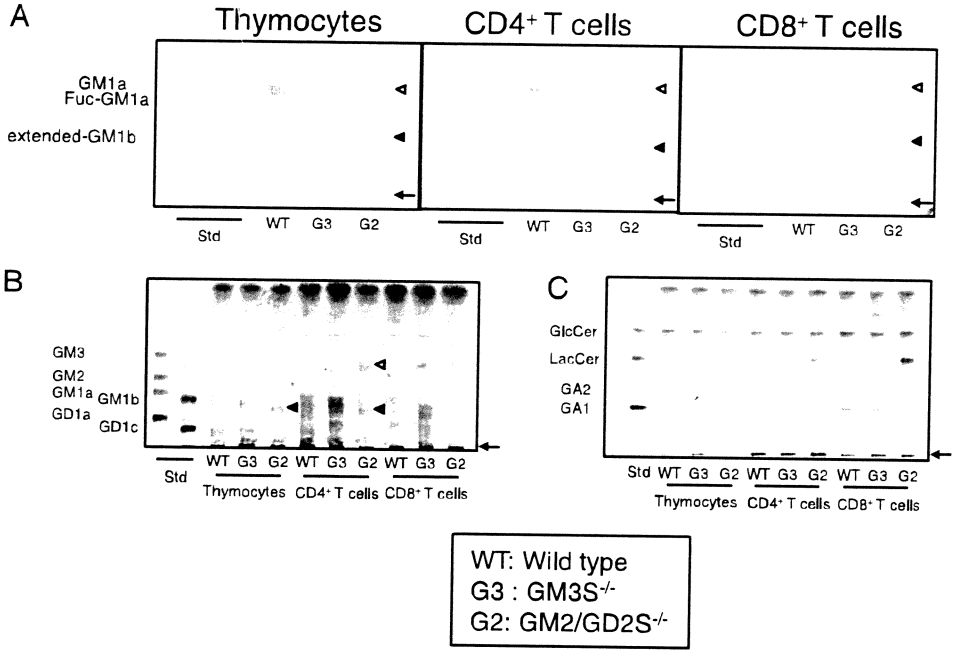


Fig. 3. Glycosphinogolipid expression patterns in thymocytes and peripheral primary CD4+ T and CD8+ T cells in WT, GM3S$^{-/-}$, and GM2/GD2S$^{-/-}$ mice. Neutral and acidic lipids were obtained from thymocytes, CD4+ T cells, and CD8+ T cells of WT, GM3S$^{-/-}$ (G3), and GM2/GD2S$^{-/-}$ (G2) mice. (*A*) The acidic lipids were separated on HPTLC plates and were stained with HRP-conjugated choleragenoid (CTx-B). An arrow indicates the origin for TLC. White and black arrowheads indicate GM1a and extended-GM1b bands, respectively. (*B* and *C*) Acidic (*B*) and neutral (*C*) lipids were separated on HPTLC plates and visualized with orcinol-sulfuric acid. White and black arrowheads in (*B*) indicate GM3 and GD3 bands, respectively. Fuc-GM1a, fucosylated GM1a; std, standard lipids.

mice (Fig. 5*A*). Although both types of mice challenged with OVA exhibited airway infiltration of inflammatory cells including eosinophils and lymphocytes, the numbers of infiltrating cells were significantly lower in GM3 null mice (Fig. 5*B*). Serum OVA-specific IgE levels were greatly increased on days 3 and 5 after OVA challenge in WT mice, but not in GM3S null mice (Fig. 5*C*). Decreased levels of Th2 cytokines in the bronchoalveolar lavage (BAL) fluids were also observed in GM3S null mice (Fig. 5*D*). In adoptive transfer experiments, CD4+ T cells isolated from OVA-sensitized WT and GM3S null mice were transferred into naive WT mice, and the recipient mice were challenged with OVA. Infiltration of inflammatory cells, particularly eosinophils and lymphocytes, was suppressed in the recipient mice of CD4+ T cells from GM3S null mice (Fig. 5*E*). In the recipient mice of CD4+ T cells from GM2/GD2 synthase null mice, there was no difference in the numbers of infiltrated cells compared with those of recipient mice of CD4+ T cells from WT mice (Fig. 5*F*). These results indicate that the immune function of CD4+ T cells in vivo is selectively deficient in GM3S null mice.

Discussion

In the present study, we determined in great detail the ganglioside expression patterns of primary T cells, specifically those of immature thymocytes and mature peripheral CD4+ T cells and CD8+ T cells. Our most important finding was that distinct expression of gangliosides exists in CD4+ T cells and CD8+ T cells, and defines the immune function of each T-cell subset. CD4+ T cells preferentially express a-series gangliosides, and cells isolated from GM3S null mice exhibit severe impairments in TCR-mediated cytokine production and clonal expansion, but can be rescued by reintroducing a-series gangliosides. Similarly, CD8+ T cells preferentially express o-series GSLs, and cells isolated from GM2/GD2S null mice exhibit severe impairments in TCR-mediated cytokine production and clonal expansion. They can be rescued by reintroducing o-series gangliosides. These results suggest that CD4+ T-cell and CD8+ T-cell subsets require a-series and o-series ganglioside expression, respectively, to undergo activation upon TCR ligation.

Why are CD4+ T cells and CD8+ T cells dependent on expression of distinct gangliosides for proper immune function?

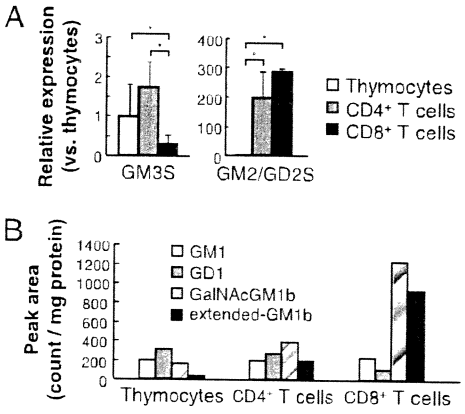


Fig. 4. Distinct expression of ganglioside species during T-cell repertoire selection. (*A*) Gene expression of GM3S and GM2/GD2S was determined by quantitative real-time PCR analysis. Data represent the relative gene expression in peripheral T-cell subsets compared with that in thymocytes (set to 1.0 separately for each target gene). *$P < 0.05$. (*B*) Gangliosides of mouse thymocytes and CD4+ and CD8+ T cells analyzed by LC-MS. Peak areas of GM1, GD1, GalNAcGM1b, and extended-GM1b were determined in the mass chromatograms obtained by C30 column chromatography-MS with GM3 (NeuAc, d18:1–14:0) as an internal standard. GM1 includes GM1a [*N*-glycolylneuraminic acid (NeuGc)] and GM1b (NeuGc), each carrying d18:1–16:0, –18:0, –20:0, –22:0, –24:1, and –24:0. GD1 includes GD1b (NeuGc) and GD1c (NeuGc) each carrying d18:1–16:0, –18:0, –20:0, –22:0, –24:1, and –24:0. GD1a was not detectable in any of the three cell types.

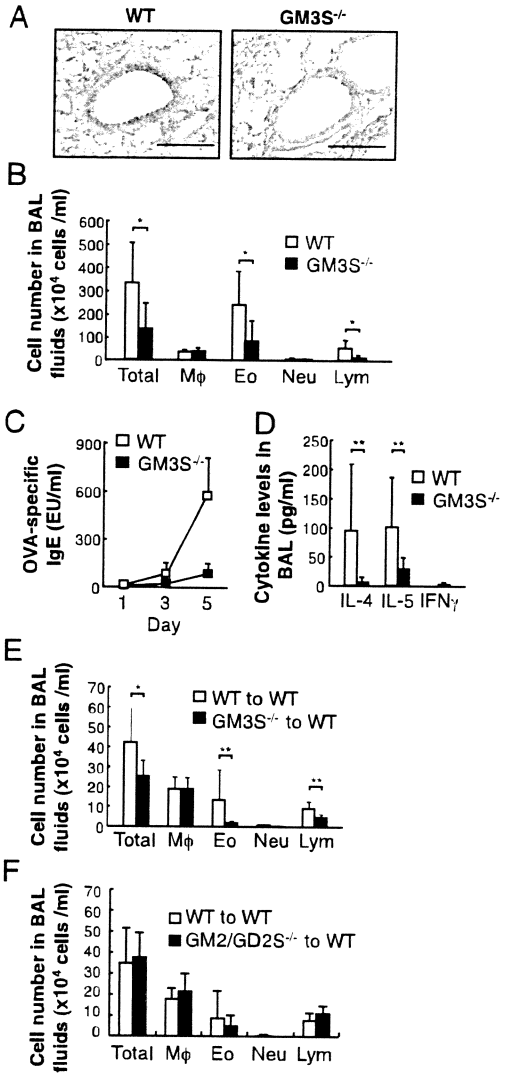


Fig. 5. Allergic airway inflammation in GM3S null mice. (*A* and *B*) Sensitized WT and GM3S null mice were challenged with OVA. Five days after the challenge, BAL fluid and lung tissues were collected. The representative lung sections stained with PAS (*A*) and the numbers of total cells (Total), macrophages (Mϕ), eosinophils (Eo), neutrophils (Neu), and lymphocytes (Lym) in BAL fluids (*B*) are shown. (WT, $n = 7$; GM3S null, $n = 9$). (Scale bar in *A*, 200 μm.) (*C*) Sera from sensitized WT and GM3S null mice were obtained at 1 (WT, $n = 6$; GM3S null, $n = 6$), 3 (WT, $n = 6$; GM3S null, $n = 6$) and 5 d (WT, $n = 6$; GM3S null, $n = 6$) after OVA challenge. OVA-specific IgE in the sera was measured. (*D*) Cytokine levels in BAL fluid (WT, $n = 6$; GM3S null, $n = 6$) were measured 1 d after challenge. (*E* and *F*) Cell numbers in BAL fluid of mice adoptively transferred with $CD4^+$ T cells. $CD4^+$ T cells from sensitized WT and GM3S null mice (*E*) or GM2/GD2S null mice (*F*) were transferred to naive WT mice. BAL fluid was obtained from the recipient mice 5 d after OVA challenge [(*E*) WT recipient, $n = 6$; GM3S null recipient, $n = 7$; (*F*) WT recipient, $n = 10$; GM2/GD2S null recipient, $n = 6$]. The numbers of total cells (Total), macrophages (Mϕ), eosinophils (Eo), neutrophils (Neu), and lymphocytes (Lym) in BAL fluid were counted. $^*P < 0.05$, $^{**}P < 0.01$.

Although there are some commonalities between the mechanisms of TCR-mediated signaling in $CD4^+$ T cells and $CD8^+$ T cells, the two subsets do have different cellular and molecular modifications. CD4 and CD8 can localize to lipid rafts by palmitoylation in their juxtamembrane region (10, 11), yet raft localization seems not to be determined by lipid modification alone (11, 12). To ensure that CD4 and CD8 undergo proper intracellular trafficking and successful localization on the plasma membrane, it might be vital for CD4/CD8 to interact with rafts carrying a specific ganglioside. CD28, a B7-type costimulatory molecule, provides functional differences between $CD4^+$ T cells and $CD8^+$ T cells (13, 14). In human and mouse $CD4^+$ T cells, CD28 promotes the clustering of CTx-B–detectable rafts at the immunological synapse through its downstream signaling molecule protein kinase Cθ (15). However, $CD8^+$ T cells do not reorient CTx-B–detectable rafts to the T-cell/antigen-presenting cell (APC) interface during activation (4, 16). Considering the combined information, we speculate that ganglioside compositions in rafts necessary for signaling events mediated by TCR and costimulatory molecules differ between $CD4^+$ T cells and $CD8^+$ T cells.

Ganglioside expression in primary T cells has previously been studied using biochemical analyses (TLC and HPLC) of whole T-cell populations. However, whole T-cell populations are truly a "mixed population," so any such results would be of limited value to study specific T-cell subsets. In contrast, we separated $CD4^+$ T cells and $CD8^+$ T cells from cell mixtures isolated from lymph nodes and spleen and then performed TLC and LC-MS analyses. Previously, FACS analyses with monoclonal antibodies (mAbs) against several ganglioside species determined that mature peripheral $CD4^+$ T cells and $CD8^+$ T cells express differential species of gangliosides (17, 18). Our LC-MS analysis (Fig. 4*B* and Figs. S4 and S5) demonstrated that expression of GalNAcGM1b and extended-GM1b is much higher in $CD8^+$ T cells than in $CD4^+$ T cells. $CD4^+$ T cells express a larger amount of GD1c than $CD8^+$ T cells do.

Staining with CTx-B, commonly used to detect GM1a and visualize rafts, has demonstrated that $CD8^+$ T cells express higher levels of GM1a in the rafts than $CD4^+$ T cells (19). However, this toxin also reacts to other gangliosides including fucosylated-GM1a and extended-GM1b, both of which have a monosialo-ganglio-triose structure, Galβ1-3GalNAcβ1-4(SAα2-3)Galβ1- (6). In fact, we were able to detect two CTx-B–reactive gangliosides, GM1a and extended GM1b in T cells with different quantities in individual T-cell subsets (Fig. 3*A*). The presence in a single cell of a variety of rafts with different gangliosides has been suggested (4, 5). Cross-linking gangliosides using CTx-B or a homolog, the heat-labile enterotoxin of *Escherichia coli*, can induce apoptosis in $CD8^+$ T cells but not in $CD4^+$ T cells (20), which results from the induction of caspase-dependent signaling caused by activation of NF-κB and c-Myc (20). Although this process is known to proceed in a Fas- and p55 tumor necrosis factor receptor-independent pathway (21), the events in rafts following the ganglioside cross-linking remain undetermined. Considering the differences in the expression of CTx-B–binding ganglioside species between $CD4^+$ T cells and $CD8^+$ T cells (Fig. 3*A*), it seems possible that apoptosis by CTx-B cross-linking may involve extended-GM1b rafts and not GM1a rafts. This result strongly suggests that each T-cell subset has unique rafts in the plasma membrane and that these rafts provide distinct functions in different intracellular events following receptor-mediated stimulation.

FACS analyses have revealed that $CD4^+$ T cells and $CD8^+$ T cells each include subpopulations expressing a particular GSL not observed in the rest of the population. GA1-positive $CD8^+$ T cells exhibit more robust activation via the TCR and play a critical role in CD40/CD28 costimulated and blockade-resistant allograft rejection, compared with GA1-negative $CD8^+$ T cells (22, 23). These findings imply that each subpopulation of $CD4^+$ T cells and $CD8^+$ T cells has a unique ganglioside expression pattern in its rafts, which may be responsible for exerting specific functions of Th and Tc effector cells. GA1-positive mouse $CD8^+$ T cells produce higher levels of IFN-γ in vitro upon TCR stimulation than GA1-negative $CD8^+$ T cells, and both clonal expansion of $CD8^+$ T cells and cytotoxic T-cell–

dependent allograft rejection are suppressed by administration of anti-GA1 mAb in vivo (22). It remains unclear whether, in addition to GA1, the other o-series species expressed in primary $CD8^+$ T cells are essential for TCR-mediated activation. In mouse $CD4^+$ T cells, few studies have addressed whether expression of a-series gangliosides is indispensable for TCR-mediated activation. Human $CD4^+$ T cells isolated from peripheral blood mainly express GM3 (24), which would form GM3-containing rafts available as a platform for TCR signal transduction. The importance of GM3-containing rafts may be corroborated by the observation that GM3 forms a complex with CD4 and Lck on plasma membranes and is coimmunoprecipitated with ZAP-70 after cross-linking with anti-CD3 plus anti-CD28 mAb (24, 25). Consequently, the future challenge will be to examine immune responses in primary T-cell subpopulations separated on the basis of ganglioside species.

Mouse $CD4^+$ T cells and $CD8^+$ T cells activated by anti-CD3 antibody exhibit different profiles for *N*-linked glycans (26). In addition, differentially *N*-glycosylated TCR complexes have been observed in $CD4^+$ T cells compared with $CD8^+$ T cells, which might affect the functional avidity of TCR-transduced T cells (27, 28). The CD4 and CD8 coreceptors, which enhance the TCR–MHC interaction upon binding, have also been shown to be glycosylated (29). These findings, combined with multiple lines of evidence that gangliosides interact with *N*-linked glycans of glycoproteins (30), suggest that a specific ganglioside species expressed on the plasma membrane of $CD4^+$ T and $CD8^+$ T cells might be responsible for the interaction between the TCR and CD4/CD8, to ensure the induction of proper TCR signaling.

Roles of GSLs in TCR signaling and T-cell activation have also been studied using inhibitors of GSL biosynthesis (31). We previously demonstrated that treatment of Jurkat cells with D-*threo*-1-phenyl-2-decanoylamino-3-morpholino-1-propanol (D-PDMP), an inhibitor of GlcCerS (32), preferentially reduces the levels of GSLs in rafts without affecting SM or cholesterol levels. The alteration of raft lipid content results in the up-regulation of TCR signaling via GPI-anchored protein (31). In contrast, treatment of human peripheral blood lymphocytes with this inhibitor attenuated TCR signaling and T-cell activation, indicated by reduction in the expression of markers for T-cell activation and IFN-γ secretion (33).

Activated human T cells are increased in GM1a levels (34, 35). Studies in cells from patients with systemic lupus erythematosus, an autoimmune rheumatic disease characterized by abnormalities in T-cell activation, have determined that the expression of a raft-associated ganglioside, GM1a, is increased in $CD4^+$ T cells, but not in $CD8^+$ T cells, compared with controls (36, 37). It is thought that GM1a expression is enhanced in self-reactive $CD4^+$ T cells, which causes persistence of abnormal cell activation (37, 38). We demonstrated that allergic airway responses caused by OVA inhalation were improved in GM3S null mice, which lack GM1a, resulting in dysfunction of $CD4^+$ T cells. This finding, as well as a recent report in which airway inflammation is suppressed by administration of antisense oligonucleotides against GM3S (39), suggests that inhibition of a-series ganglioside synthesis would be a powerful choice for a treatment of allergic airway diseases.

Recently, novel $CD4^+$ T-cell subsets, in addition to Th1 and Th2 cells, Th17 and regulatory T (Treg), have been described. In allergic airway inflammation, the balance between effector Th2 cells and suppressive Treg cells is skewed toward Th2 predominance (40). Th17 cells have been suggested to contribute to neutrophilic, steroid-resistant severe asthma and to enhance Th2-mediated airway inflammation, although a role for the cells in asthma remains to be determined (41). Reportedly, GM3S null mice exhibit a decreased number of Th17 cells skewed by in vitro culture (42). Because the adoptive transfer experiments confirmed the marked reduction of allergic responses in WT mice that received a whole $CD4^+$ T-cell population from sensitized GM3S null mice (Fig. 5*E*), we are underway to identify which $CD4^+$ T-cell subset is affected in GM3S null mice in vivo.

The present study demonstrates that the functional repertoire selection from double-positive ($CD4^+CD8^+$) to single-positive cells is accompanied by selective GSL expression in individual T-cell subsets and this GSL selection process would be critical for the formation of a functional microcluster and/or lipid rafts in mature T cells. These findings may open up a strategy for targeting specific T-cell subpopulations to treat immune diseases by controlling ganglioside expression in lipid rafts.

Materials and Methods

Experimental Animals. All animals were maintained in accordance with the guidelines of the Tohoku Pharmaceutical University for the care and use of laboratory animals. C57BL/6 mice were obtained from Japan SLC. The GM3S null and GM2/GD2S null mice were generated as previously described (8, 43). Both types of null mice were backcrossed with C57BL/6 mice over >11 generations. Mice were analyzed for the *GM3S* and *GM2/GD2S* genotypes by PCR as described previously (8, 43).

T-Cell Purification. Thymus, spleen, and lymph nodes were collected from WT, GM3S null, and GM2/GD2S null mice. Detailed methods can be found in *SI Materials and Methods*.

T-Cell Activation. For antibody-mediated activation, T-cell subsets purified by negative selection were incubated with 0.1 μg/mL of anti-CD3ε antibody (145-2C11) in the presence of 0.2 μg/mL of anti-CD28 (PV-1) antibody for 72 h. For GSL supplementation experiments the cells were pretreated with the indicated GSLs for 2 h before TCR-mediated stimulation. For the antigen-specific proliferative response assays, $CD4^+$ T cells and $CD8^+$ T cells were prepared from the spleen 7 d after immunization with OVA conjugated with trinitrophenyl (TNP) (Biosearch Technologies). The cells were cocultured with mitomycin C (MMC)-treated WT splenocytes for 72 h in the presence or absence of TNP-OVA antigen. For mixed lymphocyte reactions (MLR), $CD4^+$ T and $CD8^+$ T cells were cocultured for 72 h with MMC-treated splenocytes from BALB/c mice. Cell proliferation was measured by 2,3-bis-(2-methoxy-4- nitro-5-sulfophenyl)-2H-tetrazolium-5-carboxanilide (XTT) assay with a cell proliferation kit (MD Biosciences), according to the manufacturer's instructions.

Allergen-Induced Airway Inflammation. Airway inflammation was generated as previously described (44). Detailed methods can be found in *SI Materials and Methods*.

Preparation of $CD4^+$ T Cells for Adoptive Transfer. On day 17, spleens collected from sensitized WT, GM3S null, and GM2/GD2S null mice were excised, and the splenocytes were disaggregated. The washed splenocytes were resuspended and cultured in the presence of 200 μg/mL OVA. Three days after the culture, $CD4^+$ T cells were purified by positive selection on an autoMACS separator (Miltenyi Biotec), using anti-mouse CD4 (L3T4) MicroBeads (Miltenyi Biotec) according to the manufacturer's protocol. The $CD4^+$ T cells (2×10^6 cells/ 200 μL in saline) were transferred to naive WT mice by tail vein injection. Three days after the injection, the recipient mice were aerosol challenged; BAL fluids were collected 5 d after the challenge as described above.

ELISA. Concentrations of IL-2 and IFN-γ in culture supernatants were measured by ELISA as described elsewhere (45), using two types of anti-mouse IL-2 mAbs and anti-mouse IFN-γ mAb. Serum levels of OVA-specific IgE were measured with ELISA according to published methods (42). IL-4 and IL-5 contents in BAL fluid were measured using an ELISA kit (R&D Systems) according to the manufacturer's protocol.

Lipid Analysis. Lipid analysis was performed as described previously (31). Detailed methods can be found in *SI Materials and Methods*.

Liquid Chromatography–Mass Spectrometry (LC-MS). LC-MS analyses of ganglioside species were performed as described previously (46) with modifications as follows. Detailed methods can be found in *SI Materials and Methods*.

Quantitative Real-Time PCR. Total RNA was isolated using TRI Reagent (Molecular Research Center). Detailed information can be found in *SI Materials and Methods*.

Statistics. Values in the text are the means ± SD. Data were compared using Student's *t* test for two-group comparison or ANOVA for multigroup comparison. Significant differences were post hoc analyzed using Scheffé's test. Differences were considered significant at $P < 0.05$.

ACKNOWLEDGMENTS. We thank Shiro Ono and Yoshiko Mori for helpful technical advice and Elizabeth A. Sweeney and James C. Paulson for critical review of the manuscript. We also thank Yukari Tamekawa and Masumi Toyosawa for assistance with mouse breeding and genotyping and Masaki Saito for providing the gene-targeting mice. This work was supported by research grants from the Core Research for Evolutional Science and Technology division of the Japan Science and Technology Agency (to J.-i.I. and M.N.), a Grant-in-Aid for Scientific Research (B) (to J.-i.I.), the Mizutani Research Foundation for Glycoscience (J.-i.I.), The Naito Foundation (J.-i.I.), and the ONO Medical Research Foundation (J.-i.I.).

1. Simons K, Ikonen E (1997) Functional rafts in cell membranes. *Nature* 387:569–572.
2. Dykstra M, Cherukuri A, Sohn HW, Tzeng SJ, Pierce SK (2003) Location is everything: Lipid rafts and immune cell signaling. *Annu Rev Immunol* 21:457–481.
3. Harder T, Rentero C, Zech T, Gaus K (2007) Plasma membrane segregation during T cell activation: Probing the order of domains. *Curr Opin Immunol* 19:470–475.
4. Kovacs B, et al. (2002) Human CD8$^+$ T cells do not require the polarization of lipid rafts for activation and proliferation. *Proc Natl Acad Sci USA* 99:15006–15011.
5. Gómez-Móuton C, et al. (2001) Segregation of leading-edge and uropod components into specific lipid rafts during T cell polarization. *Proc Natl Acad Sci USA* 98: 9642–9647.
6. Nakamura K, Suzuki M, Inagaki F, Yamakawa T, Suzuki A (1987) A new ganglioside showing choleragenoid-binding activity in mouse spleen. *J Biochem* 101:825–835.
7. Degroote S, Wolthoorn J, van Meer G (2004) The cell biology of glycosphingolipids. *Semin Cell Dev Biol* 15:375–387.
8. Yoshikawa M, et al. (2009) Mice lacking ganglioside GM3 synthase exhibit complete hearing loss due to selective degeneration of the organ of Corti. *Proc Natl Acad Sci USA* 106:9483–9488.
9. Takamiya K, et al. (1996) Mice with disrupted GM2/GD2 synthase gene lack complex gangliosides but exhibit only subtle defects in their nervous system. *Proc Natl Acad Sci USA* 93:10662–10667.
10. Balamuth F, Brogdon JL, Bottomly K (2004) CD4 raft association and signaling regulate molecular clustering at the immunological synapse site. *J Immunol* 172: 5887–5892.
11. Pang DJ, Hayday AC, Bijlmakers MJ (2007) CD8 raft localization is induced by its assembly into CD8alpha beta heterodimers, not CD8alpha alpha homodimers. *J Biol Chem* 282:13884–13894.
12. Popik W, Alce TM (2004) CD4 receptor localized to non-raft membrane microdomains supports HIV-1 entry. Identification of a novel raft localization marker in CD4. *J Biol Chem* 279:704–712.
13. Kroczek RA, Mages HW, Hutloff A (2004) Emerging paradigms of T-cell co-stimulation. *Curr Opin Immunol* 16:321–327.
14. Greenwald RJ, Freeman GJ, Sharpe AH (2005) The B7 family revisited. *Annu Rev Immunol* 23:515–548.
15. Bi K, et al. (2001) Antigen-induced translocation of PKC-theta to membrane rafts is required for T cell activation. *Nat Immunol* 2:556–563.
16. O'Keefe JP, Blaine K, Alegre ML, Gajewski TF (2004) Formation of a central supramolecular activation cluster is not required for activation of naive CD8+ T cells. *Proc Natl Acad Sci USA* 101:9351–9356.
17. Marusić A, Markotić A, Kovačić N, Müthing J (2004) Expression of glycosphingolipids in lymph nodes of mice lacking TNF receptor 1: Biochemical and flow cytometry analysis. *Carbohydr Res* 339:77–86.
18. Nakamura K, Suzuki H, Hirabayashi Y, Suzuki A (1995) IV3 alpha (NeuGc alpha 2-8NeuGc)-Gg4Cer is restricted to CD4+ T cells producing interleukin-2 and a small population of mature thymocytes in mice. *J Biol Chem* 270:3876–3881.
19. de Mello Coelho V, et al. (2004) Quantitative differences in lipid raft components between murine CD4+ and CD8+ T cells. *BMC Immunol*, 10.1186/1471-2172-5-2.
20. Nashar TO, Williams NA, Hirst TR (1996) Cross-linking of cell surface ganglioside GM1 induces the selective apoptosis of mature CD8+ T lymphocytes. *Int Immunol* 8: 731–736.
21. Salmond RJ, et al. (2002) CD8+ T cell apoptosis induced by Escherichia coli heat-labile enterotoxin B subunit occurs via a novel pathway involving NF-kappaB-dependent caspase activation. *Eur J Immunol* 32:1737–1747.
22. Trambley J, et al. (1999) Asialo GM1(+) CD8(+) T cells play a critical role in costimulation blockade-resistant allograft rejection. *J Clin Invest* 104:1715–1722.
23. Sorice M, et al. (1997) Evidence for the existence of ganglioside-enriched plasma membrane domains in human peripheral lymphocytes. *J Lipid Res* 38:969–980.
24. Garofalo T, et al. (2002) Association of GM3 with Zap-70 induced by T cell activation in plasma membrane microdomains: GM3 as a marker of microdomains in human lymphocytes. *J Biol Chem* 277:11233–11238.
25. Barbat C, et al. (2007) p56lck, LFA-1 and PI3K but not SHP-2 interact with GM1- or GM3-enriched microdomains in a CD4-p56lck association-dependent manner. *Biochem J* 402:471–481.
26. Comelli EM, et al. (2006) Activation of murine CD4+ and CD8+ T lymphocytes leads to dramatic remodeling of N-linked glycans. *J Immunol* 177:2431–2440.
27. Rossi NE, et al. (2008) Differential antibody binding to the surface alphabetaTCR.CD3 complex of CD4+ and CD8+ T lymphocytes is conserved in mammals and associated with differential glycosylation. *Int Immunol* 20:1247–1258.
28. Kuball J, et al. (2009) Increasing functional avidity of TCR-redirected T cells by removing defined N-glycosylation sites in the TCR constant domain. *J Exp Med* 206: 463–475.
29. Marth JD, Grewal PK (2008) Mammalian glycosylation in immunity. *Nat Rev Immunol* 8:874–887.
30. Hakomori SI (2008) Structure and function of glycosphingolipids and sphingolipids: Recollections and future trends. *Biochim Biophys Acta* 1780:325–346.
31. Nagafuku M, et al. (2003) Reduction of glycosphingolipid levels in lipid rafts affects the expression state and function of glycosylphosphatidylinositol-anchored proteins but does not impair signal transduction via the T cell receptor. *J Biol Chem* 278: 51920–51927.
32. Inokuchi J, Radin NS (1987) Preparation of the active isomer of 1-phenyl-2-decanoylamino-3-morpholino-1-propanol, inhibitor of murine glucocerebroside synthetase. *J Lipid Res* 28:565–571.
33. Blank N, Schiller M, Gabler C, Kalden JR, Lorenz HM (2005) Inhibition of sphingolipid synthesis impairs cellular activation, cytokine production and proliferation in human lymphocytes. *Biochem Pharmacol* 71:126–135.
34. Tani-ichi S, et al. (2005) Structure and function of lipid rafts in human activated T cells. *Int Immunol* 17:749–758.
35. Tuosto L, et al. (2001) Organization of plasma membrane functional rafts upon T cell activation. *Eur J Immunol* 31:345–349.
36. Jury EC, Kabouridis PS, Flores-Borja F, Mageed RA, Isenberg DA (2004) Altered lipid raft-associated signaling and ganglioside expression in T lymphocytes from patients with systemic lupus erythematosus. *J Clin Invest* 113:1176–1187.
37. Dong L, et al. Increased expression of ganglioside GM1 in peripheral CD4+ T cells correlates soluble form of CD30 in systemic lupus erythematosus patients. *J Biomed Biotechnol*, 10.1155/2010/569053.
38. Kabouridis PS, Jury EC (2008) Lipid rafts and T-lymphocyte function: Implications for autoimmunity. *FEBS Lett* 582:3711–3718.
39. Karman J, et al. (2010) Reducing glycosphingolipid biosynthesis in airway cells partially ameliorates disease manifestations in a mouse model of asthma. *Int Immunol* 22:593–603.
40. Shalaby KH, Martin JG (2010) Overview of asthma; the place of the T cell. *Curr Opin Pharmacol* 10:218–225.
41. Lloyd CM, Hessel EM (2010) Functions of T cells in asthma: More than just T(H)2 cells. *Nat Rev Immunol* 10:838–848.
42. Zhu Y, et al. (2011) Lowering glycosphingolipid levels in CD4+ T cells attenuates T cell receptor signaling, cytokine production, and differentiation to the Th17 lineage. *J Biol Chem* 286:14787–14794.
43. Yamashita T, et al. (2005) Interruption of ganglioside synthesis produces central nervous system degeneration and altered axon-glial interactions. *Proc Natl Acad Sci USA* 102:2725–2730.
44. Okuyama K, Wada K, Chihara J, Takayanagi M, Ohno I (2008) Sex-related splenocyte function in a murine model of allergic asthma. *Clin Exp Allergy* 38:1212–1219.
45. Takeuchi N, et al. (2004) Anti-HER-2/neu immune responses are induced before the development of clinical tumors but declined following tumorigenesis in HER-2/neu transgenic mice. *Cancer Res* 64:7588–7595.
46. Ikeda K, Taguchi R (2010) Highly sensitive localization analysis of gangliosides and sulfatides including structural isomers in mouse cerebellum sections by combination of laser microdissection and hydrophilic interaction liquid chromatography/electrospray ionization mass spectrometry with theoretically expanded multiple reaction monitoring. *Rapid Commun Mass Spectrom* 24:2957–2965.

Peptides 32 (2011) 421–427

Contents lists available at ScienceDirect

Peptides

journal homepage: www.elsevier.com/locate/peptides

Review

Dermorphin tetrapeptide analogs as potent and long-lasting analgesics with pharmacological profiles distinct from morphine

Hirokazu Mizoguchi[a], Giacinto Bagetta[b], Tsukasa Sakurada[c], Shinobu Sakurada[a,*]

[a] Department of Physiology and Anatomy, Tohoku Pharmaceutical University, 4-4-1 Komatsushima, Aoba-ku, Sendai 981-8558, Japan
[b] Department of Pharmacobiology, University of Calabria, Arcavacata di Rende, Cosenza 87036, Italy
[c] First Department of Pharmacology, Daiichi College of Pharmaceutical Sciences, 22-1 Tamagawa-cho, Minami-ku, Fukuoka 815-8511, Japan

ARTICLE INFO

Article history:
Received 4 May 2010
Received in revised form
21 November 2010
Accepted 21 November 2010
Available online 30 November 2010

Keywords:
Dermorphin analog
Analgesics
μ-Opioid receptor
κ-Opioid receptor
Dynorphins
Dependence

ABSTRACT

Dermorphin (Tyr-D-Ala-Phe-Gly-Tyr-Pro-Ser-NH_2) is a heptapeptide isolated from amphibian skin. With a very high affinity and selectivity for μ-opioid receptors, dermorphin shows an extremely potent antinociceptive effect. The structure–activity relationship studies of dermorphin analogs clearly suggest that the N-terminal tetrapeptide is the minimal sequence for agonistic activity at μ-opioid receptors, and that the replacement of the D-Ala^2 residue with D-Arg^2 makes the tetrapeptides resistant to enzymatic metabolism. At present, only a handful of dermorphin N-terminal tetrapeptide analogs containing D-Arg^2 have been developed. The analogs show potent antinociceptive activity that is greater than that of morphine with various injection routes, and retain high affinity and selectivity for μ-opioid receptors. Interestingly, some analogs show pharmacological profiles that are distinct from the traditional μ-opioid receptor agonists morphine and [D-Ala^2,NMePhe^4,Gly-ol^5]enkephalin (DAMGO). These analogs stimulate the release of dynorphins through the activation of μ-opioid receptors. The activation of κ-opioid receptors by dynorphins is suggested to reduce the side effects of μ-opioid receptor agonists, e.g., dependence or antinociceptive tolerance. The dermorphin N-terminal tetrapeptide analogs containing D-Arg^2 may provide a new target molecule for developing novel analgesics that have fewer side effects.

© 2010 Elsevier Inc. All rights reserved.

Contents

1. Preface 421
2. Dermorphin 422
3. Endogenous dermorphins 423
4. Synthetic dermorphin analogs 423
5. Distinct antinociceptive profiles of dermorphin tetrapeptide analogs 424
6. Adverse effects of dermorphin tetrapeptide analogs 425
   6.1. Respiratory depression 425
   6.2. Antinociceptive tolerance 425
   6.3. Dependence liability 425
7. Conclusion 425
   Acknowledgements 425
   References 425

1. Preface

Morphine, one of the oldest analgesics in the history of human beings, is still the best analgesic in the clinic, especially for cancer pain and post-operative pain. Its analgesic effect is mediated through μ-opioid receptors, which are mainly involved in the endogenous pain control systems among the three major subtypes of opioid receptors. Beside its potent analgesic effect, morphine also has several side effects, including constipation, itchiness, respiratory depression, antinociceptive tolerance, physical dependence, and psychological dependence. These side effects of morphine seriously affect its effectiveness in the clinic. Therefore, new analgesics that are more potent and have fewer side effects than morphine have been explored. At present, several μ-opioid receptor agonists along with morphine, e.g., fentanyl, oxycodone, and methadone, are available as analgesics in the clinic. However, the pharmacological

* Corresponding author. Tel.: +81 22 727 0124; fax: +81 22 727 0125.
E-mail address: s-sakura@tohoku-pharm.ac.jp (S. Sakurada).

0196-9781/$ – see front matter © 2010 Elsevier Inc. All rights reserved.
doi:10.1016/j.peptides.2010.11.013

Table 1
Endogenous opioid peptides.

Endogenous μ-opioid peptides	
Endomorphin-1	Tyr^1-Pro-Trp-Phe^4-NH_2
Endomorphin-2	Tyr^1-Pro-Phe-Phe^4-NH_2
β-Endorphin	Tyr^1-Gly-Gly-Phe-Met^5-Thr-Ser-Glu-Lys-Ser^{10}-Gln-Thr-Pro-Leu-Val^{15}-Thr-Leu-Phe-Lys-Asn^{20}-Ala-Ile-Ile-Lys-Asn^{25}-Ala-Tyr-Lys-Lys-Gly^{30}-Gln^{31}-OH
Dermorphin	Tyr^1-D-Ala-Phe-Gly-Tyr^5-Pro-Ser^7-NH_2
Endogenous δ-opioid peptides	
[Met^5]Enkephalin	Tyr^1-Gly-Gly-Phe-Met^5-OH
[Leu^5]Enkephalin	Tyr^1-Gly-Gly-Phe-Leu^5-OH
Endogenous κ-opioid peptides	
Dynorphin A	Tyr^1-Gly-Gly-Phe-Leu^5-Arg-Arg-Ile-Arg-Pro^{10}-Lys-Leu-Lys-Trp-Asp^{15}-Asn-Gln^{17}-OH
Dynorphin B	Tyr^1-Gly-Gly-Phe-Leu^5-Arg-Arg-Gln-Phe-Lys^{10}-Val-Val-Thr^{13}-OH
α-Neo-endorphin	Tyr^1-Gly-Gly-Phe-Leu^5-Arg-Lys-Tyr-Pro-Lys^{10}-OH
β-Neo-endorphin	Tyr^1-Gly-Gly-Phe-Leu^5-Arg-Lys-Tyr-Pro^9-OH

characteristics of these analgesics are quite similar to morphine, and their intrinsic activities are similar to or lower than morphine [24]. Unfortunately, most of the side effects of morphine, as well as its analgesic effects, are mediated through μ-opioid receptors [39]. Therefore, more valuable μ-opioid receptor agonists than morphine as analgesics are still not available in the clinic.

During the past two decades, selective δ-opioid receptor agonists (TAN-67, SNC80, etc.) or selective κ-opioid receptor agonists (U-50, 488H, TRK-820, etc.) have been developed as new analgesics that have fewer side effects than morphine [2,27,57,58]. However, none of these compounds are used in the clinic as analgesics because their analgesic effects are much weaker than morphine. The low intrinsic activity of ligands mediated through δ- or κ-opioid receptors and the low density of δ- or κ-opioid receptors in the site involved in pain transmission limit their analgesic effect [14,19]. Theoretically, there is no possibility that selective δ-opioid receptor agonists or selective κ-opioid receptor agonists can be better analgesics than morphine in the clinic.

Like [D-Ala^2,NMePhe^4,Gly-ol^5]enkephalin (DAMGO), β-endorphin or dermorphin, several μ-opioid receptor agonists that have higher intrinsic activity than morphine are available [23,24]. However, all of those compounds are peptides; therefore, none of those compounds were originally expected to be effective after peripheral injection. Interestingly, dermorphin and its analogs were unexpectedly effective after peripheral injection [40]. In the present article, the antinociceptive profiles of dermorphin analogs are reviewed. Dermorphin and its analogs may provide a new target molecule for developing novel analgesics that have higher intrinsic activity and fewer side effects than morphine.

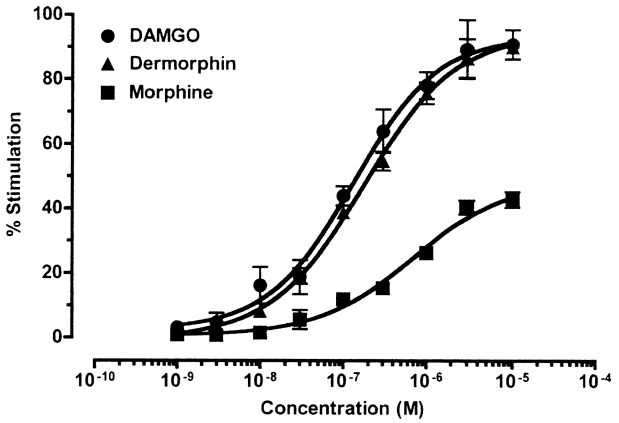


Fig. 1. The increase in [^{35}S]GTPγS binding by DAMGO, dermorphin or morphine in spinal cord membranes obtained from ICR mice. Membranes were incubated with 50 pM [^{35}S]GTPγS and 30 μM GDP in the absence/presence of various concentrations (1 nM–10 μM) of DAMGO, dermorphin or morphine for 2 h at 25 °C. Non-specific binding was measured in the presence of 10 μM unlabeled GTPγS. The data are expressed as the percentage of basal [^{35}S]GTPγS binding measured in the presence of GDP and in the absence of agonist, and represent the mean ± S.E.M. for at least three independent experiments. The concentration-effect curves were calculated with GraphPad Prism, a computer-assisted curve-fitting program. The maximum stimulation with DAMGO, dermorphin or morphine is 93.77%, 94.90% or 49.55%, respectively.

2. Dermorphin

Dermorphin (Tyr-D-Ala-Phe-Gly-Tyr-Pro-Ser-NH_2) is a heptapeptide isolated from amphibian skin [26]. As shown in Table 1, the amino acid sequence of dermorphin is quite different from the other endogenous opioid peptides. Dermorphin does not contain the common N-terminal sequence for the traditional endogenous opioid peptides (Tyr-Gly-Gly-Phe), and its sequence is completely different from that of the endomorphins, which were identified as endogenous μ-opioid peptides that also do not contain the common sequence. Interestingly, dermorphin contains D-Ala (D-isomer amino acid) in its sequence. In the opioid receptor binding assay using the mouse brain, dermorphin shows a very high affinity for μ-opioid receptors with a low affinity for δ-opioid receptors (Table 2) [12]. Without any significant affinity for κ-opioid receptors, dermorphin shows a higher selectivity for μ-opioid receptors than morphine. The intrinsic activity of dermorphin for G-protein activation is similar to that of DAMGO and higher than that of morphine (Fig. 1), suggesting that dermorphin, as well as DAMGO, is a full agonist for μ-opioid receptors, whereas morphine is a partial agonist for that receptor. With a high affinity and intrinsic activity for μ-opioid receptors, dermorphin shows a strong and prolonged antinociceptive effect with various injection routes. After i.c.v. injection, dermorphin is approximately 200 times more potent than morphine for antinociception [11]. Unlike other pep-

Table 2
Affinities of ligands for μ-, δ- and κ-opioid receptors in mouse brain.

Ligands	IC_{50} values with their 95% confidence intervals (nM)		
	[^{3}H]DAMGO (μ)	[^{3}H]DPDPE (δ)	[^{3}H]U-69,593 (κ)
Morphine	2.84 (2.57–3.14)	133 (100–176)	141 (114–174)
Dermorphin	0.76 (0.69–0.83)	73.5 (59.1–91.4)	>1000
Endomorphin-1	2.86 (2.49–3.28)	n.d.	n.d.
[D-Ala^2]Deltorphin II	n.d.	2.29 (1.98–2.66)	n.d.
U-50,488H	n.d.	n.d.	0.76 (0.60–0.95)

Membranes obtained from ICR mouse whole brain without the cerebellum were incubated at 25 °C for 2 h with 1 nM of [^{3}H]DAMGO, [^{3}H]DPDPE or [^{3}H]U-69,593 in the absence/presence of various concentrations (0.03–1000 nM) of the agonists. Non-specific binding was measured in the presence of 10 μM naloxone, DPDPE or U-69,593 for the [^{3}H]DAMGO, [^{3}H]DPDPE or [^{3}H]U-69,593 binding assays, respectively. The IC_{50} values with their 95% confidence intervals for the agonists in each binding assay were calculated with GraphPad Prism, a computer-assisted curve-fitting program. n.d., not determined.

Table 3
Dermorphin and its endogenous analogs.

Dermorphin	Tyr^1-D-Ala-Phe-Gly-Tyr^5-Pro-Ser^7-NH_2
[Hyp^6]Dermorphin	Tyr^1-D-Ala-Phe-Gly-Tyr^5-Hyp^6-Ser^7-NH_2
[Lys^7]Dermorphin	Tyr^1-D-Ala-Phe-Gly-Tyr^5-Pro-Lys^7-NH_2
[Lys^7]Dermorphin-OH	Tyr^1-D-Ala-Phe-Gly-Tyr^5-Pro-Lys^7-OH
[Trp^4,Ans^7]Dermorphin	Tyr^1-D-Ala-Phe-Trp^4-Tyr^5-Pro-Ans^7-NH_2
[Trp^4,Ans^7]Dermorphin-OH	Tyr^1-D-Ala-Phe-Trp^4-Tyr^5-Pro-Ans^7-OH
[Trp^4,Ans^5]Dermorphin(1-5)-OH	Tyr^1-D-Ala-Phe-Trp^4-Ans^5-OH

tidic analgesics, dermorphin shows potent antinociceptive effects with peripheral injection routes, such as s.c. and i.v. injections [40]. Although the blood–brain barrier (BBB) permeability of dermorphin is markedly lower than for morphine, dermorphin still has a four-fold more potent antinociceptive effect than morphine after s.c. injection [31]. The peripherally-administered dermorphin is mainly degraded to the deamidated N-terminal tetrapeptide (dermorphin[1-4]-OH) by cleaving enzymes in the blood, lever, brain, or spinal cord [30]. However, its rate of degradation is more than 30 times slower than for other endogenous opioid peptides [50]. Moreover, dermorphin[1-4]-OH, the main metabolite of dermorphin, does not have remarkable agonistic activity for μ-opioid receptors [17]. The potency of dermorphin[1-4]-OH for inhibiting the guinea pig ileum contraction is only 1/525 of dermorphin. Therefore, the potent and prolonged antinociceptive effect of dermorphin may be due to its slow degradation, but not to its active metabolites.

3. Endogenous dermorphins

At present, seven endogenous analogs of dermorphin have been identified (Table 3). Unlike dermorphin, three of the endogenous analogs do not have a C-terminus that is protected by amidation. Without the C-terminal amidation, the affinity of these peptides for μ-opioid receptors is dramatically reduced by 5–63 fold [29]. Dermorphin is degraded by enzymes that cleave its C-terminal amino acid [30]. Since C-terminal amidation prevents this degradation by cleaving enzymes, endogenous dermorphin analogs that contain C-terminal amidation may have more potent agonistic activity for μ-opioid receptors than the analogs that lack C-terminal amidation.

Among the endogenous dermorphin analog identified, [Lys^7]dermorphin has been suggested to have high BBB permeability [31]. The antinociceptive effect of s.c.-administered [Lys^7]dermorphin is 6.6 times stronger than dermorphin, whereas the effect of i.c.v.-administered [Lys^7]dermorphin is almost identical to dermorphin, suggesting that BBB permeability of [Lys^7]dermorphin is higher than dermorphin. Moreover, the duration of the antinociceptive effect of [Lys^7]dermorphin is 2 times longer than dermorphin. Since [Lys^7]dermorphin is more resistant than dermorphin to the cleaving enzymes in the brain [29], the slow degradation of [Lys^7]dermorphin may be responsible for its prolonged antinociceptive effect [31]. It is note worthy that [Lys^7]dermorphin has two binding sites on μ-opioid receptors: one is a [Lys^7]dermorphin high-affinity site and the other is a [Lys^7]dermorphin low-affinity site [29]. Interestingly, [Trp^4,Asn^7]dermorphin, one of the endogenous dermorphin analogs, has a very high affinity for the [Lys^7]dermorphin low-affinity μ-opioid receptors. [Trp^4,Asn^7]dermorphin administered i.c.v. is 7 times more potent than [Lys^7]dermorphin as an inducer of catalepsy, whereas the antinociceptive effect of i.c.v.-administered [Trp^4,Asn^7]dermorphin is only 1/80 of [Lys^7]dermorphin. Moreover, [Trp^4,Asn^7]dermorphin is 2 times more potent than [Lys^7]dermorphin as a μ-opioid receptor agonist in the mouse vas deference or guinea pig ileum. This evidence clearly suggests that the pharmacological profile of the [Lys^7]dermorphin high-affinity μ-opioid receptors is quite different with that of the [Lys^7]dermorphin low-affinity ([Trp^4,Asn^7]dermorphin high-affinity) μ-opioid receptors. In fact, the antinociceptive effect of i.c.v.-administered [Lys^7]dermorphin is potently suppressed by pretreatment with the μ_1-opioid receptor antagonist naloxonazine, whereas the cataleptic response of i.c.v.-administered [Lys^7]dermorphin is not affected by naloxonazine [31]. The [Lys^7]dermorphin high-affinity μ-opioid receptors may be μ_1-opioid receptors that are mainly involved in central antinociception, whereas the [Lys^7]dermorphin low-affinity ([Trp^4,Asn^7]dermorphin high-affinity) μ-opioid receptors may be μ_2-opioid receptors that are involved in the cataleptic response and smooth muscle contraction.

4. Synthetic dermorphin analogs

Since the discovery of dermorphin, more than 100 dermorphin analogs have been synthesized, and their structure–activity relationships have been well established. The remarkable characteristic of the structure of dermorphin is the presence of a D-isomer amino acid (D-Ala) located between two aromatic amino acids (Tyr^1 and Phe^3 residues) in its sequence. Interestingly, the D-Ala^2 residue is essential for the agonistic activity of dermorphin for μ-opioid receptors, since an analog with the D-Ala^2 residue replaced by L-Ala^2 ([L-Ala^2]dermorphin) is almost inactive [17]. The affinity of [L-Ala^2]dermorphin for μ-opioid receptors is more than 4000 times lower than dermorphin. Ordinarily, the N-terminal fragments of dermorphin have reduced opioid activity compared to the native heptapeptide (dermorphin) because of the lost C-terminal amino acids [16]. The N-terminal hexapeptide (dermorphin[1–6]) and pentapeptide (dermorphin[1–5]) of dermorphin retain approximately half of the affinity for μ-opioid receptors compared to dermorphin. The N-terminal tetrapeptide of dermorphin (dermorphin[1-4]) still has a moderate affinity for μ-opioid receptors (approximately 1/20 of dermorphin), whereas the N-terminal tripeptide of dermorphin (dermorphin[1–3]) does not have any significant affinity for μ-opioid receptors. The N-terminal tetrapeptide of dermorphin may be the minimal sequence required for agonistic activity at μ-opioid receptors.

The most fundamental finding in structure–activity relationship studies for dermorphin analogs is that replacement of the D-Ala^2 residue with D-Arg^2 may increase the selectivity of dermorphin analogs for μ-opioid receptors involved in central antinociception, but not in their peripheral effects. In fact, the antinociceptive effect of i.c.v.-administered [D-Arg^2]dermorphin is only 4 times weaker than that of dermorphin, although [D-Arg^2]dermorphin is 26 times weaker than dermorphin as an inhibitor of the guinea pig ileum contraction [11]. Unlike i.c.v.-administered [D-Arg^2]dermorphin, which shows a weaker antinociceptive effect than dermorphin, s.c.-administered [D-Arg^2]dermorphin shows an equipotent antinociceptive effect with dermorphin [46]. The evidence clearly suggests that the substitution with the D-Arg^2 residue in dermorphin increases its BBB permeability. More interestingly, the N-terminal tetrapeptide of [D-Arg^2]dermorphin ([D-Arg^2]dermorphin[1-4]) shows a 2.2 time more potent antinociceptive effect than [D-Arg^2]dermorphin at supraspinal sites [11], whereas the antinociceptive effect of dermorphin[1-4] is 1/4 of dermorphin [3]. Deamidated [D-Arg^2]dermorphin[1-4], [D-Arg^2]dermorphin[1-4]-OH, also shows a very potent and long-lasting antinociceptive effect [46,48]. [D-Arg^2]dermorphin[1-4]-OH is the main and most potent active metabolite of [D-Arg^2]dermorphin [45]. Since [D-Arg^2]dermorphin[1-4] and [D-Arg^2]dermorphin[1-4]-OH are enzymatically very stable [5,45], their potent and long-lasting antinociceptive effect may be due to their high resistance to enzymatic degradation.

Table 4
Synthetic dermorphin analogs containing D-Arg^2.

[D-Arg^2]Dermorphin	Tyr^1-D-Arg^2-Phe-Gly-Tyr^5-Pro-Ser^7-NH_2
[D-Arg^2]Dermorphin[1-4]	Tyr^1-D-Arg^2-Phe-Gly^4-NH_2
[D-Arg^2]Dermorphin[1-4]-OH	Tyr^1-D-Arg^2-Phe-Gly^4-OH
[D-Arg^2,β-Ala^4]Dermorphin[1-4] (TAPA-NH_2)	Tyr^1-D-Arg^2-Phe-β-Ala^4-NH_2
[D-Arg^2,β-Ala^4]Dermorphin[1-4]-OH (TAPA)	Tyr^1-D-Arg^2-Phe-β-Ala^4-OH
N$^\alpha$-Amidino-[D-Arg^2,β-Ala^4]Dermorphin[1-4]-OH (Amidino-TAPA)	$H_2NC(=NH)$-Tyr^1-D-Arg^2-Phe-β-Ala^4-OH
N$^\alpha$-Amidino-[D-Arg^2,Meβ-Ala^4]Dermorphin[1-4]-OH (ADAMB)	$H_2NC(=NH)$-Tyr^1-D-Arg^2-Phe-Meβ-Ala^4-OH
[D-Arg^2,Sar^4]Dermorphin[1-4]-OH (TAPS)	Tyr^1-D-Arg^2-Phe-Sar^4-OH
[D-Arg^2,Lys^4]Dermorphin (DALDA)	Tyr^1-D-Arg^2-Phe-Lys^4-NH_2
[Dmt^1,D-Arg^2,Lys^4]Dermorphin ([Dmt^1]DALDA)	$(CH_3)_2$Tyr^1-D-Arg^2-Phe-Lys^4-NH_2

Dmt, dimethyl-tyrosine; Meβ-Ala, methyl-β-Ala.

With the above information, many N-terminal tetrapeptide analogs of dermorphin containing D-Arg^2 have been developed as new analgesics (Table 4). The most remarkable molecule for a new analgesic is [D-Arg^2,β-Ala^4]dermorphin[1-4]-OH (Tyr-D-Arg-Phe-β-Ala-OH: TAPA) [4]. TAPA shows an extremely potent and long-lasting antinociception, which is 2000 times, 1100 times and 9.1 times greater than that of morphine after i.c.v., i.t. and s.c. injections, respectively [4,43,49]. TAPA has a very high affinity and selectivity for μ-opioid receptors [43] and its antinociceptive effect is selectively mediated by μ-opioid receptors [4,43]. However, the bioavailability of TAPA was unexpectedly low, and the magnitude of the antinociception induced by TAPA administered p.o. was reduced to a level comparable to morphine [7]. Sasaki et al. developed the C-terminal amidated form of TAPA, [D-Arg^2,β-Ala^4]dermorphin[1-4]-NH_2 (Tyr-D-Arg-Phe-β-Ala-NH_2: TAPA-NH_2) [44]. TAPA-NH_2 has a high affinity for μ-opioid receptors, which is comparable to TAPA, and shows a greater selectivity for μ-opioid receptors than TAPA. TAPA-NH_2 also shows a more potent antinociceptive effect than morphine, which is mediated by μ-opioid receptors; however, its potency is still weaker than that of TAPA [25]. The structure–activity relationships study for dermorphin analogs showed that N$^\alpha$-amidination strengthens the antinociceptive activities of dermorphin analogs [15]. Based on this evidence, N$^\alpha$-amidinated TAPA N$^\alpha$-amidino-[D-Arg^2,β-Ala^4]dermorphin[1-4]-OH ($H_2NC(=NH)$-Tyr-D-Arg-Phe-β-Ala-OH: amidino-TAPA) was developed [33]. Amidino-TAPA retained high affinity and selectivity for μ-opioid receptors [22], and produced a more potent antinociception than TAPA after both s.c. and p.o. injections [7,33]. N$^\alpha$-Amidino-[D-Arg^2,Meβ-Ala^4]dermorphin[1-4]-OH ($H_2NC(=NH)$-Tyr-D-Arg-Phe-Meβ-Ala-OH: ADAMB) is a more potent derivative of TAPA for antinociception [33]. The potencies of ADAMB for antinociception are 37 times and 3.8 times higher than those of morphine after s.c. and p.o. injections, respectively.

Another remarkable candidate molecule for a new analgesic is [D-Arg^2,Lys^4]dermorphin (Tyr-D-Arg-Phe-Lys-NH_2: DALDA) [52]. DALDA has two positively charged amino acids in its sequence, and shows an extremely high selectivity for μ-opioid receptors. Unfortunately, its antinociceptive effect in the spinal cord is only 14 times higher than morphine, and relatively very low compared to TAPA or its derivatives [54]. However, unlike other μ-opioid receptor agonists, DALDA is highly restricted in distribution to the placenta, and may be a promising opioid analgesic for obstetrical use [55]. [Dmt^1,D-Arg^2,Lys^4]Dermorphin ($(CH_3)_2$Tyr-D-Arg-Phe-Lys-NH_2: [Dmt^1]DALDA), a DALDA derivative containing 2′,6′-dimethyl-Tyr, is a most potent derivative of DALDA as a μ-opioid receptor agonist [51]. [Dmt^1]DALDA shows an extremely potent antinociception, especially in the spinal cord. The potencies of [Dmt^1]DALDA for antinociception are 218 times, 119 times and 5148 times higher than those of morphine after s.c., i.c.v. and i.t. injections, respectively [32]. Interestingly, these [D-Arg^2]dermorphin[1-4] derivatives developed as new analgesics, contain the common sequence Tyr-D-Arg-Phe. This common sequence may be essential for the production of an extremely potent and prolonged antinociceptive effect. [D-Arg^2,Sar^4]dermorphin[1-4]-OH (Tyr-D-Arg-Phe-Sar-OH: TAPS) is another new analgesic that contains this common sequence [47]. With a high affinity and selectivity for μ-opioid receptors [59], TAPS produces an extremely potent antinociceptive effect with various injection routes. The antinociceptive effect produced by i.c.v., i.t., s.c. and p.o. administrations of TAPS was 600 times, 393 times, 21 times and 1.5 times more potent than that produced by morphine, respectively [18,33,34,47–49].

5. Distinct antinociceptive profiles of dermorphin tetrapeptide analogs

Interestingly, some of the dermorphin tetrapeptide analogs containing D-Arg^2 have antinociceptive profiles that are distinct from traditional μ-opioid receptor agonists. The antinociceptive effects of i.t.-administered [Dmt^1]DALDA, TAPS, TAPA, TAPA-NH_2, and amidino-TAPA are potently suppressed by the κ-opioid receptor antagonist nor-binaltorphimine, although those peptides are very selective for μ-opioid receptors and do not have any significant affinity for κ-opioid receptors [18,22,51,56,59, unpublished observations]. This phenomenon is also observed with the endogenous μ-opioid peptide endomorphin-2, which causes the release of dynorphin A via activation of μ-opioid receptors [41]. Like endomorphin-2, the above peptides also evoke the spinal release of dynorphins through μ-opioid receptors, and the released dynorphins subsequently stimulate κ-opioid receptors. Intriguingly, the released dynorphins are variable with these peptides. TAPS and TAPA-NH_2 cause the release of dynorphin B [18,unpublished observation], whereas TAPA causes the release of α-neo-endorphin [unpublished observation]. On the other hand, similarly to endomorphin-2, [Dmt^1]DALDA causes the release of dynorphin A [56]. Amidino-TAPA causes the release of all three endogenous κ-opioid peptides: dynorphin A, dynorphin B and α-neo-endorphin [22]. In addition, [Dmt^1]DALDA and amidino-TAPA evoke the spinal release of [Met^5]enkephalin and [Leu^5]enkephalin, respectively [22,56]. In fact, their spinal antinociceptive effects are also attenuated by the δ-opioid receptor antagonists naltriben and naltrindole. The traditional μ-opioid receptor agonists, such as DAMGO and morphine, do not have these effects. Therefore, the distinct antinociceptive profiles of these opioid peptides, which include the release of the endogenous opioid peptides, may be mediated by the activation of distinct μ-opioid receptors that are insensitive to traditional μ-opioid receptor agonists. Since the evidence supporting the distinct antinociceptive profiles of these opioid peptides is only from behavioral pharmacological experiments, more direct evidence from neurochemical or molecular biological experiments is needed to prove the distinctness of their antinociceptive profiles.

The μ-opioid receptor gene MOR-1 was first cloned in 1993 [8,60], and since then 33 splice variants have been identified in mouse MOR-1 mRNA [9,10,13,37,38]. Although the distributions of most of the splice variants in the rodent central nervous system have been described [9,10,35–38], the selectivity and intrinsic

activity of μ-opioid receptor agonists for each splice variant and the physiological roles of each splice variant are still unknown. We have recently found that the spinal antinociceptive effect of amidino-TAPA, which has a distinct antinociceptive profile (see above), is mediated through the activation of the MOR-1J, MOR-1K and MOR-1L, which are amidino-TAPA-sensitive and DAMGO-insensitive splice variants of MOR-1 [20]. Interestingly, the release of the endogenous κ-opioid peptides dynorphin A, dynorphin B and α-neo-endorphin and the endogenous δ-opioid peptide [Leu^5]enkephalin in the spinal cord by amidino-TAPA was eliminated under conditions that cause the desensitization of the MOR-1J, MOR-1K and MOR-1L, suggesting that the distinct antinociceptive profile of amidino-TAPA is mediated through the activation of amidino-TAPA-sensitive and DAMGO-insensitive MOR-1 splice variants [unpublished observations]. The distinct antinociceptive profiles of the other D-Arg^2-containing dermorphin tetrapeptide analogs may also be mediated by the activation of specific splice variants of MOR-1 that are insensitive to DAMGO or morphine.

6. Adverse effects of dermorphin tetrapeptide analogs

Beside its potent antinociceptive effect, morphine shows many side effects in the clinic, e.g., constipation (inhibition of gastrointestinal transit), itchiness, catalepsy, respiratory depression, antinociceptive tolerance, physical dependence, and psychological dependence. Those side effects, as well as its analgesic effect, are mediated through the activation of μ-opioid receptors. Therefore, it has long been considered that it is theoretically impossible to develop potent analgesics without severe side effects. However, as mentioned above, several new analgesics, which have antinociceptive profiles distinct from morphine, have been developed. As described below, some of these analogs also show different profiles for their side effects than morphine.

6.1. Respiratory depression

Morphine shows significant respiratory depression in the clinic at doses 10 times higher than the analgesic dose (AD). In rodents, the morphine-induced respiratory depression is observed at doses of $10 \times AD_{50}$, $30 \times AD_{50}$, and $5 \times AD_{80}$ after s.c., i.t. and i.c.v. administration, respectively [34,53,54]. Unlike morphine, TAPS does not induce respiratory depression even at a more than 30 times higher dose than the AD_{80} after i.c.v. administration [34]. Interestingly, relatively low doses of TAPS (up to $10 \times AD_{80}$) injected i.c.v. cause respiratory stimulation. The lack of respiratory depression with TAPS may be a clinical benefit as an analgesic. In contrast, DALDA injected i.t. causes respiratory depression at a dose of $3 \times AD_{50}$ [54]. [Dmt^1]DALDA at a dose of $32 \times AD_{50}$ after i.t. injection, does not show respiratory depression; however, s.c.-administered [Dmt^1]DALDA, in contrast, causes respiratory depression at $10 \times AD_{50}$ [53,54].

6.2. Antinociceptive tolerance

Like morphine, most of the dermorphin tetrapeptide analogs containing D-Arg^2 cause antinociceptive tolerance. However, the characteristics of their antinociceptive cross-tolerance to morphine are variable. TAPS injected s.c. shows antinociceptive cross-tolerance in rats that have developed antinociceptive tolerance to morphine, whereas morphine injected s.c. does not show antinociceptive cross-tolerance in rats that have developed antinociceptive tolerance to TAPS [42]. In contrast, morphine injected s.c. and i.c.v., but not i.t., shows antinociceptive cross-tolerance in mice that have developed antinociceptive tolerance to TAPA, whereas TAPA injected s.c., i.c.v. and i.t. does not show antinociceptive cross-tolerance in mice that have developed antinociceptive tolerance to morphine [6]. Interestingly, [Dmt^1]DALDA shows the same characteristics as TAPA for the antinociceptive cross-tolerance to morphine. Morphine injected s.c. shows antinociceptive cross-tolerance in mice that have developed antinociceptive tolerance to [Dmt^1]DALDA, whereas [Dmt^1]DALDA injected s.c. does not show marked antinociceptive cross-tolerance in mice that have developed antinociceptive tolerance to morphine [1,61]. The evidence that TAPA and [Dmt^1]DALDA, but not TAPS, are still effective for producing antinociception under the condition of morphine antinociceptive tolerance, suggests a clinical benefit for TAPA and [Dmt^1]DALDA as analgesics.

6.3. Dependence liability

Morphine is well known to develop the both physical dependence and psychological dependence. The physical dependence liability of the dermorphin tetrapeptide analogs containing D-Arg^2 has only been evaluated for TAPA and TAPS [4,28]. Like morphine, chronic s.c. treatment with TAPA or TAPS causes physical dependence, and withdrawal symptoms are observed after their abrupt withdrawal. However, the withdrawal symptoms for TAPA and TAPS are relatively milder than those for morphine, suggesting that the physical dependence liability of TAPA and TAPS is lower than that of morphine. Regarding the psychological dependence liability, no research has been conducted on the dermorphin tetrapeptide analogs containing D-Arg^2. However, we have recently found that unlike morphine, amidino-TAPA lacks the psychological dependence liability [21]. As described above, amidino-TAPA causes the release of dynorphins via activation of μ-opioid receptors. The activation of κ-opioid receptors by the released dynorphins may block the psychological dependence from amidino-TAPA, since amidino-TAPA shows a remarkable rewarding effect in prodynorphin-knockout mice [21]. The other dermorphin tetrapeptide analogs mentioned above also cause the release of dynorphins via activation of μ-opioid receptors. Although it has not been determined at present, those analogs may also lack the psychological dependence liability.

7. Conclusion

The dermorphin N-terminal tetrapeptide analogs containing D-Arg^2 show antinociceptive activity that is greater than that of morphine with various injection routes, even after peripheral injections. Some analogs have distinct antinociceptive profiles from the traditional μ-opioid receptor agonist morphine. They stimulate the release of dynorphins through the activation of distinct μ-opioid receptors. The activation of κ-opioid receptors by the released dynorphins is suggested to reduce the side effects of the μ-opioid receptor agonists. The dermorphin N-terminal tetrapeptide analogs containing D-Arg^2 may provide a new target molecule for developing novel analgesics that have fewer side effects and more therapeutic benefits than morphine.

Acknowledgements

This work was supported by a Grant-in-Aid for Scientific Research (C) [KAKENHI 21600013 and 22600009] from the Japan Society for the Promotion of Science, and a Matching Fund Subsidy for Private Universities from the Ministry of Education, Culture, Sports, Science, and Technology Japan (2010–2014).

References

[1] Ben Y, Smith AP, Schiller PW, Lee NM. Tolerance develops in spinal cord, but not in brain with chronic [Dmt^1]DALDA treatment. Br J Pharmacol 2004;143:987–93.

[2] Bilsky EJ, Calderon SN, Wang T, Bernstein RN, Davis P, Hruby VJ, et al. SNC 80, a selective, nonpeptidic and systemically active opioid δ agonist. J Pharmacol Exp Ther 1995;273:359–66.
[3] Broccardo M, Erspamer V, Falconieri Erspamer G, Improta G, Linari G, Melchiorri P, et al. Pharmacological data on dermorphins, a new class of potent opioid peptides from amphibian skin. Br J Pharmacol 1981;73:625–31.
[4] Chaki K, Kawamura S, Kisara K, Sakurada S, Sakurada T, Sasaki Y, et al. Antinociception and physical dependence produced by [D-Arg^2]dermorphin tetrapeptide analogues and morphine in rats. Br J Pharmacol 1988;95:15–22.
[5] Chaki K, Sakurada S, Sakurada T, Kisara K, Suzuki K. N-terminal tetrapeptide of dermorphin and D-Arg-substituted tetrapeptides: inactivation process of the antinociceptive activity by peptidase. Life Sci 1990;46:1671–8.
[6] Chaki K, Sakurada S, Sakurada T, Nakata N, Kisara K, Watanabe H, et al. Antinociceptive cross-tolerance between [D-Arg^2]-dermorphin tetrapeptide analogs and morphine. Peptides 1990;11:139–44.
[7] Chaki K, Sakurada S, Sakurada T, Sato T, Kawamura S, Kisara K, et al. Comparison of the antinociceptive effects of new [D-Arg^2]-dermorphin tetrapeptide analogs and morphine in mice. Pharmacol Biochem Behav 1988;31:439–44.
[8] Chen Y, Mestek A, Liu J, Hurley A, Yu L. Molecular cloning and functional expression of a μ-opioid receptor from rat brain. Mol Pharmacol 1993;44:8–12.
[9] Doyle GA, Sheng XR, Lin SS, Press DM, Grice DE, Buono RJ, et al. Identification of three mouse μ-opioid receptor (MOR) gene (Oprm1) splice variants containing a newly identified alternatively spliced exon. Gene 2007;388:135–47.
[10] Doyle GA, Sheng XR, Lin SS, Press DM, Grice DE, Buono RJ, et al. Identification of five mouse μ-opioid receptor (MOR) gene (Oprm1) splice variants containing a newly identified alternatively spliced exon. Gene 2007;395:98–107.
[11] Kisara K, Sakurada S, Sakurada T, Sasaki Y, Sato T, Suzuki K, et al. Dermorphin analogues containing D-kyotorphin: structure-antinociceptive relationships in mice. Br J Pharmacol 1986;87:183–9.
[12] Krumins SA. Characterization of dermorphin binding to membranes of rat brain and heart. Neuropeptides 1987;9:93–102.
[13] Kvam T-M, Baar C, Rakvåg TT, Kaasa S, Krokan HE, Skorpen F. Genetic analysis of the murine μ opioid receptor: increased complexity of Oprm gene splicing. J Mol Med 2004;82:250–5.
[14] Mansour A, Khachaturian H, Lewis ME, Akil H, Watson SJ. Anatomy of CNS opioid receptors. Trends Neurosci 1988;11:308–14.
[15] Marastoni M, Salvadori S, Balboni G, Borea PA, Marzola G, Tomatis R. Synthesis and activity profiles of new dermorphin-(1-4) peptide analogues. J Med Chem 1987;30:1538–42.
[16] Melchiorri P, Erspamer GF, Erspamer V, Guglietta A, De Castiglione R, Faoro F, et al. Synthetic peptides related to the dermorphins. II. Synthesis and biological activities of new analogues. Peptides 1982;3:745–58.
[17] Melchiorri P, Negri L. The dermorphin peptide family. Gen Pharmacol 1996;27:1099–107.
[18] Mizoguchi H, Ito K, Watanabe H, Watanabe C, Katsuyama S, Fujimura T, et al. Contribution of spinal μ_1-opioid receptors and dynorphin B to the antinociception induced by Tyr-D-Arg-Phe-Sar. Peptides 2006;27:2786–93.
[19] Mizoguchi H, Narita M, Nagase H, Tseng LF. Activation of G-proteins in the mouse pons/medulla by β-endorphin is mediated by the stimulation of μ- and putative ε-receptors. Life Sci 2000;67:2733–43.
[20] Mizoguchi H, Watanabe C, Higashiya T, Takeda S, Moriyama K, Yonezawa A, et al. Involvement of mouse μ-opioid receptor splice variants in the spinal antinociception induced by the dermorphin tetrapeptide analog amidino-TAPA. Eur J Pharmacol; in press.
[21] Mizoguchi H, Watanabe C, Osada S, Yoshioka M, Aoki Y, Natsui S, et al. Lack of a rewarding effect and a locomotor-enhancing effect of the selective μ-opioid receptor agonist amidino-TAPA. Psychopharmacology (Berl) 2010;212:215–25.
[22] Mizoguchi H, Watanabe C, Watanabe H, Moriyama K, Sato B, Ohwada K, et al. Involvement of endogenous opioid peptides in the antinociception induced by the novel dermorphin tetrapeptide analog amidino-TAPA. Eur J Pharmacol 2007;560:150–9.
[23] Mizoguchi H, Wu HE, Narita M, Loh HH, Nagase H, Tseng LF. Loss of μ-opioid receptor-mediated G-protein activation in the pons/medulla of mice lacking the exons 2 and 3 of μ-opioid receptor gene. Neurosci Lett 2002;335:91–4.
[24] Mizoguchi H, Wu HE, Narita M, Sora I, Hall SF, Uhl GR, et al. Lack of μ-opioid receptor-mediated G-protein activation in the spinal cord of mice lacking Exon 1 or Exons 2 and 3 of the MOR-1 gene. J Pharmacol Sci 2003;93:423–9.
[25] Mizoguchi H, Yuhki M, Watanabe H, Hayashi T, Sakurada C, Yonezawa A, et al. Differential involvement of μ_1-opioid receptors in dermorphin tetrapeptide analogues-induced antinociception. Eur J Pharmacol 2004;486:19–24.
[26] Montecucchi PC, De Castiglione R, Piani S, Gozzini L, Erspamer V. Amino acid composition and sequence of dermorphin, a novel opiate-like peptide from the skin of *Phyllomedusa sauvagei*. Int J Pept Protein Res 1981;17:275–83.
[27] Nagase H, Hayakawa J, Kawamura K, Kawai K, Takezawa Y, Matsuura H, et al. Discovery of a structurally novel opioid κ-agonist derived from 4,5-epoxymorphinan. Chem Pharm Bull (Tokyo) 1998;46:366–9.
[28] Nakata N, Sakurada S, Sakurada T, Kisara K, Sasaki Y, Suzuki K. Physical dependence of a dermorphin tetrapeptide analog, [D-Arg^2, Sar^4]-dermorphin (1-4) in the rat. Pharmacol Biochem Behav 1986;24:27–31.
[29] Negri L, Erspamer GF, Severini C, Potenza RL, Melchiorri P, Erspamer V. Dermorphin-related peptides from the skin of *Phyllomedusa bicolor* and their amidated analogs activate two μ opioid receptor subtypes that modulate antinociception and catalepsy in the rat. Proc Natl Acad Sci USA 1992;89:7203–7.
[30] Negri L, Improta G. Distribution and metabolism of dermorphin in rats. Pharmacol Res Commun 1984;16:1183–94.
[31] Negri L, Lattanzi R, Melchiorri P. Production of antinociception by peripheral administration of [Lys^7]dermorphin, a naturally occurring peptide with high affinity for μ-opioid receptors. Br J Pharmacol 1995;114:57–66.
[32] Neilan CL, Nguyen TM, Schiller PW, Pasternak GW. Pharmacological characterization of the dermorphin analog [Dmt^1]DALDA, a highly potent and selective μ-opioid peptide. Eur J Pharmacol 2001;419:15–23.
[33] Ogawa T, Miyamae T, Murayama K, Okuyama K, Okayama T, Hagiwara M, et al. Synthesis and structure–activity relationships of an orally available and long-acting analgesic peptide, N$^{\alpha}$-amidino-Tyr-D-Arg-Phe-MeβAla-OH (ADAMB). J Med Chem 2002;45:5081–9.
[34] Paakkari P, Paakkari I, Vonhof S, Feuerstein G, Sirén AL. Dermorphin analog Tyr-D-Arg^2-Phe-sarcosine-induced opioid analgesia and respiratory stimulation: the role of μ_1-receptors? J Pharmacol Exp Ther 1993;266:544–50.
[35] Pan Y-X, Xu J, Bolan E, Abbadie C, Chang A, Zuckerman A, et al. Identification and characterization of three new alternatively spliced μ-opioid receptor isoforms. Mol Pharmacol 1999;56:396–403.
[36] Pan Y-X, Xu J, Bolan E, Chang A, Mahurter LA, Rossi G, et al. Isolation and expression of a novel alternatively spliced μ opioid receptor isoform, MOR-1F. FEBS Lett 2000;466:337–40.
[37] Pan Y-X, Xu J, Bolan E, Moskowitz HS, Xu M, Pasternak GW. Identification of four novel exon 5 splice variants of the mouse μ-opioid receptor gene: functional consequences of C-terminal splicing. Mol Pharmacol 2005;68:866–75.
[38] Pan Y-X, Xu J, Mahurter L, Bolan E, Xu M, Pasternak GW. Generation of the μ opioid receptor (MOR-1) protein by three new splice variants of the Oprm gene. Proc Natl Acad Sci USA 2001;98:14084–9.
[39] Pasternak GW, Wood PJ. Multiple μ opiate receptors. Life Sci 1986;38:1889–98.
[40] Puglisi-Allegra S, Castellano C, Filibeck U, Oliverio A, Melchiorri P. Behavioural data on dermorphins in mice. Eur J Pharmacol 1982;82:223–7.
[41] Sakurada S, Hayashi T, Yuhki M, Orito T, Zadina JE, Kastin AJ, et al. Differential antinociceptive effects induced by intrathecally administered endomorphin-1 and endomorphin-2 in the mouse. Eur J Pharmacol 2001;427:203–10.
[42] Sakurada S, Nakata N, Sakurada T, Chaki K, Kawamura S, Kisara K, et al. Tolerance and cross-tolerance to the antinociceptive effects of [D-Arg^2]-dermorphin tetrapeptide analogue and morphine. Neuropharmacology 1993;32:689–93.
[43] Sakurada S, Takeda S, Sato T, Hayashi T, Yuki M, Kutsuwa M, et al. Selective antagonism by naloxonazine of antinociception by Tyr-D-Arg-Phe-β-Ala, a novel dermorphin analogue with high affinity at μ-opioid receptors. Eur J Pharmacol 2000;395:107–12.
[44] Sasaki Y, Ambo A, Suzuki K. Studies on analgesic oligopeptides: VII. Solid phase synthesis and biological properties of Tyr-D-Arg-Phe-β-Ala-NH_2 and its fluorinate aromatic amino acid derivatives. Chem Pharm Bull (Tokyo) 1991;39:2316–8.
[45] Sasaki Y, Hosono M, Matsui M, Fujita H, Suzuki K, Sakurada S, et al. On the degradation of dermorphin and D-Arg^2-dermorphin analogs by a soluble rat brain extract. Biochem Biophys Res Commun 1985;130:964–70.
[46] Sasaki Y, Matsui M, Fujita H, Hosono M, Taguchi M, Suzuki K, et al. The analgesic activity of D-Arg^2-dermorphin and its N-terminal tetrapeptide analogs after subcutaneous administration in mice. Neuropeptides 1985;5:391–4.
[47] Sasaki Y, Matsui M, Taguchi M, Suzuki K, Sakurada S, Sato T, et al. D-Arg^2-dermorphin tetrapeptide analogues. A potent and long-lasting analgesic activity after subcutaneous administration. Biochem Biophys Res Commun 1984;120:214–8.
[48] Sato T, Sakurada S, Sakurada T, Furuta S, Chaki K, Kisara K, et al. Opioid activities of D-Arg^2-substituted tetrapeptides. J Pharmacol Exp Ther 1987;242:654–9.
[49] Sato T, Sakurada S, Takahashi N, Sakurada T, Tan-No K, Wako K, et al. Contribution of spinal μ_1-opioid receptors to morphine-induced antinociception. Eur J Pharmacol 1999;369:183–7.
[50] Scalia S, Salvadori S, Marastoni M, Bortolotti F, Tomatis R. Reversed-phase HPLC study on the in vitro enzymic degradation of dermorphin. Peptides 1986;7:247–51.
[51] Schiller PW, Nguyen TM, Berezowska I, Dupuis S, Weltrowska G, Chung NN, et al. Synthesis and in vitro opioid activity profiles of DALDA analogues. Eur J Med Chem 2000;35:895–901.
[52] Schiller PW, Nguyen TM, Chung NN, Lemieux C. Dermorphin analogues carrying an increased positive net charge in their "message" domain display extremely high μ opioid receptor selectivity. J Med Chem 1989;32:698–703.
[53] Shimoyama M, Kuwaki T, Nakamura A, Fukuda Y, Shimoyama N, Schiller PW, et al. Differential respiratory effects of [Dmt^1]DALDA and morphine in mice. Eur J Pharmacol 2005;511:199–206.
[54] Shimoyama M, Shimoyama N, Zhao GM, Schiller PW, Szeto HH. Antinociceptive and respiratory effects of intrathecal H-Tyr-D-Arg-Phe-Lys-NH_2 (DALDA) and [Dmt^1] DALDA. J Pharmacol Exp Ther 2001;297:364–71.
[55] Szeto HH, Clapp JF, Desiderio DM, Schiller PW, Grigoriants OO, Soong Y, et al. In vivo disposition of dermorphin analog (DALDA) in nonpregnant and pregnant sheep. J Pharmacol Exp Ther 1998;284:61–5.
[56] Szeto HH, Soong Y, Wu D, Qian X, Zhao GM. Endogenous opioid peptides contribute to antinociceptive potency of intrathecal [Dmt^1]DALDA. J Pharmacol Exp Ther 2003;305:696–702.
[57] Takemori AE, Ikeda M, Portoghese PS. The μ, κ and δ properties of various opioid agonists. Eur J Pharmacol 1986;123:357–61.
[58] Tseng LF, Narita M, Mizoguchi H, Kawai K, Mizusuna A, Kamei J, et al. Delta-1 opioid receptor-mediated antinociceptive properties of a nonpeptidic delta

opioid receptor agonist, (−)TAN-67, in the mouse spinal cord. J Pharmacol Exp Ther 1997;280:600–5.
[59] Vonhof S, Barone FC, Price WJ, Paakkari P, Millison JH, Feuerstein GZ, et al. Receptor binding and biological activity of the dermorphin analog Tyr-D-Arg^2-Phe-Sar (TAPS). Eur J Pharmacol 2001;416:83–93.
[60] Wang JB, Imai Y, Eppler CM, Gregor P, Spivak CE, Uhl GR. μ opiate receptor: cDNA cloning and expression. Proc Natl Acad Sci USA 1993;90:10230–4.
[61] Zhao GM, Wu D, Soong Y, Shimoyama M, Berezowska I, Schiller PW, et al. Profound spinal tolerance after repeated exposure to a highly selective μ-opioid peptide agonist: role of δ-opioid receptors. J Pharmacol Exp Ther 2002;302:188–96.

European Journal of Pharmacology 651 (2011) 66–72

Contents lists available at ScienceDirect

European Journal of Pharmacology

journal homepage: www.elsevier.com/locate/ejphar

Neuropharmacology and Analgesia

Involvement of mouse μ-opioid receptor splice variants in the spinal antinociception induced by the dermorphin tetrapeptide analog amidino-TAPA

Hirokazu Mizoguchi [a], Chizuko Watanabe [a], Takayuki Higashiya [a], Satoshi Takeda [a], Kaori Moriyama [a], Akihiko Yonezawa [a], Takumi Sato [b], Takaaki Komatsu [c], Tsukasa Sakurada [c], Shinobu Sakurada [a,*]

[a] Department of Physiology and Anatomy, Tohoku Pharmaceutical University, 4-4-1 Komatsushima, Aoba-ku, Sendai 981-8558, Japan
[b] Department of Pharmacology, Nihon Pharmaceutical University, 10281 Komuro, Ina-machi, Kitaadachi-gun, Saitama 362-0806, Japan
[c] First Department of Pharmacology, Daiichi College of Pharmaceutical Sciences, 22-1 Tamagawa-cho, Minami-ku, Fukuoka 815-8511, Japan

ARTICLE INFO

Article history:
Received 20 February 2010
Received in revised form 2 October 2010
Accepted 16 October 2010
Available online 31 October 2010

Keywords:
Antinociception
Acute tolerance
mu-Opioid receptor
Opioid peptides
Splice variants
Spinal cord

ABSTRACT

The involvement of the mouse μ-opioid receptor (mMOR-1) splice variants in the antinociceptive effect of intrathecally (i.t.) administered N^{α}-amidino-Tyr-D-Arg-Phe-β-Ala (amidino-TAPA) and [D-Ala^2,N-MePhe^4, Gly-ol^5]enkephalin (DAMGO) was investigated in mice by monitoring the recovery from acute antinociceptive tolerance to amidino-TAPA and DAMGO. A single i.t. pretreatment with DAMGO produced an acute antinociceptive tolerance, which peaked at 2 h and disappeared within 5 h after the pretreatment. In contrast, a single i.t. pretreatment with amidino-TAPA produced an acute antinociceptive tolerance, which disappeared within 3 h after the pretreatment. The concomitant i.t. pretreatment with an antisense oligodeoxynucleotide (ODN) for exon-1, exon-12, exon-13 or exon-14 of mMOR-1 maintained the acute antinociceptive tolerance to amidino-TAPA for 24 h after the pretreatment. On the other hand, the concomitant i.t. pretreatment with an antisense ODN for exon-1 of mMOR-1, but not an antisense ODN for exon-12, exon-13 or exon-14 of mMOR-1, maintained the acute antinociceptive tolerance to DAMGO for 24 h after the pretreatment. The present results suggest that the spinal antinociception of amidino-TAPA is partially mediated through the activation of the amidino-TAPA-sensitive and DAMGO-insensitive mMOR-1 splice variants MOR-1J, MOR-1K and MOR-1L, which contain the sequence encoded by exon-12, exon-13 and exon-14, respectively.

© 2010 Elsevier B.V. All rights reserved.

1. Introduction

N^{α}-Amidino-Tyr-D-Arg-Phe-β-Ala (amidino-TAPA) is an N-terminal tetrapeptide derivative of dermorphin. It has a very high affinity and selectivity for μ-opioid receptors, and produces an extremely potent and long-lasting antinociception (Mizoguchi et al., 2007; Ogawa et al., 2002). The antinociceptive potency of amidino-TAPA is 10-fold, 1.2-fold or 650-fold higher than that of morphine after subcutaneous, oral or intrathecal (i.t.) injections, respectively. Unlike the traditional μ-opioid receptor agonist DAMGO, the antinociceptive effect of i.t.-administered amidino-TAPA is mediated through the release of the endogenous κ-opioid peptides dynorphin A, dynorphin B and α-neo-endorphin and the endogenous δ-opioid peptide [Leu^5] enkephalin via activation of μ-opioid receptors in the spinal cord (Mizoguchi et al., 2007). The distinct antinociceptive profiles of amidino-TAPA may be mediated by the activation of distinct μ-opioid receptors that are sensitive to amidino-TAPA but insensitive to DAMGO.

Since the initial cloning of the μ-opioid receptor gene MOR-1 (Chen et al., 1993; Wang et al., 1993), 33 splice variants have been identified in mouse MOR-1 (mMOR-1) mRNA (Doyle et al., 2007a,b; Kvam et al., 2004; Pan et al., 2001, 2005). The sequence variability of the splice variants is found in the sequences of the N-terminal and first transmembrane region, and in the sequence of the intracellular C-terminal region. The selectivities and intrinsic activities of various μ-opioid receptor agonists for 6 of the splice variants (MOR-1, 1A, 1C, 1D, 1E, and 1F), that contain the sequences encoded by exon-1, have been described in CHO cells over-expressing each of these splice variants (Pasternak, 2004). However, no remarkable differences in the selectivity and intrinsic activity of any μ-opioid receptor agonist were observed among the splice variants examined. For the other splice variants, the selectivity and intrinsic activity of μ-opioid receptor agonists is still unknown. Although the distribution of most of the splice variants in the rodent central nervous system have been described (Doyle et al., 2007a,b; Pan et al., 1999, 2000, 2001, 2005), the physiological roles of each splice variant are still unknown.

A single intracerebroventricular or i.t. injection of opioid receptor agonists induces a rapid and short-term reduction of their antinociceptive effect, the so-called "acute antinociceptive tolerance" (Narita et al., 1995, 1996; Suh and Tseng, 1990; Wu et al., 2001, 2003). The development of acute antinociceptive tolerance is considered to

* Corresponding author. Tel.: +81 22 727 0124; fax: +81 22 727 0125.
E-mail address: s-sakura@tohoku-pharm.ac.jp (S. Sakurada).

0014-2999/$ – see front matter © 2010 Elsevier B.V. All rights reserved.
doi:10.1016/j.ejphar.2010.10.049

be a receptor-dependent phenomenon. We have previously reported that the acute antinociceptive tolerance to a δ-opioid receptor agonist is caused by the internalization and degradation of the δ-opioid receptor following the single treatment with a δ-opioid receptor agonist (Narita et al., 1996, 1997a,b). The recovery from the acute antinociceptive tolerance to a δ-opioid receptor agonist is produced by newly synthesized δ-opioid receptors, which are associated with the natural turnover of δ-opioid receptors. Therefore, the suppression of the synthesis of new δ-opioid receptors can maintain the acute antinociceptive tolerance to an δ-opioid receptor agonist.

The present study was conducted to identify the mMOR-1 splice variants involved in the spinal antinociceptive effect of amidino-TAPA, but not DAMGO, by monitoring the recovery from acute antinociceptive tolerance to amidino-TAPA and DAMGO.

2. Materials and methods

All experiments were performed following the approval of the Ethics Committee for Animal Experiments at Tohoku Pharmaceutical University and according to the National Institutes of Health Guide for the Care and Use of Laboratory Animals. Every effort was made to minimize the number and any suffering of the animal used in the following experiments.

2.1. Animals

Male ddY mice (Japan SLC, Hamamatsu, Japan) weighing 22–25 g were used. The animals were housed in a room maintained at 22–23 °C and 50–60% relative humidity with an alternating 12-h light/dark cycle. Food and water were available *ad libitum*. Mice were used only once.

2.2. Assessment of antinociception

Antinociception was determined with the tail-flick test (D'Amour and Smith, 1941). For measurement of the latency of the tail-flick response, mice were gently held by hand with their tail positioned in an apparatus (Ugo Basile, Italy) for radiant heat stimulation on the ventral surface of the tail. The intensity of the heat stimulus was adjusted so that the animal withdrew its tail after 2.5–3.5 s. The inhibition of the tail-flick response was expressed as the percent maximal possible effect, % MPE, which was calculated as follows: $[(T_1 - T_0)/(T_2 - T_0)] \times 100$, where T_0 and T_1 are the tail-flick latencies before and after the treatments, respectively, and T_2 is the cutoff time, set at 10 s to avoid injury to the tail. The antinociceptive effect was represented as the mean ± S.E.M. for at least 10 mice. The dose–response curves and ED_{50} values with their 95% confidence intervals were calculated with a computer-assisted curve-fitting program (GraphPad Prism; GraphPad Software, Inc., San Diego, CA).

2.3. Intrathecal injection

The i.t. injection was performed following the method described by Hylden and Wilcox (1980) using a 29-gauge stainless-steel needle attached to a 50-μl Hamilton microsyringe. For i.t. injections, drugs were dissolved in sterile artificial cerebrospinal fluid (aCSF) containing 126.6 mM NaCl, 2.5 mM KCl, 2.0 mM $MgCl_2$, and 1.3 mM $CaCl_2$. The volume for the i.t. injections was 5 μl.

2.4. Drugs

The drugs used were amidino-TAPA (Peptides Institute, Osaka, Japan) and DAMGO (Sigma-Aldrich, St. Louis, MO). Antisense phosphorothioate-linked oligodeoxynucleotides (ODNs) for exon-1, exon-12, exon-13, and exon-14 of mMOR-1, which were purchased from The Midland Certified Reagent Company (Midland, TX), had the following sequences: 5'-GCC CAC TAC ACA CAC GAT AGA-3' (antisense ODN for exon-1), 5'-GTG AAG CAC TGT CTT CTA AAG GGG-3' (antisense ODN for exon-12), 5'-TCA GTC TTT ATC AGC TCA CCG CCA-3' (antisense ODN for exon-13) and 5'-TAT TTT GAT TTT CAG TTG ATT C-3' (antisense ODN for exon-14).

2.5. Statistical analyses

The statistical significance of differences between the groups was assessed with a one-way analysis of variance (ANOVA) and a two-way ANOVA followed by Dunnett's test and Bonferroni's test, respectively.

3. Results

3.1. Acute antinociceptive tolerance to DAMGO and amidino-TAPA

Groups of mice were injected i.t. with DAMGO (10 pmol), amidino-TAPA (2 pmol) or aCSF, and the antinociceptive effects induced by DAMGO and amidino-TAPA were measured. The i.t. administration of DAMGO or amidino-TAPA resulted in a marked antinociception with approximately equal efficacy (87.54% and 85.38% MPE for DAMGO and amidino-TAPA, respectively, at their peak-effect time) at the doses used (Fig. 1). The antinociceptive effect of amidino-TAPA developed rapidly, reached its maximal effect at 10 min after the treatment, and then disappeared slowly by 120 min. A more prolonged antinociceptive effect was observed for amidino-TAPA than for DAMGO, whose antinociceptive effect peaked at 10 min and disappeared by 45 min after the treatment. In the following experiments, to identify the acute antinociceptive tolerance to DAMGO or amidino-TAPA, the antinociceptive effects of i.t.-administered DAMGO (10 pmol) or amidino-TAPA (2 pmol) were measured 10 min after the treatment in mice receiving the various pretreatments.

Groups of mice were pretreated i.t. with aCSF or DAMGO (10 pmol) 1, 2, 3, 4, 5, or 6 h before the i.t. treatment with DAMGO (10 pmol), and the antinociception induced by DAMGO was measured 10 min after the treatment. The mice pretreated with DAMGO 1 h before showed an antinociceptive effect of DAMGO treatment that was equipotent to mice pretreated with aCSF (Fig. 2A). However, in mice pretreated with DAMGO 2 h before, the antinociceptive effect of DAMGO was dramatically suppressed compared with mice pretreated

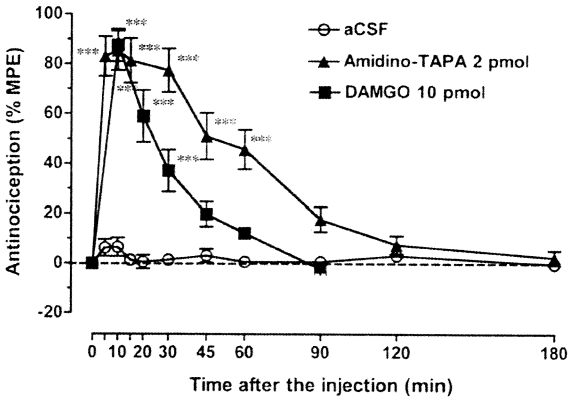


Fig. 1. Antinociceptive effects of DAMGO and amidino-TAPA in the ddY mouse spinal cord. Groups of mice were injected i.t. with DAMGO (10 pmol) or amidino-TAPA (2 pmol), and the tail-flick inhibition induced by DAMGO or amidino-TAPA was measured for 90 or 180 min, respectively. The antinociceptive effect was calculated as the mean ± S.E.M for at least 10 mice. The statistical significance of the differences between the groups was assessed with a two-way ANOVA followed by Bonferroni's test. The *F* values of the two-way ANOVA for DAMGO and amidino-TAPA against aCSF were $F[1,126] = 134.7$ ($P<0.001$) and $F[1,180] = 340.4$ ($P<0.001$), respectively. ***$P<0.001$ vs. the aCSF-treated group.

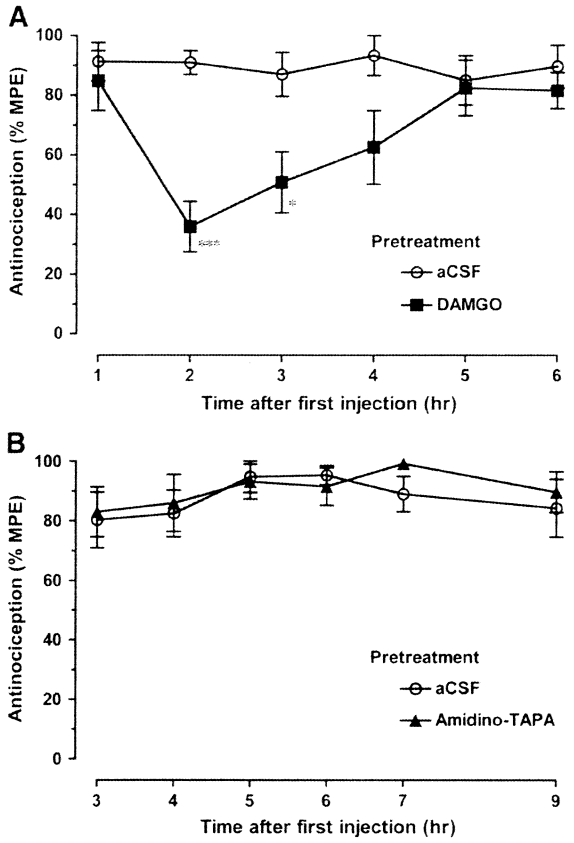


Fig. 2. Acute antinociceptive tolerance to DAMGO and amidino-TAPA in the ddY mouse spinal cord. (A) Groups of mice were pretreated i.t. with aCSF or DAMGO (10 pmol) 1, 2, 3, 4, 5, or 6 h before the i.t. treatment with DAMGO (10 pmol), and the antinociception induced by DAMGO was measured 10 min after the treatment. (B) Groups of mice were pretreated i.t. with aCSF or amidino-TAPA (2 pmol) 3, 4, 5, 6, 7, or 9 h before the i.t. treatment with amidino-TAPA (2 pmol), and the antinociception induced by amidino-TAPA was measured 10 min after the treatment. The antinociceptive effect was calculated as the mean ± S.E.M for at least 10 mice. The statistical significance of the differences between the groups was assessed with a two-way ANOVA followed by Bonferroni's test. (A) The F value of the two-way ANOVA was $F[1,124] = 21.90$ ($P<0.001$). $^{*}P<0.05$, $^{***}P<0.001$ vs. the aCSF-pretreated group. (B) The F value of the two-way ANOVA was $F[1,117] = 0.3782$ ($P = 0.5397$).

with aCSF. The suppression of DAMGO-induced antinociception (acute antinociceptive tolerance to DAMGO) gradually disappeared. At 5 h after the pretreatment with DAMGO, the antinociceptive effect of DAMGO treatment had completely recovered to the same magnitude observed in mice pretreated with aCSF.

Other groups of mice were pretreated i.t. with aCSF or amidino-TAPA (2 pmol) 3, 4, 5, 6, 7, or 9 h before the i.t. treatment with amidino-TAPA (2 pmol), and the antinociception induced by amidino-TAPA was measured 10 min after the treatment. In contrast to DAMGO, the antinociceptive effect of amidino-TAPA in mice pretreated with amidino-TAPA was exactly equipotent with that in mice pretreated with aCSF at all time points measured after the pretreatment (Fig. 2B). In other words, no suppression of amidino-TAPA-induced antinociception after the pretreatment with amidino-TAPA (acute antinociceptive tolerance to amidino-TAPA) was observed at any time point tested. Together with the evidence that the antinociceptive effect of amidino-TAPA is long-lasting and it takes 2 h to return the nociceptive threshold to the baseline level after the treatment, the present results suggests the possibility that the acute antinociceptive tolerance to amidino-TAPA develops rapidly and disappears within 3 h. To investigate this possibility, the acute antinociceptive tolerance to amidino-TAPA 3 h after the pretreatment was determined under conditions where the new synthesis of most of the mMOR-1 splice variants had been suppressed by the pretreatment with an antisense ODN for exon-1 of mMOR-1. Groups of mice pretreated i.t. with aCSF or an antisense ODN for exon-1 of mMOR-1 (5 μg) 24 h before, were injected i.t. with aCSF or amidino-TAPA (2 pmol) 3 h before the i.t. treatment with amidino-TAPA (2 pmol), and the tail-flick inhibition induced by amidino-TAPA was measured at 10 min after the treatments. Like the data presented in Fig. 2B, no suppression of amidino-TAPA-induced antinociception at 3 h after the pretreatment with amidino-TAPA (acute antinociceptive tolerance to amidino-TAPA) was observed in mice pretreated with aCSF 24 h before (data not shown). However, in mice pretreated with an antisense ODN for exon-1 of mMOR-1 24 h before, a marked suppression of amidino-TAPA-induced antinociception at 3 h after the pretreatment with amidino-TAPA (the acute antinociceptive tolerance to amidino-TAPA) was observed.

3.2. Retention of the acute antinociceptive tolerance to DAMGO or amidino-TAPA by co-pretreatment with exon-specific antisense ODNs for mMOR-1

The mMOR-1 splice variants involved in the acute antinociceptive tolerance to DAMGO or amidino-TAPA in the mouse spinal cord were determined using the exon-specific antisense ODNs for mMOR-1. Groups of mice were pretreated i.t. with aCSF, an antisense ODN for exon-1 of mMOR-1 (5 μg), μ-opioid receptor agonists (10 pmol of DAMGO or 2 pmol of amidino-TAPA), or μ-opioid receptor agonists in combination with an antisense ODN for exon-1 of mMOR-1 24 h before the i.t. treatment with μ-opioid receptor agonists (10 pmol of DAMGO or 2 pmol of amidino-TAPA), and the tail-flick inhibition induced by μ-opioid receptor agonists was measured at 10 min after the treatments. The pretreatment with an antisense ODN for exon-1 of mMOR-1 24 h before did not alter the antinociception induced by either DAMGO or amidino-TAPA (Fig. 3). The antinociception induced by DAMGO and amidino-TAPA also was not affected by the 24-h pretreatment with DAMGO and amidino-TAPA, respectively. The acute antinociceptive tolerance to DAMGO and amidino-TAPA was not observed 24 h after the pretreatment with DAMGO and amidino-TAPA, respectively. In contrast, the antinociception induced by DAMGO or amidino-TAPA was significantly attenuated by the concomitant pretreatment with the antisense ODN for exon-1 of mMOR-1 and either DAMGO or amidino-TAPA, respectively. The acute antinociceptive tolerance to DAMGO or amidino-TAPA was still maintained for 24 h after the pretreatment by the concomitant pretreatment with the antisense ODN for exon-1 of mMOR-1.

The involvement of MOR-1J (splice variant containing the sequence encoded by exon-12), MOR-1K (splice variant containing the sequence encoded by exon-13) and MOR-1L (splice variant containing the sequence encoded by exon-14) in the acute antinociceptive tolerance to DAMGO or amidino-TAPA in the mouse spinal cord was also investigated on the same experimental schedule, using antisense ODNs for exon-12, exon-13 and exon-14 of mMOR-1, respectively. The pretreatment with antisense ODNs for either exon-12, exon-13 or exon-14 of mMOR-1 24 h before did not alter the antinociception induced by either DAMGO or amidino-TAPA (Figs. 4–6). Amidino-TAPA-induced antinociception was significantly attenuated by the concomitant pretreatment with amidino-TAPA and antisense ODNs for either exon-12, exon-13 or exon-14 of mMOR-1 (Figs. 4B, 5B, 6B), whereas DAMGO-induced antinociception was not altered by the concomitant pretreatment with DAMGO and antisense ODNs for either exon-12, exon-13 or exon-14 of mMOR-1 (Figs. 4A, 5A, 6A). The acute antinociceptive tolerance to amidino-TAPA, but not to DAMGO, was maintained for 24 h after the pretreatment by antisense ODNs for either exon-12, exon-13 or exon-14 of mMOR-1.

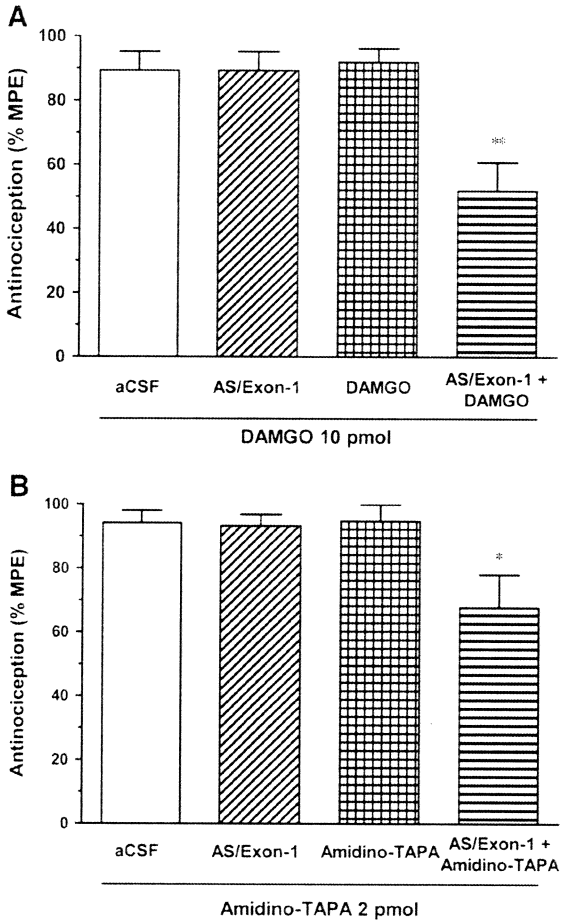


Fig. 3. Effects of an antisense ODN for exon-1 of mMOR-1 on the acute antinociceptive tolerance to DAMGO and amidino-TAPA in the ddY mouse spinal cord. (A) Groups of mice were pretreated i.t. with aCSF, an antisense ODN for exon-1 of mMOR-1 (AS/Exon-1: 5 μg), DAMGO (10 pmol) or DAMGO in combination with AS/Exon-1 24 h before the i.t. treatment with DAMGO (10 pmol), and the tail-flick inhibition induced by DAMGO was measured at 10 min after the treatments. (B) Groups of mice were pretreated i.t. with aCSF, AS/Exon-1 (5 μg), amidino-TAPA (2 pmol) or amidino-TAPA in combination with AS/Exon-1 24 h before the i.t. treatment with amidino-TAPA (2 pmol), and the tail-flick inhibition induced by amidino-TAPA was measured at 10 min after the treatments. The antinociceptive effect was calculated as the mean ± S.E.M for at least 10 mice. The statistical significance of the differences between the groups was assessed with a one-way ANOVA followed by Dunnett's test. (A) The F value of the one-way ANOVA was $F[3,35] = 8.836$ ($P<0.001$). $^{**}P<0.01$ vs. the aCSF-pretreated group. (B) The F value of the one-way ANOVA was $F[3,36] = 4.271$ ($P<0.05$). $^{*}P<0.05$ vs. the aCSF-pretreated group.

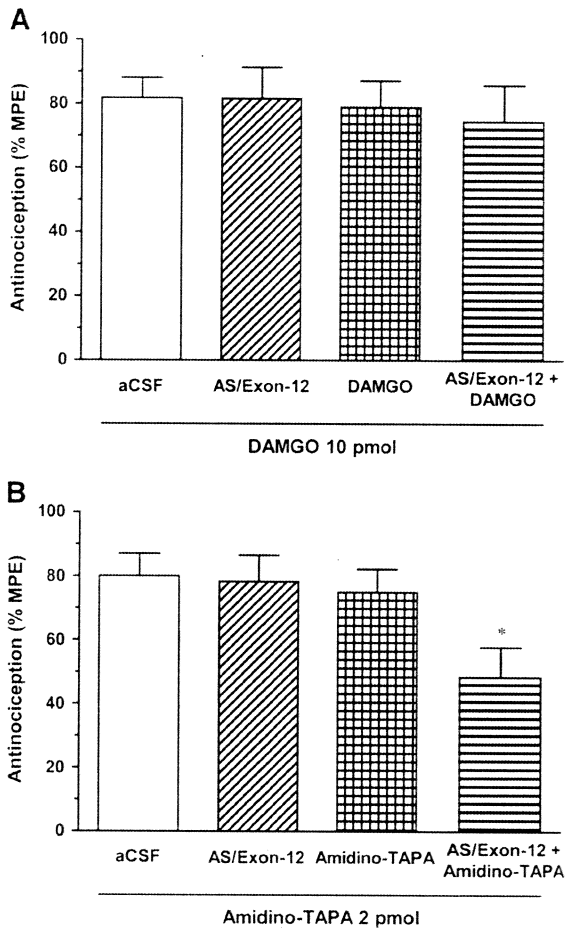


Fig. 4. Effects of an antisense ODN for exon-12 of mMOR-1 on the acute antinociceptive tolerance to DAMGO and amidino-TAPA in the ddY mouse spinal cord. (A) Groups of mice were pretreated i.t. with aCSF, an antisense ODN for exon-12 of mMOR-1 (AS/Exon-12: 5 μg), DAMGO (10 pmol) or DAMGO in combination with AS/Exon-12 24 h before the i.t. treatment with DAMGO (10 pmol), and the tail-flick inhibition induced by DAMGO was measured at 10 min after the treatments. (B) Groups of mice were pretreated i.t. with aCSF, AS/Exon-12 (5 μg), amidino-TAPA (2 pmol) or amidino-TAPA in combination with AS/Exon-12 24 h before the i.t. treatment with amidino-TAPA (2 pmol), and the tail-flick inhibition induced by amidino-TAPA was measured at 10 min after the treatments. The antinociceptive effect was calculated as the mean ± S.E.M for at least 10 mice. The statistical significance of the differences between the groups was assessed with a one-way ANOVA followed by Dunnett's test. (A) The F value of the one-way ANOVA was $F[3,36] = 0.1393$ ($P = 0.9358$). (B) The F value of the one-way ANOVA was $F[3,76] = 3.444$ ($P<0.05$). $^{*}P<0.05$ vs. the aCSF-pretreated group.

4. Discussion

Amidino-TAPA has a very high affinity and selectivity for μ-opioid receptors, and shows an extremely potent and long-lasting antinociception that is mediated by μ-opioid receptors (Mizoguchi et al., 2007; Ogawa et al., 2002). Unlike the traditional μ-opioid receptor agonist DAMGO, amidino-TAPA has a distinct spinal antinociceptive mechanism that is mediated by the release of the endogenous δ-opioid peptide [Leu^5]enkephalin and the endogenous κ-opioid peptides dynorphin A, dynorphin B and α-neo-endorphin, which is initiated by the activation of spinal μ-opioid receptors (Mizoguchi et al., 2007). An antinociception that is mediated through the release of endogenous opioid peptides in the spinal cord is also observed for the other selective μ-opioid receptor agonists endomorphin-2 (Mizoguchi et al., 2006b; Sakurada et al., 2001), Tyr-D-Arg-Phe-Sar (TAPS: Mizoguchi et al., 2006a) and dimethyl-Tyr-D-Arg-Phe-Lys-NH_2 ([Dmt^1]DALDA: Szeto et al., 2003). The evidence clearly suggests that these selective μ-opioid receptor agonists stimulate different μ-opioid receptors than DAMGO to produce the antinociception. At present, 33 splice variants for mMOR-1 have been identified (Doyle et al., 2007a, b; Kvam et al., 2004; Pan et al., 2001, 2005). The release of endogenous opioid peptides by the above μ-opioid receptor agonists may be mediated by the activation of specific splice variants of mMOR-1 that are insensitive to DAMGO. In the present study, the mMOR-1 splice variants involved in the spinal antinociception of amidino-TAPA, but not DAMGO, were identified by monitoring the recovery from the acute antinociceptive tolerance to amidino-TAPA.

Acute antinociceptive tolerance is the rapid and temporary reduction of the antinociceptive effect of opioid receptor agonists observed after a single pretreatment with the same agonist. In the present study, the pretreatment with DAMGO caused the reduction of its antinociceptive effect (acute antinociceptive tolerance), which peaked at 2 h and disappeared by 5 h after the pretreatment. The

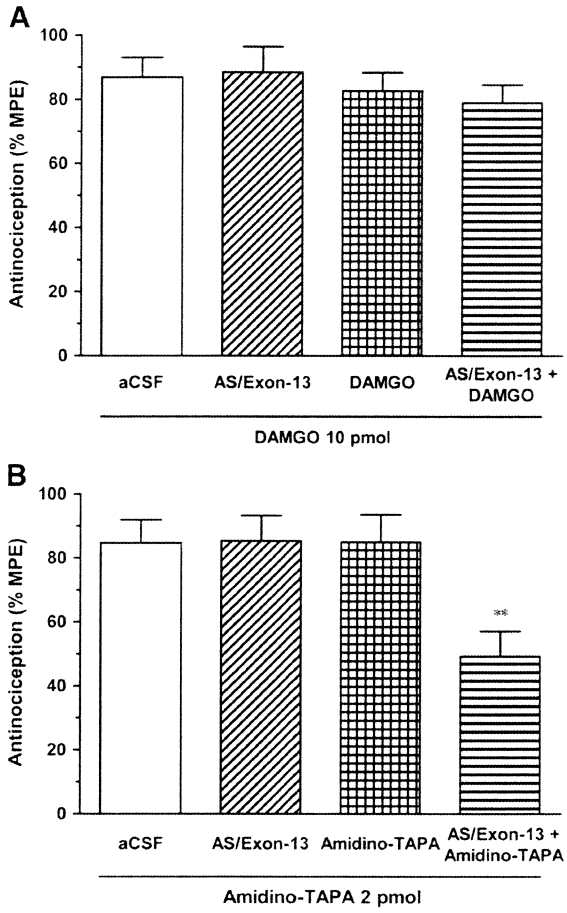


Fig. 5. Effects of an antisense ODN for exon-13 of mMOR-1 on the acute antinociceptive tolerance to DAMGO and amidino-TAPA in the ddY mouse spinal cord. (A) Groups of mice were pretreated i.t. with aCSF, an antisense ODN for exon-13 of mMOR-1 (AS/Exon-13: 5 μg), DAMGO (10 pmol) or DAMGO in combination with AS/Exon-13 24 h before the i.t. treatment with DAMGO (10 pmol), and the tail-flick inhibition induced by DAMGO was measured at 10 min after the treatments. (B) Groups of mice were pretreated i.t. with aCSF, AS/Exon-13 (5 μg), amidino-TAPA (2 pmol) or amidino-TAPA in combination with AS/Exon-13 24 h before the i.t. treatment with amidino-TAPA (2 pmol), and the tail-flick inhibition induced by amidino-TAPA was measured at 10 min after the treatments. The antinociceptive effect was calculated as the mean ± S.E.M for at least 10 mice. The statistical significance of the differences between the groups was assessed with a one-way ANOVA followed by Dunnett's test. (A) The F value of the one-way ANOVA was $F[3,36] = 0.4406$ ($P = 0.7253$). (B) The F value of the one-way ANOVA was $F[3,36] = 5.065$ ($P < 0.01$). $^{**}P < 0.01$ vs. the aCSF-pretreated group.

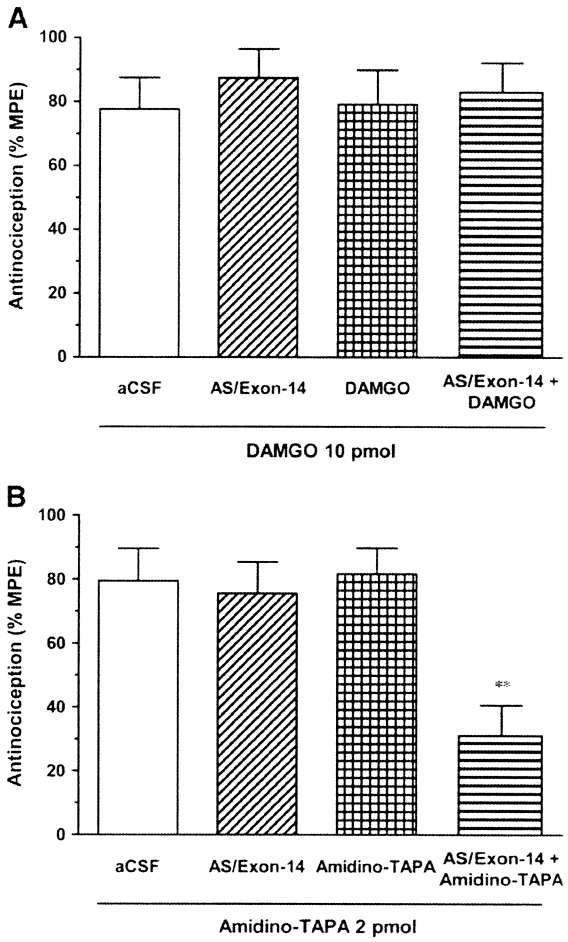


Fig. 6. Effects of an antisense ODN for exon-14 of mMOR-1 on the acute antinociceptive tolerance to DAMGO and amidino-TAPA in the ddY mouse spinal cord. (A) Groups of mice were pretreated i.t. with aCSF, an antisense ODN for exon-14 of mMOR-1 (AS/Exon-14: 5 μg), DAMGO (10 pmol) or DAMGO in combination with AS/Exon-14 24 h before the i.t. treatment with DAMGO (10 pmol), and the tail-flick inhibition induced by DAMGO was measured at 10 min after the treatments. (B) Groups of mice were pretreated i.t. with aCSF, AS/Exon-14 (5 μg), amidino-TAPA (2 pmol) or amidino-TAPA in combination with AS/Exon-14 24 h before the i.t. treatment with amidino-TAPA (2 pmol), and the tail-flick inhibition induced by amidino-TAPA was measured at 10 min after the treatments. The antinociceptive effect was calculated as the mean ± S.E.M for at least 10 mice. The statistical significance of the differences between the groups was assessed with a one-way ANOVA followed by Dunnett's test. (A) The F value of the one-way ANOVA was $F[3,36] = 0.1991$ ($P = 0.8963$). (B) The F value of the one-way ANOVA was $F[3,36] = 6.497$ ($P < 0.01$). $^{**}P < 0.01$ vs. the aCSF-pretreated group.

duration of acute antinociceptive tolerance to opioid receptor agonists is variable depending on the subtype of the opioid receptors. Unlike the μ-opioid receptor agonist DAMGO, the acute antinociceptive tolerance to the δ-opioid receptor agonist [D-Ala^2]deltorphin II and the κ-opioid receptor agonist U-50,488H both peaked at 3–6 h, but disappeared by 12 h and 24 h after the pretreatment, respectively (Narita et al., 1997a; unpublished observation). The development of acute antinociceptive tolerance to δ-opioid receptor agonist is caused by the internalization and degradation of δ-opioid receptors, and the recovery from the acute antinociceptive tolerance is produced by the newly synthesized δ-opioid receptors (Narita et al., 1997a). The duration of the acute antinociceptive tolerance to opioid receptor agonists may depend on the turnover speed of the opioid receptor, which is identical for each opioid receptor subtype. In the present study, the pretreatment with amidino-TAPA did not show any reduction of its antinociceptive effect (acute antinociceptive tolerance) at 3–9 h after the pretreatment. The antinociceptive effect of amidino-TAPA is long-lasting and it takes 2 h to completely return the nociceptive threshold to the baseline level after the treatment. Based on the above evidence, the present results suggest the possibility that the acute antinociceptive tolerance to amidino-TAPA develops rapidly and disappears within 3 h. To investigate this possibility, the acute antinociceptive tolerance to amidino-TAPA at 3 h after the pretreatment was determined under conditions where the new synthesis of most of the mMOR-1 splice variants had been suppressed by the pretreatment with antisense ODN for exon-1 of mMOR-1. Under these conditions, amidino-TAPA showed a marked acute antinociceptive tolerance, suggesting that the acute antinociceptive tolerance to amidino-TAPA developed rapidly and disappeared within 3 h. The suggestion that the duration of acute antinociceptive tolerance to amidino-TAPA is much shorter than that to DAMGO is another piece of evidence to support the hypothesis that amidino-TAPA stimulates different μ-opioid receptors than DAMGO.

By monitoring the recovery from the acute antinociceptive tolerance to DAMGO and amidino-TAPA, the involvement of mMOR-1 splice variants in the acute antinociceptive tolerance to DAMGO or amidino-TAPA was determined using exon-specific antisense ODNs for mMOR-1. In general, the prolonged pretreatment (usually 4 days) with antisense ODNs for opioid receptors is required to desensitize the opioid receptors (Narita et al., 1997b). Because antisense ODNs for the opioid receptor itself do not have any effect on existing opioid receptors on the cell membrane surface, it should take 3–4 days to desensitize existing opioid receptors with endogenous opioid peptides. In fact, a single 24-h pretreatment with an antisense ODN for exon-1 of mMOR-1 did not alter DAMGO-induced antinociception, although a 4-day pretreatment with the same antisense ODN significantly suppressed the DAMGO-induced antinociception (unpublished observation). However, a single 24-h but concomitant pretreatment with an antisense ODN for exon-1 of mMOR-1 and DAMGO suppressed DAMGO-induced antinociception, suggesting that the suppression of the synthesis of new mMOR-1 splice variants containing the sequence encoded by exon-1 can maintain the acute antinociceptive tolerance to DAMGO for 24 h after the pretreatment, which usually disappeared within 5 h after the pretreatment. This is a simple but accurate method for desensitizing a specific subtype of opioid receptor with a single pretreatment. In the present study, the concomitant pretreatment with an antisense ODN for exon-1 of mMOR-1 and amidino-TAPA maintained the acute antinociceptive tolerance to amidino-TAPA for 24 h after the pretreatment, suggesting that the splice variants of mMOR-1 that are desensitized by pretreatment with amidino-TAPA, as well as DAMGO, are the splice variants containing the sequence encoded by exon-1. Most of the splice variants for mMOR-1 identified contain the sequence encoded by exon-1 (Doyle et al., 2007a,b; Kvam et al., 2004; Pan et al., 2001, 2005). Pasternak and his colleagues described the selectivity and intrinsic activity of various μ-opioid receptor agonists for mMOR-1 splice variants containing the sequences encoded by exon-1 (Bolan et al., 2004; Pan et al., 1999, 2000; Pasternak, 2004). However, no remarkable differences in the selectivity and intrinsic activity of any μ-opioid receptor agonists were observed among the mMOR-1 splice variants examined. Therefore, in the present study, we focused on the other mMOR-1 splice variants, MOR-1J, MOR-1K or MOR-1L, which contain the sequence encoded by exon-12, exon-13 or exon-14, respectively. We found that amidino-TAPA-induced antinociception is significantly suppressed by a 24-h concomitant pretreatment with amidino-TAPA and an antisense ODN for either exon-12, exon-13 or exon-14 of mMOR-1. The suppression of the new synthesis of MOR-1J, MOR-1K or MOR-1L can maintain the acute antinociceptive tolerance to amidino-TAPA for 24 h after the pretreatment, suggesting that the splice variants of mMOR-1 desensitized by pretreatment with amidino-TAPA are MOR-1J, MOR-1K and MOR-1L. In contrast, DAMGO-induced antinociception was not affected by a 24-h concomitant pretreatment with DAMGO and an antisense ODN for either exon-12, exon-13 or exon-14 of mMOR-1, suggesting that MOR-1J, MOR-1K and MOR-1L are not the splice variants desensitized by pretreatment with DAMGO. In other words, these splice variants are amidino-TAPA-sensitive and DAMGO-insensitive mMOR-1 splice variants.

At present, the physiological roles of the 33 identified splice variants of mMOR-1 are still unclear. We have previously found that, unlike DAMGO, amidino-TAPA induces the release of the endogenous κ-opioid peptides dynorphin A, dynorphin B and α-neo-endorphin and the endogenous δ-opioid peptide [Leu^5]enkephalin in the spinal cord to produce the antinociception. In the present study, we have identified the amidino-TAPA-sensitive and DAMGO-insensitive mMOR-1 splice variants, MOR-1J, MOR-1K and MOR-1L, in the spinal cord. Together with the previous observations, the present results suggest the possibility that the release of endogenous opioid peptides by amidino-TAPA is mediated by the amidino-TAPA-sensitive and DAMGO-insensitive mMOR-1 splice variants MOR-1J, MOR-1K and MOR-1L.

5. Conclusion

In conclusion, the spinal antinociception of amidino-TAPA is partially mediated through the activation of the distinct mMOR-1 splice variants MOR-1J, MOR-1K or MOR-1L, which contain the sequence encoded by exon-12, exon-13 or exon-14, respectively. These splice variants are amidino-TAPA-sensitive and DAMGO-insensitive mMOR-1 splice variants, which may be responsible for the distinct antinociceptive properties of amidino-TAPA.

Acknowledgements

This work was supported by a Grant-in-Aid for Scientific Research (C) [KAKENHI 21600013 and 22600009] from the Japan Society for the Promotion of Science, and a Matching Fund Subsidy for Private Universities from the Ministry of Education, Culture, Sports, Science, and Technology Japan (2010–2014).

References

Bolan, E.A., Pan, Y.X., Pasternak, G.W., 2004. Functional analysis of MOR-1 splice variants of the mouse mu opioid receptor gene *Oprm*. Synapse 51, 11–18.

Chen, Y., Mestek, A., Liu, J., Hurley, A., Yu, L., 1993. Molecular cloning and functional expression of a μ-opioid receptor from rat brain. Mol. Pharmacol. 44, 8–12.

D'Amour, F.E., Smith, D.L., 1941. A method for determining loss of pain sensation. J. Pharmacol. Exp. Ther. 72, 74–79.

Doyle, G.A., Sheng, X.R., Lin, S.S., Press, D.M., Grice, D.E., Buono, R.J., Ferraro, T.N., Berrettini, W.H., 2007a. Identification of three mouse μ-opioid receptor (MOR) gene (Oprm1) splice variants containing a newly identified alternatively spliced exon. Gene 388, 135–147.

Doyle, G.A., Sheng, X.R., Lin, S.S., Press, D.M., Grice, D.E., Buono, R.J., Ferraro, T.N., Berrettini, W.H., 2007b. Identification of five mouse μ-opioid receptor (MOR) gene (Oprm1) splice variants containing a newly identified alternatively spliced exon. Gene 395, 98–107.

Hylden, J.L., Wilcox, G.L., 1980. Intrathecal morphine in mice: a new technique. Eur. J. Pharmacol. 67, 313–316.

Kvam, T.M., Baar, C., Rakvåg, T.T., Kaasa, S., Krokan, H.E., Skorpen, F., 2004. Genetic analysis of the murine μ opioid receptor: increased complexity of Oprm gene splicing. J. Mol. Med. 82, 250–255.

Mizoguchi, H., Ito, K., Watanabe, H., Watanabe, C., Katsuyama, S., Fujimura, T., Sakurada, T., Sakurada, S., 2006a. Contribution of spinal μ_1-opioid receptors and dynorphin B to the antinociception induced by Tyr-D-Arg-Phe-Sar. Peptides 27, 2786–2793.

Mizoguchi, H., Watanabe, H., Hayashi, T., Sakurada, W., Sawai, T., Fujimura, T., Sakurada, T., Sakurada, S., 2006b. Possible involvement of dynorphin A (1–17) release via μ_1-opioid receptors in spinal antinociception by endomorphin-2. J. Pharmacol. Exp. Ther. 317, 362–368.

Mizoguchi, H., Watanabe, C., Watanabe, H., Moriyama, K., Sato, B., Ohwada, K., Yonezawa, A., Sakurada, T., Sakurada, S., 2007. Involvement of endogenous opioid peptides in the antinociception induced by the novel dermorphin tetrapeptide analog amidino-TAPA. Eur. J. Pharmacol. 560, 150–159.

Narita, M., Narita, M., Mizoguchi, H., Tseng, L.F., 1995. Inhibition of protein kinase C, but not of protein kinase A, blocks the development of acute antinociceptive tolerance to an intrathecally administered μ-opioid receptor agonist in the mouse. Eur. J. Pharmacol. 280, R1–R3.

Narita, M., Mizoguchi, H., Kampine, J.P., Tseng, L.F., 1996. Role of protein kinase C in desensitization of spinal δ-opioid-mediated antinociception in the mouse. Br. J. Pharmacol. 118, 1829–1835.

Narita, M., Mizoguchi, H., Kampine, J.P., Tseng, L.F., 1997a. The effect of pretreatment with a δ_2-opioid receptor antisense oligodeoxynucleotide on the recovery from acute antinociceptive tolerance to δ_2-opioid receptor agonist in the mouse spinal cord. Br. J. Pharmacol. 120, 587–592.

Narita, M., Mizoguchi, H., Nagase, H., Tseng, L.F., 1997b. Use of antisense oligodeoxynucleotide to δ-opioid receptor mRNA in the study of turnover of δ-opioid receptors in the spinal cord of the mouse. Psychopharmacology 133, 347–350.

Ogawa, T., Miyamae, T., Murayama, K., Okuyama, K., Okayama, T., Hagiwara, M., Sakurada, S., Morikawa, T., 2002. Synthesis and structure-activity relationships of an orally available and long-acting analgesic peptide, N^{α}-amidino-Tyr-D-Arg-Phe-MeβAla-OH (ADAMB). J. Med. Chem. 45, 5081–5089.

Pan, Y.X., Xu, J., Bolan, E., Abbadie, C., Chang, A., Zuckerman, A., Rossi, G., Pasternak, G.W., 1999. Identification and characterization of three new alternatively spliced μ-opioid receptor isoforms. Mol. Pharmacol. 56 936-403.

Pan, Y.X., Xu, J., Bolan, E., Chang, A., Mahurter, L.A., Rossi, G., Pasternak, G.W., 2000. Isolation and expression of a novel alternatively spliced mu opioid receptor isoform, MOR-1F. FEBS Lett. 466, 337–340.

Pan, Y.X., Xu, J., Mahurter, L., Bolan, E., Xu, M., Pasternak, G.W., 2001. Generation of the mu opioid receptor (MOR-1) protein by three new splice variants of the Oprm gene. Proc. Natl. Acad. Sci. U.S.A. 98, 14084–14089.

Pan, Y.X., Xu, J., Bolan, E., Moskowitz, H.S., Xu, M., Pasternak, G.W., 2005. Identification of four novel exon 5 splice variants of the mouse μ-opioid receptor gene: functional consequences of C-terminal splicing. Mol. Pharmacol. 68, 866–875.

Pasternak, G.W., 2004. Multiple opiate receptors: déjà vu all over again. Neuropharmacology 47, 312–323.

Sakurada, S., Hayashi, T., Yuhki, M., Orito, T., Zadina, J.E., Kastin, A.J., Fujimura, T., Murayama, K., Sakurada, C., Sakurada, T., Narita, M., Suzuki, T., Tan-no, K., Tseng, L.F., 2001. Differential antinociceptive effects induced by intrathecally administered endomorphin-1 and endomorphin-2 in the mouse. Eur. J. Pharmacol. 427, 203–210.

Suh, H.H., Tseng, L.F., 1990. Lack of antinociceptive cross-tolerance between intracerebroventricularly administered β-endorphin and morphine or DPDPE in mice. Life Sci. 46, 759–765.

Szeto, H.H., Soong, Y., Wu, D., Qian, X., Zhao, G.M., 2003. Endogenous opioid peptides contribute to antinociceptive potency of intrathecal [Dmt[1]]DALDA. J. Pharmacol. Exp. Ther. 305, 696–702.

Wang, J.B., Imai, Y., Eppler, C.M., Gregor, P., Spivak, C.E., Uhl, G.R., 1993. μ Opiate receptor: cDNA cloning and expression. Proc. Natl. Acad. Sci. U.S.A. 90, 10230–10234.

Wu, H.E., Hung, K.C., Mizoguchi, H., Fujimoto, J.M., Tseng, L.F., 2001. Acute antinociceptive tolerance and asymmetric cross-tolerance between endomorphin-1 and endomorphin-2 given intracerebroventricularly in the mouse. J. Pharmacol. Exp. Ther. 299, 1120–1125.

Wu, H.E., Darpolor, M., Nagase, H., Tseng, L.F., 2003. Acute antinociceptive tolerance and partial cross-tolerance to endomorphin-1 and endomorphin-2 given intrathecally in the mouse. Neurosci. Lett. 248, 139–142.

Psychopharmacology (2010) 212:215–225
DOI 10.1007/s00213-010-1946-0

ORIGINAL INVESTIGATION

Lack of a rewarding effect and a locomotor-enhancing effect of the selective μ-opioid receptor agonist amidino-TAPA

Hirokazu Mizoguchi · Chizuko Watanabe · Shin Osada · Maya Yoshioka · Yuta Aoki · Sanae Natsui · Akihiko Yonezawa · Syu-ichi Kanno · Masaaki Ishikawa · Tsukasa Sakurada · Shinobu Sakurada

Received: 14 February 2010 / Accepted: 29 June 2010 / Published online: 4 August 2010
© Springer-Verlag 2010

Abstract
Rationale and objectives Psychological dependence is one of the worst side effects of morphine. It limits the clinical availability of morphine and non-patient morphine users suffer from addiction. An analgesic, which is more potent than morphine but without the liability of psychological dependence, has long been sought in the clinic. We have recently developed a new μ-opioid receptor agonist, N^{α}-amidino-Tyr-D-Arg-Phe-β-Ala (amidino-TAPA), as a potent analgesic with an antinociceptive profile that is distinct from morphine, including the release of endogenous κ-opioid peptides. The activation of κ-opioid receptors has been suggested to suppress the development of psychological dependence by μ-opioid receptor agonists. In the present study, the psychological dependence liability and the related locomotor-enhancing effect of amidino-TAPA were evaluated.

Results Amidino-TAPA injected subcutaneously produced an extremely potent and longer lasting antinociception than morphine in ddY mice, prodynorphin-knockout mice, and wild-type C57BL/6J mice. Unlike subcutaneously injected morphine, which had potent locomotor-enhancing and rewarding effects at antinociceptive doses in ddY mice, amidino-TAPA injected subcutaneously did not induce significant locomotor-enhancing and rewarding effects at antinociceptive or even higher doses in ddY mice. In wild-type C57BL/6J mice, amidino-TAPA showed the same pharmacological profile (potent antinociception, lack of locomotor-enhancing and rewarding effects) as in ddY mice. However, amidino-TAPA produced potent locomotor-enhancing and rewarding effects at antinociceptive doses in prodynorphin-knockout mice.
Conclusions The present results suggest that amidino-TAPA is a potent analgesic without the liability of psychological dependence because it releases endogenous κ-opioid peptides.

Keywords Antinociception · Psychological dependence · Peptides · μ-Opioid receptor · κ-Opioid receptor · Transmitter release

H. Mizoguchi · C. Watanabe · S. Osada · M. Yoshioka · Y. Aoki · S. Natsui · A. Yonezawa · S. Sakurada (✉)
Department of Physiology and Anatomy, Tohoku Pharmaceutical University,
4-4-1 Komatsushima, Aoba-ku,
Sendai 981-8558, Japan
e-mail: s-sakura@tohoku-pharm.ac.jp

S.-i. Kanno · M. Ishikawa
Department of Clinical Pharmacotherapeutics, Tohoku Pharmaceutical University,
4-4-1 Komatsushima, Aoba-ku,
Sendai 981-8558, Japan

T. Sakurada
First Department of Pharmacology, Daiichi College of Pharmaceutical Sciences,
22-1 Tamagawa-cho, Minami-ku,
Fukuoka 815-8511, Japan

Introduction

N^{α}-amidino-Tyr-D-Arg-Phe-β-Ala (amidino-TAPA) is an N-terminal tetrapeptide analog of dermorphin (Tyr-D-Ala-Phe-Gly-Tyr-Pro-Ser-NH_2). Because of its high affinity and selectivity for μ-opioid receptors, amidino-TAPA produces an extreme potent and long-lasting antinociception in mice (Ogawa et al. 2002a, b; Mizoguchi et al. 2007). Its potency for antinociception in mice is approximately 10 times and 400 times higher than that of morphine by the subcutaneous (s.c.) and intrathecal injection routes, respectively

(Mizoguchi et al. 2007; Ogawa et al. 2002a, b; Sato et al. 1999). Unlike most peptidic analgesics, which are generally ineffective by oral administration, amidino-TAPA is effective for antinociception by oral administration with a slightly higher potency than morphine (Ogawa et al. 2002a, b). Interestingly, amidino-TAPA has an antinociceptive mechanism in the spinal cord that is distinct from the traditional μ-opioid receptor agonist [D-Ala^2-N-Me-Phe^4, Gly-ol^5]-enkephalin (DAMGO) (Mizoguchi et al. 2007). Unlike DAMGO, the antinociception induced by amidino-TAPA is mediated through the release in the spinal cord of the endogenous κ-opioid peptides dynorphin A, dynorphin B, and α-neo-endorphin and the endogenous δ-opioid peptide [Leu^5]enkephalin, which are released by the activation of μ-opioid receptors.

Psychological dependence is one of the major side effects of narcotic analgesics, such as morphine, and it limits distribution and clinical applications of narcotic analgesics. The development of psychological dependence on narcotic analgesics is generally induced by the repeated reinforcement of their rewarding effect via μ-opioid receptors (Herz and Spanagel 1995). It is well known that the rewarding effect of μ-opioid receptor agonists is mediated by the disinhibition of mesolimbic dopaminergic neurons, which projects from the ventral tegmental area to the nucleus accumbens (Spanagel et al. 1992). The activation of μ-opioid receptors located on the γ-aminobutyric acid (GABA)ergic neurons in the ventral tegmental area by μ-opioid receptor agonists causes the reduction of GABA release in this area, which subsequently induces the disinhibition of mesolimbic dopaminergic neurons and the enhancement of dopamine release from these neurons in the nucleus accumbens (Johnson and North 1992a). On the terminal of these mesolimbic dopaminergic neurons in the nucleus accumbens, dynorphinergic nerve fibers that inhibit the release of dopamine are localized (Spanagel et al. 1990, 1992). Therefore, the activation of κ-opioid receptors suppresses the development of psychological dependence to μ-opioid receptor agonists (Funada et al. 1993). Interestingly, the same type of neuronal network regulates the nigrostriatal dopaminergic neurons, which project from the substantia nigra to the striatum (Enrico et al. 1998). By the same mechanism as the mesolimbic dopaminergic neurons, the activation of μ-opioid receptors by μ-opioid receptor agonists in the substantia nigra promotes disinhibition of nigrostriatal dopaminergic neuron and increases the release of dopamine in the striatum, which results in enhancement of locomotor activity (Johnson and North 1992b). Like the rewarding effect in the nucleus accumbens, the locomotor-enhancing effect of μ-opioid receptor agonists is also regulated by the inhibitory neurons of the κ-opioid system in the striatum (Narita et al. 1993).

We have recently developed amidino-TAPA as a new analgesic that has a pharmacological profile that is distinct from the traditional μ-opioid receptor agonists, including the release of endogenous κ-opioid peptides. The evidence strongly suggests that amidino-TAPA has less psychological dependence liability. In the present study, the rewarding and locomotor-enhancing effects of amidino-TAPA injected s.c. were evaluated in mice.

Materials and methods

All experiments were performed following the approval of the Ethics Committee for Animal Experiments at Tohoku Pharmaceutical University and according to the National Institutes of Health Guide for the Care and Use of Laboratory Animals. Every effort was made to minimize the number and any suffering of the animals used in the following experiments.

Animals

Male ddY mice (Japan SLC, Hamamatsu, Japan), C57BL/6J mice (The Jackson Laboratory, Bar Harbor, ME, USA), and prodynorphin-knockout mice (B6.129S4-Pdyn^{tm1Ute}; The Jackson Laboratory) weighing 22–25 g were used. The prodynorphin-knockout mice, which originated on a B6/129 (C57BL/6J × 129S6/SvEvTac) background, have been backcrossed for eight generation onto the C57BL/6J background by the supplier. Therefore, C57BL/6J mice were used as the wild-type mice for the prodynorphin-knockout mice. The deletion of the prodynorphin gene in the prodynorphin-knockout mice was confirmed with the polymerase chain reaction before they were used. The animals were housed in a room maintained at 22–23°C and 50–60% relative humidity with an alternating 12-h light/dark cycle. Food and water were available ad libitum. Mice were used only once.

Antinociception

Antinociception was determined with the thermal tail-flick test (D'Amour and Smith 1941). For measurement of the latency of the tail-flick response, mice were gently held by hand with their tail positioned in an apparatus (Ugo Basile, Italy) for radiant heat stimulation on the ventral surface of the tail. The intensity of the heat stimulus was adjusted so that the animal withdrew its tail after 2.5–3.5 s. The inhibition of the tail-flick response was expressed as the percent maximal possible effect, %MPE, which was calculated as follows: $[(T_1-T_0)/(T_2-T_0)]\times 100$, where T_0 and T_1 are the tail-flick latencies before and after the treatments, respectively, and T_2 is the cutoff time, set at 10 s to avoid injury to the tail. The antinociceptive effect was

represented as the mean±SEM for at least 10 mice. The dose–response curves and ED_{50} values with their 95% confidence intervals were calculated with a computer-associated curve-fitting program (GraphPad Prism; GraphPad Software, Inc., San Diego, CA, USA).

Conditioned place preference

The conditioned place preference (CPP) test was conducted by the method of Bardo et al. (1984) with a minor modification (Suzuki et al. 1999). The apparatus consisted of a shuttle box (15 cm wide×30 cm long×15 cm high), which was made of acrylic resin board and divided into two equal-sized compartments. One compartment was white with a textured floor, and the other was black with a smooth floor to create equally preferred compartments. The pre-conditioning test and the post-conditioning test were performed as follows: the partition separating the two compartments was raised to 7 cm above the floor, a neutral platform was inserted along the seam separating the compartments, and mice that had not been treated with either drugs or saline were then placed on the platform. The time spent in each compartment during a 900-s session was recorded automatically using an infrared sensor beam (KN-80, Natsume Seisakusyo Co., Tokyo, Japan). Twelve mice in each group were used for the pre-conditioning test, and eight mice in each group, which had no strong preference (less than 100 s more time spent in one compartment than the other) for either the white or black compartment, were selected for the conditioning session. The mice used in the conditioning session, spent 446.4±15.41 s in the white compartment and 453.6±15.47 s in the black compartment in the pre-conditioning test. Groups of mice were allocated to their respective conditioning compartments based on their pre-conditioning test data, and conditioning sessions (three for drug and three for saline) were conducted once per day for 6 days. Immediately after the s.c. treatment with morphine or saline, or 60 min after the s.c. treatment with amidino-TAPA or saline, these animals were placed for 1 h in the compartment opposite to that in which they had spent more time during the pre-conditioning test. On alternate days, these animals received saline or drugs and then were placed in the other compartment for 1 h. On day 7, the post-conditioning test was performed. The CPP score represents the time spent in the drug-conditioned compartment minus that spent in the saline-conditioned compartment. All sessions were conducted under conditions of dim illumination (200 lx lamp) and white masking noise.

Locomotor activity

The locomotor activity of mice was measured with an activity monitoring system (NS-AS01; Neuroscience Inc., Tokyo, Japan). Briefly, the activity monitor was composed of an infrared ray sensor place over an open-top box (34.5 cm wide×40.3 cm long×17.7 cm high), a single amplification circuit, and a control circuit. The sensor can detect the movement of animals on the basis of released infrared rays associated with their body temperature. Counts of locomotor activity were collected in 10-min intervals for 3 h before treatment for habituation and for 3 or 6 h after the treatment with morphine or amidino-TAPA, respectively. The data were analyzed with a computer-associated analyzing system (Multidigital 32-port Counter System; Neuroscience Inc.)

Drugs

The drugs used were amidino-TAPA (Peptide Institute, Osaka, Japan), morphine hydrochloride (Sankyo, Tokyo, Japan), and naloxone hydrochloride (Sigma-Aldrich, St. Louis, MO, USA).

Statistical analyses

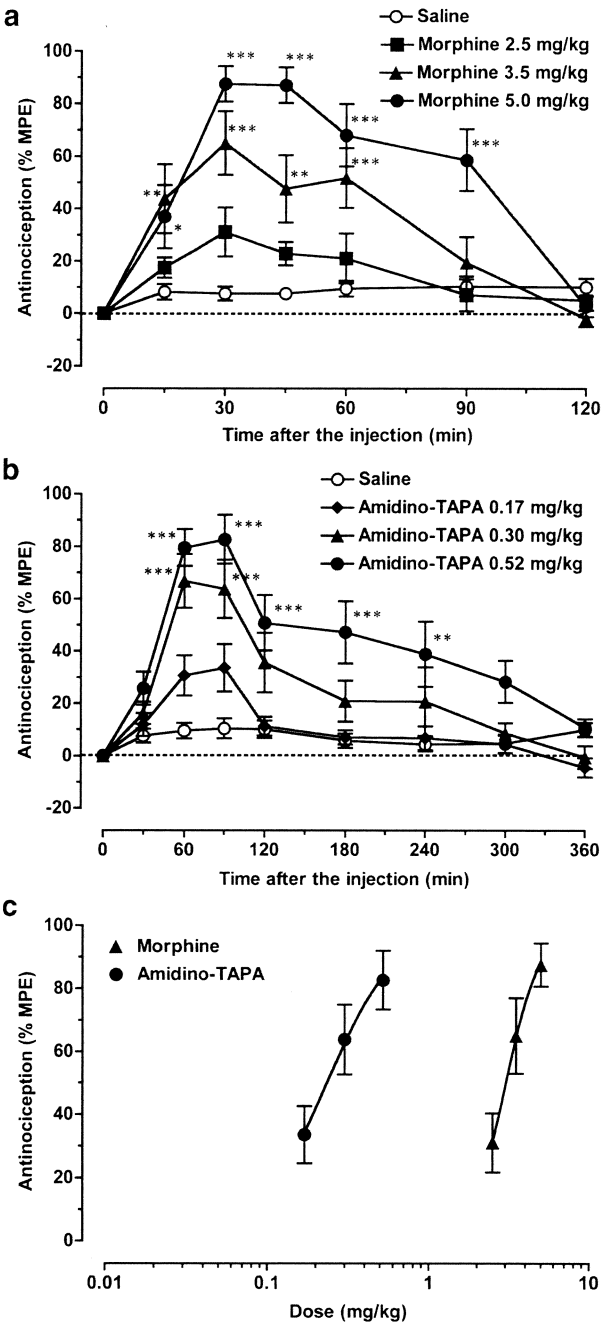
The statistical significance of differences between the groups was assessed with a one-way analysis of variance (ANOVA) followed by Dunnett's test or with a two-way ANOVA followed by Bonferroni's test.

Results

The antinociceptions induced by morphine and amidino-TAPA

Groups of ddY mice were injected s.c. with saline, morphine (2.5–5.0 mg/kg), or amidino-TAPA (0.17–0.52 mg/kg), and the inhibition of the tail-flick response induced by morphine or amidino-TAPA was measured. The s.c. administration of morphine or amidino-TAPA resulted in a dose-dependent antinociception (Fig. 1a, b). The antinociceptive effect of amidino-TAPA started 30 min after the treatment, reached its maximal effect at 90 min, and then disappeared slowly by 360 min. The antinociceptive effect of amidino-TAPA was more prolonged than that of morphine, which disappeared by 120 min after the treatment. The ED_{50} values of morphine and amidino-TAPA for antinociception at the peak-effect time were 3.028 and 0.2336 mg/kg, respectively (Fig. 1c). The antinociceptive effect of amidino-TAPA was approximately 13 times more potent than that of morphine in ddY mice.

We previously reported that intrathecally administered amidino-TAPA causes the release of the endogenous κ-opioid peptides dynorphin A, dynorphin B, or α-neo-endorphin in the spinal cord to produce the antinociception



◀ **Fig. 1** Antinociceptive effects of morphine and amidino-TAPA in ddY mice. Groups of mice were injected s.c. with saline, morphine (**a** 2.5–5.0 mg/kg), or amidino-TAPA (**b** 0.17–0.52 mg/kg), and inhibition of the tail-flick response induced by morphine or amidino-TAPA was measured for 120 or 360 min. The antinociceptive effect was represented as the mean±SEM for at least 10 mice. The statistical significance of the differences between the groups was assessed with a two-way ANOVA followed by Bonferroni's test. The dose–response curves and ED_{50} values with their 95% confidence intervals (**c**) for morphine and amidino-TAPA at their peak-effect time were calculated with GraphPad Prism, a computer-associated curve-fitting program. **a** The F value of the two-way ANOVA for morphine was $F[3, 252]=42.37$ ($p<0.001$). $^{*}p<0.05$, $^{**}p<0.01$, $^{***}p<0.001$ vs. the saline-treated group. **b** The F value of the two-way ANOVA for amidino-TAPA was $F[3, 324]=46.66$ ($p<0.001$). $^{**}p<0.01$, $^{***}p<0.001$ vs. the saline-treated group. **c** The ED_{50} values for morphine and amidino-TAPA with their 95% confidence intervals were 3.028 (2.692–3.406) and 0.2336 (0.1692–0.3226) mg/kg, respectively

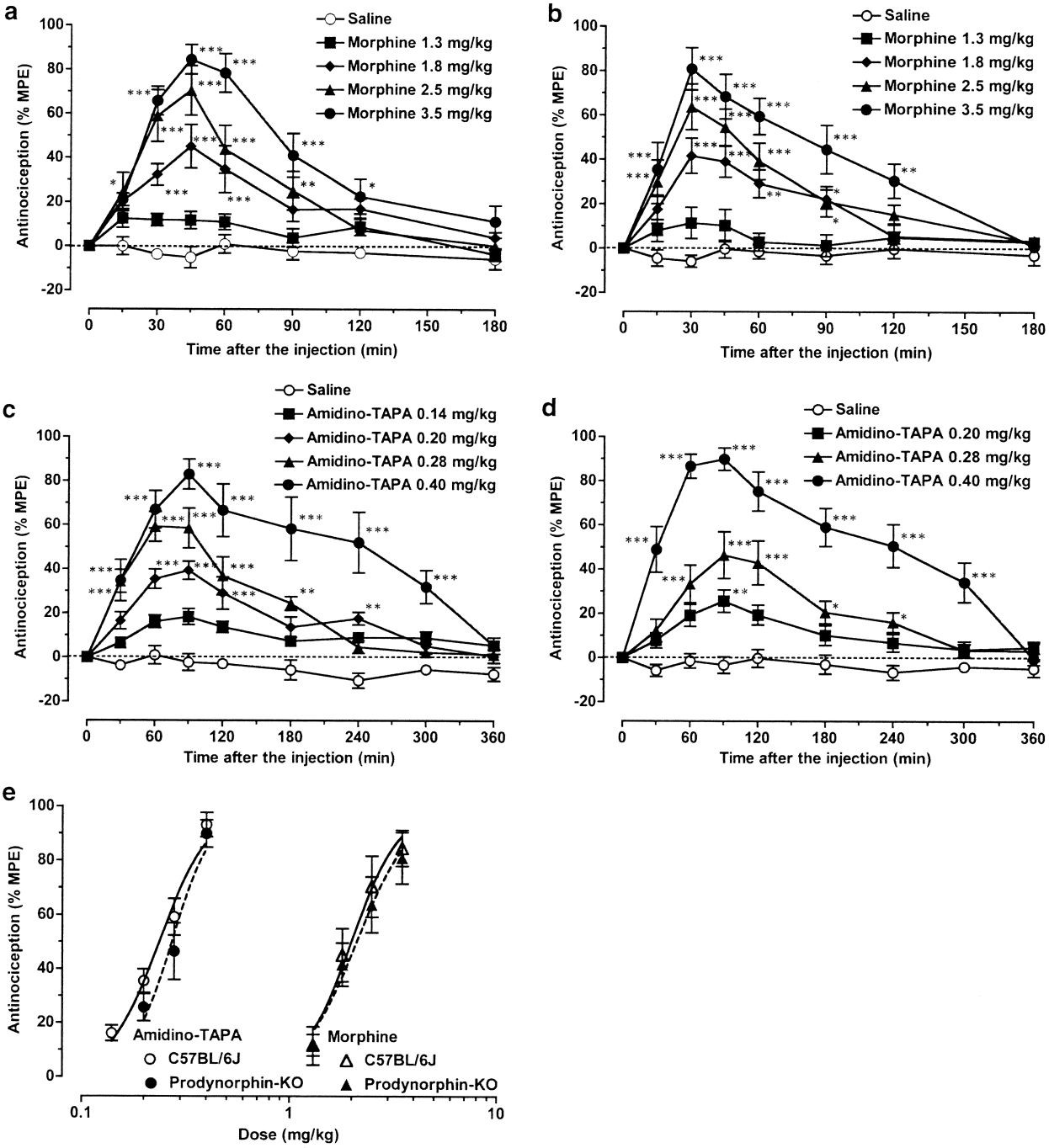
(Mizoguchi et al. 2007). To elucidate the involvement of endogenous κ-opioid peptides in the antinociception induced by s.c.-administered amidino-TAPA, prodynorphin-knockout mice, which lack the precursor for the endogenous κ-opioid peptides, and wild-type C57BL/6J mice were used. Groups of C57BL/6J mice and prodynorphin-knockout mice were injected s.c. with saline, morphine (1.3–3.5 mg/kg), or amidino-TAPA (0.14–0.40 mg/kg), and the inhibition of the tail-flick response induced by morphine or amidino-TAPA was measured. In both C57BL/6J mice and prodynorphin-knockout mice, the s.c.-administered morphine or amidino-TAPA resulted in a dose-dependent antinociception with the same antinociceptive profiles observed in ddY mice (Fig. 2a–d). The ED_{50} value of morphine in C57BL/6J mice and prodynorphin-knockout mice for antinociception at the peak-effect time was 1.992 and 2.116 mg/kg, respectively,

Fig. 2 Antinociceptive effects of morphine and amidino-TAPA in ▶ C57BL/6J mice and prodynorphin-knockout mice. Groups of C57BL/6J mice (**a** and **c**) and prodynorphin-knockout mice (**b** and **d**) were injected s.c. with saline, morphine (**a** and **b** 1.3–3.5 mg/kg), or amidino-TAPA (**c** and **d** 0.14–0.40 mg/kg), and inhibition of the tail-flick response induced by morphine or amidino-TAPA was measured for 180 and 360 min. The antinociceptive effect was represented as the mean±SEM for at least 10 mice. The statistical significance of the differences between the groups was assessed with a two-way ANOVA followed by Bonferroni's test. The dose–response curves and ED_{50} values with their 95% confidence intervals (**e**) for morphine and amidino-TAPA at their peak-effect time were calculated with GraphPad Prism, a computer-associated curve-fitting program. **a** The F value of the two-way ANOVA for morphine in C57BL/6J mice was $F[4, 360]=65.54$ ($p<0.001$). $^{*}p<0.05$, $^{**}p<0.01$, $^{***}p<0.001$ vs. the saline-treated group. **b** The F value of the two-way ANOVA for morphine in prodynorphin-knockout mice was $F[4, 360]=61.43$ ($p<0.001$). $^{*}p<0.05$, $^{**}p<0.01$, $^{***}p<0.001$ vs. the saline-treated group. **c** The F value of the two-way ANOVA for amidino-TAPA in C57BL/6J mice was $F[4, 405]=96.35$ ($p<0.001$). $^{**}p<0.01$, $^{***}p<0.001$ vs. the saline-treated group. **d** The F value of the two-way ANOVA for amidino-TAPA in prodynorphin-knockout mice was $F[3, 324]=145.5$ ($p<0.001$). $^{*}p<0.05$, $^{**}p<0.01$, $^{***}p<0.001$ vs. the saline-treated group. **e** The ED_{50} values for morphine with its 95% confidence interval in C57BL/6J mice and prodynorphin-knockout mice were 1.992 (1.655–2.399) and 2.116 (1.756–2.548) mg/kg, respectively. The ED_{50} values for amidino-TAPA with its 95% confidence intervals in C57BL/6J mice and prodynorphin-knockout mice were 0.2374 (0.1926–0.2926) and 0.2727 (0.1112–0.6688) mg/kg, respectively

whereas the ED_{50} value of amidino-TAPA in C57BL/6J mice and prodynorphin-knockout mice for antinociception at the peak-effect time was 0.2374 and 0.2727 mg/kg, respectively (Fig. 2e). The antinociceptive effects of both morphine and amidino-TAPA were equipotent in C57BL/6J mice and prodynorphin-knockout mice.

Rewarding effect of morphine and amidino-TAPA

The rewarding effects of morphine and amidino-TAPA were evaluated with the CPP test in ddY mice. Groups of ddY mice were conditioned for 6 days to the black and white compartments with saline, morphine (1.3–5.0 mg/kg, s.c.),



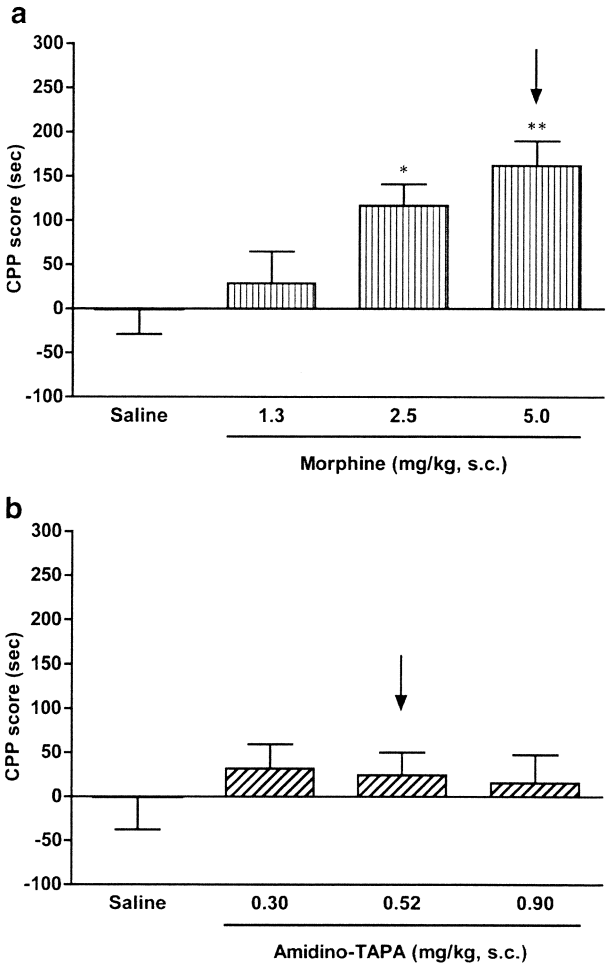


Fig. 3 Rewarding effects of morphine and amidino-TAPA on conditioned place preference (*CPP*) in ddY mice. In conditioning sessions (three for drug and three for saline), groups of mice were conditioned to the black and white compartments for 1 h with saline and various s.c. doses of morphine (**a** 1.3–5.0 mg/kg) or amidino-TAPA (**b** 0.30–0.90 mg/kg). During the test session, the time spent in each compartment during a 900-s session was recorded without any injection. The rewarding effect of morphine or amidino-TAPA is represented as the CPP score, which is the time spent in the drug-conditioned compartment minus the time spent in the saline-conditioned compartment. The *arrows* indicate the doses that show an 80–90% antinociception. *Each column* represents the mean±SEM for 7–16 mice. The statistical significance of the differences between the groups was assessed with a one-way ANOVA followed by the Dunnett's test. **a** The F value of the one-way ANOVA for morphine was $F[3, 35]=5.807$ ($p<0.01$). $*p<0.05$, $**p<0.01$ vs. the saline-conditioned group. **b** The F value of the one-way ANOVA for amidino-TAPA was $F[3, 36]=0.1839$ ($p=0.9066$)

or amidino-TAPA (0.30–0.90 mg/kg, s.c.), and on day 7, the greater (or less) amount of time spent in drug-conditioned compartment than saline-conditioned compartment during a 900-s test session without any injection was recorded as the CPP score. Morphine resulted in a dose-dependent increase in the CPP score and showed a significant CPP score compared to saline at an 80–90% analgesic dose (5 mg/kg), which is indicated by an arrow (Fig. 3a). On the contrary, amidino-TAPA did not show a significant CPP score at an 80–90% analgesic dose (0.52 mg/kg) or even at higher doses (Fig. 3b).

To elucidate the involvement of endogenous κ-opioid peptides in the lack of a rewarding effect of s.c.-administered amidino-TAPA, prodynorphin-knockout mice and C57BL/6J mice were used for the CPP test. In both C57BL/6J mice and prodynorphin-knockout mice, morphine resulted in a dose-dependent increase in the CPP score and showed a significant CPP score at an 80–90% analgesic dose (3.5 mg/kg), as observed in ddY mice (Fig. 4a, b). In prodynorphin-knockout mice, the morphine (3.5 mg/kg)-induced significant CPP score was completely eliminated by the concomitant administration of the μ-opioid receptor antagonist naloxone (0.5 mg/kg), which did not show any effect on the CPP score by itself (Fig. 4b). In C57BL/6J mice, amidino-TAPA did not show a significant CPP score at an 80–90% analgesic dose (0.4 mg/kg) or even at higher doses, as observed in ddY mice (Fig. 4c). However, amidino-TAPA caused a dose-dependent increase in the CPP score in prodynorphin-knockout mice and showed a significant CPP score at an 80–90% analgesic dose (0.4 mg/kg) and at higher doses (Fig. 4d). The amidino-TAPA (0.8 mg/kg)-induced significant CPP score in prodynorphin-knockout mice was completely eliminated by the concomitant administration of naloxone (0.5 mg/kg).

Locomotor-enhancing effect of morphine and amidino-TAPA

Groups of ddY mice were injected s.c. with saline, morphine (2.5–5.0 mg/kg), or amidino-TAPA (0.30–0.90 mg/kg), and the locomotor activity was measured for 180 or 360 min. Morphine increased the locomotor activity in a dose-dependent manner and showed a significant locomotor enhancement at an 80–90% analgesic dose (5 mg/kg), which is indicated by an arrow (Fig. 5a). On the contrary, amidino-TAPA did not increase locomotor activity at an 80–90% analgesic dose (0.52 mg/kg) or even at higher doses (Fig. 5b).

To elucidate the involvement of endogenous κ-opioid peptides in the lack of a locomotor-enhancing effect of s.c.-administered amidino-TAPA, prodynorphin-knockout mice and C57BL/6J mice were used. In both C57BL/6J mice and prodynorphin-knockout mice, morphine increased the locomotor activity in a dose-dependent manner and showed a significant locomotor enhancement at 5.0 mg/kg, which is a 1.4-fold higher dose than an 80–90% analgesic dose (Fig. 6a, b). In prodynorphin-knockout mice, morphine (5.0 mg/kg)-induced locomotor enhancement was completely eliminated by concomitant administration of nalox-

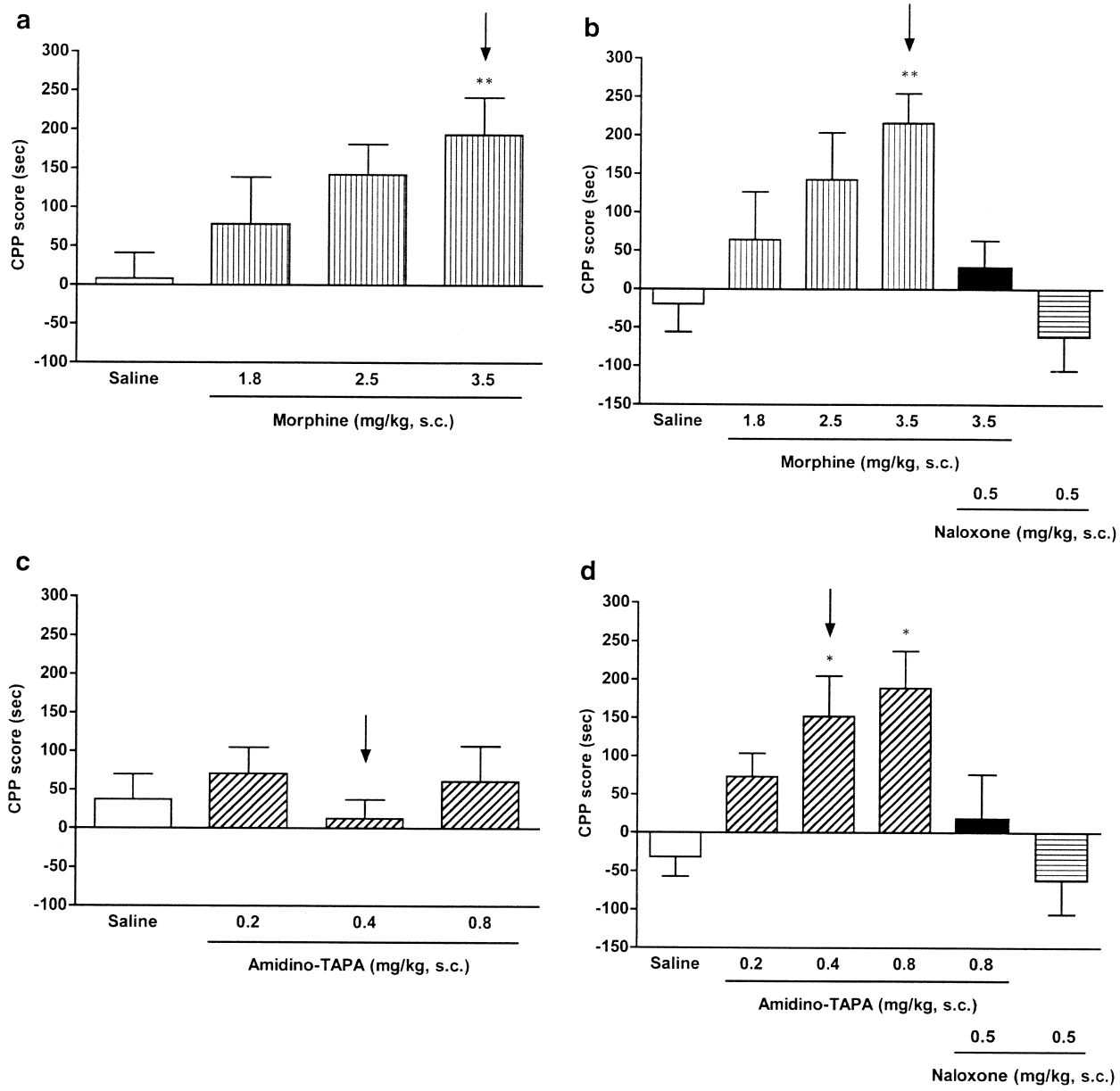


Fig. 4 Rewarding effects of morphine and amidino-TAPA on conditioned place preference (*CPP*) in C57BL/6J mice and prodynorphin-knockout mice. During conditioning sessions (three for drug and three for saline), groups of C57BL/6J mice (**a** and **c**) and prodynorphin-knockout mice (**b** and **d**) were conditioned to the black and white compartments for 1 h with saline and various s.c. doses of morphine (**a** and **b** 1.8–3.5 mg/kg) or amidino-TAPA (**c** and **d** 0.2–0.8 mg/kg). Naloxone (0.5 mg/kg) was concomitantly administered s.c. with saline, morphine, or amidino-TAPA. On the test session, the time spent in each compartment during a 900-s session was recorded without any injection. The rewarding effect of morphine or amidino-TAPA is represented as the CPP score, which is the time spent in the drug-conditioned compartment minus the time spent in the saline-conditioned compartment. The *arrows* indicate the doses that show an 80–90% antinociception. *Each column* represents the mean±SEM for 7–16 mice. The statistical significance of the differences between the groups was assessed with a one-way ANOVA followed by the Dunnett's test. **a** The F value of the one-way ANOVA for morphine in C57BL/6J mice was $F[3, 36]=3.817$ ($p<0.05$). $^{**}p<0.01$ vs. the saline-conditioned group. **b** The F value of the one-way ANOVA for morphine in prodynorphin-knockout mice was $F[5, 63]=4.702$ ($p<0.01$). $^{**}p<0.01$ vs. the saline-conditioned group. **c** The F value of the one-way ANOVA for amidino-TAPA in C57BL/6J mice was $F[3, 26]=0.5052$ ($p=0.6821$). **d** The F value of the one-way ANOVA for amidino-TAPA in prodynorphin-knockout mice was $F[5, 62]=3.905$ ($p<0.01$). $^{*}p<0.05$ vs. the saline-conditioned group

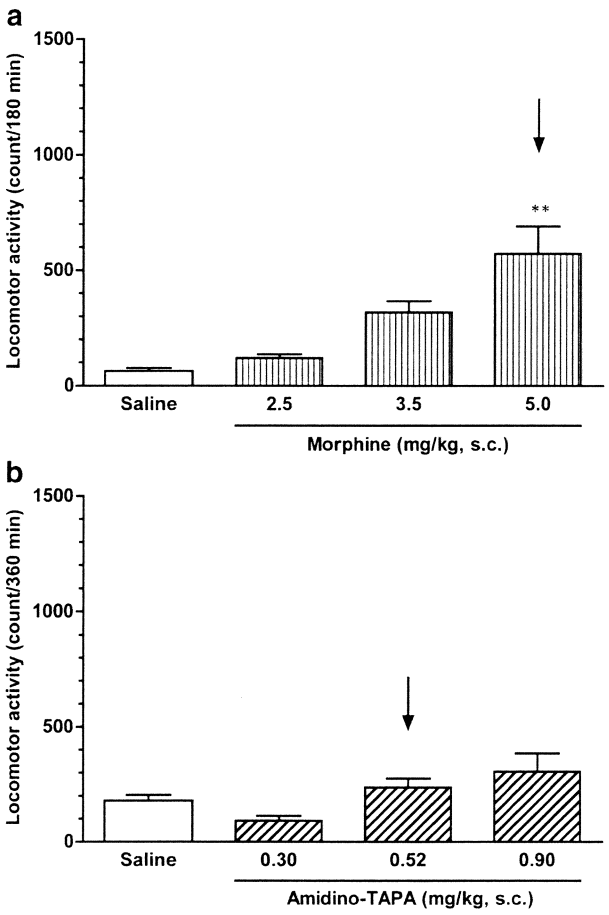


Fig. 5 Locomotor-enhancing effects of morphine and amidino-TAPA in ddY mice. Groups of mice were injected s.c. with saline, morphine (**a** 2.5–5.0 mg/kg), or amidino-TAPA (**b** 0.30–0.90 mg/kg), and the locomotor activity was measured for 180 or 360 min. The *arrows* indicate the doses that show an 80–90% antinociception. *Each column* represents the mean±SEM for at least 10 mice. The statistical significance of the differences between the groups was assessed with a one-way ANOVA followed by Dunnett's test. **a** The F value of the one-way ANOVA for morphine was $F[3, 46]=6.383$ ($p<0.01$). $^{**}p<0.01$ vs. the saline-treated group. **b** The F value of the one-way ANOVA for amidino-TAPA was $F[3, 35]=3.597$ ($p<0.05$)

one (0.5 mg/kg), which did not show any effect on locomotor activity by itself (Fig. 6b). In C57BL/6J mice, amidino-TAPA did not increase locomotor activity at doses up to 0.80 mg/kg, which is a 2-fold higher dose than an 80–90% analgesic dose (Fig. 6c). However, amidino-TAPA increased locomotor activity in a dose-dependent manner in prodynorphin-knockout mice and showed a significant locomotor enhancement at 0.80 mg/kg (Fig. 6d). Amidino-TAPA (0.80 mg/kg)-induced locomotor enhancement in prodynorphin-knockout mice was completely eliminated by concomitant administration of naloxone (0.5 mg/kg).

Discussion

The μ-opioid receptor agonists that are commonly used in the clinic as narcotic analgesics have both potent analgesic and rewarding effects. Since the rewarding effect as well as the analgesic effect of narcotic analgesics is mediated through μ-opioid receptors (Herz and Spanagel 1995), there are currently no opioid analgesics available in the clinic that have high potency and efficacy for antinociception without a rewarding effect. Amidino-TAPA is a selective μ-opioid receptor agonist that we have recently developed as a new peptidic analgesic (Ogawa et al. 2002a, b; Mizoguchi et al. 2007). In the present study, amidino-TAPA injected s.c. was approximately 13 times more potent than morphine in a behavioral assay for antinociception. Generally, peptidic analgesics are ineffective after peripheral injection because they are rapidly degraded by enzymes and penetrate poorly into the central nervous system through the blood–brain barrier. However, unlike other peptidic analgesics, amidino-TAPA is very resistant to enzymatic degradation and is transported into the central nervous system through the blood–brain barrier via the adsorption-mediated endocytosis system (Deguchi et al. 2004). The distinct pharmacokinetic profile of amidino-TAPA could lead to extremely potent antinociception after peripheral injection. It should be noted from the present study that unlike morphine, which showed remarkable rewarding and locomotor-enhancing effects at analgesic doses, amidino-TAPA injected s.c. did not show any rewarding effect or locomotor-enhancing effect at analgesic or even higher doses. We have previously reported that the endogenous μ-opioid peptide endomorphin-2 injected intracerebroventricularly showed a potent antinociceptive effect without a rewarding effect (Tseng et al. 2000; Narita et al. 2001). However, endomorphin-2 is ineffective via peripheral injection routes. Therefore, the present study suggests that amidino-TAPA is the first μ-opioid receptor agonist, which lacks the rewarding effect, but is effective after peripheral injection.

As we reported previously, amidino-TAPA has a pharmacological profile that is distinct from the traditional μ-opioid receptor agonists, including the release of endogenous κ-opioid peptides via activation of μ-opioid receptors (Mizoguchi et al. 2007). The activation of κ-opioid receptors is well known to suppress the development of psychological dependence on and the locomotor-enhancing effect of μ-opioid receptor agonists (Funada et al. 1993; Narita et al. 1993). In fact, endomorphin-2 given intracerebroventricularly, which causes the release of dynorphin A via activation of μ-opioid receptors at a supraspinal site (Tseng et al. 2000; Sakurada et al. 2008), does not show a remarkable rewarding effect, but produces a prominent aversive effect rather than a rewarding effect (Narita et al. 2001; Wu et al. 2004). The activation of κ-

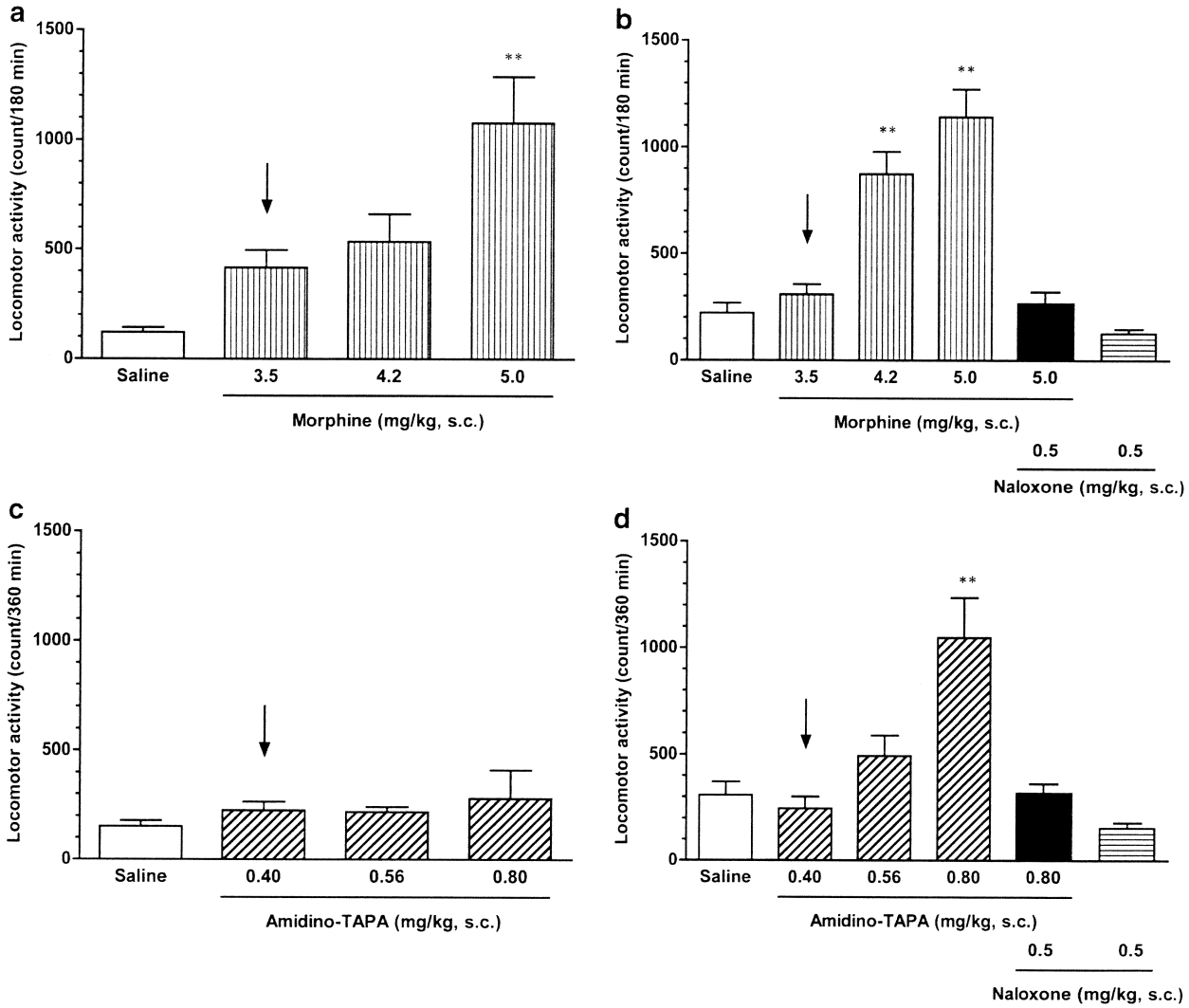


Fig. 6 Locomotor-enhancing effects of morphine and amidino-TAPA in C57BL/6J mice and prodynorphin-knockout mice. Groups of C57BL/6J mice (**a** and **c**) and prodynorphin-knockout mice (**b** and **d**) were injected s.c. with saline, morphine (**a** and **b** 3.5–5.0 mg/kg), or amidino-TAPA (**c** and **d** 0.40–0.80 mg/kg), and the locomotor activity was measured for 180 or 360 min. Naloxone (0.5 mg/kg) was concomitantly administered s.c. with saline, morphine, or amidino-TAPA. The *arrows* indicate the doses that show an 80–90% antinociception. *Each column* represents the mean±SEM for at least 10 mice. The statistical significance of the differences between the groups was assessed with a one-way ANOVA followed by Dunnett's test. **a** The F value of the one-way ANOVA for morphine in C57BL/6J mice was $F[3, 36]=9.558$ ($p<0.001$). $^{**}p<0.01$ vs. the saline-treated group. **b** The F value of the one-way ANOVA for morphine in prodynorphin-knockout mice was $F[5, 54]=28.54$ ($p<0.001$). $^{**}p<0.01$ vs. the saline-treated group. **c** The F value of the one-way ANOVA for amidino-TAPA in C57BL/6J mice was $F[3, 36]=0.5544$ ($p=0.6485$). **d** The F value of the one-way ANOVA for amidino-TAPA in prodynorphin-knockout mice was $F[5, 54]=11.68$ ($p<0.001$). $^{**}p<0.01$ vs. the saline-treated group

opioid receptors by dynorphins or other κ-opioid receptor agonists in the nucleus accumbens leads to the decreased release of dopamine from the mesolimbic dopaminergic neuron and shows an aversive effect (Spanagel et al. 1992). Indeed, the endomorphin-2-induced aversive effect was completely suppressed by a κ-opioid receptor antagonist or an antiserum against dynorphin A (Narita et al. 2001; Wu et al. 2004). Moreover, the aversive effect of endomorphin-2 microinjected into the nucleus accumbens shell was completely suppressed by co-microinjection of the μ-opioid receptor antagonist CTOP (D-Phe-Cys-Tyr-D-Trp-Orn-Thr-Pen-Thr-NH_2) or antiserum against dynorphin A (Terashvili et al. 2004). The evidence clearly suggests that increased release of dynorphin A via activation of μ-opioid receptors in the

nucleus accumbens is involved in the aversive effect (or lack of the remarkable rewarding effect) of endomorphin-2. The lack of the rewarding effect of amidino-TAPA observed in the present study may be mediated by the same mechanism as for endomorphin-2. Therefore, in the present study, to confirm the involvement of endogenous κ-opioid peptides in the lack of a rewarding effect and a locomotor-enhancing effect of amidino-TAPA, prodynorphin-knockout mice, which lack the prodynorphin gene (Sharifi et al. 2001), were used. In the prodynorphin-knockout mice, amidino-TAPA produced remarkable rewarding and locomotor-enhancing effects at doses of amidino-TAPA that did not show any rewarding effect or locomotor-enhancing effect in wild-type C57BL/6J mice. The rewarding and locomotor-enhancing effects of amidino-TAPA observed in prodynorphin-knockout mice were completely abolished by the μ-opioid receptor antagonist naloxone. The evidence clearly suggests that although the selective μ-opioid receptor agonist amidino-TAPA has rewarding and locomotor-enhancing effects by stimulating μ-opioid receptors, the distinct pharmacological effect of amidino-TAPA, i.e., the release of endogenous κ-opioid peptides, may block its rewarding effect and locomotor-enhancing effect by stimulating κ-opioid receptors. Endomorphin-2 causes the release of only dynorphin A as an endogenous κ-opioid peptide (Tseng et al. 2000; Sakurada et al. 2001, 2008), whereas amidino-TAPA can cause the release of not only dynorphin A but also dynorphin B and α-neo-endorphin (Mizoguchi et al. 2007). At present, it is not clear which endogenous κ-opioid peptides are involved in the lack of rewarding and locomotor-enhancing effects of amidino-TAPA. Extensive research will be required to make clear the exact mechanisms for the lack of rewarding and locomotor-enhancing effects by amidino-TAPA.

Our previous finding that the antinociceptive effect of intrathecally administered amidino-TAPA was significantly suppressed in prodynorphin-knockout mice compared to wild-type mice suggests that the spinal antinociceptive effect of amidino-TAPA is mediated partially through the spinal release of dynorphins (Mizoguchi et al. 2007). However, in the present study, the antinociceptive effect of amidino-TAPA injected s.c. was unexpectedly not reduced in prodynorphin-knockout mice. The present evidence suggests that the release of dynorphins is not the main component for the production of antinociception for s.c.-administered amidino-TAPA. At present, the reason for this apparent discrepancy is not clear. Unlike the spinal cord, the regions involved in the antinociception induced by s.c.-administered amidino-TAPA may not contain the special μ-opioid receptors involved in the release of dynorphins.

In contrast to endomorphin-2, which produces a prominent aversive effect rather than a rewarding effect (Narita et al. 2001; Wu et al. 2004), amidino-TAPA did not show either a rewarding effect or an aversive effect. Amidino-TAPA causes the release of dynorphin A, dynorphin B, α-neo-endorphin, and [Leu^5]enkephalin via activation of μ-opioid receptors (Mizoguchi et al. 2007), whereas endomorphin-2 causes the release of dynorphin A and [Met^5]enkephalin but not dynorphin B, α-neo-endorphin, or [Leu^5]enkephalin (Tseng et al. 2000; Sakurada et al. 2001). The evidence clearly suggests that amidino-TAPA stimulates more or different types of μ-opioid receptors (μ-opioid receptor subclasses) than endomorphin-2. In fact, amidino-TAPA-induced antinociception is suppressed by the selective μ_2-opioid receptor antagonist D-Pro^2-Tyr-W-MIF-1, which is ineffective against endomorphin-2-induced antinociception (Watanabe et al. 2005; unpublished observation). By activating more or different types of μ-opioid receptors, amidino-TAPA may show a neutral effect on motivation, i.e., may not show either a rewarding effect or an aversive effect. The aversive effect of a medicine seriously affects a patient's compliance to a regular schedule of medication. From this point of view, amidino-TAPA may be better than endomorphin-2 as a potent analgesic that lacks a rewarding effect.

In conclusion, unlike the traditional narcotic analgesic morphine, the selective μ-opioid receptor agonist amidino-TAPA did not show a rewarding effect or a locomotor-enhancing effect after peripheral injection. The release of endogenous κ-opioid peptides via activation of μ-opioid receptors, identified as a pharmacological profile of amidino-TAPA distinct from morphine, may be responsible for the lack of rewarding and locomotor-enhancing effects of amidino-TAPA.

Acknowledgments This work was supported by a Grant-in-Aid for Scientific Research (C) [KAKENHI 21600013 and 22600009] from the Japan Society for the Promotion of Science and a Matching Fund Subsidy for Private Universities from the Ministry of Education, Culture, Sports, Science and Technology Japan.

References

Bardo MT, Miller JS, Neisewander JL (1984) Conditioned place preference with morphine: the effect of extinction training on the reinforcing CR. Pharmacol Biochem Behav 21:545–549

D'Amour FE, Smith DL (1941) A method for determining loss of pain sensation. J Pharmacol Exp Ther 72:74–79

Deguchi Y, Naito Y, Ohtsuki S, Miyakawa Y, Morimoto K, Hosoya K, Sakurada S, Terasaki T (2004) Blood–brain barrier permeability of novel [D-Arg^2]dermorphin (1-4) analogs: transport property is related to the slow onset of antinociceptive activity in the central nervous system. J Pharmacol Exp Ther 310:177–184

Enrico P, Mura MA, Esposito G, Serra P, Migheli R, De Natale G, Desole MS, Miele M, Miele E (1998) Effect of naloxone on morphine-induced changes in striatal dopamine metabolism and

glutamate, ascorbic acid and uric acid release in freely moving rats. Brain Res 797:94–102

Funada M, Suzuki T, Narita M, Misawa M, Nagase H (1993) Blockade of morphine reward through the activation of κ-opioid receptors in mice. Neuropharmacology 32:1315–1323

Herz A, Spanagel R (1995) Endogenous opioids and addiction. In: Tseng LF (ed) The pharmacology of opioid peptides. Harwood Academic, Singapore, pp 445–462

Johnson SW, North RA (1992a) Opioids excite dopamine neurons by hyperpolarization of local interneurons. J Neurosci 12:483–488

Johnson SW, North RA (1992b) Two types of neurone in the rat ventral tegmental area and their synaptic inputs. J Physiol (London) 450:455–468

Mizoguchi H, Watanabe C, Watanabe H, Moriyama K, Sato B, Ohwada K, Yonezawa A, Sakurada T, Sakurada S (2007) Involvement of endogenous opioid peptides in the antinociception induced by the novel dermorphin tetrapeptide analog amidino-TAPA. Eur J Pharmacol 560:150–159

Narita M, Takahashi Y, Takamori K, Funada M, Suzuki T, Misawa M, Nagase H (1993) Effects of κ-agonist on the antinociception and locomotor enhancing action induced by morphine in mice. Jpn J Pharmacol 62:15–24

Narita M, Ozaki S, Ioka M, Mizoguchi H, Nagase H, Tseng LF, Suzuki T (2001) Different motivational effects induced by the endogenous μ-opioid receptor ligands endomorphin-1 and -2 in the mouse. Neuroscience 105:213–218

Ogawa T, Miyamae T, Murayama K, Okuyama K, Okayama T, Hagiwara M, Sakurada S, Morikawa T (2002a) Synthesis and structure–activity relationships of an orally available and long-acting analgesic peptide, N^{α}-amidino-Tyr-D-Arg-Phe-MeβAla-OH (ADAMB). J Med Chem 45:5081–5089

Ogawa T, Miyamae T, Okayama T, Hagiwara M, Sakurada S, Morikawa T (2002b) Structure–activity relationships (SAR) of [D-Arg^2]dermorphin(1-4) analogues, N^{α}-amidino-Tyr-D-Arg-Phe-X. Chem Pharm Bull 50:771–780

Sakurada S, Hayashi T, Yuhki M, Orito T, Zadina JE, Kastin AJ, Fujimura T, Murayama K, Sakurada C, Sakurada T, Narita M, Suzuki T, Tan-no K, Tseng LF (2001) Differential antinociceptive effects induced by intrathecally administered endomorphin-1 and endomorphin-2 in the mouse. Eur J Pharmacol 427:203–210

Sakurada S, Sawai T, Mizoguchi H, Watanabe H, Watanabe C, Yonezawa A, Morimoto M, Sato T, Komatsu T, Sakurada T (2008) Possible involvement of dynorphin A release via μ_1-opioid receptor on supraspinal antinociception of endomorphin-2. Peptides 29:1554–1560

Sato T, Sakurada S, Takahashi N, Sakurada T, Tan-No K, Wako K, Kisara K (1999) Contribution of spinal μ_1-opioid receptors to morphine-induced antinociception. Eur J Pharmacol 369:183–187

Sharifi N, Diehl N, Yaswen L, Brennan MB, Hochgeschwender U (2001) Generation of dynorphin knockout mice. Mol Brain Res 86:70–75

Spanagel R, Herz A, Shippenberg TS (1990) The effects of opioid peptides on dopamine release in the nucleus accumbens: an in vivo microdialysis study. J Neurochem 55:1734–1740

Spanagel R, Herz A, Shippenberg TS (1992) Opposing tonically active endogenous opioid systems modulate the mesolimbic dopaminergic pathway. Proc Natl Acad Sci USA 89:2046–2050

Suzuki T, Kishimoto Y, Misawa M, Nagase H, Takeda F (1999) Role of the κ-opioid system in the attenuation of the morphine-induced place preference under chronic pain. Life Sci 64:PL1-7

Terashvili M, Wu HE, Leitermann RJ, Hung KC, Clithero AD, Schwasinger ET, Tseng LF (2004) Differential conditioned place preference responses to endomorphin-1 and endomorphin-2 microinjected into the posterior nucleus accumbens shell and ventral tegmental area in the rat. J Pharmacol Exp Ther 309:816–824

Tseng LF, Narita M, Suganuma C, Mizoguchi H, Ohsawa M, Nagase H, Kampine JP (2000) Differential antinociceptive effects of endomorphin-1 and endomorphin-2 in the mouse. J Pharmacol Exp Ther 292:576–583

Watanabe H, Nakayama D, Ito K, Watanabe C, Mizoguchi H, Fujimura T, Murayama K, Kawamura S, Sato T, Sakurada C, Sakurada T, Sakurada S (2005) A Tyr-W-MIF-1 analog containing D-Pro^2 acts as a selective μ_2-opioid receptor antagonist in the mouse. J Pharmacol Exp Ther 312:1075–1081

Wu HE, MacDougall RS, Clithero AD, Leitermann RJ, Terashvili M, Tseng LF (2004) Opposite conditioned place preference responses to endomorphin-1 and endomorphin-2 in the mouse. Neurosci Lett 365:157–161

Respirology

ORIGINAL ARTICLE

Gender differences in transcriptional regulation of IL-5 expression by bronchial lymph node cells in a mouse model of asthma

KANA WADA, KAORI OKUYAMA, YUICHI OHKAWARA, MOTOAKI TAKAYANAGI AND ISAO OHNO

Department of Pathophysiology, Tohoku Pharmaceutical University, Sendai, Japan

ABSTRACT

Background and objective: **The severity of asthma after puberty is higher in women than in men. Increased numbers of eosinophils in the airways of female mice after antigen challenge was associated with increased levels of T helper (Th)2 cytokines at the site of inflammation, and in human and mouse studies, the profile of cytokines produced by immune cells from women showed greater Th2 predominance. The aim of this study was to investigate gender differences in the development of Th2 immune responses.**

Methods: **Male and female C57BL/6 mice were sensitized with ovalbumin. Cells prepared from bronchial lymph nodes were cultured in the absence or presence of ovalbumin. Cytokine concentrations in the culture supernatants were measured, and IL-5 and GATA-binding protein 3 (GATA-3) gene expression were evaluated. T-cell subsets were analysed using specific surface markers.**

Results: **The concentrations of IL-4, IL-5, IL-13 and IL-10, but not interferon-γ or transforming growth factor-β_1, were higher in cell supernatants from female mice than in those from male mice. IL-5 and GATA-3 gene expressions were higher in cells from women than in cells from men. The numbers of $CD3^+CD4^+T1/ST2^+$ cells, but not $CD3^+CD4^+$ or $CD4^+CD25^+$ cells, were significantly higher in cells from women than in cells from men.**

Conclusions: **Greater antigen-induced Th2 cytokine production by bronchial lymph node cells from female mice was associated with enhanced Th2 cell differentiation and increased expression of the Th2-specific transcription factor, GATA-3.**

Key words: asthma, bronchial lymph node, GATA-binding protein 3 (GATA-3), gender difference, T helper 2 cytokine.

Correspondence: Isao Ohno, Department of Pathophysiology, Tohoku Pharmaceutical University, 4-4-1 Komatsushima, Aoba-ku, Sendai 981-8558, Japan. Email: iohno@tohoku-pharm.ac.jp

Received 28 September 2009; invited to revise 5 November 2009, 8 December 2009; revised 25 November 2009, 8 December 2009; accepted 9 December 2009 (Associate Editor: Toby Maher).

© 2010 The Authors
Journal compilation © 2010 Asian Pacific Society of Respirology

SUMMARY AT A GLANCE

Gender differences in the development of Th2 immune responses were investigated. Increased antigen-induced production of Th2 cytokines in lymphocytes from female mice was associated with larger numbers of Th2 cells and greater expression of GATA-3 compared with cells from male mice.

INTRODUCTION

Bronchial asthma is a chronic airway disease characterized by the accumulation and activation of inflammatory cells such as eosinophils and mast cells. The behaviour of inflammatory cells in asthmatic airways is tightly regulated by a network of T helper type 2 (Th2) cytokines, such as IL-4, IL-5 and IL-13, which are produced mainly by Th2 cells.[1–3] GATA-binding protein 3 (GATA-3) is a member of the GATA family of zinc finger proteins, which bind to the WGATAR (W = A/T; R = A/G) DNA sequence. GATA-3 is one of the transcription factors that plays a critical role in Th2 cell differentiation and the production of Th2 cytokines.[4–6] The pathogenic roles of this molecule in asthma have been demonstrated in studies on asthmatic subjects, as well as in animal models.[7–12] There is also increasing evidence that $CD4^+CD25^+$ regulatory T cells (Tregs) play a key role in regulating asthmatic airway inflammation.[13–18]

The prevalence and severity of asthma are greater in boys than in girls, but this gender difference is reversed after puberty,[19–22] which strongly suggests that sex hormones play a role in the pathogenesis of the disease.[23,24] However, the mechanisms underlying gender differences in the prevalence and severity of asthma are not fully understood. It has been reported that the interferon (IFN)-γ: IL-4 ratio was significantly greater in supernatants of phytohemagglutinin-stimulated T-cell cultures from men compared with those from women, and that supplementation of these T-cell cultures with sex hormones did not modify the secretion of these cytokines.[25,26] In addition, we recently showed that, in splenocyte transfer

Respirology (2010) **15**, 629–635
doi: 10.1111/j.1440-1843.2010.01721.x

experiments, allergen-induced airway inflammation in female recipients of splenocytes transferred from female donors was more severe than that with any other gender combination of recipients and donors. Furthermore, splenocytes from sensitized female mice produced more IL-5 on stimulation with a specific antigen than those from sensitized male mice.[27]

Therefore, we hypothesized that gender differences in asthma may be attributable to differences in Th2 cytokine production at the site of inflammation. To address this hypothesis, the proportion of T-cell subsets (Th2 cells and Tregs), gene expression and production of Th2 cytokines and GATA-3 gene expression in bronchial lymph node cells were compared between sensitized male and female mice. T1/ST2 was used as a surface marker for Th2 cells, as it is preferentially expressed on the surface of murine Th2 cells, and plays an important role in the activation of Th2 cells, including proliferation and Th2 cytokine production.[28,29]

METHODS

Animals

Specific pathogen-free, male and female, C57BL/6 (B6) mice were purchased from CLEA Japan, Inc. (Tokyo, Japan). All experiments were approved by and conformed to the guidelines of the Committee on Animal Experiments at Tohoku Pharmaceutical University.

Isolation of bronchial lymph nodes

B6 mice, aged 6–8 weeks, were sensitized and made to inhale antigen, as previously described.[27] Briefly, mice were sensitized by intraperitoneal injections of chicken ovalbumin (OVA) (Grade V, Sigma Chemical Co., St. Louis, MO, USA) (8 μg/mouse), adsorbed with aluminium hydroxide (Wako Pure Chemical Industries, Osaka, Japan) on days 0 and 5. On day 17, mice were challenged twice with aerosolized OVA (5% in saline) for 1 h, within a 4-h interval. Twenty-four hours after the last allergen challenge, bronchial lymph nodes (BLN) were harvested from 5 to 10 mice and pooled for each experiment.[30]

Preparation and culture of bronchial lymph node cells

Bronchial lymph node cells were prepared from BLN as previously described,[31] with minor modifications. BLN cells were resuspended at 5×10^6 cells/mL in complete medium consisting of RPMI 1640 (Gibco BRL, Rockville, MD, USA) with 10% fetal bovine serum (ICN Biomedicals, Inc., Aurosa, OH, USA), 55 μM 2-mercaptoethanol (Wako Pure Chemical Industries), 2 mg/mL $NaHCO_3$, 50 U/mL penicillin G (Meijiseika, Tokyo, Japan), 50 μg/mL streptomycin sulphate (Meijiseika) and 2 mmol/L L-glutamine (Wako Pure Chemical Industries). Cell viability was >98%, as determined by trypan blue dye exclusion. Cells were cultured at 1×10^7 cells/well in 24-well culture plates (MICROPlate, Asahi Techno Glass, Chiba, Japan) in the presence or absence of OVA (200 μg/mL). At the indicated time points, culture samples were centrifuged after counting the viable cells. Supernatants were stored at −80°C for measurement of cytokines by ELISA, and the cells were subjected to RNA extraction and analysis of lymphocyte subsets by flow cytometry.

Measurement of cytokine concentrations

IL-4, IL-5, IL-10, IL-13, IFN-γ and transforming growth factor (TGF)-β_1 concentrations in the supernatants were measured using specific ELISA kits (R&D Systems, Minneapolis, MN, USA), according to the manufacturer's protocol. The sensitivities of detection were 2 pg/mL for IL-4, 7 pg/mL for IL-5, 4 pg/mL for IL-10, 1.5 pg/mL for IL-13, 2 pg/mL for IFN-γ and 2.9 pg/mL for TGF-β_1.

Evaluation of gene expression

IL-5 and GATA-3 gene expressions were evaluated by RT-PCR, as previously described.[32] Briefly, total RNA was extracted from BLN cells before and after culture with OVA. cDNA was synthesized from total RNA and amplified using specific primers (Table 1). The PCR products were electrophoresed and visualized by ethidium bromide staining. mRNA expression was quantified as the ratio of the band intensities of the target genes to that of GAPDH on the digitized images, using NIH imageJ software (National Institutes of Health, Bethesda, MD, USA).

Flow cytometric analysis

$CD3^+CD4^+$ and $CD3^+CD4^+T1/ST2^+$ subsets of BLN cells were analysed as previously described.[33] Briefly, the cells were pre-incubated with anti-CD16/CD32 ($F_c\gamma$III/II receptor; BD Biosciences PharMingen, San Diego, CA, USA) to reduce non-specific binding of the following antibodies: anti-T1/ST2-fluorescein isothiocyanate (clone DJ8, 0.8 μg/10^6 cells) (Morwell Diagnostic, Zurich, Switzerland), anti-CD3e-allophycocyanin (clone 145-2C11, 0.8 μg/10^6 cells) (BD Biosciences PharMingen), anti-CD4-R-phycoerythrin (PE) (clone GK1.5, 0.5 μg/10^6 cells) (BD Biosciences PharMingen) or isotype control antibodies, which were added directly to the cells. Tregs were identified as $CD4^+CD25^+$ cells, using a mouse regulatory T-cell staining kit (eBioscience, San Diego, CA, USA), according to the manufacturer's protocol. Cells were counted on a FACScan instrument (BD Biosciences PharMingen) and data were analysed using Cell Quest software (BD Biosciences PharMingen).

Data analysis and statistics

Data are presented as means ± SD. Differences between two groups were assessed for statistical significance using the non-parametric Mann–Whitney

© 2010 The Authors
Journal compilation © 2010 Asian Pacific Society of Respirology

Table 1 Primer sequences used for PCR amplification

Gene		Sequence	Denaturation °C	Denaturation s	Annealing °C	Annealing s	Extension °C	Extension s	Number of cycles	Product size (bp)
IL-5	Sense	5′-CTCACCGAGCTCTGT TGACAAG-3′	94	45	64	45	72	60	33	251
	Antisense	5′-GAACTCTTGCAGGTAA TCCAGG-3′								
GATA-3	Sense	5′-GGAGGACTTCCCCAA GAGCA-3′	95	30	67	60	72	60	34	169
	Antisense	5′-CATGCTGGAAGGGTG GTGAG-3′								
GAPDH	Sense	5′-TGATGACATCAAGAAG GTGGTGAAG-3′	94	60	67	60	72	60	25	249

GAPDH, glyceraldehyde 3-phosphate dehydrogenase; GATA, GATA-binding protein 3.

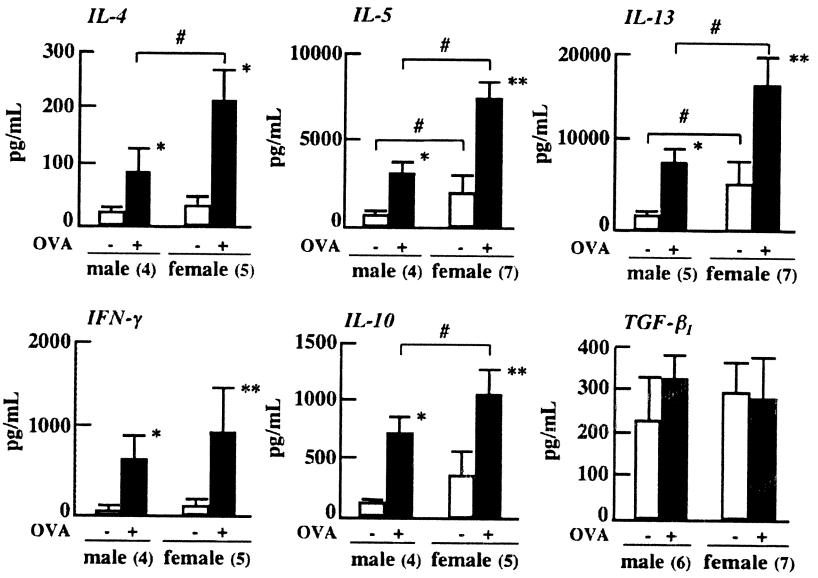


Figure 1 Gender differences in cytokine production by bronchial lymph node (BLN) cells. BLN cells from sensitized male and female mice were cultured with (closed bars) or without (open bars) ovalbumin (OVA) for 72 h. The concentrations of IL-4, IL-5, IL-13, interferon (IFN)-γ, IL-10 and transforming growth factor (TGF)-β_1 in the culture supernatants were measured. Data from four to seven independent experiments (shown in parentheses) are expressed as mean ± SD. $*P < 0.05$, $**P < 0.01$ compared with BLN cells cultured without OVA. $\#P < 0.05$, comparing BLN cells from male and female mice.

U-test, and those between time points were assessed using the Wilcoxon matched pairs test or the Kruskal–Wallis test. All statistical analyses were performed using Prism4 software (GraphPad Software, San Diego, CA, USA). A *P*-value < 0.05 was considered significant.

RESULTS

Cytokine concentrations in culture supernatants of bronchial lymph node cells

As shown in Figure 1, for both male and female mice, the levels of IL-4, IL-5, IL-13, IFN-γ and IL-10, but not TGF-β_1, were significantly higher in supernatants of BLN cells cultured in the presence of OVA than in those cultured in the absence of OVA. In the presence of OVA, IL-4, IL-5, IL-13 and IL-10 levels in BLN cells of female mice were significantly higher than those in BLN cells of male mice (IL-4, 213 ± 66.9 vs. 96.8 ± 38.4 pg/mL, $P < 0.05$; IL-5, 7391 ± 446 vs. 2977 ± 597 pg/mL, $P < 0.05$; IL-13, 15763 ± 3471 vs. 7209 ± 1664 pg/mL, $P < 0.05$; IL-10, 1080 ± 191 vs. 695 ± 145 pg/mL, $P < 0.05$). On the other hand, there were no significant differences in the concentrations of IFN-γ or TGF-β_1 between female and male mice. In the absence of OVA, significantly higher concentrations of IL-5 and IL-13 were observed in cells from female mice compared with those from male mice (IL-5, 1916 ± 998 vs. 570 ± 220 pg/mL, $P < 0.05$; IL-13, 4976 ± 2735 vs. 1453 ± 301 pg/mL, $P < 0.05$).

Expression of IL-5 and GATA-binding protein 3 (GATA-3) mRNA in bronchial lymph node cells

In both male and female mice, expression of IL-5 mRNA in BLN cells after 24 h of culture with OVA was

© 2010 The Authors
Journal compilation © 2010 Asian Pacific Society of Respirology

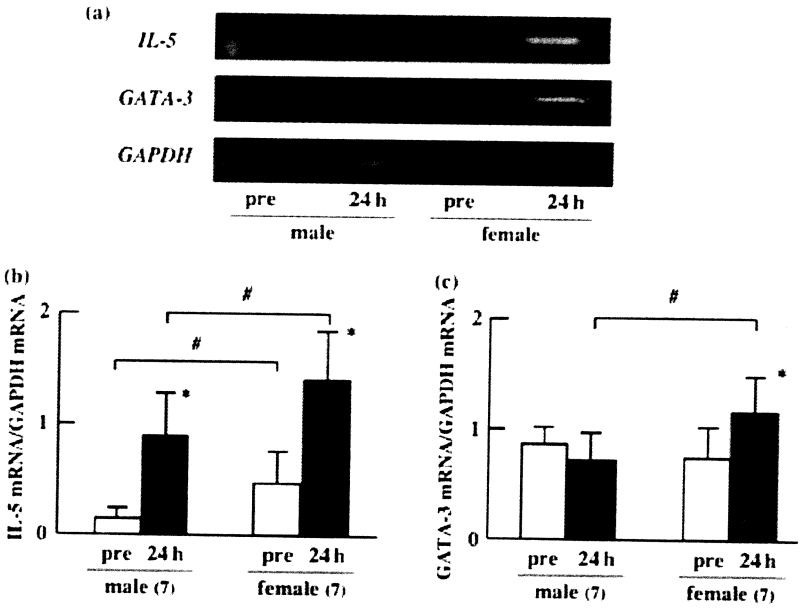


Figure 2 Gender differences in the expression of IL-5 and GATA-3 mRNA in bronchial lymph node (BLN) cells. BLN cells from sensitized male and female mice were analysed before (pre) and after 24 h of culture with ovalbumin. Total RNA was extracted and subjected to RT-PCR with primers for IL-5, GATA-3 and glyceraldehyde 3-phosphate dehydrogenase (GAPDH). (a) Representative photographs showing gel electrophoresis of RT-PCR products. (b) The ratios of IL-5 relative to GAPDH mRNA and (c) GATA-3 relative to GAPDH mRNA were determined. Data from seven independent experiments (shown in parentheses) are expressed as mean ± SD. *$P < 0.05$ compared with pre; #$P < 0.05$, comparing BLN cells from male and female mice. GATA, GATA-binding protein 3.

significantly higher than that before culture with OVA (male: 0.9 ± 0.4 vs. 0.1 ± 0.1, $P < 0.05$; female: 1.4 ± 0.5 vs. 0.5 ± 0.3, $P < 0.05$) (Fig. 2a). Comparing IL-5 mRNA expression between BLN cells from male and female mice, before or after culture with OVA, expression was significantly greater in female than in male mice (before: 0.5 ± 0.3 vs. 0.1 ± 0.1, $P < 0.05$; after: 1.4 ± 0.5 vs. 0.9 ± 0.4, $P < 0.05$) (Fig. 2b).

There was no significant difference in GATA-3 mRNA expression between BLN cells from male and female mice before culture with OVA. However, GATA-3 mRNA expression was significantly increased in cells from female mice, after culture with OVA compared with before culture (1.2 ± 0.3 vs. 0.7 ± 0.3, $P < 0.05$). In contrast, there was no increase in GATA-3 mRNA expression in cells from male mice. Therefore, GATA-3 mRNA expression was significantly higher in female- compared with male-derived BLN cells, after culture with OVA (1.2 ± 0.3 vs. 0.7 ± 0.3, $P < 0.05$) (Fig. 2c).

T-cell subsets in bronchial lymph node cells

There was no significant difference between the genders in the numbers of viable cells after 24 and 72 h of culture with OVA (data not shown).

There was a tendency for the proportion of $CD3^+CD4^+$ cells to increase after culture with OVA, in both male and female mice, but the increase was not statistically significant, except for male mice after 72 h of culture. In addition, there was no significant difference in the proportion of $CD3^+CD4^+$ cells between the genders at any time point.

There was a tendency for the proportion of $CD3^+CD4^+T1/ST2^+$ cells to increase after culture with OVA in both male and female mice; however, the increase did not reach statistical significance, except for male mice after 72 h of culture. Comparing the proportion of $CD3^+CD4^+T1/ST2^+$ BLN cells between males and females after 24 h of culture with OVA, female-derived BLN cells showed a significantly higher proportion compared with male-derived BLN cells (2.1 ± 0.2% vs. 1.2 ± 0.2%, $P < 0.05$) (Fig. 3).

The proportion of $CD4^+CD25^+$ BLN cells was significantly increased after 72 h of culture with OVA compared with that before culture, for both male and female cells (male: 3.7 ± 1.2% vs. 1.5 ± 0.4%, $P < 0.05$; female: 3.2 ± 1.1% vs. 1.4 ± 0.5%, $P < 0.05$). However, there were no significant differences between the genders at any time point (Fig. 3).

DISCUSSION

In this study, we demonstrated gender differences in Th2 cell differentiation, Th2 cytokine production and GATA-3 gene expression in BLN cells. When cultured with OVA, BLN cells from female mice produced significantly greater amounts of IL-4, IL-5 and IL-13, but not IFN-γ or TGF-β_1, than those from male mice. The results for IL-5 and IFN-γ production are in

© 2010 The Authors
Journal compilation © 2010 Asian Pacific Society of Respirology

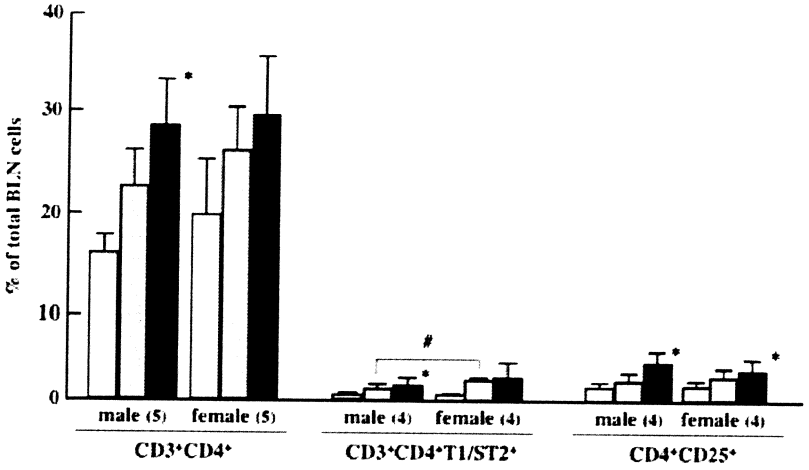


Figure 3 Gender differences in the proportion of T-cell subsets in bronchial lymph node (BLN) cells. BLN cells from sensitized male and female mice were analysed for the proportions of $CD3^+CD4^+$, $CD3^+CD4^+T1/ST2^+$ and $CD4^+CD25^+$ cells before (pre) (open bars), and after 24 h (striped bars) and 72 h (closed bars) of culture with ovalbumin. The numbers of $CD3^+CD4^+$, $CD3^+CD4^+T1/ST2^+$ and $CD4^+CD25^+$ cells are shown as percentages of the total number of BLN cells. Data from four to five independent experiments (shown in parentheses) are expressed as mean ± SD. $^*P < 0.05$ compared with pre, $\#P < 0.05$, comparing BLN cells from male and female mice.

accordance with our previous findings that the expression of IL-5, but not IFN-γ, in culture supernatants of splenocytes from sensitized female mice was significantly greater than that from sensitized male mice, after culture with antigen. However, there were no significant differences between the genders in the amounts of IL-4 or IL-13 in the splenocyte cultures.[27] The discrepancy between BLN cells and splenocytes, in terms of gender differences in IL-4 and IL-13 production, may be attributable to the *in vivo* prestimulation of BLN cells and the different location of the cells. Seymour *et al.* recently reported that in an asthma model of *in vitro* stimulation with antigen, production of IL-5 and IL-13 by homogenized lung tissue of female mice was significantly greater than that from lung tissue of male mice.[34] The present findings on BLN cells are also supported by the recent observation that the Th1 : Th2 cytokine (IFN-γ : IL-4) ratio was significantly higher in supernatants of phytohemagglutinin-stimulated T-cell cultures from men compared with those from women.[25,26]

We also investigated whether the greater production of Th2 cytokines, particularly IL-5, by female BLN cells was associated with enhanced expression of the GATA-3 gene. Before culture with OVA, IL-5 mRNA expression in female-derived BLN cells was greater than that in male-derived BLN cells, while GATA-3 mRNA expression and the proportion of Th2 cells were similar. These results suggest greater transcription of the IL-5 gene in females, but the mechanisms involved remain to be delineated. After culture with OVA, IL-5 and GATA-3 mRNA expressions and the proportion of Th2 cells were significantly greater in cells from female mice compared with those from male mice. Hayashi *et al.* previously reported that IL-4, but not IFN-γ, mRNA expression in splenocytes of sensitized female mice was higher than that in male mice; however, they did not investigate production of cytokine protein, Th2 cell subsets or transcription factors such as GATA-3.[35] The mechanisms by which transcription of GATA-3 was enhanced in female compared with male mice were not investigated in the present study, although activation of oestrogen receptor α is known to increase GATA-3 expression in $CD4^+$ T cells and breast cancer cells.[36,37] Unexpectedly, the increase in IL-5 mRNA expression was not accompanied by increased GATA-3 mRNA expression in male-derived BLN cells. It is possible that in male mice, other transcription factors such as c-Maf and NF-AT may be of greater importance for the regulation of IL-5 gene expression.[4] The gender differences in protein expression and binding activity to the target genes of GATA-3 require further exploration.

There were no gender differences in the percentages of $CD4^+CD25^+$ cells at any time point, while the percentage increased in both genders after 72 h of culture with OVA. Melgert *et al.* investigated the effect of allergen challenge on the numbers of $CD4^+$ and $CD4^+CD25^+$ cells in lung tissue in a murine model of allergic asthma. The number of $CD4^+$ T cells after challenge was significantly higher in female mice than in male mice, although Th2 cells were not identified. The percentage of $CD4^+CD25^+$ cells in females was lower after PBS challenge and similar after OVA challenge.[38] The authors assumed that the lower number of cells with an inactive Treg phenotype produced less suppression of Th2 responses following allergen challenge, resulting in greater numbers of eosinophils in the airways of female mice. Further characterization of $CD4^+CD25^+$ cells by distinguishing Tregs[39,40] from activated $CD4^+$ cells is needed in order to elucidate the role of Tregs in gender differences in asthma.

© 2010 The Authors
Journal compilation © 2010 Asian Pacific Society of Respirology

In conclusion, this is the first study to demonstrate gender differences in antigen-induced Th2 cell differentiation and Th2 cytokine gene expression in BLN cells from sensitized mice. Furthermore, these differences correlated with greater expression of the GATA-3 gene in female mice. We are in the process of investigating gender differences in the regulation of GATA-3 expression, including STAT-6 activation and differences related to interactions with the Th1-specific transcription factor, T-bet.[4,5] Studies on the transcriptional regulation of cytokine expression in each gender would increase our understanding of the pathogenesis of diseases that demonstrate gender differences, such as asthma and autoimmune diseases.

ACKNOWLEDGEMENTS

This work was supported in part by a Grant-in-Aid for High Technology Research Program from the Ministry of Education, Culture, Sports, Science and Technology of Japan.

REFERENCES

1 Kay AB. Asthma and inflammation. *J. Allergy Clin. Immunol.* 1991; **87**: 893–910.
2 Bousquet J, Jeffery PK, Busse WW *et al.* Asthma: from bronchoconstriction to airways inflammation and remodeling. *Am. J. Respir. Crit. Care Med.* 2000; **161**: 1720–45.
3 Ngoc PL, Gold DR, Tzianabos AO *et al.* Cytokines, allergy, and asthma. *Curr. Opin. Allergy Clin. Immunol.* 2005; **5**: 161–6.
4 Zhou M, Ouyang W. The function role of GATA-3 in Th1 and Th2 differentiation. *Immunol. Res.* 2003; **28**: 25–37.
5 Ho IC, Pai SY. GATA-3—not just for Th2 cells anymore. *Cell. Mol. Immunol.* 2007; **4**: 15–29.
6 Barnes PJ. Role of GATA-3 in allergic diseases. *Curr. Mol. Med.* 2008; **8**: 330–4.
7 Nakamura Y, Ghaffar O, Olivenstein R *et al.* Gene expression of the GATA-3 transcription factor is increased in atopic asthma. *J. Allergy Clin. Immunol.* 1999; **103**: 215–22.
8 Caramori G, Lim S, Ito K *et al.* Expression of GATA family of transcription factors in T cells, monocytes and bronchial biopsies. *Eur. Respir. J.* 2001; **18**: 466–73.
9 Kiwamoto T, Ishii Y, Morishima Y *et al.* Transcription factors T-bet and GATA-3 regulate development of airway remodeling. *Am. J. Respir. Crit. Care Med.* 2006; **174**: 142–51.
10 Yamashita N, Tashimo H, Ishida H *et al.* Involvement of GATA-3-dependent Th2 lymphocyte activation in airway hyperresponsiveness. *Am. J. Physiol. Lung Cell. Mol. Physiol.* 2006; **290**: L1045–51.
11 Finotto S, De Sanctis GT, Lehr HA *et al.* Treatment of allergic airway inflammation and hyperresponsiveness by antisense-induced local blockade of GATA-3 expression. *J. Exp. Med.* 2001; **193**: 1247–60.
12 Lee CC, Huang HY, Chiang BL. Lentiviral—mediated GATA-3 RNAi decreases allergic airway inflammation and hyperresponsiveness. *Mol. Ther.* 2008; **16**: 60–5.
13 Xystrakis E, Boswell SE, Hawrylowicz CM. T regulatory cells and the control of allergic disease. *Expert Opin. Biol. Ther.* 2006; **6**: 121–33.
14 Larché M. Coexpression of TGF-beta1 and IL-10 enables regulatory T cells to completely suppress airway hyperreactivity. *Chest* 2007; **132**: 1007–14.
15 Kearley J, Barker JE, Robinson DS *et al.* Resolution of airway inflammation and hyperreactivity after in vivo transfer of $CD4^+CD25^+$ regulatory T cells is interleukin 10 dependent. *J. Exp. Med.* 2005; **202**: 1539–47.
16 Joetham A, Takeda K, Taube C *et al.* Naturally occurring lung CD4(+)CD25(+) T cell regulation of airway allergic responses depends on IL-10 induction of TGF-beta. *J. Immunol.* 2007; **178**: 1433–42.
17 Matsumoto K, Inoue H, Fukuyama S *et al.* Decrease of interleukin-10-producing T cells in the peripheral blood of severe unstable atopic asthmatics. *Int. Arch. Allergy Immunol.* 2004; **134**: 295–302.
18 Hartl D, Koller B, Mehlhorn AT *et al.* Quantitative and functional impairment of pulmonary $CD4^+CD25^{hi}$ regulatory T cells in pediatric asthma. *J. Allergy Clin. Immunol.* 2007; **119**: 1258–66.
19 The ENFUMOSA Study Group. The ENFUMOSA cross-sectional European multicentre study of the clinical phenotype of chronic severe asthma. *Eur. Respir. J.* 2003; **22**: 470–7.
20 Siroux V, Curt F, Oryszczyn MP *et al.* Role of gender and hormone-related events on IgE, atopy, and eosinophils in the Epidemiological Study on the Genetics and Environment of Asthma, bronchial hyperresponsiveness and atopy. *J. Allergy Clin. Immunol.* 2004; **114**: 491–8.
21 Almqvist C, Worm M, Leynaert B; Working Group of GA2LEN WP 2.5 Gender. Impact of gender on asthma in childhood and adolescence: a GA2LEN review. *Allergy* 2008; **63**: 47–57.
22 Chen W, Mempel M, Schober W *et al.* Gender difference, sex hormones, and immediate type hypersensitivity reactions. *Allergy* 2008; **63**: 1418–27.
23 Balzano G, Fuschillo S, Melillo G *et al.* Asthma and sex hormones. *Allergy* 2001; **56**: 13–20.
24 Mitchell VL, Gershwin LJ. Progesterone and environmental tobacco smoke act synergistically to exacerbate the development of allergic asthma in a mouse model. *Clin. Exp. Allergy* 2007; **37**: 276–86.
25 Girón-González JA, Moral FJ, Elvira J *et al.* Consistent production of a higher TH1 : TH2 cytokine ratio by stimulated T cells in men compared with women. *Eur. J. Endocrinol.* 2000; **143**: 31–6.
26 Jarefors S, Bennet L, You E *et al.* Lyme borreliosis reinfection: might it be explained by a gender difference in immune response? *Immunology* 2006; **118**: 224–32.
27 Okuyama K, Wada K, Chihara J *et al.* Sex-related splenocyte function in a murine model of allergic asthma. *Clin. Exp. Allergy* 2008; **38**: 1212–19.
28 Löhning M, Stroehmann A, Coyle AJ *et al.* T1/ST2 is preferentially expressed on murine Th2 cells, independent of interleukin 4, interleukin 5, and interleukin 10, and important for Th2 effector function. *Proc. Natl. Acad. Sci. USA* 1998; **95**: 6930–5.
29 Meisel C, Bonhagen K, Löhning M *et al.* Regulation and function of T1/ST2 expression on $CD4^+$ T cells: induction of type 2 cytokine production by T1/ST2 cross-linking. *J. Immunol.* 2001; **166**: 3143–50.
30 Nahori MA, Lagranderie M, Lefort J *et al.* Effects of Mycobacterium bovis BCG on the development of allergic inflammation and bronchial hyperresponsiveness in hyper-IgE BP2 mice vaccinated as newborns. *Vaccine* 2001; **19**: 1484–95.
31 Vermaelen KY, Carro-Muino I, Lambrecht BN *et al.* Specific migratory dendritic cells rapidly transport antigen from the airways to the thoracic lymph nodes. *J. Exp. Med.* 2001; **193**: 51–60.
32 Okuyama K, Yamashita M, Kitabatake Y *et al.* Ciglitazone inhibits the antigen-induced leukotrienes production independently of PPAR? in RBL-2H3 mast cells. *Eur. J. Pharmacol.* 2005; **521**: 21–8.
33 Kropf P, Herath S, Klemenz R *et al.* Signaling through the T1/ST2 molecule is not necessary for Th2 differentiation but is important for the regulation of type 1 responses in nonhealing Leishmania major infection. *Infect. Immun.* 2003; **71**: 1961–71.
34 Seymour BW, Friebertshauser KE, Peake JL *et al.* Gender differences in the allergic response of mice neonatally exposed to environmental tobacco smoke. *Dev. Immunol.* 2002; **9**: 47–54.

© 2010 The Authors
Journal compilation © 2010 Asian Pacific Society of Respirology

35 Hayashi T, Adachi Y, Hasegawa K *et al.* Less sensitivity for late airway inflammation in males than females in BALB/c mice. *Scand. J. Immunol.* 2003; **57**: 562–7.
36 Lambert KC, Curran EM, Judy BM *et al.* Estrogen receptor alpha (ERalpha) deficiency in macrophages results in increased stimulation of CD4+ T cells while 17beta-estradiol acts through ERalpha to increase IL-4 and GATA-3 expression in CD4+ T cells independent of antigen presentation. *J. Immunol.* 2005; **175**: 5716–23.
37 Fang SH, Chen Y, Weigel RJ. GATA-3 as a marker of hormone response in breast cancer. *J. Surg. Res.* 2009; **157**: 290–5.
38 Melgert BN, Postma DS, Kuipers I *et al.* Female mice are more susceptible to the development of allergic airway inflammation than male mice. *Clin. Exp. Allergy* 2005; **35**: 1496–503.
39 Tournoy KG, Provoost S, Van Hove C *et al.* The role of immune tolerance in asthma pathogenesis. *Curr. Allergy Asthma Rep.* 2006; **6**: 437–43.
40 Vignali DA, Collison LW, Workman CJ. How regulatory T cells work. *Nat. Rev. Immunol.* 2008; **8**: 523–32.

© 2010 The Authors
Journal compilation © 2010 Asian Pacific Society of Respirology

Original Paper

International Archives of Allergy and Immunology

Int Arch Allergy Immunol 2010;152:342–352
DOI: 10.1159/000288287

Received: July 7, 2009
Accepted after revision: September 22, 2009
Published online: February 26, 2010

The Involvement of μ-Opioid Receptors in the Central Nervous System in the Worsening of Allergic Airway Inflammation by Psychological Stress in Mice

Kaori Okuyama[a] Kana Wada[a] Shinobu Sakurada[b] Hirokazu Mizoguchi[b]
Hiroshi Komatsu[c] Ichiro Sora[c] Gen Tamura[d] Yuichi Ohkawara[a]
Motoaki Takayanagi[a] Isao Ohno[a]

Departments of [a]Pathophysiology and [b]Physiology and Anatomy, Tohoku Pharmaceutical University, [c]Department of Biological Psychiatry, Tohoku University Graduate School of Medicine, and [d]Division of Respiratory Medicine, Airway Institute, Sendai, Japan

Key Words
Bronchial asthma · Psychological stress · μ-Opioid receptors · Morphine

Abstract
Background: Psychological stress has a recognized association with asthma symptoms. However, the mechanisms linking stress to the exacerbation of asthma are not well defined. μ-Opioid receptors (MOR) have been shown to be involved in the shift of the immune system toward a Th2-predominant response caused by psychological stress. ***Objective:*** To test the hypothesis that MOR play a role in the worsening of allergic airway inflammation evoked by psychological stress. ***Methods:*** Sensitized mice were exposed to restraint stress followed by antigen challenge. The levels of corticosterone and ovalbumin (OVA)-specific IgE in the blood and the levels of inflammatory cells and cytokine contents in bronchoalveolar lavage fluid were compared between stressed and nonstressed mice. The effects of MOR gene deletion and MOR antagonists/agonists were also investigated. ***Results:*** Stress exposure was confirmed by an increase in corticosterone levels. Although OVA-specific IgE levels were not significantly different, the numbers of inflammatory cells and Th2 cytokine levels after antigen challenge in stressed mice were significantly higher than in nonstressed mice. MOR gene deletion ameliorated the stress-induced worsening of antigen-induced airway inflammation, and the administration of morphine, a MOR agonist, reproduced the stress-induced antigen-induced airway inflammation. Selective blocking of MOR in the central nervous system (CNS) significantly reduced stress-induced inflammatory exacerbation, but the blocking of peripheral MOR did not. ***Conclusions:*** MOR in the CNS are involved in psychological stress-induced aggravation of allergic airway inflammation.

Copyright © 2010 S. Karger AG, Basel

Introduction

Bronchial asthma is a chronic airway inflammatory disease characterized by the accumulation and activation of inflammatory cells, such as eosinophils and mast cells, in the bronchial wall and airway lumen. The behavior of inflammatory cells in asthmatic airways is tightly regulated by a network of Th2 cytokines such as IL-4, IL-5 and

KARGER
Fax +41 61 306 12 34
E-Mail karger@karger.ch
www.karger.com

© 2010 S. Karger AG, Basel
1018–2438/10/1524–0342$26.00/0

Accessible online at:
www.karger.com/iaa

Correspondence to: Prof. Isao Ohno
Department of Pathophysiology
Tohoku Pharmaceutical University
4-4-1 Komatsushima, Aoba-ku, Sendai 981-8558 (Japan)
Tel. +81 22 727 0127/Fax +81 22 727 0128, E-Mail iohno@tohoku-pharm.ac.jp

IL-13. Inflammatory mediators released from these cells upon stimulation, such as arachidonic acid metabolites and reactive oxygen species, evoke the airway narrowing and airway hyper-responsiveness observed in asthmatics [1–4].

Various clinical studies have demonstrated an association between psychological stress and aggravation of asthma symptoms [5, 6]. For example, one study found that 20–35% of asthmatics experience exacerbation of symptoms during periods of stress [7]. In childhood asthma, high levels of ongoing chronic stress combined with an acutely negative life event increase the risk of asthma attacks [8]. Furthermore, psychological stress has effects on the inflammatory and immune responses implicated in asthma, such as Th2 cytokines. For example, chronic stress caused by academic examinations was shown to increase IL-5 production and eosinophil accumulation after antigen inhalation in college students with mild asthma [9, 10]. However, the precise mechanisms linking psychological stress to exacerbation of asthma are not well understood.

Psychological stress upregulates the production of endogenous opioids, including endorphins, enkephalins and dynorphins. These endogenous opioids exert their effects, such as analgesia, neuroendocrine functions and immunoregulation, through binding to opioid receptors consisting of 3 subtypes, μ, δ and κ [11, 12]. The hypothalamic-pituitary-adrenal (HPA) axis and sympathetic and adrenomedullary (SAM) system are activated by opioids in stressful conditions through the binding of ligands to μ-opioid receptors (MOR). Activation of the HPA axis and SAM system results in enhanced secretion of cortisol and catecholamines, respectively [13–15]. These stress hormones have been reported to shift the immune response from Th1 to Th2 by downregulating Th1 cytokine expression [16]. MOR are also expressed on inflammatory cells, including T cells, monocytes/macrophages and dendritic cells [17, 18]. The activation of MOR on T cells was reported to induce the differentiation of Th2 cells and a shift from Th1 to Th2 responses [19–21]. Furthermore, we recently reported that psychological stress, in this case 'restraint stress', exacerbated antigen-induced airway inflammation in wild-type mice but not in MOR gene knockout (MORKO) mice [22].

These findings led us to hypothesize that MOR play an important role in the worsening of allergic airway inflammation caused by psychological stress. To address this hypothesis, we examined the effects of opioid receptor antagonists, as well as MORKO, on stress-induced asthma exacerbation and the potential of MOR agonists to exacerbate allergic airway inflammation using a murine model of asthma. In addition, to clarify which MOR in the central nervous system (CNS) or on inflammatory cells are involved in such exacerbation, the effects of intracerebroventricular and intraperitoneal injection of MOR antagonists were investigated.

Materials and Methods

Animals

Specific pathogen-free female C57BL/6 mice were purchased from Japan SLC (Hamamatsu, Japan). MORKO mice were generated as described previously [23]. Congenic MORKO mice backcrossed with C57BL/6 mice [24], and wild-type C57BL/6 mice (Japan SLC) were used as controls in this study. Animals were housed under a 12-hour light/dark cycle at a constant temperature (22 ± 2°C). Sterilized food and water were available ad libitum. All experiments described below were approved by the Committee of Animal Experiments at Tohoku Pharmaceutical University and conformed to its guidelines.

Protocols for Sensitization, Challenge and Stress Exposure

Mice 6–8 weeks of age were sensitized and made to inhale antigen as described previously [22, 25], but with a minor modification. Briefly, mice were sensitized by intraperitoneal injections of chicken ovalbumin (OVA; grade V, Sigma, St. Louis, Mo., USA; 8 μg/mouse) adsorbed with aluminum hydroxide (Wako Pure Chemical Industries, Osaka, Japan; 4 mg/mouse) on days 0 and 5. For restraint stress, each mouse was placed in a 50-ml conical centrifuge tube with multiple ventilation holes for 6 h a day. Mice were not physically squeezed and felt no pain. This restraint allowed the mice to rotate from a supine to prone position, but not to turn their heads toward their tails or to consume food and water [22]. Restraint stress is generally regarded as inducing psychological stress in animals [26]. On day 30, stressed mice in 50-ml conical centrifuge tubes were left in the plastic chambers for 6 h. For the first hour of the period, aerosolized OVA flowed through the chambers so that the mice in the tubes were exposed to OVA. Stressed mice were further exposed to the restraint stress on 6 consecutive days, days 31–36, at the same time each day. Nonstressed mice were only deprived of food and water for the same period of time as the stressed mice were exposed to stress. Deprivation of food and water has been used as a nonstress condition in other rodent experiments that investigated the effect of restraint stress [27, 28]. Before and immediately after the restraint stress on day 30, and immediately after the restraint stress on days 32 and 36, a retro-orbital blood sample was taken from the mice after anesthetization with diethylether (Wako) and stored on ice until further processing. Blood was collected from nonstressed mice in the same way. Plasma samples separated from blood samples were stored at –80°C for corticosterone concentration measurements by enzyme immunoassay (EIA). On day 37, stressed and nonstressed mice were challenged with aerosolized OVA or saline (second challenge). Before and after the second challenge, as shown in figure 1a, bronchoalveolar lavage (BAL) was performed as described previously [22, 25]. Briefly, the lungs were dissected and the trachea

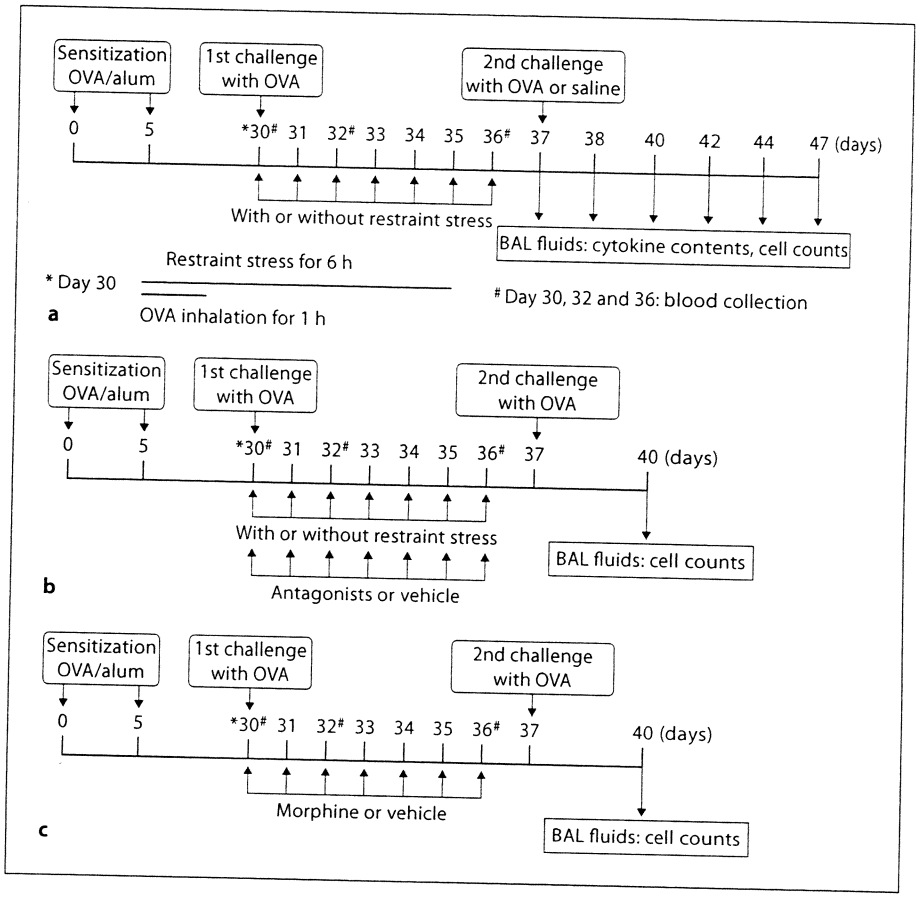


Fig. 1. Diagrammatic representation of the protocols for sensitization, challenge and stress exposure. **a** Stress exposure protocol. **b** Stress exposure plus opioid receptor antagonists protocol. **c** μ-Opioid receptor agonist protocol.

was cannulated with a polyethylene tube (Becton Dickinson, Sparks, Md., USA). The lungs were lavaged twice by the injection of 0.25 ml of cold saline through the tube, and the recovered saline was pooled. Approximately 0.4 ml of instilled fluid was consistently recovered from each mouse. BAL fluid was processed for the measurement of cytokine contents and for counting total cells and cell differentials. After centrifugation of BAL fluid, supernatants were stored at −80°C for cytokine measurements by ELISA (fig. 1a). In experiments with opioid receptor antagonists (fig. 1b), β-funaltrexamine (β-FNA; (a MOR antagonist; Tocris, Bristol, UK), naltrindole (a δ-opioid receptor antagonist; Sigma), nor-binaltorphimine (nor-BNI; a κ-opioid receptor antagonist; Sigma) and naloxone methiodide (a nonselective opioid receptor antagonist; Sigma) were intraperitoneally or intracerebroventricularly administered 1 h before each period of stress at the dose indicated [29–31] to the stressed and nonstressed mice. These mice were then exposed to OVA on day 37 (second challenge). In experiments with the MOR agonist (fig. 1c), morphine hydrochloride (Sankyo, Tokyo, Japan; 0.3, 1, 3 and 10 mg/kg body weight) was administered subcutaneously to the nonstressed mice instead of stress exposure. These mice were then exposed to OVA on day 37 (second challenge). The antagonists and agonist were dissolved in sterilized calcium- and magnesium-free phosphate-buffered saline (PBS; Wako), which was used as a control for the agents.

Corticosterone Assays

The corticosterone concentration in plasma was measured using an EIA kit (Assay Designs Inc., Ann Arbor, Mich., USA) according to the manufacturer's protocol. The sensitivity was 32 pg/ml.

OVA-Specific IgE Measurement

Serum levels of OVA-specific IgE on day 37 before the second challenge were measured with ELISA, as described previously [32].

Cytokine Assays

IL-4, IL-5, IL-13 and IFN-γ concentrations in the BAL fluid were measured using an ELISA kit (R&D Systems, Minneapolis, Minn., USA) according to the manufacturer's protocol. The sensitivity of detection was 2 pg/ml for IL-4 and IFN-γ, 7 pg/ml for IL-5 and 1.5 pg/ml for IL-13.

Statistical Analysis

Data are expressed as means ± SD. The number values are from multiple independent experiments with 2–4 mice. Significant differences between two groups were determined using the nonparametric Mann-Whitney U test. Significant differences in corticosterone concentrations in plasma after stress exposure, in the cell counts in BAL fluid during the time period after the second challenge and in BAL fluid from mice treated with various

doses of morphine were determined using one-way analysis of variance followed by Bonferroni's test. These analyses were performed using Prism 4 (GraphPad Software, San Diego, Calif., USA). A p value of less than 0.05 was considered significant.

Results

The Effect of Restraint Stress on Plasma Corticosterone Concentrations

While there were no significant differences in corticosterone concentrations between stressed and nonstressed mice before stress exposure, corticosterone concentrations in stressed mice were significantly higher than in nonstressed mice after the 1st, 3rd and 7th stress exposure [1st exposure: 368.7 ± 135.9 (n = 7) vs. 223.7 ± 53.2 ng/ml (n = 7), $p < 0.05$; 3rd exposure: 228.0 ± 53.3 (n = 5) vs. 144.2 ± 17.9 ng/ml (n = 5), $p < 0.05$; 7th exposure: 197.7 ± 52.0 (n = 4) vs. 89.5 ± 10.2 ng/ml (n = 4), $p < 0.05$] (fig. 2). Corticosterone concentrations after the 1st stress exposure were significantly increased in both stressed (restraint stress with food and water deprivation) and nonstressed (only food and water deprivation) mice compared to concentrations before the 1st stress exposure. The increase in nonstressed mice could have been due to food and water deprivation. Therefore, the differences in concentrations between stressed and nonstressed mice would only reflect the effect of the restraint stress. Although corticosterone concentrations tended to decrease with repeated exposure to stress in the stressed group and over time in the nonstressed group, this decrease did not reach significance (fig. 2).

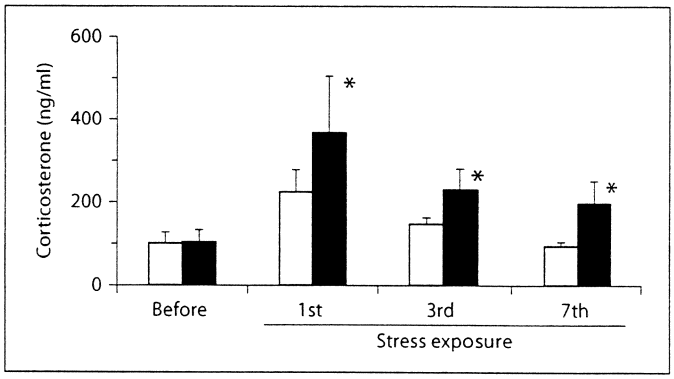


Fig. 2. The effect of restraint stress on blood corticosterone concentrations. Blood was collected from stressed (black bars) and nonstressed (white bars) mice before the 1st stress and after the 1st, 3rd and 7th stress exposure, and the corticosterone levels in blood were measured by EIA. Data are expressed as means ± SD (n = 4–7). * $p < 0.05$ compared to nonstressed mice.

The Effect of Restraint Stress on OVA-Specific IgE in Plasma

The levels of OVA-specific IgE in stressed mice were not significantly different from those in nonstressed mice [5.1 ± 2.0 (n = 8) vs. 6.4 ± 2.0 EU/ml (n = 7)] on day 37 before the second challenge.

Worsening of Antigen-Induced Airway Inflammation due to Restraint Stress

In stressed mice, the numbers of total cells, eosinophils and lymphocytes in BAL fluid 3 days after the second OVA challenge (day 40) were significantly increased compared to those before the second OVA challenge (day 37) [day 40 (n = 11) vs. day 37 (n = 6) in the stress/OVA group: total cells, 178.8 ± 88.9 vs. 35.9 ± 19.0 × 10^4 cells/ml, $p < 0.01$; eosinophils, 131.9 ± 77.6 vs. 22.5 ± 18.5 × 10^4 cells/ml, $p < 0.01$; lymphocytes, 22.8 ± 10.9 vs. 3.8 ± 2.2 × 10^4 cells/ml, $p < 0.05$] (fig. 3b). However, the second challenge with saline in stressed mice did not increase the numbers of those cells [day 40 (n = 6) vs. day 37 (n = 9) in the stress/saline group: total cells, 16.1 ± 9.4 vs. 36.6 ± 20.7 × 10^4 cells/ml; eosinophils, 0.7 ± 1.4 vs. 16.8 ± 14.2 × 10^4 cells/ml; lymphocytes, 2.1 ± 2.5 vs. 5.0 ± 4.1 × 10^4 cells/ml] nor of macrophages and neutrophils. In stressed mice, there were significant differences in the numbers of total cells ($p < 0.01$), eosinophils ($p < 0.01$) and lymphocytes ($p < 0.01$) between the OVA and saline challenge on day 40. On the other hand, in nonstressed mice, there was no statistically significant increase in the numbers of total cells, eosinophils and lymphocytes, nor of macrophages and neutrophils, in BAL fluid at any time point after the second OVA challenge compared to the numbers of cells before the second OVA challenge (day 37) [day 40 (n = 10) vs. day 37 (n = 6) in the nonstress/OVA group: total cells, 85.4 ± 33.4 vs. 54.3 ± 21.4 × 10^4 cells/ml; eosinophils, 52.0 ± 29.2 vs. 41.2 ± 27.8 × 10^4 cells/ml; lymphocytes, 12.3 ± 5.6 vs. 7.8 ± 3.9 × 10^4 cells/ml] (fig. 3a). There was also no significant increase in the numbers of inflammatory cells after the second challenge with saline [day 40 (n = 6) vs. day 37 (n = 8) in the nonstress/saline group: total cells, 21.6 ± 4.2 vs. 51.4 ± 33.1 × 10^4 cells/ml; eosinophils, 2.8 ± 2.7 vs. 29.7 ± 28.0 × 10^4 cells/ml; lymphocytes, 4.0 ± 1.8 vs. 6.4 ± 3.5 × 10^4 cells/ml]. However, in nonstressed mice, there were significant differences in the numbers of total cells ($p < 0.01$), eosinophils ($p < 0.01$) and lymphocytes ($p < 0.01$) between the OVA and saline challenge on day 40. Comparing the numbers of inflammatory cells between stressed and nonstressed mice on

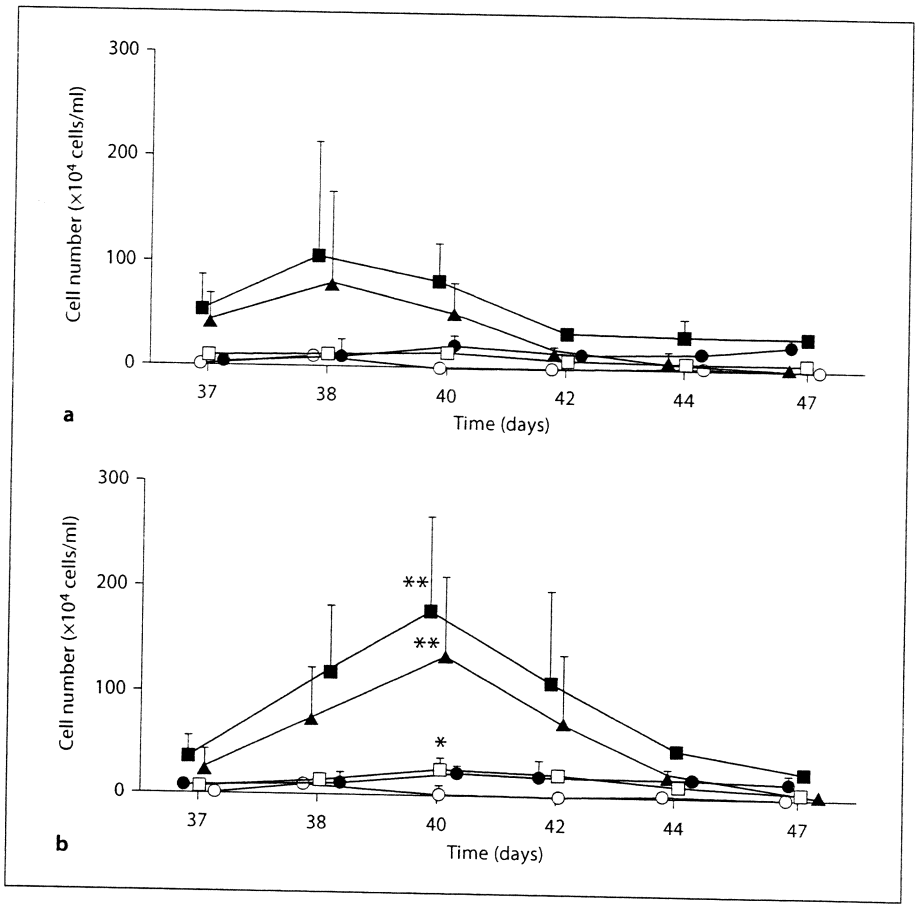


Fig. 3. Time course of changes in cell numbers in the BAL fluid from stressed and nonstressed mice after the second OVA inhalation. In the BAL fluid from nonstressed (**a**) and stressed (**b**) mice challenged with OVA, the numbers of total cells (■), macrophages (●), eosinophils (▲), neutrophils (○) and lymphocytes (□) were counted at the time points indicated. Data are expressed as means ± SD (n = 6–11). * $p < 0.05$, ** $p < 0.01$ compared to prior to the challenge (day 37).

day 40 (3 days after the second OVA challenge), significant differences were found in numbers of total cells ($p < 0.01$), eosinophils ($p < 0.01$) and lymphocytes ($p < 0.05$), while there were no significant differences in the numbers of any type of cell between the groups on day 37 (before the second challenge). Therefore, in the following experiments in this study, the numbers of inflammatory cells in BAL fluid were evaluated on day 40.

The levels of IL-4, IL-5 and IL-13 in BAL fluid from stressed and OVA-challenged mice were significantly higher than those in nonstressed and OVA-challenged mice on day 38 (1 day after the second OVA challenge; table 1). In stressed mice, the levels of these cytokines were decreased on day 40 (3 days after the second challenge) and were below the limit of detection on day 42 (5 days after the second challenge), while these cytokines were not detected on either day 40 or 42 in nonstressed mice. Similar levels of IL-13 were detected even after the saline challenge in stressed and nonstressed mice, although the levels were significantly lower than those in the OVA-challenged mice. The presence of IL-13 in saline-challenged mice could be due to the effect of the first OVA challenge on day 30. IFN-γ was detected in stressed and nonstressed mice only on day 38, after the second OVA challenge, when the levels were not significantly different between the groups (table 1).

Table 1. Cytokine contents in BAL fluids from the stressed and nonstressed B6 mice on day 38

2nd challenge	IL-4 pg/ml	IL-5 pg/ml	IL-13 pg/ml	IFN-γ pg/ml
Nonstressed				
OVA	3.7 ± 4.0	10.9 ± 8.4	50.6 ± 49.3	3.5 ± 0.5
Saline	0.0 ± 0.0	0.0 ± 0.0	23.3 ± 7.5	0.0 ± 0.0
Stressed				
OVA	26.5 ± 7.2**	23.1 ± 10.2*	195.3 ± 133.7*	4.3 ± 1.4
Saline	0.0 ± 0.0	0.0 ± 0.0	26.8 ± 15.8	0.0 ± 0.0

Data are expressed as means ± SD (n = 4–7). * $p < 0.05$, ** $p < 0.01$ compared to the nonstressed mice.

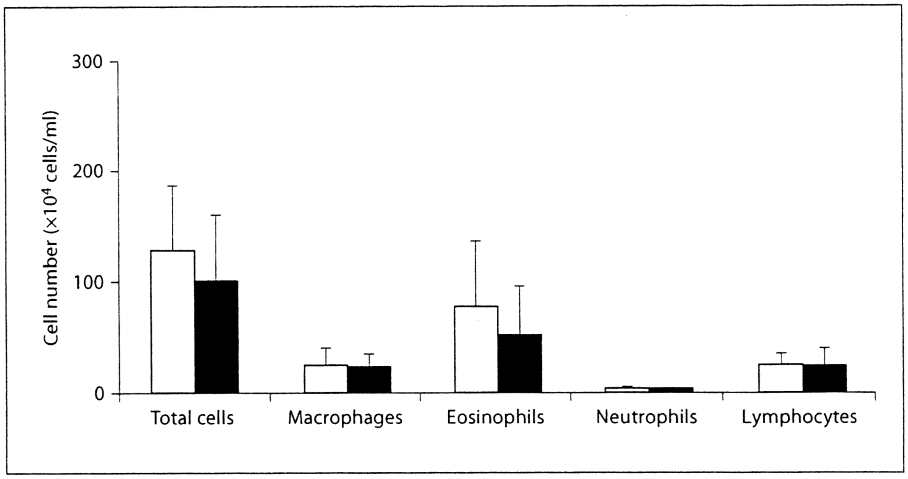


Fig. 4. Comparison of cell numbers in BAL fluids between stressed and nonstressed MORKO mice after the second OVA challenge. The numbers of total cells, macrophages, eosinophils, neutrophils and lymphocytes in BAL fluids from stressed (black bars) and nonstressed (white bars) MORKO mice 3 days after OVA challenge were counted. Data are expressed as means ± SD (n = 7).

Table 2. Cytokine contents in BAL fluids from the stressed and nonstressed MORKO mice on day 38

	IL-4 pg/ml	IL-5 pg/ml	IL-13 pg/ml	IFN-γ pg/ml
Nonstressed	29.6 ± 19.7	36.8 ± 14.1	41.8 ± 41.8	12.8 ± 4.1
Stressed	21.4 ± 13.8	36.8 ± 2.5	92.1 ± 71.4	10.5 ± 0.5

Data are expressed as means ± SD (n = 4–7).

Abolishment of Restraint Stress-Induced Aggravation in MORKO Mice

In both stressed and nonstressed MORKO mice, there were no significant increases in the numbers of any type of cell in BAL fluids on day 40 (3 days after the second OVA challenge) compared to those on day 37 (before the second challenge), and there was no significant difference in the numbers of any type of cell in BAL fluid between stressed and nonstressed MORKO mice on either day 37 (data not shown) or day 40 (fig. 4). The levels of IL-4, IL-5, IL-13 and IFN-γ in BAL fluid of stressed MORKO mice were not significantly different from those of nonstressed MORKO mice on day 38 (1 day after the second OVA challenge; table 2).

Worsening of Antigen-Induced Airway Inflammation by Morphine, a MOR Agonist

To investigate whether MOR activation exacerbates antigen-induced airway inflammation, we examined the effect of administration of the MOR agonist morphine as a replacement for restraint stress in wild-type mice without stress. The systemic administration of morphine (1 mg/kg) produced significant increases in the numbers of total cells, eosinophils and lymphocytes in BAL fluid compared to the administration of PBS [morphine (1 mg/kg) (n = 9) vs. PBS (n = 11) in the nonstress/OVA group: total cells, 277.8 ± 107.0 vs. 164.9 ± 86.5 × 10^4 cells/ml, $p < 0.05$; eosinophils, 192.0 ± 73.2 vs. 118.4 ± 71.3 × 10^4 cells/ml, $p < 0.05$; lymphocytes, 55.0 ± 32.9 vs. 25.1 ± 18.1 × 10^4 cells/ml, $p < 0.05$). However, doses of 0.3, 3 and 10 mg/kg morphine did not produce significant effects on the numbers of any types of cells in BAL fluid compared with PBS (fig. 5). In contrast to the results for wild-type mice, in MORKO mice, administration of morphine (1 mg/kg) did not significantly affect the numbers of inflammatory cells in BAL fluid compared with PBS administration (data not shown).

Inhibitory Effects of Antagonists for μ-, but Not κ- and δ-Opioid Receptors on Stress-Induced Aggravation

To investigate whether other opioid receptors, such as κ- and δ-receptors, rather than MOR were involved in stress-induced exacerbation of antigen-induced airway inflammation, we examined the effect of systemic administration of antagonists for opioid receptors in wild-type mice. The increase in total cells, but not eosinophils and lymphocytes, in BAL fluid from stressed mice treated with PBS was abolished in stressed mice treated with β-FNA (10 mg/kg, i.p.), a MOR antagonist [PBS (n = 7) vs. β-FNA (n = 8) in the stress/OVA group: total cells 291.1 ± 106.7 vs. 172.7 ± 83.5 × 10^4 cells/ml, $p < 0.05$]. Treatment with nor-BNI (10 mg/kg, i.p.), a κ-opioid receptor antagonist, and naltrindole (10 mg/kg, i.p.), a δ-

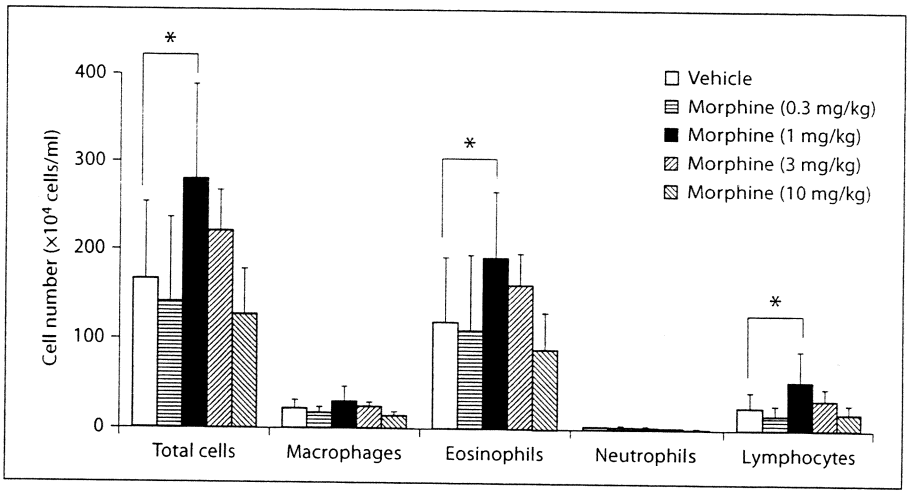


Fig. 5. The effect of morphine on cell numbers in the BAL fluid after the second OVA challenge. The numbers of total cells, macrophages, eosinophils, neutrophils and lymphocytes in the BAL fluid from vehicle- or morphine-treated mice 3 days after OVA challenge were counted. Data are expressed as means ± SD (n = 9–11). * $p < 0.05$.

opioid receptor antagonist, had no significant effect on the increase in total cells, eosinophils and lymphocytes in BAL fluid from stressed mice (data not shown).

Abolishment of Stress-Induced Aggravation by a MOR-Selective Antagonist in the CNS

The above results revealed that MOR were involved in stress-induced aggravation of antigen-induced airway inflammation. Since MOR are expressed not only in the CNS [11, 12], but also on immune cells [17, 18], as a next step, we investigated which MOR present in the CNS or on immune cells are involved in aggravation, by intracerebroventricular injection of β-FNA to selectively antagonize MOR in the CNS, and by intraperitoneal injection of naloxone methiodide for opioid receptors, including MOR, in the periphery. The increase in the numbers of total cells, eosinophils and lymphocytes in the BAL fluid caused by restraint stress was abolished by intracerebroventricular administration of β-FNA (5 nmol/mouse) [PBS (n = 7) vs. β-FNA (n = 7) in the stress/OVA group: total cells, 297.5 ± 119.1 vs. 124.6 ± 42.5 × 10^4 cells/ml, $p < 0.01$; eosinophils, 217.3 ± 84.0 vs. 91.2 ± 39.9 × 10^4 cells/ml, $p < 0.01$; lymphocytes, 45.6 ± 21.8 vs. 18.3 ± 8.4 × 10^4 cells/ml, $p < 0.05$). Stressed mice that were injected intracerebroventricularly with β-FNA showed similar levels of cells to nonstressed mice that were injected intracerebroventricularly with vehicle (fig. 6a). By contrast, treatment with a peripherally restricted opioid antagonist, naloxone methiodide (10 mg/kg), did not reduce the increase in the inflammatory cells in BAL fluid of stressed mice that were treated intraperitoneally with vehicle, and stressed mice that were injected intraperitoneally with naloxone methiodide still showed a significant increase in the numbers of total cells and eosinophils compared to nonstressed mice that were injected intraperitoneally with vehicle (fig. 6b).

Discussion

The present study demonstrated for the first time that MOR in the CNS are involved in psychological stress-induced aggravation of airway inflammation in a murine model of allergic asthma using MORKO mice and MOR antagonists/agonists.

The effect of restraint stress as a model of psychological stress was confirmed by the findings shown in figure 2, in which the levels of corticosterone, one of the stress hormones [33], were significantly higher in stressed mice than in nonstressed mice. Corticosterone levels in both stressed (restraint stress + deprivation of food and water) and nonstressed (only food and water deprivation) groups declined with repeated stress, although the decline was not statistically significant. It has been suggested that repeated stress induces a state of hyporesponsiveness of the HPA axis, whereby corticosterone secretion is attenuated [34]. In other rodent models, repeated stress ranging from 4 to 14 days was required to induce worsening of allergic airway inflammation [22, 35–37]. By contrast, short-term restraint stress reduced allergic airway inflammation [22, 35]; therefore, prolonged period of repeated stress was used in this study, as in our previous study [22]. Allergen-induced airway inflammation in stressed mice was more severe than in nonstressed mice, in association with greater amounts of Th2 cytokines. These findings are consistent with previous reports using

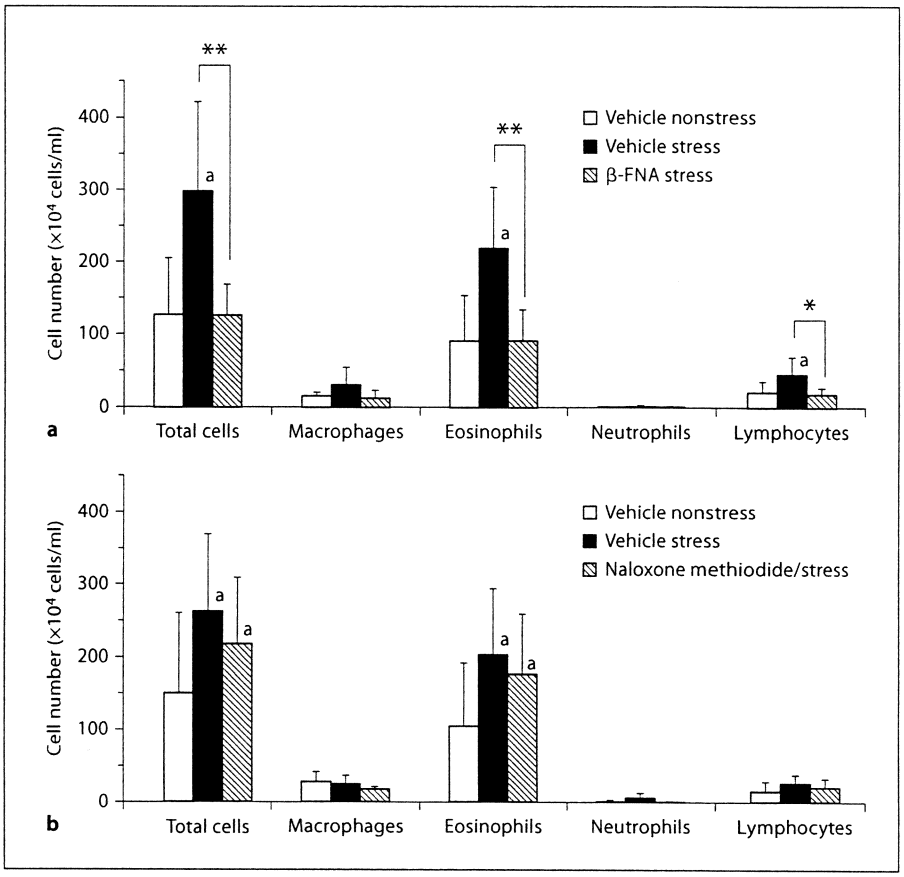


Fig. 6. The effects of antagonists for central MOR and peripheral opioid receptors on cell numbers in the BAL fluid after OVA challenge. The numbers of total cells, macrophages, eosinophils, neutrophils and lymphocytes in the BAL fluid from stressed and nonstressed mice 3 days after OVA challenge were counted. β-FNA (5 nmol/mouse, intracerebroventricular) (**a**) and naloxone methiodide (10 mg/kg, i.p.) (**b**) were administered before each stress exposure. Data are expressed as means ± SD (n = 7). * $p < 0.05$, ** $p < 0.01$. [a] $p < 0.05$ compared to vehicle/nonstressed mice.

mouse models with different types of psychological stress, such as sound stress, restraint stress and forced swim stress [22, 35]. All experiments described here were conducted in B6 mice. There are several pieces of evidence that support the idea that allergic inflammatory responses in airways vary widely in different strains of mice [38]. BALB/c mice have been commonly used for mouse models of allergic asthma. To ensure that the effect of restraint stress was not specific to B6 mice, we previously analyzed the same protocol in BALB/c mice [22]. While the results of the experiments using BALB/c mice were similar to those obtained using B6 mice, stress was relatively more effective in B6 mice. Furthermore, the genetic background of the MORKO mice used in the current study was B6.

In MORKO mice, the numbers of inflammatory cells in BAL fluid were not significantly different from those in wild-type mice under nonstressed conditions, although the levels of IL-4 and IL-5 were significantly higher. The reason for the differences in cytokine levels between MORKO and wild-type mice was not determined. However, in contrast to the results for wild-type mice, no significant worsening of inflammatory cell numbers and cytokine levels in BAL fluid was observed in MORKO mice under stress conditions. These results suggest that MOR are involved not in the development but the exacerbation of allergen-induced airway inflammation. The involvement of MOR in stress-induced aggravation of allergic airway inflammation was further investigated by the replacement of stress with a MOR agonist, morphine. As shown in figure 5, the administration of 1 mg/kg morphine, but not of 0.3, 3 or 10 mg/kg, induced an increase in inflammatory cells in BAL fluid after the second allergen challenge. The analgesic effect exerted by 1 mg/kg morphine was similar to that evoked by the restraint stress used in this study [39]. Administration of 0.3 mg/kg might not be sufficient to stimulate MOR. Administration of higher doses of morphine could have desensitized MOR, an idea that is supported by findings that repeated administration of morphine at doses of 3 mg/kg or 10 mg/kg for 5–7 days resulted in tolerance to morphine-induced analgesia [40, 41]. There are several pieces

of evidence showing that desensitization of MOR via the activation of protein kinase C and internalization of MOR via activation of arrestin are major mechanisms that reveal antinociceptive tolerance due to chronic treatment with morphine [42, 43]. The MOR-dependent morphine effect was confirmed by the loss of the effect in MORKO mice. Severe asthma exacerbations related to the use of opioids such as heroin and morphine (a heroin metabolite) have received attention as a public health issue. The possible mechanisms have been thought to be sensitization against opioid antigen and pharmacological degranulation of mast cells independent of opioid receptors [44, 45]. The results of the current study suggest the possibility that opioid use exacerbates allergen-induced asthma attacks through MOR activation.

Endogenous opioids released upon exposure to psychological stress are able to bind to 3 subtypes of opioid receptors, i.e. μ, δ and κ [12, 13]. MOR involvement was pharmacologically investigated with opioid receptor antagonists specific for each subtype. The simultaneous administration of β-FNA, a MOR antagonist, with restraint stress significantly reduced the number of total cells in BAL fluid compared to the simultaneous administration of vehicle. However, the reduction in the numbers of eosinophils and lymphocytes was not statistically significant, the reason for which will be discussed below. On the other hand, naltrindole, a δ-opioid receptor antagonist, and nor-BNI, a κ-opioid receptor antagonist, showed no significant effects on the increase in total cells, nor on eosinophils and lymphocytes, under the stress conditions. These observations suggest that subtypes of opioid receptors other than MOR are unlikely to be involved in stress-induced aggravation of airway inflammation.

Opioid-induced immunomodulation is thought to be mediated centrally by MOR localized in the CNS and peripherally by MOR expressed on immune cells [46]. To clarify which MOR contribute to stress-induced aggravation, MOR in the CNS were selectively antagonized by intracerebroventricular injection of β-FNA, and MOR in the periphery were selectively antagonized by intraperitoneal injection of naloxone methiodide, a nonselective opioid receptor antagonist that is unable to pass through the blood-brain barrier. Stress-induced aggravation was significantly reduced by intracerebroventricular injection of β-FNA, but not by intraperitoneal injection of naloxone methiodide. These results indicate that the MOR involved in stress-induced aggravation could be localized in the CNS. The participation of the CNS in stress-induced aggravation of airway inflammation and obstruction has been suggested in previous reports. Rosenkranz et al. [47] showed that activation in the anterior cingulated cortex and insula in response to asthma-relevant emotional stimuli, demonstrated by functional magnetic resonance imaging, was associated with airway inflammation and obstruction in asthmatics exposed to antigen. This study suggests a functional link between emotion-processing circuits in the brain and peripheral physiological processes relevant to airway inflammation and narrowing subsequent to antigen exposure in the lungs [47]. Joachim et al. [48] reported that, in asthmatics, stress perception was correlated with serum levels of brain-derived neurotrophic factor involved in central stress processing and, furthermore, that forced expiratory volume in 1 s was negatively correlated with brain-derived neurotrophic factor. In contrast to intracerebroventricular administration (fig. 6a), intraperitoneal administration of β-FNA showed no significant effects on the numbers of eosinophils and lymphocytes, as mentioned above. This lack of effect might be due to the fact that the intraperitoneal dose of β-FNA in the CNS was not sufficient to antagonize MOR in the CNS.

It has become increasingly apparent that psychological stress increases the frequency, duration and severity of asthmatics' symptoms by enhancing airway inflammatory responses to environmental triggers such as inhaled allergen, characterized by further skewing of the balance toward a Th2-dominant cytokine profile [49]. Students with asthma showed increases in eosinophils and IL-5 in sputum and enhanced and reduced production of Th2 and Th1 cytokines, respectively, by mononuclear cells in peripheral blood during exam periods compared to non-exam periods [9, 10, 50]. It has been reported that lower socioeconomic status and more stressful life events are associated with higher levels of Th2 cytokine production and eosinophil counts in peripheral blood [51–53]. In animal models of asthma, various types of psychological stress such as electrical footshock stress, sound stress, restraint stress and forced swim stress have been shown to exacerbate allergen-induced airway inflammation [22, 35–37]. The HPA axis and SAM system have been proposed as relevant pathways through which stress modifies inflammatory/immune responses to induce asthma exacerbation. Stimulation of the HPA axis and SAM system results in the release of stress hormones corticosterone and catecholamine, which have the potential to shift immune responses to Th2 predominance [33, 34, 54]. However, the psycho-neuro-endocrino-immunological cascade in the worsening of asthma symptoms due to psychological stress is not fully understood. There

are only a few reports suggesting interactions between psychological stress and peripheral neuronal responses. Joachim et al. [55, 56] used a murine model to show that increased expression of substance P and its interaction with NK-1 receptors in diseased airways were involved in sound stress-aggravated airway inflammation.

In summary, the present study identified for the first time that MOR are one group of candidates in the CNS linking psychological stress to the worsening of allergen-induced airway inflammation. The mechanism by which the activation of MOR in the CNS was triggered by psychological stress to induce immune alterations favoring asthmatic exacerbations should be further investigated, paying particular attention to activation of the HPA axis and SAM system.

Acknowledgments

This article was checked for correct English usage by American Journal Experts (Certification Number: 0805-16C9-6EE3-7CA3-5EB1). This work was supported by Grants-in-Aid for Scientific Research (No. 16616007 and 19590909 to I.O.) and by the High Technology Research Program of the Ministry of Education, Culture, Sports, Science and Technology of Japan.

References

1 Bousquet J, Jeffery PK, Busse WW, Johnson M, Vignola AM: Asthma: from bronchoconstriction to airways inflammation and remodeling. Am J Respir Crit Care Med 2000; 161:1720–1745.
2 Holgate ST: Airway inflammation and remodeling in asthma: current concepts. Mol Biotechnol 2002;22:179–189.
3 Kay AB: The role of T lymphocytes in asthma. Chem Immunol Allergy 2006;91:59–75.
4 Barnes PJ: Immunology of asthma and chronic obstructive pulmonary disease. Nat Rev Immunol 2008;8:183–192.
5 Rietveld S, Everaerd W, Creer TL: Stress-induced asthma: a review of research and potential mechanisms. Clin Exp Allergy 2000; 30:1058–1066.
6 Chetta A, Foresi A, Marangio E, Olivieri D: Psychological implications of respiratory health and disease. Respiration 2005;72: 210–215.
7 Isenberg SA, Lehrer PM, Hochron S: The effects of suggestion and emotional arousal on pulmonary function in asthma: a review and a hypothesis regarding vagal mediation. Psychosom Med 1992;54:192–216.
8 Sandberg S, Paton JY, Ahola S, McCann DC, McGuinness D, Hillary CR, Oja H: The role of acute and chronic stress in asthma attacks in children. Lancet 2000;356:982–987.
9 Kang DH, Coe CL, McCarthy DO, Jarjour NN, Kelly EA, Rodriguez RR, Busse WW: Cytokine profiles of stimulated blood lymphocytes in asthmatic and healthy adolescents across the school year. J Interferon Cytokine Res 1997;17:481–487.
10 Liu LY, Coe CL, Swenson CA, Kelly EA, Kita H, Busse WW: School examinations enhance airway inflammation to antigen challenge. Am J Respir Crit Care Med 2002;165:1062–1067.
11 Lopez-Carderon A, Ariznavarreta C, Chen CL: Influence of chronic restraint stress on pro-opiomelanocortin mRNA and β-endorphin in the rat hypothalamus. J Mol Endocrinol 1991;7:197–204.
12 Drolet G, Dumont EC, Gosselin I, Kinkead R, Laforest S, Trottier L-F: Role of endogenous opioid system in the regulation of the stress response. Prog Neuropsychopharmacol Biol Psychiatry 2001;25:729–741.
13 Akil H, Watson SJ, Young E, Lewis ME, Khachaturian H, Walker JM: Endogenous opioids: biology and function. Annu Rev Neurosci 1984;7:223–255.
14 Buckingham JC: Stimulation and inhibition of corticotropin releasing factor secretion by β endorphin. Neuroendocrinology 1986;42: 148–152.
15 Kiritsy-Roy JA, Appel NM, Bobbitt FG, Van Loon GR: Effects of μ-opioid receptor stimulation in the hypothalamic paraventricular nucleus on basal and stress-induced catecholamine secretion and cardiovascular responses. J Pharmacol Exp Ther 1986;239: 814–822.
16 Elenkov IJ, Chrousos GP: Stress hormones, Th1/Th2 patterns, pro/anti-inflammatory cytokines and susceptibility to disease. Trends Endocrinol Metab 1999;10:359–368.
17 Chuang TK, Killam KF, Chuang LF, Kung HF, Sheng WS, Chao CC, Yu L, Chuang RY: μ opioid receptor gene expression in immune cells. Biochem Biophys Res Commun 1995;216:922–930.
18 Makarenkova VP, Esche C, Kost NV, Shurin GV, Rabin BS, Zozulya AA, Shurin MR: Identification of δ- and μ-type receptors on human and murine dendritic cells. J Neuroimmunol 2001;117:68–77.
19 Sacerdote P, Manfredi B, Gaspani L, Panerai AE: The opioid antagonist naloxone induces a shift from type 2 to type 1 cytokine pattern in BALB/c mice. Blood 2000;95:2031–2036.
20 Wang J, Charboneau R, Barke RA, Loh HH, Roy S: μ-opioid receptor mediates chronic restraint stress-induced lymphocyte apoptosis. J Immunol 2002;169:3630–3636.
21 Roy S, Wang J, Gupta S, Charboneau R, Loh HH, Barke RA: Chronic morphine treatment differentiates T helper cells to Th2 effector cells by modulating transcription factors GATA 3 and T-bet. J Neuroimmunol 2004; 147:78–81.
22 Okuyama K, Ohwada K, Sakurada S, Sato N, Sora I, Tamura G, Takayanagi M, Ohno I: The distinctive effects of acute and chronic psychological stress on airway inflammation in a murine model of allergic asthma. Allergol Int 2007;56:29–35.
23 Sora I, Takahashi N, Funada M, Ujike H, Revay RS, Donovan DM, Miner LL, Uhl GR: Opiate receptor knockout mice define μ receptor roles in endogenous nociceptive responses and morphine-induced analgesia. Proc Natl Acad Sci USA 1997;94:1544–1549.
24 Hall FS, Li XF, Goeb M, Roff S, Hoggatt H, Sora I, Uhl GR: Congenic C57BL/6 μ-opiate receptor (MOR) knockout mice: baseline and opiate effects. Genes Brain Behav 2003; 2:114–121.
25 Kumagai K, Ohno I, Okada S, Ohkawara Y, Suzuki K, Shinya T, Nagase H, Iwata K, Shirato K: Inhibition of matrix metalloproteinases prevents allergen-induced airway inflammation in a murine model of asthma. J Immunol 1999;162:4212–4219.
26 Posevitz V, Vizler C, Benyhe S, Duda E, Borsodi A: Restraint stress and anti-tumor immune response in mice. Acta Biol Hung 2003;54:167–176.
27 Mercado AM, Padgett DA, Sheridan JF, Marucha PT: Altered kinetics of IL-1α, IL-1β, and KGF-1 gene expression in early wounds of restrained mice. Brain Behav Immun 2002;16:150–162.

28 Ashcraft KA, Hunzeker J, Bonneau RH: Psychological stress impairs the local CD8+ T cells response to mucosal HSV-1 infection and allows for increased pathogenicity via a glucocorticoid receptor-mediated mechanism. Psychoneuroendocrinology 2008;33:951–963.
29 Tseng RJ, Padgett DA, Dhabhar FS, Engler H, Sheriden JF: Stress-induced modulation of NK activity during influenza viral infection: role of glucocorticoids and opioids. Brain Behav Immun 2005;19:153–164.
30 Hiramatsu M, Inoue K, Ambo A, Sasaki Y, Kameyama T: Long-lasting antinociceptive effects of a novel dynorphin analogue, Tyr-D-Ala-Phe-Leu-Argψ (CH_2NH) Arg-NH_2, in mice. Br J Pharmacol 2001;132:1948–1956.
31 Baamonde A, Lasta A, Juárez L, García-Suárez O, Meana A, Hidelgo A, Menéndez L: Endogenous β-endorphin induces thermal analgesia at the initial stage of a murine osteosarcoma. Peptides 2006;27:2778–2785.
32 Ohwada K, Kanako W, Okuyama K, Ohkawara Y, Sugaya T, Takayanagi M, Ohno I: The involvement of type 1a angiotensin II receptors in the regulation of airway inflammation in a murine model of allergic asthma. Clin Exp Allergy 2007;37:1720–1727.
33 Wright RJ: Stress and atopic disorders. J Allergy Clin Immunol 2005;116:1301–1306.
34 Wright RJ, Cohen RT, Cohen S: The impact of stress on the development and expression of atopy. Curr Opin Allergy Clin Immunol 2005;5:23–29.
35 Forsythe P, Ebeling C, Gordon JR, Befus AD, Vliagoftis H: Opposing effects of short- and long-term stress on airway inflammation. Am J Respir Crit Care Med 2004;169:220–226.
36 Joachim RA, Quarcoo D, Arck PC, Herz U, Renz H, Klapp BF: Stress enhances airway reactivity and airway inflammation in an animal model of allergic bronchial asthma. Psychosom Med 2003;65:811–815.
37 Datti F, Datti M, Antunes E, Teixeira NA: Influence of chronic unpredictable stress on the allergic responses in rats. Physiol Behav 2002;77:79–83.
38 Whitehead GS, Walker JKL, Berman KG, Foster WM, Schwartz DA: Allergen-induced airway disease is mouse strain dependent. Am J Physiol Lung Cell Mol Physiol 2003;285:L32–L42.
39 Homayoun H, Dehpour AR: Differential contribution of cholecystokinin receptors to stress-induced modulation of seizure and nociception thresholds in mice. Pharmacol Biochem Behav 2004;78:209–215.
40 Li S, Lee ML, Brunchas MR, Chan GC, Storm DR, Chavkin C: Calmodulin-stimulated adenylyl cyclase gene deletion affects morphine responses. Mol Pharmacol 2006;70:1742–1749.
41 Tsuchiya T, Takeuchi T, Hayashida K, Shimizu H, Ando K, Harada E: Milk-derived lactoferrin may block tolerance to morphine analgesia. Brain Res 2006;1068:102–108.
42 Zeitz KP, Malmberg AB, Gilbert H, Basbaum AI: Reduced development of tolerance to the analgesic effects of morphine and clonidine in PKC gamma mutant mice. Pain 2001;94:245–253.
43 Bohn LM, Lefkowitz RJ, Caron MG: Differential mechanisms of morphine antinociceptive tolerance revealed in βarrestin-2 knock-out mice. J Neurosci 2002;22:10494–10500.
44 Cygan J, Trunsky M, Corbridge T: Inhaled heroin-induced status asthmaticus: five cases and a review of the literature. Chest 2000;117:272–275.
45 Krantz AJ, Hershow RC, Prachand N, Hayden DM, Franklin C, Hryhorczuk DO: Heroin insufflation as a trigger for patients with life-threatening asthma. Chest 2003;123:510–517.
46 Wei G, Moss J, Yuan CS: Opioid-induced immunosuppression: is it centrally mediated or peripherally mediated? Biochem Pharmacol 2003;65:1761–1766.
47 Rosenkranz MA, Busse WW, Johnstone T, Swenson CA, Crisafi GM, Jackson MM, Bosch JA, Sheridan JF, Davidson RJ: Neural circuitry underlying the interaction between emotion and asthma symptom exacerbation. Proc Natl Acad Sci USA 2005;102:13319–13324.
48 Joachim RA, Noga O, Sagach V, Hanf G, Fliege H, Kocalevent RD, Peters EM, Klapp BF: Correlation between immune and neuronal parameters and stress perception in allergic asthmatics. Clin Exp Allergy 2008;38:283–290.
49 Chen E, Miller GE: Stress and inflammation in exacerbations of asthma. Brain Behav Immun 2007;21:993–999.
50 Höglund CO, Axén J, Kemi C, Jernelöv S, Grunewald J, Müller-Suur C, Smith Y, Grönneberg R, Eklund A, Stierna P, Lekander M: Changes in immune regulation in response to examination stress in atopic and healthy individuals. Clin Exp Allergy 2006;36:982–992.
51 Chen E, Fisher EB, Bacharier LB, Strunk RC: Socioeconomic status, stress, and immune markers in adolescents with asthma. Psychosom Med 2003;65:984–992.
52 Chen E, Hanson MD, Paterson LQ, Griffin MJ, Walker HA, Miller GE: Socioeconomic status and inflammatory processes in childhood asthma: the role of psychological stress. J Allergy Clin Immunol 2006;117:1014–1020.
53 Chen E, Chim LS, Strunk RC, Miller GE: The role of the social environment in children and adolescents with asthma. Am J Respir Crit Care Med 2007;176:644–649.
54 Chrousos GP: Stress, chronic inflammation, and emotional and physical well-being: concurrent effects and chronic sequelae. J Allergy Clin Immunol 2000;106:S275–S291.
55 Joachim RA, Sagach V, Quarcoo D, Dinh QT, Arck PC, Klapp BF: Neurokinin-1 receptor mediates stress-exacerbated allergic airway inflammation and airway hyperresponsiveness in mice. Psychosom Med 2004;66:564–571.
56 Joachim RA, Cifuentes LB, Sagach V, Quarcoo D, Hagen E, Arck PC, Fischer A, Klapp BF, Dinh QT: Stress induces substance P in vagal sensory neurons innervating the mouse airways. Clin Exp Allergy 2006;36:1001–1010.

平成22年度～平成26年度私立大学戦略的研究基盤形成支援事業研究成果報告書

平成27年5月発行

編集　私立大学戦略的研究基盤形成支援事業（創薬研究）運営委員会
発行　東北薬科大学
〒981-8558　仙台市青葉区小松島4-4-1
TEL　022-234-4181
印刷　株式会社東北プリント